

AD-A186 490

UNITED STATES AIR FORCE RESEARCH INITIATION PROGRAM  
1984 RESEARCH REPORTS (U) SOUTHEASTERN CENTER FOR  
ELECTRICAL ENGINEERING EDUCATION INC S W D PEELE

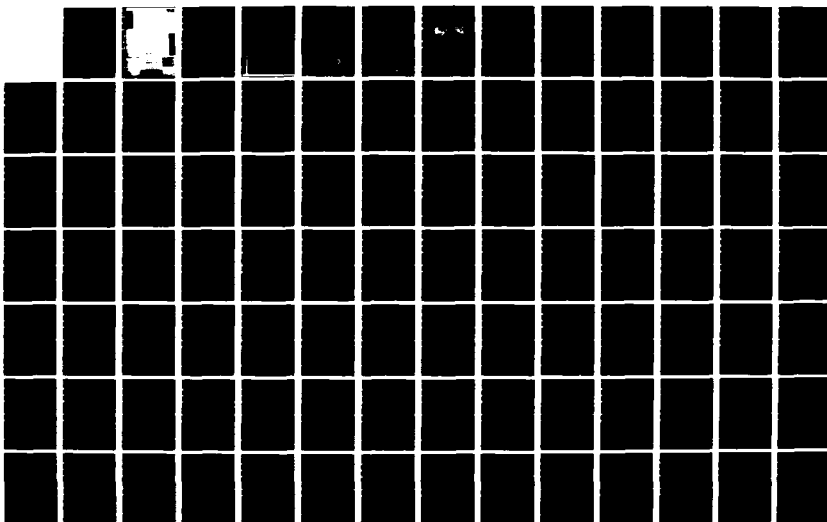
01/11

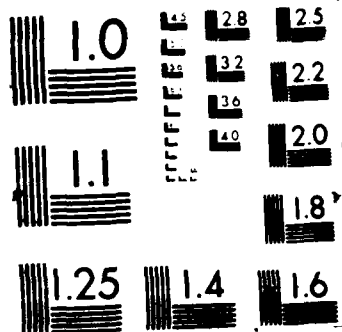
UNCLASSIFIED

MAY 86 AFOSR-TR-87-1721 F49620-82-C-0035

F/G 15/1

NL







AD-A186 490

AFOSR

SCIEE

USAF RESEARCH INITIATION PROGRAM

1984

RESEARCH REPORTS

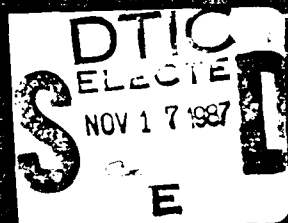
VOLUME II

CONDUCTED BY  
THE SOUTHEASTERN CENTER FOR  
ELECTRICAL ENGINEERING EDUCATION

PROF. WARREN D. PEELE  
PROGRAM DIRECTOR, SCIEE

MAJ. AMOS OTIS  
PROGRAM MANAGER, AFOSR

DTIC FILE COPY



This document has been approved  
for public release and sale; its  
distribution is unlimited.

UNCLASSIFIED

SECURITY CLASSIFICATION OF THIS PAGE

## REPORT DOCUMENTATION PAGE

Form Approved  
OMB No. 0704-0188

1a. REPORT SECURITY CLASSIFICATION <b>UNCLASSIFIED</b>			1b. RESTRICTIVE MARKINGS		
2a. SECURITY CLASSIFICATION AUTHORITY			3. DISTRIBUTION/AVAILABILITY OF REPORT  Approved for public release; distribution unlimited.		
2b. DECLASSIFICATION/DOWNGRADING SCHEDULE					
4. PERFORMING ORGANIZATION REPORT NUMBER(S)			5. MONITORING ORGANIZATION REPORT NUMBER(S)  <b>AFOSR-TR. 87-1721</b>		
6a. NAME OF PERFORMING ORGANIZATION The Southeastern Center for Electrical Engineering Education		6b. OFFICE SYMBOL (if applicable)	7a. NAME OF MONITORING ORGANIZATION Air Force Office of Scientific Research/XOT		
6c. ADDRESS (City, State, and ZIP Code) 11th & Massachusetts Ave. St. Cloud, Florida 32769			7b. ADDRESS (City, State, and ZIP Code) Building 410 Bolling AFB, DC 20332		
8a. NAME OF FUNDING/SPONSORING ORGANIZATION  AFOSR		8b. OFFICE SYMBOL (if applicable)  XOT	9. PROCUREMENT INSTRUMENT IDENTIFICATION NUMBER  F49620-82-C-0035		
8c. ADDRESS (City, State, and ZIP Code)  Building 410 Bolling AFB, DC 20332			10. SOURCE OF FUNDING NUMBERS		
			PROGRAM ELEMENT NO. 61102F	PROJECT NO. 2301	TASK NO. D5
11. TITLE (Include Security Classification) USAF Research Initiation Program - Volume 2					
12. PERSONAL AUTHOR(S) Prof. Warren D. Peele					
13a. TYPE OF REPORT Interim		13b. TIME COVERED FROM _____ TO _____		14. DATE OF REPORT (Year, Month, Day) May 86	
15. PAGE COUNT					
16. SUPPLEMENTARY NOTATION					
17. COSATI CODES			18. SUBJECT TERMS (Continue on reverse if necessary and identify by block number)		
FIELD	GROUP	SUB-GROUP			
19. ABSTRACT (Continue on reverse if necessary and identify by block number)  (SEE REVERSE)					
20. DISTRIBUTION/AVAILABILITY OF ABSTRACT <input checked="" type="checkbox"/> UNCLASSIFIED/UNLIMITED <input type="checkbox"/> SAME AS RPT <input type="checkbox"/> DTIC USERS			21. ABSTRACT SECURITY CLASSIFICATION <b>UNCLASSIFIED</b>		
22a. NAME OF RESPONSIBLE INDIVIDUAL Amos Otis, Major, Program Manager			22b. TELEPHONE (Include Area Code) (202) 767-4971		22c. OFFICE SYMBOL XOT

## Research Initiation Program - 1984

For several years prior to 1983, AFOSR conducted a special follow-on funding program for Summer Faculty Research Program (SFRP) participants; this was popularly known as the AFOSR Minigrant Program. That program was superseded in 1983 by the Research Initiation Program conducted by SCEE.

To compete for a 1984 Research Initiation Program award, SFRP participants must submit a complete proposal and proposed budget either during or promptly after their SFRP appointment periods. Awards to the 1984 participants may extend through 15 December 1985.

Each proposal was evaluated for technical excellence, with special emphasis on relevance to continuation of the SFRP effort, as determined by the Air Force laboratory/center. The final selection of awards was the responsibility of AFOSR.

The most effective proposals were those which were closely coordinated with the SFRP Effort Focal Point and which followed the SFRP effort with proposed research having strong prospects for later sustained funding by the Air Force laboratory/center.

The maximum award under the Research Initiation Program is \$12,000 plus cost-sharing up to a matching total amount.

The mechanics of applying for a Research Initiation Program award are as follows:

- (1) Research Initiation Program proposals of \$12,000 plus cost-sharing were to be submitted after August 1, 1984 but no later than November 1, 1984.
- (2) Proposals were evaluated and the final award decision was the responsibility of AFOSR after consultation with the Air Force Laboratory/center.
- (3) The total available funding limited the number of awards to approximately half the number of 1984 SFRP participants.
- (4) Subcontracts were negotiated with the employing institution, designating the SFRP participant as Principal Investigator, with the period of award having a start date no earlier than September 1, 1984 and a completion date no later than December 15, 1985.

Employing institutions were encouraged to cost-share since the program was designed as a research initiation procedure. Budgets included, where applicable, Principal Investigator time, graduate assistant and support effort, equipment and expendable supplies, travel and per diem costs, conference fees, indirect costs, and computer charges.

Volumes I, II, III, and IV of the 1984 Research Initiation Program Report contain copies of reports on the 89 subcontract efforts awarded under this program.

AFOSR-TR- 87-1721

①

DTIC  
ELECTE  
NOV 17 1987  
S E D

This document has been approved  
for public release and sale in  
distribution is unlimited.

87

D

1984 USAF/SCEEE RESEARCH INITIATION PROGRAM

Conducted by  
Southeastern Center for  
Electrical Engineering Education  
under

USAF Contract Number F49620-82-C-0035

RESEARCH REPORTS

Volume II of IV

submitted to  
Air Force Office of Scientific Research  
Bolling Air Force Base  
Washington, DC

BY  
Southeastern Center for  
Electrical Engineering Education  
May 1986

Accession For	
NTIS GRA&I	<input checked="" type="checkbox"/>
DTIC TAB	<input checked="" type="checkbox"/>
Unannounced	<input type="checkbox"/>
Justification	
By	
Distribution/	
Availability Codes	
Dist	Avail and/or Special
A-1	



This document has been approved  
for public release and sale in  
unlimited quantities

DTIC  
ELECTE  
NOV 17 1987  
D



SCEEE  
©  
1986

## INTRODUCTION.

### Research Initiation Program - 1984

For several years prior to 1983, AFOSR conducted a special follow-on funding program for Summer Faculty Research Program (SFRP) participants; this was popularly known as the AFOSR Minigrant Program. That program was superceded in 1983 by the Research Initiation Program conducted by SCEEE.

To compete for a 1984 Research Initiation Program award, SFRP participants must submit a complete proposal and proposed budget either during or promptly after their SFRP appointment periods. Awards to the 1984 participants may extend through 15 December 1985.

Each proposal was evaluated for technical excellence, with special emphasis on relevance to continuation of the SFRP effort, as determined by the Air Force laboratory/center. The final selection of awards was the responsibility of AFOSR.

The most effective proposals were those which were closely coordinated with the SFRP Effort Focal Point and which followed the SFRP effort with proposed research having strong prospects for later sustained funding by the Air Force laboratory/center.

The maximum award under the Research Initiation Program is \$12,000 plus cost-sharing up to a matching total amount.

The mechanics of applying for a Research Initiation Program award are as follows:

- (1) Research Initiation Program proposals of \$12,000 plus cost-sharing were to be submitted after August 1, 1984 but no later than November 1, 1984.
- (2) Proposals were evaluated and the final award decision was the responsibility of AFOSR after consultation with the Air Force Laboratory/center.
- (3) The total available funding limited the number of awards to approximately half the number of 1984 SFRP participants.
- (4) Subcontracts were negotiated with the employing institution, designating the SFRP participant as Principal Investigator, with the period of award having a start date no earlier than September 1, 1984 and a completion date no later than December 15, 1985.

Employing institutions were encouraged to cost-share since the program was designed as a research initiation procedure. Budgets included, where applicable, Principal Investigator time, graduate assistant and support effort, equipment and expendable supplies, travel and per diem costs, conference fees, indirect costs, and computer charges.

Volumes I, II, III, and IV of the 1984 Research Initiation Program Report contain copies of reports on the 89 subcontract efforts awarded under this program.

RESEARCH REPORTS  
1984 USAF-SCEEE RESEARCH INITIATION PROGRAM

<u>VOLUME I</u> <u>REPORT NO.</u>	<u>TITLE</u>	<u>RESEARCH ASSOCIATE</u>
1.	AN ANALYTICAL STUDY OF TWO-STAGE LIGHT GAS GUN PERFORMANCE	Dr. Robert W. Courter
2.	A LOW-COST LOCAL-AREA NETWORK for DESKTOP COMPUTERS	Dr. Myron A. Calhoun
3.	DEVELOPMENT of PREDICTION MODELS for HUMAN TORQUE STRENGTH	Dr. S. Deivanayagam
4.	THE ROLE of ANTIOXIDANT NUTRIENTS in PREVENTING HYPERBARIC OXYGEN DAMAGE to the RETINA	Dr. William L. Stone
5.	THE INFULUENCE of MELTING and REACTANT COMSUMPTION on TEMPERATURE TRANSIENTS in SPHERICAL and CYLINDRICAL CHARGES of EAK	Dr. John W. Sheldon
6.	GEOSTROPHIC ADJUSTMENT in a THREE- DIMENSIONAL MESOSCALE NUMERICAL MODEL of the ATMOSPHERE	Dr. Keith L. Seitter
7.	Report not received on time. Will be provided when available.	Dr. William Czelen
8.	EFFECTS of TEMPERATURE and REACTANT SOLVATION UPON the RATES of GAS-PHASE ION-MOLECULE REACTIONS	Dr. Peter M. Hierl
9.	EFFECTS of NUCLEAR RADIATION on the OPTICAL CHARACTERISTICS of LASER COMPONENTS	Dr. Hermman Donnert
10.	A REVIEW of COMPUTER SIMULATIONS for AIRCRAFT-SURFACE DYNAMICS	Dr. George R. Doyle, Jr.
11.	COMPUTATIN OF TRANSONIC PROJECTILE AERODYNAMICS	Dr. Chen-Chi Hsu
12.	DEVELOPMENT of an ADAPTIVE GRID GENERATION TECHNIQUE for TRANSONIC PROJECTILE BASE FLOW PROBLEMS	Dr. Chris Reed
13.	Report not received on time. Will be provided when available.	Dr. Kendall Nygard



RESEARCH REPORTS  
1984 USAF-SCEEE RESEARCH INITIATION PROGRAM

VOLUME II  
REPORT NO.

TITLE

RESEARCH ASSOCIATE

- |     |   |                              |
|-----|---|------------------------------|
| 26. | ALTERNATIVE COMPUTATIONAL METHODS for SEPARATED FLOWS about PITCHED FLAT SURFACES.                                    | Dr. Larry A. Glasgow         |
| 27. | NO TITLE  | Dr. Hendrik F. Hamka         |
| 28. | FUNCTIONAL ROLE of SEROTONIN in the CEREBELLAR GLOMERULAR SYNAPSE   | Dr. Deborah Armstrong        |
| 29. | CHOLINE and ETHANOLAMINE PHOSPHOTRANSFERASE ACTIVITIES in GLOMERULAR PARTICLES ISOLATED FROM BOVINE CEREBELLAR CORTEX | Dr. Robert V. Dorman         |
| 30. | DYNAMICS OF LARGE SCALE VORTEX STRUCTURES and QUASI-LARGE SCALE STRUCTURES in the WAKE of a SPLITTER PLATE            | Dr. Paul H. Chiu             |
| 31. | FLOW PHYSICS THROUGH A PIERCED MEMBRANE.  | Dr. Louis C. Chow            |
| 32. | COMPUTATIONAL STUDIES of RAMJET COMBUSTOR FLOW FIELDS   | Dr. K.M. Isaac               |
| 33. | FREE STREAM TURBULENCE EFFECTS on TURBULENT HEAT and MOMENTUM TRANSFER  | Dr. Paavo Sepri              |
| 34. | STUDY of COLD REACTING and COMBUSTING FLOWS AROUND BLUFF-BODY COMBUSTORS  | Dr. Richard S. Tankin        |
| 35. | NUMERICAL MODELING of MULTIPHASE TURBULENT RECIRCULATING FLOWS in SUDDEN-EXPANSION RAMJET GEOMETRY                    | Dr. Albert Tong              |
| 36. | SiC FIBER REINFORCED GLASS-CERAMIC COMPOSITES in the ZIRCONIA/MAGNESIUM ALUMINOSILICATE SYSTEM.                       | Dr. Charles H. Drummond, III |

Volume III

- |     |  |                      |
|-----|--|----------------------|
| 37. | ARYLOXY SUBSTITUTED PYROMELLITIC DIANHYDRIDES                              | Dr. William F. Feld  |
| 38. | ANGLE RESOLVED ION-SCATTERING STUDY of GaAs SURFACES the EXPERIMENT DESIGN | Dr. Thomas P. Graham |

RESEARCH REPORTS  
1984 USAF-SCEEE RESEARCH INITIATION PROGRAM

<u>VOLUME I</u> <u>REPORT NO.</u>	<u>TITLE</u>	<u>RESEARCH ASSOCIATE</u>
14.	USE of BAYESIAN DECISION THEORY in ASSESSING the POTABILITY of GROUND WATER BASED DRINKING WATER SUPPLIES	Dr. Stephan J. Nix
15.	DESIGN of a DIGITAL EW PASSIVE RECEIVER	Dr. William S. McCormick
16.	DUAL CHANNEL FFT SYSTEM ANALYSIS FACILITY for EVALUATING INTEGRATED COMMUNICATION SYSTEMS	Dr. Paul B. Griesacker
17.	FAR-INFRARED ABSORPTION PROFILES for DISTRIBUTED SHALLOW DONORS in GaAs-GaAlAs HETEROSTRUCTURES	Dr. Ronald L. Greene
18.	EFFECT of POLE PIECES on the AXIAL MAGNETIC FIELD in TRAVELING WAVE TUBES	Dr. James D. Patterson
19.	ENHANCING MPC-DSS to INCLUDE AUTOMATIC RESCHEDULING and ADAPTIVE PERFORMANCE MEASURES	Dr. Philip S. Chong
<u>Volume II</u>		
20.	PARAMETRIC STABILITY in COST ESTIMATING MODELS	Dr. Thomas R. Gulledge, Jr.
21.	ANALYSIS of AIR FORCE VEHICLE CONDITION RATINGS FROM HISTORICAL DATA	Dr. Bruce N. Janson
22.	THE DEVELOPMENT of COMPUTATIONAL EFFICIENCIES in CONTINUUM FINITE ELEMENT CODES USING MATRIX DIFFERENCE EQUATIONS	Dr. Harold C. Sorensen
23.	CENTRIFUGE MODEL STUDY and FINITE ELEMENT ANALYSIS OF BURIED CONCRETE BOX CULVERTS	Dr. Yong S. Kim
24.	EFFECTS of FLUID SHIFTS and HYPOVOLEMIA in INDIVIDUALS with DIFFERENT WORKING CAPACITIES WHILE RESTING at a FIVE DEGREE DECLINATION	Dr. William G. Squires
25.	STRUCTURE OF MOLTEN IMIDAZOLIUM CHLORIDE	Dr. R.D. Murphy

RESEARCH REPORTS  
1984 USAF-SCEEE RESEARCH INITIATION PROGRAM

<u>VOLUME III</u> <u>REPORT NO.</u>	<u>TITLE</u>	<u>RESEARCH ASSOCIATE</u>
39.	THERMAL DECOMPOSTITION STUDIES of SOME SILAHYDROCARBONS	Dr. Vijay K. Gupta
40.	SILANE-TREATED SILICA FILLERS for USE in FULRORSILICONE ELASTOMERS	Dr. Larry M. Ludwick
41.	RAMAN SPECTROSCOPIC STUDIES in EXTRINSIC P-TYPE SILICON	Dr. James Schneider
42.	GRAIN SIZE CONTROL in META STABLE BETA TITANIUM ALLOYS	Dr. Isaac Weiss
43.	THE IMPACT of EXPERT SYSTEMS on PERFORMANCE and COGNITIVE STRATEGIES in DIAGNOSTIC INFERENCE	Dr. Sallie E. Gordon
44.	EFFECTS of ENRICHING a COMPUTER-INSTRUCTED PROCEDURALIZED TASK with EXPLANATORY INFORMATION	Dr. Krystine B. Yaworsky
45.	SPECIFICATION SEARCHES in COVARIANCE STRUCTURE MODELING	Dr. Robert MacCallum
46.	A COMPUTATIONAL MODEL of the HUMAN CARDIOPULMONARY SYSTEM	Dr. David Reynolds
47.	DEVELOPMENT of an OPTIMAL TESTING PROTOCOL for the USAF CRITERION TASK SET (CTS)	Dr. Robert E. Schlegel
48.	CONSTRUCTION of CONCEPT-ATOMS	Dr. Yin-Min Wei
49.	DEVELOPMENT of a HIGH-FREQUENCY LUNG VENTILATION MODEL for TESTING UNDER HYPOBARIC CONDITIONS	Dr. Mukul R. Banerjee
50.	BRILLOUIN SPECTROSCOPY in SYSTEMS of BIOLOGICAL SIGNIFICANCE	Dr. Raj M. Krishnan
51.	STABILIZATION of MODE-LOCKED LASERS	Dr. Odis P. McDuff
52.	RAMAN SPECTROSCOPY of CAROTENOIDs and OTHER MOLECULES in UNSTIMULATED and STIMULATED, CULTURED Y-1 MOUSE ADRENAL TUMOR CELLS	Dr. James J. Mrotek

RESEARCH REPORTS  
1984 USAF-SCEEE RESEARCH INITIATION PROGRAM

<u>VOLUME III</u> <u>REPORT NO.</u>	<u>TITLE</u>	<u>RESEARCH ASSOCIATE</u>
53.	MILITARY FAMILY STRESS and JOB PERFORMANCE	Dr. Lena Wright Myers
54.	Report not received on time. Will be provided when available	Dr. Walter Salter
55.	Report not received on time. Will be provided when available	Dr. William Thomas
56.	EVALUATION and VALIDATION of ADA PROGRAMMING SUPPORT ENVIRONMENTS	Dr. Mike Burlakoff
57.	KINETICS of HOMOGENEOUS GAS PHASE OXIDATION of HYDRAZINE in AIR	Dr. Datta V. Naik
58.	SOFTWARE CORRECTIONS and EXTENSIONS for an INTEGRATED PARTICLE SIZING SYSTEM	Dr. Arthur M. Sterling
<u>Volume IV</u>		
59.	PREDICTING GASEOUS PHASE ADSORPTION of ORGANIC VAPORS by MICROPOROUS ADSORBENTS	Dr. Martin D. Werner
60.	NO TITLE	Dr. Frank P. Colby, Jr.
61.	SOLAR HARD X-RAY BURSTS and TYPE-II RADIO EMISSIONS	Dr. Gabriel Kojoian
62.	THE PASSIVE MODE LOCKING of an $\text{Nd}^{3+}$ : YAG LASER WITH a TWO-PHOTON ABSORBER	Dr. Nabil M. Lawandy
63.	PLASMA GENERATION and DIAGNOSTICS for IONOSPHERIC PLASMA SIMULATION	Dr. Bernard McIntyre
64.	STUDY of UNIFIED COMPLEX SUSCEPTIBILITY OVER MILLIMETER and INFRARED REGIONS VIA KRAMERS-KRONIG RELATIONSHIP	Dr. Ken Tomiyama
65.	DETERMINATION of PROFESSIONAL LITERATURE RESOURCES RELATING to USAF FAMILY and LIFE STYLE ATTRIBUTES AND ATTITUDES: SUPPORT for INTERPRETING AFSS DATA	Dr. L.W. Buckalew

RESEARCH REPORTS  
1984 USAF-SCEE RESEARCH INITIATION PROGRAM

<u>VOLUME IV</u> <u>REPORT NO.</u>	<u>TITLE</u>	<u>RESEARCH ASSOCIATE</u>
66.	DIFFERENT CAREER STAGES: DIFFERENT DEGREES of COMMITMENT	Dr. Jan Leeman Brooks
67.	A MULTILEVEL EXAMINATION of LEADERSHIP EFFECTS WITH THE ORGANIZATIONAL ASSESSMENT PACKAGE	Dr. Kevin W. Mossholder
68.	FUSE and SURFACE TRACKING SWITCH MODELS for the SHIVA STAR INDUCTIVE PULSE COMPRESSION SYSTEM	Dr. R. Gerald Colclaser
69.	MODELING the THERMAL LAYER	Dr. Arthur A. Kovitz
70.	DIGITAL INTERPOLATION BASED on FUNCTIONAL ITERATION	Dr. Aldy T. Fam
71.	Report not received on time. Will be provided when available.	Dr. Brian Holmes
72.	NUMERICAL CHARACTERIZATION of MICROSTRIP DISCONTINUITIES on THICK SUBSTRATES	Dr. Robert W. Jackson
73.	A SUBOPTIMUM EXTRAPOLATOR for IMPROVED SPECTRAL ESTIMATION	Dr. Lonnie C. Ludeman
74.	HANDLING FACTS with NON-CONSTANT GROUND TERMS in a KNOWLEDGE-BASED SYSTEM	Dr. John T. Minor
75.	STRUCTURAL MODIFICATION to ENHANCE the ACTIVE VIBRATION CONTROL of LARGE SPACE STRUCTURES	Dr. Franklin E. Eastep
76.	CONSISTENT SHEAR LAG MODELING of DAMAGE in UNIDIRECTIONAL COMPOSITE LAMINATES	Dr. Walter F. Jones
77.	NUMERICAL SIMULATION of a SUPERSONIC INLET FLOW	Dr. Meng-Sing Liou
78.	RECONFIGURATION of FLIGHT CONTROL SYSTEM of UNMANNED RESEARCH VEHICLE	Dr. Kuldip S. Rattan
79.	ANALYSIS of ARMOR BRACKETRY	Dr. Hemen Ray

RESEARCH REPORTS  
1984 USAF-SCEEE RESEARCH INITIATION PROGRAM

<u>VOLUME IV</u> <u>REPORT NO.</u>	<u>TITLE</u>	<u>RESEARCH ASSOCIATE</u>
80.	ESTIMATING SPEED of MENTAL ROTAION THROUGH ITEM PACING	Dr. David F. Lohman
31.	DEVELOPMENT and IMPLEMENTATION of COST-EFFECTIVENESS and UTILITY METHOD- OLOGIES for the AF PERFORMANCE MEASUREMENT PROJECT	Dr. Robert Vance
82.	A SCANNING ELECTRON MICROSCOPICAL STUDY of PERIOSTEUM from SUBHUMAN PRIMATES	Dr. Gwendolyn B. Howze
83.	AN INVESTIGATION of TEST BIAS on the ARMED SERVICES VOCATIONAL APTITUDE BATTERY (ASVAB) FOR MALES and FEMALES.	Dr. Cynthia A. Ford
84.	MODERNIZATION of AGING HIGH-ALTITUDE ENGINE TEST CELLS	Dr. Doyle E. Hasty
85.	EFFECTS of PYRIDOSTIGMINE in the DIET UPON SIMPLE and COMPLEX BEHAVIORS in the MONGOLIAN GERBIL (MERIONES UNGUICULATUS)	Dr. Arthur Harriman
86.	SYNTHESIS of TRIFLATE and CHLORIDE SALTS of ALKYL N,N BIS (2,2,2-TRIFLUOROETHYL) AMINES	Dr. Gloria L. Anderson
87.	LIQUID ROCKET INSTABILITY MODEL DEVELOPMENT	Dr. Charles E. Mitchell
88.	LAMINARIZATION in HIGHLY ACCELERATED FLOW	Dr. Brian Vick
89.	FUTURE TACTICAL AIR CONTROL SYSTEM DATABASE DESIGN	Dr. William Perrizo

FINAL REPORT

PARAMETRIC STABILITY IN COST ESTIMATING MODELS

Prepared For

The Air Force Office of Scientific Research  
AFOSR/XOT

and submitted to

The Southeastern Center of Electrical Engineering Education

Contract No. F49620-82-C-0035

Subcontract No. 84 RIP 20

Prepared by: Thomas R. Gullledge, Jr.

Academic Rank: Assistant Professor

Department and Department of Quantitative Business Analysis  
University: Louisiana State University

Date: September 10, 1985

FOR OFFICIAL USE ONLY

This document contains data which may be considered contractor sensitive.  
The data may not be disclosed outside the U.S. Government without prior  
written permission from McDonnell Aircraft Company.

# ABSTRACT

The purpose of this research was twofold. The first part involved extending a previous cost model for the C141 program to include the F4 program. The second part involved checking parameter stability across programs. If key parameters are stable, then the model can be used to predict across programs using the methodology suggested in [21] and [22]. This research suggests that the key parameters are stable across programs.



## INTRODUCTION

In recent years, there has been an increased interest in researching the made-to-order production situation. Made-to-order production is characterized by a contractual agreement that specifies the number of units to be produced in a fixed time horizon. Many early researchers examined this situation [1,2,3,11,14,15,17,18,19], but they did not present definitive functional forms that were suitable for application. The first truly applicable planning models have only appeared recently [7,8,20,21,22,23,24, 25]. In particular, the model presented by Womer and Gulledge conforms with economic theory, conforms with actual cost behavior on made-to-order programs, and the parameters may be estimated from available cost data. This model was developed under the support of the Air Force Business Research Management Center [22], and is currently available on the COPPER IMPACT computer network. A description of the model is included in Appendix A. The rationale for this type of model is simple. Figure 1 delineates two approaches for estimating the total price of an aircraft in a given program. The usual approach allocates overhead in the plant based on direct labor estimates. Since only a part of overhead costs are fixed, a more realistic allocation scheme involves separating total cost into fixed and variable cost, modeling the variable cost, and then distributing the fixed cost to the production units. This methodology is advocated by Balut [6]. In either case, in the absence of current contractor data, some method is needed to model the direct or variable cost profiles so that DoD planners can analyze many programs simultaneously for various procurement quantities. The model that is analyzed in this research can be used to generate either direct or variable cost profiles.

However, model implementation often involves analyzing programs for which data is scarce, so the question that is addressed in this research

# ESTIMATING APPROACHES

PROGRAM COSTS

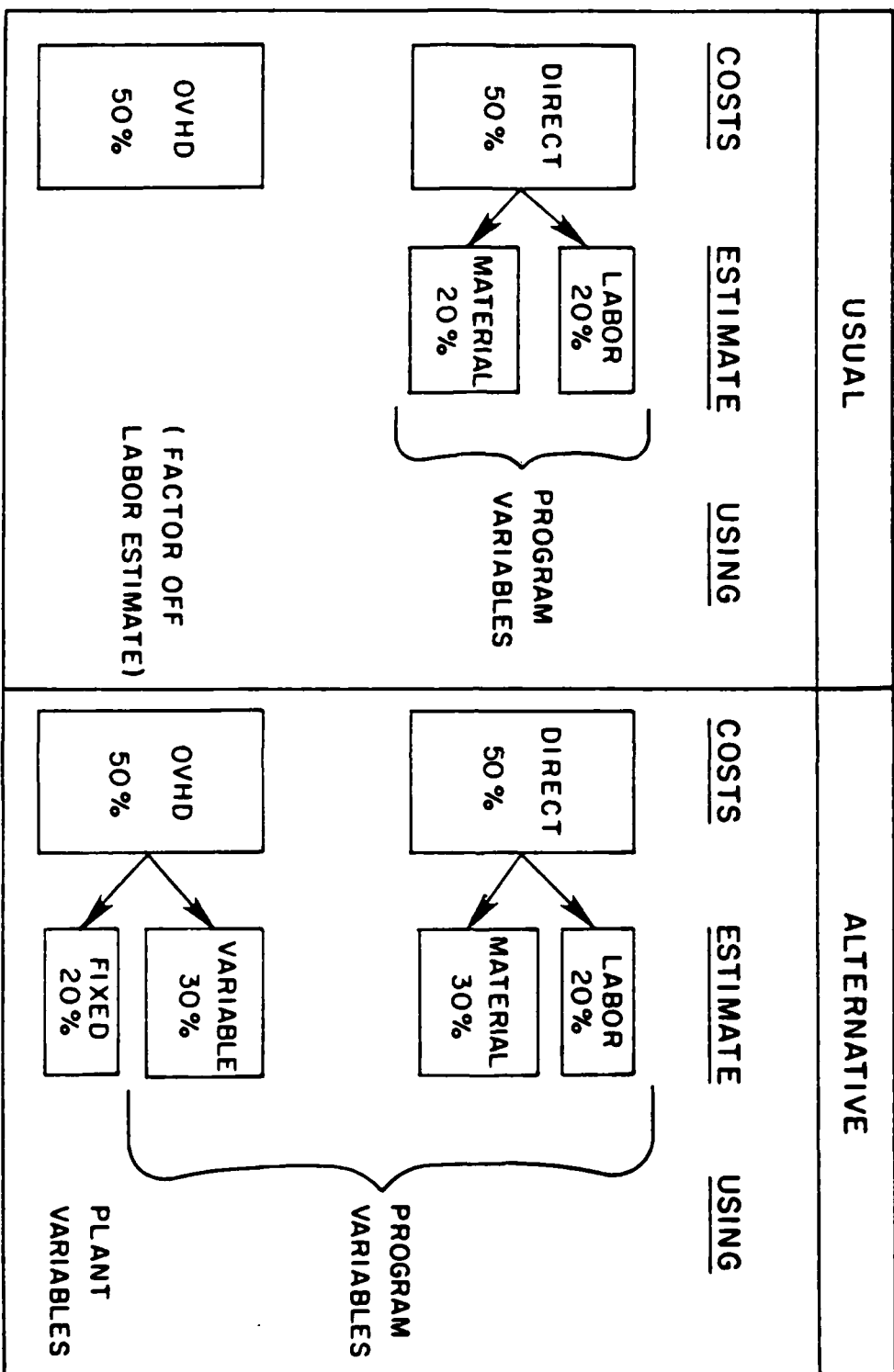


Figure 1. Alternative Estimating Approaches (Source: S.J. Balut).

concerns the application of an existing model to new programs. Of course some quantities are inherently different across programs; e.g., no one expects an F4 aircraft to cost the same as a C141 aircraft. These problems can be handled by rescaling the model as presented in [22]. Learning curve estimates are needed for the model, but these are often also available by analogy with similar programs. The crucial estimate is probably the factor returns parameter. Very little is known about its true value since we have limited experience in estimating this parameter. This research examines, in particular, the stability of this parameter.

During the summer of 1984, Gullledge and Harmon initiated research where the Womer and Gullledge model was applied to the A and B models of the F4 program. The results of this research are promising. It appears that the parameters for the F4 program are surprisingly similar to those for the C141 program. However, because of time limitations the equality hypothesis was not formally tested. This research is documented in Harmon's final report to the Air Force Office of Scientific Research, and it was published as his Masters Thesis at the University of Cincinnati. This work extends that research.

#### THE MODEL

The model that is used in the analysis that follows is a modification of the model in Appendix A. It is based on the belief that model specification should be based on economic theory. That is, in lieu of empirical specification, a behavioral assumption is stated, a theoretical model is specified, and an estimable cost function is derived. Consider the following definitions:

- $C$  = discounted program cost measured in units of the variable composite resource,  
 $i$  = the sequence number of an airframe,  
 $C_i$  = discounted variable cost of a single airframe,  
 $n$  = the total number of airframes in the production program,  
 $T_{di}$  = the delivery date for airframe  $i$ ,  
 $V$  = the average number of airframes in the production process in the facility at time  $t$ ,  
 $t_{si}$  = the date work begins on airframe  $i$ ; work on all airframes in the same lot is assumed to begin at the lot release date,  
 $q_i(t)$  = production rate at time  $t$  on airframe  $i$ ,  
 $Q_i(t)$  = cumulative production on airframe  $i$  at time  $t$ ,  
 $x_i(t)$  = rate of resource use at time  $t$  on airframe  $i$ ,  
 $\delta$  = a parameter describing learning prior to airframe  $i$ ,  
 $\epsilon$  = a parameter describing learning on airframe  $i$ ,  
 $\gamma$  = a parameter describing returns to the variable resources,  
 $\alpha$  = a parameter associated with decreases in labor productivity as an airframe nears completion,  
 $\nu$  = a parameter describing returns to the length of the production line,  
 $\rho$  = the discount rate,  
 $A$  = a constant.

The production function is assumed to be of the following form:

$$q_i(t) = A(1-\frac{1}{2})^{\delta} Q_i^{\epsilon}(t) (t_{di}-t)^{\alpha} x^{1/\gamma}(t) V^{\nu}. \quad (1)$$

The following parametric assumptions are made:

$$0 \leq \alpha \leq 1, \quad 0 \leq \epsilon \leq 1, \quad 0 \leq \delta \leq 1, \quad \nu < 0, \quad \gamma > 1.$$

The model is

$$\begin{aligned} \text{Min } C &= \sum_{i=1}^n \int_{t_{si}}^{t_{di}} x_i(t) e^{-\rho t} dt \\ \text{ST: } q_i(t) &= A(i-k_2)^{\delta} Q_i^{\epsilon}(t) (t_{di}-t)^{\alpha} x^{1/\gamma}(t) V^{\nu} \\ Q_i(t_{di}) &= 1 \quad i = 1, 2, \dots, n \\ Q_i(t_{si}) &= 0 \quad i = 1, 2, \dots, n. \end{aligned}$$

The solution for this model is very similar to that presented in Appendix A.

The basic estimable relationship is

$$\begin{aligned} \sum_{i=k_j}^{n_j} [X_i(T_2) - X_i(T_1)] &= \sum_{i=k_j}^{n_j} \beta_0 (i-k_2)^{-\gamma\delta} \Gamma^{-\gamma} [\rho(t_{di}-t_{si})/(\gamma-1), \beta_1] \\ &\quad V^{-\gamma\nu}(T_1, T_2) \{ \Gamma[\gamma\rho(t_{di}-T_1)/(\gamma-1), \beta_1] \} \\ &\quad - \Gamma[\gamma\rho(t_{di}-T_2)/(\gamma-1), \beta_1] \} \end{aligned} \quad (3)$$

where

$T_1$  = the beginning date of the period of observation,

$T_2$  = the ending date of the period of observation,

$\beta_0$  = a scaling factor,

$\beta_1$  =  $\alpha\gamma/(\gamma-1)+1$ ,

$n_j$  = the last airframe sequence number in the lot,

$k_j$  = the first airframe sequence number in the lot,

and

$\Gamma(\cdot)$  is the incomplete gamma function.

#### THE F4 AIRFRAME PROGRAM

The F4 Phantom was developed as a twin-engined two-seat long-range all weather missile fighter for the U.S. Navy. The Phantom operated as a high-performance fighter, attack, and reconnaissance aircraft for the U.S.

Navy, U.S. Air Force, and U.S. Marine Corps. The Phantom was also placed in service with the Royal Navy, Royal Air Force, Royal Australian Air Force, the Imperial Iranian Air Force, the Republic of Korea Air Force, the Israeli Air Force, and the Federal German Luftwaffe. This application examines only the first 10 production job orders of F4A's, F4B's, and F4C's all of which were placed in service by the U.S. armed forces. These aircraft were produced in the late 1950's and the early 1960's. In total, 791 aircraft were analyzed.

The F4 program cost history [13] contains data on primary manufacturing labor hours on blocks of airframes within job orders within contracts. In Harmon's analysis, this data was organized by individual blocks of airframes. The result was 617 observations for estimation. Since some of the data is reported as common hours for airplanes in multiple blocks, it is necessary to assign some hours to the blocks using somewhat arbitrary weighting schemes. For this reason, in this application the data is organized by job order.

The data analysis problems at this stage of the analysis were formidable. Actual delivery schedules were not available, so actual acceptance schedules were used. For all job orders there were small quantities of labor hours that were allocated to the lot after the schedule indicated that all aircraft had been accepted. These were extremely small quantities, but still they were redistributed evenly over all production periods. Also, for the first two job orders there was a 27 month period for which McDonnell Aircraft Company did not report direct manufacturing hours. The model was still initialized at  $t=0$ , but the first observation for the estimation does not occur until time period 27.

Job order 720 of contract 62-0383 presented special problems. This job order contained 147 F4-B aircraft. The acceptance schedule separated these aircraft into two groups, 29 and 118 aircraft. The data on labor hours was separated into two groups in the program cost history, but an examination of the data suggested problems associated with the allocation to the 29 aircraft. It appeared that too many hours were allocated to the 29 aircraft, and there was one observation that was an obvious copy and/or accounting error. Therefore the model was estimated using several data configurations.

The model was estimated with the 29 and 118 aircraft reported separately, and with both the outlier included and excluded. The analysis was repeated with the two groups of aircraft combined. By separating the data the number of observations was increased, but the decision was still made to combine the observations and estimate the job order as a complete group of observations. After all data adjustments, the data set contained 236 observations on 791 aircraft. The decision was also made to leave the extreme observation in the data set. This is discussed in a later section of the report.

#### ANALYSIS

Since the C141 program was selected as the standard of comparison, it seemed pertinent to reexamine that program. One of the problems noted in that estimation was that the discount rate was apparently not statistically different from zero [22,p.121-122]. After extensive simulations, it was resolved that the nonsignificance was false; i.e., an artifact of the estimation procedure. The problem was caused by a high correlation between the  $\rho$  and  $\gamma$  estimates. Therefore,  $\rho$  was fixed at its estimated value and the parameters were reestimated. The results of this estimation are presented in Table 1.

Table 1  
Parameter Estimates and Asymptotic Standard Errors

<u>Parameter</u>	<u>Estimate</u>	<u>Standard Error</u>
$\beta_0$	1.1460	.67300
$\beta_1$	3.0490	.4545
$\delta^1$	0.4848	.06550
$\gamma$	1.0016	.000298
$\nu$	-0.4408	.160750

These estimates are in close agreement with those presented in [22]. These estimates will be the standard of comparison for the F4 estimates.

The first F4 estimates were made without any consideration of the differences in the three different aircraft models included in the analysis. The results of this estimation are presented in Table 2.

Table 2  
Parameter Estimates and Asymptotic Standard Errors

<u>Parameter</u>	<u>Estimate</u>	<u>Standard Error</u>
$\beta_0$	11.0300	1.4100
$\beta_1$	4.1730	0.5045
$\delta^1$	0.3169	0.0432
$\gamma$	1.0032	0.0004
$\nu$	0.2131	0.0494

These estimates agree with expectations with the exception of the estimate for  $\nu$ . Our expectations were that our hypothesis about the production cost driver with respect to the average number of units in the plant was probably weak theoretically, and therefore could be difficult to verify empirically. However, a significant positive coefficient was not expected. Our suspicion is that the positive sign follows from not considering the model differences in the 791 aircraft.



To investigate this hypothesis it was necessary to devise a methodology to capture the differences in the models. Intuition suggests that there should be a difference in cost, and this difference should scale the cost function up or down. The first thing that comes to mind is dummy variable regression, but this concept is not clearly defined in nonlinear regression for a model that does not have an additive intervention effect. Since the cost function is shifted in scale by the model changes, the obvious parameter to alter is the scale parameter,  $\beta_0$ . FORTRAN code was written to incorporate a different scaling factor for each production model of the F4 (The complete code with the data is included in Appendix B). The results of the estimation with the different scaling factors are presented in Table 3.

Table 3  
Parameter Estimates and Asymptotic Standard Errors

<u>Parameter</u>	<u>Estimate</u>	<u>Standard Error</u>
$\beta_{01}$	5.0440	0.8795
$\beta_{02}$	5.4610	1.1850
$\beta_{03}$	3.5640	0.9835
$\delta^1$	4.1470	0.4510
$\delta^1$	0.3894	0.0466
$\gamma$	1.0033	0.0004
$\nu$	-0.0003	0.0549

In this table  $\beta_{01}$  is the scaling factor for the F4-A's,  $\beta_{02}$  is the scaling factor for the F4-B's, and  $\beta_{03}$  is the scaling factor for the F4-C's. These estimates agree with a priori expectations. The estimate for  $\nu$  is negative, but not significantly different from zero. We could restrict  $\nu$  to be equal to zero, but since the residual variance was computed with 229 degrees of freedom, it would have little impact on the estimates.

One thing worth noting is that the consideration of model differences caused a significant reduction in the error sum of squares. The residual

error variance for the estimation presented in Table 2 was .7773 while that for Table 3 was .6594.

#### PREDICTABILITY AND RESIDUAL ANALYSIS

Since the seven parameter model seems more appropriate, all the analysis that follows concerns only that model. A plot of the predicted versus the actual values is presented in Figure 2 (the solid line is the predicted). This plot has several characteristics that should be discussed. First, there is the obvious outlier that was noted earlier in the report. The model was estimated two ways:

1. outlier in the data,
2. outlier corrected.

Surprisingly, the outlier had very little impact on the values of the estimates. Since no real reason could be assigned to the occurrence of the observation, and since the observation had negligible impact, it was left in the data.

The second characteristic concerns the way the model predicts low in the early time periods. The figure is misleading in that it visually assigns equal weight to the early and latter periods. In fact, the early time periods represent a very small number of aircraft relative to the latter time periods. In any case, the model suggested that labor hours be reduced, but McDonnell Aircraft Company correctly chose not to reduce its work force. A shortcoming of this model is that it does not include hiring and firing penalties. This is certainly an area where the research needs to be extended.

The original plan was to analyze the residuals using the methodology presented in [5]; i.e., analyze the projected residuals. For several

# AGGREGATED ACTUALS VERSUS PREDICTED 7 PARAMETER MODEL

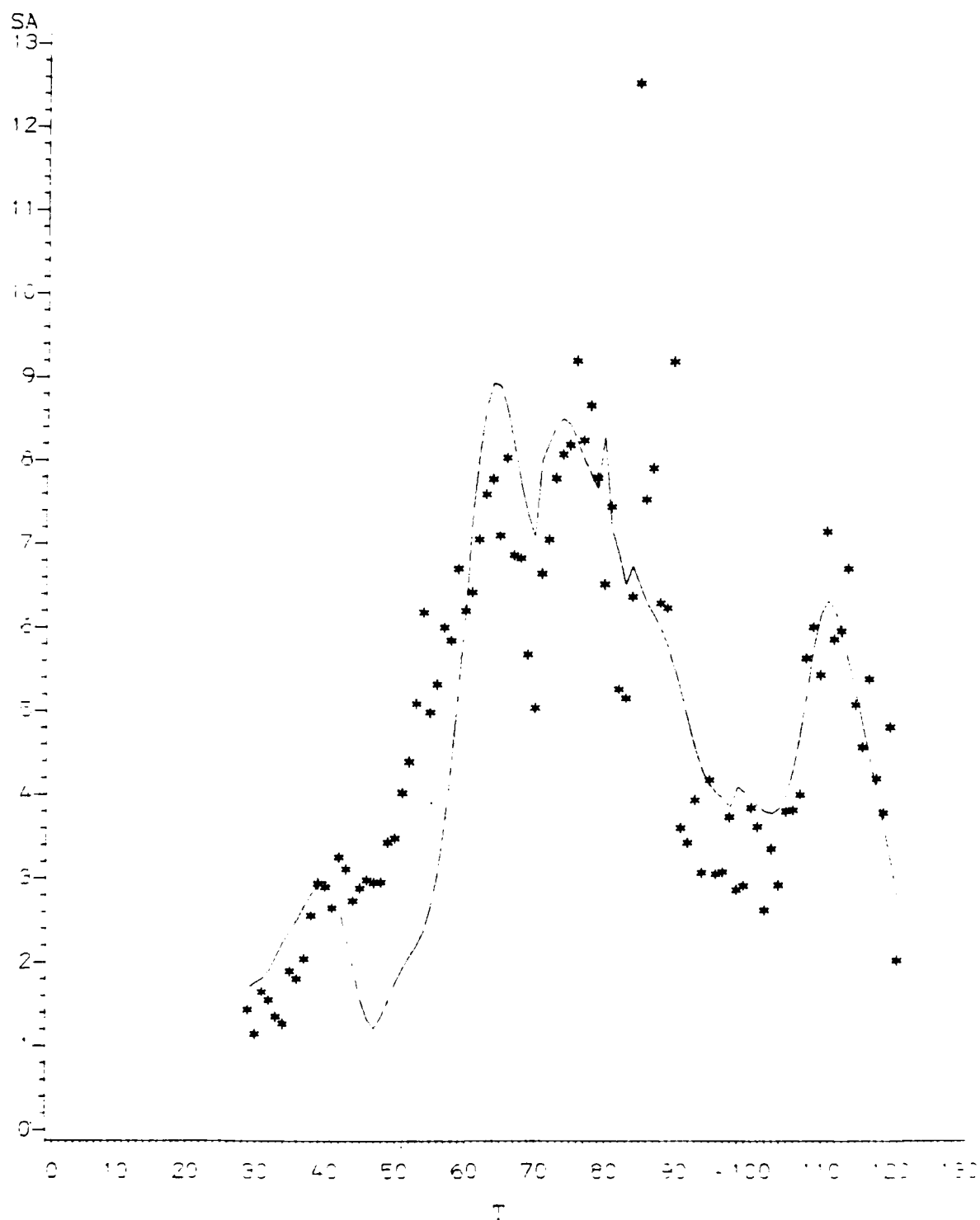


Figure 2.

reasons, ordinary residual analysis techniques were used. The first reason is related to an analytical problem, and the second concerns practicality. The analytical problem is that the projected residuals require the second derivative of the sum of squares function. In this case that would be the second derivative of a function that contains incomplete gamma functions. Of course, the derivatives could be obtained numerically, but the programming effort could not be justified in the short research period. The decision to use ordinary residual analysis was reenforced by Cook and Tsai's observation: "further investigation may be needed to determine the best approach in nonlinear regression, but it does appear that the alternative types of residuals will all suffer from the same shortcomings as the ordinary residuals [5, p.9]."

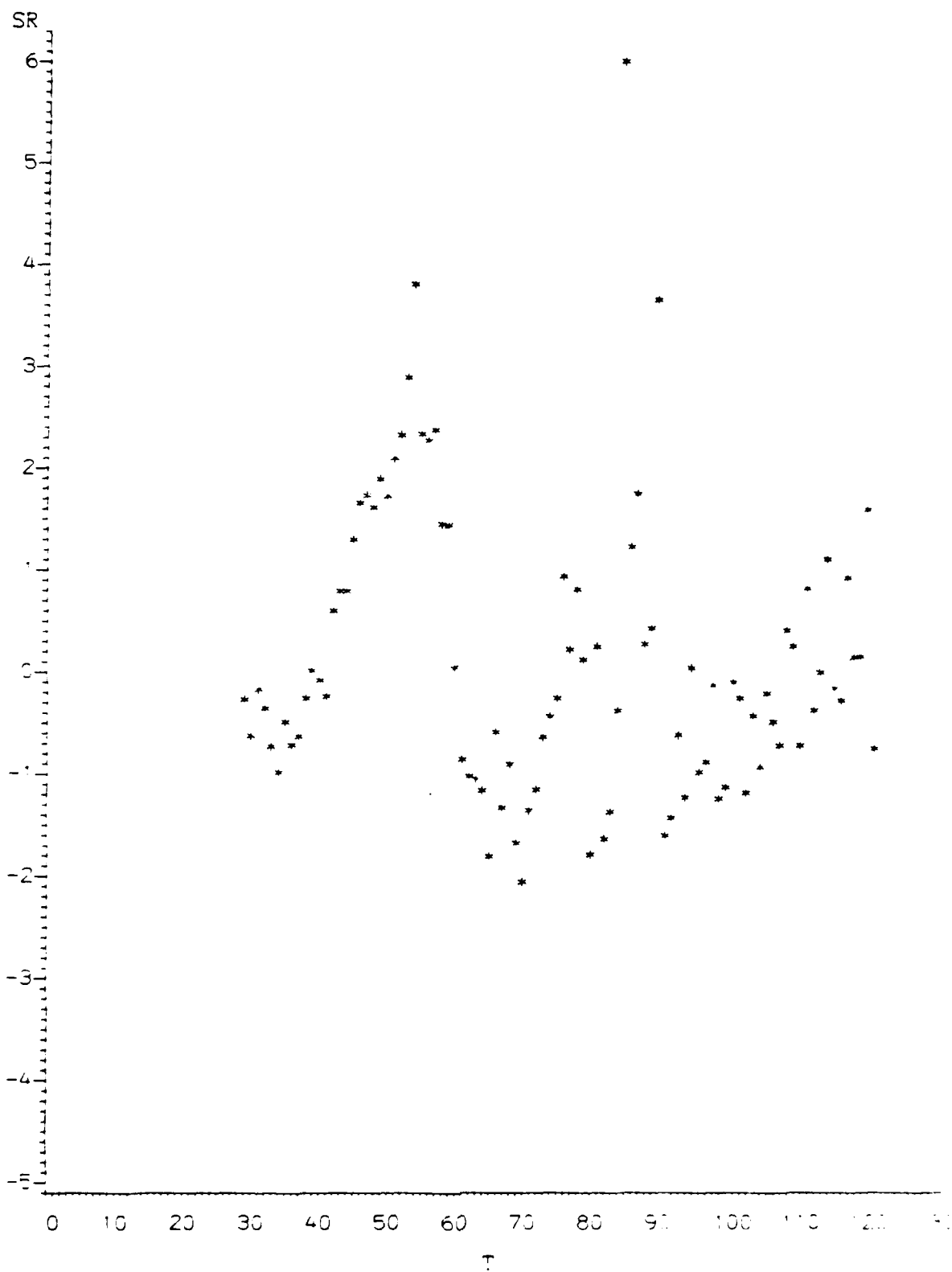
The ordinary residual analysis was straightforward, and the results are predictable from Figure 3. The long string of positive residuals associated with the underprediction is clearly discernible in Figure 3. With the outlier excluded, the latter residuals pass the usual randomness tests, even though there is one short period of time late in the program where the model predicts high. All other things considered, one would have to be satisfied with this model's fit given the nature of the data. That is, this data was not generated within the context of an experimental design; it is actual accounting data.

#### COMPARISON WITH THE C141 MODEL

In examining the data in Tables 1 and 2, it is obvious that it makes no sense to compare the scale parameters;  $\beta_0$ ,  $\beta_{01}$ ,  $\beta_{02}$ ,  $\beta_{03}$ . In fact these parameters are expected a priori to be different. The learning parameter,  $\delta$ , appears to be different in both models, but the scale parameter,  $\gamma$ , appears to be very close across models. However, this visual analysis is

# AGGREGATED RESIDUALS

7 PARAMETER MODEL



20.15

Figure 3.

misleading. If the method of Ratkowsky [16, chapter 7] is used to compare parameters across models, neither the  $\gamma$  nor  $\delta$  estimates are significantly different. The result with the learning parameter is surprising, but the result with the scale parameter agrees with our earlier research. At this time, no logical reason can be assigned to the statistical equivalence of the learning parameters. This is another area where additional research is desperately needed.

#### CONCLUSIONS

The promised deliverables of this research project are summarized below:

1. extend the Womer and Gulledge model to include the F4 airframe program,
2. design a methodology for including model changes within the model,
3. subject the model to extensive diagnostic checking,
4. test for parametric stability across the F4 and C141 programs.

All of the above items have been addressed favorably in the research project. The positiveness of this application reaffirms our commitment to our current research project. Balut, Womer, and Gulledge are currently incorporating this model within a more comprehensive model for repricing aircraft. This model will be used to model variable program costs while other methods will be used to distribute in-plant fixed cost. The proposed model will be a direct competitor with the present multiple regression models that are being used by the Air Force and the Navy.

As a final note, the principal investigator offered to work with Aeronautical Systems Division Personnel in the implementation of this model or a more comprehensive repricing model. That offer is repeated, just for the record.

## REFERENCES

- [1] Alchian, A. A. "Costs and Outputs," in the Allocation of Economic Resources edited by M. Abramovitz, Stanford, CA: Stanford University Press, 1959.
- [2] Alchian, A. A. "Reliability of Progress Curves in Airframe Production," Econometrica, Vol. 31 (October, 1963), 679-93.
- [3] Asher, H. "Cost Quantity Relationships in the Airframe Industry," Rand Report, No. R-291, Santa Monica, CA, 1959.
- [4] Assistant Secretary of Defense (Program Analysis and Evaluation) "Acceptance Rates and Tooling Capacity of Selected Military Aircraft" Washington, D.C., 1974.
- [5] Cook, R.D. and Chih-Ling Tsai. "Residuals in Nonlinear Regression," To Appear in Biometrika.
- [6] Balut, Stephen J. "Redistributing Fixed Overhead Costs," Concepts, Vol. 4 (1981), 63-76.
- [7] Gullledge, Thomas R., Jr.; Norman K. Womer; and M. Murat Tarimcilar. "A Discrete Dynamic Optimization Model for Made-to-Order Cost Analysis," Accepted for publication in Decision Sciences, 1984.
- [8] Gullledge, Thomas R., Jr.; Norman K. Womer; and James R. Dorroh. "Learning and Cost in Airframe Production: A Multiple Output Production Function Approach," Naval Research Logistics Quarterly, Vol. 31 (March, 1984), 67-85.
- [9] Gullledge, Thomas R., Jr.; N. K. Womer; and J. D. Camm. "Learning and Production Costs: An Application to A Fighter Airframe Program," Paper Prepared for the DoD/FAI Acquisition Research Symposium, Richmond, Virginia, 1985.
- [10] Gullledge, Thomas R., Jr. "Specification and Estimation of Dynamic Cost Functions for Airframe Production Programs," Unpublished Ph.D. thesis. Clemson University, Clemson, South Carolina, 1981.
- [11] Hirshleifer, J. "The Firm's Cost Function: A Successful Reconstruction?" Journal of Business, Vol. 35 (July, 1962), 235-255.
- [12] Large, J. P., et al. "Production Rate and Production Costs," Rand Report, No. R-1609-PA&E Santa Monica, CA, 1974.
- [13] McDonnell Aircraft Company, Department 015. F-4 Cost Data, Report 7290, McDonnell Douglas Corporation, 1972.
- [14] Oi, W. Y. "The Neoclassical Foundations of Progress Functions," The Economic Journal, Vol. 77 (September, 1967), 579-594.

- [15] Preston, L. E. and E. C. Keachie. "Cost Functions and Progress Functions," "American Economic Review", Vol. 47 (February, 1965), 31-86.
- [16] Ratkowsky, D. A. Nonlinear Regression Modeling. New York: Marcel Dekker, 1983.
- [17] Rosen, Sherwin. "Learning by Experience as Joint Production," Quarterly Journal of Economics, Vol. 86 (August, 1972), 366-382.
- [18] Smith, Larry L. "An Investigation of Changes in Direct Labor Requirements Resulting from Changes in Airframe Production Rate," Unpublished doctoral dissertation, University of Oregon, Eugene, 1976.
- [19] Washburn, A. R. "The Effects of Discounting Profits in the Presence of Learning in the Optimization of Production Rates." AIIE Transactions, Vol. 4 (1972), 205-213.
- [20] Womer, N. K. and Thomas R. Gulledge, Jr. "A Dynamic Cost Function for an Airframe Production Program," Engineering Costs and Production Economics, Vol. 7 (1983), 213-27.
- [21] Womer, N. K. "A Cost Function for Military Airframes," Proceedings of the Ninth Annual DOD/FAI Acquisition Research Symposium, Annapolis, Maryland, 1980.
- [22] Womer, N. K. and Thomas R. Gulledge, Jr. Final Report: Cost Functions for Airframe Production Programs. Research project jointly supported by the Air Force Business Research Management Center under Contract F33615-81-K-5116 and the Office of Naval Research under Contract N00014-75-C-0451, 1982.
- [23] Womer, N. K. "Estimating Learning Curves from Aggregate Monthly Data," Management Science, Vol. 30 (August, 1984), 982-92.
- [24] Womer, N. K. "Learning Curves, Production Rate, and Program Costs," Management Science, Vol. 25 (April, 1979), 312-19.
- [25] Womer, N. K. "Some Propositions on Cost Functions," Southern Economic Journal, Vol. 47 (April 1981), 1111-1119.



Appendix A

## A DYNAMIC COST FUNCTION FOR AN AIRFRAME PRODUCTION PROGRAM

Norman K. Womer

Clemson University, Clemson, South Carolina, U.S.A.

and Thomas R. Gulledge, Jr.\*

Louisiana State University, Baton Rouge, Louisiana, U.S.A.

---

### ABSTRACT

*This research represents an extension of previous work in the area of estimating military airframe program costs. The effort is unique in that it yields a model of the production process that considers the impact of learning, production rate, and (implicitly) facility size on total program costs. To provide an empirical test of model validity*

*the parameters are estimated for the C141 airframe program. The model's use as a prototype for models of ongoing production programs is illustrated by estimating the cost impact of exogenous changes in the program delivery schedules, e.g. the "crashes" and "stretch-outs" that frequently characterize military airframe production programs.*

---

### 1. INTRODUCTION

The history of cost estimation in the military airframe industry consists mostly of inaccurate estimates that are insensitive to many production decisions. Congressional concern and the need for better planning capabilities provide the impetus for new research in this area. The approach favored by the Department of Defense is one of estimating parametric cost equations which attempt to model cost as a function of only a few aircraft design and performance characteristics. These models often yield useful planning estimates, but Large and Gillespie [1] show that the models may produce

estimates that can be off by as much as 100%. The real limitation of these models is their inability to consider production policy changes which may occur prior to or during the life of a program. To improve upon these techniques, new models must be developed that demonstrate a better understanding of the factors and forces that determine cost.

In contrast to the parametric cost estimating approach, this research involves modeling the production factors that influence cost during an airframe program. In particular, the influences of production rate, learning, and delivery schedules are studied. A modeling effort with this stated purpose requires considerable knowledge of both the planning and production stages in any airframe program.

Before production, a tentative production schedule is developed to help in labor force

---

\*Correspondence to: Thomas R. Gulledge, Jr., Department of Quantitative Business Analysis, 3181 CEBA, Louisiana State University, Baton Rouge, Louisiana 70803, U.S.A.

planning, tooling, facility needs, ordering of long lead time items, etc. This early period of time is called the planning stage. The tentative production schedule is designed to cover the life of the project, but the formal agreements between the government and the contractor usually cover just one year. The reason is that annual congressional funding, changing national needs, or other exogenous impacts are continually varying throughout the life of the program. This period of changing situations is called the production period. The essence of this research is its ability to capture the relationship between total program cost and both endogenous and exogenous production rate changes during the production period. There is now general agreement that both learning and production rate changes impact total program costs. In the former case, it is usually assumed that production costs fall with cumulative production experience. In the latter, the direction and magnitude of the impact on total cost is less certain. Empirical studies have shown that changes in production rate may be associated with increases, decreases, and no change in total program costs.

## 2. HISTORICAL PERSPECTIVE

Traditional neoclassical economic theory explores the relationship between cost and output rate. With the introduction of Wright's [2] seminal work, a new dimension was added to the empirical study of cost. Wright's paper represents the foundation for many of the progress function studies that are prevalent in the engineering literature. In many instances these early engineering cost studies seemed to contradict neoclassical economic theory. Economic theory purports output rate to be an important determinant of cost, but in most of these engineering studies cost was modeled only as a function of cumulative output. In those studies which considered other variables as determinants of program

costs, output rate was often found to be unimportant in predicting cost (see Alchian [3] and Large et al. [4]). There is a remarkable shortage of literature that recognizes the problem or attempts to link the traditional economic approach to the industrial engineering approach. Early researchers such as Asher [5], Alchian [6, 7], Preston and Keachie [8], Oi [9], and Hirshleifer [10] considered the problem in a loose heuristical fashion, and in general their results lacked rigor. Rosen [11] represented the first attempt to solve the problem directly. His work included the theoretical specification of a market structure, the statement of a criterion function, and a straightforward recursive solution to the problem. Although this work is quite noteworthy, it stops short of functional forms sufficiently precise for empirical estimation.

The first real applications oriented integration of the economic and engineering approaches came with the work of Washburn [12] and Womer [13-16]. The present research effort represents the refinement of a more general model [13] for military airframes, so that it may be used to explain the production and cost behavior of a particular airframe project.

## 3. THE C141 PROGRAM

The C141 program produced 284 aircraft during the six-year period from 1962 to 1968. Only one model of the aircraft was produced. Data for this study is drawn from two sources. Orsini [17] reports direct man-hours per quarter for each of the 12 lots in the C141 program. He also reports a delivery schedule for the aircraft by month. Orsini attributes these data to the "C141 Financial Management Reports" maintained by the Air Force Plant Representative Office located at the Lockheed - Georgia facility. The schedule of actual aircraft acceptances by month as reported in the OASD (PA&E)

publication "Acceptance Rates and Tooling Capacity for Selected Military Aircraft" [18] was used to check the Orsini delivery data.

These data, like much data on aircraft production, provide labor hours for a period of time (quarterly) and dates and quantities of deliveries. Unfortunately, there is no available information which relates output to the period of time over which labor hours are observed. One approach to this problem, used by Orsini, is to make some assumption about the pace of production on the program and aggregate the quarterly data across lots. In addition to being arbitrary, this approach reduces 91 potential observations to 24. Our approach to the data problem is to construct a detailed production model of the aircraft to be delivered in any month. The model is then aggregated to explain the data, rather than the other way around.

Preliminary analysis of the data revealed two additional data problems. First, there were two instances, late in the program, where a small number of labor hours were expended on a production lot after the schedule indicated delivery. This probably is a situation where deliveries were made out of sequence. To remedy this problem the labor hours for the last quarter of lots 9 and 10 were aggregated with those of the previous quarter. This reduced the number of observations by two.

The other problem is that in lots 2 through 8, delivery of the aircraft seems to lag the last expenditure of labor hours by an average of four months. For the other five lots labor hours are expended up to the last month of delivery. To overcome this problem, the deliveries of aircraft in lots 2 through 8 were advanced by four months.

With these adjustments 89 observations on labor hours for 24 quarters for 12 lots were used. These observations, together with the number of aircraft delivered each month, constitute the data for the study.

#### 4. PRODUCTION COST DRIVERS

This section discusses four ways in which costs are affected by production decisions. The concept of production cost drivers provides the rationale for the model which follows. That is, the model contains components that attempt to capture the effects of each of the production cost drivers.

The first production cost driver is the concept of learning by doing. The idea is that as the cumulative number of airframes produced becomes larger, the unit costs (or at least labor hours) decrease. This component is the only production cost driver that is sometimes included in parametric cost estimates. It is commonly discussed in both the industrial engineering and the operations research literature, but the learning curve is only rarely mentioned in the production and cost related economics literature.

To introduce the concept of learning and the other production cost drivers the analysis follows Washburn [12] by adopting the concept of a production line as a frame of reference. Learning by doing affects cost by influencing efficiency at each position on the production line. That is, as the number of airframes passing each position on the line increases, yielding more experience, the efficiency at the position increases, thus lowering labor cost. Notice that this process implies that at any point in time the experience on the production line may vary dramatically, e.g. in the C141 program as much as two years elapsed between the lot release date and delivery of an airframe.

The second production cost driver is a different learning effect. Over time learning how to produce more efficiently may take place due to events other than experience at a position on the production line. For example, early in a production program labor hours may be spent to learn how to produce more efficiently. Later in the program this may result in increased efficiency independent

of experience at a point on a line. If this is the case, positions at the end of the line work more efficiently on the same airframe than positions at the beginning of the line. This effect may be related to experience at other locations on the production line. That is, a position late in the production line may benefit from the experience of earlier positions, thus work at later positions proceeds more efficiently than work at early positions on the same airframe.

A third production cost driver is the speed of the production line. Unless there is a learning compensation, increasing the speed of the line is expected to require more labor at each position on the line. Furthermore, due to diminishing returns, the additional labor required is expected to be more than in proportion to the increase in speed. Anyone who has observed the activity around an airframe during production recognizes the likelihood of diminishing returns to labor on that airframe.

The fourth cost driver is the length of the production line. One way to increase delivery rate is to increase the number of positions on the production line, reducing the amount of work to be done at each position, and increasing the total amount of work accomplished per unit of time. If alternative length production lines are planned, this driver may not be a source of variation in unit costs. However, if the length of the line is changed on short notice, unit costs may be affected. For example, increasing the length of the line may result in crowded facilities, overused tools, and inefficient use of other fixed resources. These factors adversely affect the efficiency of production and may result in increased unit costs. This last effect involves an interaction among the airframes that are in the facility at the same point in time. The model of production described in the next section represents an attempt to capture these effects in an estimable analytic model.

## 5. THE MODEL

The model augments a homogeneous production function with a learning hypothesis. The discounted cost of production is minimized subject to a production function constraint, and the optimal time path of resource use is derived. Since factor prices are assumed to be constant over the relevant time period, cost is measured in the units of the variable resource. The variables used in the analysis are:

- $i$  = an index for a batch of airframes in the same lot ( $j$ ) all of which are to be delivered at time  $t_j$ ,
- $n_j$  = the number of batches in lot  $j$ ,
- $m$  = the total number of lots in the production program,
- $D_{ij}$  = the number of airframes in batch  $i$  of lot  $j$ ,
- $E_{ij}$  = a measure of experience prior to the midpoint of batch  $i$ , i.e.,

$$E_{ij} = \sum_{k=1}^{j-1} \sum_{h=1}^{n_j} D_{hk} + \sum_{h=1}^{i-1} D_{hj} + \frac{1}{2} D_{ij}.$$

- $V$  = the number of airframes in the production process in the facility at time  $t$ ,
  - $t_j$  = date work begins for all the batches of lot  $j$ ,
  - $t_{ij}$  = date work ends for batch  $i$  of lot  $j$ ,
  - $q_{ij}(t)$  = production rate at time  $t$  on batch  $i$  of lot  $j$ ,
  - $Q_{ij}(t)$  = cumulative production on batch  $i$  of lot  $j$  at time  $t$ , i.e.,
- $$\int_{t_j}^t q_{ij}(\tau) d\tau,$$
- $x_{ij}(t)$  = rate of resource use at time  $t$  on batch  $i$  of lot  $j$ ,
  - $\delta$  = a parameter describing learning prior to batch  $i$ ,
  - $\epsilon$  = a parameter describing learning on batch  $i$ .

- $\gamma$  = a parameter describing returns to the variable resources,
- $\alpha$  = a parameter associated with decreases in labor productivity as a batch of airplanes nears completion,
- $\nu$  = a parameter describing returns to the length of the production line,
- $\eta$  = a parameter describing returns to the size of the batch,
- $\rho$  = the discount rate,
- $C$  = discounted variable program cost,
- $C^*$  = discounted variable costs for a single batch of airframes.

The production function is assumed to be of the following form:

$$q_{ij}(t) = A V^\nu D_{ij}^\eta E_{ij}^\delta Q_{ij}^\epsilon(t) (t_{ij} - \tau)^\alpha x_{ij}^{1-\gamma}(t), \quad (1)$$

where  $A$  is a constant. The input  $x$  is assumed to be a composite of many inputs whose use rate is variable throughout the production period.

This production function includes the production cost drivers described in the previous section, it conforms to economic production theory, and it also accommodates the fact that the nature of work along the production line changes from position to position. On the other hand, it is still a very simple function, and it can only be expected to describe such a complex production process with some error.

The term  $E_{ij}^\delta$  describes learning by doing in producing a given batch  $i$  in lot  $j$ . A priori,  $\delta$  is expected to be between 0 and 1. The terms  $Q_{ij}^\epsilon(t)$  and  $(t_{ij} - \tau)^\alpha$  represent attempts to describe learning that occurs over time during the process of producing batch  $i$  of lot  $j$ . These terms also admit the possibility that the nature of work changes as the airframe moves down the production line. In particular, it is assumed that as the batch delivery date is approached it is more difficult to substitute labor for time in the production process. Both  $\epsilon$  and  $\alpha$  are expected to be

between 0 and 1. Still one more term  $t^\lambda$  would have been useful to include in the production function to model this effect. Unfortunately, a solution has not been found for the resulting control problem if time is included in this way. Elsewhere [19], specifications of this type have been dealt with extensively.

The terms  $D_{ij}^\eta$  and  $X_{ij}^{1-\gamma}(t)$  together capture the effect of the speed of the production line. The  $D_{ij}^\eta$  term represents the number of airframes in the batch (the number of positions on the line occupied by the batch), while  $X_{ij}^{1-\gamma}(t)$  captures the effect of applying more labor to any given number of positions. The expectation is for  $\eta$  to be between 0 and 1 and  $\gamma$  to be greater than 1. Below, it is seen that the effect of learning during the batch and the effect of the number of airframes in a batch cannot be separated with our data.

Finally the term  $V^\nu$  is intended to capture the effect of assembling alternative numbers of airframes in the same facility. It is assumed that assembling more airframes in the same facility results in a slight decrease in efficiency ( $\nu$  is negative and small).

Although the objective of the firm is a function of the wording of the contract, one goal of most contracts is to induce the firm to minimize discounted cost. The problem may be stated as:

$$\text{Min } C = \sum_{j=1}^m \sum_{i=1}^{n_j} \int_{t_j}^{t_{ij}} x_{ij}(t) e^{-\rho t} dt \quad (2)$$

subject to

$$q_{ij}(t) = A V^\nu D_{ij}^\eta E_{ij}^\delta Q_{ij}^\epsilon(t) (t_{ij} - \tau)^\alpha x_{ij}^{1-\gamma}(t),$$

$$i = 1, 2, \dots, n_j$$

$$j = 1, 2, \dots, m$$

$$Q_{ij}(t_{ij}) = D_{ij}, \quad i = 1, 2, \dots, n_j$$

$$Q_{ij}(t_j) = 0, \quad j = 1, 2, \dots, m$$

Since total cost is monotone nondecreasing and the subproblems are additive, the solution can be obtained by minimizing each of the subproblems. The problem may then be stated as:

$$\text{Min } C' = \int_{t_j}^{t_{ij}} x_{ij}(t) e^{-\rho t} dt \quad (3)$$

subject to

$$\begin{aligned} q_{ij}(t) &= A V^{\nu} D_{ij}^{\delta} E_{ij}^{\epsilon} Q_{ij}^{\epsilon}(t) (t_{ij} - t)^{\alpha} x_{ij}^{1/\gamma}(t), \\ Q_{ij}(t_{ij}) &= D_{ij}, \\ Q_{ij}(t_j) &= 0. \end{aligned}$$

This problem is an optimal control problem which may be solved directly by minimizing the Hamiltonian function. However, the problem can easily be transformed into the problem of Lagrange, which can be solved using classical variational techniques. At this point the redundant  $ij$  subscripts are dropped. Solving the constraint for  $x(t)$  yields

$$x(t) = q^{\gamma}(t) A^{-\gamma} V^{-\nu\gamma} D^{-\eta\gamma} E^{-\delta\gamma} Q^{-\epsilon\gamma}(t) (t_{ij} - t)^{-\alpha\gamma} \quad (4)$$

A transformation is desired that yields one state variable and one control variable, the control variable being the time rate of change of the state variable. Let

$$Z(t) = A^{-1} V^{-\nu} D^{-\eta} E^{-\delta} Q^{1-\epsilon}(t) / (1 - \epsilon). \quad (5)$$

This implies that

$$z(t) = A^{-1} V^{-\nu} D^{-\eta} E^{-\delta} Q^{-\epsilon}(t) q(t). \quad (6)$$

For the transformed problem  $Z(t)$  is the new state variable, and its time derivative,  $z(t)$ , is the control variable. Formation of the new objective functional requires absorbing the constraint. After using (4) and (6), an expression is obtained for  $x(t)$  in terms of the new control variable, i.e.

$$x(t) = z^{\gamma}(t) (t_{ij} - t)^{-\gamma\alpha}. \quad (7)$$

After substituting into the objective functional and setting the boundary conditions, the following transformed problem is obtained:

$$\text{Min } C' = \int_{t_j}^{t_{ij}} z^{\gamma}(t) (t_{ij} - t)^{-\gamma\alpha} e^{-\rho t} dt = \int_{t_j}^{t_{ij}} I(z, t) dt \quad (8)$$

subject to

$$\begin{aligned} Z(0) &= 0, \\ Z(t_{ij}) &= A^{-1} V^{-\nu} D^{1-\epsilon-\eta} E^{-\delta} / (1 - \epsilon). \end{aligned}$$

Since the intermediate function,  $I$ , does not depend explicitly on the state variable, the Euler equation is

$$\frac{\partial I}{\partial z} = \gamma z^{\gamma-1}(t) (t_{ij} - t)^{-\gamma\alpha} e^{-\rho t} = K_0. \quad (9)$$

After solving the Euler equation, the following expression is obtained for optimal  $z(t)$ :

$$z(t) = K_1 (t_{ij} - t)^{\gamma\alpha/(\gamma-1)} e^{\rho t/(\gamma-1)}. \quad (10)$$

This also provides a solution for the optimum time path of resource usage, i.e.

$$x(t) = K_1^{\gamma} (t_{ij} - t)^{\alpha\gamma/(\gamma-1)} e^{\rho t\gamma/(\gamma-1)}. \quad (11)$$

This optimal solution to the problem is only of transient significance since the value of the constant  $K_1$  is unknown. What is needed is an optimal expression for  $x(t)$  that is in terms of the variables and parameters of the original problem. To obtain the constant, notice that

$$Z(t) = \int K_1 (t_{ij} - \tau)^{\alpha\gamma/(\gamma-1)} e^{\rho\tau/(\gamma-1)} d\tau + K_2. \quad (12)$$

Let  $\omega = \rho(t_{ij} - \tau)/(\gamma - 1)$ , then

$$\begin{aligned} Z(u) &= \int K_1 [(\gamma-1)/\rho]^{\alpha\gamma/(\gamma-1)} \omega^{\alpha\gamma/(\gamma-1)} \\ &\quad e^{-\omega} \rho t_{ij}/(\gamma-1) J d\omega + K_2 \end{aligned} \quad (13)$$

where  $J$  is the Jacobian of the transformation. Now,  $u(t_j) = \rho(t_{ij} - t)/(\gamma - 1)$  and  $u(t_{ij}) = 0$ , so choosing 0 and  $u$  as the limits of integration the appropriate integral is

$$Z(u) = K_3 \int_0^u \omega^{\alpha\gamma/(\gamma-1)} e^{-\omega} d\omega + K_4. \quad (14)$$

Integration of this expression yields

$$Z(u) = K_3 \Gamma[u, \alpha\gamma/(\gamma-1) + 1] + K_4 \quad (15)$$

where  $\Gamma$  is the incomplete gamma function. To satisfy the initial condition that  $Z[u(t_j)] = 0$ , let

$$Z(u) = -K_3 \{ \Gamma[\rho(t_{ij} - t_j)/(\gamma - 1), \alpha\gamma/(\gamma - 1) + 1] - \Gamma[u, \alpha\gamma/(\gamma - 1) + 1] \}. \quad (16)$$

Also let

$$-K_3 = A^{-1} V^{-\nu} E^{-\delta} D^{1-\epsilon-\eta} (1-\epsilon)^{-1} \Gamma^{-1} [\rho(t_{ij} - t_j)/(\gamma - 1), \alpha\gamma/(\gamma - 1) + 1], \quad (17)$$

then this implies that  $Z$  also satisfies the final condition,  $Z[u(t_{ij})] = A^{-1} V^{-\nu} E^{-\delta} D^{1-\epsilon-\eta} (1-\epsilon)^{-1}$ . Also, note that

$$z(t) = \frac{dZ(u)}{dt} = K_3 [\rho(t_{ij} - t)/(\gamma - 1)]^{\alpha\gamma/(\gamma - 1)} e^{-\rho(t_{ij} - t)/(\gamma - 1)} [-\rho/(\gamma - 1)]. \quad (18)$$

After substituting for  $K_3$ , the following expression is obtained:

$$z(t) = A^{-1} V^{-\nu} E^{-\delta} D^{1-\epsilon-\eta} (1-\epsilon)^{-1} \Gamma^{-1} \left[ \frac{\rho(t_{ij} - t)}{(\gamma - 1)}, \frac{\alpha\gamma}{\gamma - 1} + 1 \right] \times \left( \frac{\rho(t_{ij} - t)}{(\gamma - 1)} \right)^{\alpha\gamma/(\gamma - 1)} e^{-\rho(t_{ij} - t)/(\gamma - 1)} \left( \frac{\rho}{\gamma - 1} \right). \quad (19)$$

This formulation for optimum  $z(t)$  along with (10) provides a direct solution for  $K_1$ . Substitution for  $K_1$  in (11) yields the following optimum time path of resource use:

$$x_{ij}(t) = B V^{-\nu} E^{-\delta} D^{\gamma(1-\epsilon-\eta)} \Gamma^{-\gamma} [\rho(t_{ij} - t)/(\gamma - 1), \alpha\gamma/(\gamma - 1) + 1] \times (t_{ij} - t)^{\alpha\gamma/(\gamma - 1)} e^{-\gamma\rho(t_{ij} - t)/(\gamma - 1)}, \quad (20)$$

and  $\Gamma[\rho(t_{ij} - t_j)/(\gamma - 1), \alpha\gamma/(\gamma - 1) + 1]$  is the incomplete gamma function. This is the optimal time path for resource use on any batch of airframes.

Since the data presented in the C141 study are quarterly data, the quantity of interest

is the total resource use over a quarterly period. If  $T_k$  and  $T_l$  represent the beginning and ending dates for the quarterly period for some batch  $i$ , the appropriate expression is:

$$X(T_k) - X(T_l) = \int_{T_l}^{T_k} x(t) dt, \quad (21)$$

and using (11) the integral is

$$X(T_k) - X(T_l) = \int_{T_l}^{T_k} K_1^{\gamma} (t_{ij} - t)^{\alpha\gamma/(\gamma - 1)} e^{\gamma\rho t/(\gamma - 1)} dt. \quad (22)$$

Let  $y = \gamma\rho(t_{ij} - t)/(\gamma - 1)$ , then

$$X(T_k) - X(T_l) = -K_1^{\gamma} \int_{\gamma\rho(t_{ij} - T_l)/(\gamma - 1)}^{\gamma\rho(t_{ij} - T_k)/(\gamma - 1)} [(\gamma - 1)/\gamma\rho]^{\alpha\gamma/(\gamma - 1)} \times y^{\alpha\gamma/(\gamma - 1)} e^{-y} e^{\gamma\rho t_{ij}/(\gamma - 1) - (\gamma - 1)/\gamma\rho} dy. \quad (23)$$

Notice that this is a form of the incomplete gamma function. Integration of (23) yields the following expression for resources used during the interval:

$$X(T_k) - X(T_l) = K_1^{\gamma} \left[ \left( \frac{\gamma - 1}{\gamma\rho} \right)^{\alpha\gamma/(\gamma - 1) + 1} e^{\gamma\rho t_{ij}/(\gamma - 1)} \times \{ \Gamma[\gamma\rho(t_{ij} - T_l)/(\gamma - 1), \alpha\gamma/(\gamma - 1) + 1] - \Gamma[\gamma\rho(t_{ij} - T_k)/(\gamma - 1), \alpha\gamma/(\gamma - 1) + 1] \} \right]. \quad (24)$$

Substituting for  $K_1$  and performing the necessary algebra leaves an expression that represents the optimum amount of resource use over an interval of time for an individual batch of airframes, i.e.

$$X_{ij}(T_k) - X_{ij}(T_l) = A V^{-\nu} E^{-\delta} D^{\gamma(1-\epsilon-\eta)} (1-\epsilon)^{-1} \Gamma^{-\gamma} [\rho(t_{ij} - t_j)/(\gamma - 1),$$



$$\alpha\gamma/(\gamma-1)+1 \left( \frac{\rho}{\gamma-1} \right)^{\gamma(\alpha+1)-1} \\ \times \gamma^{-\alpha\gamma/(\gamma-1)-1} \{ \Gamma[\gamma\rho(t_{ij}-T_l)/(\gamma-1), \\ \alpha\gamma/(\gamma-1)+1] - \\ \Gamma[\gamma\rho(t_{ij}-T_k)/(\gamma-1), \alpha\gamma/(\gamma-1)+1] \}. \quad (25)$$

Since the data presented by Orsini [17] are quarterly data, the quantity of interest is the total resource use over a quarterly period. If  $T_k$  and  $T_l$  represent the beginning and ending dates for the quarterly period for some batch  $i$ , the appropriate expression is:

$$X(T_k) - X(T_l) = \int_{T_l}^{T_k} x(t) dt, \quad (26)$$

and using (4) the integral is

$$X_{ij}(T_k) - X_{ij}(T_l) = B'E_{ij}^{-\delta} \gamma D_{ij}^{\gamma(1-\epsilon-\eta)} \\ \times \Gamma^{-\gamma}[\rho(t_{ij}-t_l)/(\gamma-1), \alpha\gamma/(\gamma-1)+1] V^{-\gamma\nu} \\ \times \{ \Gamma[\gamma\rho(t_{ij}-T_l)/(\gamma-1), \alpha\gamma/(\gamma-1)+1] - \\ \Gamma[\gamma\rho(t_{ij}-T_k)/(\gamma-1), \alpha\gamma/(\gamma-1)+1] \}. \quad (27)$$

Because of the nature of the data it is impossible to observe the quantity on the left side of eqn. (27). What is observable is direct manhours per lot. This means that the observed quantity is

$$\sum_{i=1}^{n_j} [X_{ij}(T_k) - X_{ij}(T_l)] \quad (28)$$

where there are  $n_j$  batches in lot  $j$ . For this study, the sum is the observed values of labor hours that are reported in Orsini's data set. This sum and the number of aircraft delivered each month are the variables that are used to test empirically the validity of the model.

## 6. EMPIRICAL RESULTS

To explore the applicability of the theoretical specification, the parameters in (27)

are estimated using the C141 data. Let  $\beta_0 = \beta'$  and  $\beta_1 = \alpha\gamma/(\gamma-1) + 1$ . Furthermore, since  $\epsilon$  and  $\eta$  cannot be independently estimated let  $\lambda = \epsilon + \eta$ . The model may be restated as:

$$\sum_{i=1}^{n_j} X_{ij}(t_k) - X_{ij}(T_l) = \sum_{i=1}^{n_j} \beta_0 E_{ij}^{-\delta} D_{ij}^{\gamma(1-\lambda)} V^\nu \\ \times \Gamma^{-\gamma}[\rho(t_{ij}-t_l)/(\gamma-1), \beta_1] \\ \times \{ \Gamma[\gamma\rho(t_{ij}-T_l)/(\gamma-1), \beta_1] \\ - \Gamma[\gamma\rho(t_{ij}-T_k)/(\gamma-1), \beta_1] \}. \quad (29)$$

Since the monthly delivery dates for each batch within each lot are known, it is possible to estimate the parameters in (29) using nonlinear least squares.

TABLE 1

Parameter estimates and asymptotic standard errors

Parameters	Estimates	Standard error
$\beta_0$	1.251	0.9
$\beta_1$	3.280	0.73
$\delta$	0.2809	0.11
$\lambda$	0.2924	0.25
$\gamma$	1.022	0.009
$\nu$	-0.34	0.17
$\rho$	0.0289	0.008

The results of this regression are presented in Table 1. It does not appear that all of the parameters are significantly different from zero, i.e. the asymptotic standard errors for  $\beta_0$ ,  $\epsilon$  and  $\nu$  seem large, but restricting these parameters to 0 generates large increases in the residual sum of squares. All of the signs of the estimated parameters agree with a priori expectations. In particular, notice that the value of  $\gamma$  is significantly greater than 1, indicating that the production function does exhibit decreasing returns to the variable factor. The estimated value of the learning parameter is also consistent with a priori expectations. A  $\delta$  value of 0.28 is consistent with an 83% learning curve.

In addition, the estimate for  $\beta_1$  has a most

interesting interpretation with respect to the optimal time path of resource use. Notice in (29) that  $\beta_1$  is the argument of a gamma function. A gamma function with parameter  $\beta_1 = 3.280$  generates a time path for resource use that is consistent with our knowledge of labor productivity patterns for "lots" of airframes. In most cases resource use rises at an increasing rate from time  $t_j$  to an inflection point, after which it continues to rise, but at a decreasing rate. Eventually resource usage reaches a maximum and declines thereafter. Simulated time paths of resource use rate and cumulative resource usage for fixed  $V$  are presented in Figs 1 and 2. The eventual decline in resource use rate is attributed to a decrease in the marginal product of labor as the delivery date for a batch approaches. That is, before components of the airframe are assembled, adding more labor easily increases the production rate; but after most of the components are assembled, crowding makes it more difficult to increase production rate on a batch by adding more labor. In fact, the rate of labor use on the batch must fall

to provide the optimal production rate. In addition, the time-consuming testing procedures that precede delivery may not be compressed by more labor. Therefore, there is a period of time near the end of a project where labor cost is significantly reduced.

As observed this functional form generates a time path of resource use for a batch of airframes that conforms to a better understanding of the production process. However, it is possible to observe the time path of resource use for the entire program. Figure 3 illustrates the predicted time path of resource use for the program and the actual resources used. While the model fits the data well ( $R^2 = 0.69$ ), the model shows more variation with time than exhibited by the data. This is particularly true for the period between quarter 14 and quarter 19 where the model predicts somewhat fewer man-hours than used. Perhaps this is because the model included no penalty for hiring or firing costs. Therefore, even though the model predicts that the workforce should decline and then rise again, the company (correctly)

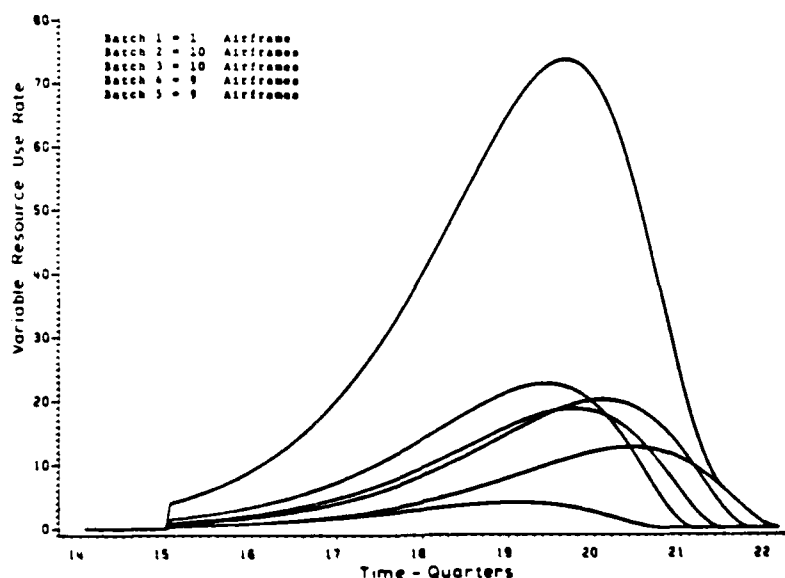


Fig. 1. Simulated optimal time path of resource use rate for a given lot of airframes and the 5 batches within the lot.

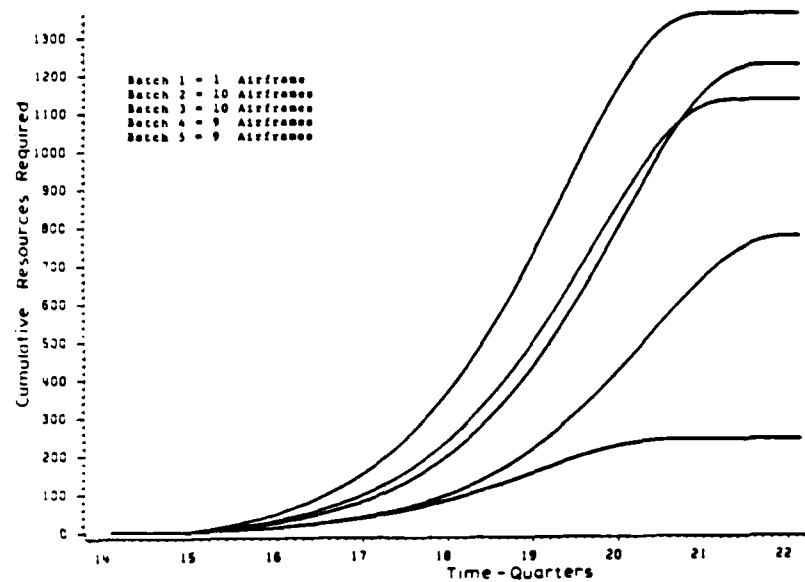


Fig. 2. Simulated optimal time path of cumulative resource usage for a given lot of airframes.

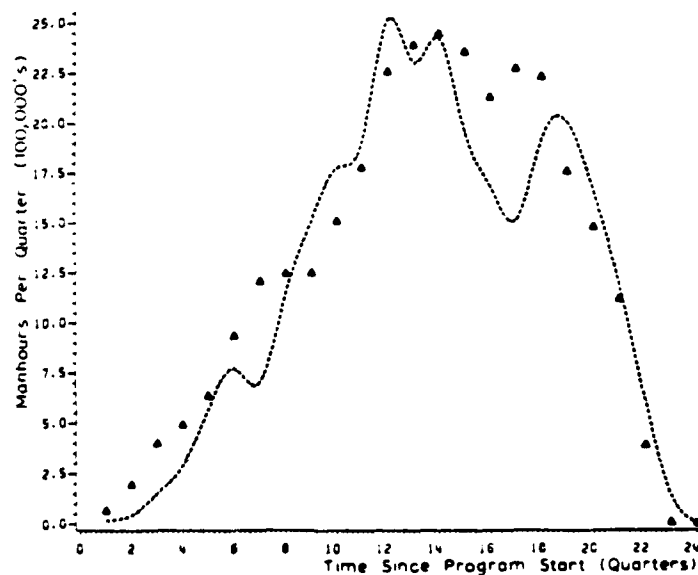


Fig. 3. Predicted time path of resource use for the C141 program and the actual resources used ( $\Delta$  = actual).

chose to maintain a higher workforce over the relatively brief slump. If this is true, then a more appropriate delivery schedule should have permitted substantial savings on the program. These questions are investigated further in the next section.

## 7. SENSITIVITY ANALYSES

To illustrate further the sensitivity of the model to changes in the delivery schedule the time path of resource use is plotted (eqn. (20) summed over  $i$  and  $j$ ) for several hypothetical alternative delivery schedules. Each of the alternatives represents a small discrete change to the actual delivery schedules.

The first alternative, Fig. 4, has the first airframe in the program delivered one month later. This causes the rate of resource use to be lowered early in the program, but it is increased as the new delivery date is approached. The net effect is a small increase in predicted program cost. This delivery schedule change operates by adding one month to the first batch, increasing  $t_{11}$ , by increasing  $(t_{11} - t_1)$ , the time from pro-

gram start until first delivery; and by increasing  $V$  during quarters 5 and 6. The effect of delaying this delivery seems to be to increase the learning applicable to the first unit by providing more time prior to delivery. This effect is offset by the fact that  $V$  increases (the number of positions on the line increases). The net effect is a slight rise in program cost and a delay in program costs (and benefits).

The second sensitivity analysis illustrates a shortcoming of combining the airframes into batches. In this instance, the effect of delivering the last airframe one month early is examined. This results in reducing the time to work on the last airframe and the time for learning. It also results in an increase in  $V$  during the period when the last airframe was completed. These changes all argue for slightly higher program costs for this alternative. However, if the last airframe is combined with the previous batch of airframes, this also has the effect of reducing the number of batches and increasing the size of the augmented batch. This last effect tends to offset the others, resulting in a very slight

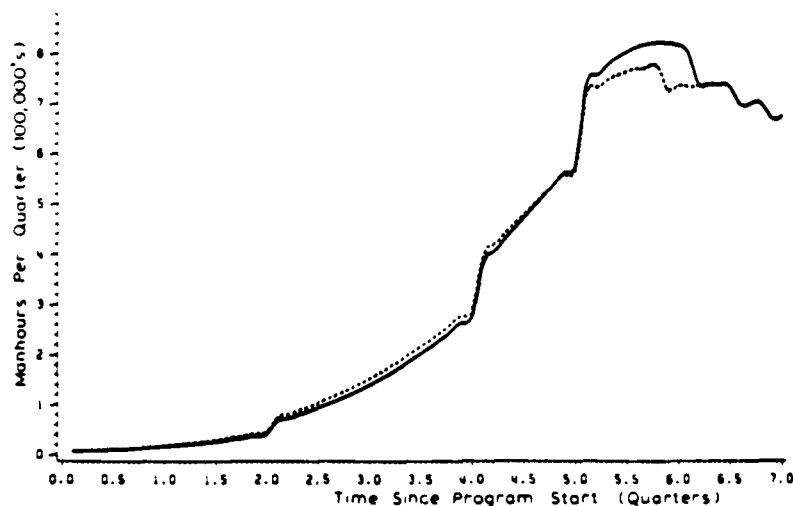


Fig. 4. Predicted time path of resource use when the first airframe is delivered one month late (solid line represents the delayed delivery).



Fig. 5. Predicted time path of resource use when the first airframe is delivered one month early (solid line is altered delivery).

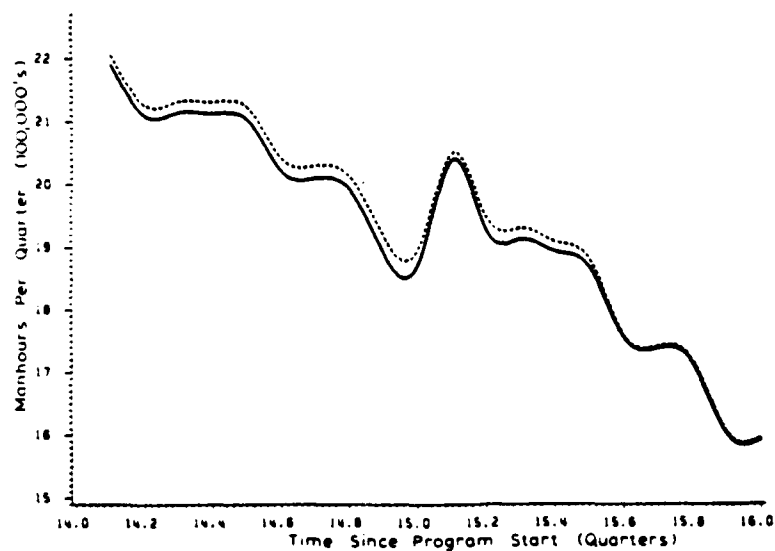


Fig. 6. Predicted time path of resource use when the delivery rate is altered during the program (solid line is altered delivery).

uniform decrease in the time path of resource use. This is illustrated in Fig. 5.

Next, consider the advancement of the delivery of one airframe in the middle of the program. Between the middle of quarter 14 and the middle of quarter 15 deliveries on the C141 program increased from seven per month to nine per month. Only in the first month of quarter 15 were eight air frames delivered. Fig. 6 illustrates the effect of increasing this period where the delivery rate was eight to an entire quarter. Here deliveries are increased by one in the last month of quarter 14 and decreased by one in the second month of quarter 15. This decreases the time available for learning, but it also decreases  $V$ . The net effect is a uniform decrease in the time path of resource use on the program.

The next simulation considers the effect of changing lot release dates on the program. In Fig. 7 the lot release date for the last lot is delayed until the start of quarter 16. In addition to preventing expenditures on

the last lot in quarter 15,  $V$  is lower during that quarter, reducing cost for other lots. Also this effectively shifts the work on the last lot to periods of time when  $V$  is lower, but these effects are partly offset by the compressed schedule for the last lot. The effect of these changes is a reduction of the time path in quarter 15 coupled with a very small increase in expenditures starting in quarter 16. The net effect of these changes is to reduce program cost.

Finally the effect of an early start on a lot in the middle of the program is considered. In Fig. 8 the release date for lot 7 is moved from the beginning of quarter 11 to the beginning of quarter 10. This increases resource use in quarter 10 by permitting work to take place on lot 7, and resource use is also increased for the other lots because  $V$  is higher. Later in the program resource use is decreased due to the lengthening of lot 7. The net effect of these changes is to raise program costs.

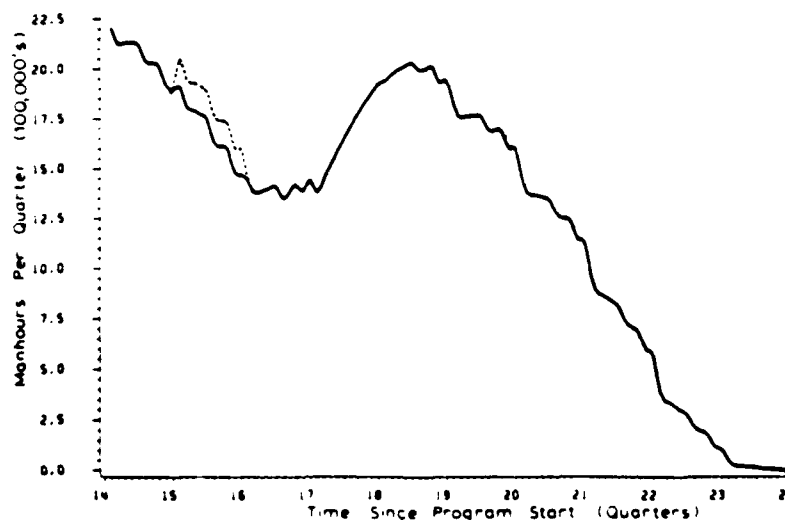


Fig. 7. Predicted time path of resource use when the lot release date is altered during the program (solid line is altered time path).

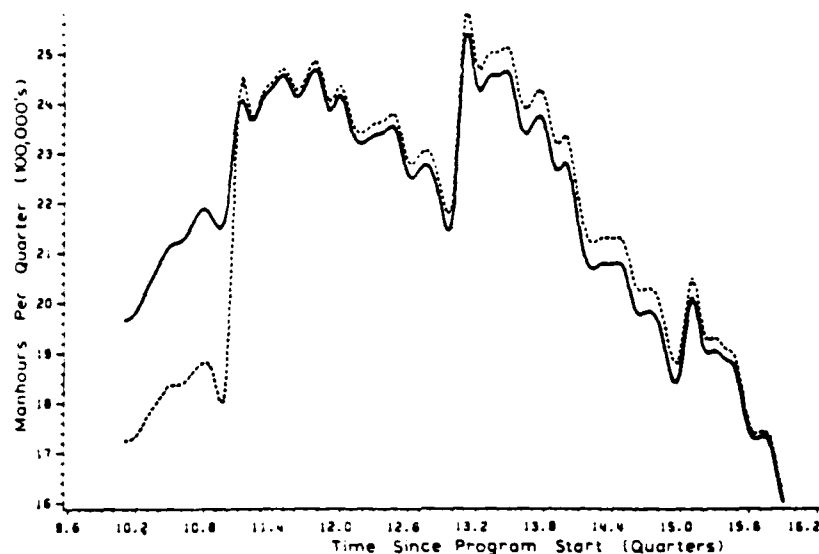


Fig. 8. Predicted time path when a lot in the middle of the program is started early (solid line is altered value).

## 8. SUMMARY

The objective of this study was to provide a model of airframe production that is well grounded in theory, estimated from actual data and sensitive to exogenous delivery schedule effects. In this paper the rationale for such a model is provided, the functional form is derived, the estimation procedure and the parameter estimates are reported, and the sensitivity of the estimated model to delivery schedule changes is examined.

The sensitivity analyses clearly imply that alternative delivery schedules would have resulted in lower costs for the C141 program. In addition, some of these schedules are associated with airframes being delivered to the customer sooner. If so, it is important to ask, "Why were these lower cost and higher benefit schedules not chosen?"

Certainly one possibility is that the decision makers have better insight than the model as to what is best. There are several areas in which flaws in the model may be important. One is the lack of consideration of hiring and firing costs, and a second is the incomplete interaction among the batches

that is permitted in the model. To elaborate, the model permits work on a batch neither to start later than the lot release date nor to end sooner than the delivery date. From the point of view of the single batch, neither of these events would ever be optimal; but, if starting late or ending early could affect  $V$ , then from the point of view of the program, they may be attractive. As it is now,  $V$  is completely determined by the lot release dates and delivery schedule. Of course, more and better data might permit more accurate and different estimated parameters.

On the other hand, it is also possible that with a tool which permits decision makers to grasp the program implications of funding cuts, stretchouts, and of altered delivery schedules more optimal decisions will be made. Management science is based on possibilities such as these.

## ACKNOWLEDGEMENTS

This work was supported in part by the Office of Naval Research under Contract N00014-75-C-0451 and by the Air Force Business Research Management Center under Contract F33615-81-K-5116.

## REFERENCES

- 1 Large, J.P. and Gillespie, K.M.S., 1977. A Critique of Airframe Cost Models, R-2194-AF, The Rand Corporation, Santa Monica, California.
- 2 Wright, T.P., 1936. Factors affecting the cost of airplanes, *Journal of Aeronautical Science*, 3: 122-128.
- 3 Alchian, A.A., 1963. Reliability of progress curves in airframe production, *Econometrica*, 31: 679-693.
- 4 Large, J.P., Koffmayer, K. and Kontrovich, F., 1974. Production Rate and Production Costs, R-1609-PA&E, The Rand Corporation, Santa Monica, California.
- 5 Asher, H., 1956. Cost-Quantity Relationships in the Airframe Industry, R-291, The Rand Corporation, Santa Monica, California.
- 6 Alchian, A.A., 1959. Costs and outputs, in Abramovitz, M. (ed.), *The Allocation of Economic Resources*, Stanford University Press, Stanford, California, 23-40.
- 7 Alchian, A.A. and Allen, W.R., 1964. *Exchange and Production Theory in Use*, Wadsworth, Belmont, California.
- 8 Preston, L.E. and Keachie, E.C., 1974. Cost functions and progress functions: an integration, *American Economic Review*, 54: 100-106.
- 9 Oi, W.Y., 1967. The neoclassical foundations of progress functions, *Economic Journal*, 77: 579-594.
- 10 Hirshleifer, J., 1962. The firm's cost function: a successful reconstruction, *Journal of Business*, 35: 235-255.
- 11 Rosen, S., 1972. Learning by experience as joint production, *Quarterly Journal of Economics*, 86: 366-382.
- 12 Washburn, A.R., 1972. The effects of discounting profits in the presence of learning in the optimization of production rates, *AIIE Transactions*, 4: 205-213.
- 13 Womer, N.K., 1979. Learning curves, production rate, and program costs, *Management Science*, 25: 312-319.
- 14 Womer, N.K., 1980. A cost function for military airframes, Occasional Paper Series, Department of Industrial Management, Clemson University, Clemson, South Carolina.
- 15 Womer, N.K., 1981a. Learning curves and monthly data, Occasional Paper Series, Department of Industrial Management, Clemson University, Clemson, South Carolina.
- 16 Womer, N.K., 1981b. Some propositions on cost functions, *Southern Economic Journal*, 47: 1111-1119.
- 17 Orsini, J.A., 1970. An analysis of theoretical and empirical advances in learning curve concepts since 1966, Master's Thesis, Air Force Institute of Technology, Wright-Patterson AFB, Ohio.
- 18 Assistant Secretary of Defence (Program and Evaluation), 1974. *Acceptance Rates and Tooling Capacity for Selected Military Aircraft*, Washington, D.C.
- 19 Gullledge, T.R., Jr., 1981. Specification and estimation of dynamic cost functions for airframe production programs, Ph.D. Thesis, Clemson University, Clemson, South Carolina.

(Received October 18, 1982; accepted December 30, 1982)



Appendix B

```
// EXEC FORTGCLG,TIME=20
//PCRT.SYSIN DD *
```

```
C
C
C *****
C ***** MAIN *****
C *****
C *
C *
C *
C *
C * NONLINEAR LEAST SQUARES . THIS PROGRAM CALCULATES NONLINEAR LEAST*
C * SQUARES ESTIMATES OF THE REVISED MODEL BY WOMER AND GULLEDGE *
C * USING MARQUARDT'S COMPLEXISE. *
C *
C *
C *
C * NOTE..THIS PROGRAM IS SET UP TO TAKE A MAXIMUM OF 500 OBSERVATIONS *
C * (TIME PERIODS ON LOIS) AND 1000 INDIVIDUAL DELIVERY TIMES (STORED*
C * IN ARRAY DT) . *
C * IF MORE THAN THIS IS REQUIRED DIMENSION STATEMENTS MUST BE *
C * CHANGED IN BOTH THE MAIN AND SUBROUTINE 'MODEL' *
C *
C *
C * A DESCRIPTION OF THE VARIABLES IS GIVEN IN THE SUBROUTINES. *
C *
C *****
```

```
C
C
C EXTERNAL MODEL
C COMMON /AREA1/ X(500,6)
C COMMON /AREA2/ DT(1000)
C COMMON /AREA3/ LN(500)
C DIMENSION Y(500),TH(7),DIFF(7),SCRAT(3000),SIGNS(7),DIFZ(7)
C REAL SIGNS/4*1.0,0.0,2*1.0/,DIFF/3*.01,-.001,-.01,2*.01/,
C & DIFZ/3*.01,-.001,-.01,2*.01/
C INTEGER START1,QUIT1
C NPROB=1
C NP=7
C ESP1=.00001
C ESP2=.005
C MIT=200.
C FLAM=.01
C FNU=10.
C READ(5,*)NOB,TH(1),TH(2),TH(3),TH(4),TH(5),TH(6),TH(7),NUMLOT
C L1=0
C DO 20 J=1,NUMLOT
C READ(5,*)LTJ
C DO 21 L=1,LTJ
C L1=L1+1
C READ(5,*)Y(L1),X(L1,1),X(L1,2),X(L1,3),X(L1,4),X(L1,5),X(L1,6)
C & LN(L1)
21 CONTINUE
C START1=X(L1,2)+1
C QUIT1=X(L1,4)
C DO 100 K=START1,QUIT1
C READ(5,*)DT(K)
100 CONTINUE
20 CONTINUE
C CALL UWHAUS(NPROB,MODEL,NOB,Y,NP,TH,DIFF,SIGNS,ESP1,ESP2,MIT,FLAM,
C & FNU,SCRAT)
```

STCP  
END

```

C
C
C
C      SUBROUTINE MODEL(NPRCE,TH,P,NOB,NP)
C
C THIS IS A USER SUPPLIED SUBROUTINE THAT EVALUATES A GIVEN FUNCTION
C (F) FOR DIFFERENT VALUES OF THE PARAMETERS (TH).
C
C      NPROB = PROBLEM NUMBER-SCALAR
C      TH    = PARAMETER VALUES-DIMENSIONED AT TH(NP)
C      F     = PREDICTED VALUES FROM REGRESSION EQUATION,
C              DIMENSIONED AT F(NOB)
C      NOB   = SAMPLE SIZE-SCALAR
C      NP    = NUMBER OF UNKNOWN PARAMETERS-SCALAR
C      X     = IND. VARIABLE MATRIX-DIMENSIONED AT X(NCB,NP)
C      X(I,1) = END OF TIME PERIOD (OBSERVATION I)
C      X(I,2) = NO. DELIVERED PRIOR TO THIS LOT
C      X(I,3) = PERIOD WORK BEGAN ON THE LOT
C      X(I,4) = SEQUENCE NUMBER OF THE LAST AIRFRAME IN THE LOT
C      X(I,5) = AVG. NO. IN HOUSE DURING THE PERIOD
C      X(I,6) = START OF THE PERIOD
C      TH(1) = B0.....THE CONSTANT TERM
C      TH(2) = DELTA.....THE LEARNING PARAMETER
C      TH(3) = B1.....ALPHA/(GAMMA-1.) +1.
C      TH(4) = GAMMA-1.....FACTORS TO SCALE (LESS 1. SO THAT GAMMA >1)
C      TH(5) = B0.....THE DISCOUNT PARAMETER
C      TH(6) = H.....THE PARAMETER ASSOCIATED WITH AVG. IN HOUSE
C              (ALL TH(I) ARE RESTRICTED TO THE SIGN OF INITIALIZATION)
C      NUMLOT = NUMBER OF LOTS
C      L1Q    = NUMBER OF OBSERVATIONS (TIME PERIODS) FOR A LOT
C      LN     = AN ARRAY THAT DEFINES THE LOT NUMBERS
C
COMMON /AREA1/ X(500,6)
COMMON /AREA2/ DT(1000)
COMMON /AREA3/ LN(500)
DIMENSION F(1),Y(1),TH(1)
INTEGER START,QUIT
BHC=.001706
B2=BHC/TH(4)
IF (B2.L1.0.) PRINT 19
19  FORMAT(' ERROR.....B2<0')
DO 910 I=1,NOB
IF (LN(I).EQ.10) K=7
IF (LN(I).EQ.9) K=6
IF (LN(I).LE.8) K=7
IF (LN(I).LE.6) K=6
IF (LN(I).LE.2) K=1
CT=X(I,1)
Q1N=X(I,2)+.5
U=0.
START=X(I,2)+1
QUIT=X(I,4)
T0=X(I,3)
V=X(I,5)
CT1=X(I,6)
DO 920 J1=START,QUIT
TH=DT(J1)
IF (DT(J1).LE.C.) PRINT 17

```

```

17  FORMAT('ERROR..... A IT IS <=0')
    IF (CT1.GE.TH) GO TO 920
    IF (CT.LE.TH) GO TO 925
    BT = (TH-CT1) * (TH(4) + 1.) * F2
    E4 = GAM1(TH(3), BT)
    GO TO 930
925  BT = (TH-CT) * (TH(4) + 1.) * R2
    ET1 = BT + (TH(4) + 1.) * R2
    E4 = GAM1(TH(3), BT1) - GAM1(TH(3), BT)
930  EQ = Q1N ** (-TH(2) * (TH(4) + 1.))
    EV = V ** (- (TH(4) + 1.) * TH(5))
    F2 = R2 * (TH - T0)
    IF (F2.LT.0.0) PRINT 18
18   FORMAT('ERROR.....F2 <0')
    E = GAM1(TH(3), F2)
    E = E ** (- (TH(4) + 1.))
    U = U + TH(K) * EQ * E * E4 * EV
920  Q1N = Q1N + 1.
    F(I) = U
910  CONTINUE
    RETURN
    END

```

```

C
C
C
C      SUBROUTINE UNHAUS(NPROB,MODEL,NOB,Y,NP,TH,DIFF,SIGNS,ESP1,ESP2,
      @HIT,FLAM,FNU,SCRAT)

```

```

C
C      *****
C      ***** MARQUARITS COMPROMISE *****
C      *****

```

```

C      MARQUARIT, DONALD W. 'AN ALGORITHM FOR LEAST SQUARES ESTIMATION OF
C      NONLINEAR PARAMETERS.' J. SOC. INDUST. APPL. MATH. VOL. XI
C      (JUNE, 1963), 431-34.

```

```

C      LAMBDA LARGE=STEEPEST DESCENT---SHIFT TO LINEARIZATION

```

```

C      NPROB  =PROBLEM NUMBER-SCALAR
C      MODEL  =NAME OF SUBROUTINE--MUST DECLARE AS EXTERNAL IN MAIN
C              LINE-USER SUPPLIED SUBROUTINE TO COMPUTE THE FITTED
C              VALUES FROM THE REGRESSION EQUATION.
C      NOB    = NUMBER OF OBSERVATIONS-SCALAR
C      Y(I)   =VECTOR OF OBSERVATIONS ON THE DEPENDENT VARIABLE-
C              DIMENSIONED AT Y(NOB)
C      NP     =NUMBER OF UNKNOWN PARAMETERS-SCALAR
C      TH     =VECTOR OF PARAMETERS-DIMENSIONED AT TH(NP)
C      DIFF   =RELATIVE STEP SIZE IN NUMERICAL DIFFERENTIATION-SAY .01
C              DIMENSIONED AT DIFF(NP)
C      SIGN   = 0. FOR UNRESTRICTED SEARCH,
C              = 1. SIGN OF I TH PARAMETER MUST NOT CHANGE-
C              DIMENSIONED AT SIGN(NP)
C      ESP1   = TERMINATION VALUE OF SUM OF SQUARES S(THETA)-
C              SAY 10.**-07-SCALAR
C      ESP2   = TERMINATION BASED ON PARAMETERS-SAY 10.**-03
C      HIT    = MAXIMUM NO OF ITERATIONS-SCALAR
C      FLAM   = LAMBDA EQUALS APPROX 0.01-SCALAR
C      FNU    = GAMMA EQUALS APPROX 10.-SCALAR
C      SCRAT  = STORAGE AREA. MAIN LINE DIMENSION GE
C              5*NP*NP**2+2*NOB*NOB*NP

```

```

C
  DIMENSION SCRAT(1),TH(1),I(1),DIFF(1),SIGNS(1)
  IA=1
  IB=IA+NP
  IC=IB+NP
  ID=IC+NP
  IE=ID+NP
  IF=IE+NP
  IG=IF+NOB
  IH=IG+NCB
  II=IH+NP*NOB
  IJ=IH
  CALL HAUS59(NPROB,MODEL,NCB,Y,NP,TH,DIFF,SIGNS,EPS1,EPS2,MIT
  @,FLAM,FNU,SCRAT(IA),SCRAT(IB),SCRAT(IC),SCRAT(ID),
  @SCRAT(IE),SCRAT(IF),SCRAT(IG),SCRAT(IH),SCRAT(II),
  @SCRAT(IJ))
  RETURN
  END

C
C
C
  SUBROUTINE HAUS59(NPROB,MODEL,NCB,Y,NQ,TH,DIFZ,SIGNS,EP1S,EP2S,
  @MIT,FLAM,FNU,Q,P,E,PHI,TE,F,R,A,D,DELZ)

C
C  NPROB = VARIABLE INDICATING THE PROBLEM NUMBER
C  MODEL = SUBROUTINE WHICH COMPUTES THE VALUES OF THE MODEL
C  NCB   = NUMBER OF OBSERVATIONS
C  Y     = VECTOR OF OBSERVED FUNCTION VALUES
C  NP    = NUMBER OF UNKNOWN PARAMETERS.
C         NP IS BIGGER THAN 1 AND SMALLER THAN 11 IN THE PROGRAM.
C  TH    = VECTOR OF PARAMETER VALUES
C  DIFF  = VECTOR OF DERIVATIVES IN TH. IT IS USED TO CALCULATE
C         THE NUMERICAL DERIVATIVES OF THE FUNCTION.
C  SIGNS = VECTOR INDICATING THE EXISTENCE OF A PRIORI SIGN
C         RESTRICTIONS.
C  EPS1  = RELATIVE CHANGE OF THE FUNCTION CRITERION
C  EPS2  = PARAMETER CONVERGENCE CRITERION
C  MIT   = MAXIMUM NUMBER OF ITERATIONS
C  FLAM  = STARTING VALUE FOR LAMDA
C  FNU   = VALUE OF NQ TO REDUCE LAMDA
C  SCRAT = TEMPORARY STORAGE FOR USE BY UMHAUS

C
C  DIMENSION TH(NQ),DIFZ(NQ),SIGNS(NQ),Y(NCB)
C  DIMENSION Q(NQ),P(NQ),E(NQ),PHI(NQ),TE(NQ)
C  DIMENSION F(NCB),R(NCB)
C  DIMENSION A(NQ,NQ),D(NQ,NQ),DELZ(NBO,NQ)

C
C  COMMON /AREA1/X(500,6)
C  COMMON /AREA3/LN(500)
C  DIMENSION TH(1),DIFZ(1),SIGNS(1),Y(1),Q(1),P(1),E(1)
  @PHI(1),TE(1),F(1),R(1),A(1),D(1),DELZ(1),SUMO(100),SUMP(100)
  NP=NQ
  NPRCB=NPR30
  NOB=NBO
  EPS1=EP1S
  EPS2=EP2S
  NPSQ=NP*NP
  NSCRAC=5*NP+NPSQ+2*NOB+NP*NOB
  PRINT 1000,NPROB,NOB,NP,NSCRAC
  PRINT 1001

```

```

      CALL GASS60(1,NP,TH,TEMP,TEMP)
      PRINT 1002
      CALL GASS60(1,NP,DIFZ,TEMP,TEMP)
      IF (MIN0(NP-1,50-NP,NOE-AP,MIT-1,999-MIT)) 99,15,15
15    IF (FNU-1.0) 99,99,16
16    CONTINUE
      DO 19 I=1,NP
      TEMP=AES(DIFZ(I))
      IF (AMIN1(1.0-TEMP,AES(TH(I)))) 99,99,19
19    CONTINUE
      GA=FLAM
      MIT=1
      LACS=0
      IF (EPS1) 5,70,70
5      EPS1=0
70     SSQ=0
      CALL MODEL(NPROB,TH,F,NCB,NP)

C
C *****          R(I)=Y(I)-F(TH)          *****
C ***** INITIAL SUM OF SQUARES *****
C
      DO 90 I=1,NOB
      R(I)=Y(I)-F(I)
90    SSQ=SSQ+R(I)*R(I)
      PRINT 1003,SSQ

C
C ***** BEGIN ITERATION *****
C
100   GA=GA/FNU
      INTCNT=0
      PRINT 1004,NIT
101   JS=1-NOB
      DO 130 J=1,NP
      TEMP=TH(J)
      P(J)=DIFZ(J)*TH(J)
      TH(J)=TH(J)+P(J)
      Q(J)=0
      JS=JS+NCB
      CALL MODEL(NPROB,TH,DELZ(JS),NOB,NP)
      IJ=JS-1

C
C ***** NUMERICAL EVALUATIONS OF DERIVATIVES *****
C
      DO 120 I=1,NOB
      IJ=IJ+1
      DELZ(IJ)=DELZ(IJ)-P(I)
120   Q(J)=Q(J)+DELZ(IJ)*R(I)
      Q(J)=Q(J)/P(J)

C
C ***** Q=X1*R (STEEPEST DESCENT) *****
C
130   TH(J)=TEMP
      IF (LAOS) 131,131,414
131   DO 150 I=1,NP
      DO 151 J=1,I
      SUM=0.
      KJ=NOB*(J-1)
      KI=NOB*(I-1)
      DO 160 K=1,NOB
      EI=KI+1

```

```

      KJ=KJ+1
160  SUM=SUM+DELZ (KI) *DELZ (KJ)
      TEMP=SUM/(P(I)*P(J))
      JI=J+NP*(I-1)
      D(JI)=TEMP
      IJ=I+NP*(J-1)
151  D(IJ)=TEMP
150  E(I)=SQRT(D(JI))
666  CONTINUE
      DO 153 I=1,NP
      IJ=I-NP
C
C ***** SCALING OF XTRANSICSE X MATRIX TO C-1/2XTRANS X D-1/2 *****
C ***** SCALING OF XTRANS R TO D-1/2 XTRANS R *****
C ***** ADD LAMDA I TO SCALED XTRANS X MATRIX *****
C
      DO 153 J=1,I
      IJ=IJ+NP
      A(IJ)=D(IJ)/(E(I)*E(J))
      JI=J+NP*(I-1)
153  A(JI)=A(IJ)
C
C ***** A= SCALED MOMENT MATRIX *****
C
      II=-NP
      DO 155 I=1,NP
      P(I)=Q(I)/E(I)
      PHI(I)=P(I)
      II=NP+1+II
155  A(II)=A(II)+GA
      I=1
C
C ** CALCULATE THE DETERMINANT AND INVERSE OF C-1/2 XTRANS X D-1/2+LA **
C
      CALL MATIN(A,NP,P,I,DET)
C
C ***** P/E=CCFFECTION VECTOR *****
C
      STEP=1.0
      SUM1=0.
      SUM2=0.
      SUM3=0.
      DO 231 I=1,NP
      SUM1=P(I)*PHI(I)+SUM1
      SUM2=P(I)*P(I)+SUM2
      SUM3=PHI(I)*PHI(I)+SUM3
231  PHI(I)=P(I)
      TEMP=SUM1/SQRT(SUM2*SUM3)
      TEMP=AMIN1(TEMP,1.0)
      TEMP=57.295*ACOS(TEMP)
      PRINT 1041,DET,TEMP
170  DO 220 I=1,NP
      P(I)=PHI(I)*STEP/E(I)
      TB(I)=TB(I)+P(I)
220  CONTINUE
      PRINT 7000
7000  FORMAT(///' TEST POINT PARAMETER VALUES')
      PRINT 2006,(TB(I),I=1,NI)
      DO 221 I=1,NP
      IF (SIGNS(I)) 221,221,222

```

```

222 IF (SIGN(1.0,TH(I))*SIGN(1.0,TB(I))) 663,221,221
221 CONTINUE
    SUMF=0.
    CALL MCDEL(NPFOB,TB,F,NCE,NP)
    DO 230 I=1,NOB
    R(I)=Y(I)-F(I)
230 SUMF=SUMF+R(I)*R(I)
    PRINT 1043,SUMB
    IF (SUMF-(1.0+EPS1)*SSQ) 662,662,663
C
C ***** IF ANGLE LESS THAN 30 DEG THEN DECREASE STEP SIZE *****
C
663 IF (AMIN1(TEMP-30.0,GA)) 665,665,664
665 STEP=STEP/2.0
    INTCNT=INTCNT+1
    IF (INTCNT-36) 170,2700,2700
664 GA=GA*FNU
    INTCNT=INTCNT+1
    IF (INTCNT-36) 666,2700,2700
662 PRINT 1007
    DO 669 I=1,NP
669 TH(I)=TB(I)
    CALL GASS60(1,NP,TH,TEMP,TEMP)
    PRINT 1040,GA,SUMB
    IF (EPS2) 229,229,225
229 IF (EPS1) 270,270,265
C
C ***** PARAMETER CONVERGENCE CRITERION *****
C
225 DO 240 I=1,NP
    IF (ABS(P(I))/(1.E-20+ABS(TH(I)))-EPS2) 240,240,241
241 IF (EPS1) 270,270,265
240 CONTINUE
    PRINT 1009,EPS2
    GO TO 280
C
C ***** SUM OF SQUARES CONVERGENCE CRITERION *****
C
265 IF (ABS(SUMB-SSQ)-EPS1*SSQ) 266,266,270
266 PRINT 1010,EPS1
    GO TO 280
270 SSQ=SUMB
    NIT=NIT+1
    IF (NIT-NIT) 100,100,280
2700 PRINT 2710
2710 FORMAT (// 50H0*** THE SUM OF SQUARES CANNOT BE REDUCED TO THE
    @// 55H SUM SQUARES AT THE END OF THE LAST ITERATION - STOP / )
C
C ***** END ITERATION *****
C
C ***** FINAL FUNCTION VALUES AND RESIDUALS *****
C
280 PRINT 1036
    PRINT 1036
    PRINT 1011
    PRINT 1036
    DO 342 I=1,NOB
342 WRITE(3,*) Y(I),F(I),R(I),X(I,1),LN(I)
    DO 810 JLP=1,100
    SUMC(JLP)=0.0

```



```

810  SUMF(JLP)=0.0
      DO 820 ILP=1,NOB
        JLF=X(ILP,1)
        SUMC(JLP)=SUMO(JLP)+Y(IIP)
820  SUMF(JLP)=SUMF(JLP)+F(IIF)
      DO 845 JLP=1,100
        IF(SUMO(JLP).EQ.0.0) GO TO 850
        PRINT 840,JLP,SUMO(JLF),SUMP(JLP)
840  FORMAT(' ',1X,I4,9X,F12.6,2X,F12.6)
845  CONTINUE
850  CONTINUE
      SSQ=SUMB
      IDF=NCB-NP
      PRINT 1015
      I=0
      CALL MATIN(D,NP,P,I,DET)
      DO 7692 I=1,NP
        II=I+NP*(I-1)
7692  E(I)=SQRT(D(II))
      DO 340 I=1,NP
        JI=I+NP*(I-1)-1
        IJ=I+NP*(I-2)
        DO 340 J=I,NP
          JI=JI+1
          A(JI)=D(JI)/(E(I)*E(J))
          IJ=IJ+NP
340  A(IJ)=A(JI)
      CALL GASS60(3,NP,TEMP,TEMP,A)
      PRINT 1016
      CALL GASS60(1,NP,E,TEMP,TEMP)
      IF(IDF)341,410,341
341  SDEV=SSQ/IDF
      PRINT 1014,SDEV,IDF
      SDEV=SQRT(SDEV)
      DO 391 I=1,NP
        P(I)=TH(I)+2.0*E(I)*SDEV
391  TB(I)=Ta(I)-2.0*E(I)*SDEV
      PRINT 1036
      PRINT 1039
      PRINT 1036
      PRINT 1038
      DO 423 I=1,NP
423  PRINT 1037,I,TH(I),TB(I),P(I)
      LACS=1
      GO TO 101
414  DO 415 K=1,NOB
        TEMP=0.
        DO 420 I=1,NP
          DO 420 J=1,NP
            ISUB=K+NOB*(I-1)
            DEBUG1=DELZ(ISUB)
C
C ***** DEBUG1=DELZ(K+NOB*(I-1)) *****
C
          ISUB=K+NOB*(J-1)
          DEBUG2=DELZ(ISUB)
C
C ***** DEBUG2=DELZ(K+NOB*(J-1)) *****
C
          IJ=I+NP*(J-1)

```

```

420  DEBUG3=D(IJ)/(DIFZ(I)*TH(I)*DIFZ(J)*TH(J))
      TEMP=TEMP+DEBUG1*DEBUG2*DEBUG3
      TEMP=2.0*SQRT(TEMP)*SIEV
      B(K)=F(K)+TEMP
415  F(K)=F(K)-TEMP
      PRINT 1008
      IE=0
      DO 425 I=1,NOB,10
      IE=IE+10
      IF (NOB-IE) 430,435,435
430  IE=NOB
435  PRINT 2001,(R(J),J=I,IE)
425  PRINT 2006,(F(J),J=I,IE)
410  PRINT 1033, NPROB
      GO TO 9999
      99  PRINT 1034
      GO TO 410
1000  FORMAT(' NONLINEAR ESTIMATION, PROBLEM NUMBER ',I3, '//I5,
a)  ' OBSERVATIONS, ',I5,' PARAMETERS ',I14,' SCRATCH REQUIRED')
1001  FORMAT('// ' INITIAL PARAMETER VALUES')
1002  FORMAT('// ' PROPORTIONS USED IN CALCULATING DIFFERENCE QUOTIENTS')
1003  FORMAT('// ' INITIAL SUM OF SQUARES = ',E12.4)
1004  FORMAT('////////'*****'
a)  ' ITERATION NO. ',I4, '//')
1007  FORMAT('///' PARAMETER VALUES VIA REGRESSION')
1008  FORMAT('///' APPROXIMATE CONFIDENCE LIMITS FOR EACH FUNCTION VALUE'
a)
1009  FORMAT('////' ITERATION STOPS - RELATIVE CHANGE IN EACH',
a)  ' PARAMETER LESS THAN ',E12.4)
1010  FORMAT('////' ITERATION STOPS - RELATIVE CHANGE IN SUM OF',
a)  ' SQUARES LESS THAN ',E12.4)
1011  FORMAT('** OBSERVED *** FITTED *** RESIDUAL **')
1012  FORMAT(3E12.4)
1014  FORMAT('///' VARIANCE OF RESIDUALS = ',E12.4,1X,I4,
a)  ' DEGREES OF FREEDOM')
1015  FORMAT('////' CORRELATION MATRIX')
1016  FORMAT('////' NORMALIZING ELEMENTS')
1033  FORMAT('///' END OF PROBLEM NO. ',I3)
1034  FORMAT('///' PARAMETER ERROR')
1036  FORMAT(' ')
1039  FORMAT('///' INDIVIDUAL CONFIDENCE LIMITS FOR EACH PARAMETER ',
a)  '(CN LINEAR HYPOTHESIS) ')
1037  FORMAT(I4,3E12.4)
1038  FORMAT(' I TH(I) CONFIDENCE LIMITS ')
1040  FORMAT('///' LAMEDA = ',E10.3,30X,' SUM OF SQUARES AFTER',
a)  ' REGRESSION = ',E15.7)
1041  FORMAT('///' DETERMINANT = ',E12.4,6X,' ANGLE IN SCALED COORD. = ',
a)  'P5.2,' DEGREES')
1043  FORMAT('///' TEST POINT SUM OF SQUARES = ',E12.4)
2001  FORMAT (/5E12.4, //5E12.4)
2006  FORMAT (/5E12.4, //5E12.4)
9999  RETURN
      END

```

C  
C  
C

```

SUBROUTINE MATIN(A,NV/R,E,NB,DET)
DIMENSION A(NVAR,1),B(NVAR,1)
PIVCTM=A(1,1)
DET=1.0

```

```

DO 550 ICOL=1,NVAR
PIVCT=A(ICOL,ICOL)
PIVOTM=AMIN1(PIVCT,PIVCTM)
DET=PIVOT*DET
C
C ***** DIVIDE PIVCT ROW BY PIVOT ELEMENT *****
C
A(ICCL,ICOL)=1.0
PIVCT=AMAX1(PIVOT,1.E-20)
PIVOT=A(ICCL,ICCL)/PIVCT
DO 350 L=1,NVAR
350 A(ICOL,L)=A(ICOL,L)*PIVCT
IF(NB.EQ.0) GC TO 371
DO 370 L=1,NB
370 B(ICCL,L)=B(ICOL,L)*PIVCT
C
C ***** REDUCE NON-PIVOT ROWS *****
C
371 DO 550 L1=1,NVAR
IF(L1.EQ.ICOL) GC TO 550
T=A(L1,ICOL)
A(L1,ICCL)=0.
DO 450 L=1,NVAR
450 A(L1,L)=A(L1,L)-A(ICCL,L)*T
IF(NB.EQ.0) GO TO 550
DO 500 L=1,NB
500 B(L1,L)=B(L1,L)-B(ICCL,L)*T
550 CONTINUE
RETURN
END
C
C
C
SUBROUTINE GASS60(ITYIE,NQ,A,B,C)
C
C THE ONLY FUNCTION OF THIS SUBPROGRAM IS TO CARRY OUT
C VARIOUS PRINTING TASKS. IT PRINTS THE VALUES OF VARIOUS QUANTITIES
C THAT ARE PASSED IN THE ARGUMENT LIST OVER THE RANGE LOW TO LUP,
C WHERE LUP IS THE NUMBER OF PARAMETERS (VARIABLE UP TO 10).
C
DIMENSION A(NQ),B(NQ),C(NQ,NQ)
NP=NQ
NR=NR/10
LOW=1
LUP=10
10 IF(NR) 15,20,30
15 RETURN
20 LUP=NP
IF(LCW.GT.LUP) RETURN
30 PRINT 500,(J,J=LOW,LUP)
GO TO (40,60,80),ITYIE
40 PRINT 600,(A(J),J=LCW,LUP)
GO TO 100
60 PRINT 600,(B(J),J=LCW,LUP)
GO TO 40
80 DO 90 I=LOW,LUP
90 PRINT 720,I,(C(J,I),J=LCW,LUP)
LOW2=LUP+1
IF(LOW2.GT.NP) GO TO 100
DO 95 I=LOW2,NP

```

```

95  PRINT 720,I,(C(J,I),J=LCW,LUP)
100  LOW=LOW+10
    LOF=LOF+10
    NR=NR-1
    GO TO 10
500  FORMAT(/5I12,/,5I12)
600  FORMAT(/5E12.4,/,5E12.4)
720  FORMAT(1H0,I3,1X,5F12.4,/,5X,5F12.4)
    RETURN
    END

```

```

C
C
C

```

```

    FUNCTION GAMI(A,X)
C***REVISION OCTOBER 1, 1980
C***CATEGORY NO. B5F
C***KEYWORD(S) GAMMA FUNCTION, INCOMPLETE GAMMA FUNCTION, SPECIAL FUNCTION
C***DATE WRITTEN JULY 1977
C***AUTHOR FULLERTON W. (LASI)
C***PURPOSE - COMPUTES THE INCOMPLETE GAMMA FUNCTION
C***DESCRIPTION
C JULY 1977 EDITION. W. FULLERTON, C3, LOS ALAMOS SCIENTIFIC LAB.
C
C EVALUATE THE INCOMPLETE GAMMA FUNCTION DEFINED BY
C
C  $GAMI = \int_{T=C}^{T=X} \exp(-T) * T^{(A-1.0)} dt$ 
C
C GAMMA IS EVALUATED FOR POSITIVE VALUES OF A AND NON-NEGATIVE VALUES
C OF X. A SLIGHT DETERIORATION OF 2 OR 3 DIGITS ACCURACY WILL OCCUR
C WHEN GAMMA IS VERY LARGE OR VERY SMALL, BECAUSE LOGARITHMIC VARIABLES
C ARE USED.
C
C***ROUTINES CALLED GAMIT,ALNGAM
    IF (A.LE.0.0) PRINT 970
    IF (X.LT.0.0) PRINT 970
970  FORMAT(' ***** GAMMA.....A MUST BE GT 0 AND X GE 0')
    GAMI=0.0
    IF (X.EQ.0.0) RETURN
C
C THE ONLY ERROR POSSIBLE IN THE EXPRESSION BELOW IS A FATAL OVERFLOW.
C
    FACTOR=EXP(ALNGAM(A)+A*21CG(X))
    GAMI=FACTOR*GAMIT(A,X)
    RETURN
    END

```

```

C
C
C

```

```

    FUNCTION ALNGAM(X)
C
C***REVISION OCTOBER 1, 1980
C***CATEGORY NO. B5F,B3
C***KEYWORD(S) LOGARITHM, GAMMA FUNCTION, SPECIAL FUNCTION
C***DATE WRITTEN JUNE 1977
C***AUTHOR FULLERTON W. (LASI)
C***PURPOSE
C COMPUTES THE LOG OF THE ABSOLUTE VALUE OF THE GAMMA FUNCTION.
C***DESCRIPTION
C JUNE 1977 EDITION. W. FULLERTON, C3, LOS ALAMOS SCIENTIFIC LAB.
C

```

```

C SQ2PIL = ALOG(SQRT(2.*PI)), SQPI2L = ALOG (SQRT(PI/2.))
C
C***ROUTINES CALLED  B9LGMC,GAMMA,B1MACH
  DATA SQ2PIL / 0.9189385332 0467274E0/
  DATA SQPI2L / 0.2257913526 4472743E0/
  DATA PI / 3.1415926535 8979324E0/
  DATA XMAX,DXREL /0.,0./
  IF (XMAX.NE.0.) GO TO 10
  XMAX=B1MACH(2)/ALOG (B1MACH(2))
  DXREL=SQRT(B1MACH(4))
10  Y=ABS(X)
  IF (Y.GT. 10.0) GO TO 20
C
C  ALOG (AES (GAMMA(X))) FOR  ABS(X).LE.10.0
C
  ALNGAM=ALOG(AES(GAMMA(X)))
  RETURN
C
C  ALOG (ABS (GAMMA(X))) FOR  ABS(X).GT. 10.0
C
20  IF (Y.GT. XMAX) PRINT 971
971  FORMAT(' ***** ALNGAM  ABS(X) CAUSES OVERFLOW')
  IF (X.GT.0.) ALNGAM=SQ2PIL+(X-0.5)*ALOG(X)-X+B9LGMC(Y)
  IF (X.GT.0.) RETURN
  SINPIY=ABS(SIN(PI*Y))
  IF (SINPIY.EQ.0.) PRINT 972
972  FORMAT(' ***** ALNGAM... X IS NEGATIVE')
  IF (ABS((X-AINT(X-0.5))/X).LT.DXREL) PRINT 973
973  FORMAT(' ***** ALNGAM...LT HALF PRECISION')
  ALNGAM=SQPI2L+(X-0.5)*ALOG(Y)-X-ALOG(SINPIY)-B9LGMC(Y)
  RETURN
  END
C
C
C
  FUNCTION GAMIT(A, X)
C***REVISION OCTOBER 1, 1980
C***CATEGORY NO.  B5F
C***KEYWORD(S)  TRICOMI-S, INCOMPLETE GAMMA FUNCTION,
C  GAMMA FUNCTION, SPECIAL FUNCTION
C***DATE WRITTEN  JULY 1977
C***AUTHOR  FULLERTON W. (LPSI)
C***PURPOSE
C  COMPUTES TRICOMI-S FORM OF THE INCOMPLETE GAMMA FUNCTION.
C***DESCRIPTION
C  JULY 1977 EDITION.  W. FULLERTON, C3, LOS ALAMOS SCIENTIFIC LAB.
C
C  EVALUATE TRICOMI-S INCOMPLETE GAMMA FUNCTION DEFINED BY
C
C  GAMIT = X**(-A)/GAMMA(A) * INTEGRAL T = 0 TO X OF EXP(-T) * T**(A-1.)
C
C  AND ANALYTIC CONTINUATION FOR A .LE. 0.0.  GAMMA(X) IS THE COMPLETE
C  GAMMA FUNCTION OF X.  GAMIT IS EVALUATED FOR ARBITRARY REAL VALUES OF
C  A AND FOR NON-NEGATIVE VALUES OF X (EVEN THOUGH GAMIT IS DEFINED FOR
C  X .LT. 0.0), EXCEPT THAT FOR X = 0 AND A .LE. 0.0, GAMIT IS INFINITE,
C  A FATAL ERROR.
C
C  A SLIGHT DETERIORATION OF 2 OR 3 DIGITS ACCURACY WILL OCCUR WHEN
C  GAMIT IS VERY LARGE OR VERY SMALL IN ABSOLUTE VALUE, BECAUSE LOG-
C  ARITHMIC VARIABLES ARE USED.  ALSO, IF THE PARAMETER A IS VERY CLOSE

```

C TO A NEGATIVE INIEGER (BUT NOT A NEGATIVE INTEGER), THERE IS A LOSS  
C OF ACCURACY, WHICH IS REPORTED IF THE RESULT IS LESS THAN HALF  
C MACHINE PRECISION.

C REP. -- W. GAUTSCHI, AN EVALUATION PROCEDURE FOR INCOMPLETE GAMMA  
C FUNCTIONS. ACM TRANS. MATH. SOFTWARE.

C\*\*\*ROUTINES CALLED R9LGIC,YECLR,ALNGAM,R9LGIT,R9GMIT,ALGAMS,GAML,  
C R1MACH

```

DATA ALNEPS, SQEPS, BCT / 3*0.0 /
IF (ALNEPS.NE.0.0) GO TO 10
ALNEPS=-ALOG (R1MACH(3))
SQEPS=SQRT (R1MACH(4))
BOT=ALOG (R1MACH(1))
10 IF (X.LI.0.0) PRINT 974
974 FORMAT (' ***** GAMIT...X IS NEGATIVE')
IF (X.NE.0.0) ALX=ALOG (X)
SGA=1.0
IF (A.NE.0.0) SGA=SIGN (1.0,A)
ALNTA=AINT (A+0.5*SGA)
AEPS=A-AINTA
IF (X.GT.0.0) GO TO 20
GAMIT=0.0
IF (AINTA.GT.0.0.OR.AEPS.NE.0.0) GAMIT=GAMB (A+1.0)
RETURN
20 IF (X.GT.1.0) GO TO 40
IF (A.GE. (-0.5).OR.AEPS.NE.0.0) CALL ALGAMS (A+1.0,ALGAP1,
1SGNGAM)
GAMIT=B9GMIT (A,X,ALGAP1,SGNGAM,ALX)
RETURN
40 IF (A.LI.X) GO TO 50
T=B9IGIT (A,X,ALNGAM (A+1.0))
GAMIT=EXP (T)
RETURN
50 ALNG=B9LGIC (A,X,ALX)

```

```

10 IF (ALNG.EQ.0) PRINT 974
974  FORMAT(' ***** GAMIT...I IS NEGATIVE')
    IF (X.NE.0.0) ALX=ALOG(X)
    SGA=1.0
    IF (A.NE.0.0) SGA=SIGN(1.C,A)
    AINTA=AINT(A+0.5*SGA)
    AEPS=A-AINTA
    IF (X.GT.0.0) GO TO 20
    GAMIT=0.0
    IF (AINTA.GT.0.0.OR.AEPS.NE.0.0) GAMIT=GAMR(A+1.0)
    RETURN
20  IF (X.GT.1.0) GO TO 40
    IF (A.GE.(-0.5).OR.AEPS.NE.0.0) CALL ALGAMS(A+1.0,ALGAP1,
1  SGNGAM)
    GAMIT=B9GMIT(A,X,ALGAP1,SGNGAM,ALX)
    RETURN
40  IF (A.LT.X) GO TO 50
    T=B9IGIT(A,X,ALNGAM(A+1.0))
    GAMIT=EXP(T)
    RETURN
50  ALNG=B9LGIC(A,X,ALX)

```

```

C
C EVALUATE GAMIT IN TERMS OF PLCG(GAMIC(A,X))

```

```

H=1.0
IF (AEPS.EQ.0.0.AND.AINTA.LE.0.0) GO TO 60
CALL ALGAMS(A+1.0,AIGAF1,SGNGAM)
T=ALOG (ABS (A) )+AING-AIGAF1
IF (T.GT.ALNEPS) GO TO 70
IF (T.GT. (-ALNEPS) ) H=1.0-SGA*SGNGAM*EXP (T)
IF (ABS (H) .GT. SLEPS) GO TO 60
PRINT 975
975 FORMAT (' ***** GAMIT... IT HALF PRECISION')
60 T=-A*ALX+ALOG (ABS (H) )
GAMIT=SIGN (EXP (T) ,H)
RETURN
70 T=T-A*ALX
GAMIT=-SGA*SGNGAM*EXP (T)
RETURN
END

```

```

60 T=-A*ALX+ALOG (ABS(H))
   GAMIT=SIGN (EXP (T),H)
   RETURN
70 T=T-A*ALX
   GAMIT=-SGA*SGNGAM*EXP (T)
   RETURN
   END

```

C  
C  
C

FUNCTION B9LGMC(X)

C  
C\*\*\*REVISION OCTOBER 1, 1980

```

C***CATEGORY NO. B5F
C***KEYWORD(S) CORRECTION FACTOR, LOG GAMMA, SPECIAL FUNCTION
C***DATE WRITTEN AUGUST 1977
C***AUTHOR FULLERTON W. (LASI)
C***PURPOSE
C COMPUTES THE LOG GAMMA CORRECTION FACTOR SO THAT
C  $\text{ALOG}(\text{GAMMA}(X)) = \text{ALOG}(\text{SQRT}(2*\text{PI})) + (X-.5)*\text{ALOG}(X) - X + \text{R9LGMC}(X)$ 
C***DESCRIPTION
C AUGUST 1977 EDITION. W. FULLERTON, C3, LOS ALAMOS SCIENTIFIC LAB.
C
C COMPUTE THE LOG GAMMA CORRECTION FACTOR FOR X .GE. 10.0 SO THAT
C  $\text{ALOG}(\text{GAMMA}(X)) = \text{ALOG}(\text{SQRT}(2*\text{PI})) + (X-.5)*\text{ALOG}(X) - X + \text{R9LGMC}(X)$ 
C
C SERIES FOR ALGM ON THE INTERVAL 0. TO 1.00000E-02
C WITH WEIGHTED ERROR 3.4CE-16
C LCG WEIGHTED ERROR 15.47
C SIGNIFICANT FIGURES REQUIRED 14.39
C DECIMAL PLACES REQUIRED 15.86
C
C
C

```

```

C***ROUTINES CALLED CSEVL, F1PACH, INITS
      DIMENSION ALGMC(6)
      DATA ALGMC( 1) / .166389480 45186E0 /
      DATA ALGMC( 2) / -.0000138494 817606E0 /
      DATA ALGMC( 3) / .0000000098 108256E0 /
      DATA ALGMC( 4) / -.0000000000 180912E0 /
      DATA ALGMC( 5) / .0000000000 000622E0 /
      DATA ALGMC( 6) / -.0000000000 000003E0 /
      DATA NALGM, XBIG, XMAX / 0, 2*0.0 /
      IF (NALGM.NE.0) GO TO 10
      NALGM=INITS(ALGMC,6,F1PACH(3))
      XBIG=1.0/SQRT(F1PACH(3))
      XMAX=EXP(AMIN1(ALOG(F1PACH(2)/12.0),-ALOG(12.0*F1PACH(1))))
10      IF (X.LT.10.0) PRINT 976
976      FORMAT(' ***** R9LGMC....X MUST BE GE 10')
      IF (X.GE.XMAX) GO TO 20
      R9LGMC=1.0/(12.0*X)
      IF (X.LT.XBIG) R9LGMC=CSEVL(2.0*(10./X)**2-1.,ALGMC,NALGM)/X
      RETURN
20      R9LGMC=0.0
      PRINT 977
977      FORMAT(' ***** R9LGMC....X TOO BIG, UNDERFLOW')
      RETURN
      END

```

```

C
C
C
      FUNCTION GAMR(X)
C***REVISION OCTOBER 1, 1980
C***CATEGORY NO. B5F
C***KEYWORD(S) RECIPROCAL GAMMA FUNCTION, GAMMA FUNCTION SPECIAL FUNCTION
C***DATE WRITTEN JULY 1977
C***AUTHOR FULLERTON W. (LASI)
C***PURPOSE COMPUTES THE RECIPROCAL OF THE GAMMA FUNCTION.
C***DESCRIPTION
C JULY 1977 EDITION. W. FULLERTON, C3, LOS ALAMOS SCIENTIFIC LAB.
C THIS ROUTINE, NOT GAMMA(X), SHOULD BE THE FUNDAMENTAL ONE.
C
C***ROUTINES CALLED ALGAMS, XERCLR, GAMMA, XSETP, XGETF
      GAMR=0.0

```

```

      IF (X.LE.0.0.AND.AINT(X).EQ.X) RETURN
      IF (ABS(X).GT.10.0) GO TO 10
      GAMB=1.0/GAMMA(X)
      RETURN
10    CALL ALGAMS(X,ALNGX,SGNGX)
      GAMR=SGNGX*EXP(-ALNGX)
      RETURN
      END

C
C
C
      SUBROUTINE ALGAMS(X,AIGAM,SGNGAM)
C***REVISION OCTOBER 1, 1980
C***CATEGORY NO. B5F
C***KEYWORD(S) LOGARITHM,GAMMA FUNCTION,SPECIAL FUNCTION
C***DATE WRITTEN JULY 1977
C***AUTHOR FULLERTON W. (LASI)
C***PURPOSE
C COMPUTES LCG (ABS (GAMMA(X))) .
C***DESCRIPTION
C JULY 1977 EDITION. W. FULLERTON, C3, LOS ALAMOS SCIENTIFIC LAB.
C EVALUATE LCG ABS (GAMMA(X)) AND RETURN THE SIGN OF GAMMA(X) IN SGNGAM
C SGNGAM IS EITHER +1.0 OR -1.0.
C***ROUTINES CALLED ALNGAM
      ALGAM=ALNGAM(X)
      SGNGAM=1.0
      IF (X.GT.0.0) RETURN
      INT=AMOD(-AINT(X),2.0)+0.1
      IF (INT.EQ.0) SGNGAM=-1.0
      RETURN
      END

C
C
C
      FUNCTION R9GMIT(A,X,AIGAP1,SGNGAM,ALX)
C***REVISION OCTOBER 1, 1980
C***CATEGORY NO. B5F
C***KEYWORD(S) TRICOMI-S,INCOMPLETE GAMMA FUNCTION,GAMMA FUNCTION,
C SPECIAL FUNCTION,SMALL X
C***DATE WRITTEN JULY 1977
C***AUTHOR FULLERTON W. (LASI)
C***PURPOSE
C COMPUTES TRICOMI-S INCOMPLETE GAMMA FUNCTION FOR SMALL X.
C***DESCRIPTION
C JULY 1977 EDITION. W. FULLERTON, C3, LOS ALAMOS SCIENTIFIC LAB.
C COMPUTE TRICOMI-S INCOMPLETE GAMMA FUNCTION FOR SMALL X.
C***ROUTINES CALLED ALNGAM,SLMACH
      DATA EPS,BOT /2*0.0/
      IF (EPS.EQ.0.0) EPS=0.5*R1MACH(3)
      IF (BOT.EQ.0.0) BOT=ALCG(1MACH(1))
      IF (X.LE.0.0) PRINT 978
978  FORMAT(' ***** R9GMIT....X MUST BE GT 0. ')
      MA=A+0.5
      IF (A.LT.0.0) MA=A-0.5
      AEPS=A-FLOAT(PA)
      AE=A
      IF (A.LT.(-0.5)) AE=AEPS
      T=1.0
      TE=AE
      S=T

```



```

DO 20 K=1,200
FK=K
TE=-X*TE/FK
T=TE/(AE+FK)
S=S+T
IF (ABS(T).LT.EPS*ABS(S))GC TO 30
20 CONTINUE
PRINT 979
979 FORMAT(' ***** R9GMIT....NO CONVERGENCE IN 200 TERMS')
30 IF (A.GE.(-0.5))ALGS=-ALGAF1+ALOG(S)
IF (A.GE.(-0.5))GC TO 60
ALGS=-ALNGAM(1.0+AEPS)+ALOG(S)
S=1.0
M=-MA-1
IF (M.EQ.0) GO TO 50
T=1.0
DO 40 K=1,M
T=X*T/(AEPS-FLCAT(M+1-K))
S=S+T
IF (ABS(T).LT.EPS*ABS(S))GC TO 50
40 CONTINUE
50 R9GMIT=0.0
ALGS=-FLCAT(MA)*ALOG(X)+ALGS
IF (S.EQ.0.0.OR.AEPS.EQ.0.0)GO TO 60
SGNG2=SGNGAM*SIGN(1.0,S)
ALG2=-X-ALGAP1+ALOG(AIS(S))
IF (ALG2.GT.307) R9GMIT = SGNG2*EXP(ALG2)
IF (ALGS.GT.307) R9GMIT = R9GMIT + EXP(ALGS)
RETURN
60 R9GMIT=EXP(ALGS)
RETURN
END

```

C  
C  
C

```

FUNCTION R9LGIT(A,X,ALGAP1)
C***REVISION OCTOBER 1, 1980
C***CATEGORY NO. B5F
C***KEYWORDS(S) TRICOMI-S, INCOMPLETE GAMMA FUNCTION, LOGARITHM,
C PERRON-S CONTINUED FRACTION, SPECIAL FUNCTION
C***DATE WRITTEN JULY 1977
C***AUTHOR FULLERTON W. (LASI)
C***PURPOSE
C COMPUTES THE LOG OF TRICOMI-S INCOMPLETE GAMMA FUNCTION WITH
C PERRON-S CONTINUED FRACTION FOR LARGE X AND FOR A .GE. X.
C***DESCRIPTION
C JULY 1977 EDITION. W. FULLERTON, C3, LOS ALAMOS SCIENTIFIC LAB.
C
C COMPUTE THE LOG OF TRICOMI-S INCOMPLETE GAMMA FUNCTION WITH PERRON-S
C CONTINUED FRACTION FOR LARGE X AND FOR A .GE. X.
C***ROUTINES CALLED R1MACH
DATA EPS, SQEPS / 2*0.0 /
IF (EPS.EQ.0.0) EPS = 0.5*R1MACH(3)
IF (SQEPS.EQ.0.0) SQEPS = SQRT(R1MACH(4))
IF (X.LE.0.0.OR.A.LT.X)PRINT *80
980 FORMAT(' ***** R9LGIT....X MUST BE GT 0. LE A')
AX=A+X
A1X=AX+1.0
B=C.0
P=1.0

```

```

      S=P
      DO 20 K=1,200
      FK=K
      T=(A+FK)*X*(1.0+R)
      R=1/((A1+FK)*(A1X+FK)-T)
      P=R*P
      S=S+P
      IF (ABS(P).LT.EPS*S) GO TO 30
20    CONTINUE
      PRINT 981
981   FORMAT(' ***** R9LGIT.... NO CONVERGENCE IN 200 TERMS')
30    HSTAR=1.0-1*S/A1X
      IF (HSTAR.LT.S*EPS) PRINT 982
982   FORMAT(' ***** R9LGIT.... LT HALF PRECISION')
      R9LGIT=-X-ALGAP1-ALOG(HSTAR)
      RETURN
      END

C
C
C
      FUNCTION R9LGIC(A,X,A1X)
C***REVISION OCTOBER 1, 1980
C***CATEGORY NO. B5F
C***KEYWORD(S) LOGARITHM, COMPLEMENTARY INCOMPLETE GAMMA FUNCTION,
C SPECIAL FUNCTION, LARGE X
C***DATE WRITTEN JULY 1977
C***AUTHOR FULLERTON W. (LPSI)
C***PURPOSE
C COMPUTES THE LOG COMPLEMENTARY INCOMPLETE GAMMA FUNCTION FOR LARGE
C X AND FOR A .LE. X.
C***DESCRIPTION
C JULY 1977 EDITION. W. FULLERTON, C3, LOS ALAMOS SCIENTIFIC LAB.
C
C COMPUTE THE LOG COMPLEMENTARY INCOMPLETE GAMMA FUNCTION FOR LARGE X
C AND FOR A .LE. X.
C***ROUTINES CALLED R1MACH
      DATA EPS /0.0/
      IF (EPS.EQ.0.0) EPS=0.5*R1MACH(3)
      XPA=X+1.0-A
      XMA=X-1.0-A
      R=0.0
      P=1.0
      S=P
      DO 10 K=1,200
      FK=K
      T=FK*(A-FK)*(1.0+R)
      R=-T/((XMA+2.0*FK)*(XPA+2.0*FK)+T)
      P=R*P
      S=S+P
      IF (ABS(P).LT.EPS*S) GO TO 20
10    CONTINUE
      PRINT 983
983   FORMAT(' ***** R9LGIC.... NO CONVERGENCE IN 200 TERMS')
20    R9LGIC=A*A1X-X+ALOG(S/XPA)
      RETURN
      END

C
C
C
      FUNCTION INITS(C3,MCS,ETA)

```

```

C***REVISION OCTOBER 1, 1980
C***CATEGORY NO. B5R
C***KEYWORD(S) ORTHOGONAL SERIES, INITIALIZE, SPECIAL FUNCTION
C***DATE WRITTEN APRIL 1977
C***AUTHOR FULLERTON W. (LASI)
C***PURPOSE
C INITIALIZES AN ORTHOGONAL SERIES SO THAT IT DEFINES THE NUMBER
C OF TERMS TO CARRY IN THE SERIES TO MEET A SPECIFIED ERROR.
C***DESCRIPTION
C APRIL 1977 VERSION. W. FULLERTON, C3, LOS ALAMOS SCIENTIFIC LAB.
C
C INITIALIZE THE ORTHOGONAL SERIES SO THAT INITS IS THE NUMBER OF TERMS
C NEEDED TO INSURE THE ERROR IS NO LARGER THAN ETA. ORDINARILY, ETA
C WILL BE CHOSEN TO BE ONE-TENTH MACHINE PRECISION.
C
C INPUT ARGUMENTS --
C OS      ARRAY OF NOS COEFFICIENTS IN AN ORTHOGONAL SERIES.
C NOS      NUMBER OF COEFFICIENTS IN OS.
C ETA      REQUESTED ACCURACY OF SERIES.
C

```

```

      DIMENSION OS(NOS)
      IF (NOS.LT.1) PRINT 984
984  FORMAT(' ***** INITS.....# OF COEFF LT 1')
      ERR=0.
      DO 10 II=1,NOS
      I=NOS+1-II
      ERR=ERR+ABS(OS(I))
      IF (ERR.GT.ETA) GO TO 20
10   CONTINUE
20   IF (I.EQ.NOS) PRINT 985
985  FORMAT(' ***** INITS.....ETA MAY BE TOO SMALL')
      INITS=I
      RETURN
      END

```

```

C
C
C

```

```

      FUNCTION CSEVL(X,CS,N)
C***REVISION OCTOBER 1, 1980
C***CATEGORY NO. B5R
C***KEYWORD(S) CHEBYSHEV, SPECIAL FUNCTION, FNLIB
C***DATE WRITTEN APRIL, 1977
C***AUTHOR FULLERTON W. (LASI)
C***PURPOSE
C EVALUATE THE N-TERM CHEBYSHEV SERIES CS AT X.
C***DESCRIPTION
C APRIL 1977 VERSION. W. FULLERTON, C-3, LOS ALAMOS SCIENTIFIC LABORATORY
C INSTALLED ON THE VAX BY DOLORES MONTANO, C-3, 5/80.
C
C EVALUATE THE N-TERM CHEBYSHEV SERIES CS AT X. ADAPTED FROM
C R BROUCKE, ALGORITHM 446, C.A.C.M., 16, 254 (1973). ALSO SEE FOX
C AND PARKER, CHEBYSHEV POLYS IN NUMERICAL ANALYSIS, OXFORD PRESS, P. 56.
C
C INPUT ARGUMENTS --
C X      VALUE AT WHICH THE SERIES IS TO BE EVALUATED.
C CS     ARRAY OF N TERMS OF A CHEBYSHEV SERIES. IN EVAL-
C        UATING CS, ONLY HALF THE FIRST COEF IS SUMMED.
C N      NUMBER OF TERMS IN ARRAY CS.
C

```

```

      DIMENSION CS(1)

```

```

IF(N.LT.1)PRINT 986
986  FORMAT(' ***** CSEVL.....# OF TERMS LE 0. ')
IF(N.GT.1000)PRINT 987
987  FORMAT(' ***** CSEVL.....# OF TERMS GT 1000 ')
IF(X.LT.-1.0.OR.X.GT.1.0)PRINT 988
988  FORMAT(' ***** CSEVL.....X OUTSIDE (-1,+1) ')
      B1=0.
      B0=0.
      TWOX=2.*X
      DO 10 I=1,N
      B2=B1
      B1=B0
      NI=N+1-I
      B0=TWOX*B1-B2+CS(NI)
10    CONTINUE
      CSEVL=0.5*(B0-B2)
      RETURN
      END

C
C
C
C      REAL FUNCTION R1MACH(I)
C
C      SINGLE-PRECISION MACHINE CONSTANTS
C      R1MACH(1) = B**(EMIN-1), THE SMALLEST POSITIVE MAGNITUDE.
C      R1MACH(2) = B**EMAX*(1 - B**(-T)), THE LARGEST MAGNITUDE.
C      R1MACH(3) = B**(-T), THE SMALLEST RELATIVE SPACING.
C      R1MACH(4) = B**(1-T), THE LARGEST RELATIVE SPACING.
C      R1MACH(5) = LCG10(B)
C
C      REAL RMACH(5)
C
C      MACHINE CONSTANTS FOR THE IBM 3033 AT CLEMSON UNIVERSITY.
C
C      DATA RMACH(1) / 20010C0C0 /
C      DATA RMACH(2) / 27FFFFFFFF /
C      DATA RMACH(3) / 23B10CCCC /
C      DATA RMACH(4) / 23C1000C0 /
C      DATA RMACH(5) / 241134413 /
C      R1MACH = RMACH(I)
C      RETURN
C      END
C
C
C
C      INTEGER FUNCTION I1MACH(I)
C
C      I/O UNIT NUMBERS.
C      I1MACH( 1) = THE STANDARD INPUT UNIT.
C      I1MACH( 2) = THE STANDARD OUTPUT UNIT.
C      I1MACH( 3) = THE STANDARD PUNCH UNIT.
C      I1MACH( 4) = THE STANDARD ERROR MESSAGE UNIT.
C
C      WORDS.
C      I1MACH( 5) = THE NUMBER OF BITS PER INTEGER STORAGE UNIT.
C      I1MACH( 6) = THE NUMBER OF CHARACTERS PER INTEGER STORAGE UNIT.
C
C      INTEGERS.
C      ASSUME INTEGERS ARE REPRESENTED IN THE S-DIGIT, BASE-A FORM
C      SIGN ( X(S-1)*A**(S-1) + ... + X(1)*A + X(0) )

```

```

C      WHERE 0 .LE. X(I) .LT. A FOR I=0,...,S-1.
C      IMACH( 7) = A, THE BASE.
C      IMACH( 8) = S, THE NUMBER OF BASE-A DIGITS.
C      IMACH( 9) = A**S - 1, THE LARGEST MAGNITUDE.
C
C      FLOATING-POINT NUMBERS.
C      ASSUME FLOATING-POINT NUMBERS ARE REPRESENTED IN THE T-DIGIT,
C      BASE-B FORM
C          SIGN (B**E)*( (X(1)/B) + ... + (X(T)/B**T) )
C          WHERE 0 .LE. X(I) .LT. B FOR I=1,...,T,
C          0 .LT. X(1), AND EMIN .LE. E .LE. EMAX.
C      IMACH(10) = B, THE BASE.
C
C      SINGLE-PRECISION
C      IMACH(11) = T, THE NUMBER OF BASE-B DIGITS.
C      IMACH(12) = EMIN, THE SMALLEST EXPONENT E.
C      IMACH(13) = EMAX, THE LARGEST EXPONENT E.
C
C      DOUBLE-PRECISION
C      IMACH(14) = T, THE NUMBER OF BASE-B DIGITS.
C      IMACH(15) = EMIN, THE SMALLEST EXPONENT E.
C      IMACH(16) = EMAX, THE LARGEST EXPONENT E.
C
C      INTEGER IMACH(16), OUTPUT
C      EQUIVALENCE (IMACH(4),OUTPUT)
C
C      MACHINE CONSTANTS FOR THE IBM 3033 AT CLEMSON UNIVERSITY.
C
C      DATA IMACH( 1) / 5 /
C      DATA IMACH( 2) / 6 /
C      DATA IMACH( 3) / 2 /
C      DATA IMACH( 4) / 3 /
C      DATA IMACH( 5) / 32 /
C      DATA IMACH( 6) / 4 /
C      DATA IMACH( 7) / 2 /
C      DATA IMACH( 8) / 31 /
C      DATA IMACH( 9) / 27FFFFFF /
C      DATA IMACH(10) / 16 /
C      DATA IMACH(11) / 6 /
C      DATA IMACH(12) / -64 /
C      DATA IMACH(13) / 63 /
C      DATA IMACH(14) / 14 /
C      DATA IMACH(15) / -64 /
C      DATA IMACH(16) / 63 /
C      IF (I.LT.1.OR.I.GT.16) GO TO 10
C      IMACH=IMACH(I)
C      RETURN
10  WRITE(OUTPUT,9000)
9000 FORMAT(' ERROR      1 IN IMACH - I OUT OF BOUNDS')
C      RETURN
C      END
//GO.F103P001 DD DSN=QMGUI1.OUTPUT,DISP=SHR
//GC.SYSIN DE *
236 5.079 3871 4.138 .003315 .002408 5.507 3.602 10
17
1.19548 28. C. 0. 7. 23.000 27. 1
0.87208 29. C. 0. 7. 23.000 28. 1
1.36017 30. C. 0. 7. 23.000 29. 1
1.26328 31. C. 0. 7. 22.500 30. 1
1.00719 32. C. 0. 7. 22.000 31. 1

```

0.89211	33.	C.	0.	7.	22.000	32. 1
1.27575	34.	C.	0.	7.	22.000	33. 1
1.14815	35.	C.	0.	7.	21.500	34. 1
1.15231	36.	C.	0.	7.	21.000	35. 1
1.24936	37.	C.	0.	7.	20.500	36. 1
1.02576	38.	C.	0.	7.	20.000	37. 1
0.90939	39.	C.	0.	7.	43.500	38. 1
0.58287	40.	C.	0.	7.	43.000	39. 1
0.45301	41.	C.	0.	7.	42.500	41. 1
0.37731	42.	C.	0.	7.	41.500	42. 1
0.21011	43.	C.	0.	7.	40.000	43. 1
0.11133	44.	C.	0.	7.	38.000	44. 1

31.5  
35.5  
37.5  
39.5  
41.5  
43.5  
44.5  
34

0.23904	28.	7.	0.	23.	23.000	27. 2
0.26792	29.	7.	0.	23.	23.000	28. 2
0.28405	30.	7.	0.	23.	23.000	29. 2
0.28837	31.	7.	0.	23.	22.500	30. 2
0.33922	32.	7.	0.	23.	22.000	31. 2
0.37202	33.	7.	0.	23.	22.000	32. 2
0.61544	34.	7.	0.	23.	22.000	33. 2
0.64844	35.	7.	0.	23.	21.500	34. 2
0.88443	36.	7.	0.	23.	21.000	35. 2
1.30476	37.	7.	0.	23.	20.500	36. 2
1.90464	38.	7.	0.	23.	20.000	37. 2
1.96346	39.	7.	0.	23.	43.500	38. 2
1.94893	40.	7.	0.	23.	43.000	39. 2
2.37299	41.	7.	0.	23.	42.500	40. 2
2.21135	42.	7.	0.	23.	41.500	41. 2
1.90135	43.	7.	0.	23.	40.000	42. 2
2.00296	44.	7.	0.	23.	38.000	43. 2
2.02364	45.	7.	0.	23.	108.000	44. 2
1.89796	46.	7.	0.	23.	105.500	45. 2
1.76414	47.	7.	0.	23.	102.500	46. 2
1.82274	48.	7.	0.	23.	101.000	47. 2
1.58376	49.	7.	0.	23.	101.000	48. 2
1.49733	50.	7.	0.	23.	101.000	49. 2
1.39265	51.	7.	0.	23.	101.000	50. 2
1.36656	52.	7.	0.	23.	101.000	51. 2
1.29265	53.	7.	0.	23.	99.500	52. 2
0.75652	54.	7.	0.	23.	98.000	53. 2
0.36923	55.	7.	0.	23.	97.500	54. 2
0.11657	56.	7.	0.	23.	95.500	55. 2
0.09666	57.	7.	0.	23.	94.000	56. 2
0.06745	58.	7.	0.	23.	94.000	57. 2
0.03575	59.	7.	0.	23.	93.500	58. 2
0.04195	60.	7.	0.	23.	165.000	59. 2
0.02468	61.	7.	0.	23.	164.500	60. 2

42.50  
43.50  
44.50  
45.33  
45.67  
46.25

46.50  
46.75  
47.25  
47.50  
47.75  
53.25  
53.50  
53.75  
57.50  
55.50  
30

0.01967	39.	23.	38.	47.	43.500	38. 3
0.10990	40.	23.	38.	47.	43.000	39. 3
0.42763	41.	23.	38.	47.	42.500	40. 3
0.51955	42.	23.	38.	47.	41.500	41. 3
0.61842	43.	23.	38.	47.	40.000	42. 3
0.77169	44.	23.	38.	47.	38.000	43. 3
0.96280	45.	23.	38.	47.	108.000	44. 3
1.05265	46.	23.	38.	47.	105.500	45. 3
1.18733	47.	23.	38.	47.	102.500	46. 3
1.58118	48.	23.	38.	47.	101.000	47. 3
1.80794	49.	23.	38.	47.	101.000	48. 3
2.22878	50.	23.	38.	47.	101.000	49. 3
2.35663	51.	23.	38.	47.	101.000	50. 3
2.71505	52.	23.	38.	47.	101.000	51. 3
3.47529	53.	23.	38.	47.	99.500	52. 3
2.59432	54.	23.	38.	47.	98.000	53. 3
2.91105	55.	23.	38.	47.	97.500	54. 3
2.70636	56.	23.	38.	47.	95.500	55. 3
2.11521	57.	23.	38.	47.	94.000	56. 3
1.90967	58.	23.	38.	47.	94.000	57. 3
1.36859	59.	23.	38.	47.	93.500	58. 3
1.42259	60.	23.	38.	47.	165.000	59. 3
1.45556	61.	23.	38.	47.	164.500	60. 3
1.12204	62.	23.	38.	47.	163.500	61. 3
0.70945	63.	23.	38.	47.	162.500	62. 3
0.23030	64.	23.	38.	47.	161.000	63. 3
0.17782	65.	23.	38.	47.	156.500	64. 3
0.07716	66.	23.	38.	47.	150.500	65. 3
0.03211	67.	23.	38.	47.	142.500	66. 3
0.0000	68.	23.	38.	47.	131.500	67. 3

56.25  
56.50  
56.75  
61.50  
62.50  
63.50  
64.33  
64.67  
65.13  
65.25  
65.38  
65.50  
65.63  
65.75  
65.88  
66.17  
66.33  
66.50  
66.66

100.33  
100.44  
100.56  
100.67  
100.78  
100.89  
101.11  
101.22  
101.33  
101.44  
101.56  
101.67  
101.78  
101.89  
102.10  
102.20  
102.30  
102.40  
102.50  
102.60  
102.70  
102.80  
102.90  
103.11  
103.22  
103.33  
103.44  
103.56  
103.67  
103.78  
103.89  
104.10  
104.20  
104.30  
104.40  
104.50  
104.60  
104.70  
104.80  
104.90  
105.10  
105.20  
105.30  
105.40  
105.50  
105.60  
105.70  
105.80  
105.90  
106.11  
106.22  
106.33  
106.44  
106.55  
106.67  
106.78  
106.89  
107.11  
107.22  
107.33



3.05223	95.	341.	82.	464.	534.000	94. 9
3.07767	96.	341.	82.	464.	525.000	95. 9
3.74317	97.	341.	82.	464.	513.500	96. 9
2.72778	98.	341.	82.	464.	962.000	97. 9
2.51151	99.	341.	82.	464.	945.500	98. 9
3.05881	100.	341.	82.	464.	925.000	99. 9
2.11725	101.	341.	82.	464.	901.500	100. 9
1.71578	102.	341.	82.	464.	874.000	101. 9
1.87150	103.	341.	82.	464.	841.000	102. 9
1.34397	104.	341.	82.	464.	806.000	103. 9
1.10247	105.	341.	82.	464.	771.500	104. 9
0.73111	106.	341.	82.	464.	736.000	105. 9
0.45439	107.	341.	82.	464.	828.500	106. 9
0.38147	108.	341.	82.	464.	1170.500	107. 9
0.64337	109.	341.	82.	464.	1143.000	108. 9
0.14513	110.	341.	82.	464.	1109.000	109. 9

94.17  
 94.33  
 94.50  
 94.67  
 94.83  
 95.11  
 95.22  
 95.33  
 95.44  
 95.56  
 95.67  
 95.78  
 95.89  
 96.11  
 96.22  
 96.33  
 96.44  
 96.56  
 96.67  
 96.78  
 96.89  
 97.11  
 97.22  
 97.33  
 97.44  
 97.56  
 97.67  
 97.78  
 97.89  
 98.17  
 98.33  
 98.50  
 98.67  
 98.83  
 99.11  
 99.22  
 99.33  
 99.44  
 99.56  
 99.67  
 99.78  
 99.89  
 100.11  
 100.22

93.40  
93.47  
93.53  
93.60  
93.67  
93.73  
93.80  
93.87  
93.93  
94.14  
94.29  
94.43  
94.57  
94.71  
94.86

8

0.06254	84.	338.	83.	339.	575.500	83. 7
0.13461	85.	338.	83.	339.	560.500	84. 7
0.09029	86.	338.	83.	339.	547.000	85. 7
0.08536	87.	338.	83.	339.	536.000	86. 7
0.08822	88.	338.	83.	339.	526.500	87. 7
0.09829	89.	338.	83.	339.	516.500	88. 7
0.23207	90.	338.	83.	339.	505.500	89. 7
0.04995	91.	338.	83.	339.	497.000	90. 7

91.50  
19

0.00135	78.	339.	77.	341.	185.500	77. 8
0.00151	79.	339.	77.	341.	176.500	78. 8
0.00170	80.	339.	77.	341.	164.500	79. 8
0.00107	81.	339.	77.	341.	151.000	80. 8
0.00112	82.	339.	77.	341.	141.500	81. 8
0.02237	83.	339.	77.	341.	255.500	82. 8
0.24645	84.	339.	77.	341.	175.500	83. 8
0.11348	85.	339.	77.	341.	560.500	84. 8
0.14740	86.	339.	77.	341.	547.000	85. 8
0.13638	87.	339.	77.	341.	536.000	86. 8
0.12935	88.	339.	77.	341.	526.500	87. 8
0.19003	89.	339.	77.	341.	516.500	88. 8
0.03224	90.	339.	77.	341.	505.500	89. 8
0.01442	91.	339.	77.	341.	497.000	90. 8
0.02303	92.	339.	77.	341.	482.000	91. 8
0.01145	93.	339.	77.	341.	558.000	92. 8
0.00754	94.	339.	77.	341.	544.500	93. 8
0.00213	95.	339.	77.	341.	534.000	94. 8
0.00255	96.	339.	77.	341.	525.000	95. 8

94.50  
96.50  
28

0.02944	83.	341.	82.	464.	255.500	82. 9
0.80573	84.	341.	82.	464.	575.500	83. 9
1.45618	85.	341.	82.	464.	560.500	84. 9
1.30307	86.	341.	82.	464.	547.000	85. 9
1.14949	87.	341.	82.	464.	536.000	86. 9
1.71016	88.	341.	82.	464.	526.500	87. 9
2.93737	89.	341.	82.	464.	516.500	88. 9
2.13736	90.	341.	82.	464.	505.500	89. 9
2.83715	91.	341.	82.	464.	497.000	90. 9
3.91784	92.	341.	82.	464.	482.000	91. 9
2.66468	93.	341.	82.	464.	558.000	92. 9
3.80929	94.	341.	82.	464.	544.500	93. 9

87.91  
88.10  
88.20  
88.30  
88.40  
88.50  
88.60  
88.70  
88.80  
88.90  
89.08  
89.17  
89.25  
89.33  
89.42  
89.50  
89.58  
89.67  
89.75  
89.83  
89.92  
90.08  
90.17  
90.25  
90.33  
90.42  
90.50  
90.58  
90.67  
90.75  
90.83  
90.92  
91.08  
91.17  
91.25  
91.33  
91.42  
91.50  
91.58  
91.67  
91.75  
91.83  
91.92  
92.08  
92.15  
92.23  
92.31  
92.38  
92.46  
92.54  
92.62  
92.69  
92.77  
92.85  
92.92  
93.07  
93.13  
93.20  
93.27  
93.33

83.10  
83.20  
83.30  
83.40  
83.50  
83.60  
83.70  
83.80  
83.90  
84.06  
84.13  
84.19  
84.25  
84.31  
84.38  
84.44  
84.50  
84.56  
84.63  
84.69  
84.75  
84.82  
84.88  
84.94  
85.06  
85.13  
85.19  
85.25  
85.31  
85.38  
85.44  
85.50  
85.56  
85.63  
85.69  
85.75  
85.82  
85.88  
85.94  
86.08  
86.15  
86.23  
86.31  
86.39  
86.46  
86.54  
86.62  
86.69  
86.77  
86.85  
86.92  
87.09  
87.18  
87.27  
87.36  
87.45  
87.55  
87.64  
87.73  
87.82

80.18  
80.24  
80.29  
80.35  
80.41  
80.47  
80.53  
80.59  
80.65  
80.71  
80.76  
80.82  
80.88  
80.94  
81.11  
81.22  
81.33  
81.44  
81.55  
81.67  
81.78  
81.89  
25

0.03193	70.	191.	69.	338.	229.000	69. 6
0.34971	71.	191.	69.	338.	219.000	70. 6
0.90940	72.	191.	69.	338.	211.000	71. 6
1.76691	73.	191.	69.	338.	205.000	72. 6
2.72692	74.	191.	69.	338.	199.000	73. 6
3.85694	75.	191.	69.	338.	191.500	74. 6
5.12589	76.	191.	69.	338.	180.500	75. 6
6.94414	77.	191.	69.	338.	167.000	76. 6
6.85761	78.	191.	69.	338.	185.500	77. 6
6.11974	79.	111.	69.	338.	176.500	78. 6
7.26889	80.	191.	69.	338.	164.500	79. 6
5.21449	81.	191.	69.	338.	151.000	80. 6
5.15660	82.	191.	69.	338.	141.500	81. 6
6.32066	83.	191.	69.	338.	255.500	82. 6
11.42129	84.	191.	69.	338.	275.500	83. 6
5.83803	85.	191.	69.	338.	560.500	84. 6
6.37578	86.	191.	69.	338.	547.000	85. 6
4.92702	87.	191.	69.	338.	536.000	86. 6
4.31611	88.	191.	69.	338.	526.500	87. 6
5.97020	89.	191.	69.	338.	516.500	88. 6
1.20556	90.	191.	69.	338.	505.500	89. 6
0.43470	91.	191.	69.	338.	497.000	90. 6
0.00000	92.	191.	69.	338.	482.000	91. 6
0.39775	93.	191.	69.	338.	558.000	92. 6
0.36704	94.	191.	69.	338.	544.500	93. 6

80.50  
81.33  
81.67  
82.10  
82.20  
82.30  
82.40  
82.50  
82.60  
82.70  
82.80  
82.90

6.07048	72.	119.	59.	191.	211.000	71. 5
5.99359	73.	119.	59.	191.	205.000	72. 5
5.38045	74.	119.	59.	191.	199.000	73. 5
5.28531	75.	119.	59.	191.	191.500	74. 5
3.12728	76.	119.	59.	191.	180.500	75. 5
1.72110	77.	119.	60.	191.	167.000	76. 5
0.94430	78.	119.	61.	191.	185.500	77. 5
0.39982	79.	119.	62.	191.	176.500	78. 5
0.17868	80.	119.	63.	191.	164.500	79. 5
0.04702	81.	119.	64.	191.	151.000	80. 5

75.25  
 75.50  
 75.75  
 76.07  
 76.14  
 76.21  
 76.29  
 76.36  
 76.43  
 76.50  
 76.57  
 76.64  
 76.71  
 76.79  
 76.86  
 76.93  
 77.07  
 77.13  
 77.20  
 77.27  
 77.33  
 77.40  
 77.47  
 77.53  
 77.60  
 77.67  
 77.73  
 77.80  
 77.87  
 77.93  
 78.08  
 78.17  
 78.25  
 78.33  
 78.42  
 78.50  
 78.58  
 78.67  
 78.75  
 78.83  
 78.92  
 79.12  
 79.25  
 79.37  
 79.50  
 79.62  
 79.75  
 79.87  
 80.06  
 80.12

69.73  
 69.82  
 69.91  
 70.09  
 70.18  
 70.27  
 70.36  
 70.45  
 70.55  
 70.64  
 70.73  
 70.82  
 70.91  
 71.09  
 71.18  
 71.27  
 71.36  
 71.45  
 71.55  
 71.64  
 71.73  
 71.82  
 71.91  
 72.14  
 72.29  
 72.43  
 72.57  
 72.71  
 72.86  
 73.14  
 73.29  
 73.43  
 73.57  
 73.71  
 73.86  
 74.14  
 74.29  
 74.43  
 74.57  
 74.71  
 74.86  
 75.14  
 75.29  
 75.43  
 75.57  
 75.71  
 75.86

22

0.09440	60.	119.	59.	191.	165.000	59. 5
0.21798	61.	119.	59.	191.	164.500	60. 5
0.50545	62.	119.	59.	191.	163.500	61. 5
0.72456	63.	119.	59.	191.	162.500	62. 5
1.01639	64.	119.	59.	191.	161.000	63. 5
1.61539	65.	119.	59.	191.	156.500	64. 5
1.86886	66.	119.	59.	191.	150.500	65. 5
2.41520	67.	119.	59.	191.	142.500	66. 5
2.61123	68.	119.	59.	191.	131.500	67. 5
2.96616	69.	119.	59.	191.	121.000	68. 5
4.75018	70.	119.	59.	191.	229.000	69. 5
5.71782	71.	119.	59.	191.	219.000	70. 5

65.83  
67.25  
67.50  
67.75  
69.50  
29

0.00996	47.	47.	46.	119.	102.500	46.	4
0.02965	48.	47.	46.	119.	101.000	47.	4
0.08344	49.	47.	46.	119.	101.000	48.	4
0.30266	50.	47.	46.	119.	101.000	49.	4
0.63845	51.	47.	46.	119.	101.000	50.	4
1.00236	52.	47.	46.	119.	101.000	51.	4
1.40825	53.	47.	46.	119.	99.500	52.	4
1.62892	54.	47.	46.	119.	98.000	53.	4
2.03716	55.	47.	46.	119.	97.500	54.	4
3.17816	56.	47.	46.	119.	95.500	55.	4
3.62862	57.	47.	46.	119.	94.000	56.	4
4.72402	58.	47.	46.	119.	94.000	57.	4
4.78499	59.	47.	46.	119.	93.500	58.	4
4.86147	60.	47.	46.	119.	165.500	59.	4
5.34870	61.	47.	46.	119.	164.500	60.	4
5.96560	62.	47.	46.	119.	163.500	61.	4
6.34085	63.	47.	46.	119.	162.500	62.	4
5.85055	64.	47.	46.	119.	161.500	63.	4
6.24051	65.	47.	46.	119.	156.500	64.	4
4.91988	66.	47.	46.	119.	150.500	65.	4
4.38904	67.	47.	46.	119.	142.500	66.	4
3.07483	68.	47.	46.	119.	131.500	67.	4
2.07644	69.	47.	46.	119.	121.000	68.	4
1.87063	70.	47.	46.	119.	229.000	69.	4
0.99034	71.	47.	46.	119.	219.000	70.	4
0.80919	72.	47.	46.	119.	211.000	71.	4
0.31633	73.	47.	46.	119.	205.000	72.	4
0.08406	74.	47.	46.	119.	199.000	73.	4
0.05670	75.	47.	46.	119.	191.500	74.	4

67.11  
67.22  
67.33  
67.44  
67.56  
67.67  
67.78  
67.89  
68.09  
68.18  
68.27  
68.36  
68.45  
68.55  
68.64  
68.73  
68.82  
68.91  
69.09  
69.18  
69.27  
69.36  
69.45  
69.55  
69.64



107.44  
107.56  
107.67  
107.78  
107.89  
108.11  
108.22  
108.33  
108.44  
108.56  
108.67  
108.78  
108.89  
109.17  
109.33  
109.50  
109.67  
109.83  
110.50

32

0.13513	98.	464.	97.	791.	962.000	97.	10
0.40428	99.	464.	97.	791.	945.500	98.	10
0.79447	100.	464.	97.	791.	925.000	99.	10
1.50403	101.	464.	97.	791.	901.500	100.	10
0.90932	102.	464.	97.	791.	874.000	101.	10
1.48901	103.	464.	97.	791.	841.000	102.	10
1.57734	104.	464.	97.	791.	806.000	103.	10
2.70526	105.	464.	97.	791.	771.500	104.	10
3.09044	106.	464.	97.	791.	736.000	105.	10
3.55258	107.	464.	97.	791.	828.500	106.	10
5.25950	108.	464.	97.	791.	1170.500	107.	10
5.37162	109.	464.	97.	791.	1143.000	108.	10
5.29467	110.	464.	97.	791.	1109.000	109.	10
7.15675	111.	464.	97.	791.	1074.500	110.	10
5.86912	112.	464.	97.	791.	1033.500	111.	10
5.96496	113.	464.	97.	791.	990.500	112.	10
6.71579	114.	464.	97.	791.	951.500	113.	10
5.08034	115.	464.	97.	791.	908.500	114.	10
4.57877	116.	464.	97.	791.	926.000	115.	10
5.39298	117.	464.	97.	791.	827.500	116.	10
4.19785	118.	464.	97.	791.	785.500	117.	10
3.79263	119.	464.	97.	791.	741.000	118.	10
4.82061	120.	464.	97.	791.	697.000	119.	10
2.02787	121.	464.	97.	791.	660.500	120.	10
3.42786	122.	464.	97.	791.	627.500	121.	10
3.26986	123.	464.	97.	791.	1502.500	122.	10
1.90001	124.	464.	97.	791.	1464.500	123.	10
0.83112	125.	464.	97.	791.	1423.000	124.	10
0.81505	126.	464.	97.	791.	1376.500	125.	10
0.43529	127.	464.	97.	791.	1329.500	126.	10
0.15642	128.	464.	97.	791.	1278.000	127.	10
0.05032	129.	464.	97.	791.	1226.500	128.	10

112.13  
112.25  
112.38  
112.50  
112.63  
112.75  
112.88  
113.05

113.11  
113.16  
113.21  
113.26  
113.32  
113.37  
113.42  
113.47  
113.53  
113.58  
113.63  
113.68  
113.74  
113.79  
113.84  
113.89  
113.95  
114.04  
114.07  
114.11  
114.14  
114.18  
114.21  
114.25  
114.29  
114.32  
114.36  
114.39  
114.43  
114.46  
114.50  
114.54  
114.57  
114.61  
114.64  
114.68  
114.71  
114.75  
114.79  
114.82  
114.86  
114.89  
114.93  
114.96  
115.04  
115.08  
115.12  
115.15  
115.19  
115.23  
115.27  
115.31  
115.35  
115.38  
115.42  
115.46  
115.50  
115.54  
115.58  
115.62

115.65  
115.69  
115.73  
115.77  
115.81  
115.85  
115.88  
115.92  
115.96  
116.04  
116.08  
116.12  
116.16  
116.20  
116.24  
116.28  
116.32  
116.36  
116.40  
116.44  
116.48  
116.52  
116.56  
116.60  
116.64  
116.68  
116.72  
116.76  
116.80  
116.84  
116.88  
116.92  
116.96  
117.04  
117.09  
117.13  
117.17  
117.22  
117.26  
117.30  
117.35  
117.39  
117.43  
117.48  
117.52  
117.57  
117.61  
117.65  
117.70  
117.74  
117.78  
117.83  
117.87  
117.91  
117.96  
118.04  
118.08  
118.12  
118.16  
118.20

118.24  
118.28  
118.32  
118.36  
118.40  
118.44  
118.48  
118.52  
118.56  
118.60  
118.64  
118.68  
118.72  
118.76  
118.80  
118.84  
118.88  
118.92  
118.96  
119.04  
119.08  
119.13  
119.17  
119.21  
119.25  
119.29  
119.33  
119.38  
119.42  
119.46  
119.50  
119.54  
119.58  
119.63  
119.67  
119.71  
119.75  
119.79  
119.83  
119.88  
119.92  
119.96  
120.04  
120.08  
120.13  
120.17  
120.21  
120.25  
120.29  
120.33  
120.38  
120.42  
120.46  
120.50  
120.54  
120.58  
120.63  
120.67  
120.71  
120.75

120.79  
120.83  
120.88  
120.92  
120.96  
121.06  
121.12  
121.18  
121.24  
121.29  
121.35  
121.41  
121.47  
121.53  
121.59  
121.65  
121.71  
121.76  
121.82  
121.88  
121.94  
122.05  
122.11  
122.16  
122.21  
122.26  
122.32  
122.37  
122.42  
122.47  
122.53  
122.58  
122.63  
122.68  
122.74  
122.79  
122.84  
122.89  
122.95  
123.05  
123.11  
123.16  
123.21  
123.26  
123.32  
123.37  
123.42  
123.47  
123.53  
123.58  
123.63  
123.68  
123.74  
123.79  
123.84  
123.89  
123.95  
124.06  
124.13  
124.19

124.25  
124.31  
124.38  
124.44  
124.50  
124.56  
124.63  
124.69  
124.75  
124.81  
124.88  
124.94  
125.05  
125.09  
125.14  
125.18  
125.33  
125.27  
125.32  
125.36  
125.41  
125.45  
125.50  
125.55  
125.59  
125.64  
125.68  
125.73  
125.77  
125.82  
125.86  
125.91  
125.95  
126.05  
126.11  
126.16  
126.21  
126.26  
126.31  
126.36  
126.42  
126.47  
126.53  
126.58  
126.63  
126.68  
126.74  
126.79  
126.84  
126.89  
126.95  
127.06  
127.11  
127.17  
127.22  
127.28  
127.33  
127.39  
127.44  
127.50

127.56  
127.61  
127.67  
127.72  
127.78  
127.83  
127.88  
127.94  
128.09  
128.18  
128.27  
128.36  
128.45  
128.54  
128.64  
128.73  
128.82  
128.91  
129.50

//

1984-85 Research Initiation Program

Sponsored by the

AIR FORCE OFFICE OF SCIENTIFIC RESEARCH

Conducted by the

SOUTHEASTERN CENTER FOR ELECTRICAL ENGINEERING EDUCATION

Final Report

ANALYSIS OF AIR FORCE VEHICLE CONDITION RATINGS FROM HISTORICAL DATA

Prepared by:	Bruce N. Janson
Academic Rank:	Assistant Professor
Address:	Department of Civil Engineering Carnegie-Mellon University Pittsburgh, PA 15213
USAF Research:	Capt. James R. Van Scotter, USAF
Date:	July 25, 1985



## ANALYSIS OF AIR FORCE VEHICLE CONDITION RATINGS FROM HISTORICAL DATA

### ABSTRACT

The method used by the U.S. Air Force to record historical information on the use, maintenance and repair needs of their vehicles is the Vehicle Information Management System (VIMS). A large number of data elements are recorded daily and compiled monthly for most every vehicle at each Air Force base around the world. One factor that is assigned monthly to each vehicle on the basis of current information is the vehicle's condition rating known as the Replacement Code. Its primary determinants are age, accumulated use, and the cost of a one-time repair if it is needed. As a vehicle's age, use and repair needs indicate a decline in its operational reliability, the condition rating of the vehicle is successively downgraded through a sequence of alphabetic replacement codes, the specifics of which will be further described in later sections.

The replacement code is the primary indicator to a vehicle fleet manager and base-level command of the need for new vehicle procurements. As such, the use of this rating as a guideline for vehicle buy allocations has a direct impact on both the cost and functional capability of base fleets. Considering that the Air Force owns and operates over 100,000 vehicles of roughly 330 different types at both major and minor installations around the world, it is important that the replacement code be a valid measure of a vehicle's condition and anticipated performance. The purpose of this research was to assess the economic validity of the replacement code as a repair or replace indicator, and to evaluate the sensitivity of repair or replace decisions to possible changes in its calculation.

## ANALYSIS OF AIR FORCE VEHICLE CONDITION RATINGS FROM HISTORICAL DATA

### 1 Introduction

Effective vehicle monitoring systems are necessary to track the use, maintenance and condition of a vehicle fleet. These systems can also be used to assist vehicle fleet managers in forecasting inventory needs for new vehicles and parts. The reliability of such forecasts will have significant impacts on vehicle buy decisions and the accuracy of capability assessments. Since the condition of a vehicle is often a prime determinant in how it is used, maintained and repaired, and when it is scheduled to be replaced, the useful life of a vehicle, from procurement to salvage, is affected by both its actual and rated conditions. Examples of equipment maintenance and replacement research are [2,5,12,13,14].

The method used by the U.S. Air Force to record historical information on the use, maintenance and repair needs of their vehicles is the Vehicle Information Management System (VIMS). A large number of data elements are recorded daily and compiled monthly for most every vehicle at each Air Force base around the world. One factor that is assigned monthly to each vehicle on the basis of current information is the vehicle's condition rating known as the Replacement Code. Its primary determinants are age, accumulated use, and the cost of a one-time repair if it is needed. As a vehicle's age, use and repair needs indicate a decline in its operational reliability, the condition rating of the vehicle is successively downgraded through a sequence of alphabetic replacement codes, the specifics of which will be further described in later sections.

The replacement code is the primary indicator to a vehicle fleet manager and base-level command of the need for new vehicle procurements. As such, the use of this rating as a guideline for vehicle buy allocations has a direct impact on both the cost and functional capability of base fleets. Considering that the Air Force owns and operates over 100,000 vehicles of roughly 330 different types at both major and minor installations around the world, it is important that the replacement code be a valid measure of a vehicle's condition and anticipated performance.

From May through July of 1984, this researcher worked with the USAF at the Logistics Management Center at Gunter AFS. The objective of that research was to develop a prototype vehicle fleet analysis system for the Zenith Z-100 micro-computer that could retrieve and utilize VIMS data. During that 10-week research engagement, we identified several potential difficulties with the replacement code as a single measure of a vehicle's condition, reliability, expected future performance and economic value. Several needs for further research to evaluate and recommend improvements to the design and/or use of the vehicle replacement code were identified.

The purpose of this research was to assess the economic validity of the replacement code as a repair or replace indicator, and to evaluate the sensitivity of repair or replace decisions to possible changes in its calculation. Since the replacement code is meant to be a reliable measure of a vehicle's present condition, this indicator should react to significant changes in a vehicle's current performance, but not to incidental repair needs or small variations in other operational costs. An explanation of the replacement code is given first that clarifies the successive ordering of these alphabetic ratings. Then, a description and analysis of the one-time repair limit — a key factor in the determination of a vehicle's replacement code — compares it to the calculated salvage value of a vehicle based upon engineering economic principles.

The importance of accounting for price changes in a one-time repair limit is discussed, and it is shown that price changes are accounted for in VIMS by adjustments to a vehicle's standard price. However, the analysis of VIMS data in this study revealed that these adjustments to standard prices appear to be very inconsistent. Hence, a specific recommendation of this study is to examine whether changes in suppliers' prices are being properly updated and utilized within VIMS for calculating one-time repair limits. Section 6 explains how data was retrieved from a VIMS historical record file for a particular base and organized into a usable dataset. Section 7 then examines the impact that small price adjustments to the one-time repair limit might have on the number of vehicles exceeding this limit. Section 8 concludes this report with a summary and recommendations.

## 2 Review of the Air Force Vehicle Replacement Code

The Replacement Code (RC) is updated and recorded monthly for each vehicle of a base fleet in the monthly historical record file of the Vehicle Information Management System (VIMS). These records are usually maintained on a current VIMS tape for the most recent 12 months. A large number of data items are recorded to this database, but only a select few pertain to the determination of the replacement code. A necessary task in the data analysis portion of this research was to retrieve the following selected data elements from the VIMS tape for a given base and place these into a manageable database.

1. Vehicle Registration Number (VRN)
2. Management Code (MC)
3. Vehicle Equivalents (VEQ)
4. Acceptance Date (AD)
5. Standard Price (SP)
6. Replacement Code (RC)
7. Life Expectancy (LE)
8. One-Time Repair Cost Limit (OTL)
9. One-Time Repair Cost Exceeded (OTX)
10. One-Time Repair Cost Price (OTP)
11. Use Code (UC)
12. Average Daily Use (ADU)
13. Cumulative Use (CU)
14. Direct Labor Cost for Repairs (DLC)
15. Total Parts Cost for Repairs (TPC)

Details pertaining to the retrieval of this data from the VIMS data file are discussed in a later section.

The vehicle replacement code is primarily a function of upon three basic criteria -- age, use and one-time repair. The age of a vehicle can be calculated from its Acceptance Date (AD), which is the date at which the vehicle was actually

delivered to a base by its supplier. Both month and year are recorded in the acceptance date. The year of the acceptance date usually agrees with a vehicle's model year, which is the first two digits of its Vehicle Registration Number (VRN).

A vehicle's AD year can easily be one year later than the model year in cases where a late year purchase carries the acceptance date into the following year. In a few instances, however, the AD year can be very different from the MY if a vehicle has been depot repaired or reassigned to a completely different base. An analysis of VIMS data showed that the one-time repair limit, which will be explained later, is always computed on the basis of the acceptance date, even when it differs from the model year substantially.

The use of a vehicle can be recorded in terms of four different units — miles (M), hours (H), units (U) and kilometers (K). A vehicle's Use Code (UC) indicates the particular units in which the Cumulated Use (CU) and the Average Daily Use (ADU) of that vehicle were recorded. A vehicle's use is always measured in units that are consistent with the Average Annual Standard specified in the Air Force 77-310 Motor Vehicle Management Manual [6], or Technical Order 36A-1-1301 [8], if one is available for that particular vehicle type.

In assigning a replacement code to a particular vehicle, both the age and use of the vehicle are compared against their expected lifetime values. The Life Expectancy (LE) of a vehicle is given in years as one of the data elements in the VIMS historical record file. The lifetime expected use (LEU) of a vehicle equals the life expectancy of the vehicle times its average Annual Use Standard (AUS), where  $LEU = LE \cdot AUS$ . Unfortunately, the annual use standard for each vehicle is not recorded as a data element in the VIMS historical record file. This omission makes it very awkward to associate the correct AUS values in AFM 77-310 with the vehicles found in a VIMS historical record file.

Section V of Technical Order 00-25-249 [7] on Vehicle Replacement Codes contains descriptions of the replacement codes as listed in Table 1. Some wording changes, particularly the replacement of Miles/Kilometers with Use, have been made for consistency. It is unclear in TO 00-25-249 whether the Use criterion is ever used to determine the replacement codes of vehicles for which

**Table 1: Vehicle Replacement Codes**

The following descriptions are found in Section V of TO 00-25-249. See TO 36A-1-1301 for vehicle life expectancies and lifetime expected use standards, and AFM 77-310 for additional information.

Abbreviations used are: LE = life expectancy (in years); LEU = lifetime expected use (in M/H/U/K); OTL = one-time repair limit (in dollars).

1. **A - Age, Use and One-Time Repair.** Vehicle has exceeded both its LE and LEU; also requires repairs that would exceed its OTL, and the vehicle repair authority has decided that only minimum essential repairs will be made.
2. **B - Age and One-Time Repair.** Vehicle has exceeded its LE, also requires repairs that would exceed its OTL, and it has been decided that only minimum essential repairs will be made.
3. **C - Use and One-Time Repair.** Vehicle has exceeded its LEU, also requires repairs that would exceed its OTL, and it has been decided that only minimum essential repairs will be made.
4. **D - One-Time Repair.** Vehicle requires repairs that would exceed its OTL, and it has been decided that only minimum essential repairs will be made.
5. **F - Obsolete.** Vehicle has been declared obsolete. Vehicle maintenance will manually enter this code into VIMS upon notification.
6. **G - Age and Use.** Both LE and LEU have been exceeded.
7. **H - Age.** Life expectancy has been exceeded.
8. **J - Use.** Lifetime expected use has been exceeded.
9. **K - Age and Use, 1 Year.** Both LE and LEU will be exceeded within 1 year.
10. **L - Age, 1 Year.** Life expectancy will be exceeded within one year.
11. **M - Use, 1 Year.** Lifetime expected use will be exceeded within one year.
12. **N - Age and Use, 2 Years.** Both LE and LEU will be exceeded within 2 years.
13. **P - Age, 2 Years.** Life expectancy will be exceeded within two years.
14. **Q - Use, 2 Years.** Lifetime expected use will be exceeded within two years.
15. **R - Age, Mid-Life.** Vehicle's age has exceeded one-half of its LE.
16. **S - Depot Repaired Vehicles.** Vehicle was depot repaired less than 3 years ago; see paragraph 5-22 for further instructions.
17. **T - Other.** Assign to vehicles whenever codes A-S or U do not apply.
18. **U - Warranty.** Assign to vehicles under new or remanufacture warranty; does not apply to depot repaired vehicles.

Table 2: Replacement Code Criteria

Code		Basic Criteria				Time Variables				Special Categories		
#	RC	AGE	USE	OTL	ZL	1Y	2Y	HL	WRN	DR	OBS	OTHER
1	A	X	X	X	X							
2	B	X		X	X							
3	C		X	X	X							
4	D			X	X							
5	F										X	
6	G	X	X		X							
7	H	X			X							
8	J		X		X							
9	K	X	X			X						
10	L	X				X						
11	M		X			X						
12	N	X	X				X					
13	P	X					X					
14	Q		X				X					
15	R	X						X				
16	S									X		
17	T											X
18	U								X			

Key: RC = replacement code  
 AGE = age of vehicle (in years).  
 USE = cumulated use (in M/H/U/K).  
 OTL = one-time repair limit (in dollars).

ZL = zero life expectancy or lifetime expected use remaining.  
 1Y = 1 yr life " " " " "  
 2Y = 2 yr life " " " " "  
 HL = half life expectancy or lifetime expected use remaining.  
 WRN = vehicle under warranty (essentially full life remaining).

DR = vehicle depot repaired less than 3 years ago.  
 OBS = vehicle declared obsolete.  
 Other = whenever codes A-S or U do not apply.

use is measured in hours. Nevertheless, it is easier to comprehend the successive nature of these replacement codes by observing their common criteria as shown Table 2, where an 'X' indicates that the criterion in a given column applies to the replacement code in a given row.

The replacement codes listed in Tables 1 and 2 are mutually exclusive, since all criteria for any one replacement code must be met simultaneously. It is also explained in TO 00-25-249 that sending a vehicle to Depot Repair will revert its replacement code from a letter below L, back up to the letter S, and then down to P. For this reason, all vehicles with replacement codes F, S and T must be treated as special cases. Obsolete and Other are two additional categories used for vehicles with special circumstances that nullify the standard criteria.

The time variables ZL, 1Y, 2Y, and HL shown in Table 2 can apply to either the life expectancy or the lifetime expected use of a vehicle, as is suggested by the assignment rules for the replacement codes. In terms of life expectancy, ZL (or zero life remaining) implies that the age of the vehicle as measured from its acceptance date has exceeded the life expectancy of the vehicle. In comparison, ZL in terms of LEU implies that the cumulated use of the vehicle has exceeded its lifetime expected use. Life expectancies (in years) and lifetime expected use standards are specified in TO 36A-1-1301 and AFM 77-310 as mentioned above.

Times at which a vehicle has less than one year, two years or half of its life expectancy remaining are directly apparent from the vehicle's age and LE values. It is also clear as to when a vehicle's current CU has exceeded half of its LEU. However, it is unclear as to when a vehicle is said to have less than one or two years of its LEU remaining, since this could be based either on the standard annual use standard (AUS) or upon its own average annual use record. It is more accurate to classify a vehicle as being within one year of its LEU when the difference between its LEU and CU values is less than its own average annual use as compared to simply being within one AUS of its LEU.

Within the time variable columns of Table 2, a vehicle's replacement code goes down and upward as it gets older. Its transition upward depends, however, upon how intensely it is used.



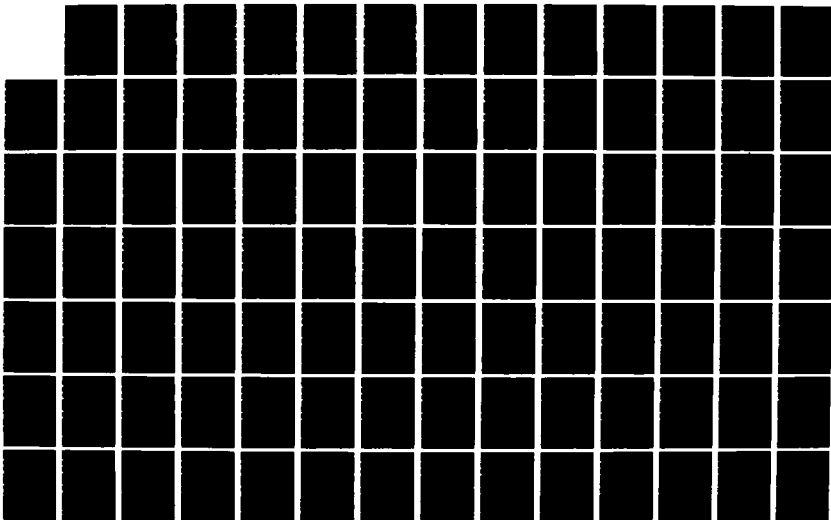
AD-A186 490

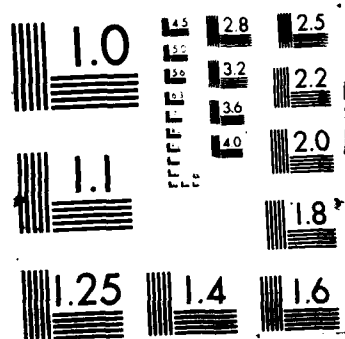
UNITED STATES AIR FORCE RESEARCH INITIATION PROGRAM  
1984 RESEARCH REPORTS (U) SOUTHEASTERN CENTER FOR  
ELECTRICAL ENGINEERING EDUCATION INC 5 W D PEELE  
MAY 86 AFOSR-TR-87-1721 F49620-82-C-0035 F/G 15/1

02/11

UNCLASSIFIED

NL





less than its AGE times its AUS, then it will be assigned codes R, P, L, H, B and possibly A throughout its lifetime. If a vehicle's use is continually greater than its AGE times its AUS, then it will be assigned codes Q, M, J, C and possibly A throughout its lifetime. A vehicle whose use follows the prescribed AUS fairly closely year after year will probably be assigned codes R, N, K, G and possibly A during its lifetime.

The procedure by which a vehicle's average annual use standard is estimated is not investigated in this research. This value depends upon the fleet size needed at an Air Force base in order to cover all assigned functions, and the intensity of use that a vehicle receives on these assignments. The determination of an optimal fleet size involves many factors including the characteristics of daily demands for those vehicles, their reliability, and their critical need in the event of an emergency response. As a rule, it is more costly to operate a fleet size in excess of the number of vehicles required to cover all functions with adequate allowance for out-of-commission vehicles.

It is assumed in this research that the annual use standards estimated by the Air Force for its vehicles correctly reflect the trade-offs between fleet size cost and preparedness in that organization. However, the tremendous variety of Air Force base locations and operating conditions does introduce some doubt as to whether a single use standard is appropriate for the same vehicle type at all installations. It is recognized here that a strong need for policy standardization within the Air Force does require that certain simplifying assumptions be made that lead to uniform management directives. Moreover, an analysis of how operating conditions, maintenance procedures and usage intensity affect the useful life of Air Force vehicles is beyond the scope of this research.

The life expectancy of a vehicle and its lifetime expected use are both dependent upon the average annual use of the vehicle and its economical time of replacement. Given that the average annual use of a vehicle is taken to be known and fixed, as opposed to being determined simultaneously with the vehicle's optimal replacement age, the optimal replacement time of a vehicle can be determined theoretically on the basis of its expected operations and maintenance costs. Unfortunately, there is insufficient data in one 12-month VIMS dataset with

which to estimate the optimal replacement age, or useful life expectancy, of any given vehicle type.

Alternatively, the One-Time Repair Limit (OTL) that is updated monthly in the VIMS records can be examined on the basis of available data, and its calculation can be modified to better reflect the current economic value of a vehicle. In the next section of this report is explained the current procedure used by the Air Force to calculate a vehicle's one-time repair limit. Section 4 shows that the current formula is similar to, but consistently higher than, an alternative calculation of OTL based upon engineering economic calculations of a vehicle's salvage value.

### 3 Explanation of the One-Time Vehicle Repair Limit

Currently, the One-Time Repair Limit (OTL) is primarily an indicator of age and use. It does not reflect the expected operation and maintenance expenses of that particular vehicle type in future years. TO 00-25-249 specifies that OTL for a given vehicle should be calculated on the basis of two different but related ratios. One formula uses AGE/LE ratio, while the other formula uses the CU/LEU ratio. Otherwise, both formulas, as shown by equations (1) and (2), are identical.

$$\begin{aligned} \text{OTL}_1 &= \text{SP} \cdot (1 - 0.9 \cdot \text{AGE}/\text{LE}) && \text{for AGE} \leq \text{LE} \\ \text{OTL}_1 &= \text{SP} \cdot (0.1) && \text{for AGE} > \text{LE} \end{aligned} \quad (1)$$

$$\begin{aligned} \text{OTL}_2 &= \text{SP} \cdot (1 - 0.9 \cdot \text{CU}/\text{LEU}) && \text{for CU} \leq \text{LEU} \\ \text{OTL}_2 &= \text{SP} \cdot (0.1) && \text{for CU} > \text{LEU} \end{aligned} \quad (2)$$

$$\text{OTL} = \text{Min} [\text{OTL}_1, \text{OTL}_2] \quad (3)$$

where, SP = Standard Price (of a new vehicle, in dollars)

AGE = Current Date - Acceptance Date (in months)

LE = Life Expectancy (in months)

CU = Cumulated Use (in M/H/U/K units)

LEU = Lifetime Expected Use (in M/H/U/K units)

In the above formulas, LE is multiplied by 12 to convert it to months, and LEU equals LE (in years) times the annual use standard. After calculating both  $\text{OTL}_1$  and  $\text{OTL}_2$ , the lower of the two is taken as the OTL for that vehicle in that month as given by equation (3).

Figure 1 shows the OTL values for a hypothetical vehicle with a standard has a standard price of \$10,000 and a life expectancy of 10 years. It is very straightforward to calculate  $OTL_1$  for any vehicle on the basis of its life expectancy and its age calculated from VIMS records. On a graph such as Figure 1,  $OTL_1$  can be drawn as a line connecting the standard price at time 0 to 10% of the SP at time LE. For vehicle ages beyond LE,  $OTL_1$  is set to 10% of the standard price, as given by equation (1) and shown by the values for  $OTL_1$  in Table 3.

By comparison,  $OTL_2$  is a function of a vehicle's use, and it will not be straight line unless the vehicle receives the identical amount of use in every month. Moreover, it is not possible to calculate  $OTL_2$  directly from VIMS data because the annual use standard for each vehicle type is not included in the VIMS dataset. The graph of  $OTL_2$  shown in Figure 1 is based on hypothetical use data for this example vehicle shown in Table 3. Note that in Figure 1,  $OTL_2$  is always greater than or equal to  $OTL_1$ . Only at times when the total cumulated use of a vehicle exceeds its age times its annual use standard will  $OTL_2$  will be lower than  $OTL_1$ . Otherwise,  $OTL_1$  will always be lower, which was found to be the case for all vehicle records examined in this study for one particular base.

As explained in the next section, the reasoning behind a one-time repair limit is that it reflects the salvage value of a vehicle at that time. One implication of using the above formulas to determine the one-time repair limit is that the salvage value of a vehicle, no matter how old, is assumed to be atleast 10% of its standard price, which is a common rule for equipment depreciation accounting [4]. A maintenance related reason for the 10% minimum is, however, that it insures the allowance of minimal repairs to vehicles that are needed and are still operational past their expected lifetimes. Otherwise, a very usable vehicle could be left out-of-commission because of needing relatively inexpensive repairs.

#### 4 Alternative Calculation of the One-Time Repair Limit

The purpose of setting one-time repair limits on vehicles is to potentially avoid uneconomical repair expenditures on a vehicle beyond its salvage value. The calculation of salvage value for a given vehicle in a given year requires that the

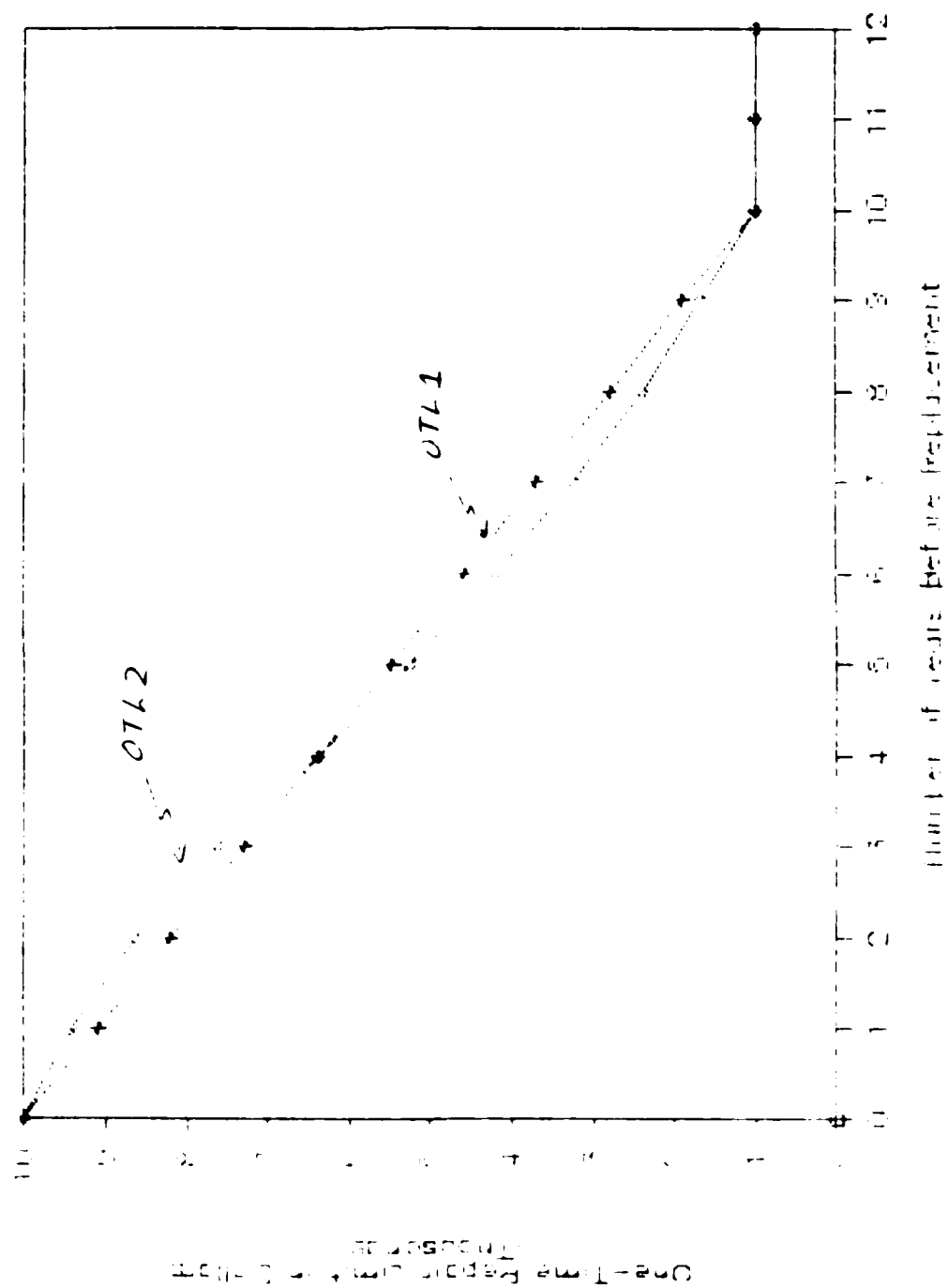
Table 3: Calculations of  $OTL_1$  and  $OTL_2$

Listed below are values of annual and cumulated use for a hypothetical vehicle with a standard price of \$10000.

Year	Annual Miles	Total Miles	OTL2 Dollars	OTL1 Dollars	OTL Dollars
1	5000	5000	9437.5	9100.0	9100.0
2	7000	12000	8650.0	8200.0	8200.0
3	9000	21000	7637.5	7300.0	7300.0
4	11000	32000	6400.0	6400.0	6400.0
5	10000	42000	5275.0	5500.0	5275.0
6	9500	51500	4206.3	4600.0	4206.3
7	8500	60000	3250.0	3700.0	3250.0
8	7500	67500	2406.3	2800.0	2406.3
9	6500	74000	1675.0	1900.0	1675.0
10	6000	80000	1000.0	1000.0	1000.0
11	0	80000	1000.0	1000.0	1000.0
12	0	80000	1000.0	1000.0	1000.0

Note: For vehicle in this example, AUS = 8000 mi/yr and LE = 10 yrs.

Figure 1: Comparison of OTL1 and OTL2



principles of life cycle costing be applied correctly. Textbooks such as [3] and [11] explain the engineering economic principles that are the basis for present value and uniform annual value calculations used in life cycle costing and replacement scheduling of transit equipment [1,9,10].

The calculation of a one-time repair limit based upon engineering economics is equivalent to determining the salvage value of the vehicle in any period. Data required to make this calculation are the vehicle's original purchase price or standard price, its expected operation and maintenance cost in each period, and an appropriate discount rate or opportunity cost of capital for the equipment owning organization. If inflation is accounted for within the analysis, then the cash flows in this stream can be expressed in current dollars at time 0 or in "then-current" dollars for each of the time periods. Accounting for inflation requires that a suitable equipment cost price index be available for the analysis period.

The final key assumptions to the calculation of a vehicle's salvage value based upon engineering economics are that:

1. This vehicle can be replaced by an equivalent vehicle at the time that the salvage value of this vehicle equals zero, and that this replacement process can continue forever.
2. The standard price of the replacement vehicle (expressed in time 0 discounted dollars) will equal the time 0 price of the current vehicle.
3. The operation and maintenance costs of the replacement vehicle (expressed in time 0 discounted dollars) will equal the time 0 costs of the current vehicle.

Given that these assumptions are valid, the key to determining a vehicle's economically efficient replacement time is to evaluate the equivalent uniform annual cost (EUAC) of expenditures on this vehicle for alternative replacement times over a realistic planning horizon. In terms of economic efficiency, the optimal replacement time is the one that results in the lowest EUAC.

In order to calculate EUAC values for the \$20,000 hypothetical vehicle represented in Figure 1, an assumed set of operations and maintenance costs for this vehicle in each year are listed in Table 4. These annual costs were chosen to represent a typical vehicle expenditure history in which there is a uniform base amount, a slowly increasing gradient of minor repair costs after the first year, and



a more sharply increasing gradient of repair costs after the mid-life of the vehicle. The optimal time to replace this vehicle so as to operate at the minimum EUAC point is 14 years. These EUAC values are listed in Table 4 and shown as a graph in Figure 2.

An explanation of the formula used to calculate the EUAC values for this vehicle is given in Appendix A. One assumption made in calculating these EUAC values is that the expected salvage value of a vehicle at its optimal replacement time will be zero, which is basically true of a rational salvage market if we accept the premise that Brealey and Myers prescribe as the Fundamental Financial Concept of Efficient Capital Markets: [4, pg. 265]

"If capital markets are efficient, then the purchase or sale of any security at the prevailing market price is a zero-NPV transaction."

Given the salvage market to be efficient, then the one-time repair limit that should be placed upon a vehicle at any time preceeding its replacement date should be equal to the vehicle's salvage value at that time. Salvage values for the example vehicle are also listed in Table 4, where it is shown to equal zero at the end of year 10. The formula used to calculate these salvage values is also explained in Appendix A.

The justification for performing a one-time vehicle repair is that this one-time repair will return the vehicle to the average operating condition of similar vehicles of common age and use. This vehicle is then expected to perform as well as any similar vehicle that could have been purchased at the salvage value. Given that the one-time repair being considered will return a vehicle to average working condition for its remaining lifetime, then the one-time repair limit should equal the salvage value of an average working vehicle of similar type at that point in time. The alternative would be to salvage the vehicle and purchase a different new or used one. However, if the salvage market is working properly, then the value of the unrepaired vehicle should exactly equal the salvage value of a similar working vehicle minus the cost of repairs. The Air Force can validly operate within these principles since they effectively control the salvage values of their own vehicles by setting their own vehicle lifetimes and one-time repair limits.

Table 4: Calculations of Equivalent Uniform Annual  
Costs and Economic Salvage Values

Listed below are hypothetical cash flows for this example vehicle.

SP = Standard Price at Time 0 = 10000  
 UB = Annual Base O & M Cost = 500  
 G1 = Annual O & M Cost Grad = 100  
 Y1 = Year in which G1 begins = 2  
 G2 = Annual O & M Cost Grad = 220  
 Y2 = Year in which G2 begins = 6  
 i = Annual Discount Rate = 0.10

t = Time of Replacement = 10  
 UACt = UAC if held to time t = 2736.82  
 CPVt = CPV if held to time t = 16816.59

Replace Time	Cash Flow	CPV	EUAC	Salvage Value
0	10000.0	10000.0	10000.0	10000.0
1	500.0	10454.5	11500.0	8763.2
2	600.0	10950.4	6309.5	7502.7
3	700.0	11476.3	4614.8	6216.1
4	800.0	12022.7	3792.8	4900.9
5	900.0	12581.6	3319.0	3554.2
6	1220.0	13270.2	3046.9	2392.8
7	1540.0	14060.5	2888.1	1435.2
8	1860.0	14928.2	2798.2	701.9
9	2180.0	15852.7	2752.7	215.3
10	2500.0	16816.6	2736.8	0.0
11	2820.0	17805.0	2741.3	0.0
12	3140.0	18805.5	2760.0	0.0
13	3460.0	19807.7	2788.5	0.0
14	3780.0	20803.1	2823.9	0.0
15	4100.0	21784.6	2864.1	0.0

Note: All cash flow, EUAC and salvage values are expressed in undiscounted dollars for each year. Each cost present value (CPV) amount equals the sum of discounted cash flows up to the end of the year shown.

Figure 2: Uniform Annual Cost (EUAC)

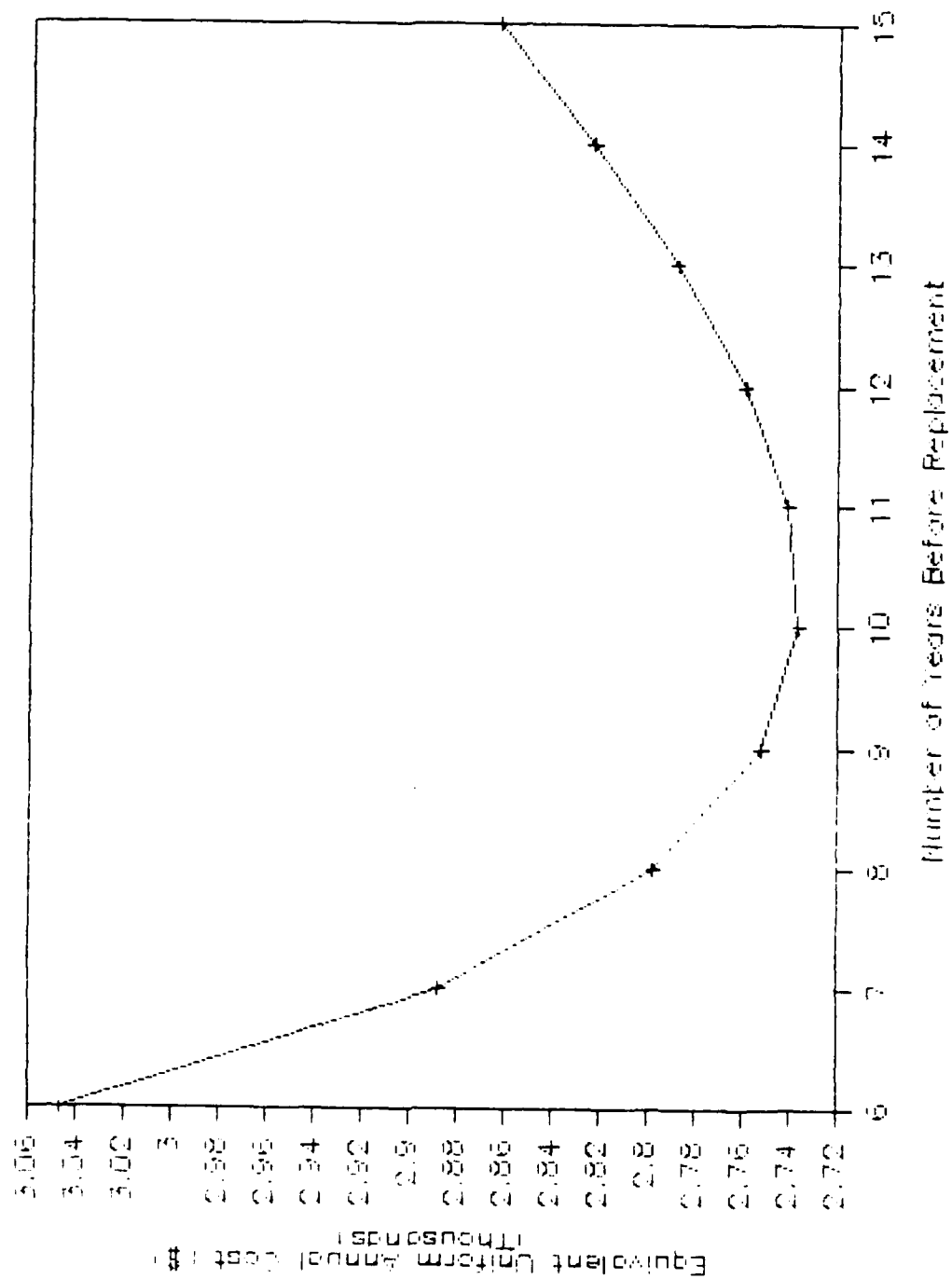
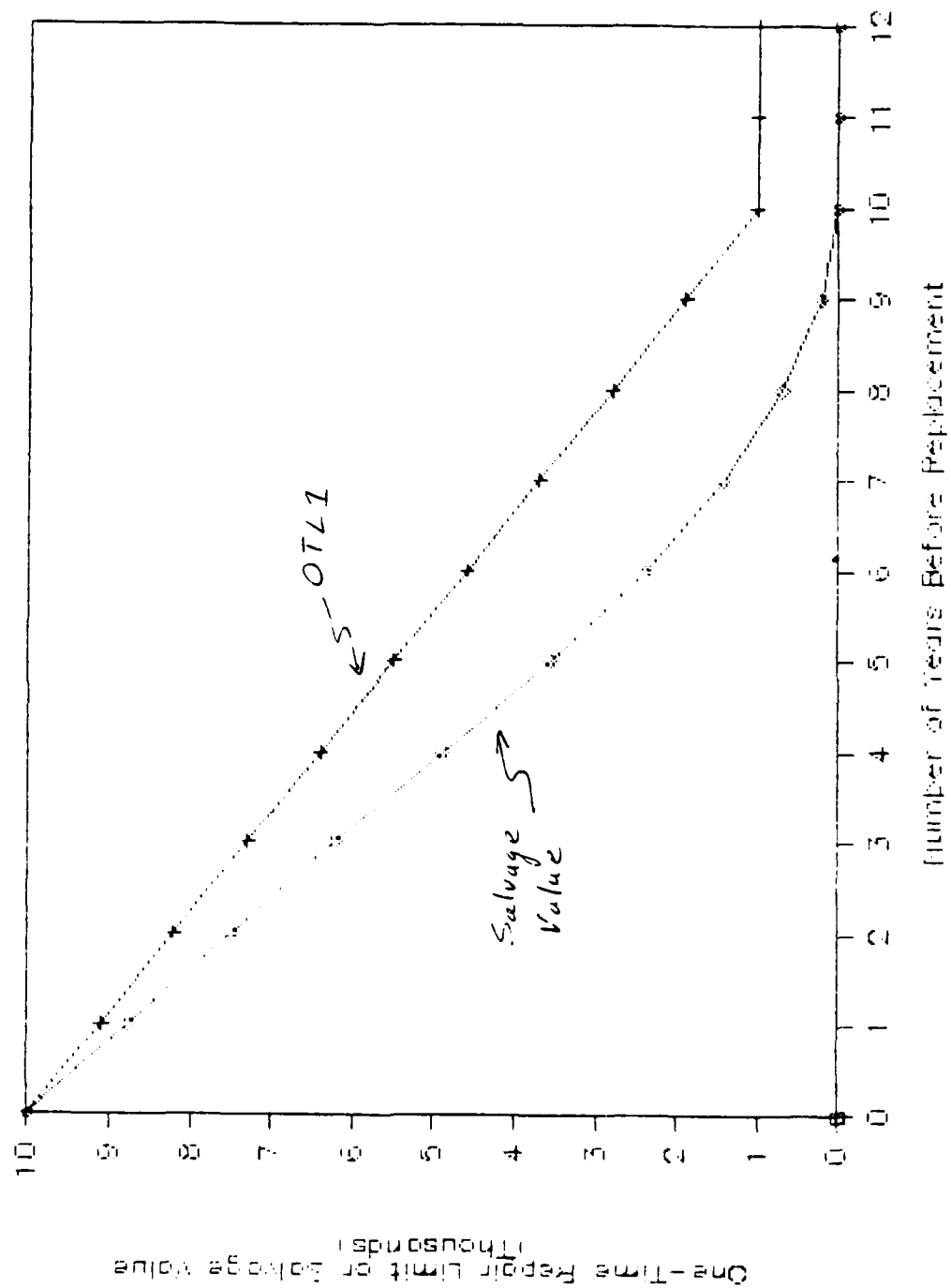


Figure 3: OTL1 versus Salvage Value



Theoretically, EUAC curves and salvage values could be estimated for each Air Force vehicle type based upon historical records of operations and maintenance expenditures for similar vehicles. If this were done, the life expectancy of a vehicle, as specified in TO 36A1-1-1301, should agree approximately with the year corresponding to the lowest point of its EUAC curve. Although there does not exist enough data currently available with which to estimate EUAC values for an actual Air Force vehicle type, we can compare the salvage values listed in Table 4 with the values for  $OTL_1$  given in Table 1 as shown by the graph in Figure 3. The  $OTL_1$  values are consistently higher than salvage values for corresponding years, but we can see by this comparison that  $OTL_1$  is a reasonable approximation to economically efficient salvage values. The major reason for any difference is that  $OTL_1$  is drawn to 10% of a vehicle's standard price at the time of replacement rather than zero.

Having shown some economic validity to the straightforward calculation of  $OTL_1$  given by equation (1), attention must now be given to the fact that both sets of values shown in Figure 3 fail to include the proper treatment of price changes in both repair and replacement costs of a given vehicle. Equipment price changes can occur for a variety of reasons such as technological differences between older vehicles and their replacements, or changes in contract agreements between the Air Force and its suppliers. General inflation or selective input price changes to the vehicle manufacturing industry can also have an impact. Whatever the reason for price changes, it is important to calculate the one-time repair limit in "then-current" dollars for the period in which a repair is being considered. Unless one-time repair limits are adjusted for price changes, a vehicle could be denied an economically justified repair for exceeding a limit based on non-current prices.

The Statistical Abstract of the United States contains producers price indexes for many industrial sectors of the U.S. economy. Price index values for the Transportation Equipment sector for the years 1970-1980 are listed below.

**Producer Price Index Values for Transportation Equipment**

Year	1970	1973	1974	1975	1976	1977	1978	1979	1980
Index	100.0	110.0	120.0	135.3	144.5	154.2	165.9	179.8	197.9

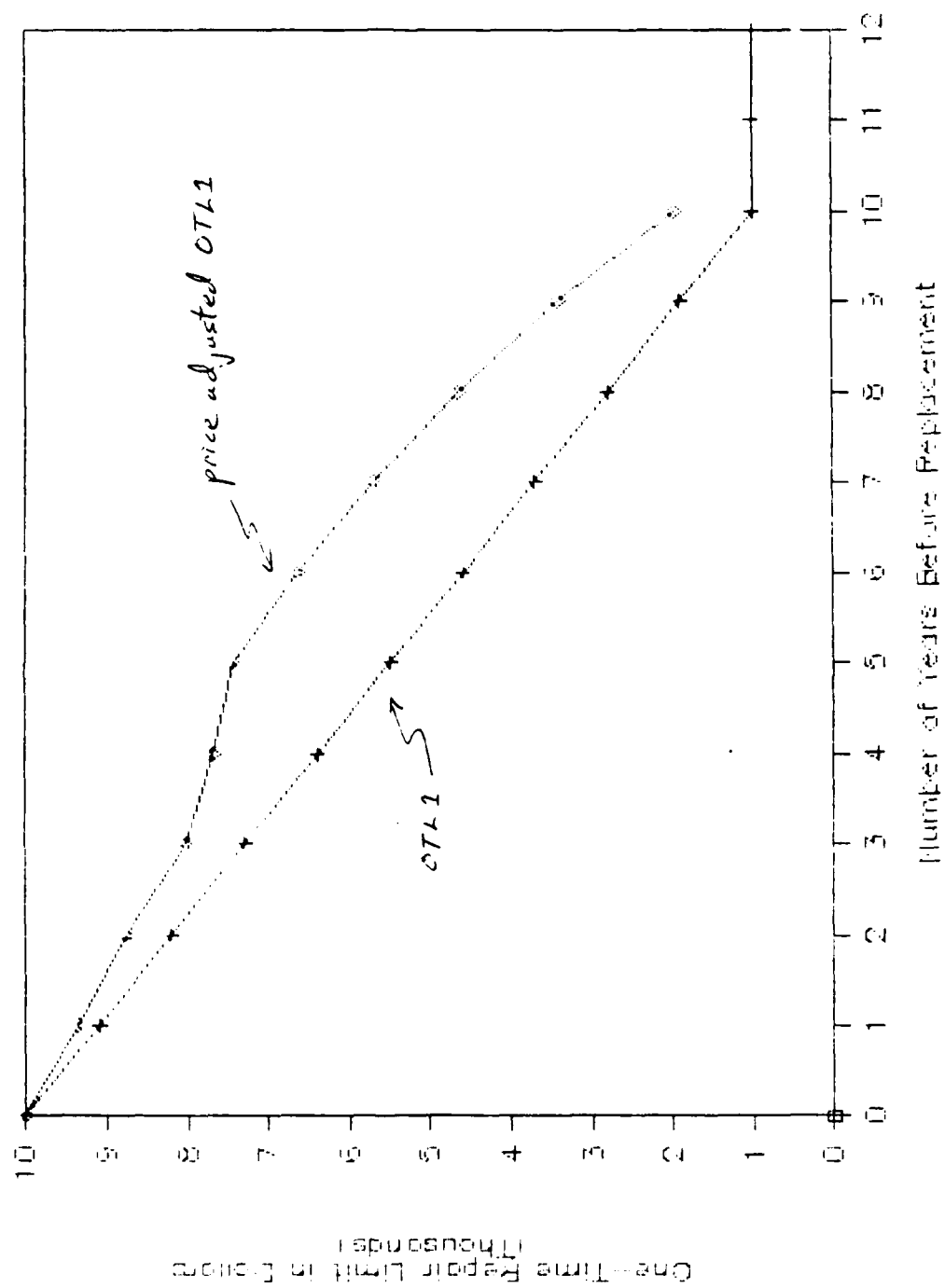
Source: Statistical Abstract of United States (1982-83). The values have been adjusted proportionately so that 1970 equals 100.

Since the above index equals 100 for 1970, each value shown represents the equivalent cost in that year of a comparable equipment expenditure valued at \$100 in 1970. In Figure 3 above, if time 0 corresponds to the end of 1970, then time 10 equals the end of 1980. Figure 4 shows both the straightline  $OTL_1$  values from Figure 1 and their inflated values after multiplication by the above index values. Note that by the end of year 10 (or 1980), the inflated one-time repair limit is almost twice the value of the uninflated limit.

The same graph of inflated one-time repair limits shown in Figure 4 can be obtained by multiplying the standard price of the vehicle by the index value for each year and drawing the  $OTL_1$  line for that year based upon this amount. This method of annually updating the standard price of a replacement vehicle so that  $OTL$  values are adjusted proportionately is used by VIMS. Hence, the Standard Price that appears in each monthly vehicle record of the VIMS database can be referred to more appropriately as a Replacement Price.

A caution is provided here concerning economically valid changes in a vehicle's  $OTL$  value whenever a change in its standard price reflects technological differences in the replacement vehicle. The effects of general inflation on price levels can often be disregarded from standard engineering economic calculations since, if inflation affects all cash flows in an alternatives analysis to the same degree, then proper analyses with and without adjustments for inflation will result in the same preferred alternative. For example, the optimal replacement time of a vehicle is not affected by general price inflation. Similarly, if a replacement vehicle is technologically and functionally equivalent to the current vehicle, then a supplier's price increase must be responded to by an increase in the one-time repair limit of the current vehicle. However, if a replacement vehicle has been selected that is technologically superior to the current vehicle, and its higher price is acceptable based upon the benefits to be derived from its enhanced capabilities, then the current vehicle might be considered obsolete and thus warrant an even lower one-time repair limit, or an earlier replacement time, than would otherwise be assigned.

Figure 4: OTL1 and Price Adjusted OTL1



Currently, an obsolete designation can be assigned to the replacement code of a vehicle, which effectively reduces its OTL to zero, since no significant repair work can be authorized. Ideally, the optimal replacement time for the current vehicle should be altered in response to the greater benefits of its technologically superior replacement. However, significant modifications to the current VIMS database and OTL calculations would be required to isolate the effects of these benefit and quality factors on replacement vehicle prices. Hence, the current method of updating the Standard Price based upon the most recently acquired price for a replacement vehicle is a practical alternative.

The primary conclusions of this section are that:

1. Setting one-time repair limits for equipment is a valid method of preventing repair expenditures beyond the current economic value of a vehicle.
2. The economic value of a vehicle, as reflected in its salvage value, can theoretically be determined from the life cycle costs of similar vehicles.
3. The current OTL formula used by the Air Force is similar to, but somewhat higher than, the salvage value of a vehicle based upon engineering economic calculations. Hence, OTL appears to be a generous estimation of a vehicle's true economic value.
4. Since the OTL formula used by the Air Force is based upon a vehicle's standard price, one-time repair limits are affected by any changes to a vehicle's standard price because of general inflation, selective price changes to specific equipment, or technological differences in replacement vehicles. Whatever the reason for price changes, each vehicle's standard price must be adjusted appropriately so that its one-time repair limit is a value comparable to "then-current" dollars at any given time.

The impact of price adjustments to the one-time repair limit on recent repair or replace decisions at a given Air Force base will be examined next by searching a VIMS historical record file for instances in which vehicles had approached or exceeded their OTL's over the last year. The purpose of this analysis is to assess the sensitivity of repair or replace decisions to the one-time repair limit. In short, if a improved method of treating price and technological changes in vehicles were added to the VIMS calculation of OTL values, how much of an impact might this have had on recent repair or replace decisions.



## 5 Retrieval of Data from the VIMS Historical Record File

Initially, all 6507 monthly vehicle assignment, maintenance and use records on tape ARAD6T in file ARADOF were copied to a hard disk file using a tape copy utility on the mainframe computer. Since each record has length 700 (i.e. contains 700 characters), a very large temporary storage allocation was required on the hard disk to store this entire dataset. However, since only a select number of data fields would be required to perform the investigations of this research, a subset of required data elements listed in Table 5 were extracted from this large file and written to a smaller file by program ARADO1 as discussed next.

Listings of all computer programs used in this study to breakout, examine, process, summarize and display the data are included in Appendix B. Each of these programs was written in standard FORTRAN. Initially, ARADO1 is used to produce smaller files of required data elements, but no changes whatsoever were made to the data in this reduction process. Hence, ARADO1 preserves all data entries exactly as they were copied from the ARAD6T tape in this first step of the conversion process.

In scanning through the files produced from ARADO1, it was observed that the consistency of the records was dramatically different for vehicle classes other than D, E and L. There were roughly 20 'K' vehicles preceeding 'L' vehicles in the file, and then some more vehicles with 'K' in their VRN's but not in their mangement codes. There were also many 'X' and 'P' class vehicles in the end of the file with missing management codes or LE values. Hence, the records for vehicle classes other than D, E and L were deleted from the files. This left a total of slightly less than 4000 vehicle records in the dataset to be used in the analysis. The records for these vehicles were then divided into three separate files containing:

1530 records for 135 D vehicles  
1048 records for 95 E vehicles  
1264 records for 117 L vehicles.

Table 5: Data Retrieved from the ARADOF File of the ARAD6T  
Tape of Monthly Air Force VIMS Vehicle Records

Item#	Field	#Chars	Units	Field Name	Abbrev
	2X				
1	3-10 0X	8	Alphanumeric	Vehicle Registration Number	VRN
2	11-14 33X	4	Alphanumeric	Management Code	MC
3	48-50 30X	3	Whole Vehicles	Vehicle Equivalents	VEQ
4	81-84 9X	4	Year/Month	Acceptance Date	AD
5	94-99 0X	6	Whole Dollars	Standard Price	SP
6	100 9X	1	Alpha	Replacement Code	RC
7	110-111 6X	2	Whole Years	Life Expectancy	LE
8	118-123 0X	6	Whole Dollars	One-Time Repair Cost Limit	OTL
9	124 0X	1	" "no;"="yes	One-Time Repair Cost Exceeded	OTX
10	125-131 165X	7	Whole Cents	One-Time Repair Cost Price (Current estimate if applies)	OTP
11	297 0X	1	M/H/U/K	Use Code	UC
12	298-300 0X	3	M/H/U/K	Average Daily Use	ADU
13	301-306 98X	6	M/H/U/K	Cummulative Use	CU
14	395-400 18X	6	Whole Cents	Direct Labor Cost for Repairs (excluding accidents)	DLC
15	419-425	7	Whole Cents	Total Parts Cost for Repairs (excluding accidents)	TPC

Note: All of the above values that can change on a monthly basis are shown as "this month" values. These include RC, OTL, OTX, OTP, DLC and TPC. CU accumulates continuously, and ADU is computed on the basis of CU. ADU is not month specific.

### 5.1 Reformating the Records

Program ARADO2 is used as a second step in the conversion process reduce the files from ARADO1 to an essential number of records. The first and last records for each vehicle were always retained, and among the others, only records in which a significant data element changed were written.

1. The following data elements never vary:

- Vehicle Registration Number (VRN).
- Management Code (MC).
- Life Expectancy (LE).
- Use Code (UC).

2. The following data elements are expected to change monthly, and a change in any of them would not cause the record to be written.

- Average Daily Use (ADU).
- Cumulative Use (CU).
- One-Time Repair Cost Limit (OTL).
- One-Time Repair Cost Exceeded (OTX).

3. The following data elements can change monthly, and if so, the record was written.

- Acceptance Date (AD).
- Standard Price (SP).
- Replacement Code (RC).

4. The record was written whenever the One-Time Repair Price (OTP) exceeded the One-Time Repair Limit.

5. The Total Parts Cost for Repairs (TPC) and the Direct Labor Cost for Repairs (DLC) do change monthly, and these were accumulated as running totals and simply printed each time a record was otherwise written.

Whenever a record is written, its first item is the number of the record for this vehicle in the ARADO1 file (e.g., 1 = first monthly record, and 12 = 12th monthly record). Each vehicle should have 12 records for each of 12 months in a year, except for new or salvaged vehicles during the year.

Other adjustments to the data by ARADO2 include deleting the first character of the Total Parts Cost, since it was always found to be a zero or a bracket. The One-Time Repair Price (OTR), the Direct Labor Cost (DLC) and the Total Parts Cost (TPC) were converted from whole cents into whole dollars. In addition, all numeric data elements were written in integer form, and thus all leading zeros were striped away. The output files from ARADO2 were thus of a better form for both visual scanning to numerical analyses.

Note that the Standard Price is included in the set of values that can change monthly. It was anticipated that the standard price of a vehicle would probably show one or two changes in each 12-month period so as to reflect price adjustments in the designated replacement vehicle. However, the adjustments to standard prices found on this VIMS tape revealed many inconsistencies. Changes to standard prices occurred most often in the last monthly records for some but not all vehicles. Instances of both price increases and decreases were found, and sometimes in records other than the last. Furthermore, among vehicles of the same type and model year with the same standard price in the first record, some did not receive any change while others received a range of changes. For example, listed below are the standard prices found in the first and last monthly records of ten D541 vehicles in this dataset.

#### Standard Prices from Monthly Records of Ten D541 Vehicles

Vehicles Model Year	First Record's Standard Price	Last Record's Standard Price
'667	\$7143	\$2857
'672	\$7143	\$4669
'672	\$4237	\$4237
'673	\$4237	\$4676
'674	\$4237	\$4676
'675	\$4237	\$4676
'676	\$7143	\$7143
'677	\$7143	\$6877
'677	\$7143	\$5572
'679	\$4237	\$4676

Note that the price given in the first record for each vehicle is either \$4237 or \$7143, which logically indicates two different D541 vehicle models. By comparison, prices that appear in the last monthly records for these same vehicles

show a great variety of changes. Without examining the records for the following year, it is unclear as to whether these last record prices become the first record prices of the following year's data, or whether these last record prices can be ignored. Nevertheless, the fact that such widely varied price changes are frequently observed in the VIMS data suggests that reasons for these changes need to be investigated. These changes certainly reflect price adjustments for reasons other than general inflation, suppliers' prices changes or technological differences in replacement vehicles.

#### 6 Analysis of Vehicles Exceeding Their One-Time Repair Limits

In previous sections was discussed the method by which the one-time repair limit is calculated in VIMS and how adjustments are made to a vehicle's standard price that cause proportional changes in the OTL values for these vehicles. Inconsistencies were noted in the standard price changes observed in the last monthly records for these vehicles, as can be seen by paging through the records shown in Appendix C. However, it was found that OTL values in the vehicle records did most always agree with whatever standard price was given as explained next.

Before compiling statistics for vehicles that had exceeded their one-time repair limits, the OTL values found in the data were compared to equations (1-3). It was found in the data for D, E and L vehicles that OTL was always computed on the basis of a vehicle's age from its acceptance date, and never upon its use. This indicates that either (1) vehicles are not being used anywhere close to their annual use standards, or (2) the VIMS computation of OTL is not computing  $OTL_2$  properly before selecting  $OTL_1$  as the lower of the two. Not one case was found in 3842 records for 347 vehicles where the value of OTL selected had been calculated on the basis of vehicle use.

The fact that  $OTL_1$  is lower than  $OTL_2$  for most all vehicles during their lifetimes is not unexpected. The vehicle shown in Figure 1 has an annual use standard of 8000 miles per year. However, in the first year, it was only used 5000 miles. Even if this vehicle were used 9000 miles in each of the following 3 years,  $OTL_1$  would still have been lower than  $OTL_2$ . Hence, we see that if the use of a

vehicle falls behind its standard or expected use up to that point in time, which is very probable for most vehicles at some age, then  $OTL_1$  is likely to remain lower than  $OTL_2$  for the remainder of that vehicle's life.

A few cases were found among roughly 10 vehicles in which  $OTL$  was different from  $OTL_1$ , but not because it was computed on the basis of vehicle use. These cases simply indicated a very inconsistent calculation of  $OTL$ , such as changing the age of the vehicle midstream. Moreover, the acceptance date remained the basis for  $OTL$  values, even when the model year of the vehicle and its acceptance date differed substantially, e.g. by as much as ten years. This use of the acceptance date may be the intended policy for cases in which a vehicle is returned from depot repair.

In order to examine just how sensitive repair or replace decisions might be to the one-time repair limit, program ARADO2 extracted a vehicle's record whenever its One-Time Repair Price (OTP) exceeded its one-time repair limit. Vehicles that had exceeded their one-time repair limits in a previous year would not be identified in this analysis. Listed in Table 6 are the numbers of D, E and L vehicles that had a OTP value greater than  $OTL$  recorded. The vehicles were grouped according to the percentage range by which their OTP exceeded their  $OTL$ . Within this one 12-month period, 10% of the D, E and L vehicles at this base had been estimated to require repairs that exceeded their one-time repair limits. More importantly, the total standard price of replacement vehicles for cases in which OTP was within 25% its  $OTL$  summed to \$146,000.

Previous discussions showed how dramatically the effects of inflation can change a vehicle's replacement price, and how varied the standard prices assigned to seemingly identical model vehicles can be. Given the margin for error that exists in properly adjusting standard prices for inflation and technological change, the \$146,000 worth of vehicles found above to have had exceeded their one-time repair limits by less than 25% might well have fallen within slightly inflated or otherwise adjusted limits. This indicates that the dollar amount involved in decisions to deny repair of Air Force vehicles because of the one-time repair limit is sensitive to the proper treatment of standard price changes.

Table 6: Analysis of Vehicles That Exceeded Their  
One-Time Repair Limits Within the Last Year

\*\*\* TOTAL NUMBER OF VEHICLES IN CLASS D = 135  
\*\*\* NUMBER OF D VEHICLES EXCEEDING OTL = 18

RANGE	No. of Vehicles	Total SP	Total OTL	Total OTP
0- 5%	0	0	0	0
5- 10%	0	0	0	0
10- 15%	0	0	0	0
15- 20%	2	76446	7645	8882
20- 25%	0	0	0	0
25- 50%	5	137423	14934	19592
50-100%	5	57713	6937	12207
100-500%	3	17208	3952	9994

\*\*\* TOTAL NUMBER OF VEHICLES IN CLASS E = 95  
\*\*\* NUMBER OF E VEHICLES EXCEEDING OTL = 13

RANGE	No. of Vehicles	Total SP	Total OTL	Total OTP
0- 5%	4	38926	3894	4001
5- 10%	1	10196	1020	1093
10- 15%	1	10196	1020	1123
15- 20%	1	10196	1020	1194
20- 25%	0	0	0	0
25- 50%	2	18534	1854	2364
50-100%	2	16676	1668	2921
100-500%	2	16676	1668	4044

\*\*\* TOTAL NUMBER OF VEHICLES IN CLASS L = 117  
\*\*\* NUMBER OF L VEHICLES EXCEEDING OTL = 4

RANGE	No. of Vehicles	Total SP	Total OTL	Total OTP
0- 5%	0	0	0	0
5- 10%	0	0	0	0
10- 15%	0	0	0	0
15- 20%	0	0	0	0
20- 25%	1	25927	2593	3162
25- 50%	2	33147	3315	4304
50-100%	0	0	0	0
100-500%	1	7220	722	1921

Note: RANGE = (OTP-OTL)\*100/OTL = percent y which OTL  
was found to exceed OTP. All other columns show  
totals for vehicles within these ranges.

It is also interesting to note by scanning through the output from ARADO2 that, for many vehicles, the one year accumulation of direct labor and total parts costs over the last 12 months of records shown, exceeded a vehicle's one-time repair limit while the repairs in any one month did not. It may have been preferable to retire those problem vehicles rather than continue with repairs. Both of these difficulties with the current use of the one-time repair limit require further analysis in order to determine their impact on the efficient allocation of vehicle buy expenditures.

## 7 Summary and Recommendations

Improved forecasts of vehicle repair and replacement needs could assist vehicle fleet managers and base commanders in preparing for future needs rather than having to react to sudden shortfalls in vehicle availability. This study recommends that the current procedure used to adjust the standard price of vehicles, which in turn affects their one-time repair limits be examined more thoroughly for its economic validity. While it is correct to adjust standard prices to reflect the price differences of replacement vehicles, the data indicates that current adjustments to the standard prices are very inconsistent and of such a magnitude as to have a significant impact on the dollar amount of the repair or replace decisions that they are affecting. The analysis showed that vehicles had exceeded their one-time repair limits by less than 25% in a significant number of cases. As a result, those vehicles were potentially denied repair and retired from service at times when repair may have been the preferred alternative.

Several aspects of the vehicle replacement code were also identified in this report as assumptions or rules that may not be universally appropriate to the wide range of daily vehicle uses, operating conditions, and mission support requirements of all Air Force installations. For example, a different weight or critical priority associated with the economic cost of vehicle downtime can greatly affect the best timing of replacement for that vehicle. The critical nature of some vehicles at certain bases may warrant special treatment, but any variance from standard replacement policies must be balanced against demands for uniform treatment within the vehicle buy program.



In many organizations, standardized procedures that lead to uniform management directives are often developed as cost effective responses to the need for efficiency, often at some compromise to special needs and circumstances. The Air Force vehicle buy program is a case in which the advantages of policy standardization are quite apparent. However, while the replacement code can provide for a consistent classification of vehicle conditions, it also overlooks the performance records and special requirements of individual vehicles. Hence, the implications of using a standardized replacement code on the cost and frequency of vehicle replacements in the vehicle buy program should also be examined.

While it is important to recognize the inherent difficulties with using a categorical vehicle condition rating for all vehicles as opposed to treating individual vehicles on a case-by-case basis, the approach of this research was to accept the need for a standardized index and thus look for ways in which the validity of this index could be improved. It appears that adjustments to standard prices currently maintained in VIMS may not be accounting for supplier's price changes in the correct manner, and that improvements in this regard are very possible after reasons for inconsistencies in the price adjustments are explained. Another concern mentioned in this report is the method by which vehicle life expectancies are estimated, since this depends upon engineering economic principles as explained.

The ultimate objective of improvements sought to current procedures is to increase the cost effectiveness of expenditures on vehicles and vehicle fleet management costs throughout the Air Force. To this end, repair or replace indicators such as the replacement code that are of direct consequence to the vehicle buy program should be designed to best reflect both the true economic value of a vehicle and its importance to emergency preparedness that the Air Force must consider in its vehicle fleet management directives.

#### Acknowledgements

The author would like to thank Major Dan King and Capt. James Van Scotter of the Air Force Logistics Management Center at Gunter AFS for their help in obtaining and explaining the Air Force documents and data used in this research.

## REFERENCES

1. Armour R.F. (1980) An Economic Analysis of Transit Bus Replacement. *Transit Journal*, Winter 1980.
2. Aronson J.E. and Aronofsky J.S. (1984) A Decision Support System for the Optimization of Equipment Replacement Models. Technical Report 83-OR-7. Department of Operations Research and Engineering Management, Southern Methodist University, Dallas, Texas.
3. Au T. and Au T.P. (1983) *Engineering Economics for Capital Investment Analysis*. Allyn and Bacon, Inc.
4. Brealey R.A. and Myers S.C. (1984) *Principles of Corporate Finance*. McGraw-Hill Book Company, New York.
5. Chand S. and Sethi S. (1979) Planning Horizon Procedures for Machine Replacement Models with Several Possible Replacement Alternatives. *Naval Research Logistics Quarterly* 29(3), pp. 483-493.
6. Department of the Air Force (1983) Air Force Manual 77-310 (Volume I): Acquisition, Management and Use of Motor Vehicles. Washington, D.C.
7. Department of the Air Force (1979) Air Force Technical Order 00-25-049: Maximum Repair Allowances, Repair Codes, and Priority Buy Program for USAF Vehicles. Washington, D.C.
8. Department of the Air Force (1979) Air Force Technical Order 36A-1-1301: Vehicle Management Index File. Washington, D.C.
9. Foerster, J., Miller F., Kosinski M. and Rueda A. (1983) Management Tools for Bus Maintenance — Current Practices and New Methods. Urban Transportation Center, University of Illinois at Chicago Circle, Final Report to the Urban Mass Transportation Administration.
10. Kliem B. and Goeddel D. (1983) Management Tools for Improving Maintenance Performance. *Bus Maintenance Improvement*. Transportation Research Board Special Report #198, Washington D.C.
11. Newnan D.G. (1983) *Engineering Economic Analysis*, (Second Edition). Engineering Press, San Jose, CA.
12. Pierskala W.P. and Voelker J.A. (1976) A Survey of Maintenance Models: The Control and Surveillance of Deteriorating Systems. *Naval Research Logistics Quarterly* 23(3), pp. 353-388.
13. Rapp B. (1974) *Models for Optimal Investment and Maintenance Decisions*. Halsted Press, Stockholm, Sweden.
14. Sethi S. and Chand S. (1979) Planning Horizon Procedures for Machine Replacement Models. *Management Science* 25(2), pp. 140-151.

#### Appendix A: Engineering Economic Calculations

Calculations of equivalent uniform annual cost and vehicle salvage values discussed earlier in this report were performed with the following formulas.

Given the cost in each period  $C_t$  for  $t=0$  to  $N$  periods, the cost present value (CPV) of these expenditure amounts at time 0 equals:

$$CPV = \sum_{t=0}^N C_t * [P|F, i, t] = \sum_{t=0}^N C_t / (1+i)^t$$

Having found CPV at time 0, EUAC is easily calculated as:

$$EUAC = CPV * [U|P, i, N] = CPV * i(1+i)^N / (1+i)^N - 1$$

The time for which EUAC has its minimum value is the optimal replacement time of a vehicle. In an efficient capital market, all activities can supposedly take place at minimum cost. Hence, the salvage value of a vehicle at any time prior to its replacement time is the difference in the present value at time  $t$  of its remaining operation and maintenance costs and the present value at time  $t$  of the minimum EUAC times the remaining number of years. For example, if the optimal replacement time of a vehicle were at the end of year 10, the the economic salvage value of this vehicle at the end of year 7 (given that it has performed and is likely to perform as expected and currently has no unusual repair needs) can be calculated as:

$$SV_t = \sum_{t=8}^{10} EUAC^* / (1+i)^{t-7} - \sum_{t=8}^{10} C_t / (1+i)^{t-7}$$

Special formulas can be used to simplify the above calculations for uniformly increasing gradients of expenditures. Additional explanation can be found in Au and Au [3].

#### Appendix B: Programs Used to Retrieve and Tabulate Vehicle Data from the VIMS Tape

The following pages contain listings of four programs used to retrieve the data from tape used in this study and perform various calculations. The general purpose and use of these programs were explained in the report.

A sample of roughly 40 records output by ARADO1 are shown following its listing. Records for different vehicles can be distinguished by changes in the last four digits of the VRN. Since there were 12 records for most every vehicle, and not every record was needed, program ARADO2 was used to identify and write out only the required records as also explained in the report. The output from ARADO2 for D, E and L vehicles is in Appendix C.

Program ARADO3 was used to identify and group vehicles that exceeded their one-time repair limits within the past year. Program ARADO4 was used to check whether the one-time repair limit for any vehicle was ever calculated on the basis of use instead of age.

C \* PROGRAM ARAD01 TO RETRIEVE DATA FIELDS FROM THE ARAD6T TAPE \*  
 C B. JANSON, CARNEGIE-MELLON UNIVERSITY, PITTSBURGH, PA 15213  
 C

IMPLICIT INTEGER (A-Z)  
 DOUBLE PRECISION IFILE4,IFILE7,VR(20)

C  
 C UNIT 4 = DISK INPUT  
 C UNIT 5 = TERMINAL INPUT  
 C UNIT 6 = TERMINAL OUTPUT  
 C UNIT 7 = DISK OUTPUT  
 C

C Listed below are the data elements stored in the VRN vector.  
 C

Field#	#Chars	Units	Data Element Name	Abbrev.
1	8	Alphanumeric	Vehicle Registration Number	VRN
2	4	Alphanumeric	Management Code	MC
3	3	Whole Vehicles	Vehicle Equivalents	VEQ
4	4	Year/Month	Acceptance Date	AD
5	6	Whole Dollars	Standard Price	SP
6	1	Alpha	Replacement Code	RC
7	2	Whole Years	Life Expectancy	LE
8	6	Whole Dollars	One-Time Repair Cost Limit	OTL
9	1	" "=no;"-=yes	One-Time Repair Cost Exceeded	OTX
10	7	Whole Cents	One-Time Repair Cost Price	OTP
11	1	M/H/U/K	Use Code	UC
12	3	M/H/U/K	Average Daily Use	ADU
13	6	M/H/U/K	Cummulative Use	CU
14	6	Whole Cents	Direct Labor Cost for Repairs	DLC
15	7	Whole Cents	Total Parts Cost for Repairs	TPC

C  
 C OPEN(UNIT=6,DEVICE='TTY')  
 C WRITE(6,401)  
 C 401 FORMAT(/1X,'\*\*\* AIR FORCE VEHICLE CONDITION RESEARCH \*\*\* ')  
 C WRITE(6,503)  
 C 503 FORMAT(/1X,'TYPE INPUT FILENAME AND PRESS RETURN'/)  
 C READ (6,400) IFILE4  
 C WRITE(6,504)  
 C 504 FORMAT(/1X,'TYPE OUTPUT FILENAME AND PRESS RETURN'/)  
 C READ (6,400) IFILE7  
 C WRITE(6,505)  
 C 505 FORMAT(/1X,'HOW MANY RECORDS TO SKIP FROM THE INPUT FILE?'/)  
 C READ (6,\*) M  
 C WRITE(6,506)  
 C 506 FORMAT(/1X,'HOW MANY RECORDS TO READ FROM THE INPUT FILE?'/)  
 C READ (6,\*) N  
 C 400 FORMAT(A10)

C  
 C OPEN(UNIT=4,DEVICE='DSK',FILE=IFILE4)  
 C OPEN(UNIT=7,DEVICE='DSK',FILE=IFILE7)

C  
 C IF(M.EQ.0) GO TO 1  
 C DO 5 I=1,M  
 C 5 READ (4,100) (VR(J),J=1,15)

C  
 C 1 DO 10 I=1,N  
 C READ (4,100) (VR(J),J=1,15)  
 C 100 FORMAT(2X,A8,A4,33X,A3,30X,A4,9X,A6,A1,9X,A2,6X,  
 C > A6,A1,A7,165X,A1,A3,A6,88X,A6,18X,A7)  
 C WRITE(7,110) (VR(J),J=1,15)  
 C 110 FORMAT(A8,1X,A4,1X,A3,1X,A4,1X,A6,1X,A1,1X,A2,1X,

> A6,1X,A1,1X,A7,1X,A1,1X,A3,1X,A6,1X,A6,1X,A7)  
10 CONTINUE

C  
999 STOP  
END

\*\*\* Output from ARAD01 \*\*\*

VRN	MC	VEO	AD	SP	RC	LE	OTL	OTX	OTP	UC	ADU	CU	DLC	TPC
72D00924	D522	055	7202	082527	D	17	030098	-	0000000	H	000	000700	000000	0000000
72D00924	D522	055	7202	082527	D	17	029734	-	0000000	H	000	000700	000000	0000000
72D00924	D522	055	7202	082527	D	17	029370	-	0000000	H	000	000700	000000	0000000
72D00924	D522	055	7202	082527	D	17	029006	-	0000000	H	000	000700	000000	0000000
72D00924	D522	055	7202	038804	D	17	013467	-	0000000	H	000	000700	000000	0000000
67D00471	D541	016	1167	007143	B	12	000714	-	0000000	H	001	003244	000000	{022794
67D00471	D541	016	1167	007143	B	12	000714	-	0154495	H	001	003251	066564	{008893
67D00471	D541	016	1167	007143	B	12	000714	-	0000000	H	001	003269	000000	0000000
67D00471	D541	016	1167	007143	B	12	000714	-	0000000	H	001	003289	000000	0000000
67D00471	D541	016	1167	007143	B	12	000714	-	0000000	H	001	003281	000000	0000000
67D00471	D541	016	1167	007143	B	12	000714	-	0000000	H	001	003270	000000	{004212
67D00471	D541	016	1167	007143	B	12	000714	-	0000000	H	000	003270	033763	{008670
67D00471	D541	016	1167	007143	B	12	000714	-	0000000	H	000	003292	000000	0000000
67D00471	D541	016	1167	007143	B	12	000714	-	0000000	H	001	003291	019798	{008894
67D00471	D541	016	1167	007143	B	12	000714	-	0000000	H	001	003296	000000	0000000
67D00471	D541	016	1167	007143	B	12	000714	-	0000000	H	000	003310	004292	0000000
67D00471	D541	016	1167	002857	B	12	000286	-	0000000	H	000	003338	000000	0000000
72D00390	D541	016	7209	007143	D	12	001339	-	0000000	H	001	002526	000000	0000000
72D00390	D541	016	7209	007143	D	12	001295	-	0000000	H	001	002527	002064	0000000
72D00390	D541	016	7209	007143	D	12	001250	-	0000000	H	001	002533	000000	0000000
72D00390	D541	016	7209	007143	D	12	001205	-	0000000	H	000	002533	000000	{004052
72D00390	D541	016	7209	007143	D	12	001161	-	0000000	H	000	002541	072511	{003458
72D00390	D541	016	7209	007143	D	12	001116	-	0000000	H	000	002548	004180	0000000
72D00390	D541	016	7209	007143	D	12	001071	-	0000000	H	000	002560	014772	0000000
72D00390	D541	016	7209	007143	D	12	001027	-	0000000	H	016	002562	033138	0000000
72D00390	D541	016	7209	007143	D	12	000982	-	0000000	H	013	002568	018766	{034896
72D00390	D541	016	7209	007143	D	12	000938	-	0000000	H	010	002570	017816	{022732
72D00390	D541	016	7209	007143	D	12	000893	-	0000000	H	007	002578	036483	{008132
72D00390	D541	016	7209	004669	D	12	000554	-	0000000	H	005	002578	002653	0000000
72D00432	D541	016	7210	004237	D	12	000821	-	0000000	H	000	002387	007740	0000000
72D00432	D541	016	7210	004237	D	12	000794	-	0000000	H	001	002416	000000	0000000
72D00432	D541	016	7210	004237	D	12	000768	-	0000000	H	001	002450	008216	0000000
72D00432	D541	016	7210	004237	D	12	000741	-	0000000	H	001	002444	009834	{039302
72D00432	D541	016	7210	004237	D	12	000715	-	0000000	H	001	002464	000000	0000000
72D00432	D541	016	7210	004237	D	12	000689	-	0000000	H	001	002474	000000	0000000
72D00432	D541	016	7210	004237	D	12	000662	-	0000000	H	001	002460	014243	{004212
72D00432	D541	016	7210	004237	D	12	000636	-	0000000	H	001	002461	031578	{009108
72D00432	D541	016	7210	004237	D	12	000609	-	0000000	H	000	002470	000000	0000000
72D00432	D541	016	7210	004237	D	12	000583	-	0000000	H	000	002475	000000	0000000
72D00432	D541	016	7210	004237	D	12	000556	-	0000000	H	000	002517	000000	0000000
72D00432	D541	016	7210	004237	D	12	000530	-	0000000	H	001	002589	009551	0000000
73D00698	D541	016	7404	004237	D	12	001298	-	0000000	H	001	000809	035604	0000000
73D00698	D541	016	7404	004237	D	12	001271	-	0000000	H	405	000809	000000	0000000
73D00698	D541	016	7404	004237	D	12	001245	-	0000000	H	378	0008769	015677	{005104
73D00698	D541	016	7404	004237	D	12	001218	-	0000000	H	305	0008781	000000	0000000
73D00698	D541	016	7404	004237	D	12	001192	-	0000000	H	230	000866	000000	0000000
73D00698	D541	016	7404	004237	D	12	001165	-	0000000	H	157	0009015	021947	0000000
73D00698	D541	016	7404	004237	D	12	001139	-	0000000	H	083	0009051	020047	{009750
73D00698	D541	016	7404	004237	D	12	001112	-	0000000	H	009	0009051	018465	0000000

C \* PROGRAM ARADO2 TO REFORMAT DATA FIELDS FROM THE ARAD6T TAPE \*  
 C B. JANSON, CARNEGIE-MELLON UNIVERSITY, PITTSBURGH, PA 15213

C

IMPLICIT INTEGER (A-Z)  
 DOUBLE PRECISION IFILE4,IFILE7

C

C UNIT 4 = DISK INPUT  
 C UNIT 5 = TERMINAL INPUT  
 C UNIT 6 = TERMINAL OUTPUT  
 C UNIT 7 = DISK OUTPUT

C

C Listed below are the variable names used in this program.

#Chars	Units	Variable Name	Abbrev.
4	Alphanumeric	Veh. Reg. Number (1st half)	VRN1
4	Alphanumeric	Veh. Reg. Number (2nd half)	VRN2
4	Alphanumeric	Management Code	MC
3	Whole Vehicles	Vehicle Equivalents	VEQ
4	Year/Month	Acceptance Date	AD
6	Whole Dollars	Standard Price	SP
1	Alpha	Replacement Code	RC
2	Whole Years	Life Expectancy	LE
6	Whole Dollars	One-Time Repair Cost Limit	OTL
1	" "=no;"-=yes	One-Time Repair Cost Exceeded	OTX
7	Whole Cents	One-Time Repair Cost Price	OTP
1	M/H/U/K	Use Code	UC
3	M/H/U/K	Average Daily Use	ADU
6	M/H/U/K	Cummulative Use	CU
6	Whole Cents	Direct Labor Cost for Repairs	DLC
6	Whole Cents	Total Parts Cost for Repairs	TPC

C

C Notes: OTP, DLC and TPC are converted to whole dollars in this program.  
 C Both DLC and TPC are input for individual months, but are summed over  
 C preceeding months and output that way. Other than the first and last  
 C records, which are output for every vehicle, only records in which a  
 C vehicle's acceptance data, standard price, or replacement code changed,  
 C or in which a one-time repair price was recorded, are written to the  
 C output file. Vehicle Equivalents are not written to the output file.

C

```

OPEN(UNIT=6,DEVICE='TTY')
WRITE(6,401)
401 FORMAT(/1X,'*** AIR FORCE VEHICLE CONDITION RESEARCH *** ')
WRITE(6,503)
503 FORMAT(/1X,'TYPE INPUT FILENAME AND PRESS RETURN'/)
READ (6,400) IFILE4
WRITE(6,504)
504 FORMAT(/1X,'TYPE OUTPUT FILENAME AND PRESS RETURN'/)
READ (6,400) IFILE7
WRITE(6,506)
506 FORMAT(/1X,'HOW MANY RECORDS TO READ FROM THE INPUT FILE?'/)
READ (6,*) N
400 FORMAT(A10)

```

C

```

OPEN(UNIT=4,DEVICE='DSK',FILE=IFILE4)
OPEN(UNIT=7,DEVICE='DSK',FILE=IFILE7)

```

C

```

NV=0
REC=1
VREC=1
READ (4,100) VRN11,VRN21,MC1,VEQ1,AD1,SP1,RC1,LE1,OTL1,OTX1,OTP1,
> UC1,ADU1,CU1,DLC1,TPC1

```

```

      OTP1=OTP1/100
      DLC1=DLC1/100
      TPC1=TPC1/100
      WRITE(7,110) VREC,VRN11,VRN21,MC1,AD1,SP1,RC1,LE1,OTL1,OTX1,OTP1,
> UC1,ADU1,CU1,DLC1,TPC1
111 REC=REC+1
      IF(REC.GT.N) GO TO 999
      READ (4,100) VRN12,VRN22,MC2,VEQ2,AD2,SP2,RC2,LE2,OTL2,OTX2,OTP2,
> UC2,ADU2,CU2,DLC2,TPC2
      OTP2=OTP2/100
      DLC2=DLC2/100
      TPC2=TPC2/100
      IF(VRN22.EQ.VRN21) GO TO 210
      IF(PRNT.NE.1)
> WRITE(7,110) VREC,VRN11,VRN21,MC1,AD1,SP1,RC1,LE1,OTL1,OTX1,OTP1,
> UC1,ADU1,CU1,DLC1,TPC1
      WRITE(7,*)
      PRNT=0
      VREC=1
      DLCT=DLC2
      TPCT=TPC2
      WRITE(7,110) VREC,VRN12,VRN22,MC2,AD2,SP2,RC2,LE2,OTL2,OTX2,OTP2,
> UC2,ADU2,CU2,DLC2,TPC2
      GO TO 222
C
210 PRNT=0
      VREC=VREC+1
      DLCT=DLCT+DLC2
      TPCT=TPCT+TPC2
      IF(AD2.EQ.AD1.AND.SP2.EQ.SP1.AND.RC2.EQ.RC1.AND.OTP2.LT..8*OTL2)
> GO TO 222
      PRNT=1
      WRITE(7,110) VREC,VRN12,VRN22,MC2,AD2,SP2,RC2,LE2,OTL2,OTX2,OTP2,
> UC2,ADU2,CU2,DLC2,TPC2
C
222 VRN11=VRN12
      VRN21=VRN22
      MC1=MC2
      AD1=AD2
      SP1=SP2
      RC1=RC2
      LE1=LE2
      OTL1=OTL2
      OTX1=OTX2
      OTP1=OTP2
      UC1=UC2
      ADU1=ADU2
      CU1=CU2
      DLC1=DLC2
      TPC1=TPC2
      GO TO 111
C
100 FORMAT(A4,A4,1X,A4,1X,I3,1X,I4,1X,I6,1X,A1,1X,I2,1X,
> I6,1X,A1,1X,I7,1X,A1,1X,I3,1X,I6,1X,I6,2X,I6)
110 FORMAT(3X,I3,1X,A4,A4,1X,A4,1X,I4,1X,I6,1X,A1,1X,I2,1X,
> I6,1X,A1,1X,I6,1X,A1,1X,I3,1X,I6,1X,I5,2X,I5)
C
999 STOP
      END

```



0 • PROGRAM ARAD03 TO EXAMINE VEHICLES THAT HAVE EXCEEDED THEIR •  
 0 • ONE-TIME REPAIR LIMITS WITHIN THE PAST 12 MONTHS OF RECORDS •  
 0 9. JANSON, CARNEGIE-MELLON UNIVERSITY, PITTSBURGH, PA 15213  
 0

IMPLICIT INTEGER (A-Z)  
 DOUBLE PRECISION (FILE4,IFILE7,RANGE(8))  
 DIMENSION NUMVEH(8),TSP(8),TOTL(8),TOTP(8)

UNIT 4 = DISK INPUT  
 UNIT 5 = TERMINAL INPUT  
 UNIT 6 = TERMINAL OUTPUT  
 UNIT 7 = DISK OUTPUT

Listed below are the variable names used in this program.

#Chars	Units	Variable Name	Abbrev.
4	Alphanumeric	Ven. Reg. Number (1st half)	VRN
4	Alphanumeric	Ven. Reg. Number (2nd half)	VRN
4	Alphanumeric	Management Code	MC
4	Year/Month	Acceptance Date	AD
6	Whole Dollars	Standard Price	SP
1	Alpha	Replacement Code	RC
2	Whole Years	Life Expectancy	LE
6	Whole Dollars	One-Time Repair Cost Limit	OTL
1	" " = no; "-" = yes	One-Time Repair Cost Exceeded	OTX
7	Whole Cents	One-Time Repair Cost Price	OTP
1	M/H/U/K	Use Code	UC
3	M/H/U/K	Average Daily Use	ADU
6	M/H/U/K	Cumulative Use	CU
6	Whole Cents	Direct Labor Cost for Repairs	DLC
6	Whole Cents	Total Parts Cost for Repairs	TPC

0 Note: OTP, DLC and TPC are converted to whole dollars in this program.  
 0 Both DLC and TPC are now cumulative over preceeding months as summed  
 0 in program ARAD02.  
 0

```

    OPEN(UNIT=6,DEVICE='TTY')
    WRITE(6,401)
401 FORMAT(1X,'*** AIR FORCE VEHICLE CONDITION RESEARCH ***')
    WRITE(6,503)
503 FORMAT(1X,'TYPE INPUT FILENAME AND PRESS RETURN')
    READ(6,400) IFILE4
    WRITE(6,504)

504 FORMAT(1X,'TYPE OUTPUT FILENAME AND PRESS RETURN')
    READ(6,400) IFILE7
    WRITE(6,506)
506 FORMAT(1X,'HOW MANY RECORDS TO READ FROM THE INPUT FILE?')
    READ(6,*) N
400 FORMAT(A10)
  
```

```

    OPEN(UNIT=4,DEVICE='DSK',FILE=IFILE4)
    OPEN(UNIT=7,DEVICE='DSK',FILE=IFILE7)
  
```

```

    DO 10 I=1,N
      NUMVEH(I)=0
      TSP(I)=0
      TOTL(I)=0
10 TOTP(I)=0
  
```

```

    RANGE(1)=' 0- 50'
  
```

21140

```

RANGE(2)=' 5- 10%'
RANGE(3)=' 10- 15%'
RANGE(4)=' 15- 20%'
RANGE(5)=' 20- 25%'
RANGE(6)=' 25- 50%'
RANGE(7)=' 50-100%'
RANGE(8)='100-500%'

C
REC=0
NVEHS=1
111 REC=REC+1
IF(REC.GT.N) GO TO 999
READ(4,100) VREC,VRN1,VRN2,MC,AD,SP,RC,LE,OTL,OTX,OTP,
> UC,ADU,CU,OLC,TPC
IF(VRN1.EQ.' ') NVEHS=NVEHS+1
IF(VRN1.EQ.' ') GO TO 111
IF(OTL.LT.10) GO TO 111
IF(OTP.GT.0.AND.OTP.LT.OTL) WRITE(6,601)
601 FORMAT(/1X,'*** OTP FOUND THAT IS LESS THAN OTL. ***'/)
IF(OTP.LT.OTL) GO TO 111
IF(OTP.GE.OTL*2.00) ORANGE=8
IF(OTP.LT.OTL*2.00.AND.OTP.GE.OTL*1.50) ORANGE=7
IF(OTP.LT.OTL*1.50.AND.OTP.GE.OTL*1.25) ORANGE=6
IF(OTP.LT.OTL*1.25.AND.OTP.GE.OTL*1.20) ORANGE=5
IF(OTP.LT.OTL*1.20.AND.OTP.GE.OTL*1.15) ORANGE=4
IF(OTP.LT.OTL*1.15.AND.OTP.GE.OTL*1.10) ORANGE=3
IF(OTP.LT.OTL*1.10.AND.OTP.GE.OTL*1.05) ORANGE=2
IF(OTP.LT.OTL*1.05.AND.OTP.GE.OTL*1.00) ORANGE=1
NUMVEH(ORANGE)=NUMVEH(ORANGE)+1
TSP(ORANGE)=TSP(ORANGE)+SP
TOTL(ORANGE)=TOTL(ORANGE)+OTL
TOTP(ORANGE)=TOTP(ORANGE)+OTP
GO TO 111

C
100 FORMAT(1X,13,1X,A4,A4,1X,A4,1X,14,1X,16,1X,A1,1X,12,1X,
> 16,1X,A1,1X,15,1X,A1,1X,13,1X,16,1X,15,2X,15)

C
999 NVEHS=NVEHS+1
WRITE(7,109) NVEHS
109 FORMAT(/1X,'TOTAL NUMBER OF VEHICLES = ',13//
> ' RANGE NUMVEH TSP TOTL TOTP'/)
WRITE(7,110) RANGE(1),NUMVEH(1),TSP(1),TOTL(1),TOTP(1),I=1,8)
110 FORMAT(A8,2X,15,19,17,17)
STOP
END

```

C • PROGRAM ARADO<sup>4</sup> TO COUNT THE NUMBER OF VEHICLE RECORDS THAT •  
 C • ONE-TIME REPAIR LIMIT IS A FUNCTION OF USE RATHER THAN AGE •  
 C B. JANSEN, CARNEGIE-MELLON UNIVERSITY, PITTSBURGH, PA 15213  
 C

IMPLICIT INTEGER (A-Z)  
 DOUBLE PRECISION IFILE4,IFILE7  
 REAL AGE,LE,OTLX

C  
 C UNIT 4 = DISK INPUT  
 C UNIT 5 = TERMINAL INPUT  
 C UNIT 6 = TERMINAL OUTPUT  
 C UNIT 7 = DISK OUTPUT

C Listed below are the variable names used in this program.

#Chars	Units	Variable Name	Abbrev.
2	Year	VRN Model Year (Chars 1-2)	MY
2	Alphanumeric	Veh. Reg. Number (Chars 3-4)	VRN1
4	Alphanumeric	Veh. Reg. Number (Chars 5-8)	VRN2
4	Alphanumeric	Management Code	MC
3	Whole Vehicles	Vehicle Equivalents	VEQ
4	Year	Acceptance Date	ADY
4	Month (1-12)	Acceptance Date	ADM
6	Whole Dollars	Standard Price	SP
1	Alpha	Replacement Code	RC
2	Whole Years	Life Expectancy	LE
6	Whole Dollars	One-Time Repair Cost Limit	OTL
1	" "=no;"-=yes	One-Time Repair Cost Exceeded	OTX
7	Whole Cents	One-Time Repair Cost Price	OTP
1	M/H/U/K	Use Code	UC
3	M/H/U/K	Average Daily Use	ADU
6	M/H/U/K	Cumulative Use	CU
6	Whole Cents	Direct Labor Cost for Repairs	DLC
6	Whole Cents	Total Parts Cost for Repairs	TPC

C PEN(UNIT=6,DEVICE='TTY')  
 C WRITE(6,401)  
 C 401 FORMAT(/IX,'\*\*\* AIR FORCE VEHICLE CONDITION RESEARCH \*\*\* ')  
 C WRITE(6,503)  
 C 503 FORMAT(/IX,'TYPE INPUT FILENAME AND PRESS RETURN'/)  
 C READ (6,400) IFILE4  
 C WRITE(6,504)  
 C 504 FORMAT(/IX,'TYPE OUTPUT FILENAME AND PRESS RETURN'/)  
 C READ (6,400) IFILE7  
 C WRITE(6,506)  
 C 506 FORMAT(/IX,'HOW MANY RECORDS TO READ FROM THE INPUT FILE?'/)  
 C READ (6,\*) N  
 C 400 FORMAT(A10)  
 C  
 C OPEN(UNIT=4,DEVICE='DSK',FILE=IFILE4)  
 C OPEN(UNIT=7,DEVICE='DSK',FILE=IFILE7)  
 C  
 C REC=1  
 C VREC=1  
 C TIME=1  
 C READ (4,100) MY1,VRN11,VRN21,MC1,VEQ1,ADY1,ADM1,SP1,RC1,LE1,  
 C > OTL1,OTX1,OTP1,UC1,ADU1,CU1,DLC1,TPC1  
 C 100 FORMAT(I2,A2,A4,IX,A4,IX,I3,IX,I2,I2,IX,I6,IX,A1,IX,I2,IX,  
 C > I6,IX,A1,IX,I7,IX,A1,IX,I3,IX,I6,IX,I6,2X,I6)  
 C  
 C IF(ADY1.LT.60) GO TO 111

```

      IF (ABS(MY1-ADY1).LE.1) GO TO 205
      WRITE(7,109) VRN21,MY1,ADY1
109  FORMAT(/1X,'>>> MY NOT EQUAL TO ADY: VRN21 = ,A4,2X,4HMY = ,I3,
> 2X,5HADY = ,I3,
      ADY1=MY1
      ADM1=7
      C
      C
205  AGE=(83-ADY1)*12 / (6+TIME-ADM1)
      LE=LE1*12
      IF (AGE.LE.LE) OTLX=SP1*(1.0-0.9*AGE/LE)
      IF (AGE.GT.LE) OTLX=0.1*SP1
      IF (ABS(OTLX-OTL1).GT.SP1/LE)
      >      WRITE(7,110) VRN21,SP1,OTL1,OTLX,AGE,LE
110  FORMAT(/1X,'*** OTL1 NOT EQUAL TO OTL: ',3X,5HVRN = ,A4/5X,4HSP = ,
> 16,2X,5HOTL = ,16,2X,5HOTL1 = ,F7.0,2X,5HAGE = ,F5.0,2X,4HLE = ,F5.0)
      C
111  REC=REC+1
      IF (REC.GT.N) GO TO 999
      READ (4,100) MY2,VRN12,VRN22,MC2,VEQ2,ADY2,ADM2,SP2,RC2,LE2,
      >      OTL2,CTX2,OTP2,UC2,ADU2,CU2,DLC2,TPC2
      IF (VRN22.EQ.VRN21) GO TO 210
      VREC=0
      TIME=0
      C
210  VREC=VREC+1
      TIME=TIME+1
      IF (ADY2.LT.60) GO TO 111
      IF (ABS(MY2-ADY2).LE.1) GO TO 215
      WRITE(7,109) VRN22,MY2,ADY2
      ADY2=MY2
      ADM2=7
      C
      C
215  AGE=(83-ADY2)*12 / (6+TIME-ADM2)
      LE=LE2*12
      IF (AGE.LE.LE) OTLX=SP2*(1.0-0.9*AGE/LE)
      IF (AGE.GT.LE) OTLX=0.1*SP2
      IF (ABS(OTLX-OTL2).GT.SP2/LE)
      >      WRITE(7,110) VRN22,SP2,OTL2,OTLX,AGE,LE
      C
      MY1=MY2
      VRN11=VRN12
      VRN21=VRN22
      MC1=MC2
      ADY1=ADY2
      ADM1=ADM2
      SP1=SP2
      RC1=RC2
      LE1=LE2
      OTL1=OTL2
      CTX1=CTX2
      OTP1=OTP2
      UC1=UC2
      ADU1=ADU2
      CU1=CU2
      DLC1=DLC2
      TPC1=TPC2
      GO TO 111
      C
999  STOP
      END

```

### Appendix C Listing of Output from Program ARADO2

The following pages contain the output files from program ARADO2. The records shown for D, E and L class vehicles are all records in which a significant data element to this study changed within the 12-month period of data shown by this tape for a particular base.

The columns contain, from the left to right, the following data items.

Units	Variable Name	Abbrev.
1. Integer	Monthly Record Number (1-12)	
2. Alphanumeric	Vehicle Registration Number	VRN2
3. Alphanumeric	Management Code	MC
4. Year/Month	Acceptance Date	AD
5. Whole Dollars	Standard Price	SP
6. Alpha	Replacement Code	RC
7. Whole Years	Life Expectancy	LE
8. Whole Dollars	One-Time Repair Cost Limit	OTL
9. " "no;"="yes	One-Time Repair Cost Exceeded	OTX
10. Whole Cents	One-Time Repair Cost Price	OTP
11. M/H/U/Y	Use Code	UC
12. M/H/U/Y	Average Daily Use	ADU
13. M/H/U/Y	Cummulative Use	CU
14. Whole Cents	Direct Labor Cost for Repairs	DLC
15. Whole Cents	Total Parts Cost for Repairs	TPC

Data items OTP, DLC and TPC are converted from whole cents, as they are recorded to the VIMS tape, to whole dollars in this output. Both DLC and TPC are input for individual months, but are summed over preceeding months and output that way. Other than the first and last records, which are output for every vehicle, only records in which a vehicle's acceptance date, standard price, or replacement code changed, or in which a one-time repair price was recorded, are written to the output file. Vehicle equivalents, a data item originally retrieved by ARADO1 from the VIMS tape, is not written to the ARADO2 output files since it was not needed for this study.

1	72D00924	D542	7202	82527	D	17	30098	-	O	H	0	700	0	0
5	72D00924	D542	7202	38804	D	17	13467	-	O	H	0	700	0	0
1	67D00471	D541	7143	7143	B	12	714	-	O	H	1	3244	0	227
2	67D00471	D541	7143	7143	B	12	714	-	1544	H	1	3251	665	315
12	67D00471	D541	7143	2957	B	12	296	-	O	H	0	3338	1241	531
1	72D00390	D541	7209	7143	D	12	1339	-	O	H	1	2526	0	0
12	72D00390	D541	7209	4669	D	12	554	-	O	H	5	2578	2019	730
1	72D00432	D541	7210	4237	D	12	821	-	O	H	0	2387	77	0
12	72D00432	D541	7210	4237	D	12	530	-	O	H	1	2589	809	526
1	73D00698	D541	7404	4237	D	12	1298	-	O	H	1	50809	356	0
12	73D00698	D541	7404	4676	D	12	1111	-	O	H	517	9500	1647	433
1	73D00901	D541	7301	4237	D	12	900	-	O	H	1	841	0	0
12	73D00901	D541	7301	4676	D	12	672	-	O	H	1	971	268	78
1	75D00361	D541	7506	4237	R	12	1668		O	H	0	1981	0	0
12	75D00361	D541	7506	4676	R	12	1520		O	H	1	2128	1694	612
1	75D00378	D541	7506	4237	R	12	1668		O	H	2	2870	0	0
12	75D00378	D541	7506	4676	R	12	1520		O	H	4	3478	1953	932
1	75D00400	D541	7506	4237	R	12	1668		O	H	2	14037	41	0
4	75D00400	D541	7506	4237	R	12	1589		2431	H	2	14141	745	1194
12	75D00400	D541	7506	4676	R	12	1520		O	H	2	14499	1606	1591
1	75D00417	D541	7506	4237	R	12	1668		O	H	359	19020	0	0
12	75D00417	D541	7506	4676	R	12	1520		O	H	1	1390	1866	733
1	75D00423	D541	7506	4237	R	12	1668		O	H	3	12779	526	130
3	75D00423	D541	7506	4237	R	12	1615		2350	H	2	12807	1804	782
12	75D00423	D541	7506	4676	R	12	1520		O	H	2	15152	2459	985
1	76D00246	D541	7608	7143	R	12	3438		O	H	4	965	0	0
12	76D00246	D541	7608	7143	R	12	2946		O	H	0	697	234	41
1	76D00247	D541	7608	7143	R	12	3438		O	H	1	993	0	0
12	76D00247	D541	7608	7143	R	12	2946		O	H	1	1505	635	479
1	76D00248	D541	7608	7143	R	12	3438		O	H	4	1104	0	0
12	76D00248	D541	7608	7143	R	12	2946		7738	H	09	1249	3392	3662
1	76D00292	D541	7609	7143	R	12	3482	0	O	H	8	2559	0	0
12	76D00292	D541	7609	7143	R	12	2991	0	O	H	3	1848	1286	222
1	77D00045	D541	7708	7143	T	12	3973	0	O	H	1	3940	443	391
2	77D00045	D541	7708	7143	R	12	3929	0	O	H	1	3978	509	391
12	77D00045	D541	7708	6877	R	12	3353	0	O	H	0	4200	1662	961
1	77D00046	D541	7708	7143	T	12	3973	0	O	H	1	3381	0	0
2	77D00046	D541	7708	7143	P	12	3929	0	O	H	1	3389	123	2
12	77D00046	D541	7708	6877	R	12	3353	0	O	H	1	3495	1208	994
1	77D00106	D541	7710	7143	T	12	4063	0	O	H	4	4704	314	510
4	77D00106	D541	7710	7143	R	12	3929	0	O	H	6	5095	788	708
12	77D00106	D541	7710	6877	R	12	3438	0	O	H	2	5597	2152	1215

1	77D00108	D541	7710	7143	T	12	4063	0	0	H	0	4410	0	500
4	77D00108	D541	7710	7143	R	12	3929	0	0	H	209	11706	498	523
12	77D00108	D541	7710	6877	R	12	3438	0	0	H	46	5632	1944	1069
1	77D00134	D541	7709	7143	T	12	4018	0	0	H	1	2048	41	0
3	77D00134	D541	7709	7143	R	12	3929	0	0	H	2	2139	41	0
12	77D00134	D541	7709	5572	R	12	2751	0	0	H	1	2208	664	433
1	77D00135	D541	7709	7143	T	12	4018	0	0	H	10	3179	0	0
3	77D00135	D541	7709	7143	R	12	3929	0	0	H	2	3299	41	229
12	77D00135	D541	7709	5572	R	12	2751	0	0	H	0	3288	776	297
1	78D00367	D541	7904	4237	T	12	2886	0	0	H	43	3319	564	188
12	78D00367	D541	7904	4676	T	12	2864	0	0	H	1	1216	2054	776
1	78D00368	D541	7904	4237	T	12	2886	0	0	H	4	5791	211	50
12	78D00368	D541	7904	4676	T	12	2864	0	0	H	73	6347	2493	1242
1	78D00369	D541	7904	4237	T	12	2886	0	0	H	3	2429	46	41
12	78D00369	D541	7904	4676	T	12	2864	0	0	H	3	1688	2218	962
1	72D00150	D547	7202	13369	L	12	1922	0	0	H	73	3072	351	6
7	72D00150	D547	7202	13369	L	12	1420	0	0	H	1	3257	1122	415
1	70D00350	D548	7001	13369	B	9	1337	-	0	H	1	3598	0	0
12	70D00350	D548	7001	3298	B	9	330	-	0	H	0	3638	346	18
1	70D00353	D548	7005	13369	B	9	1337	-	0	H	0	3213	0	0
12	70D00353	D548	7005	3298	B	9	330	-	0	H	1	3325	186	0
1	70D00639	D548	7005	13369	B	9	1337	-	0	H	0	1001	0	0
12	70D00639	D548	7005	2831	B	9	283	-	0	H	16	3137	392	14
1	70D00640	D548	7004	13369	B	9	1337	-	0	H	8	3304	681	37
12	70D00640	D548	7004	2831	B	9	283	-	0	H	20	308	1691	875
1	72D00150	D548	7202	13369	H	9	1337	0	0	H	1	3289	105	30
4	72D00150	D548	7202	13369	H	9	1337	0	1866	H	1	3335	619	1024
5	72D00150	D548	7202	2977	H	9	298	0	0	H	1	3350	661	1024
1	72D00158	D548	7202	13369	B	9	1337	-	0	H	17	2153	0	0
12	72D00158	D548	7202	2977	B	9	298	-	0	H	1	273	609	134
1	72D00232	D548	7201	13369	D	12	1838	-	0	H	0	308	92	0
8	72D00232	D548	7201	13369	B	9	1337	-	0	H	6	372	589	636
12	72D00232	D548	7201	2977	B	9	298	-	0	H	1	388	1287	682
1	72D00240	D548	7204	13369	B	9	1337	-	0	H	0	1230	567	0
6	72D00240	D548	7204	13369	B	9	1337	-	2029	H	0	1235	1538	245
12	72D00240	D548	7204	2977	B	9	298	-	0	H	1	1265	1585	245
1	78D00189	D548	7807	13369	R	9	6684	0	0	H	7	1358	0	0
12	78D00189	D548	7807	2831	R	9	1156	0	0	H	4	1601	887	745
1	78D00190	D548	7807	13369	R	9	6684	0	0	H	2	3053	0	0
12	78D00190	D548	7807	2831	R	9	1156	0	0	H	3	3737	396	303
1	78D00191	D548	7807	13369	R	9	6684	0	0	H	6	3890	0	0
12	78D00191	D548	7807	2831	R	9	1156	0	0	H	2	4582	1340	1061

1	79D00168	D548	7904	13369	T	9	7687	0	0	H	2	1007	0	0
4	79D00168	D548	7904	13369	R	9	7353	0	0	H	3	870	133	18
12	79D00168	D548	7904	11397	R	9	5509	0	0	H	0	817	326	44
1	79D00590	D548	7910	13369	T	12	9609	0	0	H	0	336	41	0
10	79D00590	D548	7910	13369	R	9	7353	0	0	H	0	378	226	0
12	79D00590	D548	7910	2831	R	9	1510	0	0	H	1	407	242	0
1	71D00512	D560	7109	13369	B	9	1337	-	0	H	3	1866	0	0
12	71D00512	D560	7109	2922	B	9	292	-	0	H	0	2130	501	948
1	71D00520	D560	7109	13369	B	9	1337	-	0	H	7	2540	0	0
12	71D00520	D560	7109	2922	B	9	292	-	0	H	0	4287	218	111
1	71D00570	D560	7110	13369	D	12	1588	-	0	H	0	3480	0	0
5	71D00570	D560	7110	13369	B	12	1337	-	0	H	93	3486	20	3
7	71D00570	D560	7110	13369	B	12	1337	-	2565	H	99	4120	542	1600
12	71D00570	D560	7110	2922	B	9	292	-	0	H	35	4693	667	1615
1	71D00672	D560	8306	13369	D	12	13285	-	0	H	0	1110	123	17
12	71D00672	D560	8306	2922	D	9	2630	-	0	H	3	1350	1002	1045
1	71D00685	D560	7111	13369	B	9	1337	-	0	H	1	3235	0	0
4	71D00685	D560	7111	13369	B	9	1337	-	1781	H	1	3243	1154	608
12	71D00685	D560	7111	2922	B	9	292	-	0	H	1	3331	1986	1263
1	73D00157	D560	7306	13369	B	9	1337	-	0	H	0	2699	134	0
12	73D00157	D560	7306	2922	B	9	292	-	0	H	0	2788	886	457
1	73D00418	D560	7305	13369	B	9	1337	-	0	H	1	4057	0	0
3	73D00418	D560	7305	13369	B	9	1337	-	2577	H	2	4151	250	2124
12	73D00418	D560	7305	2922	B	9	292	-	712	H	0	4223	634	2777
1	73D00419	D560	7305	13369	B	9	1337	-	0	H	0	4275	196	0
6	73D00419	D560	7305	13369	B	9	1337	-	2605	H	1	4020	943	1381
12	73D00419	D560	7305	2922	B	9	292	-	0	H	6	4752	1147	1768
1	74D00137	D560	7412	13369	D	9	1894	-	0	H	2	2548	92	28
7	74D00137	D560	7412	13369	B	9	1337	-	0	H	9	2939	768	149
12	74D00137	D560	7412	2922	B	9	292	-	0	H	2	1579	1174	689
1	74D00156	D560	7412	13369	D	9	1894	-	0	H	23	3166	0	0
7	74D00156	D560	7412	13369	B	9	1337	-	0	H	1	3255	40	0
10	74D00156	D560	7412	13369	B	9	1337	-	1556	H	1	3255	321	1007
12	74D00156	D560	7412	2922	B	9	292	-	0	H	1	3278	321	1007
1	74D00185	D560	7409	13369	D	9	1560	-	0	H	2	1730	51	0
4	74D00185	D560	7409	13369	B	9	1337	-	0	H	2	1871	61	0
5	74D00185	D560	7409	13369	B	9	1337	-	1758	H	2	1871	621	838
12	74D00185	D560	7409	2922	B	9	292	-	0	H	2	1937	621	1574
1	74D00186	D560	7412	13369	D	9	1894	-	0	H	21	1820	0	0
7	74D00186	D560	7412	13369	B	9	1337	-	0	H	2	2018	124	183
12	74D00186	D560	7412	2922	B	9	292	-	0	H	0	1967	459	195
1	75D00013	D560	7510	13369	P	9	3008		0	H	0	2847	0	0
5	75D00013	D560	7510	13369	L	9	2562		0	H	14	4033	1202	159
12	75D00013	D560	7510	2922	L	9	390		0	H	0	4047	1400	172
1	75D00014	D560	7510	13369	P	9	3008		0	H	1	3842	0	0



5	75D00014	D560	7510	13369	L	9	2562	0 H	1	3987	863	133
12	75D00014	D560	7510	2922	L	9	390	0 H	1	4053	1118	1424
1	75D00015	D560	7510	13369	P	9	3008	0 H	1	5571	93	0
5	75D00015	D560	7510	13369	L	9	2562	0 H	2	5666	846	30
12	75D00015	D560	7510	2922	L	9	390	0 H	3	5829	1003	411
1	75D00016	D560	7510	13369	P	9	3008	0 H	3	3825	176	0
5	75D00016	D560	7510	13369	L	9	2562	0 H	1	3877	176	0
12	75D00016	D560	7510	2922	L	9	390	0 H	1	3959	350	30
1	75D00017	D560	7510	13369	P	9	3008	0 H	1	3478	0	0
5	75D00017	D560	7510	13369	L	9	2562	0 H	2	3567	195	39
12	75D00017	D560	7510	2922	L	9	390	0 H	1	3851	1146	872
1	76D00098	D560	7612	13369	R	9	4568 0	0 H	1	1490	0	0
7	76D00098	D560	7612	13369	P	9	3899 0	0 H	2	1800	336	1301
12	76D00098	D560	7612	11397	P	9	2849 0	0 H	1	1860	1565	2092
1	76D00100	D560	7612	13369	R	9	4568 0	0 H	2	2069	0	0
7	76D00100	D560	7612	13369	P	9	3899 0	0 H	1	2176	233	10
12	76D00100	D560	7612	11397	P	9	2849 0	0 H	1	2168	338	10
1	76D00159	D560	7701	13369	R	9	4679 0	0 H	0	1167	603	20
8	76D00159	D560	7701	13369	P	9	3899 0	0 H	1	1260	2207	60
12	76D00159	D560	7701	11397	P	9	2944 0	0 H	1	1299	3146	1364
1	79D00158	D560	7906	13369	T	9	7910 0	0 H	10	1995	103	0
6	79D00158	D560	7906	13369	R	9	7353 0	0 H	3	2256	298	600
12	79D00158	D560	7906	11397	R	9	5698 0	0 H	1	2364	1148	706
1	79D00159	D560	7906	13369	T	9	7910 0	0 H	29	1545	0	0
6	79D00159	D560	7906	13369	R	9	7353 0	0 H	1	1593	1354	3321
12	79D00159	D560	7906	11397	R	9	5698 0	0 H	2	1799	2562	5076
1	79D00160	D560	7906	13369	T	9	7910 0	0 H	2	1834	0	0
6	79D00160	D560	7906	13369	R	9	7353 0	0 H	2	2066	198	13
12	79D00160	D560	7906	11397	R	9	5698 0	0 H	2	2230	1402	787
1	83D00129	D560	8212	13369	U	9	12589 0	0 H	4	215	0	283
6	83D00129	D560	8212	13369	T	9	12032 0	0 H	6	645	154	283
12	83D00129	D560	8212	13369	T	9	11364 0	0 H	2	1185	332	382
1	83D00130	D560	8212	13369	U	9	12589 0	0 H	9	335	15	0
6	83D00130	D560	8212	13369	T	9	12032 0	0 H	6	764	285	14
12	83D00130	D560	8212	13369	T	9	11364 0	0 H	2	1078	332	14
1	62D02108	D569	6201	67986	B	21	6799 -	0 H	1	2200	0	0
12	62D02108	D569	6201	12260	B	10	1226 -	0 H	3	2285	0	0
1	62D02117	D569	6212	67986	B	18	6799 -	0 H	4	1540	0	0
12	62D02117	D569	6212	12260	B	10	1226 -	0 H	7	1027	2398	2758
1	62D02122	D569	6212	67986	B	18	6799 -	0 H	1	1314	185	0
12	62D02122	D569	6212	12260	B	10	1226 -	0 H	1	1545	2812	2264
1	67D00758	D569	6708	67986	B	10	6799 -	0 H	1	3483	340	0
12	67D00758	D569	6708	23941	B	10	2394 -	0 H	0	3533	1357	3387
1	80D01155	D569	8103	67986	T	10	53709 0	0 H	1	616	20	0

12	80D01155	D569	8103	67986	T	10	48100	0	0	H	2	921	1254	1381
1	82D00103	D569	8111	67986	T	10	57788	0	0	H	3	479	0	0
12	82D00103	D569	8111	67141	T	10	51531	0	0	H	6	854	448	141
1	82D00104	D569	8111	67986	T	10	57788	0	0	H	1	410	0	0
12	82D00104	D569	8111	67141	T	10	51531	0	0	H	1	637	666	375
1	82D00105	D569	8111	67986	T	10	57788	0	0	H	2	619	0	0
12	82D00105	D569	8111	67141	T	10	51531	0	0	H	20	986	752	404
1	66D01373	D570	6601	114646	B	10	11465	-	0	H	0	1430	0	0
12	66D01373	D570	6601	41591	B	10	4159	-	0	H	1	1548	2523	2226
1	66D01385	D570	6601	114646	B	10	11465	-	0	H	1	1147	0	0
12	66D01385	D570	6601	41591	B	10	4159	-	0	H	1	1147	0	0
1	84D00600	D570	8401	32812		10	0	0	0	H	0	3	0	0
2	84D00600	D570	8401	70789	T	10	70258	0	0	H	0	3	0	0
6	84D00600	D570	8401	70789	T	10	68134	0	0	H	35	180	416	145
1	80D00123	D572	8003	29355	T	10	20548	0	0	H	2	272	30	0
12	80D00123	D572	8003	28668	T	10	17702	0	0	H	1	1048	1356	784
1	80D00124	D572	8003	29355	T	10	20548	0	0	H	4	845	20	0
12	80D00124	D572	8003	28668	T	10	17702	0	0	H	1	1010	856	189
1	80D00977	D572	8007	29355	U	10	21429		0	H	1	636	185	0
12	80D00977	D572	8007	28668	U	10	18563		0	H	1	765	556	294
1	80D00978	D572	8007	29355	T	12	22750		0	H	1	630	98	360
12	80D00978	D572	8007	28668	T	10	18563		0	H	1	731	1320	1275
1	80D01025	D592	8012	54971	T	12	41915	0	0	H	2	1664	168	76
5	80D01025	D592	8012	54971	T	12	40541	0	0	H	184	1811	1643	390
1	80D00287	D594	8004	54398	T	12	41138	0	0	H	104	1087	0	586
12	80D00287	D594	8004	51640	T	12	35502	0	0	H	0	1173	2990	1856
1	80D01025	D594	8012	54971	T	12	44320	0	0	H	1	1376	159	0
7	80D01025	D594	8012	54971	T	12	42259	0	0	H	3	1605	1286	213
1	83D00242	D594	8307	56941	U	12	0	0	0	H	0	21	41	0
9	83D00242	D594	8307	54398	U	12	51338	0	0	H	2	397	800	514
11	83D00242	D594	8307	56941	T	12	53026	0	0	H	2	458	1142	572
1	70D01080	D595	7007	30738	B	12	3074	-	0	H	1	2550	154	14
7	70D01080	D595	7007	30738	B	12	3074	-	4038	H	398	2601	2163	1413
10	70D01080	D595	7007	19457	B	12	1946	-	0	H	1	2659	2950	1497
12	70D01080	D595	7007	19457	B	12	1946	-	0	H	1	2700	3086	1497
1	70D01084	D595	7007	30738	B	12	3074	-	0	H	28	5137	165	0
10	70D01084	D595	7007	19457	B	12	1946	-	0	H	0	2882	1322	463
12	70D01084	D595	7007	19457	B	12	1946	-	0	H	0	52300	2593	793
1	75D00521	D598	7501	12128	P	10	2850	0	0	H	1	28	0	0
8	75D00521	D598	7501	12128	L	10	2213	0	0	H	13	1010	273	0
12	75D00521	D598	7501	8750	L	10	1334	0	0	H	1	42	273	0
1	67D01748	D604	6701	10213	B	12	1021	-	0	H	0	558	0	0

12	67D01748	D604	6701	10213	B	12	1021	-	O	H	0	599	329	0
1	72D01168	D606	7211	5431	D	12	1086	-	O	U	0	0	41	0
12	72D01168	D606	7211	1680	D	12	220	-	O	U	0	0	140	35
1	75D00462	D606	7510	5431	R	12	2274		O	U	1	0	0	0
12	75D00462	D606	7510	5431	R	12	1901		O	U	1	0	433	129
1	80D00212	D606	8005	5431	T	12	4141		O	U	0	0	10	34
12	80D00212	D606	8005	4851	T	12	3365		O	U	0	0	259	39
1	72D00572	D620	7301	12257	B	10	1226	-	O	U	0	0	0	0
12	72D00572	D620	7301	17960	B	10	1796	-	O	U	0	0	326	377
1	77D00425	D620	7706	12257	R	10	5546	0	O	U	0	0	0	0
12	77D00425	D620	7706	17960	R	10	6645	0	O	U	0	0	263	0
1	77D00428	D620	7707	12257	R	10	5638	0	O	U	14	0	0	0
12	77D00428	D620	7707	17960	R	10	6780	0	O	U	14	0	134	7
1	79D00214	D626	7907	37839	T	12	24832	0	O	H	2	1311	315	0
5	79D00214	D626	7907	29252	T	12	18465	0	O	H	1	1394	1823	2236
1	79D00215	D626	7907	37839	T	12	24832	0	O	H	1	1197	316	327
5	79D00215	D626	7907	29252	T	12	18465	0	O	H	1	1365	802	656
1	72D00533	D631	7209	40247	B	10	4025	-	O	H	1	1889	258	732
12	72D00533	D631	7209	14911	B	10	1491	-	O	H	0	1994	2523	2080
1	72D01194	D631	7205	40247	B	10	4025	-	O	H	8	3432	0	0
12	72D01194	D631	7205	14352	B	10	1435	-	O	H	0	3618	2121	2230
1	72D01197	D631	7201	40247	B	10	4025	-	O	H	9	6690	103	0
8	72D01197	D631	7201	40247	B	10	4025	-	O	H	2	6808	731	610
1	82D00200	D631	8210	40247	U	10	37530	0	O	H	1	191	0	0
12	82D00200	D631	8210	44477	U	10	37805	0	O	H	2	629	735	877
1	69D01332	D632	6910	63077	B	10	6308	-	O	H	1	4570	0	0
3	69D01332	D632	6910	63077	B	10	6308	-	7326	H	1	4745	2164	3485
7	69D01332	D632	6910	63077	B	10	6308	-	O	H	7	4795	3126	3492
1	69D01333	D632	6910	63077	B	10	6308	-	O	H	1	6074	206	0
12	69D01333	D632	6910	20469	B	10	2047	-	O	H	0	6239	3013	2957
1	79D00214	D632	7907	37839	T	12	26487	0	O	H	1	1105	0	0
7	79D00214	D632	7907	37839	T	12	25068	0	O	H	3	1287	1037	315
1	79D00215	D632	7907	37839	T	12	26487	0	O	H	2	1046	237	10
7	79D00215	D632	7907	37839	T	12	25068	0	O	H	1	1194	878	78
1	71D00178	D640	7101	83514	B	10	8351	-	O	H	19	3810	0	0
12	71D00178	D640	7101	30024	B	10	3002	-	O	H	54	3591	4151	2250
1	80D01098	D653	8008	49864	T	12	38956	0	O	H	6	1601	0	0
12	80D01098	D653	8008	55937	T	12	39855	0	O	H	3	1607	1494	561
1	80D01099	D653	8008	49864	T	12	38956	0	O	H	112	1466	454	122
12	80D01099	D653	8008	55937	T	12	39855	0	O	H	4	1930	2269	1310

1	66D00192	D655	6604	62341	B	12	6234	-	O	H	2	593	87	0
8	66D00192	D655	6604	62341	B	12	6234	-	7799	H	10	717	2571	4466
12	66D00192	D655	6604	13562	B	12	1356	-	O	H	2	942	4115	4503
1	66D01294	D655	6605	62341	B	15	6234	-	O	H	2	7203	41	96
12	66D01294	D655	6605	12570	B	12	1257	-	O	H	2	7475	2394	2466
1	75D00290	D655	7501	62341	R	12	22599	0	O	H	1	1582	2654	543
12	75D00290	D655	7501	27613	R	12	8111	0	O	H	1	1785	6211	5814
1	66D01241	D660	6611	29653	D	20	7413	-	O	U	0	0	0	0
1	66D01241	D660	6611	29653	D	20	7413	-	O	U	0	0	0	0
1	79D00564	D667	7911	87344	T	12	63324		O	H	1	1123	681	49
12	79D00564	D667	7911	892	T	12	585		O	H	0	1210	4378	2025
1	63D00801	D676	6310	19600	B	17	1960	-	O	H	0	3357	0	0
10	63D00801	D676	6310	19394	B	17	1939	-	O	H	0	3421	861	146
12	63D00801	D676	6310	4836	B	17	484	-	O	H	0	3421	861	923
1	81D00224	D676	8403	19600	T	17	19600	0	O	H	0	144	42	0
2	81D00224	D676	8403	19394	T	17	19308	0	O	H	0	149	42	0
4	81D00224	D676	8403	16936	T	17	16712	0	O	H	0	149	42	0
1	70D00991	D680	7010	17113	D	15	4022	-	O	H	0	1012	0	0
10	70D00991	D680	7010	24674	D	15	4688	-	O	H	3	1032	748	43
11	70D00991	D680	7010	17113	D	15	3166	-	O	H	1	829	1295	608
12	70D00991	D680	7010	9055	D	15	1630	-	O	H	1	829	1295	608
1	69D00235	D682	6901	4808	D	25	2298	-	O	U	0	0	0	0
8	69D00235	D682	6901	2263	D	25	1034	-	O	U	0	0	36	0
12	69D00235	D682	6901	2263	D	25	1007	-	O	U	0	0	36	0
1	69D01501	D684	8012	3428	D	25	3109	-	O	U	0	0	0	0
6	69D01501	D684	8012	8667	D	25	7731	-	O	U	0	0	0	0
12	69D01501	D684	8012	2667	D	25	2331	-	O	U	0	0	0	0
1	70D01924	D701	7001	101379	B	12	10138	-	O	U	0	0	0	0
10	70D01924	D701	7001	117664	B	12	11766	-	O	U	0	0	1344	266
11	70D01924	D701	7001	101379	B	12	10138	-	O	U	0	0	1344	266
12	70D01924	D701	7001	24250	B	12	2425	-	O	U	0	0	1344	266
1	66D02755	D705	6601	48267	B	10	4827	-	O	H	1	2698	134	0
5	66D02755	D705	6601	67247	B	10	6725	-	O	H	0	2676	134	0
12	66D02755	D705	6601	23500	B	10	2350	-	O	H	1	2684	607	66
1	67D00933	D707	6704	88667	B	10	8867	-	O	U	0	0	0	0
10	67D00933	D707	6704	300491	B	10	30049	-	O	U	0	0	134	1493
11	67D00933	D707	6704	88667	B	10	8867	-	O	U	0	0	134	1493
12	67D00933	D707	6704	86064	B	10	8606	-	O	U	0	0	182	1673
1	70D01966	D715	7012	14941	D	15	3661	-	O	U	0	0	0	0
10	70D01966	D715	7012	17794	D	15	3559	-	O	U	0	0	0	0
11	70D01966	D715	7012	14941	D	15	2913	-	O	U	0	0	0	0
12	70D01966	D715	7012	6360	D	15	1208	-	O	U	0	0	0	0
1	76D00466	D717	7601	10039	R	15	5521	0	O	U	0	0	0	0
12	76D00466	D717	7601	2163	R	15	1071	0	O	U	0	0	93	0
1	71D00167	D718	7101	9019	D	15	2255	-	O	U	0	0	41	0

10	71D00167	D718	7101	9798	D	15	2009	-	O	U	0	0	326	751
11	71D00167	D718	7101	9019	D	15	1804	-	O	U	0	0	326	751
12	71D00167	D718	7101	2300	D	15	448	-	O	U	0	0	326	751
1	79D00547	D718	8003	9019	T	15	7215		O	U	0	0	0	0
10	79D00547	D718	8003	9798	T	15	7397		O	U	0	0	67	0
11	79D00547	D718	8003	9019	T	15	6764		O	U	0	0	67	0
12	79D00547	D718	8003	7210	T	15	5371		O	U	0	0	67	0
1	66D00397	D720	6612	39889	B	15	3989	-	O	M	7	19386	0	0
10	66D00397	D720	6612	46803	B	15	4680	-	O	M	8	20640	1508	552
11	66D00397	D720	6612	39889	B	15	3989	-	O	M	7	20743	1679	558
12	66D00397	D720	6612	12566	B	15	1257	-	O	M	6	20743	1679	558
1	64D00062	D731	6408	37869	B	17	3787	-	O	M	28	45556	412	277
12	64D00062	D731	6408	7407	B	17	741	-	O	M	8	46063	2554	1498
1	66D00835	D731	6612	37869	D	17	4622	-	O	M	9	45487	114	11
7	66D00835	D731	6612	37869	B	17	3787	-	O	M	9	46818	1243	169
12	66D00835	D731	6612	10826	B	17	1083	-	O	M	3	47631	2016	648
1	70D00830	D731	7005	37869	D	17	11472	-	O	M	19	57809	0	0
12	70D00830	D731	7005	15359	D	17	3908	-	O	M	8	60147	2626	1679
1	71D00500	D731	7107	37869	D	17	13811	-	O	M	10	44800	0	0
12	71D00500	D731	7107	28954	D	17	9155	-	O	M	4	46173	2878	973
1	72D00309	D731	7203	37869	R	17	15148	0	O	M	82	47914	0	0
12	72D00309	D731	7203	28954	R	17	10176	0	O	M	11	51514	3400	1660
1	72D00596	D731	7209	37869	D	17	16150	-	O	M	37	46347	0	0
12	72D00596	D731	7209	37869	D	17	14312	-	O	M	9	48583	3998	1015
1	80D00162	D765	8101	20855	T	15	17727	0	O	U	0	0	41	0
12	80D00162	D765	8101	19948	T	15	15859	0	O	U	0	0	114	0
1	79D00519	D766	1079	45927	G	12	4593		O	H	10	327	41	0
12	79D00519	D766	1079	38821	G	12	3882		O	H	4	150	341	0
1	79D00381	D768	7902	7780	T	10	4687	0	O	H	2	519	0	0
8	79D00381	D768	7902	7780	R	10	4279	0	O	H	0	521	161	3
12	79D00381	D768	7902	13374	R	10	6954	0	O	H	6	612	421	12
1	79D00553	D768	8005	7780	T	10	5563		O	H	0	88	0	0
12	79D00553	D768	8005	6425	T	10	4064		O	H	0	110	945	524
1	78D00811	D772	7812	29068	R	8	14080	0	O	H	2	638	25	0
12	78D00811	D772	7812	18257	R	8	6960	0	O	H	0	739	763	303

1	69E00645	E801	6911	8446	B	11	845	-	O	H	15	3127	0	0
2	69E00645	E801	6911	10196	B	11	1020	-	O	H	16	2709	87	0
5	69E00645	E801	6911	10196	B	11	1020	-	O	H	16	2709	87	0
1	69E00748	E801	6912	8446	B	11	845	-	O	H	1	1338	10	0
2	69E00748	E801	6912	10196	B	11	1020	-	O	H	1	1423	122	9
4	69E00748	E801	6912	10196	B	11	1020	-	1038	H	2	1482	628	231
5	69E00748	E801	6912	10196	B	11	1020	-	1123	H	1	1484	1226	718
12	69E00748	E801	6912	5417	B	11	542	-	O	H	1	83	2058	974
1	70E00069	E801	7008	8446	B	11	845	-	O	H	2	3834	0	0
2	70E00069	E801	7008	10196	B	11	1020	-	O	H	2	3884	20	0
12	70E00069	E801	7008	5417	B	11	542	-	O	H	1	4154	921	241
1	70E00070	E801	7008	8446	B	11	845	-	O	H	1	3869	0	0
2	70E00070	E801	7008	10196	B	11	1020	-	O	H	1	3839	169	4
12	70E00070	E801	7008	5417	B	11	542	-	O	H	1	3719	862	380
1	70E00127	E801	7008	8446	B	11	845	-	O	H	0	26	254	0
2	70E00127	E801	7008	10196	B	11	1020	-	O	H	0	414	428	4
5	70E00127	E801	7008	10196	B	11	1020	-	1040	H	4	84	955	35
12	70E00127	E801	7008	5417	B	11	542	-	O	H	1	234	1385	89
1	70E00128	E801	7008	8446	B	11	845	-	O	H	2	6540	10	0
2	70E00128	E801	7008	10196	B	11	1020	-	O	H	1	6555	10	0
12	70E00128	E801	7008	5417	B	11	542	-	O	H	0	6653	477	256
1	70E00167	E801	7008	8446	B	11	845	-	O	H	1	3354	0	0
2	70E00167	E801	7008	10196	B	11	1020	-	O	H	2	3302	82	0
4	70E00167	E801	7008	10196	A	11	1020	-	O	H	1	17365	102	42
5	70E00167	E801	7008	10196	B	11	1020	-	O	H	214	4400	102	126
12	70E00167	E801	7008	5417	B	11	542	-	O	H	0	3407	696	682
1	70E00170	E801	7008	8446	B	11	845	-	O	H	0	5580	0	412
2	70E00170	E801	7008	10196	B	11	1020	-	1194	H	0	5600	534	552
12	70E00170	E801	7008	5417	B	11	542	-	O	H	1	5833	1010	728
1	70E00172	E801	7008	8446	B	11	845	-	O	H	2	5640	77	0
2	70E00172	E801	7008	10196	B	11	1020	-	O	H	1	5686	77	0
12	70E00172	E801	7008	5417	B	11	542	-	O	H	1	5930	784	218
1	70E00178	E801	7008	8446	B	11	845	-	O	H	1	1919	0	0
2	70E00178	E801	7008	10196	B	11	1020	-	O	H	1	2000	46	0
12	70E00178	E801	7008	5417	B	11	542	-	O	H	1	1828	796	203
1	70E00220	E801	7009	8446	B	11	845	-	O	H	2	4670	51	131
2	70E00220	E801	7009	10196	B	11	1020	-	O	H	3	4728	302	161
12	70E00220	E801	7009	5417	B	11	542	-	O	H	2	5296	1071	538
1	72E00271	E801	7209	8446	L	11	960	0	O	H	1	1910	0	0
2	72E00271	E801	7209	10196	L	11	1089	0	O	H	1	1949	0	0
4	72E00271	E801	7209	10196	H	11	1020	0	O	H	1	2021	108	5
12	72E00271	E801	7209	5417	H	11	542	0	O	H	1	2253	369	160
1	72E00684	E801	7208	8446	L	11	902	0	O	H	2	1418	15	240
2	72E00684	E801	7208	10196	L	11	1020	0	1055	H	2	1425	302	760
3	72E00684	E801	7208	10196	H	11	1020	0	O	H	2	1452	714	801
12	72E00684	E801	7208	5417	H	11	542	0	O	H	4	2067	1283	976
1	72E00685	E801	7208	8446	L	11	902	0	O	H	1	3202	0	0

2	72E00685	E801	7208	10196	L	11	1020	0	0	H	1	3210	0	0
3	72E00685	E801	7208	10196	H	11	1020	0	0	H	1	3257	0	0
11	72E00685	E801	7208	10196	H	11	1020	0	1293	H	1	3316	1148	446
12	72E00685	E801	7208	5417	H	11	542	0	0	H	1	3340	1211	449
1	72E00686	E801	7208	8446	L	11	902	0	0	H	2	4020	0	0
2	72E00686	E801	7208	10196	L	11	1020	0	0	H	2	4114	0	0
3	72E00686	E801	7208	10196	H	11	1020	0	0	H	3	4064	0	0
12	72E00686	E801	7208	5417	H	11	542	0	0	H	1	4346	538	288
1	72E00687	E801	7208	8446	L	11	902	0	0	H	8	3568	0	0
2	72E00687	E801	7208	10196	L	11	1020	0	0	H	4	3456	46	417
3	72E00687	E801	7208	10196	H	11	1020	0	1093	H	4	3543	415	419
12	72E00687	E801	7208	5417	H	11	542	0	0	H	0	3499	956	739
1	72E00688	E801	7208	8446	D	11	902	-	0	H	1	3087	244	0
2	72E00688	E801	7208	10196	D	11	1020	-	0	H	1	3087	244	0
3	72E00688	E801	7208	10196	B	11	1020	-	0	H	1	3177	254	70
10	72E00688	E801	7208	10196	H	11	1020	0	0	H	2	3446	830	120
12	72E00688	E801	7208	5417	H	11	542	0	0	H	1	3507	872	130
1	72E00689	E801	7208	8446	L	11	902	0	0	H	1	2588	0	97
2	72E00689	E801	7208	10196	L	11	1020	0	0	H	1	2550	287	190
3	72E00689	E801	7208	10196	H	11	1020	0	0	H	1	2577	287	190
12	72E00689	E801	7208	5417	H	11	542	0	0	H	1	2688	488	551
1	72E00711	E801	7310	8446	P	11	1708	0	0	H	1	4243	0	0
2	72E00711	E801	7310	10196	P	11	1993	0	0	H	1	4243	0	0
5	72E00711	E801	7310	10196	L	11	1784	0	0	H	1	2959	421	79
10	72E00711	E801	7310	10196	H	11	1437	0	0	H	2	3199	905	394
11	72E00711	E801	7310	10196	L	11	1367	0	0	H	2	3189	905	394
12	72E00711	E801	7310	5417	L	11	689	0	0	H	2	3257	1058	476
1	78E00214	E801	7801	8446	R	11	4645	0	0	H	0	817	51	75
2	78E00214	E801	7801	10196	R	11	5538	0	0	H	0	823	51	75
12	78E00214	E801	7801	5717	R	11	2716	0	0	H	1	867	352	223
1	78E00215	E801	7801	8446	R	11	4645	0	0	H	2	1326	10	0
2	78E00215	E801	7801	10196	R	11	5538	0	0	H	2	1376	10	0
12	78E00215	E801	7801	5717	R	11	2716	0	0	H	1	1579	300	202
1	82E00277	E801	8202	8446	T	11	7467	0	0	H	4	854	0	0
2	82E00277	E801	8202	10196	T	11	8945	0	0	H	3	948	0	0
12	82E00277	E801	8202	8755	T	11	7084	0	0	H	2	1532	820	1020
1	81E00230	E816	8105	17440	T	8	13189	0	0	H	1	1118	0	0
2	81E00230	E816	8105	13629	T	8	10179	0	0	H	2	1159	15	13
12	81E00230	E816	8105	14453	T	8	9440	0	0	H	2	1637	564	815
1	81E00231	E816	8105	17440	T	8	13189	0	0	H	3	596	0	0
2	81E00231	E816	8105	13629	T	8	10179	0	0	H	3	620	164	120
12	81E00231	E816	8105	14453	T	8	9440	0	0	H	1	930	438	193
1	81E00232	E816	8105	17440	T	8	13189	0	0	H	1	594	103	0
2	81E00232	E816	8105	13629	T	8	10179	0	0	H	1	630	118	0
12	81E00232	E816	8105	14453	T	8	9440	0	0	H	3	987	347	203
1	81E00233	E816	8105	17440	T	8	13189	0	0	H	2	661	0	12
2	81E00233	E816	8105	13629	T	8	10179	0	0	H	3	989	67	12
12	81E00233	E816	8105	14453	T	8	9440	0	0	H	2	1078	518	178

1	81E00234	E816	8005	17440	T	8	11227	0	0	H	1	888	0	0
2	81E00234	E816	8005	12629	T	8	8646	0	0	H	1	863	30	0
11	81E00234	E816	8005	12629	R	8	7496	0	0	H	3	1274	449	118
12	81E00234	E816	8005	14453	R	8	7814	0	0	H	2	1500	475	113
1	70E00285	E820	7011	50340	B	8	8034	-	0	H	0	600	0	0
2	70E00285	E820	7011	64057	B	8	6406	-	0	H	0	600	0	0
12	70E00285	E820	7011	19551	B	8	1955	-	0	H	9	1634	1985	1388
1	82E00001	E822	8205	23449	T	10	20987	0	0	H	0	5	0	0
11	82E00001	E822	8205	30737	T	10	25204	0	0	H	6	25	338	195
12	82E00001	E822	8205	30737	T	10	24974	0	0	H	6	25	338	195
1	82E00017	E822	8111	23449	T	10	18733	0	0	H	7	2011	0	0
2	82E00017	E822	8111	30737	T	10	23572	0	0	H	6	2331	133	145
12	82E00017	E822	8111	23449	T	10	17083	0	0	H	1	2715	616	523
1	82E00082	E822	8202	23449	T	10	20459	0	0	H	12	549	0	0
2	82E00082	E822	8202	30737	T	10	26588	0	0	H	9	455	77	0
12	82E00082	E822	8202	23449	T	10	18525	0	0	H	10	1243	1194	904
1	83E00401	E823	8212	19322	T	10	18308	0	0	H	2	195	0	0
6	83E00401	E823	8212	19322	T	10	17583	0	0	H	1	364	703	38
12	83E00401	E823	8212	19322	T	10	16714	0	0	H	1	571	976	55
1	83E00423	E824	8306	30611	T	10	30381	0	0	H	0	114	0	0
2	83E00423	E824	8306	34264	T	10	33750	0	0	H	4	454	0	0
12	83E00423	E824	8306	36820	T	10	33506	0	0	H	2	189	213	149
1	70E00546	E830	7009	8338	B	11	834	-	0	H	1	7468	0	455
2	70E00546	E830	7009	8338	B	11	834	-	1668	H	1	7480	677	536
12	70E00546	E830	7009	8338	B	11	834	-	0	H	1	6016	1522	866
1	70E00549	E830	7009	8338	A	11	834	-	0	H	1	9428	0	0
2	70E00549	E830	7009	8338	A	11	834	-	868	H	1	9496	480	0
6	70E00549	E830	7009	8338	B	11	834	-	0	H	2	81	806	80
7	70E00549	E830	7009	8338	A	11	834	-	0	H	3	9674	1006	268
12	70E00549	E830	7009	8338	A	11	834	-	0	H	129	9726	1316	413
1	70E00550	E830	7009	8338	B	11	834	-	0	H	0	1766	93	14
12	70E00550	E830	7009	8338	B	11	834	-	0	H	1	1989	1103	479
1	70E00571	E830	7009	8338	B	11	834	-	0	H	4	243	108	33
12	70E00571	E830	7009	8338	B	11	834	-	0	H	1	749	1078	673
1	72E00850	E830	7203	8338	H	11	834	0	0	H	1	6197	77	0
12	72E00850	E830	7203	8338	H	11	834	0	0	H	2	6643	260	4
1	72E00851	E830	7203	8338	H	11	834	0	0	H	2	250	0	0
6	72E00851	E830	7203	8338	H	11	834	0	1349	H	3	481	716	172
12	72E00851	E830	7203	8338	H	11	834	0	0	H	78	8817	1093	357
1	72E00852	E830	7203	8338	H	11	834	0	0	H	1	3837	0	0
12	72E00852	E830	7203	8338	H	11	834	0	0	H	1	4138	731	1328
1	72E00853	E830	7203	8338	H	11	834	0	0	H	11	8066	0	0
6	72E00853	E830	7203	8338	H	11	834	0	1071	H	3	7064	882	872
9	72E00853	E830	7203	8338	B	11	834	-	0	H	2	7169	1177	1489
10	72E00853	E830	7203	8338	B	11	834	-	2376	H	2	7200	2167	1582



12	72E00853	E830	7203	8338 B 11	834 -	O H	1	7314	2416	1654
1	72E00854	E830	7203	8338 G 11	834 O	O H	1	9469	72	0
2	72E00854	E830	7203	8338 H 11	834 O	O H	2	8930	72	161
5	72E00854	E830	7203	8338 G 11	834 O	O H	1	9028	266	161
8	72E00854	E830	7203	8338 G 11	834 O	O H	2	9053	307	161
1	72E00855	E830	7203	8338 H 11	834 O	O H	18	5018	0	0
12	72E00855	E830	7203	8338 H 11	834 O	O H	1	4974	634	232
1	72E00856	E830	7203	8338 H 11	834 O	O H	1	2883	0	0
6	72E00856	E830	7203	8338 H 11	834 O	1572 H	1	3017	724	568
12	72E00856	E830	7203	8338 H 11	834 O	O H	1	3067	1194	725
1	76E00188	E830	7603	8338 R 11	3335	O H	4	3109	20	10
12	76E00188	E830	7603	8337 R 11	2710	O H	2	1551	1351	724
1	78E00646	E830	7909	17440 T 11	11970 O	O H	2	2486	0	0
2	78E00646	E830	7909	13629 T 11	9262 O	O H	2	2899	148	364
8	78E00646	E830	7909	13629 R 8	6857 O	O H	3	2931	430	483
12	78E00646	E830	7909	12638 R 8	5885 O	O H	1	2934	1840	2830
1	78E00648	E830	7909	17440 T 11	11970 O	O H	1	1333	0	0
2	78E00648	E830	7909	13629 T 11	9262 O	O H	1	1491	118	121
9	78E00648	E830	7909	13629 R 8	6857 O	O H	3	2138	428	516
12	78E00648	E830	7909	12638 R 8	5885 O	O H	3	2515	721	584
1	78E00476	E831	7811	17440 R 9	8284 O	O H	0	2338	0	0
2	78E00476	E831	7811	13629 R 8	6346 O	O H	0	2346	0	0
12	78E00476	E831	7811	12638 R 8	4700 O	O H	0	2419	444	48
1	78E00478	E831	7811	17440 R 8	8284 O	O H	1	2223	0	0
2	78E00478	E831	7811	13629 R 8	6346 O	O H	1	2272	0	0
12	78E00478	E831	7811	12638 R 8	4700 O	O H	1	2244	376	253
1	78E00488	E831	7811	17440 R 8	8284 O	O H	3	2434	0	0
2	78E00488	E831	7811	13629 R 8	6346 O	O H	3	2434	0	0
12	78E00488	E831	7811	12638 R 8	4700 O	O H	1	2671	1035	621
1	69E01156	E832	6902	23449 B 10	2345 -	O H	0	2285	0	0
2	69E01156	E832	6902	30737 B 10	3074 -	O H	0	2285	487	1355
12	69E01156	E832	6902	9697 B 10	970 -	O H	1	1434	2099	2069
1	70E00484	E832	7101	23449 B 10	2345 -	O H	1	241	36	0
2	70E00484	E832	7101	30737 B 10	3074 -	O H	1	251	36	0
5	70E00484	E832	7101	30737 B 10	3074 -	O H	1	251	36	0
1	70E00485	E832	7101	23449 B 10	2345 -	O H	0	3176	0	2
2	70E00485	E832	7101	30737 B 10	3074 -	O H	0	3188	77	2
12	70E00485	E832	7101	9697 B 10	970 -	O H	0	3281	554	107
1	70E00979	E832	7005	23449 B 10	2345 -	O H	14	2866	443	149
2	70E00979	E832	7005	30737 B 10	3074 -	O H	9	2886	720	161
12	70E00979	E832	7005	9697 B 10	970 -	O H	24	2924	1402	487
1	70E00980	E832	7005	23449 B 10	2345 -	O H	1	4414	15	0
2	70E00980	E832	7005	30737 B 10	3074 -	O H	1	4414	15	0
12	70E00980	E832	7005	9697 B 10	970 -	O H	18	6648	337	18
1	73E00702	E832	7303	23449 H 10	2345 O	O H	1	2629	0	0

2	73E00702	E832	7303	30737	H	10	3074	0	0	H	1	2642	5	0
12	73E00702	E832	7303	9697	H	10	970	0	0	H	1	1497	753	3103
1	75E00183	E832	7507	23449	R	10	6566	0	0	H	1	1876	0	0
2	75E00183	E832	7507	30737	P	10	8376	0	0	H	1	1876	0	89
12	75E00183	E832	7507	9697	P	10	1915	0	0	H	0	1956	2472	5052
1	75E00189	E832	7507	23449	R	10	6566	0	0	H	1	1296	0	0
2	75E00189	E832	7507	30737	P	10	8376	0	0	H	1	1302	0	0
12	75E00189	E832	7507	9697	P	10	1915	0	0	H	1	1483	811	352
1	75E00202	E832	7508	23449	R	10	6742	0	0	H	1	388	0	0
2	75E00202	E832	7508	30737	R	10	8606	0	0	H	2	187	0	7
3	75E00202	E832	7508	30737	P	10	8376	0	0	H	3	187	0	7
12	75E00202	E832	7508	9697	P	10	1988	0	0	H	17	1177	1746	3223
1	75E00205	E832	7508	23449	R	10	6742	0	0	H	1	4833	0	0
2	75E00205	E832	7508	30737	R	10	8606	0	0	H	1	4863	138	0
3	75E00205	E832	7508	30737	P	10	8376	0	0	H	1	4874	226	101
12	75E00205	E832	7508	9697	P	10	1988	0	0	H	1	5014	789	470
1	75E00220	E832	7508	23449	R	10	6742	0	0	H	1	955	30	0
2	75E00220	E832	7508	30737	R	10	8606	0	0	H	1	966	40	0
3	75E00220	E832	7508	30737	P	10	8376	0	0	H	1	998	40	0
12	75E00220	E832	7508	9697	P	10	1988	0	0	H	2	1216	914	401
1	77E00164	E832	7711	23449	R	10	11490	0	0	H	1	1531	46	269
2	77E00164	E832	7711	30737	R	10	14831	0	0	H	1	1531	46	269
12	77E00164	E832	7711	12501	R	10	5094	0	0	H	1	1803	854	817
1	77E00169	E832	7711	23449	R	10	11490	0	0	H	1	713	0	0
2	77E00169	E832	7711	30737	R	10	14831	0	0	H	1	713	0	0
12	77E00169	E832	7711	12501	R	10	5094	0	0	H	1	958	1699	1285
1	77E00170	E832	7711	23449	R	10	11490	0	0	H	3	1381	25	0
2	77E00170	E832	7711	30737	R	10	14831	0	0	H	1	1396	66	23
12	77E00170	E832	7711	12501	R	10	5094	0	0	H	8	1439	738	1269
1	77E00174	E832	7711	23449	R	10	11490	0	0	H	70	1940	0	0
2	77E00174	E832	7711	30737	R	10	14831	0	0	H	33	1976	92	254
12	77E00174	E832	7711	12501	R	10	5094	0	0	H	1	0	1396	3052
1	77E00186	E832	7711	23449	R	10	11490	0	0	H	1	971	0	0
2	77E00186	E832	7711	30737	R	10	14831	0	0	H	1	1031	0	0
12	77E00186	E832	7711	12501	R	10	5094	0	0	H	1	1113	354	314
1	77E00193	E832	7711	23449	R	10	11490	0	0	H	1	1456	108	32
2	77E00193	E832	7711	30737	R	10	14831	0	0	H	1	1481	180	64
12	77E00193	E832	7711	12501	R	10	5094	0	0	H	1	1631	1135	780
1	71E00217	E834	7201	30611	B	10	3061	-	0	H	1	3184	0	106
2	71E00217	E834	7201	34264	B	10	3426	-	0	H	1	3184	92	142
3	71E00217	E834	7201	34264	B	10	3426	-	0	H	1	3184	82	142
1	71E00227	E834	7201	30611	B	10	3061	-	0	H	1	4375	0	0
2	71E00227	E834	7201	34264	B	10	3426	-	0	H	1	4375	0	0
7	71E00227	E834	7201	34264	B	10	3426	-	0	H	31	4569	855	132
1	71E00261	E834	7202	30611	B	10	3061	-	0	H	0	1996	103	0
2	71E00261	E834	7202	34264	B	10	3426	-	0	H	0	2000	144	13

5	71E00261	E834	7202	34264	B	10	3426	-	O H	0	2046	221	13
1	70E00118	E834	7207	30611	H	10	3061	0	O H	2	2225	0	42
2	70E00118	E834	7207	34264	H	10	3426	0	O H	2	2244	20	42
7	70E00118	E834	7207	34264	H	10	3426	0	O H	1	156	253	48
1	71E00227	E835	7201	34264	B	10	3426	-	O H	21	4586	278	0
5	71E00227	E835	7201	23321	B	10	2332	-	O H	2	4647	745	322
1	70E00118	E835	7207	34264	H	10	3426	0	O H	1	156	136	16
5	70E00118	E835	7207	23321	H	10	2332	0	O H	28	2549	307	125
1	62E02558	E841	6203	9892	B	15	989	-	O H	0	0	41	0
12	62E02558	E841	6203	9892	B	15	989	-	O H	0	0	232	27
1	93E00792	E841	9310	15592	U	15	15514	0	O H	0	1	0	0
2	93E00792	E841	9310	17906	U	15	17628	0	O H	0	1	0	0
8	93E00792	E841	9310	15592	U	15	14968	0	O H	0	15	310	0
1	67E01196	E842	6703	22222	B	15	2222	-	O H	0	795	0	0
11	67E01196	E842	6703	21792	B	15	2179	-	O H	0	805	97	0
12	67E01196	E842	6703	21792	B	15	2179	-	O H	0	805	97	0
1	92E00083	E853	9202	23449	T	10	20459	0	O H	4	1855	0	17
2	92E00083	E853	9202	30737	T	10	26588	0	O H	4	1855	282	73
12	92E00083	E853	9202	23449	T	10	17296	0	O H	3	2624	914	266
1	70E00942	E902	7206	30671	R	17	12674	0	O H	1	1983	154	0
12	70E00942	E902	7206	16451	R	17	6000	0	O H	24	2149	1410	814
1	65E00407	E935	6501	144423	H	10	14442		O H	0	214	0	0
2	65E00407	E935	6501	160427	H	10	16043		O H	0	214	0	0
12	65E00407	E935	6501	160427	H	10	16043		O H	0	214	0	0
1	66E01106	E935	6608	144423	H	10	14442	0	O H	5	397	464	398
2	66E01106	E935	6608	160427	H	10	16043	0	O H	4	464	464	398
3	66E01106	E935	6608	160427	G	10	16043	0	O H	3	33791	464	442
5	66E01106	E935	6608	160427	H	10	16043	0	O H	235	525	923	543
12	66E01106	E935	6608	38751	H	10	3875	0	O H	22	1438	2212	372
1	67E01166	E935	6701	144423	B	10	14442	-	O H	4	757	10	0
2	67E01166	E935	6701	160427	B	10	16043	-	O H	3	815	10	0
10	67E01166	E935	6701	160427	H	10	16043		O H	5	824	1633	432
12	67E01166	E935	6701	38751	H	10	3875		O H	15	1042	1706	432
1	84E00150	E935	8405	160427	U	10	0	0	O H	0	8	0	0
2	84E00150	E935	8405	123600	U	10	122673	0	O H	0	8	0	0
1	66E00792	E952	6607	9339	B	8	934	-	O H	1	3664	93	0
12	66E00792	E952	6607	9339	B	8	934	-	O H	1	3826	1213	562
1	66E00795	E952	6608	9339	B	8	934	-	O H	243	3438	0	0
12	66E00795	E952	6608	9339	B	8	934	-	O H	16	3592	348	10
1	70E01341	E954	7009	12210	B	10	1221	-	O H	0	625	149	1
6	70E01341	E954	7009	12210	B	10	1221	-	O H	1	680	324	75
1	69E00413	E956	6909	47421	B	12	4742	-	O H	3	4211	77	0
2	69E00413	E956	6909	45700	B	12	4570	-	O H	2	4293	77	0
10	69E00413	E956	6909	45700	B	12	4570	-	O H	1	4385	1404	1273

1	75E00556	E956	7501	47421	R	12	17190	O H	1	3030	0	0
2	75E00556	E956	7501	45700	R	12	16281	O H	1	3052	0	0
12	75E00556	E956	7501	16034	R	12	5297	O H	0	3155	2311	4195
1	74E00524	E957	7403	47421	R	12	14226	O H	0	1968	20	0
2	74E00524	E957	7403	45700	R	12	13424	O H	1	1993	20	126
12	74E00524	E957	7403	45700	P	12	11139	O H	0	2011	843	429
12	74E00524	E957	7403	25670	P	12	5936	O H	0	2034	843	429
1	74E00546	E957	7409	47421	R	12	16005	O H	1	2473	93	9
2	74E00546	E957	7409	45700	R	12	15138	O H	1	2508	108	9
12	74E00546	E957	7409	25670	R	12	6899	O H	11	2720	1174	1508
1	76E00037	E957	7609	47421	R	12	23118	O H	1	166	0	0
2	76E00037	E957	7609	45700	R	12	21993	O H	1	189	128	91
12	76E00037	E957	7609	25670	R	12	10749	O H	14	1731	1871	4140
1	76E00038	E957	7609	47421	R	12	23118	O H	1	1266	0	43
2	76E00038	E957	7609	45700	R	12	21993	O H	1	13	226	341
12	76E00038	E957	7609	25670	R	12	10749	O H	13	1530	1357	938
1	82E00707	E957	8205	47421	T	12	43272	O H	4	179	25	0
2	82E00707	E957	8205	45700	T	12	41416	O H	5	288	107	0
12	82E00707	E957	8205	39893	T	12	33660	O H	5	458	920	2359
1	83E00050	E957	8306	47421	T	12	43568	O H	9	888	0	0
2	83E00050	E957	8306	45700	T	12	41701	O H	7	888	15	0
12	83E00050	E957	8306	39893	T	12	33909	O H	9	288	1231	790
1	83E00052	E957	8307	47421	T	12	43864	O H	3	182	134	68
2	83E00052	E957	8307	45700	T	12	41987	O H	3	192	213	83
12	83E00052	E957	8307	39893	T	12	34158	O H	30	454	620	506

1	77L00290	L113	7701	112434	T	15	68585	0	O M	27	48061	0	0
5	77L00280	L113	7701	152934	T	15	90231	0	O M	41	18460	760	2181
7	77L00280	L113	7701	152934	T	15	98702	0	O M	483	51348	1332	2351
1	77L00292	L113	7701	112434	T	15	68585	0	O M	22	58632	97	147
5	77L00292	L113	7701	152934	T	15	90231	0	O M	31	61039	940	201
7	77L00292	L113	7701	152934	T	15	98702	0	O M	21	61884	2251	995
1	77L00290	L114	7701	152934	T	15	87937	0	O M	557	51348	310	232
5	77L00280	L114	7701	152934	T	15	84878	0	O M	92	53475	873	318
1	77L00292	L114	7701	152934	T	15	87937	0	O M	21	62104	31	0
5	77L00292	L114	7701	152934	T	15	84878	0	O M	18	63690	903	25
1	65L00671	L125	6500	15000	H	16	1500	0	O H	0	1786	0	0
2	65L00671	L125	6500	113935	H	16	11394	0	O H	0	1794	0	0
11	65L00671	L125	6500	15000	H	16	1500	0	O H	2	1907	747	151
1	70L00696	L130	7011	106644	R	16	30660	0	O H	1	2201	469	44
2	70L00696	L130	7011	113935	R	16	32222	0	O H	2	2247	643	44
12	70L00696	L130	7011	38274	R	16	9030	0	O H	1	2504	1843	442
1	70L00698	L130	7011	106644	R	16	30660	0	O H	5	1459	0	0
2	70L00698	L130	7011	113935	R	16	32222	0	O H	5	1459	0	0
12	70L00698	L130	7011	38274	R	16	9030	0	O H	0	1474	0	0
1	71L00007	L130	7101	106644	R	16	31660	0	O H	1	4004	207	0
2	71L00007	L130	7101	113935	R	16	33290	0	O H	1	4033	207	140
12	71L00007	L130	7101	38274	R	16	9389	0	O H	1	4173	1905	2838
1	71L00065	L130	7110	106644	R	16	36159	0	O H	1	3178	0	0
2	71L00065	L130	7110	113935	R	16	38097	0	O H	1	3194	0	0
12	71L00065	L130	7110	38274	R	16	11004	0	O H	1	3361	1193	377
1	72L00721	L130	7212	106644	S	16	43157	0	O H	87	2620	165	78
2	72L00721	L130	7212	113935	S	16	45574	0	O H	97	2634	288	97
12	72L00721	L130	7212	38274	S	16	13516	0	O H	1	2898	1423	353
1	73L01243	L130	7303	106644	R	16	44657	0	O H	2	258	941	173
2	73L01243	L130	7303	113935	R	16	47176	0	O H	2	283	1955	342
4	73L01243	L130	7303	113935	S	16	46108	0	O H	2	417	2877	776
12	73L01243	L130	7303	38274	S	16	14054	0	O H	2	866	5476	5158
1	73L01437	L133	7310	91779	R	15	38088	0	O H	2	3969	258	15
2	73L01437	L133	7310	99305	R	15	40715	0	O H	2	5038	947	82
12	73L01437	L133	7310	22225	R	15	8001	0	O H	7	4222	3316	1286
1	79L00123	L133	7905	91779	T	15	68834	0	O H	2	1837	278	417
2	79L00123	L133	7905	99305	T	15	73982	0	O	0	0	278	417
12	79L00123	L133	7905	55364	T	15	38478	0	O H	2	2366	2869	1213
1	79L00124	L133	7905	91779	T	15	68834	0	O H	1	1433	0	0
2	79L00124	L133	7905	99305	T	15	73982	0	O H	1	1492	0	0
12	79L00124	L133	7905	55364	T	15	38478	0	O H	2	1769	4502	3621
1	64L00022	L143	6407	381768	L	19	38177	0	O H	1	2670	249	0
2	64L00022	L143	6407	426582	H	19	42658	0	O H	1	2670	249	329
10	64L00022	L143	6407	426582	S	12	42658	0	O H	10	2960	1332	407
11	64L00022	L143	6407	426582	H	12	42658	0	O H	10	2960	1332	407

1	79L00031	L143	7908	381768	T	12	269624	0	0	H	1	1453	2442	0
2	79L00031	L143	7908	426582	T	12	298607	0	0	H	1	1468	2442	1
12	79L00031	L143	7908	151894	T	12	96832	0	0	H	0	1528	12312	20164
1	80L00383	L143	8101	381768	T	12	310186	0	0	H	0	550	1152	0
2	80L00383	L143	8101	426582	T	12	343932	0	0	H	0	597	1721	0
12	80L00383	L143	8101	151894	T	12	112971	0	0	H	9	763	7036	9704
1	84L00094	L143	8404	426582	U	12	423916	0	0	H	0	13	633	295
2	84L00094	L143	8404	151894	U	12	149995	0	0	H	0	31	770	1312
1	84L00096	L143	8405	247000	U	12	245456	0	0	H	0	4	0	0
1	84L00096	L143	8405	247000	U	12	245456	0	0	H	0	4	0	0
1	74L00343	L145	7405	223486	S	12	69839	0	0	H	37	3192	227	0
2	74L00343	L145	7405	172171	S	12	52727	0	0	H	28	3287	2005	150
12	74L00343	L145	7405	146039	S	12	35597	0	0	H	1	3446	7856	17461
1	74L00344	L145	7405	223486	R	12	69839	0	0	H	1	2974	855	54
2	74L00344	L145	7405	172171	R	12	52727	0	0	H	1	3016	1843	171
12	74L00344	L145	7405	146039	P	12	35597	0	0	H	0	3142	7832	15455
1	74L00345	L145	7405	223486	S	12	69839	0	0	H	1	2806	368	0
2	74L00345	L145	7405	172171	S	12	52727	0	0	H	2	2859	974	168
12	74L00345	L145	7405	146039	S	12	35597	0	0	H	0	8829	11390	22283
1	74L00351	L145	7406	223486	S	12	71236	0	0	H	1	3114	206	840
2	74L00351	L145	7406	172171	S	12	53803	0	0	H	1	3321	647	840
12	74L00351	L145	7406	146039	S	12	36510	0	0	H	1	2756	5296	3557
1	75L00393	L145	7506	223486	S	12	87998	0	0	H	4	3461	165	219
2	75L00393	L145	7506	172171	S	12	66716	0	0	H	2	3582	1068	964
12	75L00393	L145	7506	146039	S	12	47463	0	0	H	9	4371	6259	5834
1	75L00394	L145	7506	223486	R	12	87998	0	0	H	2	2846	0	0
2	75L00394	L145	7506	172171	R	12	66716	0	0	H	2	2926	821	254
12	75L00394	L145	7506	146039	R	12	47463	0	0	H	2	3507	7097	3889
1	75L00395	L145	7506	223486	R	12	87998	0	0	H	3	5312	242	0
2	75L00395	L145	7506	172171	R	12	66716	0	0	H	3	5312	1392	1746
12	75L00395	L145	7506	146039	R	12	47463	0	0	H	6	5887	9755	9824
1	75L00565	L145	7509	223486	R	12	92188	0	0	H	1	1350	0	0
2	75L00565	L145	7509	172171	R	12	69944	0	0	H	1	1350	0	0
12	75L00565	L145	7509	146039	R	12	50201	0	0	H	4	2579	9763	7260
1	75L00566	L145	7510	223486	R	12	93585	0	0	H	2	3703	0	0
2	75L00566	L145	7510	172171	R	12	71021	0	0	H	2	3703	0	0
8	75L00566	L145	7510	172171	R	12	64564	0	0	H	2	3703	0	0
1	75L00567	L145	7509	223486	R	12	92188	0	0	H	2	1782	486	197
2	75L00567	L145	7509	172171	R	12	69944	0	0	H	2	1819	711	244
12	75L00567	L145	7509	146039	R	12	50201	0	0	H	2	2363	4522	1762
1	75L00568	L145	7509	223486	R	12	92188	0	0	H	0	3547	0	0
2	75L00568	L145	7509	172171	R	12	69944	0	0	H	0	3547	0	0
8	75L00568	L145	7509	172171	R	12	63488	0	0	H	0	3547	0	0
1	74L00203	L149	7403	45268	R	12	13580	0	0	M	66	55872	181	835
2	74L00203	L149	7403	23281	R	12	8308	0	0	M	51	55897	1305	972

8	74L00203	L149	7403	28281	L	10	3040	O M	9	57393	1700	2291
9	74L00203	L149	7403	28281	D	10	2828 -	O M	9	57393	2418	2611
10	74L00203	L149	7403	28281	B	10	2828 -	O M	8	57618	2952	2739
12	74L00203	L149	7403	12350	B	10	1235 -	O M	7	58321	3426	2995
1	74L00230	L149	7407	45268	R	12	14712	O M	212	45828	453	257
2	74L00230	L149	7407	28281	R	12	9015	O M	147	46743	607	265
8	74L00230	L149	7407	28281	L	10	3889	O M	70	51294	2237	2867
12	74L00230	L149	7407	12350	L	10	1328	O M	37	54991	2710	3388
1	74L00113	L151	7404	28054	L	10	4699 O	O M	20	6540	46	234
2	74L00113	L151	7404	29534	L	10	4725 O	O M	11	6549	1578	235
11	74L00113	L151	7404	29534	H	10	2953 O	O M	43	14562	3113	1408
12	74L00113	L151	7404	12511	H	10	1251 O	O M	51	15774	3198	1538
1	74L00120	L151	7412	28054	H	8	2805	O M	35	56815	206	22
2	74L00120	L151	7412	29534	H	8	2953	O M	26	57030	349	133
8	74L00120	L151	7412	29534	L	10	5168	O M	5	57882	1557	1568
12	74L00120	L151	7412	16342	L	10	2370	O M	5	58598	2137	2304
1	76L00496	L151	7607	28054	P	8	5961	O M	23	66008	0	0
2	76L00496	L151	7607	29534	L	8	5999	O M	19	67664	51	0
8	76L00496	L151	7607	29534	R	10	9377	O M	34	72596	490	299
12	76L00496	L151	7607	12511	R	10	3597	O M	36	76807	758	513
1	67L00561	L273	6709	91442	H	10	9144	O H	25	4116	187	0
2	67L00561	L273	6709	103212	H	10	10321	O H	19	4101	412	19
12	67L00561	L273	6709	34802	H	10	3480	O H	0	905	2056	1987
1	67L00566	L273	6709	91442	B	10	9144 -	O H	70	2876	0	0
1	67L00566	L273	6709	91442	B	10	9144 -	O H	70	2876	0	0
1	67L00651	L273	6710	91442	B	10	9144 -	O H	4	2879	0	0
2	67L00651	L273	6710	103212	B	10	10321 -	O H	1	2898	154	0
12	67L00651	L273	6710	34802	B	10	3480 -	O H	1	3034	1966	1278
1	67L01377	L273	6703	91442	S	10	9144	O H	1	5481	123	0
2	67L01377	L273	6703	103212	S	10	10321	O H	24	5517	123	0
12	67L01377	L273	6703	34802	S	10	3480	O H	1	3470	2019	1545
1	72L00986	L275	7210	91442	H	10	9144 O	O H	53	3273	0	0
2	72L00986	L275	7210	103212	H	10	10321 O	O H	40	3277	0	0
12	72L00986	L275	7210	34802	H	10	3480 O	O H	10	3749	3689	4540
1	72L01025	L275	7201	91442	H	10	9144 O	O H	1	4458	124	3036
2	72L01025	L275	7201	103212	H	10	10321 O	O H	1	4520	308	3036
12	72L01025	L275	7201	34802	H	10	3480 O	O H	4	4899	4041	5457
1	72L01027	L275	7210	91442	H	10	9144 O	O H	1	4075	0	0
2	72L01027	L275	7210	103212	H	10	10321 O	O H	1	4075	0	0
6	72L01027	L275	7210	103212	S	10	10321	O H	0	9	313	0
7	72L01027	L275	7210	103212	H	10	10321	O H	0	51	460	1120
12	72L01027	L275	7210	34802	H	10	3480	O H	2	409	1295	2055
1	72L01028	L275	7210	91442	H	10	9144 O	O H	1	3294	0	22
2	72L01028	L275	7210	103212	H	10	10321 O	O H	1	3294	277	93
12	72L01028	L275	7210	34802	H	10	3480 O	O H	2	0	1386	1574
1	72L01029	L275	7210	91442	H	10	9144 O	O H	14	3569	439	0
2	72L01029	L275	7210	103212	H	10	10321 O	O H	9	3632	439	0

12	72L01029	L275	7210	34802	H 10	3480	O	H	1	3849	2558	1256
1	72L01030	L275	7210	91442	H 10	9144	O	H	1	3817	643	95
2	72L01030	L275	7210	103212	H 10	10321	O	H	1	3822	920	958
12	72L01030	L275	7210	34802	H 10	3480	O	H	4	4099	2912	3116
1	72L01031	L275	7210	91442	H 10	9144	O	H	1	3858	0	0
2	72L01031	L275	7210	103212	H 10	10321	O	H	1	3892	0	0
12	72L01031	L275	7210	34802	H 10	3480	O	H	1	4177	1744	1948
1	73L01154	L275	7301	91442	H 10	9144	O	H	1	2776	124	0
2	73L01154	L275	7301	103212	H 10	10321	O	H	2	28037	575	19
12	73L01154	L275	7301	34802	H 10	3480	O	H	1	3164	3676	8339
1	73L01155	L275	7303	91442	H 10	9144	O	H	2	411	0	0
2	73L01155	L275	7303	103212	H 10	10321	O	H	1	465	236	0
12	73L01155	L275	7303	34802	H 10	3480	O	H	31	3433	2026	4285
1	73L01180	L275	7303	91442	H 10	9144	O	H	1	2651	0	0
2	73L01180	L275	7303	103212	H 10	10321	O	H	1	2684	1134	26
12	73L01180	L275	7303	34802	H 10	3480	O	H	1	3178	2927	1505
1	73L01181	L275	7304	91442	H 10	9144	O	H	1	3582	82	0
2	73L01181	L275	7304	103212	H 10	10321	O	H	4	3600	291	0
12	73L01181	L275	7304	34802	H 10	3480	O	H	1	3665	1087	665
1	73L01182	L275	7304	91442	H 10	9144	O	H	1	3987	0	134
2	73L01182	L275	7304	103212	H 10	10321	O	H	1	3993	955	313
12	73L01182	L275	7304	34802	H 10	3480	O	H	1	4394	3197	1829
1	73L01183	L275	7304	91442	S 10	9144	O	H	0	56	258	9
2	73L01183	L275	7304	103212	S 10	10321	O	H	1	80	535	21
12	73L01183	L275	7304	34802	S 10	3480	O	H	1	415	2560	1791
1	73L01210	L275	7504	91442	P 10	23546	O	H	5	3409	497	275
2	73L01210	L275	7504	103212	P 10	25803	O	H	4	3425	517	275
11	73L01210	L275	7504	103212	L 10	18836	O	H	2	3857	2797	4386
12	73L01210	L275	7504	34802	L 10	6090	O	H	2	3895	2977	4431
1	75L00080	L275	7506	91442	P 10	24918	O	H	1	2878	247	22
2	75L00080	L275	7506	103212	P 10	27351	O	H	2	2902	596	22
12	75L00080	L275	7506	45882	P 10	8718	O	H	2	3222	2276	1773
1	75L00082	L275	7506	91442	P 10	24918	O	H	2	4332	0	0
2	75L00082	L275	7506	103212	P 10	27351	O	H	2	2484	97	107
12	75L00082	L275	7506	45882	P 10	8718	O	H	6	4838	1182	516
1	75L00674	L275	7512	91442	R 10	29033	O	H	2	3456	0	0
2	75L00674	L275	7512	103212	R 10	31996	O	H	1	3478	164	227
7	75L00674	L275	7512	103212	P 10	28125	O	H	1	3646	524	2240
12	75L00674	L275	7512	45882	P 10	10782	O	H	1	3793	1345	3029
1	75L00691	L275	7512	91442	R 10	29033	O	H	1	1845	0	0
2	75L00691	L275	7512	103212	R 10	31996	O	H	1	1847	0	0
7	75L00691	L275	7512	103212	P 10	28125	O	H	1	1958	391	25
12	75L00691	L275	7512	45882	P 10	10782	O	H	1	27432	809	536
1	75L00693	L275	7512	91442	R 10	29033	O	H	1	3837	154	0
2	75L00693	L275	7512	103212	R 10	31996	O	H	2	3906	154	0
7	75L00693	L275	7512	103212	P 10	28125	O	H	2	4072	1370	197



12	75L00693	L275	7512	45882	P	10	10782	O H	1	4189	1617	1124
1	75L00698	L275	7512	91442	R	10	29033	O H	1	4341	185	1000
2	75L00698	L275	7512	103212	R	10	31996	O H	4	4189	328	1000
7	75L00698	L275	7512	103212	P	10	28125	O H	2	4451	1625	1736
12	75L00698	L275	7512	45882	P	10	10782	O H	2	4607	2387	1826
1	75L00700	L275	7512	91442	R	10	29033	O H	3	3754	0	0
2	75L00700	L275	7512	103212	R	10	31996	O H	3	3840	400	324
7	75L00700	L275	7512	103212	P	10	28125	O H	1	3897	855	905
12	75L00700	L275	7512	45882	P	10	10782	O H	1	4033	2252	1448
1	75L00701	L275	7511	91442	R	10	28347	O H	0	1751	0	0
2	75L00701	L275	7511	103212	R	10	31222	O H	0	1751	0	0
6	75L00701	L275	7511	103212	P	10	28125	O H	0	1751	0	0
9	75L00701	L275	7511	103212	P	10	25803	O H	0	1751	0	0
1	82L00590	L275	8211	91442	U	10	85955	O H	3	696	20	0
2	82L00590	L275	8211	103212	U	10	96245	O H	3	818	30	0
5	82L00590	L275	8211	103212	T	10	93923	O H	3	1088	500	192
12	82L00590	L275	8211	81084	T	10	69530	O H	4	1667	1228	1689
1	82L00591	L275	8211	91442	U	10	85955	O H	4	704	237	0
2	82L00591	L275	8211	103212	U	10	96245	O H	3	788	648	0
5	82L00591	L275	8211	103212	T	10	93923	O H	3	1020	1031	532
12	82L00591	L275	8211	81084	T	10	69530	O H	3	1574	2097	1015
1	82L00592	L275	8211	91442	U	10	85955	O H	0	107	521	0
2	82L00592	L275	8211	103212	U	10	96245	O H	1	153	705	33
5	82L00592	L275	8211	103212	T	10	93923	O H	1	357	1057	33
12	82L00592	L275	8211	81084	T	10	69530	O H	29	746	2478	1367
1	82L00593	L275	8211	91442	U	10	85955	O H	8	1019	0	0
2	82L00593	L275	8211	103212	U	10	96245	O H	8	1242	0	0
5	82L00593	L275	8211	103212	T	10	93923	O H	4	1077	810	2724
12	82L00593	L275	8211	81084	T	10	69530	O H	9	1750	2001	3926
1	82L00597	L275	8211	91442	U	10	85955	O H	3	570	134	0
2	82L00597	L275	8211	103212	U	10	96245	O H	3	680	503	0
5	82L00597	L275	8211	103212	T	10	93923	O H	2	692	767	246
12	82L00597	L275	8211	81084	T	10	69530	O H	2	1266	3150	1011
1	83L00849	L275	8403	80402	U	10	80402	O H	0	33	83	0
2	83L00849	L275	8403	103212	U	10	102438	O H	1	89	83	0
4	83L00849	L275	8403	81084	U	10	79260	O H	1	3310	83	0
1	83L00866	L275	8403	80402	U	10	80402	O H	0	16	0	0
2	83L00866	L275	8403	103212	U	10	102438	O H	0	75	0	0
4	83L00866	L275	8403	81084	U	10	79260	O H	2	215	96	0
1	83L00873	L275	8403	80402	U	10	80402	O H	0	21	0	0
2	83L00873	L275	8403	103212	U	10	102438	O H	0	91	83	0
4	83L00873	L275	8403	81084	U	10	79260	O H	3	204	199	0
1	83L00874	L275	8403	80402	U	10	80402	O H	0	19	0	0
2	83L00874	L275	8403	103212	U	10	102438	O H	0	90	146	0
4	83L00874	L275	8403	81084	U	10	79260	O H	3	238	178	0
1	67L00075	L276	6701	100836	B	11	10084	O H	0	1925	0	0
2	67L00075	L276	6701	100814	B	11	10081	O H	0	1930	92	7

12	67L00075	L276	6701	25392	B	11	2539	-	O	H	0	1960	1719	1033
1	84L00049	L276	8406	93610	U	11	93610	0	O	H	0	502	0	0
1	84L00049	L276	8406	93610	U	11	93610	0	O	H	0	502	0	0
1	74L00609	L278	7408	39734	R	12	3846		O	H	0	3565	0	0
2	74L00609	L278	7408	31102	R	12	10108		O	H	1	28395	308	691
12	74L00609	L278	7408	19356	R	12	4818		O	H	0	2864	308	2045
1	82L00435	L305	8210	56472	U	14	53749	0	O	M	48	230	0	0
4	82L00435	L305	8210	56472	T	14	52842	0	O	M	49	230	272	28
5	82L00435	L305	8210	56472	T	14	52539	0	O	M	60	230	272	28
1	61L00753	L350	6110	71453	B	19	7145	-	O	H	0	1442	0	0
2	61L00753	L350	6110	104380	B	19	10438	-	O	H	0	1610	71	25
12	61L00753	L350	6110	19866	B	16	2987	-	O	H	2	1592	1511	924
1	68L00909	L350	6806	71453	L	16	10830		O	H	48	5777	0	0
2	68L00909	L350	6806	104380	L	16	15331		O	H	28	3010	0	0
12	68L00909	L350	6806	39400	L	16	2940		O	H	103	5352	1051	272
1	63L00171	L351	363	25927	H	16	2593	0	O	M	16	18874	145	315
12	63L00171	L351	363	7220	H	16	722	0	O	M	51	21601	2851	1987
1	64L00714	L351	6403	25927	L	20	3371		O	M	12	48069	10	0
8	64L00714	L351	6403	25927	H	16	2593		O	M	20	51296	1080	1179
12	64L00714	L351	6403	7220	H	16	722		O	M	181	52691	2158	1248
1	65L00736	L351	6507	25927	B	16	2593	-	O	M	5	119306	0	0
5	65L00736	L351	6507	25927	B	16	2593	-	3334	M	8	120266	665	2600
12	65L00736	L351	6507	7220	B	16	722	-	O	M	6	121177	999	2750
1	65L00763	L351	6501	25927	B	16	2593	-	O	M	10	117091	62	0
12	65L00763	L351	6501	7220	B	16	722	-	970	M	8	120916	1942	2053
1	65L00774	L351	6507	25927	B	16	2593	-	O	M	6	29536	0	0
10	65L00774	L351	6507	25927	H	16	2593		O	M	2	30435	766	1281
12	65L00774	L351	6507	7220	H	16	722		O	M	3	30699	1296	2622
1	65L00837	L351	6507	25927	B	16	2593	-	O	M	11	44799	149	0
10	65L00837	L351	6507	25927	H	16	2593		O	M	12	46686	1418	371
12	65L00837	L351	6507	7220	H	16	722		O	M	8	46865	1517	420
1	65L00892	L351	6511	25927	B	16	2593	-	O	M	11	55279	17	0
10	65L00892	L351	6511	25927	H	16	2593		O	M	7	57518	2127	2430
12	65L00892	L351	6511	7220	H	16	722		1921	M	8	58055	2877	3533
1	65L01112	L351	6511	25927	H	16	2593		O	M	9	40450	180	168
9	65L01112	L351	6511	25927	H	16	2593		3162	M	10	42632	1250	2627
12	65L01112	L351	6511	7220	H	16	722		O	M	6	43697	1276	2627
1	65L01113	L351	6511	25927	B	16	2593	-	O	M	5	61258	154	316
10	65L01113	L351	6511	25927	H	16	2593		O	M	18	62610	1162	955
12	65L01113	L351	6511	7220	H	16	722		O	M	6	45825	1289	1045
1	68L00543	L351	1068	25927	B	16	2593	-	O	M	7	18233	278	503
12	68L00543	L351	1068	7600	B	16	2593	-	O	M	3	19594	760	780
1	68L00570	L351	6811	25927	P	16	4537		O	M	17	55445	340	181
6	68L00570	L351	6811	25927	L	16	3930		O	M	7	56617	1845	1193

12	68L00570	L351	6811	7600	L	16	938	0	M	84	58441	3274	2086
1	68L00572	L351	6811	25927	P	16	4537	0	0	M	10	33070	0
6	68L00572	L351	6811	25927	L	16	3930	0	0	M	8	1217	1230
12	68L00572	L351	6811	7600	L	16	938	0	0	M	6	2890	2394
1	70L00550	L351	7003	25927	R	16	6482	0	0	M	4	51962	72
10	70L00550	L351	7003	25927	P	16	5388	0	0	M	4	52761	1409
12	70L00550	L351	7003	7600	P	16	1508	0	0	M	4	52923	1510
1	70L00554	L351	7003	25927	R	16	6482	0	0	M	15	39740	0
10	70L00554	L351	7003	25927	P	16	5388	0	0	M	18	43216	1776
12	70L00554	L351	7003	7600	P	16	1508	0	0	M	15	44411	2043
1	70L00555	L351	7003	25927	R	16	6482	0	0	M	7	39720	536
10	70L00555	L351	7003	25927	P	16	5388	0	0	M	6	41434	1673
12	70L00555	L351	7003	7600	P	16	1508	0	0	M	30	43894	2273
1	70L00556	L351	7003	25927	R	16	6482	0	0	M	5	46364	441
10	70L00556	L351	7003	25927	P	16	5388	0	0	M	14	49927	2661
12	70L00556	L351	7003	7600	P	16	1508	0	0	M	11	50997	3058
1	70L00558	L351	7003	25927	R	16	6482	0	0	M	18	22545	129
10	70L00558	L351	7003	25927	P	16	5388	0	0	M	20	26422	1790
12	70L00558	L351	7003	7600	P	16	1508	0	0	M	15	27355	1795
1	70L00561	L351	7003	25927	R	16	5631	0	0	M	0	9101	0
3	70L00561	L351	7003	25927	P	16	5388	0	0	M	5	9929	328
5	70L00561	L351	7003	7600	P	16	1508	0	0	M	11	10474	521
1	70L00589	L351	7004	25927	R	16	6603	0	0	M	9	38552	0
11	70L00589	L351	7004	25927	P	16	5388	0	0	M	8	41248	1198
12	70L00589	L351	7004	7600	P	16	5266	0	0	M	6	41248	1358
1	70L00591	L351	7004	25927	R	16	6603	0	0	M	10	38919	0
11	70L00591	L351	7004	25927	P	16	5388	0	0	M	14	42422	1351
12	70L00591	L351	7004	7600	P	16	1544	0	0	M	11	42568	1409
1	70L00592	L351	7004	25927	R	16	6603	0	0	M	14	53953	72
11	70L00592	L351	7004	25927	P	16	5388	0	0	M	7	55621	893
12	70L00592	L351	7004	7600	P	16	1544	0	0	M	8	55722	956
1	75L00230	L351	7505	25927	R	16	14017	0	0	M	179	30350	0
12	75L00230	L351	7505	11165	R	16	5460	0	0	M	10	32682	2002
1	75L00251	L351	7506	25927	R	16	14138	0	0	M	3	7450	0
12	75L00251	L351	7506	11165	R	16	5513	0	0	M	3	7928	550
1	76L00020	L351	7607	25927	T	16	15718	0	0	M	3	13731	0
12	76L00020	L351	7607	15126	T	16	8390	0	0	M	4	15073	125
1	76L00060	L351	7603	25927	T	16	15232	0	0	M	14	23922	154
5	76L00060	L351	7603	25927	T	16	14746	0	0	M	14	25301	1070
1	76L00061	L351	7603	25927	T	16	15232	0	0	M	11	27335	0
9	76L00061	L351	7603	25927	R	16	14260	0	0	M	15	30572	960
12	76L00061	L351	7603	15126	R	16	8107	0	0	M	17	31857	1382
1	80L00070	L351	8002	25927	T	16	20944	0	0	M	7	11207	0
12	80L00070	L351	8002	32102	T	16	24277	0	0	M	12	15117	1089

1	63L00028	L363	6402	23981	L	20	3028	0	0	U	0	0	10	0
9	63L00028	L363	6402	23981	H	20	2398	0	0	U	0	0	259	316
12	63L00028	L363	6402	6983	H	20	698	0	0	U	0	0	342	316
1	59L01114	L389	5908	112870	D	25	15689	-	0	U	0	0	0	0
10	59L01114	L389	5908	112870	L	25	12641		0	U	0	0	40	0
12	59L01114	L389	5908	35000	L	25	3710		0	U	0	0	40	0
1	63L00577	L461	8306	9760	T	25	9672	0	0	U	0	0	376	114
8	63L00577	L461	8306	9760	T	25	9467		0	U	0	0	376	114
1	65L00943	L461	6506	9760	R	25	3406	0	0	U	0	0	0	0
12	65L00943	L461	6506	2673	R	25	845	0	0	U	0	0	121	0
1	68L00678	L461	6805	9760	R	25	4431	0	0	U	0	0	0	0
12	68L00678	L461	6805	2673	R	25	1125	0	0	U	0	0	1011	1752
1	68L00691	L461	6806	9760	R	25	4460		0	U	0	0	0	0
12	68L00691	L461	6806	2673	R	25	1133		0	U	0	0	257	6
1	69L00442	L461	6903	9760	R	25	4724		0	U	0	0	0	0
12	69L00442	L461	6903	2730	R	25	1231		0	U	0	0	539	0
1	69L00516	L461	6903	9760	R	25	4724		0	U	0	0	0	0
12	69L00516	L461	6903	2730	R	25	1231		0	U	0	0	102	5
1	80L00300	L461	8006	9760	T	25	8677	0	0	U	0	0	185	0
12	80L00300	L461	8006	9064	T	25	7759	0	0	U	0	0	417	0
1	68L00420	L486	6902	4003	R	25	1925		0	U	0	0	0	0
2	68L00420	L486	6902	4113	R	25	1966		0	U	0	0	0	0
12	68L00420	L486	6902	3575	R	25	1602		0	U	0	0	98	0
1	68L00421	L486	6902	4003	R	25	1925		0	U	0	0	0	0
2	68L00421	L486	6902	4113	R	25	1966		0	U	0	0	0	0
12	68L00421	L486	6902	3575	R	25	1602		0	U	0	0	117	0
1	68L00422	L486	6902	4003	R	25	1925		0	U	0	0	0	0
2	68L00422	L486	6902	4113	R	25	1966		0	U	0	0	20	0
12	68L00422	L486	6902	3575	R	25	1602		0	U	0	0	93	0
1	63L00780	L504	8310	86000		10	0	0	0	H	0	55	0	0
2	63L00780	L504	8310	77714	T	10	77131	0	0	H	0	55	0	0
7	63L00780	L504	8310	77714	H	10	74217		0	H	5	219	709	1056
8	63L00780	L504	8310	77714	T	10	73634		0	H	5	226	709	1056
9	63L00780	L504	8310	77714	T	10	73051		0	H	2	389	746	1056

1984 USAF-SCEEE RESEARCH INITIATION PROGRAM

Sponsored by the  
AIR FORCE OFFICE OF SCIENTIFIC RESEARCH

Conducted by  
SOUTHEASTERN CENTER FOR ELECTRICAL ENGINEERING EDUCATION

FINAL TECHNICAL REPORT

THE DEVELOPMENT OF COMPUTATIONAL EFFICIENCIES IN  
CONTINUUM FINITE ELEMENT CODES USING MATRIX DIFFERENCE EQUATIONS

Prepared By:	Dr. Harold C. Sorensen
Academic Rank:	Associate Professor
Department and University:	Civil and Environmental Engineering Washington State University
Research Location:	Civil and Environmental Engineering Washington State University
USAF Research Focal Point:	Dr. Timothy J. Ross
Date Submitted:	November 25, 1985
Contract No.:	F49620-82-C-0035
Subcontract No.:	84 RIP 22
Subcontract Term:	11/16/84-11/15/85 (12 months)
Amount Granted:	\$12,000

THE DEVELOPMENT OF COMPUTATIONAL EFFICIENCIES IN  
CONTINUUM FINITE ELEMENT CODES USING MATRIX DIFFERENCE EQUATIONS

by  
Harold C. Sorensen

ABSTRACT

The feasibility of using the Matrix Difference Equation (MDE) theory to effect computational efficiencies in continuum finite element codes has been investigated in this research. The study was centered around the SAMSON2 code, which is a state-of-the-art 2-D code for use in dynamic structural analyses of plane and axisymmetric solids undergoing development within AFWL/NTE.

The SAMSON2 code uses explicit time integration and is particularly suited to the analysis of large displacement, large strain problems involving nonlinear material behavior and structure-media interface (SMI) problems.

The MDE method is applicable only to longitudinally periodic structures within simply supported or guided ends. The use of the MDE method is limited to linear elastic structures (small-displacement theory) for which the principle of superposition is valid. Equilibrium is not satisfied by the method. An approximate solution to the system of equations developed in any problem solution is obtained by a least squares technique. The method involves a Guyan matrix reduction which introduces errors. The eigensolutions obtained by the method are unreliable for the high half of the range of frequencies and should be discarded.

Because of the errors and approximations in the MDE method, the restrictions on geometric and material linearities, and its applicability only to

longitudinal periodic structures, it is concluded that the MDE method has a low potential for improving the computational efficiency of the SAMSON2 code.

Further study of the MDE method with regard to large displacement, large strain type finite element computer codes is not recommended. However, the MDE method could be further studied for usefulness in linear finite element solutions.

#### ACKNOWLEDGMENTS

Grateful appreciation is hereby expressed to the Air Force Systems Command, Air Force Office of Scientific Research and the Southeastern Center for Electrical Engineering Education for providing the financial support for this project.

Thanks go to the Air Force Weapons Laboratory, Kirtland, AFB for the opportunity to begin this study during a summer faculty research appointment for the P.I.

Special thanks go to Dr. Arthur Guenther (AFWL) for his support of this project and to Dr. Timothy J. Ross (AFWL/NTE) for originating the idea for this study and for his continued encouragement and support during the research period.



## 1. INTRODUCTION

The proposed research project was initiated during the summer 1984 when the P.I. (Dr. Harold C. Sorensen) spent eight weeks at AFWL/NTE, KAFB, NM as a participant in the AFOSR/SCEEE summer faculty research program. Two graduate students (S. S. Miller and R. L. Bigelis) accompanied the P.I. and worked for ten weeks toward the accomplishment of the objective of this research.

During the summer period, the P.I. became familiar with the principles and concepts of the MDE method and with the theory and operation of the SAMSON2 code. One graduate student (S. S. Miller) became very familiar with the logic of the finite element portion of the SAMSON2 code in a programming sense. He is capable of changing the code as it becomes necessary to do so. The other graduate student (R. L. Bigelis) became very familiar with the slideline concept and theory. He is capable of working with the code in this area.

The Matrix Difference Equation (MDE) method has been developed by P. H. Denke, et al. (Ref. 1) at the Douglas Aircraft Corporation and has been shown by them to reduce computational costs associated with elastic analyses of spatially periodic structures. The term "periodic structure" means a structure modeled as a linear array of identical substructures. There must also be a plane of symmetry in each substructure which is one of the key factors in the development of the method.

In the MDE method, the finite element method is applied to one of the identical substructures to obtain a mechanical impedance matrix. A matrix difference equation is derived from the impedance matrix, based on conditions of equilibrium and compatibility at the substructure boundaries. The order of the difference equation is reduced by eliminating the force variables and introducing substructure displacement modes. The solution is found by

calculating the eigenvalues and eigenvectors of a related characteristic equation. The result is a closed form expression in the longitudinal coordinate. The method is considered to be general and applicable to complex structures because of the finite element basis.

A brief summary of the MDE method is as follows.

The finite element model is given in Figure 1.

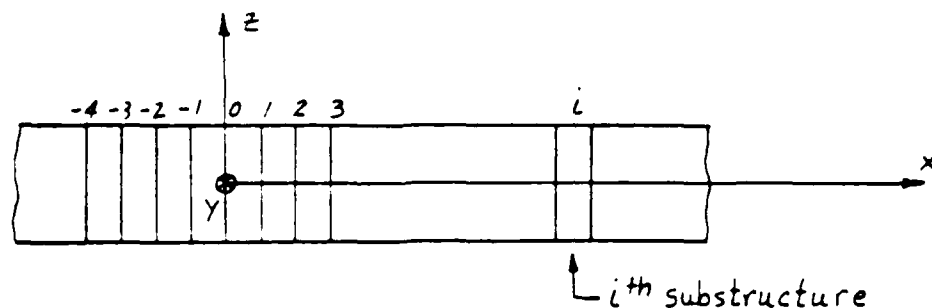


Figure 1. The structure idealized as a linear array of identical substructures.

The linear equation of motion for one substructure in harmonic motion can be written in the following form.

$$\underline{A} \underline{\Delta} = \underline{P}_u \quad (1)$$

where  $\underline{A}$  is the mechanical impedance matrix,  $\underline{\Delta}$  is a column matrix of complex displacement amplitudes and  $\underline{P}_u$  is a column matrix of complex external load amplitudes in the unconstrained degrees of freedom.

The impedance matrix is given by

$$\underline{A} = \underline{K} - \omega^2 \underline{M} + i\omega \underline{C} \quad (2)$$

where  $\omega$  = frequency,  $i = \sqrt{-1}$  and  $\underline{K}$ ,  $\underline{M}$  and  $\underline{C}$  = square symmetric stiffness, mass and damping matrices for the substructure derived by standard finite element procedures.

By eliminating the interior degrees of freedom of the substructure, Eq. 1 may be written as

$$\underline{A}_B \underline{\Delta}_B = \underline{P}_{u_B} \quad (3)$$

where

$$\underline{A}_B = \underline{K}_B - \omega^2 \underline{M}_B + i\omega \underline{C}_B \quad (4)$$

In Eq. 3 and Eq. 4, the subscript  $B$  refers to equivalent boundary matrices associated with the boundary degrees of freedom.

Through an appropriate modal transformation Eq. 3 can be written as

$$\hat{\underline{A}}_B \hat{\underline{\Delta}}_B = \hat{\underline{P}}_{u_B} \quad (5)$$

Equation 5 can be partitioned as follows

$$\begin{bmatrix} \hat{\underline{A}}_{\sim Bll} & \hat{\underline{A}}_{\sim Blr} \\ \hat{\underline{A}}_{\sim Brl} & \hat{\underline{A}}_{\sim Brr} \end{bmatrix} \begin{Bmatrix} \hat{\underline{\Delta}}_{\sim Bl} \\ \hat{\underline{\Delta}}_{\sim Br} \end{Bmatrix} = \begin{Bmatrix} \hat{\underline{p}}_{\sim uBl} \\ \hat{\underline{p}}_{\sim uBr} \end{Bmatrix} \quad (6)$$

where the subscripts  $l$  and  $r$  refer to the left and right boundaries of the substructure, respectively.

By expanding Eq. 6 and retaining the force variables,  $\hat{\underline{p}}_{\sim uB}$ , the following matrix difference can be obtained.

$$\hat{\underline{y}}_{\sim}^{(i+1)} - \hat{\underline{N}}_{\sim} \hat{\underline{y}}_{\sim}^{(i)} = \underline{0} \quad (7)$$

where

$$\hat{\underline{N}}_{\sim} = \begin{bmatrix} -\hat{\underline{A}}_{\sim Brr} \hat{\underline{A}}_{\sim Blr} & \hat{\underline{A}}_{\sim Brl} - \hat{\underline{A}}_{\sim Brr} \hat{\underline{A}}_{\sim Blr}^{-1} \hat{\underline{A}}_{\sim Bll} \\ -\hat{\underline{A}}_{\sim Blr}^{-1} & -\hat{\underline{A}}_{\sim Blr}^{-1} \hat{\underline{A}}_{\sim Bll} \end{bmatrix} \quad \& \quad \hat{\underline{y}}_{\sim}^{(i)} = \begin{Bmatrix} \hat{\underline{p}}_{\sim uBr}^{(i)} \\ \hat{\underline{\Delta}}_{\sim Br}^{(i)} \end{Bmatrix} \quad (8)$$

A solution to Eq. 7 is

$$\hat{\underline{y}}_{\sim k}^{(i)} = \hat{\underline{G}}_{\sim k} \hat{\lambda}_k^{(i)} \quad (9)$$

where  $\hat{\underline{G}}_{\sim k}$  is a column matrix and  $\hat{\lambda}_k^{(i)}$  is a scalar.

Substituting Eq. 9 into Eq. 7 gives

$$(\hat{\underline{N}} - \hat{\lambda}_k \underline{I}) \hat{\underline{G}}_k = \underline{0} \quad (10)$$

Equation 10 is a characteristic equation which can be solved for the eigenvalues  $\hat{\lambda}_k$  and the eigenvectors  $\hat{\underline{G}}_k$ .

The above formulation with force variables retained is useful for solving small problems involving limited numbers of degrees of freedom.

If Eq. 6 is again expanded, but this time with the force variables,  $\hat{\underline{p}}_{uB}$ , eliminated, the following difference equation can be obtained.

$$\hat{\underline{A}}_{Br\ell} \hat{\underline{\Delta}}_{Br}^{(i)} + (\hat{\underline{A}}_{B\ell\ell} + \hat{\underline{A}}_{Brr}) \hat{\underline{\Delta}}_{Br}^{(i+1)} + \hat{\underline{A}}_{B\ell r} \hat{\underline{\Delta}}_{Br}^{(i+2)} = \underline{0} \quad (11)$$

Equation 11 is solved by the substitution of

$$\hat{\underline{\Delta}}_{Brk} = \hat{\underline{G}}_{\Delta k} \hat{\lambda}_k^{(i)} \quad (12)$$

where  $\hat{\underline{G}}_{\Delta k}$  is a column matrix of displacement eigenvectors. This substitution gives the following equation.

$$\left[ \hat{\underline{A}}_{Br\ell} \hat{\lambda}_k^2 + (\hat{\underline{A}}_{B\ell\ell} + \hat{\underline{A}}_{Brr}) \hat{\lambda}_k + \hat{\underline{A}}_{B\ell r} \right] \hat{\underline{G}}_{\Delta k} = \underline{0} \quad (13)$$

Equation 13 is a characteristic equation in which the matrices are only half as large as those in Eq. 10, and is, therefore, worth solving even though it is quadratic in  $\hat{\lambda}$ .

In the solution for the natural frequencies and the mode shapes for the total structure, a boundary stiffness matrix,  $\underline{K}_B$ , and a boundary mass matrix,  $\underline{M}_B$ , are developed for one substructure. These two matrices have the following form.

$$\underline{K}_B = \left[ \begin{array}{cc|cc} p_{aa} & p_{ab} & g_{aa} & g_{ab} \\ p_{ab}^T & p_{bb} & -g_{ab}^T & g_{bb} \\ \hline g_{aa} & -g_{ab} & p_{aa} & -p_{ab} \\ g_{ab}^T & g_{bb} & -p_{ab}^T & p_{bb} \end{array} \right] \quad (14)$$

$$\underline{M}_B = \left[ \begin{array}{cc|cc} m_{aa} & m_{ab} & n_{aa} & n_{ab} \\ m_{ab}^T & m_{bb} & -n_{ab}^T & n_{bb} \\ \hline n_{aa} & -n_{ab} & m_{aa} & -m_{ab} \\ n_{ab}^T & n_{bb} & -m_{ab}^T & m_{bb} \end{array} \right] \quad (15)$$

Then two matrices are defined as follows

$$\underline{k}_v = \left[ \begin{array}{c|c} P_{aa} + g_{aa} \cos \theta_v & g_{ab} \sin \theta_v \\ \hline g_{ab}^T \sin \theta_v & P_{bb} + g_{bb} \cos \theta_v \end{array} \right] \quad (16)$$

$$\underline{m}_v = \left[ \begin{array}{c|c} m_{aa} + n_{aa} \cos \theta_v & n_{ab} \sin \theta_v \\ \hline n_{ab}^T \sin \theta_v & m_{bb} + n_{bb} \cos \theta_v \end{array} \right] \quad (17)$$

where

$$\theta_v = \frac{\pi v}{S} \quad v = 0, 1, 2, \dots, S \quad (18)$$

and where  $S$  is the number of substructures in the structure. Thus one  $\underline{k}_v$  matrix and one  $\underline{m}_v$  matrix are defined for each value of the integer  $v$ .

The following characteristic equation is used in the solution of a structure with simply supported or guided ends.

$$\left( \underline{k}_v - \tilde{\omega}_{k_v}^2 \underline{m}_v \right) \tilde{G}_{\Delta k_v} = \underline{0} \quad (19)$$

The matrices  $\underline{k}_v$  and  $\underline{m}_v$  are square of order  $n$ , where  $n$  is the number of boundary degrees of freedom on one substructure boundary. Therefore, Eq. 19

produces  $n$  values of the eigenvalue  $\tilde{\omega}_{kv}$  and of the eigenvector  $\tilde{q}_{kv}$  for each choice of the integer  $v$ . The eigenvalues which are obtained from Eq. 19 for each value of the integer  $v$  are coupled in that they range from low values to high values in a definite pattern. The complete solution to the problem is obtained by evaluating Eq. 19 over the entire range of the integer  $v$ .

During the summer period, after studying the theory of the MDE method, the P.I. applied the technique in the solution of a simply supported beam. A beam type finite element was used in the solution. While working through the solution of this simple linear, elastic symmetric problem, many questions arose as to why the method worked in predicting natural frequencies and mode shapes of the simple beam. These questions concerned: (1) the definitions of  $\theta_v$  and the matrices  $\underline{k}_v$  and  $\underline{m}_v$ ; (2) the basis of the associated characteristic equation; (3) why the natural frequencies occur in patterns of high-low pairs; (4) how the method could be revised to account for unsymmetrical elements; (5) how to incorporate nonlinear effects into the method; etc. Hence, it was concluded that additional study of the MDE method should be undertaken to ascertain the answers to these and related questions. However, this initial study of the MDE method provided enough background on the method to conclude that, if it can be extended to the nonlinear region and incorporated into computer codes like SAMSON2, extremely efficient computations could result.

The MDE method is based on a harmonic modal solution for which the damping matrix is defined as a linear function of the mass and the stiffness (proportional damping). The linear elastic solution process involves an explicit force balance technique. Hence, the following question needs to be



answered. Can the explicit force balance technique in MDE be extended to the nonlinear case?

The SAMSON2 code, developed by T. Belytschko and R. R. Robinson (Ref. 2) of the IIT Research Institute, uses an explicit time integration technique incorporating central finite difference equations to determine nodal accelerations, velocities and displacements resulting from the application of external loads. Strains, stresses and internal forces are determined from these nodal parameters through the use of constitutive equations and material properties. This finite difference technique can exhibit stability problems if the integration time step is too large. In many problems, many small elements are used to obtain the desired calculational accuracy and small time steps are used to guarantee the stability of the finite difference solution. This combination of many elements and many small time steps over the desired time interval results in a major computational task. Hence, there is a need to determine and implement more efficient techniques to reduce the computational effort required in solving these types of problems.

Implicit analysis schemes require matrix operations on a structure stiffness matrix in order to obtain the eigensolutions to any given problem. These implicit schemes do not exhibit computational stability problems in the solution process but they require operations, such as matrix inversion, on relatively large matrices. Explicit time integration techniques are subject to stability problems but do not require the use of matrix operations. The optimum solution technique, therefore, would be one which would use the best part of each type of solution, i.e., an implicit solution scheme with operations on a stiffness matrix of relatively low order. The MDE method has the potential of becoming the optimum solution technique.

During the summer 1984, it was learned that the higher order elements which presently exist in the SAMSON2 code do not work properly. It was also learned that, if these elements could be used in the solutions of problems, the computational process would be more efficient. Hence, it was concluded that, by studying the finite element theory for the higher order elements and comparing this theory to the higher order element definitions in the code and then correcting any errors existing in the code, the code would be more efficient. This study would also provide the necessary background in the finite element logic of the code in order to know where and how to incorporate the MDE approach into the code as MDE is developed.

While at AFWL, it also was learned that the slideline model in the SAMSON2 code does not work as well as it was originally intended. Hence, it was concluded that a study should be initiated (1) to investigate the slideline model in order to change it to be more compatible with real world problems and (2) to begin the development of a finite element to replace the slideline model. This study would also provide the necessary background in the structure-media interface (SMI) concept in order to develop an SMI element which will be compatible with the MDE approach and the numerical integration schemes of the SAMSON2 code.

The slideline in the SAMSON2 code has no stiffness. Therefore, it has no harmonic solution, and the following question concerning the slideline concept needs to be answered. How is the slideline to be incorporated into the MDE method which involves a harmonic solution?

### II. OBJECTIVE

Finite element computer codes which are used to solve problems containing a large number of elements are expensive to run. The objective of this research is to effect computational efficiencies in numerical algorithms of continuum finite element codes using the matrix difference equation (MDE) approach. The research will center around the SAMSON2 code, but the general theory should be adaptable to other continuum finite element codes. The SAMSON2 code is a state-of-the-art research tool undergoing development within AFWL/NTE and is a two-dimensional code used for the dynamic analyses of plane and axisymmetric solids. The SAMSON2 code uses explicit time integration and is particularly suited for the analysis of large displacement, large strain problems involving nonlinear material behavior and structure-media interface (SMI) conditions.

During this study, material published by Dr. P. H. Denke and others at the McDonnell Douglas Corporation will be reviewed to determine the applicability of the MDE method to the solution of problems important to the AFWL. Much of what follows are amplifications and physical explanations of the original work.

### III. SCOPE

The scope of the work in this report deals with the study of the MDE theory to obtain the answers to the following questions.

1. What is the basis for the definition of  $\theta_v$ ?
2. From where are the matrices  $k_v$  and  $m_v$  derived, and why do they work as defined?
3. Why do high-low frequency pairs occur for the different values of  $\nu$ ?

## 17. RESEARCH FINDINGS

The purpose of this section is to provide the results obtained by performing work associated with the scope of this report.

Question 1. What is the basis for the definition of  $\Theta_v$ ?

The definition for  $\Theta_v$  (see p. 11) can be obtained by solving for the free lateral vibrations of a prismatic bar. This solution can be found in any textbook on vibrations (Ref. 3). Only enough of the development is presented here to show how  $\Theta_v$  is defined.

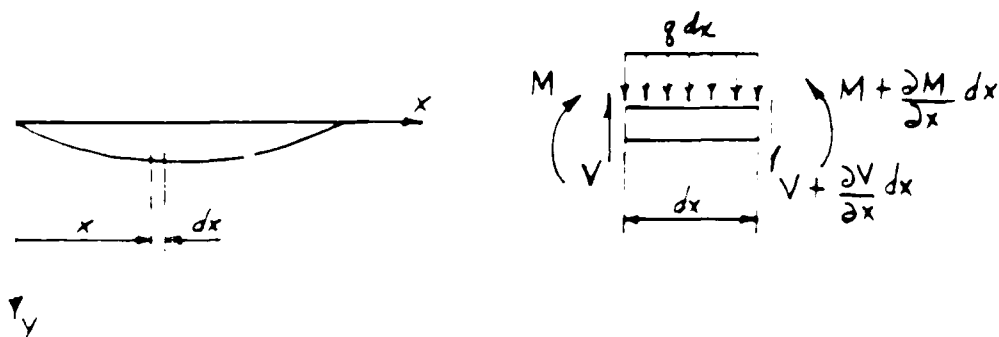


Fig. 2. Laterally Loaded Prismatic Beam

The motion of a vibrating beam is described by the partial differential equation (free vibrations,  $EI = \text{constant}$ )

$$a^2 \frac{\partial^4 y}{\partial x^4} = - \frac{\partial^2 y}{\partial t^2} \quad (20)$$

where  $a^2 = \frac{EI}{\gamma}$

$EI$  = beam flexural stiffness

$\gamma$  = mass per unit length of the beam

and in which shear and rotary inertia have been neglected. The general solution to this equation is

$$y(x,t) = (C_1 \cosh kx + C_2 \sinh kx + C_3 \cos kx + C_4 \sin kx) A' \cos(\omega t - \phi) \quad (21)$$

where  $\omega = a k^2 \quad (22)$

For a simply supported beam, the boundary conditions are

$$1) y(0,t) = 0 \quad 2) y(l,t) = 0 \quad 3) \frac{\partial^2 y}{\partial x^2}(0,t) = -\frac{M}{EI} = 0 \quad 4) \frac{\partial^2 y}{\partial x^2}(l,t) = -\frac{M}{EI} = 0$$

From BC1 and BC3,  $C_1 = C_3 = 0$ .

From BC2 and BC4,

$$0 = C_2 \sinh kl + C_4 \sin kl \quad (23)$$

$$0 = C_2 \sinh kl - C_4 \sin kl \quad (24)$$

For a nontrivial solution, the determinant of the coefficients in Equations 23 and 24 must be zero. Hence,

$$\sinh kl \sin kl = 0 \quad (25)$$

Equation 25 can be satisfied provided  $\sin kl = 0$ .

Therefore,  $kl = n\pi$  (26)  
 $n = 1, 2, 3, \dots$

and  $k^2 = \frac{n^2\pi^2}{l^2}$  (27)

We now see from Equations 22 and 27 that a simply supported beam has an infinite number of natural frequencies and modes of vibration.

Note that in Equation 26,  $n$  is the number of half sine waves in the simply supported beam associated with each of the various natural modes. This equivalency for  $n$  can be verified by the following procedure.

Substitution of Equation 26 into either of Equations 23 or 24 gives  $C_2 = 0$ . Hence the general solution, Equation 21, reduces to

$$y(x,t) = C_n \sin \frac{n\pi x}{l} \cos(\omega_n t - \phi) \quad (28)$$

Note that the term  $\sin \frac{n\pi x}{l}$  is a shape function for which only the amplitude varies with time. Plots of  $y = \sin \frac{n\pi x}{l}$  for  $n = 1, 2, 3$  are as follows:

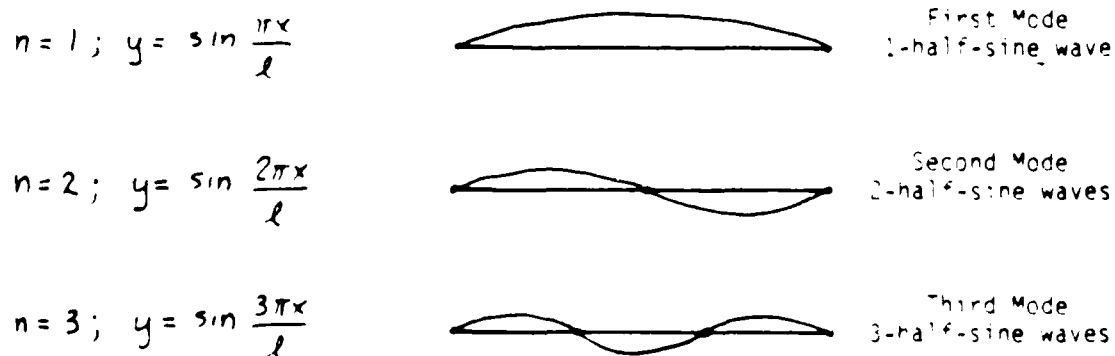


Fig. 3. Mode Shape Patterns

Mode shape patterns similar to those in Fig. 3 can be obtained for a finite number of the mode shapes for a simply supported beam if the length,  $l$ ,

of the beam is represented by a finite number of equal length segments,  $s$ , where  $s$  is associated with the number of modes shapes desired. Then  $x$  in the sine term of Equation 28 is represented by a number,  $n$ , of the segments within the range of values of  $s$ .

For example, if the number of mode shapes desired is 3, then  $s = 3$  and the length of each segment is  $\frac{l}{3}$ , and the beam is represented as shown in Fig. 4. We can write

$$kx = \frac{n\pi x}{l} = n\pi \left(\frac{x}{l}\right) \equiv v\pi \left(\frac{l}{s}\right) = \theta_v l \quad (29)$$

where  $kx \equiv \theta_v l$ ,  $n \equiv v$  and  $\frac{x}{l} \equiv \frac{l}{s}$  where  $v$  is the number of particular segments which locate a particular point along the beam. Hence

$y = \sin \frac{v\pi l}{s} \equiv \sin \frac{n\pi x}{l}$  and the first three mode shape patterns are as shown. It is concluded from Equation 29, that

$$\theta_v = \frac{v\pi}{s} \quad v = 0, 1, 2, \dots, s \quad (30)$$

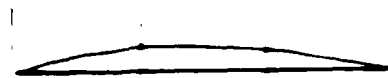
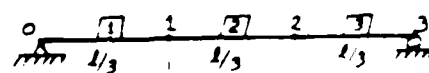
which is the symbolism used in the MDE theory.

$$s = 3; \quad l = 0, 1, 2, 3$$

$$v = 1; \quad y = \sin \frac{\pi l}{s}$$

$$v = 2; \quad y = \sin \frac{2\pi l}{s}$$

$$v = 3; \quad y = \sin \frac{3\pi l}{s}$$



First Mode  
1-half-sine wave



Second Mode  
2-half-sine waves



Third Mode  
3-half-sine waves

Fig. 4. Mode Shape Patterns

Question 2. From where are the matrices  $\underline{k}_v$  and  $\underline{m}_v$  derived, and why do they work as defined?

The matrices  $\underline{k}_v$  and  $\underline{m}_v$  (see p. 11) are derived from the substructure stiffness matrix  $\underline{K}_B$  and the substructure mass matrix  $\underline{M}_B$ , respectively, by a transformation of the form

$$\underline{k}_v = \underline{I}_s^T \underline{K}_B \underline{I}_s \quad \text{and} \quad \underline{m}_v = \underline{I}_s^T \underline{M}_B \underline{I}_s$$

The coordinate transformation matrix,  $\underline{I}_s$ , is defined as

$$\underline{I}_s = \begin{bmatrix} \underline{I}_a a & 0 \\ 0 & \underline{I}_b b \\ \underline{I}_a b & 0 \\ 0 & \underline{I}_b a \end{bmatrix}$$

where  $\underline{I}_a$  and  $\underline{I}_b$  are unit matrices have  $n_a$  the number of a-type displacements and  $n_b$  the number of b-type displacements rows, respectively, and where the scalars  $a$  and  $b$  are defined as

$$a = \cos \left( \frac{\pi}{4} - \frac{\theta_v}{2} \right)$$

$$b = \sin \left( \frac{\pi}{4} - \frac{\theta_v}{2} \right)$$

$$\theta_v = \frac{\pi v}{S} \quad v = 0, 1, 2, \dots, S$$

The two different substructure displacement types are illustrated in Fig. 5. The transverse plane midway between the substructure boundaries is designated as the median cross-section. Type a displacements (vectors) are symmetric about the median cross-section and type b displacements are antisymmetric.



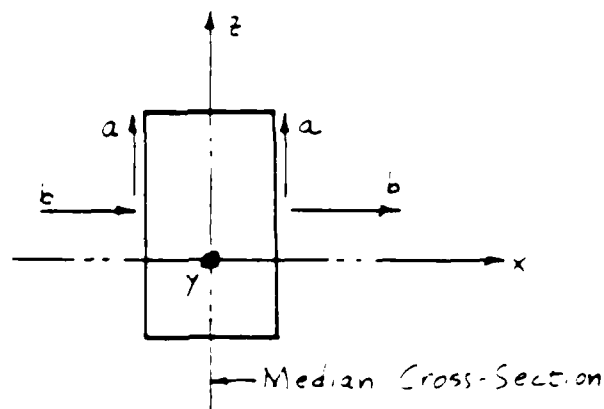


Fig. 6. Substructure Displacement Classification

The transformation,  $\underline{I}_s$ , has more rows than columns and, therefore, reduces the size of the problem. The forms of the scalars,  $a$  and  $b$ , have been chosen to preserve the symmetry and the antisymmetry properties of the  $a$ -type and  $b$ -type displacements through the transformation. The zeros in the transformation are also required in order to preserve the displacements in the proper order, i.e.,  $a$ -type transform to  $a$ -type and  $b$ -type transform to  $b$ -type. In order for  $\underline{B}_v$  and  $\underline{m}_v$  to work as defined, they must be associated with the original substructure. A summary of the transformation procedure required to show this association is as follows.

$$\underline{\Delta}_B^{(c)} = \underline{I}_s \underline{\bar{\Delta}}_B^{(c)} \quad (31)$$

where  $\underline{\Delta}_B^{(c)}$  is the matrix of the substructure boundary displacements (global sense) and  $\underline{\bar{\Delta}}_B^{(c)}$  is the matrix of the transformed substructure boundary displacements (local sense).

Upon substitution

$$\begin{Bmatrix} \underline{\Delta}_{B2a}^{(c)} \\ \underline{\Delta}_{B2b}^{(c)} \\ \underline{\Delta}_{B1a}^{(c)} \\ \underline{\Delta}_{B1b}^{(c)} \end{Bmatrix} = \begin{bmatrix} \underline{I}_{a^2} & 0 \\ 0 & \underline{I}_{b^2} \\ \underline{I}_{a^b} & 0 \\ 0 & \underline{I}_{b^a} \end{bmatrix} \begin{Bmatrix} \underline{\bar{\Delta}}_{B2a}^{(c)} \\ \underline{\bar{\Delta}}_{B2b}^{(c)} \\ \underline{\bar{\Delta}}_{B1a}^{(c)} \\ \underline{\bar{\Delta}}_{B1b}^{(c)} \end{Bmatrix} \quad (32)$$

In Equation 32,  $\underline{\Delta}_B^{(i)}$  is partitioned according to a and b type displacements on the left and right sides of the substructure. The matrix  $\bar{\underline{\Delta}}_B^{(i)}$  has two partitions to correspond to the partitioning of  $\underline{I}_S$ . The matrices  $\bar{\underline{\Delta}}_{Ba}^{(i)}$  and  $\bar{\underline{\Delta}}_{Bb}^{(i)}$  have  $n_a$  rows and  $n_b$  rows in order to be conformable with  $\underline{I}_a$  and  $\underline{I}_b$ .

Expanding Equation 32 gives

$$\underline{\Delta}_{Ba}^{(i)} = \bar{\underline{\Delta}}_{Ba}^{(i)} \cos\left(\frac{\pi}{4} - \frac{\theta_v}{2}\right) \quad (33)$$

$$\underline{\Delta}_{Bb}^{(i)} = \bar{\underline{\Delta}}_{Bb}^{(i)} \sin\left(\frac{\pi}{4} - \frac{\theta_v}{2}\right) \quad (34)$$

$$\underline{\Delta}_{Bra}^{(i)} = \bar{\underline{\Delta}}_{Ba}^{(i)} \sin\left(\frac{\pi}{4} - \frac{\theta_v}{2}\right) \quad (35)$$

$$\underline{\Delta}_{Brb}^{(i)} = \bar{\underline{\Delta}}_{Bb}^{(i)} \cos\left(\frac{\pi}{4} - \frac{\theta_v}{2}\right) \quad (36)$$

Combining Equation 33 with 35 and Equation 34 with 36 gives

$$\frac{\underline{\Delta}_{Bra}^{(i)}}{\underline{\Delta}_{Ba}^{(i)}} = \frac{\sin \frac{\pi}{4} \left(1 - \frac{2\nu}{5}\right)}{\cos \frac{\pi}{4} \left(1 - \frac{2\nu}{5}\right)} \quad (37)$$

$$\frac{\underline{\Delta}_{Brb}^{(i)}}{\underline{\Delta}_{Bb}^{(i)}} = \frac{\cos \frac{\pi}{4} \left(1 - \frac{2\nu}{5}\right)}{\sin \frac{\pi}{4} \left(1 - \frac{2\nu}{5}\right)} \quad (38)$$

where, for example,  $\Delta_{Bra_j}^{(i)}$  means the  $j$ th a-type displacement on the right hand boundary of the  $i$ th substructure and  $\theta_2 = \frac{2\pi}{5}$ .

Equation 37 shows that the substructure is constrained so that the ratio of an a-type displacement on the right hand boundary to the corresponding displacement on the left hand boundary has a constant value for all degrees of freedom. This ratio depends on the integer  $\nu$ . The b-type displacements are similarly restrained. The constraints implied by the transformation,  $\underline{T}_S$ , are shown for three values of  $\nu$  in Figures 6, 7 and 8.

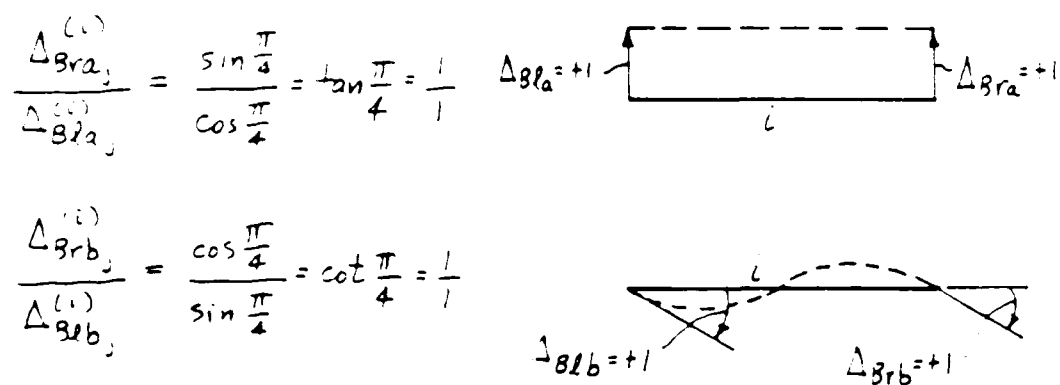


Fig. 6. Substructure Constraints for  $\nu = 0$

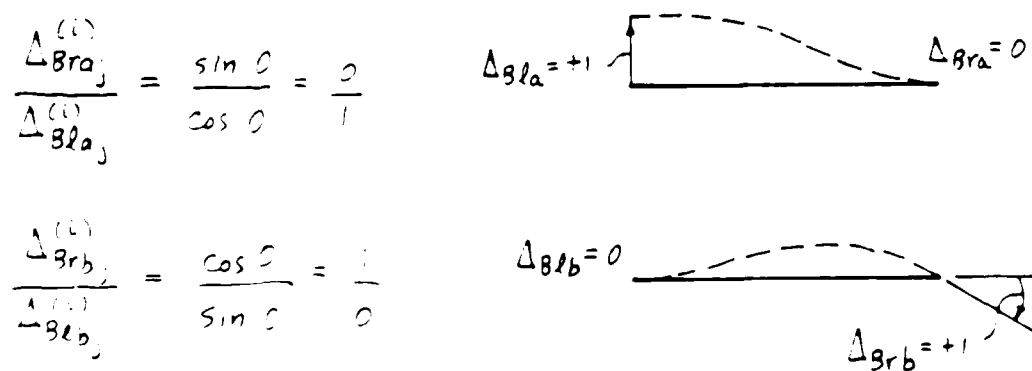
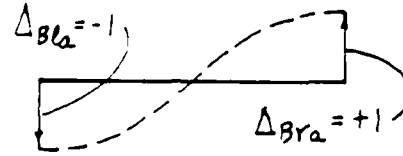


Fig. 7. Substructure Constraints for  $\nu = \frac{5}{2}$

$$\frac{\Delta_{Bra_j}^{(i)}}{\Delta_{Bla_j}^{(i)}} = \frac{\sin \frac{-\pi}{4}}{\cos \frac{-\pi}{4}} = \tan \frac{-\pi}{4} = -\frac{1}{1}$$



$$\frac{\Delta_{Brb_j}^{(i)}}{\Delta_{Blb_j}^{(i)}} = \frac{\cos \frac{-\pi}{4}}{\sin \frac{-\pi}{4}} = \cot \frac{-\pi}{4} = -\frac{1}{1}$$

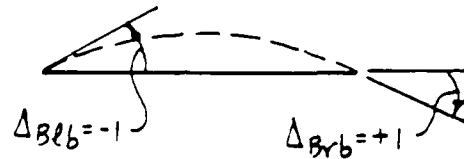


Fig. 8. Substructure Constraints for  $\nu = 5$

These constraints can be realized physically by mechanical linkages that require the ratios to have the values shown. In particular from Fig. 7 for  $\nu = \frac{5}{2}$ , all a-type displacements on the right hand boundary and b-type displacements on the left hand boundary are constrained to be zero as shown. Similarly from Fig. 6, the a-type and b-type displacements have equal magnitudes with the same sign and from Fig. 8, the displacements have the same magnitudes but opposite signs. Therefore, the constrained structure is a real structure, and its stiffness and mass matrices are positive definite, for all values of  $\nu$ .

Upon substitution of  $\underline{K}_B$  and  $\underline{I}_S$ , the matrix  $\underline{k}_\nu$  becomes

$$\underline{k}_\nu = \begin{bmatrix} p_{aa}(a^2+b^2) + g_{aa} * 2ab & g_{ab}(a^2-b^2) \\ g_{ab}^T(a^2-b^2) & p_{bb}(a^2+b^2) + g_{bb} * 2ab \end{bmatrix} \quad (39)$$

Noting that  $a^2 + b^2 = 1$  ;  $a^2 - b^2 = \sin \theta_v$  ;  $2ab = \cos \theta_v$

$$\underline{k}_v = \begin{bmatrix} p_{aa} + g_{aa} \cos \theta_v & g_{ab} \sin \theta_v \\ g_{ab}^T \sin \theta_v & p_{bb} + g_{bb} \cos \theta_v \end{bmatrix} \quad (40)$$

Similarly

$$\underline{m}_v = \begin{bmatrix} m_{aa} + n_{aa} \cos \theta_v & n_{ab} \sin \theta_v \\ n_{ab}^T \sin \theta_v & m_{bb} + n_{bb} \cos \theta_v \end{bmatrix} \quad (41)$$

Thus  $\underline{k}_v$  and  $\underline{m}_v$  are stiffness and mass matrices of the original substructure modified by the constraints implied by the transformations. These constraints can be physically realized. Therefore,  $\underline{k}_v$  and  $\underline{m}_v$  are stiffness and mass matrices of a real structure. They are therefore positive definite, and the eigenvalues  $\tilde{\omega}_{kv}^2$  of the frequency equation

$$\left[ \underline{k}_v - \tilde{\omega}_{kv}^2 \underline{m}_v \right] \underline{G}_{\Delta kv} = \underline{0} \quad (42)$$

are real and positive. The corresponding eigenvectors  $\underline{G}_{\Delta kv}$  are real.

Question 3. Why do high-low frequency pairs occur for the different values of  $\nu$ ?

The answer to this question is found by examining the solution to Equation 13, which is rewritten here for continuity.

$$\left[ \hat{A}_{\sim B l r} \hat{\lambda}_k^2 + (\hat{A}_{\sim B l l} + \hat{A}_{\sim B r r}) \hat{\lambda}_k + \hat{A}_{\sim B r l} \right] \hat{G}_{\Delta k} = 0 \quad (13)$$

The  $\hat{A}$  matrices in this equation are of order  $\hat{n}$  and the characteristic equation has  $2\hat{n}$  eigensolutions, since it is quadratic.

By dividing the  $\hat{\lambda}_k$  and rearranging the terms in Equation 13, the characteristic equation can be written in the following form

$$\left( \hat{A}_{\sim B r l} \frac{1}{\hat{\lambda}_k} + \hat{A}_{\sim B l l} + \hat{A}_{\sim B r r} + \hat{A}_{\sim B r l} \hat{\lambda}_k \right) \hat{G}_{\Delta k} = 0 \quad (43)$$

For a nontrivial solution of the characteristic equation to exist, the determinant of the coefficient matrix must be zero, i.e.,

$$\left| \hat{A}_{\sim B r l} \frac{1}{\hat{\lambda}_k} + \hat{A}_{\sim B l l} + \hat{A}_{\sim B r r} + \hat{A}_{\sim B r l} \hat{\lambda}_k \right| = 0 \quad (44)$$

The rows and the columns in a determinant may be interchanged without changing its value.

Therefore,

$$\left| \hat{A}_{\sim B r l}^T \frac{1}{\hat{\lambda}_k} + \hat{A}_{\sim B l l}^T + \hat{A}_{\sim B r r}^T + \hat{A}_{\sim B l r}^T \hat{\lambda}_k \right| = 0 \quad (45)$$

The boundary impedance matrix can be written in partitioned form as

$$\hat{\tilde{A}}_B = \begin{bmatrix} \hat{\tilde{A}}_{Bll} & \hat{\tilde{A}}_{Blr} \\ \hat{\tilde{A}}_{Br l} & \hat{\tilde{A}}_{Brr} \end{bmatrix} \quad (46)$$

This impedance matrix is symmetric, therefore

$$\hat{\tilde{A}}_{Blr} = \hat{\tilde{A}}_{Br l}$$

$$\hat{\tilde{A}}_{Bll}^T = \hat{\tilde{A}}_{Bll}$$

$$\hat{\tilde{A}}_{Blr}^T = \hat{\tilde{A}}_{Blr}$$

$$\hat{\tilde{A}}_{Brr}^T = \hat{\tilde{A}}_{Brr}$$

Hence, if  $\hat{\lambda}_k$  in Equation 45 is replaced by  $1/\hat{\lambda}_k$ , the characteristic equation is still satisfied. Therefore, if  $\hat{\lambda}_k$  is an eigenvalue, then its reciprocal,  $1/\hat{\lambda}_k$ , is also an eigenvalue.

Let  $\hat{\lambda}_k \equiv \hat{\lambda}_{lk}$  be an eigenvalue of the characteristic equation, and let  $\hat{\lambda}_{gk} \equiv 1/\hat{\lambda}_{lk} \equiv 1/\hat{\lambda}_k$  for which  $\hat{\lambda}_{gk}$  must also be an eigenvalue. Hence

$$\hat{\lambda}_{lk} * \hat{\lambda}_{gk} = 1 \quad (47)$$

The conclusion is that the eigenvalues occur in reciprocal pairs, such that, one of the values is associated with a low(er) frequency and one with a

great(er) frequency. The subscripts  $l$  and  $g$  refer to "lower" and "greater" as implied in the definitions.

A study of the SAMSON2 code was conducted concurrently with the study of the MDE method. The study concerning the SAMSON2 code has not been completed at this writing and is currently supported by funding provided by the Air Force Weapons Laboratory. However, the SAMSON2 study has progressed far enough to form the conclusion that the results of the SAMSON2 study will not change the findings pertinent to the MDE method as stated in this report. The intermediate results available at this time from the SAMSON2 study will not be reported here but will be discussed in detail in a final report to the AFWL in 1986.



## 7. DISCUSSION

The SAMSON2 code is a two-dimensional code to be used for dynamic structural analysis of plane and axisymmetric solids. The program uses explicit time integration and is particularly suited to the analysis of large displacement, large strain problems involving nonlinear material behavior and structure-media (SMI) problems.

In contrast, the Matrix Difference Equation (MDE) method is a hybrid approach that can be expected to increase the efficiency of the finite element analysis only for a particular class of structures. The MDE method is applicable only to periodic structures and is based on the following assumptions.

1. The structure is represented by a finite element model.
2. The model is longitudinally periodic which requires the axis of a linear array of identical substructures to be a straight line.
3. Strains are linear functions of displacements, stresses are linear functions of strains and loads are linear functions of stresses (i.e., geometric and material linearity).
4. Forcing functions are sinusoidal functions of time of a single frequency. Forcing functions include external loads, support displacements and element unassembled deformations. Each forcing function can have its own amplitude and phase angle. Responses to forcing functions of different frequencies can be separately calculated and superimposed in the time domain because of the assumed linearity.
5. The substructure is symmetric about a median plane normal to the longitudinal axis (i.e., longitudinal symmetry).
6. The ends of the structure are simply supported or guided according to generalized definitions.

7. The assembled substructure damping matrix is a linear combination of the assembled mass and stiffness matrices (i.e., proportional damping).

An advantage of the MDE method compared to conventional finite-element analysis is that the responses in the MDE method, such as displacements, are given in closed-form exponential and sinusoidal functions of the longitudinal coordinate. As a result, a significant cost savings in computing should be realized compared to the conventional approach. For example, all of the natural modes and frequencies of a periodic structure of a particular type can be found by calculating the eigensolutions of characteristic equations equal in order to the number of degrees of freedom on one substructure boundary.

An advantage of the MDE approach compared to differential equation analysis employing ordinary or partial differential equations with constant coefficients is that while the structure must be longitudinally periodic, it need not be uniform in any direction, and any boundary conditions can exist along the edges.

However, the SAMSON2 code does not fall into either the category of conventional finite element analysis or that of linear ordinary or partial differential equations with constant coefficients. Therefore, the advantages previously mentioned are not applicable to the SAMSON2 code. In fact, it is the opinion of the writer that the MDE method cannot be incorporated successfully into the SAMSON2 code because the MDE method is too restrictive in its development and use. A list of disadvantages of the MDE method pertinent to the SAMSON2 code is as follows:

1. The structure must be longitudinally periodic. (The SAMSON2 code is used frequently for the solutions of axisymmetric problems.)

2. The structure must have pinned or guided ends. (Too restrictive for SAMSON2.) The solutions to problems with other end conditions by the MDE method are very complicated.
3. The MDE method is founded on linearity. (In direct conflict with the nonlinear capability in SAMSON2.)
4. The substructures must be symmetrical about a median line. (This would eliminate the use of some elements in SAMSON2, e.g., all forms of the triangular element.)
5. Only sinusoidal forcing functions may be used with the MDE method. (It would be difficult to model the high amplitude pressure wave used in the SAMSON2 code as a sine wave.)
6. The MDE method requires the use of a stiffness matrix. (SAMSON2 is based on explicit time integration for which there is no requirement to compute a stiffness matrix.)
7. Weighting factors are needed to obtain solutions by the MDE method for end conditions other than pinned ends or guided ends. These weighting factors have not been derived.
8. The equilibrium condition used in the MDE method results in untransformed forces that only approximately satisfy equilibrium at a loaded boundary. (Dynamic equilibrium is satisfied in the SAMSON2 code through the use of the equation of motion.)
9. The MDE method requires the use of the principle of superposition. Hence, only small displacements are allowed. (Large displacements must be allowed in the code because of the extremely high magnitudes of loads in AFWL problems.) It is the opinion of the writer that the extension of the MDE method to incorporate nonlinear capabilities would be an enormous task.

10. In conventional finite element procedures, a set of equations is solved based on one independent equation per degree of freedom, i.e., per unknown displacement in the problem. In the MDE method, a coordinate transformation is performed to reduce the number of unknowns (displacements) in the problem in order to reduce the computational time required in the solution (refer to the discussion on p. 20).

In MDE, the number of end conditions is equal to twice the number of degrees of freedom on one substructure boundary. Hence, the actual number of scalar equations available for the solution is  $2n$ , where  $n$  = the number of degrees of freedom per substructure boundary. After the transformation is applied, the number of unknowns is  $2\hat{n}$ , where  $\hat{n}$  = the number of transformed degrees of freedom per substructure boundary.

Thus, in the MDE method, there exist  $2n$  scalar equations and  $2\hat{n}$  unknowns with the number of equations greater than the number of unknowns. Consequently, no solution exists that exactly satisfies all of the equations. However, an approximate solution is obtained based on the method of least squares, which is applicable when a set of real equations has more equations than unknowns. The least squares method gives a solution for which the sum of the squares of the residuals (errors) of the equations being solved is a minimum.

11. The eigenvalues obtained in the MDE method occur in reciprocal related pairs; one low frequency value and one high frequency value. The higher frequency values and the corresponding mode shapes produced by the MDE method tend to be inaccurate and unreliable (the error is greater than 25% even in relatively small problems) and should be discarded. (In many problems of interest to the Air Force the higher frequencies of vibration can contribute significantly to the solution.) The errors result from

several approximations inherent in the MDE method. A discussion of several approximations is given briefly in the following paragraphs.

Errors are attributed to the substructure mass matrix, which is approximate. This mass matrix approximation is associated with the Guyan transformation used in the MDE method as discussed in the following paragraphs.

A Guyan transformation (Ref. 4) is used in the MDE method to reduce the size of the problem. Just as it is necessary to reduce the size of the stiffness matrix for the static structural analysis, the simultaneous reduction of the nondiagonal mass matrix for natural mode analysis is also required.

The general static structural equations

$$\underline{F} = \underline{K} \underline{X} \quad (\text{Force} = \text{stiffness} * \text{displacement})$$

can be arranged, so that after partitioning, the following form exists.

$$\begin{bmatrix} \underline{F}_B \\ \underline{F}_I \end{bmatrix} = \begin{bmatrix} \underline{K}_{BB} & \underline{K}_{BI} \\ \underline{K}_{IB} & \underline{K}_{II} \end{bmatrix} \begin{bmatrix} \underline{X}_B \\ \underline{X}_I \end{bmatrix} \quad \begin{array}{l} B = \text{boundary} \\ I = \text{interior} \end{array} \quad (48)$$

Upon expansion, the two resulting equations are

$$\underline{F}_B = \underline{K}_{BB} \underline{X}_B + \underline{K}_{BI} \underline{X}_I \quad (49)$$

$$\underline{F}_I = \underline{K}_{IB} \underline{X}_B + \underline{K}_{II} \underline{X}_I \quad (50)$$

From Equation 50

$$\underline{X}_I = \underline{K}_{II}^{-1} (\underline{F}_I - \underline{K}_{IB} \underline{X}_B) \quad (51)$$

Substituting Equation 51 into Equation 49 gives

$$\underline{F}_B^E = \underline{K}_B \underline{X}_B \quad (52)$$

where  $\underline{K}_B = \underline{K}_{BB} - \underline{K}_{BI} \underline{K}_{II}^{-1} \underline{K}_{IB}$  (53)

and  $\underline{F}_B^E = \underline{F}_B - \underline{K}_{BI} \underline{K}_{II}^{-1} \underline{F}_I$  (54)

Note in Equation 54 that  $\underline{F}_B$  is a matrix of actual loads applied to the boundary, while  $\underline{F}_B^E$  is a matrix of equivalent boundary loads.

In a Guyan reduction the internal forces,  $\underline{F}_I$ , are eliminated, i.e.,  $\underline{F}_I = \underline{0}$ . Hence, with  $\underline{F}_I = \underline{0}$ , Equations 51 through 54 give

$$\underline{X}_I = - \underline{K}_{II}^{-1} \underline{K}_{IB} \underline{X}_B \quad (55)$$

$$\underline{F}_B^E = \underline{F}_B = \underline{K}_B \underline{X}_B \quad (56)$$

and  $\underline{K}_B = \underline{K}_{BB} - \underline{K}_{BI} \underline{K}_{II}^{-1} \underline{K}_{IB}$  (57)

By comparing Equations 51 and 55, one can see that an error exists in calculating interior displacements, because the effects of the interior loads are not included in a Guyan transformation, i.e.,  $\underline{F}_I = \underline{0}$ .

The Guyan transformation,  $\underline{T}_G$ , which produces Equation 55 is

$$\underline{T}_G = \begin{bmatrix} \underline{I} \\ -\underline{K}_{II}^{-1} \underline{K}_{IB} \end{bmatrix} \quad (58)$$

or in equation form,  $\underline{X} = \underline{T}_G \underline{X}_B$ , or

$$\begin{bmatrix} \underline{X}_B \\ \underline{X}_I \end{bmatrix} = \begin{bmatrix} \underline{I} \\ -\underline{K}_{II}^{-1} \underline{K}_{IB} \end{bmatrix} \underline{X}_B \quad (59)$$

If the structure energies are written  $T = \frac{1}{2} \dot{\underline{X}}^T \underline{M} \dot{\underline{X}}$  (kinetic energy) and  $V = \frac{1}{2} \underline{X}^T \underline{K} \underline{X}$  (potential energy) and the Guyan transformation,  $\underline{T}_G$ , is used, the result is (Ref. 5)

$$T = \frac{1}{2} \dot{\underline{X}}_B^T (\underline{T}_G^T \underline{M} \underline{T}_G) \dot{\underline{X}}_B = \frac{1}{2} \dot{\underline{X}}_B^T \underline{M}_R \dot{\underline{X}}_B \quad (60)$$

$$V = \frac{1}{2} \underline{X}_B^T (\underline{T}_G^T \underline{K} \underline{T}_G) \underline{X}_B = \frac{1}{2} \underline{X}_B^T \underline{K}_R \underline{X}_B \quad (61)$$

from which the reduced stiffness is seen to be

$$\underline{K}_R = \underline{T}_G^T \underline{K} \underline{T}_G \quad (62)$$

and the reduced mass matrix is seen to be

$$\underline{M}_R = \underline{I}_G^T \underline{M} \underline{I}_G \quad (63)$$

Evaluation of Equation 62 gives

$$\underline{K}_R = \underline{K}_{BB} - \underline{K}_{BI} \underline{K}_{II}^{-1} \underline{K}_{IB} \equiv \underline{K}_B \quad (64)$$

which is identical to Equation 57.

If the nondiagonal mass matrix is taken as

$$\underline{M} = \begin{bmatrix} \underline{M}_{BB} & \underline{M}_{BI} \\ \underline{M}_{IB} & \underline{M}_{II} \end{bmatrix} \quad (65)$$

the reduced mass matrix resulting from Equation 63 is

$$\underline{M}_R = \underline{M}_{BB} - \underline{M}_{BI} \underline{K}_{II}^{-1} \underline{K}_{IB} - (\underline{K}_{II}^{-1} \underline{K}_{IB}) (\underline{M}_{IB} - \underline{M}_{II} \underline{K}_{II}^{-1} \underline{K}_{IB}) \quad (66)$$

From Equation 64 it can be seen that in the case of the reduced stiffness matrix, none of the structural complexity is lost by the Guyan transformation, since all elements of the original stiffness matrix contribute. However, in the reduced mass matrix, combinations of stiffnesses and mass elements appear. The result is that the eigensolution problem is not exactly preserved.



Applying the Guyan reduction in the MDE method to the dynamic problem results in another approximation, which is associated with inertia loads. As previously discussed, the Guyan reduction is based on the assumption that interior displacements result from imposed boundary displacements and not from interior loads which are assumed to be zero. Hence, in the dynamic case, large interior inertia loads can be acting even if no external loads are applied to interior nodes.

#### VI. CONCLUSIONS

Based on the previous discussion, it is concluded that the potential for the Matrix Difference Equation method to effect any significant computational efficiencies in the SAMSON2 finite element code being developed at AFWL/NTE is very low.

#### VII. RECOMMENDATIONS

It is hereby recommended that financial support by the Air Force for future research on the MDE method for possible incorporation into large displacement, large strain type finite element codes be discontinued.

Future work to determine the feasibility of the MDE method for incorporation into more conventional linear elastic finite element codes, because of the reduction in the order matrices used in the MDE method, could be supported.

VIII. REFERENCES

1. P. H. Denke, G. R. Eide and J. Pickard, "Matrix Difference Equation Analysis of Vibrating Periodic Structures," AIAA Journal, Vol. 13, No. 2, 1975, pp. 160-166.
2. T. Belytschko and R. R. Robinson, "SAMSON2: A Nonlinear Two-Dimensional Structure/Media Interaction Computer Code," AFWL Final Report, No. AFWL-TR-81-109, January 1982.
3. G. L. Downey and G. M. Smith, Advanced Dynamics, International Textbook Company, 1960.
4. R. J. Guyan, "Reduction of Stiffness and Mass Matrices," AIAA Journal, Vol. 3, No. 2, p. 380, 1965.
5. R. W. Clough and J. Penzien, Dynamics of Structures, McGraw-Hill Book Company, 1975.

AD-A186 498

UNITED STATES AIR FORCE RESEARCH INITIATION PROGRAM

03/11

1984 RESEARCH REPORTS (U) SOUTHEASTERN CENTER FOR

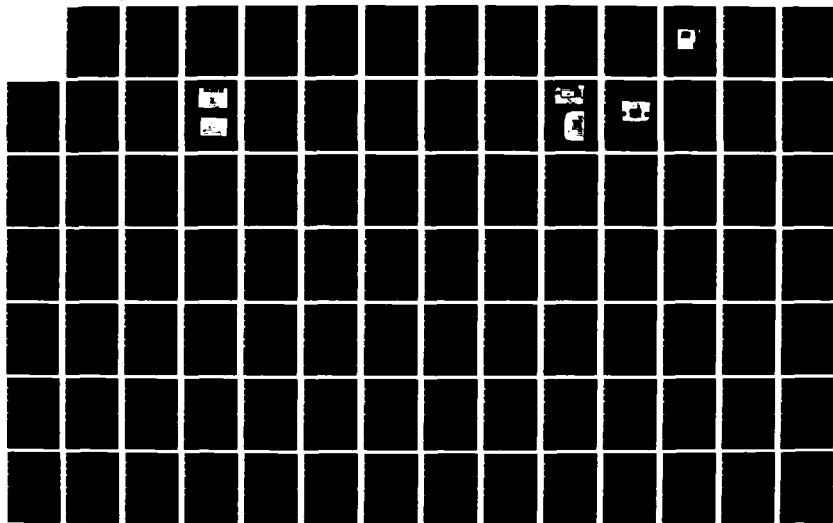
ELECTRICAL ENGINEERING EDUCATION INC S W D PEELE

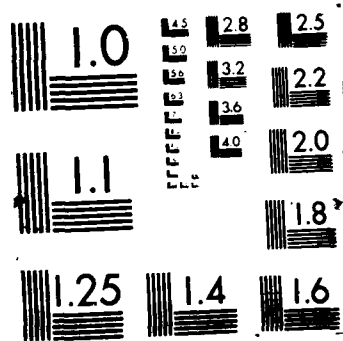
UNCLASSIFIED

MAY 86 AFOSR-TR-87-1721 F49620-82-C-0035

F/G 15/1

NL





IX. BIBLIOGRAPHY

1. C. S. Desai and J. F. Abel, Introduction to the Finite Element Method, Van Nostrand Reinhold Company, 1972.
2. O. C. Zienkiewicz, The Finite Element Method in Engineering Science, McGraw-Hill Book Company, London, 1971.
3. G. Sengupta, "Vibration of Periodic Structures," The Shock and Vibration Digest, Vol. 12, No. 3, March 1980.
4. T. J. R. Hughes and T. Belytschko, "A Précis of Developments in Computational Methods of Transient Analysis," Journal of Applied Mechanics, Vol. 50, December 1983, pp. 1033-1041.
5. D. E. Newland, Random Vibrations and Spectral Analysis, Longman, 1975.
6. D. G. Fertig, Dynamics and Vibration of Structures, John Wiley and Sons, Inc., 1973.
7. J. E. Bowles, Foundation Analysis and Design, Third Edition, McGraw-Hill Book Company, 1982.
8. W. F. Chen, Plasticity in Reinforced Concrete, McGraw-Hill Book Company, 1982.
9. R. L. Burden, D. J. Faires and A. C. Reynolds, Numerical Analysis, Second Edition, Prindle, Weber and Schmidt Publishers, Boston, 1978.
10. S. H. Crandall, Engineering Analysis -- A Survey of Numerical Procedures, McGraw-Hill Book Company, 1956.
11. R. R. Craig, Jr., Structural Dynamics, John Wiley and Sons, Inc., 1981.
12. C. P. Johnson, R. R. Craig, Jr. and A. Yarigicoglu, "Quadratic Reduction for the Eigenproblem," International Journal for Numerical Methods in Engineering, Vol. 15, 1980, pp. 911-923.
13. K-J Bathe, Finite Element Procedures in Engineering Analysis, Prentice-Hall, Inc., 1982.
14. S. Timoshenko and D. H. Young, Vibration Problems in Engineering, Third Edition, D. Van Nostrand Co., Inc., 1955.

1985 USAF-SCEEE RESEARCH INITIATION PROGRAM

Sponsored by the

AIR FORCE OFFICE OF SCIENTIFIC RESEARCH

Conducted by the

SOUTHEASTERN CENTER FOR ELECTRICAL ENGINEERING EDUCATION

FINAL REPORT

CENTRIFUGE MODEL STUDY AND FINITE ELEMENT ANALYSIS

OF

BURIED CONCRETE BOX CULVERTS

Prepared by:	Dr. Yong S. Kim
Academic Rank:	Assistant Professor
Department and University:	Department of Civil and Mechanical Engineering McNeese State University
Research Period:	January 1, 1985 - November 30, 1985
Contract No.:	F49620-82-C-0035

# ABSTRACT

The centrifuge model technique is used to evaluate the behavior of a 5-in. X 5-in. concrete box culvert under a 4-in. backfill soil.

Two different types of soil installations are studied: embankment and trench. Results of the centrifuge model study for both installations are compared with each other, and with predictions of a finite element code, CANOE (Culvert Analysis and Design).

Furthermore, the influence of soil stiffness for backfill is studied using finite element analyses. The results of CANOE analyses including nonlinear constitutive models for characterizing culvert and soil, incremental construction and free vertical movement with a symmetric mesh are reported.

## SECTION I

### INTRODUCTION

#### A. Purpose

During the past decade, research on soil-structure interaction of circular culverts under embankments was performed by numerous research groups. Empirical data on soil pressure distributions and structural stresses and deflections has been collected for shallow to moderate depth installations. As a result, the soil-structure interaction problems of circular culverts embedded in embankments are better understood, and new design and analysis procedures are being proposed. However, research on box culverts has been limited, and the behavior of box culverts is not well understood. Due to an increased number of box culvert projects (i.e., protective structures), a better understanding of soil-structure interaction and more accurate calculation of soil pressure distributions and concrete section behavior are required. The purpose of this research is, therefore, to study the behavior of buried box culverts under embankments using centrifuge modeling technique and numerical simulations.

#### B. Objective

The primary objective of this study is to investigate the soil-structure interaction problems of concrete box culverts under backfills. More specifically, the objectives of this study are to:

1. Develop an experimental technique to simulate the behavior of a prototype box culvert in a centrifuge.



2. Conduct a preliminary series of centrifuge model experiments on a small capacity centrifuge in order to determine the influence of installation types (embankment and trench) on the behavior of the box culvert.

3. Predict the behavior of the box culvert using finite element analysis.

4. Gain experience necessary for model studies in a large capacity centrifuge.

#### C. Scope

With these objectives in mind, the research is reported in the following sections. They contain a description of the centrifuge facility used for model study; design and fabrication of an accompanying testing apparatus; investigation of the influence of installation types using a centrifuge model technique and finite element analysis; and investigation of the influence of soil types using finite element analysis. Finally, some potential topics for future research in this area are mentioned.

## SECTION II

### CENTRIFUGE MODEL STUDY

#### A. Fundamentals of Centrifuge Modeling

One of the most ideal approaches for obtaining information on the behavior of prototype structures is full-scale model testing. A full scale model with the necessary instrumentation (i.e. soil stress meters, pore water pressure transducers, settlement gages and strain gages, etc.) could give the best results for estimating prototype behavior.

Unfortunately, full-scale model testing has serious major drawbacks: mainly, cost and time of construction and operation. Because of these reasons, small scale model testing is becoming a favorite testing method in geotechnical engineering.

However, use of small scale model tests in the laboratory is severely limited when the gravity body force of the structure itself is the principal load on the system, such as in dams and embankments. This limitation is due to two major factors. One is that soil characteristics are nonlinear and overburden dependent, and the other involves stress magnitudes. The stresses in a small scale model due to its own weight are much smaller in magnitude than those in the corresponding prototype system. To eliminate these deficiencies, the centrifuge modeling technique has been used since 1931. The increase in unit weight is achieved by placing a model in a centrifuge and spinning it to produce an acceleration field that is equivalent to an artificial gravitational field. In this way the state of stress at every point in the model under an artificial gravitational field is

equal to that at the homologous point in the prototype. This technique has been applied to a variety of geotechnical problems (slope stability, reinforced earth, foundation design, offshore gravity platforms, rockfill dams, tunnels, and buried circular pipes) reported elsewhere (References 1,2,3,4 and 5). Table 2.1 summarizes the scaling rules that have been developed for relating the behavior of the centrifuge model and an equivalent full scale geotechnical structure.

## 8. The Centrifuge and Monitoring Systems

### 1. The Centrifuge

The University of California, Davis' geotechnical centrifuge (Schaevitz Type B-8-0 rotary accelerator) was used for the present model study. It was designed to apply controlled centrifugal accelerations up to 175 g's or 10,000 g-lbs at a nominal radius of 39 inches. It is capable of reaching a maximum speed of 390 RPM.

The centrifuge includes a welded steel framework to prevent vibration. Sub-assemblies including the drive motor, the timing belt drive, the RPM pick-up, the rotating arm assembly, and the terminal box for control and test connections are supported within this framework.

There are two types of buckets available to carry the model; the Schaevitz stationary type and the swing-up type. In this study the swing-up bucket was used. This bucket is held by two arms attached to the spokes by two pivots. This permits the soil surface to remain perpendicular to the vector sum of centrifuge acceleration and the acceleration due to gravity.

Table 2.1 Scaling Relations (Reference 6)

Quantity	Full Scale (Prototype)	Centrifugal Model at $n$ g's
Linear Dimension	1	$1/n$
Area	1	$1/n^2$
Volume	1	$1/n^3$
Time		
In Dynamic Terms	1	$1/n$
In Diffusion Cases	1	$1/n^2$
In Viscous Flow Cases	1	1
Velocity (Distance/Time)	1	1
Acceleration (Distance/Time <sup>2</sup> )	1	$n$
Mass	1	$1/n^3$
Force	1	$1/n^2$
Energy	1	$1/n^3$
Stress (Force/Area)	1	1
Strain (Displacement/Unit Length)	1	1
Density	1	1
Energy Density	1	1
Frequency		
In Dynamic Terms	1	$n$

Hydraulic and electrical services are available to the model in flight. The hydraulic lines may be used to conduct compressed air or fluids from the outside control area to the model. Eighteen electrical channels are available for sending power to and receive signals from transducers which monitor behavior of the model. Electrical signals are transmitted to the centrifuge rotor and then to the model in flight through a stack of slip rings. Hydraulic services are transmitted through four rotary journals. A general view of the centrifuge and control panel is shown in Figure 2.1.

## 2. Photographic and Video Recording Systems

A still photographic system is available to permanently record selected moments of the centrifuge model tests. A camera is mounted near the hub of the centrifuge. Thus, still photographs can be taken with an on-board camera-flash unit by remote control during the tests. The photographs may be used later for analyses. In this study a photographic system was not used. However, a Sony television camera and video recording device were used as the monitoring system. This video camera was mounted near the hub of the centrifuge. It provided not only a continuous and instantaneous monitor of the test while in progress but also a permanent, replayable record of the model tests.

## C. Model Box, Concrete Box Culvert and Strain Gages

A centrifuge model box which had been used in a prior investigation at The University of California, Davis was used to contain the soil model. The model box was made of 1/4 inch thick



Figure 2.1 A View of the Centrifuge

aluminum alloy, and was designed to operate under a maximum centrifugal loading of 100 g. The dimensions of the model box were 15 inches long by 15 inches wide by 10 inches high.

The model box culvert was made of Quikrete, a commercial ready-to-use sand (topping) mix, with water-cement ratio of 0.15 (by weight). The model box culvert consisted of a roof, floor, and two side walls and the exterior dimension of the culvert were 9 inches (length) by 5 inches (width) by 5 inches (height). The thickness of these slabs was 0.4 inch.

A commercial strain gage (Gage Type CEA-13-125UW-120) made by Measurements Group, Inc. was used to measure the strains on the surfaces of the culvert. The strain gages were placed at the mid-section of the culvert. Figures 2.2 and 2.3 show the dimensions of the model box culvert and location of the strain gages, respectively. Symmetry was assumed.

#### D. Microcomputer Based Data Acquisition System

At least fourteen strain gages (seven exterior and seven interior gages) were required to measure the strains for the model study. However, these instruments faced two very difficult problems: 1) a limited number of slip rings were available for data transmission and, 2) brush noise caused by dynamic vibration occurred in the area in which the brush is in contact with the slip ring. To overcome these problems, a microcomputer-based time division data acquisition system (which works as a synchronized channel selector as shown in Figure 2.4) was designed by Li (Reference 7) and installed by Ju (Reference 8) for

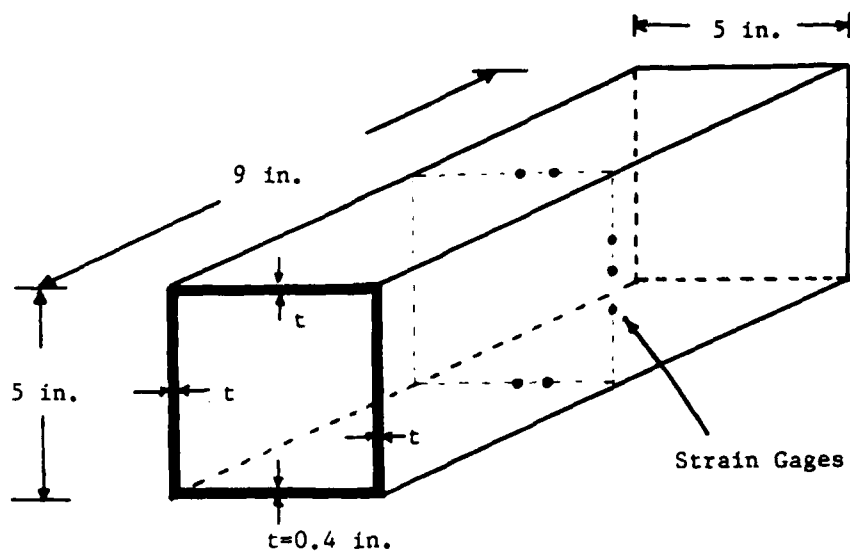


Figure 2.2 Dimensions of the Model Box Culvert

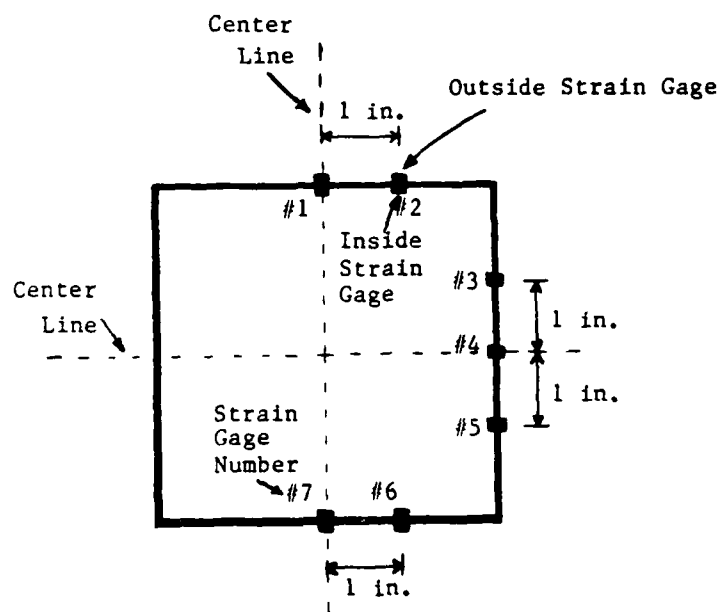


Figure 2.3 Locations of the Strain Gages



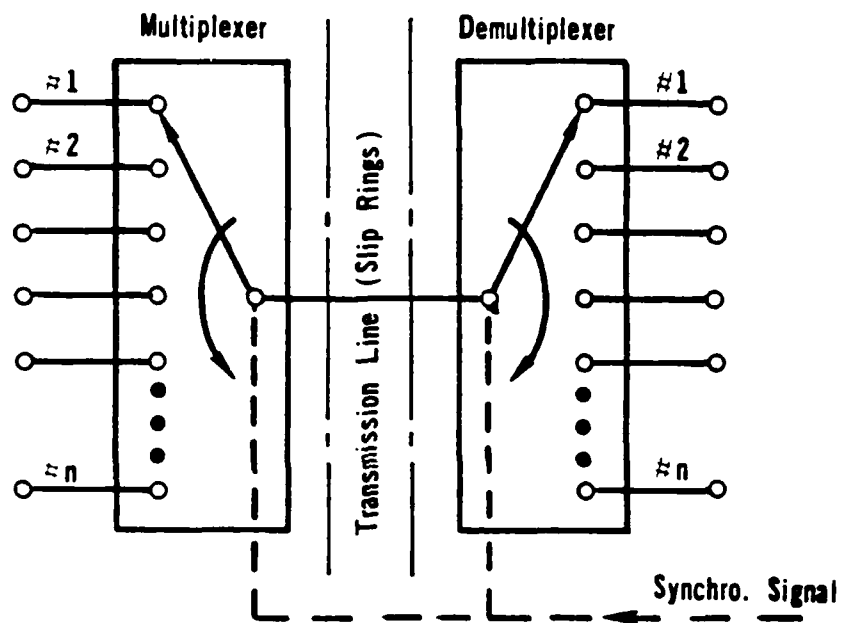


Figure 2.4 A Time Division Multiplexer - Demultiplexer Unit  
(Reference 9)

the model study. Details of the system are described in Reference 9, and a brief description of the system is illustrated below.

Referring to Figure 2.5, the transducers are connected to the corresponding signal conditioning. Conditioned signals are picked up in a sequential order by the 16-channel multiplexer and then fed through the voltage follower which is linked to a pair of slip rings. Signals transmitted through the slip rings are received by the A-D converter which is connected to a microcomputer. The synchronization signal comes from a pulse generator (output from a channel of the D-A converter). Each pulse causes the shifting of one channel of the multiplexer. At any given instant only one channel of the 16-channel multiplexer is connected to A-D converter. For this system, the synchronization and the demultiplexing functions are executed by software programming. Note that channel 0 of the multiplexer is connected to a fixed voltage, and serves as a reference mark for the computer to identify the position of all channels. Under a specified sampling rate, the computer automatically acquires data from all the channels and converts signal voltages to actual physical quantities to be stored, processed or tabulated by the printer. Figures 2.6 and 2.7 show the multiplexer and data acquisition system utilizing a Radio Shack TRS-80 Model I microcomputer and a printer, respectively.

#### E. Soil Properties

The soil used in this study is Monterey No.0 sand which is classified as SP in the Unified Soil Classification System. The sand has a specific gravity of 2.65 and a mean grain diameter of about 0.45

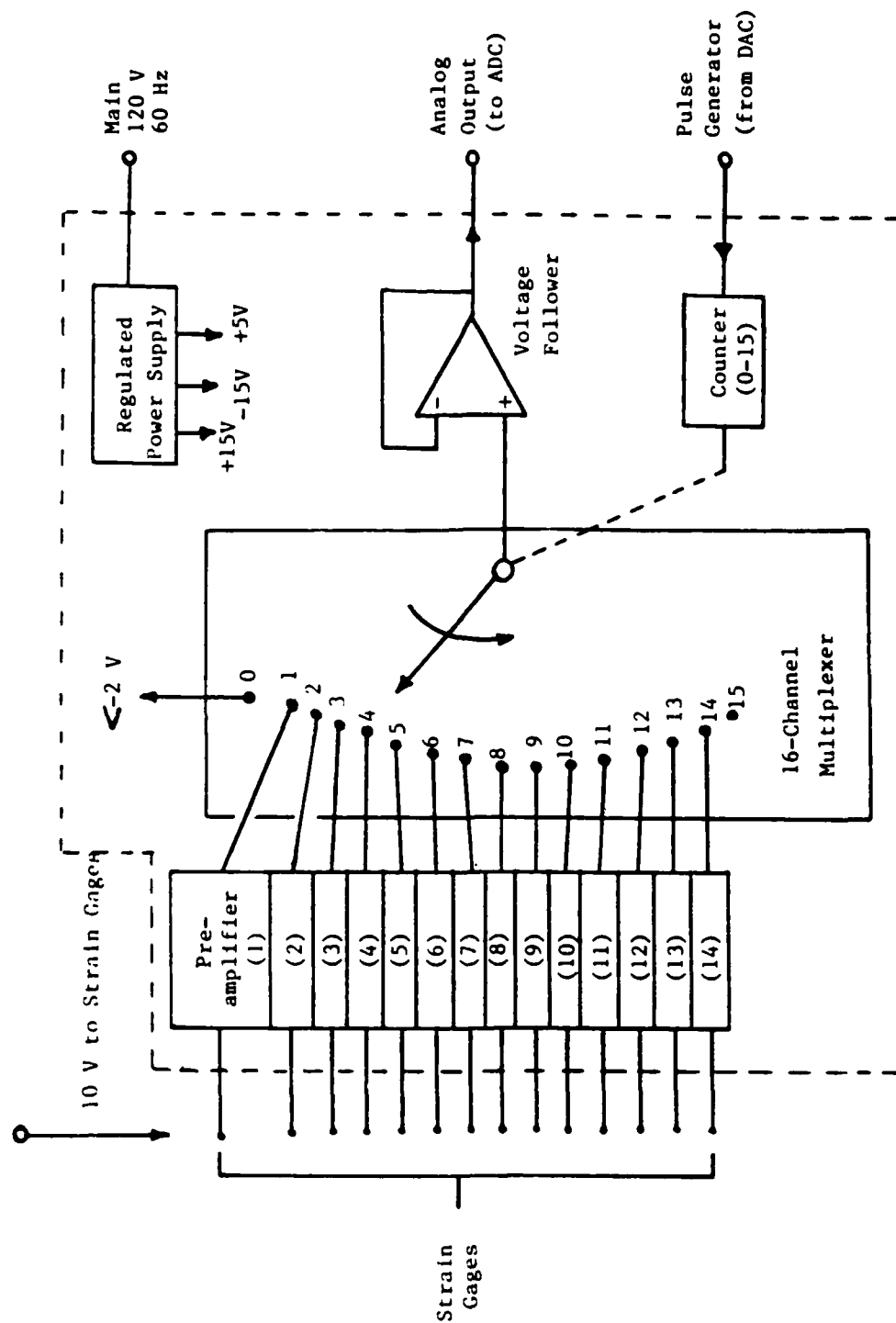


Figure 2.5 A Schematic of a Microcomputer Based Data Acquisition System

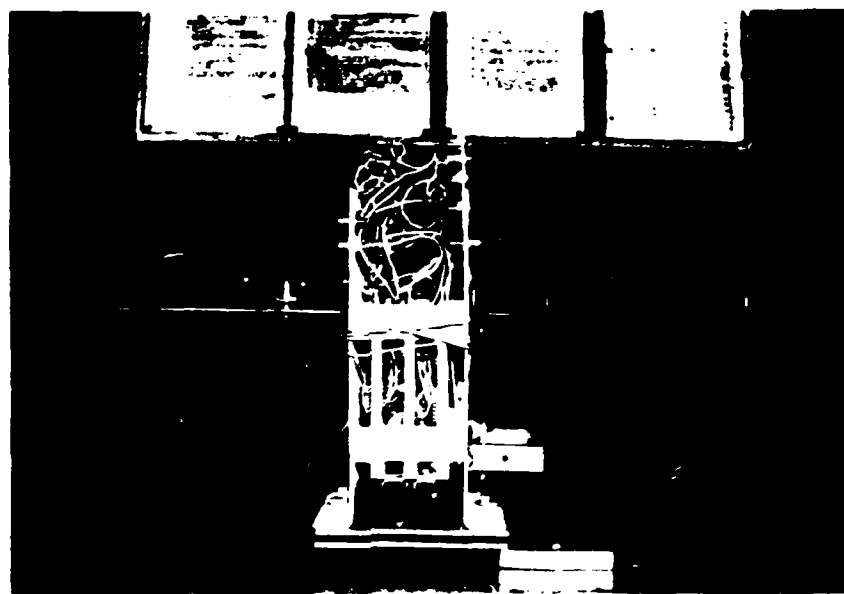


Figure 2.6 A View of Multiplexer

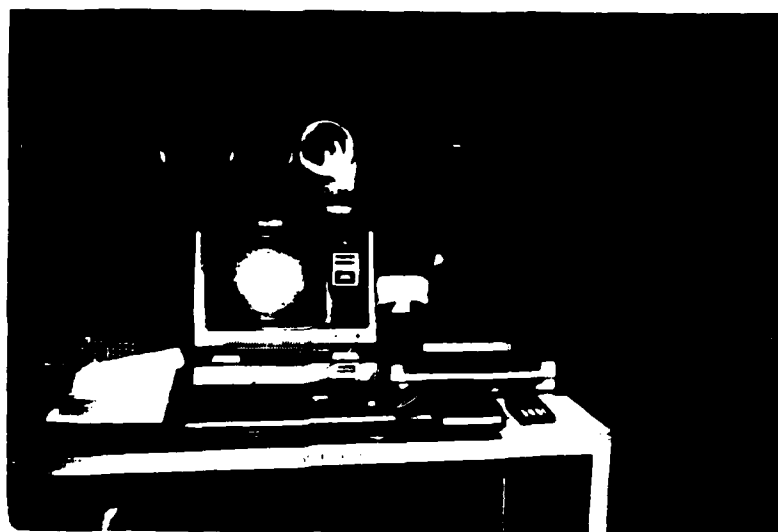


Figure 2.7 A View of a Microcomputer Based Data Acquisition System

mm. Figure 2.8 shows the grain size distribution and Figures 2.9 and 2.10 show the data obtained from the triaxial compression tests for Monterey No.0 sand. The laboratory tests were performed by Yang (Reference 10).

#### F. Model Preparation

The following steps are involved in preparing a model:

- 1) The concrete model box culvert was instrumented, and was then placed in the selected installation type (embankment or trench) as shown in Figures 2.11, 2.12 and 2.13.
- 2) Monterey No.0 sand was pluviated in the direction normal to the axis of the culvert (see Figure 2.14).
- 3) The completed sample was then transferred to the centrifuge and placed in one of the two swing-up buckets.
- 4) Instrumentation (T.V. monitor and multiplexer) was securely fastened, and both static and dynamic balancing of the rotating arm were performed prior to testing, thus completing preparation of the model system for centrifuge testing (see Figure 2. 15).

After a model was placed in the swing-up bucket and all required instrumentation was securely mounted in the centrifuge, the model package was slowly brought up to a rotating speed of 195 rpm, equivalent to 60 gravitational pulls.

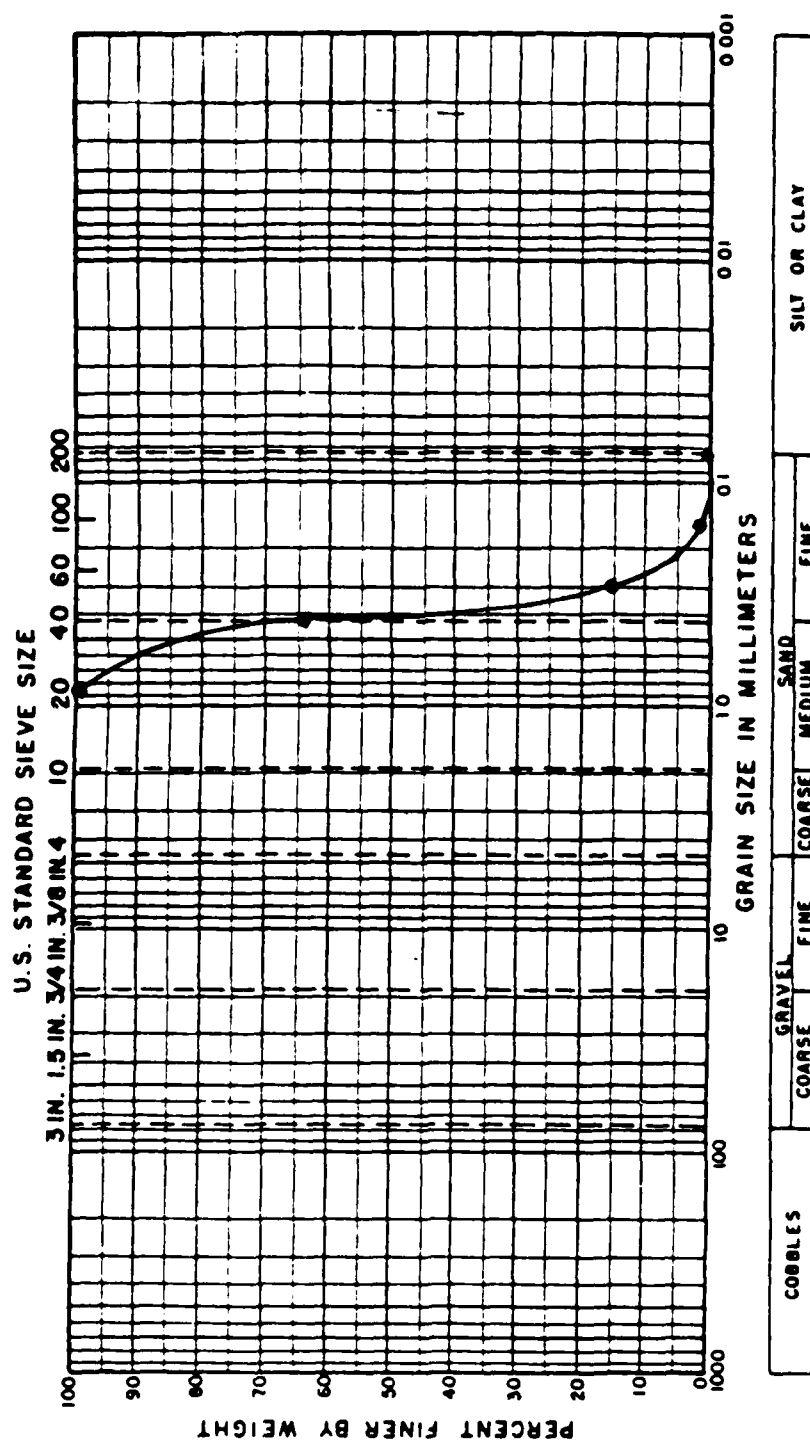


Figure 2.8 Particle Size Distribution for Monterey No.0 Sand (Reference 15)

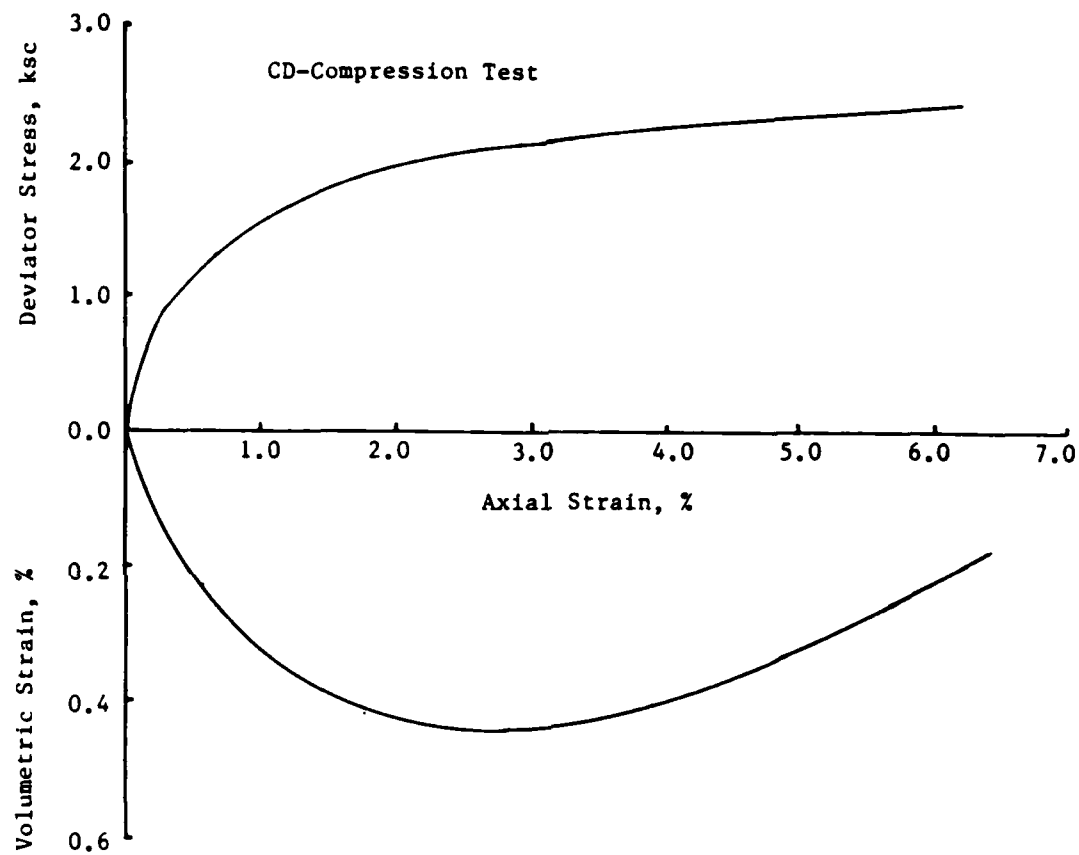


Figure 2.9 Stress-Strain and Volume-Change Curves from CD Triaxial Tests on Monterey No.0 Sand (Reference 15)

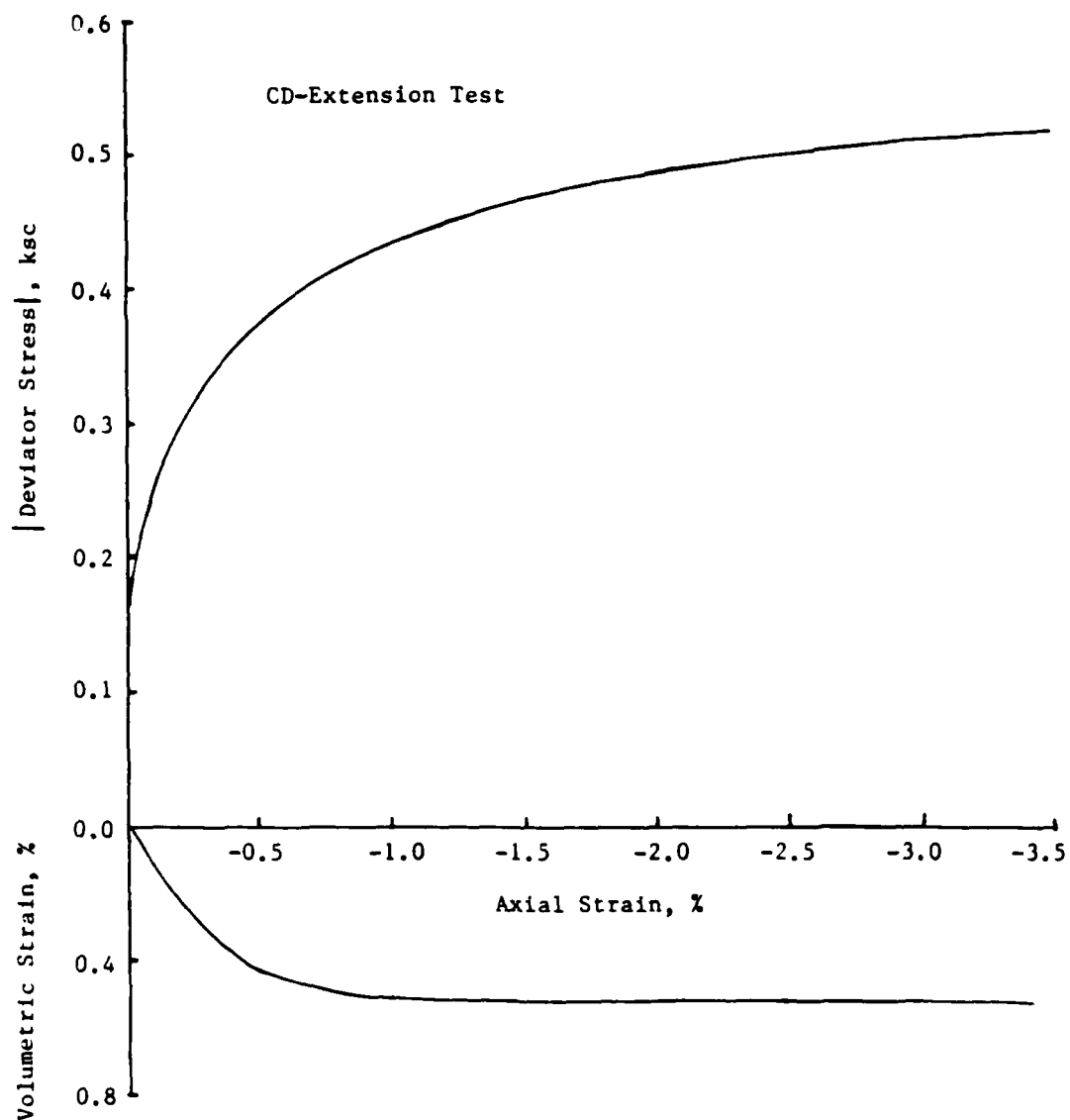


Figure 2.10 Stress-Strain and Volume-Change Curves from CD Triaxial Tests on Monterey No.0 Sand (Reference 15)



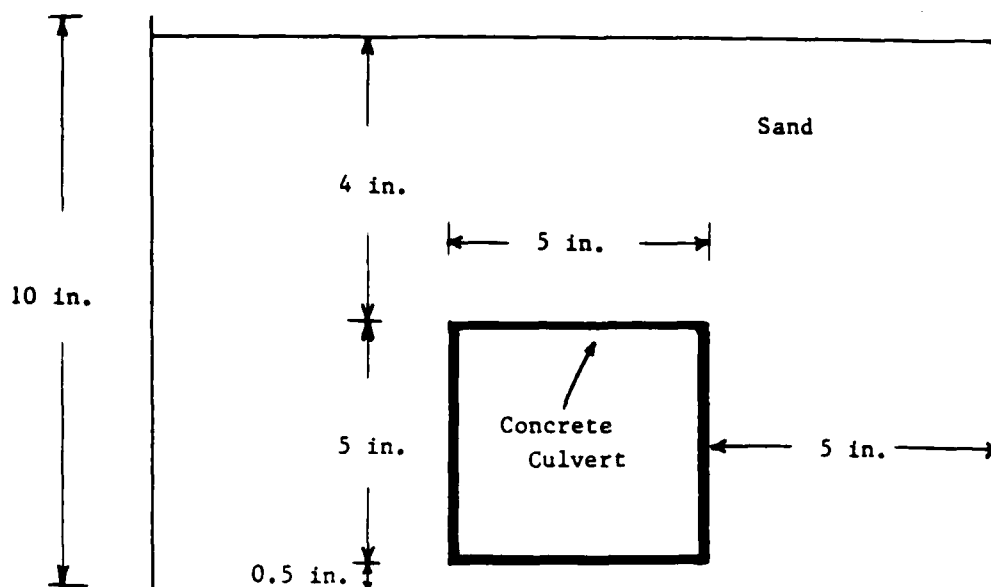


Figure 2.11 Dimensions of Model Package: Embankment Condition

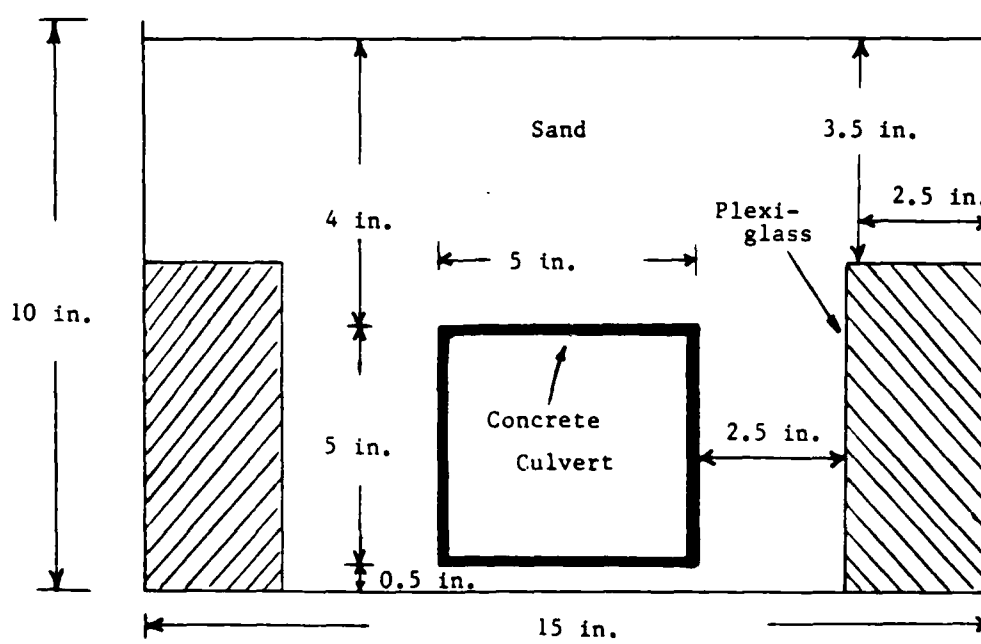


Figure 2.12 Dimensions of Model Package: Trench Condition



Figure C.14 A View of Model Preparation



Figure C.15 A View of Instrumented Concrete Box Culvert  
in the Model Box

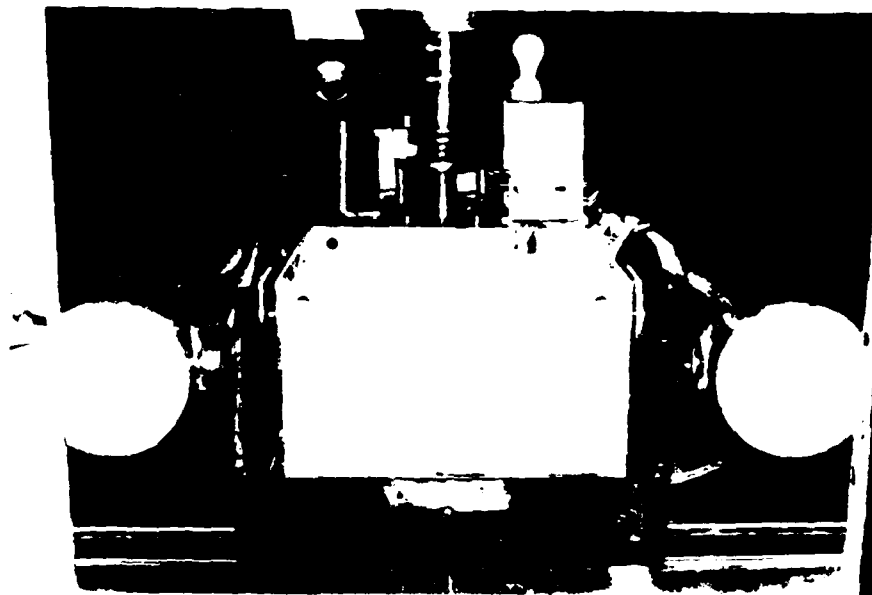


Figure 2.15 A View of Model Package in the Swing-Bucket

### SECTION III

#### FINITE ELEMENT ANALYSIS

##### A. Description of the Computer Code

The computer code, CANDE (Culvert ANalysis and DEsign), used in this study was developed by Katona et al. (References 11 and 12). The basic assumptions of the program are: plane strain geometry and loading, small displacement theory, and quasistatic response. The following description summarizes salient features of CANDE used in the analysis.

##### 1. Modeling of Culvert

The box culvert was modeled as a series of straight line segments with a one-dimensional beam-column bending element comprising each segment. This bending element employs a plane-strain formulation which neglects shearing deformations. Two nodes with three degrees of freedom per node (horizontal and vertical displacement and a rotation) define each element. At each node, cubic and linear displacement approximations were used in calculations of displacements in the transverse and axial directions, respectively. Figure 3.1 shows the coordinate system of the beam element.

##### 2. Modeling of Soil

Nonconforming quadrilateral and triangular elements were used to represent the soil (see Figure 3.2). The quadrilateral, defined by four nodes with two degrees of freedom (horizontal and vertical

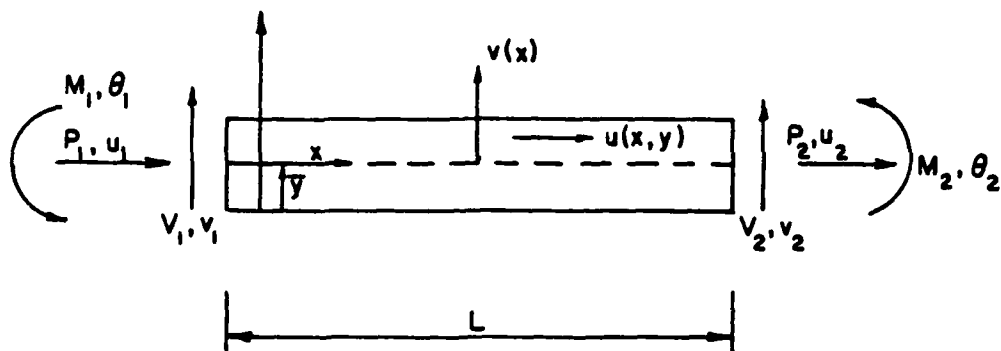


Figure 3.1 Coordinate System for Beam Element in CANDE

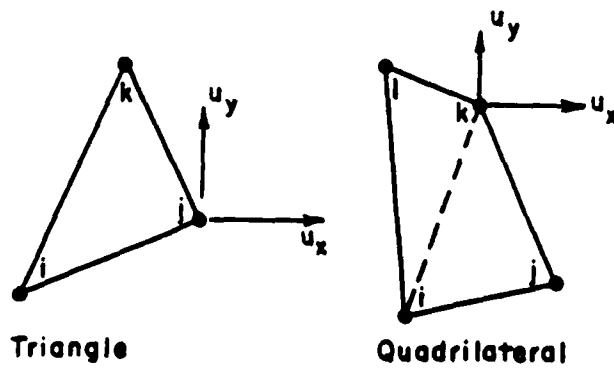


Figure 3.2 Element Types Used for Soil Model in CANDE

displacements) per node comprise two triangles with complete, quadratic, interpolation functions specified within each triangle. Application of appropriate constraints and static condensation procedures result in a four-node quadrilateral element (Reference 11).

There are four material characterizations available for the soil properties: linear elastic; incremental elastic (overburden dependent); extended-Hardin; and Duncan's hyperbolic stress-strain relationship, which employs tangent Young's modulus and tangent bulk modulus formulations (References 12,13 and 14).

### 3. Modeling of Slip

A constrained finite element formulation, which is based on a generalized principle of virtual work, was used to model the relative movement of the soil with respect to the pipe at the soil-culvert interface, and relative movement of the soil with respect to the soil-soil interface (i.e., trench). An interface element is defined by a set of paired nodes joining two elements as shown in Figure 3.3. The paired nodes, which have two degree of freedom per node (vertical and horizontal displacement), initially take the same position in space before any loading, but are assigned to separate elements. Therefore, each node responds individually under any applied loading. In addition, a third node, which is assigned between the paired nodes, provides normal and shear forces existing between the paired nodes. It should be observed that these interface forces arise only from the adjoining element interaction and applied forces at the paired nodes.

#### 4. Modeling of Incremental Construction

CANDE uses incremental iterative solution techniques to represent the placing of the culvert and embankment in a series of soil layers as shown in Figure 3.4. The basis of the techniques is superposition of solutions from successive soil layers and a newly added layer. At each increment, iterative calculations determine soil and culvert moduli until equilibrium is approximated within an allowable error.

#### B. Finite Element Parameters

##### 1. Finite Element Mesh and Boundary Conditions

The finite element grid with boundary conditions used in this study is shown in Figure 3.5. Since the model and its loading is symmetric, only half of the model was analyzed. Boundary conditions on the culvert used in the analysis are shown in the figure: a fixed movement condition in the horizontal direction and free movement condition in the vertical direction. The culvert was represented by 20 beam-column elements, and the soil by 110 quadrilateral elements.

##### 2. Soil-Culvert Interface and Incremental Solution Procedure

A fixed condition was used at the soil-culvert interface. Although it is possible to represent the slip between the continuum and beam elements, a current study has demonstrated that the influence of slip conditions for this particular geometrical configuration are insignificant (Reference 15). Due to large amounts of CPU (Central Processing Unit) time, and substantial computational costs when slip

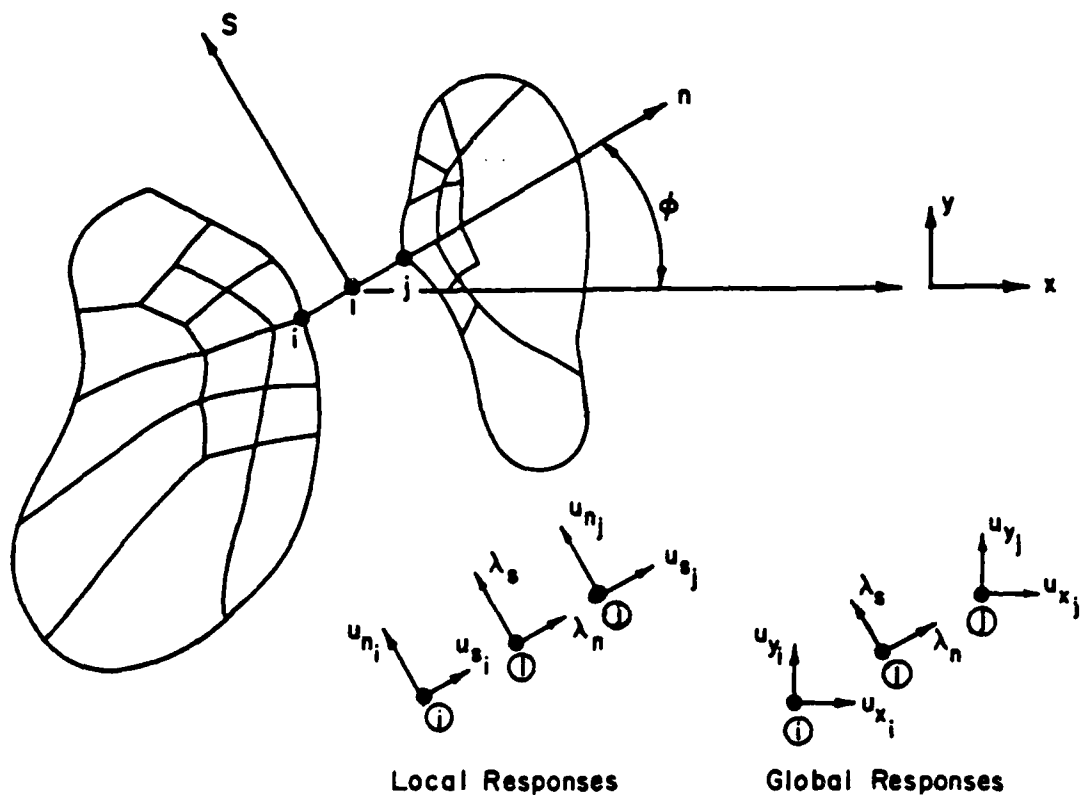


Figure 3.3 Nodes for Constraint Interface Element in CANDE

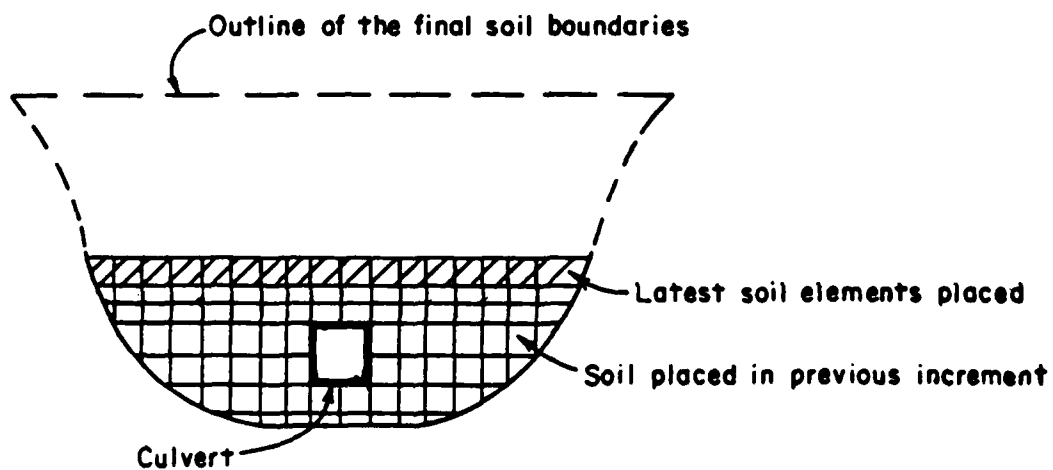


Figure 3.4 Incremental Construction



Number of Nodes: 142

Number of Beam Elements: 20

Number of Quadrilateral Elements: 110

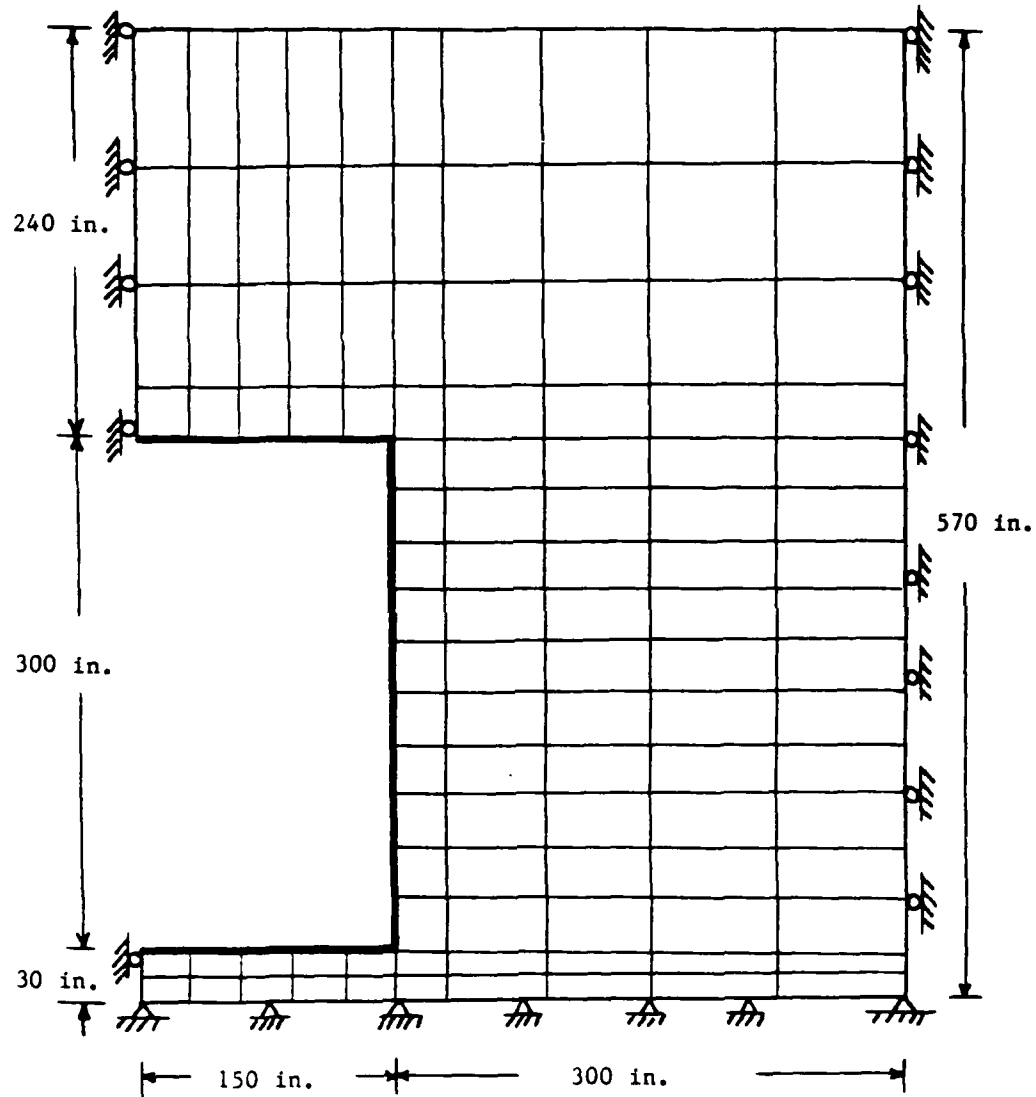


Figure 3.5 Symmetric Mesh

was allowed, the fixed condition was used for the analysis.

The incremental solution procedure for embankment and trench simulated the actual installation process of placing soil layers in a series of lifts. Figures 3.6 and 3.7 show the construction increment numbers of element groups entering sequentially into the system. The first construction increment included placing all bedding pad, in situ soil, and the box culvert elements. Subsequent increments, numbers 2 through 10, were gravity loaded elements of fill soil.

### 3. Material Properties

The soil model employed in the study is a characterization proposed by Duncan et al. (References 13 and 14) which has had a substantial history of development and application over the last decade. This soil model characterizes soil behavior with a variable tangent Young's modulus and tangent bulk modulus. Eight parameters are needed to define a particular soil in loading:  $K$ ,  $n$ ,  $R_f$ ,  $c$ ,  $\theta$ , and  $\Delta\theta$  for the tangent Young's modulus; and  $K_b$  and  $m$  for the tangent bulk modulus. These parameters can be determined from data obtained by conventional triaxial tests. Table 3.1 shows the parameters used for Monterey No.0 sand in the analysis. These parameters were determined by Duncan (Reference 13).

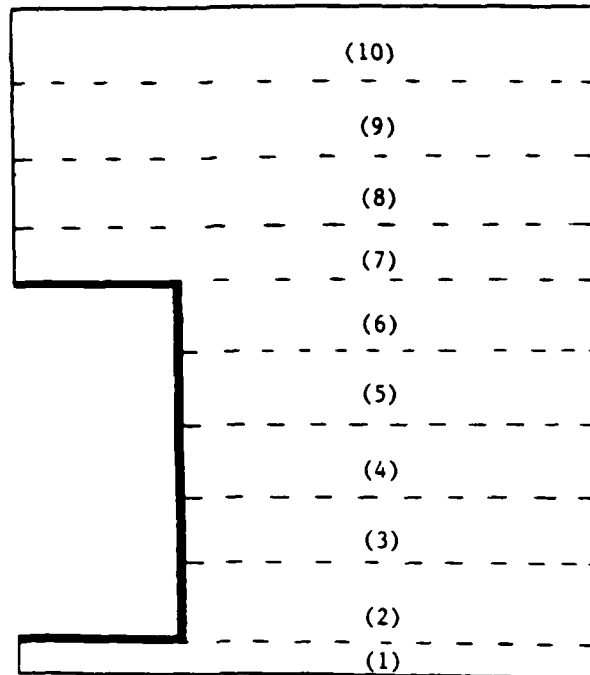


Figure 3.6 Soil Layers and Construction Increments  
for Embankment Soil Installation

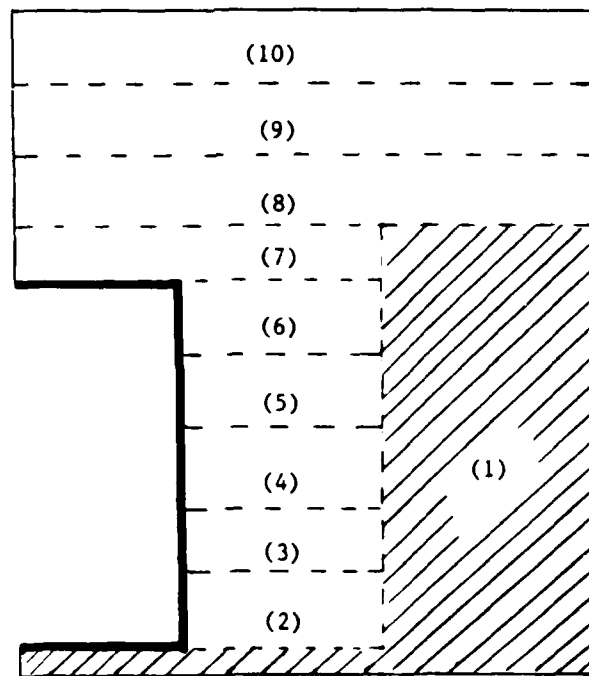


Figure 3.7 Soil Layers and Construction Increments  
for Trench Soil Installation

Table 3.1 Duncan's Soil Parameters for Monterey No.0 Sand  
(Reference 13)

Cohesion, $c$	0.0
Friction Angle, $\phi$	35.0°
Modulus Number, $K$	920.0
Modulus Exponent, $n$	0.79
Failure Ratio, $R_f$	0.96

## SECTION IV

### RESULTS AND DISCUSSION

This section presents results from the numerical analysis and centrifuge model study whose purpose was to investigate the influence of installation types (embankment and trench) and soil types on the structural behavior of a typical box culvert. The input parameters for the centrifuge model study are same as those in the Section II. The numerical results obtained from CANDE in Section IV.8 are based on the input parameters discussed in the Section III.8.3 and the input parameters used for the study of soil type influence are described in Section IV.C.

#### A. The Influence of Installation Type

##### 1. Bending Moment Distribution

The bending moments developed in the concrete culvert were determined from the results of centrifuge model study and predictions of numerical analyses. Figures 4.1 to 4.9 visually report the variation of moments with depth of fill for nine locations. Figure 4.10 shows the bending moments around the culvert under a simulated fill height of 20 feet.

Figure 4.1 shows the moments for the midspan of the top slab. The moments are initially negligible, and subsequently increase almost linearly with the backfilling process. All the moments are positive throughout the incremental constructions due to the vertical soil pressure which induced inward deflection of the top slab. No negative

moments were detected during the first six construction increments at which the fill height reached the same elevation of the top span of the culvert. This indicates that the box culvert was rigid enough to resist the inward forces on the sides of the culvert under lateral soil pressure.

The largest moment is developed at the upper corner of the culvert as shown in Figure 4.3. As expected, the moments are negative throughout the backfill process.

Figures 4.7 and 4.9 show the moments developed at the corner and midspan of the bottom slab of the culvert, respectively. The results are interesting since the magnitude of those moments are much smaller than the moments at the corner and midspan of the top slab of the culvert. This confirms that the soil pressure exerted on the bottom slab is a function of bedding parameters which are important for culvert design.

The comparison between the results of centrifuge model study and numerical predictions is made on the figures. Typically, Figure 4.10 shows the compared moments around the culvert under fill height of 20 feet. Although agreement between these two results are not excellent in magnitude, centrifuge model and finite element results are in moderately good agreement for shape.

No major difference in structural behavior was observed under two different installation types, embankment and trench. This result may indicate that the influence of the installation type to overall behavior of the box culvert is minimal although the installation type is one of the more important parameters to be considered for circular culverts. However, it should be pointed out that the embankment

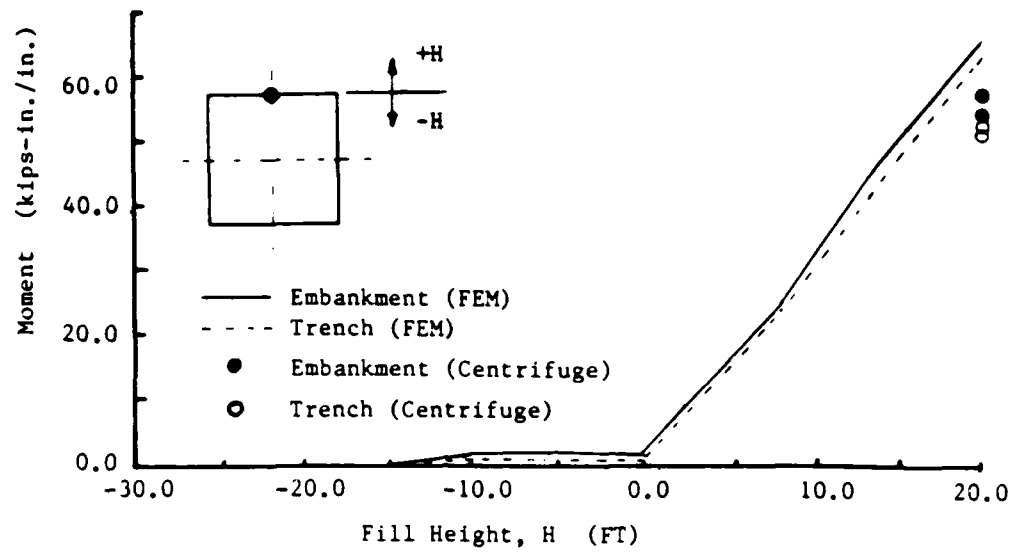


Figure 4.1 Culvert Bending Moments at Strain Gage #1

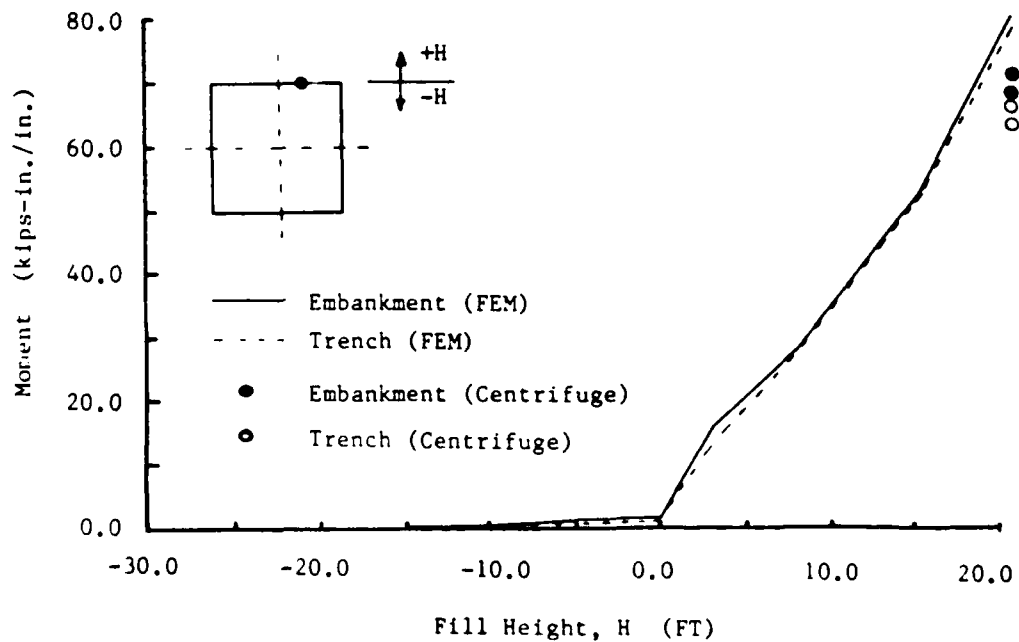


Figure 4.2 Culvert Bending Moments at Strain Gage #2

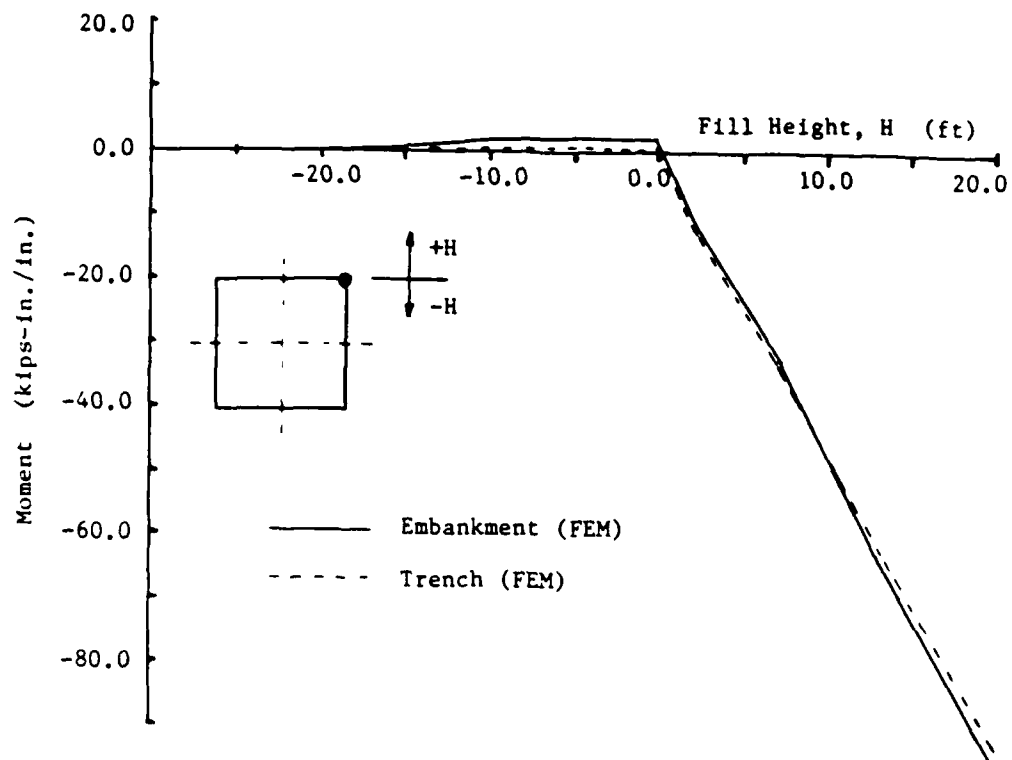


Figure 4.3 Culvert Bending Moments at the Upper Corner

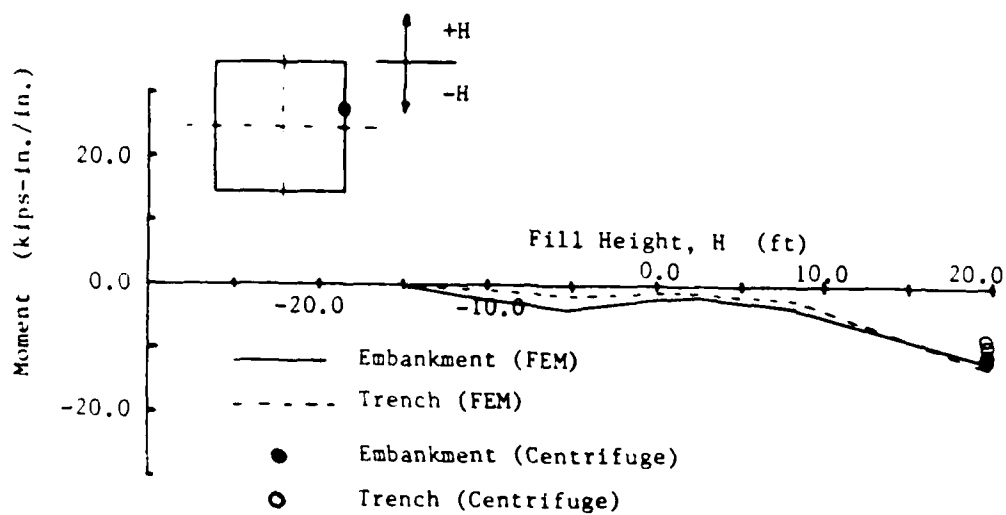


Figure 4.4 Culvert Bending Moments at Strain Gage #3



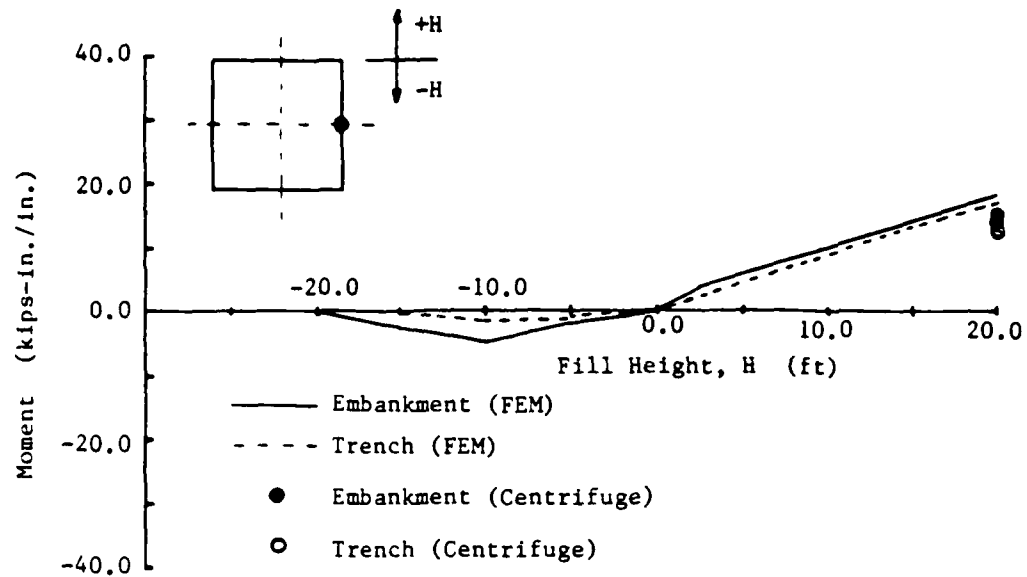


Figure 4.5 Culvert Bending Moments at Strain Gage #4

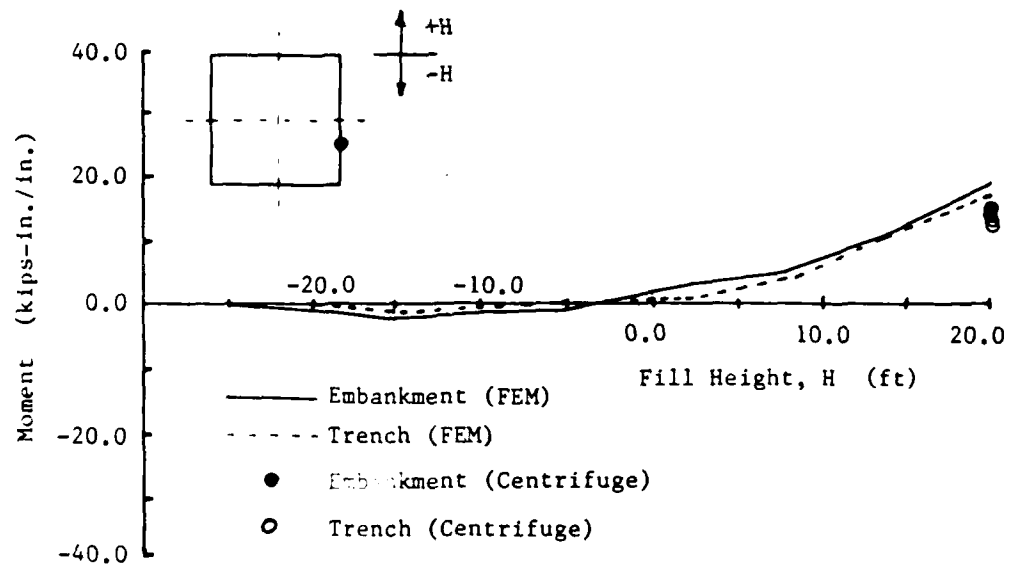


Figure 4.6 Culvert Bending Moments at Strain Gage #5

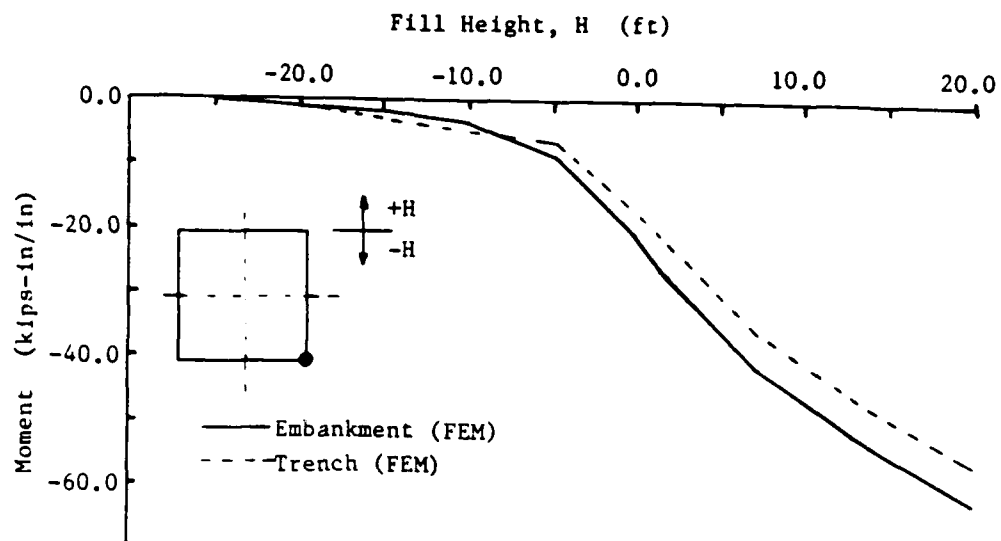


Figure 4.7 Culvert Bending Moments at Bottom Corner

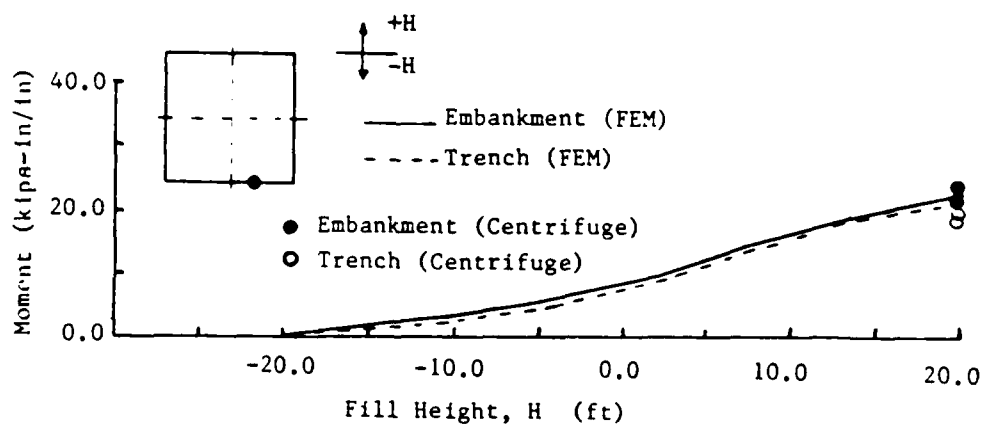


Figure 4.8 Culvert Bending Moments at Strain Gage #6

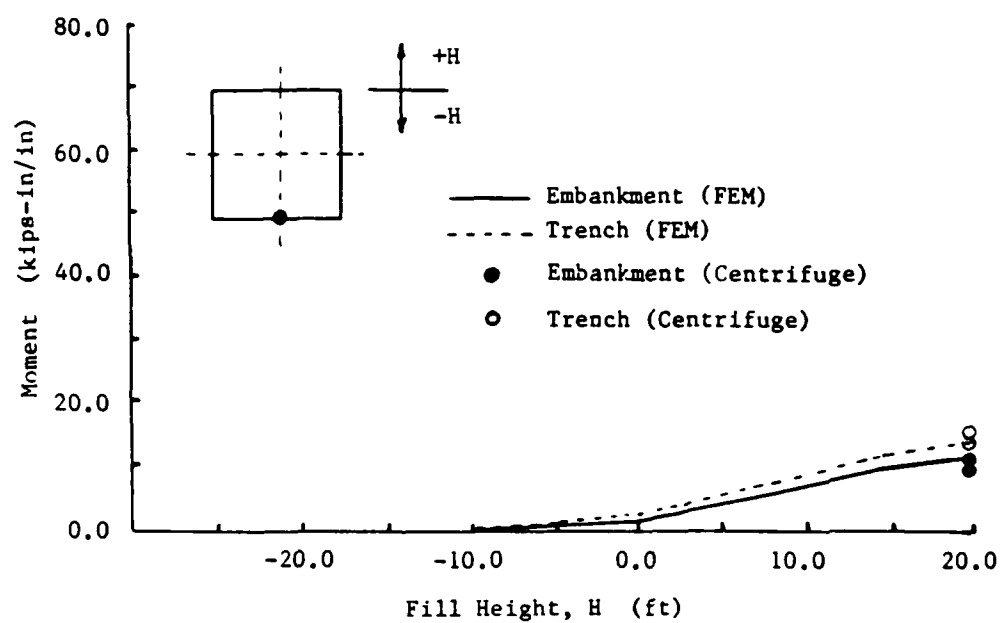


Figure 4.9 Culvert Bending Moments at Strain Gage #7

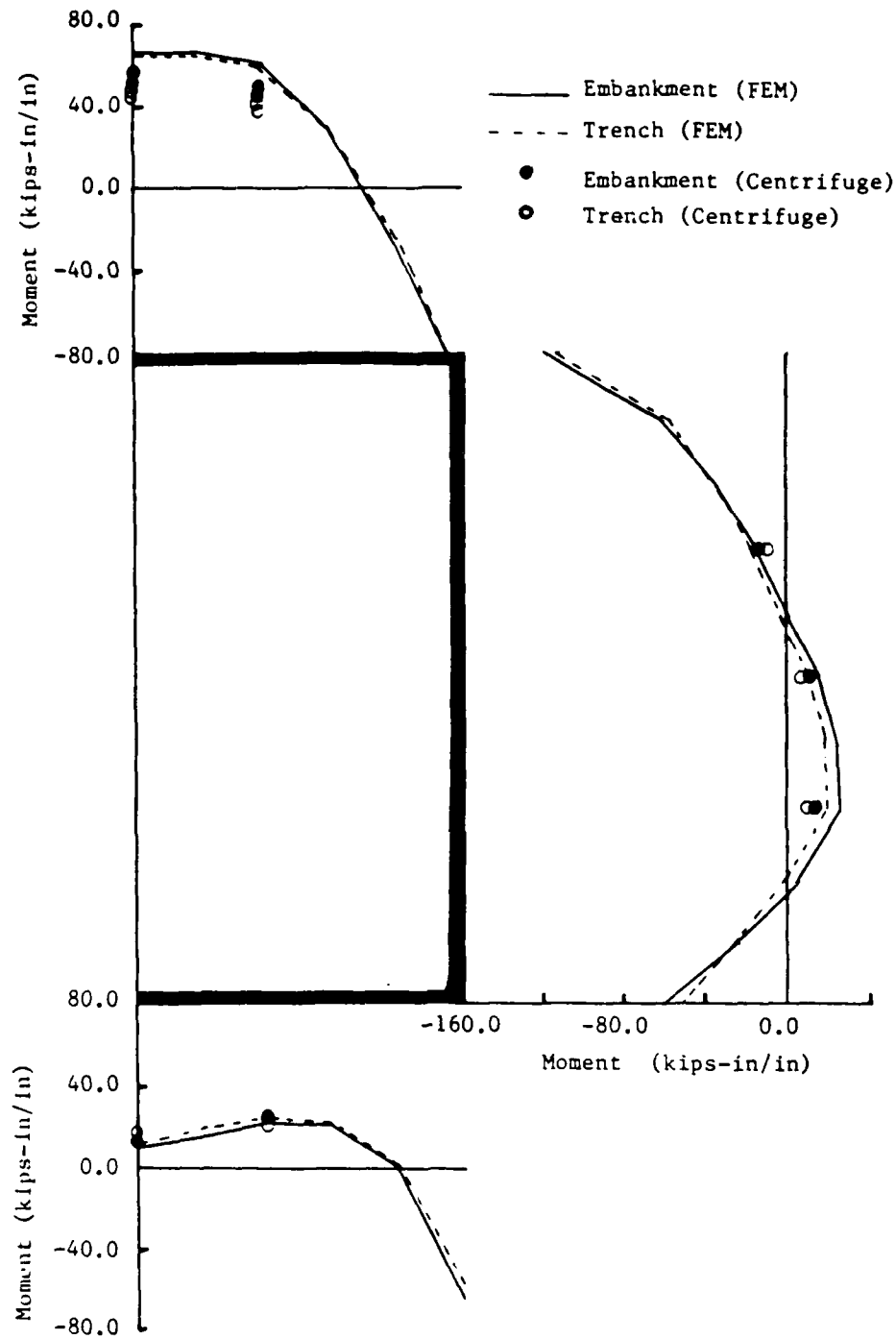


Figure 4.10 Bending Moments around the Culvert  
at Fill Height = 20 ft

condition produces slightly greater loading conditions.

## 2. Thrust Distribution

The thrusts developed in the concrete box culvert were determined from the results of the centrifuge model study and predictions of numerical analyses. Figures 4.11 to 4.15 report the variation of thrusts with depth of fill for five locations, while Figure 4.16 shows the thrusts around culvert under fill height of 20 feet.

Figures 4.11 and 4.12 show the thrusts at the midspan and corner of the top slab of the box culvert. The thrusts begin with compressive (positive) forces, but once the depth of fill height exceeds the crown height of the culvert, the thrusts become tensile (negative) forces.

A larger thrust was observed at midspan of the vertical wall as shown in Figure 4.13. No compressive (positive) forces were detected during the early incremental constructions. A drastic increase of tensile (negative) forces may be observed as further backfill is placed over the box culvert.

The thrust distribution around the culvert for fill heights under 20 feet is shown in Figure 4.16. All thrusts are tensile (negative) forces and the largest tensile force occurred at approximately one-third of the vertical wall height from the bottom.

The results of centrifuge model study are plotted on the figures. They are similar to those in Section IV.A.1: moderately good agreement in shape, but not excellent agreement in magnitude.

Again, no measure difference in structural behavior is observed between embankment and trench installations except that the embankment

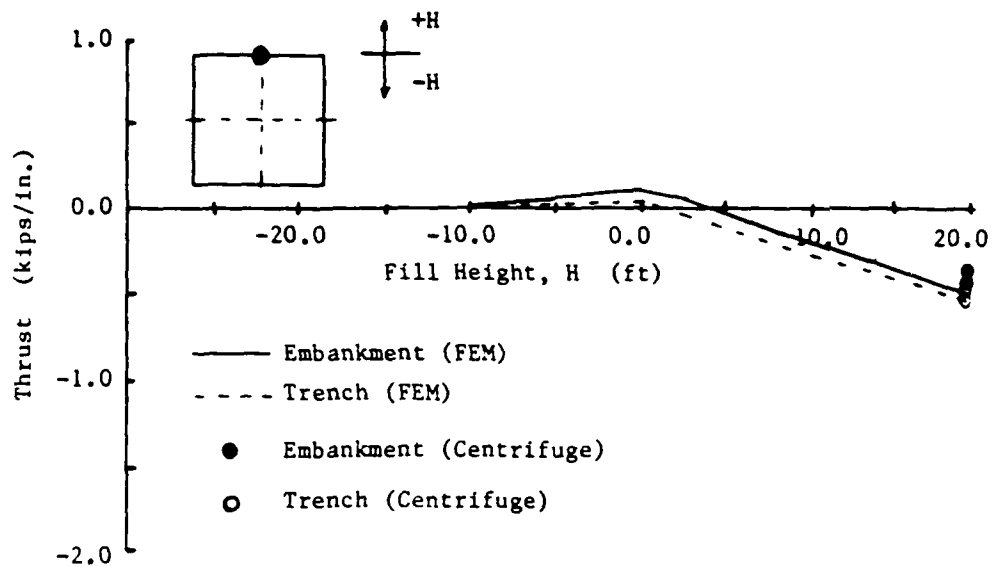


Figure 4.11 Culvert Thrusts at Strain Gage #1

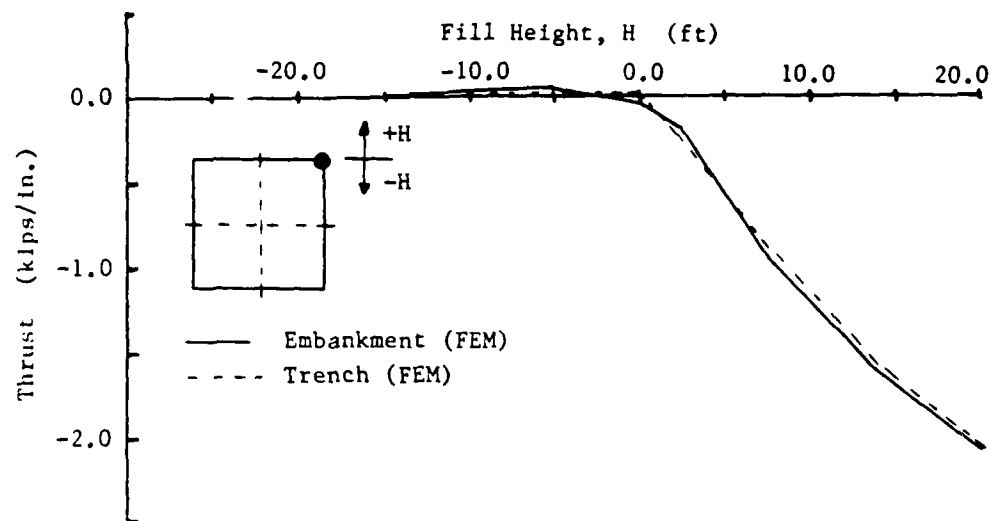


Figure 4.12 Culvert Thrusts at Upper Corner

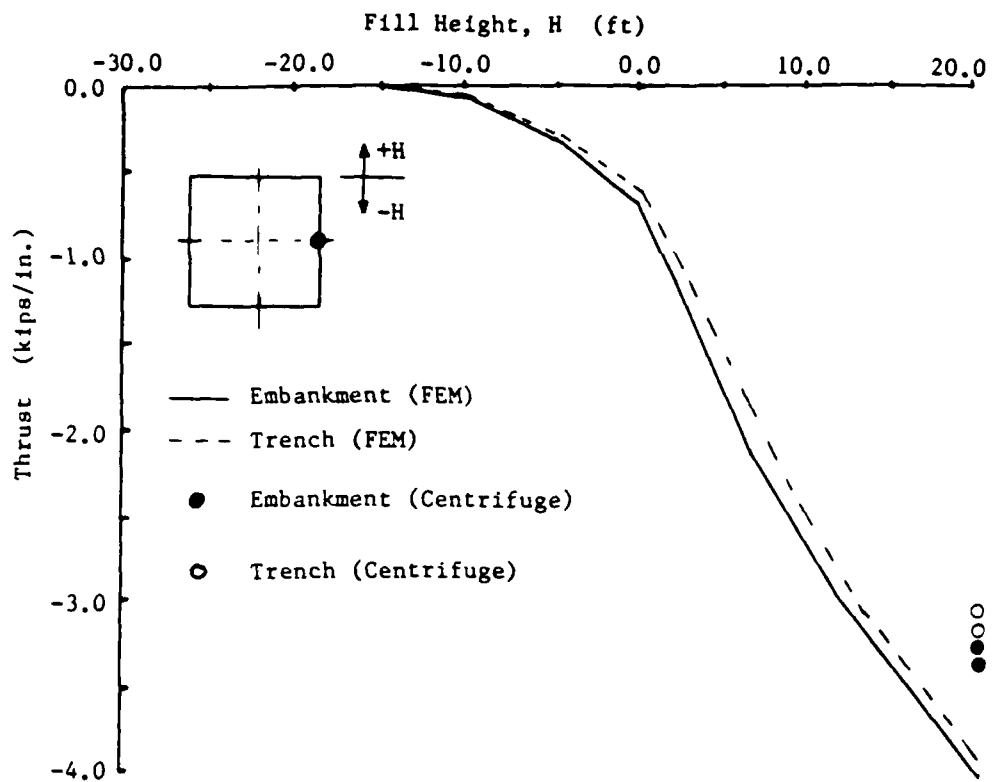


Figure 4.13 Culvert Thrusts at Strain Gage #4

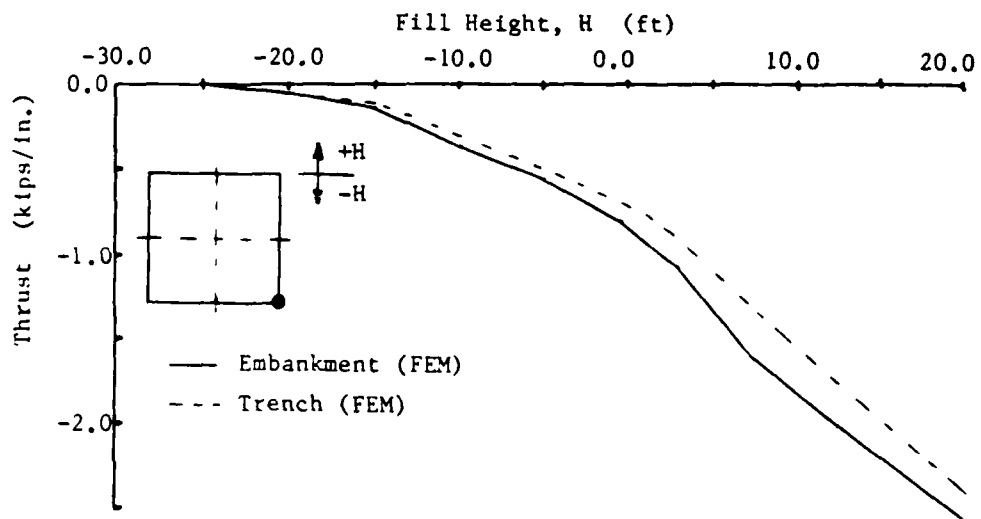


Figure 4.14 Culvert Thrusts at Bottom Corner

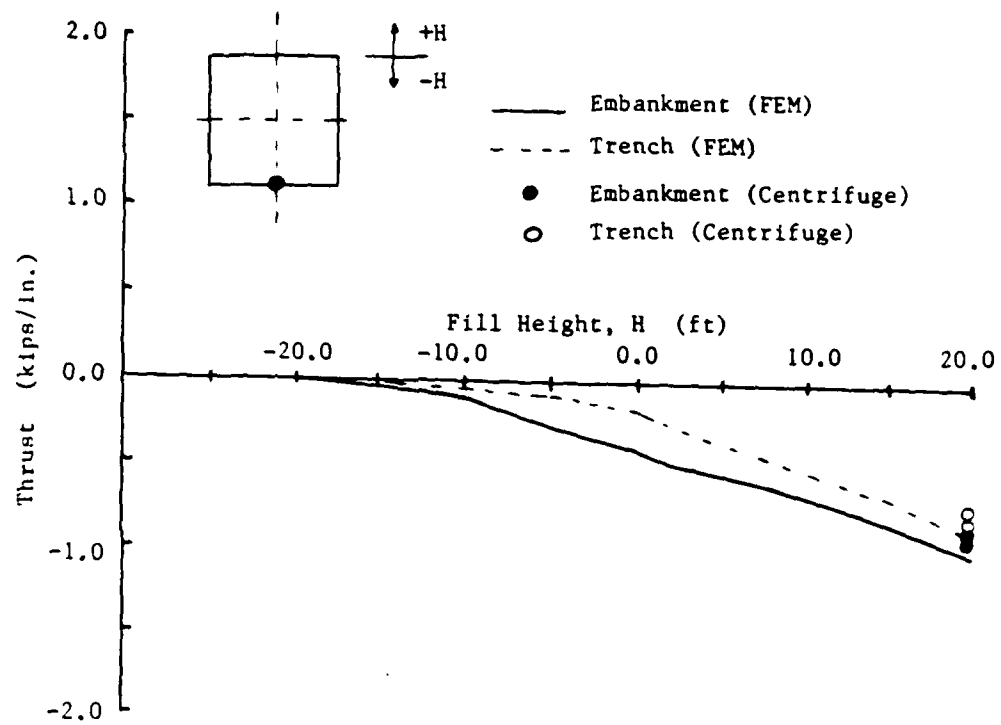


Figure 4.15 Culvert Thrusts at Strain Gage #7



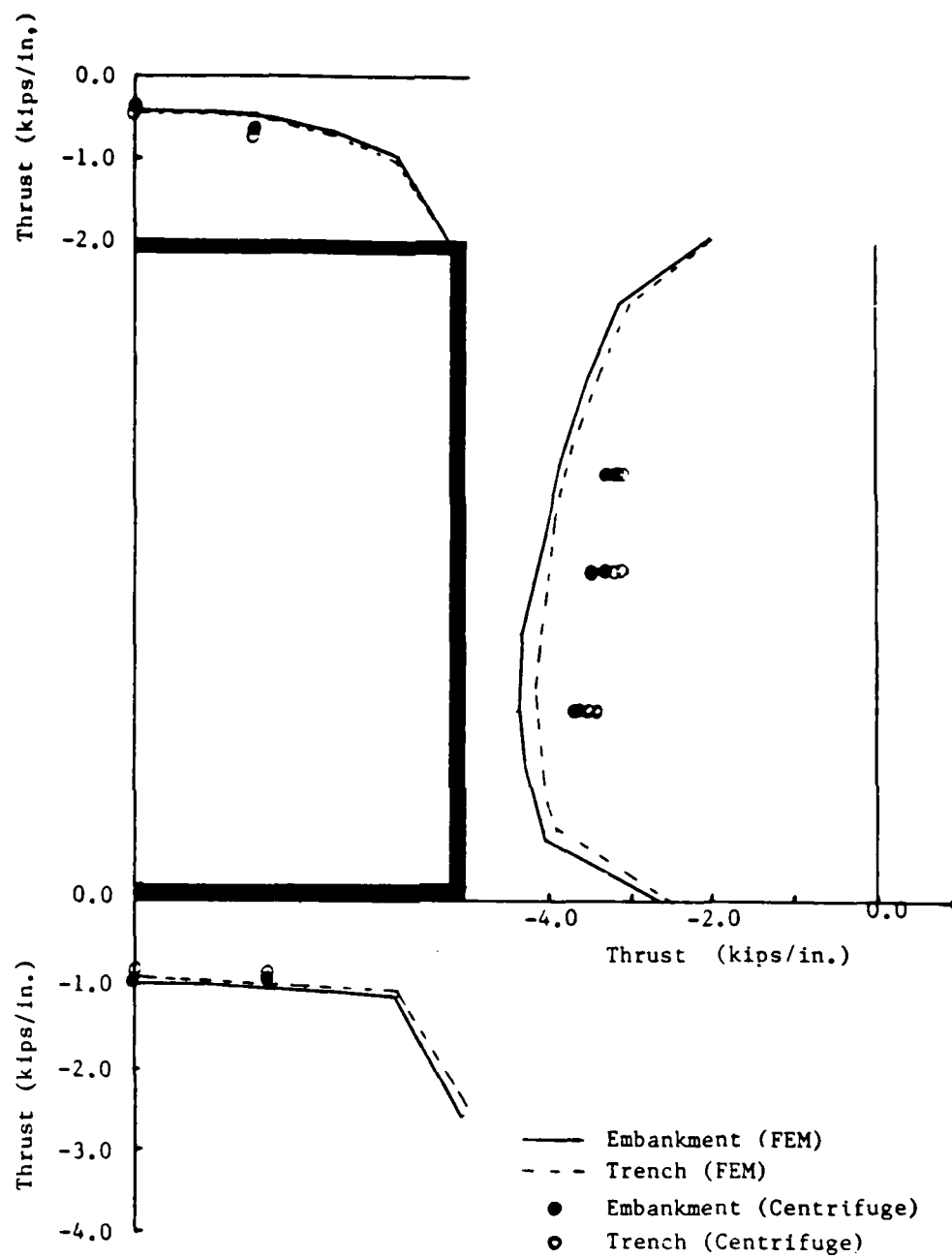


Figure 4.16 Thrusts around the Culvert  
at Fill Height = 20 ft

condition produces slightly larger magnitudes.

#### B. The Influence of Soil Type

This subsection presents the predictions of numerical analyses which investigated the influence of soil type on the behavior of the box culvert. Since no major difference in structural behavior was found between embankment and trench soil installation, only embankment condition was considered for the remainder of the investigation. Two soil types were considered: coarse aggregate (GW type soil) and silty sand (SM type soil). The input parameters for the soil model in CANOE were chosen from standard Duncan's soil parameters in Reference 13. Table 4.1 shows Duncan's hyperbolic parameters used in the analysis.

##### 1. Soil Pressure Distribution

The variation of normal soil pressure at the midspan of the top slab with depth of fill is plotted in Figure 4.17. As can be seen from the figure, GW soil type (coarse aggregate) exhibits lower values of normal soil pressure until the fill height reaches approximately 7 feet. Beyond this it starts to show high values of soil pressure. At a fill height of 20 feet, the soil pressure of GW soil type is almost twice as large as the soil pressure of SM type soil (silty sand). More deformation of the culvert would be expected from higher soil pressure as will be seen later.

The normal soil pressure distribution around the culvert under a fill height of 20 feet is shown in Figure 4.18. This figure reveals an interesting observation. Much higher soil pressure is developed around

Table 4.1 Representative Parameter Values of the Modified  
Duncan Model (References 12 and 13)

	GW Soil	SM Soil
Cohesion, $c$	0.0	0.0
Friction Angle, $\phi$	33.0°	32.0°
Modulus Number, $K$	200.0	300.0
Modulus Exponent, $n$	0.4	0.25
Failure Ratio, $R_f$	0.7	0.7
Bulk Modulus Number, $K_b$	50.0	250.0
Bulk Modulus Number, $m$	0.2	0.0

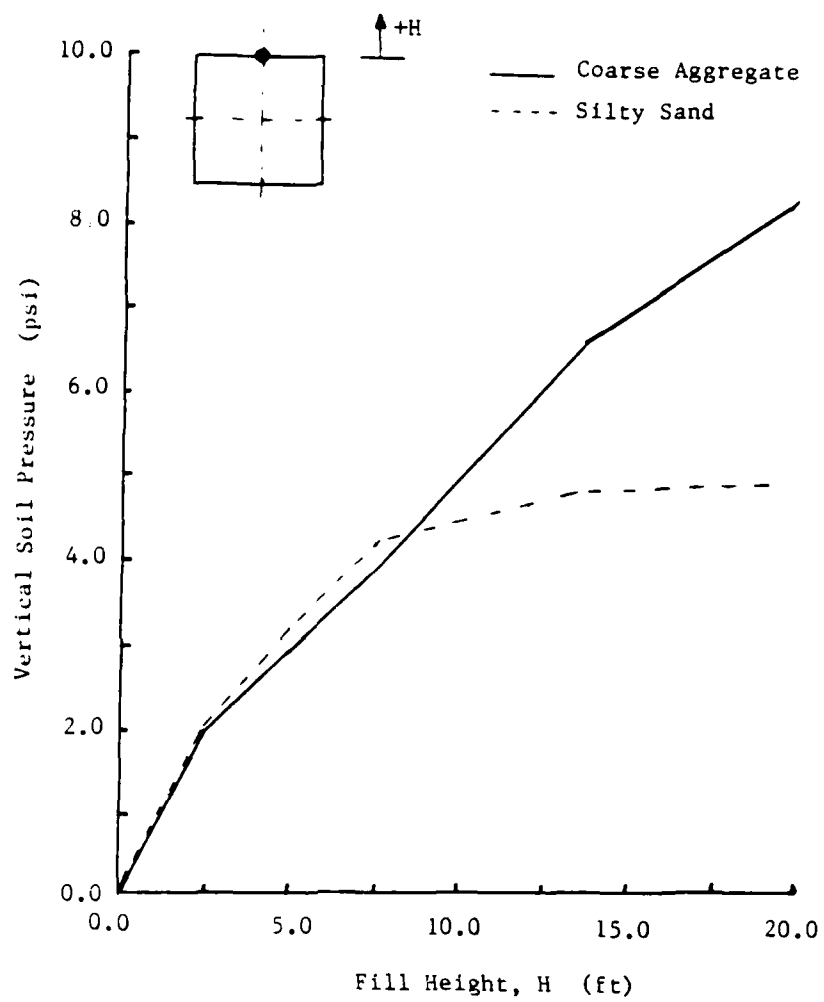


Figure 4.17 Vertical Soil Pressure at Crown

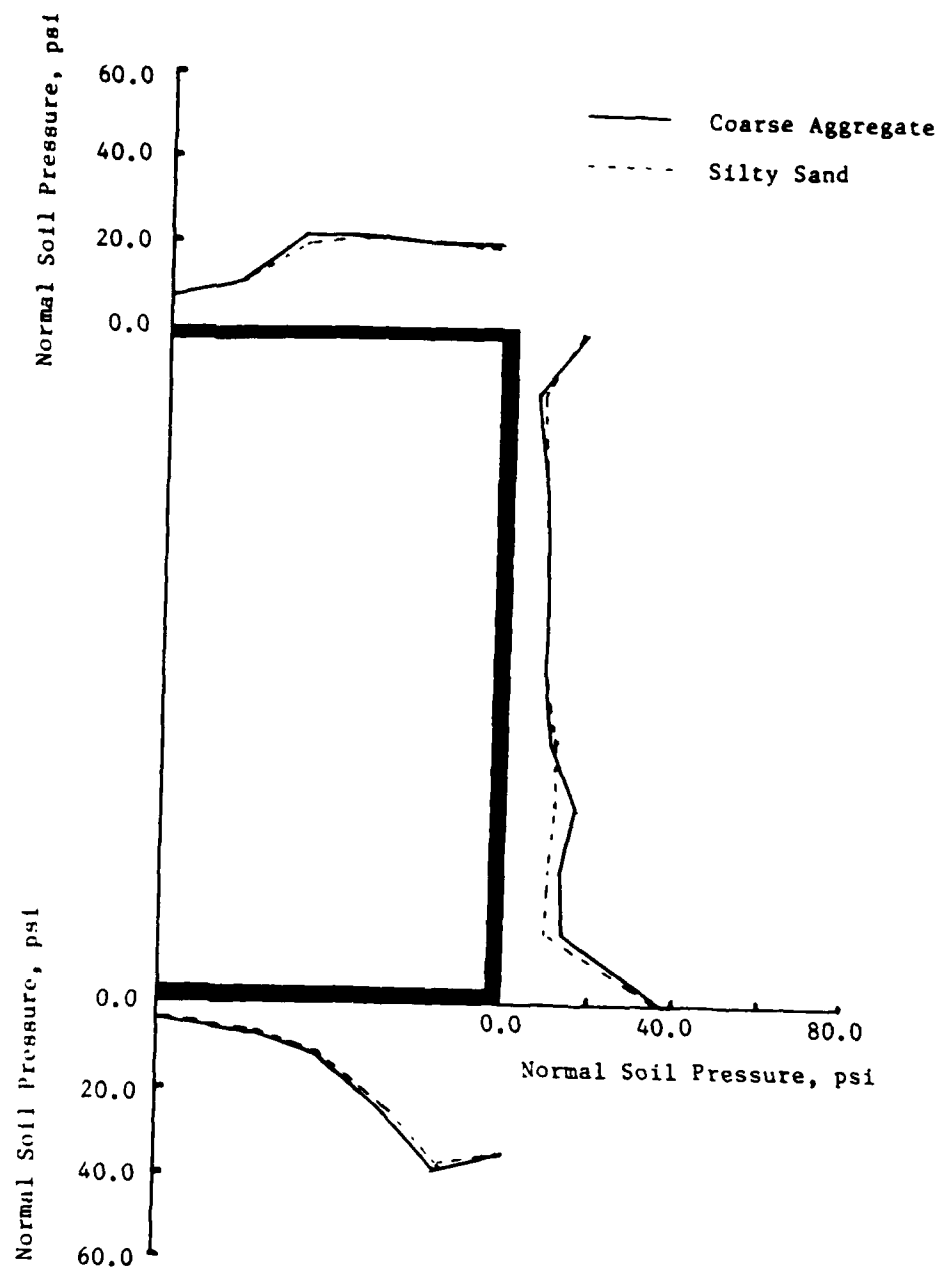


Figure 4.18 Soil Pressure Distribution around the Culvert at Fill Height = 20 ft

the bottom of the culvert. One possible explanation is that since the culvert deforms downward, it is more likely to mobilize passive pressures in the soil adjacent to the bottom corner, with a resultant higher coefficient of soil pressure than is characteristic of the active state.

## 2. Shape of the Deformed Culvert

Figure 4.19 shows crown deformation versus the depth of fill. SM soil type (silty sand) shows a rising crown deflection until the fill height reaches the crown level of the culvert, followed by a downward linear deformation due to the vertical soil pressure of backfill. By comparison, GW soil type (coarse aggregate) shows no rising crown deflection. The deflection of GW soil type at 20 feet of fill height is about two times larger than the deflection of SM soil type. With the soil pressure previously observed, this confirms that greater deflection of the culvert would be developed from the higher soil pressure.

Figure 4.20 shows the final shape of deformed culvert under the fill height of 20 feet. From this comparison study it is evident that the type of soil is one of major factors governing the behavior of a box culvert, and is an important factor for analysis and design of a box culvert.

## 3. Bending Moment and Thrust Distribution

Figures 4.21 to 4.25 report the bending moments versus the depth of fill at five locations, and Figure 4.26 shows the bending moment

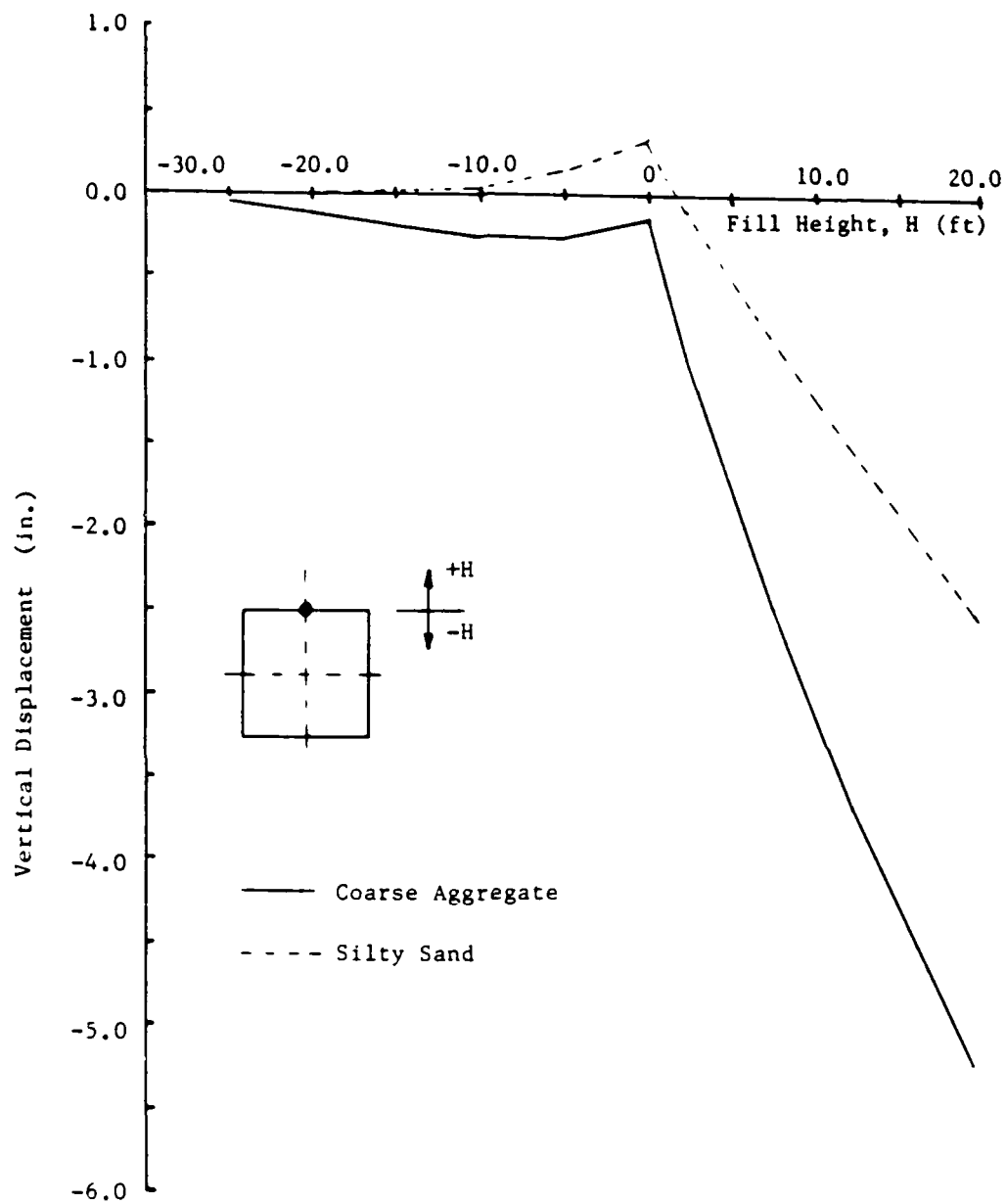


Figure 4.19 Crown Deflection vs. Fill Height

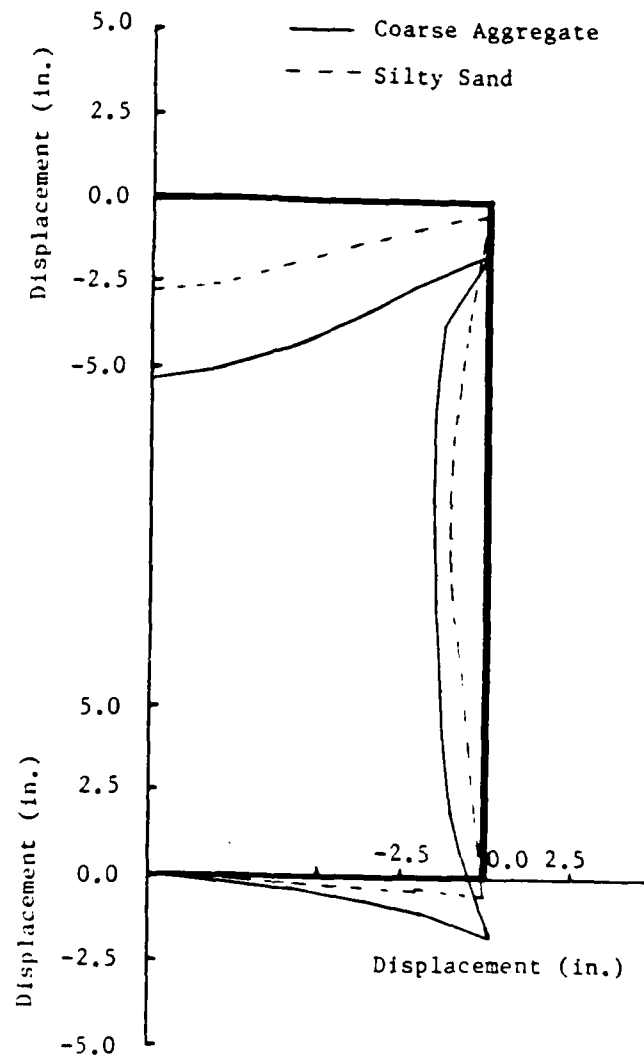


Figure 4.20 Deformed Box Culvert under Fill Height = 20 ft



distribution around culvert under a fill height of 20 feet. Also Figures 4.27 to 4.31 report thrust variations with the depth of fill at five locations. Figure 4.32 shows the thrust distribution around the culvert under fill height of 20 feet.

As expected, the results are similar in shape to those moments and thrusts shown in the previous section. At the end of the last construction increment, positive moments are observed at the midspans of the top slab, vertical wall and bottom slab. Also, negative moments are observed at the top and bottom corners. Finally, the top corner proves to be the most critical section.

Again, all thrusts are tensile (negative) forces under the fill height of 20 feet, and the most critical section is observed to occur one-third of vertical wall height from the bottom.

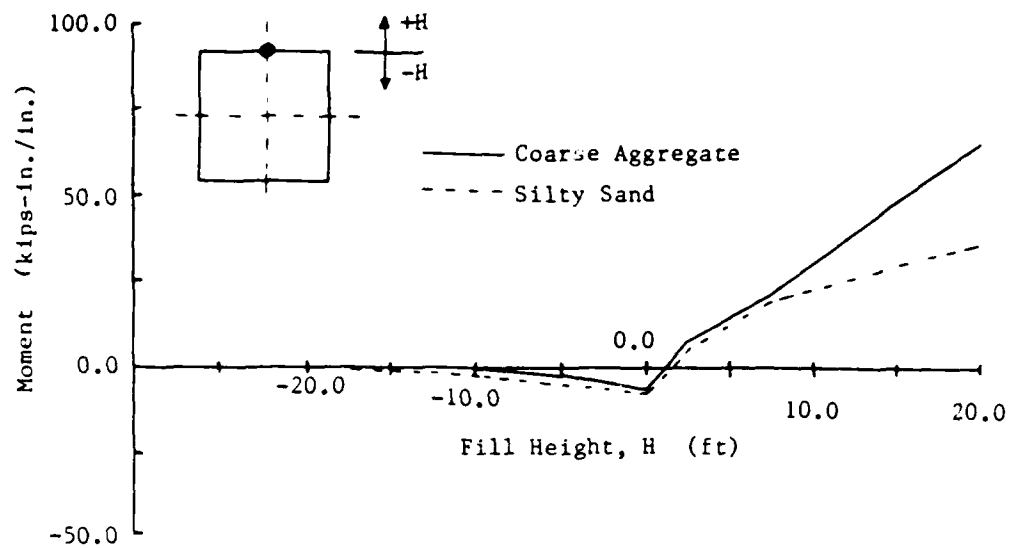


Figure 4.21 Culvert Bending Moments at Strain Gage #1

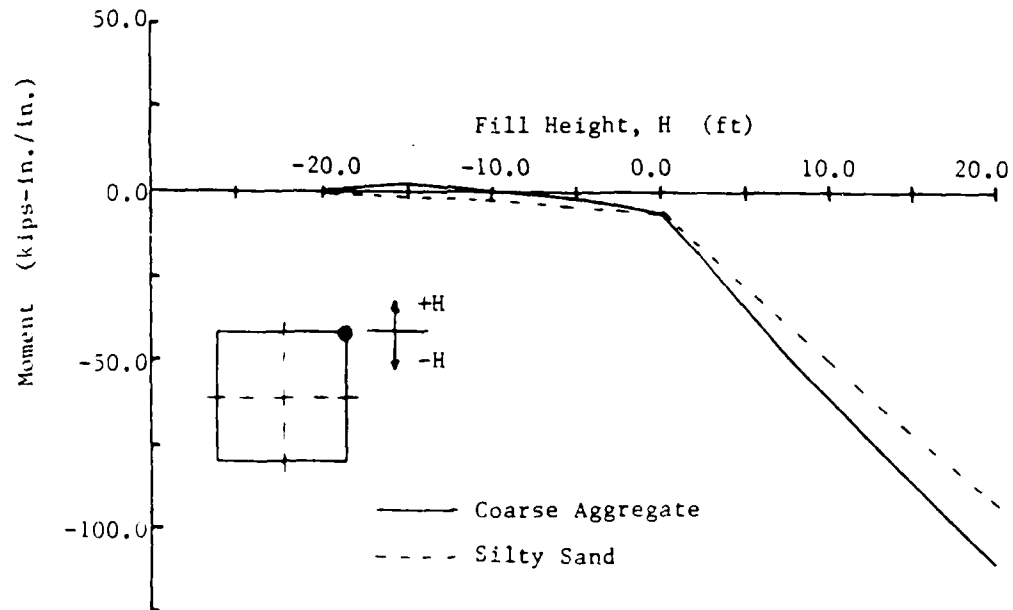


Figure 4.22 Culvert Bending Moments at the Upper Corner

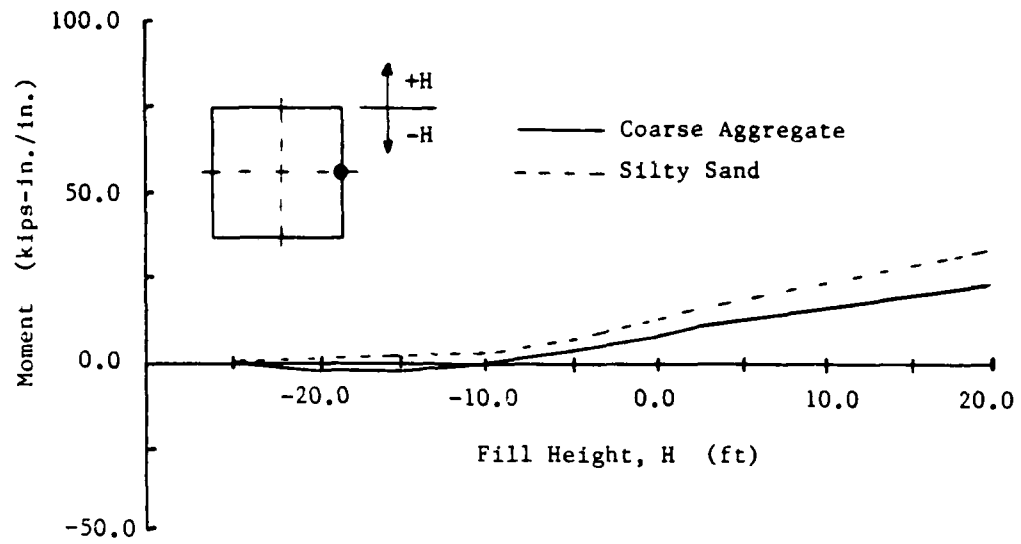


Figure 4.23 Culvert Bending Moments at Strain Gage #4

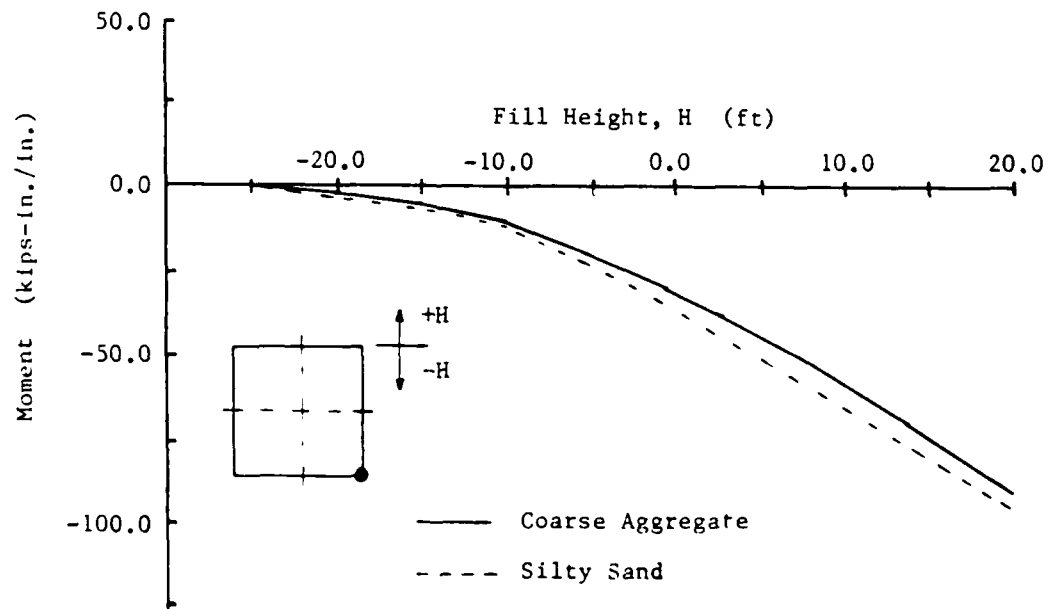


Figure 4.24 Culvert Bending Moments at Bottom Corner

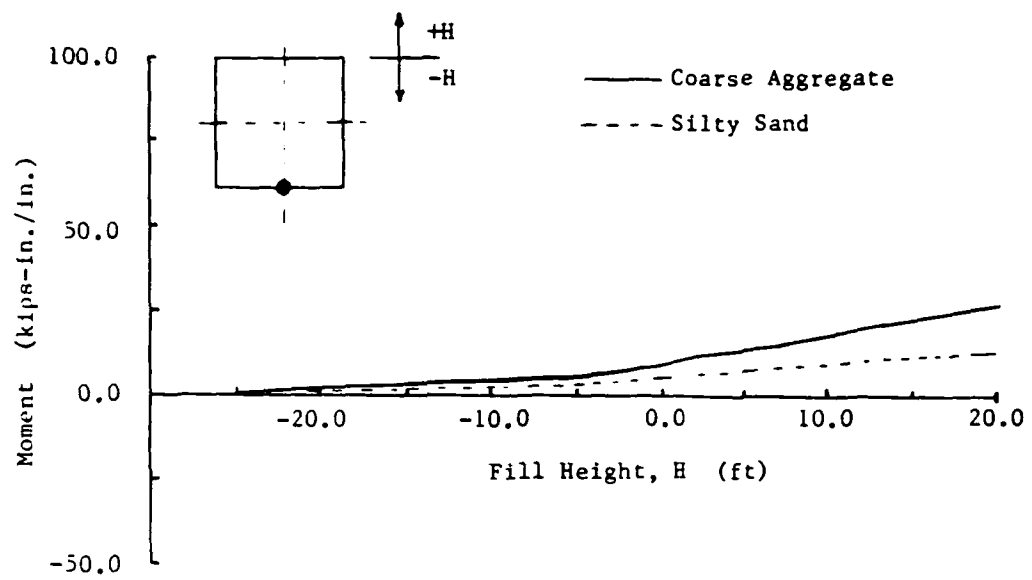


Figure 4.25 Culvert Bending Moments at Strain Gage #7

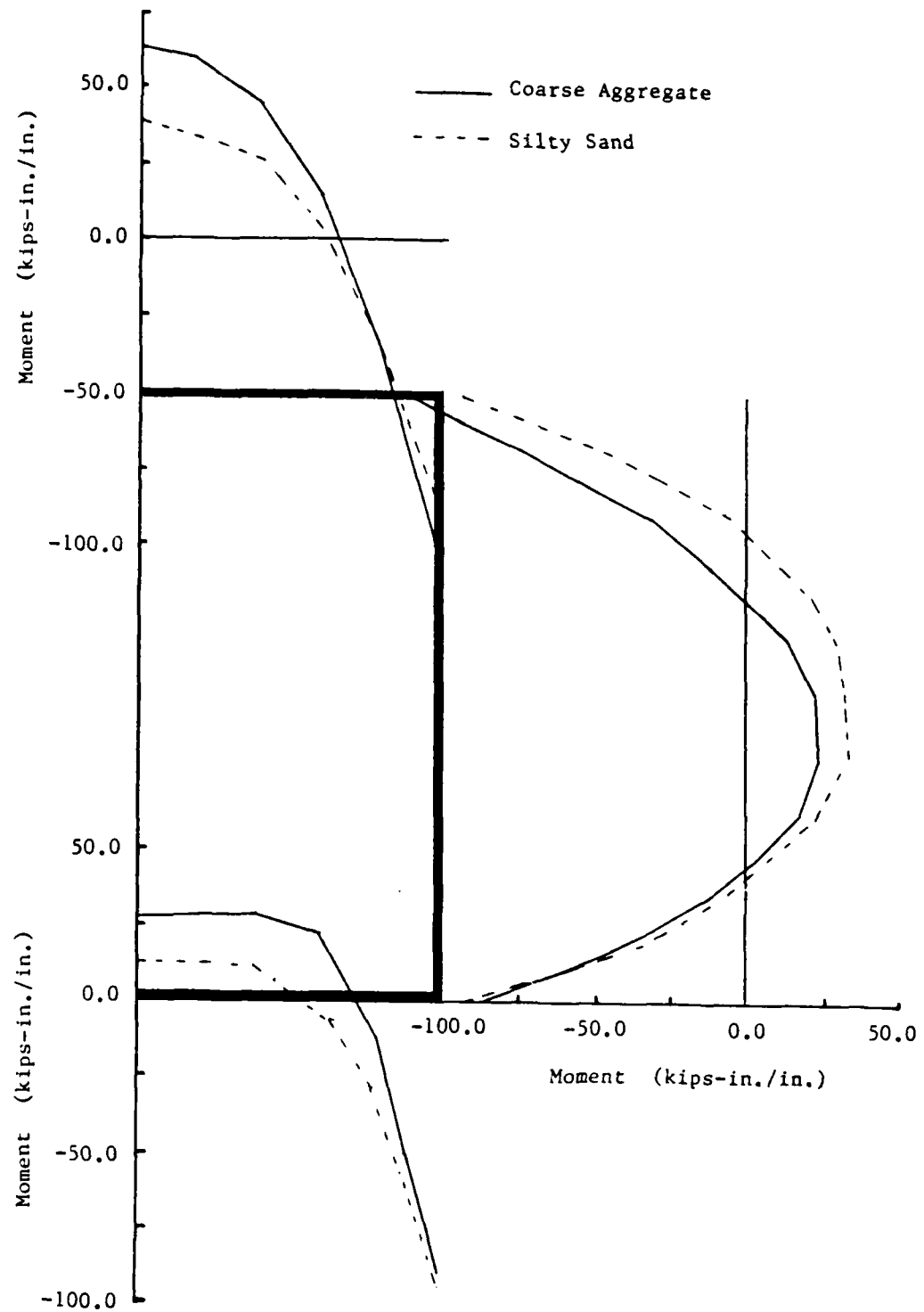


Figure 4.26 Bending Moments around the Culvert  
at Fill Height = 20 ft

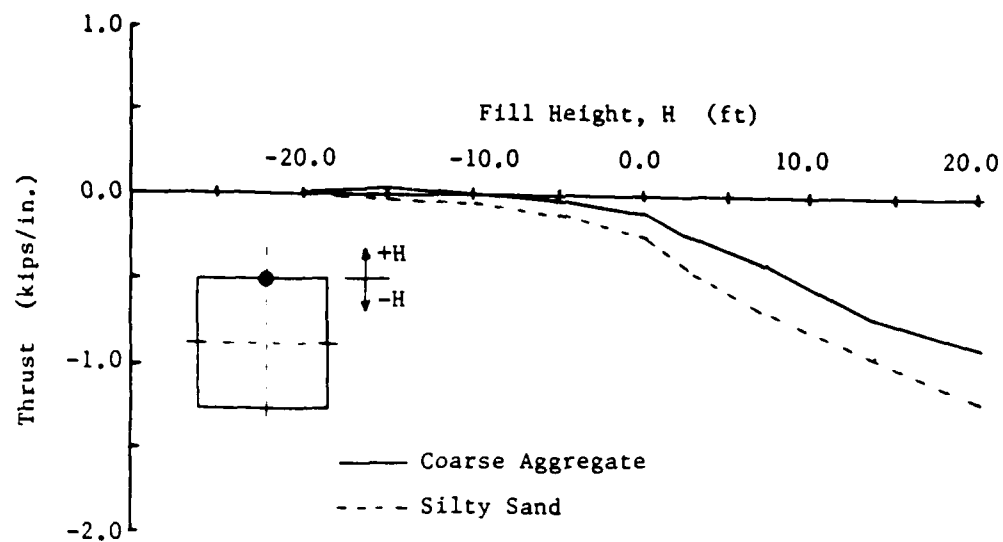


Figure 4.27 Culvert Thrusts at Strain Gage #1

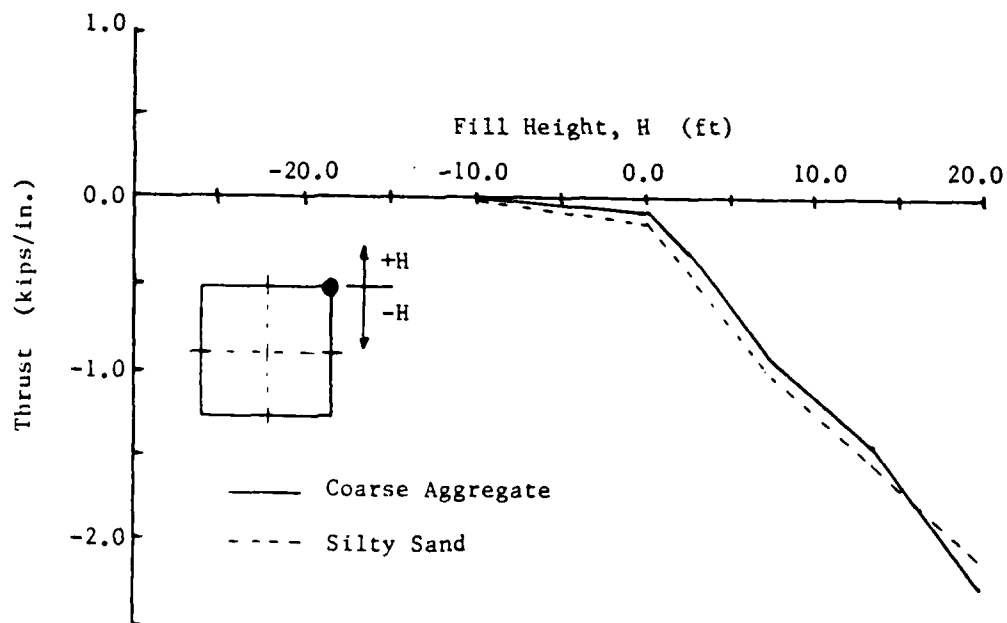


Figure 4.28 Culvert Thrusts at Upper Corner

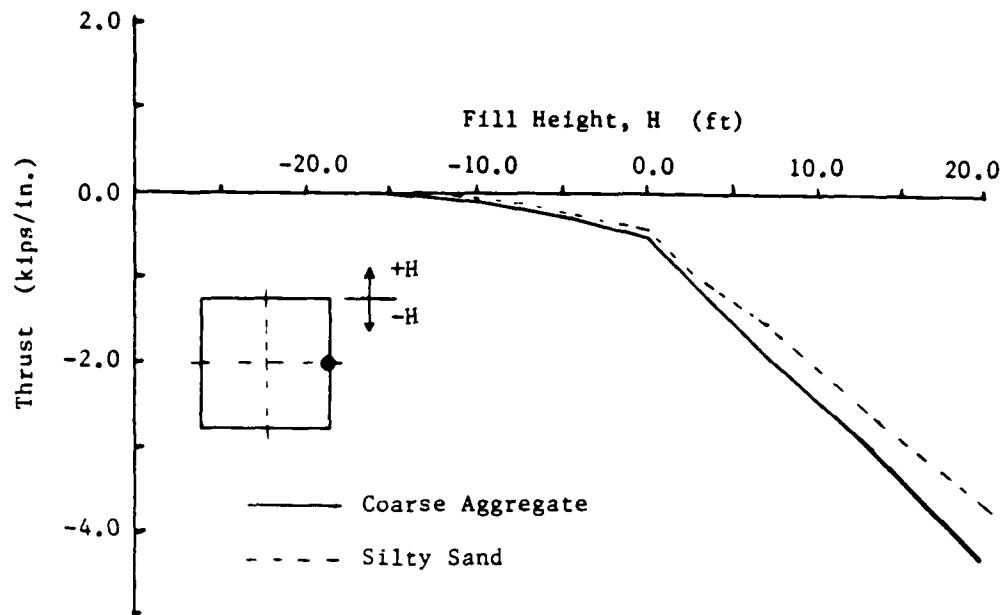


Figure 4.29 Culvert Thrusts at Strain Gage #4

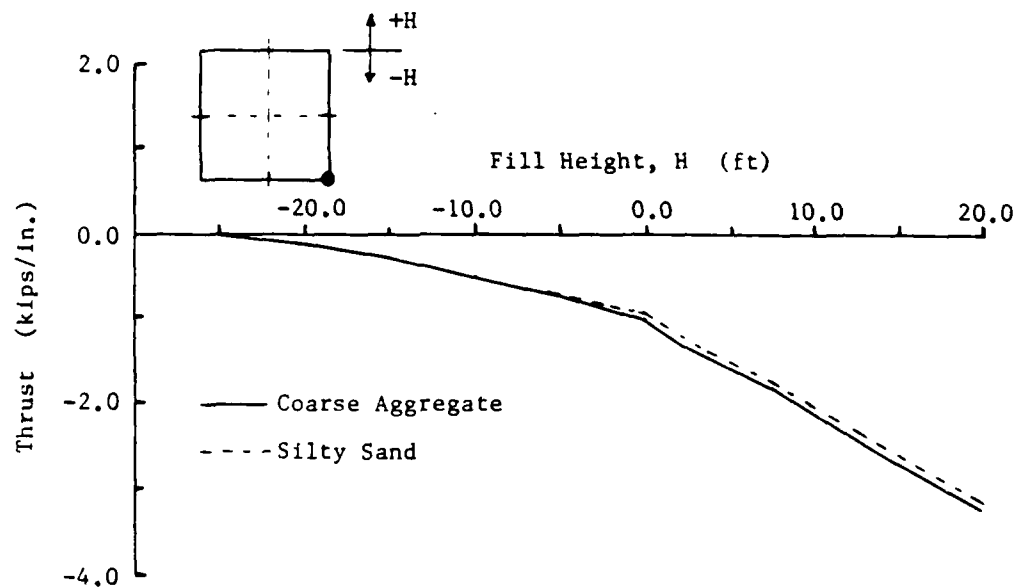


Figure 4.30 Culvert Thrusts at Bottom Corner

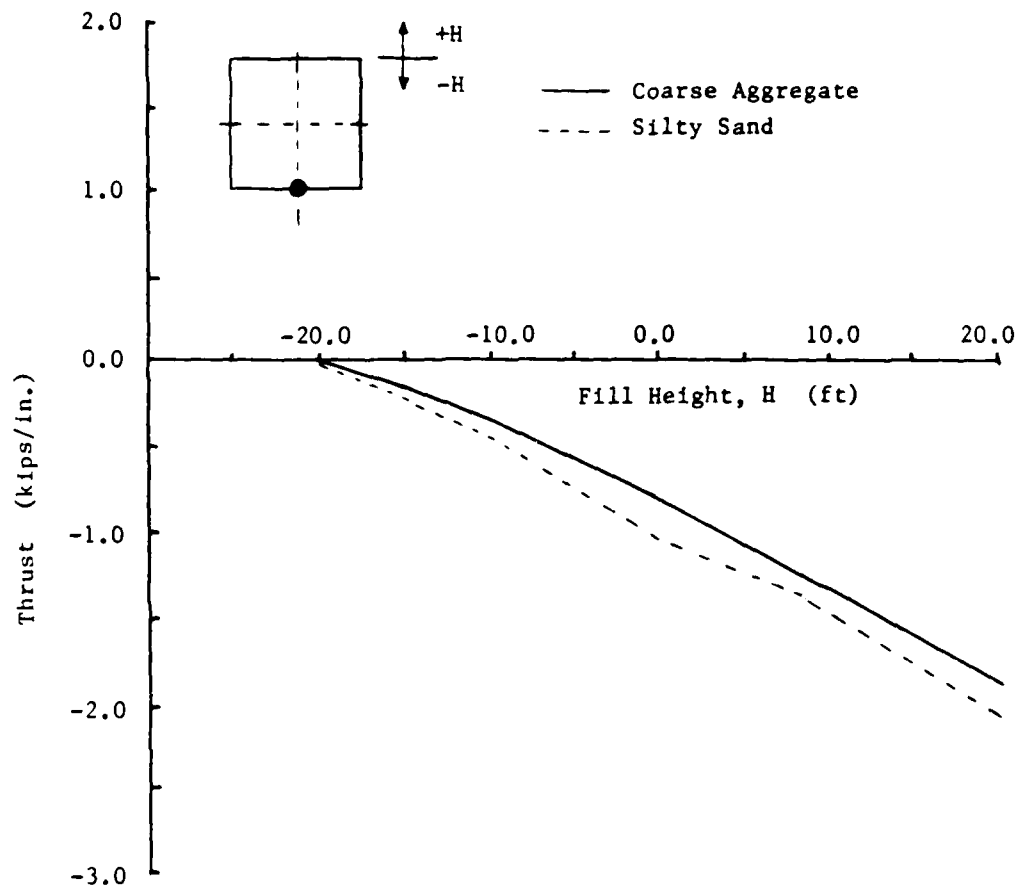


Figure 4.31 Culvert Thrusts at Strain Gage #7



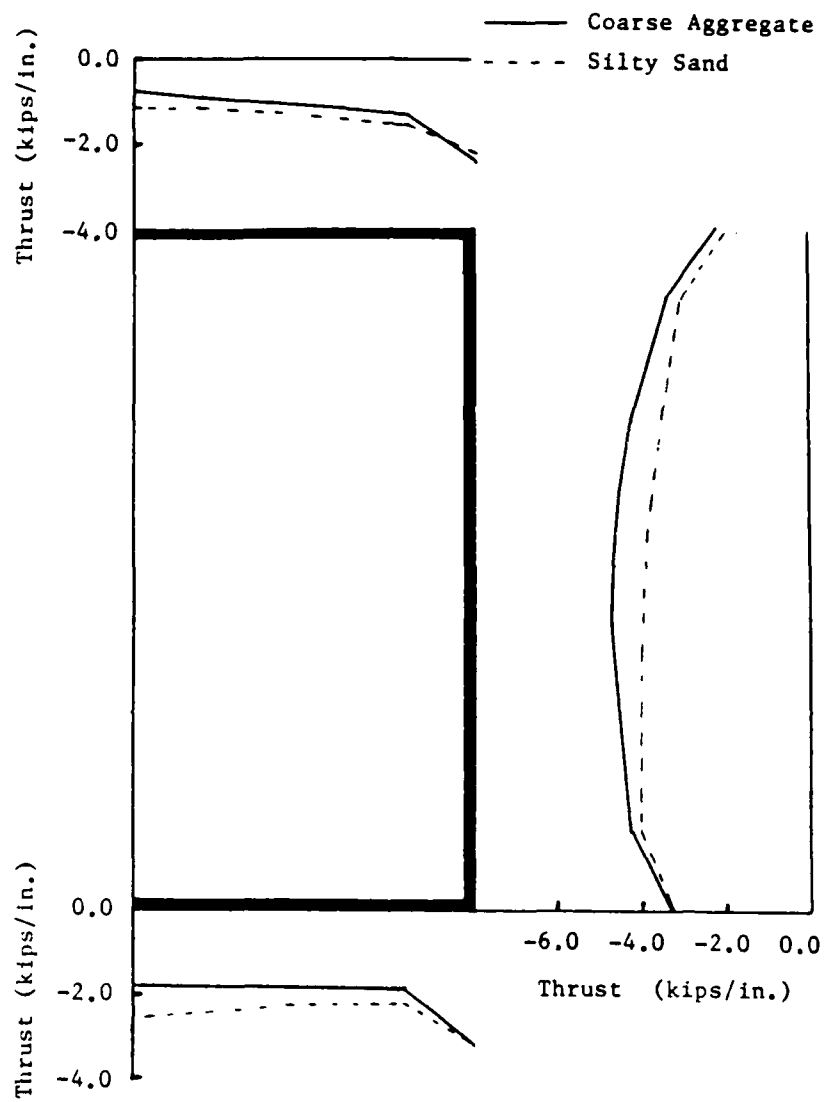


Figure 4.32 Thrusts around the Culvert  
at Fill Height = 20 ft

## SECTION V

### SUMMARY, CONCLUSIONS AND RECOMMENDATIONS

#### A. Summary and Conclusion

This report presents an investigation of the behavior of a concrete box culvert under backfill loads. A centrifuge model technique is used to simulate a prototype structural box culvert, and the measured structural responses are compared with predictions of finite element analyses. Findings and conclusions from this investigation are as follows:

1. The results of the centrifuge model study agree moderately well in shape, but some differences in magnitude are observed when they are compared with the results of finite element analyses.

2. No major difference in structural behavior is observed between trench and embankment soil installation from both the centrifuge model study and numerical analyses except that embankment soil installation produces slightly higher loadings.

3. Maximum bending moment is observed at the upper corner of the culvert as expected.

4. Centrifuge model study and numerical analyses show that all thrusts around the culvert below a fill height of 20 feet are negative (tensile) forces due to deflection of the slab members by soil pressures.

5. Significantly different shapes of the deformed culverts are observed from the finite element analyses when different soil stiffness is used in CANDE. This indicates that soil type is one of important

parameters to be considered in the analysis and design of a culvert.

#### B. Recommendations

Recommendations for further research based on this study are as follows:

1. The results of centrifuge model study presented in this report are based on the preliminary investigation for the feasibility study of a box culvert in a centrifuge. More comprehensive (extensive) research including culverts of other sizes and geometries, reinforcement, and different soil types and compaction for backfills and bedding parameters is required in order to gain a better understanding of the behavior of a box culvert.

2. In order to achieve accurate model details mentioned in (1) above, a much larger centrifuge is preferable.

3. Once reasonable information is obtained from the comprehensive centrifuge model study and numerical analyses, a field study is necessary to verify the results of centrifuge model study and predictions of finite element analyses.

#### REFERENCES

1. Coles, C.K., "Centrifuge Models of a Spile-Reinforced Tunnel," M.S. Thesis, University of California, Davis, June, 1982.
2. Kim, M.M. and Ko, H.Y., "Centrifugal Testing of Soil Slope Models," Transportation Research Record 872, pp. 7-15, 1982.
3. Rowe, P.W. and Craig, W.H., "Application of Models to the Prediction of Offshore Gravity Platform Foundation Performance," International Conference on Offshore Site Investigation, pp. 269-281, Graham and Trotman, London, 1980.
4. Shen, C.K., Kim, Y.S., Bang, S. and Mitchell, J., "Centrifuge Modeling of a Lateral Earth Support," Proceedings of the ASCE, Journal of the Geotechnical Engineering Division, Vol. 108, No. GT9, pp. 1150-1164, September, 1982.
5. James, R.G., and Larsen, H., "Centrifugal Model Tests of Buried Rigid Pipes," Proceedings of the Ninth International Conference on Soil Mechanics and Foundation Engineering, Tokyo, Japan, 1977.
6. Scott, R.F., and Morgan, N.R., "Feasibility and Desirability of Constructing a Very Large Centrifuge for Geotechnical Studies," Report 760-170 NSF, California Institute of Technology and JPL, March, 1977.
7. Li, X.S., Personal communication, Department of Civil Engineering, University of California, Davis, California, 1985.
8. Ju, Personal communication, Department of Civil Engineering, University of California, Davis, California, 1985.
9. Shen, C.K., Li, X.S. and Kim, Y.S., "Microcomputer Based Data Acquisition Systems for Centrifuge Modeling," Proceedings of the ASTM, Geotechnical Testing Journal, Volume 7, Number 4, pp. 200-204, December, 1984.
10. Yang, F., Personal communication, Department of Civil Engineering, University of California, Davis, California, 1985.
11. Katona, M.G., Smith, J.M., Odello, R.J., and Allgood, J.R., "CANDE - A Modern Approach for the Structural Design and Analysis of Buried Culverts," Report No. FHWA/RD-77/5, Federal Highway Administration, Washington, D.C., October, 1976.
12. Katona, M.G., Vittes, P.D., Lee, C.H., and Ho, H.T., "CANDE-1980: Box Culverts and Soil Models," Report No. FHWA/RD-80/172, Federal Highway Administration, Washington, D.C., May, 1981.

13. Duncan, J.M., et al., "Strength, Stress-Strain and Bulk Modulus Parameters for Finite Element Analyses of Stresses and Movements in Soil Masses," Report No. UCB/GT/78-02, National Science Foundation, April, 1978.
14. Wong, K.S. and Duncan, J.M., "Hyperbolic Stress-Strain Parameters for Nonlinear Finite Element Analysis of Stresses and Movements in Soil Masses," Report No. TE-74-3, University of California, Berkeley, July, 1974.
15. Gardner, M.P. and Jeyapalan, K., "Preliminary Analysis of the Behavior of Reinforced Concrete Box Culverts," Report No. FHWA/TX-82/50+326-1, September, 1982.

1984 USAF-SCEEE FACULTY SUMMER SUPPORT PROGRAM

Sponsored by the

AIR FORCE OFFICE OF SCIENTIFIC RESEARCH

Conducted by the

SOUTHEASTERN CENTER FOR ELECTRICAL ENGINEERING EDUCATION

FINAL REPORT

EFFECTS OF FLUID SHIFTS AND HYPOVOLEMIA IN INDIVIDUALS

WITH DIFFERENT WORKING CAPACITIES WHILE RESTING

AT A FIVE DEGREE DECLINATION

Prepared by:	William G. Squires, Ph.D.
Academic Department:	Biology
University:	Texas Lutheran College
Research Location:	Aerospace Physiology Laboratory, Biomedical Division, Crew Technology Branch
USAF Research Contact:	Sarah Nunneley, Ph.D.
Date:	1985
Contract No.:	84 RIP 24 F49620-82-C-0035

EFFECTS OF FLUID SHIFTS AND HYPOVOLEMIA IN INDIVIDUALS WITH  
DIFFERENT WORKING CAPACITIES WHILE RESTING  
AT A FIVE DEGREE DECLINATION

by

William G. Squires

ABSTRACT

Data from actual space flight studies have demonstrated functional abnormalities and changes of the cardiovascular system immediately post-flight. Interest lies in what occurs to the body during exposure to zero gravity that could account for these post-flight alterations in cardiovascular functions. During zero gravity or head-down rest, the hydrostatic intra- and extravascular pressure gradients that are normally present in the upright position are abolished or minimized. This causes a headward shift of body fluids from the lower portions of the body cavity. This massive fluid shift induces adaptive changes in other body systems, such that re-exposure to normal gravitational forces produces signs of orthostatic intolerance. These adaptive changes include the following: inhibition of the renin-angiotensin and ADH systems, diuresis, decreased blood volume, weight loss associated with diuresis and decreased blood volume, inhibition of sympathetic activity due to decreased levels of circulating catecholamines and increased activity of the carotid sinus nerve, decreased stroke volume, no change (or slight increase) in arterial pressure, cardiac output, or the contractile state of the heart, compensatory

bradycardia, increased right and left atrial filling pressures and central venous pressure, increased left ventricular end-diastolic volume and left ventricular ejection fraction, decreased leg volumes and increased forearm volumes.

Preliminary studies were done on a dog and the expected changes in the cardiovascular parameters were found. Contractility of the heart increased, left ventricular pressure increased, left ventricular end-diastolic pressure increased, heart rate decreased, renal blood flow and carotid blood flow increased, and systemic arterial pressure increased after the dog was tilted five degrees head-down for one hour.



## I. INTRODUCTION:

The major focus of the experiment was to compare responses to zero gravity and orthostatic tolerance post-tilt between individuals with different fitness levels. Understanding the mechanisms involved required elucidation of changes in plasma renin-angiotensin levels, plasma catecholamine levels, body fluid shifts, and segmental volume changes. As a result, further significance could be drawn from this study regarding the use of the head-down tilt method as a means of pre-flight preparation for the pilot.

With the advent of manned space flight new questions have arisen as to the effects of zero gravity on human cardiovascular function. The adaptive responses of man to this new type of environment involve many interrelated and complex organ systems. Data from actual space flight studies have shown no signs of severe cardiovascular impairment but functional abnormalities and changes of the cardiovascular system have been demonstrated immediately post-flight.<sup>6,9,24,30,31,32</sup> Interest lies in what occurs to the body during exposure to zero gravity that could account for these post-flight alterations in cardiovascular function.

Because of time, method, and other limitations during actual space flight studies, it is necessary to develop ground-based simulations of weightlessness. Bed rest and water immersion both produce the same human responses as those seen with prolonged exposure to zero gravity. However, recent

Russian and American studies have demonstrated that a slightly head-down position (from  $-4^{\circ}$  to  $-6^{\circ}$ ) produces effects qualitatively similar to those of bed rest except that the adaptation is accelerated. During short-term experiments head-down tilt produces a greater degree of cardiovascular deconditioning than horizontal bed rest of equal duration. Water immersion has also been used to simulate zero gravity, though there are problems inherent in this technique. Prolonged immersion is logistically difficult because of skin lesions due to maceration and presence of hydrostatic pressures alters respiratory mechanisms. The temperature of the bath is also critical. Thermoregulatory mechanisms disturb the hydrostatic effects if the bath is not theroneutral, i.e., kept at  $33-35^{\circ}$  C. In general, the comparisons of the effects of space flight and head-down tilt support the use of tilt as a simulation method for cardiovascular studies since it, rather than bed rest and water immersion, most closely resembles conditions during weightlessness.

During normal erect posture most blood volume is usually maintained below the level of the heart. Under zero gravity or head-down rest there is a headward shift of body fluids from the lower portions of the body.<sup>5,6,10,18,40,44</sup> Therefore, blood tends to pool in the thoracic cavity. This massive fluid shift induces adaptive changes in other body systems. These changes are referred to in Figure 1.

# PHYSIOLOGICAL RESPONSES TO HEAD-DOVE TILTING (-30°)

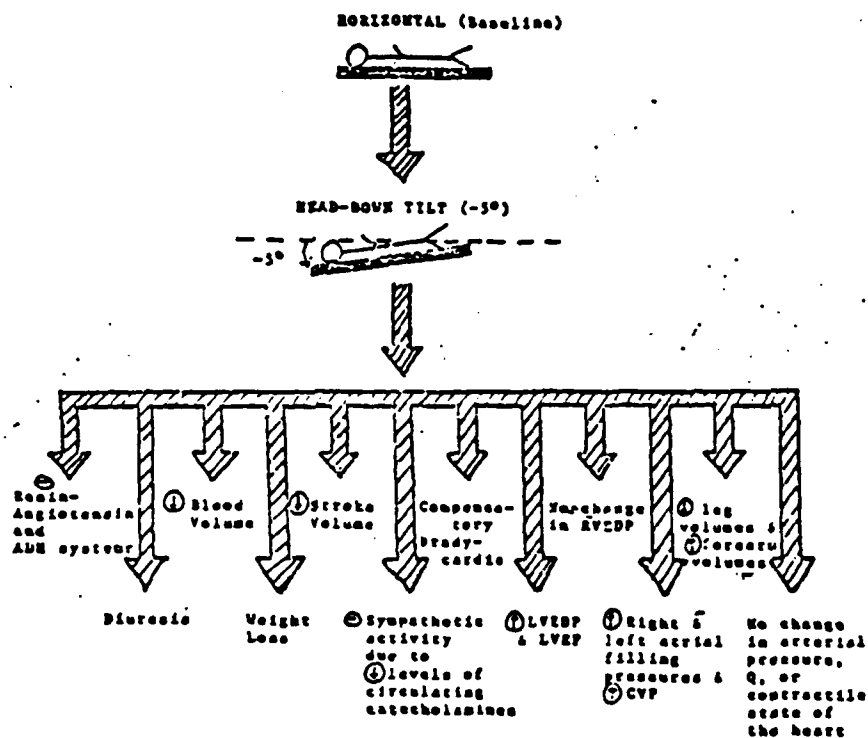


FIGURE 1

Due to the ambitious nature of this project, time limitations and necessary approval of this protocol from the Human Use Committee, this study was not carried out last summer but was done this summer under the same USAF-SCEEE Summer Support Program sponsored by the Air Force Office of Scientific Research. What follows is the protocol for this experiment.

However, a preliminary study involving dog models was undertaken last summer and results showed the expected relative changes in the cardiovascular system of the dog when it was

tilted 5° head-down.

A study similar to the one outlined here using trained and untrained dogs instead of human subjects as the experimental models was also completed in the summer of 1985.

## II. OBJECTIVES:

The objects of this experiment are to determine if individuals of different working capacities respond differently to head-down tilting and to elucidate the time course of volume changes in the right and left heart, so that a correlation between these changes with other biochemical and physiological changes may be made. In this way a clearer understanding of the mechanisms involved with volume regulation might be brought forth. Basically, this study was a continuation of last year's work.

## III. PROCEDURES:

A. Human Study: The experiment will use a 2 D echo cardiovascular imaging technique that will measure volume changes in the left heart. Individuals undertaking this protocol will undergo a baseline stress test and 2 D echocardiogram. One week prior to the actual declination study the subject will perform a maximal exercise stress test on the bicycle ergometer so that aerobic capacity can be determined.

The subject will be asked to report to the bedrest facility at 0800 hours on a pre-selected day. He will spend approximately 28 hours in the facility and will be released by approximately 1200 hours the following day. Upon entering the

bedrest facility the subject will recline in a horizontal position on a tilt-table. He will be instrumented with a standard twelve lead ECG, blood pressure cuff and strain gauges to measure anthropomorphic changes. The subject will then be tilted 5° head-down and data collection will take place every 15 minutes for the first hour, every 30 minutes for the next two hours, and once every hour until 1700 hours. No data will be collected during the night. The following morning at 0800 hours there will be another collection of data. At 0900 hours the subject will return to the horizontal position upon which data will also be collected. A post- maximal exercise stress test on the bicycle ergo meter will be conducted and left heart functioning will be studied.

#### TIMELINE

<u>ONE WEEK PRIOR:</u>		(Pre) Max Exercise Stress Test (bicycle ergometer)	1200	Data collection; radioisotope imaging and blood samples
		1st pass Thallium injection (individual attenuations)	1200-1300	Lunch
		MUGA --- Technetium injection	1300-1700	Data collection; radioisotope imaging and blood sample <u>every hour</u>
		Max VO <sub>2</sub> measurement with radioisotope imaging	(hourly)	
<u>TIME</u>	<u>ACTIVITY</u>		1700-1800	Dinner
0800-0900	Briefing and preparation of the subject		1800-0800 (next day)	Rest in tilt position; no data collection during the night
	Isotope (technetium) injection		0900-1000	Isotope (technetium) injection
0900	Horizontal - baseline measurements			RETURN TO HORIZONTAL
	TILT			Data collection; radioisotope imaging and blood sample
0915			1000-1100	(Post) Max Exercise Stress Test (bicycle ergometer)
0930	Data collection; radioisotope imaging and blood samples			Max VO <sub>2</sub> measurement with radioisotope imaging
0945			1200	Dinner
1000				
1030	Data collection; radioisotope imaging and blood samples			
1100				

FIGURE 2

The approach taken in this protocol will allow elucidation of the time course of volume changes left heart and possible correlation between these changes with other biochemical and physiological changes.

B. Dog Study: A healthy mongrel dog (17.6 kg) was used as an experimental animal. The animal was anesthetized with thiamyl sodium (10 mg/kg i.v.) and ventilated under positive pressure through a cuffed endotracheal tube with a standard volume animal respirator (Harvard Apparatus, Waltham, MA). The animal was positioned on the right side and an incision was made on the left hind leg to expose the saphenous vein into which a catheter was inserted. The catheter was connected to a two-way stopcock so that additional thiamyl sodium could be added to effect. The dog was then placed on its side and a small neck incision was made. The right common carotid was exposed and a pulsed Doppler flow probe tied into place. Careful attention was paid to assure normal carotid artery flow velocity with no constriction. The pulsed Doppler flow probe was calibrated in terms of Doppler frequency shift. A baseline zero can be established and a linear relationship between flow and frequency shift has been established in vivo.<sup>17</sup> A Doppler flow probe was also placed on the right femoral artery under direct vision. Precaution was taken to prevent arterial constriction. The dog was again positioned on the right side and a left flank incision made through which the left renal

artery was identified and encircled with a pulsed Doppler flow probe. As with the other flow probes, careful attention was taken to avoid constriction of the artery. A catheter was inserted into the dog's urinary bladder so that urine output could be measured. Next, a catheter was inserted into the left femoral artery and threaded up into the aorta for measurement of the systemic arterial pressure (Stratham p23Db pressure transducer). Electrocardiographic (ECG) lead AVF was established through a needle lead in all four limbs. A left thoracotomy was performed through the fifth intercostal space and the heart was suspended in a pericardial cradle. With the aid of a purse string suture, a solid state pressure transducer (Koingsberg P-7, Pasadena, CA) was inserted through a stab wound into the left ventricular apex.

The instrumentation allowed for measurement of left ventricular pressure (LVP), left ventricular and diastolic pressure (LVDP), systemic arterial, systolic and diastolic pressures (SP and DP), heart rate (HR), renal, carotid and femoral artery blood flow (RF, CF, FF), urine output and calculation of the first derivative of left ventricular pressure (LVdP/dt). Recordings were made on an eight channel recorder (Gould brush mark 200).

Following instrumentation, control baseline measurements were made for five minutes of LVP, LVDP, SP, DP, HR, CF, RF, and FF with the dog in the horizontal position. The dog was then tilted 5° head-down. Measurements were taken every five

minutes for one hour. After one hour head-down the dog was then brought back up to the horizontal position and measurements were taken at five and seven minutes post-tilt. After the last measurements were made, the dog was euthanized with a saturated solution of potassium chloride.

#### IV. RESULTS:

The results obtained from this experiment show the expected changes in the cardiovascular parameters. The contractility of the heart increased, left ventricular pressure increased, left ventricular end diastolic pressure increased, heart rate increased, RF and CF increased, and SP and DP increased after the dog was tilted 5° for one hour. Most of the changes occurred during the first 30 minutes head-down and then leveled out for the rest of the hour. When the dog was brought back up to the horizontal position, no change in the readings were evident within five and seven minutes.

#### V. RECOMMENDATIONS:

Despite the many studies on man's adaptation to simulated zero gravity, no conclusive evidence exists as to the effect of physical fitness on this response to zero gravity. Although objective comparisons of athletes and non-athletes give variable results, it has been suggested that the more physically fit person (high  $VO_2$ ) is less tolerant to orthostatic stress when volume depleted as a result of diuresis during head-down rest. This loss of blood volume is analogous to heat-related volume loss.<sup>6,18,19,33</sup>



The investigators in this study would eventually like to find out if, in fact, there are relative physiological and biochemical changes between trained and untrained subjects, dog and human, and if so, to what degree these parameters vary when the subjects go from the horizontal position to a 5° head-down position. Understanding the mechanisms involved requires elucidation of changes in plasma renin-angiotensin levels, plasma catecholamine levels and body fluid shifts. As a result, further significance could be drawn from this study regarding the use of the head-down tilt method as a means of pre-flight preparation for the pilot.

Studies have shown that increased activity of the carotid sinus nerve due to hypervolemia<sup>23,35</sup> or manual stimulation with electrodes<sup>42</sup> results in a reflex decrease in the force of atrial systole by a decrease in sympathetic activity to the heart and an increase in efferent vagal activity to the heart. A suggestion for follow-up research would be to isolate the carotid sinus nerve in an animal model. A small neck incision could be made to expose the left internal carotid artery at its origin where there is a bulbous enlargement, the carotid sinus, which is about 3 mm in diameter and 4 mm in length.<sup>25</sup> It contains an afferent fiber called either the carotid sinus nerve or the Hering nerve which is a branch of the glossopharyngeal nerve (IX). A microelectrode could then be placed on the carotid sinus nerve to measure its electrical activity. Then one could determine if it was stimulation of

the carotid sinus nerve or the reduction in circulating catecholamines that decreases sympathetic activity to the heart resulting in an attenuation of the force of atrial systole.

### Acknowledgement

The author would like to thank the Air Force Office of Scientific Research and the Southeastern Center for Electrical Engineering Education for the opportunity to work on an exciting and mind-stimulating project for the summer. I am grateful for the many things I learned and the interesting experiences I had at Brooks AFB/SAM while honing my research skills. In particular, I would like to acknowledge the Aerospace Physiology Division of the Crew Technology Branch for its hospitality, guidance, patience and excellent working conditions.

Finally, I would like to thank Dr. Carter Alexander for suggesting this area of research, and I would like to acknowledge the collaboration and excellent guidance of Dr. Russell Burton and Dr. Sarah Nunneley.

## REFERENCES

1. Abel, F.L., J.H. Pierce, and W.G. Guntheroth, "Baroreceptors influence on postural changes in blood pressure and carotid blood flow." Am. J. Physiol. Vol. 205(2), pp. 360-364, 1963.
2. Abel, F.L. and J.A. Waldhausen, "Influence of posture and passive tilting on venous return and cardiac output." Am. J. Physiol. Vol. 215(5), pp. 1058-1066, 1968.
3. Auger, R.G., J.E. Zehr, R.G. Siekert, and W.E. Segar. "Position effect on antidiuretic hormone: blood levels in bedrest patients." Arch. Neurol. Vol 23, pp. 513-517, 1970.
4. Bevegard, S., J. Castendørs, and L. Lindblad. "Effect of changes in blood volume distribution on circulatory variables and plasma renin activity in man." Acta Physiol. Scand. Vol. 99, pp. 237-245, 1977.
5. Blomqvist, C.G., J.V. Nixon, R.L. Johnson, J.H. Mitchell. "Early cardiovascular adaptation to zero gravity simulated by head-down tilt." Acta Astronautica Vol. 7, pp. 543-553, 1980.
6. Blomqvist, C.G. and H.L. Stone. "Cardiovascular adjustments to gravitational stress." Handbook of Physiology--The Cardiovascular System IV, in publication.
7. Bonde-Peterson, F., Y. Suzuki, and T. Sadamoto. "Cardiovascular responses to isometric exercise during simulated zero gravity." The Physiologist pp. 37-38.
8. Brennan, L.A., R.L. Malvin, K.E. Jochim, and D.E. Roberts. "Influence of right and left atrial receptors on plasma concentrations of ADH and renin." Am. J. Physiol. Vol. 221(1), pp. 273-278, 1971.
9. Buderer, M.C., J.A. Rummel, E.L. Michel, D.G. Mauldin, and C.F. Sawin. "Exercise cardiac output following Skylab mission." Aviat. Space Environ. Vol. 47(4), pp. 365-372, 1976.
10. Epstein, M. "Cardiovascular and renal effects of head-out water immersion in man." Circ. Res. Vol. 39(5), pp. 619-628, 1976.

11. Gazenko. O.G., et al. "Effects of various counter-measures against the adverse effects of weightlessness on central circulation in the healthy man." Aviat. Space Environ. Med. Vol. 53(6), pp. 523-530, 1982.
12. Gomez-Sanchez, C., D.C. Kim, N.M. Kaplan. "A radio-immunoassay for plasma aldosterone by immunologic purification." J. Clin. Endocrin. Metab. Vol. 36, pp. 795-798, 1973.
13. Goodall, McC., M. McCally, and J.D. Graveline. "Urinary adrenaline and noradrenaline response to simulated weightless state." Am. J. Physiol. Vol. 206(2), pp. 431-436, 1964.
14. Graveline, D.E. and M. McCally. "Body fluid distribution: implications for zero gravity." Aerosp. Med. Vol. 33 (11), pp. 1281-1290, 1962.
15. Greenleaf, J.E., D. Sciaraffa, E. Schwartz, L.C. Kiel, and P.J. Brock. "Exercise training hypotension: implications for plasma volume, renin, and vasopressin." J. Appl. Physiol.: Respirat. Environ., Exercise Physiol. Vol. 51(2), pp 298-305, 1981.
16. Haber, E., T. Koerner, L.B. Page, B. Klenian, and A. Purnode. "Application of a radioimmunoassay for angiotensin I to the physiological measurements of plasma renin activity in normal human subjects." J. Clin. Endocrinol. Metab. Vol. 29, pp. 1349-1355, 1969.
17. Hartley, C.J., H.G. Hanley, R.M. Lewis, and F.S. Cole. "Synchronized pulsed Doppler blood flow and ultrasonic dimension measurement in conscious dogs." Ultrasound in Med. and Biol. pp. 99-110, 1978.
18. Katkov, V.E., V.V. Chestukkin, R.I. Lapteva, V.A. Yakovleva, V.M. Mikhailov, O. Kh. Zybin, and V.N. Utkin. "Central and cerebral hemodynamics and metabolism of the healthy man during head-down tilting." Aviat. Space Environ. Med. Vol. 50(2), pp. 147-153, 1979
19. Klein, K.E., H.M. Wegmann, and P. Kuklinski. "Athletic endurance training - advantage." Aviat. Space Environ. Med. Vol. 48(3), pp. 215-222, 1977.
20. Klein, K.E., H.M. Wegmann, H. Bruner, and L. Voght. "Physical fitness and tolerance to environmental extremes." Aerosp. Med. Vol. 40(9), pp. 998-1001. 1969.

21. Lamb, L.E., R.L. Johnson, P.M. Stevens, and B.E. Welch. "Cardiovascular deconditioning from space cabin simulator confinement." Aerosp. Med. Vol 35, pp. 420-428, 1964.
22. Liu, C.T., H.E. Hoff, and R.A. Huggins. "Circulatory and respiratory responses to platural changes in the hemorrhagic dog." J. Appl. Physiol. Vol 27(4), pp. 460-464, 1969.
23. Mancia, G., J.T. Shepherd, and D.E. Donald. "Interplay among carotid sinus, cardiopulmonary, and carotid body reflexes in dogs." Am. J. Physiol. Vol. 230(1), pp. 19-24, 1976.
24. Michel, E.L., J.A. Rummel, and C.F. Sawin. "Skylab experiment M-171 'metabolic activity' - results of the first manned mission." In Biomedical Results from Skylab. (Edited by R.S. Johnston and L.F. Dietlein), pp. 284-312, NASA, Washington, D.C.
25. Miller, M.E. "The head." In Guide to the Dissection of the Dog, p. 289, Ithaca, New York.
26. Miller, P.B., R.L. Johnson, and L.E. Lamb. "Effects of four weeks of absolute bed rest on circulatory functions in man." Aerosp. Med. Vol. 42, pp. 1194-1200, 1964.
27. Myhre, L.G., D.K. Brown, F.G. Hall, and D.B. Dill. "The use of carbon monoxide and T-1824 for determining blood volume." Clin. Chem. Vol. 14, pp. 1197-1205, 1969.
28. Nickel, J.F., L. Levine, and J.A. Gagnon. "Effects of acute passive tilting on arterial pressure, renal hemodynamics, and urinary electrolyte excretion in the dog." J. Appl. Physiol. Vol. 9, pp. 176-184, 1956.
29. Nixon, J.V., R. Gordon Murray, C. Bryant, R.L. Johnson, J.H. Mitchell, O. Bryan Holland, C. Gomez-Sanchez, P. Vergne-Marini, and C.G. Blomqvist. "Early cardiovascular adaptation to simulated zero gravity." J. Appl. Physiol. Respirat. Environ. Exercise Physiol. Vol. 46(3), pp. 541-548, 1979.
30. Rummel, J.A., E.L. Michel, and C.A. Berry. "Physiological response to exercise after space flight - Apollo 7 to Apollo 11." Aerosp. Med. Vol. 44(3), pp. 235-238, 1973.

31. Rummel, J.A., C.F. Sawin, M.C. Buderer, D.G. Mauldin, and E.L. Michel. "Physiological response to exercise after space flight - Apollo 14 through Apollo 17." Aviat. Space Environ. Med. Vol. 46(5), pp. 679-683, 1975.
32. Rummel, J.A., E.L. Michel, C.F. Sawin, and M.C. Buderer. "Medical experiment M-171: results from the second manned Skylab mission." Aviat. Space Environ. Med. Vol. 47(10), pp. 1056-1060, 1976.
33. Saiki, H., N. Masayuki, M. Sudoh, M. Abe, Y. Taketomi, and M. Naruse. "Effect of athletic training on physical fitness under hypodynamics." The Physiologist, pp. 39-40.
34. Saltin, B., G. Blomqvist, J.H. Mitchell, R.L. Johnson, Jr., K. Wildenthal, and C.B. Chapman. "Response to exercise after bed rest and after training: a longitudinal study of adaptive changes in oxygen transport and body composition." Circ. Suppl. Vol. 7, pp. 1-78, 1968.
35. Sarnoff, S.J., J.P. Gilmore, S.K. Brockman, J.H. Mitchell, R.J. Linden. "Regulation of ventricular contraction by the carotid sinus: its effect on atrial and ventricular dynamics." Circ. Res. Vol. 8, pp. 1123-1136, 1960.
36. Siggers, D.C., C. Salter, and P.A. Toseland. "A double isotope dilution method for differential determination of adrenaline and noradrenaline in plasma." Clinica Chemica Acta. Vol. 30, pp. 373-376, 1970.
37. Stegemann, J., U. Meier, W. Skipka, W. Hartleif, B. Hemmer, and U. Tibes. "Effects of a multi-hour immersion with intermittent exercise on urinary excretion and tilt-table tolerance in athletes and nonathletes." Aviat. Space Environ. Med. Vol. 46(1), pp. 26-29, 1975.
38. Stone, H.L. "Cardiac function and exercise training in conscious dogs." J. Appl. Physiol.: Respirat. Environ. Exercise Physiol. Vol. 42(6), pp. 824-832, 1977.
39. Tipton, C.M., R.A. Carey, W.C. Eastim, and H.H. Erickson. "A submaximal test for dogs: evaluation of effects of training, detraining, and cage confinement." J. Appl. Physiol. Vol. 37(2), pp. 271-275, 1974.

40. Tipton, C.M., A.R. Hargens, P.D. Gollnick, S.J. Mubarak, M.R. Gonsalves, and B.J. Tucker. "Influence of head-down tilt on muscle function and Starling forces." Med. Sci. Sports Exercise, Vol. 13(2), p. 102, 1981.
41. Torphy, D.E. "Effects of short-term bed rest and water immersion on plasma volume and catecholamine response to tilting." Aerosp. Med. Vol. 37, pp. 383-387, 1966.
42. Vatner, S.F., D. Franklin, and E. Braunwald. "Effects of anesthesia and sleep on circulatory response to carotid sinus nerve stimulation." Am. J. Physiol. Vol. 230(1), pp. 19-24, 1976.
43. Vogt, F.B. and P.C. Johnson. "Study of effect of water immersion on healthy adult male subjects: plasma volume and fluid-electrolyte changes." Aerosp. Med. Vol. 38, pp. 447-452, 1965.
44. Wilkens, R.W., S.E. Bradley, and C.K. Friedland. "The acute circulatory effects of the head-down position (negative G) in normal man, with a note on some measures designed to relieve cranial congestion in this position." J. Clin. Invest. Vol. 29, pp. 940-949, 1950.
45. Williams, J.A. and J. Fine. "Measurement of blood volume with a mass apparatus." N. Eng. J. Med. Vol. 264, pp. 842-848, 1961.



STRUCTURE OF MOLTEN IMIDAZOLIUM CHLORIDE

Final Technical Report Submitted to the

SOUTHEASTERN CENTER FOR ELECTRICAL ENGINEERING EDUCATION

Under the Research Initiation Program

Sponsored by the

AIR FORCE OFFICE OF SCIENTIFIC RESEARCH

Subcontract Number:	84 RIP 25
Principal Investigator:	R. D. Murphy
Academic Rank:	Professor
Department and University:	Department of Physics University of Missouri-Kansas City
Starting Date:	November 1, 1984
Report Date:	January 15, 1986

## I. INTRODUCTION

This is the final technical report for Subcontract Number 84 RIP 25 under the Research Initiation Program. The research discussed here is an outgrowth of the author's 1984 work<sup>1</sup> as a Summer Faculty Research Participant in the Chemical Sciences Directorate of the Frank J. Seiler Research Laboratory. Research at the Seiler Laboratory has identified a very interesting class of room-temperature molten salts which appear to have a number of most promising applications. The salts which have been studied<sup>2</sup> are mixtures of aluminum chloride and methylethylimidazolium chloride (MEIC), which at least in some concentration ranges are liquid at temperatures well below room temperature.

The substantial promise shown by these liquids has prompted a great deal of effort to determine and understand their chemical and physical properties. Careful measurements of their phase diagram, conductivity, viscosity<sup>3</sup>, nuclear magnetic resonance<sup>4</sup> properties, and transport numbers<sup>5</sup> have recently been published. The NMR studies have provided information about the structure of the melts, and a systematic analysis of the concentration dependence of the chemical shifts has strongly suggested the existence in the melts of structure, i.e. a tendency of the ions in solution to form clusters. Specifically, Fannin *et al.*<sup>4</sup> have proposed that the anions and cations tend to form "chains" of ions of alternating sign. The Monte Carlo calculations of the author<sup>1</sup> lent

considerable support to this picture of the structure of the fluid. In addition, a simple but physically reasonable explanation for the occurrence of this structure in terms of the known behavior of other molten salts<sup>6,7</sup> was proposed.<sup>1</sup>

Although these preliminary results are physically quite plausible and most encouraging, what has been lacking is a direct comparison with experiment. In particular, although the Monte Carlo code produces a quite specific prediction of the liquid structure factor of the current model of MEIC, there have been no experimental studies of the structure of this substance. In general, theoretical work is essential to understanding the X-ray (or neutron) scattering studies of the structure of liquids. For these reasons, the author proposed under the Research Initiation Program a coordinated theoretical and experimental program to study the structure of one of the simplest of the molten salts of interest, namely pure molten MEIC.

## II. PROGRESS MADE UNDER CONTRACT

The experimental portion of the work was done, primarily by Dr. Fred Ross, at the University of Missouri Research Reactor. Liquid X-ray scattering is very different from the X-ray diffraction patterns produced by a crystalline solid. In particular, the intensity is very much less, the Bragg lines are missing, and the "signal" from the liquid is comparable in magnitude to the "noise" from the glass X ray capillary

tubes used to hold the sample; this "noise" must of course be measured and subtracted out. For these reasons, a conventional GE XRD-6 X ray diffractometer was modified as follows: first, a heating stage was constructed to keep the sample molten during the measurements; second, a new detector mounting to bring the detector to a near position for higher intensities was constructed; third, the tubes containing the samples were mounted in contact with temperature sensors to monitor heating; fourth, the scanning in scattering angle and the data collection were automated and computerized to permit the long run times needed to acquire satisfactory statistics.

Problems and frustrating delays were encountered with the equipment, particularly the electronic instrumentation, and with the MEIC (which is notoriously difficult to handle because of its air sensitivity). Nonetheless, the following three major, concrete experimental results, the third of which was not proposed because it was thought to be too difficult, were accomplished. First, X-ray scattering data from molten MEIC just above its melting temperature were obtained. Second, Bragg diffraction lines from crystalline MEIC were observed in the same runs when the temperature was lowered to just below melting. Third, crystals of MEIC were grown; pictures taken with a precession camera showed the spots characteristic of crystalline (but not single-crystal) material. Some samples are apparently good enough to permit crystal structure determination.

Due to the aforementioned delays, the experimental data were obtained only very near the end of the contract period. There were delays, too, in acquiring the "theoretical equipment" (an IBM PC and software) needed for the purposes noted in the proposal, namely: contact with the experimental setup and the capability to transfer files of experimental data; storage, plotting, curve-fitting, and analysis of experimental data; and communication with and file transfer to and from the computer facilities at the Seiler Laboratory. Although these problems have now been overcome, time has not yet permitted the detailed analysis of the experimental MEIC data which is required. But substantial computational work on the extension and refinement of the model<sup>1</sup> of a molten salt has continued. The results, which are even more striking than was previously realized, will be presented at the March 1986 meeting of the American Physical Society.<sup>8</sup>

### III. FUTURE WORK

The work which needs to be done most immediately is: first, the X-ray crystallography of crystalline MEIC; secondly, obtaining better statistics for the liquid phase and analyzing the data theoretically. It is the author's firm belief that structure studies will be of increased importance in the study of the molten salts under investigation as possible battery electrolytes at the Seiler Laboratory. There are a number of worthwhile extensions of this work, which, like the work here discussed, are coordinated theoretical and

experimental efforts. The most immediately and obviously important are:

1. It would be highly desirable to do neutron diffraction studies of the crystalline phase of MEIC and neutron scattering studies of its molten phase, since neutron techniques yield information complementary to that obtained by X-ray diffraction. This experimental work could quite well be done at the University of Missouri Research Reactor: this facility has the highest neutron flux of all reactors in American universities and was recently identified by the National Science Foundation as a major materials research center. The author could perform the theoretical work necessary to interpret the neutron data.

2. Because of the intended application of these molten salts as electrolytes in batteries, the question of their transport properties, e.g. their viscosity, electrical conductivity, and mobility, is crucial. As soon as reasonably accurate intermolecular potentials are determined, the molecular dynamics method should be applied to study these transport properties.

3. Finally, of course, it must be noted that the actual melts of greatest interest are more complex: they include aluminum chloride in varying proportions. All of the above steps (computer studies of the structure accompanied by X-ray and if possible neutron diffraction experiments and calculation of the transport properties) should be taken in the case of these melts. Although this is a rather large task, it is

feasible. The initial steps we have taken under the current contract represent a necessary first step and a very good start on this project and the author feels that the preliminary results discussed here strongly justify extension of the present effort.

#### IV. SUMMARY AND CONCLUSIONS

Under this Research Initiation Program contract, we have obtained experimental data on the molten phase of MEIC and, although it was not expected, on its crystalline phase. The author has continued, refined, and extended Monte Carlo calculations on clustering phenomena in molten salts. Experimental equipment has been modified to study X-ray scattering from liquids, and "theoretical equipment" has been acquired to make possible close coordination between theoretical and experimental efforts at the University of Missouri and interaction, particularly computational, with the Seiler Laboratory. The major goal of the Research Initiation Program has been fully achieved: within the budget permitted by the RIP (and with some contributions from the University of Missouri), we have laid the foundation for further work, and we feel that the results we have achieved justify extension of this work. We are most grateful to the Air Force Office of Scientific Research for this program; to SCEEE for its most efficient management of it; and to the Seiler Laboratory, especially Dr. John Wilkes, for their hospitality and interest in and support of this project.

#### REFERENCES

1. J. S. Wilkes, J. A. Levisky, R. A. Wilson, and C. L. Hussey, *Inorg. Chem.* 21, 1263 (1982).
2. A. A. Fannin, Jr., D. A. Floreani, L. A. King, J. S. Landers, B. J. Piersma, D. J. Stech, R. L. Vaughn, J. S. Wilkes, and J. L. Williams, *J. Phys. Chem.* 88, 2614 (1984).
3. A. A. Fannin, Jr., L. A. King, J. A. Levisky, and J. S. Wilkes, *J. Phys. Chem.* 88, 2609 (1984).
4. R. O. Watts and I. J. McGee, Liquid State Chemical Physics, (John Wiley and Sons, New York, 1976), pp. 80-87.
5. C. J. Dymek and L. A. King, *J. Electrochem. Soc.* 132, 1375 (1985).
6. J. P. Hansen and I. R. McDonald, *Phys. Rev. A* 11, 2111 (1975).
7. M. L. Saboungi, A. Rahman and M. Blander, *J. Chem. Phys.* 80, 2141 (1984).
8. R. D. Murphy, *Bull. Am. Phys. Soc.* (to appear).



1984-85 RESEARCH INITIATION PROGRAM

Sponsored by the  
AIR FORCE OFFICE OF SCIENTIFIC RESEARCH

Conducted by the  
SOUTHEASTERN CENTER FOR ELECTRICAL ENGINEERING EDUCATION

FINAL TECHNICAL REPORT

Project 84 RIP 26

ALTERNATIVE COMPUTATIONAL METHODS FOR SEPARATED FLOWS  
ABOUT PITCHED FLAT SURFACES

Prepared by:	Larry A. Glasgow
Academic Rank:	Associate Professor
Department and University:	Department of Chemical Engineering Kansas State University
USAF Contact:	Major John M. Walker FJSRL, USAF Academy Colorado Springs, CO 80840
Date:	October 17, 1985

## INTRODUCTION

The calculation of incompressible flows over airfoils is of immense practical importance to designers concerned with improved aerodynamic efficiency at maneuvering speeds. The most frequently used approach to this problem at present utilizes the two-dimensional Reynolds equation for the mean velocity field in conjunction with a suitable assumption for the Reynolds "stress", i.e., the turbulent inertia tensor. In this method of attack upon the problem, the Navier-Stokes and continuity equations are written

$$\frac{\partial u_i}{\partial t} + u_j \frac{\partial u_i}{\partial x_j} = \frac{1}{\rho} \frac{\partial \sigma_{ij}}{\partial x_j} \quad (1)$$

and

$$\frac{\partial u_i}{\partial x_i} = 0 \quad (2)$$

where  $u_i$  is the instantaneous velocity and  $\sigma_{ij} = -p\delta_{ij} + 2\mu s_{ij}$  ( $\delta_{ij}$  is the Kronecker delta). The Reynolds decomposition is performed in the usual fashion by letting  $u = U + u'$ ; the equations resulting from these substitutions are time-averaged and simplified by noting that the linear terms in the fluctuating quantities are zero for a statistically stationary process. It is important to note that the Reynolds-averaging procedure must be long compared to the characteristic time scales of the turbulence, yet short when compared to the characteristic times of transient phenomena of interest. In some unsteady flow applications, these requirements will be mutually incompatible. Nevertheless, the result of the procedure described above is the Reynolds momentum equation:

$$\frac{\partial U_i}{\partial t} + U_j \frac{\partial U_i}{\partial x_j} = \frac{1}{\rho} \frac{\partial}{\partial x_j} (-p\delta_{ij} + 2\mu s_{ij} - \rho u'_i u'_j) \quad (3)$$

It is, of course, the introduction of the  $-\rho u_i u_j$  terms that defines the closure problem of turbulence and constitutes the major difficulty confronting any analyst wishing to employ this method of attack upon the problem. In order for the Reynolds equation to be used for the calculation of airfoil flows of interest it is necessary to introduce some kind of approximation for  $\tau_{ij} = -\rho u_i u_j$ . The simplest possibilities are descendents of Boussinesq's eddy viscosity model or Prandtl's mixing length model. In the former, turbulent momentum transport is modeled by analogy with Newton's law of viscosity--it is assumed that the required components of the turbulent inertia tensor can be represented by transverse gradients of the mean velocity field, multiplied by a turbulent or eddy viscosity. Of course this type of model is seriously deficient since turbulence is a characteristic of the flow and not of the fluid. It has been noted by many fluid dynamicists, including Tennekes and Lumley [1972], that gradient transport models are not appropriate for turbulent flow with multiple length or velocity scales. Prandtl's mixing length model is of the same general nature, except that it was formulated by analogy with the kinetic theory of gases instead of Newton's law of viscosity. Although it depends upon the mean flow gradient in nonlinear fashion, it could hardly be considered a major improvement since fluid particles in turbulence exchange momentum in continuous fashion and not intermittently as is the case with colliding gas molecules. Except under Knudsen flow conditions, the smallest length scales in turbulence (of the order of the Kolmogorov microscale) are many times larger than the molecular mean free path. Despite these obvious and debilitating fundamental deficiencies such models are widely used; Hegna [1981], for example, chose to let

$$\rho u_i u_j = 2\epsilon_m S_{ij} = \epsilon_m \left( \frac{\partial u_i}{\partial x_j} + \frac{\partial u_j}{\partial x_i} \right) \quad (4)$$

with  $\epsilon_m$  represented by

$$\begin{aligned}\epsilon_i &= \mu(k_1 y D_L)^2 \left( \frac{\partial U}{\partial y} - \frac{\partial v^2}{\partial x} \right) \frac{1}{Re} \\ \epsilon_o &= \mu k_2 u_e \delta^* Re \gamma\end{aligned}\quad (5)$$

with

$$\begin{aligned}D_L &= 1 - \exp\left(-\frac{y}{A} \left| \frac{\partial U}{\partial y} \right|_{y=0} Re\right)^{1/2} \\ \gamma &= (1 - 5.5(y/\delta)^6)^{-1} \\ \delta^* &= \int_0^\delta (1 - U/U_e) dy\end{aligned}\quad (6)$$

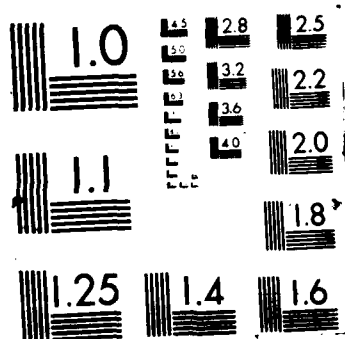
The switch from inner to outer models is made when  $\epsilon_i$  first exceeds  $\epsilon_o$ . The gross deficiencies of such a model are obvious and need not be recited here. It is important to remember, however, that this approach is essentially empirical curve-fitting since as Lumley [1980] has pointed out, what is being calculated is the behavior of a fluid with a "different constitutive relation." Indeed, Jobe and Hankey [1980] obtained constants for the above eddy viscosity model for attached flows with constant adverse pressure gradient by adjusting  $k_1$ ,  $k_2$ , and  $A^+$  until calculated and experimental drag coefficients and velocity profiles matched. Thus the results of this type of modeling may produce nearly the correct drag and mean velocity under certain defined or standard conditions, but extrapolation can be dangerous, particularly in situations where there are multiple length and/or velocity scales or additional driving forces such as buoyancy. Despite the well known problems there is currently a huge effort underway in this exact area--the review paper by Kline et al. [1981] gives some indication of the work of investigators working with the Reynolds equation and turbulence models. There are many legitimate questions that should be asked about the value of further work in this area--H. W. Liepmann [1979], for example, says these efforts "will be of passing interest only."

UNCLASSIFIED

UNITED STATES AIR FORCE RESEARCH INITIATION PROGRAM  
1984 RESEARCH REPORTS (U) SOUTHEASTERN CENTER FOR  
ELECTRICAL ENGINEERING EDUCATION INC S M D PEELE  
MAY 86 AFOSR-TR-87-1721 F49620-82-C-0035 F/G 15/

NL

[illegible]



how gradient transport models used in conjunction with the Reynolds equation will contribute either to our understanding of turbulence or our ability to model the important phenomena.

Assuming that a suitable closure has been achieved, the analyst is still confronted with the task of solving an intractable partial differential equation. Finite difference methods used for problems of this type can be explicit, implicit, or hybrid. Explicit methods are generally easier to program although they are subject to the Courant stability condition which restricts the time increment to

$$\Delta t < \Delta x / (U + a) \quad (7)$$

$U + a$  is the sum of the convection velocity in the x-direction and the speed of sound; a similar restriction exists in the y-direction. Deiwert and Bailey [1984] suggest that explicit methods are a good choice if the time increment constraints are compatible with flow frequency-- $\Delta t$  as given by (7) cannot be of the same order as  $f^{-1}$ . Generally speaking, the thin shear layers found at high Re result in a prohibitive Courant condition and implicit or hybrid methods must be used. Beam and Warming [1978] have devised an ADI sequence for treating the compressible Navier-Stokes equations in conservation-law form; although the alternating-direction implicit or Peaceman-Rachford [1955] method is readily implemented for linear parabolic PDE's such as the heat conduction equation, the nonlinear character of the Navier-Stokes equations is a serious obstacle. Beam and Warming used a truncated Taylor series expansion to achieve linearization but they also caution that the cross-spatial derivatives (e.g.,  $\partial u_1 / \partial x_2$ ) complicate construction of an efficient algorithm. They employ an explicit representation for these terms without adversely affecting numerical stability.

An alternative hybrid method developed by MacCormack [1978] and used by Hegna [1981], Shang [1978], and others, utilizes equation splitting--an explicit formulation is used for regions dominated by convection and the shear layer is treated implicitly. Deiwert and Bailey [1984] note that it is difficult to efficiently implement this procedure on modern array processors. They also note that finite difference methods in general suffer from aliasing of high frequency energy to larger-scale motions since the grid or mesh with N nodal points can at most support N/2 harmonics of the form  $e^{ikx}$ .

There are alternatives to the Reynolds equation-turbulence modeling approach; these include sub-grid scale closure models, direct numerical simulation of the Navier-Stokes equations, and the spectral method. Deardorff [1970] has been the principal proponent of sub-grid scale closure--in this method, the large scale motions are explicitly obtained from the Navier-Stokes equations. The very small scale motions are treated statistically and in this manner the Reynolds number limitations of a total numerical simulation are avoided. Orszag [1977], among others, speaks in favor of this approach, noting that the dissipative eddies are less than satisfactory. For purposes of illustration we now consider Deardorff's treatment of planar Poiseuille flow. First, the dependent variables are averaged spatially over the grid spacing:

$$\bar{u}(x,y,z,t) = (1/\Delta x \Delta y \Delta z) \int_{x_1 - \frac{1}{2}\Delta x_1}^{x_1 + \frac{1}{2}\Delta x_1} \int \int u(x,y,z,t) dx dy dz \quad (8)$$

The Navier-Stokes equations can then be written:

$$\frac{\partial u_i}{\partial t} = - \frac{\partial}{\partial x_j} (u_i u_j + u_i' u_j') - \frac{1}{3} \delta_{ij} u_1' u_1' - \frac{\partial}{\partial x_1} (p/\rho_0 u^{*2} + \frac{1}{3} u_1' u_1') \quad (9)$$



In (9), the terms  $u'_i u'_j$  represent deviations from the grid-volume means, i.e., the sub-grid scale turbulent inertia tensor; its components are modeled as

$$u'_i u'_j - (1/3)\delta_{ij} u'_i u'_i = -K \left( \frac{\partial u_i}{\partial x_j} + \frac{\partial u_j}{\partial x_i} \right) \quad (10)$$

where  $K$  is the sub-grid scale eddy coefficient. It is assumed that

$$K(x,y,z,t) = (c\Delta)^2 \left( \frac{\partial u_i}{\partial x_j} \left( \frac{\partial u_i}{\partial x_j} + \frac{\partial u_j}{\partial x_i} \right) \right)^{1/2} \quad (11)$$

Certainly in this respect, the SGS model is not that much superior to first-order turbulence modeling used in conjunction with the Reynolds momentum equation. Deardorff found that a value of  $c=0.10$  provided realistic results in the integration; larger values were found to produce excessive energy in the sub-grid scale motions. It is essential to remember that this method has been applied to channel flows and atmospheric phenomena--its application to thin shear flows such as turbulent boundary layers will be considerably more difficult.

One would anticipate great difficulty in the direct simulation of the Navier-Stokes equations, since in the past 150 years, only about 75 analytic solutions to the equations have been found--a tribute to the intractability of simultaneous nonlinear partial differential equations. The pursuit of numerical solutions to the full set of equations is hindered by the rapid increase in degrees of freedom (nodal points in finite difference methods) with Reynolds number. Schumann et al. [1980], Liepmann [1979], and Orszag [1977] have all noted that the required degrees of freedom scales with  $Re^{9/4}$ . If it were possible to deal with a flow where  $Re=100$  with 1000 interior mesh points, the scaling law suggests that  $Re=10^4$  would require about  $3 \times 10^7$  mesh points. In fact, Orszag notes that an order of magnitude increase in computational power will permit an increase in  $Re$  of only 2.15

times and Schumann et al. note that a brute-force simulation on a 10 MIPS machine for  $Re=10^4$  would require about 3 years computing time. There are grounds for optimism, however, for free flows and flows in decay, where either the  $Re$  is small or the large scale motions can be treated independently of the dissipative structure. There is less reason to be optimistic about success in direct simulation of flows about objects; for turbulent boundary layers or laminar boundary layers undergoing transition, the rapid changes in the streamwise direction cause difficulties in resolution. Furthermore, the downstream or outflow boundary conditions would appear to require complete specification in the wake region--with the concomitant danger that the flow will be over-specified and the results of the direct simulation set in advance.

It appears that for the present purposes, the probability of "success" with either direct simulation or sub-grid scale closure methods is very small. And although the Reynolds equation with turbulence modeling has been and is being widely employed, it too suffers from some serious problems which can be summarized as follows:

- 1) Correct parameters for the eddy viscosity model(s) will have to be determined for any flow that differs in pressure gradient from those previously treated.
- 2) There is reason to question implementation of down stream boundary conditions due to the danger of over-specification and the possible upstream propagation of artificial velocity constraints.
- 3) The averaging process used to obtain the Reynolds equation from Navier-Stokes automatically entails loss of information and it is not at all clear how pervasive this will be with respect to the integral-scale motions.

It is clear, however that the governing PDE will be wrong the instant any first-order closure scheme is incorporated for the turbulent inertia tensor.

4) Deiwert and Bailey [1984], among others, have noted that the application of the Reynolds equation has been limited to two-dimensional flows without freestream turbulence or other perturbation. This type of simulation has resulted in cyclic unsteadiness with a single dominant frequency. More complicated flows will necessitate removal of the Reynolds-averaging restriction.

5) Discrepancies at higher angles of attack in Reynolds equation modeling have been noted by Cebeci et al. [1984] and Shang [1984].

#### REVIEW OF LITERATURE

For the above reasons the decision was made to explore the spectral methods described in the monograph of Gottlieb and Orszag [1977] and the review of Gottlieb et al. [1984]. Spectral methods have become increasingly popular in recent years resulting in studies of transitional fluid flows [20,32,39], incompressible fluid flow simulations [14,22,25,34,35,36,38,53,54], and most recently for complicated compressible flow fields which include shock waves [12,13,18,45,46]. Interest in spectral methods is due in part to the increased accuracy available for a given number of independent degrees of freedom (i.e. the number of mesh nodes for a finite difference method) in comparison to finite difference techniques; for example see Haidvogel et al. [1980] or Dennis and Quartapelle [1982] for comparisons of accuracy. The spectral methods are often referred to as being infinite-order accurate, that is, if after  $N$  terms the error decreases more rapidly than any power of  $1/N$ . Orszag [1971] states that it is possible to decrease the computational time and storage by an order of magnitude. The advent of

the fast Fourier transform in the mid 60's allowed the development of spectral methods, since rapid evaluation of trigonometric polynomial coefficients became possible. Much of the work done with respect to fluid dynamics in the area of interest has involved the use of the pseudo-spectral techniques also known as "collocation" or the "method of selected points" (Lanczos [1956]).

Spectral methods represent the solution to the problem as a truncated series of eigenfunctions for the independent variable. The type of series expansion used is based upon the type of boundary condition that is to be satisfied. for example, a periodic boundary condition would suggest the use of a Fourier series representation for the solution. Gottlieb and Orszag [1977] and Orszag [1977] suggest the following series representations:

<u>Boundary Conditions</u>	<u>Series Representation</u>
periodic	$\exp(inx)$
inviscid	$\sin(nx)$ or $\cos(nx)$
no-slip	Chebyshev ( $T_n(x)$ ) or Legendre ( $P_n(x)$ )

Pseudospectral techniques are deemed the most likely to be appropriate for the problem under consideration; that of computation of separated flow on a pitched airfoil. The principal concept behind pseudospectral calculations as stated by Orszag [1980] is to simply transform freely between physical ( $x_j$ ) and spectral ( $a_n$ ) representations, evaluating each term in whatever representation that term is most accurately, and simply evaluated. Pseudospectral computations have several advantages over spectral algorithms: 1) For complex geometry the solution of the spectral (Galerkin) method requires at least twice the number of fast Fourier transforms than that of the pseudospectral method (collocation); 2) Pseudospectral techniques have significant advantages over spectral techniques when considering

nonlinear partial differential equations since spectral methods can be very computationally expensive in the evaluation of nonlinear partial differential equations.

In order to demonstrate the spectral method consider the one dimensional transient equation:

$$\frac{\partial u}{\partial t} = \frac{\partial^2 u}{\partial x^2} \quad (12)$$

with the boundary and initial conditions

$$u(0,t) = u(\pi,t) = 0$$

$$u(x,0) = f(x) \quad (13)$$

the analytic solution to this problem can be shown to be

$$u(x,t) = \sum_{n=1}^{\infty} \left\{ \frac{2}{\pi} \int_0^{\pi} f(x) \sin(nx) dx \right\} \sin(nx) \exp(-n^2 t) \quad (14)$$

Therefore, let  $u_N$  be the spectral approximation to  $u$ , so that the solution can be approximated as

$$u_N(x,t) = \sum_{n=1}^N a_n(t) \sin(nx) \quad (15)$$

Substituting back into equation (12) results in

$$\frac{da_n(t)}{dt} = -n^2 a_n(t) \quad (16)$$

and this set of ordinary differential equations are solved with respect to the initial conditions  $a_n(0) = \frac{2}{\pi} \int_0^{\pi} f(x) \sin(nx) dx$  ( $n=1, \dots, N$ ). Gottlieb and Orszag [1977] have shown for this example that  $u(x,t) - u_N(x,t)$  goes to zero more rapidly than  $\exp(-N^2 t)$  for any  $t > 0$  and  $N \rightarrow \infty$ . It can be seen that the spectral approximation of  $u(x,t)$  that results is a truncation of the exact solution to  $N$  terms. In contrast to this exceedingly good approximation it is possible to construct a spectral method that will arrive at extremely poor results; therefore care must be exercised in the construction of a spectral approximation.

The pseudospectral method is typically chosen over the spectral methods when considering a nonlinear equation. For example consider

$$\frac{\partial u}{\partial t} = \exp(xu) \frac{\partial u}{\partial x} + \frac{\partial^2 u}{\partial x^2} \quad (17)$$

let the approximation  $u_N(x,t)$  to  $u(x,t)$  be

$$u_N(x,t) = \sum_{n=1}^N a_n(t) \psi_n(x) \quad (18)$$

where  $\psi_n(x)$  is an orthonormal function. Then the spectral approximation will be

$$\frac{da_n(t)}{dt} = \int \psi_n \left\{ \exp[x \sum a_n \psi_n] \sum a_n \psi_n' + \sum a_n \psi_n'' \right\} dx \quad (19)$$

It is seen that these equations for  $a_n(t)$  are computationally complex due to the resulting integro-differential equation for  $a_n(t)$ . Therefore, consider the pseudospectral method. First,  $N$  collocation points  $(x_1, x_2, \dots, x_N)$  lying within the computational domain are introduced. The approximation (18) is forced to satisfy the governing partial differential equation (17). For example, the following steps would be followed; 1) Determine  $N$  coefficients  $a_n(t)$  such that

$$u_N(x_j, 0) = \sum_{n=1}^N a_n(0) \psi_n(x_j) \quad (20)$$

2) Evaluate each term of the governing partial differential equation in either physical or spectral space, whichever gives the most accurate and easily obtainable approximation. For example,  $\exp(x_j u_N(x_j, t))$  is evaluated in physical space since the value for  $u_N(x_j, t)$  is known and the partial derivatives are evaluated in spectral space since this results in the most accurate representation. 3) Integrate in time with respect to  $u_N(x_j, t)$  using the "leap-frog" method or another suitable choice. 4) Repeat steps

1)-3) until the time integration is completed. From this example pseudo-spectral methods are seen to be much easier to apply to nonlinear equations than corresponding spectral techniques.

The application of boundary conditions in a spectral method can determine the solution's stability. Gottlieb et al. [1981] state that incorrect boundary treatments may give strong instabilities in contrast to finite-difference methods in which this would appear as relatively weak oscillations. Moin and Kim [1980] note that fully explicit pseudospectral solution of the incompressible Navier-Stokes equation have an inherent numerical problem for viscous flows involving solid boundaries, due to enforcing no-slip conditions at the walls. Rudy and Stridwerda [1981] presented a study of inflow and outflow boundary conditions for compressible Navier-Stokes equations of flow past a flat plate. This study, conducted for finite-difference methods of solution, indicates that errors in the data specified at the inflow boundary condition can significantly affect the solution obtained. Gottlieb and Orszag [1977] note spectral methods are extremely sensitive to the formulation of boundary conditions, for example, when improper boundary conditions are imposed, the solution is likely to be "explosively" unstable.

Convergence of the spectral (Galerkin) method has been demonstrated for a Fourier representation with periodic boundary conditions by Hald [1981]. Maday and Quarteroni [1982] have provided stability results and "optimal" convergence rates for Galerkin and pseudospectral approximations (using trigonometric polynomials) for the stationary Navier-Stokes equation with periodic boundary conditions. Canuto [1984] analyzed explicit and implicit methods of imposing boundary conditions for Chebyshev and Legendre approximations of elliptic problems ensuring stability and convergence for these methods. Canuto and Quarteroni [1984] give stability and "optimal"

convergence rates for Chebyshev collocation approximations of variable coefficient elliptic problems with Dirichlet or Neumann-type boundary conditions. Pasciak [1980] investigated spectral and pseudospectral representations of advection equations with the intention of introducing a framework in which finite elements analysis can be applied to spectral methods. In addition error estimates are given for fully discrete explicit pseudospectral as well as semidiscrete spectral and pseudospectral methods.

Some additional considerations are necessary. In the case of a discontinuity, the rate of convergence in the region of the discontinuity is seriously degraded, but spectral approximations are still normally more accurate than corresponding finite difference representations [10]. Additionally, the error is localized better by the spectral method such that less local dissipation is required to smooth the discontinuities. If dissipation or a filtering technique is not used Gibb's phenomena is seen in the region of the discontinuity, and, the resulting error from the lack of smoothing pollutes the solution globally [40]. Majda *et al.* [1978] have shown for general linear hyperbolic Cauchy problems with nonsmooth initial data that the appropriate smoothing techniques applied to the equation results in stability and that this smoothing combined with smoothing of the initial data gives rise to infinite order accuracy away from the discontinuities of the exact solution. The most prominent examples of discontinuities that have been examined by spectral methods are treatments of shock waves [12,13,18,33,45,46,50,55]. A variety of filters and dissipation functions have been used to damp the oscillations occurring in the solution due to the discontinuity. For example, one sided Schumann filter [12,33], von Hann window filter [18,46], second and fourth-order artificial viscosity [45,50], artificial density [50] as well as the method of



Boris and Book [1976], originally developed for the construction of finite difference algorithms involving strong shocks [55], have been able to produce an accurate smooth solution for this type of problem. In addition, Gottlieb et al. [1981] used a low-pass spectral filter to remove the high frequency waves that lead to instability and a "cosmetic" filter (a one-sided Schumann filter) to find a nonoscillatory numerical solution.

The spectral and pseudospectral methods have been used successfully to model wakes [33], internally separated flows [22], flow past flat plates [36,53,54] and transonic flows past airfoils [13,50]. The areas of concern to the present work are: representation of two dimensional flow past a pitched plate, problems encountered due to imposition of boundary conditions, and separation that is certain to occur [27].

Both Plotkin [1982] and Kumar and Yajnik [1980] considered separated flow based on the stream function equation

$$\psi_y \psi_{yyx} - \psi_x \psi_{yyy} = Re^{-1} \psi_{yyyy} \quad (21)$$

One of the problems that Kumar and Yajnik note about this problem is the presence of reverse flow--the equation is said to be of mixed-parabolic type. The theory of such equations is not sufficiently developed to indicate boundary conditions that permit solution. Furthermore, the steady-state equation considered by both Plotkin and Kumar and Yajnik must be replaced by a more general representation:

$$(\psi_y \frac{\partial}{\partial x} - \psi_x \frac{\partial}{\partial y}) \nabla \psi = Re^{-1} \nabla^2 \psi \quad (22)$$

This stream function equation was used by Mei and Plotkin [1984] in determining confined laminar wakes.

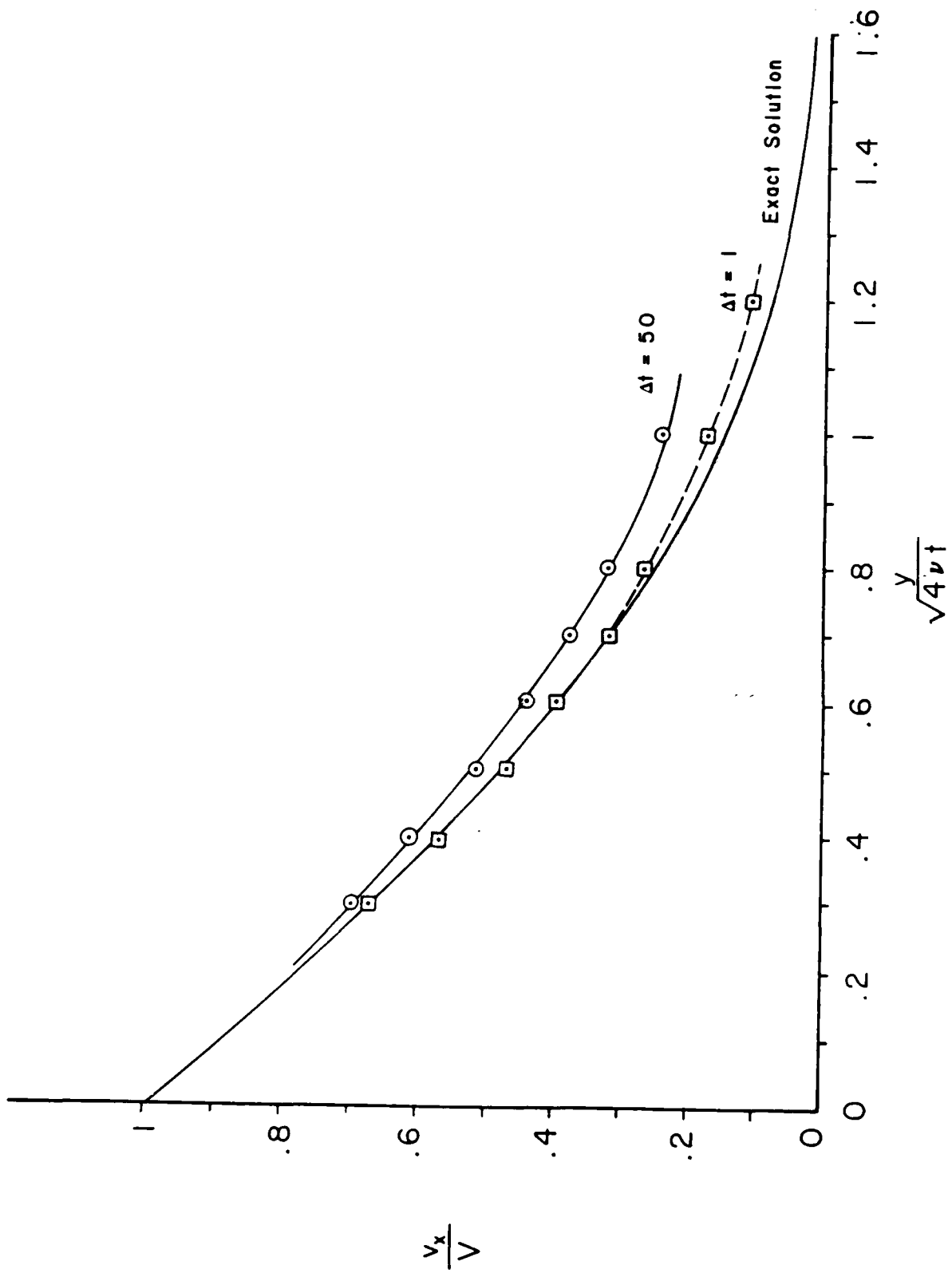
Symmetric flow past a flat plate has been treated by Orszag [1971] and Taylor and Murdock [1980],[1981]. Planar flow has been investigated by Moin and Kim [1980], Orszag and Kells [1980] and Kleiser [1982]. Taylor and

Murdock studied the flow over a flat plate in a range of  $1.2 \times 10^5 < Re < 3.8 \times 10^5$ , which is well within the turbulent flow regime. The velocity profile was solved as perturbation about the Blasius velocity profile. Taylor and Murdock used a mesh of  $17 \times 17$  to solve for the velocity profile, while Orszag used nine collocation points to approximate a one dimensional boundary layer, both studies resulted in accurate approximations.

The treatments of transonic flow by Gottlieb et al. [1984b] and Streett et al. [1985] are interesting in that spectral methods (Chebyshev collocation) are being used. The treatment of transonic flow over an airfoil can be viewed as state-of-the-art in the use of spectral methods because of the difficulty posed by the sharp shock gradients and the computational competition with finite difference methods. Again, it is seen that separation causes difficulty as Streett et al. note that the potential equation which is being solved becomes a mixed elliptic-hyperbolic type and admits weak solutions with discontinuities. Streett et al. use artificial viscosity with a directional bias introduced in the potential equation in the supersonic region to suppress the appearance of compression and expansion shocks due to the presence of a supersonic bubble. It is apparent that the use of multigrid techniques has made spectral methods for steady compressible flow competitive with finite difference methods for problems of aerodynamic interest.

#### SOME ILLUSTRATIVE NUMERICAL EXAMPLES

Successful application of spectral method is still something of an art-experience in the selection of appropriate series expansions is a virtual necessity. To illustrate this point and the method in general, a number of



$$\phi = \frac{v_z}{(p_0 - p_L)R^2/4\mu L} ; \quad \xi = \frac{r}{R} ; \quad \tau = \frac{\mu t}{\rho R^2}$$

at  $\tau=0$  a pressure gradient  $(p_0 - p_L)/L$  is impressed upon the system. This is a more interesting problem because of the variable coefficient  $1/\xi$ . The analytic solution for this problem is

$$\phi = (1-\xi^2) - 8 \sum_{n=1}^{\infty} \frac{J_0(\alpha_n \xi)}{\alpha_n^3 J_1(\alpha_n)} e^{-\alpha_n^2 \tau} \quad (27)$$

The pseudospectral approximation,  $\phi_n$ , to the solution,  $\phi$ , was represented by a Chebyshev polynomial expansion with the coefficients being determined at each time step. Nine terms were included in the series and a time increment of 0.001 was used for integration of equation (26) with an Euler predictor

$$\bar{\phi}(t_2, \xi) - \phi(t_1, \xi) = \int_{t_1}^{t_2} \left( 4 + \frac{1}{\xi} \frac{\partial}{\partial \xi} \left( \xi \frac{\partial \phi}{\partial \xi} \right) \right) dt \quad (28)$$

Table 1 illustrates the results obtained for this problem integrated with  $\tau=0.05$ . It should be noted that a fairly accurate solution was obtained even though few terms were used in the series approximation of the solution. Though this problem may be more demanding than Stokes first problem due to the presence of a variable coefficient it also cannot be regarded as a demanding test.

The classical Gratez thermal entrance length problem was selected as the final example--primarily because the exact solution is known. However, this is a more strenuous test of the method because of the initial discontinuity (producing an infinite Nusselt number). The governing equation after insertion of the parabolic velocity distribution is

$$\text{RePr}[1-r^{*2}] \frac{\partial \theta}{\partial z^*} = \frac{1}{r^*} \frac{\partial}{\partial r^*} \left( r^* \frac{\partial \theta}{\partial r^*} \right) \quad (29)$$

$\xi$	$\phi(0.05, \xi)$	$\phi_N(0.05, \xi)$	% Error
1	0	0	0
0.9239	0.1054	0.07848	25.5
0.7071	0.2056	0.1796	12.6
0.3827	0.1941	0.1998	3.0
0	0.2000	0.2032	1.6

Table 1: Comparison of Pseudospectral prediction of unsteady laminar flow to the analytical solution with 4 terms of the series being retained. (Eq. (27)).

The difficulty arising at the wall where  $r=R$  is apparent. It was also thought likely that the Euler predictor used previously would prove inadequate, so the fourth-order Adams-Bashforth method was used in its place, although the Euler expression was used to get started. Some oscillatory behavior was detected originally in the approximate solution and this was dealt with by incorporation of limited digital filtering. The predictor formulation is again

$$\theta(r^*, z_2^*) = \theta(r^*, z_1^*) + \int_{z_1^*}^{z_2^*} \frac{1}{\text{RePr}(r^* r^{*3})} \frac{\partial}{\partial r^*} (r^* \frac{\partial \theta}{\partial r^*}) dz^* \quad (30)$$

where

$$\theta = \sum a_n(z^*) F_n(r^*)$$

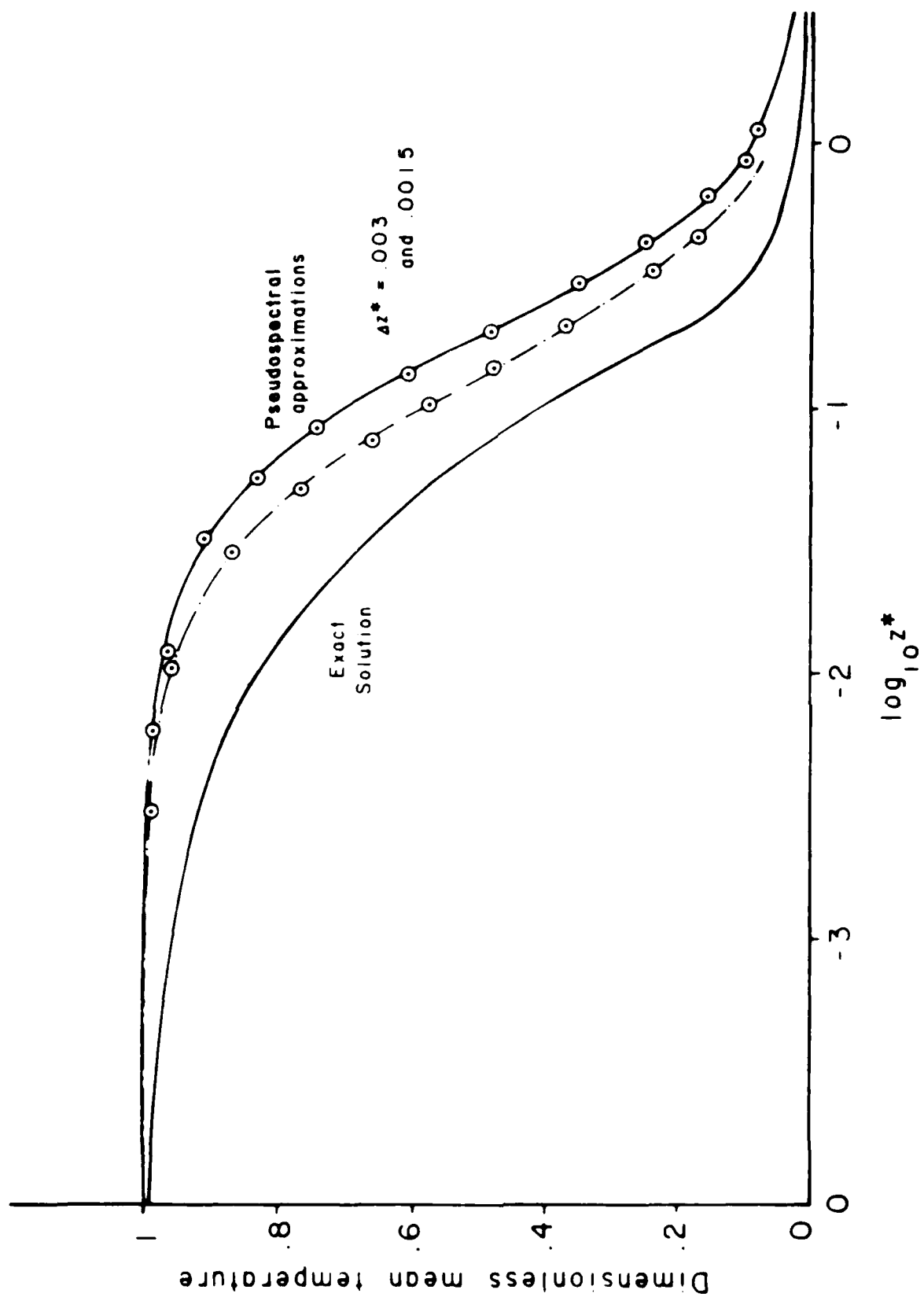
Figure 2 illustrates the results obtained using a dimensionless axial ( $z^*$ ) increment of 0.003; the abscissa is dimensionless axial distance and the ordinate is dimensionless mean temperature. The approximate solution is qualitatively good, but quantitatively disappointing. Clearly a reduced step-size would be necessary in order to produce an acceptable approximation.

#### EXTERNAL SEPARATED FLOWS

Consider the two dimensional incompressible Navier Stokes equation for flow past a pitched flat plate expressed in terms of the stream function

$$\frac{\partial}{\partial t} \nabla^2 \psi + (\psi_y \frac{\partial}{\partial x} - \psi_x \frac{\partial}{\partial y}) \nabla^2 \psi = \nu \nabla^4 \psi \quad (31)$$

The transient response of the flow to a periodic forcing function is the ultimate goal, but the first step is to consider the steady state solution. A Fourier spectral solution for the steady state form of equation (31) was presented by Mei and Plotkin [1984] for confined laminar wakes. The use of the Fourier spectral method by Mei and Plotkin was made possible due to



periodic boundary conditions. In the present study a pseudospectral approximation will be used based on orthogonal Chebyshev or Legendre polynomials. Relating the collocation points to the structure of Chebyshev or Legendre polynomials results in good approximations. It should be noted that it is possible to use equally-spaced Chebyshev collocation, but as the number of data points increase beyond 10 Chebyshev interpolation rapidly decreases in accuracy [52]. This decrease in accuracy is not a problem when considering a Legendre expansion.

The problem with equally spaced points for the Chebyshev collocation can be avoided if interpolation points on the interval  $(-1,1)$  are chosen to be

$$x_j = \cos\left(\frac{\pi j}{N}\right); \quad (j=0,1,\dots,N) \quad (32)$$

for a  $N$ th order Chebyshev polynomial approximation. A Chebyshev polynomial of degree  $n$  is defined as

$$T_n(x) = \cos(n \arccos(x)) \quad (33)$$

it follows that

$$T_n(x_j) = \cos\left(\frac{\pi j n}{N}\right); \quad (j=0,1,\dots,N)$$

The Chebyshev polynomials lend themselves to the use of the Fourier transform to determine interpolation coefficients. The Legendre polynomials do not lend themselves to the Fourier transform, but, Taylor *et al* [1984] have shown that in general the fast Fourier transform and Crout reduction with partial pivoting require approximately the same amount of computational time if the defining matrix for the Crout reduction is not changed. Therefore it should be possible to use either Chebyshev polynomials with a fast Fourier transform or Legendre polynomials with Crout reduction and partial pivoting.

The question then arises which of these polynomial approximations would be most appropriate under the conditions being considered. The Chebyshev



polynomials have the advantage of concentrating the collocation points in the regions of  $x=-1$  and  $x=1$ . While the Legendre can be defined at any point in the system, but are typically equally spaced. Pseudospectral Chebyshev methods are commonly seen used in the literature this is in part due to the availability of fast Fourier transforms (FFT's) and a general belief that direct matrix inversion is not as fast as the FFT. It was decided to use Chebyshev polynomials on the basis of the availability of the FFT. The use of Chebyshev collocation will ensure that a large number of interpolation points are near the plate in the region of the greatest gradient. Finlayson [1980] notes that collocation may not be satisfactory when the solution domain contains steep gradients, which is the situation that is expected with thin shear layers.

The Falkner Skan equation was used as a tool to estimate the accuracy of the pseudospectral approximation for separated flow present on the back side of an inclined plate. Based on a fourth order Runge-Kutta solution of the Falkner Skan equation ( $\beta = 0.125$ )

$$f''' + f f'' + \beta (1 - f'^2) = 0 \quad (35)$$

with boundary conditions

$$\begin{aligned} f(0) &= 0, \quad f'(0) = 0 \\ f'(\infty) &= 1, \quad f(\infty) = 0 \end{aligned} \quad (36)$$

a Chebyshev interpolation function was evaluated for  $N=10, 20$  and  $40$ . The evaluation was based on a comparison of the first and second derivatives found using a pseudospectral evaluation and those obtained by the Runge-Kutta method. The coefficients for the pseudospectral approximation are obtained by a Fourier transform. Three separate observations were made from these evaluations: 1) In one trial the data used for the value of  $f(\eta)$  at each collocation point was rounded to three significant figures with  $N=20$ .

This resulted in large oscillations of the first derivative as suggested by Osher [1984] and Majda et al. [1978]. 2) Increasing the number of collocation points from 10 to 20 to 40 did not significantly affect the accuracy of the resulting approximations. 3) The accuracy of a derivative decreased approximately one order of magnitude for each increase in the order of differentiation. A compilation of these results is presented in Tables 2 and 3.

Based upon the above, it was decided to use a steady state stream function vorticity representation for the flow

$$\frac{\partial u}{\partial x} \frac{\partial \psi}{\partial y} - \frac{\partial u}{\partial y} \frac{\partial \psi}{\partial x} = \nu \left( \frac{\partial^2 u}{\partial x^2} + \frac{\partial^2 u}{\partial y^2} \right) \quad (37)$$

$$u = \frac{1}{2} \left( \frac{\partial^2 \psi}{\partial x^2} - \frac{\partial^2 \psi}{\partial y^2} \right) \quad (38)$$

with the boundary conditions

$$\psi(x,0) = \psi_x(x,0) = \psi_y(x,0) = 0 \quad 1 \leq x \leq a \quad (39)$$

$$\psi(x,\infty) = \psi(\infty,y) = \psi_{\text{free stream}} \quad (40)$$

$$u(\infty,y) = u(x,\infty) = 0 \quad (41)$$

$$\omega(x,0) = \frac{1}{\nu} \frac{\partial \psi}{\partial y^2} \quad 1 \leq x \leq a \quad (42)$$

Then the stream function and vorticity can be approximated by

$$\begin{aligned} \psi(x,y) &= \sum_{n=0}^N a_n(x) f_n(y) \\ \omega(x,y) &= \sum_{n=0}^N g_n(x) f_n(y) \end{aligned} \quad (43)$$

This representation was chosen to make use of the increased accuracy of pseudospectral approximations along the axis in which the greatest amount of change will occur. Gottlieb et al. [1984a] note that a finite difference representation is typically used along the vertical axis and a pseudo spectral representation along the horizontal axis. The solution is split

$\eta$	$f'(\eta)$	KK	N 10	N 20	N 20 (3 significant figures)	N 40
0 1958		0 025576	0 024552	0 024773	0 023739	0 023847
0 7639		0 072826	0 074226	0 072494	0 084111	0 073005
1 649		0 067062	0 065499	0 066957	0 079243	0 067009
2 764		0 088610	0 086654	0 088983	0 071295	0 088778
4 000		0 45786	0 45962	0 45794	0 45309	0 45790
5 236		0 84314	0 84205	0 84291	0 85391	0 84302
6 351		0 98166	0 98236	0 98171	0 94579	0 98163
7 236		0 99963	0 99931	0 99964	1 05521	0 99965
7 804		1 00106	1 00118	1 00105	1 07258	1 00111
8 000		1 00116	1 00101	1 00119	0 95798	1 00130

Table 2 Comparisons of the first derivative of the Falkner Skan equation for a 4th order Runge Kutta method and Chebyshev collocation where N represents the number of terms retained in the series expansion

$\eta$	$f''(\eta)$	RK	N=10	N=20	N=20 3 significant figures	N=40
0.1958		0.11855	0.11514	0.13321	0.14046	0.13404
0.7639		0.04837	0.04922	0.04922	0.02698	-0.04577
1.649		0.06256	0.06346	0.06193	0.07137	0.05968
2.764		0.22016	0.21912	0.21990	0.18439	0.22008
4.000		0.35247	0.35299	0.35490	0.1807	0.35865
5.236		0.22321	0.22364	0.22300	0.17815	0.22307
6.351		0.04637	0.04527	0.04592	0.09232	0.04413
7.236		0.00537	0.00632	0.00530	0.14462	0.00500
7.804		$8 \times 10^{-4}$	$1.1 \times 10^{-4}$	$7.5 \times 10^{-4}$	0.68487	$6.5 \times 10^{-4}$
8.000		$3.5 \times 10^{-4}$	0.00103	0.00121	-2.82886	0.00721

Table 3: Comparisons of the second derivative of the Palkner-Skan Equation for a 4th order Runge-Kutta method and Chebyshev collocation where N represents the number of terms retained in the series expansion.

into an upper and lower region for above and below the plate and having the numerical boundary conditions

$$\begin{aligned}\omega^u(x,0) &= \omega^l(x,0) & a < x < -a \\ \psi^u(x,0) &= \psi^l(x,0) & a < x < -a\end{aligned}\quad (44)$$

where the superscripts  $u$  and  $l$  refer to the upper and lower regions respectively.

The following computational scheme was then used to evaluate the flow. The mesh nodes for the stream function were initialized using an equation given in Lamb [1945] that has been corrected for the angle of attack and transformed to Cartesian coordinates (Appendix A). The vorticity was initialized as zero everywhere except on the plate where a first order finite difference evaluation was performed based on methods found in Roache [1972]

$$\omega(x,0) = \frac{2(\psi_{w+1} - \psi_w)}{\Delta n^2} + O(\Delta n) \quad (45)$$

where  $\Delta n$  is the distance from the wall ( $w$ ) to the mesh node normal to the wall ( $w+1$ ). The following steps were then followed in obtaining a solution:

- 1) Determine the pseudospectral coefficients to the Chebyshev polynomials at each  $(x, y_j)$  combination.
- 2) Starting at the leading edge of the flow field evaluate the derivatives with respect to  $y$  for that column.
- 3) Equation (37) is solved with respect to  $\omega$  for a finite difference representation of the  $x$  derivative.
- 4) Equation (38) is solved with respect to  $\psi$  for a finite difference representation of the  $x$  derivative.
- 5) Steps 3) and 4) are repeated for each value of  $\omega$  and  $\psi$  in the column.
- 6) Move to the next column and repeat steps 2) through 5).
- 7) Repeat for the second region.

8) Satisfy the numerical boundary conditions.

9) Continue steps 1) through 8) until convergence is achieved.

In order to estimate the accuracy of the above algorithm a central finite difference algorithm for the stream function representation (22) was developed. The successive under relaxation algorithm was based on the same boundary conditions as given by equations (39)-(40).

Both the finite difference and pseudospectral algorithms were explosively unstable. The fact that both algorithms were unstable suggests that improper boundary conditions are being applied.

#### LITERATURE CITED

- [1] Beam, R. M., R. F. Warming. AIAA J. 16:393 (1978).
- [2] Boris, J. P., and D. L. Book. J. Comp. Phys. 20:397 (1976)
- [3] Canuto, C., Computing Methods in Applied Sciences and Engineering VI, pp. 335-351, Elsevier Science Pub. (N. Holland) (1984).
- [4] Canuto, C. and A. Quarteroni. Spectral Methods for Partial Differential Equations, pp. 55-78, SIAM Philadelphia (1984).
- [5] Cebeci, T., K. Stewartson and J. H. Whitelaw, Numerical and Physical Aspects of Aerodynamic Flows II, pp. 1-40, Springer-Verlag, New York (1984).
- [6] Deardorff, J. W. J. Fluid Mech., 41:453 (1970).
- [7] Derivent, G. S. and H. E. Bailey. Numerical and Physical Aspects of Aerodynamic Flows II, pp. 63-78, Springer-Verlag, New York (1984).
- [8] Dennis, S. C. R. and L. Quartapelle. J. Comp. Phys. 52:448 (1983).
- [9] Finlayson, B. Nonlinear Analysis in Chemical Engineering, McGraw-Hill, New York (1980).
- [10] Gottlieb, D. and S. A. Orszag. Numerical Analysis of Spectral Methods: Theory and Applications, SIAM, Philadelphia (1977).
- [11] Gottlieb, D., M. Y. Hussaini and S. A. Orszag. Spectral Methods for Partial Differential Equations, pp. 1-54, SIAM, Philadelphia (1984a).
- [12] Gottlieb, D., L. Lustman and S. A. Orszag. SIAM, J. Sci. Stat. Comput. 2:296 (1981).
- [13] Gottlieb, D., L. Lustman and C. Streett. Spectral Methods for Partial Differential Equations, pp. 79-95, SIAM, Philadelphia (1984b).
- [14] Haidvogel, D. B., A. R. Robinson and E. E. Schulman. J. Comp. Phys. 34:1 (1980).
- [15] Hald, O. H. J. Comp. Phys. 40:305 (1981).
- [16] Hegna, H. A., AFWAL-TR-81-3053 (October 1981).
- [17] Hegna, H. A., AIAA 82-0092 (January 1982).
- [18] Hussaini, M. Y. and T. A. Zang. Spectral Methods for Partial Differential Equations, pp. 119-140, SIAM, Philadelphia (1984).
- [19] Jobe, C. E. and W. L. Hankey. AIAA J. 18:1394 (1980).
- [20] Kleiser, J. Lecture Notes in Physics Vol. 170, pp. 280-285, Springer-Verlag, New York (1982).
- [21] Kline, S. J., R. L. Wooley. J. Fluids Engr. 100:180 (1978).

- [22] Kumar, A. and K. S. Yajnik. J. Fluid Mech. 97:27 (1980).
- [23] Lamb, H. Hydrodynamics, Dover, New York (1945).
- [24] Lanczos, C. Applied Analysis, Prentics Hall Inc. Englewood Cliffs, N.J. (1956).
- [25] Leonard, A. and A. Wrey. Lecture Notes in Physics Vol. 170, pp. 335-342, Springer-Verlag, New York (1982).
- [26] Liepmann, H. W. Amer. Scientist, 67:221 (1979).
- [27] Lugt, H. J. and H. J. Haussling. J. Fluid Mech. 65:711 (1974).
- [28] Lumley, J. L. Prediction Methods for Turbulent Flows, pp. 1-32, Hemisphere, Washington (1980).
- [29] MacCormack, R. W. An Efficient Numerical Method for Solving the Time-Dependent Compressible Navier-Stokes Equations at High Reynolds Numbers, NASA TM 73129.
- [30] Maday, Y. and A. Quarteroni. SIAM J. Numer. Anal. 19:761 (1982).
- [31] Majda, A., J. McDonough and S. Osher. Math. Comp. 32:1041 (1978).
- [32] Marcus, P. S., S. A. Orszag and A. T. Patera. Lecture Notes in Physics Vol. 170, pp. 371-376, Springer-Verlag (1982).
- [33] Mei, R. W. and A. Plotkin. AIAA 84-1616 (June 1984).
- [34] Moin, P. Lecture Notes in Physics Vol. 170 pp. 55-76, Springer-Verlag, New York (1982).
- [35] Moin, P. and J. Kim. J. Comp. Phys. 35:381 (1980).
- [36] Orszag, S. A. Stud. Appl. Math. 50:293 (1971).
- [37] Orszag, S. A. Handbook of Turbulence, pp. 281-314, Plenum, New York (1977).
- [38] Orszag, S. A. J. Comp. Phys. 37:70 (1980).
- [39] Orszag, S. A. and L. C. Kells. J. Fluid Mech. 96:159 (1980).
- [40] Osher, S. Spectral Methods for Partial Differential Equations, pp. 209-216, SIAM, Philadelphia (1984).
- [41] Pasciak, J.E. Math. Comp. 35:1081 (1980).
- [42] Peaceman, D. W., H. H. Rachford. J. Soc. Indust. Appl. Math. 3:28 (1955).
- [43] Roache, P. J. Computational Fluid Dynamics, Hermosa Pub., Albuquerque (1982).



- [44] Rudy, D. H. and J. C. Strikwerda. *Comp. and Fluids*, 9:327 (1981).
- [45] Sakell, L. *AIAA J.*, 22:929 (1984).
- [46] Salas, M. D., T.A. Zang and M. Y. Hussaini. *Lecture Notes in Physics* Vol. 170, pp. 461-467, Springer-Verlag, New York (1982).
- [47] Schumann, U., Grotzbach, G., and L. Kleiser. *Prediction Methods for Turbulent Flows*, pp. 123-258, Hemisphere, Washington (1980).
- [48] Shang, J. S. *AIAA J.*, 16:496 (1978).
- [49] Shang, J. S. *AIAA* 84-1549 (June 1984).
- [50] Streett, C. L., T. A. Zang and M. Y. Hussaini. *J. Comp. Phys.* 57:43 (1985).
- [51] Taylor, T. D. *Spectral Methods for Partial Differential Equations*, pp. 257-267, SIAM, Philadelphia, (1984).
- [52] Taylor, T. D., R. S. Hirsh and M. M. Nadworny. *Comp. and Fluids*, 12:1 (1984).
- [53] Taylor, T. D. and J. W. Murdock. *Lecture Notes in Mathematics* Vol. 771, pp. 519-537, Springer-Verlag, New York, (1980).
- [54] Taylor, T. D. and J. W. Murdock. *Comp. & Fluids* 9:255 (1981).
- [55] Taylor, T. D., R. B. Myers and J. H. Albert. *Comp. & Fluids*, 9:469 (1981).
- [56] Tennekes, H. and J. L. Lumley. *A First Course in Turbulence*, MIT, Cambridge (1972).

## Appendix A

Lamb [1945] gives the following representation for the stream function for flow past a flat plate pitched at angle of  $45^\circ$

$$\psi = -\frac{cq_0}{\sqrt{2}} \sinh \xi (\cos \eta - \sin \eta) \quad (A1)$$

whose edges are located at  $x = \pm c$  and where  $q_0$  is the free stream velocity. This equation was derived from the relation describing fluid motion relative to an elliptic cylinder

$$\psi = -c \left\{ v \sinh \xi \cos \eta - u \sinh \xi \sin \xi \right\} \quad (A2)$$

where  $u$  and  $v$  are the  $x$  and  $y$  components of velocity with respect to the plate. Then  $\psi$  can be represented as

$$\psi = -c q_0 \cos \theta \sinh \xi \{ \tan \theta \cos \eta - \sin \eta \} \quad (A3)$$

where  $\theta$  is the angle of attack for the plate. Cartesian coordinates and elliptic coordinates are related in the following fashion

$$x = c \cosh(\xi) \cos(\eta) \quad (A4)$$

$$y = c \sinh(\xi) \sin(\eta) \quad (A5)$$

The following relation

$$\frac{x^2}{c^2 \cos^2 \eta} - \frac{y^2}{c^2 \sin^2 \eta} = 1 \quad (A6)$$

along with the definition of a point on a hyperbola and the relation of  $\sinh$  to  $\cosh$  define the following relations for the stream function in Cartesian coordinates

$$\psi = -q_0 \cos \theta \left\{ \tan \theta \sqrt{x^2 - \frac{1}{4}(\sqrt{(c+x)^2 + y^2} - \sqrt{(c-x)^2 + y^2})^2} - y \right\} \quad (A7)$$

for  $x > 0$ , and

$$\psi = q_0 \cos \theta \left\{ \tan \theta \sqrt{x^2 - \frac{1}{4}(\sqrt{(c+x)^2 + y^2} - \sqrt{(c-x)^2 + y^2})^2} - y \right\} \quad (A8)$$

for  $x < 0$ .

SCEEE

Final report on subcontract 84 RIP 27 by  
H.P. Hamerka, Department of Chemistry,  
University of Pennsylvania

During a stay at the Frank J. Seiler Research Laboratory in the summer of 1984 I completed a calculation of ESR coupling constants for a series of small organic radicals, namely methyl, allyl, ethyl and vinyl. My research efforts supported by subcontract 84 RIP 27 involved the extension of these calculations to larger systems, varying from the phenyl radical to mono-, di- and tri-nitro phenyl and benzyl radicals.

During the past year we have accumulated an extensive amount of theoretical data on the radicals mentioned above, varying from phenyl to trinitro-benzyl. Unfortunately we found that the procedure that gave us satisfactory theoretical results for the smaller radicals did not lead to good agreement with the experimental data for the larger radicals.

In order to improve the accuracy of our calculations we first developed a method for removing higher-order spin contaminations from the UHF results. This led to some improvements but we did not judge these improvements as sufficient. We concluded that the discrepancies are due to the small non-orthogonality between the unpaired orbital and the orbitals of the other spins. We are now engaged in calculations where these non-orthogonality effects are determined so that they can be eliminated.

We hope that the latter calculations will lead to improved agreement between theory and experiment so that we can feel confident about publishing our results. However, we have not yet reached that stage.

We plan to continue work on this problem and we hope to obtain satisfactory results within the next year.

1985 USAF-SCEEE RESEARCH INITIATION PROGRAM

Sponsored by the

AIR FORCE OFFICE OF SCIENTIFIC RESEARCH

Conducted by the

SOUTHEASTERN CENTER FOR ELECTRICAL ENGINEERING EDUCATION

FINAL REPORT

FUNCTIONAL ROLE OF SEROTONIN IN THE  
CEREBELLAR GLOMERULAR SYNAPSE

Prepared by:	Dr. Deborah Armstrong
Academic Rank:	Assistant Professor
Department and University:	Division of Life Sciences University of Texas at San Antonio
Date:	APRIL 12, 1986
Contract No:	84 RIP 28

FUNCTIONAL ROLE OF SEROTONIN IN THE  
CEREBELLAR GLOMERULAR SYNAPSE

by

Deborah L. Armstrong, Ph.D

ABSTRACT

Stimulation of the dorsal raphe resulted in modulation of granule cell spontaneous activity. This provides support for the proposal that serotonin functions as a transmitter in the granular layer of the cerebellar cortex, however, the diversity of the observed responses does not permit a precise determination of the nature of the activated synapses. Of the eleven cells that responded consistently, six displayed decreased spontaneous activity, three were excited by the stimulation, and four cells displayed a biphasic response of initial excitation followed by inhibition. The iontophoretic application of serotonin decreased the spontaneous activity of the majority of cells tested and this effect could not be blocked by methysergide. Several cells were excited by serotonin application and this effect could be blocked by methysergide.

## I. INTRODUCTION

Based on evidence from anatomical, physiological, and biochemical studies serotonergic efferents of the brain stem raphe nuclei contribute to the mossy fiber system innervation of the cerebellar glomeruli. The anatomical mapping includes fluorescent histochemistry (4,13) and autoradiography following intracisternal injection of  $^3\text{H}$ -serotonin (7). In both cases labeling was identified within structures resembling the large mossy fiber rosette terminal (25). Additional orthograde transport studies (6,8,12), use of retrogradely transported horseradish peroxidase (8,21) and immunocytochemistry (5) have verified the existence of 5-HT fibers within the cerebellum, however, the innervation is complex. Chan-Palay (8) describes three distinct systems: mossy fibers, fine axons that ascend to the molecular layer and bifurcate in manner resembling parallel fibers, and finally, a diffuse axonal system that innervates both the deep cerebellar nuclei and the cerebellar cortex.

Physiological studies to determine the functional significance of these serotonergic fibers are scarce and concentrate on Purkinje cell responses to raphe stimulation or iontophoresis of serotonergic agents (7,21-24). However, they do demonstrate that serotonergic mechanisms probably play a role in modulating cerebellar cortical activity. Obviously, a more thorough investigation of serotonergic transmission in the granular layer is needed.

The results of recent uptake studies utilizing an

isolated glomerular preparation have shown that a high affinity uptake system for serotonin does exist in this region (26). These studies are part of an ongoing project to identify cerebellar glomerular neurotransmitter systems and their interactions with one another. The positive results of these experiments have provided a solid base on which to begin an investigation of the physiological responses of cerebellar granule cells to serotonergic stimulation.

## II. OBJECTIVES

The primary objective of this research initiation project was to determine the response of granule cells to raphe stimulation. Since the dorsal raphe is such a well defined cluster of serotonergic cells in the rat we elected to begin with this particular nucleus. It is also one of four raphe nuclei that anatomical studies have shown to project to the cerebellar cortex. An initial sampling of recording electrode placements in the lateral hemisphere foli was planned to determine whether or not specific regions were more likely to contain responsive cells. To strengthen the proposal that responses were indeed mediated via activation of serotonergic synapses a second group of experiments was planned in which recordings made with multibarrel electrodes would enable the iontophoretic application of serotonergic receptor antagonists during stimulation evoked responses. These experiments would aid in determining the functional role of serotonin in information processing at the level of the cerebellar glomerular synapse.

### III. GRANULE CELL RESPONSE TO RAPHE NERVE STIMULATION

The majority of experiments examining serotonin's influence on cerebellar activity have dealt with Purkinje or subcortical cell responses to raphe stimulation. Utilizing extracellular recording techniques, Strahlendorf et al (22) have reported that stimulation of the raphe centralis superior or inferior produces initial bursting of fastigial and Purkinje cells followed by reduced spontaneous activity lasting up to 1600 msec. When stimulation of the sensorimotor cortex or radial nerve was applied during this period of raphe conditioning evoked spike activity was suppressed to an even greater extent than spontaneous activity, leading to the suggestion that serotonin modulates the ratio of spontaneous activity (noise) to evoked activity (specific responses to afferent signals) (24). Since very little information is known about the possible role of serotonin in the modulation of granule cell activity our initial experiments were planned to simply investigate the direct affect of raphe stimulation on granule cells.

### METHODS

Adult Sprague-Dawley rats from Holtzman suppliers were used. Animals were anesthetized with urethane (1.5 mg/kg body weight) injected intraperitoneally and supplemented as needed. Rectal temperature was continuously monitored and body temperature maintained at 37-0.5 C by means of a heating pad equipped with a negative feedback circuit. After placement in



a stereotaxic headholder and exposure of the skull surface the calvaria bone was removed to expose the lateral aspects of the vermis and the cerebellar hemisphere. After removal of the overlying dura matter a 1% solution of agar in physiological saline was placed on the cortical surface to prevent drying and reduce surface noise. An additional hole was made in the skull for positioning of the stimulating electrode, coordinates: A -6.5, L +1.0, V 6.5-7.0, into the dorsal raphe (14). Extracellular recordings were made with glass capillary electrodes drawn and broken to a tip diameter of 5-10  $\mu$ m (1 to 5 Megohm impedances), filled with 3 M NaCl saturated with fast green for later verification of electrode tip placement. Unit activity and field potentials were amplified by a high input impedance preamplifier and audio amplifier, displayed on a Tektronix storage oscilloscope for photography, and then fed into a window discriminator (20) for signal sorting. Data was stored on magnetic tape for further analysis or relayed to a chart recorder for on line observations. The recording electrode microdrives were tilted to facilitate electrode penetration into the crowns of the cerebellar folia. Concentric bipolar stimulating electrodes (Rhodes Medical Instruments, Inc.) were used to apply single rectangular pulses (60 Hz), 0.5 msec in duration and ranging from 0-500 nA intensity, using a WPI Programmable stimulator.

## RESULTS

The response to dorsal raphe stimulation was not as robust as we had anticipated. Out of the 87 cells sampled in

the granule layer only 11 responded consistently to stimulation. Six of these cells displayed decreased spontaneous activity, three were excited by the stimulation and four cells displayed a biphasic response of initial excitation followed by a long period of suppressed activity. The location of these cells in the intermediate to far lateral anterior lateral hemisphere corresponded to areas expected to have significant innervation by serotonergic fibers (5) although they were not concentrated in any one folia or defined region.

Figure 1 illustrates the response of a cell whose spontaneous activity was suppressed by raphe stimulation. The high frequency, low amplitude action potentials of this cell found at a depth of 560  $\mu$ m below the surface suggest that it is indeed a granule cell(9). With increasing stimulus intensities the degree of suppression increases to a maximum duration of 230 msec.

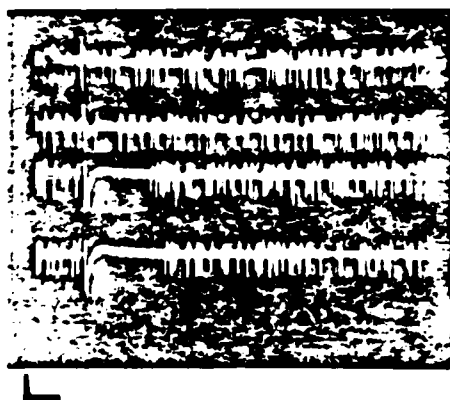


Fig. 1. Response of granule cell to single pulse stimulation of the dorsal raphe. Each trace formed by three beam sweeps. Stimulus indicated by artifact to the left of each trace. From top to bottom traces indicate: control baseline, 20, 30, and 50uA stimulus intensity. Scale markers denote 100msec and 1mv.

Figure 2 illustrates the biphasic type response that was observed in four cells. This type of response resembles that of Purkinje cells as described by Strahlendorf et al (22). The average latency for onset of the stimulatory phase was 25 msec, followed by a longer (200-250 msec) inhibition. The pure excitatory response that was observed in three cells had a much shorter latency (10-15 msec) as illustrated in Figure 3. It is interesting to note that this effect was apparent in granular layer regions displaying lower spontaneous activity. It is possible that this response was masked at other sites by ongoing background stimulation.

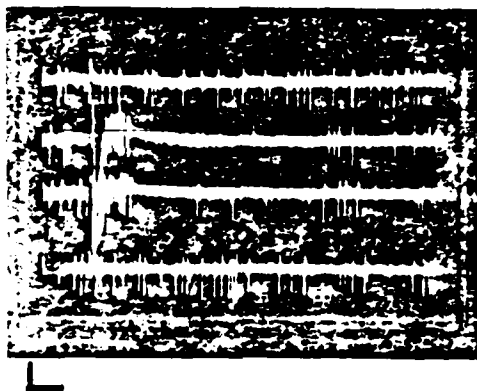


Fig 2. Example of granule cell responding to dorsal raphe stimulation with initial bursting activity followed by a long period of suppressed activity. Top and bottom traces are control baseline sweeps. Second and third middle traces display response to 20 and 30 uA stimulus intensity. Scale markers denote 50 msec and 1mV.

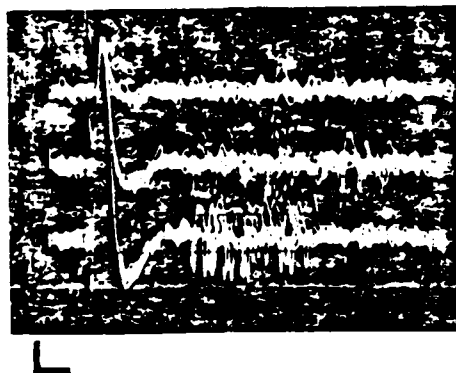


Figure 3. Example of granule layer cell activated by dorsal raphe stimulation. Each trace formed by five beam sweeps. From top to bottom the traces indicate: control baseline, 30, 40, and 60 uA stimulus intensity. Scale markers denote 5msec and 1mV.

The small number of cells encountered in the granular layer that responded to our stimulation was disappointing. However, the highest number of responsive cells were identified during the latter part of the research period following some procedural modifications. We now believe that our original stimulating arrangement may have been causing some damage to the raphe neurons, thus lessening the probability of producing normal stimulus responses. Because of time limitations we proceeded with the iontophoretic studies alone rather than combined with stimulation effects.

#### IV. IONTOPHORESIS OF SEROTONERGIC AGENTS

At best one could say that the literature on neuronal responses to local application of serotonergic compounds is

varied and, in some cases, actually contradictory and confusing. Part of the problem can be attributed to the existence of more than one class of serotonin receptor (18,19). An attempt has been made to categorize these classes, 5-HT<sub>1</sub> and 5-HT<sub>2</sub>, into inhibitory and excitatory receptors, respectively (1) and this does aid in organizing the literature, however, it is the more rigorous use of intracellular recording techniques that show the most promise for determining serotonin's synaptic functions. One clear picture that is emerging is the important role of K<sup>+</sup> conductance in the mediation of serotonin's effects (15-17).

To begin our investigation of the effects of local application of serotonin in the granular layer, we wanted to replicate the findings reported by Bloom et al (7) who described increased activity of granule cells in response 5-HT iontophoresis. This would be expected if the transmitter were stimulating postsynaptic receptors of mossy fiber synapses within the glomeruli. A multibarrel recording arrangement was employed to test for the effects of serotonergic receptor antagonists during transmitter application.

#### METHODS

Seven barrel glass capillary pipette electrodes (Frederick Haer) were drawn and broken to a tip diameter of 6-10  $\mu$ m. Two of the outer barrels were filled with 1.0 monosodium glutamate and 0.15 M NaCl. The NaCl barrel was used for current balancing and control ejections. The other barrels contained combinations of 5-hydroxy-tryptamine creatinine sulfate (0.5

M) and receptor antagonists including cyproheptadine HCl (14.6 mM), methysergide maleate (0.01 M) M). The pH of all chemicals used were adjusted as needed and each solution was filtered (Millipore Corp., 0.22  $\mu$ m). The chemicals were electrophoretically applied to neurons by calibrated DC currents using a Neurophore BH-2 microiontophoresis system (Medical Systems Corp.). Control procedures for assessing microiontophoretic effects were carried out. A retaining current of 5 nA was utilized to prevent the spontaneous diffusion of active ions from the capillary barrels. To study the interaction between chemicals one was applied continuously while the other was applied at regular intervals.

#### RESULTS

A total of 33 cells were tested with serotonergic agents and glutamate. Five of these cells did not display a reliable response to glutamate and are excluded from this discussion. Of the remaining 28, the majority, nineteen, were inhibited by 5-HT. An example of this response is illustrated in Figure 4. The reduction in activity is significant and endures beyond the period of drug application. At higher doses ( $> 50$  nAmps) several cells oscillated in activity before returning to a normal baseline. Application of methysergide using current levels that did not directly affect cell activity had no or very little affect on this suppression of activity. There are several reports in the literature of 5-HT receptor antagonists having minimal affect on serotonin induced inhibition (1,15,16).

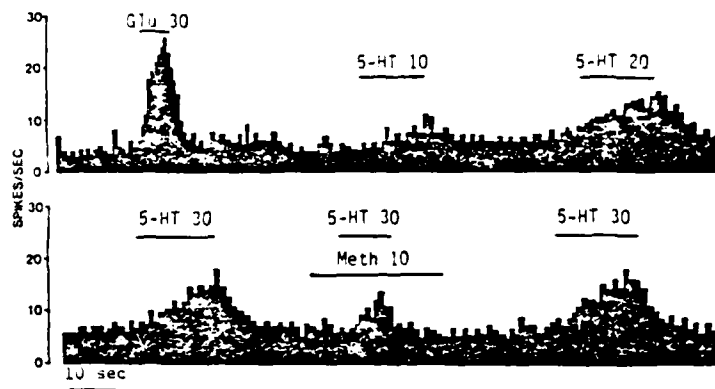


Figure 5. Example of increased activity of granule cell in response to serotonin application. This effect could be partially blocked by ejection of methysergide (Meth).

#### RECOMMENDATIONS

Despite the limited number of cells that responded to stimulation the results are very exciting in terms of providing a frame work for deliniating distinct serotonergic pathways based on the type of response illicited in granule cells. The prolonged inhibitory response indicates a type of humoral modulation that could be mediated by the fine serotonergic fibers that do not appear to make definite synaptic contacts with target cells within the granular and molecular layers. The fact that some granule cells did respond with short latency bursts supports the idea of serotonergic mossy fiber innervation. At the present time we are concentrating on integrating the stimulation and iontophoretic techniques as we had originally planned.

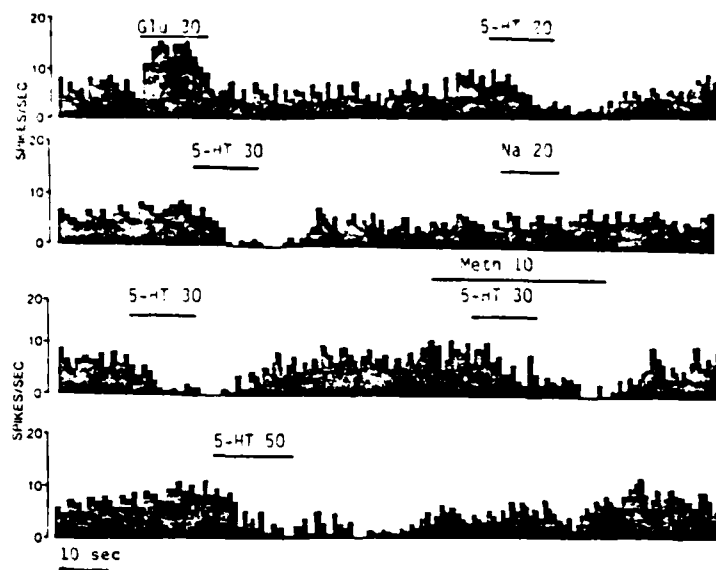


Figure 4. Reduction of granule cell activity in response to pulses of serotonin (5-HT). Rows are from continuous strip chart record of activity (spikes/sec) of single cell. Bars indicate duration and intensity (nAmps) of current application. Application of 5-HT receptor antagonist methysergide (Meth) did not block inhibitory effect. Glu indicates glutamate.

Of the nine cells that were not inhibited by 5-HT, seven displayed increased activity and two were not affected by any level of 5-HT ejection current. Figure 5 illustrates this excitatory response and as can be seen the effect could be blocked by methysergide. The excitatory response differed from that produced by glutamate in that it was not as immediate in onset and offset, however, the excitation never display the long duration that characterized the inhibitory responses.



## REFERENCES

1. Aghajanian, G. K. and R. Y. Wang. Physiology and Pharmacology of central serotonergic neurons. In: Psychopharmacology: A Generation of Progress. M. A. Lipton, A. DiMascio and K. F. Killam (eds.) Raven Press, New York, 1978.
2. Aghajanian, G.K. and C.P. Vandermaelen. Intracellular recordings from serotonergic dorsal raphe neurons: pacemaker potentials and the effect of LSD. Brain Res. 238: 463-469, 1982.
3. Aghajanian, G.K. and J.M. Lakoski. Hyperpolarization of serotonergic neurons by serotonin and LSD: studies in brain slices showing increased K<sup>+</sup> conductance. Brain Res. 305: 181-185, 1984.
4. Anden, N. E., K. Fuxe and U. Ungerstedt. Monoamine pathways to the cerebellum and cerebral cortex. Experientia 23: 838-839, 1967.
5. Bishop, G. A., R. H. Ho and J. S. King. Localization of serotonin immunoreactivity in the deep cerebellar nuclei of the opossum. Neurosci. Abstr. 10: 750, 1984.
6. Bobillier, P., S. Sequin, F. Petitjean, D. Salvert, M. Touret and M. Jouvet. The raphe nuclei of the cat brainstem: A topographical atlas of their efferent projections as revealed by autoradiography. Brain Res. 113: 449-486, 1976.
7. Bloom, F. E., B. J. Hoffer, G. P. Siggins, J. L. Barker and R. A. Nicoll. Effects of serotonin on central neurons: microiontophoretic application. Fed. Proc. 31: 97-106, 1976.
8. Chan-Palay, V. Cerebellar Dentate Nucleus: Organization, Cytology and Transmitters. Berlin: Springer-Verlag, 1977.
9. Eccles, J. C., M. Ito and J. Szentagothai. The Cerebellum as a Neuronal Machine. Springer-Verlag, New York, 1967.
10. Eccles, J. C., K. Sasaki, and P. Strata. The potential fields generated in the cerebellar cortex by a mossy fiber volley. Exp. Brain Res. 3: 58-80, 1967.
11. Eccles, J. C., K. Sasaki and P. Strata. A comparison of the inhibitory actions of Golgi cells and of basket cells. Exp. Brain Res. 3: 81-94, 1967.

12. Halaris, A. E., B. E. Jones and R. Moore. Axonal transport in serotonin neurons of the midbrain raphe. Brain Res. 66: 555-574, 1976.
13. Hokfelt, T. and K. Fuxe. Cerebellar monoamine nerve terminals, a new type of afferent fibers to the cortex cerebelli. Exp. Brain Res. 9: 63-73, 1969.
14. Konig, J. P. F. and R. A. Klippel. The Rat Brain: A Stereotaxic Atlas of the Forebrain and Lower Parts of the Brain Stem. Baltimore: Williams and Wilkins, 1963.
15. McCall, R. B. and G. K. Aghajanian. Serotonergic facilitation of facial motoneuron excitation. Brain Res. 169: 11-27, 1967.
16. McCall, R.B. Serotonergic excitation of sympathetic preganglionic neurons: a microiontophoretic study. Brain Res. 289: 121-127, 1983.
17. Park, M.R., J.A. Gonzales-Vegas and S.K. Kitai. Serotonergic excitation from dorsal raphe stimulation recorded intracellularly from rat caudate-putamen. Brain Research 243: 49-58, 1982.
18. Peroutka, S. J., R. M. Lebovitz and S. H. Snyder. Two distinct central serotonin receptors with different physiological functions. Science 212: 827-829, 1981.
19. Peroutka, S. J. and S. H. Snyder. Multiple serotonin receptors: differential binding of (<sup>3</sup>H)5-hydroxytryptamine, (<sup>3</sup>H)Lysergic Acid Diethylamide and (<sup>3</sup>H)Spiroperidol. Mol. Pharmacol 16: 687-699, 1979.
20. Peterson, R. C., A. D. Simpson, M. J. Wayner and H. Yagi. A window discriminator for sorting electrical signals. Physiol. Behav. 4: 865-867, 1969.
21. Shinnar, S., R. J. Maciewicz and R. J. Shofer. A raphe projection to cat cerebellar cortex. Brain Res. 97: 139-143, 1973.
22. Strahlendorf, J. C., H. K. Strahlendorf and C. D. Barnes. Modulation of cerebellar neuronal activity by raphe stimulation. Brain Res. 169: 565-569, 1979.
23. Strahlendorf, J. C. and G. D. Hubbard. Serotonergic interactions with rat cerebellar purkinje cells. Brain Res. Bull. 11: 265-269, 1983.

24. Strahlendorf J. C., H. K. Strahlendorf and C. D. Barnes. Comparative aspects of raphe-induced modulation of evoked and spontaneous cerebellar unit activity. In: The Role of Peptides and Amino Acids as Neurotransmitters, pgs. 217-225. Alan Liss, New York, 1981.
25. Szentagothai, J. Glomerular synapses, complex synaptic arrangements, and their operational significance. The Neurosciences. 427-443, 1970.
26. Terrian, D.M., W.I. Butcher, P.H. Wu and D.L. Armstrong. Isolation of glomeruli from areas of bovine cerebellum and comparison of <sup>3</sup> serotonin uptake. Brain Res. Bull. 14: 469, 1985.

### Acknowledgement

The author would like to thank the USAF School of Aerospace Medicine, the Southeastern Center for Electrical Engineering Education and Air Force Office of Scientific Research for providing the support needed to carry out and complete this research project. A special thank you goes to Dr. David Terrian for his helpful ideas and support throughout the past two years.

CHOLINE AND ETHANOLAMINE PHOSPHOTRANSFERASE  
ACTIVITIES IN GLOMERULAR PARTICLES ISOLATED  
FROM BOVINE CEREBELLAR CORTEX

Robert V. Dorman\*, Scott B. Bischoff\*\* and David M. Terran\*\*

\*Dept. Biological Sciences, Kent State University,  
Kent, OH 44242

\*\*USAF School of Aerospace Medicine, Clinical Sciences  
Division, Brooks AFB, TX 78235

Correspondence to: Dr. Robert V. Dorman  
Dept. Biological Sciences  
Kent State University  
Kent, OH 44242

Running title: Lipid Metabolism in Cerebellar Glomeruli

# ABSTRACT

Isolated cerebellar glomeruli provide a relatively homogenous subcellular fraction, which can be used to study the biochemical events related to chemical transmission within a well-characterized central synapse. Choline and ethanolamine phosphotransferase activities were identified and partially characterized in this nerve ending preparation. Choline phosphotransferase associated with the glomerular particles required  $Mg^{2+}$ , while ethanolamine phosphotransferase required  $Mn^{2+}$  for optimal activities. Both enzymes were inhibited by exogenous  $Ca^{2+}$ . The apparent  $V_{max}$  values were 35.9 and 10.0 nmol/hr/mg protein for the choline and ethanolamine phosphotransferases, respectively. The apparent  $K_m$  value for the CDPcholine substrate was 28.5  $\mu M$ , and the  $K_m$  for CDPethanolamine was 8.6  $\mu M$ . Neither enzyme responded to the various adenine nucleotides, neurotransmitters or neurotransmitter agonists tested. However, exposure of the glomerular particles to cytidine nucleotides inhibited ethanolamine phosphotransferase activity and stimulated choline phosphotransferase activity.

## INTRODUCTION

The cerebellar glomeruli consist of the large terminals of the mossy fibers, granule cell dendrites, Golgi cell terminals and dendrites and a protective glial sheath (1-3). The synaptic connections in this complex have been described (4). Methods have been reported for the isolation of intact and functional glomerular particles (5-7). The enriched glomerular fraction provides a useful model for the investigation of synaptic events, since the isolated glomeruli retain their morphological and functional integrity. The mossy fiber terminals retain many of their synaptic connections and are filled with synaptic vesicles (5,6,8). The glomerular particles respire, actively transport neurotransmitters and amino acids and they contain the enzymes involved in mitochondrial function and neurotransmitter synthesis (6-9). Terrian et al.(8) have recently described an improved method for the purification of cerebellar glomeruli.

Choline and ethanolamine phosphotransferases were identified and partially characterized in the purified glomerular fraction in order to further assess the metabolic capabilities of this unique nerve ending preparation. Choline phosphotransferase (CDPcholine: 1,2-diradylglycerol 3-phosphate phosphotransferase; EC 2.3.7.2) and ethanolamine phosphotransferase (CDPethanolamine: 1,2-diradylglycerol ethanolamine phosphotransferase; EC 2.3.7.1) catalyze the final steps in the synthesis of the choline and

ethanolamine glycerophospholipids, respectively. The enzymes catalyze the transfer of either phosphocholine or phosphoethanolamine from the cytidine nucleotide carrier to a diglyceride acceptor (10). These enzymes have been identified in other CNS membrane preparations. They are most active in cerebral microsomes (11-13) and they have been assayed in isolated neurons and glia (14). They have also been identified in purified CNS myelin (15,16), microsomes prepared from the hypomyelinated brains of jumpy and quaking mutant mice (17,18), and cerebral synaptosomes (19,20). It has been suggested that the phosphotransferases associated with synaptosomes may be involved in the membrane events related to neurotransmission, since they are influenced by neurotransmitters and cAMP (20).

The isolated cerebellar glomeruli were used to show the presence of choline and ethanolamine phosphotransferases in cerebellum, since they have not yet been identified in cerebellar membrane preparations. Also, the phosphotransferases were partially characterized prior to assessing their potential involvement in synaptic events in this nerve ending preparation. Phosphotransferase activities were measured in the presence of neurotransmitters thought to be endogenous to cerebellar glomeruli, their agonists and nucleotides implicated in either stimulus-secretion coupling, or phospholipid synthesis.



## EXPERIMENTAL PROCEDURES

### MATERIALS

The [methyl- $^{14}\text{C}$ ]-cytidine diphosphocholine and the Aquasol II were obtained from New England Nuclear, while the [ethanolamine-1,2- $^{14}\text{C}$ ]-cytidine diphosphoethanolamine was purchased from ICN. The radioactive cytidine nucleotides were diluted with unlabeled CDPcholine and CDPethanolamine (Sigma Chemical Co.). The neurotransmitters, neurotransmitter agonists, adenine and cytidine nucleotides, 1,2-diolein and Ficoll 400 were purchased from Sigma Chemical Co.

### ISOLATION OF CEREBELLAR GLOMERULI

A purified glomeruli fraction (PGF) was prepared from bovine cerebellar cortex. Cerebella were obtained at a slaughterhouse within 15 minutes of sacrifice. They were placed in ice for transport and the vermal cortices were removed by dissection. This tissue was rinsed in ice-cold saline and minced with scissors prior to manual homogenization in 9 volumes of 0.3 M sucrose, using a modified Dounce homogenizer, according to the method of Hayes et al.(5). Magnesium ions (1 mM  $\text{MgSO}_4$ ) were included in all solutions used in the preparation of the PGF. The procedures used to isolate the enriched glomeruli fraction have

recently been described by Terrian et al.(8). A number of sub-fractions were obtained during the preparation of the PGF, including the crude nuclear and crude mitochondrial fractions. These fractions contain the microsomal elements. Medullated fibers were separated from the crude glomeruli fraction in order to obtain the purified glomeruli fraction. Each of these sub-fractions was assayed for choline and ethanolamine phosphotransferase activities. Aliquots of each PGF preparation were taken for determination of protein concentration (21). The remainder was diluted with 9 volumes of 10 mM Tris-HCl buffer, pH 7.45, prior to estimation of choline and ethanolamine phosphotransferase activities.

#### PHOSPHOTRANSFERASE ASSAYS

Choline and ethanolamine phosphotransferase assays were performed for 30 minutes at 37°C in a total volume of 1.0 ml. Typical incubations contained 1-2 mg PGF protein and 20 to 80  $\mu$ M [ $^{14}$ C]CDPcholine or [ $^{14}$ C]CDPethanolamine (each at 2 nCi/nmol) in 10 mM Tris-HCl buffer, pH 7.45. Choline phosphotransferase assays normally contained 100 mM MgCl<sub>2</sub>, while ethanolamine phosphotransferase assays included 10 mM MnCl<sub>2</sub>. The neurotransmitters, neurotransmitter agonists, cytidine and adenine nucleotides were present at 1 mM concentrations. The 1,2-diolein was suspended by high speed vortexing for five minutes in 10 mM

Tris-HCl (pH 7.45), in the presence of 0.022% Triton X-100. The 1,2-diolein concentrations ranged from 0.5 to 10 mM, in order to determine  $K_m$  values for the diglyceride substrate. Triton X-100 was found to provide for greater phosphotransferase activities than either Brij 35 or Tween 80 and had a final concentration of 0.02% in the incubations which included 1,2-diolein. Some of the glomerular preparations were exposed to 5 mM Tris buffer for 60 min at 4°C for lysis of the vesicles according to Lai and Clark (22). All reactions were stopped by the addition of 5 ml of chloroform: methanol (2:1, v:v) and the total lipids were extracted and washed according to Folch et al.(23).

The radioactivity in the total lipid extract was used as the measure of phosphotransferase activities after thin layer chromatography (24) was used to show that the [ $^{14}C$ ]CDPcholine labeled only the choline glycerophospholipids and the [ $^{14}C$ ]CDPethanolamine labeled only the ethanolamine glycerophospholipids. The incorporation of radiolabeled substrates was determined by liquid scintillation counting in a Beckman LS-230 counter, with Aquasol II as the cocktail. F-tests were performed to show significant differences in phosphotransferase activities due to exposure of the PGF to neurotransmitters, transmitter agonists or nucleotides. Student's t-test was then used to determine which treatment groups were significantly different from untreated controls.

## RESULTS

### Characterization of Phosphotransferase Activities in the PGF

Choline and ethanolamine phosphotransferase activities were detected in all membrane fractions isolated from bovine cerebellar cortex, including the purified glomeruli fraction. The phosphotransferases were partially characterized in the PGF. The incorporation of radiolabeled precursors into their respective phospholipids were enzymic, since both activities were abolished by exposure to 100°C for ten minutes. Also, the rates of isotope incorporation were linear over 30 minutes of incubation, and the activities were dependent on protein concentrations, between 0.2 and 3.0 mg glomerular protein (data not shown). Both phosphotransferase enzymes exhibited a pH optimum near 8.0 (Figure 1). Routine assays were then carried out at 37°C, for 30 minutes, at pH 7.45, in the presence of 1-2 mg glomerular protein.

The cation requirements of the phosphotransferases were determined. Choline phosphotransferase was most active in the presence of 100 mM MgCl<sub>2</sub>, while ethanolamine phosphotransferase activity was optimal in the presence of 10 mM MnCl<sub>2</sub>. Both phosphotransferases were inhibited by Ca<sup>2+</sup> in the presence of optimal concentrations of either Mg<sup>2+</sup> or Mn<sup>2+</sup> (Table I).

### Distribution of Phosphotransferases in Subcellular Fractions

Choline and ethananoiamine phosphotransferase activities were identified in all particulate fractions isolated during the preparation of the PGF (Table I). The phosphotransferase activities in the crude nuclear and crude mitochondrial fractions were almost twice that of the homogenate. The supernatant recovered following sedimentation of the crude glomeruli fraction contained phosphotransferase activities that were about 10% of those found in the homogenate (data not shown). When the crude glomeruli fraction was further purified by sedimentation through 1.2 M sucrose, the medullated fiber fraction exhibited a decline in phosphotransferase activities when compared to the crude glomeruli fraction, while the activities in the purified glomeruli fraction were about doubled compared to the crude preparation. The purified glomeruli fraction had phosphotransferase activities which were comparable to those in the homogenate. Also, hypotonic lysis of the PGF particles by the method of Lai and Clark (22) did not significantly alter the activity of either enzyme.

### Kinetic Parameters and Treatment Effects

Estimates of  $K_m$  and  $V_{max}$  values were made for both enzymes

in the PGF. Vmax values were determined in the presence of 10 mM 1,2-diolein and either 100  $\mu$ M CDPcholine or CDPethanolamine. The Km values were determined using various concentrations of diglyceride and nucleotide substrates. The results are shown in Table III. The apparent Vmax value for the choline phosphotransferase was 3.5 times greater than the value for the ethanolamine phosphotransferase. The apparent Km values for the choline phosphotransferase were 2.9 mM for the diglyceride substrate and 28.6  $\mu$ M for the CDPcholine. Ethanolamine phosphotransferase exhibited similar Km values for the 1,2-diolein and the cytidine nucleotide.

Isolated glomeruli were exposed to exogenous neurotransmitters, neurotransmitter agonists and nucleotides which have been implicated in transmission processes and the effects of the treatments on phosphotransferase activities were determined (Figure 2). Exogenous diglycerides were not added to the incubations and CDPcholine and CDPethanolamine concentrations were 20  $\mu$ M. ATP and cAMP (1 mM) had no effect on the activity of either enzyme, when compared to untreated controls. Equimolar concentrations (1 mM) of the neurotransmitters norepinephrine (NE), 5-hydroxytryptamine (5-HT) and gamma-aminobutyric acid (GABA), and the transmitter agonists muscimol, quisqualic acid and carbamylcholine, also had no effect on the activity of either phosphotransferase. However, cytidine nucleotides induced significant and opposite effects on the enzyme activities. Choline

phosphotransferase activity was increased 37% by CTP ( $p < 0.01$ ), 45% by CDP ( $p < 0.01$ ) and 44% by CMP ( $p < 0.001$ ) when compared to untreated controls. Conversely, ethanolamine phosphotransferase activity was inhibited 20% by CTP ( $p < 0.01$ ), 15% by CDP ( $p < 0.01$ ) and 35% by CMP ( $p < 0.001$ ) when compared to controls.

## DISCUSSION

The ability to isolate cerebellar glomeruli as a relatively homogenous subcellular fraction has enabled investigators to study the biochemical events underlying synaptic transmission within a central synapse that has been extensively characterized. Choline and ethanolamine phosphotransferase enzyme activities were identified in isolated glomerular particles as part of continuing studies of the biochemical events related to synaptic activities in this nerve ending preparation. The enzymes were partially characterized, in order to determine their general requirements, prior to assessing their involvement in glomerular functions by testing the effects of neurotransmitters and nucleotides believed to be endogenous to cerebella glomeruli. Also, there are no known reports on phosphotransferase activities in the cerebellum.

Most of the requirements of the PGF enzymes were similar to those for phosphotransferases from other regions and subcellular fractions of the CNS. Enzyme activities were dependent on protein concentrations, were linear over 30 minutes of incubation and were abolished by exposure to 100°C for ten minutes. Both enzymes had a pH optimum near 8.0, which is consistent with reported values (11, 15). Ethanolamine phosphotransferase required 10 mM  $Mn^{2+}$  for optimal activity, which is similar to values reported for brain microsomes (25), purified CNS myelin



(16) and synaptosomes isolated from cerebral cortex (20). However, choline phosphotransferase required 100 mM  $Mg^{2+}$ , which is 2 to 10 times greater than values reported for other CNS membrane preparations (11, 20, 26). Both enzymes were inhibited by  $Ca^{2+}$ , as has been shown in rat brain microsomes (11), isolated neurons and glia (14) and cerebral synaptosomes (20).

Phosphotransferase activities were measured in all particulate fractions isolated during the preparation of the PGF, in order to determine the subcellular distribution of the enzymes in cerebellar cortex. Both enzymes were present in all fractions and the distributions were similar to those reported for other CNS regions. The crude nuclear and crude mitochondrial fractions were the most active and this is consistent with results from other brain regions, since these fractions contain the microsomal elements of the cerebellar cortex (5) and the microsomal fraction is the most enriched source of phosphotransferase activities in nerve tissues (11, 13, 16). However, nuclear envelopes and mitochondrial fractions also contain these enzymes (12, 19, 26) and these membrane bounded organelles are also found in the crude nuclear and mitochondrial fractions. Sedimentation of the crude glomeruli fraction through 1.2 M sucrose separates the medullated fibers from the purified glomeruli and resulted in a moderate enrichment of the activities in the PGF, since the medullated fibers contained lower activities than the purified glomeruli.

Although there was no enrichment of enzyme activities in the PGF when compared to homogenate, there were substantial activities in the PGF. Further work is required to determine which of the PGF membranes contain the phosphotransferases, since the PGF includes neuronal and glial constituents and subcellular membrane components, such as mitochondria and endoplasmic reticulum. Regardless of the relative contributions of the various membrane components, it is clear that the purified glomeruli fraction isolated from cerebellar cortex is able to synthesize choline and ethanolamine glycerophospholipids.

The kinetic parameters for the enzymes were similar to those reported for other nerve ending preparations. The apparent  $V_{max}$  value for the choline phosphotransferase in the PGF was 3.5 times greater than the  $V_{max}$  for the ethanolamine phosphotransferase. The greater activity of the choline phosphotransferase is consistent with the previously observed differences in the relative distribution of these enzymes in other CNS membrane preparations (11-14) and reflects the uneven distribution of the choline and ethanolamine glycerophospholipids in cerebellar cortex (27). The activities of these enzymes in the PGF were less than the activities in brain microsomes (28), but they were similar to those reported for cerebral synaptosomes (20). Both enzymes had comparable affinities for the diglyceride and cytidine nucleotide substrates and these apparent  $K_m$  values were similar to those

described in cerebral synaptosomes (20).

Even though the observed characteristics of the PGF enzymes were similar to those reported for other nerve ending preparations, the mechanisms involved in control of their activities may be different. The phosphotransferases in the PGF were unaffected by 1 mM ATP and cAMP, in the presence of subsaturating concentrations of diglycerides and CDPcholine and CDP-ethanolamine. However, adenine nucleotides have been shown to affect phosphotransferase activities in other membrane preparations. Both phosphotransferases are inhibited by ATP in rat liver microsomes (29-31), but only ethanolamine phosphotransferase activity is inhibited in chicken brain microsomes (32). Also, 1 mM ATP stimulates choline phosphotransferase activity, but not ethanolamine phosphotransferase activity in cerebral synaptosomes and the same effect is observed in the presence of 1  $\mu$ M cAMP (20). These effects may be related to chemical transmission processes observed in cerebral synaptosomes. However, such influences were not expressed in the isolated glomeruli, since ATP and cAMP had no effect on the activity of either enzyme under the present experimental conditions.

The neurotransmitters NE, 5-HT and GABA, and the transmitter agonists muscimol, quisqualic acid and carbamylcholine, also had no effect on the activity of either phosphotransferase enzyme in isolated cerebellar glomeruli. These chemicals were chosen because they have been implicated in nervous system

function in general and glomerular function in particular (33,34). Subsaturating concentrations of diglycerides and CDPcholine and CDPethanolamine were used in all the treatment experiments, because the enzymes are unlikely to be saturated in vivo, and subsaturating substrate concentrations should allow for the observance of either competitive or noncompetitive treatment effects. Treatment concentrations of 1 mM were chosen because such concentrations have been shown to be effective in other membrane preparations (20,32). Therefore, the lack of transmitter effects on the activities of these enzymes is interpreted to indicate that neither enzyme is involved in receptor mediated processes in this nerve ending preparation. However, more extensive screening must be done in order to eliminate the possibility that the phosphotransferases are involved in the transmission processes related to a particular neurotransmitter.

Although neither phosphotransferase responded to neurotransmitters or agonists, they were both affected by exogenous cytidine nucleotides. The presence of 1 mM CTP, CDP or CMP stimulated choline phosphotransferase activity and inhibited ethanolamine phosphotransferase activity in the PGF. Although there is no known role for the cytidine compounds in neurotransmission, they appear to be involved in the regulation of choline and ethanolamine glycerophospholipid synthesis in cerebellar glomeruli. This regulation may be directly expressed at the

level of the enzymes, or it may involve control of endogenous substrate levels. For example, cytidine nucleotides have been shown to alter the rate of phosphatidic acid formation in rat brain homogenates (35), which may affect the availability of endogenous diglycerides. Also, we found that CTP, CDP and CMP stimulated the incorporation of [14C]acetate into cerebral diglycerides in vitro and in vivo (unpublished results). The cytidine nucleotides may also affect the endogenous levels of CDPcholine or CDPethanolamine, as has been shown in virus infected HeLa cells (36). Further work must be done to clarify the effects of the cytidine nucleotides, since these compounds appear to be involved in the control mechanisms for the synthesis of the major phospholipid constituents of the associated membranes.

Acknowledgements: We would like to thank Mary Beth Hofstetter for her excellent technical help. This work was supported in part by the U.S. Air Force: AFOSR/AFSC, F49620-22-C-0035 (RVD) and a grant from AFOSR #2312W3 (DMT).

## FIGURE LEGENDS

Figure 1. The effects of pH on the activities of choline and ethanolamine phosphotransferase enzymes in the purified glomeruli fraction. The assays were performed as described in the Experimental Procedures, while the buffer pH was varied from 6.0 to 9.0. Choline phosphotransferase assays included 100 mM MgCl<sub>2</sub>, while ethanolamine phosphotransferase assays included 10 mM MnCl<sub>2</sub>. The results are given as the mean values of at least three separate determinations.

Figure 2. The effects of nucleotides, neurotransmitters and neurotransmitter agonists on choline and ethanolamine phosphotransferase activities in the purified glomeruli fraction. The assays included 20  $\mu$ M [<sup>14</sup>C]CDPcholine or [<sup>14</sup>C]CDPethanolamine. The neurotransmitters, transmitter agonists and nucleotides were included at 1 mM concentrations. Diglycerides were not added to the incubations and the assays were performed as previously described. The results were obtained from at least six separate determinations. (NE)norepinephrine, GABA(gamma-aminobutyric acid, 5-HT(5-hydroxytryptamine); (\*p < 0.01; \*\*p < 0.001 compared to untreated controls; Student's t-test).

## REFERENCES

1. Hamori, J. 1965. Identification in cerebellar isles of Golgi II axon endings by aid of experimental degeneration, pages 291-292, in Titlebalch, M.(ed.), Proc. of the Third European Regional Conference of Electron Microscopy, Pub. House of the Czechoslovak Acad. of Sci., Prague.
2. Hamori, J. and Szentagothai, J. 1966. Participation of Golgi neuron processes in the cerebellar glomeruli: an electron microscope study. Exp. Brain Res. 2:35-48.
3. Fox, C. A., Hillman, D. E., Siegesmund, K. A. and Dutta, C. R. 1967. The primate cerebellar cortex: a Golgi and electron microscope study. Prog. Brain Res. 25:174-225.
4. Szentogothai, J. 1970. Glomerular synapses, complex synaptic arrangements, and their operational significance, pages 427-443, in Schmitt, F.O.(ed.), The Neurosciences: Second Study Program, Rockefeller Univ. Press, New York.
5. Hajos, F., Tapia, R., Wilkin, G., Johnson, A.L. and Balazs, R. 1974. Subcellular fractionation of rat cerebellum: an electron microscopic and biochemical investigation. I. Preservation of large fragments of the cerebellar glomeruli. Brain Res. 70:261-279.
6. Tapia, R., Hajos, F., Wilkin, G., Johnson, A. and Balazs, R. 1974. Subcellular fractionation of rat cerebellum: an electron microscopic and biochemical investigation. Brain Res. 70:285-299.



7. Hamberger, A., Hansson, H.-A., Lazarewicz, J. W., Lundh, T. and Sellstrom, A. 1975. The cerebellar glomerulus: isolation and metabolic properties of a purified fraction. *J. Neurochem.* 27:267-272.
8. Terrian, D. M., Butcher, W. I., Wu, P. H. and Armstrong, D. L. 1985. Isolation of glomeruli from areas of bovine cerebellum and comparison of [3H]serotonin uptake. *Brain Res. Bull.* 14:469-475.
9. Wilson, J. E., Wilkin, G. P. and Balazs, R. 1976. Metabolic properties of a purified preparation of large fragments of the cerebellar glomeruli: glucose metabolism and amino acid uptake. *J. Neurochem.* 26:957-965.
10. Van den Bosch, H. 1974. Phosphoglyceride metabolism. *Ann. Rev. Biochem.* 43:243-277.
11. McCaman, R. E. and Cook, K. 1966. Intermediary metabolism of phospholipids in brain tissue. III. Phosphocholine-glyceride transferase. *J. Biol. Chem.* 241:3390-3394.
12. Ansell, G. B. and Metcalfe, R. F. 1968. Labelling of brain phosphatidylethanolamine and ethanolamine plasmalogen from cytidine diphosphate ethanolamine in vitro. *Biochem. J.* 109:29.
13. Goracci, G., Horrocks, L. A., and Porcellati, G. 1978. Studies of rat brain choline and ethanolamine phosphotransferases using labeled alkylacylglycerol as substrate with evidence for reversibility of the reaction. *Adv. Exp. Med. Biol.* 101:269-278.
14. Freysz, L. and Mandel, P. 1974. Etude comparative de la biosynthese des phosphatidylcholines dans les neurones et les

- cellules gliales de cerveau de poulet. Febs. Lett. 40:110-113.
15. Toews, A. D., Horrocks, L. A. and King, J. S. 1976. Simultaneous isolation of purified microsomal and myelin fractions from rat spinal cord. J. Neurochem. 27:25-31.
  16. Wu, P.-S. and Ledeen, R. W. 1980. Evidence for the presence of CDP-ethanolamine: 1,2-diacyl-sn-glycerol ethanolaminephosphotransferase in rat central nervous system myelin. J. Neurochem. 35:659-666.
  17. Dorman, R. V., Freysz, L. and Horrocks, L. A. 1977. Synthesis of ethanolamine phosphoglycerides by microsomes from the brains of jimpy and quaking mice. J. Neurochem. 29:231-233.
  18. Schneider, W. J. and Vance, D. E. 1978. Activities of choline kinase, cholinephosphate cytidyltransferase and CDP-choline: 1,2-diacylglycerol cholinephosphotransferase in brain from normal and quaking mice. J. Neurochem. 30:1599-1601.
  19. Possmayer, F., Kleine, L., Duwe, G., Stewart-DeHaan, J., Wong, T., MacPherson, C. F. C. and Harding, P. G. R. 1979. Differences in the subcellular and subsynaptosomal distribution of the putative endoplasmic reticulum markers NADPH-cytochrome c reductase, estrone sulfate sulfohydrolase and CDP-choline-diacylglycerol cholinephosphotransferase in rat brain. J. Neurochem. 32:889-906.
  20. Strosznajder, J., Radomska-Pyrek, A. and Horrocks, L. A. 1979. Choline and ethanolamine glycerophospholipid synthesis in isolated synaptosomes of rat brain. Biochim. Biophys. Acta 574:48-56.
  21. Lowry, O.H., Rosebrough, N. J., Farr, A. L. and Randall, R. J.

1951. Protein measurement with the Folin phenol reagent. *J. Biol. Chem.* 193:265-275.
22. Lai, J. C. K. and Clark, J. B. 1976. Preparation and properties of mitochondria derived from synaptosomes. *Biochem. J.* 154:423-432.
23. Folch, J., Lees, M. and Sloane-Stanley, G. H. 1957. A simple method for the isolation and purification of total lipids from animal tissues. *J. Biol. Chem.* 226:497-509.
24. Horrocks, L. A. and Sun, G. Y. 1972. Ethanolamine plasmalogens, pages 223-231, in Rodnight, R. and Marks, N. (eds.), *Research Methods in Neurochemistry*, Plenum Press, New York.
25. Roberti, R., Binaglia, L., Francescangeli, E., Goracci, G. and Porcellati, G. 1975. Enzymic synthesis of 1-alkyl-2-acyl-sn-glycero-3-phosphorylethanolamine through ethanolaminephosphotransferase activity in neuronal and glial cells of rabbit in vitro. *Lipids* 3:121-127.
26. Baker, R. R. and Chang, H.-I. 1982. Cholinephosphotransferase activities in microsomes and neuronal nuclei isolated from immature rabbit cerebral cortex: the use of endogenously generated diacylglycerols as substrate. *Can. J. Biochem.* 60:724-733.
27. Geison, R. L., Flangas, A. L. and Kornguth, S. E. 1974. Total glycerophospholipid fatty acid and phospholipid class composition of nerve ending and related fractions from fetal and adult pig cerebellum and adult pig whole brain cortex. *Lipids* 9:756-764.
28. Radomska-Pyrek, A., Strosznajder, J., Dabrowiecki, Z., Chojnacki,

- T. and Horrocks, L. A. 1976. Effects of free fatty acids on the enzymic synthesis of diacyl and ether types of choline and ethanolamine phosphoglycerides. *J. Lipid Res.* 17:657-662.
29. De Kruyff, B., Van Golde, L. M. G. and Van Deenen, L. L. M. 1970. Utilization of diacylglycerol species by cholinephosphotransferase, ethanolaminephosphotransferase and diacylglycerol acyltransferase in rat liver microsomes. *Biochim. Biophys. Acta* 210:425-435.
30. Sribney, M., Knowles, C. L. and Lyman, E. M. 1976. Regulation of phosphatidylcholine synthesis in rat liver endoplasmic reticulum. *Biochem. J.* 156:507-514.
31. Liteplo, R. G. and Sribney, M. 1977. Inhibition of rat liver CDPethanolamine: 1,2-diacylglycerol ethanolaminephosphotransferase activity by ATP and pantothenic acid derivatives. *Can. J. Biochem.* 55:1049-1056.
32. Freysz, L., Horrocks, L. A. and Mandel, P. 1976. Ethanolamine and choline phosphotransferases of chicken brain, pages 252-268, in Gatt, S., Freysz, L. and Mandel, P. (eds.), *Enzymes of Lipid Metabolism*, Plenum Press, New York.
33. Levi, G. 1984. Release of putative transmitter amino acids, pages 463-509, in Lajtha, A. (ed.), *Handbook of Neurochemistry*, Vol. 6, Plenum Press, New York.
34. Chan-Palay, V. 1977. The indoleamine afferent axons to the cerebellum, pages 330-453, in *Cerebellar Dentate Nucleus: Organization, Cytology and Transmitters*, Springer-Verlag, New York.

35. Possmayer, F. and Mudd, J. B. 1971. The regulation of sn-glycerol-3-phosphate acylation by cytidine nucleotides in rat brain cerebral hemispheres. *Biochim. Biophys. Acta* 239:217-233.
36. Choy, P. C., Paddon, H. B. and Vance, D. E. 1980. An increase in cytoplasmic CTP accelerates the reaction catalyzed by CTP:phosphocholine cytidyltransferase in poliovirus-infected HeLa cells. *J. Biol. Chem.* 255:1070-1073.
37. Eisenthal, R. and Cornish-Bowden, A. 1974. The direct linear plot. A new graphical procedure for estimating enzyme kinetic parameters. *Biochem. J.* 139:715-720.

TABLE I

CATION DEPENDENCE OF CHOLINE AND ETHANOLAMINE  
PHOSPHOTRANSFERASE ENZYMES IN THE PURIFIED  
GLOMERULI FRACTION

nmol/hr/mg protein  $\pm$  S.D.

ADDITION (mM)		CHOLINE PHOSPHOTRANSFERASE	ETHANOLAMINE PHOSPHOTRANSFERASE
none		3.07 $\pm$ 0.03	0.11 $\pm$ 0.01
MgCl <sub>2</sub>	1.0	0.18 $\pm$ 0.04	0.86 $\pm$ 0.17
	10.0	2.06 $\pm$ 0.36	0.84 $\pm$ 0.12
	20.0	2.10 $\pm$ 0.33	0.77 $\pm$ 0.09
	100.0	4.34 $\pm$ 0.48	0.79 $\pm$ 0.03
	200.0	4.30 $\pm$ 0.07	nd
MnCl <sub>2</sub>	0.1	1.54 $\pm$ 0.03	0.73 $\pm$ 0.01
	1.0	2.38 $\pm$ 0.16	1.25 $\pm$ 0.12
	10.0	2.37 $\pm$ 0.18	1.28 $\pm$ 0.27
	20.0	2.06 $\pm$ 0.16	1.14 $\pm$ 0.22
	50.0	nd	0.71 $\pm$ 0.04
CaCl <sub>2</sub>	50.0	nd	0.35 $\pm$ 0.01
	200.0	0.04 $\pm$ 0.01	nd

Incubations were performed at 37°C for 30 minutes in 10 mM Tris-HCl buffer (pH 7.45), containing 1-2 mg PGF protein and 40  $\mu$ M [14C]CDPcholine or 20  $\mu$ M [14C]CDPethanolamine (each at 2 nCi/nmol). The incubations containing CaCl<sub>2</sub> also contained optimal concentrations of either MnCl<sub>2</sub> or MgCl<sub>2</sub>. The total lipids were extracted and counted as described in Experimental Procedures. The results are expressed as nmol of isotope incorporated/hour/mg glomerular protein. nd = not determined.

TABLE II

CHOLINE AND ETHANOLAMINE PHOSPHOTRANSFERASE  
ACTIVITIES IN SUBCELLULAR FRACTIONS  
ISOLATED FROM CEREBELLAR CORTEXnmol/hr/mg protein  $\pm$  S.D.

FRACTIONS	CHOLINE PHOSPHOTRANSFERASE	ETHANOLAMINE PHOSPHOTRANSFERASE
HOMOGENATE	3.42 $\pm$ 0.85	1.76 $\pm$ 0.66
NUCLEAR FRACTION	6.45 $\pm$ 0.58	3.18 $\pm$ 0.57
MITOCHONDRIAL FRAC.	5.64 $\pm$ 0.92	2.45 $\pm$ 0.29
CRUDE GLOMERULI	1.51 $\pm$ 0.15	1.19 $\pm$ 0.21
MEDULLATED FIBERS	1.07 $\pm$ 0.24	0.87 $\pm$ 0.18
PURIFIED GLOMERULI	3.56 $\pm$ 0.36	1.89 $\pm$ 0.40

Assays were performed as described in Experimental Procedures. Each subfraction was isolated during the preparation of the PGF and all were suspended in 10 mM Tris-HCl (pH 7.45) and immediately assayed. The results represent the activities determined in at least three separate subfraction preparations.

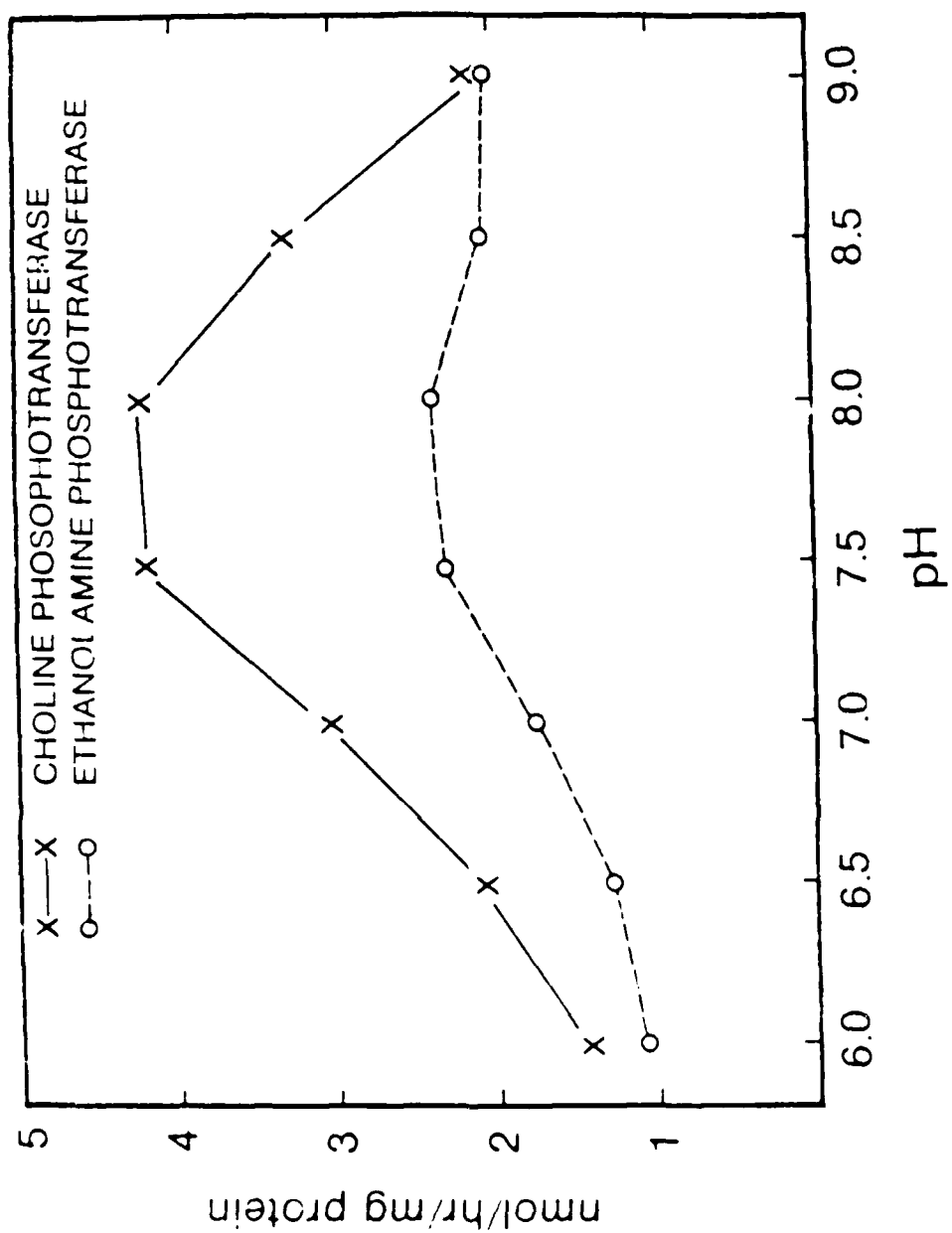
TABLE III

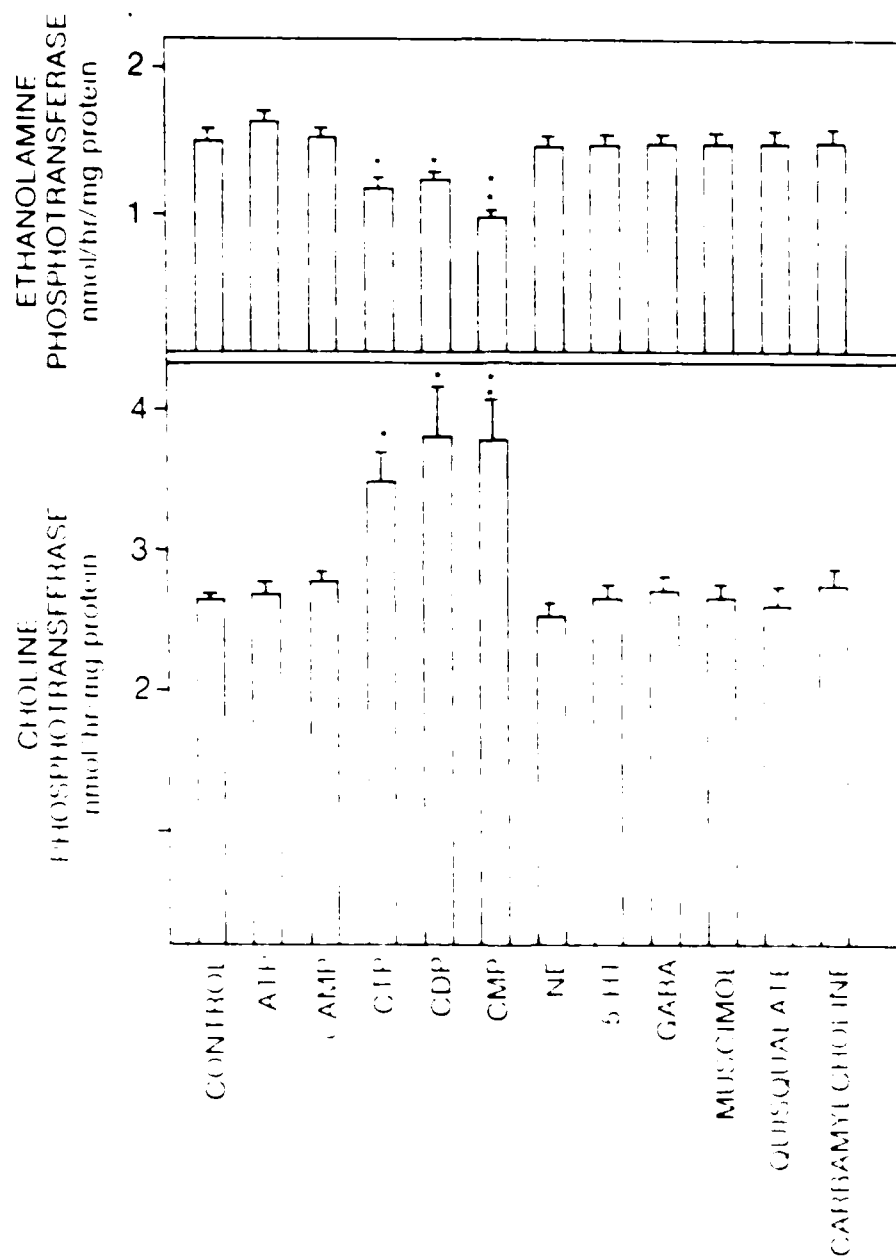
ESTIMATES OF  $K_m$  AND  $V_{max}$  VALUES FOR CHOLINE AND  
ETHANOLAMINE PHOSPHOTRANSFERASE ENZYMES  
IN THE PURIFIED GLOMERULI FRACTION

	CHOLINE PHOSPHOTRANSFERASE	ETHANOLAMINE PHOSPHOTRANSFERASE
$V_{max}$ nmol/hr/mg protein	25.9	10.9
$K_m$		
1,2-diols (mM)	2.9	2.1
CDPcholine ( $\mu$ M)	28.6	---
CDPethanolamine ( $\mu$ M)	---	6.5

Assays were performed as described in Experimental Procedures, except exogenous diglycerides (1,2-diols) were included at concentrations from 0.5 to 10.0 mM, and [ $^{14}$ C]CDPcholine and [ $^{14}$ C]CDPethanolamine concentrations were varied from 5 to 100  $\mu$ M. The apparent  $K_m$  and  $V_{max}$  values were estimated from the results of four separate experiments, according to Eisenthal and Cornish-Bowden (57).







**Dynamics of Large Scale Vortex Structures  
And Quasi-Large Scale Structures in  
the Wake of a Splitter Plate**

**Part I - Structure of Steady Base Flow**

by

**Steven A. Lottes and Paul H.H. Chiu**

**Department of Mechanical Engineering  
The University of Illinois at Chicago  
Chicago Illinois**

**May 1, 1986**

# ABSTRACT

This study is an integral part of the research on vortex shedding from a splitter plate that separates a low speed hot flow and a high speed cold. This paper extends Goldstein, Cheng, Kovitz, and Chiu's wake solutions to the flow configuration involving the asymmetric mixing of two streams of different velocity with prescribed temperature and velocity ratio at the trailing edge of the plate. The predicted wake structure in the proximity of the trailing edge reveals momentum transport from faster to slower stream which shifts the point of zero shear from the center of the wake into the slower hot stream. Effects of coupling between energy and momentum due to property variation in the presence of steep temperature gradients are also found to be significant. A two sided mixing layer structure of the trailing wake and its probable effects on vortex shedding is described and research in progress for Part II is discussed.

## INTRODUCTION

The physical mechanisms and conditions for the generation of large scale dynamic structures and subsequent growth or damping within the wake of bluff bodies has become an important area basic research with application to the engineering of combustors. Fuel efficiency, noise generation, including rumble which may lead to mechanical damage or shortened component life, and the ability of the bluff body to stabilize the flame may all be greatly affected by the generation and subsequent shedding of large scale structures from the wakes of bluff bodies.

Many experimental researchers have reported that combustion suppresses vortex shedding from the wakes of bluff bodies [1-4]. However, experimental studies at Wright Aeronautical Propulsion Laboratory by Roquemore et al. [5-8] with bluff body stabilized combustion in a long cylindrical tunnel produced much evidence of vortex shedding. Sturgess and Syed [9] proposed that the vortex shedding was the result of acoustic interaction with the natural frequencies of the long combustion tunnel. Experiments by Roquemore et al. [10] using a unique laser sheet-lighting technique showed the formation and rolling up process of vortices on the wake interface of an unducted bluff body combustor operated in a cold flow mode. When operated with combustion disturbances grew and propagated along the interface to the tip of the wake, but the characteristic rolling up observed in the cold flow was absent in the hot flow cases. These experiments are providing much information about

the types of large scale dynamic structures that occur in bluff body wakes and the conditions under which they occur in the flow field.

Theoretical work, based on knowledge gained in experiments, is needed to identify the physical mechanisms which lead to the formation of the various large scale structures in bluff body wakes and to determine the parameters which control the growth rates of these structures. Efforts at analysis or direct numerical simulation of these flows are hampered by their complexity including their fundamental 3-dimensional nature as revealed in the films of Roquemore et al. [10]. Even 2-dimensional unsteady computations use large amounts of computing resources; 3-dimensional unsteady computations with enough nodes to avoid grid sensitivity are prohibitively expensive on current large computers. Under these circumstances theoretical studies which deal with a simplified geometry and concentrate on a few of the characteristics of the flow considered most important, such as the presence of shear layer with a large temperature gradient across the layer.

In an initial analytical effort in the study of disturbance formation and growth, Chiu [11] simplified the geometry by considering the interaction of two semi-infinite streams. Additional simplifying assumptions were the absence of body or viscous forces with the shear layer idealized as a vortex sheet in the presence of an initial step temperature difference across the streams. Results of the analysis yielded stability conditions, and disturbance growth rates and propagation velocities

for the idealized flow. In particular, in the absence of mass injection, the flow is always unstable, even in the presence of a temperature difference across the streams. However, as the temperature ratio approaches infinity, the rate of disturbance growth approaches zero. If effects of viscous damping were taken into account another point of neutral stability at some finite temperature ratio would be expected.

The work reported here seeks to relax three of the major simplifying assumptions of Chiu's initial study. These include the assumption of an infinitely thin vortex sheet, the assumption of semi-infinite streams, and the assumption of an inviscid fluid model. The geometry is kept simple by considering the flow in the wake of a splitter plate (figure 1). The free-stream velocities of the upper and lower streams are different producing a shear layer in the downstream of the plate. The temperatures of the two streams are also different. For definiteness, the upper stream is taken to be fast and cold compared to the lower stream. The gravity vector is assumed not to have a component in the computational plane, and therefore, this choice of free-stream velocities and temperatures has no implications in regards to the effects of buoyancy on the stability or other characteristics of the flow. The choice is meant to correspond in some important aspects to an incoming stream of cold air interacting with a hot slower moving stream in the recirculation zone behind a bluff body in a bluff body combustor.

The planned basis for this work was the work of Goldstein [12], and later that of Kovitz [13], and Chiu [14]. These

researchers developed solutions in the form of universal functions for the flow in the near wake of a flat plate which matched Blasius profiles at the trailing edge of the plate. The near wake is considered to be a prime candidate breeding ground for vortices or other large scale structures which grow and propagate into the downstream, therefore use of these earlier methods along with judicious use of modern computational methods appears to offer the opportunity to make substantial progress on the problems of interest in this study. Unfortunately the solutions generated in this earlier work could not be used as the steady state basis of the current study, because that work assumed the flowfield to be symmetric about the centerline (the free-stream velocities of the streams were assumed to be equal), and certain property variations were assumed small, in particular the density-viscosity product, to allow decoupling of the momentum and energy equations. In fact as the temperature of air at atmospheric pressure varies from 300K to 1200K, property variations can be quite significant; the density-viscosity product varies, for example, by 56 percent. With the availability of computers and modern computational techniques, decoupling of the momentum and energy equations is not required to obtain a solution.

The effects of shear and of property variation due to large temperature gradients in the flowfield are considered to be of central importance in the study of the growth of disturbances at the interface between the two streams. Therefore, this study has been divided into two parts. The first part pro-



vides a steady flow generalization of earlier work which allows for streams of different velocities, and takes better account of property variation within the flowfield. The second part encompasses the unsteady stability analysis of the generalized splitter plate wake flow.

The remainder of this paper will deal with Part I. The formulation of the steady flow problem with its generalizations are presented, followed by a discussion of applicable numerical techniques. The formulation leads to a sequence of systems of ordinary differential equations. A computer program which solves the zero order system is included in the appendix. Solutions of the zero order system are presented and discussed.

### OBJECTIVES

The objectives of this part of the research effort are to produce a solution procedure in the form of a computer program for a generalized steady state near plate wake flow problem. The results will provide new near wake flow solutions for steady flow as well as a basis for stability analysis of the near plate wake region. The generalization will relax the assumptions of Kovitz [13] that the freestream velocities of the two streams are equal, and that the density-viscosity product is constant.

## MATHEMATICAL FORMULATION

### Problem Definition and Method of Analysis

The near wake region of a splitter plate is considered as shown in figure 1. The subscript 1 refers to the upper half plane, while 2 refers to the lower half plane.  $U_1$  and  $U_2$  are the free-stream velocities. Blasius profiles are assumed at the coordinate origin at the trailing edge of the plate. The temperature profiles are taken to be uniform at the origin. For definiteness  $U_1$  is taken to be greater than or equal to  $U_2$  and  $T_2$  is taken to be greater than or equal to  $T_1$ . The methods of analysis of Goldstein [12] and subsequently Kovitz [13] are applied to the governing equations. In this approach a Howarth transformation is applied to the governing equations which yields an incompressible form of the continuity equation. The additional assumption of constant density-viscosity product, not applied here, yields an incompressible momentum equation and decouples momentum and energy equations. This study does not make this constant property assumption and consequently leaves the momentum and energy equations coupled. The equations are nondimensionalized in the same way as Kovitz [13] so that the base solution can be compared with his to partially verify the computer program. Although the flow is not self similar, a similarity type transformation is performed to reduce the dependence of the  $y$ -profiles on the streamwise position and to put the equations in a form that can be easily matched to Blasius profiles at the origin. A series solution in terms of

streamwise coordinate and functions of the cross-stream coordinate is then assumed. Substitution into the governing equations yields a sequence of systems of ordinary differential equations, each of which is relatively simple to solve numerically from solutions of the systems of lower order.

#### Assumptions

The assumptions are similar to those of Kovitz [13], with the exception of those already noted and the condition of no chemical reaction. These assumptions are also consistent with those frequently used in stability analysis of similar types of flows [15].

- a. The flow is assumed to be 2-dimensional, initially laminar, and governed by boundary layer type equations.
- b. There are no external or body forces.
- c. The mean pressure is constant.
- d. There is no chemical reaction.
- e. Stoke's hypothesis holds: bulk viscosity =  $-2\mu/3$
- f. The fluid is a perfect gas.

#### Governing Equations

For convenience the flowfield is divided into an upper and a lower half plane, and governing equations are formulated for each half plane. To economize on notation and presentation of equations, only equations for the upper half plane are given since those for the lower half plane are exactly the same if the y-coordinate for the lower half plane is taken to be poin-

ting downward. Other notation includes a  $\hat{\phantom{x}}$  appearing over variables to denote a physical plane variable, a  $\tilde{\phantom{x}}$  to denote a Howarth transformed variable, and no over symbol to denote a nondimensionalized transformed variable. A coordinate subscript denotes differentiation with respect to that coordinate, and a prime denotes differentiation with respect to  $\eta$ .

Under the assumptions given, the governing equations are:

$$\begin{aligned}(\hat{\rho}\hat{u})_{\hat{x}} + (\hat{\rho}\hat{v})_{\hat{y}} &= 0 \\ \hat{\rho}\hat{u}\hat{u}_{\hat{x}} + \hat{\rho}\hat{v}\hat{u}_{\hat{y}} &= (\hat{\lambda}\hat{u}_{\hat{x}})_{\hat{x}} \\ \hat{\rho}\hat{c}_p(\hat{u}\hat{T}_{\hat{x}} + \hat{v}\hat{T}_{\hat{y}}) - (\hat{\lambda}\hat{T}_{\hat{x}})_{\hat{x}} &= 0 \\ \hat{P} &= \hat{\rho}\hat{R}\hat{T}\end{aligned}$$

The Howarth Transform is:

$$\begin{aligned}\tilde{x} &= \hat{x}, & \tilde{y} &= \int_0^{\hat{y}} \hat{\rho}(\hat{x}, y) / \rho_1 dy \\ \tilde{u} &= \hat{u}, & \tilde{v} &= \rho_1 / \tilde{\rho} (\tilde{v} - \tilde{u} \partial \tilde{y} / \partial \tilde{x})\end{aligned}$$

Applying the transform yields:

$$\begin{aligned}\tilde{u}_{\tilde{x}} + \tilde{v}_{\tilde{y}} &= 0 \\ \tilde{u}\tilde{u}_{\tilde{x}} + \tilde{v}\tilde{u}_{\tilde{y}} &= -(\tilde{\rho}\tilde{u}_{\tilde{x}} / \rho_1) \tilde{u}_{\tilde{x}} \\ \tilde{u}\tilde{T}_{\tilde{x}} + \tilde{v}\tilde{T}_{\tilde{y}} &= 1 / (\rho_1 \tilde{c}_p) (\tilde{\rho}\tilde{\lambda}_{\tilde{x}} / \rho_1) \tilde{T}_{\tilde{x}} \\ \tilde{P} &= \tilde{\rho}\tilde{R}\tilde{T}\end{aligned}$$

#### Nondimensionalization

The following nondimensional variables are defined:

$$\begin{aligned}x &= \tilde{x} / (4L), & y &= \sqrt{R} \tilde{y} / (4L) \\ u &= \tilde{u} / U_1, & v &= \sqrt{R} \tilde{v} / U_1 \\ \theta &= \tilde{T} / T_1, & R &= 4\rho_1 U_1 L / \mu_1 \\ \rho &= \tilde{\rho} / \rho_1, & \tilde{\lambda} &= \tilde{\lambda} / \mu_1 \\ \lambda &= \tilde{\lambda} / \lambda_1, & c_p &= \tilde{c}_p / c_{p1}\end{aligned}$$

Substituting these definitions into the Howarth transformed equations yields:

$$u_{\eta} + v_{\eta} = 0$$

$$u u_{\eta} + v u_{\eta} = (\rho_{\lambda} u_{\eta})_{\eta}$$

$$u \theta_{\eta} + v \theta_{\eta} = 1/(c_p P_r) (\rho_{\lambda} \theta_{\eta})_{\eta}$$

$$\rho = \Omega_T / \theta, \quad \text{where } \Omega_T = T_1 / T_2$$

Now consider the stream function defined by:

$$\gamma_{\eta} = u, \quad \text{and} \quad -\gamma_{\eta} = v$$

Assume that this stream function can be written in the form:

$$\gamma = \epsilon^{-1/3} f(\epsilon, \eta) \quad \text{then} \quad u = \epsilon f' / 3$$

where

$$\epsilon = x^{1/3}, \quad \text{and} \quad \eta = y x^{-1/3} / m$$

Matching Blasius profiles at the origin requires that  $m=3$ .

Transforming to  $(\eta, \epsilon)$  coordinates and substituting the stream function into the governing equations satisfies the continuity equation identically and yields the following momentum and energy equations:

$$(\rho_{\lambda} f'')' + 2ff'' - f'^3 = \epsilon(f' \partial f' / \partial \epsilon - f'' \partial f / \partial \epsilon)$$

$$(\rho_{\lambda} \theta')' + 2f\theta' = (1/P_r c_p) \epsilon(f' \partial \theta / \partial \epsilon - \theta' \partial f / \partial \epsilon)$$

For large  $\epsilon$ , these equations could be solved numerically using free-stream values of the upper and lower streams as boundary conditions and continuity of variables and their gradients at the centerline as junction conditions. However, a solution for small  $\epsilon$  is sought here which requires matching the Blasius velocity profiles as  $\epsilon \rightarrow 0$  and  $\eta \rightarrow \infty$  for small constant  $y$ . To find a small  $\epsilon$  solution, expand the dependent variables in series about  $\epsilon = 0$ :

$$f(\eta, \epsilon) = \sum \epsilon^j f_j(\eta), \quad \theta(\eta, \epsilon) = \sum \epsilon^j \theta_j(\eta)$$

To handle property variation, approximate data for  $\rho_\mu$  and  $\rho_\lambda$  as third degree polynomials:

$$\rho_\mu = \sum_{j=0}^3 a_j \theta^j, \quad \rho_\lambda = \sum_{j=0}^3 a_j \theta^j$$

Using the expansion of  $\theta$ , write:

$$\theta_2 = \sum C_j \epsilon^j, \quad \text{where} \quad \begin{aligned} C_0 &= \theta_2, \\ C_1 &= 2\theta_0 \theta_1, \\ C_2 &= 2\theta_0 \theta_2 + \theta_1^2, \\ C_3 &= 2\theta_0 \theta_3 + \theta_1 \theta_2, \dots \end{aligned}$$

$$\theta^3 = \sum D_j \epsilon^j, \quad \text{where} \quad \begin{aligned} D_0 &= \theta_2^3, \\ D_1 &= 3\theta_0 \theta_1, \\ D_2 &= 3\theta_0 \theta_2 + 3\theta_1 \theta_1, \\ D_3 &= 3\theta_0 \theta_3 + 6\theta_0 \theta_1 \theta_2 + \theta_1^3, \dots \end{aligned}$$

Substitution of these series into the polynomial approximations for  $\rho_\mu$  and  $\rho_\lambda$  yields:

$$\rho_\mu = \sum E_j \epsilon^j, \quad \rho_\lambda = \sum F_j \epsilon^j$$

where:

$$\begin{aligned} E_0 &= a_0 + a_1 \theta_0 + a_2 C_0 + a_3 D_0 \\ E_j &= a_1 \theta_j + a_2 C_j + a_3 D_j \quad \text{for } j > 0 \\ F_0 &= a_0 + a_1 \theta_0 + a_2 C_0 + a_3 D_0 \\ F_j &= a_1 \theta_j + a_2 C_j + a_3 D_j \quad \text{for } j > 0 \end{aligned}$$

Since  $c_p$  variation is small compared to other parameters and does not affect the zero order system,  $c_p$  is taken to be constant and equal to its mean value over the temperature interval. Normalized by the free-stream value of the upper stream, this value is slightly greater than one. To simplify the equations of higher order, the product  $P_r c_p$ , which is close to one for air in the range 300-1200K, is taken to be one. Substitution of the series into the momentum and energy equations yields equations of the form:

$$\mathcal{D}_j \epsilon^j = 0,$$

$$\mathcal{H}_j \epsilon^j = 0,$$

Since  $\epsilon$  is arbitrary,  $G_j = 0$  and  $H_j = 0$  for all  $j$ , which yields the following sets of equations (nonhomogeneous terms have been moved to the right hand side):

Order $j$	Momentum Equations:	$G_j = 0$
0:	$E_0 f_0'' + (2f_0 + E_0) f_0' - (f_0)^2$	$= 0$
1:	$E_0 f_1'' + (2f_0 + E_0) f_1' - 3f_0 f_1 + 3f_0' f_1$	$= -E_1 f_0'' - E_1 f_0'$
2:	$E_0 f_2'' + (2f_0 + E_0) f_2' - 4f_0 f_2 + 4f_0' f_2$	$= -E_1 f_1'' - E_1 f_1' - E_2 f_0'' - E_2 f_0' - 3f_1 f_1' + (f_1)^2$
3:	$E_0 f_3'' + (2f_0 + E_0) f_3' - 5f_0 f_3 + 5f_0' f_3$	$= -E_1 f_2'' - E_1 f_2' - E_2 f_1'' - E_2 f_1' - E_3 f_0'' - E_3 f_0' - 3f_1 f_2' - 4f_2 f_1' + 5f_1 f_2$

Order $j$	Energy Equations:	$H_j = 0$
0:	$F_0 \theta_0'' + (2f_0 + F_0) \theta_0'$	$= 0$
1:	$F_0 \theta_1'' + (2f_0 + F_0) \theta_1' - f_0 \theta_1$	$= -F_1 \theta_0'' - (F_1 + 3f_1) \theta_0'$
2:	$F_0 \theta_2'' + (2f_0 + F_0) \theta_2' - 2f_0 \theta_2$	$= -F_1 \theta_1'' - (F_1 + 3f_1) \theta_1' + f_1 \theta_1 - F_2 \theta_0'' - (F_2 + 4f_2) \theta_0'$
3:	$F_0 \theta_3'' + (2f_0 + F_0) \theta_3' - 3f_0 \theta_3$	$= -F_1 \theta_2'' - (F_1 + 3f_1) \theta_2' + 2f_1 \theta_2 - F_2 \theta_1'' - (F_2 + 4f_2) \theta_1' + f_2 \theta_1 - F_3 \theta_0'' - (F_3 + 5f_3) \theta_0'$

With proper boundary and junction conditions, these coupled pairs of ordinary differential equations can be solved numerically for each order in succession beginning with order zero.

#### Boundary and Junction Conditions

To discuss junction conditions, upper and lower stream variables must be distinguished even though the equations are



the same. Therefore lower stream variables will be identified with an overbar in the discussion to follow. A primary objective of this part of the research is to find steady state solutions to be used as a basis for analyzing the stability of the interface between the two streams in Part II. Because the interface occurs at  $y=0$ , solutions for small  $y$  are sought, which match the Blasius velocity profiles at trailing edge of the plate as  $x$  approaches zero.

#### Boundary Conditions to Match Blasius Velocity Profiles at $x=0$

The Blasius velocity profile at  $x=0$  is given by [12]:

$$u_0 = a_1 y + a_2 y^4 + a_7 y^7 + \dots$$

where

$$a_1 = \alpha/2, \quad a_4 = -0.5\alpha^2/4!, \quad a_7 = 5.5\alpha^3/7!, \quad \dots$$

and  $\alpha = 1.32824$

The limiting process to match the Blasius velocity profile allows  $x=\xi^2$  to approach zero while holding  $y=3\xi\eta$  constant at some small value. With  $u=\xi f'/3=\xi\xi^{j+1}f_j/3$ , the limit  $u \rightarrow u_0$  as  $x \rightarrow 0$  and  $y=\text{constant}$  is equivalent to:

$$\lim_{\substack{\eta \rightarrow \infty \\ \xi\eta = \text{const.}}} \xi\xi^j f_{j-i} = \xi\xi^j a_j 3^{j+1} \eta^j, \quad j=1,2,\dots$$

Matching powers of  $\xi$  in the limit requires that:

$$\lim_{\eta \rightarrow \infty} f_{j-i}/\eta^j = 3^{j+1} a_j$$

in particular as  $\eta \rightarrow \infty$ :

$$\begin{aligned} f_0/\eta &\rightarrow 5.97708, & f_1/\eta^2 &\rightarrow 0 \\ f_2/\eta &\rightarrow 0, & f_3/\eta^2 &\rightarrow -8.93136 \end{aligned}$$

The upper and lower stream velocity profiles at  $x=0$  are related

by:

$$u_0(|y|)/U_1 = \bar{u}_0(|y|)/U_2 \quad \text{or} \quad \bar{u}_0 = u_0/\Omega$$

where:  $\Omega = U_1/U_2$

Consequently, the boundary conditions for the lower stream becomes:

$$\lim_{\eta \rightarrow \infty} \bar{f}_{j-1}/\eta^2 = 3^{j-1}a_j/\Omega$$

in particular as  $\eta \rightarrow \infty$ :

$$\begin{aligned} \bar{f}_0/\eta &\rightarrow 5.97708/\Omega, & \bar{f}_1/\eta^2 &\rightarrow 0 \\ \bar{f}_2/\eta &\rightarrow 0, & \bar{f}_3/\eta^2 &\rightarrow -8.93136/\Omega \end{aligned}$$

Because the inlet temperature is taken to be uniform in each stream in this study, the boundary conditions for  $\theta_j$  and  $\bar{\theta}_j$  are simply:

$$\begin{aligned} \theta_0 &\rightarrow \Omega\tau, & \bar{\theta}_0 &\rightarrow 1, & \text{as } \eta &\rightarrow \infty \\ \theta_j &\rightarrow 0, & \bar{\theta}_j &\rightarrow 0, & \text{as } \eta &\rightarrow \infty \end{aligned}$$

#### Junction Conditions at the Interface Between the Streams

The junction conditions are derived from the continuity of streamlines, velocity, shear stress, temperature, and temperature gradient at the interface between the two streams.

Without loss of generality, take  $f(0,0)=0$ , assigning the dividing streamline the value 0. Continuity of streamlines requires that  $f_j(0)=\bar{f}_j(0)$ , and therefore:

$$f(0,0) = f_0(0) = \bar{f}_0(0) = 0$$

To obtain sufficient conditions to solve the systems of order  $j > 0$ , assume that the deviation of the zero streamline from the  $\epsilon$ -axis is negligibly small for small  $\epsilon$ . According to Crane [16], relaxing this assumption requires taking into consider-

ation terms in the Navier Stokes equations which were neglected under the boundary layer flow assumption. This small deviation assumption is adequate for stability analysis and to determine initial growth rate of disturbances, but would not be adequate to follow long term evolution of disturbances into large rolled up vortices in the downstream of the flow. Using this assumption yields:

$$f_j(0) = \bar{f}_j(0) = 0, \quad \text{for } j > 1$$

Continuity of velocity,  $u=\bar{u}$  at  $\eta=0$ , yields:

$$f'_j(\xi, 0) = \bar{f}'_j(\xi, 0)$$

and so  $f_j(0) = \bar{f}_j(0)$  for all  $j$

The choice of lower stream  $\eta$  coordinate as positive downward requires that gradients match in magnitude but have opposite sign at  $\eta=0$ . Continuity of shear stress yields therefore:

$$\bar{f}''_j(\xi, 0) = -f''_j(\xi, 0)$$

and so  $\bar{f}'_j(0) = -f'_j(0)$  for all  $j$

Similarly, continuity of temperature and temperature gradient at  $\eta=0$  yields:

$$\bar{\theta}_j(0) = \theta_j(0)$$

$$\bar{\theta}'_j(0) = -\theta'_j(0) \quad \text{for all } j$$

### NUMERICAL METHOD

In the previous section, the problem was formulated as a sequence of systems of ordinary differential equations, each system containing four equations. Because these systems are not initial value problems, straight forward numerical integration to obtain a solution is not possible, and iterative techniques must be used. Two such techniques, the Shooting Method, and the Integral Method were considered, and a hybrid combination of the two was implemented for solution of the zero order system. The shooting method is discussed in most textbooks on numerical analysis; it generally converges rapidly once the guessed parameters at the initial point are sufficiently close to the solution. In this problem the obvious candidate for the initial point is the interface between the two streams with the guessed parameters being the junction values of the variables. The presence of four unknown parameters ( $f_0, f_0', \theta_0, \theta_0'$ ) at the initial point ( $\eta=0$ ) makes successful implementation of a shooting method a very difficult task. The integral method has been successfully used by Minkowicz to obtain solutions to a variety of boundary layer problems where application of other methods would have been very difficult, see for example [17]. The integral method converts the system of differential equations into integral equations and proceeds by iteratively improving guesses of the unknown functions over the problem interval through successive numerical evaluation of the integrals. When under-relaxation is used, this method is not nearly as sensitive to the initial guess as the shooting method. Eval-

uation of junction parameters for the momentum equations proved to be a problem with the integral method because differences of large nearly equal numbers were involved, which resulted in unacceptable loss of computational significance. As a result of these difficulties, a hybrid algorithm using the shooting method to solve the momentum equations and the integral method to solve the energy equations was developed.

#### Shooting Algorithm for Momentum Equations

The momentum equations are coupled to the energy equations via the functions  $E_1$ ,  $\bar{E}_1$ , and their derivatives appearing in the coefficients of the momentum equations. During one overall iteration, these functions are computed from the latest tentative solution of the energy equations and held constant during solution of the momentum equations.

For computational convenience in the solution of the zero order system,  $f_0'(0)$  is taken as given instead of the parameter  $\Omega_0$ . This approach further reduces the shooting method to one with only one unknown quantity at the initial point. The value of  $\Omega_0$  is then computed from the converged solution. This method will not work for solution of the higher order systems, however, because the value of  $\Omega_0$  is fixed by the solution of the zero order system. The higher order systems require the use of a two parameter shooting method.

The shooting method uses a Runge Kutta algorithm to compute the functions  $f_0$ ,  $f_0'$ , and  $f_0''$  over the interval  $(0, \infty)$ , starting at  $\eta=0$ , using the differential equation, the known

values  $f_0(0)$ ,  $f_0'(0)$ , and the guessed value  $f_0'(0)$ . In practice, computation stops at some finite  $\eta=\eta_0$  which is sufficiently large so that functions have reached their asymptotic behavior to within a desired tolerance.  $\eta_0 = 4$  was found to be sufficiently large in this study. The known boundary value at the end of the interval,  $\eta=\infty$ , is then compared with the computed result and used to compute an improved guess of  $f_0'(0)$  as follows:

Let  $s$  = current guess of  $f_0'(0)$

$s^-$  = value of  $s$  from previous iteration

$s^+$  = improved  $s$  computed from current iteration results

Treat  $f_0'(\infty)$  as a function of  $s$ , then:

$$f_0'(\infty, s^+) = f_0'(\infty, s) + \partial f_0' / \partial s (s^+ - s) = a$$

where  $a = 5.97708$

Estimate the partial derivative as:

$$b = [f_0'(\infty, s) - f_0'(\infty, s^-)] / [s - s^-] = \partial f_0' / \partial s$$

Solve the Taylor expansion for  $s^+$  giving:

$$s^+ = s - [f_0'(\infty, s) - a] / b$$

Using the iteration formula above, iteration continues until:

$$(s^+ - s) / s < 10^{-6}$$

Upon convergence profiles for the upper stream are known along with the values at  $\eta=0$ , therefore, the Runge Kutta algorithm can be used to compute the profiles over the lower stream. The results of the lower stream computation are then used to compute  $\Omega_\infty$  according to:

$$\Omega_\infty = a / f_0'(\infty)$$

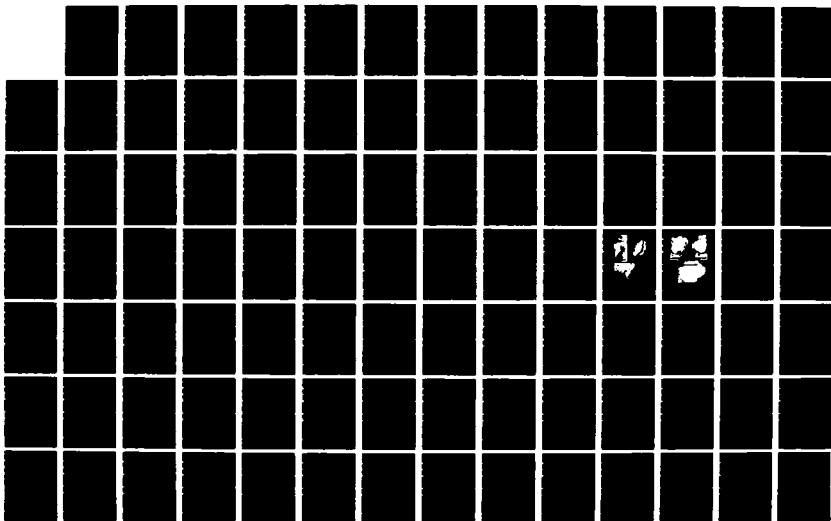
AD-A186 498

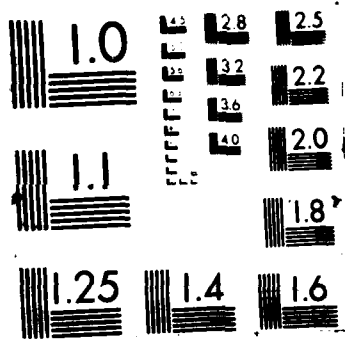
UNITED STATES AIR FORCE RESEARCH INITIATION PROGRAM  
1984 RESEARCH REPORTS (U) SOUTHEASTERN CENTER FOR  
ELECTRICAL ENGINEERING EDUCATION INC 5 W D PEELE  
MAY 86 AFOSR-TR-87-1721 F49628-82-C-8835 F/G 15/1

05/11

UNCLASSIFIED

NL







### Integral Method for Energy Equations

This section will present the integral equations for the zero order energy equations. Derivation of the method for higher orders is similar.

To simplify notation, define:

$$\overline{R}_e = (2\overline{f}_0 + \overline{F}_0)/\overline{F}_0, \quad R_e = (2f_0 + F_0)/F_0$$

$$\beta(\eta) = \exp\left[-\int_0^\eta R_e(s) ds\right], \quad \overline{\beta}(\eta) = \exp\left[-\int_0^\eta \overline{R}_e(s) ds\right]$$

$$I(\eta) = \int_0^\eta \beta(t) dt, \quad \overline{I}(\eta) = \int_0^\eta \overline{\beta}(t) dt$$

The zero order energy equations can be converted into the following integral equations:

$$\theta_0(\eta) = \theta_0(0)\beta(\eta)$$

$$\overline{\theta}_0(\eta) = -\overline{\theta}_0(0)\overline{\beta}(\eta)$$

$$\theta_0(\eta) = \theta_0(0) + \theta_0'(0)I(\eta)$$

$$\overline{\theta}_0(\eta) = \overline{\theta}_0(0) - \overline{\theta}_0'(0)\overline{I}(\eta)$$

Application of boundary and junction conditions leads to:

$$\theta_0'(0) = [\alpha_T - 1]/[I(\infty) + \overline{I}(\infty)]$$

$$\overline{\theta}_0'(0) = [I(\infty) + \alpha_T \overline{I}(\infty)]/[I(\infty) + \overline{I}(\infty)]$$

The integral method computation proceeds as follows:

1. Guess  $\theta_0$ ,  $\overline{\theta}_0$ ,  $\theta_0'$ , and  $\overline{\theta}_0'$  for  $\eta = 1$  to  $\infty$ .
2. Use current guesses of  $\theta_0$ ,  $\overline{\theta}_0$ ,  $\theta_0'$ , and  $\overline{\theta}_0'$  to compute  $F_0$ ,  $F_0'$ ,  $\overline{F}_0$ , and  $\overline{F}_0'$  over the interval.
3. Use results of step 2 and current tentative solution of momentum equations to compute  $R_e$  and  $\overline{R}_e$ .
4. Using numerical integration by trapezoidal rule compute  $\beta$ ,  $\overline{\beta}$ ,  $I$ , and  $\overline{I}$ .

5. From the values of  $I$  and  $\bar{I}$  at the end of the interval compute  $\theta_0(0)$  and  $\theta_0'(0)$ .
6. Use results of step 4 and 5 to compute new profiles of  $\theta_0(\eta)$ ,  $\theta_0'(\eta)$ ,  $\bar{\theta}_0(\eta)$ , and  $\bar{\theta}_0'(\eta)$  over the domain.
7. If iteration has not converged, go to step 2.

#### Hybrid Algorithm for Zero Order System

The hybrid algorithm uses the shooting method to solve the momentum equations and the integral method to solve the energy equations in succession, repeating the process until convergence of the entire coupled system is obtained. A Fortran program implementing this algorithm is listed in the appendix. The results of a computation can be saved on disk for later input as known coefficient functions in a program which solves the equations which arise in stability analysis of the flow.

The program is written in Microsoft Fortran for an IBM PC or compatible computer. The universality of Fortran however allows uploading to a mainframe computer with minor modifications in print and disk storage routines.

## RESULTS AND DISCUSSION

A central issue in this research is whether or not property variation within the flowfield has a significant effect on flow dynamics which might also affect the stability of the flow. If the  $\mu$  constant assumption is valid for flows with a large temperature gradient, then the momentum equation can be decoupled from the energy equation, and temperature variations within the flow would have negligible effects on the dynamics of the flow. This proposition would mean that a flow with combustion would be dynamically equivalent to some isothermal flow. Figure 12 shows the normalized density viscosity product versus normalized temperature for air at atmospheric pressure in the range 300K to 1200K. Assuming  $\mu$  constant approximates these curves as a constant one. From the degree of variation shown in figure 12, a property variation effect on the flow would appear to be expected. Such an effect would mean that a flow with combustion fed with a cold air stream is fundamentally different from any isothermal flow no matter how inlet velocities, etc. are adjusted to achieve Reynolds number similarity between the cold and combusting flows. The computer program developed here solves only the zero order system of equations for the flowfield variables. The solution does, however, give the leading term in the series expansion of these variables, and is sufficient to investigate the main effects of property variation in a steady flow.

The zero order system of equations was solved for a variety of flow conditions using the program listed in the appen-

dix. Runs for isothermal flow ( $T_1/T_2 = 1$ ) with a symmetric wake ( $U_1/U_2 = 1$ ) were made and compared with the results of Goldstein [12], which were re-computed to more significant figures and tabulated by Kovitz [13], verifying the programs capability to solve the momentum equations against a known solution.

Runs were subsequently made for temperature ratios,  $T_1/T_2$ , of 1, .5, and .25. For computational convenience these runs were made holding  $f_0'(0)$  constant at 2.  $f_0'(0)$  is proportional to the leading term of the shear stress along the centerline, and therefore, these runs represent flows with an approximately constant centerline shear stress. Results are shown plotted in figures 2-6. These plots show profiles for the leading term of the stream function, u velocity, u velocity gradient in  $\eta$  direction, temperature, and temperature gradient over both the upper and lower streams. For clarity, the lower stream variables are plotted in terms of the upper stream independent variable  $\eta = -\bar{\eta}$ .

If property variation had negligible effect on flow dynamics, figures 2-4 would show no variation as the temperature ratio decreased. However, these figures do show significant changes in the steady flow of the hot stream as the temperature of the hot fluid is doubled (green lines) and then quadrupled (red lines) as compared to the free stream value of the upper stream. As the temperature of the lower stream increases, the velocity profiles become steeper, which means that the stress in the hot stream increases in magnitude. Since both streams are transporting momentum into the wake toward the

velocity minimum, there is a layer across which the stress reverses sign (figure 4). As temperature increases in the lower stream, this layer becomes thinner and the stress difference across it increases. Whether these differences would have a stabilizing or unstabilizing on the flow is not known.

Temperature profiles are shown in figure 5. These profiles show a smooth transition from the free-stream value of the upper stream to that of the lower stream as expected. They converge to one as  $\eta \rightarrow (-\infty)$  because the temperatures are normalized by the free-stream value of the hot lower stream. Figure 6 shows temperature gradient profiles. These are always negative because the lower stream was chosen to be the hot stream, and so temperature decreases as  $\eta$  increases. These plots also show that as the temperature difference across the streams increases, the profiles steepen, while the thickness of the thermal layer across which the change occurs remains the same. This behavior is due to the step nature of the inlet temperature profiles.

Numerous computer runs were also made for isothermal but asymmetric plate wake flows with varying velocity ratios. The purpose of these runs was to study the steady state effects of having streams of unequal velocities interact across the near plate wake. The results of 300 such runs were collected and are shown plotted in figures 7 to 10.

Figure 7 shows  $f_0'(0)$ , which is proportional to the leading term of the shear stress, versus the velocity ratio. As expected, the shear increases as the velocity ratio increases.

The point of minimum  $u$  velocity at the rear edge of the plate must move from the centerline out to the free-stream of the slower stream as the two streams adjust to each other in the downstream of the wake. Because the lower stream was chosen as the slower stream, the point of minimum velocity therefore occurs in the lower stream. The position of this point in terms of  $(x,y)$  in the near wake region is actually governed by the need to match the Blasius profiles of the incoming streams which determined the definition of  $\eta$ :

$$\eta = y/(3x^{1/3})$$

The point of  $u$  velocity minimum is determined by:

$$f_0''(\eta_{min}) = 0$$

This point, in terms of the  $\eta$  coordinate, is fixed for a given velocity ratio  $U_1/U_2$ , and represents the depth of penetration of the kinematic effects of the faster upper stream into the slower lower stream by transport of momentum through shear forces. From the equation relating  $\eta$ ,  $x$ , and  $y$ :

$$y_{min} = 3\eta_{min} x^{1/3}$$

In terms  $(x,y)$  coordinates,  $\eta_{min}$  gives the rate at which the point of zero shear moves into the hot stream as  $x$  is increased from zero at the trailing edge of the plate.

Figure 8 shows the relation between  $\eta_{min}$  and velocity ratio. As velocity ratio increases,  $\eta_{min}$  also increases, meaning that at fixed  $x$ , the point of zero shear moves deeper and deeper into the hot stream. This shift could have a significant effect on the stability of the flow, and might account for some of the stabilizing effect of the hot stream.

Figures 9 and 10 show the effect of velocity ratio on the leading term of  $u$  velocity at the point of velocity minimum and on the centerline. As the velocity of the lower stream relative to the upper stream decreases, the  $u$  velocity at the velocity minimum also decreases as expected. This effect is less apparent at the centerline where transfer of momentum from the upper stream maintains a higher velocity.

### CONCLUSION

Goldstein, Cheng, Kovitz, and Chiu's wake solutions were extended to the asymmetric mixing of two streams of different velocity with prescribed temperature and velocity ratio at the trailing edge of the plate. The predicted wake structure in the proximity of the trailing edge revealed momentum transport from faster to slower stream which shifts the point of minimum velocity from the center of the wake into the slower hot stream.

Remarkably, the flow configuration near the trailing edge has a slow speed region sandwiched between the upper and lower regions which both have velocities higher than the central slow speed region. As a result, flow in this region is expected to have a propensity to double sided vortex shedding. However, this dynamic configuration starts at the trailing edge and terminates at the point when the minimum velocity in the wake approaches the free stream velocity of the slower stream. This dynamic configuration is a unique characteristic of the trailing edge wake. This structure is distinctly different from a conventional shear layer without a minimum velocity point in the layer. This two sided mixing region structure is conjectured to have vortex shedding characteristics which are significantly different from a conventional single sided mixing layer. These and other aspects will be studied in Part II of the present research program.

Effects of coupling between energy and momentum due to property variation in the presence of steep temperature gradients were also found to be significant.



The problem formulation, based on the methods of the previous researchers, lead to a sequence of systems of ordinary differential equations which allowed such frugal use of computer resources that solution on an IBM PC with math co-processor chip is feasible. While solution of the stability problem in Part II of this research, which will use the program developed here as its base, may require uploading to a mainframe computer, the initial development of this program on a PC was much more efficient than working on a mainframe shared by a large user community.

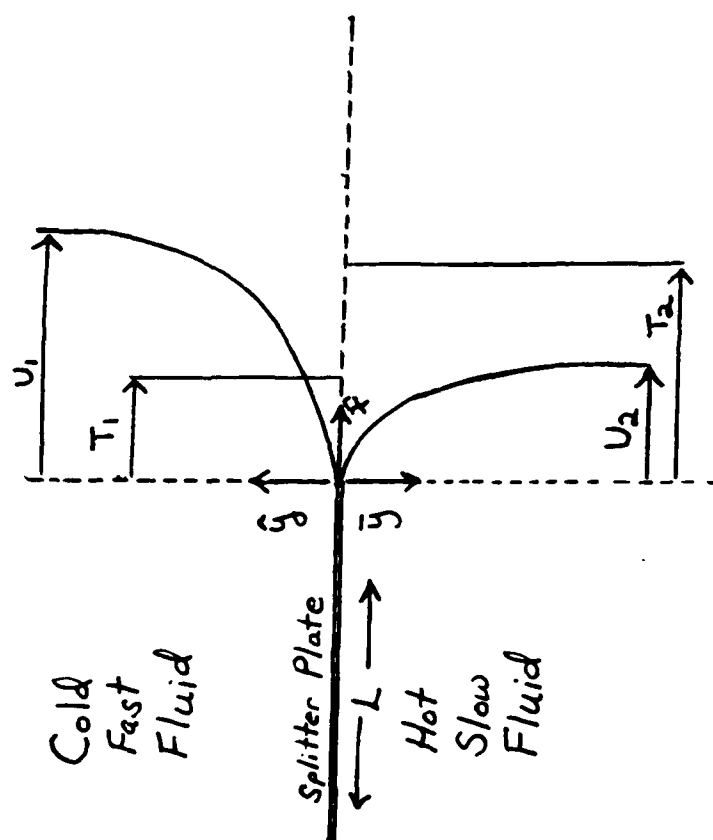


Fig. 1 - Inlet Velocity and Temperature Profiles

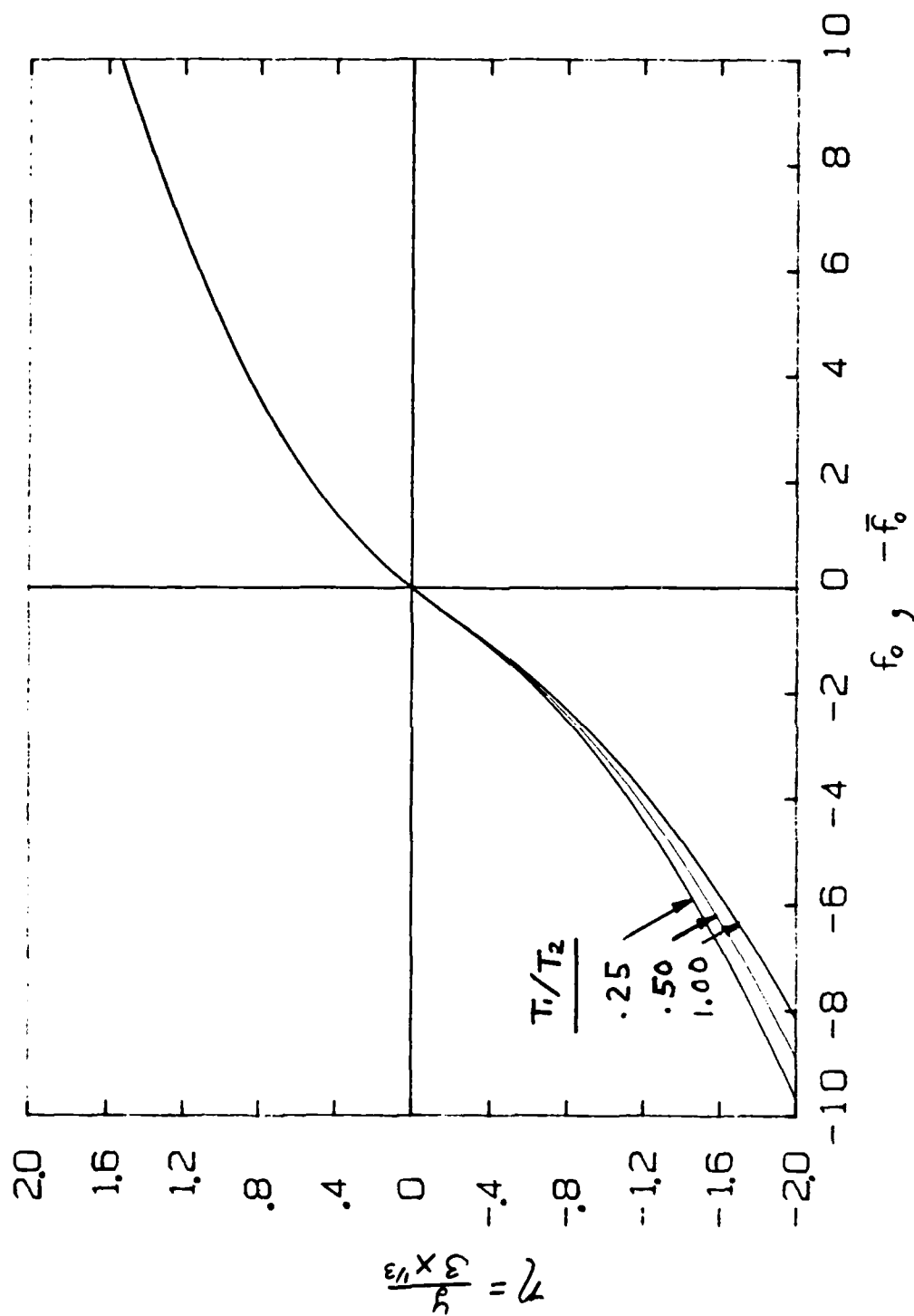


Fig. 2: Stream Function Profiles

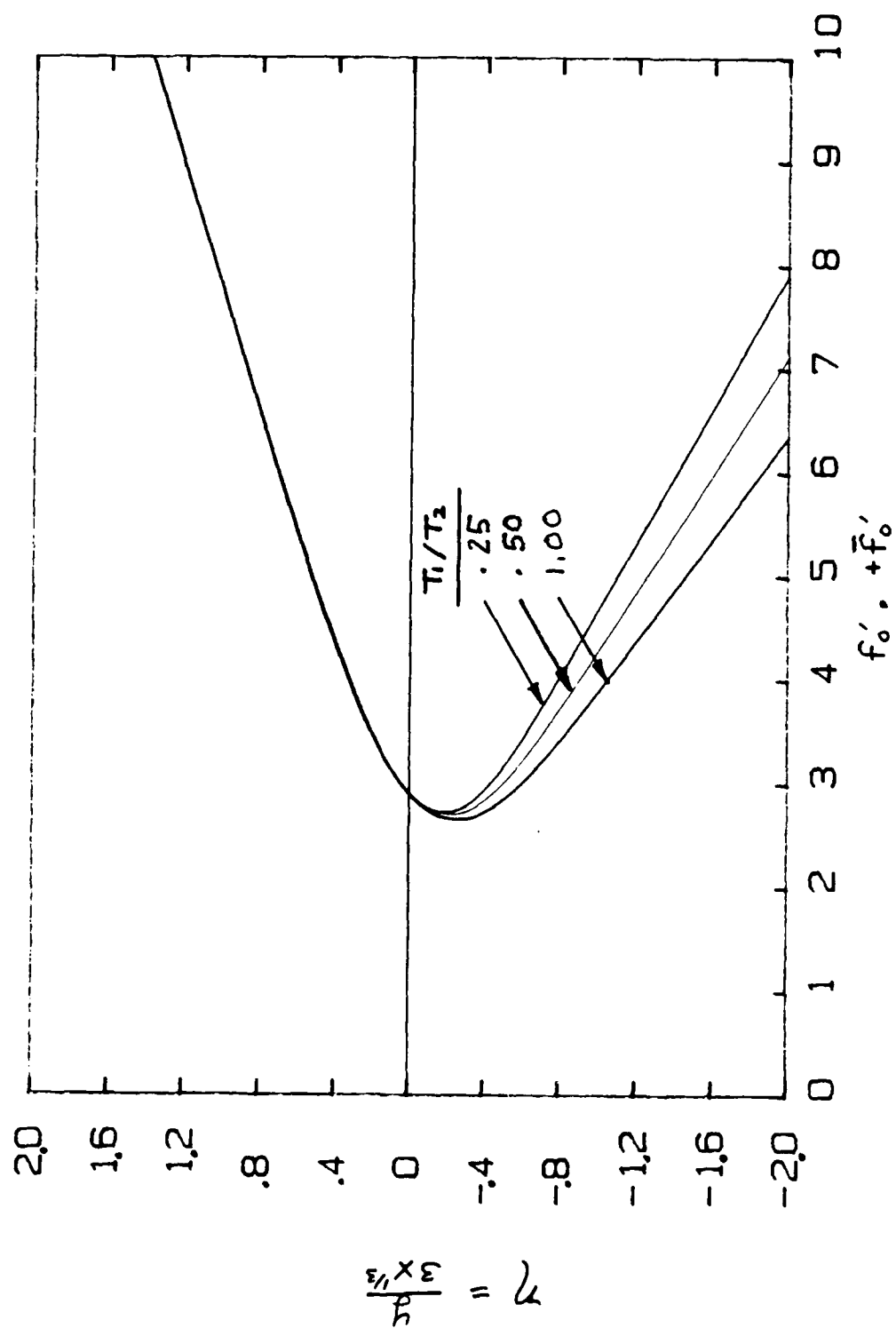


Fig. 3: Zero Order Velocity Profiles

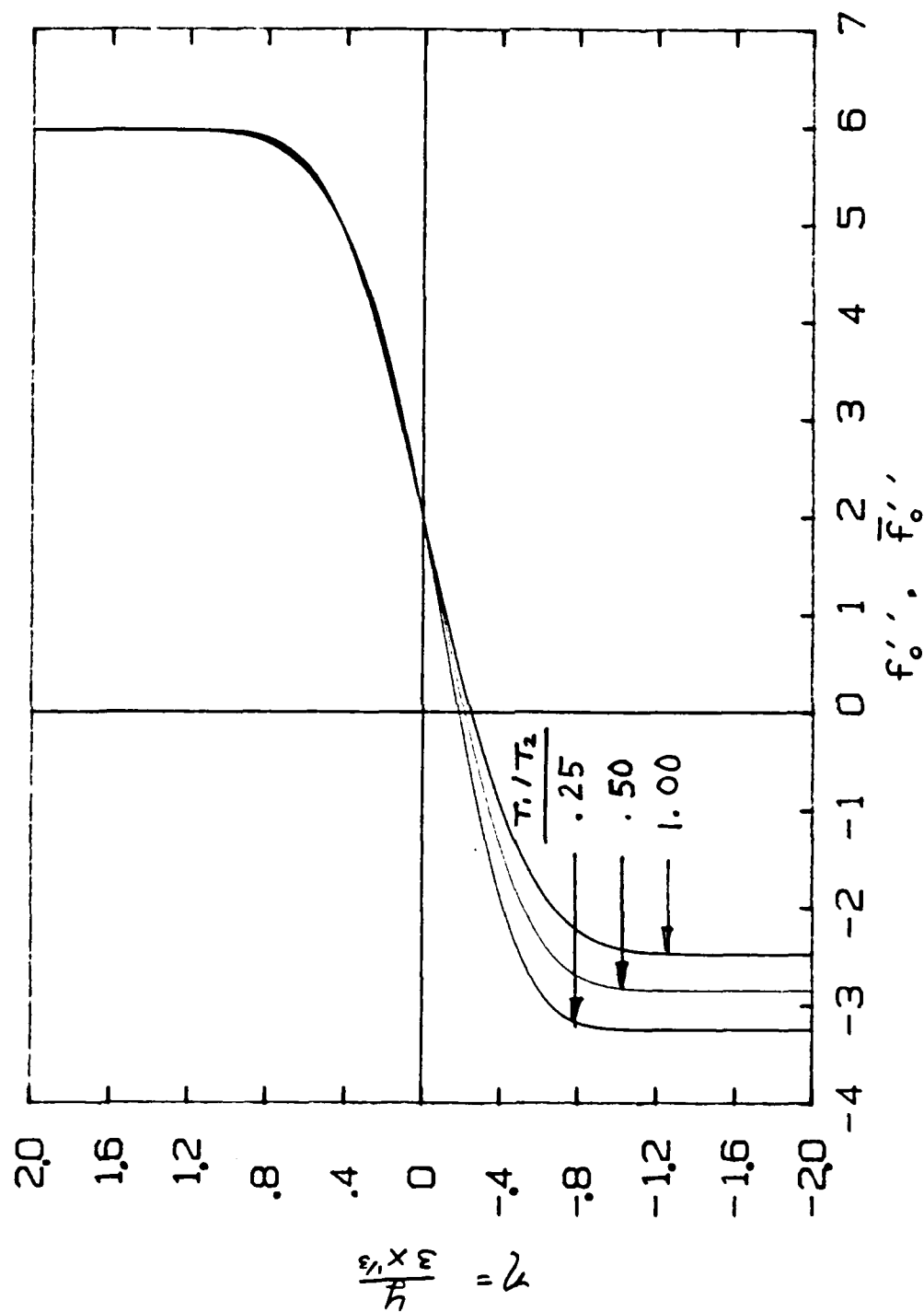


Fig. 4: Zero Order Vel. Grad. Profiles

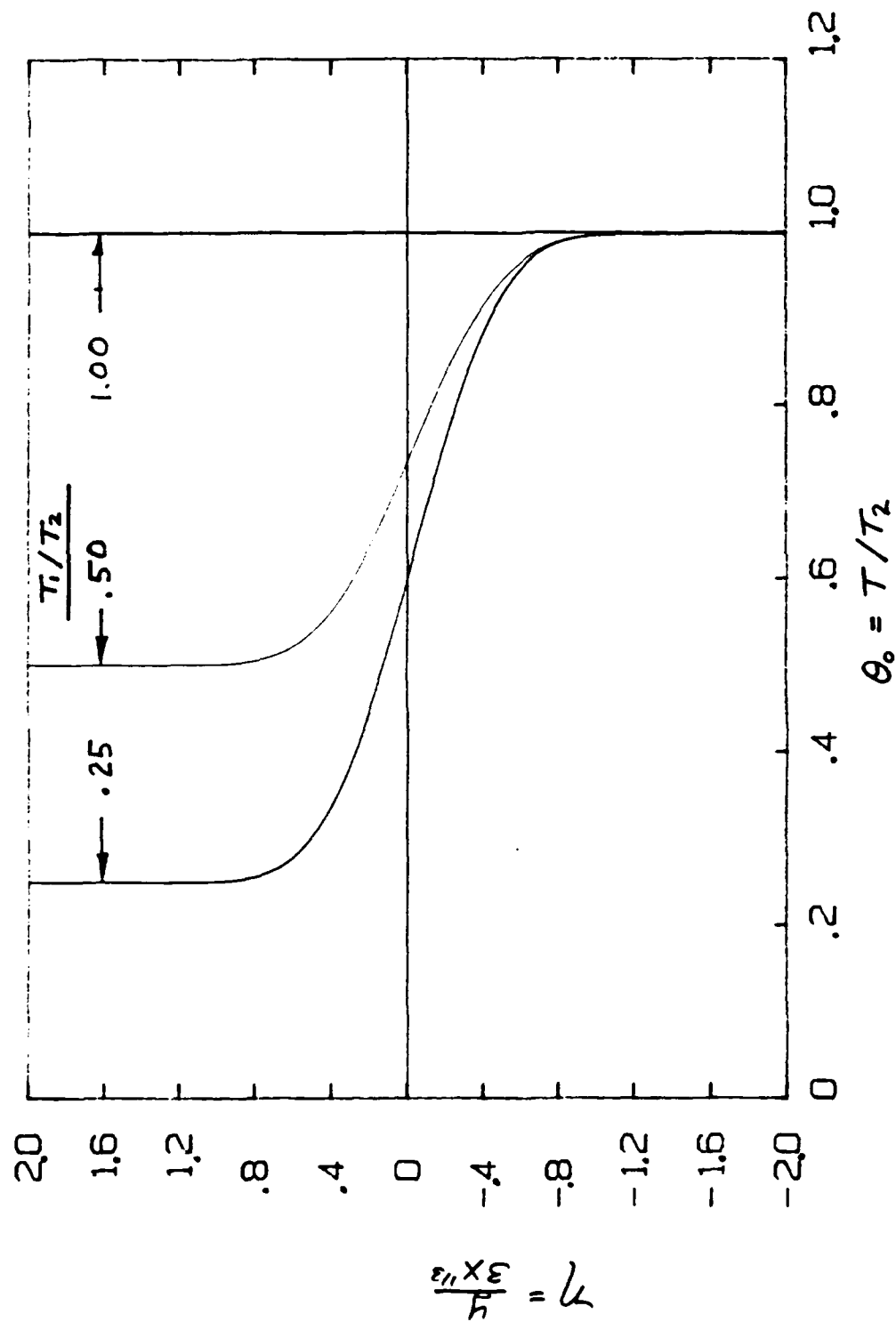


Fig. 5 : Temperature Profiles

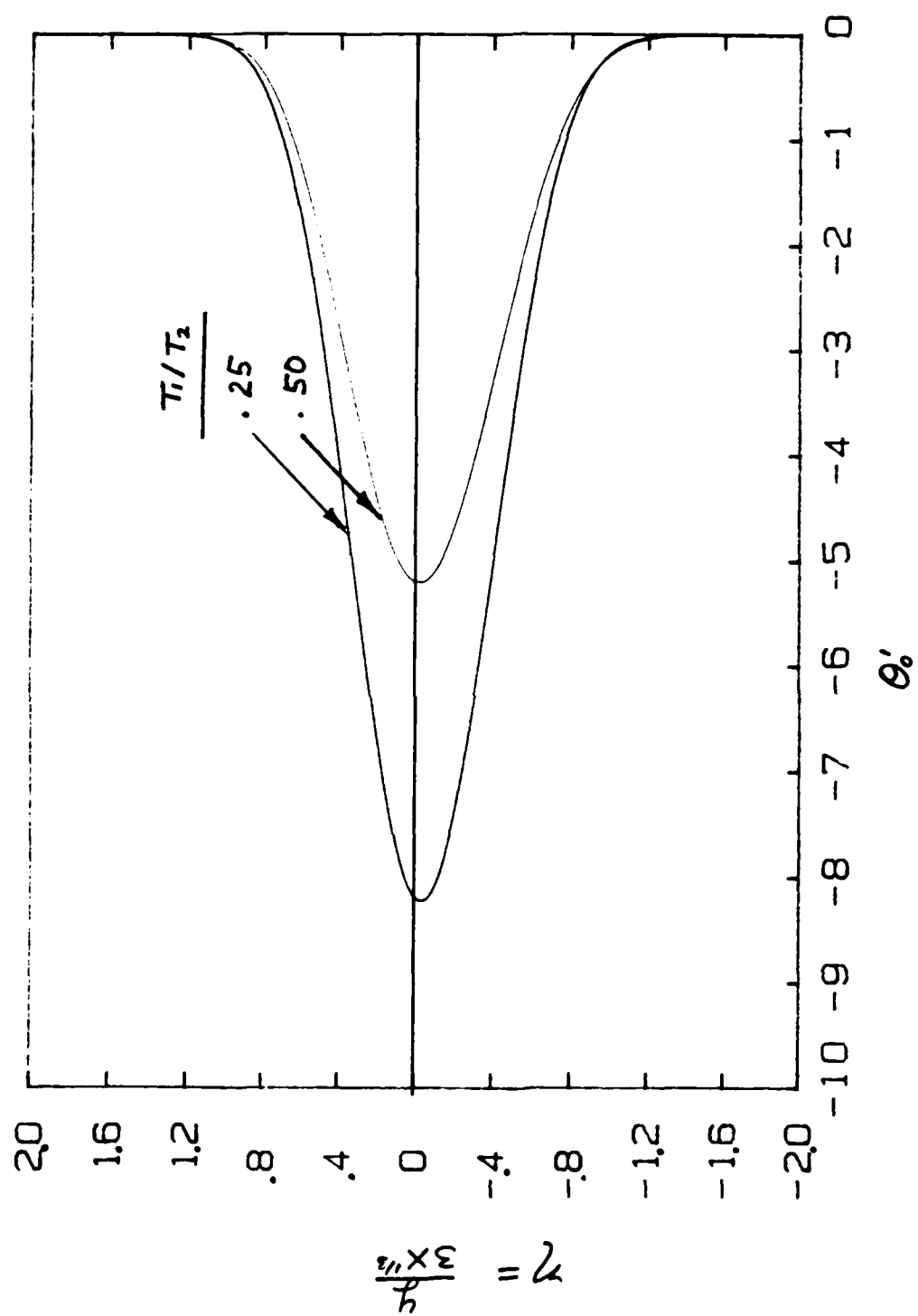


Fig.6 : Temperature Gradient Profiles

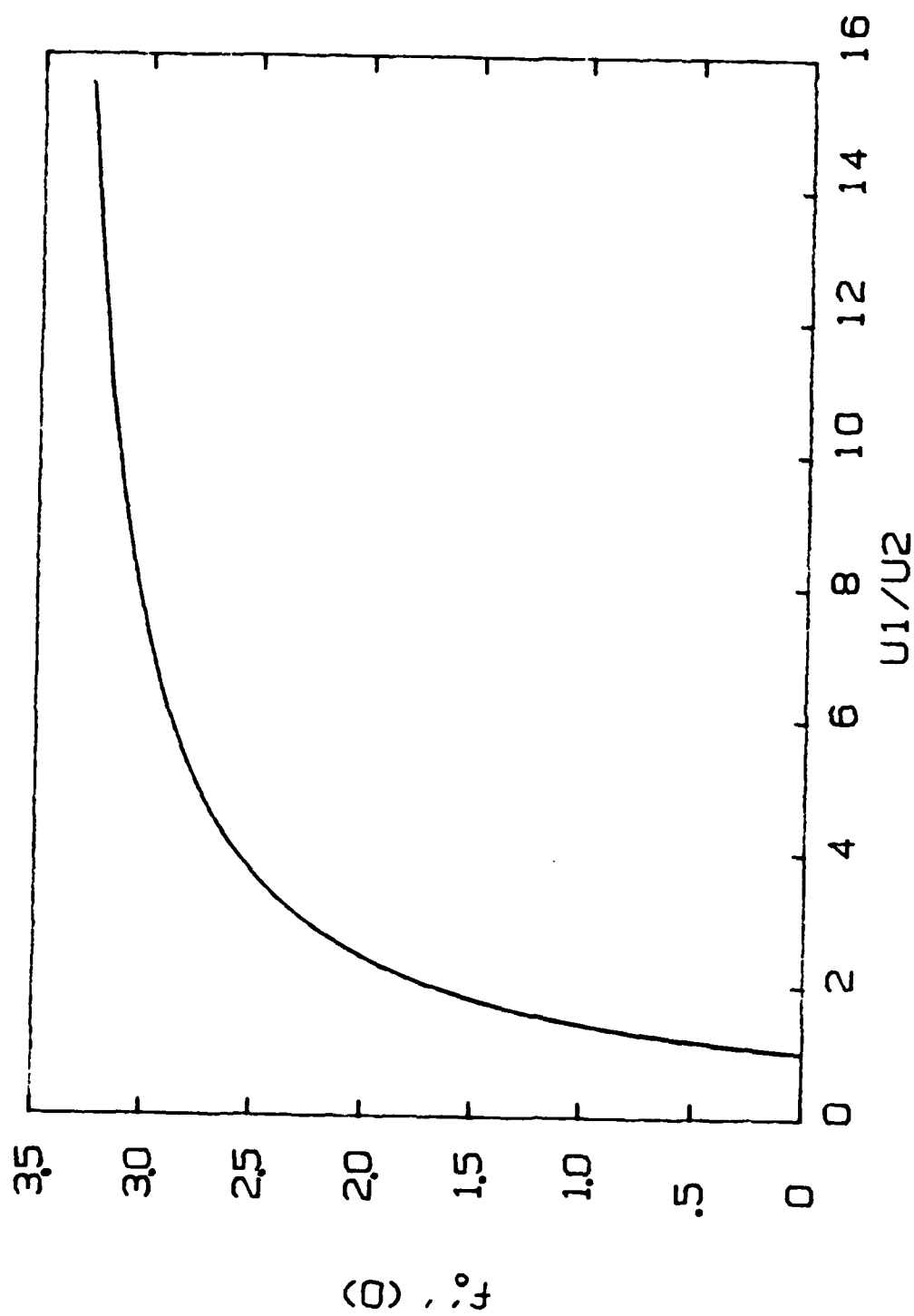


Fig. 7 :  $f''(0)$  vs. Velocity Ratio



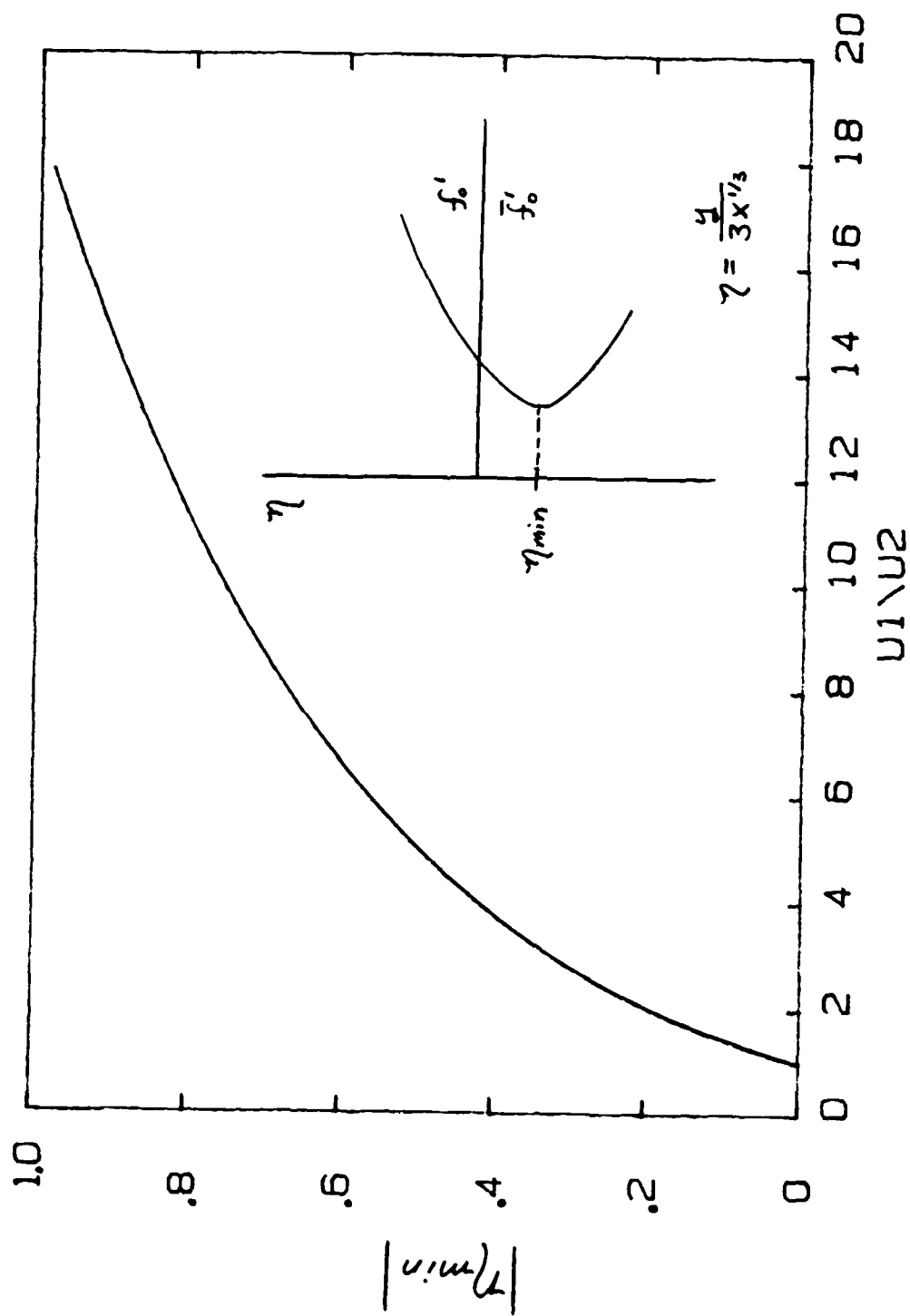


Fig. 8 : Velocity Ratio vs.  $\eta_{min}$

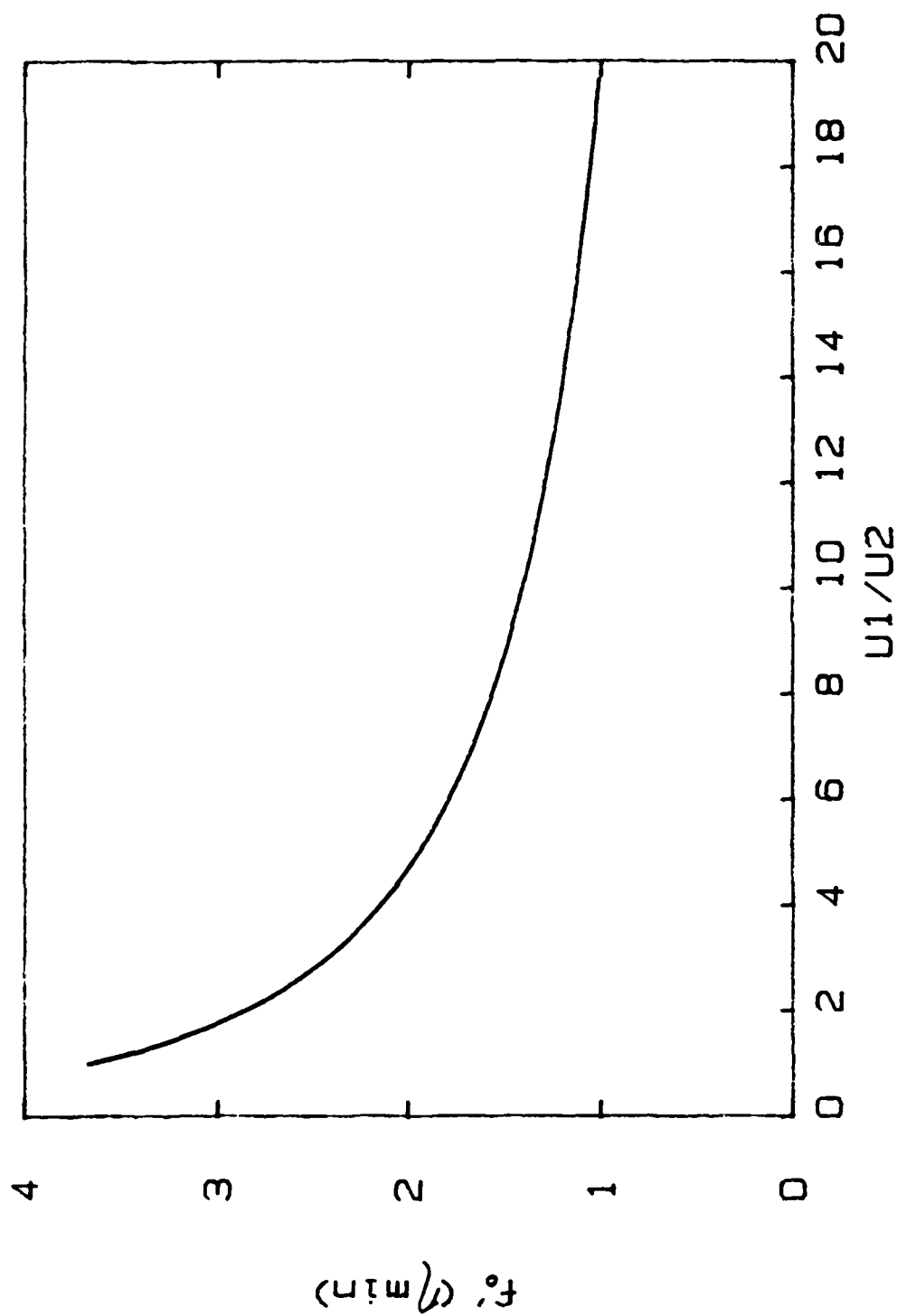


Fig. 9 : Min.  $f'_0$  vs. Velocity Ratio

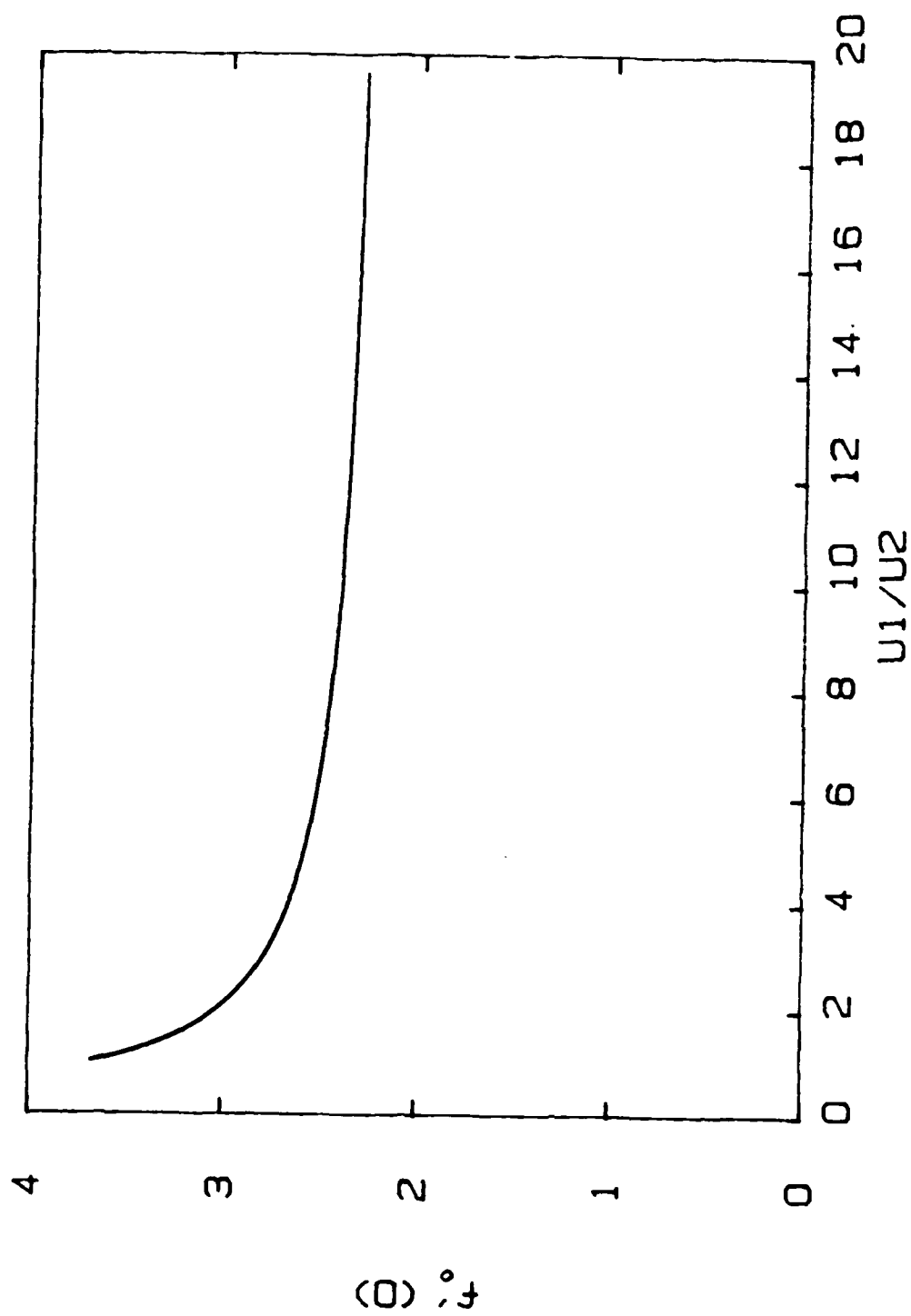


Fig. 10:  $f'(0)$  vs. Velocity Ratio

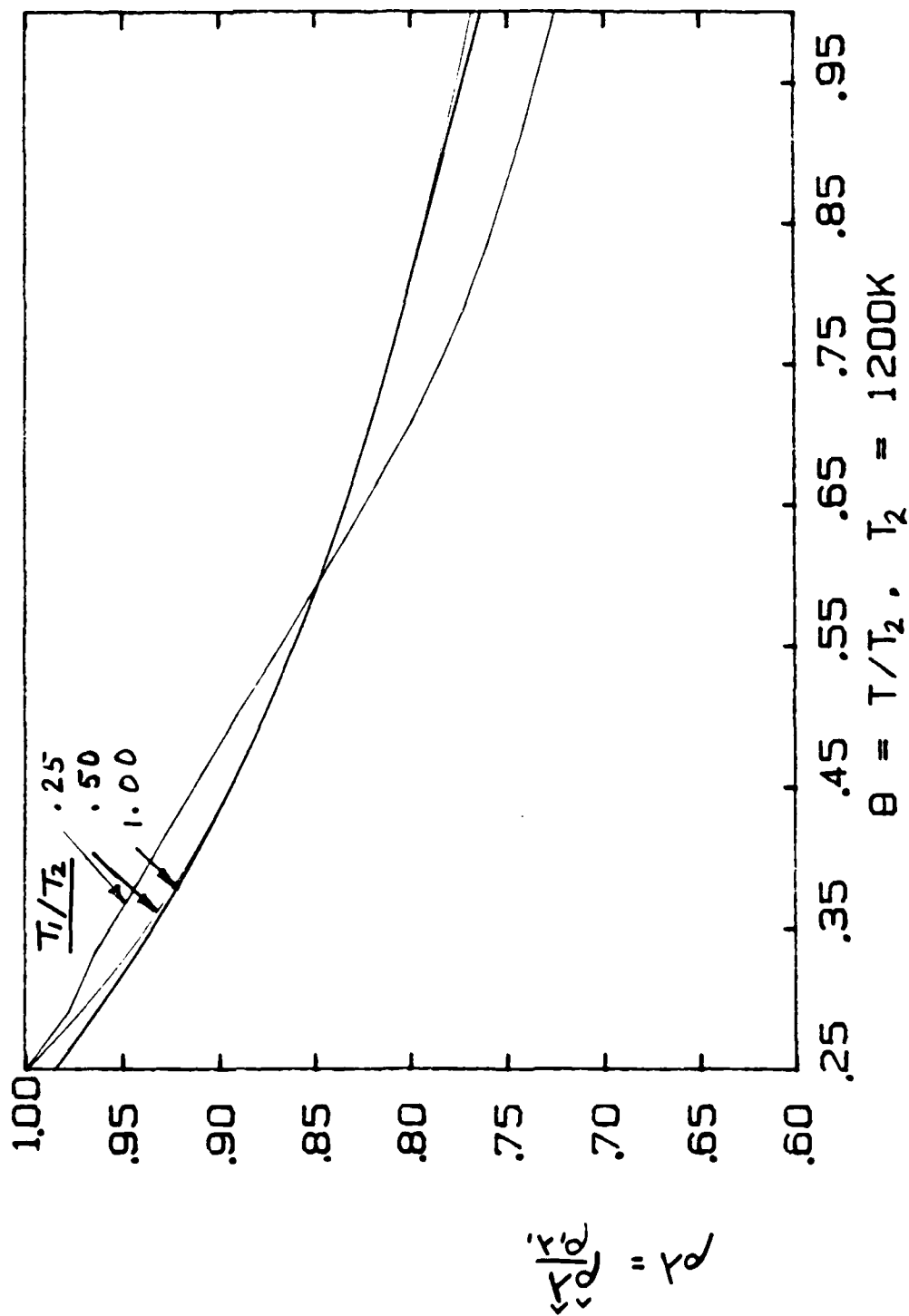


Fig. 11 : Density \* Conductivity for Air

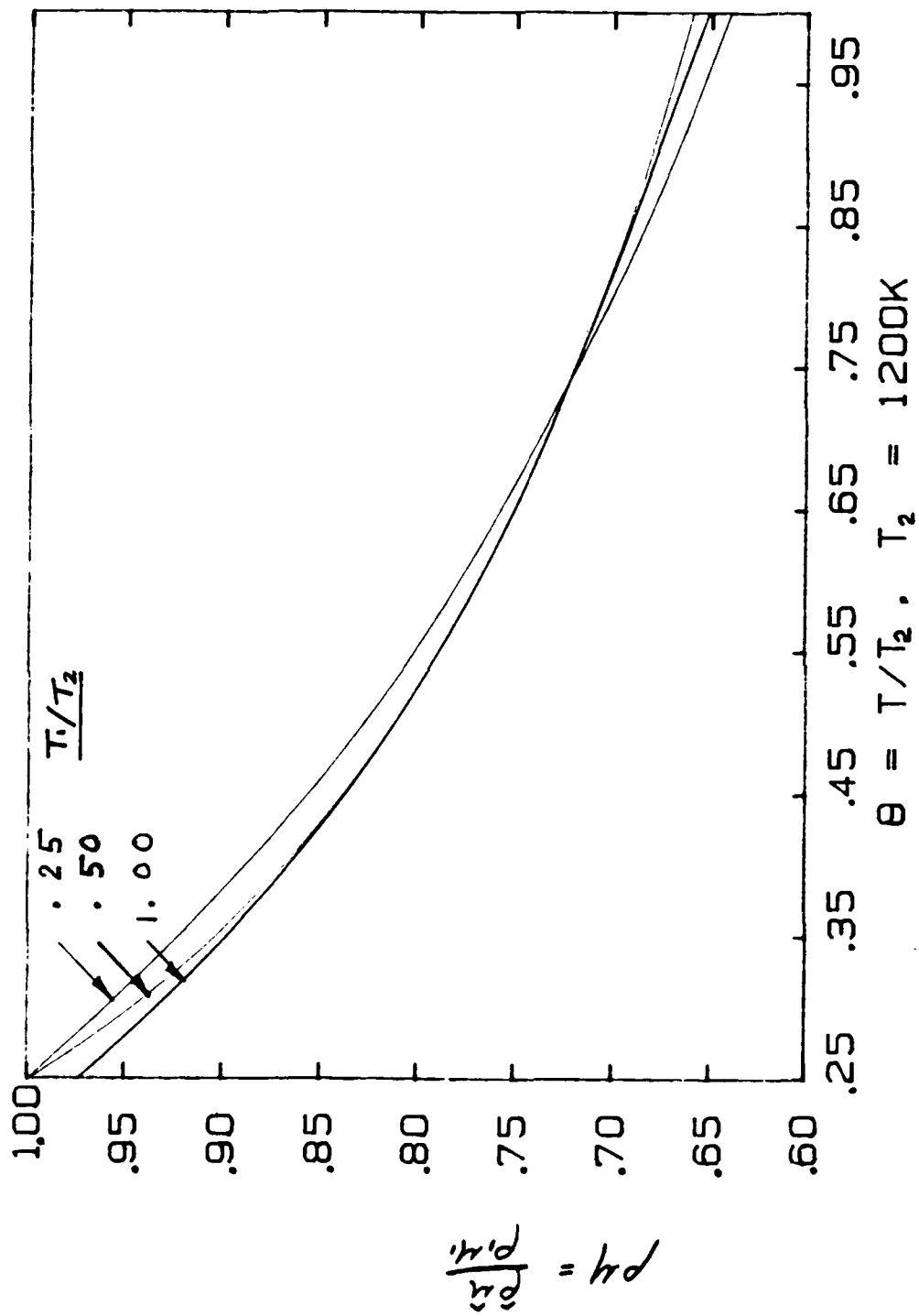


Fig.12: Density \* Viscosity for Air

## REFERENCES

1. Fujii, S., and K. Eguchi, "A Comparison of Cold and Reacting Flows Around a Bluff-Body Flame Stabilizer," J. Fluids Eng., Vol. 103, p. 328, June 1981.
2. Masri, A.R., and R.W. Bilger, "Turbulent Diffusion Flames of Hydrocarbon Fuel Stabilized as a Bluff-Body," Presented at the 21st Combustion Symposium (International), Ann Arbor, Michigan, August 1984.
3. Williams, C.G., H.C. Hottel, and A.C. Scurlock, "Flame Stabilization and Propagation in High Velocity Gas Streams," Third Symposium on Combustion and Flame and Explosion Phenomena, 1949, p. 21.
4. Kaskan, W.E., and A.E. Noreen, "High Frequency Oscillations of a Flame Held by a Bluff-Body," Trans. Am. Soc. Mech. Engrs., August 1955, p. 885.
5. Roquemore, W.M., et. al., "Utilization of Laser Diagnostics to Evaluate Combustor Models," ASARD No. 353, Combustion Problems in Turbine Engines, Sept. 1981, Vol. 19, pp. 1151-1157.
6. Roquemore, W.M., et. al., "Influence of the Vortex Shedding Process of a Bluff-Body Diffusion Flame," AIAA-83-0335, January 1983.
7. Roquemore, W.M., and R.L. Britton, "Investigation of the Dynamic Behavior of a Bluff-Body Diffusion Flame Using Flame Emission," AIAA-82-0178, January 1982.
8. Roquemore, W.M., R.P. Bradley, J.S. Stutrud, C.M. Reeves, and L. Krishnamurthy, "Preliminary Evaluation of a Combustor for Use in Modeling and Diagnostics Development," ASME 80-B1-93.
9. Sturgess, G.J., and S.A. Syed, "Dynamic Behavior of Turbulent Flow in a Widely-Spaced Co-Axial Jet Diffusion Flame Combustor," AIAA-83-0575, January, 1983.
10. Roquemore, W.M., R.S. Tankin, H.H. Chiu, and S.A. Lottes, "The Role of Vortex Shedding in a Bluff-Body Combustor, paper presented at the ASME 105th Winter Annual Meeting, Symposium on Experimental Measurements and Techniques in Turbulent Reactive Flows.
11. Chiu, H.H., Dynamics of Vortex Shedding and Quasi-large Scale Structures in a Bluff-Body Combustor, Final Report 1984 USAB SCEEE Summer Faculty Research Program, October 1984.

12. Goldstein, S., "Concerning Some Solutions of the Boundary Layer Equations in Hydrodynamics," Proc. Cambridge Phil. Soc., Vol. 26, 1930, pp. 1-30.
13. Kovitz, A.A., "Ignition in the Laminar Wake of a Flat Plate," PhD Thesis, Princeton University, 1956.
14. Cheng, S.I., and H.H. Chiu, "Mixing and Chemical Reaction in an Initially Non-Uniform Temperature Field," Int. J. Heat Mass Transfer, Vol. 1, pp. 280-293.
15. Lin, C.C., Theory of Hydrodynamic Stability, Cambridge University Press, 1955.
16. Crane, L.J., "The Laminar and Turbulent Mixing of Jets of Compressible Fluid. Part II The Mixing of Two Semi-infinite Streams, J. Fluid Mech., 1957.
17. Minkowycz, W.J., and P. Cheng, "Free Convection About a Vertical Cylinder Embedded in a Porous Medium," Int. J. Heat Mass Transfer, Vol. 19, pp. 805-813, 1976.

C Splitter Plate Wake  
C with Large Temperature Gradient  
C Solution of Zeroth Order Functions

C Author: S.A. Lettes,

Nov. 15, 1985

C This routine solves the zero order system of differential  
C equations for a nonsymmetric plate wake using the shooting  
C method with a Runge-Kutta routine for the momentum equations  
C and the integral method for the energy equations.

$$E f''' + (2f + E')f'' - f' = 0$$

$$\bar{E} \bar{f}''' + (2\bar{f} + \bar{E}')\bar{f}'' - \bar{f}' = 0$$

$$F \theta + (2f + F')\theta' = 0$$

$$\bar{F} \bar{\theta} + (2\bar{f} + \bar{F}')\bar{\theta}' = 0$$

C B.C.s:  $f(0) = 0, \quad f''(m) = 5.97708$

$$\bar{f}(0) = 0, \quad \bar{f}''(m) = 5.97708/(U1/U2)$$

$$f'(0) = \bar{f}'(0), \quad f'''(0) = -\bar{f}'''(0)$$

$$\theta(m) = T1/T2, \quad \bar{\theta}(m) = 1$$

$$\theta(0) = \bar{\theta}(0), \quad \theta'(0) = -\bar{\theta}'(0)$$

C Main Variable Assignments:

$$f - F0, \quad \bar{f} - F0B, \quad f' - F0P, \quad \bar{f}' - F0PB,$$

$$f'' - F0PP, \quad \bar{f}'' - F0PPB$$

$$\theta - T0, \quad \bar{\theta} - T0B, \quad \theta' - T0P, \quad \bar{\theta}' - T0PB,$$

$$E - EV, \quad \bar{E} - EVB, \quad E' - EVP, \quad \bar{E}' - EVPB,$$

$$F - ET, \quad \bar{F} - ETB, \quad F' - ETP, \quad \bar{F}' - ETPB,$$

$$T1/T2 - T1DT2$$

$$U1/U2 - U1DU2$$

C Inputs: User is prompted for the inputs, which are entered as  
C integers or floating point numbers with decimal point  
C separated by commas.

C 1)  $f''(0)$

C 2) Guess for  $f'(0)$ .

C 3) Length of interval.

C 4) Step size and print step size.



```

C          5) Temperature ratio  $T_1/T_2$ 
C
C      Outputs: The program prints function values
C              and slopes over the interval.
C
C          U1\U2
C
C      -----
C      Initialization and collection of inputs
C      -----
C
$NOFLOATCALLS
$LARGE
$DEBUG
      IMPLICIT REAL*8 (A-H,O-Z)
      CHARACTER*64 FNAME
      CHARACTER*18 UPPER,LOWER
      CHARACTER*10 NAME
C
      DIMENSION Y(3),F(3)
      COMMON/VECTF/F0(801),F0B(801),F0P(801),F0PB(801),
1          F0PP(801),F0PPB(801),F0B(801),F0B(802),X(801)
      COMMON/VECTT/T0(801),T0B(801),T0P(801),T0PB(801),
1          T0B(801),T0B(801)
      COMMON/EV/EV(1601),EVB(1601),EVP(1601),EVPB(1601)
      COMMON/ET/ET(801),ETB(801),ETP(801),ETPB(801)
      COMMON/PROP/AV0,AV1,AV2,AV3,AK0,AK1,AK2,AK3
      COMMON/PARM/DX,IXE,IXE2,IPB,ITMAX,RF,T1DT2,T00,XL,IFP,
1          UPPER,LOWER,U1DU2,U1DU2B
      COMMON/PARMS/Y0,YPPL,YPO0,YPO1,YPP0
      Read initial values, guesses, and parameters.
C
      WRITE(*,1)
1      FORMAT(10X,'Zero Order Plate Wake'//)
      WRITE(*,3)
3      FORMAT(1X,'Enter T1DT2: ')
      READ(*,60)T1DT2
      WRITE(*,5)
5      FORMAT(10X,'Enter DDf(0): ')
      READ(*,60)YPP0
      WRITE(*,7)
7      FORMAT(10X,'Enter guesses for Df(0): ')
      READ(*,60)YPO0,YPO1
      WRITE(*,9)
9      FORMAT(10X,'Enter x1: ')
      READ(*,60)XL
      WRITE(*,11)
11     FORMAT(//10X,'Enter no. of points and points/prints: ')
      READ(*,40)IXE,IPB
      WRITE(*,13)
13     FORMAT(10X,'For full print enter 1, abbreviated print enter 0: ')
      READ(*,40)IFP
40     FORMAT(5I9)
60     FORMAT(4F14.9)
C
C      Set constants

```

```

C      UPPER='Upper Half Plane'
      LOWER='Lower Half Plane'
      IXE2=2*IXE-1
      YO=0.
      YPPL=5.97708
      ITHAX=1000
      DX=XL/(IXE-1)
      DO 52 I=1,IXE
52     X(I)=(I-1)*DX
C      RF = Relaxation factor used in temperature field computation
      RF=.3

C
C      Set Initial Guess for Temperature Dependent Coefficients
C
      DO 70 I=1,IXE
      ET(I)=1.
      ETP(I)=0.
      ETB(I)=1.
      ETPB(I)=0.
70     CONTINUE
      DO 72 I=1,IXE2
      EV(I)=1.
      EVP(I)=0.
      EVB(I)=1.
      EVPB(I)=0.
72     CONTINUE

C
C      Initial Guess of Centerline Temp Fn
C
      T00=(T1DT2+1)/2

C
C      Initialize Coefficients for Property Computation
C
C      Taylor Series for Normalized Density*Viscosity
C
      TVP=T1DT2**3
      TM=(T1DT2+1)/2
      BV0=TVP/TM**3
      BV1=-.3*TVP/TM**1.3
      BV2=.195*TVP/TM**2.3
      BV3=-.897*TVP/TM**3.3/6
      AV0=BV0-TM*(BV1-TM*(BV2-TM*BV3))
      AV1=BV1-TM*(2*BV2-3*BV3*TM)
      AV2=BV2-3*BV3*TM
      AV3=BV3

C
C      Taylor Series for Density*Conductivity
C
      TKP=T1DT2**1.9
      BK0=TKP/TM**1.9
      BK1=-.19*TKP/TM**1.19
      BK2=.11305*TKP/TM**2.19
      BK3=-.0825265*TKP/TM**3.19
      AK0=BK0-TM*(BK1-TM*(BK2-TM*BK3))
      AK1=BK1-TM*(2*BK2-3*BK3*TM)

```

```

      AK2=BK2-3*BK3*TM
      AK3=BK3
C
      CALL VELOCITY
      CALL TEMP
C
      DO 80 I=1,IXE
      FS(I)=FO(I)
      FSB(I)=FOB(I)
      TS(I)=TO(I)
      TSB(I)=TOB(I)
80    CONTINUE
      U1DU25=U1DU2
C-----
C
C      Main Iteration Loop
C
C      The program alternately computes the velocity and temperature
C      fields beginning with the velocity field. The velocity and
C      temperature fields are computed iteratively in subroutines.
C
C      Because  $f'(0)$  is specified for convenience in the computation,
C      the velocity ratio U1DU2 is computed from the results.
C
C      Overall convergence is checked by verifying that the maximum
C      stream function change and change in U1DU2 is below a preset
C      tolerance level after an intervening temperature computation,
C      and that the maximum change in temperature is below a preset
C      tolerance after an intervening velocity computation.
C-----
      DO 200 IT=1,ITMAX
C
      CALL VELOCITY
      CALL TEMP
C
      CHGMX=DABS(U1DU2-U1DU25)/U1DU2
      DO 110 I=2,IXE
      D1=DABS(FO(I)-FS(I))/FO(I)
      D2=DABS(TO(I)-TS(I))/TO(I)
      D3=DABS(FOB(I)-FSB(I))/FOB(I)
      D4=DABS(TOB(I)-TSB(I))/TOB(I)
      CHGMX=DMAX1(D1,D2,D3,D4,CHGMX)
      FS(I)=FO(I)
      TS(I)=TO(I)
      FSB(I)=FOB(I)
      TSB(I)=TOB(I)
110    CONTINUE
      U1DU25=U1DU2
      WRITE(*,120)CHGMX
120    FORMAT(/10X,' ***** CHGMX=',B16.4,' *****'/)
      IF(CHGMX.LE.1D-7)80 TO 300
200    CONTINUE
C-----
C
C      Check and print results
C-----

```

```

C
300  CALL VPRINT(FO,1,IXE,'FO      ')
      CALL VPRINT(FOB,1,IXE,'FOB    ')
      CALL VPRINT(FOP,1,IXE,'FOP    ')
      CALL VPRINT(FOPB,1,IXE,'FOPB  ')
      CALL VPRINT(FOPP,1,IXE,'FOPP  ')
      CALL VPRINT(FOPPB,1,IXE,'FOPPB ')
      CALL VPRINT(TO,1,IXE,'TO      ')
      CALL VPRINT(TOB,1,IXE,'TOB    ')
      CALL VPRINT(TOP,1,IXE,'TOP    ')
      CALL VPRINT(TOPB,1,IXE,'TOPB  ')
      WRITE(*,305)UIDU2

```

```

305  FORMAT(/1X,'----- UIDU2 = ',B16.8,' -----'/)

```

```

C -----
C
C      Write Results on Disk
C -----
C

```

```

2999  WRITE(*,3000)
3000  FORMAT(1X,'Enter 1 to save results on disk: ')
      READ(*,3001)ISAVE
3001  FORMAT(I5)
      IF(ISAVE.NE.0)THEN

```

```

          FNAME='D:N.O'
          CALL WDISK(X,FNAME,IXE)
          FNAME='D:FO.X'
          CALL WDISK(FO,FNAME,IXE)
          FNAME='D:FOP.X'
          CALL WDISK(FOP,FNAME,IXE)
          FNAME='D:FOPP.X'
          CALL WDISK(FOPP,FNAME,IXE)
          FNAME='D:FOB.X'
          CALL WDISK(FOB,FNAME,IXE)
          FNAME='D:FOPB.X'
          CALL WDISK(FOPB,FNAME,IXE)
          FNAME='D:FOPPB.X'
          CALL WDISK(FOPPB,FNAME,IXE)
          FNAME='D:TO.X'
          CALL WDISK(TO,FNAME,IXE)
          FNAME='D:TOB.X'
          CALL WDISK(TOB,FNAME,IXE)
          FNAME='D:TOP.X'
          CALL WDISK(TOP,FNAME,IXE)
          FNAME='D:TOPB.X'
          CALL WDISK(TOPB,FNAME,IXE)

```

```

      ENDIF

```

```

      STOP
      END

```

```

C -----
C
C      Velocity Distribution Computation
C -----
C

```

```

      SUBROUTINE VELOCITY

```

```

      IMPLICIT REAL*8 (A-H,O-Z)

```

```

CHARACTER*64 FNAME
CHARACTER*18 UPPER,LOWER
CHARACTER*10 NAME
DIMENSION Y(3),F(3)
COMMON/VECTF/FO(801),FOB(801),FOP(801),FOPB(801),
1      FOPP(801),FOPPB(801),FB(801),FBB(802),X(801)
COMMON/EV/EV(1601),EVB(1601),EVP(1601),EVPB(1601)
COMMON/PROP/AV0,AV1,AV2,AV3,AK0,AK1,AK2,AK3
COMMON/PARM/DX,IXE,IXE2,IPS,ITMAX,RF,T1DT2,T00,XL,IFP,
1      UPPER,LOWER,U1DU2,U1DU2S
COMMON/PARMS/Y0,YPPL,YP00,YP01,YPPO

C
JX=1
Y(1)=YPPO
Y(2)=YP00
Y(3)=Y0
CALL RUNGE0(Y,JX,IXE,DX,X,FO,FOP,FOPP,EV,EVP,0)
YPPL0=Y(1)
WRITE(*,81)
81  FORMAT(/IX,'Velocity Computation Iteration'/)
I=0
WRITE(*,90)I,YP00,YPPL0
90  FORMAT(IX,I4,' FPO=',G18.12,' FPPL=',G18.12)
C
DO 300 I=1,ITMAX
JX=1
Y(1)=YPPO
Y(2)=YP01
Y(3)=Y0
CALL RUNGE0(Y,JX,IXE,DX,X,FO,FOP,FOPP,EV,EVP,0)
YPPL1=Y(1)
A=(YPPL1-YPPL0)/(YP01-YP00)
YPPL0=YPPL1
YP00=YP01
YP01=YP00-(YPPL1-YPPL)/A
ERR=DABS((YPPL-YPPL1)/YPPL)
WRITE(*,100)I,YP00,YPPL0,ERR
100 FORMAT(IX,I4,' FPO=',G18.12,' FPPL=',G18.12,' ERR=',G12.4)
IF(ERR.LT.1D-8)GO TO 1000
300 CONTINUE
1000 FO(1)=Y0
FOP(1)=YP01
FOPP(1)=YPPO
JX=1
Y(1)=YPPO
Y(2)=YP01
Y(3)=Y0
CALL RUNGE0(Y,JX,IXE,DX,X,FO,FOP,FOPP,EV,EVP,1)
IF(IFP.EQ.1)CALL PRINT(X,FO,FOP,FOPP,IXE,IPS,UPPER)
C
FOB(1)=Y0
FOPB(1)=YP01
FOPPB(1)= -YPPO
JX=1
Y(1)= -YPPO
Y(2)=YP01

```

```

Y(3)=Y0
CALL RUNGE0(Y,JX,IXE,DX,X,F0B,F0PB,F0PPB,EVB,EVPB,1)
IF(IFP.EQ.1)CALL PRINT(X,F0B,F0PB,F0PPB,IXE,IPB,LOWER)
YPPLB=Y(1)
U1DU2=YPPL/YPPLB
WRITE(*,1300)U1DU2
1300 FORMAT(/1X,'U1DU2= ',B16.8/)
RETURN
END

```

```

C-----
C
C   Temperature Distribution Computation
C-----
C

```

# SUBROUTINE TEMP

```

IMPLICIT REAL*8 (A-H,O-Z)
CHARACTER*64 FNAME
CHARACTER*18 UPPER,LOWER
CHARACTER*10 NAME

```

```

DIMENSION A(801),AB(801)
DIMENSION RT(801),RTB(801)
DIMENSION SESRT(801),SESRTB(801)
DIMENSION SRT(801),SRTB(801)

```

```

COMMON/VECTT/T0(801),TOB(801),TOP(801),TOPB(801),
1      TB(801),TSB(801)
COMMON/VECTF/F0(801),F0B(801),F0P(801),F0PB(801),
1      F0PP(801),F0PPB(801),FB(801),FSB(802),X(801)
COMMON/PARM/DX,IXE,IXE2,IPS,ITMAX,RF,TIDT2,T00,XL,IFP,
1      UPPER,LOWER,U1DU2,U1DU28
COMMON/EV/EV(1601),EVB(1601),EVP(1601),EVPB(1601)
COMMON/ET/ET(801),ETB(801),ETP(801),ETPB(801)
COMMON/PROP/AV0,AV1,AV2,AV3,AK0,AK1,AK2,AK3
WRITE(*,401)

```

```

401 FORMAT(/1X,'Temperature Field Computation Iteration')

```

```

C
DO 500 IRT=1,ITMAX
DO 420 I=1,IXE
RT(I)=(2*F0(I)+ETP(I))/ET(I)
RTB(I)=(2*F0B(I)+ETPB(I))/ETB(I)
420 CONTINUE
C

```

```

IF(IFP.EQ.1)THEN
CALL VPRINT(RT,1,IXE,'RT      ')
CALL VPRINT(RTB,1,IXE,'RTB    ')
ENDIF

```

```

CALL TRPINT(RT,SRT,IXE,1)
CALL TRPINT(RTB,SRTB,IXE,1)

```

```

C
C
C
C
C
Compute SRT =  $\int_0^{XE} RT \, dx$  , SRTB =  $\int_0^{XE} RTB \, dx$ 
C

```

```

DO 450 I=1,IXE
  A(I)=DEXP(-BRT(I))
  AB(I)=DEXP(-BRTB(I))
450 CONTINUE
  CALL TRPINT(A,SESRT,IXE,1)
  CALL TRPINT(AB,SESRTB,IXE,1)

C
C   Compute new centerline temperature.
C
  TOONEM=(SESRT(IXE)+T1DT2*SESRTB(IXE))/(SESRT(IXE)+SESRTB(IXE))
  RDT00=DABS((TOONEM-T00)/T00)
  T00=T00 + RF*(TOONEM-T00)
  TOP0=(T1DT2-1)/(SESRT(IXE)+SESRTB(IXE))

C
C   Compute new temperature and temperature gradient profiles.
C
  DO 470 I=1,IXE
    TO(I)=TOP0*SESRT(I)+T00
    TOB(I)=-TOP0*SESRTB(I)+T00
    TOP(I)=TOP0*A(I)
    TOPB(I)=-TOP0*AB(I)
470 CONTINUE

C
  IF(IFP.EQ.1)THEN
    CALL VPRINT(TO,1,IXE,'TO NEW ')
    CALL VPRINT(TOB,1,IXE,'TOB NEW ')
    CALL VPRINT(TOP,1,IXE,'TOP NEW ')
    CALL VPRINT(TOPB,1,IXE,'TOPB NEW ')
  ENDIF

C
C   Recalculate property dependent part of coefficient RT.
C
  DO 472 I=1,IXE
    ET(I)=AK0+TO(I)*(AK1+TO(I)*(AK2+TO(I)*AK3))
    ETB(I)=AK0+TOB(I)*(AK1+TOB(I)*(AK2+TOB(I)*AK3))
    ETP(I)=TOP(I)*(AK1+TO(I)*(2*AK2+TO(I)*3*AK3))
    ETPB(I)=TOPB(I)*(AK1+TOB(I)*(2*AK2+TOB(I)*3*AK3))
472 CONTINUE

C
  IF(IFP.EQ.1)THEN
    CALL VPRINT(ET,1,IXE,'ET NEW ')
    CALL VPRINT(ETB,1,IXE,'ETB NEW ')
    CALL VPRINT(ETP,1,IXE,'ETP NEW ')
    CALL VPRINT(ETPB,1,IXE,'ETPB NEW ')
  ENDIF

C
  WRITE(*,480)ITERT,TOONEM,RDT00
480 FORMAT(5X,I4,' TOONEM=',B18.9,' RDT00=',B12.3)
  IF(RDT00.LE.1D-8)GO TO 600
500 CONTINUE

C
C   Set ready to return to momentum iteration
C
C   Recalculate property dependent part of coefficients
  for momentum equations
C

```

```

600 DO 610 I=1,IXE
    J=2*I-1
    EV(J)=AV0+T0(I)*(AV1+T0(I)*(AV2+T0(I)*AV3))
    EVB(J)=AV0+TOB(I)*(AV1+TOB(I)*(AV2+TOB(I)*AV3))
    EVP(J)=TOP(I)*(AV1+T0(I)*(2*AV2+T0(I)*3*AV3))
    EVPB(J)=TOPB(I)*(AV1+TOB(I)*(2*AV2+TOB(I)*3*AV3))
610 CONTINUE
    DO 620 I=2,IXE2-1,2
    EV(I)=(EV(I-1)+EV(I+1))/2
    EVB(I)=(EVB(I-1)+EVB(I+1))/2
    EVP(I)=(EVP(I-1)+EVP(I+1))/2
    EVPB(I)=(EVPB(I-1)+EVPB(I+1))/2
620 CONTINUE
C
    IF(IFP.EQ.1)THEN
        CALL VPRINT(EV,1,IXE,'EV NEW ')
        CALL VPRINT(EVB,1,IXE,'EVB NEW ')
        CALL VPRINT(EVP,1,IXE,'EVP NEW ')
        CALL VPRINT(EVPB,1,IXE,'EVPB NEW ')
    ENDIF
C
    RETURN
    END
C
C -----
C
C Runge Kutta Routine to Compute f0, f0b and derivatives
C -----
C
SUBROUTINE RUNGE0(Y,JX,IXE,DX,X,Y0,YOP,YOPP,EV,EVP,IS)
IMPLICIT REAL*8 (A-H,O-Z)
DIMENSION Y(6),F(6),X(801),Y0(801),YOP(801),YOPP(801)
DIMENSION EV(1601),EVP(1601)
N=3
DO 30 I=2,IXE
    DO 10 M=1,4
        CALL RUNGE(N,Y,F,JX,DX,M)
        F(1)=(-(2*Y(3)+EVP(JX))*Y(1)+Y(2)+Y(2))/EV(JX)
        F(2)=Y(1)
        F(3)=Y(2)
10    CONTINUE
        CALL RUNGE(N,Y,F,JX,DX,5)
        IF(IS.EQ.1)THEN
            Y0(I)=Y(3)
            YOP(I)=Y(2)
            YOPP(I)=Y(1)
        ENDIF
30    CONTINUE
    RETURN
    END
C
C -----
C
C Runge Kutta Half Step Routine
C -----
C
SUBROUTINE RUNGE(N,Y,F,JX,DX,M)

```



```

      IMPLICIT REAL*8 (A-H,O-Z)
      DIMENSION Y(3),F(3),Q(3)
      GO TO (1,4,5,3,7),M
1     DO 2 I=1,M
2       Q(I) = 0.
      A = .5
      RETURN
3     A = 1.7071067811865475244
4     JX = JX + 1
5     DO 6 I=1,M
      Y(I) = Y(I) + A*(F(I)*DX - Q(I))
6     Q(I) = 2.*A*DX*F(I) + (1.-3.*A)*Q(I)
      A = .2928932188134524756
      RETURN
7     DO 8 I = 1,M
8     Y(I) = Y(I) + DX*F(I)/6. - Q(I)/3.
      RETURN
      END

```

```

C-----
C
C      Subroutine for local integral of a function
C      using the trapezoidal rule.
C-----

```

```

C
C      F - Vector containing input function
C      SF - Vector containing output local integral
C           SF(I)= integral from LLIM to IX.
C      NP - Number of points, including end points in
C           the interval for integration.
C      DX - Step size: X distance between points.
C      LLIM - F index for lower limit for integration
C
C      SUBROUTINE TRPINT(F,SF,NP,LLIM)
C

```

```

      IMPLICIT REAL*8 (A-H,O-Z)
      CHARACTER*10 UPPER,LOWER
      COMMON/PAIR/DX,IXE,IXE2,IPB,ITMAX,RF,T1DT2,T00,XL,IFP,
1      UPPER,LOWER,U1DU2,U1DU2S
      DIMENSION F(801),SF(801)
      SF(LLIM)=0.
      DO 100 I=LLIM+1,LLIM+NP-1
100    SF(I)=SF(I-1) + DX* (F(I-1) + F(I))/2.
      RETURN
      END

```

```

C-----
C
C      Save a Vector on Disk
C-----

```

```

C
C      SUBROUTINE WDISK(V,FILE,IMAX)
C      IMPLICIT REAL*8 (A-H,O-Z)
C      CHARACTER*64 FILE
C      DIMENSION V(801)
C      OPEN (6,FILE=FILE,STATUS='NEW',ACCESS='SEQUENTIAL')
10    WRITE(6,10) (V(I),I=1,IMAX)
      FORMAT(1X,F10.12)

```

```

CLOSE(6)
RETURN
END

C-----
C
C      Subroutine to do table output to printer
C-----
C
SUBROUTINE PRINT(X,B,BP,BPP,IXE,IPS,REGION)
IMPLICIT REAL*8 (A-H,O-Z)
DIMENSION X(801),B(801),BP(801),BPP(801)
CHARACTER*18 REGION
WRITE(*,1)
1  FORMAT(1X,/26X,'Table of Function Values')
WRITE(*,3)REGION
3  FORMAT(28X,A18,
1//6X,'x',20X,'DDf',17X,'Df',15X,'f'/)
WRITE(*,1200)(X(I),BPP(I),BP(I),B(I),I=1,IXE-1,IPS)
WRITE(*,1200)X(IXE),BPP(IXE),BP(IXE),B(IXE)
RETURN
1200 FORMAT(1X,B15.7,2X,B19.12,2X,B19.12,2X,B19.12)
END

C-----
C
C      Subroutine to do vector output to printer
C-----
C
SUBROUTINE VPRINT(V,IO,LP,NAME)
IMPLICIT REAL*8 (A-H,O-Z)
CHARACTER*18 UPPER,LOWER
COMMON/PAVM/DX,IXE,IXE2,IPS,ITMAX,RF,T1DT2,T00,XL,IFP,
1      UPPER,LOWER,U1DU2,U1DU2S
DIMENSION V(801)
CHARACTER*10 NAME
WRITE(*,5)NAME
5  FORMAT(/5X,'VARIABLE: ',A12/)
IX=IO
IF(IX.GT.IXE)RETURN
WRITE(*,90)(I,DX*(I-1),NAME,V(I),I=IX,LP-1,IPS)
IF(LP.EQ.IXE)GO TO 60
50  WRITE(*,90)LP,DX*(LP-1),NAME,V(LP)
RETURN
60  WRITE(*,98)IXE,DX*(IXE-1),NAME,V(IXE)
RETURN
90  FORMAT(4X,'I= ',I3,6X,'X= ',B12.4,6X,A10,'=',1X,B22.14)
98  FORMAT(4X,'IE ',I3,6X,'E= ',B12.4,6X,A10,'=',1X,B22.14)
END

```

Flow Physics Through a Pierced Membrane

Final Report

to

Southeastern Center for Electrical Engineering Education

by

L.C. Chow (Principal Investigator)

D.E. Tilton (Graduate Student)

Washington State University  
Pullman, WA 99164-2920

December 31, 1985

AF Contract F49620-82-C-0035  
Subcontract 84 RIP 31

ABSTRACT:

The objective of this research was to further investigate the feasibility of a flexible radiator for rejecting large quantities of waste heat in space. An experiment designed to assess the potential damages caused by micrometeoroids was carried out. This involved piercing different membrane materials with various needles and computing corresponding mass loss rates for two cases. In one case a layer of condensate covered the membrane. In the other case, the test section was filled with superheated steam only. From the data obtained it is concluded that mass loss for the condensate case is high, but not critical. It is believed that gravity may account for a large percentage of this high mass loss rate. For the superheated steam case, mass loss is very low and would not significantly effect radiator performance. Considering the radiator's intended operation, total mass loss rates would probably not be significant. Therefore the flexible radiator concept is sound and should be further developed.

## INTRODUCTION:

Advancing space technology, especially defense applications indicates a need to develop new space radiators capable of rejecting large quantities of waste heat. One suggested radiator for this purpose is to be constructed in the shape of a large cylinder, from a lightweight flexible material.<sup>1</sup> Hot components will be sprayed with water. This water would flash vaporize and fill the cylinder causing it to extend into space. As the vapor cooled it would condense on the cylinder wall where it could be pumped out of the radiator. A constant retraction force would be applied to pull the radiator back inside the spacecraft as the volume decreased due to condensation. This force would also be used to keep the two phase mixture inside at constant saturation pressure and temperature.

Unlike radiators with rigid structures this radiator is only exposed to the harmful space environment when it is in operation. Even though this is a relatively short period of time, the radiators susceptibility to damage from micrometeoroids must be evaluated. These particles travel through space at approximately 20 km/s. Since the radiator is lightweight and flexible, it is probable that punctures will occur. No previous research has been done to determine what will happen to the internal fluid and vapor under these circumstances. The experiment conducted was designed to simulate this situation. In this manner, the extent of potential damage and its effects on radiator performance could be determined.

## EXPERIMENTAL APPARATUS & PROCEDURES

The experimental apparatus is represented by the schematic diagram in Figure 1. The test section, located in the bell jar of the Veeco Ve-400 vacuum machine, is a double walled stainless steel vessel. It has an aluminum membrane holder on the bottom. An electrically controlled 15 watt solenoid, bolted to a cross-member in the test section, is used to pierce the membrane using a needle attachment threaded into the plunger. Constant temperature water is pumped from the Neslab EX-100 Excal constant temperature bath through the outer wall of the vessel to keep the internal contents at constant conditions. This water is also circulated through the copper coils in the steam generation vessel for the same purpose. The temperature is monitored in both vessels using type T thermocouples and an Omega 21764 digital thermometer. The two Celesco E1PD pressure transducers, located on the top of each vessel are linked to a Hewlett Packard 7100 B strip chart recorder using Celesco CD10 carrier demodulators.

After a new membrane has been installed, the entire system is evacuated. The bell jar is pumped down to 0.1 mm Hg using a Duo Seal model 1397 mechanical vacuum pump. The steam generation vessel and test section are evacuated using a Duo Seal model 1402 auxiliary mechanical pump to approximately the same pressure. Then a given amount of water is added using a calibrated syringe. The location of water addition for each case is indicated in Figure 1. Either superheated steam or saturated steam with a condensate layer covering one side of the membrane will

occupy the test section. The other side of the membrane will be exposed to the vacuum environment in the bell jar. For both cases, the valve between the test section and the steam generation vessel is closed at the time of the test. When the desired conditions in the test section are obtained, the solenoid is activated to puncture the membrane. For the condensate case, there is no pressure or temperature drop as condensate is expelled from the test section. Therefore, the mass loss rate is calculated by estimating the time it takes for the entire condensate layer to leak out. Sample data collected for this case is given in Table 1, where  $T_{sat}$  is the saturation temperature,  $V_{add}$  is the volume of liquid added, and  $t$  is the time required to expell the entire layer of condensate. For the steam case the pressure loss versus time is recorded by the strip chart recorder. The temperature and pressure,  $T_1$  and  $P_1$  are noted just prior to puncture. As vapor escapes from the test section the pressure in the bell jar increases. This pressure rise is monitored by the pressure thermocouple gage in the vacuum test machine. As soon as this pressure rises above 1.0 mm Hg, the mass loss rate begins to decrease. Therefore the test is ended and the new temperature and pressure in the test section,  $T_2$  and  $P_2$  are recorded. The time is read from the strip chart recorder plot. Sample data collected for this case is given in Table 2.

## RESULTS AND DISCUSSION

In the case where a condensate layer was covering the membrane, it was predicted that the hole might seal itself by the following process. At the instant of puncture, a small percentage of liquid would flash vaporize when suddenly exposed to a vacuum. It would absorb its latent heat of vaporization from the remaining water in the vicinity of the hole, causing it to freeze and plug up the hole.

This process was not observed even when using the smallest needle available, which punctured a hole of  $0.029 \text{ mm}^2$ . Apparently, the water was expelled from the hole faster than the sealing process could take place. The water did freeze when it landed on the viewing mirror below the test section. Mass loss rates for this case were determined by the method shown in sample calculation #1, Appendix 1. A summary of results is given in Table 3, and graphically in Figure 2. A hole of  $.029 \text{ mm}^2$  gave a mass loss rate of approximately  $2.73 \text{ kg/hr}$ . For a 25 MW Radiator<sup>1</sup>, we can assume an operating time of one hour, a total working fluid mass of 500 kg, and a radiator size of 3 m in diameter by 100 m long. Using a probability model<sup>2,3</sup> as shown in sample calculation #2, a radiator this size can expect a 0.2% chance of being struck by a micrometeoroid large enough to puncture the hole discussed. Under these circumstances, the total reduction in mass is less than 0.6% of the total working fluid. This indicates that the mass loss associated with this case may not be significant. However, as meteoroid size decreases, the chance of puncture increases. Therefore it is possible that many smaller holes will be present. The possibility of sealing in these



smaller holes has not been ruled out. As hole size decreases, the surface tension and viscosity of the water play an increasing role in slowing down the flow rate of water. This may result in freezing before expulsion causing the hole to seal itself as discussed earlier.

The mass loss rates predicted by this experiment may be much higher than would occur in space. This is due to the fact that the pressure difference caused the membrane to curve and the puncture was located in the bottom as seen in Figure 3. On earth gravity was responsible for delivering more condensate to the vicinity of the hole. In space, the lack of a body force may greatly diminish the mass loss rates. A small amount of condensate would leak out and leave the hole exposed to steam only as seen in Figure 4. This would cause continued leakage to occur according to the steam only case.

In the steam only case, mass loss was seen to be so low that it is insignificant and will not effect radiator performance. The results for this case, obtained according to sample calculation #3, are summarized in Table 4. The experimentally determined mass loss rates versus puncture area can be seen graphically in Figure 5. The slope of this plot is the average mass flux. This value compared nicely to the theoretical<sup>4</sup> prediction from choked flow, as seen in sample calculations 4 & 5.

The experimental mass flux was  $0.1250 \text{ kg/hr mm}^2$  and the theoretical value was  $0.1216 \text{ kg/hr mm}^2$ . This is less than a 20% difference including the experimental uncertainty which is given in Appendix 2.

Assuming the same puncture conditions and radiator dimensions, the mass loss is only 0.00363 kg/hr or a  $7.25 \times 10^{-4}\%$  decrease in total mass.

This experiment is not truly representative of actual operation in that superheated steam near 70°C and 20 kPa was used experimentally. In reality, saturated steam at 70°C and 31.19 kPa would occupy the radiator. Therefore, the actual mass loss rate for this case would be higher but still insignificant.

For each of the two cases previously discussed, two different membrane materials were tested. One was a clear plastic laminate 0.152 mm thick. The other was a plastic - aluminum film laminate 0.137 mm thick. Table 5 lists material type, actual hole area,  $A$ , needle cross-sectional area,  $A_n$ , and the ratio  $A_n/A$  for each run. Due to the wide variation in the area ratio, no correlation can be made between needle size and hole size for the two materials tested. Examples of the different punctures are shown in Figures 6 and 7. The clear plastic stretched more readily and then puncture was fairly clean and round. The aluminum - plastic material ripped when the needle was forced through. Due to the irregular hole shapes area calculation was difficult. Pictures of the punctures were taken at high magnification. A grid was used to estimate the area in the photograph. This value was then reduced by the magnification factor to determine the actual puncture area. The error associated with this calculation is probably not more than 10%.

## CONCLUSIONS & RECOMMENDATIONS

From the experimental results obtained, it is concluded that damage due to micrometeoroids will not significantly effect radiator performance. The total mass loss over the entire operating period probably would not exceed two percent in the worst case. However considering the results of the condensate case it is highly desirable to minimize the thickness of the condensate layer as much as possible. This will reduce mass loss, as well as, thermal resistance to heat transfer. Also, when considering a design for liquid return, care should be taken in avoiding the delivery of condensate to the vicinity of a hole.

To more accurately determine the extent of damage in space, the condensate case should be redone in a zero-gravity environment. The effects of gravity on mass loss may be great for this case. Without gravity, the flow rate through the hole will decrease. For this reason, it is entirely possible that the sealing process discussed will occur more readily. If not, the lack of a mechanism to deliver more condensate to the vicinity of the hole, may still diminish mass loss significantly.

In any case the mass loss estimates provided here are the maximum that could possibly occur. Since these are acceptable, micrometeoroid damage will not be a problem, and the flexible radiator concept should be further researched and developed.

#### REFERENCES

- 1) L.C. Chow, E.T. Mahefkey and J.E. Yokajty, "Low Temperature Expandable Megawatt Pulse Power Radiator," AIAA 20th Thermophysics Conference, 1968, AIAA Paper 85-1076.
- 2) Meteoroid Environment Model - 1969, NASA SP-8013, 1963.
- 3) Meteoroid Damage Assessment, NASA SP-8042, 1970.
- 4) K. Oswatitsch and G. Kuerti, Gas Dynamics, Academic Press Inc., 1956, p. 51.
- 5) J.P. Holman, Thermodynamics, third edition, McGraw Hill, 1960, Steam Tables.

RUN	$T_{\text{sat}} \pm 0.2^\circ\text{C}$	$V_{\text{add}} \pm 0.2\text{cm}^3$	$t \pm 1.0 \text{ sec}$
1	70.2	5.1	5.6
2	67.1	5.1	5.4
3	68.6	6.3	6.0
4	66.8	7.0	6.0

TABLE 1: Raw Data: Condensate Case

RUN sec	$T_1 \pm 0.2^\circ\text{C}$	$P_1 \pm 0.2\text{kPa}$	$T_2 \pm 0.2^\circ\text{C}$	$P_2 \pm 0.2 \text{ kPa}$	$t \pm 0.3$
5	70.2	21.67	68.6	20.99	62.0
6	68.2	19.98	67.4	19.19	20.5
7	71.0	18.29	70.2	16.94	26.0
8	70.8	19.98	69.6	19.03	8.5
9	70.4	22.23	69.4	20.54	7.3
6	70.2	20.54	68.6	17.73	7.5
7	70.2	21.10	69.4	19.42	3.0

TABLE 2: Raw Data: Steam Case

RUN	$\dot{M} \pm 10\% \text{ kg/hr}$	$A \pm 10\% \text{ mm}^2$	$M\text{flux} \pm 20\% \text{ kg/hr mm}^2$
1	2.73	0.029	94.14
2	2.87	0.036	79.72
3	3.27	0.046	71.09
4	3.71	0.050	74.20

TABLE 3: Results: Condensate Case

RUN	$\dot{M} \pm 20\% \text{ kg/hr}$	$A \pm 10\% \text{ mm}^2$
5	0.00081	0.008
6	0.00316	0.026
7	0.00435	0.039
8	0.00898	0.080
9	0.0193	0.172
10	0.0314	0.221
11	0.0470	0.370

MASS FLUX = 0.1250 kg/hr mm<sup>2</sup>

TABLE 4: Results: Steam Case

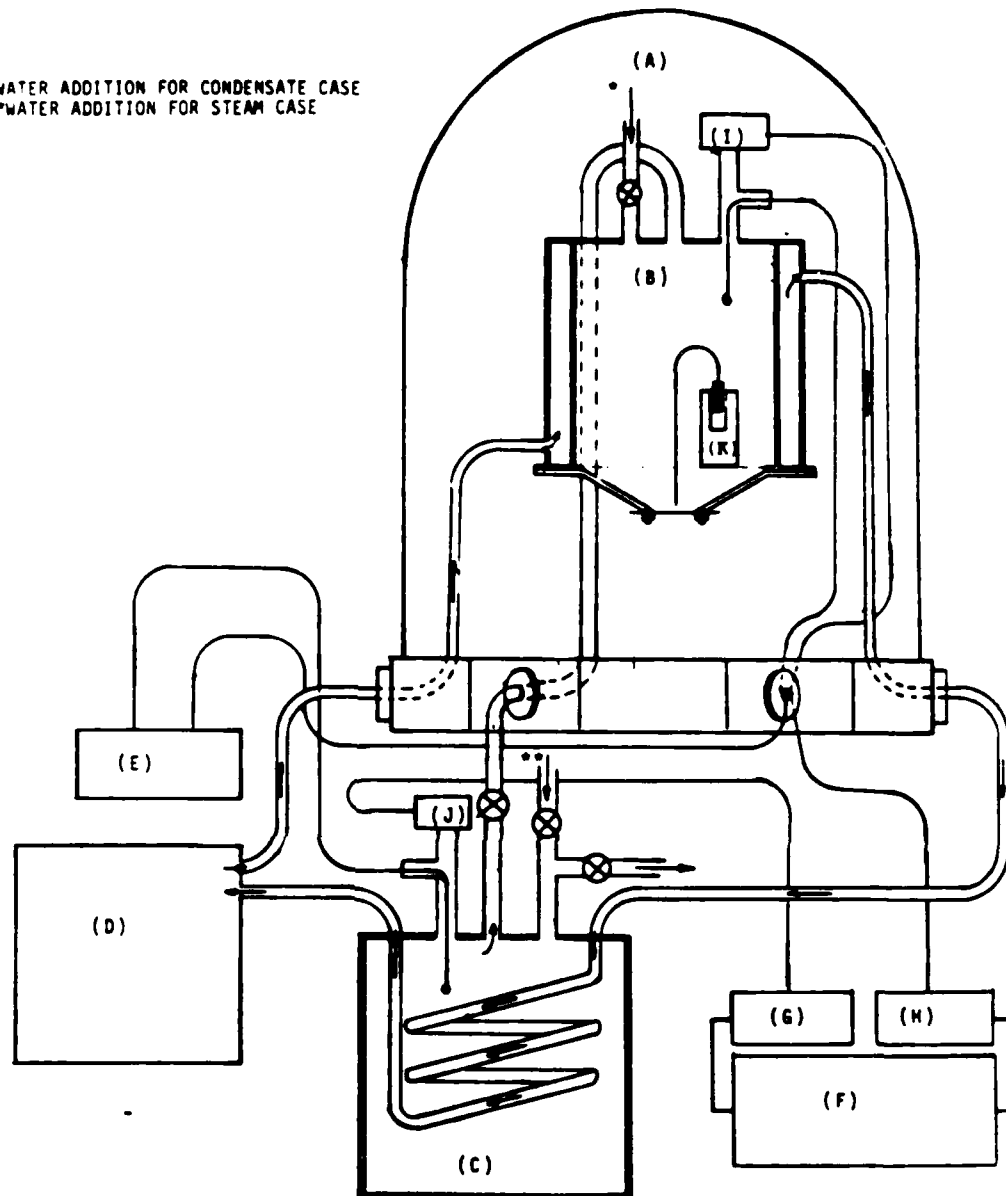
RUN	MATERIAL	A(mm <sup>2</sup> )	An(mm <sup>2</sup> )	An/A
1	C	0.114	0.029	3.93
2	C	0.257	0.036	7.14
3	C	0.114	0.046	2.46
4	A	0.257	0.050	5.14
5	C	0.114	0.008	14.25
6	A	0.257	0.026	9.88
7	A	0.621	0.039	15.92
8	A	0.456	0.080	5.70
9	C	0.311	0.172	4.72
10	A	1.267	0.221	5.73
11	A	2.011	0.370	5.43

Clear Plastic Average  $An/A = 6.50$

Aluminum-Plastic Average  $An/A = 7.97$

TABLE 5: PUNCTURE AREA AND NEEDLE AREA DATA.

\*WATER ADDITION FOR CONDENSATE CASE  
 \*\*WATER ADDITION FOR STEAM CASE



- (A)-BELL JAR, VEECO VE-400 VACUUM TEST MACHINE (V=100000cc)
- (B)-STAINLESS STEEL DOUBLE WALL TEST SECTION (V=3800cc)
- (C)-STEAM GENERATION VESSEL (V=22500cc)
- (D)-NESLAB EX-100 EXCAL CIRCULATING CONSTANT TEMPERATURE BATH
- (E)-OMEGA 21764 DIGITAL THERMOMETER
- (F)-HEWLETT PACKARD 7100B STRIP CHART RECORDER
- (G)&(H)-CELESCO CD10 CARRIER DEMODULATORS
- (I)&(J)-CELESCO E1PD PRESSURE TRANSDUCERS
- (K)-SOLENOID-NEEDLE PUNCTURE ASSEMBLY

**FIGURE 1: APPARATUS SCHEMATIC**

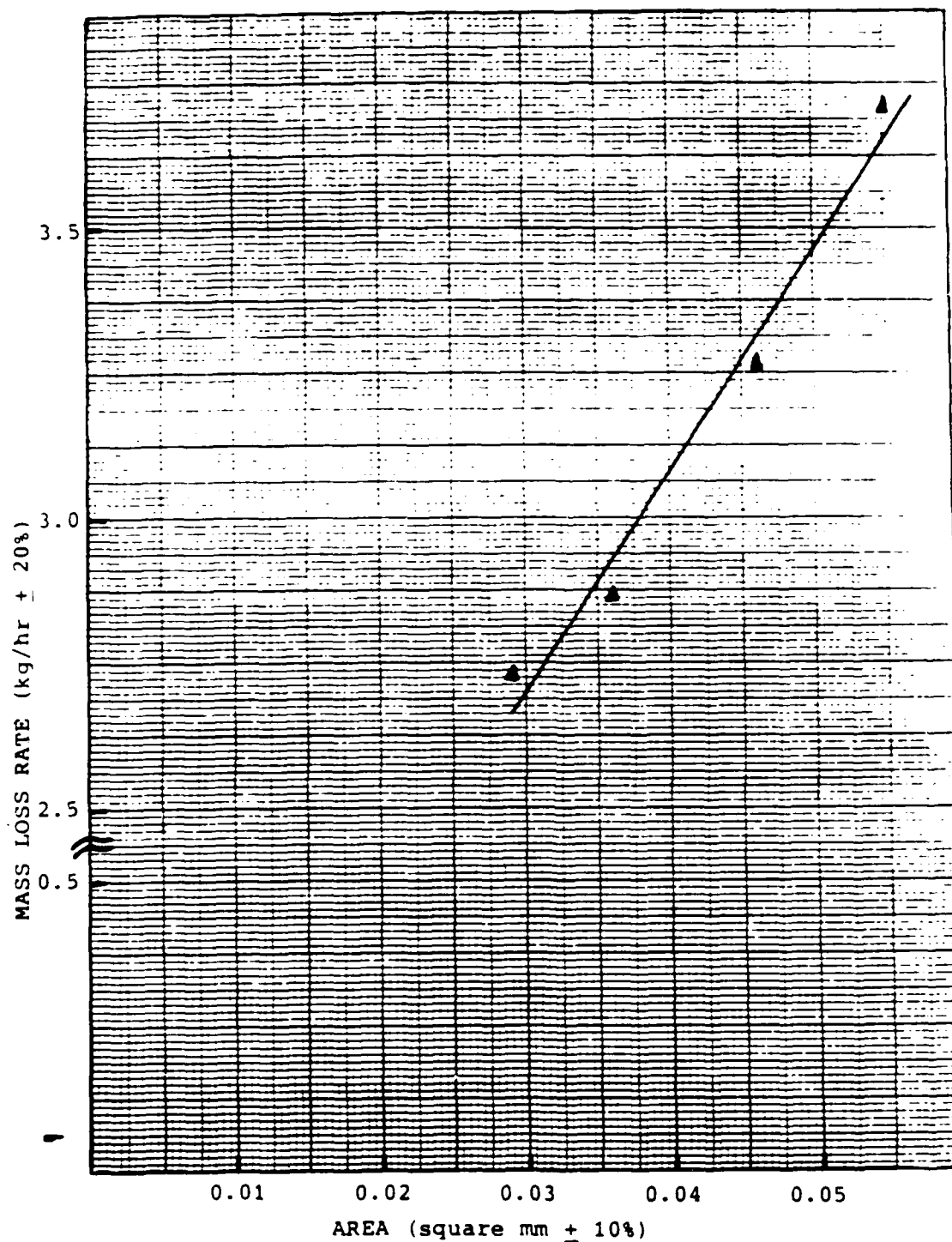


**FIGURE 2:** MASS LOSS RATE vs. PUNCTURE AREA (CONDENSATE CASE)



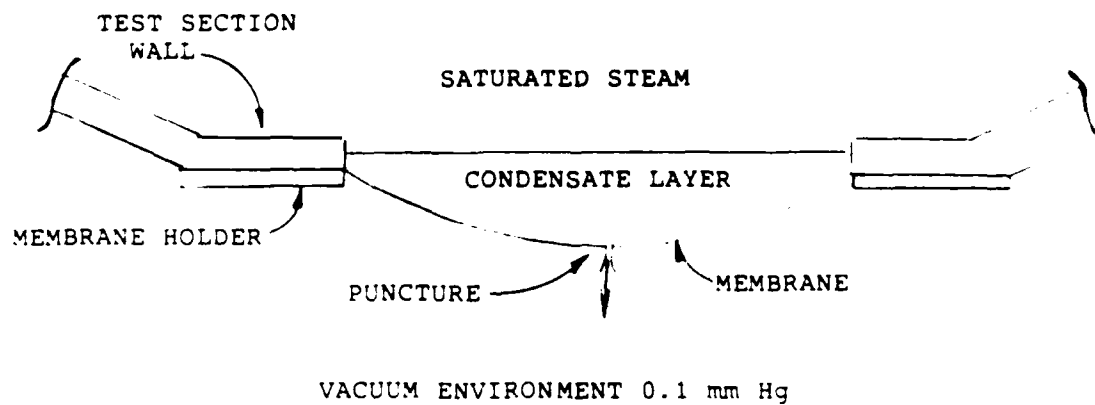


**FIGURE 3:** GRAVITATIONAL DELIVERY OF CONDENSATE TO PUNCTURE

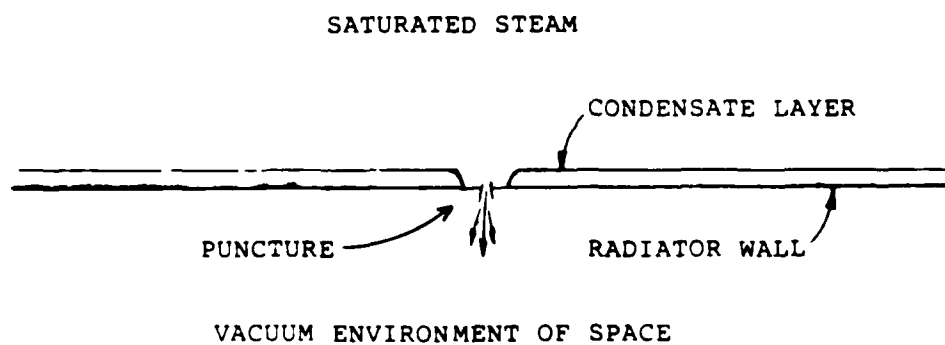


**FIGURE 4:** ZERO-G, NO CONDENSATE DELIVERY TO PUNCTURE

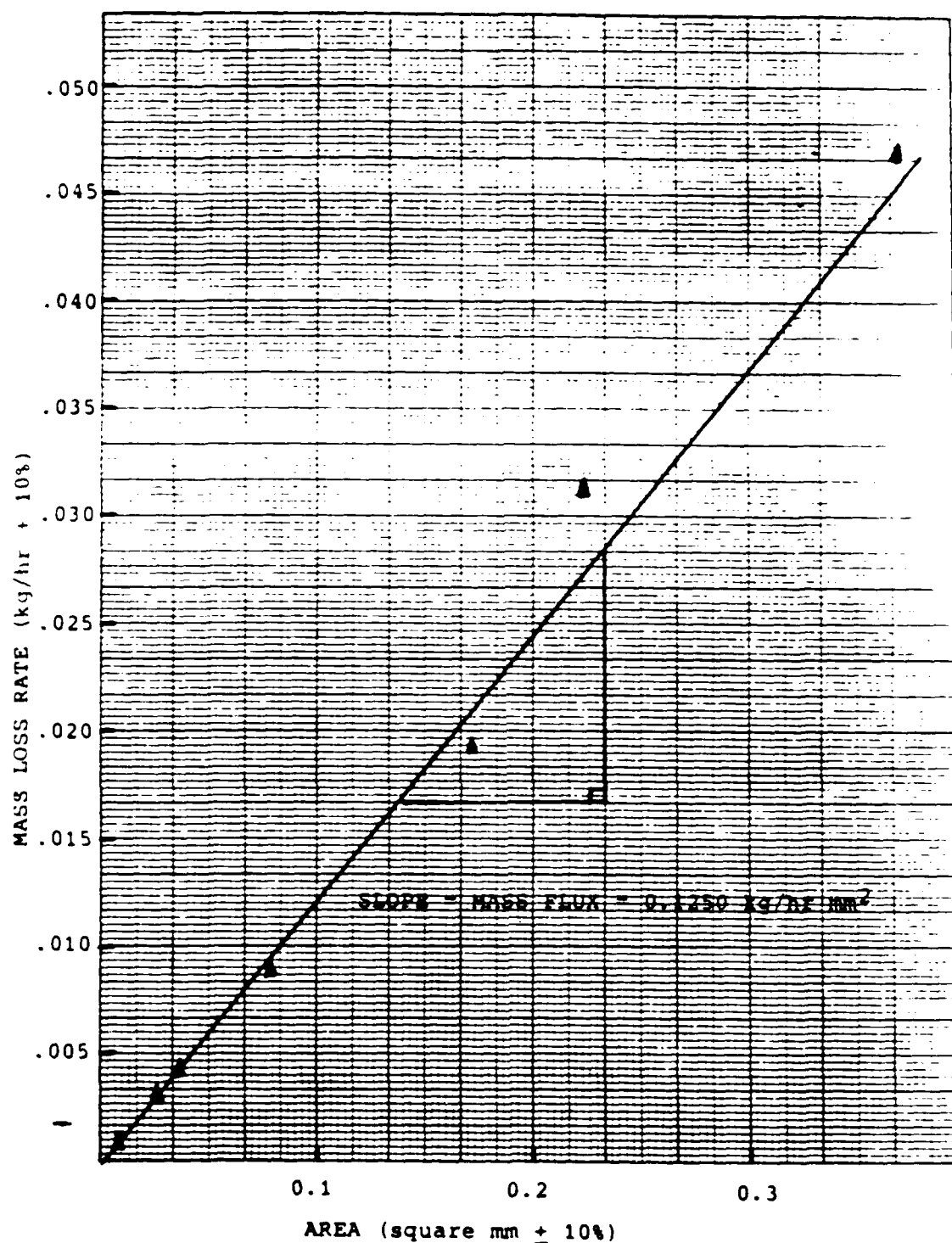


**FIGURE 5: MASS LOSS RATE vs. AREA (STEAM CASE)**



$A=0.039 \text{ mm}^2$   $D_n=0.889 \text{ mm}$



$A=0.37 \text{ mm}^2$   $D_n=1.60 \text{ mm}$



$A=0.026 \text{ mm}^2$   $D_n=0.572 \text{ mm}$

**FIGURE 6:** EXAMPLE PUNCTURES, ALUMINUM-PLASTIC LAMINATE

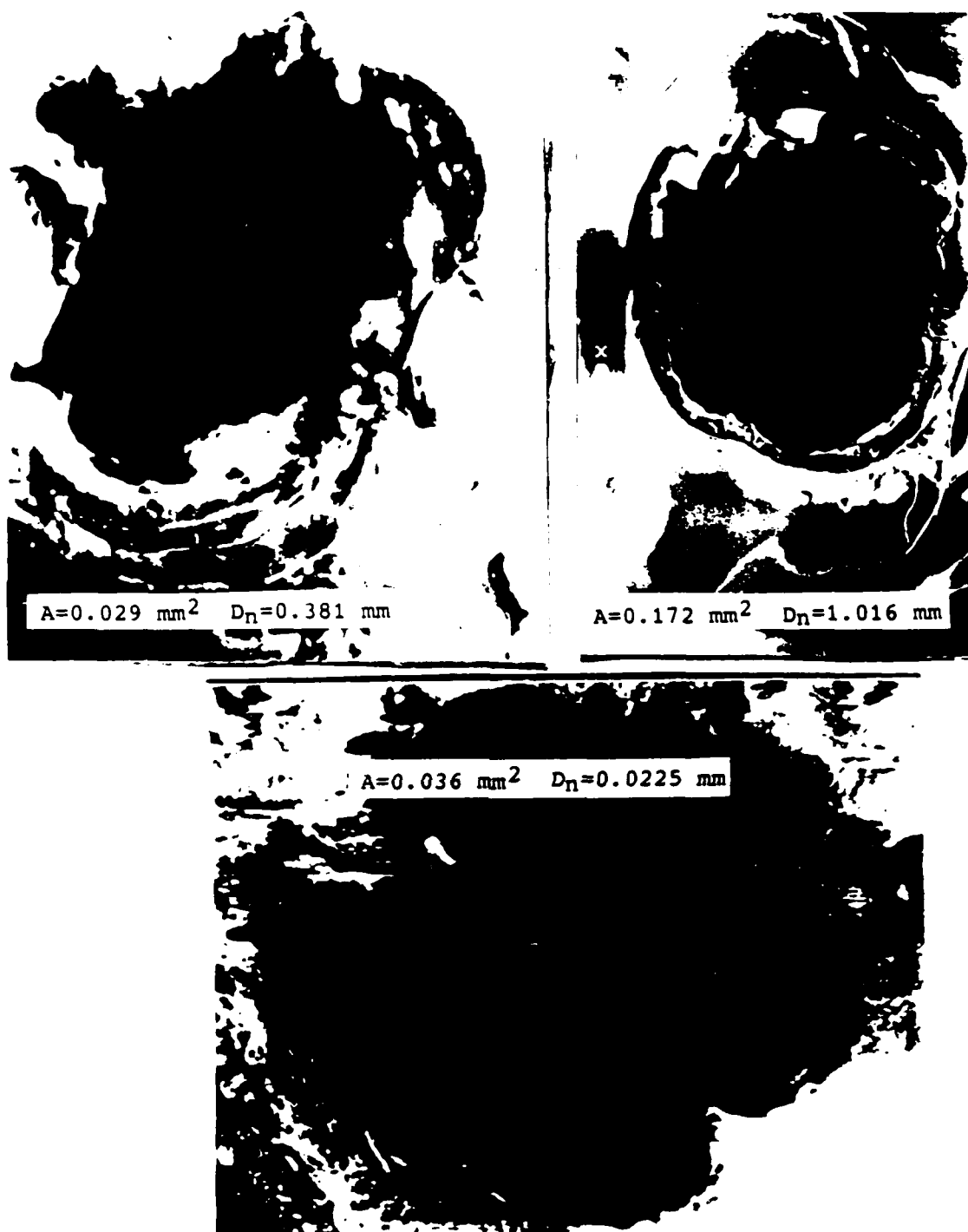


**FIGURE 7: EXAMPLE PUNCTURES, CLEAR PLASTIC LAMINATE**

APPENDIX 1  
SAMPLE CALCULATIONS

SAMPLE CALCULATIONS #1 (Condensate Case)

Raw Data:

$$T = 70.2^{\circ}\text{C}$$

$$V_{\text{added}} = 5.1 \text{ cm}^3 \text{ at } 70^{\circ}\text{C} \quad M_{\text{add}} = 4.99\text{g}$$

$$V_{\text{test sect}} = 3800 \text{ cm}^3$$

$$v_{\text{tot}} = 3800 \text{ cm}^3 / 4.99\text{g} = 761.5 \text{ cm}^3/\text{g}$$

From (5) C.P. Holman, Thermodynamics

$$v_f = 1.0228 \text{ cm}^3/\text{g}$$

$$v_g = 5042 \text{ cm}^3/\text{g}$$

$$v_{\text{tot}} = v_f + x(v_g - v_f)$$

$$761.5 = 1.0228 + x(5042 - 1.0228)$$

$$x = 0.151$$

$$(1 - x) = 0.849$$

$$\text{grams of condensate layer} = (0.849)(4.99) = 4.24 \text{ g}$$

$$\dot{m} = 4.24 \text{ g} / 5.6 \text{ sec} = 0.757 \text{ g/s}$$

$$\dot{m} = 2.73 \text{ kg/hr}$$

$$M_{\text{flux}} = \dot{m}/A$$

$$M_{\text{flux}} = 94.14 \text{ kg/hr mm}^2$$

=====

SAMPLE CALCULATION #2

Puncture Probability

From References (2) and (3) for a meteoroid of mass  $10^{-6}$  grams or less

$$\log_{10} N_t = -14.37 - 1.213 \log_{10} M$$

where  $N_t$  = Number of particles of mass,  $m$  or greater per square meter of space per second.

$M$  = Meteoroid mass in grams.

Assume a meteoroid mass density of 0.5 grams/cm<sup>3</sup> for all meteoroids.

For hole area = 0.029 mm<sup>2</sup>

Assuming the micrometeoroid has the same cross-sectional area as the hole volume of meteoroid,  $V = 0.030 \text{ mm}^3 = 3.0 \times 10^{-5} \text{ cm}^3$

$$m = 1/(5 \times 10^{-5}) \text{ grams.}$$

$$\log_{10} N_t = -14.37 - 1.213 \log_{10} 1.5 \times 10^{-5}$$

$$N_t = 3.0 \times 10^{-9} \text{ particles/m}^2\text{s}$$

ASSUME: Average radiator cross sectional area = 150m<sup>2</sup>

Operating time of 1 hour = 3600 seconds

$$\begin{aligned} \text{Number of punctures} &= N_t \times A \times t \\ &= 0.00164 \end{aligned}$$

°. There is less than a 0.2% chance that  
a puncture this size or greater will occur.

SAMPLE CALCULATION #3 (Steam only)

Raw Data:  $T_1 = 70.4^\circ\text{C}$   $T_2 = 69.4^\circ\text{C}$   
 $P_1 = 22.23 \text{ kPa}$   $P_2 = 20.54 \text{ kPa}$   
 $t = 7.3 \text{ sec}$

Since  $Z \approx 1.0$ ; Use Ideal Gas Law

$$v = \frac{RT}{P}$$

$$v_1 = 7119.3 \text{ cm}^3/\text{g}$$

$$v_2 = 7682.6 \text{ cm}^3/\text{g}$$

Volume of Test Section:  $V = 3800 \text{ cm}^3$

$$m_1 = 3800 \text{ cm}^3 / 7119.3 \text{ cm}^3/\text{g} = 0.5338 \text{ g}$$

$$m_2 = 3800 \text{ cm}^3 / 7682.6 \text{ cm}^3/\text{g} = 0.4946 \text{ g}$$

$$\dot{m} = \frac{m_1 - m_2}{t} = \frac{0.5338 - 0.4946}{7.3}$$

$$\dot{m} = 0.00536 \text{ g/s}$$

$$\dot{m} = 0.0193 \text{ g/hr}$$

From slope of  $\dot{m}$  vs a steam case plot

$$M_{\text{flux}} = 0.1250 \text{ kg/hr mm}^2$$

=====



# SAMPLE CALCULATIONS #4      Steam Case (theoretical)

From (4) Oswatitsch/Kuerti, Gas Dynamics, 1956

The mass flux of a vapor leaking from a vessel into a vacuum through an orifice is given by the choked flow equation:

$$M_{flux} = \left( \frac{2}{\gamma + 1} \right)^{\frac{\gamma}{\gamma - 1}} C_o \rho_o$$

where  $C_o$  = speed of sound at internal conditions

$\rho_o$  = vapor density at internal conditions

$\gamma$  = ratio of specific heats

For  $H_2O$  vapor at  $70^\circ C$ , 20 kPa

$$\gamma = 1.33$$

$$R = 460.6 \text{ J/kg K}$$

$$T_o = 342.2 K$$

$$C_o = (\gamma R T_o)^{\frac{1}{2}} = 457.85 \text{ m/s}$$

From Ideal Gas Law,  $Z=1.0$

$$\rho_o = \frac{P_o}{R T_o} = 0.1265 \text{ Kg/m}^3$$

$$M_{flux} = 33.78 \text{ kg/sm}^2$$

$$M_{flux} = 0.1216 \text{ Kg/hr-mm}^2$$

# SAMPLE CALCULATION #5

Experimental and theoretical comparison (Steam case)

From slope of  $\dot{m}$  vs A plot

$$\text{experimental } M_{\text{flux}} = 0.1250 \text{ kg/nr mm}^2$$

From sample calculation #2

$$\text{theoretical } M_{\text{flux}} = 0.1216 \text{ kg/nr mm}^2$$

$$\% \text{ error} = \frac{0.1250 - 0.1216}{0.1250} \times 100 = 2.27\%$$

$$\% \text{ error} = 2.27\%$$

including Uncertainty Calculation in Appendix 2

$$\% \text{ error} = \leq 20\%$$

APPENDIX 2  
UNCERTAINTY ANALYSIS

#### UNCERTAINTY ANALYSIS:

All uncertainty calculations were performed in the standard way, such that the uncertainty in any value  $F$ ,  $\omega_F$ , is given by:

$$\frac{\omega_F}{F} = \left( \left( \frac{\partial F}{\partial v_1} \omega_{v_1} \right)^2 + \left( \frac{\partial F}{\partial v_2} \omega_{v_2} \right)^2 + \dots + \left( \frac{\partial F}{\partial v_n} \omega_{v_n} \right)^2 \right)^{\frac{1}{2}}$$

Where:  $F = F(v_1, v_2, \dots, v_n)$

#### CONDENSATE CASE:

mass flow rate;  $\frac{\omega_m}{m} = 20\%$

mass flux;  $\frac{\omega_{M_{flux}}}{M_{flux}} = 25\%$

#### STEAM CASE:

mass flow rate;  $\frac{\omega_m}{m} = 10\%$

mass flux;  $\frac{\omega_{M_{flux}}}{M_{flux}} = 15\%$

#### PUNCTURE AREA:

area;  $\frac{\omega_A}{A} = 10\%$

Technical Memorandum

MAE-TM-18

Computational Studies of Ramjet Combustor Flowfields

K. M. Isaac

Department of Mechanical and Aerospace Engineering

University of Missouri-Rolla

January 1986

## ABSTRACT

Computation of combustion chamber flowfields has been of interest in recent years because of the enormous benefits to be reaped from the improvements in ramjet/turbojet engine performance. An investigation was undertaken to evaluate proposed modifications to the turbulence model to account for low turbulence Reynolds number effect and streamline curvature effect. The vehicle for this computational study was a computer program which was used to solve the fully-elliptic Navier-Stokes equations based on the methodology of Gosman et al. The program is currently capable of calculating compressible, recirculating, axisymmetric or two-dimensional, internal flows. This report describes new studies conducted on the recirculating combustor flowfield by using modified forms of the k-e turbulence model. Details of the methodology adopted for calculating compressible flow are also discussed in this report.

## NOMENCLATURE

D	-	chamber diameter
d	-	inlet diameter
f	-	constant in turbulence model
G	-	generation term in turbulence model
H	-	total enthalpy
K	-	constant in turbulence model
k	-	turbulent kinetic energy, thermal conductivity
l	-	macro length scale
S	-	source term
s	-	coordinate tangential to streamlines
n	-	coordinate normal to streamlines
u	-	velocity component in the axial direction
v	-	velocity component in the radial direction
P	-	rate of generation of turbulence energy
p	-	time-mean pressure
T	-	static temperature
R	-	gas constant
Re	-	Reynolds number
r	-	radial coordinate
x	-	axial coordinate
y	-	distance normal to the wall
$\alpha$	-	constant in turbulence model
$\beta$	-	constant in turbulence model
$\delta$	-	shear layer thickness
$\Gamma$	-	exchange coefficient
$\mu$	-	dynamic viscosity

- $\nu$  - kinematic viscosity
- $\epsilon$  - turbulent energy dissipation rate
- $\rho$  - density
- $\sigma$  - Prandtl-Schmidt number
- $\tau$  - shear stress
- $\phi$  - variable representing various flow parameters

Subscripts

- in - inlet
- ref - reference
- t - turbulent parameters



## INTRODUCTION

Combustion chamber designs for turbojet and ramjet engines that have been developed over the last few decades have resulted in improved designs having much higher levels of performance. The designers, however, are faced with trial and error procedures because of the uncertainties in predictive capability. The reasons for this are many. The interplay of several physical phenomena, such as turbulence, multiphase flow, and chemical reaction, makes the flowfield very complex and, therefore, difficult to analyze. Very often the flowfield is three-dimensional in nature, and this imposes severe limitations on the computations in terms of storage and computation time. When a computer code is successfully developed, it is often found that there are few experimental data available to prescribe the boundary conditions meaningfully or to compare with the predictions.

Some encouraging developments have taken place in recent years that address some of the problems discussed above. Good progress has been made in the numerical modeling of the (Navier-Stokes) equations governing recirculating flowfields typical of a ramjet/turbojet combustion chamber. Turbulence models capable of predicting the flowfields in a wide range of physical situations, such as free shear flows (jets and wakes), wall-bounded flows (boundary-layers), and confined jets, have been developed. Chemical reaction models of varying degrees of sophistication are currently being used for combusting flows. These models range from a reactants-and-products equilibrium chemistry model to finite-rate chemistry models with multi-step reactions involving several chemical species. Recent developments in nonintrusive experimental techniques have made it possible to make accurate measurements of mean velocity and turbulence even in highly turbulent,

recirculating flow regions. Therefore, it is now possible to accurately specify the boundary conditions for the solution of the equations; one is also able to make meaningful comparisons between experiments and predictions without unduly worrying about experimental uncertainties.

Some combustor configurations that are currently being investigated are the dump combustor and the center bluff body combustor (Figures 1 and 2). The dump combustor appears to be particularly attractive because of its ability to decelerate the flow and create recirculating zones for flame holding and flame stabilization without a significant amount of pressure loss.

#### BACKGROUND

The numerical solution of the time-averaged, fully elliptic Navier-Stokes equations poses several difficulties because of the coupled, nonlinear nature of the equations. The solution becomes particularly cumbersome when the flowfield considered is multidimensional, turbulent, compressible, and chemically reacting. Turbulence introduces additional complexities because of what is known as the 'closure' problem, which makes it necessary to resort to turbulence modeling<sup>1-12</sup>. In compressible flows, an additional equation (the energy equation) must be solved, and the fluid density becomes a variable and must be calculated from an equation of state. Chemical reaction introduces additional equations for the transport of various chemical species.

The first aspect of the problem that was dealt with in the present study was the numerical algorithm for solving the set of nonlinear, coupled, partial differential equations governing the flowfield. Solutions of the two-dimensional flow problems have been obtained in the past with vorticity and stream function as the dependent variables. A more widely used approach was developed by Patankar and Spalding<sup>13</sup> who employed the SIMPLE (Semi -

Implicit - Pressure - Linked - Equations) algorithm for solving the equations in primitive variables. Their method has several features in common with the earlier work of Harlow and Welch<sup>14</sup>. Some of the deficiencies of these methods have been widely recognized, and recently some alternative methods have been proposed<sup>15-17</sup> to overcome these deficiencies. Some of these methods are still in the development stage, and, therefore, their applicability is yet to be tested. The SIMPLE algorithm has been widely used for the solution of the Navier - Stokes equations governing parabolic as well as elliptic (recirculating) flows. Despite its shortcomings, the method has successfully predicted a wide range of flowfields. Several investigators have used the method to predict the flowfield in combustion chambers of different geometries<sup>17-22</sup>.

The problems of turbulence modeling are still intriguing investigators in the field. One approach, which has gained wide popularity, is the  $k-\epsilon$  model<sup>1</sup> in which  $k$  and  $\epsilon$  represent respectively the turbulent kinetic energy and its dissipation rate. The  $k-\epsilon$  model treats turbulence by means of transport equations for these two variables. Several versions of the  $k-\epsilon$  model are in use; however, none of them gives uniformly good results for vastly varying flow conditions. Other approaches, such as Reynolds stress models and pdf models, can be found in the literature. It appears that the  $k-\epsilon$  model offers more satisfactory results over a wide range of flow conditions in comparison to the other turbulence models, which give good predictions in some cases and perform poorly in others. Recent use by the principal investigator of a computer code for calculating compressible, recirculating flow in internal geometries has brought to the surface some deficiencies of the predictive efforts that have been expended in this area<sup>23</sup>. It was felt that predictions could be improved by using a turbulence model which takes into account the

characteristics of recirculating flows. Regions of the flowfield where the streamlines have large curvature are known to yield unrealistic predictions when the standard  $k-\epsilon$  model of turbulence is used. Furthermore, the effects of turbulence Reynolds number on the flowfield are also largely unknown. The present study was directed towards addressing these two problems.

#### THE TURBULENCE MODEL

The turbulence model that is most widely used in the prediction of flowfields in internal geometries is the  $k-\epsilon$  model in which  $k$  and  $\epsilon$  are, respectively the turbulent kinetic energy and its dissipation rate. The model prescribes these quantities in terms of the transport equations for these variables. The equations of continuity, momenta, energy, and the two transport equations for  $k$  and  $\epsilon$  are given in the appendix. The reason for representing all the equations in one general form is the ease of numerical implementation. The transport equations for  $k$  and  $\epsilon$  are reproduced below for clarity.

$$\frac{\partial}{\partial x} (\rho u k) + \frac{1}{r} \frac{\partial}{\partial r} (\rho v r k) = \frac{\partial}{\partial x} \left[ \left( \mu + \frac{\mu_t}{\sigma_k} \right) \frac{\partial k}{\partial x} \right] + \frac{1}{r} \frac{\partial}{\partial r} \left[ \left( r \left( \mu + \frac{\mu_t}{\sigma_k} \right) \frac{\partial k}{\partial r} \right) \right] + G - \rho \epsilon \quad (1)$$

$$\frac{\partial}{\partial x} (\rho u \epsilon) + \frac{1}{r} \frac{\partial}{\partial r} (\rho v r \epsilon) = \frac{\partial}{\partial x} \left[ \left( \mu + \frac{\mu_t}{\sigma_\epsilon} \right) \frac{\partial \epsilon}{\partial x} \right] + \frac{1}{r} \frac{\partial}{\partial r} \left[ r \left( \mu + \frac{\mu_t}{\sigma_\epsilon} \right) \frac{\partial \epsilon}{\partial r} \right] + C_1 \frac{\epsilon}{k} G - C_2 \frac{\rho \epsilon^2}{k} \quad (2)$$

In addition, the auxiliary relation for turbulent viscosity is given by

$$\mu_t = C_\mu \rho \frac{k^2}{\epsilon} \quad (3)$$

The terms  $\sigma_k, \sigma_\epsilon, C_1, C_2$  and  $C_\mu$  which appear in the equations for  $k, \epsilon$  and  $\mu_t$  equations, are empirical constants, which must be determined by adjusting their values to fit experimental data. The above equations apply in

regions of high turbulence Reynolds number where the molecular viscosity is negligible. The expression for the turbulent Reynolds number is

$$Re_t = u' l / \nu \quad (4)$$

in which  $u'$  is the fluctuating velocity, and  $l$  the macro length scale. (This is of the order of the transverse dimensions of the geometry)

Several investigators<sup>7,11,12</sup> previously concluded that for low turbulent Reynolds number flows, the viscous dissipation is important, and, therefore, its effects must be accounted for in the turbulence model. Jones and Launder and Chien proposed modifications to account for low turbulence Reynolds number. The essential features of the two models are the same; however, a few differences may be noticed in their detailed implementation. A brief review of the two models is given below.

#### 1. Jones and Launder Model

This model is closely related to the Harlow and Nakayama<sup>3</sup> model which also contains proposals for the way in which molecular viscosity exerts direct influence on the turbulence when the turbulence Reynolds number is low. The Jones and Launder model has been widely tested for a range of flow conditions. Their model was able to predict the observed behavior of the wall Stanton number in flows in which laminarization was present. They enlarged the model in the following three ways.

- i) Viscous diffusion of  $k$  and  $\epsilon$  was included.
- ii) The empirical constants in the transport equations were made functions of the turbulent Reynolds number.
- iii) Terms were added to account for the fact that dissipation processes are not isotropic.

The  $k$  and the  $\epsilon$  equations for this model are as follows.

turbulent kinetic energy:

(5)

Energy dissipation rate:

$$\begin{aligned} \frac{\partial}{\partial x}(\rho u \epsilon) + \frac{1}{r} \frac{\partial}{\partial r}(\rho v r \epsilon) &= \frac{\partial}{\partial x} \left[ \left( \mu + \frac{\mu_t}{\sigma_\epsilon} \right) \frac{\partial \epsilon}{\partial x} \right] + \frac{1}{r} \frac{\partial}{\partial r} \left[ r \left( \mu + \frac{\mu_t}{\sigma_\epsilon} \right) \frac{\partial \epsilon}{\partial r} \right] \\ &+ C_1' \frac{\epsilon}{k} G - C_2' \rho \frac{\epsilon^2}{k} + 2\mu \mu_t \frac{\partial^2 u}{\partial y^2} \end{aligned} \quad (6)$$

Eddy viscosity:

$$\mu_t = C_\mu' \rho \frac{k^2}{\epsilon} \quad (7)$$

Turbulent thermal conductivity:

$$k_t = C_p \mu_t / \sigma_h \quad (8)$$

In the above equation set the C's and the  $\sigma$ 's retain the values assigned to them in the standard k- $\epsilon$  model. (Table 1) The influence of the Reynolds number is introduced by way of the f's which are assigned the following forms.

$$f_1 = 1 \quad (9)$$

$$f_2 = 1 - 3 \exp(-Re_\epsilon) \quad (10)$$

$$f_\mu = \exp[-2.5 / (1 + Re_\epsilon/50)] \quad (11)$$

where  $Re_\epsilon = \rho k^2 / \mu \epsilon$  may be interpreted as the Reynolds number of turbulence. These authors made  $\epsilon$  as the isotropic part of dissipation and made it go to zero at the wall because they could achieve decisive

computational advantages. They showed that the total dissipation at the wall becomes equal to the last term on the right hand side of the energy equation. In addition they used another term  $2\mu\mu_t \frac{\partial^2 u}{\partial y^2}$  in the dissipation equation in order to obtain better agreement with experimental data. They did not offer any explanation for the presence of this term except for the fact that the inclusion of this term provided better agreement with experimental data. They chose  $f_\mu$  so that the model, when applied to the calculation of the decay of grid turbulence, accorded with experiment for both high and low turbulence intensities. The form of the function  $f_\mu$  was determined by focusing on the prediction of constant stress couette flow wherein the turbulent viscosity formula given above was not used to calculate turbulent viscosity. Instead,  $\mu_t$  was obtained by way of the Van Driest form of the mixing length formula. This practice enabled attention to be focused on the  $\epsilon$  equation which was then adjusted to produce a reasonable turbulence energy distribution in the viscous sublayer region.

## 2. Hanjelic and Launder Model

Hanjelic and Launder<sup>10</sup> discussed the specific effects of viscosity on the various transport processes. They presented numerical solutions for turbulent channel flows at low Reynolds number as well as a case of severely accelerated boundary-layer in which the turbulent shear stress becomes negligible compared with viscous stresses.

The equation for dissipative transport has been used in the following form by Hanjelic and Launder.

$$\frac{D\epsilon}{Dt} = C_{\epsilon 1} \frac{\epsilon}{k} P - C_{\epsilon 2} \frac{\epsilon^2}{k} - C_\epsilon \frac{\partial}{\partial x_k} \left\{ \frac{k}{\epsilon} \overline{U_k U_l} \frac{\partial \epsilon}{\partial x_l} \right\} \quad (12)$$

where  $P$  is the rate of generation of turbulence energy by the mean strain

rate. Tennekes and Lumley<sup>24</sup> omitted the first term in Eq. 12 on the grounds that the term containing the mean field variables were of a smaller order. However, Hanjelic and Launder argued that a positive source term must be present in the equation so as to avoid physically unacceptable form of modeling. Lumley and Khajeh Nouri<sup>25</sup> preferred to have the term  $(u_i u_i / k - 2/3 \delta_{ij})^2 \epsilon$

instead of  $P$  in Eq. 12. Hanjelic and Launder preferred to use  $P$  rather follow the argument of Lumley and Khajeh Nouri. Extensive numerical testing conducted using  $P$  has been put forth as a reason for their choice of the term  $P$  in their model. In a homogeneous decaying turbulent flow Eq. 12 becomes

$$\frac{D\epsilon}{Dt} = - C_{\epsilon 2} \frac{\epsilon^2}{k} \quad (13)$$

A consequence of this equation is that the turbulent kinetic energy decays at a rate of  $x^{-n}$  where  $x$  is the distance downstream of the grid which generates the turbulence and  $n$  is an index whose value is given by

$$n = \frac{1}{(C_{\epsilon 2} - 1)} \quad (14)$$

The variation of  $n$  behind the grid is between 1.8 and 2.5 as observed from experiments. Hanjelic and Launder assumed that this variation was entirely due to the diminution of the turbulence Reynolds number  $Re_\epsilon$ . Therefore, they argued that  $C_{\epsilon 2}$  should be a function of  $Re_\epsilon$ . The particular form of the dependence was based on the experiments of Batchelor and Townsend. Thus,

$$\frac{D\epsilon}{Dt} = - C_{\epsilon 2} f_\epsilon \epsilon^2 / k \quad (15)$$

$$f_\epsilon = 1 - \frac{0.4}{1.8} \exp \left[ - \left( \frac{Re_\epsilon}{6} \right)^2 \right] \quad (16)$$



### 3. Chien's model

Chien<sup>7</sup> added kinematic viscosity  $\nu$  to account for molecular diffusion of  $k$  and  $\epsilon$ . The dissipation term in the  $\epsilon$  equation was modified to fit the data of decaying grid turbulence at high as well as low turbulent Reynolds numbers. Chien's handling of the effect of the presence of the solid wall is different from that of previous authors. He uses Taylor series expansion of the fluctuating velocity components near the wall. He showed, by the use of the continuity equation and the no slip condition at the wall, that

$$k \sim y^2$$

$$\nu \sim y^2$$

It can be shown by Taylor series expansion near the wall that isotropic dissipation is

$$\epsilon \sim y^4$$

Chien showed that the true rate of energy dissipation is given by

$$D = 2\nu k/y^2 \quad (17)$$

in which  $\nu$  is the kinematic viscosity,  $k$  the turbulent kinetic energy and  $y$  the distance from the wall. Therefore, the low turbulent form of the  $k$  equation can be written as

$$\frac{\partial k}{\partial t} = \frac{\partial}{\partial y} \left[ \left( \nu + \frac{\nu_t}{\sigma_k} \right) \frac{\partial k}{\partial y} \right] + \nu_t \left( \frac{\partial u}{\partial y} \right)^2 - \epsilon - \frac{2\nu k}{y^2} \quad (18)$$

This equation differs from the standard form of the  $k$ - $\epsilon$  model because of the presence of the last term on the right hand side. The  $\epsilon$  equation gets modified in Chien's model as

$$\frac{\partial \epsilon}{\partial t} = \frac{\partial}{\partial y} \left[ \left( \nu + \frac{\nu_t}{\sigma_\epsilon} \right) \frac{\partial \epsilon}{\partial y} \right] + C_1 \frac{\epsilon}{k} \nu_t \left( \frac{\partial u}{\partial y} \right)^2 - \frac{\epsilon}{k} \left[ C_2 f_\epsilon \epsilon + \frac{2\nu k}{y^2} \exp(-C_4 u^* y / \nu) \right] \quad (19)$$

in which  $f_\epsilon$  is given by Eq. 16 and  $u^*$  denotes the friction velocity. Chien used  $C_\mu = 0.5$  in the above equation.

#### 4. Present Modifications of the above Models

Modified forms of the Jones and Launder model and the Chien model were used for the present study. The modifications were implemented because of the realization that wall bounded flows are different from the flow in the inviscid core of a confined jet. It is reasonable to assume that the flow is isotropic in the inviscid core region; therefore, the presently proposed model differs from those cited above in that the nonisotropy terms are absent. Moreover, the present calculations did not use terms to account for wall damping effects. Eqs. 5 and 6 were modified to reflect these changes. The term  $2\mu\left(\frac{\partial k}{\partial y}\right)^2$  was dropped from Eq. 5 and indicated earlier the term  $2\mu\mu_1\frac{\partial u}{\partial y}$  was also dropped from Eq. 6. Jones and Launder introduced the last term in Eq. 6 purely on the basis of obtaining better agreement with experimental data of wall bounded flows; it is felt that this is not a sufficient reason to introduce this term in the present calculations.

In order to investigate the usefulness of the two models in flow regimes characterized by a sudden axisymmetric expansion, a different and complete set of calculations were performed using the modified form of Chien's model. All the additional terms to account for low turbulent Reynolds number effects in Chien's model were carefully examined. It was concluded that for the present study only the term  $C_2 f_\epsilon \frac{\epsilon^2}{k}$  in Eq. 19 needs to be retained. The basis for this conclusion is the fact that in the inviscid core the other effects discussed in Chien's paper are not important.

### 5. Streamline Curvature Effects

Another aspect of the turbulence model that was investigated is the effect of streamline curvature. This is particularly important in the recirculation region where one comes across large curvature of the streamlines. Bradshaw<sup>22</sup> reviewed the experimental studies to determine the effects of streamline curvature on turbulent flows and concluded that the standard turbulence models (mixing length and  $k-\epsilon$  models) do not reflect the sensitivity of turbulence to streamline curvature. Modifications of the  $k-\epsilon$  model to account for streamline curvature were reported by Leschziner and Rodi<sup>11</sup>. These modifications are based on Gibson's algebraic stress model<sup>6</sup>. The algebraic stress equation is written in general form as

$$P_{ij} = \alpha \frac{\epsilon}{k} (\overline{u_i u_j} - \frac{2}{3} \delta_{ij} k) + \beta (P_{ij} - \frac{2}{3} \delta_{ij} P_k) + \frac{2}{3} \delta_{ij} \epsilon \quad (20)$$

In which  $P_{ij}$  is the production of turbulent stress  $\overline{u_i u_j}$ , and  $\alpha$  and  $\beta$  are constants, which assume the values of 1.5 and 0.6 respectively as given Leschziner and Rodi.<sup>11</sup> The term  $P_k$  stands for the production of turbulent kinetic energy, and  $\delta_{ij}$  is the Kronecker delta. Gibson's algebraic stress model assumes local equilibrium -- total energy supply is equal to the total energy dissipation. Under this assumption one can write  $P_k = \epsilon$ , and the above equation reduces to

$$\frac{\overline{u_i u_j}}{k} = \frac{1 - \beta}{\alpha \epsilon} P_{ij} - \frac{2}{3} \frac{\delta_{ij}}{\alpha} (1 - \alpha - \beta). \quad (21)$$

In order to see the effect of streamline curvature, this equation can be written in the streamline coordinates  $(s, n)$ , in which  $s$  is the streamwise coordinate, and  $n$  the normal coordinate.

$$P_{ss} = -2 \overline{u_s^2} \frac{\partial U_s}{\partial s} - 2 \overline{u_s u_n} \left( \frac{\partial U_s}{\partial n} + \frac{U_s}{R_c} \right) \quad (22)$$

$$P_{nn} = -2 \overline{u_n^2} \frac{\partial U_n}{\partial n} + 4 \overline{u_n u_s} \frac{U_s}{R_c} \quad (23)$$

$$P_{ns} = -\overline{u_s^2} \frac{\partial U_s}{\partial n} + (2 \overline{u_s^2} - \overline{u_n^2}) \frac{U_s}{R_c} + \overline{u_n u_s} \frac{U_r}{r} \quad (24)$$

In the above equations,  $R_c$  is the radius of curvature of the streamline, and  $U_r$  the mean velocity in the radial direction. Further simplifications are achieved by Leschziner and Rodi<sup>11</sup> by stipulating that

$$\frac{U_r}{r} = \frac{\partial U_s}{\partial s} = \frac{\partial U_n}{\partial n} = 0 \quad (25)$$

Although it appears reasonable to assume that  $\partial U_s / \partial s = \partial U_n / \partial n = 0$ , the additional assumption that  $U_r / r = 0$  does not seem to be a particularly sound one. This may be easily seen from Figure 3. The ratio  $U_r / r$  does have appreciable values in places where the streamlines have large inclinations with reference to the axis (plane) of symmetry. Therefore,  $U_r / r$  was retained in the present calculations. The modified form of the shear stress equation was obtained from Eqs. 22-24.

$$-\overline{u_s u_n} = \frac{-K_1 K_2}{[1 + 8 K_1^2 \frac{k^2}{\epsilon} \left( \frac{\partial U_s}{\partial n} + \frac{U_s}{R_c} - K_1 \frac{k}{\epsilon} \frac{U_r}{r} \right)]} \frac{k^2}{\epsilon} \left( \frac{\partial U_s}{\partial n} - \frac{U_s}{R_c} \right) \quad (26)$$

in which

$$K_1 = (1 - \beta) / \alpha, \text{ and}$$

$$K_2 = 2(1 - \alpha - \beta) / (3\alpha)$$

By comparing Eq. 26 to the expression for eddy viscosity, it can be easily seen that

$$C'_\mu = \frac{K_1 K_2}{[1 + 8 K_1^2 \frac{k^2}{\epsilon} (\frac{\partial U}{\partial n} + \frac{U}{R_c} - K_1 \frac{k}{\epsilon} \frac{U}{r})]} \quad (27)$$

Except for the retention of the term  $K_1 k \frac{U}{r}$ , the expression for  $C_\mu$  is the same as that given by Leschziner and Rodi<sup>11</sup>. The value of 0.09 was used for  $K_1 K_2$  following the argument given by these authors.

#### GOVERNING EQUATIONS AND NUMERICAL MODELING

The equations governing the compressible, axisymmetric, turbulent flow of a perfect gas can be written in a convenient form as

$$\frac{1}{r} \left[ \frac{\partial}{\partial x} (\rho u r) + \frac{\partial}{\partial r} (\rho v r) - \frac{\partial}{\partial x} (r \Gamma_\phi \frac{\partial \phi}{\partial x}) - \frac{\partial}{\partial r} (r \Gamma_\phi \frac{\partial \phi}{\partial r}) \right] = S_\phi \quad (28)$$

In the above equation the variables  $\phi$  and  $r_\phi$  assume different meanings for the equations of continuity, momentum, energy, turbulent kinetic energy and its dissipation rate. The general form of the equations given by Eq. 28 is particularly useful for their numerical solution.

For compressible flows density is also a variable and it is calculated using the equation of state for a perfect gas. For chemically reacting flows there will be additional equations for species continuity and chemical reaction rates.

The partial differential equations of continuity, momentum, energy and the turbulent quantities represented by the general form given by Eq. 28 are solved by the SIMPLE algorithm of Ref. 13. Details of the solution procedure may be found in several other references also<sup>10-12</sup>. The discretization equations are obtained by integrating the partial differential equations over the cell control volumes formed about the grid lines in the solution domain. A

lucid explanation of its advantages over other differencing methods is given by Patankar<sup>27</sup>. Suffice to state that the procedure ensures conservation of quantities such as mass, momentum and energy over any group of control volumes and therefore, over the whole computational domain. The pressure field is initially guessed and it is corrected at each iteration stage by means of a pressure correction equation. A staggered grid approach and a central/upwind differencing scheme are used in applying the equations; the advantages of these can be found in Ref. 27. A line-relaxation procedure is used for the solution of the equations. Convergence is improved by reliance on under-relaxation factors which control the variation of dependent variables from iteration to iteration. A mesh size of 21x35 was used for the present calculations. The mesh is nonuniformly arranged in order to provide better resolution in regions of high gradients of the flow variables.

The energy equation warrants particular mention. The compressible form of the energy equation was used for the present calculations and therefore, density was treated as a variable. It was calculated from the perfect gas equation of state

$$p = \rho RT$$

This method of calculating density is a departure from the previous methods in which the density is calculated using density correction equations. The present procedure makes the calculation of density more elegant and straightforward. Variations of the dynamic viscosity  $\mu$  and the thermal conductivity  $k$  with temperature are calculated using Sutherland's formulas for viscosity and thermal conductivity. They are given below.

$$\frac{\mu}{\mu_{ref}} = \left( \frac{T}{T_{ref}} \right)^{3/2} \frac{T_{ref} + 110}{T + 110} \quad (2)$$

$$\frac{k}{k_{\text{ref}}} = \left( \frac{T_{\text{ref}}}{T} \right)^{3/2} \frac{T_{\text{ref}} + 195}{T + 195} \quad (30)$$

Two methods were used for the numerical implementation of the procedure for obtaining compressible flow solutions.

The steps involved in the first method is illustrated by means of the flow diagram given in Figure 4 and may be summarized as follows:

1. Obtain a converged solution for an incompressible flow case (Mach number less than 0.2).
2. Store the solution variables on restart files in non-dimensional form.
3. Increase the inlet velocity by a small increment and repeat the solution procedure using variables stored in the non-dimensional form from the previous solution as the initial guesses; this will give a new set of non-dimensional variables to be stored on restart files.
4. Repeat steps 2 and 3 till the inlet velocity reaches the desired value in the subsonic compressible regime.

It should be noted that the non-dimensional form of the variables is particularly useful for their usage as starting values in the solution procedure. Since the solution proceeds in steps of small increments of the flow variables, faster convergence is achieved. The reason for the faster convergence may be due to the fact that the initial guesses for the flow variables are close to the true solution. Thus, special formulations for the density and pressure correction equations are avoided.

The second method was based on the use of the perfect gas equation of state in the differential form. The perfect gas equation of state may be differentiated to obtain an expression for the density change in terms of pressure and temperature. The resulting expression is

$$d\rho = \frac{d\rho}{RT} - \frac{\rho dT}{T} \quad (31)$$

The above form was used to calculate the change in density at every iteration stage. The new density was then calculated by adding this incremental change to the old value of the density. The advantage in using this method can be seen from the fact that the expression for density change involves the pressure change  $dp$ . Therefore, round-off errors may be smaller if this expression is used. It is also possible to control the change in density from iteration to iteration by means of an under-relaxation factor for density. The use of an under-relaxation factor for density was seen to improve convergence.

#### BOUNDARY CONDITIONS

In the SIMPLE procedure the boundary conditions are applied by modifying the discretization equations for the boundary cell control volumes. The no slip condition is applied for the velocities at the solid walls; at the axis of symmetry the normal derivatives of the flow variables except the radial velocity are set equal to zero. The radial velocity itself must be set equal to zero at the axis of symmetry in order to avoid multiple values of the variable there. The present code (ECFLOW) has options for three types of boundary conditions for the energy equation. The Dirichlet boundary condition is used for cases where the wall temperature is specified; the Neumann boundary condition is used for adiabatic wall cases and the Robin boundary condition is used for cases with prescribed wall heat flux. The boundary conditions for the  $k$  and the  $\epsilon$  equations are applied by means of wall functions which are used to avoid the use of extremely fine computational mesh near the wall. The rationale for the use of the wall functions is given by Chieng and Launder\*.



## RESULTS AND DISCUSSION

### Turbulence Models

An exhaustive study of turbulence models applicable to low turbulence Reynolds number regions and recirculating flow regions have been conducted. Models proposed by other investigators as well as modifications appropriate to the present problem have been tried. The influence of the various terms in the turbulence models were investigated from the point of view of their physical realism and their ability to improve predictions of the flow regimes encountered in combustion chambers.

The present study was conducted with the primary goal of predicting recirculating flowfields which are present in many internal flows associated with propulsion systems. The need for reexamining the turbulence models for this type of flowfield arises from the fact that the turbulence models rely heavily on empiricism. One severe drawback of the existing turbulence models is that they have been tested only against simple flows such as free jets and boundary-layers for which experimental data existed at the time these models were developed. The difficulty in obtaining turbulence and mean flow data in recirculating flowfields is well recognized. Hence the built-in bias in the models towards satisfying free-jet flow and boundary-layer flow phenomena.

Reliable and accurate experimental data for flowfields with high levels of turbulence are beginning to appear in literature<sup>20</sup>. The advances in non-intrusive optical flow diagnostics techniques are the major reason for this development. The present study is an attempt to use the recently available experimental data to evaluate the turbulence models that are currently being used. modifications are suggested, where appropriate, to improve the predictions.

The inviscid core that is present at the entrance of a sudden pipe

expansion is a region of low turbulent Reynolds number. However, no turbulence model exists to adequately treat this region. Hanjelic and Launder have specifically stated that their low turbulence Reynolds number model is not suitable for free-shear flows. Attempt was made in the present study to obtain a suitable form for the low turbulence Reynolds number model that can be used in the inviscid core region. Hanjelic and Launder used the term  $f_\epsilon$  given by Eq. 16 in their calculations. However, calculations performed with the sign changed in the expression (so that  $F_\epsilon$  becomes greater than 1) showed better agreement with the data for the turbulence energy decay along the center-line. This difference in the decay rate of the turbulence energy, as compared to the decay of grid turbulence may be explained on the grounds that a region of high turbulence surrounds the inviscid core and it is likely to exert significant influence on the evolution of turbulence within the inviscid core. The effect of the influence of the outer region on the flow within the inviscid core may be illustrated with the help of the sketches given in Figure 5. In all the three cases the incoming flow is assumed to be uniform (top-hat shape) with low levels of turbulence. Case (a) is a free jet in a quiescent medium. Case (b) is the flow from a hole-in-a-disk arrangement. Case (c) is the flow in a sudden pipe expansion.

The turbulence models that can be found in the literature do not take due account of the influence of the boundary conditions on the evolving flow. For example, will the decay of turbulence in the inviscid core region be the same in all the three cases illustrated in Figure 5? The present study indicates that the presence of the boundaries must be taken into consideration, not just as a local influence, but in a more global manner.

The streamline curvature modifications of Leschziner and Rodi did not improve the predictions in the recirculating flow region. The reason for this

behavior may lie in the fact that many sweeping assumptions were made in formulating this model. Omitting the term  $U_r/r$  without sound justification is one example where the assumptions are not based on valid argument. However, when this term was included in the calculations, it was seen that the solution did not converge.

The present study is inconclusive as far as the modifications to the turbulence models are concerned. Even though it has been established that the existing models are not adequate to treat turbulence in recirculating flows, certain general directions towards improving these models can be suggested based on the present study. A definite form for the improved model with the values of the empirical constants requires much further study. More experimental data on highly turbulent recirculating flows are immediately needed to correlate the models with experiments.

#### Compressible Flow Calculations

Some results from a compressible flow case with a nominal (inlet) velocity of 150 m/s are presented in Figures 6-8. The static temperature of the air at the inlet for this case was 300 °K. The temperature boundary conditions used for this case are insulated side (East) wall and constant temperature top (North) wall. Therefore, the temperature contours in this case resulted solely from compressibility effects. Contour plots of vorticity, temperature and turbulent kinetic energy are shown in these figures. All the plots are given in the non-dimensional form by using appropriate non-dimensionalizing parameters.

The vorticity contours in Figure 6 are clustered near the entrance around the step where the diameter changes from the smaller to the larger. Physically this region represents the boundary region between the inviscid core and the recirculation region. It is interesting to note that the recirculation region

is one of low vorticity; therefore, this region behaves like a free vortex.

The temperature contours are shown in Figure 7. The high temperature region lies downstream of the recirculation region and it can be seen that the rise in temperature in this region is caused by the deceleration of the flow because of the expansion and the resulting rise in static temperature. There exists a large region close to sudden expansion plane where the temperature is more or less uniform. This rapid attainment of uniformity in temperature is encouraging because it is one of the qualities that one looks for in a combustor. However, it should be cautioned that the temperature distribution in a reacting flow will depend also on the fuel-air distribution, and therefore, on the location and configuration of the fuel injectors. Another factor that will become important while considering temperature distribution in reacting flows is the wall boundary condition. As the heat transfer to the wall increases, it is expected that the region of uniform temperature seen in Figure 7 will shrink in size and move towards the center of the chamber.

The contours of turbulent kinetic energy are shown in Figure 8. Its maximum is seen to be at a downstream distance of about one diameter. Radially, the maximum occurs at the same distance as the smaller diameter of the inlet. Approximately this is the region where the expanding forward flow region and the recirculation region meet. Therefore, this constitutes the shear layer and it is natural to expect the highest levels of turbulence to occur in this region. The usefulness of the contour plots of the flow parameters to a designer can be easily seen from this figure. For the fuel air to mix to the maximum extent the fuel must enter the chamber from the periphery of the inlet.

## CONCLUSIONS

The present study has resulted in a computer code capable of predicting recirculating compressible flow in axisymmetric ducts. Some of the deficiencies of the existing turbulence models are identified in the present study and modifications are suggested. Very useful information from the compressible flow solution that could be of direct use to the designer is obtained from the present study.

In addition to improving the fluid dynamic model, several coding improvements were implemented, some of which are discussed below.

The computer code was extensively modified to make input and output more efficient. Presently all the data are input using a separate input file rather than specifying them within the program by means of source statements. This has made it possible to reduce the number of compilations necessary while conducting parametric study to see the influence of the various parameters in the governing equations. Another significant modification that was incorporated into the program is the provision for temporary storage and retrieval. This feature is very useful when the compressible flow equations are being solved.

While the program was being tested it was noticed that it took several iterations for some of the residual source sums to attain values below the ones specified as convergence criteria. As a remedy the use of double precision arithmetic was tried and this resulted in convergence with less number of iterations. All the calculations in the program presently use double precision arithmetic. It is felt that as the complexity of the calculations increase as a result of additional equations that must be solved while solving more complex flowfields, double precision arithmetic will become essential in order to preserve accuracy.

All the modifications to the program has been profusely documented

internally with the help of comment statements in order to aid other users in getting easily acquainted with the program. Other users can now run the program with a minimum investment of their time. The extensive internal documentation also facilitates future changes with little effort. Thus, calculations with a different chemical species arising, for example, from the use of fuel-air mixture, is straight forward and easy to implement. Or, as another example, a different turbulence model may be attempted by incorporating it as another option.

## REFERENCES

1. Launder, B. E. and D. B. Spalding, Mathematical Models of Turbulence, Academic Press, London, 1972.
2. Bradshaw, P., Ferriss, D. H. and Atwell, N. P., "Calculation of Boundary Layer Development Using the Turbulent Energy Equation," J. Fluid Mech., vol. 28, 1967, pp. 593-616.
3. Harlow, F. H. and Nakayama, P. I., "Transport of Turbulence Energy Decay Rate," Los Alamos Sci. Lab. Rep. LA 3854, 1968.
4. Lumley, J. L., and Khajeh Nouri, B. J., "Computational Modeling of Turbulent Transport," Adv. Geophys. Vol. 18A, 1974, pp. 169-192.
5. Wilcox, D. C. and Rubesin, M. W., "Progress in Turbulence Modeling for Complex Flow Fields including the effect of Compressibility," NASA TP 1517, 1980.
6. Gibson, M. M. and Rodi, W., "A Reynolds Stress Closure Model for Turbulence Applied to the Calculation of a Highly Curved Mixing Layer," J. Fluid Mechanics, Vol. 103, 1981.
7. Chien, K. Y., "Predictions of Channel Boundary-Layer Flows with a Low-Reynolds-Number Turbulence Model," AIAA J., Vol. 20, 1982, pp. 33-38.
8. Bywater, R. J., "Velocity Space Description of Certain Turbulent Free Shear Flow Characteristics," AIAA J., Vol. 20, No. 6, June 1982.
9. Chieng, C. C. and Launder, B. E., "On the Calculation of Turbulent Heat Transport Downstream from an Abrupt Pipe Expansion," Numerical Heat Transfer, 3, pp. 189-207, 1980.
10. Hanjelic, K. and Launder, B. E., "Contribution towards a Reynolds-stress Closure for Low Reynolds-number Turbulence," J. Fluid Mech., vol. 74, 1976, pp. 593-610.
11. Leschziner, M. A. and Rodi, W., "Calculation of Annular and Twin Parallel

- Jets Using Various Discretization Schemes and Turbulence-Model Variations," J. Fluids Engng., 103, A352, 1981.
12. Jones, W. P. and Launder, B. E., "The Prediction of Laminarization with Two-Equation Model of Turbulence," Intl. J. Heat and Mass Transfer, Vol. 15, 1972, pp. 301-304.
  13. Patankar, S. V. and Spalding, D. B., "A Calculation Procedure for Heat, Mass and Momentum Transfer in Three-Dimensional Parabolic Flows," Int. J. Heat Mass Transfer, vol. 15, 1972, pp. 1787-1806.
  14. Harlow, F. H. and Welch, J. E., "Numerical Calculation of Time-dependent Viscous Incompressible Flow," Phys. Fluids, Vol. 8, 1965, pp. 2182-2189.
  15. Raithby, G. D., "Skew Upstream Differencing Schemes for Problems Involving Fluid Flow," Computer Methods in Applied Mechanics and Engineering Vol. 9, 1976, pp. 153-164.
  16. Leonard, B. P., "Stable and Accurate Convective Modeling Procedure Based on Quadratic Upstream Interpolation," Computer Methods in Applied Mechanics and Engineering, Vol. 19, 1979, pp. 59-98.
  17. Krishnamurthy, L. and Park, S. O. "Streamline Curvature Effects in Confined Isothermal Recirculating Flowfields Behind an Axisymmetric Bluff Body: Numerical Calculations with the k- Turbulence Model," Fourth Symposium on Turbulent Shear Flows, Karlsruhe, F. R. Germany, September 1983.
  18. Gosman, A. D. and Ideraih, F. J. K., "TEACH-2E: A General Computer Program for Two-Dimensional Turbulent Recirculating Flows," Report, Dept. of Mech. Eng., Imperial College, 1976.
  19. Lilley, D. G. and Rhode, D. L. "A Computer Code for Swirling Turbulent Axisymmetric Recirculating Flows in Practical Isothermal Combustor Geometries," NASA-CR-3442, 1982.



20. Boray, R. S. and Chang, C., "Flow Studies of Dump Combustors," Fifth International Symposium on Airbreathing Engines," Bangalore, India, February 1981.
21. Sindir, M. M. and Harsha, P. T., "Assessment of Turbulence Models for Scramjet Flowfields," SAI Rept. No. 82-038-CHA, 1982.
22. Harsh, W. H., "Numerical Modeling of Ramjet Combustors," Air Force Aero Propulsion Lab. Report AFWAL-TR-82-2113, Wright Patterson Air Force Base, 1983.
23. Isaac, K. M., "Computational Study of Ramjet Combustor Flowfields," AFOSR/SCEEE Summer Faculty Research Program Report, 1984.
24. Tennekes, H. and Lumley, J. L., A First Course in Turbulence, The MIT Press, 1972.
25. Batchelor, G. K. and Townsend, A. A., "Decay of Isotropic Turbulence in the Final Period," Proc. Roy. Soc. A 194, 1948.
26. Bradshaw, P., "Effects of Streamwise Curvature on Turbulent Flows," AGARDograph No. 196, 1973.
27. Patankar, S. V., Numerical Heat Transfer and Fluid Flow, Hemisphere, Washington, DC, 1980.
28. Craig, R. R., Nejad, A. S., Hahn, E. Y., and Schwertkopf, K. G., "A General Approach for Obtaining Unbiased LDV Data in Highly Turbulent Non-reacting and Reacting Flows," AIAA-84-0366, AIAA 22nd Aerospace Sciences Meeting, 1984.

# APPENDIX

The governing equations for the conservation of mass, momentum, energy, the turbulent kinetic energy and the energy dissipation rate can be cast in the general form:

$$\frac{1}{r} \left[ \frac{\partial}{\partial x} (\rho u r \phi) + \frac{\partial}{\partial r} (\rho v r \phi) - \frac{\partial}{\partial x} (\tau_{r\phi} \frac{\partial \phi}{\partial x}) - \frac{\partial}{\partial r} (\tau_{r\phi} \frac{\partial \phi}{\partial r}) \right] = S_{\phi} \quad (1)$$

where  $\phi$  stands for the variables shown in the table. The forms for the source term  $S_{\phi}$  are also given in the table.

Table 1. The Form of the Source Term in the General Equation for  $\phi$  (Eq. (1))

$\phi$	$S_{\phi}$
$u$	$-\frac{\partial p}{\partial x} + S^u$
$v$	$-\frac{\partial p}{\partial r} + \frac{\rho w^2}{r} - \frac{2\mu v}{r^2} + S^v$
$w$	$-\frac{\rho v w}{r} - \frac{w}{r^2} \frac{\partial}{\partial r} (r\mu)$
$h$	0
$k$	$G - C_D \rho \epsilon$
$\epsilon$	$(C_1 \epsilon G - C_2 \rho \epsilon^2)/k$

The quantities  $S^u$ ,  $S^v$  and  $G$  appearing in the source terms have the following meaning.

$$S^u = \frac{\partial}{\partial x} (\mu \frac{\partial u}{\partial x}) + \frac{1}{r} \frac{\partial}{\partial r} (r\mu \frac{\partial v}{\partial x}) \quad (2)$$

$$S^v = \frac{\partial}{\partial x} (\mu \frac{\partial u}{\partial r}) + \frac{1}{r} \frac{\partial}{\partial r} (r\mu \frac{\partial v}{\partial r}) \quad (3)$$

$$G = \mu \left[ 2 \left\{ \left( \frac{\partial u}{\partial x} \right)^2 + \left( \frac{\partial v}{\partial r} \right)^2 + \left( \frac{v}{r} \right)^2 \right\} + \left( \frac{\partial u}{\partial r} + \frac{\partial v}{\partial x} \right)^2 + \left\{ r \frac{\partial}{\partial r} (w/r) \right\}^2 + \left( \frac{\partial w}{\partial x} \right)^2 \right] \quad (4)$$

$C_{\mu}$	$C_1$	$C_2$	$C_D$	$\sigma_k$	$\sigma_\epsilon$
0.09	1.44	1.92	0.96	1.0	1.2174

Table 1. Constants used in the k -  $\epsilon$  Turbulence Model

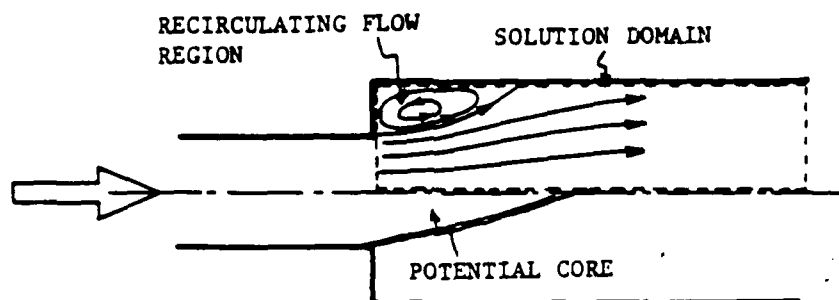


Figure 1. Schematic of Dump Combustor

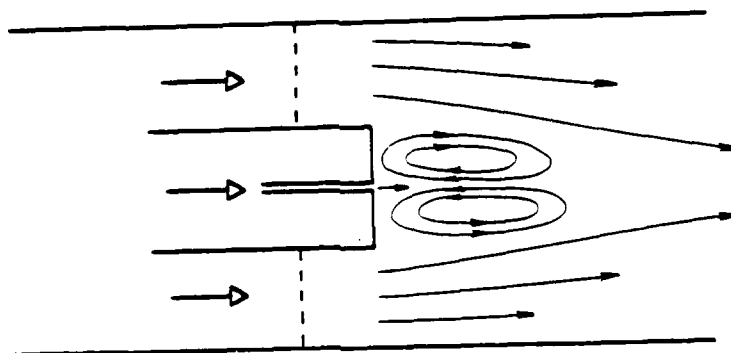


Figure 2. Schematic of Center Bluff Body Combustor

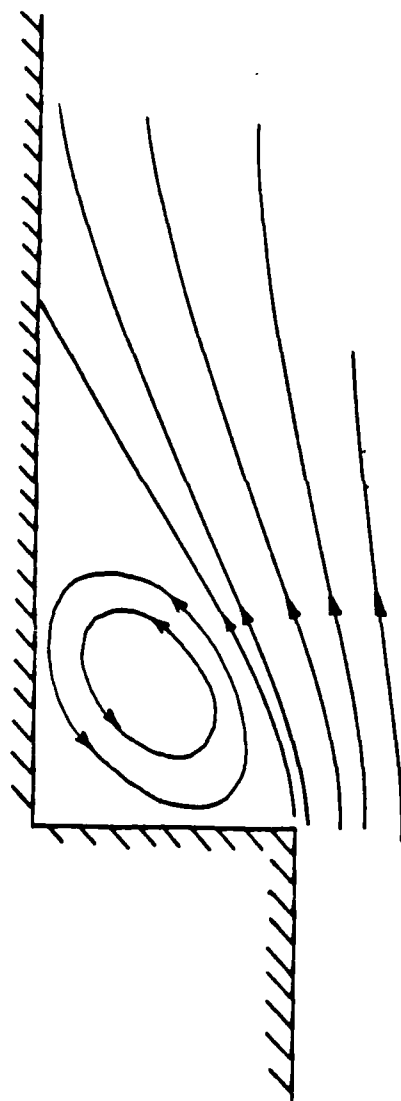


Figure 3. SCHEMATIC OF THE DUMP COMBUSTOR SHOWING THE RECIRCULATION REGION WHERE  $u_t/r$  MAY NOT BE NEGLIGIBLE

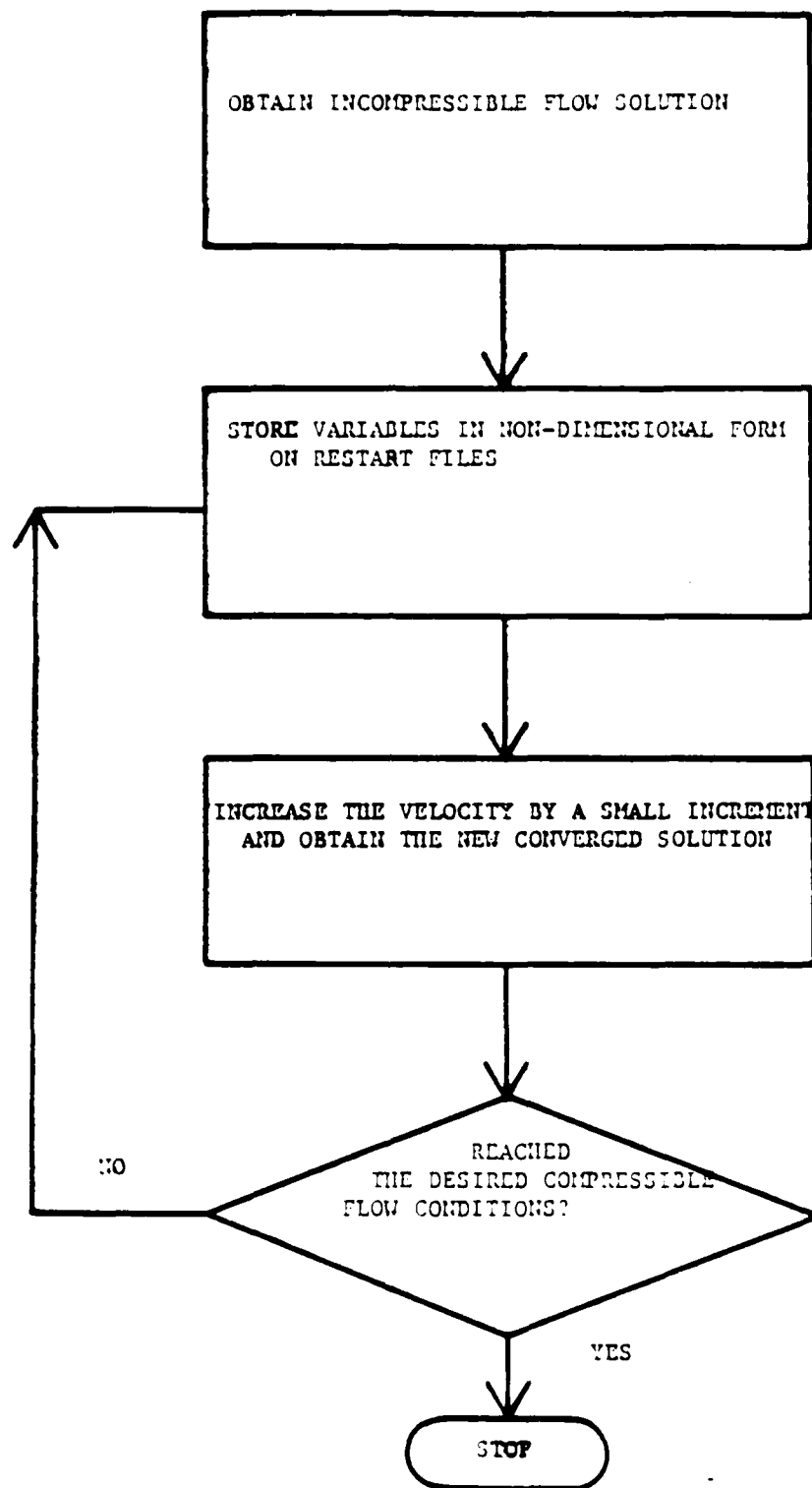


FIGURE 4 . SOLUTION PROCEDURE FOR COMPRESSIBLE NAVIER-STOKES EQUATIONS.

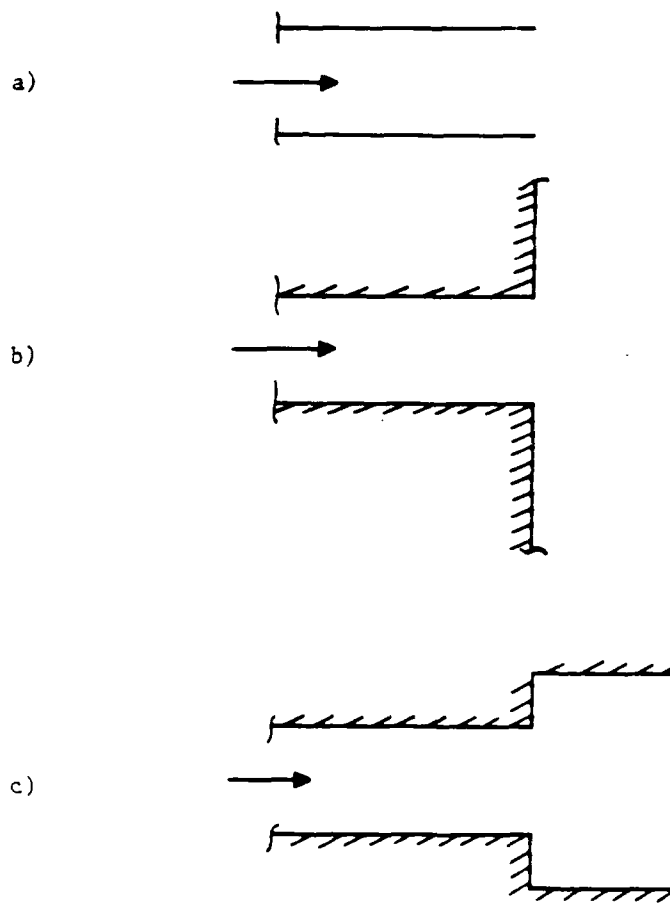


Figure 5. Different Jet Exit Conditions

- a) Free Jet in Quiescent Medium
- b) Hole-in-a-disk arrangement
- c) Confined Jet

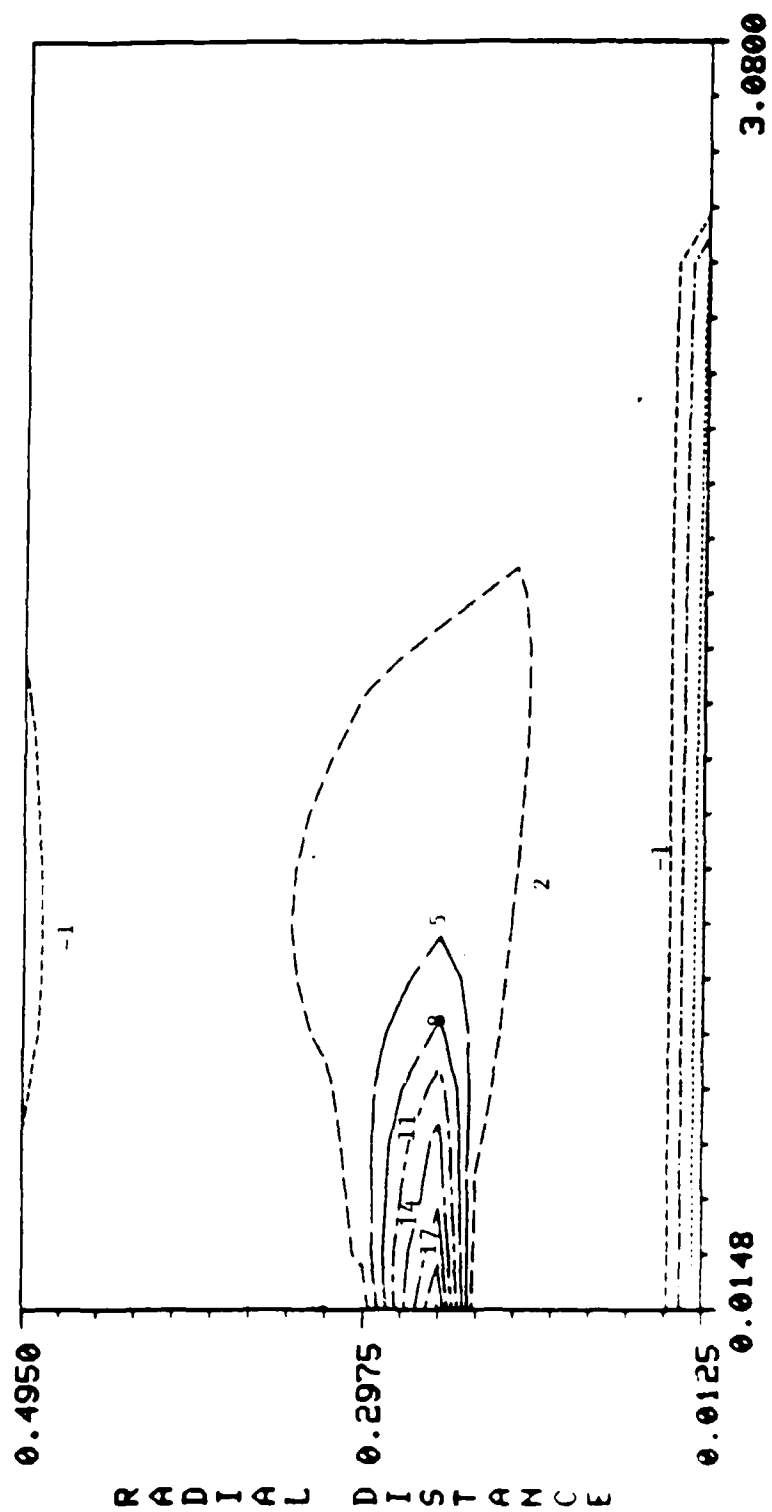


Figure 6. Non-dimensional Vorticity Contours



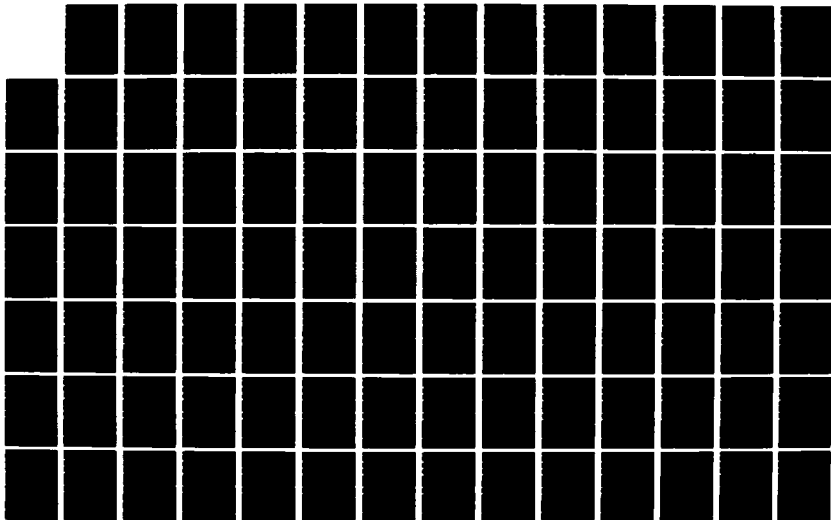
AD-A186 490

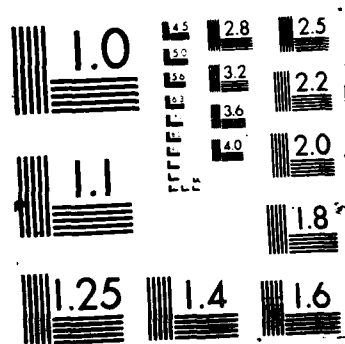
UNITED STATES AIR FORCE RESEARCH INITIATION PROGRAM  
1984 RESEARCH REPORTS (U) SOUTHEASTERN CENTER FOR  
ELECTRICAL ENGINEERING EDUCATION INC S W D PEELE  
MAY 86 AFOSR-TR-87-1721 F49620-82-C-0035 F/G 15/1

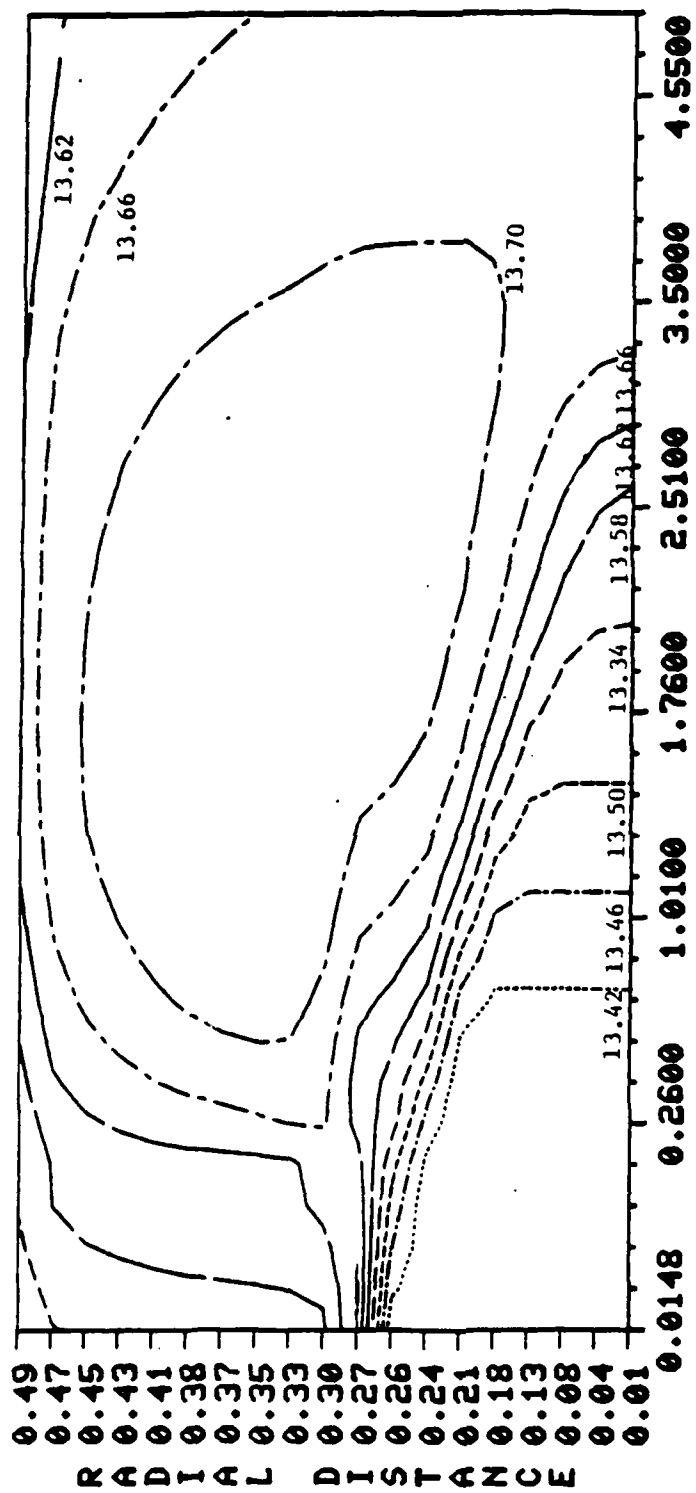
06/11

UNCLASSIFIED

NL







Axial Distance (Diameters)

Figure 7. Non-dimensional Temperature Contours

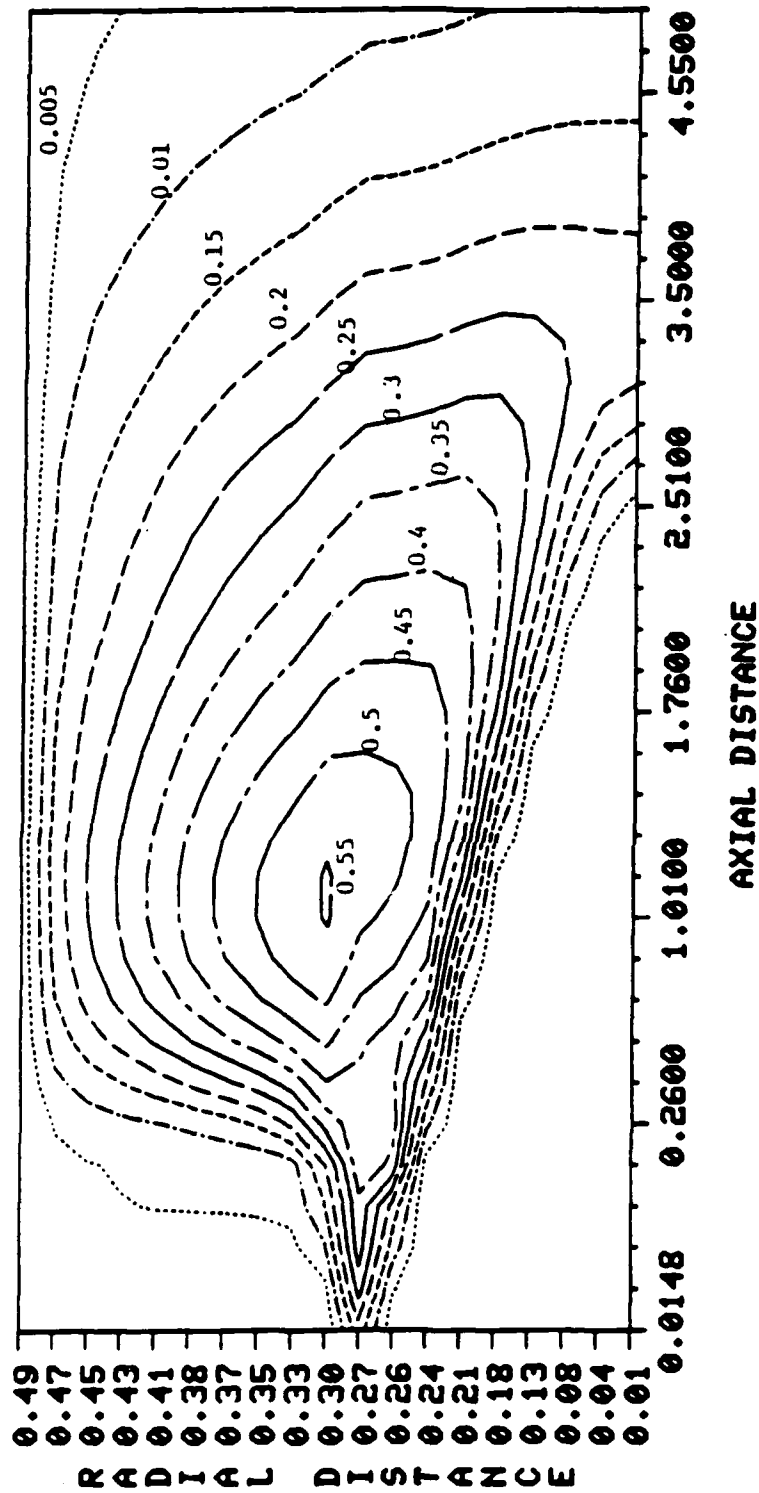


Figure 8. Non-Dimensional Turbulent Energy Contours

1985 RESEARCH INITIATION IN SCIENCE AND ENGINEERING PROGRAM

Sponsored by the

AIR FORCE OFFICE OF SCIENTIFIC RESEARCH

Conducted by the

SOUTHEASTERN CENTER FOR ELECTRICAL ENGINEERING EDUCATION

FINAL REPORT

FREE STREAM TURBULENCE EFFECTS ON TURBULENT

HEAT AND MOMENTUM TRANSFER

Prepared by:	Dr. Paavo Sepri and Mr. Baek Youn
Academic ranks:	Associate Professor and Graduate Assistant
Department and University:	School of A.M.N.E. University of Oklahoma
USAF Laboratory Location:	Air Force Wright Aeronautical Laboratories Aero-Propulsion Laboratory Turbine Engine Division Components Branch
USAF Research Contacts:	Dr. Richard Rivir and Mr. Charles D. MacArthur
Date:	August 31, 1985
Contract No.:	F49620-82-C-0035

FREE STREAM TURBULENCE EFFECTS ON TURBULENT  
HEAT AND MOMENTUM TRANSFER

By

Paavo Sepri and Baek Youn

ABSTRACT

Attention is focused on the computational predictability of turbulent boundary layers influenced by free stream turbulence (FST). One practical application lies in the area of improving turbine blade performance and enhancing the attendant lifespan. The approach herein has consisted of further scrutiny of recently published data, improved modeling of turbulent fluxes, and computations with the code STANCOOL. Four novel results have been achieved which are presented for the first time in this report. First, an analytical representation is proposed which is shown to approximate well the mean profiles of velocity and temperature throughout a turbulent boundary layer. A triple-deck exponential function is demonstrated to approximate laminar as well as turbulent profiles by appropriate changes of the parameters. FST effects are incorporated into the model by explicit variations in the coefficients. Second, through observations and fitting of data, the turbulent boundary layer is shown to be composed of three layers, for which length scales are proposed in a preliminary fashion. Third, by use of the observed triple exponential, a novel integro-differential model is proposed for the Reynolds stress and turbulent heat flux terms. Fourth, a remarkable analytical solution is found to describe a turbulent boundary layer for the case of a particular form for the Reynolds stress. Analytical expressions are derived for the turbulent Prandtl number profile for two limiting cases. Modifications of and computations with the code, STANCOOL, demonstrate improved agreement with available data for the case of a flat plate.

#### ACKNOWLEDGEMENTS

The authors gratefully acknowledge the opportunity and financial support extended to them by the Air Force Systems Command, the Air Force Office of Scientific Research, and the Southeastern Center for Electrical Engineering Education. This investigation was conducted under Contract F49620-82-C-0035. The Graduate College of the University of Oklahoma has also contributed to this investigation through cost-sharing of the expenses. Finally, the authors wish to thank Ms. Lynn Crussel for expeditious typing of the manuscript.

## 1.0 INTRODUCTION

### 1.1 Background

The transport of mass, momentum, and energy across turbulent boundary layers is a subject that is rich in practical application, and consequently it has received considerable attention in several disciplines of science and engineering. The present investigation has been motivated primarily by the continuing need for improvements in computational tools used for predicting heat transfer in the complicated aerothermal environment of turbine engines. Improvements in state-of-the-art engine design and efficiency will rely increasingly on computer codes which can predict alterations in performance and turbine blade cooling requirements under adverse thermal conditions. One goal is to increase the lifespan of turbine blades while minimizing the auxiliary power needed to cool the components effectively. For this purpose it is necessary to have accurate knowledge of heating distributions on the blade surfaces under varying operating conditions.

The present investigation is in continuation of the work initiated in 1984 by P. Sepri under the USAF-SCEEE Summer Faculty Research Program, which was conducted at the Aero-Propulsion Laboratory at Wright-Patterson Air Force Base. The final report [1] for that research, and the ensuing proposal [2] for the present study, may serve as additional background references. The particular issue under investigation concerns the increase in heat transfer that is observed to occur in turbulent boundary layers which are subjected to elevated levels of free stream turbulence (FST). Clearly, the gaseous flow around turbine blades contains a high degree of FST owing to the high mass flux which is forced through confined spaces obstructed by a sequence of engine components. The actual flow in the engine is further complicated by several factors, among which are: three dimensional mean flow, rotational



effects, non-equilibrium turbulence, transonic flow effects, corner flow interactions, strong acoustic coupling, and possibly incomplete combustion which influences fluid transport properties as well as temperature distributions. Despite the best of attempts, it is currently not possible to claim a computational capability which addresses all of these factors simultaneously and accurately.

Recent descriptions of FST effects on the structure of heated turbulent boundary layers have been reported by Simonich and Bradshaw [3], Bayley and Priddy [4], and Pedisiu, et al. [5]. Additional background material may be obtained from References [6-14]. In the present report considerable reference is made to the excellent experimental data published in the past few years by Blair [15-21]. His measurements include extensive turbulence statistics and profiles in the boundary layer adjacent to a heated flat plate, for which the FST is varied parametrically. One of the objectives of Blair's experimentation has been to produce a detailed and reliable characterization of FST effects on boundary layers of a fundamental type which may help in understanding the actual turbine flow environment.

With the availability of Blair's data, it has been of interest to compare his results with predictions from computer codes. Among the many codes developed in the industry for the purpose of calculating turbulent boundary layers [22], the one utilized for this investigation is STANCOOL, which is a modified version of STANS [23,24] developed by Crawford and Kays. This code, as well as many others, introduces a turbulent Prandtl number profile throughout the boundary layer, through which turbulent heat transport is likened to the relatively more studied momentum transport in the manner of the Reynolds analogy. The deviation in the Reynolds analogy is often described at a solid surface by the local ratio of Stanton number to half of the skin

friction coefficient,  $2St/C_f$ , which is termed the Reynolds analogy factor, with unity denoting a perfect analogy. Earlier investigations [10-14] have conflicted in their reports of the dependence of turbulent heating on the level of FST, some even claiming no effect. More recent data [3-5,18] indicate that the Reynolds analogy factor increases with increasing FST intensity.

Upon the availability of Blair's data, MacArthur [25] undertook a preliminary evaluation of the predictive capability of two options in STANCOOL. These options are comprised of a standard mixing length model and a model incorporating the turbulence kinetic energy equation [23]. Although the comparisons yielded favorable results in some cases, significant departures were noted in other cases in two respects; namely, the onset and duration of transition and the level of heating with increasing FST. Unexpectedly, MacArthur's comparisons revealed that occasionally the two computational options agreed with each other better than either did with the data. While the mixing length model does not provide for a mechanism for FST effects, it was anticipated that the kinetic energy option would introduce these effects through the external boundary condition. MacArthur's observations are also supported by the work of Winstanley, et al. [26].

Sepri and Ebert [1] continued MacArthur's initiative with the objective of seeking a turbulence model that reflects an improved prediction of FST influence on turbulent transport through the boundary layer. A preliminary turbulence model based on the work of Miyazaki and Sparrow [27] was utilized with the result of improved comparison with Blair's data. During the course of investigation, novel observations were made concerning an exponential wake structure in the turbulent boundary layer, which appeared only at the higher levels of FST.

Although the results reported by Sepri and Ebert were promising, the

preliminary model was clearly an oversimplification of a complicated phenomenon. With only one adjustable parameter in the Reynolds stress, it was not possible to obtain simultaneously a good match of the mean velocity profile as well as the skin friction variation along the wall. It became clear that the FST influenced both the wake region and the wall region in separate ways. These results and observations have lead to the present investigation, in which further improvements are sought.

## 1.2 Objectives

With the observation that FST influences the wall region as well as the wake region, it has been proposed [2] to extend the preliminary model to account for effects which were initially excluded. The study was to include five objectives, which have been addressed in phases.

First, reconsideration of the FST model used in 1984 has suggested a refinement based on the observation that inclusion of the transverse velocity at the edge of the boundary layer,  $v_e$ , would alter slightly two of the coefficients previously utilized in the model. Furthermore, a third coefficient would be introduced which would alter the Reynolds stress model in the wall region, as desired. The first objective has been to analyze this extended version of the mixing length model.

The second objective has consisted of further analysis of the exponential wake decay which was first observed in the 1984 investigation. It was evident from Blair's data [18] that the trigonometric wake function proposed by Coles [28] ceases to be an adequate representation of a turbulent boundary layer which is subjected to high levels of FST. However, the exponential function [1] serves very well under these conditions. It has been proposed [2] to analyze the turbulent boundary layer as being a composite structure consisting

of the exponential wake and a wall region, for which the functional description would be studied from Blair's data. In fact, it was suggested [2] that the turbulent boundary layer might consist of three layers, of which the outermost would comprise the decay into the free stream. In the present investigation it has emerged that the turbulent boundary layer indeed exhibits three layers, in which different physical mechanisms dominate.

The third objective has been to consider a simpler limiting case of the turbulent boundary layer with the hope of understanding better the mechanisms of transfer and to simplify the modeling of turbulent transport. The case of a uniform suction turbulent boundary layer has been suggested [2] for this purpose, in which all spatial dependences would occur in the transverse dimension ( $y$ ) only. In this case all of the describing equations may be integrated once with no additional approximations required. The resulting equations describe flux relations explicitly, among which are the Reynolds stress and turbulent heat transfer terms. This objective has been met herein as a special case of a more general formulation.

The fourth objective has been to consider the energy equation in parallel with the momentum equation, with the intention of modeling the turbulent Prandtl number profile in the boundary layer. In this connection it was observed in Blair's data that his values for  $Pr_t$  declined rapidly at the boundary layer edge. An explanation was offered by Sepri and Ebert [1] in terms of channel flow contamination of the measurements. Another goal of the present investigation has been to search the literature for other evidence (or lack thereof) of such a decline in  $Pr_t$ . Along with this task, it has been an objective to propose a model for the  $Pr_t$  profile which accounts for variations in FST.

The fifth objective has comprised of comparisons between updated mixing

length models in the code STANCOOL and Blair's data. Here, the hope has been that the effects of FST could be incorporated into an accurate, yet simple, model for the purpose of predicting the evolution of skin friction, heat transfer, and mean profiles in a turbulent boundary layer over a flat plate. Such a model has emerged from this investigation, and the comparison with the data is favorable.

### 1.3 Content

In order to meet the objectives, the investigation has proceeded in several phases. As an end result, three conclusions and descriptions have emerged which are in addition to the original objectives. These are: an analytical description which approximates the profiles of mean velocity and mean temperature throughout the turbulent boundary layer, an analytical solution to the turbulent boundary layer for a special Reynolds stress distribution, and a general formulation of Reynolds stress and turbulent heat transfer in terms of mean profiles. This last formulation does require additional closure assumptions, which are suggested for the present problem.

The first phase of investigation has consisted of further scrutiny of Blair's data with the objective of characterization of the wall layer so that the two layer modeling could commence. The details will be described later, but in essence Blair's data have revealed the existence of further exponential layers within the boundary layer, including the approach to the wall itself. These observations have been modeled in an analytical functional representation. The character of the exponential layers is seen to change explicitly with the variation of FST. The whole layer formula for the turbulent boundary layer is presented for the first time herein, and it is believed to be the most accurate representation of this kind yet achieved.

The exponential characterization of the mean profiles provides a direct means for modeling the Reynolds stress and turbulent heat transfer terms. Formal integrations of the momentum and energy equations yield formulas for these turbulent fluxes, as detailed in the subsequent section. Additional independent closure relations are required to complete the modeling, but these are directly observable from Blair's data.

After having achieved a formal relationship between the turbulent fluxes and the mean profiles, it has become apparent that a particular analytical solution may be obtained among the variables. This solution exists provided the Reynolds stress and the turbulent Prandtl number take on specific shapes, which incidentally, are not unreasonable. There are two primary benefits obtained from this analytical solution. First, it serves as an excellent check for any code such as STANCOOL. By altering only a few statements in subroutine AUX, the code may be run and checked against the analytical solution for the purpose of code verification. Second, the analytical solution displays explicitly the interrelationships among the various physical mechanisms at work in the turbulent boundary layer. In this sense, this analytical test solution serves a better function than does the originally proposed suction boundary layer. Here, the boundary layer grows in the downstream direction, and no artificial suction boundary condition is required. In addition, it is noted that no analytical solution is available for either the laminar boundary layer as described by the Blasius Equation or for the actual turbulent boundary layer. However, the analytical test case forms a remarkable middle ground between the two real flows.

Through analysis of the energy equation in parallel with the momentum equation, a formulation of  $P_{rt}$  has been achieved which may be used for more general applications. By considering limiting forms of this formulation, a

model is proposed for comparison with Blair's data. It is clear from the relationships that  $P_{rt}$  modeling in general can not be as simple as is often assumed in local gradient models. The results of  $P_{rt}$  discussions in several references are summarized.

The last part of the present investigation involves comparisons of the latest STANCOOL computations with Blair's data for the case of vanishing pressure gradient. Recommendations are presented for further investigation.

## 2.0 FORMULATION

### 2.1 Describing Equations

The basic equations utilized for the computation of a turbulent boundary layer will be listed here as a beginning point for the discussion. The initial equations will be of sufficient generality to describe many boundary layer flows, while it is not considered appropriate to begin with complete generality. The equations listed here correspond to the ones utilized in STANCOOL, and the notation is standard although it differs somewhat from that which is used by Crawford and Kays in regard to enthalpy. In dealing with gaseous boundary layers which involve significant heat transfer it is important to account for density variations throughout the boundary layer, and secondly to recognize that molecular transport coefficients depend on the local temperature. For turbulent boundary layers, the possibility of significant density fluctuations raises the unfortunate complexity of additional correlations involving this density. There are two accepted ways to treat the density variations; one is explicit, and the other is to use a mass averaged velocity decomposition, as has been introduced by Favre [29]. In accordance with the assumptions listed in the next section, the conservation of mass equation may be expressed as follows in the explicit method:

$$\frac{\partial}{\partial x_k} (\rho u_k + \langle \rho' u'_k \rangle) = 0 \quad (1)$$

Here, the subscript,  $k$ , denotes the Einstein summation convention, and the angled brackets denote the averaging process resulting in correlations between the density fluctuations and the velocity fluctuations. The other variables, without the brackets, are understood to represent mean profiles. Since the



explicit averaging process introduces additional unknown density correlations (although they may in fact be negligible in some cases), the Favre type averaging results in less cumbersome expressions. Here, we define two new variables as follows:

$$m(t,x) = \rho u(t,x) \quad (2)$$

$$n(t,x) = \rho v(t,x) \quad (3)$$

The averaging process applied to the product form yields an alternative expression for the conservation of mass equation:

$$\frac{\partial}{\partial x} (m) + \frac{\partial}{\partial y} (n) = 0 \quad (4)$$

Here, the fluctuation averages vanish by construction:

$$\langle m' \rangle = 0 = \langle n' \rangle \quad (5)$$

Of course, the formalism still must retain the identities:

$$m = \rho u + \langle \rho' u' \rangle \quad (6)$$

$$n = \rho v + \langle \rho' v' \rangle \quad (7)$$

By utilization of mass averaging, the streamwise momentum equation in the boundary layer is:

$$\frac{\partial}{\partial x} (m u) + \frac{\partial}{\partial y} (n u) + \frac{\partial}{\partial x} (p) = \frac{\partial}{\partial y} \left\{ u \left( \frac{\partial u}{\partial y} \right) - \langle n' u' \rangle \right\} \quad (8)$$

Here, additional assumptions have been made as listed in the next section. The mass averaged Reynolds stress term is  $\langle n' u' \rangle$ . In this boundary layer formulation, the momentum equation transverse to the plane of the wall reduces to the statement that the mean pressure varies only in the streamwise direction, and is prescribed by the flow external to the boundary layer. The equation for total energy, written in terms of stagnation enthalpy,  $H$ , is expressed in the boundary layer as:

$$\frac{\partial}{\partial x} (m H) + \frac{\partial}{\partial y} (n H) = \frac{\partial}{\partial y} \left\{ \frac{u}{P_r} \frac{\partial}{\partial y} (H) - \langle n' H' \rangle + G \right\} \quad (9)$$

where:  $P_r = \frac{u C_p}{k}$  (molecular Prandtl number)

$$H = h + \frac{1}{2} (u)^2$$

$$\langle n'H' \rangle = C_p \langle n'T' \rangle + u \langle n'u' \rangle$$

$$G = \left(1 - \frac{1}{P_r}\right) \frac{\partial}{\partial y} \left(\frac{1}{2} (u)^2\right)$$

It is also appropriate to record the thermal energy equation which is obtained by subtraction of the kinetic energy from the total energy equation. There results:

$$\frac{\partial}{\partial x} (m C_p T) + \frac{\partial}{\partial y} (n C_p T) = \frac{\partial}{\partial y} \left\{ k \frac{\partial}{\partial y} (T) - C_p \langle n'T' \rangle + \phi \right\} \quad (10)$$

where:  $\phi$  denotes the viscous dissipation.

Finally, the equation of state for the gaseous flow is assumed to apply:

$$p = \rho R T \quad (11)$$

## 2.2 Assumptions

For the sake of completeness, the major assumptions inherent in the above formulation will be recorded here.

- (1) The turbulence is in steady state so that its statistics are stationary.
- (2) The flow is statistically two dimensional so that there are no variations in the spanwise (z) direction. Furthermore, there is no mean flow in the spanwise direction.
- (3) The standard boundary layer assumptions are invoked so that second derivatives in the x direction are neglected in comparison to those in the y direction.

(4) All terms in the y momentum equation are negligible so that the pressure varies only in the x direction, to this order of approximation.

(5) The turbulent boundary layer is sufficiently near an equilibrium condition so that variations in turbulence structure in the x direction are negligible compared to those in the y direction.

(6) The velocity field is approximately solenoidal so that terms involving the second coefficient of viscosity in the momentum equation are negligible.

(7) Gravitational effects are negligible.

Later in the present investigation, the following additional assumptions will be employed:

(8) Density variations produce effects of secondary importance in the momentum equation.

(9) Thermal energy terms dominate the energy equation for the cases of interest. The flows under consideration here are low Mach number flows with relatively moderate heat transfer. In approximation, the contributions of turbulence kinetic energy, mean kinetic energy, and viscous dissipation are small in comparison to the thermal component. This is not to say that these energies are negligible in other equations of the hierarchy. For the sake of concreteness, the following typical magnitudes are noted:

$$\frac{C_p(T_w - T_e)}{\frac{1}{2}(u)^2} = (6000 \frac{ft^2}{s^2 \cdot R}) \frac{(30^\circ R)}{\frac{1}{2}(100 \frac{ft}{s})^2} = 36$$

(9) Although  $T'$  and  $\rho'$  are significant in this problem their contributions to the averaged ideal gas equation are negligible:

$$p = \rho RT \quad \text{where} \quad \frac{\rho' T'}{\rho T} = o(10^{-4})$$

(10) The boundary layer in this investigation will be over a flat plate so that the pressure gradient vanishes.

### 2.3 Derivations

The equations listed previously suffer from the usual closure problem well known in the study of turbulence. Although there is an infinity of correlations that might be considered, the ones of immediate concern are the lowest order ones appearing in the momentum and energy equations; namely,  $\langle n'u \rangle$  and  $\langle n'T \rangle$ . The momentum equation may be viewed as determining the evolution of the mean velocity field, provided the mean pressure, density and the Reynolds stress are supplied from other independent relations. Of course, proper boundary conditions also must be included in the solution procedure. Parallel statements may be made for the temperature field and the energy equation. The approach taken here will be to integrate Eqs. (8) and (9) formally to obtain explicit relations for the turbulent fluxes in terms of integrals and derivatives of the mean variables. This procedure does not constitute a closure scheme by itself, but it does provide a description of the unknown fluxes whenever the mean profiles can be accurately obtained from experiments, say. The method can be extended into a closure scheme, as discussed later, if appropriate additional information is inserted into the integrals of the mean profiles. It is believed that this closure method is introduced for the first time herein, although basic integral relations have appeared earlier [39].

Before embarking on the new approach, it is useful to mention the method used in the traditional mixing length hypothesis, which is also the first option provided in STANCOOL. Closure of the basic equations is effected by the following additional model:

$$\langle u'v' \rangle = \epsilon_m \frac{\partial u}{\partial y} \quad (12)$$

$$\langle v'T' \rangle = \epsilon_H \frac{\partial T}{\partial y} \quad (13)$$

where:

$$\epsilon_m = l^2 \left| \frac{\partial u}{\partial y} \right| \quad (14)$$

The turbulent Prandtl number is introduced as the ratio:

$$Pr_t = \frac{\epsilon_m}{\epsilon_H} \quad (15)$$

With these relations the system of equations becomes closed, provided the mixing length,  $l$ , and  $Pr_t$  are specified throughout the boundary layer. Of course, the closure problem has simply been shifted to the specification of these alternative unknown functions. However, several heuristic arguments may be introduced which describe these variations in approximate ways. The objective of the present investigation is to seek formulations of  $\epsilon_m$  and  $Pr_t$  which take into account the effects of FST.

The first step in the present method consists of a formal integration of the momentum (Eq. (8) and Eq. (4)) from the wall to an arbitrary location in the boundary layer. There results:

$$\langle n'u' \rangle = uu_y - \tau_w - u(n_w - \int_0^y m_x d\xi) - \int_0^y (mu)_x d\xi - p_{xy} \quad (16)$$

In this equation the subscripts  $x, y$  refer to partial differentiation in these directions respectively, and the subscript  $w$  refers to evaluation at the wall. Here,  $\tau_w$  is the local shear stress at the wall, and  $n_w$  is the local transpiration rate at the wall, which vanishes for an impermeable surface. Furthermore,  $p_x$  denotes the imposed pressure gradient, which vanishes for the case of a flat plate in the absence of external influences. For the present investigation, the case of the flat plate will be assumed henceforth, and the plate will also be taken to be impermeable, although these restrictions pose

no difficulty if generalization is desired. The physical interpretation of Eq. (16) is worth mentioning: the various terms represent the several mechanisms for momentum flux. The constant of integration,  $\tau_w$ , obtained from evaluation at the wall, may be viewed as the net effect of momentum transfer resulting from the other terms. The equation may also be interpreted as a limiting form of the control volume approach, in which the change in streamwise momentum flux is evaluated across two transverse surfaces that are infinitesimally separated in  $x$ . The term involving  $n_w$  describes the change in momentum by vertical convection through the top surface and also the wall in cases of nonvanishing transpiration. The Reynolds stress term and the molecular viscosity term represent the transfer of momentum through shearing action via turbulent and molecular motions respectively. Lastly, boundary layers with impressed pressure gradients will undergo a change in momentum flux as a result of the streamwise variation of pressure applied to the transverse control surfaces. It is important to note the satisfaction of the two limits of Eq. (16); namely, at the wall and at the boundary layer edge:

$$u \left( \frac{\partial u}{\partial y} \right)_y = 0 = \tau_w \quad (17)$$

Here, the Reynolds stress vanishes according to its limiting form near the solid surface. At the boundary layer edge:

$$\tau_w = u_e \int_0^\infty \rho_x dy - \int_0^\infty (\rho u)_x dy \quad (18)$$

The last equation is a particular form of the usual von Karman momentum integral equation. Here, at the boundary layer edge, it is assumed that the Reynolds stress vanishes along with the gradient of the mean velocity. If the mean velocity profile is specified in some manner, then Eq. (18) provides a means of determining the local wall shear. Alternatively, Eq. (18) provides a

constraint on parameters that are used in analytical approximations of the velocity field. It is interesting to note that a second integral constraint may be obtained by one further integration of Eq. (16), as follows (flat plate, impermeable wall):

$$uu = y\tau_w + \int_0^y \langle n'u' \rangle d\xi + \int_0^y \left[ \int_0^\xi (mu)_x d\zeta - u \int_0^\xi (m)_x d\zeta \right] d\xi \quad (19)$$

In the limit as  $y$  exceeds the boundary layer edge, the left hand side becomes  $uu_e$ , which is prescribed by the external flow, and the right hand side approaches a finite form achieved through integration by parts and utilization of Eq. (18) for an expression for  $\tau_w$ . Thus, Eq. (19) constitutes an additional constraint that must be satisfied by the Reynolds stress and mean velocity profiles.

The energy equation may be integrated in a parallel fashion to provide an expression for the turbulent heat transfer term. The result is as follows:

$$\langle n'H' \rangle = q_w + \frac{u}{P_r} \frac{\partial H}{\partial y} + \left(1 - \frac{1}{P_r}\right) u \frac{\partial u}{\partial y} + H \int_0^y m_x d\xi - \int_0^y (mH)_x d\xi \quad (20)$$

The physical interpretation of this equation is similar to that of the momentum equation, except that Eq. (20) describes the various mechanisms of heat and kinetic energy fluxes. If the mean velocity and mean temperature profiles were known, say by experimental means, then Eq. (20) could be used to calculate the turbulent heat flux. With turbulent heat and momentum fluxes thus determined, the turbulent Prandtl number,  $P_{rt}$ , may be directly calculated by an appropriate ratio obtained from the two.

Since no additional information has been introduced into the above discussion, it now remains to formulate a closure scheme based on these integral equations. This scheme relies on observations obtained from Blair's data, which will be presented in the next section. It turns out to be

possible to formulate rather general expressions for  $\epsilon_m$  and  $P_{rt}$ . According to experimental observations, we define the following function,  $\phi$ , to describe the mean velocity field:

$$\frac{u}{u_e} = 1 - \exp(-\phi[x,y]) \quad (21)$$

According to the no slip condition,  $\phi$  must vanish at the wall, and in order to satisfy the external boundary condition,  $\phi$  must become unbounded beyond the boundary layer edge. It is emphasized that at this point no additional assumptions have been imposed, and that Eq. (21) merely serves as a definition. The exponential form yields the following expressions upon differentiation:

$$u_x = u_e \phi_x \exp(-\phi) \quad (22)$$

$$u_y = u_e \phi_y \exp(-\phi) \quad (23)$$

Therefore,  $x$  and  $y$  derivatives of the mean velocity field are related by the following expression:

$$u_x = \frac{u_y \phi_x}{\phi_y} \quad (24)$$

From the experimental evidence presented later, it will be apparent that  $\phi$  has a benign behavior such that the ratio of its derivatives can be easily modeled. As a limiting case, and for the sake of convenience of presentation, the incompressible approximation will be discussed below. For cases of moderate heating, as in Blair's experiment, it can be shown that the variations in mean density influence the velocity field only as a small perturbation. Substitution of Eq. (24) into Eq. (16) yields the following representation for the Reynolds stress:

$$-\langle u'v' \rangle = u_\tau^2 - \nu u_y - u \int_0^y u_y \left( \frac{\phi_x}{\phi_y} \right) d\xi + 2 \int_0^y u u_y \left( \frac{\phi_x}{\phi_y} \right) d\xi \quad (25)$$



Here,  $u_\tau$  represents the friction velocity which is defined as  $(\frac{\tau_w}{\rho_w})^{1/2}$ . It now becomes evident how the Reynolds stress might be calculated in terms of the mean velocity. If the  $\phi$  function can be effectively modeled (including FST effects), then Eq. (25) may be directly utilized for the calculation of  $\langle u'v' \rangle$ . The  $x$  variation does not appear explicitly in the mean velocity profile, so that a simple integration routine may be executed at each streamwise location of the marching procedure. This method is similar to the mixing length method in that the unknown behavior of the Reynolds stress has been shifted to another unknown function. The method will be advantageous only if  $\phi$  will admit a simple and accurate modeling. This turns out to be the case. A further correspondence may be made between the original mixing length hypothesis given in Eqs. (12-14) and the modeling proposed in Eq. (25). Utilization of Eq. (18) and factorization of the velocity derivative yields the following expression:

$$-\langle u'v' \rangle = \epsilon_m \left( \frac{\partial u}{\partial y} \right) \quad (26)$$

$$\text{where: } \epsilon_m = -v + \frac{1}{\phi_y} \int_0^\infty U_y F \, d\xi + \frac{U_e}{U_y} \int_y^\infty U_y F \, d\xi - \frac{2}{U_y} \int_y^\infty U U_y F \, d\xi \quad (27)$$

and:

$$F \equiv \phi_x / \phi_y$$

Therefore, with a specification of  $\phi$ , the eddy viscosity is directly calculable. It is further interesting to note that the unknown functions  $u$ ,  $v$ , and  $\langle u'v' \rangle$  may all be directly calculated from the single unknown  $\phi$ . A similar analysis leads to a general formulation for the turbulent heat flux, which then may be used to model the turbulent Prandtl number. However, these equations will be deferred to the next section in which specific models will be discussed.

### 3.0 COMPUTATIONAL MODELS

#### 3.1 Observation of Three Layers

The first phase of the investigation has involved further scrutiny of Blair's data with the objective of extending the exponential wake model observed in 1984 to include the wall layer also. The effect of FST in the wake region was clearly displayed by a marked decrease in curvature of the exponential function as the FST was increased [1]. The pursuit of this approach has lead to a remarkable analytical approximation which describes the entire turbulent boundary layer. In Fig. 1 is displayed a comparison of Blair's data for mean velocity at  $x=84$  in. with grid configuration 4 (highest FST [18]) and a straight line least squares fit for the outer portion of the boundary layer. It is clear that the wake region follows a linear exponential decay for the velocity deficit there. In attempting to characterize the wall region, Blair's data have been subtracted from the extension of the straight line to the wall. It appeared that this difference also followed an exponential behavior. In order to highlight the behavior, the difference has been plotted in a magnified semilogarithmic format as shown in Fig. 2. It is astonishing that the previous form seems to have repeated itself on a scale which is approximately one order to magnitude smaller. A straight line curve fit is also displayed in Fig. 2 through the outer portion of this smaller region. The residue between the data closest to the wall and the second straight line has been plotted in a third semilogarithmic format, and the results are displayed in Fig. 3. Here, the characteristic length scale is approximately one order of magnitude smaller than that of the intermediate region. It is further astonishing that these data also fall on a straight line to good approximation. The scatter in the data becomes magnified in

these successive refinements. The composite function has the following analytical representation:

$$\frac{u}{u_e} = 1 - \exp(-A_1 - B_1 \eta + \exp[-A_2 - B_2 \eta + \exp\{-A_3 - B_3 \eta\}]) \quad (28)$$

where:  $\eta = \frac{y}{\delta}$  and  $\delta$  represents the local boundary layer thickness. A constraint is imposed on the coefficients in the exponentials by the no slip condition:

$$A_1 = \exp[-A_2 + \exp\{-A_3\}] \quad (29)$$

Figures 4-6 display comparisons between the above analytical function (with coefficients matched to Blair's data) and the data profiles themselves. Fig. 4 accentuates the wake region, Fig. 5 shows the usual linear comparison, and Fig. 6 (the most interesting) accentuates the wall region in a format similar to the Clauser type plot, except that the variables have not been scaled with the friction velocity. All three figures exhibit a very satisfactory agreement. The innermost comparison may be improved by another choice of  $A_3$ ,  $B_3$  above. To the authors' awareness, the above analytical expression is the first whole layer formula to describe a turbulent boundary layer to such accuracy. In Fig. 6 the influence of each of the three exponentials is also displayed. These curves indicate the sizes and locations of the three sublayers.

After the presentation of the curve fit, several questions arise which ought to be addressed. First, is the functional form adequate for describing the evolution of the boundary layer? Subsequent figures will show that all the profiles generated by Blair can be well fit by extensions of the above form. Second, how does the functional form change with varying levels of FST? Blair's data demonstrate that the outer layer coefficients depend strongly on the level of FST. Third, if there are truly three layers of

different sizes, what physical mechanisms dominate in these regions, and how do these scales evolve in the boundary layer? Possible explanations for these scales will be presented later. Fourth, what connection do these scales have to the classical notions of 'wake' and 'wall' regions? This is related to the third issue. Fifth, is the triple exponential with several adjustable coefficients simply an artifact of curve fitting, or does it contain an inherent representation of the physics of the problem? Perhaps other functions sufficiently rich in coefficients could do equally well at the fitting. A definitive answer is not presented herein, although two points are offered: (1) For the cases of high FST the linear exponentials fit very well over substantial ranges of the boundary layer. It is unlikely that any other simple function provides a better characterization. (2) Even if the triple exponential were not to comprise a fundamental representation, it nevertheless follows the data to such good accuracy that it may be used beneficially for engineering calculations. Last, how might the exponential representation be exploited for purposes of mixing length modeling which also accounts for the effects of FST? The method here will consist of utilization of Blair's data to model the  $\nu$  function described in the previous section.

### 3.2 Effect of FST

With the appearance of a special case of the triple deck exponential, it is now of interest to seek a characterization of the coefficients as a function of  $x$  location, and also to observe the variation of the function as the level of FST is varied parametrically. In 1984 [2] it was observed that the wake portion of the boundary layer could be described by a linear exponential for the higher levels of FST only. In Fig. 7 the wake is shown for the lowest level of FST (grid 0) at  $x = 84$  in. Since it can be shown that the outer portion of a laminar boundary layer decays exponentially with a quadratic

argument into the free stream, the previous linear curve fit is now extended to a quadratic one in this figure. Qualitatively it is clear that the quadratic fit is good if the free stream turbulence is at a low level, and that a linear fit is good if the FST level is high.

It is of interest to consider the extent of agreement of the previous function with the velocity profile of a laminar boundary layer. First, upstream of transition the flow is laminar, and second, a quadratic wake fit seems to be appropriate for cases of low FST. In Fig. 8 is shown the comparison between a quadratic wake fit and a numerical solution of the Blasius Equation. The agreement is excellent for the outer 80% of the laminar boundary layer. Since it can be shown that the first two terms of the inner layers are linear and quartic in  $y$ , a quartic inner exponential is assumed to describe the wall region. The results of the composite function are displayed in Figs. 9-11. The agreement is remarkably good, and could be improved by further refinement of the parameters in the wall region.

With the above observations in mind, Blair's data have been fit with least squares quadratics for various  $x$  locations and three levels of FST (grids 0, 2, and 4) in order to observe these influences on the coefficients of the exponentials. The procedure has been the same for all cases: (1) Fit the wake region first, excluding approximately the inner 25% of the boundary layer, (2) Subtract the inner data from the outer fit, (3) Fit the intermediate region to a quadratic curve, (4) Subtract the remaining data closest to the wall from the composite curve, (5) Fit a third quadratic to the innermost layer. Admittedly, this procedure introduces many coefficients, and the results are not entirely free of personal and somewhat arbitrary judgment. However, the results have been quite satisfactory. In Figures 12-15 are shown progressions of mean velocity profiles for grid 4 at  $x$  locations 12, 36, 52,

and 84 inches respectively. The analytical curves fit through the data are seen to describe the boundary layer profiles quite well, and now these functions may be used to advantage in the computational scheme. Three features are noteworthy. First, the wake region of the boundary layer scales very well with the local boundary layer thickness. This may be seen by the superposition of the curves (and data) at the various  $x$  locations, especially in the semilogarithmic wake format. Second, the inner two scales grow at a rate which is slower than the growth of  $\delta$ . This may be observed by the significant lengthening of the curves as  $x$  increases. These two observations are well known in the study of turbulent boundary layers. Third, although the intermediate portions of these curves [Figs. 12-15] are almost approximated by straight lines, it is clear from the data that there is always some amount of curvature there. The classical notion of the logarithmic layer may be regained in approximation from the analytical curve fit by an expansion in this intermediate region. However, the linear logarithmic term is only the first in the expansion, and clearly, the figures display a point of inflection.

The effects of FST are shown to be incorporated into the analytical fits in the sequence of Figures 16-23, which correspond to Blair's grid 2 and grid 0 cases. At the various  $x$  locations it may be seen from the semilogarithmic wake plots (not shown) that the boundary layer is strongly influenced by FST as the curvature term in the quadratic decreases markedly as the FST increases. The coefficients utilized in these exponentials are listed in Table 1.

As with most experiments involving turbulent boundary layers, Blair's data shown in the above plots suffer from the inability to approach close enough to the wall (into the laminar sublayer). This is caused primarily by the small

size of his apparatus. It is clear from Figs. 12-23 that the wall shear is determined predominantly by the character of the innermost wall layer. In fact, in the curve fitting, it is possible to alter the coefficients of the third layer so that  $C_f$  changes by 100% while the outer two layers appear to be unaffected in the figures. In an effort to characterize the third layer, the data of Coantic [30] and Kline, et al. [31] have been fit to the exponential representation in Figs. 24-27. These data are among those which approach farthest into the sublayer (Coantic's data even lie within unity  $y^+$ ). Since tabulations of these data were not available to the authors, there is an additional error in the plots owing to subjective reading from published graphs. Nevertheless, the curve fits appear to be very satisfactory. It may be shown that the analytical representation approaches the correct wall behavior (i.e.  $u^+ y^+$  as  $y^+ \rightarrow 0$ ). The most effective method of determining wall shear involves a full log-log plot of the velocity profile, as shown in Figs. 28 and 29 for the data of Coantic and Kline, et al. The shift in the linear portion provides  $\tau_w$  directly. However, most experimental data (including Blair's) do not extend into the linear region.

In the attempt to characterize turbulent heat transfer, it is important to fit the mean temperature profiles in parallel with those of the mean velocity. Figures 30-41 demonstrate that the previous exponential is also a good representation of the mean temperature distributions. In Table 2 are listed the corresponding coefficients for these functions. Although there are slight differences, it is apparent that on the whole the velocity and temperature profiles are very similar.

After having achieved a characterization of the mean profiles, the next phase of the investigation involves making use of this information to model the unknown Reynolds stress and turbulent heat flux terms. In this process,

the aim is to simplify the dependences of the coefficients appearing in the exponentials to account for two major effects; namely, the variations with  $x$  and with FST.

### 3.3 Turbulent Fluxes

The scrutiny of Blair's data has revealed that the mean velocity and mean temperature distributions in a turbulent boundary layer may be described well by the functional form:

$$\frac{u}{u_e} = 1 - \exp(-\phi_1 + \exp[-\phi_2 + \exp[-\phi_3]]) \quad (30)$$

where:

$$\begin{aligned} \phi_1 &= a_1 + b_1 n + c_1 n^2 ; & n &= \frac{y}{\delta} \\ \phi_2 &= a_2 + b_2 \xi + c_2 \xi^2 ; & \xi &= \frac{y}{\epsilon} \\ \phi_3 &= a_3 + b_3 \zeta + c_3 \zeta^2 ; & \zeta &= \frac{y}{\lambda} \end{aligned}$$

or equivalently:

$$\begin{aligned} \phi_1 &= A_1 + B_1 n + C_1 n^2 \\ \phi_2 &= A_2 + B_2 n + C_2 n^2 \\ \phi_3 &= A_3 + B_3 n + C_3 n^2 \end{aligned}$$

Here,  $\delta$ ,  $\epsilon$ , and  $\lambda$  represent the characteristic length scales corresponding to the three regions observed in the analytic fits of Blair's data. It remains to determine what their dependences are and how best to characterize the coefficients. It is assumed that the coefficients  $a$ ,  $b$ ,  $c$  are independent of  $x$ , and that the boundary layer evolution is scaled into the characteristic lengths, whereas the coefficients  $A$ ,  $B$ ,  $C$  cannot be independent of  $x$ . A similar expression may be written for the temperature field. In the wake region, the numbers appearing in Tables 1 and 2 indicate that the following



model is appropriate for the coefficients:

$$\begin{aligned} a_1 &= 1.45 - 0.09I_e \\ b_1 &= -1.0 + I_e \\ c_1 &= \begin{cases} 5.0 - I_e & \text{for } 0 < I_e < 5.0 \\ 0 & \text{for } I_e > 5.0 \end{cases} \end{aligned} \quad (31)$$

where:

$$\begin{aligned} I_e &= (100) \left( \frac{k_e}{u_e} \right) \\ k_e &= \langle (u')^2 + (v')^2 + (w')^2 \rangle^{1/2} |_{y>\delta} \end{aligned}$$

Although there is some scatter in the values obtained by curve fitting, the tables do indicate that these coefficients do not vary with  $x$  to first approximation. This statement is in accord with the notion that the wake region scales with the boundary layer thickness,  $\delta$ . A similar model is made for the outer layer of the mean temperature field. In this manner, the above model introduces FST explicitly into the description of the turbulent fluxes.

The behavior of the two inner layers is somewhat more difficult to describe. The traditional characterization of a turbulent boundary layer is in terms of the 'wake' and 'wall' regions only, and no mention is usually made of three distinct layers which scale with three different lengths. The terms laminar sublayer, buffer layer, and logarithmic wall layer are intended to apply within the wall layer, and all of these are assumed to be characterized by the single length scale,  $\nu/u_\tau$ . Recent investigations [32-34] have called into question the classical notion of the logarithmic wall region on the grounds that an overlap region may not exist between the wake and wall functions. In these investigations a third merging layer is discussed, but the arguments have not been widely accepted yet, and the topic is one of ongoing research. The triple exponential observed herein may have a

connection to these proposals. For the present, we make the following observations. As the solid wall is approached, the mean velocity and mean temperature fields must satisfy several constraints imposed by their Taylor series expansions about  $y=0$ . For velocity, one obtains:

$$u(x,y) = \tau_w \frac{y}{\mu} + \rho_x \frac{y^2}{2\mu} + (0)y^3 + o(y^4) + \dots \quad (32)$$

In fact, a more comprehensive argument results in a nonvanishing coefficient for the  $y^3$  term owing to an effect attributable to the  $y$  momentum equation. However, this effect is small, and will be neglected here. For an incompressible flow one may show that the effect of Reynolds stress is introduced into the expansion explicitly only in the  $y^4$  term, although the turbulence is also implicit in an increased value for  $\tau_w$ . From the Taylor series expansion, and from observation of experimental data, it is customary to utilize the friction velocity,  $u_\tau$ , in scaling both the mean velocity and the  $y$  coordinate in the wall region. Since Blair's data have thus far been presented in terms of the dimensionless ratio,  $\frac{u}{u_e}$ , we may seek to express the Taylor series expansion in that form. By such a procedure, it becomes apparent that two length scales are possible; namely:

$$\begin{aligned} \ell_1 &= \frac{\nu}{u_\tau} \\ \ell_2 &= u_e \frac{\nu}{\tau_w} \end{aligned} \quad (33)$$

The first length scale is the usual one defined by the friction velocity, whereas the second one is larger by the factor,  $\frac{u_e}{u_\tau}$ , which typically represents an increase of an order of magnitude or more. It is interesting to note that  $\ell_1$  is independent of the free stream explicitly, whereas  $\ell_2$  contains an intermediate dependence on both  $u_e$  and  $u_\tau$ . At present, it is not clear from the analytical fits of Blair's data whether or not the two inner length scales

should be identified with  $\epsilon_1$  and  $\epsilon_2$ . However, expansion of  $\frac{u}{u_\tau}$  naturally involves use of  $\epsilon_1$ , whereas expansion of  $\frac{u}{u_e}$  involves  $\epsilon_2$ . These expansions are identical through their first order terms. Higher order terms in the respective expansions begin to differ in the nature of their coefficients. However, in the triple exponential, the dominant term in each layer near the wall is the linear one. Since the form used here is  $\frac{u}{u_e}$ , both inner layers will be assumed to scale with  $\epsilon_2$ , which is in accord with the usual 'law of the wall' to first order.

In view of the exponential form and the limiting behavior imposed by the Taylor series expansion, there are now three additional constraints that must be satisfied among the coefficients of the triple exponential. By evaluation of the first derivative of velocity at the wall, one obtains the relation:

$$\frac{\tau_w}{\mu u_e} = \frac{b_1}{3} + a_1 \left( \frac{b_2}{\epsilon} + \frac{b_3 \exp(-a_3)}{\lambda} \right) \quad (34)$$

This equation indicates that the shear stress depends on all three length scales. However, since the innermost length scale is by far the smallest, one expects that the third term dominates the expression. This is also in accord with the observation that the shear stress is determined by the velocity derivative evaluated at the wall. Therefore, Eqs. (33) and (34) also support the notion that  $\lambda$  ought to be identified with  $\epsilon_2$  to first order. Thus, for convenience of the present modeling, we choose:

$$\lambda = \mu \frac{u_e}{\tau_w} \quad (35)$$

The second and third terms in the Taylor series expansion provide two further constraints on the coefficients. For a flat plate the second and third derivatives of mean velocity vanish at the wall. From these conditions, we choose to determine the curvature coefficients  $C_2$  and  $C_3$ , which are the most difficult to ascertain from curve fitting of the data as well. These results:

$$C_3 = \frac{2h_1^3 + 3g_1(h_1^2 - 2C_1) + 2A_1g_1^3 + B_3^3 A_1 \exp(-A_3)}{6A_1(2g_1 + B_3) \exp(-A_3)} \quad (36)$$

$$C_2 = \frac{1}{2} [g_1^2 + (B_3^2 - 2C_3) \exp(-A_3) + (h_1^2 - 2C_1)/A_1] \quad (37)$$

where:

$$g_1 = -B_2 - B_3 \exp(-A_3)$$

$$h_1 = -B_1 + A_1 g_1$$

In order to complete the specification of the coefficients in this model, we note the following dependences observed from curve fitting of Blair's data:

$$A_2 = 0.2 + 0.2I_e$$

$$B_2 = 2.0 + 4.0I_e \quad (38)$$

$$B_3 = b_3 \left( \frac{\delta \tau_w}{\mu u_e} \right) \quad \text{where: } b_3 \approx 1.3$$

It appears from Blair's data that the intermediate layer is influenced by the degree of FST quite strongly but that the coefficients  $A_2$ ,  $B_2$  do not depend on  $x$  appreciably. The innermost coefficients  $B_3$ ,  $C_3$  are seen to vary strongly with  $x$  as given above. Therefore, Blair's data suggest that  $\lambda$  and  $\epsilon$  are not identical.

With the mean velocity field specified as above, it now remains to formulate the model for the Reynolds stress, and similarly for  $P_{rt}$ . In order

$$\tau_w = \rho_e u_e^2 A \frac{d\delta}{dx} \quad (44)$$

A comparison of the two limits of the Reynolds stress relation (Eq. (25)) now reveals a connection between the inner and outer scales of a turbulent boundary layer and the mechanism by which FST influences the wall shear. In the wake region, FST clearly influences the rate of boundary layer growth and the character of the  $\delta$  function. The evolution of this wake region is connected with a change in the streamwise momentum deficit that is created by the wall shear as given by Eq. (44). Finally, the inner scale,  $\lambda$ , is dependent upon the local value of  $\tau_w$  as described by Eq. (35) (or perhaps Eq. (33)).

Values for the proportionate increases of the scales may be approximated from the observations that:

$$\begin{aligned} \delta &\sim x^{4/5} \\ \tau_w &\sim x^{-1/5} \end{aligned} \quad (45)$$

These usually accepted dependences are in accord with Eq. (44) above. Then it follows that:

$$\frac{\delta x}{\delta} = \frac{4}{5} \left( \frac{1}{x} \right) \quad (46)$$

For the length scales  $\ell_1$  and  $\ell_2$  it follows that:

$$\frac{\ell_1 x}{\ell_1} = \frac{1}{10} \left( \frac{1}{x} \right) \quad \text{and} \quad \frac{\ell_2 x}{\ell_2} = \frac{1}{5} \left( \frac{1}{x} \right) \quad (47)$$

more generally, for any power law dependence,

$$\ell \sim x^m$$

it follows that

$$\frac{\ell x}{\ell} = \frac{m}{x} \quad (48)$$

The important and fortuitous property of all these dependences is that  $\left( \frac{1}{x} \right)$  is

to utilize the general formula given in Eq. (25), the x and y derivatives of the specific  $\phi$  function are required, and for the present case these are:

$$-\phi_x = \eta\left(\frac{\delta x}{\delta}\right)(b_1 + 2c_1\eta) + E\left\{\xi\left(\frac{\epsilon x}{\epsilon}\right)(b_2 + 2c_2\xi) + e^{-\phi_3}\zeta\left(\frac{\lambda x}{\lambda}\right)(b_3 + 2c_3\zeta)\right\} \quad (39)$$

$$\phi_y = \frac{(b_1 + 2c_1\eta)}{\delta} + E\left\{\frac{(b_2 + 2c_2\xi)}{\epsilon} + e^{-\phi_3} \frac{(b_3 + 2c_3\zeta)}{\lambda}\right\} \quad (40)$$

where  $E = \exp(-\phi_2 + \exp[-\phi_3])$

The ratio of these two functions appears in the general Reynolds stress model given in Eq. (25). While this ratio is a complicated expression, it is interesting to observe that in each of the three successive layers the ratio is well approximated by the simpler forms:

$$y\left(\frac{\lambda x}{\lambda}\right) \quad ; \quad y\left(\frac{\epsilon x}{\epsilon}\right) \quad ; \quad y\left(\frac{\delta x}{\delta}\right) \quad (41)$$

Therefore, the Reynolds stress is essentially determined by the proportionate variation of the three length scales. Since the boundary layer thickness is a quantity which is calculated at each streamwise step in STANCOOL, the ratio  $\frac{\delta x}{\delta}$  may be directly obtained in the process. Similarly, since  $\epsilon$  and  $\lambda$  depend on  $\tau_w$ , which is also calculated, these streamwise variations may also be obtained. For present expository purposes, we proceed to an even simpler model. The von Karman momentum integral equation (Eq. (18)) may be rewritten in the more familiar form:

$$\tau_w = \rho_e u_e^2 \frac{d\theta}{dx} \quad \text{where} \quad \theta \triangleq \int_0^\infty \frac{u}{u_e} \left(1 - \frac{u}{u_e}\right) dy \quad (42)$$

Although the mean velocity profile depends on three length scales, it is clear that the momentum thickness,  $\theta$ , is predominantly determined by  $\delta$ . Therefore:

$$\theta = A\delta \quad \text{where} \quad A \equiv \text{constant} \quad (43)$$

Equation (42) becomes:

to utilize the general formula given in Eq. (25), the x and y derivatives of the specific  $\phi$  function are required, and for the present case these are:

$$-\phi_x = \eta \left( \frac{\delta x}{\delta} \right) (b_1 + 2c_1 \eta) + E \left\{ \epsilon \left( \frac{\epsilon x}{\epsilon} \right) (b_2 + 2c_2 \epsilon) + e^{-\phi_3} \zeta \left( \frac{\lambda x}{\lambda} \right) (b_3 + 2c_3 \zeta) \right\} \quad (39)$$

$$\phi_y = \frac{(b_1 + 2c_1 \eta)}{\delta} + E \left\{ \frac{b_2 + 2c_2 \epsilon}{\epsilon} + e^{-\phi_3} \frac{(b_3 + 2c_3 \zeta)}{\lambda} \right\} \quad (40)$$

$$\text{where } E = \exp(-\phi_2 + \exp[-\phi_3])$$

The ratio of these two functions appears in the general Reynolds stress model given in Eq. (25). While this ratio is a complicated expression, it is interesting to observe that in each of the three successive layers the ratio is well approximated by the simpler forms:

$$y \left( \frac{\lambda x}{\lambda} \right) ; y \left( \frac{\epsilon x}{\epsilon} \right) ; y \left( \frac{\delta x}{\delta} \right) \quad (41)$$

Therefore, the Reynolds stress is essentially determined by the proportionate variation of the three length scales. Since the boundary layer thickness is a quantity which is calculated at each streamwise step in STANCOOL, the ratio  $\frac{\delta x}{\delta}$  may be directly obtained in the process. Similarly, since  $\epsilon$  and  $\lambda$  depend on  $\tau_w$ , which is also calculated, these streamwise variations may also be obtained. For present expository purposes, we proceed to an even simpler model. The von Kármán momentum integral equation (Eq. (18)) may be rewritten in the more familiar form:

$$\tau_w = \rho_e u_e^2 \frac{d\theta}{dx} \quad \text{where} \quad \theta \triangleq \int_0^\infty \frac{u}{u_e} \left( 1 - \frac{u}{u_e} \right) dy \quad (42)$$

Although the mean velocity profile depends on three length scales, it is clear that the momentum thickness,  $\theta$ , is predominantly determined by  $\delta$ . Therefore:

$$\theta = A\delta \quad \text{where} \quad A \triangleq \text{constant} \quad (43)$$

Equation (42) becomes:

$$\tau_w \approx \rho_e u_e^2 A \frac{d\delta}{dx} \quad (44)$$

A comparison of the two limits of the Reynolds stress relation (Eq. (25)) now reveals a connection between the inner and outer scales of a turbulent boundary layer and the mechanism by which FST influences the wall shear. In the wake region, FST clearly influences the rate of boundary layer growth and the character of the  $\phi$  function. The evolution of this wake region is connected with a change in the streamwise momentum deficit that is created by the wall shear as given by Eq. (44). Finally, the inner scale,  $\lambda$ , is dependent upon the local value of  $\tau_w$  as described by Eq. (35) (or perhaps Eq. (33)).

Values for the proportionate increases of the scales may be approximated from the observations that:

$$\begin{aligned} \delta &\sim x^{4/5} \\ \tau_w &\sim x^{-1/5} \end{aligned} \quad (45)$$

These usually accepted dependences are in accord with Eq. (44) above. Then it follows that:

$$\frac{\delta_x}{\delta} = \frac{4}{5} \left( \frac{1}{x} \right) \quad (46)$$

For the length scales  $\ell_1$  and  $\ell_2$  it follows that:

$$\frac{\ell_{1x}}{\ell_1} = \frac{1}{10} \left( \frac{1}{x} \right) \quad \text{and} \quad \frac{\ell_{2x}}{\ell_2} = \frac{1}{5} \left( \frac{1}{x} \right) \quad (47)$$

more generally, for any power law dependence,

$$\ell \sim x^m$$

it follows that

$$\frac{\ell_x}{\ell} = \frac{m}{x} \quad (48)$$

The important and fortuitous property of all these dependences is that  $\left( \frac{1}{x} \right)$  is



a common factor of any power law variation in the scales, and that this factor cancels in the Reynolds stress modeling to yield from Eq. (27) the result:

$$\frac{-\langle u'v' \rangle}{U_\xi^2} = -\frac{U_y}{U_y|_0} + \frac{\frac{U_y}{\phi_y} \int_0^y U_y F d\xi + U_e \int_y^\infty U_y F d\xi - 2 \int_y^\infty U U_y F d\xi}{U_e \int_y^\infty U_y F d\xi - 2 \int_0^\infty U U_y F d\xi} \quad (49)$$

where:

$$F = \frac{m y F_1 + (n y F_2 + l y F_3) \exp(-\phi_2 + \exp[-\phi_3])}{F_1 + (F_2 + F_3) \exp(-\phi_2 + \exp[-\phi_3])}$$

$$\begin{aligned} \text{and} \quad F_1 &= b_1 + 2 c_1 n & ; \quad m &= 4/5 \\ F_2 &= b_2 + 2 c_2 n & ; \quad n &= 1/5 \\ F_3 &= (b_3 + 2 c_3 n) e^{-\phi_3} & ; \quad l &= 1/10 \end{aligned}$$

In this model, the  $x$  derivatives have cancelled, and the Reynolds stress is computable at every streamwise station explicitly. A parallel argument holds for the energy equation, from which an explicit equation may then be obtained for the  $P_{rt}$  profile throughout the boundary layer. The next section provides a more compact illustration of the procedure.

### 3.4 Particular Analytical Solution

The general procedure described above admits a particular solution which is extremely interesting for two reasons: (1) The solution thus obtained provides a means for checking the accuracy and consistency of any turbulent boundary layer code such as STANCOOL. (2) The analytical solution provides insights into the physical mechanisms at work in a turbulent boundary layer. It is emphasized, however, that this particular solution of the equations does not correspond to a realistic turbulent boundary layer because the turbulent

fluxes are artificially constructed. The solution has originated from two points of view. First, it has been observed that in the wake region at high FST, the exponential function,  $\phi$ , is linear in  $y$ . Second, one attempts to seek the simplest case for description which falls within the general realm of the problem. These points lead to consideration of the following mean velocity profile:

$$\frac{u}{u_e} = 1 - e^{-By} \quad \text{where} \quad B = B(x) \quad (50)$$

From the definition of the displacement thickness, one obtains:

$$B = \frac{1}{\delta^*} \quad (51)$$

From the conservation of mass equation, one obtains:

$$\frac{v}{u_e} = \delta_x^* [1 - (1 + \hat{\eta})e^{-\hat{\eta}}] \quad \text{where} \quad \hat{\eta} \triangleq y/\delta^* \quad (52)$$

From the momentum equation (Eq. (25)), one obtains:

$$\frac{-\langle u'v' \rangle}{u_e^2} = \delta_x^* [\hat{\eta} + \frac{1}{2}(e^{-\hat{\eta}} - 1)] e^{-\hat{\eta}} \quad (53)$$

Satisfaction of the two limits of the momentum equation results in the condition:

$$\delta_x^* = \frac{2\nu}{u_e \delta^*} \quad (54)$$

integration of which yields the growth rate:

$$\frac{\delta^*(x)}{\delta^*(0)} = \left\{ 1 + \frac{4\nu x}{u_e (\delta_0^*)^2} \right\}^{1/2} \quad (55)$$

In the turbulence kinetic energy equation and in the related Reynolds stress equation appear two terms of physical significance (among others); namely, the viscous dissipation, and turbulence production. Here, it is of interest to compute these terms for the particular analytical solution.

Although the viscous dissipation due to the turbulent fluctuations generally dominates that due to the mean velocity, the latter profile is given here explicitly since the turbulence kinetic energy has not yet been addressed in the modeling.

$$D \triangleq \mu u_y^2 = \frac{\rho u^4}{\nu} e^{-2\hat{\eta}} \quad (56)$$

The turbulence production term is:

$$P \triangleq -u_y \langle u'v' \rangle = \frac{2\rho u^4}{\nu} e^{-2\hat{\eta}} \left[ \hat{\eta} + \frac{1}{2} (e^{-\hat{\eta}} - 1) \right] \quad (57)$$

From these various profiles, one may define several weighted "characteristic" lengths, with the hope of identification with those observed from Blair's data.

$$\text{dissipation scale:} \quad \ell_D \triangleq \frac{\int_0^\infty y D dy}{\int_0^\infty D dy} = \frac{\delta^*}{2} \quad (58)$$

$$\text{production scale:} \quad \ell_P \triangleq \frac{\int_0^\infty y P dy}{\int_0^\infty P dy} = \frac{13\delta^*}{12} \quad (59)$$

$$\text{Reynolds stress scale:} \quad \ell_R \triangleq \frac{\int_0^\infty y \langle u'v' \rangle dy}{\int_0^\infty \langle u'v' \rangle dy} = \frac{13\delta^*}{6} \quad (60)$$

Before proceeding with the energy equation, a few comments of interpretation are appropriate. First, the above mathematical curiosity falls in a middle ground between laminar and turbulent flows. The square root growth rate of the boundary layer thickness ( $\delta \approx 5.3\delta^*$ ) along with similarity with respect to only one length scale (i.e.  $\delta^*$ ) are properties reminiscent of

laminar boundary layers. However, in order for such a simple profile to maintain itself, a pseudo-Reynolds stress is required to transmit a shear stress to the wall which exceeds that of the laminar case. Although this Reynolds stress (Eq. (53)) exhibits well behaved properties throughout the boundary layer, it does decrease towards the wall in proportion to  $\hat{n}$ , which is slower than the  $\hat{n}^3$  expected for an actual turbulent boundary layer. However, for illustrative purposes, none of these qualities present serious drawbacks. The view taken for zeroth order closure of the turbulent boundary layer is that the mean profiles are determined in a continuous manner by specification of the turbulent flux profiles. If the turbulent fluxes were to vanish identically, the solution would be the laminar one. As the turbulent fluxes are increased parametrically to their fully turbulent values, then the mean profiles are likewise altered continuously to their final shapes. The interpretation of the above solution is that if the Reynolds stress were to take on the form given by Eq. (53), then the mean profiles which would satisfy the equations of motion would assume the corresponding functions given above.

In order to appreciate the connection to the turbulent Prandtl number, the analytical solution will now be extended to include the energy equation as well. We explore the consequences resulting from the following mean temperature profile:

$$\frac{T - T_e}{T_w - T_e} = e^{-\beta y / \delta^*} \quad (61)$$

where  $\beta$  is a factor which permits the thermal boundary layer to grow at a rate differing from that of the momentum layer.

By utilization of the assumptions listed in Section 2.2, the energy equation may be integrated directly to give the result:

$$-\langle v'T' \rangle = \epsilon_H T_y \quad (62)$$

where

$$\epsilon_H = \left[ -\frac{2\nu}{\beta^2(1+\beta)} + \frac{2\nu}{\beta} \left( \frac{1-\beta}{\beta + \hat{n}} \right) + \frac{2\nu_H}{\tau_w(\beta+1)} u_y \right]$$

In order to achieve this result, it has been necessary to make the additional assumption that  $\beta$  is constant. It may be shown that  $\beta$  is related to the molecular Prandtl number as follows:

$$\beta^2(1 + \beta) = 2Pr \quad (63)$$

One concludes an analytical profile for  $Pr_t$ :

$$Pr_t = \frac{[e^{-\hat{n}} - 1 + 2\hat{n}]}{\left[ \frac{2}{(\beta+1)} (e^{-\hat{n}} - 1) + \frac{2}{\beta} \hat{n} \right]} \quad (64)$$

The turbulent Prandtl number is smoothly bounded by:

$$\frac{\beta(\beta+1)}{2} \sim Pr_t \sim \beta \quad (65)$$

for which the limits depend upon the choice of the molecular Prandtl number.

The analytical solution presented here will be further discussed and compared with STANCOOL calculations in Section 4.

### 3.5 Limiting Forms

Equations have now been presented for the turbulent fluxes in a sequence beginning with the general form, continuing with specific observations obtained from Blair's data, and ending with an instructive but artificial particular analytical solution. Since it does not appear possible to obtain a representation of the Reynolds stress throughout the boundary layer by analytical integration of Eq. (25), it is of interest to seek asymptotic characterizations in the two limits: near the wall and in the wake. These may

be of use in computational procedures.

The wall region is of importance owing to its immediate connection to the wall shear and heat flux, which are of practical concern. Unfortunately, it is experimentally very difficult to obtain direct measurements of Reynolds stress into the buffer layer since this region is so minute. Furthermore, the presence of the wall contaminates such measurements. From the analytical point of view, the usual argument proceeds from Taylor series expansions about  $y = 0$ . If the flow is assumed to be incompressible, and by invoking the no slip condition, the conservation of mass equation yields for the vertical velocity component:

$$v(t, \underline{x}) = \frac{\partial^2 v}{\partial y^2} \bigg|_0 \frac{y^2}{2} + o(y^3) \quad (66)$$

Since the streamwise velocity component is linear in  $y$  to first order, one concludes for the Reynolds stress:

$$\langle u'v' \rangle = c(x)y^3 + o(y^4) \quad (67)$$

One cautionary remark involves the assumption of incompressibility. If the flow were to contain significant variations of  $\frac{\partial \rho}{\partial t}$ , then the leading term above would be proportional to  $y^2$ . A second remark is that it is possible (although unlikely) that the fluctuations leading to the coefficient,  $c(x)$ , are uncorrelated so that the leading nonvanishing term actually becomes of order  $y^4$ . Here, the correct representation is assumed to be given by Eq. (67). It should be noted that the commonly accepted van Driest damping factor [35], which is also utilized in STANCOOL, results in the  $y^4$  limiting behavior.

Next, it will be shown that the general form proposed for the Reynolds stress Eq. (25) is in agreement with the limit given in Eq. (67) above. The Taylor series expansion for  $\phi$  near the wall is:

$$\phi = \phi^{(0)}(x) + \phi^{(1)}(x) y + \phi^{(2)}(x) \frac{y^2}{2} + \dots \quad (68)$$

then:

$$\phi_y = \phi^{(1)}(x) + \phi^{(2)}(x) y + \phi^{(3)}(x) \frac{y^2}{2} + \dots$$

$$\phi_x = \phi^{(0)}_x + \phi^{(1)}_x y + \phi^{(2)}_x \frac{y^2}{2} + \dots$$

Substitution of the above, together with Eq. (32), into Eq. (25) yields for the Reynolds stress:

$$-\langle u'v' \rangle = \frac{\tau_w}{\rho} - v [u^{(1)}_0 + u^{(4)}_0 \frac{y^3}{6} + \dots] - [u^{(1)}_0 y + u^{(4)}_0 \frac{y^4}{24}] \int_0^y [u^{(1)}_0 + o(y^3)] \cdot$$

$$\left[ \frac{\phi^{(0)}_x + \phi^{(1)}_x y + \dots}{\phi^{(1)}_0 + \phi^{(2)}_0 y + \dots} \right] dy + 2 \int_0^y [u^{(1)}_0 y + o(y^4)] \left[ \frac{\phi^{(0)}_x + \phi^{(1)}_x y + \dots}{\phi^{(1)}_0 + \phi^{(2)}_0 y + \dots} \right] dy \quad (69)$$

Upon integration, one obtains after some cancelation of terms:

$$-\langle u'v' \rangle = [-vu^{(4)}_0 + (u^{(1)}_0)^2 \left( \frac{\phi^{(1)}_x}{\phi^{(1)}_0} + \frac{\phi^{(0)}_x \phi^{(2)}_0}{(\phi^{(1)}_0)^2} \right)] \frac{y^3}{6} + o(y^4) \quad (70)$$

Therefore, it is verified that the use of Eq. (25) in further modeling of the Reynolds stress leads to a behavior at the wall which has the correct limiting form in regard to  $y$  dependence. However, the magnitude of the coefficient of  $y^3$  remains to be specified through the model, and this depends on the coefficients appearing in the triple deck exponential.

In the wake region, Eq. (25) leads to a directly integrable form upon noting that the inner exponentials become negligible there. In this case:

$$\frac{u}{u_e} \rightarrow 1 - e^{-\phi_1} \quad \text{for} \quad y \gg \epsilon \quad (71)$$

where  $\phi_1 = A_1 + B_1 y/\delta + C_1 (y/\delta)^2$

and  $\frac{\phi_x}{\phi_y} \rightarrow -y \left( \frac{\delta_x}{\delta} \right) \quad \text{for} \quad y \gg \epsilon \quad (72)$

Eq. (25) may be re-written as:

$$-\langle u'v' \rangle = -\nu u_y + (u_e - u) \int_0^{\infty} u_y \left( \frac{\phi_x}{\phi_y} \right) dy' + u \int_y^{\infty} u_y \left( \frac{\phi_x}{\phi_y} \right) dy' - 2 \int_y^{\infty} u u_y \left( \frac{\phi_x}{\phi_y} \right) dy'$$

The terms require the following integrations:

$$\int_y^{\infty} e^{-\phi} [B_1 + 2C_1 \frac{y}{\delta}] \left[ -y \frac{\delta_x}{\delta^2} \right] dy' \quad (73)$$

$$\text{and} \quad \int_y^{\infty} e^{-\phi} [1 - e^{-\phi}] [B_1 + 2C_1 \frac{y}{\delta}] \left[ -y \frac{\delta_x}{\delta^2} \right] dy' \quad (74)$$

These integrals may be rendered in terms of the error function and exponentials. For present purposes, however, only the case of high FST will be considered, for which:  $C_1 = 0$ . Then the above integrals are:

$$-\int_y^{\infty} e^{-A_1 - B_1 y / \delta} B_1 y \frac{\delta_x}{\delta^2} dy' = -\frac{\delta_x}{B_1} e^{-A_1 - B_1 y / \delta} \left[ \frac{B_1 y}{\delta} + 1 \right] \quad (75)$$

$$-\int_y^{\infty} e^{-2A_1 - 2B_1 y / \delta} B_1 y \frac{\delta_x}{\delta^2} dy' = -\frac{\delta_x}{4B_1} e^{-2A_1 - 2B_1 y / \delta} \left[ \frac{2B_1 y}{\delta} + 1 \right] \quad (76)$$

Under these conditions the Reynolds stress has the expression:

$$-\langle u'v' \rangle = U_y \left\{ -\nu - \frac{V_e(x)}{B_1} + \frac{U_e \delta_x}{B_1^2} \left( 1 + \frac{B_1 y}{\delta} \right) + \frac{1}{2} \frac{\delta_x}{B_1^3} U_y \right\} \quad (77)$$

Where the coefficient,  $B_1$ , depends on the degree of FST. From the momentum integral equation it is also evident that  $\delta_x$  is proportional to  $U_\tau^2$ .

Eq. (77) is in agreement with the 1984 investigation [1], in which the eddy viscosity is seen to increase linearly with  $y$  in the wake region. This earlier observation has now been shown to be a special case of the more general formulation expressed by Eq. (25).



### 3.6 The Suction Boundary Layer

The suction boundary layer was originally proposed for investigation [2] for the purpose of providing a simple limiting case of the actual boundary layer. Although this is still an interesting pursuit, and it will be described in this section, the recently obtained analytical solution presented earlier serves in this capacity even more admirably. The advantage posed by the suction boundary layer is that, by appropriate control, the flow statistics are independent of the  $x$  dimension, thereby permitting one exact integration of all the describing equations in the hierarchy. An approximation of this hypothetical flow condition could be achieved in reality through careful tailoring of upstream, downstream, and suction influences on the boundary layer. Theoretically, we envisage an infinite porous flat plate over which flows a uniform gas at a temperature differing from that of the wall. The viscous layer is maintained at a uniform and constant thickness through the agency of steady suction control. The "free stream" could be laminar or even uniformly turbulent, provided an energy mechanism maintains the turbulence. As the flow passes through the shear layer adjacent to the wall, the turbulence production terms will generate a non-vanishing Reynolds stress distribution. The thermal structure may be maintained at steady state by heat transfer mechanisms within the wall. Previous investigations concerning the suction boundary layer are mentioned by Schlichting [36] and recently by Gol'dshtik, et al. [37].

The suction boundary layer comprises a special case of the earlier equations, such that all  $x$  derivatives are taken to vanish identically. However, the wall boundary conditions now must include a non-vanishing velocity component perpendicular to the plane of the wall. The integrated form of the  $x$  momentum equation (Eq. (16)) becomes:

$$\langle n'u' \rangle = \rho u_y - \tau_w - u n_w \quad (78)$$

The conservation of mass equation yields (Eqs. (4) and (7)):

$$n = \rho v + \langle \rho'v' \rangle \equiv n_w \equiv \text{constant} \quad (79)$$

The Reynolds stress is assumed to vanish as  $y$  approaches infinity, along with the mean velocity gradient. Eq. (78) then provides an exact and explicit result for the wall shear:

$$\tau_w = -u_\infty n_w > 0 \quad \text{since} \quad n_w < 0$$

$$\text{or:} \quad \tau_w = -\rho_\infty u_\infty v_\infty \quad (80)$$

The interesting observation here is that, regardless of turbulence intensity, the wall shear is generated solely from the conversion of the mean  $x$  momentum in the free stream to the vanishing  $x$  momentum condition at the wall. Eq. (78) provides a connection between the velocity profile and the Reynolds stress distribution. If  $\frac{u}{u_\infty} = 1 - e^{-\phi}$ , then Eq. (78) becomes:

$$\begin{aligned} \langle n'u' \rangle &= [u\phi_y + n_w]u_\infty e^{-\phi} \\ \text{where} \quad \phi(0) &= 0 \quad \text{and} \quad \phi_y|_0 = -\frac{n_w}{u} \end{aligned} \quad (81)$$

Here,  $\phi$  is expected to have a form similar to the one observed in Blair's data.

An alternative interpretation of Eq. (78) leads to an explicit solution for the velocity field in terms of the Reynolds stress. By integration, one obtains:

$$\frac{u}{u_\infty} = 1 - e^\xi - \frac{e^\xi}{\tau_w} \int_0^\xi \langle n'u' \rangle e^{-\xi} d\xi \quad (82)$$

$$\text{where} \quad \xi \triangleq \int_0^y \frac{n_w}{u} dy \equiv \frac{n_w y}{u} = \frac{\rho_\infty v_\infty y}{u} < 0$$

The laminar solution is the exponential one with vanishing Reynolds stress above. For the turbulent case, the mean velocity depends continuously on the shape of the Reynolds stress.

For varying levels of FST, the coefficients implicit in the  $\psi$  function are expected to vary in a manner similar to those observed in Blair's data. In this case, the wake region of Eq. (81) reduces to the form:

$$\langle n'u' \rangle = \left[ u \left( \frac{B_1 + 2C_1(y/\delta)}{\delta} \right) + n_w \right] u_\infty e^{-A_1 - B_1(y/\delta) - C_1(y/\delta)^2} \quad (83)$$

Here,  $A_1$ ,  $B_1$ ,  $C_1$ , are assumed to depend on FST as described by Eq. (31). It is clear that length scales which characterize the FST would influence these coefficients as well as the intensity level of FST. It is further clear that such a dependence is not likely to be of a simple one dimensional kind, but that each dominant wave number in the power spectral density would exert its own influence. However, an averaged effect might be achieved by considering the longitudinal integral length scale:

$$L_f = \int_0^\Delta f(y,r) dr \quad (84)$$

where  $f = \frac{\Delta}{L_f} \langle u'(y,x)u'(y,x+r) \rangle$

Although some previous investigators [3,5,38] have claimed that turbulence transport in the boundary layer is most sensitive to integral scales of the size of  $\delta$ , it is considered here to be a topic of further research.

In parallel with the momentum equation, the energy equation (9) may also be directly integrated once to give:

$$\langle n'H' \rangle = \frac{\mu}{Pr} H_y - n_w(H-H_w) - q_w + u \left( 1 - \frac{1}{Pr} \right) u u_y \quad (85)$$

By evaluation at the wall and in the free stream, one obtains:

$$q_w = - n_w(H_\infty - H_w) = K T_y|_w \quad (86)$$

The physical interpretation of this flow situation is that the flux of total energy in the y direction remains invariant with y, whereas specific transport mechanisms may dominate in different regions. At the wall, the net energy flux is composed of a combination of thermal conduction and heat convection through the porous wall. In the momentum equation, the corresponding invariant is a combination of local shear stress and streamwise momentum flux in the y direction.

In order to arrive at an expression for  $P_{rt}$ , the following decomposition is noted:

$$\langle n'H' \rangle = C_p \langle n'T' \rangle + u \langle n'u' \rangle + v \langle n'v' \rangle + \langle n'k'^2 \rangle \quad (87)$$

For cases of dominant thermal energy content, the last two terms may be neglected to obtain from Eqs. (85) and (87):

$$C_p \langle n'T' \rangle = K T_y - n_w C_p (T - T_\infty) + \frac{n_w}{2} (U_\infty - U)^2 \quad (88)$$

The turbulent Prandtl number is then:

$$P_{rt} = \frac{\epsilon_M}{\epsilon_H} = \frac{\langle n'u' \rangle T_y}{\langle n'T' \rangle U_y} = \frac{[u U_y + n_w (U_\infty - U)] T_y}{[K T_y + n_w C_p (T_\infty - T) + \frac{n_w}{2} (U_\infty - U)^2] U_y} \quad (89)$$

This equation expresses the turbulent Prandtl number directly in terms of the mean velocity and temperature fields. The expression becomes indeterminate at both the wall and in the free stream.

The above analysis provides valuable physical insight into several of the processes at work in a turbulent boundary layer. The major difference in the

usual flat plate boundary layer is the growth of the boundary layer thickness with  $x$ , whereas this thickness is constant for the uniform suction layer. Also in the boundary layer, both the fluxes of energy and momentum are not quite invariant with respect to  $y$  as they are here, owing to the growing streamwise integral deficits.

## 4.0 RESULTS

### 4.1 STANCHEK - Analytical Comparison

The initial effort with the code STANCOOL consisted of slight alterations in format so that it would be compatible with the IBM 3081 system at the University of Oklahoma. After several weeks, the code was producing results that duplicated the computations obtained in 1984 at AFWAL/POTC by Sepri and Ebert [1]. The next phase consisted of modifications to the turbulent flux models as described in the proposal [2] for the 1985 investigation. These modifications occur primarily in the subroutine AUX. The version of STANCOOL now at OU contains five separate options in the broader category of mixing length models in the code. These are: (1) the original MLH, (2) the MLH as modified by Sepri and Ebert (denoted FST1), (3) the extended MLH as described in [2] (denoted FST2), (4) the version designed to calculate the case corresponding to the analytical solution (denoted STANCHEK), and (5) the latest turbulent flux model based on the integral relations presented earlier (denoted FST3). In this section the results of STANCHEK are discussed.

The lowest order turbulence closure rests on the notion that if the Reynolds stress distribution is presented along with the  $P_{rt}$  profile, then a boundary layer code, such as STANCOOL, may be used to calculate the mean velocity and mean temperature profiles, along with the  $C_f$  and  $S_t$  distributions on the wall. In STANCHEK,  $\langle u'v' \rangle$  and  $P_{rt}$  are modified in AUX to agree with the analytical profiles given by Eq. (53) and Eq. (64) respectively. STANCOOL is then run as usual to produce the flow field solution. Here, we compare these calculated results with the analytical solution presented in Section 3.4. This check procedure is considered to be quite useful since the number of alterations of STANCOOL consists of only approximately ten lines.

In order to set the stage, the behavior of the analytical solution will be described first. In Fig. 42 is presented a scaled schematic of the particular analytical boundary layer. The configuration of the flat plate corresponds to Blair's experiment. Shown in the figure are computer plots of  $s^*(x)$ ,  $\delta(x)$  and two mean velocity profiles located at the initial and final stations used by Blair for measurement. The square root boundary layer singularity is evident at the leading edge of the plate. The Reynolds number variation is also indicated along the abscissa. The profiles consist of the exponential given by Eq. (50). Fig. 43 displays both the Reynolds stress profile (Eq. (53)) and the mean normal velocity profile (Eq. (52)) in the boundary layer. These curves are qualitatively similar to those expected for an actual turbulent boundary layer.

The profiles of viscous dissipation (mean velocity only), turbulence production, and Reynolds stress are shown in Fig. 44. Also indicated are the various profile averaged length scales describing these mechanisms. It is clear that a turbulent boundary layer may be described by several length scales beginning with the dissipation scale, continuing with the production scale, and finally ending with the boundary layer thickness itself. For the actual turbulent boundary layer, these characteristic inner scales lie closer to the wall itself. It is suggested here that the three characteristic scales observed in the triple exponential might correspond to those of viscous dissipation, Reynolds stress, and  $\delta$ , in increasing order. However, this identification has not been firmly established herein, and it remains a subject for further investigation.

In Fig. 45 are displayed the relative growths and profiles of the mean temperature and velocity fields. The molecular Prandtl number is taken to be 0.71, so that this calculation corresponds to the case of an air flow over a heated (or cooled plate). The thermal boundary layer is seen to be

approximately 15% thicker than the viscous layer. The variation of  $P_{rt}$  in the boundary layer is shown in Fig. 46 as given by Eq. (64). The three curves correspond to molecular Prandtl numbers of 0.112, 0.71 and 3.328. For these particular cases of the analytical solution,  $P_{rt}$  approaches constant levels in the wake region of the boundary layer and beyond. However, it is important to note that such smooth  $P_{rt}$  profiles would not result if the wall temperature along the plate were not constant (e.g. a step change in temperature).

Given the analytical solution described above, it is of interest to ascertain how well STANCOOL calculates this solution. In Fig. 47 is shown a comparison of the analytical solution (symbols) with the STANCOOL result (curve) for the velocity profile at  $x = 84$  in. "Transition" is forced at the leading edge of the plate. Both profiles are presented scaled with respect to their own boundary layer displacement thicknesses. The agreement appears to be excellent in this representation. However, there are two discrepancies to be noted which are not evident in this figure. The first is shown in Fig. 48 which magnifies the wake region of the boundary layer. It is clear that STANCOOL has reproduced the exponential character of this particular solution remarkably well except at the boundary edge, near which numerical errors cause a departure of the calculation from the true nature of the decay. In Fig. 47 this departure is not apparent at all because the error magnitude is less than 1% of the free stream velocity. One might expect such a small error not to be significant; however, in fact, the calculation of the boundary layer thickness is extremely sensitive to the nature of the decay rate at the edge. This leads directly to the second discrepancy; namely, the growth rate of the boundary layer thickness as calculated by STANCOOL is approximately 6% less than that of the analytical solution. The velocity profiles in Fig. 47 are replotted in Fig. 49 with the abscissa scaled with respect to an internally calculated  $\delta^*$ . A measurable



mismatch is exhibited, which is solely due to an error in the  $\delta$  calculation in STANCOOL. This, in fact, also provides a partial explanation for some of the profile mismatches described in the earlier work of 1984 [1]. The  $\delta$  calculated by STANCOOL does not always match the actual  $\delta$  measured by Blair. A more suitable abscissa is comprised of  $y/\delta^*$ , since this is not as sensitive to small discrepancies at the boundary layer edge.

Fig. 50 further demonstrates the above discrepancy. The analytical and calculated "Reynolds stresses" in STANCHEK are in fact forced to be identical with respect to  $y/\delta$ . After computation these profiles are rescaled with respect to  $\delta^*$  and the resulting mismatch is displayed in Fig. 50. Last, Fig. 51 displays the comparison of mean temperatures obtained by using the  $P_{rt}$  profile given by Eq. (64). The discrepancy shown here is attributed to a similar difference in growth rates of the respective thermal boundary layer thicknesses. A resolution of this problem in the calculation of  $\delta$  in STANCOOL has not yet emerged, and this topic remains for further investigation. In summary, however, it is gratifying that such a simple alteration of the STANCOOL mixing length hypothesis has yielded excellent profiles except for the scaling of the boundary layer thickness.

#### 4.2 Comparison with Boundary Layer Data

Another benefit of the analytical solution is that it alerts the user of STANCOOL to another possible discrepancy in calculations of real boundary layers, although upon reflection, this possibility is obvious. Much of the profile mismatch shown in Reference [1] might be attributable to a disparity between calculated and measured boundary layer thicknesses, which is a comparison that must be considered here as well. The results presented in this section correspond to utilization of the model described by Eq. (49), and this

option in STANCOOL is the one denoted by FST3. Although this model permits the calculation of an eddy viscosity,  $\epsilon_m$ , based on mean velocity profiles, an identification with the mixing length hypothesis is not quite appropriate. First, a mixing length is not introduced in the model, and second, the resulting eddy viscosity is not entirely proportional to  $U_y$ , as it is in the MLH.

The mixing length extension described in the proposal for this investigation [2] is denoted FST2 in STANCOOL, and it has also been executed with partial success. A parametric variation of FST influence on the inner layer (denoted by C[2]) has indeed demonstrated that wall and wake regions may be separately controlled and calculated by variations of the parameters of A, B, and C. However, a rational intrinsic modeling for C has not become apparent from the study of Blair's data, whereas the formulation given by Eq. (49) has such an advantage. Since FST3 is considered superior to FST2 at this juncture, only the former results will be displayed here.

In Figs. 52 and 53 are shown Reynolds stress comparisons between Blair's data at  $x = 84$  in. and the calculated profiles utilizing FST3. In these calculations the coefficients in the exponentials are taken to have representative constant values, and no attempt has been made to match the curve fits of Blair's data at every  $x$  location. It is clear that the streamwise evolutions of these Reynolds stress profiles agree well with those measured at  $x = 84$  in. for both the bounding cases of low FST (0.25%) and high FST (5%), except for a slight mismatch of boundary layer thicknesses which was shown earlier to be attributable to STANCOOL.

Corresponding plots for mean velocity profiles are shown in Figs. 54 and 55. Here also, the calculated and measured profiles display a good agreement in the particulars of their shapes, although slight shifts in the  $\delta$ 's are observable. The mean temperature comparisons are shown in Figs. 56 and

57 with qualitatively similar results, except that the mismatch is more pronounced. This mismatch may be attributable to two causes. First, the  $P_{rt}$  profile is assumed to be unity throughout the boundary layer, because of lack of time for including the improved modeling. Second, it is not evident to what extent the discrepancy between the calculated and measured thermal thicknesses causes the observed mismatch.

These figures demonstrate that the modeling procedure has excellent promise, although there has not yet been sufficient time to bring the work to completion. Several avenues connected with the exponential structure require further investigation, and these will be discussed in Section 5.

#### 4.3 Turbulent Prandtl Number

The turbulent Prandtl number has been introduced into the study of boundary layers primarily for two reasons: (1) to highlight the strong similarity that may occur between the momentum and energy equations, and (2) to provide a convenient numerical method for obtaining solutions which involve a coupling of the velocity and temperature fields. Originally, the Reynolds analogy was meant to be applicable under the restriction of unity Prandtl number (either molecular or turbulent). Recently, computational schemes have employed  $P_{rt}$  profiles which vary significantly from unity throughout the boundary layer. It seems clear that the postulation of a  $P_{rt}$  profile can be artificial under some circumstances (as may be that of the Prandtl mixing length), and these are the cases in which the viscous and thermal boundary layers bear little similarity to each other. Even with a close resemblance, the subtle variations in  $P_{rt}$  may be difficult to model.

One example for which the viscous and thermal layers are markedly different is the case of a step increase in wall temperature in a boundary layer that

already has a developed viscous region. One might argue that in the neighborhood of the thermal jump the thermal boundary layer hypothesis is invalidated, and also that the developing thermal layer requires a certain distance in which to equilibrate. However, even substantially downstream of the jump, there will be a mismatch in thermal and viscous thicknesses. In such a circumstance, it is of interest to question the validity of the Reynolds analogy and also the significance of the turbulent Prandtl number. Even in this case, it is not obvious that the assumption of constant  $P_{rt}$  is a poor one. Recall the definition:

$$P_{rt} = \frac{\epsilon_m}{\epsilon_H} = \frac{\langle u'v' \rangle T_y}{\langle v'T' \rangle U_y} \quad (90)$$

Beyond the thermal layer the mean temperature gradient vanishes while  $\langle u'v' \rangle$  and  $U_y$  do not vanish in the larger viscous layer. However, one would also expect  $\langle v'T' \rangle$  to vanish beyond the thermal layer. Therefore, depending on the respective rates of decline, it is possible for  $P_{rt}$  to remain constant or be mildly varying. Similarly, it is possible for  $P_{rt}$  to remain constant whenever any of the four factors becomes either large or small, provided the effect is compensated appropriately by the other factors. In fact, the gross trends do compensate in just such a manner. However, we are now in a position to discuss two examples for which the gross trends do not compensate adequately, and these bring into question the general suitability of calculating heat transfer via  $P_{rt}$  modeling.

The first example has been provided during the 1984 investigation [1], in which an explanation was offered for the large decline of  $P_{rt}$  in several of the wake regions observed by Blair. Owing to asymmetries in the experiment,  $\langle u'v' \rangle$  appears to have a zero crossing external to the boundary layer before such a crossing is achieved by  $U_y$ . By the experimental arrangement,  $\langle v'T' \rangle$  and  $T_y$

never have zero crossings in this case. Consequently,  $P_{rt}$  also has a zero crossing, and the wake region  $P_{rt}$  profile declines in a sensitive manner, which is extremely difficult to model. All four factors in Eq. (90) tend to zero at differing rates. In this case, the  $P_{rt}$  behavior is not dominated at all by a similarity of  $\langle v'T' \rangle$  to  $\langle u'v' \rangle$  or of  $T_y$  to  $U_y$ . Another related observation of Blair's data has been given for the case of high FST, for which the wake decay of the mean temperature profile is exponential, whereas the decline of  $\langle v'T' \rangle$  is exponential at half that rate [1]. In reconsidering the thermal jump problem in which a smaller thermal layer is embedded within a larger viscous layer, it becomes highly questionable whether the declines of  $T_y$  and  $\langle v'T' \rangle$  are similar enough to maintain a constant  $P_{rt}$ . Clearly, the dissimilarity between momentum and energy cannot be compensated to result in a constant  $P_{rt}$ .

The second example is provided by the exact particular solution described in Section 3.4. An extension of the analysis to include variable  $\beta(x)$  leads to the explicit formula:

$$P_{rt} = \frac{\left[ \frac{2y}{\delta^*} - 1 \right] + \frac{v}{u_\tau^2} u_y}{-\frac{1}{Pr} + \frac{2}{\beta} \left\{ -1 + \frac{1}{\beta} + \frac{y}{\delta^*} \right\} + \frac{2}{\beta} \frac{v}{u_\tau^2} u_y \left[ 1 - \frac{1}{\beta + 1} \right] + \text{TERM}} \quad (91)$$

$$\text{where TERM} = \frac{\beta_x}{\delta^* x} \left\{ -\frac{2\delta^*}{\beta^3} \left( 1 + \frac{\beta y}{\delta^*} \right) + \frac{2v}{u_\tau^2} u_y \frac{\delta^*}{\beta(\beta + 1)^2} \left( 1 + \frac{y[\beta + 1]}{\delta^*} \right) \right\}$$

Although Fig. 46 exhibits mildly varying profiles of  $P_{rt}$ , these cases are chosen such that the origins for the thermal and viscous layers coincide. Even here there is a variation of  $P_{rt}$  throughout the boundary layer. For the more severe comparison of a step change in wall temperature, it is clear from Eq. (91) that the  $P_{rt}$  profile becomes more strongly varying in the  $y$  direction. Furthermore, if either  $q_w$  or  $T_w$  varies with  $x$  (as in most real cases), then the  $P_{rt}$  profile

also becomes  $x$  dependent. Although in Blair's experiments  $q_w$  was held constant, the wall temperature varied significantly with  $x$ . One may view a continuous thermal change with  $x$  to consist of a superposition of many infinitesimal jumps in wall temperature. Each such change propagates into the boundary layer in a manner similar to the embedded thermal layer described above. Therefore, the thermal boundary layer is a subtle composite of a history of upstream variations that is quite distinct from the development of the momentum layer. Although every reasonable model for  $P_{rt}$  will give results for heat transfer that may appear to be correct qualitatively, the quantitative degree of accuracy and predictability would appear to be difficult to ascertain.

In view of the foregoing two examples, it is tentatively concluded that  $P_{rt}$  modeling is an inadequate approach for turbine blade heat transfer calculations. However, the more general and novel formulations for  $\langle u'v' \rangle$  and  $\langle v'T' \rangle$  given in Eqs. (25) and (20) provide an intriguing alternative which does not suffer from the problems mentioned for  $P_{rt}$  modeling. The factors,  $\epsilon_m$  and  $\epsilon_H$ , are directly calculable in terms of modeled mean profiles (or calculated mean profiles in a marching scheme). There is no need to form a ratio of quantities which vanish at different rates; thus, the difficulty of a sensitive indeterminacy is avoided. Furthermore, wall temperature history effects may be directly incorporated into the integral scheme in which  $\langle v'T' \rangle$  is calculated via successive mean temperature (and velocity) profiles. In parallel, a modeling is not required for the Prandtl mixing length if Eq. (25) is utilized to calculate the Reynolds stress. It has become clear from study of the wake region at high FST that the eddy viscosity is not adequately represented by  $\epsilon^2 \frac{\partial u}{\partial y}$  there, but rather by a term proportional to  $y$  itself. The formulation given by Eq. (27) provides a direct means of calculating the eddy viscosity throughout the

boundary layer. These directions are proposed for further research.

In order to close the discussion of  $P_{rt}$ , a summary will be given here of several earlier works on the subject. The search for investigations dealing with  $P_{rt}$  has yielded References [37,39-71], and these may be classified into three categories: wall boundary layers, wakes and jets, and pipes and channels. A graphical summary of the relevant boundary layer trends is presented in Fig. 58. The work by Rotta [39] is often referred to as a good description of the decline of  $P_{rt}$  in the outer boundary layer. In fact, he proposed his simple function through observations of pipe data taken by Ludwig [40]. Similarly, it should be noted that the commonly accepted method for calculating  $\tau_w$  in a boundary layer utilizing the logarithmic fit with the von Karman constant,  $K$ , has originated from experimental work in pipe flow [36], in which the wall shear is more readily measured than in the boundary layer. In Fig. 58 are summarized the recent works by Simpson, et al. [41], Senda, et al. [42], Subramanian and Antonia [43], and Snijders, et al. [44]. These were directed towards measurements of  $P_{rt}$  profiles in heated turbulent boundary layers. It is seen that there are significant shifts of  $P_{rt}$  level from one experiment to another. Also, all but one of the  $P_{rt}$  profiles tend to exhibit marked declines in the wake region, except that the error band is large in both the near wall and far wake regions owing to wall interference and vanishing signals respectively. All of these measurements have been made in tunnels for which channel flow effects are presumably negligible, and they bear similarity to Blair's results. In marked contrast are the  $P_{rt}$  profiles exhibited for wakes and jets in free ambients as shown in Fig. 59. In these cases the values for  $P_{rt}$  actually tend to increase beyond the viscous layer edge. It is clear that the external behavior is strongly influenced by the relative rates at which the turbulent fluxes and mean gradients vanish. These observations further support the

conclusion promoted herein that the turbulent Prandtl number is a difficult and unreliable parameter to model, and such a methodology ought to be avoided if possible.



## 5.0 CONCLUSIONS AND RECOMMENDATIONS

The direction and content of the present investigation have been guided by the general objective of successfully calculating the evolution and characteristics of turbulent boundary layers involving heat transfer. Although many computational schemes are currently being employed, it is clear that a reliable and fundamental approach has not yet emerged in the technical community [72], and even calculations of the simplest flat plate cases are not completely satisfactory. This state of affairs points out the need for continued fundamental investigations. The specific objective herein has been to study the effects of free stream turbulence (FST) through utilization of Blair's excellent data and through computations and modifications of the code, STANCOOL.

In addition to the tasks mentioned in the proposal for this investigation [2], several other major accomplishments have come to fruition during the course of this eight month effort. First, in the search for a wall layer characterization to match the earlier exponential wake observation, an analytical approximation has been achieved which describes the complete boundary layer profiles of mean velocity and temperature. This analytical description is surprisingly comprehensive and flexible, since it is shown to match laminar as well as turbulent profiles with appropriate changes in the parameters. The effect of FST is explicitly displayed in the coefficients of the triple deck exponential. The function matches the data presented by Coantic [30] and Kline, et al. [31], as well as those of Blair [18]. It is curious that three distinct layers are observed, apparently for the first time herein.

The second accomplishment has been the expression of the Reynolds stress and turbulent heat flux profiles directly in terms of the mean velocity and temperature profiles of the boundary layer through an integro-differential relationship. Scrutiny of Blair's data has permitted a tractable formulation of

this relationship, and the model has been implemented, although this novel work has not yet come to completion. Sample results are exhibited. FST is seen to influence the wake region of the boundary layer explicitly, and the wall region implicitly.

Third, the more general formulation has lead to a remarkable particular analytical solution to the equations describing a turbulent boundary layer. This solution applies to the case of a special form of the Reynold stress distribution, which is not entirely realistic, but the solution is informative. The analytical solution may be used to check the correctness of any turbulent boundary layer code, and it also provides guidance for the interpretation of the physical mechanisms at work in a turbulent boundary layer. The solution is extended to the energy equation, and analytical profiles for  $P_{rt}$  are provided for this special case.

Fourth, the study of the suction boundary layer initially proposed is shown to be a special case of the more general formulation presented herein. This case is described, and an explicit formula is presented for the turbulent Prandtl number profile.

Fifth, STANCOOL has been made operational on the IBM 3081 system at the University of Oklahoma, and three recent modifications in turbulence modeling have been incorporated. These consist of (1) STANCHEK, which calculates the analytical test case; (2) FST2, which utilizes a separate variation of wake and wall FST effects in the boundary layer; and (3) FST3, which incorporates the more general and novel integral approach to the turbulent fluxes. These options have been run and compared with data with favorable results. However, the comparisons are not yet complete, and a question has also arisen concerning the rate of boundary layer growth as calculated by STANCOOL. These issues remain for further investigation.

Sixth, a discussion is presented concerning the modeling and calculation of  $P_{rt}$  profiles. Several formulas are given for its specification, among which are two explicit analytical ones and one general calculation procedure. A survey of the literature has revealed a disparity in reported  $P_{rt}$  profiles. The proposed calculation procedure obviates the need for introducing the  $P_{rt}$  profile altogether.

Based on the findings of this investigation, several avenues for continued study are recommended. With the novel observation of a whole layer formula, it is of great interest to perform experimental work that focuses on establishing the validity and accuracy of the triple deck exponential description. The behavior of the three associated length scales is a related topic of further research. It remains to be seen whether a set of universal coefficients in the exponential function may be obtained and how the length scales depend on the evolution of wall shear. Further calculations are recommended with the new integro-differential model for the turbulent fluxes. Although the present calculations demonstrate a good fit in quality, a better match is to be sought in regard to the boundary layer growth rate. The investigation should also be extended to include the cases of boundary layers with non-vanishing pressure gradients, since these are of practical concern. Lastly, there has not been sufficient time to explore fully the general formulation of the  $P_{rt}$  profile presented here, and if and its use is to be pursued, then its calculation in STANCOOL requires further work.

## 6.0 REFERENCES

1. Sepri, P. and Ebert, J. L., "Calculation of Enhanced Heating in Turbulent Boundary Layers Influenced by Free Stream Turbulence", 1984 USAF-SCEEE Summer Faculty Research Program, Contract No.: F49620-82-C-0035, Final Report, 27 August 1984.
2. Sepri, P., "Free Stream Turbulence Effects on Turbulent Heat Transfer", Research Proposal submitted to the AFOSR RISE Program, Subcontract No: 84RIP33, start date: 1 January 1985.
3. Simonich, J. C., and Bradshaw, P., "Effect of Free-Stream Turbulence on Heat Transfer through a Turbulent Boundary Layer", ASME Journal of Heat Transfer, Vol. 100, November 1978, pp. 671-677.
4. Bayley, F. J. and Priddy, W. J., "Effects of Free-Stream Turbulence Intensity and Frequency on Heat Transfer to Turbine Blading", ASME Journal of Engineering for Power, Vol. 103, January 1981, pp. 60-64.
5. Pedisius, A. A., Kazimekas, P.-V.A., and Slanciauskas, A. A., "Heat Transfer from a Plate to a High-Turbulence Air Flow", Heat Transfer-Soviet Research, Vol. 11, No. 5, Sept.-Oct. 1979, pp. 125-134.
6. McDonald, H. and Kreskovsky, J. P., "Effect of Free Stream Turbulence on the Boundary Layer", Int. J. Heat Mass Transfer, Vol. 17, 1974, pp. 705-716.
7. Hall, J. D., and Gibbings, J. C., "Influence of Stream Turbulence and Pressure Gradient upon Boundary Layer Transition", Journal of Mechanical Engineering Science, Vol. 14, No. 2, 1972, pp. 134-146.
8. Meier, H. U., and Kreplin, H. -P., "Influence of Freestream Turbulence on Boundary-Layer Development", AIAA Journal, Vol. 18, No. 1, January 1980, pp. 11-15.
9. Krishnamoorthy, V., "Effect of Turbulence on the Heat Transfer in a Laminar and Turbulent Boundary Layer over a Gas Turbine Blade", ASME Paper 82-GT-146, 1982, pp. 1-9.
10. Junkhan, G. H., and Serovy, G. K., "Effects of Free-Stream Turbulence and Pressure Gradient on Flat-Plate Boundary-Layer Velocity Profiles and on Heat Transfer," ASME Journal of Heat Transfer, Vol. 89, May 1967, pp. 169-176.
11. Kestin, J., "The Effect of Free-Stream Turbulence on Heat Transfer Rates", Advances in Heat Transfer, Vol. 3, ed. by T. F. Irvine, Jr., and J. P. Hartnett, Academic Press, London, 1966.
12. Sugawara, S., Sato, T., Hirosyasa, K., and Osaka, H., "The Effect of Free-Stream Turbulence on Heat Transfer from a Flat Plate", NACA Tech. Memo 1441, 1958.

13. Feiler, C. E., and Yaeger, E. B., "Effect of Large-Amplitude Oscillations on Heat Transfer", NASA Tech. Report R-142, 1962.
14. Edwards, A., and Furber, B. N., "The Influence of Free-Stream Turbulence on Heat Transfer by Convection from an Isolated Region on a Plane Surface in Parallel Air Flow", Proc.-Inst. Mech. Engrs. London, Vol. 1970, 1956, p. 941.
15. Blair, M. F., "Influence of Free-Stream Turbulence on Turbulent Boundary Layer Heat Transfer and Mean Profile Development, Parts I & II", ASME Journal of Heat Transfer, Vol. 105, February 1983, pp. 33-47.
16. Blair, M. F., "Influence of Free-Stream Turbulence on Boundary Layer Transition in Favorable Pressure Gradients", ASME Journal of Engineering for Power, Vol. 104, October, 1982, pp. 743-750.
17. Blair, M. F., "The Effect of Free-Stream Turbulence on the Turbulence Structure and Heat Transfer in Zero Pressure Gradient Boundary Layers", United Technologies Research Center Report: R82-915634-2, East Hartford, Conn., November, 1982.
18. Blair, M. F., "Final Data Report-Vol. I-Velocity and Temperature Profile Data for Zero Pressure Gradient, Fully Turbulent Boundary Layers", UTRC Report R81-914388-15, E. Hartford, Conn., January, 1981.
19. Blair, M. F., "Final Data Report-Vol. II-Velocity and Temperature Profile Data for Accelerating, Transitional Boundary Layers", UTRC Report R81-914388-16, E. Hartford, Conn., January 1981.
20. Blair, M. F., "Combined Influence of Free-Stream Turbulence and Favorable Pressure Gradients on Boundary Layer Transition and Heat Transfer", UTRC Report R81-914388-17, E. Hartford, Conn., March 1981.
21. Blair, M. F., "The Influence of Free-Stream Turbulence on the Zero Pressure Gradient Fully Turbulent Boundary Layer", UTRC Report R80-914388-12, E. Hartford, Conn., September 1980.
22. Daniels, L. D., and Browne, W. B., "Calculation of Heat Transfer Rates to Gas Turbine Blades", Int. J. Heat Mass Transfer, Vol. 24, No. 5, 1981, pp. 871-879.
23. Crawford, M. E., and Kays, W. M., "STAN5 - A Program for Numerical Computation of Two-Dimensional Internal and External Boundary Layer Flows", NASA CR-2742, November, 1976.
24. Gaugler, R. E., "Some Modifications to, and Operational Experiences with, the Two-Dimensional, Finite Difference, Boundary-Layer Code, STAN5", ASME Paper 81-GT-89, 1981, pp. 1-5.
25. MacArthur, C. D., "Prediction of Free-Stream Turbulence Effects on Boundary Layer Heat Transfer - An Evaluation of the Heat Transfer Code STAN5", 1983 USAF-SCEEE Graduate Student Summer Support Program, Contract No. F49620-82-0035, 16 September 1983.

26. Winstanley, D.K., Booth, T.C., and Dunn, M.G., "The Predictability of Turbine Vane Convection Heat Transfer", AIAA Paper No. 81-1435, July 27-29, 1981.
27. Miyazaki, H. and Sparrow, E. M., "Analysis of Effects of Free-Stream Turbulence on Heat Transfer and Skin Friction", ASME Journal of Heat Transfer, Vol. 99, November 1977, pp. 614-619.
28. Coles, D., "The Law of the Wake in the Turbulent Boundary Layer," Journal of Fluid Mechanics, Vol. 1, 1956, pp. 191-226.
29. Favre, A., "Statistical Equations of Turbulent Gases", In: "Problems of Hydrodynamics and Continuum Mechanics", SIAM, 1969, pp. 231-266.
30. Coantic, M., "Évolution, en fonction du nombre de Reynolds, de la distribution des vitesses moyennes et turbulentes dans une conduite", Comptes Rendus de Acad. des Sc., Paris, Vol. 264, Serie A, 17 mai 1967, pp. 849-852.
31. Kline, S.J., Reynolds, W.C., Schraub, F.A., and Runstadler, P.W., "The Structure of Turbulent Boundary Layers", Journal of Fluid Mechanics, vol. 30, part 4, 1967, pp. 741-773.
32. Long, R.R., and Chen, T.C., "Experimental Evidence for the Existence of the 'Mesolayer' in Turbulent Systems", Journal of Fluid Mechanics, vol. 105, 1981, pp. 19-59.
33. Afzal, N., "Mesolayer Theory for Turbulent Flows", AIAA Journal, vol. 22, No. 3, March 1984, pp. 437-439.
34. Malkus, W.V.R., "Turbulent Velocity Profiles from Stability Criteria", Journal of Fluid Mechanics, vol. 90, part 3, 1979, pp. 401-414.
35. Van Driest, E.R., "On Turbulent Flow near a Wall", Journal of the Aeronautical Sciences, Vol. 23, 1956, pp. 1007-1011.
36. Schlichting, H., Boundary Layer Theory, McGraw-Hill Book Co., 7th Ed., 1979.
37. Gol'dshtik, M.A., Kutateladze, S.S., and Lifshits, A.M., "Determination of the Turbulent Prandtl Number in an Asymptotic Boundary Layer with Suction", Izvestiya Akademii Nauk. SSSR, Mekhanika Zhidkosti i Gaza, No. 1, Jan.-Feb. 1981, pp. 74-79.
38. Meier, H.U., and Kreplin, H.P., "Influence of Freestream Turbulence on Boundary Layer Development", AIAA Journal, Vol. 18, No. 1, January 1980, pp. 11-15.
39. Rotta, J.C., "Temperaturverteilungen in der Turbulenten Grenzschicht an der Ebenen Platte", Int. J. Heat Mass Transfer, Vol. 7, 1964, pp. 215-228.

40. Ludwig, H., "Bestimmung des Verhältnisses der Austauschkoefizienten für Wärme und Impuls bei turbulenten Grenzschichten", Zeit. Flugwiss., Vol. 4, 1956, pp. 73-81.
41. Simpson, R.L., Whitten, D.G., and Moffat, R.J., "An Experimental Study of the Turbulent Prandtl Number of Air with Injection and Suction", Int. Journal of Heat and Mass Transfer, Vol. 13, 1970, pp. 125-143.
42. Senda, M., Suzuki, K., and Sato, T., "Turbulence Structure Related to the Heat Transfer in a Turbulent Boundary Layer with Injection", Turbulent Shear Flows, Vol. 2, Springer-Verlag, 1980, pp. 143-157.
43. Subramanian, C.S., and Antonia, R.A., "Effects of Reynolds Number on a Slightly Heated Turbulent Boundary Layer", Int. J. Heat Mass Transfer, Vol. 24, No. 11, 1981, pp. 1833-1846.
44. Snijders, A.L., Koppius, A.M., Nieuwelt, C., "An Experimental Determination of the Turbulent Prandtl Number in the Inner Boundary Layer for Air Flow over a Flat Plate", Int. J. Heat Mass Transfer, Vol. 26, No. 3, 1983, pp. 425-431.
45. Chen, C.P., "Determination Experimentale du Nombre de Prandtl Turbulent pres d'une Paroi Lisse", Int. J. Heat Mass Transfer, Vol. 16, 1973, pp. 1849-1862.
46. Sreenivasan, K.R., Antonia, R.A., and Chambers, A.J., "On the Variation of the Turbulent Prandtl Number in Shear Flows", Int. Comm. Heat Mass Transfer, Vol. 11, 1984, pp. 497-501.
47. Antonia, R.A., "Behaviour of the Turbulent Prandtl Number Near the Wall", Int. J. Heat Mass Transfer, Vol. 23, 1980, pp. 906-908.
48. Browne, L.W.B., and Antonia, R.A., "Measurements of Turbulent Prandtl Number in a Plane Jet", Journal of Heat Transfer, Vol. 105, August 1983, pp. 663-665.
49. Dorfman, A.Sh., "Influence of Turbulent Prandtl Number on Heat Transfer of a Flat Plate", Zhurnal Prikladnoi Mekhaniki i Tekhnicheskoi Fiziki, No. 4, July-Aug. 1984, pp. 81-85.
50. Nakayama, A., Koyama, H., and Ohsawa, S., "Momentum/Heat-Transfer Analogy for Turbulent Boundary Layers in Mild Pressure Gradients", AIAA Journal, Vol. 22, No. 6, 1984, pp. 841-844.
51. Cebeci, T., "A Model for Eddy Conductivity and Turbulent Prandtl Number", Journal of Heat Transfer, May 1973, pp. 227-234.
52. Meier, H.U. and Rotta, J.C., "Experimental and Theoretical Investigations of Temperature Distributions in Supersonic Boundary Layers", AIAA Paper No. 70-744, 1970.

53. Johnson, D.S., "Velocity and Temperature Fluctuation Measurements in a Turbulent Boundary Layer Downstream of a Stepwise Discontinuity in Wall Temperature", Journal of Applied Mechanics, Vol. 26, Trans. ASME, Series E, Vol. 81, No. 3, Sept. 1959, pp. 325-336.
54. Chan, Y.Y., "A Note on the Effect of Turbulent Prandtl Number Distribution on Compressible Turbulent Boundary Layers", C.A.S.I. Transactions, Vol. 6, No. 2, Sept. 1973, pp. 102-104.
55. Rotta, J.C., "Recent Developments in Calculation Methods for Turbulent Boundary Layers with Pressure Gradients and Heat Transfer", J. of Applied Mech., Vol. 33, June 1966, p. 429.
56. Chuang, H., and Renda, R.B., "Turbulent Prandtl Number in Thermally Stratified Shear Flows of Air", Int. J. Heat Mass Transfer, Vol. 12, 1969, pp. 1585-1594.
57. Geshev, P.I., "Influence of Heat conduction of the Wall on the Turbulent Prandtl Number in the Viscous Sublayer", Inzhenerno-Fizicheskii Zhurnal, Vol. 35, No. 2, August 1978, pp. 292-296.
58. Ginzburg, I.P., and Korneva, I.V., "Influence of Turbulent Pr Number on Friction and Heat Transfer at a Plate Immersed in a Turbulent Gas Stream", Inzhenerno-Fizicheskii Zhurnal, Vol. 9, No. 2, 1965, pp. 155-162.
59. Jischa, M., and Rieke, H.B., "About the Prediction of Turbulent Prandtl and Schmidt Numbers from Modeled Transport Equations", Int. J. Heat Mass Transfer, Vol. 22, 1979, pp. 1547-1555.
60. McEligot, D.M., Pickett, P.E., and Taylor, M.F., "Measurement of Wall Region Turbulent Prandtl Numbers in Small Tubes", Int. J. Heat Mass Transfer, Vol. 19, 1976, pp. 799-803.
61. Reynolds, A.J., "The Prediction of Turbulent Prandtl and Schmidt Numbers", Int. J. Heat Mass Transfer, Vol. 18, 1975, pp. 1055-1069.
62. Reynolds, A.J., "The Variation of Turbulent Prandtl and Schmidt Numbers in Wakes and Jets", Int. J. Heat Mass Transfer, Vol. 19, 1976, pp. 757-764.
63. Spalding, D.B., "Contribution to the Theory of Heat Transfer Across a Turbulent Boundary Layer", Int. J. Heat Mass Transfer, Vol. 7, 1964, pp. 743-761.
64. Kestin, J., and Richardson, P.D., "Heat Transfer Across Turbulent, Incompressible Boundary Layers", Int. J. Heat Mass Transfer, Vol. 6, 1963, pp. 147-189.
65. Wassel, A.T., and Catton, I., "Calculation of Turbulent Boundary Layers over Flat Plates with Different Phenomenological Theories of Turbulence and Variable Turbulent Prandtl Number", Int. J. Heat Mass Transfer, Vol. 16, 1973, pp. 1547-1563.



66. Blom, J., "An Experimental Determination of the Turbulent Prandtl Number in a Developing Temperature Boundary Layer", Fourth Int. Heat Transfer Conference, Versailles, Paris, France, August 1970.
67. Snegova, N.P., "Heat Transfer at High Prandtl Numbers in Fully Developed Turbulent Flow", Heat Transfer - Soviet Research, Vol. 3, No. 3, May-June 1971, pp. 129-133.
68. Thomas, L.C., and Ibrahim, M.B., "A Model of the Turbulent Burst Phenomenon: Predictions for Turbulent Prandtl Number", Letters in Heat and Mass Transfer, Vol. 8, 1981, pp. 357-369.
69. Anderson, P.S., Kays, W.M., and Moffat, R.J., "Experimental Results for the Transpired Turbulent Boundary Layer in an Adverse Pressure Gradient", Journal of Fluid Mechanics, Vol. 69, Part 2, 1975, pp. 353-375.
70. Pabst, O., "Die Ausbreitung heisser Gasstrahlen in bewegter Luft", F.W. Flugzeugbau, U.M. No. 8004, 8007, 1944. See: Szablewski, W., "The Diffusion of a hot air jet in air in motion", Tech. Memo. 1288, U.S. Nat. Adv. Comm. Aero., 1950.
71. Reichardt, H., "Impuls-und Wärmeaustausch in freier Turbulenz", Zeit. Angew. Math. Mech., No. 24, 1944, pp. 268-272.
72. Patel, V.C., Rodi, W., and Scheurer, G., "Turbulence Models for Near-Wall and Low Reynolds Number Flows: A Review", AIAA Journal, Vol 23, No. 9, Sept. 1985, pp. 1308-1319.

TABLE 1  
COEFFICIENTS OF TRIPLE-DECK EXPONENTIAL FUNCTION  
FIT BY LEAST SQUARES ERROR TO BLAIR'S DATA [18].

MEAN VELOCITY FIELD

$$\frac{\bar{u}}{u_e} = 1 - \exp[-\phi_1 + \exp\{-\phi_2 + \exp(-\phi_3)\}]$$

$$\text{where: } \phi_1 = A_1 + B_1 \left(\frac{Y}{\delta}\right) + C_1 \left(\frac{Y}{\delta}\right)^2$$

$$\phi_2 = A_2 + B_2 \left(\frac{Y}{\delta}\right) + C_2 \left(\frac{Y}{\delta}\right)^2$$

$$\phi_3 = A_3 + B_3 \left(\frac{Y}{\delta}\right) + C_3 \left(\frac{Y}{\delta}\right)^2$$

<u>CASE</u>										
Grid Config.	X[in]	A <sub>1</sub>	B <sub>1</sub>	C <sub>1</sub>	A <sub>2</sub>	B <sub>2</sub>	C <sub>2</sub>	A <sub>3</sub>	B <sub>3</sub>	C <sub>3</sub>
0	12	0.449	-0.537	6.067	1.801	1.513	34.70	0.0	0.0	0.0
0	36	1.596	-1.570	5.213	0.274	4.034	22.17	0.300	49.64	379.0
0	52	1.391	-0.672	4.080	0.474	5.835	22.13	0.218	76.39	251.9
0	84	1.347	-0.465	3.861	0.481	7.958	20.97	0.250	105.8	0.0
2	12	1.294	0.527	3.155	0.575	11.28	0.0	0.183	0.064	918.3
2	36	1.352	-0.012	3.783	0.505	7.295	12.70	0.214	74.84	431.5
2	52	1.299	0.306	3.604	0.545	9.926	11.25	0.214	114.5	319.1
2	84	1.220	0.822	2.922	0.753	10.31	33.13	0.049	122.6	0.0
4	12	1.064	2.662	1.451	1.404	19.86	0.0	-0.383	-9.39	1392.
4	36	1.038	3.818	0.391	1.204	19.02	117.1	-0.216	67.71	4158.
4	52	1.105	3.931	0.230	0.911	24.60	41.69	-0.011	86.78	14022.
4	84	1.105	4.474	-0.198	1.082	18.77	186.7	-0.167	192.4	1294.

TABLE 2  
COEFFICIENTS OF TRIPLE-DECK EXPONENTIAL FUNCTION  
FIT BY LEAST SQUARES ERROR TO BLAIR'S DATA [18].

MEAN TEMPERATURE FIELD

$$\frac{u}{u_e} = 1 - \exp[-\phi_1 + \exp\{-\phi_2 + \exp(-\phi_3)\}]$$

$$\text{where: } \phi_1 = A'_1 + B'_1 \left(\frac{Y}{\delta}\right) + C'_1 \left(\frac{Y}{\delta}\right)^2$$

$$\phi_2 = A'_2 + B'_2 \left(\frac{Y}{\delta}\right) + C'_2 \left(\frac{Y}{\delta}\right)^2$$

$$\phi_3 = A'_3 + B'_3 \left(\frac{Y}{\delta}\right) + C'_3 \left(\frac{Y}{\delta}\right)^2$$

<u>CASE</u>										
Grid Config.	X[in]	A' <sub>1</sub>	B' <sub>1</sub>	C' <sub>1</sub>	A' <sub>2</sub>	B' <sub>2</sub>	C' <sub>2</sub>	A' <sub>3</sub>	B' <sub>3</sub>	C' <sub>3</sub>
0	12	0.184	1.050	4.686	2.693	3.686	10.68	0.0	0.0	0.0
0	36	1.096	-0.037	2.980	0.598	9.818	28.23	0.371	35.61	1524.0
0	52	1.041	0.525	2.369	0.840	11.57	23.01	0.128	56.19	431.9
0	84	1.140	0.511	2.443	0.890	6.857	52.71	-0.0208	77.17	149.1
2	12	0.935	1.324	1.656	1.066	24.87	0.0	0.0	0.0	0.0
2	36	1.036	1.506	1.626	0.850	14.93	12.87	0.122	64.94	0.0
2	52	1.204	0.778	2.692	0.651	13.62	0.0	0.178	69.30	634.4
2	84	1.156	1.414	1.787	0.782	14.23	0.0	0.0758	100.5	0.0
4	12	1.009	1.924	0.836	0.575	19.73	30.30	0.538	-7.384	2979.0
4	36	1.147	3.355	0.799	0.927	6.954	176.9	-0.0620	91.62	195.0
4	52	1.204	3.189	0.449	1.095	8.082	43.76	-0.248	90.46	0.0
4	84	1.200	3.901	0.0	0.672	22.87	0.0	0.158	185.1	0.0

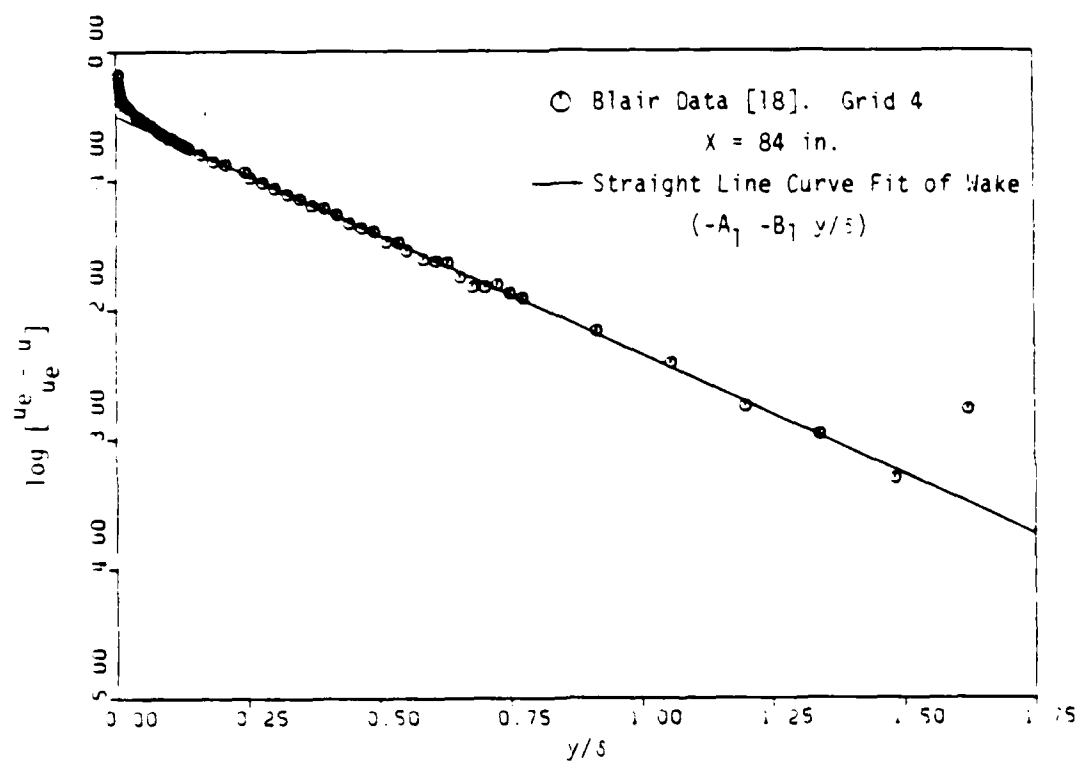


Figure 1: Semilogarithmic profile of mean velocity defect. High FST.

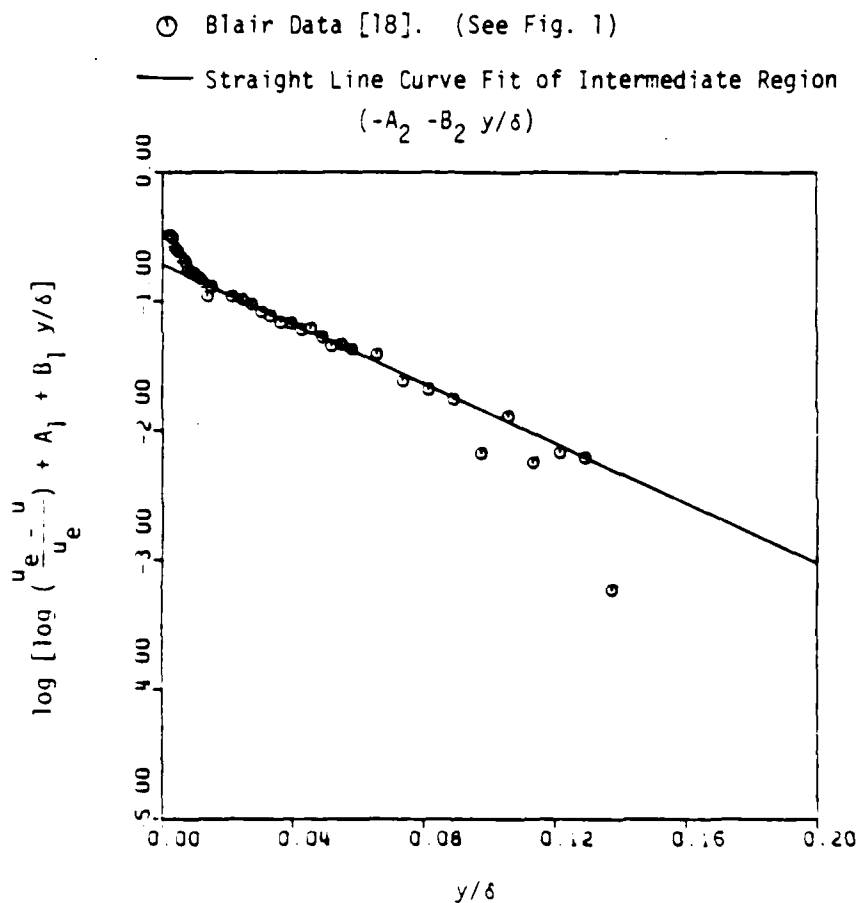


Figure 2: Semilogarithmic profile of mean velocity residue with respect to linear curve fit (see Fig. 1). High FST.

○ Blair Data [18]. (See Figs. 1 and 2)  
 — Straight Line Curve Fit of Innermost Region  
 $(-A_3 - B_3 y/\delta)$

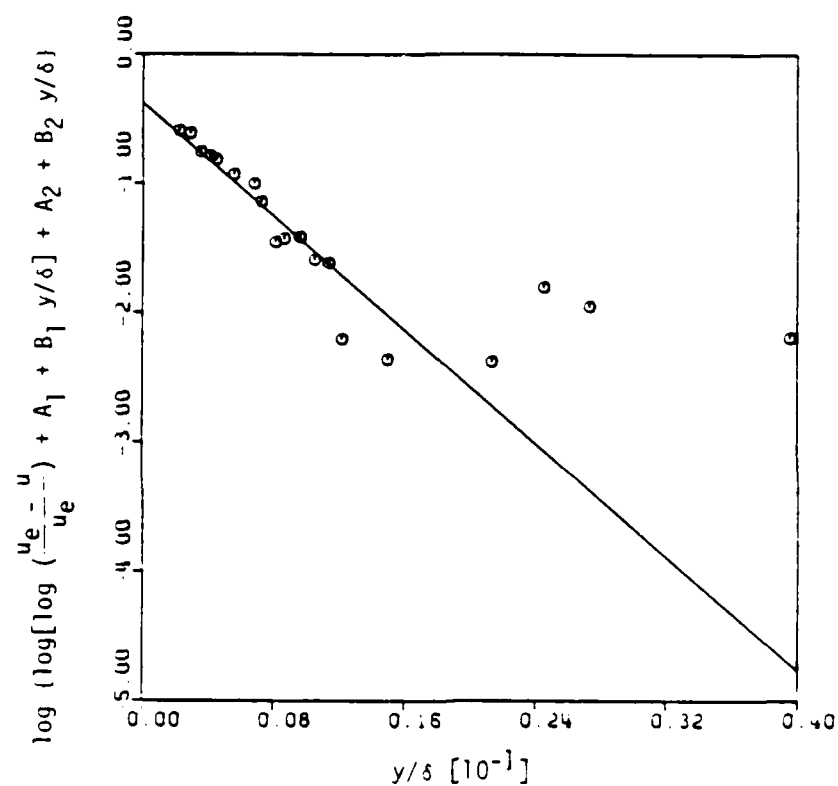


Figure 3: Semilogarithmic profile of innermost velocity region.  
 (See Figs. 1 and 2). High FST.

○ Blair Data [18]. Grid 4.  $x = 84$  in.  
 — Eq. (28)

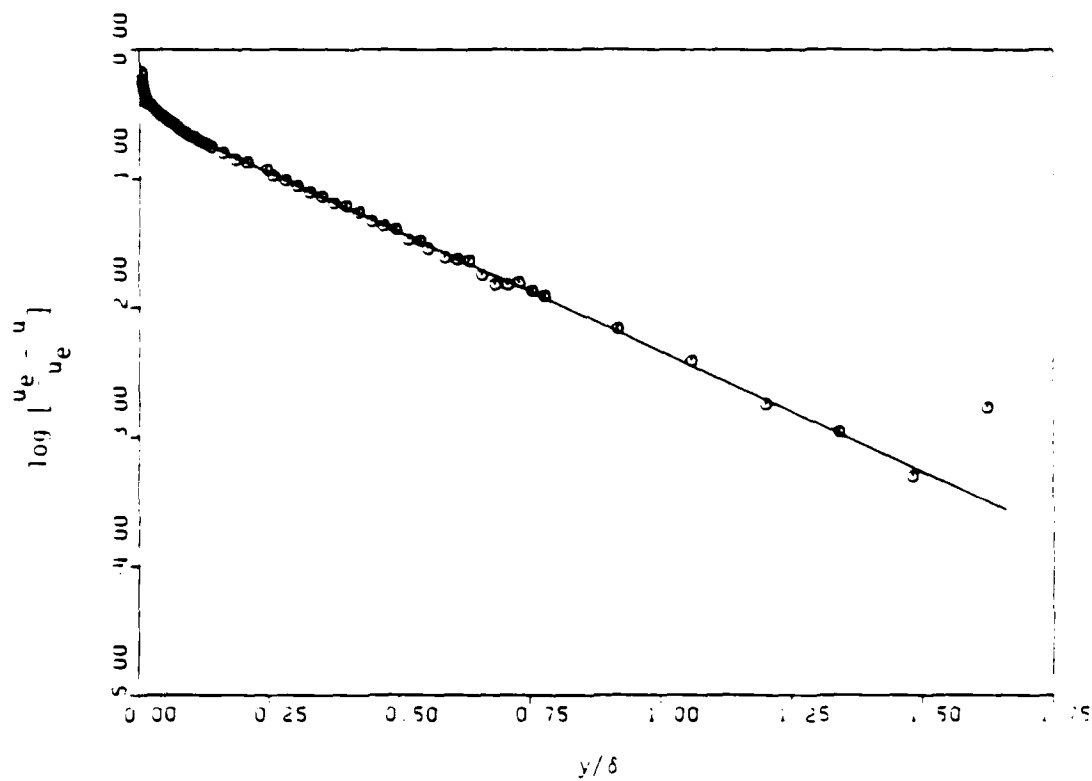


Figure 4: wake comparison of Blair's data with Eq. (28). High FST.

○ Blair Data [18]. Grid 4.  
 $x = 84$  in.  
 — Eq. (28)

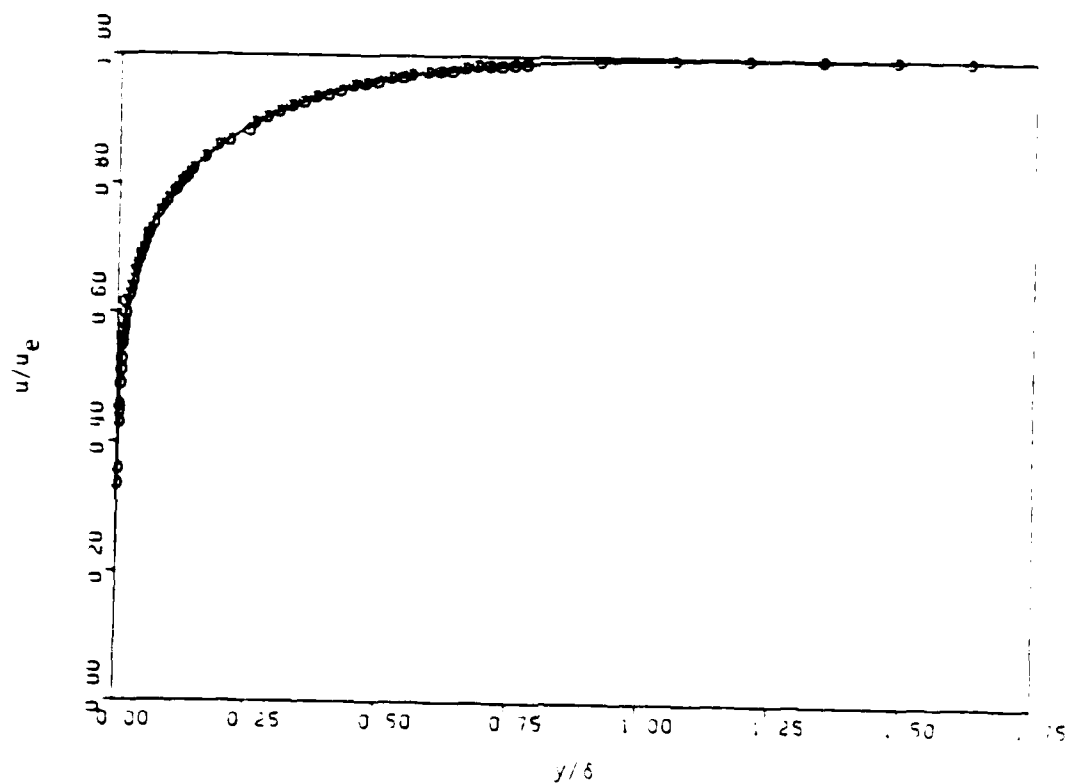


Figure 5. Linear comparison of Blair's data with Eq. (28). High FST.



○ Blair Data [18]. Grid 4.

$x = 84$  in.

— Three exponential layers.

Eq. (26)

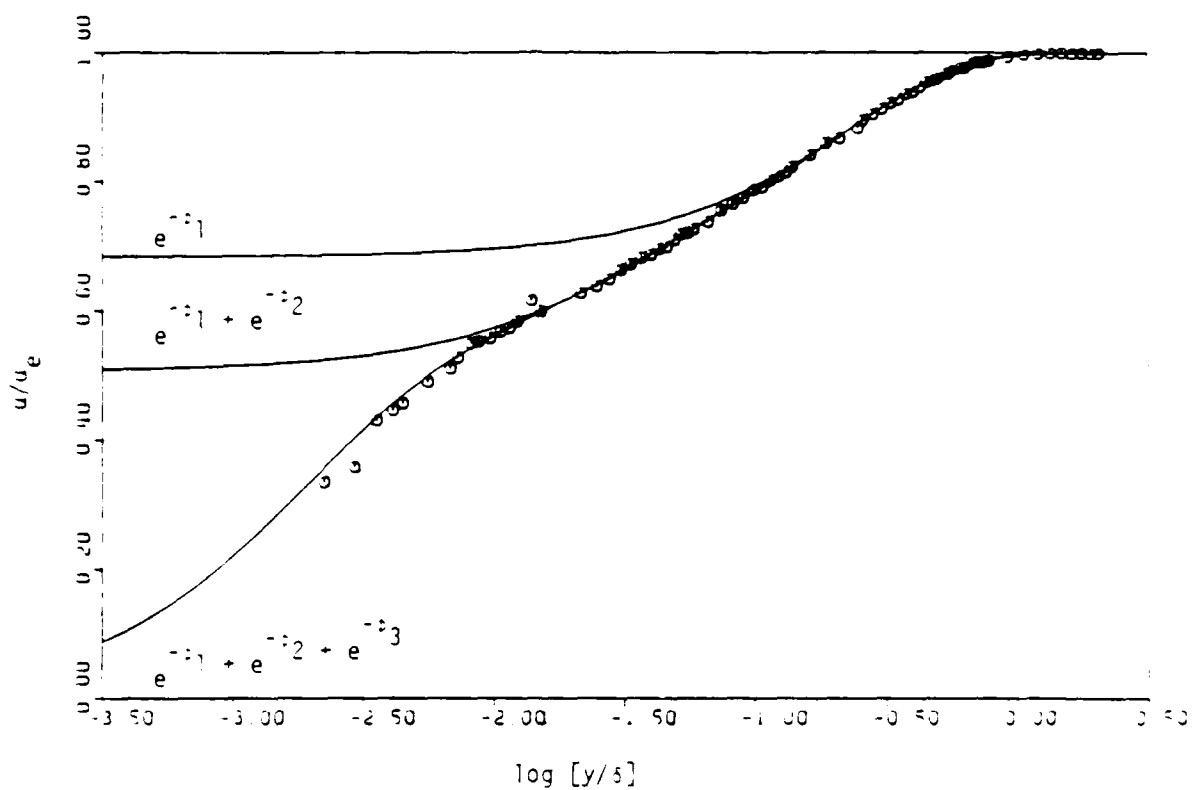


Figure 6: Semilogarithmic comparison of Blair's data with Eq. (28). High FST.

○ Blair Data [18]. Grid 0.

$x = 84$  in.

— Quadratic Curve Fit

$(-A_1 - B_1 n - C_1 n^2)$

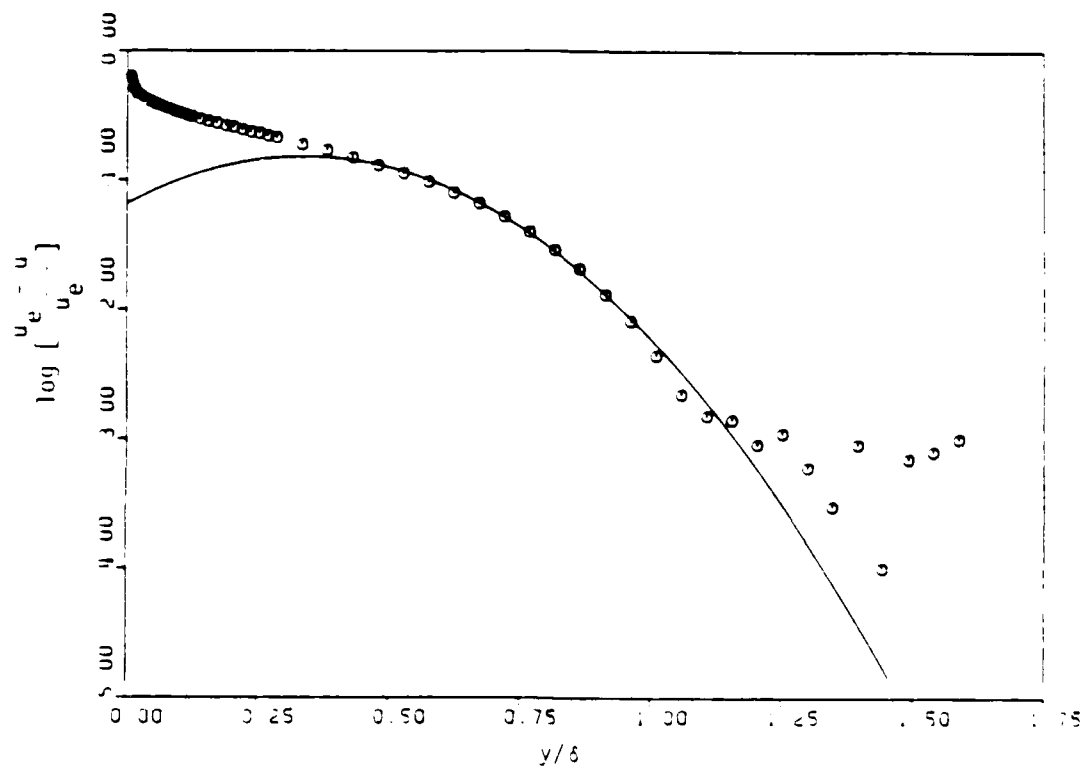


Figure 7: Quadratic fit of mean velocity wake deficit for low FST.

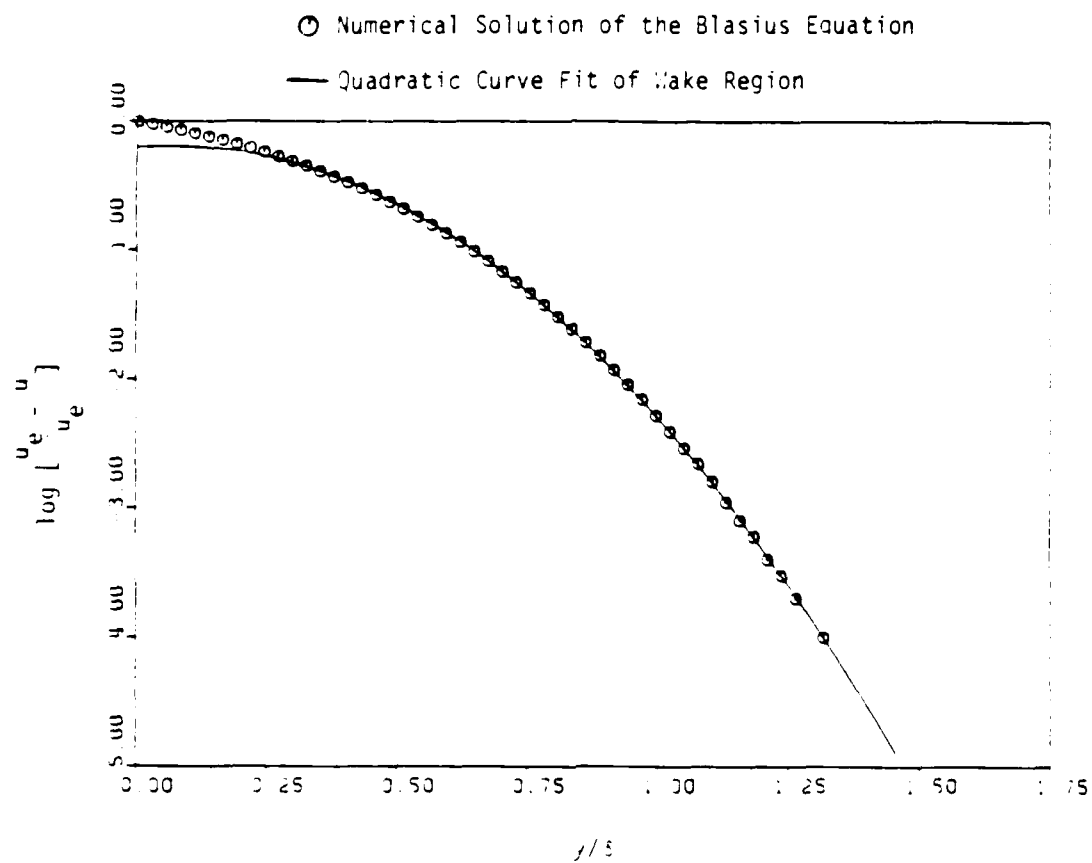


Figure 30: Laminar boundary layer fit by a quadratic wake function.

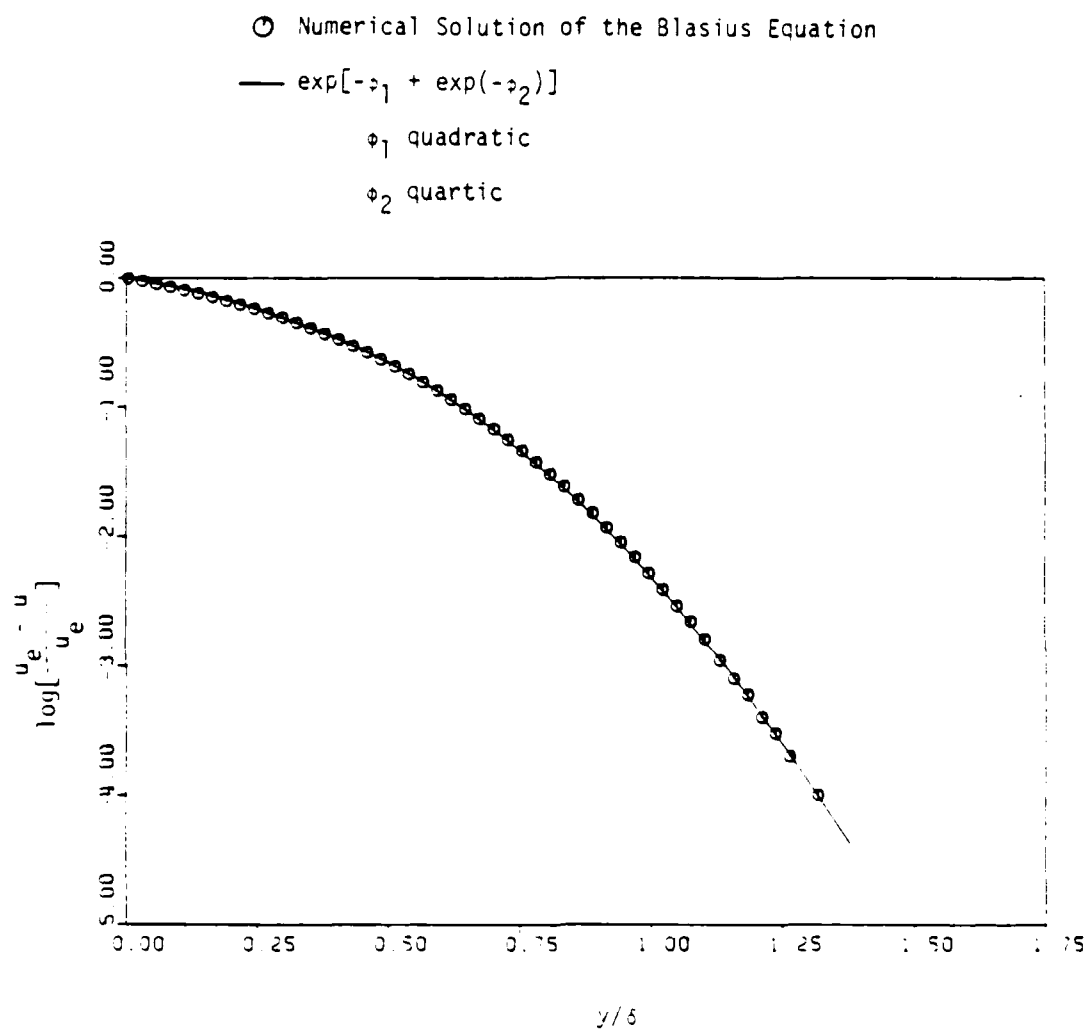


Figure 9: Blasius Solution compared with composite exponential curve fit.

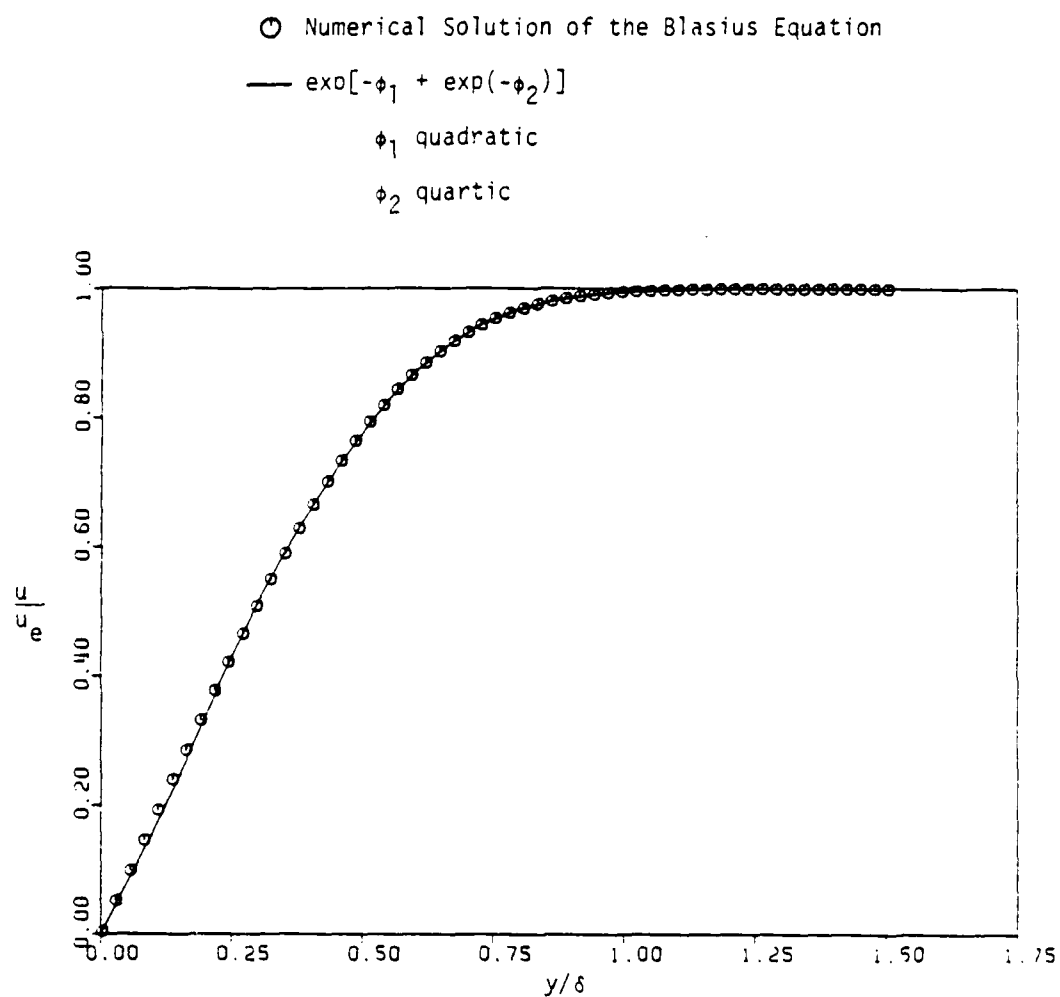


Figure 10: Blasius Solution compared with composite exponential function (linear comparison).

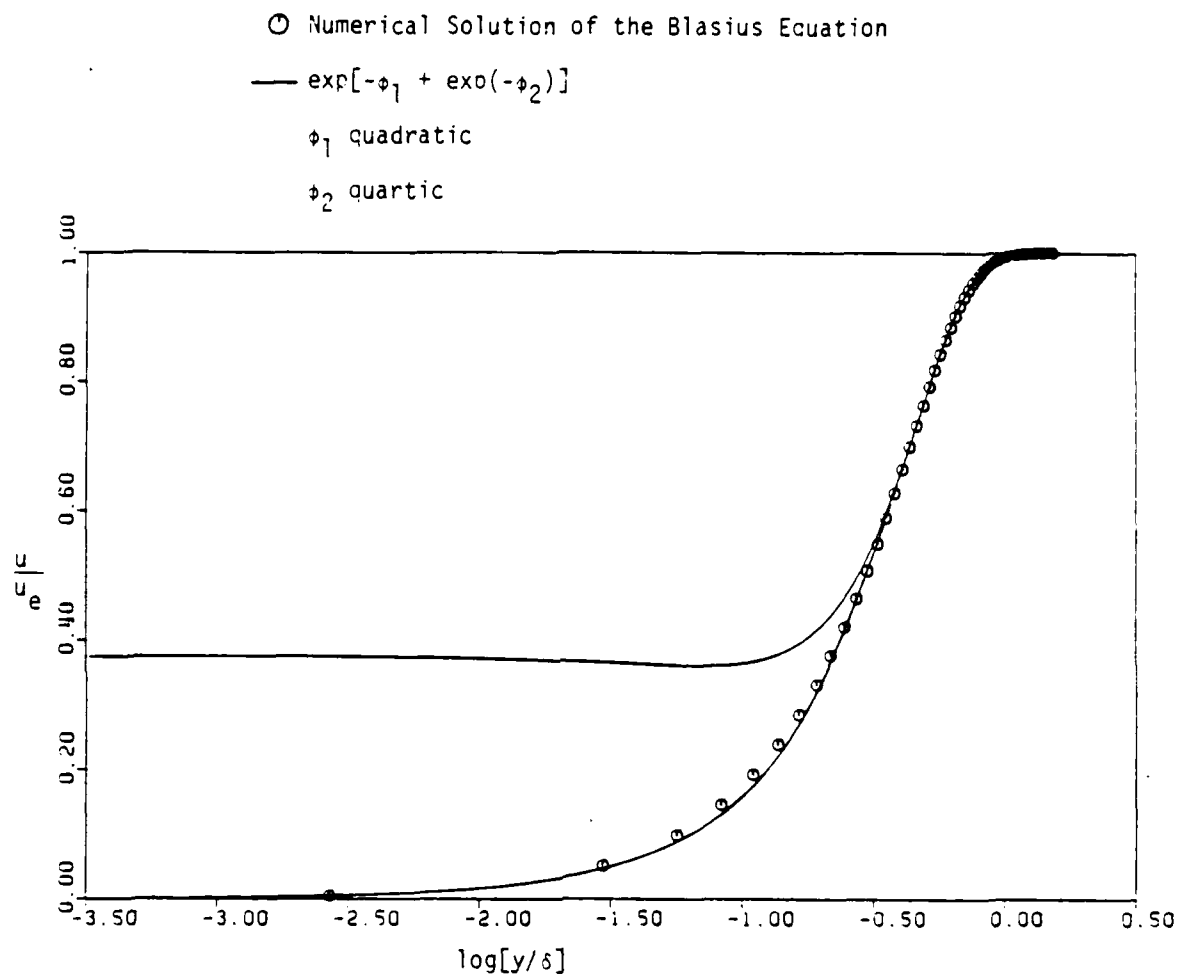


Figure 11: Blasius Solution compared sem logarithmically with composite exponential function.

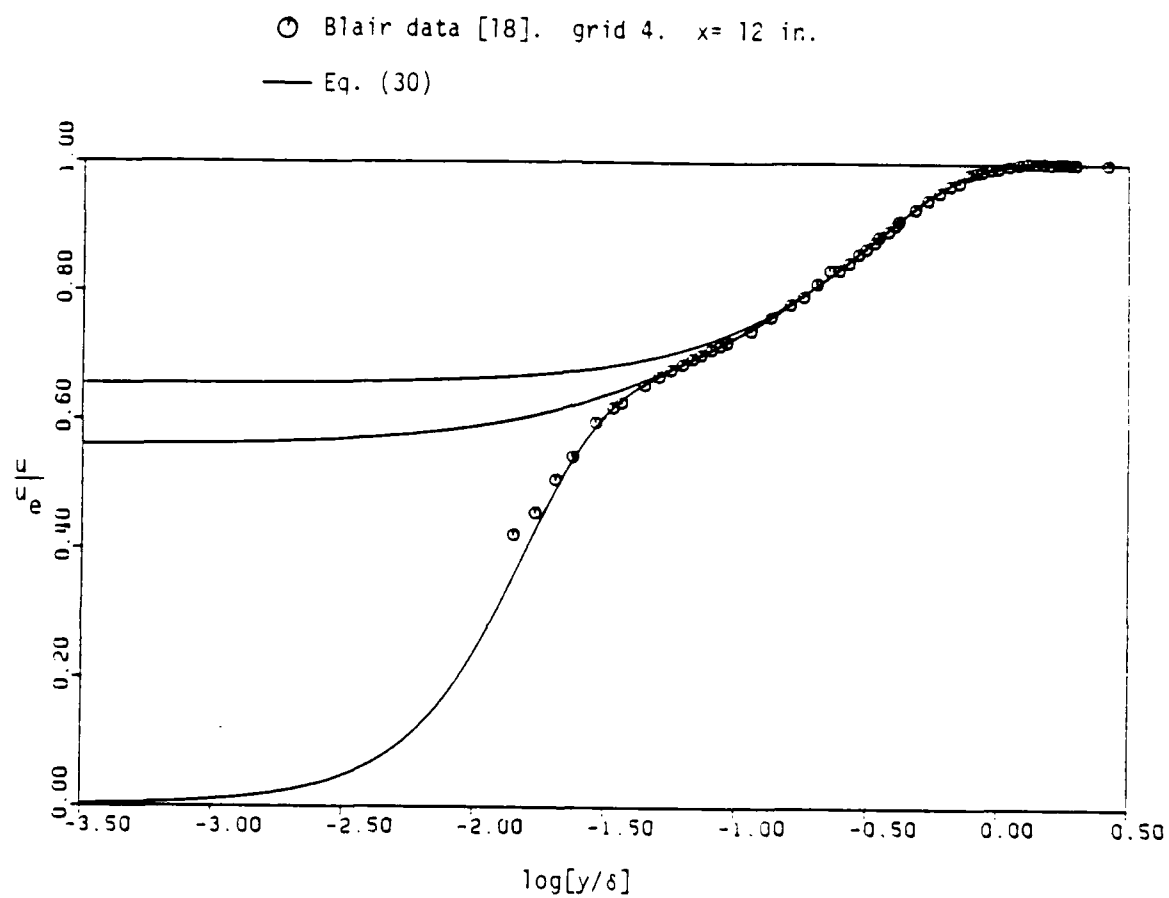


Figure 12: Velocity profile at  $x = 12$  in. Grid 4.

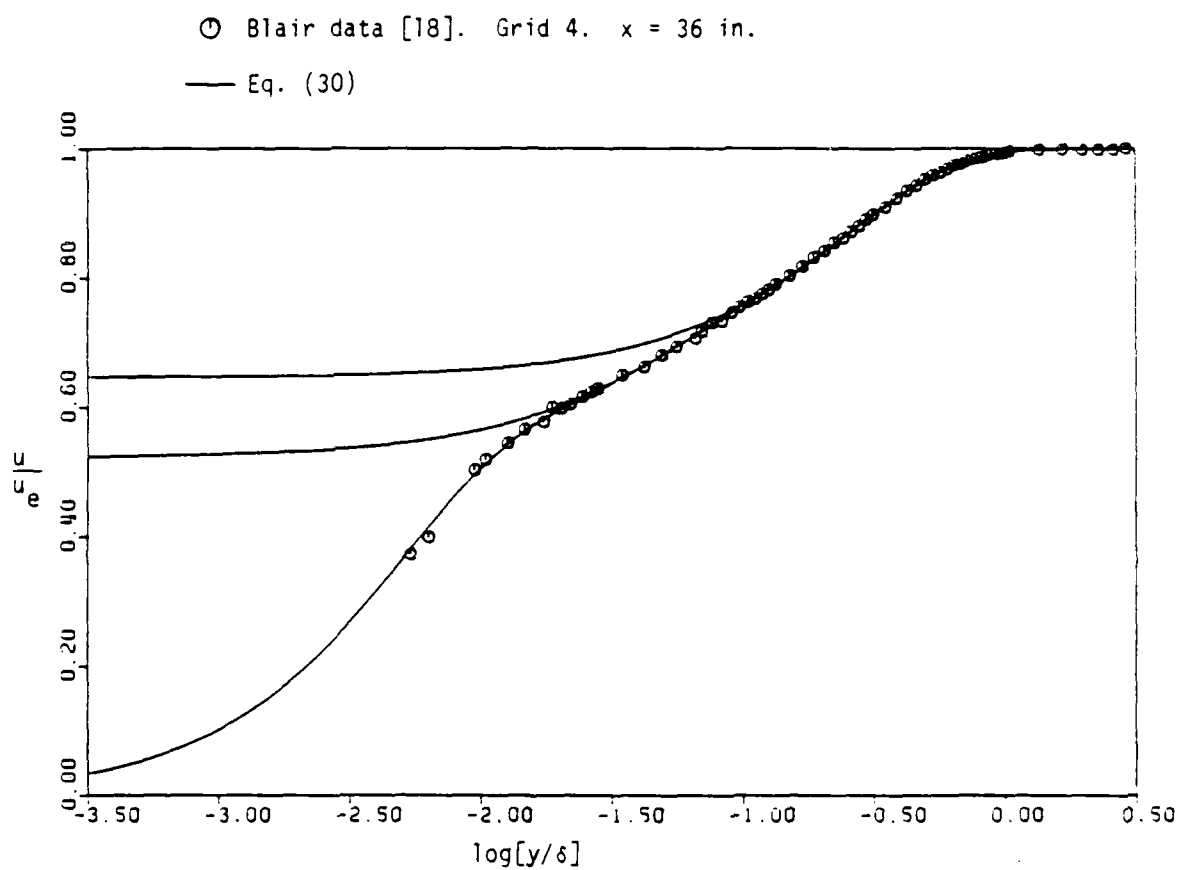


Figure 13: Velocity profile at  $x = 36$  in. Grid 4.



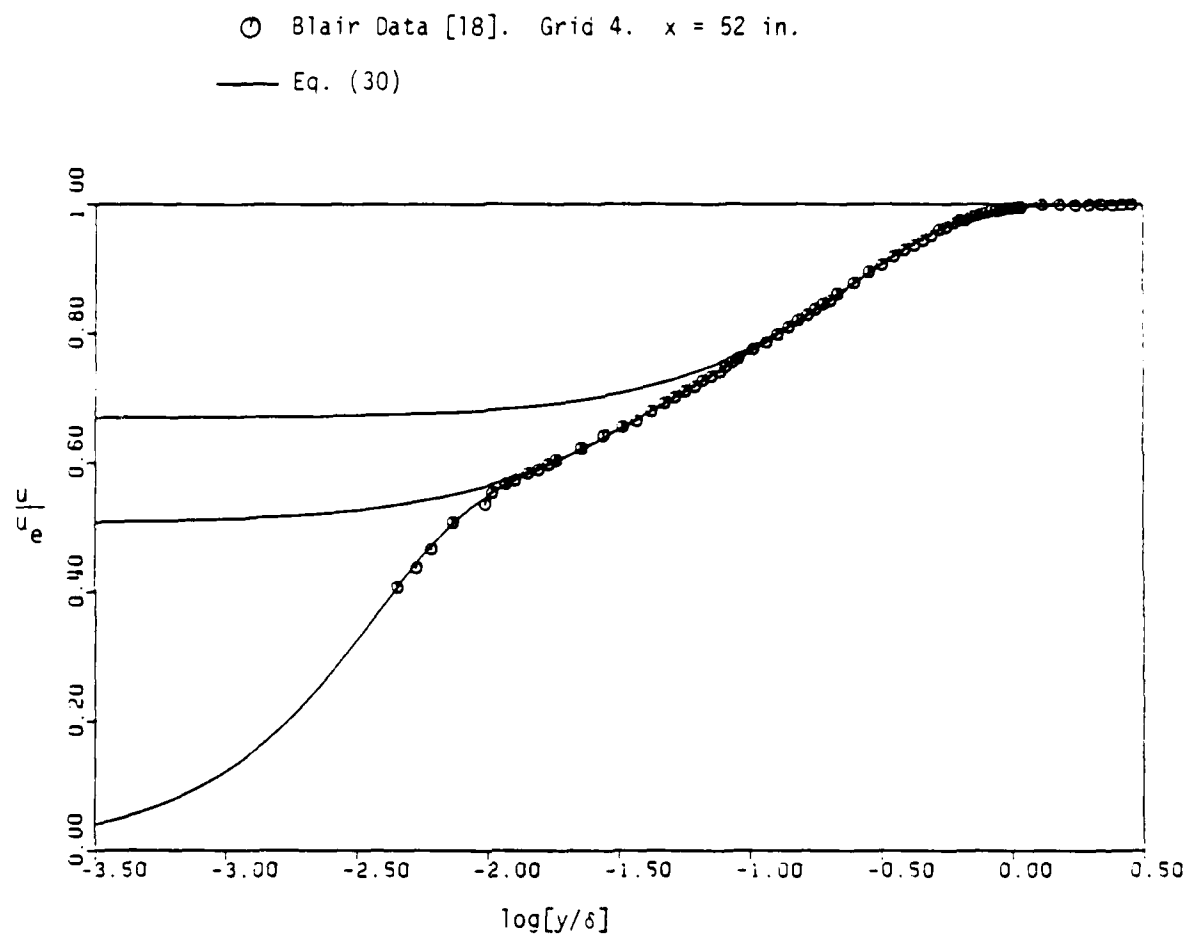


Figure 14: Velocity profile at  $x = 52$  in. Grid 4.

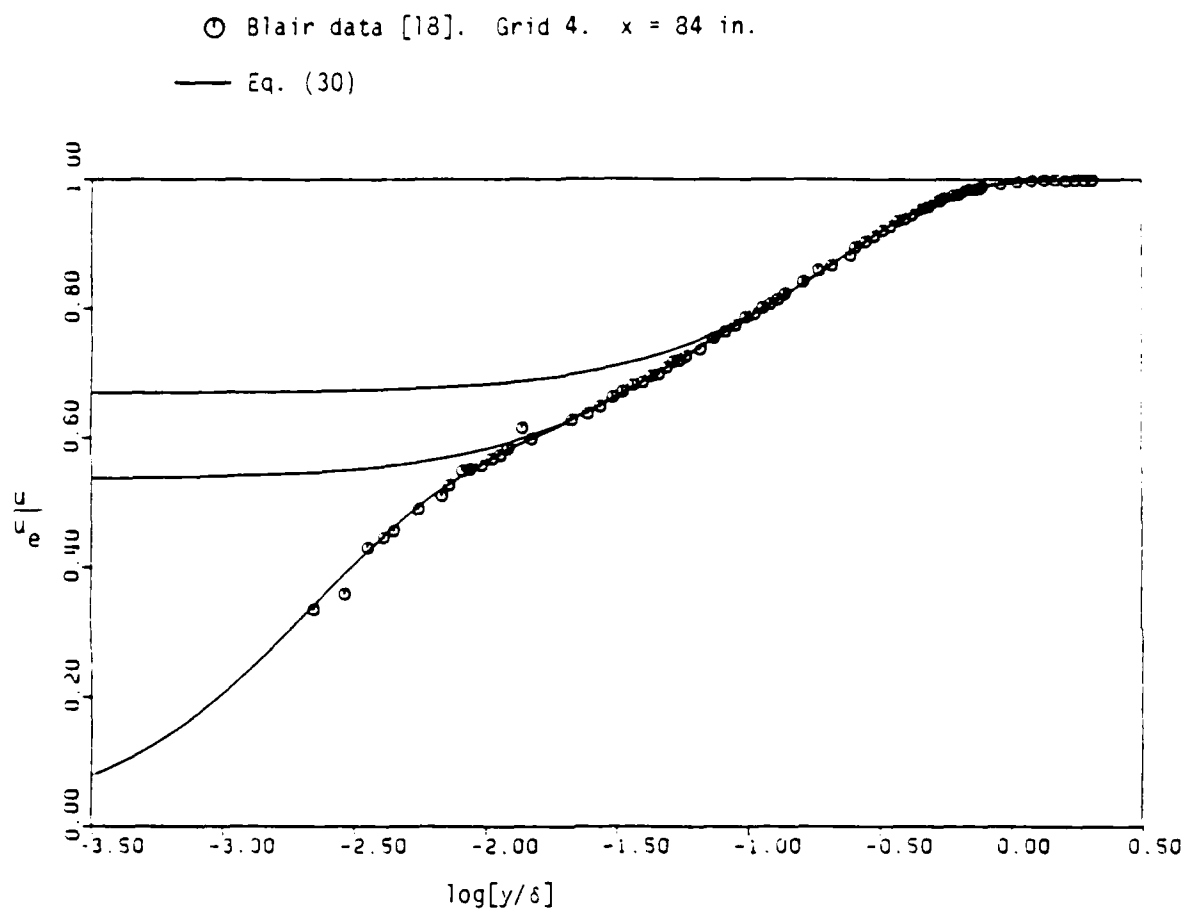


Figure 15: Velocity profile at  $x = 84$  in. Grid 4.

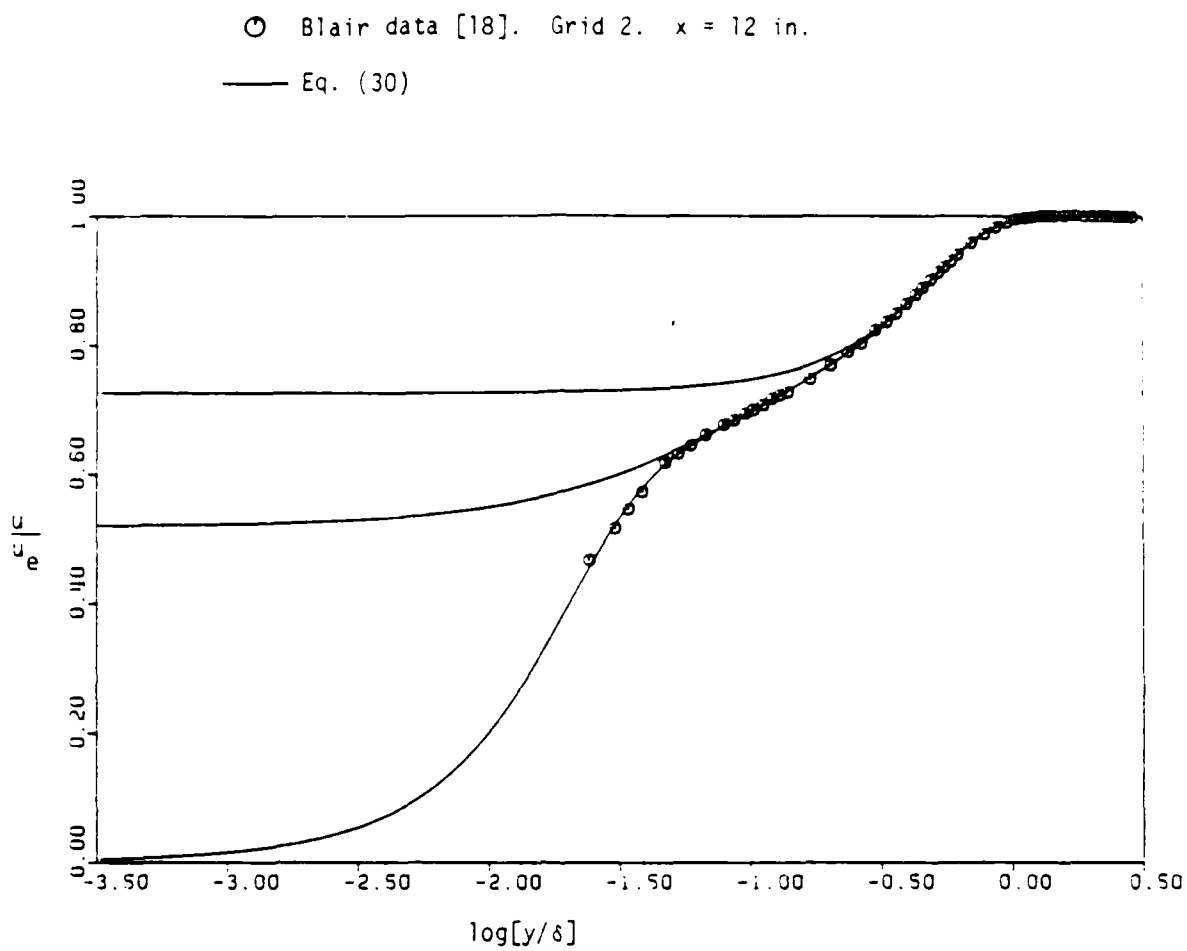


Figure 16: Velocity profile at  $x = 12$  in. Grid 2.

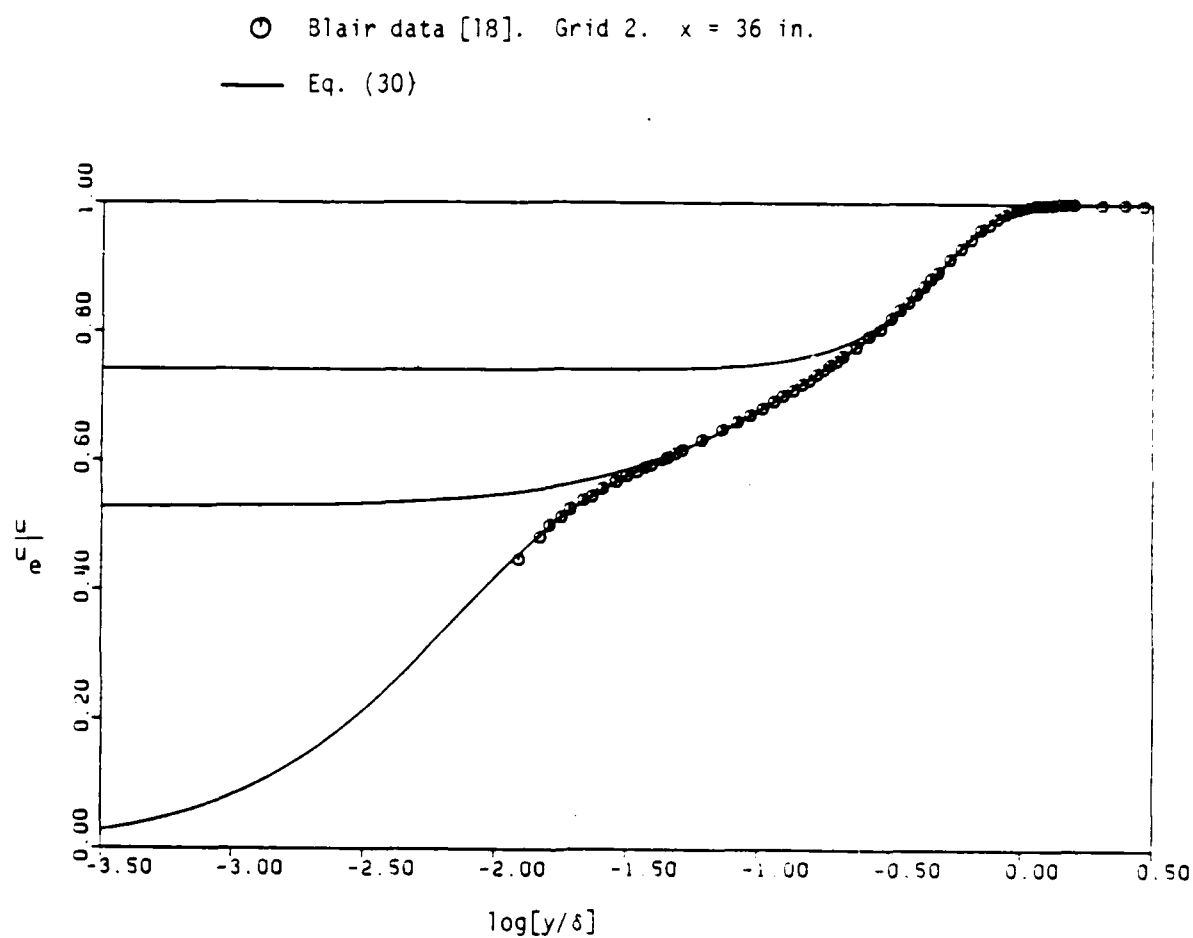


Figure 17: Velocity profile at  $x = 36$  in. Grid 2.

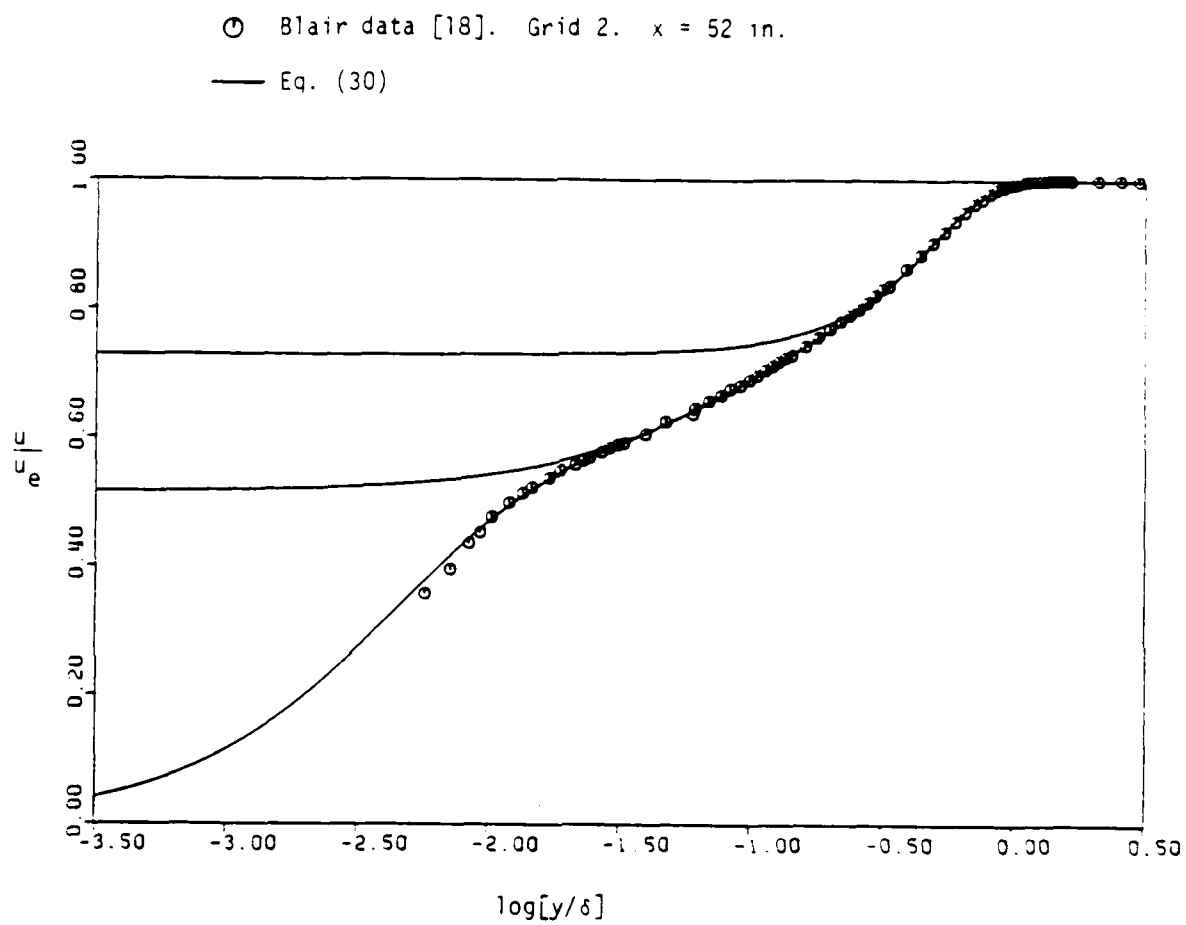


Figure 18: Velocity profile at  $x = 52$  in. Grid 2.

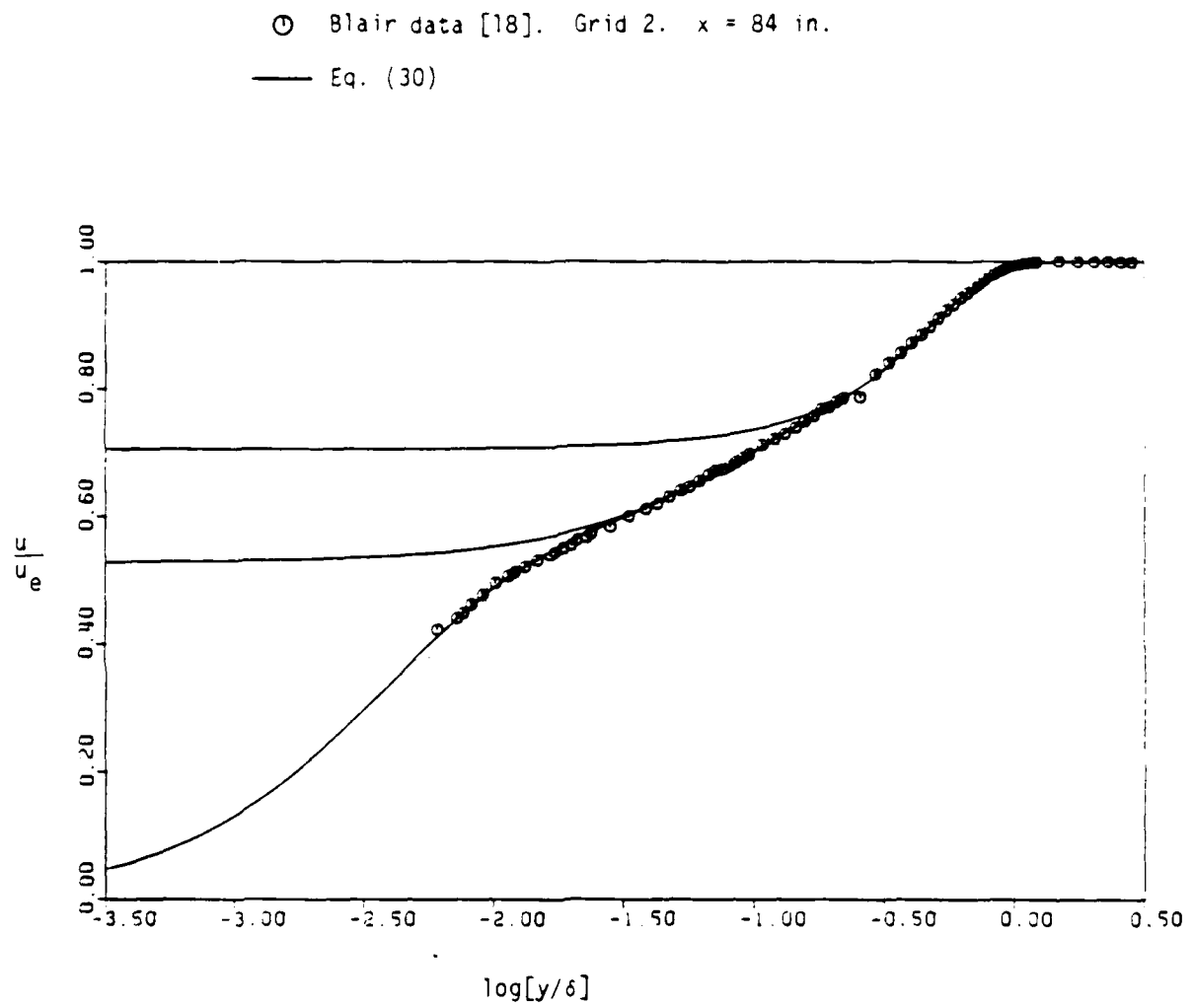


Figure 19: Velocity profile at  $x = 84$  in. Grid 2.

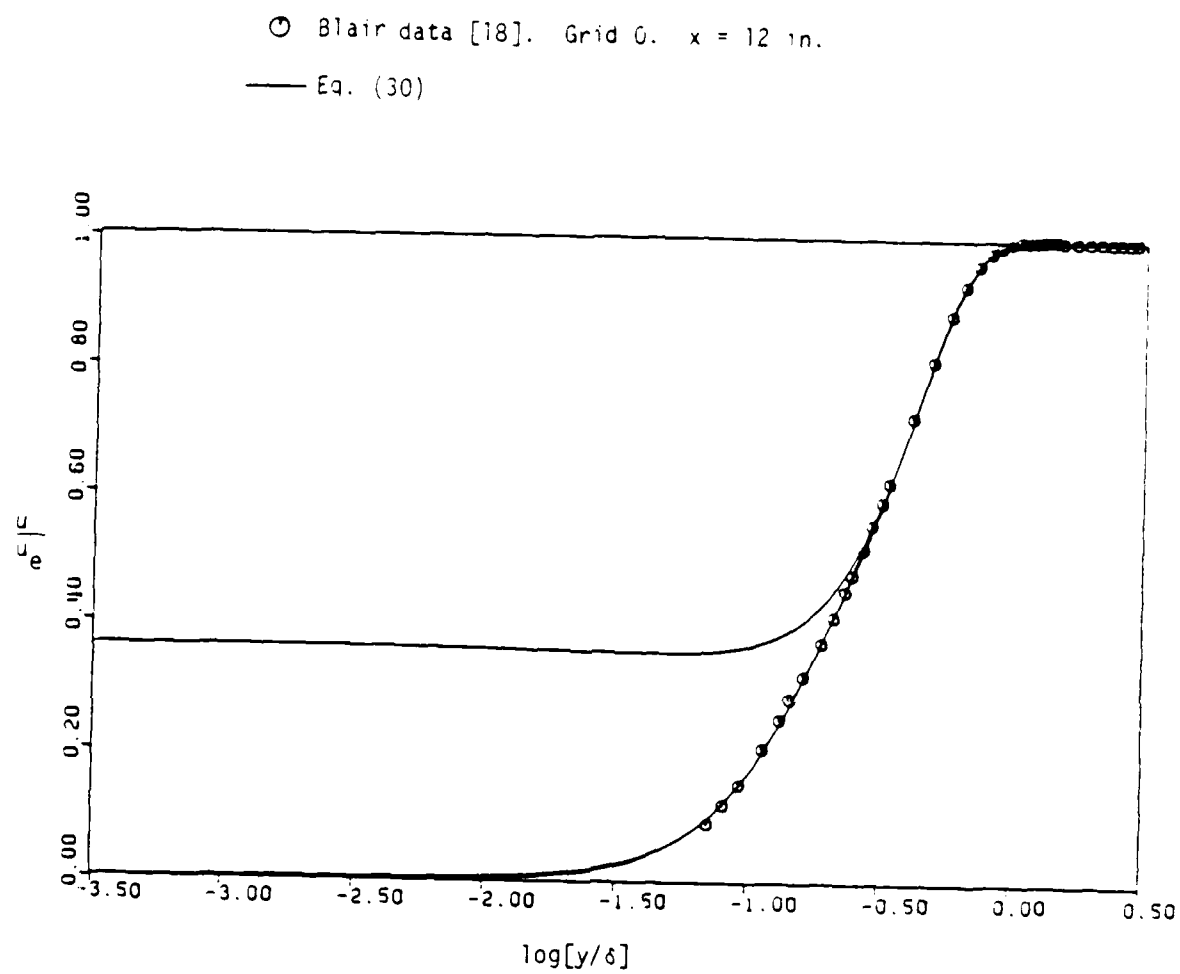


Figure 20: Velocity profile at  $x = 12$  in. Grid 0.

○ Blair Data [18]. Grid 0.  $x = 36$  in.

— Eq. (30)

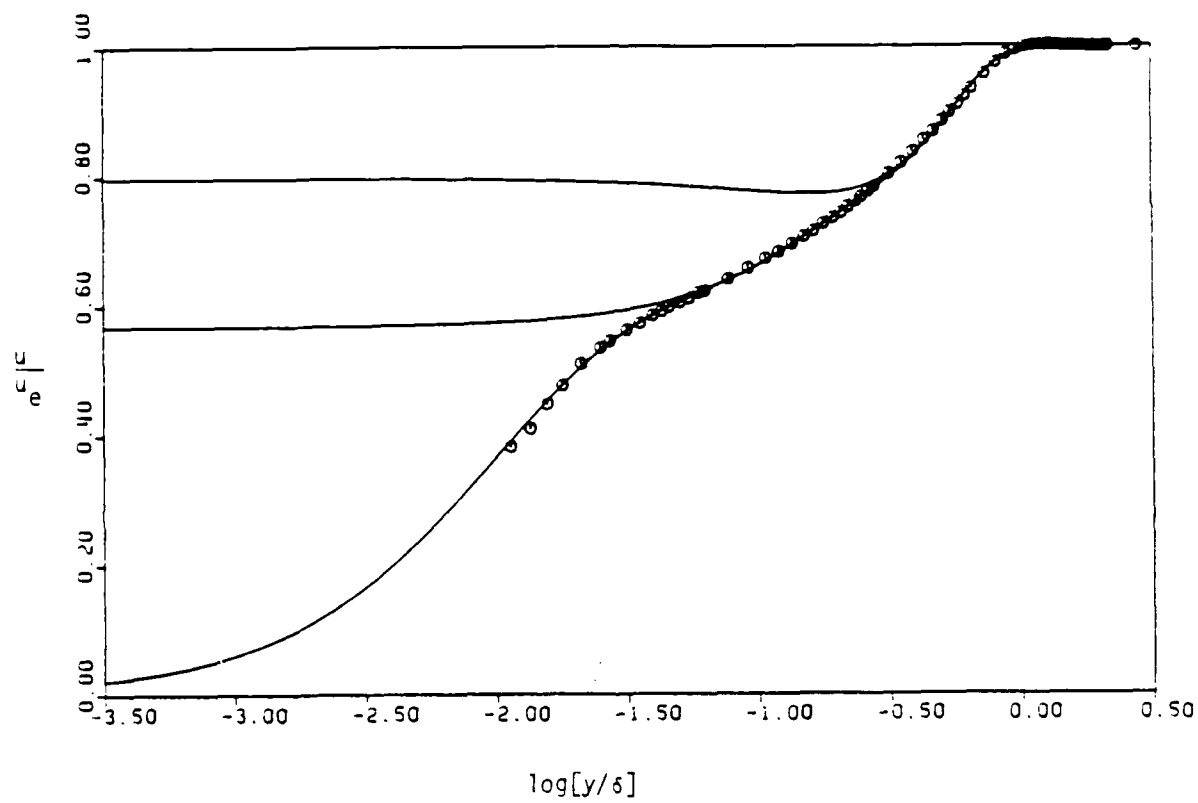


Figure 21: Velocity profile at  $x = 36$  in. Grid 0.



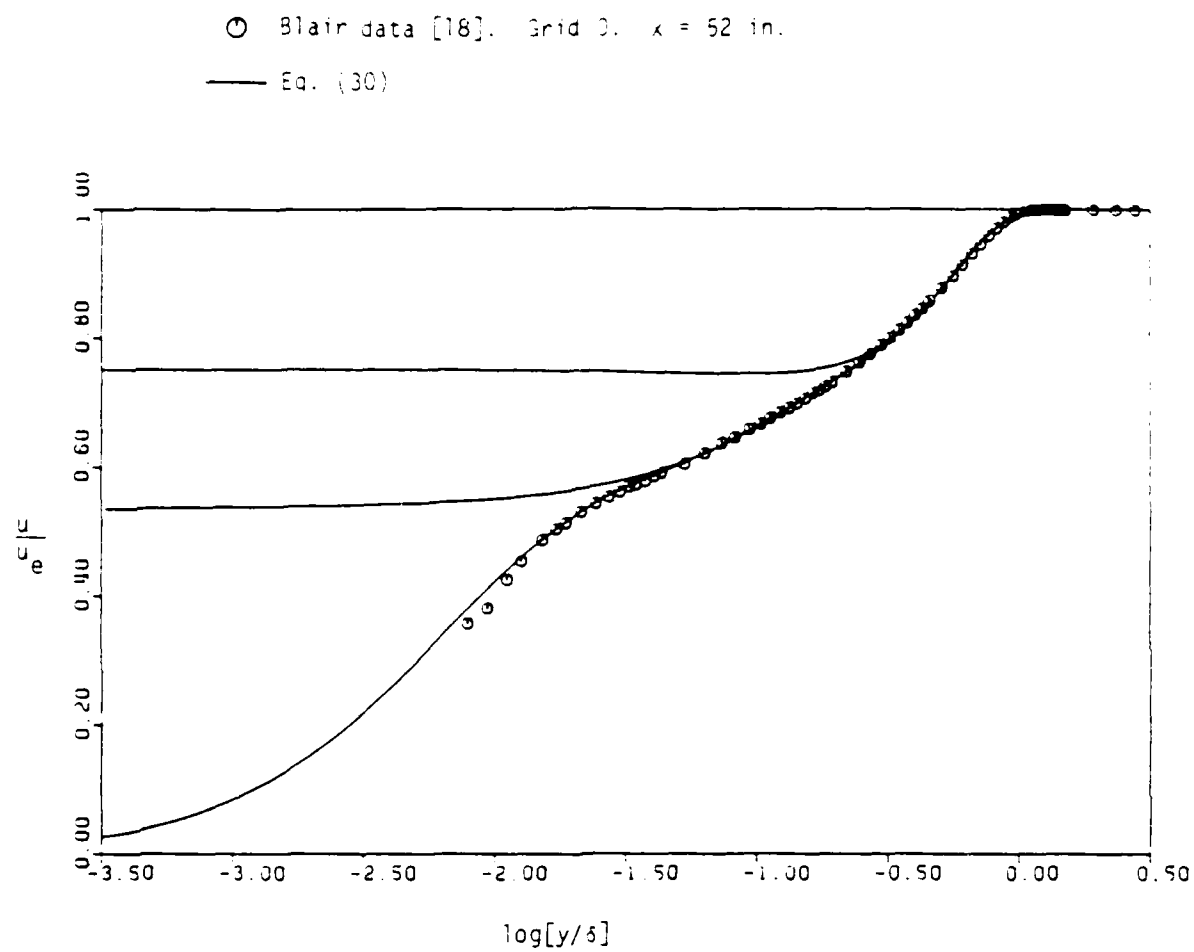


Figure 22: Velocity profile at  $x = 52$  in. Grid 0.

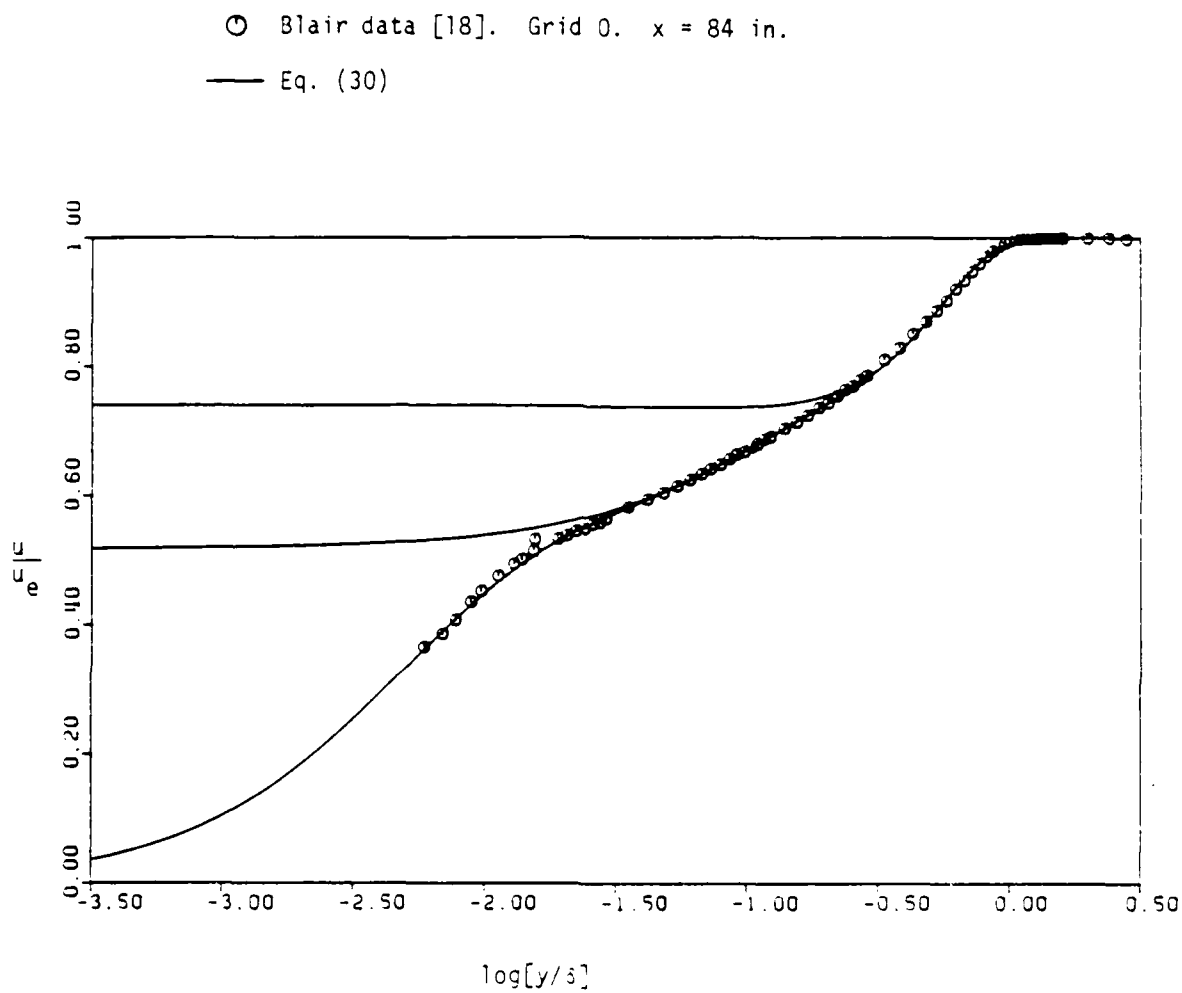


Figure 23: Velocity profile at  $x = 84$  in. Grid 0.

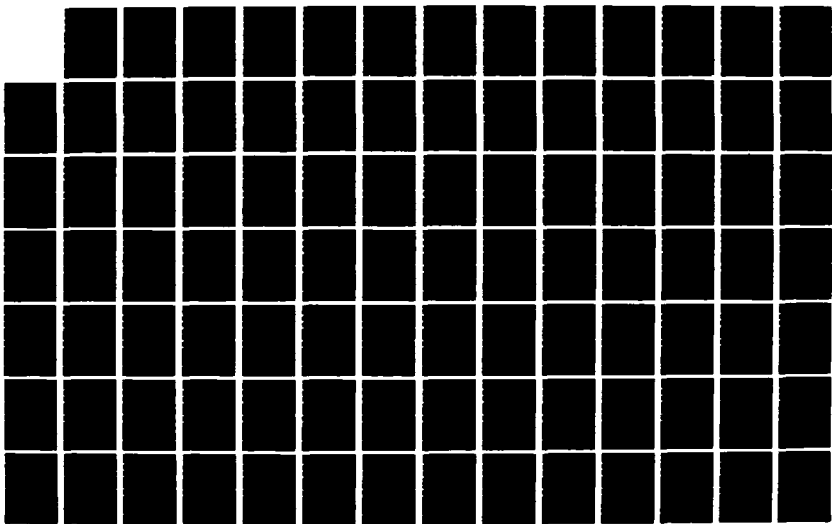
AD-A186 498

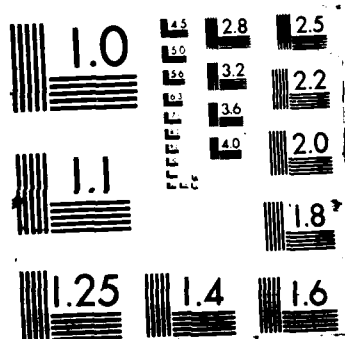
UNITED STATES AIR FORCE RESEARCH INITIATION PROGRAM  
1984 RESEARCH REPORTS (U) SOUTHEASTERN CENTER FOR  
ELECTRICAL ENGINEERING EDUCATION INC S W D PEELE  
MAY 86 AFOSR-TR-87-1721 F49620-82-C-0035 F/G 15/1

07/11

UNCLASSIFIED

NL





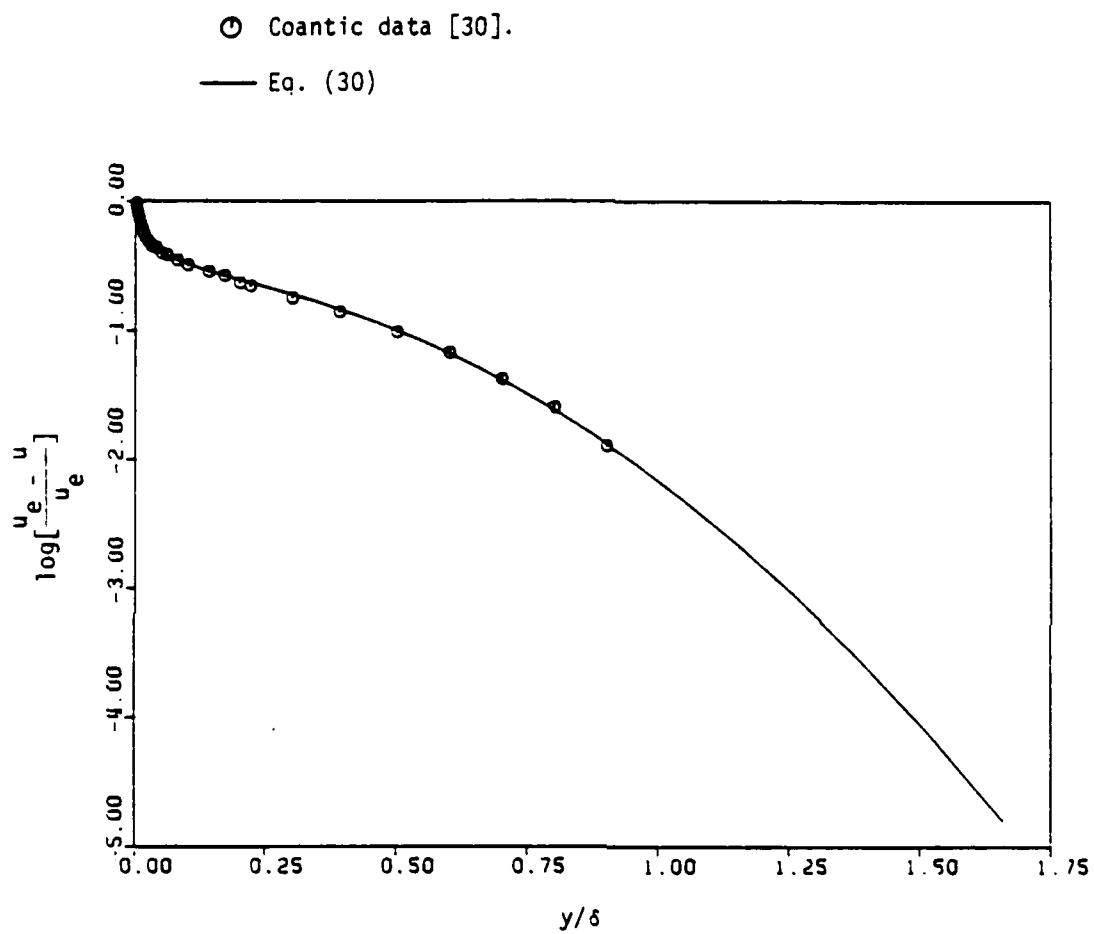


Figure 24: Wake region comparison of velocity defect with Eq. (30).  
Coantic data.

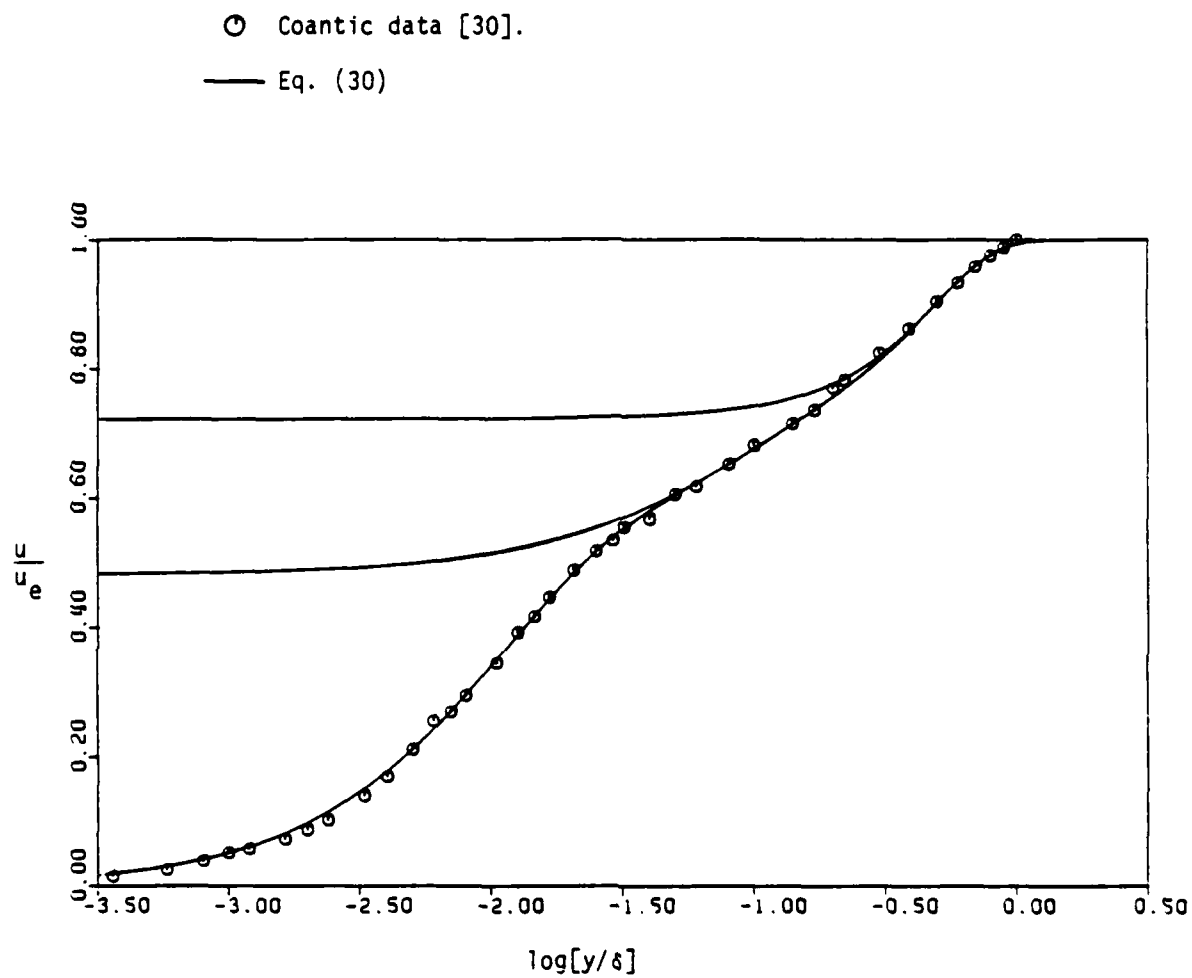


Figure 25: Wall region comparison of Coantic data with Eq. (30).

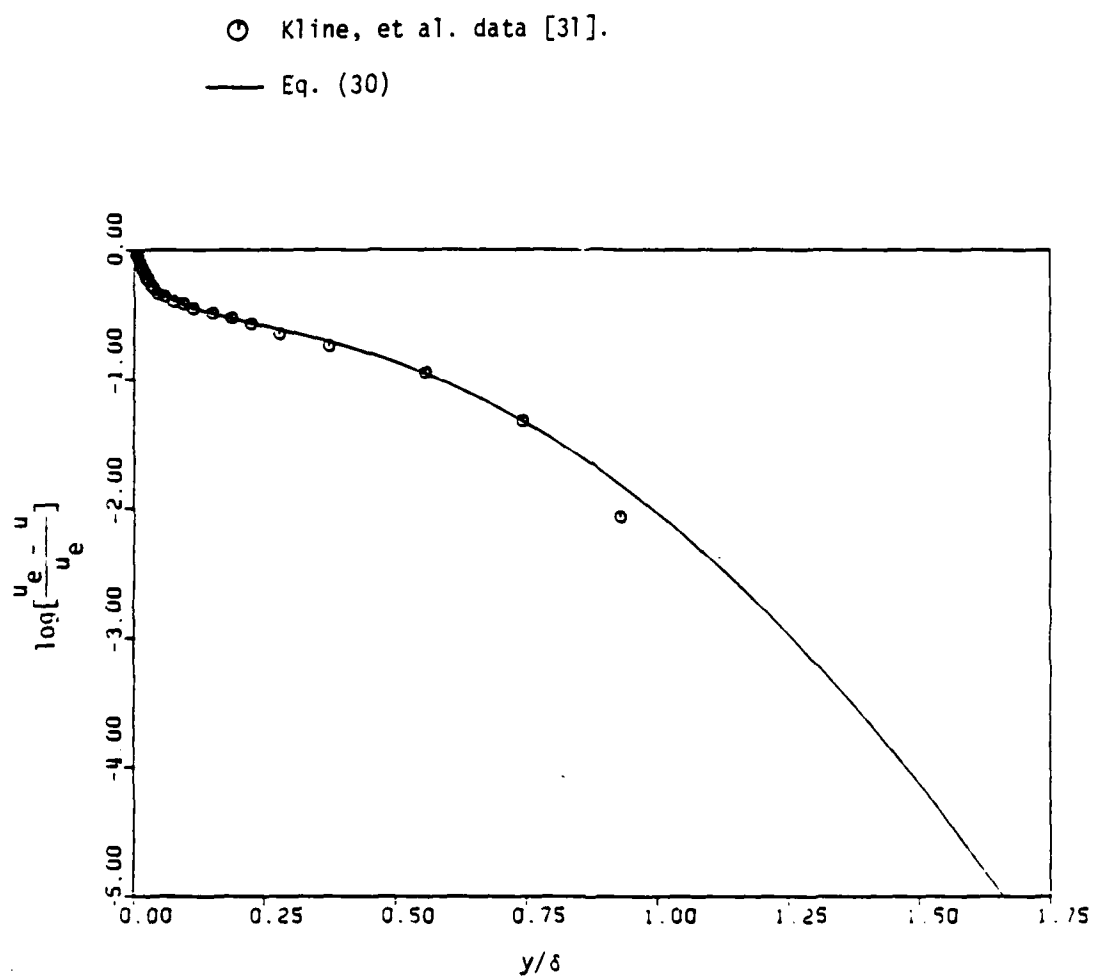


Figure 26: Wake region comparison of velocity defect with Eq. (30).  
Kline, et al. data.

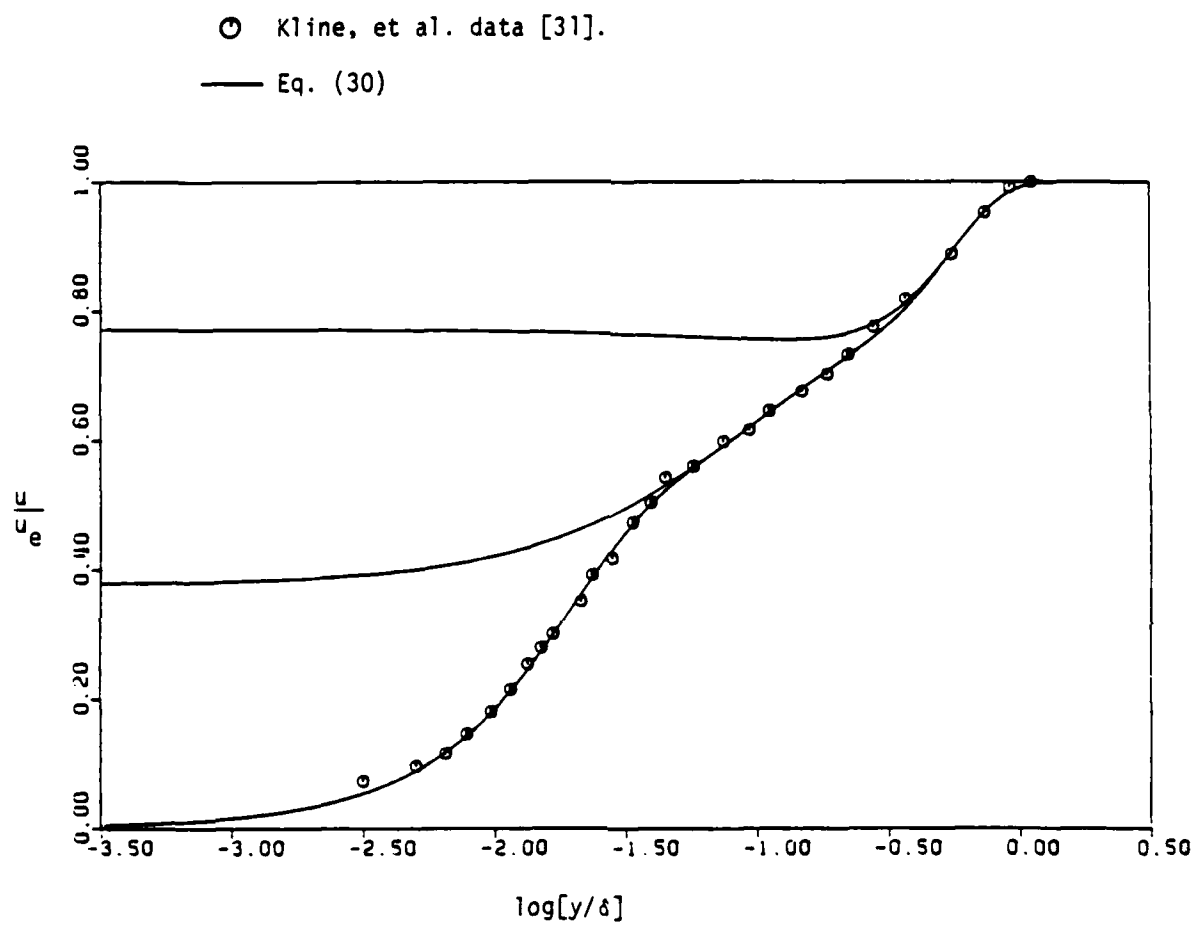


Figure 27: Wall region comparison of Kline, et al data with Eq. (30)



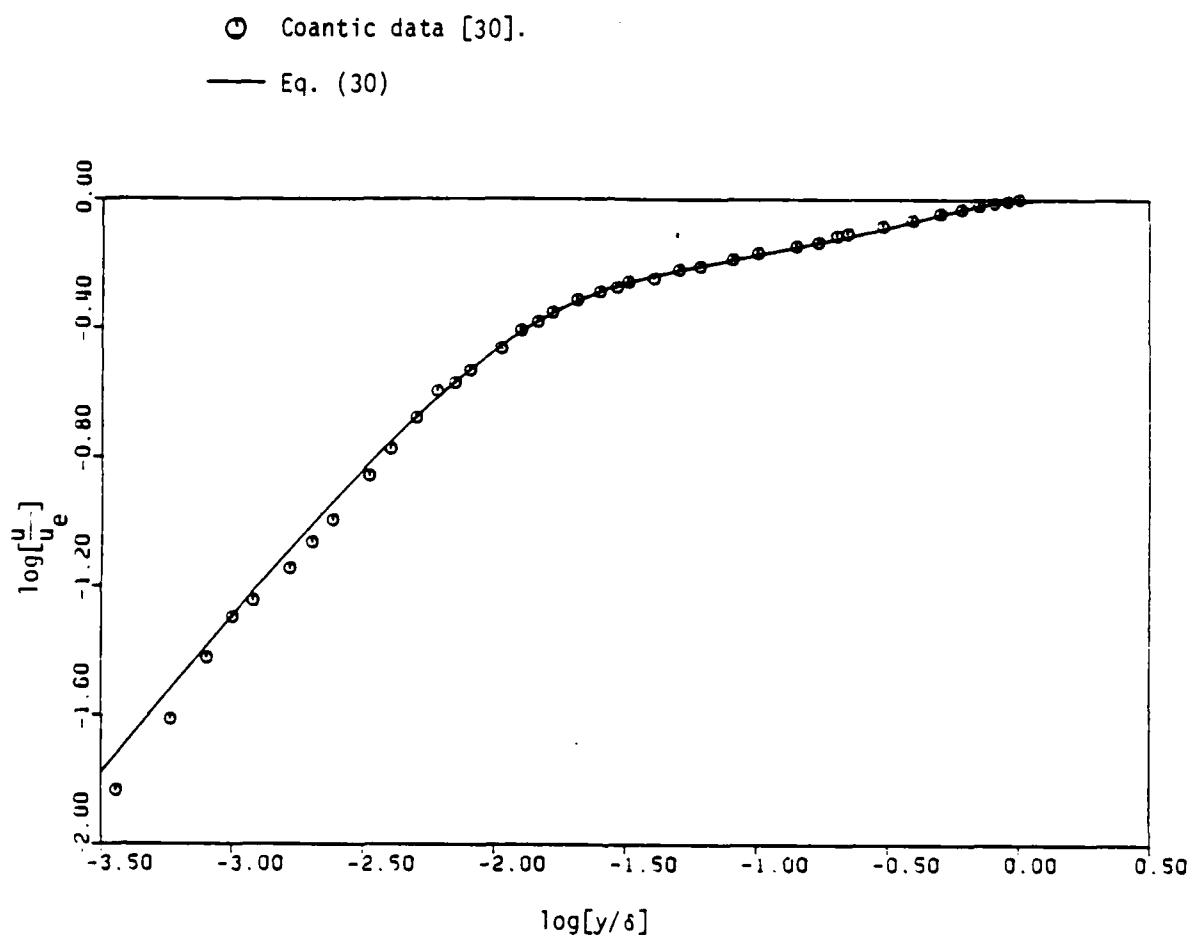


Figure 28: Logarithmic comparison of Coantic data with Eq. (30).

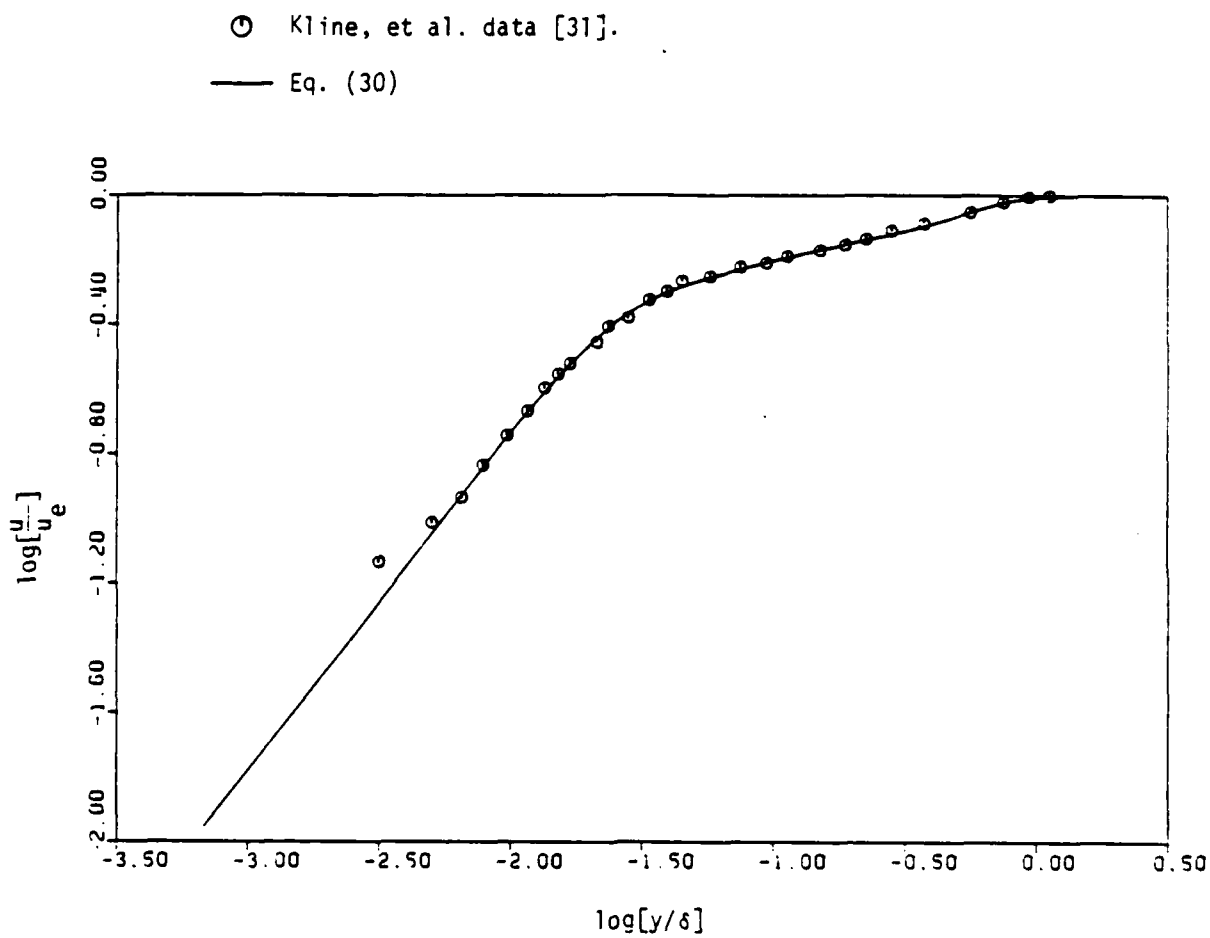


Figure 29: Logarithmic comparison of Kline, et al. data with Eq. (30).

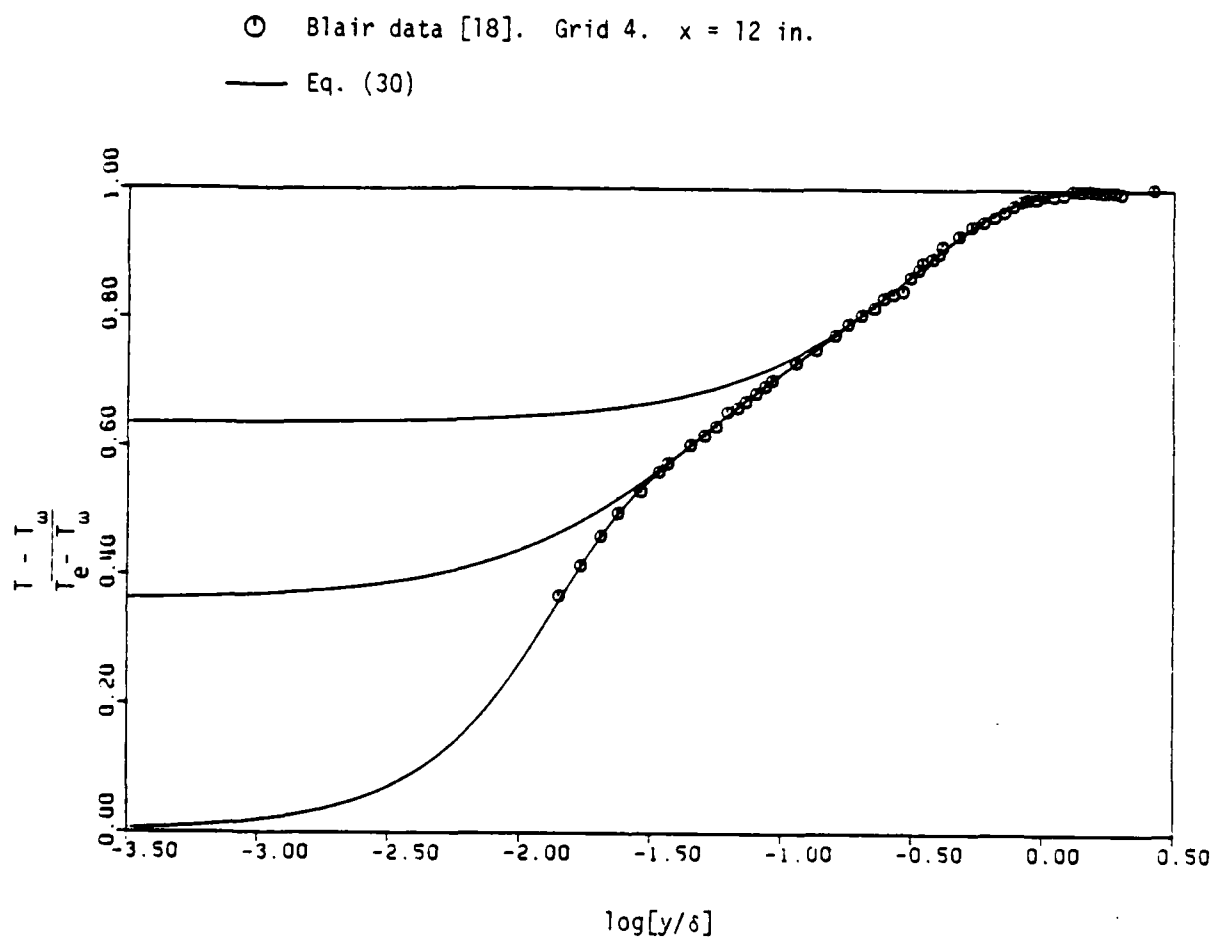


Figure 30: Temperature profile at  $x = 12$  in. Grid 4.

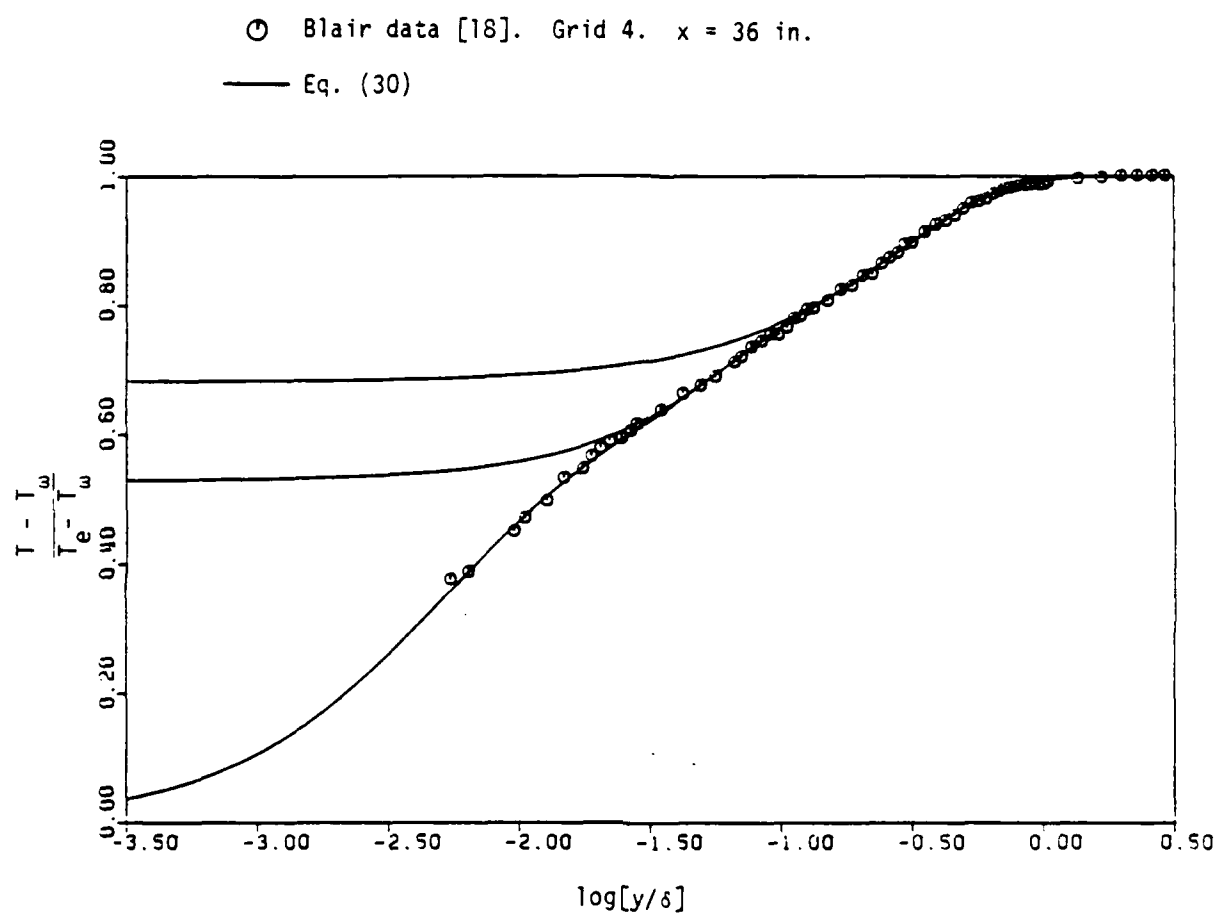


Figure 31: Temperature profile at  $x = 36$  in. Grid 4.

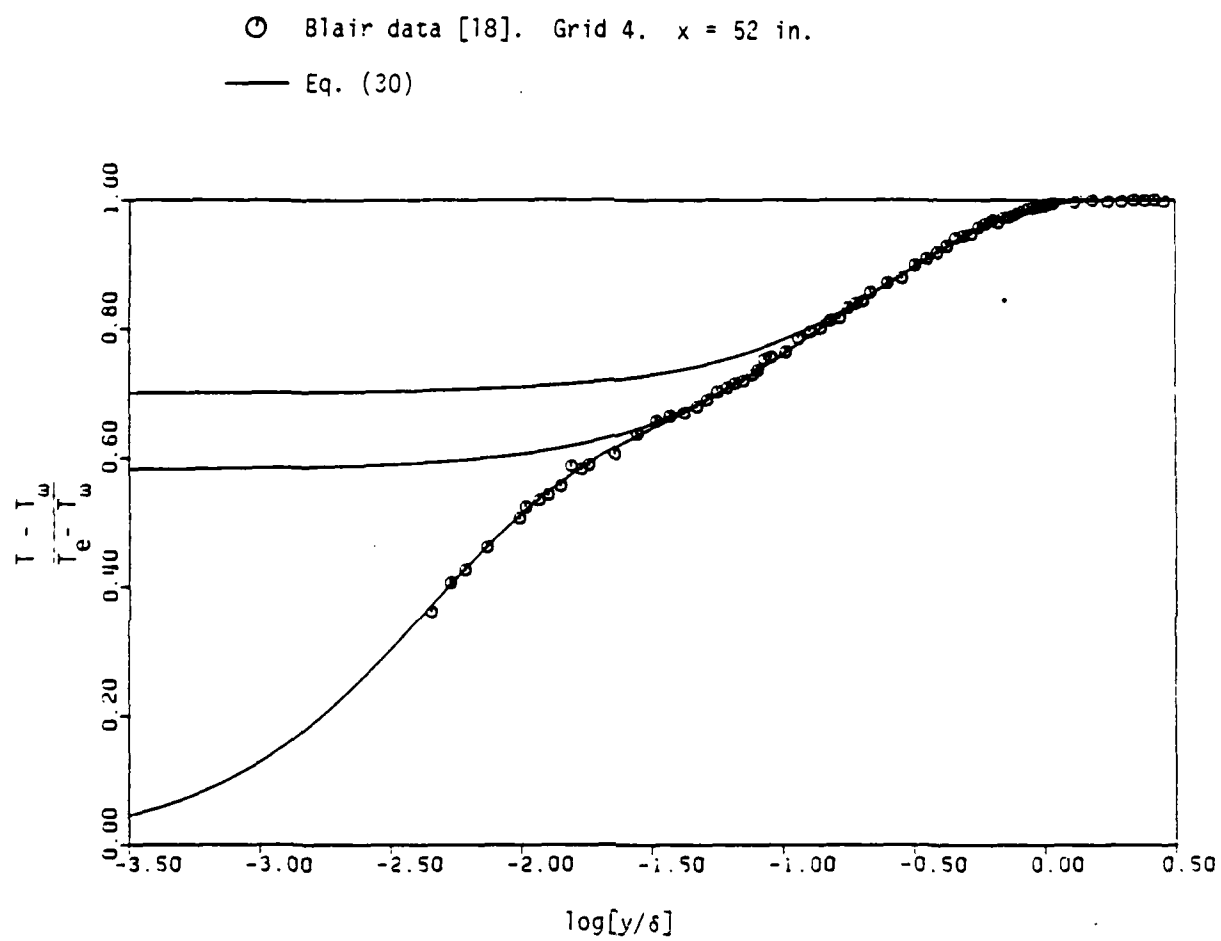


Figure 32: Temperature profile at  $x = 52$  in. Grid 4.

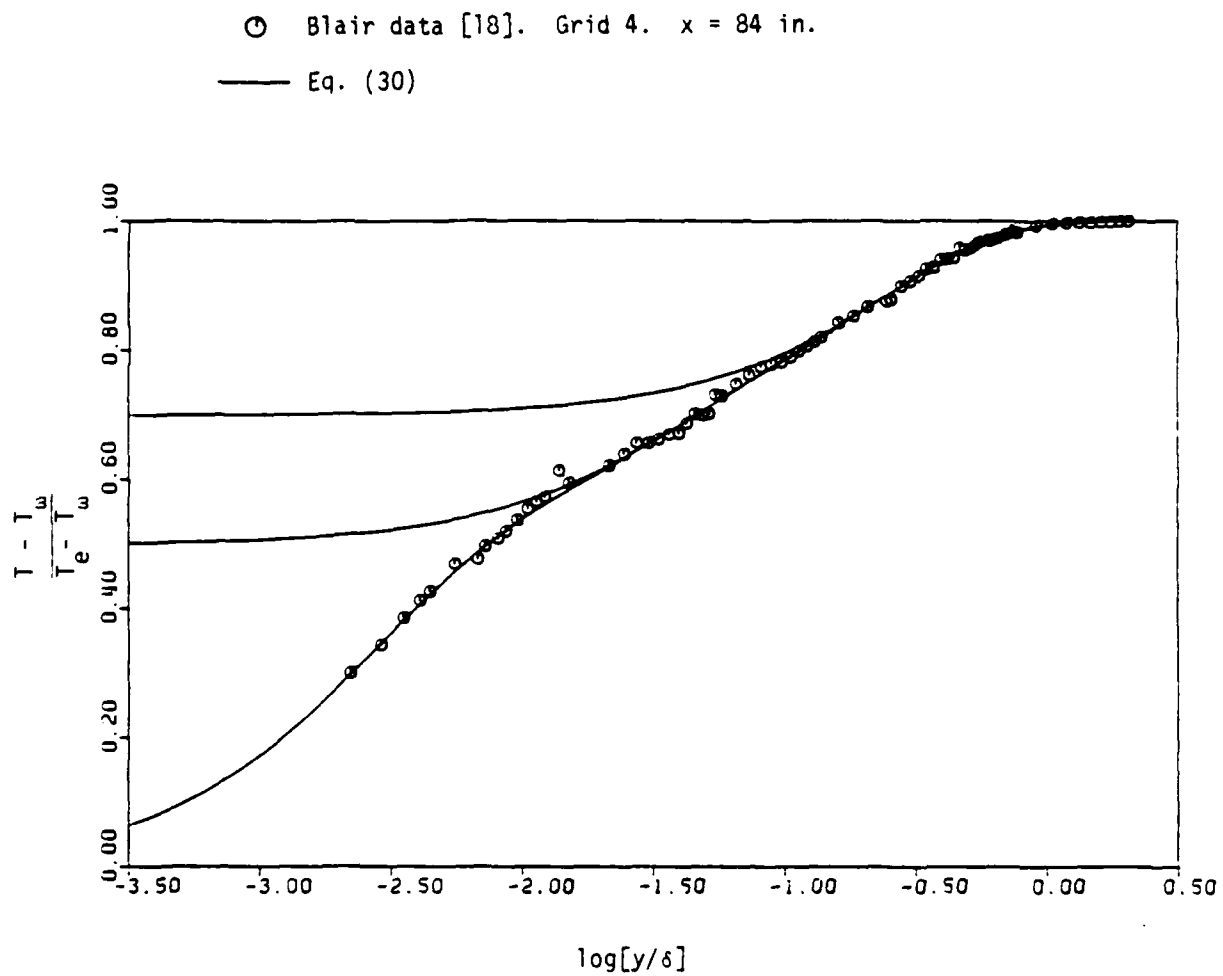


Figure 33: Temperature profile at  $x = 84$  in. Grid 4.

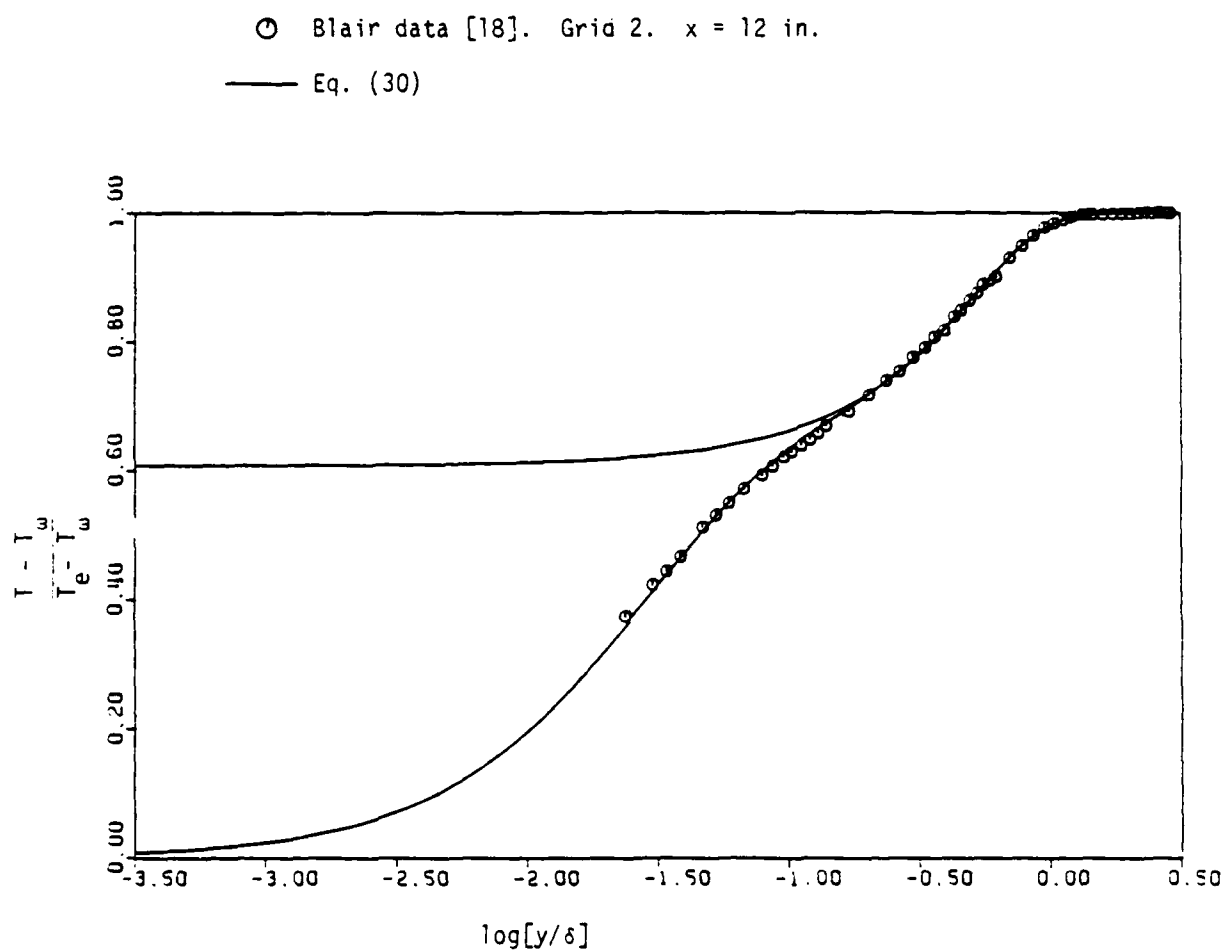


Figure 34: Temperature profile at  $x = 12$  in. Grid 2.

⊙ Blair data [18]. Grid 2.  $x = 36$  in.

— Eq. (30)

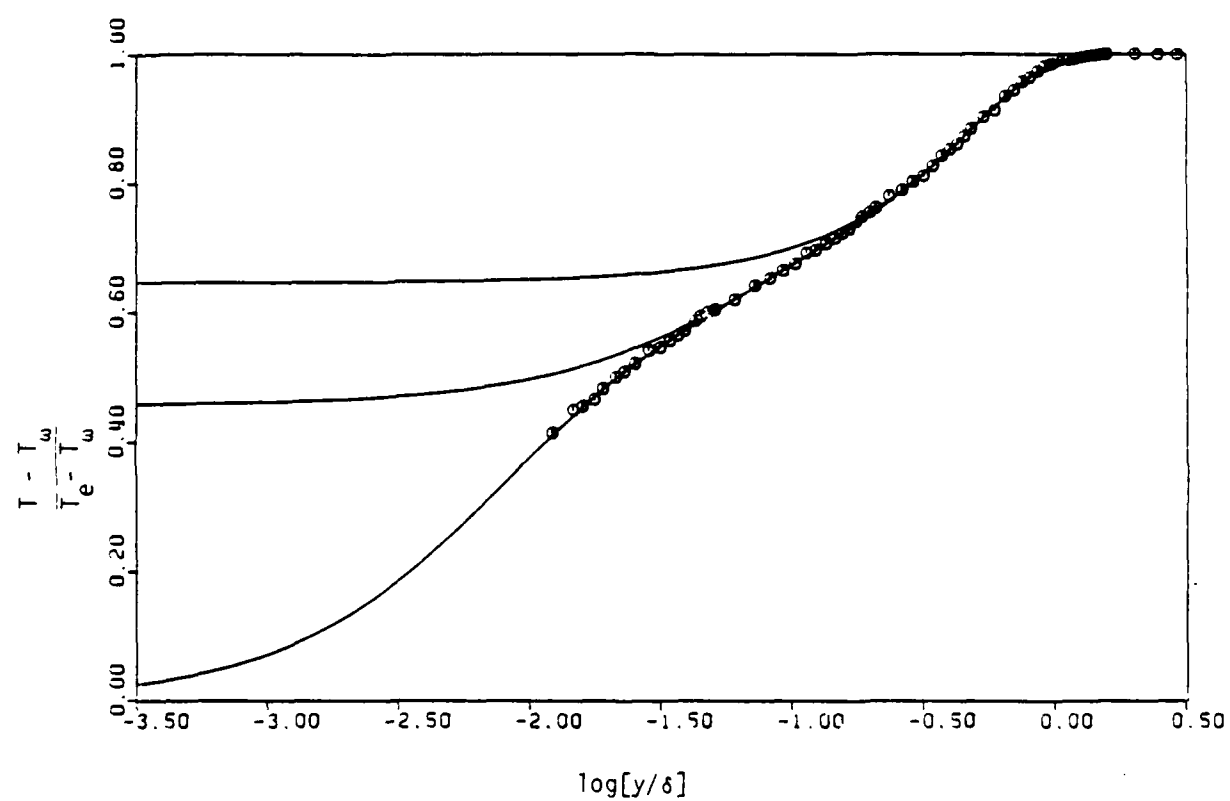


Figure 35: Temperature profile at  $x = 36$  in. Grid 2.



○ Blair data [18]. Grid 2.  $x = 52$  in.

— Eq. (30).

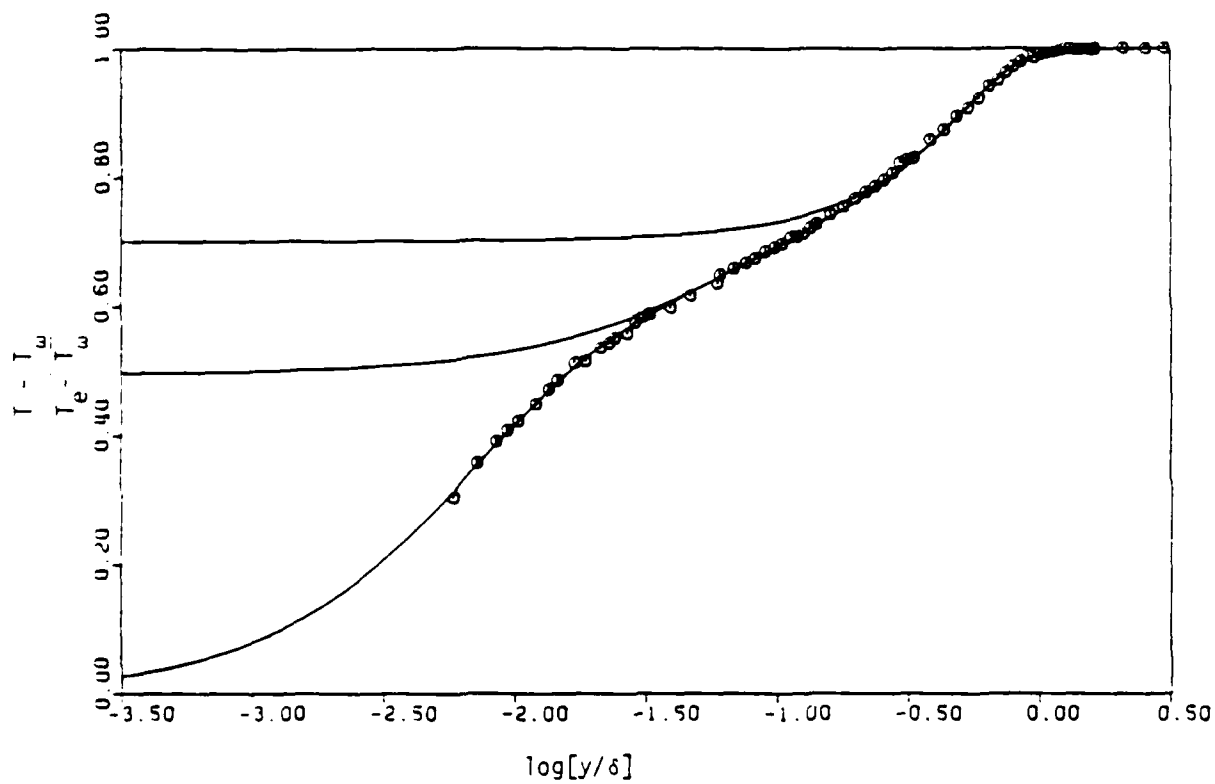


Figure 36: Temperature profile at  $x = 52$  in. Grid 2.

○ Blair data [18]. Grid 2.  $x = 84$  in.  
 — Eq. (30)

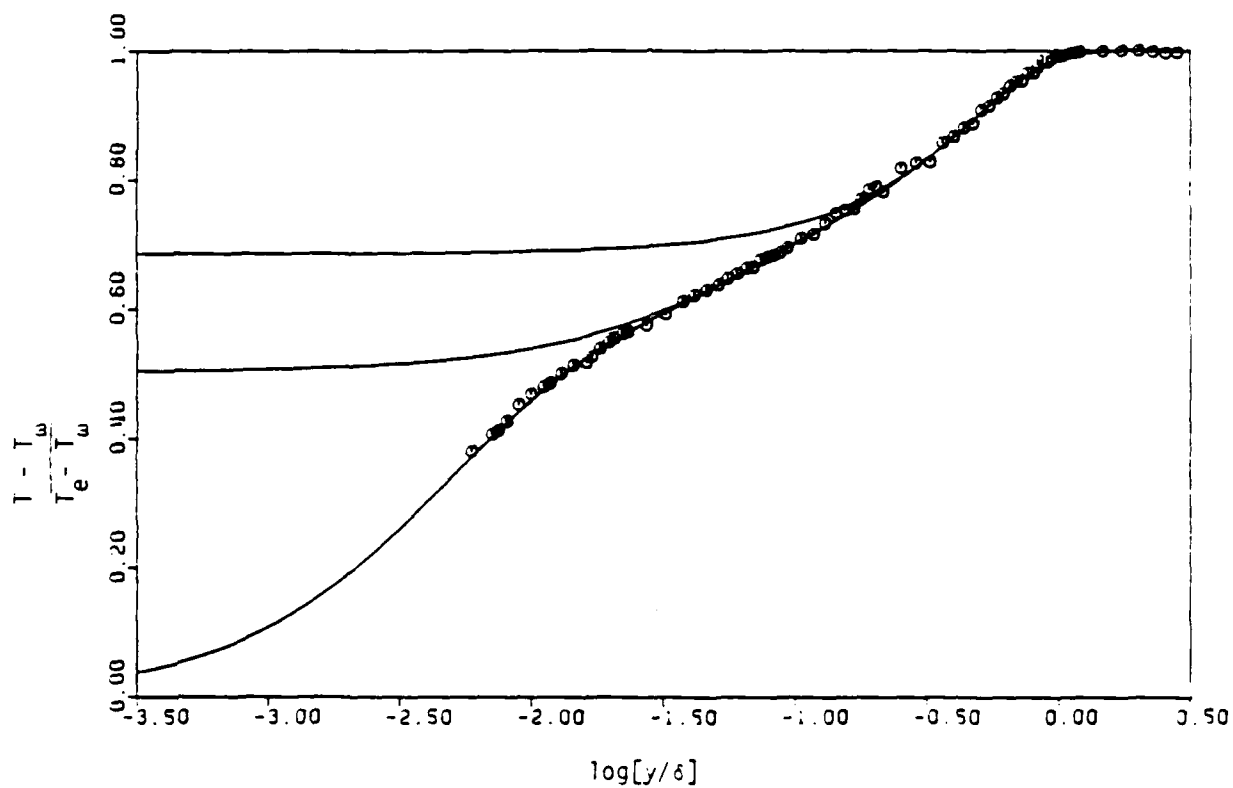


Figure 37: Temperature profile at  $x = 84$  in. Grid 2.

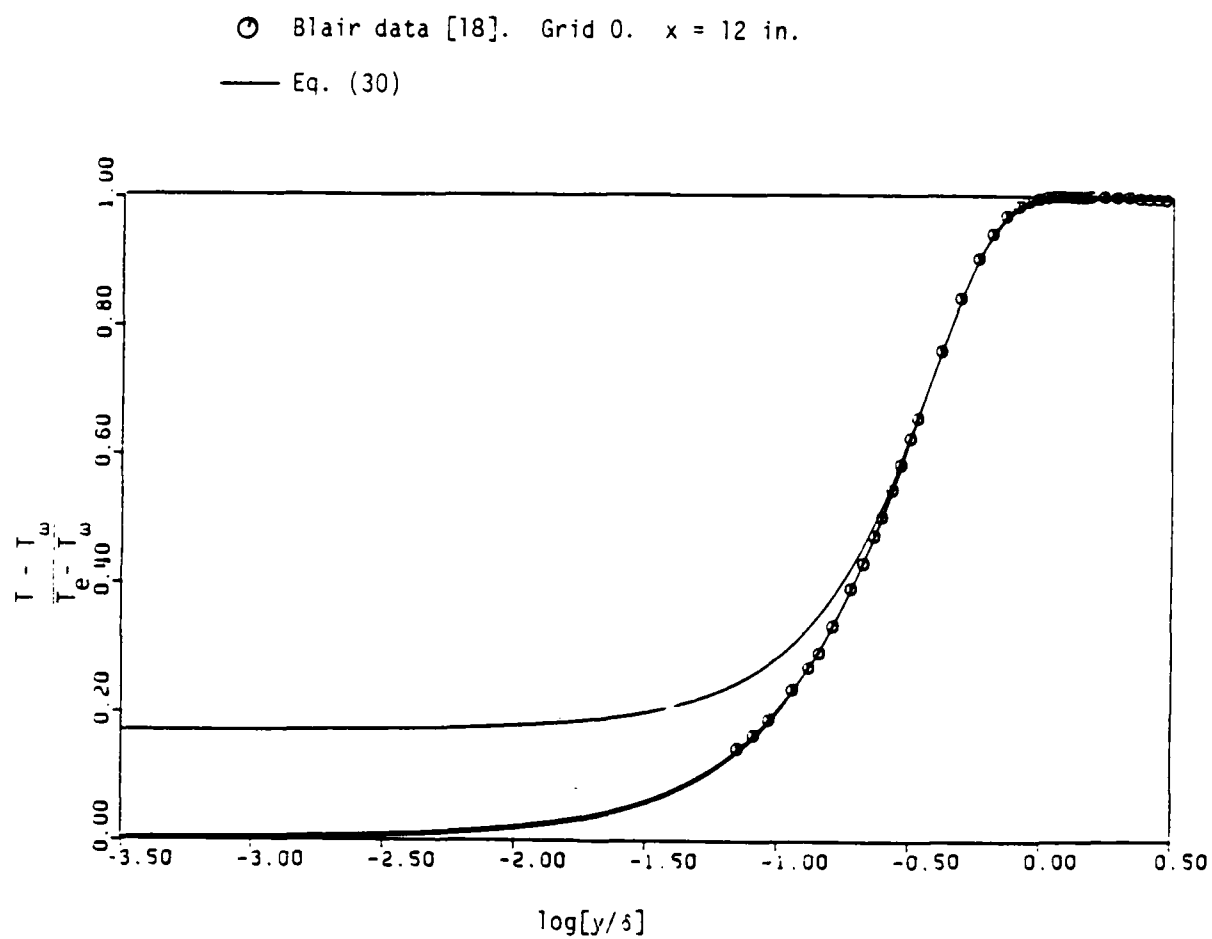


Figure 38: Temperature profile at  $x = 12$  in. Grid 0.

⊙ Blair data [18]. Grid 0.  $x = 36$  in.

— Eq. (30)

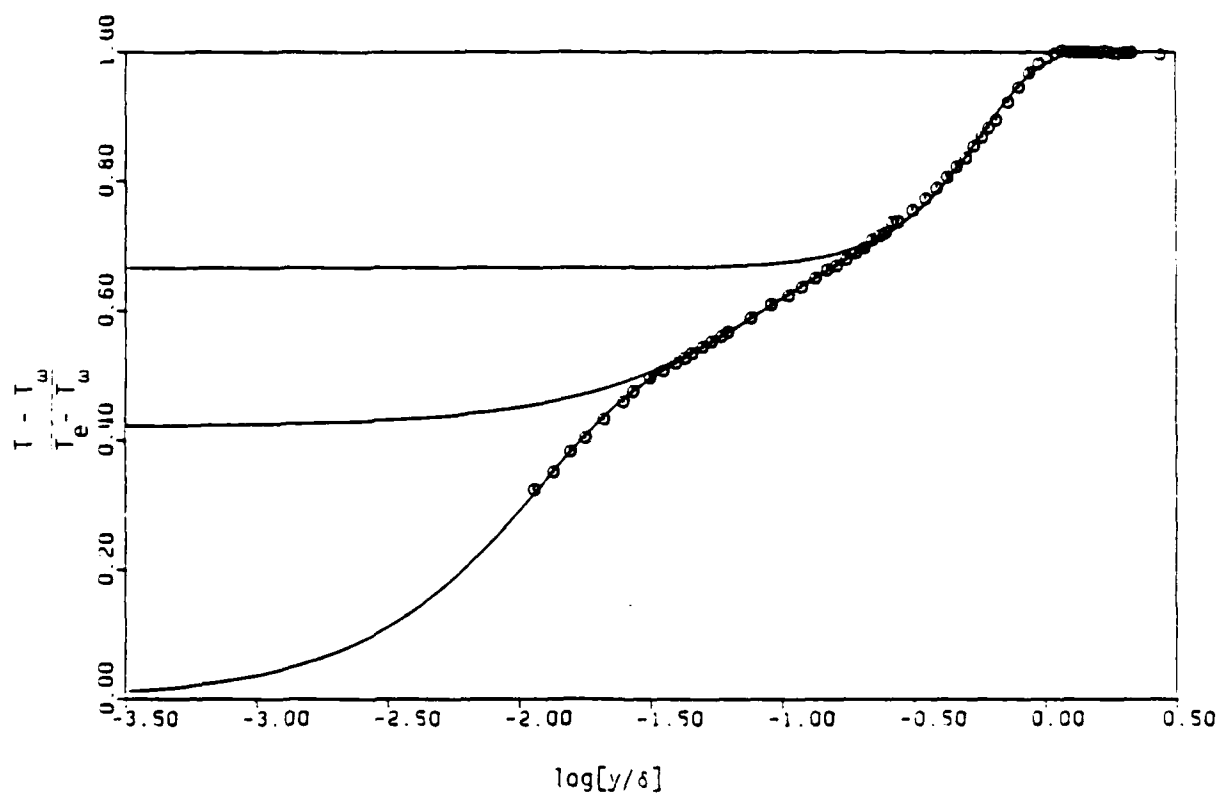


Figure 39: Temperature profile at  $x = 36$  in. Grid 0.

○ Blair data [18]. Grid 0.  $x = 52$  in.

— Eq. (30)

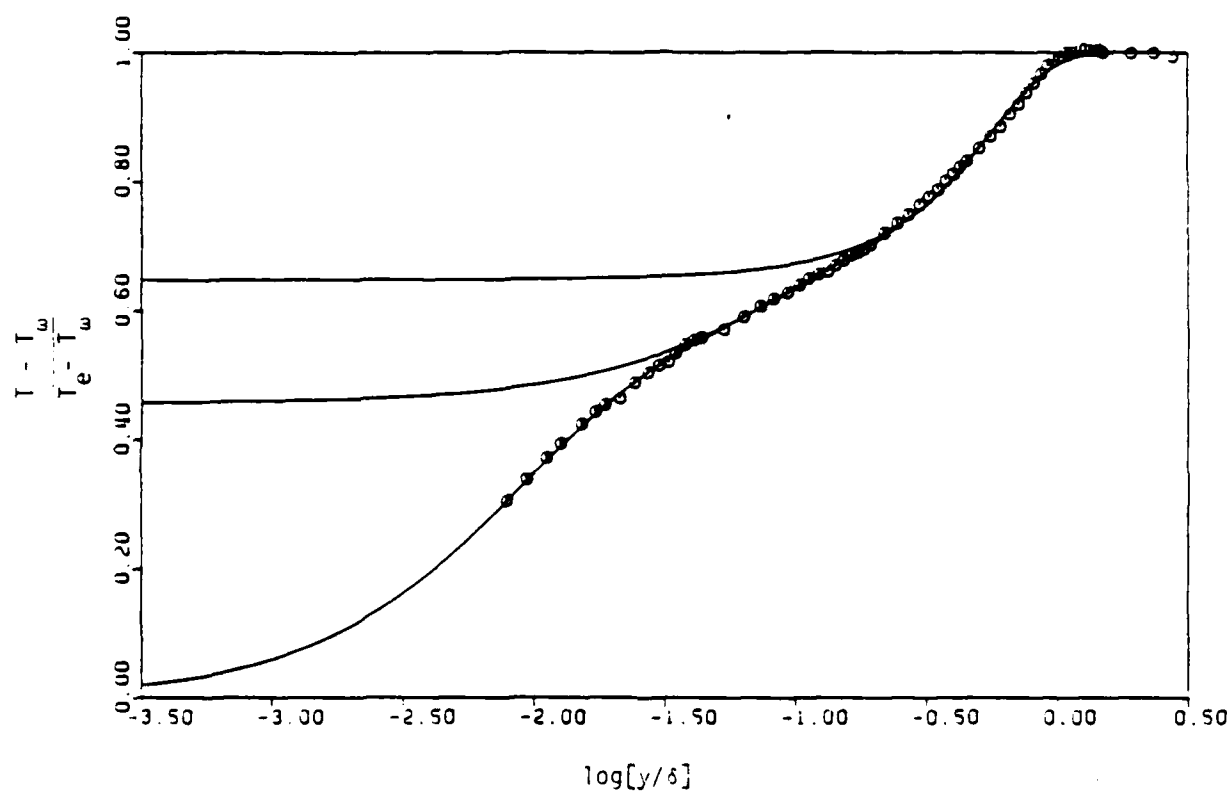


Figure 40: Temperature profile at  $x = 52$  in. Grid 0.

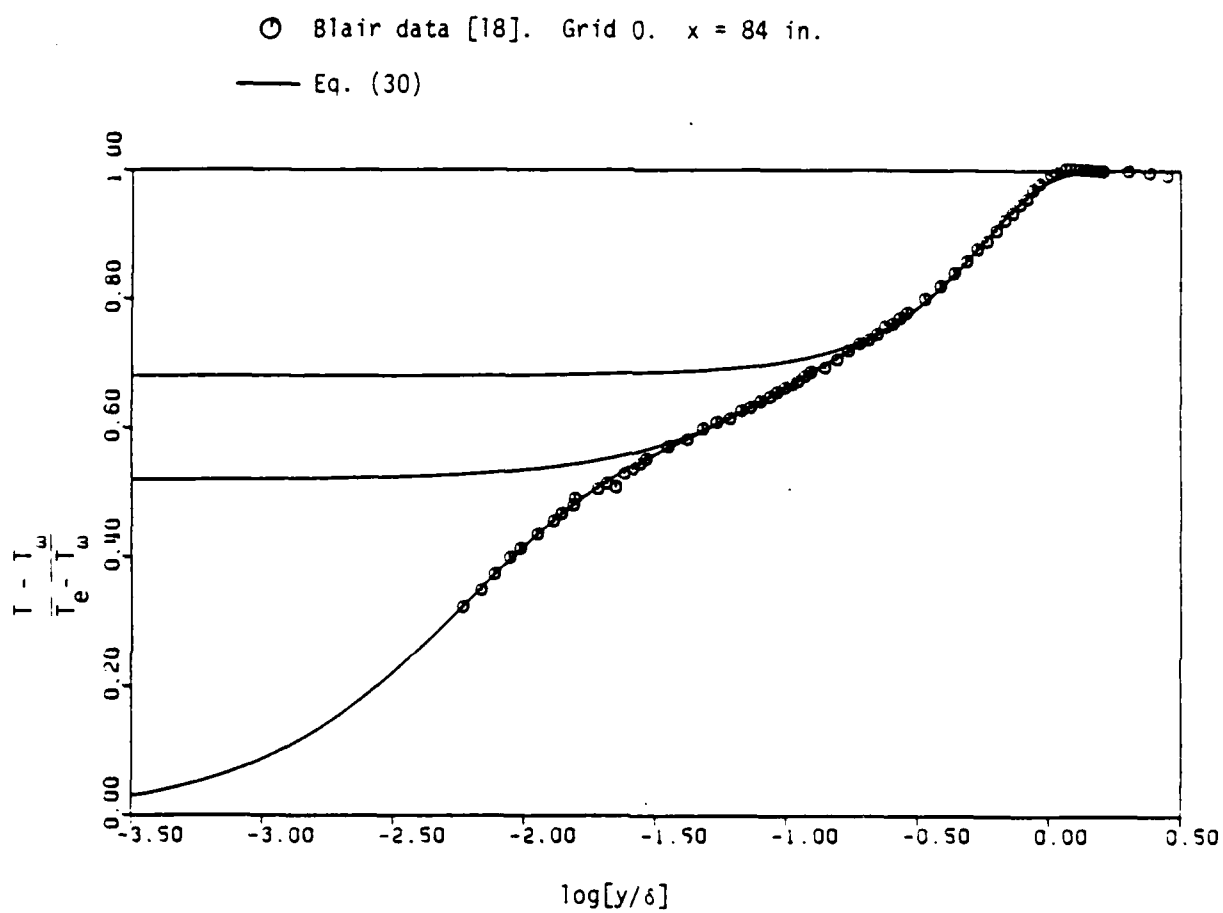


Figure 41: Temperature profile at  $x = 84$  in. Grid 0.

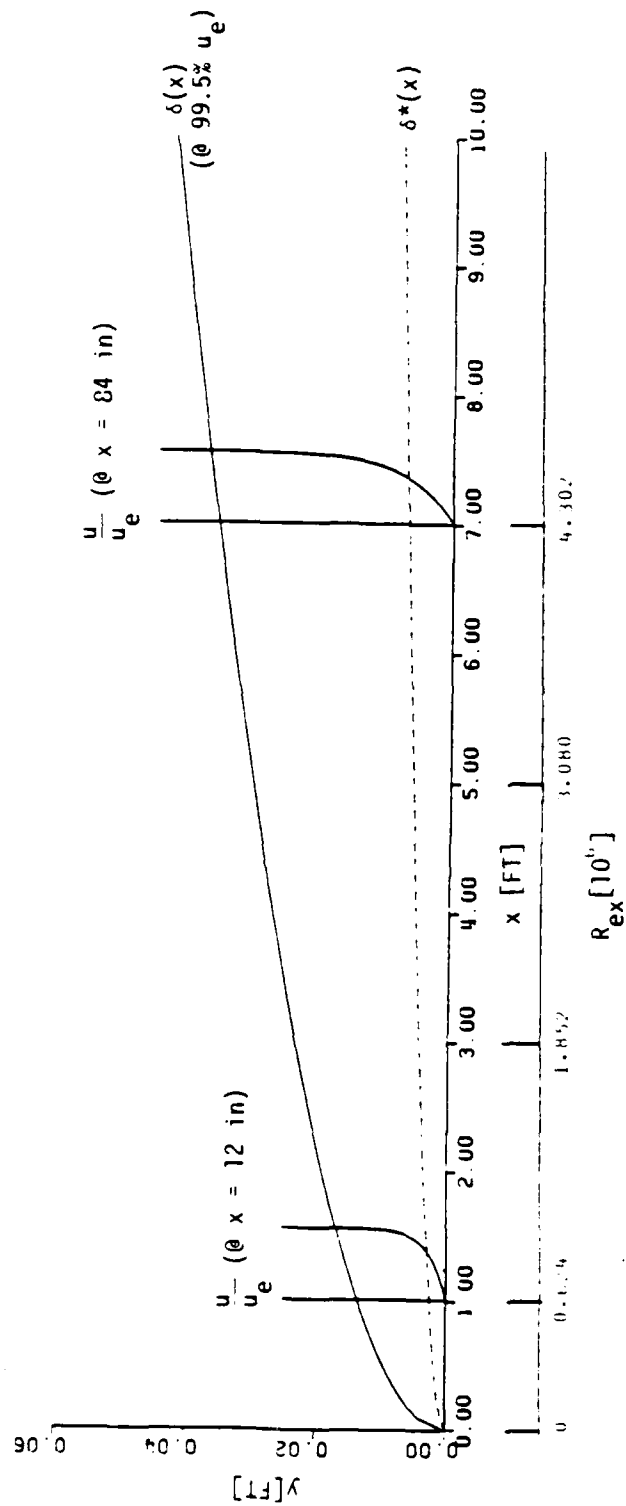


Figure 42: Analytical Test Case Corresponding to Blair's Experiment. See Eqs. (50)-(55).

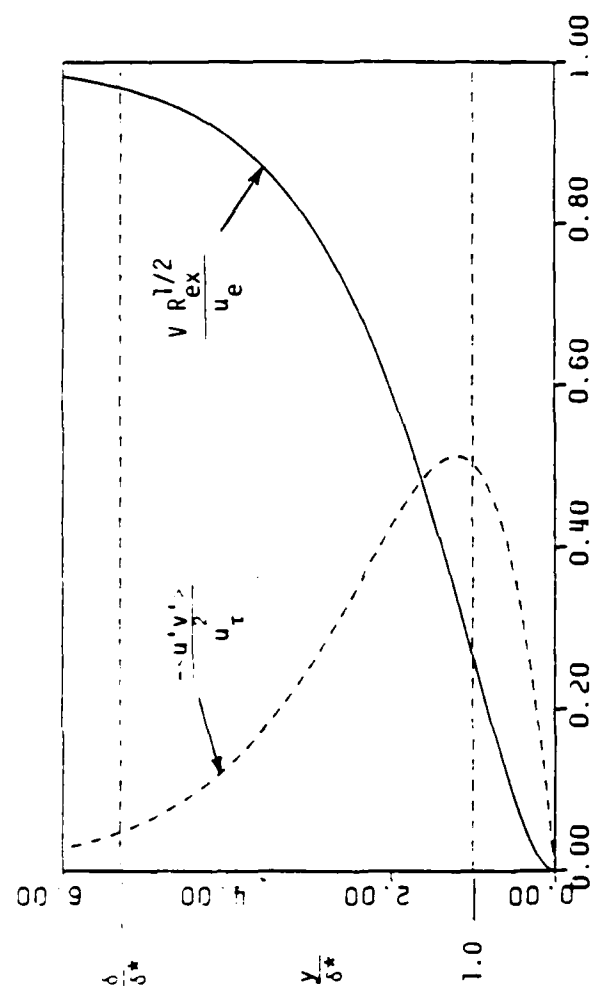


Figure 43: Analytical test case profiles for Reynolds stress and mean normal velocity component.



A = mean viscous dissipation [Eq. (56)]

B = turbulence production [Eq. (57)]

C = Reynolds stress [Eq. (53)]

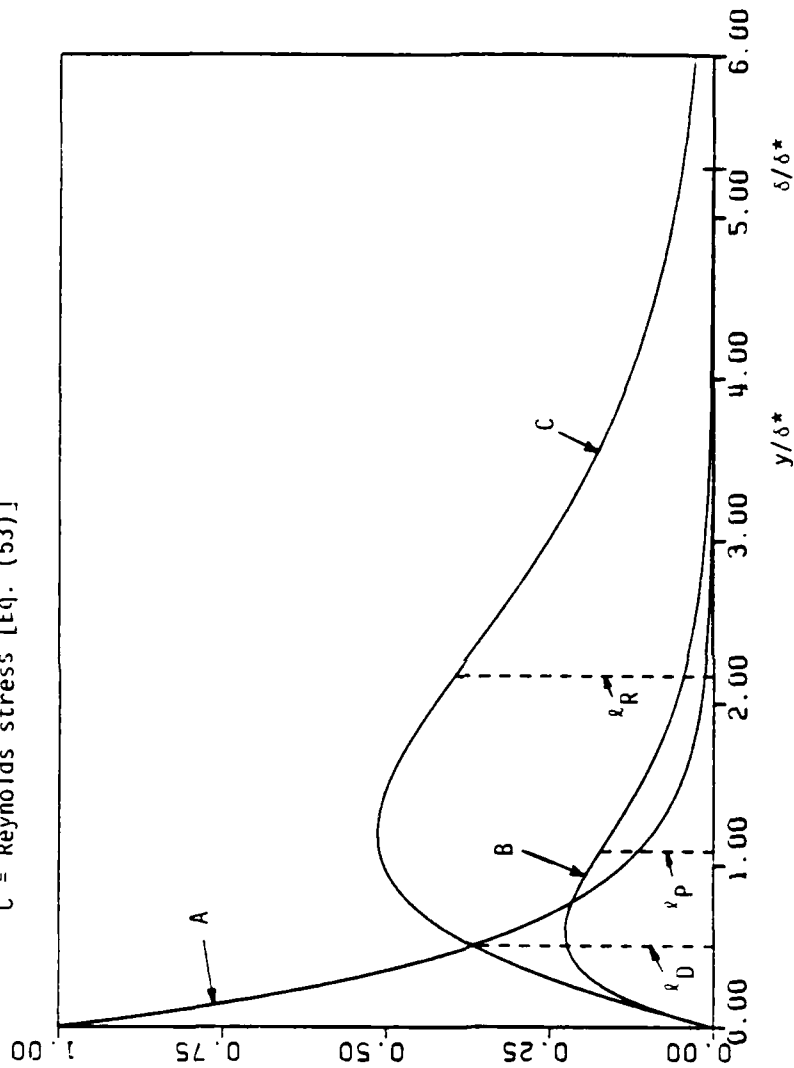


Figure 44: Turbulence related profiles of the analytical test case.

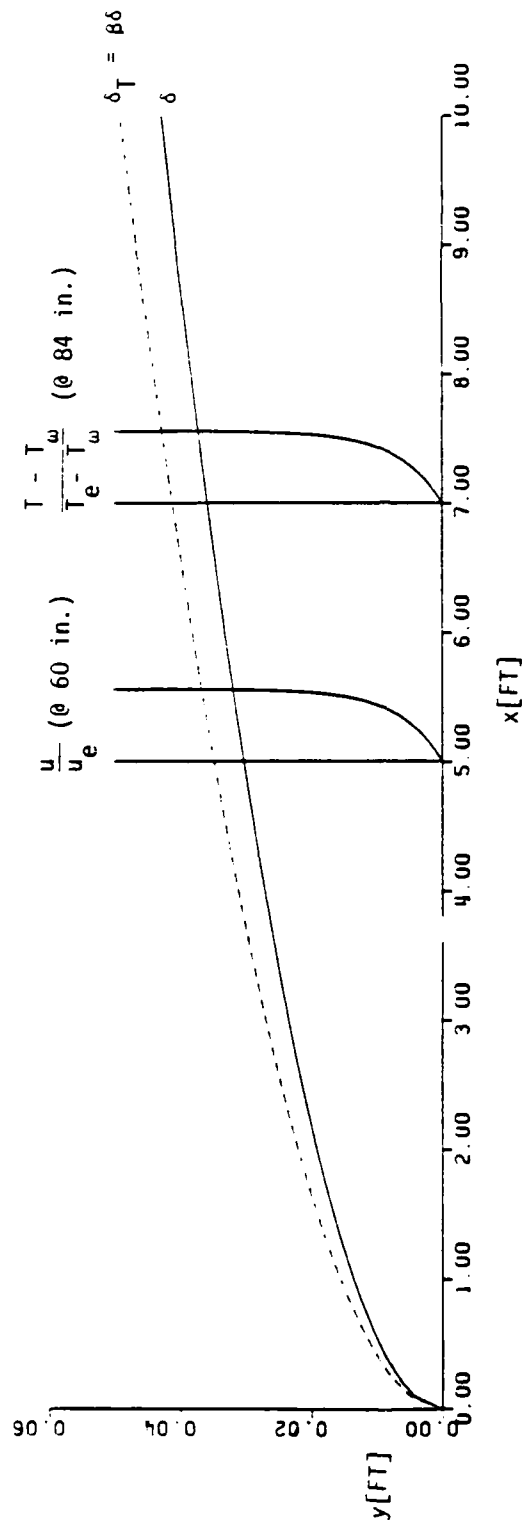


Figure 45: Comparison of thermal and velocity boundary layers for the analytical test case.  
(See Eqs. (50)-(65).)

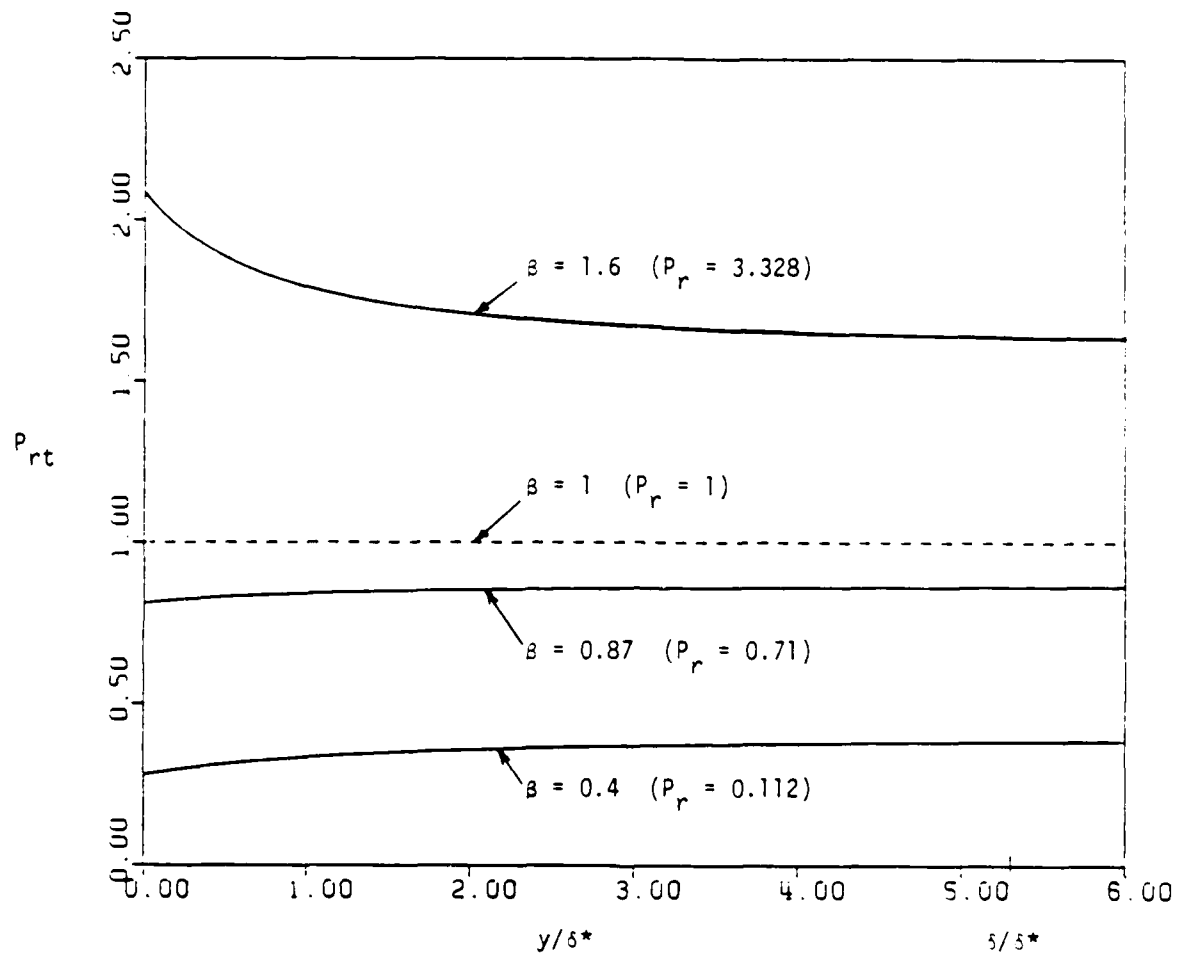


Figure 46: Turbulent Prandtl number for analytical test case. See Eq. (64).

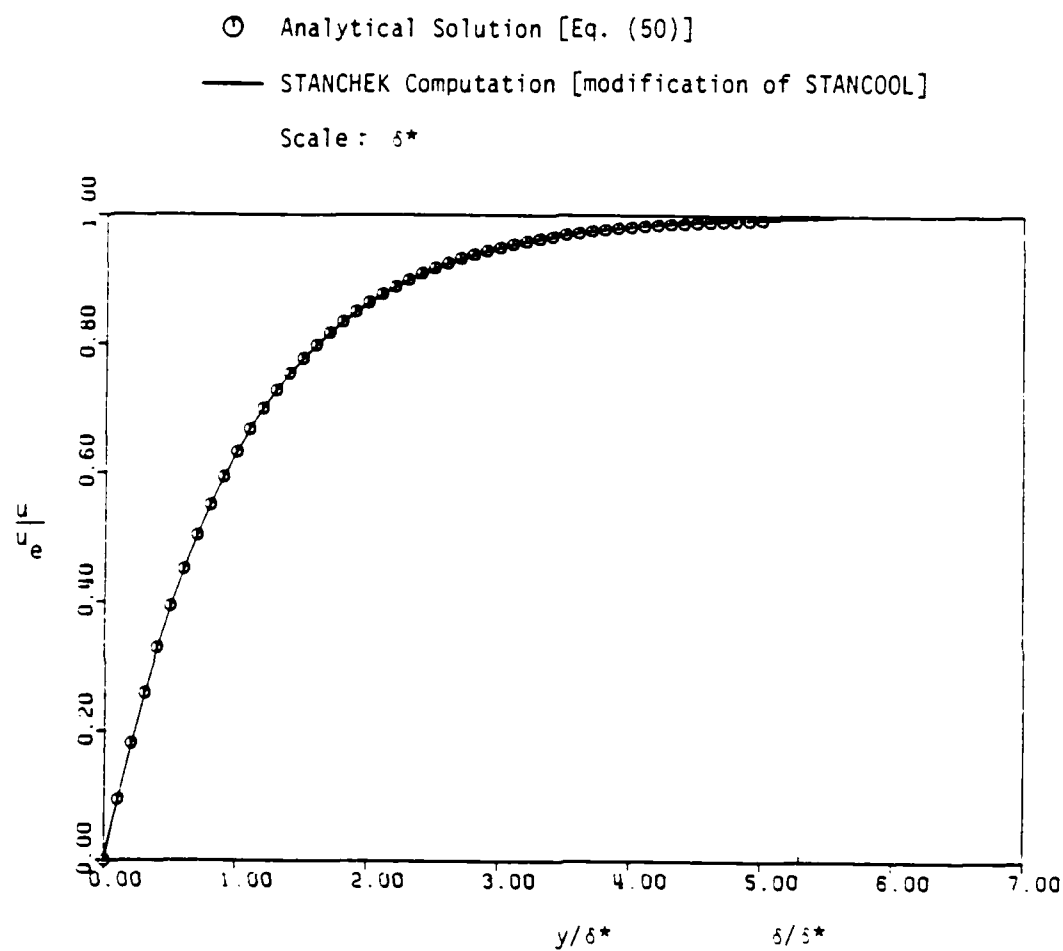


Figure 47: Comparison of STANCHEK with analytical test solution.  
Both curves are scaled with respect to their own calculated  $\delta^*$ .

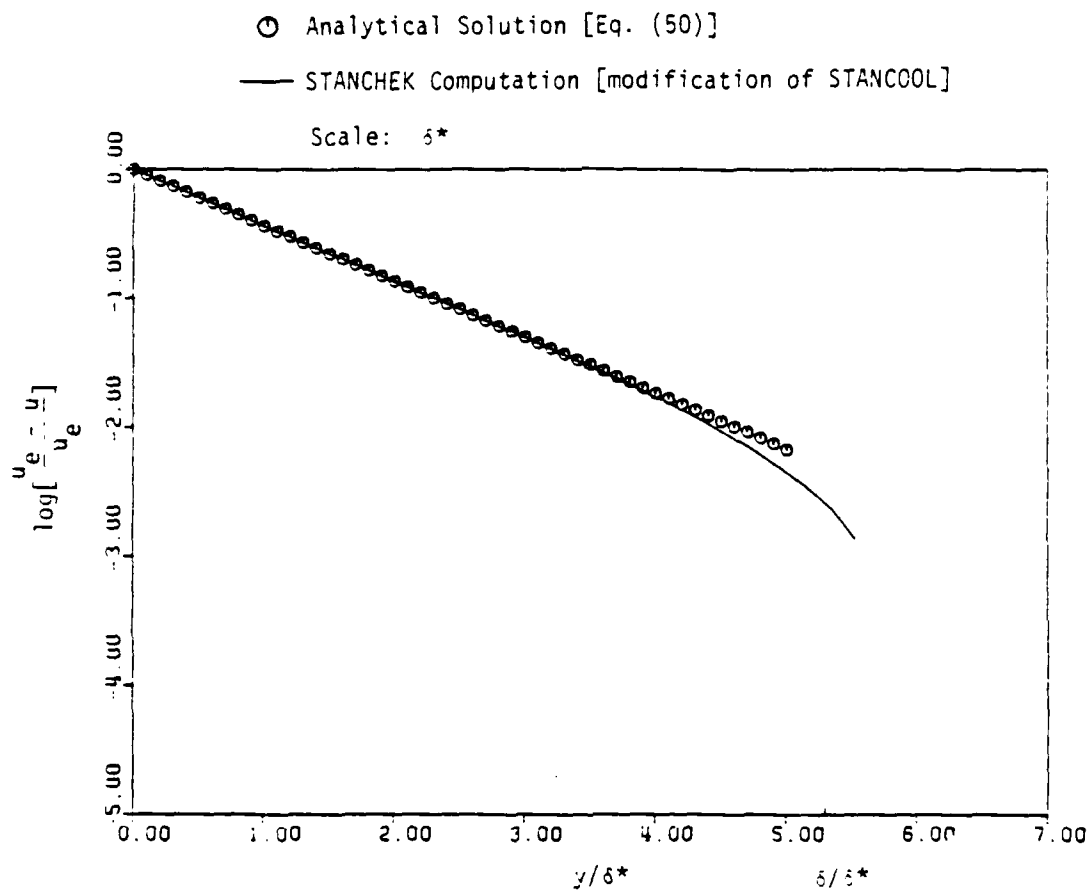


Figure 48: Wake region of analytical test case. Both curves are scaled with respect to their own calculated  $\delta^*$ .

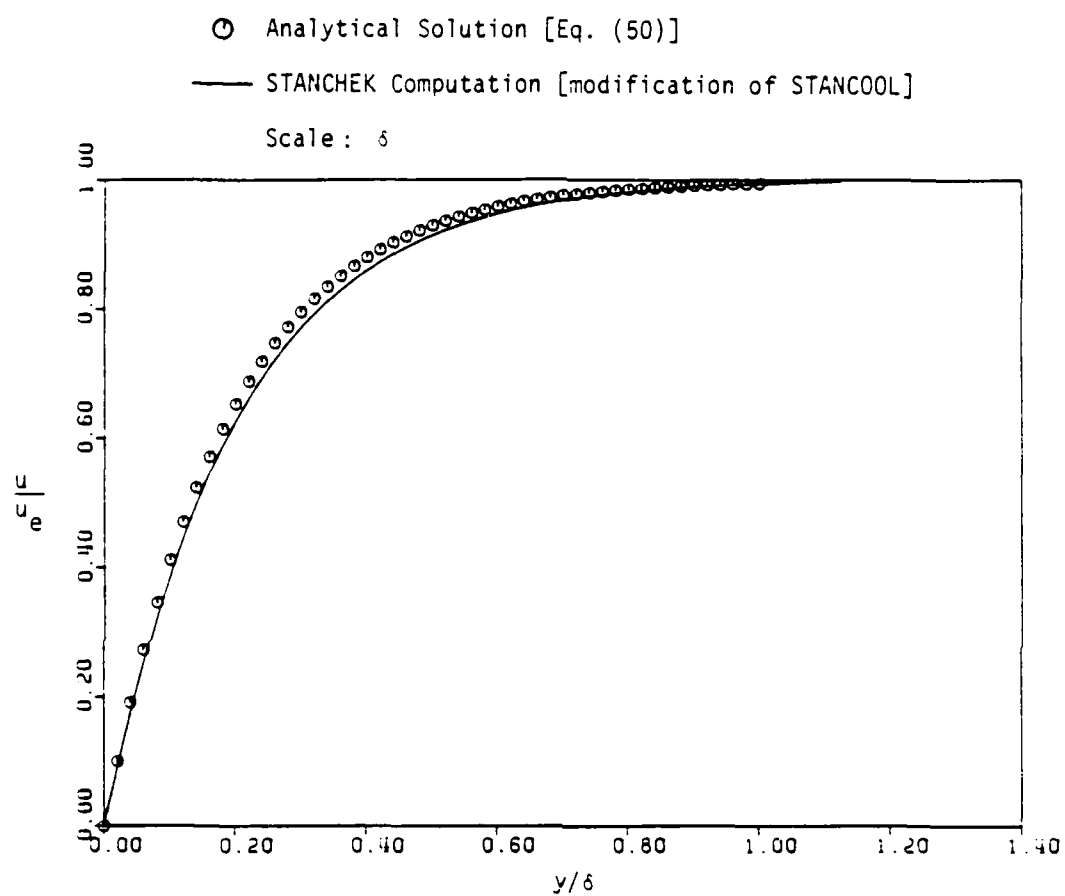


Figure 49: Comparison of STANCHEK with analytical test solution. Both curves are scaled with respect to their own calculated  $\delta$ .

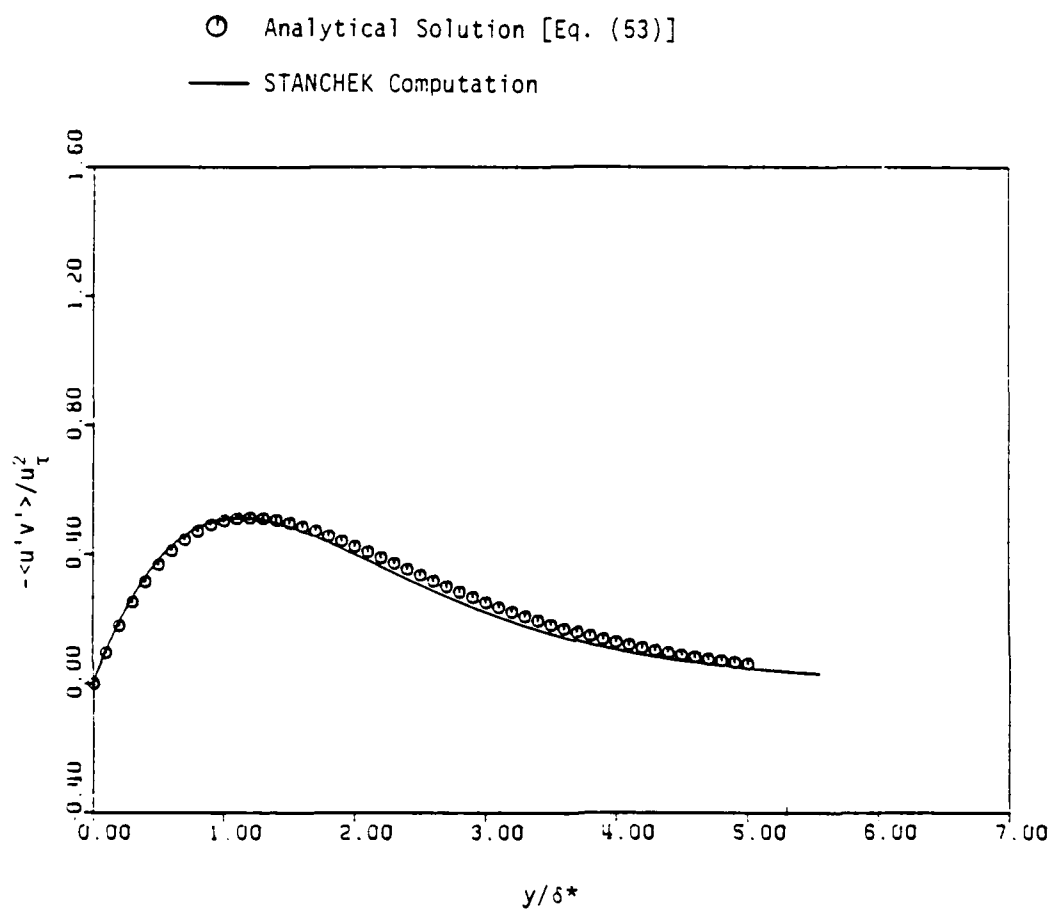


Figure 50: Comparison of STANCHEK with analytical test case Reynolds stress. [The profiles are forced to be identical in  $y/\delta$ .]

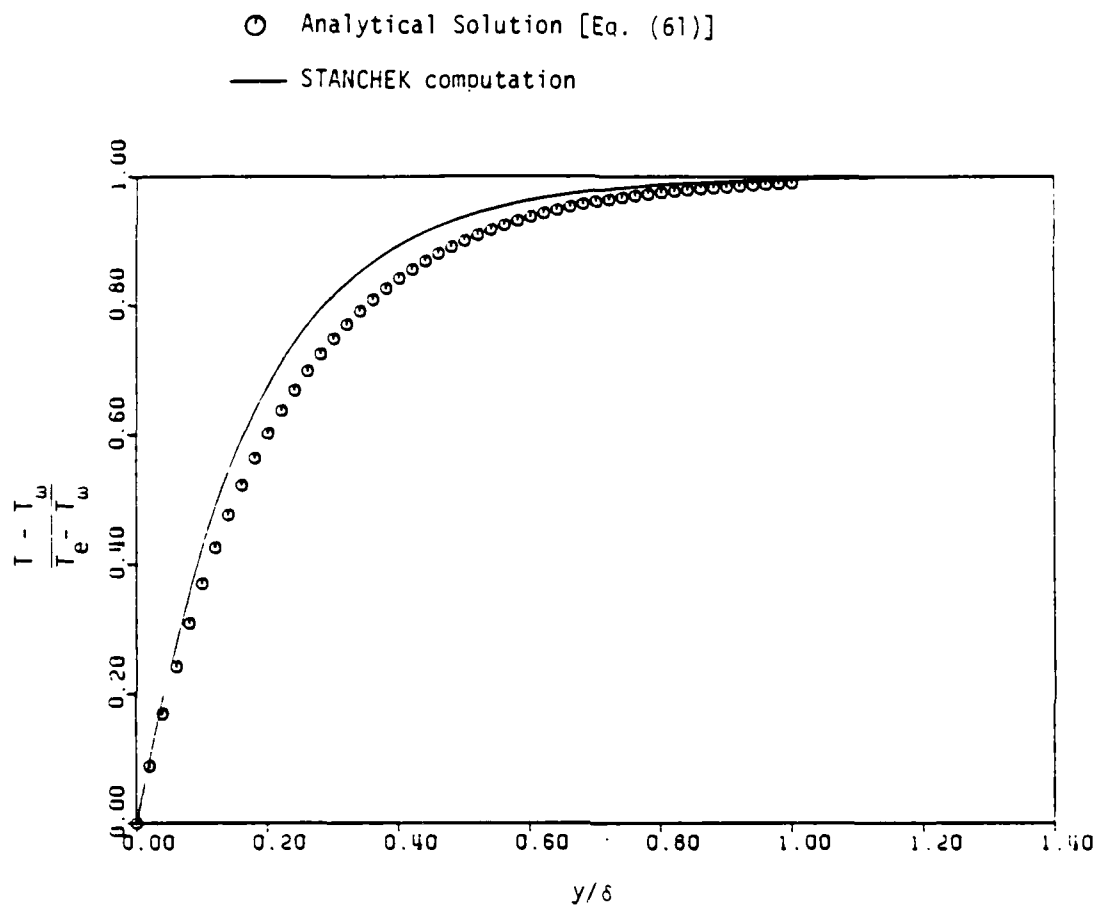


Figure 51: Comparison of STANCHEK with analytical test case temperature profile.  $P_{rt}$  according to Eq. (64).



○ Blair data [18]. Grid 0.  $x = 84$  in.

— STANCOOL computation with option FST3. [Eq. (49)]

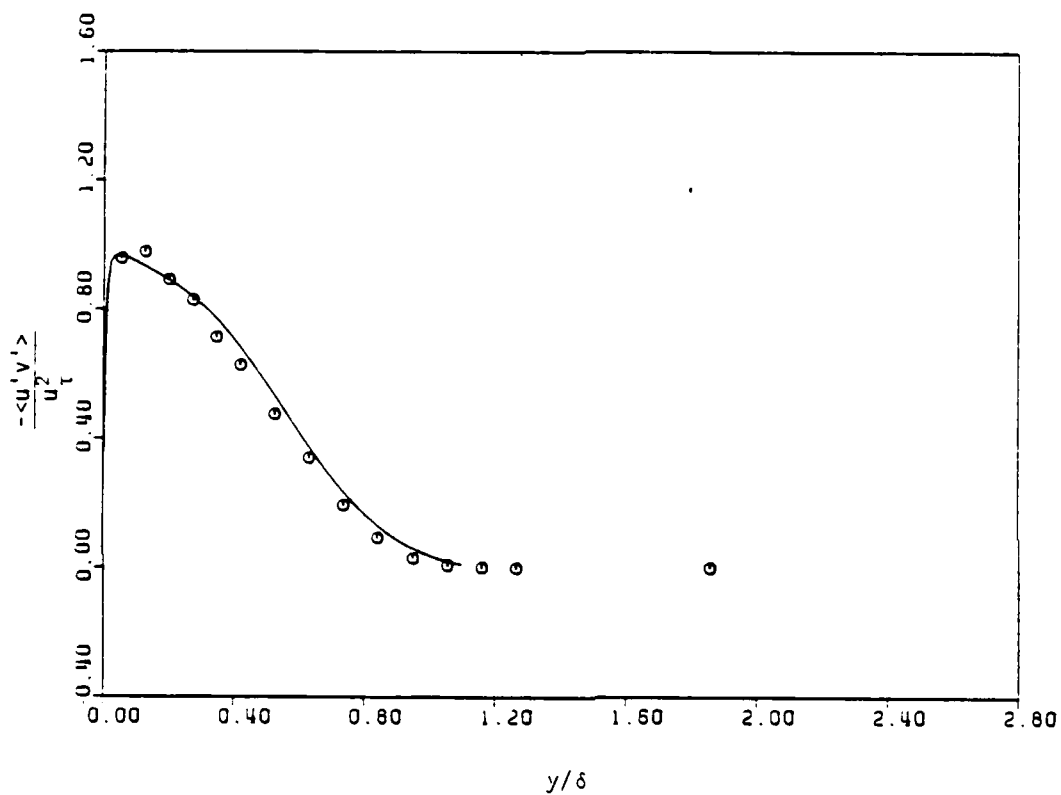


Figure 52: Calculated (FST3) and measured Reynolds stress profiles.

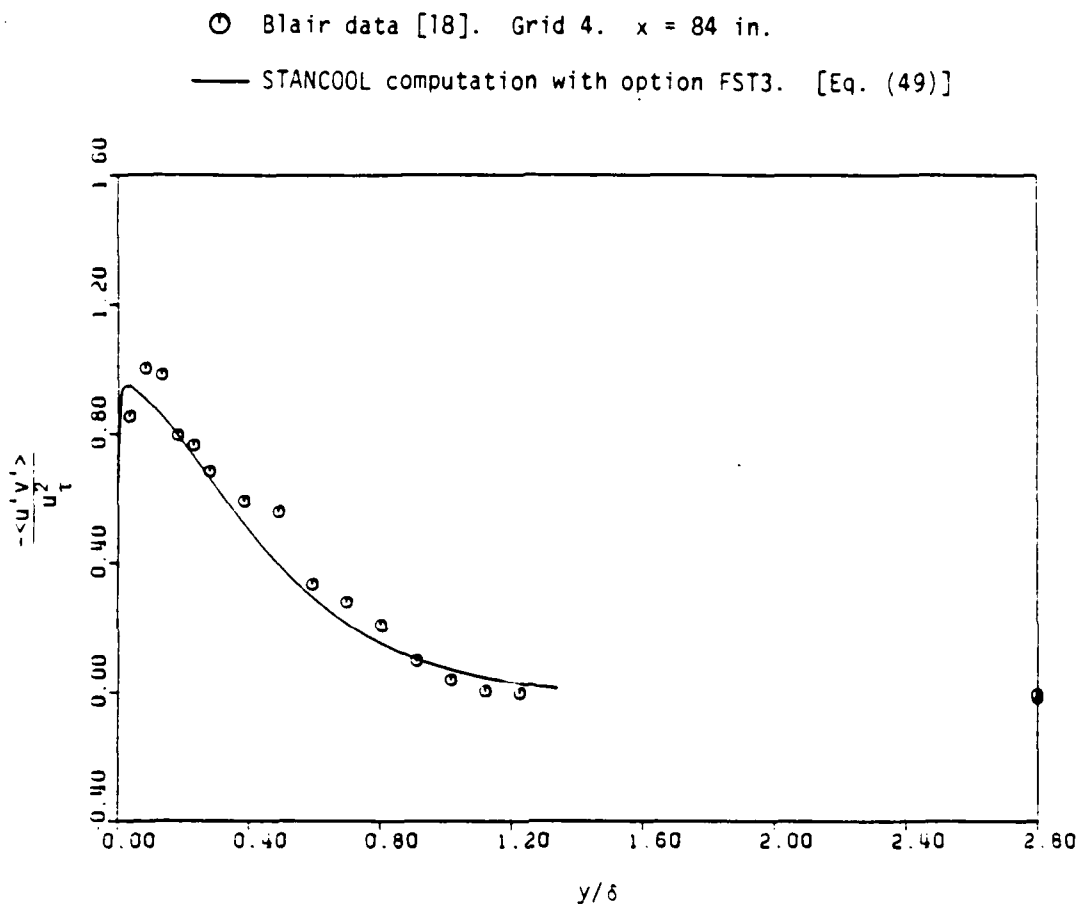


Figure 53: Calculated (FST3) and measured Reynolds stress profiles.

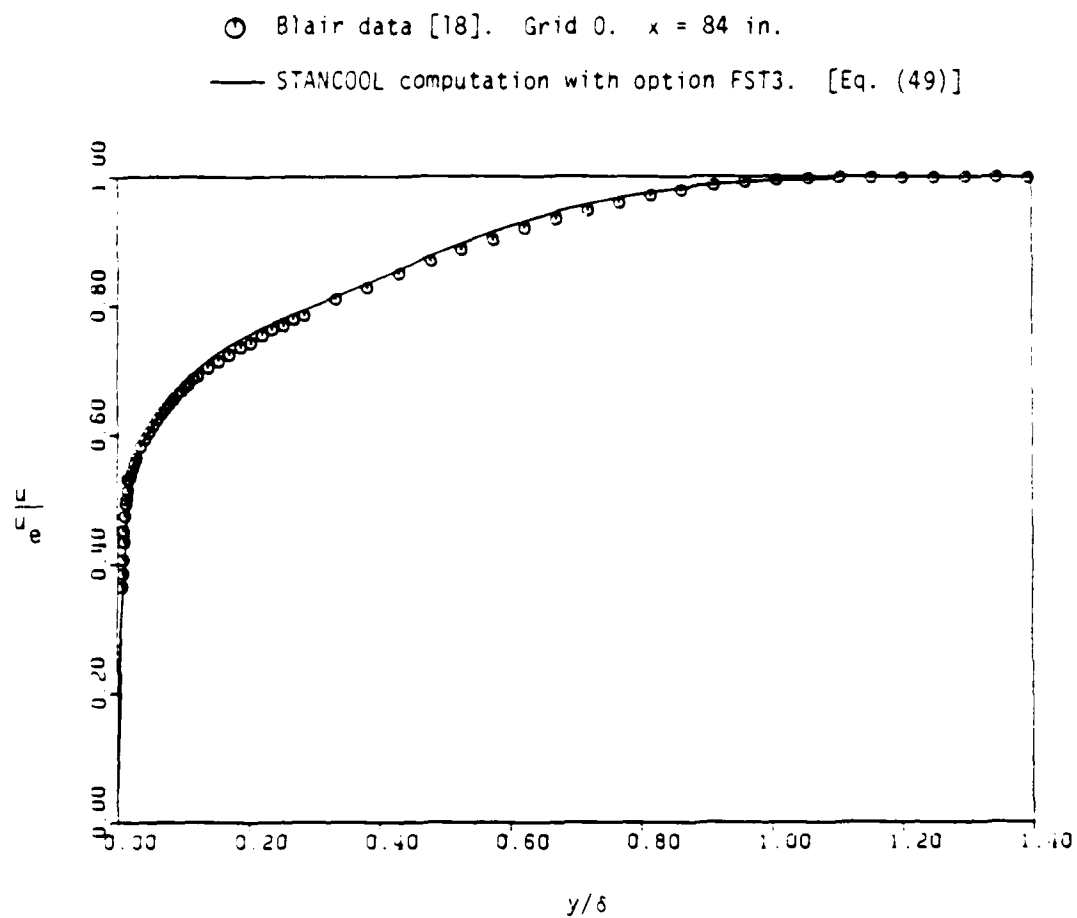


Figure 54: Calculated (FST3) and measured mean velocity profiles.

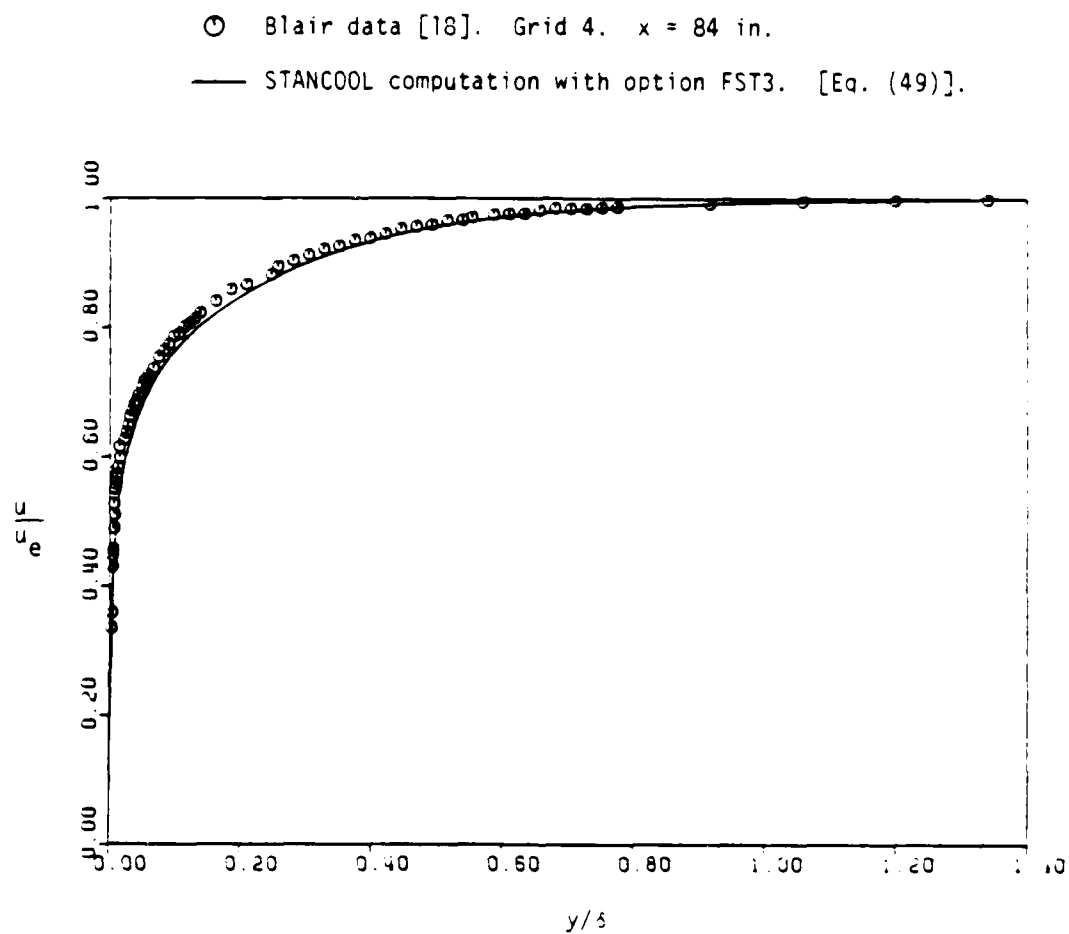


Figure 55: Calculated (FST3) and measured mean velocity profiles.

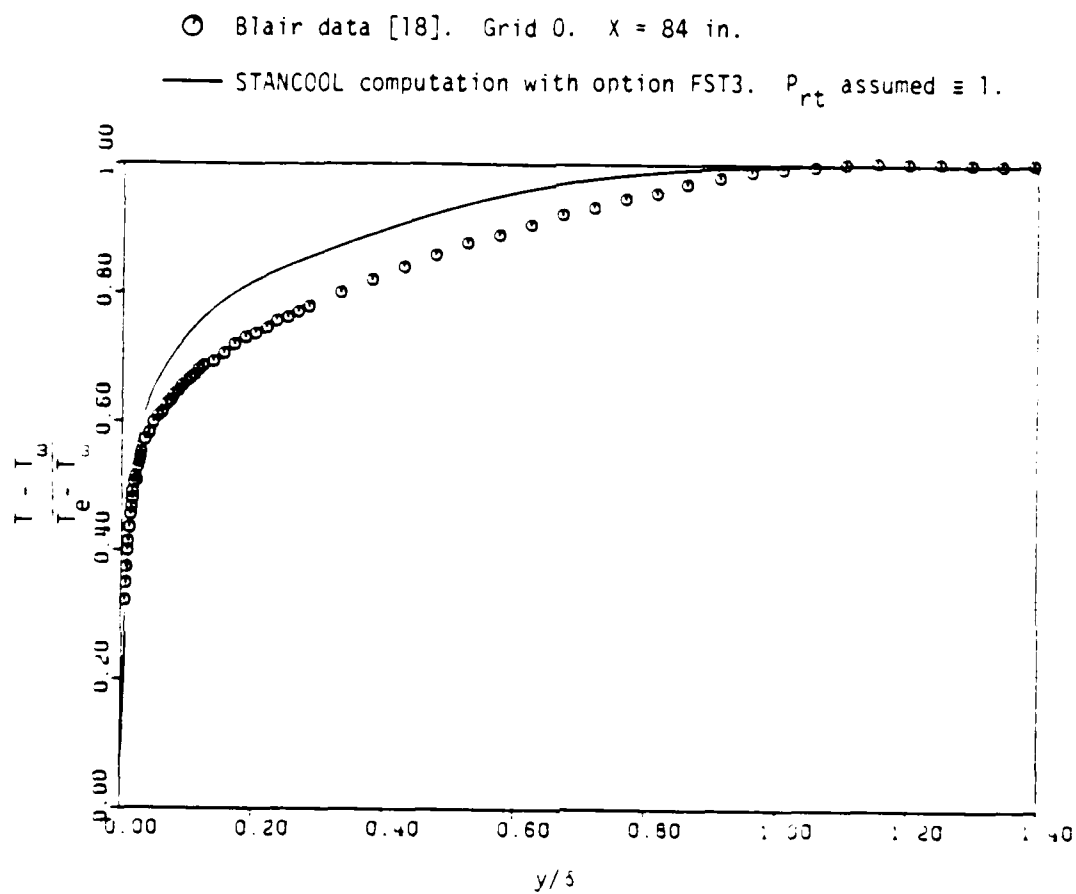


Figure 56: Calculated (FST3) and measured mean temperature profiles.  
 Unity  $P_{rt}$  assumed.

○ Blair data [18]. Grid 4.  $x = 84$  in.

— STANCOOL computation with option FST3.  $P_{rt}$  assumed  $\equiv 1$ .

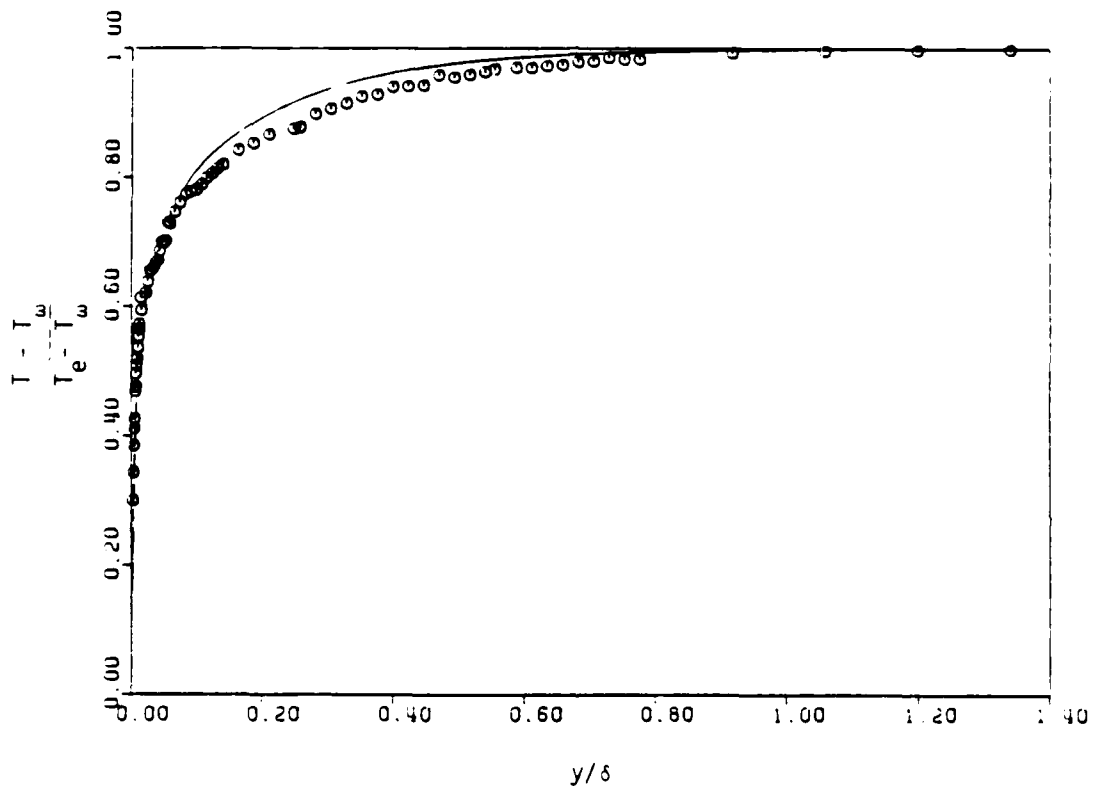


Figure 57: Calculated (FST3) and measured mean temperature profiles.  
Unity  $P_{rt}$  assumed.

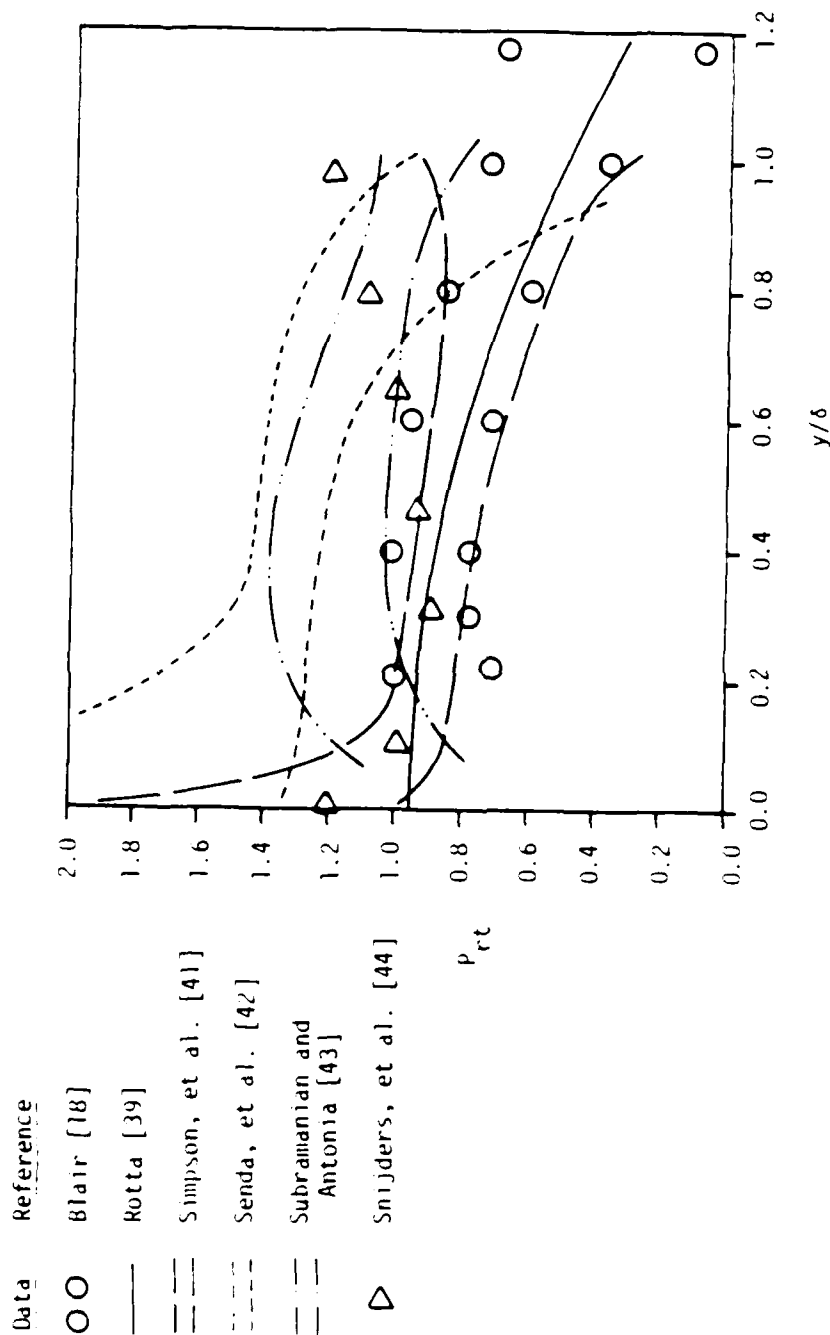


Figure 58: Summary of turbulent Prandtl number data from several references. Boundary layer flows.

Data Reference

○ Browne and Antonia [48]

□ Pabst [70]

△ Reichardt [71]

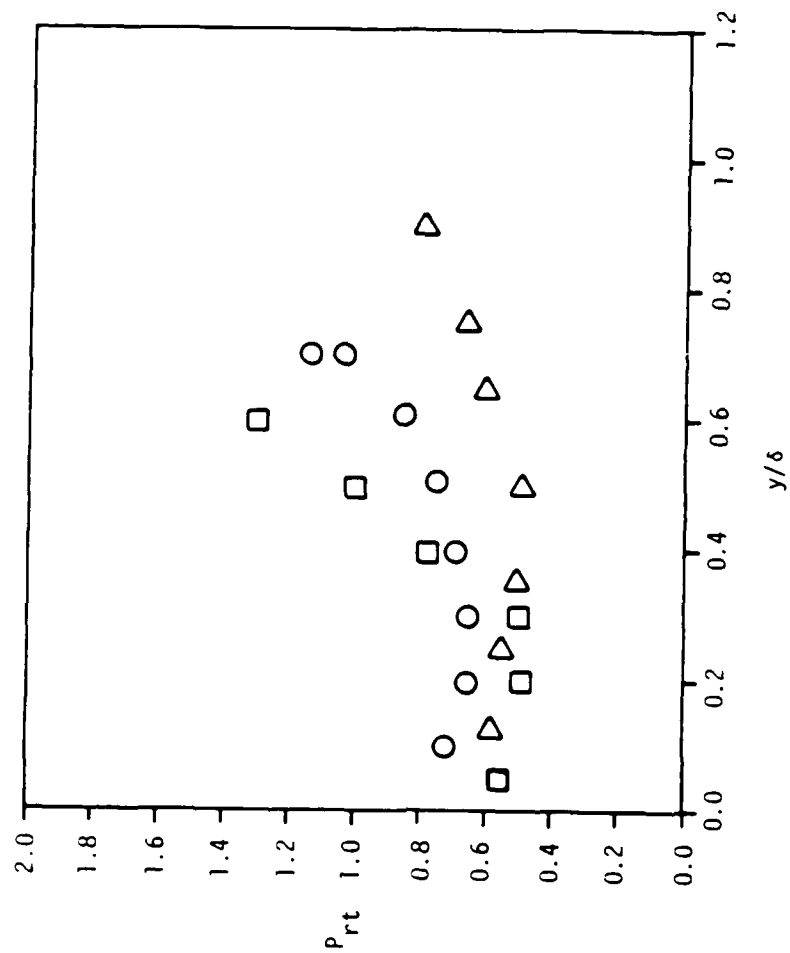


Figure 59: Turbulent Prandtl number data for turbulent jets and wakes from three references.



Study of Cold Reacting and Combusting  
Flows Around Bluff-Body Combustors

by

Xianguo Li and Richard S. Tankin

Department of Mechanical and Nuclear Engineering  
Northwestern University  
Evanston, Illinois 60201

Prepared for

Southeastern Center for Electrical Engineering Education  
Contract F49620-82-C-0035  
January 1, 1986

### Abstract

The results from visual observations and measurements of flows over axisymmetric, unducted, and vertically mounted bluff-body combustors are presented for low Reynolds number. The flow visualization is accomplished by adding  $TiCl_4$  vapor into the central gaseous propane jet for cold reacting and combustng flows, or by injecting  $TiCl_4-N_2$  mixture into the flow field behind bluff-body combustors through a 1.5 mm O.D. probe for pure annular air jet. Micron size particles of  $TiO_2$  are formed from the reaction between  $TiCl_4$  and  $H_2O$  vapor either contained in the annular air or as a product of combustion. Vertical laser light sheets provide a remarkably detailed visualization of the dynamic structures in the recirculating zone behind the bluff-body combustors. For the pure annular air jet, the length of the recirculating zone has a maximum at approximately 700~800 annular Reynolds number ( $Ra$ ) and approaches to a constant value for very large  $Ra$ . For the cold reacting flow, an empirical formula is found from thousands of the experimental data for the relation between the central jet height and the flow conditions at the nozzle exit as well as the nozzle diameters. The introduction of the central jet into the flow enlarges the recirculating zone. The vortices in the recirculating zone appear more organized, stationary and intense for attached flames compared to the cold reacting flows. However, the size of the recirculating zone and the height of the central jet are reduced by more than half. Also for the attached flames, the central jet penetrates more easily through the recirculating zone than for the cold reacting flow. For the detached flame, the height of the central jet is greatly reduced; whereas the length of the recirculating zone is increased slightly, when compared to the corresponding cold flow. It is noted that when the annular air velocity is less than 1.6 m/sec, the flame always remains attached; however, when the

annular air velocity is greater than 1.6 m/sec, the flame appears attached first for the very low central fuel velocity ( $V_{CO}$ ), becomes detached when  $V_{CO}$  exceeds a certain value, then when  $V_{CO}$  is increased further it becomes attached again. Photographs are presented to reveal the structures of the recirculating zones for the three different kinds of flows. Theoretical considerations based on Bejan's scaling method are also presented.

## 1. Introduction

Non-premixed flame stabilized by a bluff-body combustor, such as occurs when a central fuel jet issues into a surrounding annular air jet, are often used industrially. Examples of the use of such burners are in the combustion chambers of gas turbines, tubular cooler, metallurgical furnaces, aircraft jet engines, etc. Such bluff-body combustors provide good flame stabilization as well as easy control of combustion. Both the fuel and air jets leave their nozzles with considerable momenta. During the mixing process, there is transfer of mass, momentum and energy between the two jets and also between the jets and the ambient air surrounding the bluff-body combustor.

Bluff-body combustors are widely used for combustion processes requiring a fuel-rich mixture at the flame front but an overall stoichiometric or lean mixture further downstream. This type of combustor avoids pre-ignition or explosion dangers inherent in premixed combustion system and can improve the stability of overall lean flames.

From a practical point of view, it is necessary to better understand how the geometrical arrangements and operating conditions of the bluff-body combustor influence the flame processes - particularly the flame stability. It is well known that the recirculation region and large scale mixing behind the bluff-body combustor account for flame stabilization. In short, many of the characteristics of these combustors are determined by the aerodynamics of the flow. Therefore the details of the flow - particularly the recirculation zones, the location of the forward and aft stagnation points are needed to better understand the flame stabilization processes. In this study, cold reacting flow (isothermal) and combusting flow were investigated. Experiments were also conducted for pure annular air flow. These experiments give some insight into how the central fuel jet changes the recirculation zone,

especially the recirculating zone length.

Flows behind bluff-body combustors are very complicated due to separation and recirculation, exchange of mass and momentum between the two jets, the chemical reactions involving large amounts of heat release and vortex shedding. Thus these flows are very sensitive to probe interference. Therefore, laser sheet-lighting technique was used and non-intrusive measurements were made for cold reacting and combusting flows.

Though numerous experiments have been conducted on this type of combustor - either ducted (Ref. 4 and 5) or unducted (Ref. 3, 6 and 7), and numerical simulations (Ref. 8), there is still not enough understanding of the overall flow field. Therefore, flow visualization coupled with simultaneous pointwise measurements are essential for understanding the details of the flow consisting of large-scale structures.

The present experiments are visual in nature and are aimed at providing a better understanding of combustion for bluff-body combustors. The micron size  $TiO_2$  particles act as scattering media for laser sheet-lighting, providing flow visualization of the entire reacting zone. Traditionally, schlieren, shadowgraph, interferometry, and direct photography have been used in combusting flows. Unfortunately, information obtained by these methods are integrated across the flame (Ref. 10). Thus their use has been limited to a great extent to two dimensional, steady flows. By sheet-lighting the flow, a plane (vertical or horizontal) in the flame is observed. The  $TiO_2$  particles are formed as a product of the reaction between  $TiCl_4$  vapor and water vapor. Thus the  $TiO_2$  particles are formed in the reacting portion of the flame. Since the  $TiCl_4$  vapor is added to the propane (central jet), the occurrence of  $TiO_2$  will be on the rich zone of the diffusion flame. By adding the  $TiCl_4$  to dry air in the annulus, the formation of  $TiO_2$  particles would occur in the

lean zone of the flame. Records are made on either film or video tapes. To reduce the continuum radiation from the soot particles, a narrow-band pass filter centered at 5145 Å is used.

The  $\text{TiO}_2$  particles have been reported to be fairly uniform and generally in the 0.2 to 1 micron range - only a small fraction in the 2 or 3 micron range (Ref. 9). Particles in this size range follow the flow and also act as good Mie scattering center (Ref. 28). The reaction of  $\text{TiCl}_4$  with water vapor seems to be nearly instantaneous, i.e., mixing limited, thus it can be used effectively to study turbulent mixing processes (Ref. 3).

It is well known that separated recirculating flow established behind the bluff bodies stabilizes flames in high-velocity reacting systems. Zukoski and Marble (Ref. 26) in an early paper experimentally reported that the length of the recirculating zone plays an important role in flame stabilization. The dynamics of the near wake region is very important in the understanding of the mechanism of flame stabilization. For example, the size of the recirculating zone (and recirculating intensity) strongly affects the rate of production of hot products of combustion; i.e., the rate of heat release from the combustion process and thermal efficiency.

Many investigations on separated, recirculating flow for the isothermal case have been carried out over the past few decades, and a few on combusting flows (see, for example, Ref. 1, 11, 12, and 13). For most of these investigations, the bluff body was either a disk or cone of various cone angles. An exception was the study by Davis and Beer (Ref. 13) who used a cylinder as one of these bluff bodies. The annular flow in these studies was at very high Reynolds numbers. In the present experiment, cylinders were chosen as the bluff bodies and the Reynolds numbers for the annular flow varied from low to moderately high. We were limited in the annular Reynolds

number by pressure available in house air supply.

This study is an extension of the work reported by Roquemore, et al. (Ref. 3) and a result of research proposed by Tankin (Ref. 19). The main objectives are:

(1) To visually determine the behavior of the mean flow pattern for free annular air jet and central fuel jet with and without combustion under the influence of various bluff-body blockage ratios;

(2) To determine the difference between cold reacting flow and combustng flow;

(3) To measure the penetration lengths of the central jet under various flow conditions and blockage ratios;

(4) Compare the results of this study with previous measurements by other investigators.

## 2. Experimental Set-Up

The bluff-body combustor consisted of a fuel nozzle located concentric to an annular region where air flowed. The fuel nozzle was located in the center of a bluff body. The outer shell of the combustion tunnel could be translated, thus insuring the annular region and the central nozzle were concentric. This was important because small eccentricities would lead to an asymmetric flow. The design of the combustion tunnel was such that the outer rim of the combustion tunnel (outer annulus diameter) could be changed by merely changing the threaded insert. Likewise, the fuel nozzle diameter could be changed by changing threaded fuel nozzle insert. These nozzles were tapered, so that the fuel jet had a flat velocity profile at the nozzle exit and low turbulence intensity. The annular region was also tapered for the same reason.

To insure the flow would be uniform, screens and fiber glass were placed in the annular region as well as the central pipe almost 6 inches upstream of the nozzle exits. A schematic diagram of the combustion tunnel is shown in Figure 1.

The annular flow of air was controlled by a needle valve and measured with a rotameter which was calibrated with a precision wet-test meter. The calibration curve for the rotameter could be found in Appendix A. The air used in these experiments was pressurized room air. The fuel flow was measured with either of the two Gilmont rotameters that were connected in parallel. Along with the rotameters, a pressure gauge and thermocouple were installed. The fuel velocity at the nozzle exit was calculated using a computer subroutine, from equations provided by Gilmont, Co., with fuel temperature, pressure, rotameter scale reading and nozzle diameters as input parameters. The computer subroutine was titled CENFV and listed in either the Appendix B or C.

For the experiments of the cold reacting flow and combustng flow, building air flowed in the annular region and propane with small amounts of  $\text{TiCl}_4$  vapor issued from the central nozzle. For the combustng flow, the mixture was ignited. The propane flow was controlled by three valves. The propane might pass over the surface of liquid  $\text{TiCl}_4$ , which was in a stainless steel container, picking up some  $\text{TiCl}_4$  vapor. Also it was possible to have the propane by-pass the  $\text{TiCl}_4$  container.

For the case of the pure annular flow, the central fuel jet was closed and air was supplied to the annular nozzle. A small diameter probe (1.5 mm O.D.) was used to inject a mixture of dry nitrogen gas and  $\text{TiCl}_4$  vapor. The  $\text{TiCl}_4$  vapor was entrained by the nitrogen gas in the same manner as for the propane. This injected mixture, which flowed from the nozzle of the probe,



was rapidly entrained into the recirculation zone where the  $\text{TiO}_2$  particles acted as scattering centers. The recirculation zone length, which is defined as the axial distance from the bluff-body surface where the velocity is zero (stagnation point), was visually determined where approximately half of the  $\text{TiO}_2$  particles moved downwards and half moved upwards.

All the gas lines from  $\text{TiCl}_4$  container downstream consisted of stainless steel piping and stainless steel valves. Even so, there was occasional clogging of the lines. Provision was made so that  $\text{TiCl}_4$  system could easily be disconnected and cleaned. If partial blockage occurred, the fuel flow developed oscillations that were detected on the fuel rotameter. The partially plugged line or valves were cleaned by passing water through the line, followed with acetone and then air.

The optical set-up used to visualize the flow field consisted of a 4 watt argon-ion laser. The 5145 Å line was used in these experiments. When the laser light struck a glass rod, which behaved like a cylindrical lens, the light beam spread in a plane normal to the axis of the glass rod. The angle of spreading depended on the diameter of the glass rod - large diameter gave smaller angle of spread. The width of the sheet of laser could be reduced by forming a slit on the surface of the glass rod. For the cold reacting flow, where the aft stagnation point was relatively far from the nozzle, a small rod of 8 mm diameter was used. On the other hand, for the combustor flow (attached flame only), the aft stagnation point was much closer to the nozzle and a rod of 25 mm was used. The intensity of illumination in the sheet, of course, was much larger. This was fortunate because we needed more intensity to overcome the illumination of the flame. To virtually eliminate the luminous radiation from the hot carbon particles in the flame a narrow band-pass optical filter centered at 5145 Å was used. This filter had a half width

of 90 Å and reduced the light intensity at 5145 Å by 40%.

To measure lengths of the stagnation points above the nozzle, a neon helium laser (6328 Å) was mounted on a vertical traversing platform. This laser light formed a red spot due to scattering of the  $TiO_2$  particles. Attached to the traversing platform was a 3" dial gauge, thus allowing one to read the vertical position of the platform. The dial gauge was "zeroed" when the neon-helium laser was at the nozzle elevation. Also a narrow band pass filter centered at 6328 Å was considered, but was not found to be necessary.

### 3. Experimental Conditions

For the pure annular air flow, the central nozzle was blocked with a silicone type caulking compound. This was carefully done so that the surface was smooth; resulting in a configuration similar to that used by Durão and Whitelaw (Ref. 11). The ratio of the diameter of the inner annulus to the diameter of the outer annulus was either 0.57, 0.72 or 0.85; with blockage ratio 32%, 52% and 72% respectively. The Reynolds number,  $Re$ , ranged from 120 to  $4.3 \times 10^3$  - based on the exit velocity of the annular air flow and hydraulic diameter (the Reynolds number based on the diameter of the bluff-body combustor,  $Re_D$ , varied from 320 to  $1.3 \times 10^4$ ). Schematic diagrams for nozzles are shown in Figure 2.

Where flow occurred in the fuel nozzle, the Reynolds number in the annulus,  $Re$ , varied from 500 to 1900 (or  $Re_D$  from 1100 to 4500). The Reynolds number in the central fuel jet,  $Re_c$ , based on the exit velocity and the diameter of the central fuel nozzle, ranged from several tens to 1600. The flows in this study were mostly laminar, with the higher Reynolds number flow near transition to turbulence. In the case of the combustor flow, the tests were all in the laminar region (laminarization of combustor flow is quite

obvious) except for the case of detached flames.

All experiments were performed with a vertically mounted, unducted combustor. The combustor was located directly under a ventilation hood which removed  $\text{TiO}_2$ ,  $\text{HCl}$  and combustion products from the room - discharging them outside the building. Occasionally there were some air disturbances in the room which affected the flow pattern, but this was only noted at low annular air flow and even then were not significant.

For the experiments conducted on the cold reacting and combusting flows, no intrusive measurements were made. Only lasers were used and the laser light was scattered by the small particles ( $\text{TiO}_2$  and soot). For the case of the pure annular flow, an intrusive, small diameter probe was used to inject  $\text{TiCl}_4$  vapor and dry nitrogen, and thus enable one to observe the recirculation zone. This intrusive probe had some effect on the flow field, particularly at low air velocities.

As Durão and Whitelaw observed (Ref. 11) the instantaneous aft stagnation point fluctuated in spite of the low air and fuel Reynolds numbers. Thus, the aft stagnation point was obtained by taking the average of several measurements.

Measurements were made of the length of the recirculating zone for the pure annular air flow, and the axial location of the forward and aft stagnation points for the cold reacting flow and combusting flow. An attempt was made to correlate those measured quantities with exit velocities and nozzle diameters.

#### 4. Coordinate System

The origin is at the center of the combustor surface (the same elevation or plane as the nozzle exit). The z-axis is in the axial direction, positive

downstream (i.e., vertical upwards). The r-axis is radially out along the combustor surface.

## 5. Observations, Experimental Results and Discussions

This section is organized into three parts: pure annular free jet, cold reacting flow and combustor flow. In the first part, the results of measurements on the length of the recirculation zone, comparisons with the previous investigations and description of the flow field are presented. In the second part, the description of the flow for different central fuel velocities and the empirical formula about the location of the forward stagnation point with respect to flow conditions and geometries, drawn from thousands of experimental data, are given for the under-penetration of the central jet. For flow fields with combustion, the same measurements were made as for the cold reacting flow. Some phenomena observed for the combustor flow are presented in the last part. For the cold reacting and combustor flows,  $TiCl_4$  vapor was added to the central jet, which produced  $TiO_2$  particles for flow visualization.

### 5.1 Pure Annular Air Jet

The flow system for a pure, free annular air jet is shown in Figure 3 which exhibits three distinct flow regions behind the bluff body: a region of recirculation where the mean velocity along the centerline is negative and the pressure at the center of the vortices is minimum; a transition region where the velocity along the centerline accelerates to a maximum velocity and a downstream region where the velocity decays (Ref. 11, 13 and 20).

The recirculation zone is a region of subatmospheric pressure caused by the annular jet with an associated closed ring vortex in the central region

(See plate 1-b). This picture was taken with the annular air velocity of 0.4821 m/sec, and the central propane velocity of 0.0076 m/sec. A small amount of  $\text{TiCl}_4$  vapor was added into the central jet. Although this is not strictly pure annular flow, the ratio of central jet velocity to annular jet velocity is only 1.5%. This technique was used in this instance because it clearly showed the symmetry of the recirculating region. If one examines the central streamlines near the central jet exit (Plate 1-b), they are similar to those obtained for flow impinging on a flat surface. This is further evidence that the flow approaches the pure annular flow in this test. When actual data were taken for the pure annular flow, the central nozzle was plugged and a probe was used to inject the  $\text{TiCl}_4$  vapor. The small asymmetry of the vortex may be attributed to the non-eccentricity of the combustor arrangement. The bounding surface of the recirculating zone is clearly shown in Plate 1-b. To obtain this surface from pointwise measurements, it would be necessary to measure axial velocity profiles and integrate these values radially. That is,

$$M_r = \int_0^{r_1} u(r,z) \cdot 2\pi r dr = 0 \quad (1)$$

where  $M_r$  is the rate of the mass flow circulating in the recirculation zone; and  $u(r,z)$  is the z-component of the velocity at location  $r$  in the plane  $z$ . By setting  $M_r = 0$  and solving for  $r_1$ , one could determine the bounding surface of the recirculating zone.

It is obvious that it is much simpler to use flow visualization technique as described in this study to determine the bounding surface than to do it from Equation (1). However, as seen in Plate 1-b, there is some question concerning the exact location of the bounding surface at the stagnation point. Using the probe technique for supplying  $\text{TiCl}_4$  vapor, we believe, can

better define the location of the bounding surface at the stagnation point. Plate 1-c shows the sheet-lighted recirculation zone when central jet is turned off and the mixture of  $TiCl_4$  vapor and dry nitrogen gas is injected near the end of the recirculation zone ( $L_{rz}$ ) through a probe.

For the downstream region (established flow region) shown in Figure 3, the flow is fully developed, and the flow patterns as described in Ref. 24 are similar to those of single round jet with a displacement of the origin. The single round jet problem has been thoroughly studied in the past (see Ref. 25).

The measured length of the recirculating zone,  $L_{rz}$ , normalized by the bluff-body diameter,  $D_1$ , is plotted against the Reynolds number,  $Ra$  (see Figure 4). The curves show that the recirculation zone length has a maximum where the  $Ra$  is approximately 700~800 for the geometries tested. One would expect such a maximum because as  $Ra \rightarrow 0$ , the recirculation zone length goes to zero. When the flow changes from laminar to turbulent flow, one would expect the length of the recirculating zone to decrease because of increase in transfer of momentum. It was noticed in the experiments that flows appeared very steady when  $Ra$  was less than 700~800 and fluctuations appeared in flows at  $Ra$  greater than 700~800. It is believed that the data in this study at  $Ra > 800$  represent transition to turbulent flow. The data points of Durão and Whitelaw (Ref. 11) are also plotted on Figure 4. Their bluff body is a disk rather than cylinder as used in this study. However, their results are in general agreement with those of the present study. It should be noted that Durão and Whitelaw's results were obtained at much higher  $Ra$  and that their values of the length of the recirculating zone decreased slightly with increase in  $Ra$ . It appears from Figure 4 that  $L_{rz}/D_1$  approaches an asymptotic value. In the section of the study entitled "Analytical Approach", these

tendencies will be discussed in greater detail.

In Test I and Test II, the outer diameter of the annulus was kept constant and the inner diameter of the annulus was 38.5 mm and 45.2 mm respectively. This corresponds to blockage ratios of 52% and 72%. A possible explanation for the difference between the results of Test I and Test II is as follows: in Test I, the annular gap is 7.37 mm whereas in Test II it is 3.99 mm. One would expect the velocity profile at the exit to be different for Test I and II. Pope and Whitelaw (Ref. 14) in their numerical simulation mentioned that the shape of the velocity profile at the exit affects significantly the downstream flow characteristics. The results of Test III which has a blockage ratio of 32% would be expected to lie above the results of Test I (blockage of 52%). However it lies between Test I and Test II. A possible explanation for this discrepancy is that the nozzle used in Test III has a modified geometry. The inner and outer walls of the annulus are tapered  $10.8^\circ$  (see Figure 2-c). This results in a radially inward component of the velocity at the nozzle exit. Thus it is expected that the length of the recirculation zone for such a configuration will be reduced. This is in accordance with the effect of the forebody shape on the length of the recirculating zone discussed by Davies and Beer (Ref. 13). The arguments presented concerning the variation between Test I, Test II and Test III are based on conjecture.

The results of this study are compared with those of previous investigations in Table 1. The recirculation length for confined flows is significantly larger than that for unconfined flows (approximately twice as large as for unconfined flows). The agreement is reasonably good for all the investigations of unconfined annular jets as seen in Table 1. Davis and Beer (Ref. 13) obtained  $L_{rz}/D_i = 0.72$  for unconfined annular jet over a cylinder as

compared with our values of 1.00, 0.83. However their  $Ra$  was much larger than the values in this study. It should be noted that the flow near the stagnation point is more unsteady than elsewhere behind the bluff body in the experiments presented. Thus, the measured recirculation length is determined on a visual averaging of its value. As many as seven such data were taken and then numerically averaged.



Table 1. Length of recirculation zone for various flows over bluff bodies

Authors	Flow type	B.R.*	Ra	$L_{rz}/D_1$
Taylor & Whitelaw (1984)	confined disk	25%	34,000	1.75
	confined 45° cone	25%	38,100	1.55
	confined disk	50%	23,800	2.20
Winterfeld (1965)	confined disk	25%		2.0
	confined 90° cone	25%		1.9
	confined 45° cone	25%		1.7
	confined disk	4%		2.0
	confined 90° cone	4%		1.9
	confined 45° cone	4%		1.7
Fujii (1978)	confined 60° wedge	50%		1.88
Bradbury (1976)	confined flat plate	10%		1.98
Calvert (1966)	confined disk	0.56%	50,000	3.04
	confined 90° cone	0.56%	50,000	2.18
	confined 60° cone	0.56%	50,000	1.88
	confined 40° cone	0.56%	50,000	1.58
	confined 20° cone	0.56%	50,000	1.30
	confined cylinder	0.56%	50,000	1.14
Davies & Beer (1971)	unconfined annular jet, disk	25%	fully turbulent	1.52
	unconfined annular jet, 45° cone	25%		1.24
	unconfined annular jet, cylinder	25%		0.72
	unconfined annular jet, disk	54%		1.16
Durão & Whitelaw (1978)	unconfined annular jet, disk	20%	28,300	1.45
	unconfined annular jet, disk	39%	19,100	1.15
	unconfined annular jet, disk	50%	14,800	1.00
	unconfined annular jet, disk	50%	6,300	1.01
	unconfined annular jet, disk	50%	3,500	1.04
Chigier & Beer (1964)	unconfined annular jet	44%	100,000	1.10
Carmody (1964)	unconfined disk	2%	70,000	2.5
present results	unconfined annular jet, cylinder	52%	2,500	1.00
	unconfined annular jet, cylinder	72%	2,300	0.83
	unconfined annular jet, tapered cylinder (21.6°)	32%	4,300	0.91

\*B.R. means blockage ratio.

### 5.2 Cold Reacting Flow

The flow field behind bluff-body combustors could be thought of as two widely spaced jets: an annular jet and a central fuel jet (Ref. 3 and 19). A schematic diagram for the jets is shown in Figure 5. At the nozzle exit, the two jets are separated from each other, and flow independently. They behave as though no surrounding fluid exists. However the two jets soon interact due to vortices that form between the two jets (see Plate 2 and 3). As seen in the pure annular flow these vortices are set up by the annular jet and the central fuel jet. In the cold reacting flow these vortices are not stationary. There are several such vortices at any time within the recirculating region, which move usually downward and radially outward. At the edge of the recirculating zone there are vortices that are clearly observed on the shear layer (see Plate 2-a). They rapidly grow in magnitude and roll up into a spiral. In the vicinity of the aft stagnation point, some of the spiral vortices on the shear layer escape and move downstream, whereas others are recaptured by the recirculating zone. These spirals consist of air packets which are brought into the recirculating zone by the recaptured spirals. These are seen as dark regions near the aft stagnation point in the photograph. The dark region near the nozzle is the mixture of fuel and  $TiCl_4$  vapor devoid of water vapor (i.e.,  $TiO_2$  particles). Then due to the vortices existing within the recirculating zone, the packets of air and fuel mix together (also see Ref. 3).

When the central jet velocity is very small compared to the reverse flow in the recirculating zone, the central jet is turned outward. Plate 2-b shows the streak lines of the central jet as well as the recirculating zone. To achieve this, some particles of  $TiO_2$  are induced into the central propane jet. As can be seen the streamlines are similar to those of two impinging

streams. Where the central jet is turned defines the forward stagnation point.

Downstream of the aft stagnation point where the axis of the annular jet has converged at the central axis, the two jets have completely merged. The behavior of the combined jets is very similar to an equivalent single round jet. Chigier and Beer (Ref. 20) have determined the effective origin and the outside boundary of the equivalent jet as a function of the velocity ratio as well as the geometry of the nozzles for the case of air flow in the annular and central nozzles.

Two very important parameters characterizing the flow field behind a bluff-body combustor are the location of the forward and aft stagnation points. These occur where the velocity along the centerline vanishes. Since these points are usually oscillatory they are not easy to determine precisely. With probe measurements, which disturb the flow field, or laser doppler measurements, one has to interpolate the mean velocities in front of and behind the stagnation points. This introduces some uncertainty into the measurement results. We found that the forward stagnation point is stationary when it is less than half of the recirculation zone length. When the forward stagnation point reaches the half of the recirculation zone length it becomes non-stationary. The aft stagnation point has the recaptured spiral vortices in its immediate vicinity and hence is unsteady. For non-stationary fuel jet, its bounding surface is not as distinct as that of stationary fuel jet since the fuel jet is on the verge of breaking up into smaller packets.

From video tapes recorded, the flow field behind bluff-body combustors may be divided into three categories, although the numerical values of  $w$ , ratio of momentum of the central jet to the annular jet, i.e.,  $w = \rho_c V_{co}^2 A_{co} / \rho_a V_{ao}^2 A_{ao}$ , where  $A_{co}$  and  $A_{ao}$  are the central and annular nozzle exit

areas, respectively, are not exactly defined for the categorizing. The three categories are, respectively, that the annular jet is dominant; neither jet dominates and the central jet dominates.

If the central jet is weak, i.e., the momentum of the reverse flow set up by the annular jet is larger than that of the central jet. This reverse flow will force the central jet outward radially. If the momentum of the central jet is so low that it can not penetrate into the recirculation zone, the forward stagnation point is zero. In this case, the central jet is completely absorbed by the annular jet. In this regime the central jet motion is not stationary - it is pushed randomly from one side to another by the reverse flow.

If the momentum of the central jet is comparable with that of the reverse flow, neither jet dominates the flow field. The tip of the central jet which has mushroom shape is unsteady; however, the stem is very steady. When the central jet flow is increased, the forward penetration length increases and the main vortices in the recirculation region move laterally and become smaller.

If the central jet is very strong, the annular jet no longer plays an important role; the central jet dominates the flow field. The annular air is entrained into the central jet. Along the centerline no stagnation point could be found (overpenetration). As the central jet velocity is increased further, the central jet extracts more fluid from the annular jet to satisfy its entrainment requirement, and the size of the recirculating zone is reduced. At last, when the central jet velocity is so large that the central jet is completely dominant, it absorbs the annular jet totally. Then the central jet behaves as though no annular jet was present except for small vortices near the combustor surface. These small vortices are very organized

and stable.

The S-R saddle points which were computer simulation by Scott and Hankey for the flow field behind a ducted, pure annular flow (Ref. 8) are also observed in this study and presented in Plate 3-a and schematically shown in Figure 6. These saddle points occur on the centerline, the combustor surface and also the boundary of the central jet. On the centerline, such saddle points occur where flows approach either from opposite directions along the centerline and depart in a direction normal to the centerline, referred to as S-saddle point (i.e., the forward stagnation point, see point  $S_2$  in Figure 6), or from a direction normal to the centerline and departs in opposite directions along the centerline, referred to as R-saddle point (i.e., aft stagnation point, see point  $R_2$  in Figure 6). These saddle points are somewhat analogous to separation and reattachment points which occur at solid boundaries. More important is that on the boundary of the central fuel jet, S-saddle points occur as a result of the central jet entrained by the annular jet, the fuel is pulled into vortices formed at the tip and stem of the central jet, labelled as vortex A and B in Figure 6. Almost simultaneously vortex A moves towards the combustor surface while vortex C convects downstream and grows. During this time the vortex B grows and releases its fluid periodically into the region vortex C occupied previously. This probably aids the growth and convection of the vortex C. As vortex A is shed, the point  $S_2$  (forward stagnation point) oscillates along the centerline. Likewise, the saddle points  $S_2'$ ,  $S_2''$  and  $R_1$  are unsteady. On the right hand side of the central jet in Plate 3-a, vortex A is halfway to the combustor surface, Vortex C lost its identity, and vortex B was just releasing its fluid into the region close to the boundary of the recirculating zone. Thus it was not clearly shown there. On the combustor surface which is a solid boundary,

the S- and R-saddle points (separation (s) and reattachment (R)) are observed. It is noted, and also can be inferred that a stationary separation point  $S_1$  (see Figure 6) always exists at the outside edge of the combustor surface, while the reattachment point  $R_1$  moves in the radial direction along the combustor surface. A streamline originated near the point  $S_1$  will evolve into a vortex D (Figure 6) above the forward stagnation point. The separation streamline starting at the point  $S_1$  will form the boundary of the recirculating zone, and attach to the centerline. The reattaching point  $R_2$  oscillates along the centerline as vortex D is shed. The interactions between adjacent vortices as they form and move up- or downstream are very important to the understanding of mixing process hence combustion process in the recirculating zone.

It should be emphasized that all the above discussion is for annular air velocity greater than 0.5 m/sec. If less than 0.5 m/sec, the annular air is not sufficiently strong to form the usual recirculating zone presented. Plate 4-a shows the flow with fuel velocity of 0.2 m/sec, and air velocity of 0.4 m/sec. The flow field is irregular and large amounts of air intrude deep into the recirculating zone, which is not confined by an annular jet. Eddies have torn away the boundaries of the recirculating zone except the region very close to the separation point. It is interesting to note that this phenomenon never occurs for the combustor flow.

#### Experimental Results and Discussions

Using dimensional analysis, the following expression is obtained:

$$\frac{L}{D_j} = f(R_a, R_c, \frac{D_j}{D_1}, \frac{D_o - D_1}{D_1}, \frac{L_{rz}}{D_1}, \frac{V_{co}}{V_{ao}}) \quad (2)$$

where  $L$  = location of the forward stagnation point along the centerline;

$D_j$  = diameter of the central nozzle;

$D_i$  = diameter of the inner annulus;

$D_o$  = diameter of the outer annulus;

$V_{ao}$  = velocity of the annular jet at the nozzle exit;

$V_{co}$  = velocity of the central jet at the nozzle exit;

$L_{rz}$  = length of the recirculating zone;

$$R_a = \frac{V_{ao}(D_o - D_i)}{v_a}, \text{ Reynolds number of the annular jet;}$$

$$R_c = \frac{V_{co} D_j}{v_c}, \text{ Reynolds number of the central jet;}$$

By comparing Equation (2) with the experimental results shown in Figure 7 and Equation (3) below, it appears that  $L_{rz}/D_i$  and  $V_{ao}/V_{co}$  have no effect on  $\frac{L}{D_j}$ .

This could be explained as follows: the effects of  $V_{ao}$  and  $V_{co}$  have been taken into account in the parameter  $R_c$  and  $R_a$ , and that  $\frac{L_{rz}}{D_i}$  is nearly constant (see Figure 8). The forward stagnation point is strongly dependent on the geometry and the Reynolds numbers of the central jet and the annular jet.

The empirical formula shown in Figure 7, which is the result of thousands of experimental data, can be expressed in the following form:

$$\frac{L}{D_j} = A \frac{R_c}{R_a} \left(\frac{D_i}{D_j}\right)^{1.5} \left(\frac{D_o - D_i}{D_i}\right) \quad (3)$$

where  $A$  is constant, given in Table 2.

From Table 2, it seems that  $A$  depends largely on fluids used in the central and annular jets. Later on, in an analytical approach it will be shown that  $A$  is really the function of the physical properties of fluids in

the two jets. The power of  $R_a$  is always negative, i.e., as  $R_a$  increases while keeping other parameters unchanged, the central jet will be shortened. Thus, when  $R_a$  is increased,  $R_c$  should be also increased in order to maintain the central jet at the same height. Equation (3) shows that for larger  $R_c$ , i.e., larger momentum of the central jet, the height of the central jet increases, and that for smaller central nozzle diameter  $D_j$ , the forward stagnation point moves downstream if keeping fuel volume flow rate fixed, which was also noted during the experiments. The latter can be easily shown as follows:

$$V_{co} = \frac{Q_c}{\frac{\pi}{4} D_j^2}$$

where  $Q_c$  is the fuel volume flow rate. Thus the exit momentum of the central jet,  $G_c$ , is

$$G_c = \rho_c \frac{\pi}{4} D_j^2 V_{co}^2 = \rho_c \frac{Q_c^2}{\frac{\pi}{4} D_j^2}$$

Therefore if the central jet nozzle diameter is reduced, the momentum of the central jet is increased. Hence it can penetrate further into the recirculating zone.

The reason that  $L$  is normalized by  $D_j$ , not by  $L_{rz}$  or  $L_p$  as Tankin did (Ref. 3) is that for Tankin's case, the annular air velocity was very large, the aft stagnation point as reported remained almost constant, and coincided with the penetration point. However, for the present case, the annular velocity was small, the central jet had some effects on  $L_{rz}$  and  $L_p$ , whose changes will be presented in the next section. Considering the unsteady nature of the points, which results in inaccurate measurements, ratios  $L/L_{rz}$  or  $L/L_p$  will amplify measurement errors. In addition curves  $L/L_{rz}$  or  $L/L_p$



vs.  $V_{co}/V_{po}$  has been forced to pass through the point (1,1). Thus in the present case, although all the curves are similar to each other, they never coalesce into one curve. Figures 10 and 11 show curves  $L/L_{rz}$  vs.  $V_{co}/V_{po}$  and  $V_{co}/V_{ao}$  respectively. The solid curves are the results of the least square fit to the experimental data. This is obtained by rearranging the data on Cyber 730 and plotting on the Tektronic plotter. The computer program for this can be found in Appendix B.

From Eq. (3) one could understand why Roquemore & Tankin (Ref. 3) and Namazian (Ref. 7) found out that the axial location of the forward stagnation point was the function of the velocity ratio  $\frac{V_{co}}{V_{ao}}$  only because the nozzle diameters were fixed in their cases.

Table 2. Constant A and Experimental Ranges for Eq. (3)

Authors	A	$R_a$	fluid in central jet
present	1.700	500-1,900	propane
Namazian (Ref. 7)	3.083	20,000-70,000	methane
Tankin (Ref. 27)	3.125	1,250-22,500	air

---

Note: the fluid used in the annular jet is air.

### 5.3 Combusting Flows

The effect of combustion is far more than just a density change. The large amount of heat released by chemical reaction during the combustion process has significant influence on the flow field, flow properties and physical properties of the fluids. A thorough understanding of combustion

process involves the mechanism of chemical reactions and the mixing of reactants and products as well as interactions between them. The distributions of velocity, temperature and species concentrations are required for a complete description of a combustion system. Before such detailed knowledge is obtained, the global features of the system is required, which can be gained by flow visualization technique. For a bluff-body combustor, the region close to the combustor is very important to flame ignition and stabilization. In such a system, combustion processes are conventionally taken for granted to be controlled by mixing and diffusion of various components in the system (Ref. 33), i.e., chemical reactions are almost always assumed to be fast compared with the rate of mixing and the overall rate of reaction is controlled by the rate of mixing. Hence, aerodynamic aspects are emphasized here rather than chemical kinetics and the reaction mechanisms.

#### Observations

It was noticed in the experiments and video tapes that when the annular air velocity at the exit is less than 1.6 m/sec, the flame always remains attached to the combustor surface. However, when the fuel velocity is reduced below a certain value, the flame appears only in the vortex region and opens at the top, i.e., no flame exists along the centerline. The vortices within the recirculating zone entrains the fuel from the central jet. The direction of the rotation of the vortices is such that the combustion products are directed downward along the centerline. In essence, the combustion products extinguish the flame. Thus, no combustion occurs along the centerline - resulting in top-open flame. This was noticed to occur when the forward stagnation point is almost located in the plane of the combustor surface. Plate 5 shows the top-open flame. This kind of top-open flame is different

from that treated first by Lewis and von Elbe (Ref. 19), and later by many others like Law (Ref. 23).

For this top-open flame soot particles are deposited quickly on the combustor surface covering almost 80% of the surface area - the outer 20% being free of soot. After several minutes of burning, this layer may be as high as a few millimeters, having its greatest thickness at the outer edge of the layer. The formation of this soot layer could be explained as follows: since the penetration of the fuel jet is so small (nearly zero), all the soot particles that are formed are trapped in the vortices. Under steady state condition, soot particles which are continuously being formed settle on the combustor surface. The fuel is drawn outward along the combustor surface by the vortices. This fuel flow brings the soot particles outwards to form the greatest thickness of the soot layer at the outer edge of the layer. The formation of soot is discussed in Ref. 2 and 21.

The flame is predominantly yellow in color; however a blue region exists. For the case of an attached flame, this region - short in length - appears in the inner shear layer of the annular jet close to the combustor surface (see Plate 6). For a detached flame no burning appears in the vicinity of the combustor for a distance of between  $(0.5 \sim 1.0) D_1$ . The blue region appears between the upstream non-burning zone and downstream yellow flame (see Plate 7). Vortices are observed near the tip of the fuel penetration - which are highly unstable. The shedding of the vortices is noted to occur simultaneously with large oscillation of the whole flow field - including the flame.

It is interesting to note that the flame in our study always attaches to the combustor surface when the annular air velocity,  $V_{a0}$ , is less than 1.6 m/sec, no matter how the central fuel velocity,  $V_{c0}$ , is changed, either

increased or decreased. However when  $V_{a0}$  exceeds 1.6 m/sec, the flame is attached to the combustor surface for only very small  $V_{c0}$  (see Plate 6). It becomes unstable if  $V_{c0}$  is larger than a certain value, any external disturbances could lead to the flame detachment from the surface. Sirignano has presented the effect of external disturbances on axisymmetric diffusion flame (Ref. 34). In our experiments, when the flame has just detached from the surface, it is easily extinguished. In fact, blow-off was observed several times at this condition during the experiments. Plate 7 shows such detached flames. However if  $V_{c0}$  is increased further, the flame reattaches to the combustor (see Plate 8). The sizes of the recirculation zone and vortices diminish as  $V_{c0}$  continues to be increased. The yellow flame appearing near the stem of the central jet is anchored by the vortices and is reduced with a reduction of the vortex size. These vortices, rotating on their upper boundaries from the annular jet to the central jet, are well organized and have large-scale structure as seen in Plate 8-b and c. At the instant of reattachment, above this yellow flame near the combustor is a blue zone which followed by another yellow flame. The blue flame decreases with the increase of  $V_{c0}$ , and disappears at last. When the annular air jet is fully absorbed by the central jet, the vortices near the combustor surface are no longer observed. Usually the downstream yellow flame dominates the flow, occupying the whole flow region when the blue flame region is absent. Plate 8 shows this. In the photographs, the blue zone is less noticeable than it is in the laboratory perhaps due to dominance of the radiation from the yellow portion of the flame. The downstream yellow flame is severely distorted. The dark region in the flame is the intruded air.

The appearance of the blue flame reported in Reference 7 is similar to the present observation. However, Ramohalli observed (Ref. 32) that the lift-

off (detached) non-premixed flame appeared blue practically devoid of yellow flame (carbon glow). As far as the present observation is concerned, the blue flame seems to surround the yellow flame. This difference may be due to different experimental conditions between those in this study and those of Ramohalli.

The characteristics of the vortices depends on the geometry, the velocities of the central and annular jets. For  $D_j = 6.35$  mm,  $V_{ao} < 1.6$  m/sec, and small  $V_{co}$ , the size of the vortices is comparable with the recirculating zone. However, vortex size is reduced when either the annular jet velocity or the central jet velocity is increased. Plate 9-a shows such a flame (attached).

For  $D_j = 12.7$  mm and  $V_{ao} < 1.6$  m/sec (the flame is attached, see Plate 9-c); the annular vortices are believed to be always located above the forward stagnation point. When  $V_{co}$  values are low, the vortices are large and occupy the region between the forward and aft stagnation points. As  $V_{co}$  is increased, the forward stagnation point pushes the vortices ahead of it. When the forward stagnation point reaches about as high as the central nozzle diameter  $D_j$  (12.7 mm), small vortices form near the tip and stem of the central jet, and vortices due to the annular jet appear at the outside edge of the combustor surface. These annular vortices are designated as lower vortices. Initially the annular vortices which are being pushed forward by the central jet are called the upper vortices. The upper vortices are reduced in size and intensity as the forward stagnation point pushes them towards the aft stagnation point, and lose their identity as penetration of the central jet through the recirculating zone occurs. During this process the lower vortices behave very similarly to those of  $D_j = 6.35$  mm (Plate 9-a).

The development of the vortices for  $D_j = 9.45$  mm and  $V_{ao} < 1.6$  m/sec is

between the above two cases. Since the space between two jets is large enough to allow the vortices due to the annular jet (annular jet vortices) to remain more or less fixed in location. However, there is distortion of such vortices due to the vortices caused by the central jet (central jet vortices). These central jet vortices alternately shed and thus distort the annular jet vortices. The rotations of the annular jet vortices are opposite to those of the central jet vortices. Plate 9-b shows the annular jet vortices and the central jet vortices. The annular jet vortices are the outer ones and the central jet vortices are the inner pairing ones. When the central jet velocity increases, the inner vortices (central jet vortices) grow and the height of their centers increases; the outer vortices (annular jet vortices) are distorted. In this photograph, the inner vortices are asymmetrically shed (the right one is about to move downward and out along the combustor surface; the left one will grow and move upwards until it reaches an elevation of the right one), distorting the annular vortices asymmetrically. Thus, the flow field is dynamically changing, and an axisymmetrical model is inadequate for this flame. The dark region near the central nozzle exit and between the inner and outer vortices is fuel, which is turned at the forward stagnation point and moves downward to the combustor surface, then outward to the boundary of the recirculating zone, where the blue flame appears. The inner and outer vortices are green indicating they contain  $TiO_2$  particles. An important question that is not answered is why the  $TiO_2$  particles occurs in the central jet region (the inner vortices) - since  $TiO_2$  particles are formed from the reaction of  $TiCl_4$  with water vapor which is one of the combustion products. A possible explanation is that these  $TiO_2$  particles may have come from the fuel line before the nozzle exit.

For  $V_{ao} > 1.6$  m/sec, the vortices appear as the flame attaches to the

surface for low  $V_{CO}$  (the order of magnitude is centimeters per second), and no stationary vortices could be observed for detached flames. However, the flow field and flame are disturbed violently as vortices are shed near the tip of the central jet for detached flames. The shed vortices first move downward, outward and then upward along the recirculation zone boundary. The overall flame structure also moves with these shed vortices. The flame becomes attached again from the detachment if  $V_{CO}$  is increased above a certain value. Vortices due to the annular jet form near the combustor surface again. Thus, it may be regarded that the large-scale annular jet vortices in the recirculating zone are very important for the flame attachment. These vortices are not observed in the detached flame. For Test III, reattachment was not observed - blow-off usually occurs when the central jet velocity is slightly increased after the flame is detached. Probably, the spaces between the two jets, and of the entire recirculating zone are so small that only very small amount of the fluid circulates in the recirculating zone. Therefore, large bluff bodies and small central nozzles, that is, large values of  $D_1$  and  $D_1-D_2$ , have beneficial effects on the flame stabilization.

In Plate 4-b, where the blockage ratio is only 32%,  $TiO_2$  particles are added to the fuel jet, thus resulting in visualization of the streamlines. In this case, the flame boundary is smooth and extends to the combustor surface. The flame in this photograph starts at the outer edge of the combustor, contracts downstream first, then diverges as it spreads further downstream, and the flame thickness also increases downstream. The streamlines in the recirculating zone diverge before the forward stagnation point (bright horizontal zone). No streamlines in the central fuel jet reach the flame front, which is the case for the Bunsen flame as shown by Lewis and von Elbe (Ref. 29).

The flow field becomes turbulent when the flame lifts from the surface at a distance less than one diameter of the inner annulus,  $D_i$ , which was also reported in Ref. 7, and measured by Ramohalli (Ref. 32). The large fluctuations of the flow field occurs due to the vortices being shed. The small unsteady vortices in the recirculating zone have replaced the large-scale, orderly annular air jet vortices. The central jet becomes a mushroom shape (see Plate 7). The flame surface is violently distorted. The blue flame in the photographs is less noticeable than it is in the laboratory. It is clear from the photographs that the flame initiates around the aft stagnation point, where the mean velocity is very small, and the large fluctuations there are instrumental to the mixing of air and fuel. The flame is confined to a region downstream of the aft stagnation point. This differs from Namazian's finding (Ref. 7) in that he reported that the flame initiation was around the forward stagnation point, where the central jet terminated on the central axis. In his experiments, both the central and annular velocities were much larger than in the present study, and the fuel was methane. Although his geometry is similar to that of the present study, our present experimental set-up is not capable of obtaining such high velocities.

The criterion for characterizing the flow field as was done in the cold reacting flow is extremely difficult owing to the onset of combustion. For example, the flame may be attached, detached, or blown off for the same annular velocity. Beer and Chigier stated (Ref 24): "Although geometrical similarity can be maintained for studies of non-compressible fluid dynamics in isothermal system, it has to be abandoned when the system is non-isothermal or when chemical reaction plays an important role in the process investigated." The distribution of the velocity, temperature and species concentrations in the flow field affects the chemical reaction, which, in turn, influences the



flow field by releasing large amount of heat. Thus, the fluid mechanics, the heat transfer, and chemical reactions are coupled. The flow field is extremely complicated, no relationship between  $\frac{L}{D_j}$  and flow conditions as well as geometries could be found (experimental data for the combustng flow can be found in Appendix D). Such a relation requires considering the details of the flow field and chemical kinetics. According to Damköhler model (Ref. 24), five dimensionless parameters have to be considered. They are:

1. chemical reaction/bulk flow;
2. chemical reaction/molecular diffusion;
3. heat released/heat transported by bulk flow;
4. heat released/heat transported by conduction;
5. momentum transported by bulk flow/momentum transferred by viscosity (Reynolds number).

Normally it is extremely difficult to obtain empirical formula using the above five ratios due to limitations of measurement. Detailed chemical composition, temperature and velocity measurements are needed to understand the combustion process.

#### 6. Some Comparisons

This section is divided into two subsections: the first subsection presents comparisons between the pure annular free jet and the cold reacting flow. The comparisons between the cold reacting flow and combustng flow are given in the second subsection.

### 6.1 Comparison Between the Pure Annular Jet and the Cold Reacting Flow

The introduction of the central jet into the vortex region established by the annular jet changes the flow pattern in the recirculating zone substantially. It may push away the vortices, distort them, or even make the irregular small vortices take the place of the large-scale vortices present in the case of the pure annular jet. The results of this interaction between the vortices and the central jet depend on the relative magnitude of the momenta of the central and annular jets, and the space between two jets (or  $D_1 - D_j$ ). These are shown in Plate 1-b, Plate 2, 3 and 4-a as well as in Figures 3, 5 and 7.

Figure 8 shows that when the central jet velocity is increased from zero (pure annular jet) to penetration velocity (when the central jet penetrates through the recirculating zone, i.e., when  $L = L_{rz} = L_p$ ), the length of the recirculating zone,  $L_{rz}$ , increases from its value for the pure annular jet to the penetration length,  $L_p$ . At penetration,  $L = L_{rz} = L_p$ . The presence of the central jet causes the aft stagnation point to move further downstream. Thus, the central jet effectively changes the shape and extent of the recirculating zone. However, Fujii et al. (Ref. 16) found that the introduction of the central jet into the flow field behind a bluff body placed in a ducted stream shifted the recirculating zone upstream, this is contrary to our finding. Figure 8 also shows that the effect of the central nozzle diameter on the length of the recirculating zone. At the same central jet velocity,  $L_{rz}$  is larger for the larger central nozzle diameter. This is probably due to the larger momentum of the central jet, which is proportional to the nozzle exit area. When the velocity of the annular jet is increased, the influence of the central jet on the length of the recirculation zone is reduced. For large annular velocity, as reported in Ref. 3, the length of the

recirculation zone  $L_{rz}$  is almost constant, and independent of the central jet velocity. Thus,  $L_{rz} = L_p$  in this case.

## 6.2 Comparison Between Cold Reacting and Combusting Flows

The spreading of the detached and attached flames leads to two different phenomena from that of the cold reacting flow. For the attached flame, as described before, the flow is laminar, thus along the boundary of the recirculating zone, only species diffusion could occur as the means of the mass exchange across the boundary except the region very close to the combustor surface. Probably a stoichiometric fuel-air mixture occurs in the immediate vicinity of the combustor where the flame is blue. Then the flame spreads downstream along the boundary surface, converging at the central axis around the forward stagnation point developing further downstream (see Plate 9). In this case, the fluid viscosity is increased very much (approximately 10 times, see Ref. 3). Thus, compared with the cold reacting flow, this results in the faster growth of the boundary layer, which starts at the separation point (outer edge of the combustor) where its thickness is zero. Therefore, the onset of combustion reduces the recirculating zone. As observed from the experiments, the forward and aft stagnation points are moved closer to the combustor surface for the combusting flow than for the corresponding cold reacting flow (e.g., compare Plate 4-b to Plate 2-b). Figure 9 shows  $\frac{L_p}{D_i}$  vs.  $R_a$  for the cold reacting flow and the combusting flow (attached flame only). It is clear that the combustion causes the penetration length or the recirculating zone length to be reduced by more than half. Thus, it is much easier for the central fuel jet to penetrate through the recirculating zone in the combusting case. The penetration velocity increases with the annular air velocity for both cold and combusting flow cases.

However, the measured value  $V_{co}$  at penetration (i.e.,  $V_{po}$ ) and its incremental change corresponding to an incremental change in  $V_{ao}$  is much smaller in the presence of the flame (0.5 ~ 1.0 times smaller) than those for the corresponding cold reacting flow. This may be due to the corresponding reduction of the recirculating zone length in the attached flame. The shortening effect of the laminar flame on the length of the recirculating zone was also observed by Lewis and von Elbe for the flow behind the end of a small cylinder inserted into a low-velocity stream (Ref. 29). However, their results were for a premixed flame.

For the detached flame, the flow field is violently disturbed, perhaps due to the sudden expansion of combustor mixture, turbulence, and the shedding of vortices. The flame first appears in the region between the forward and aft stagnation points (closer to the aft one). It was observed that the forward stagnation point in the detached flame is shifted significantly closer to the combustor surface compared to the cold reacting flow; and the aft stagnation point moves slightly downstream. Quantitative values were not obtained due to limitations of the present experimental set-up. This finding is contrary to Namazian's result (Ref. 7), which showed that the fuel jet had greater height for the combustor flow than for the cold reacting flow. But it should be noted that Namazian used methane as fuel and the exit velocities of the fuel and air were about 10 times greater than in this study. The prolonging of the recirculating zone was also reported in the literature for bluff-body flame stabilizers inserted in premixed streams in a duct (e.g., see Ref. 15 and 30).

Due to the reduction of the recirculating zone with attached flames, the vortices sizes are also limited. However, the vortices seem more orderly, stationary, and intense. These have been presented in the previous sections.

## 7. Analytical Approach

The flow field behind a combustor is so complex that no analytical solution nor numerical solution for unducted flow are available. The present analytical approach is made possible by employing the scaling method proposed by Bejan (Ref. 31) even without knowing the details of the flow field. Due to the extreme complexities in the combustor flow case, the analyses here are only given to the pure annular air jet and the cold reacting flow cases.

The governing equations are continuity and momentum equations expressed in cylindrical coordinate as follows:

$$\frac{\partial u_r}{\partial r} + \frac{u_r}{r} + \frac{\partial u_z}{\partial z} = 0 \quad (4)$$

$$u_r \frac{\partial u_r}{\partial r} + u_z \frac{\partial u_r}{\partial z} = -\frac{1}{\rho} \frac{\partial p}{\partial r} + \nu \left( \frac{\partial^2 u_r}{\partial r^2} + \frac{1}{r} \frac{\partial u_r}{\partial r} - \frac{u_r}{r^2} + \frac{\partial^2 u_r}{\partial z^2} \right) \quad (5)$$

$$u_r \frac{\partial u_z}{\partial r} + u_z \frac{\partial u_z}{\partial z} = -\frac{1}{\rho} \frac{\partial p}{\partial z} + \nu \left( \frac{\partial^2 u_z}{\partial r^2} + \frac{1}{r} \frac{\partial u_z}{\partial r} + \frac{\partial^2 u_z}{\partial z^2} \right) \quad (6)$$

By these equations, we have assumed that the flow field is steady and axisymmetrical, and the gravitational effect is negligible.

### 7.1 Pure Annular Air Jet

By scaling method, the Equations (4)-(6) can be expressed for the flow around the recirculating zone as

$$\frac{u_r}{r} \sim \frac{u_z}{z} \quad (7)$$

$$\frac{u_r^2}{r} + u_z \frac{u_r}{z} \sim -\frac{1}{\rho_a} \frac{p}{r} + \nu_a \left( \frac{u_r}{r^2} + \frac{u_r}{z^2} \right) \quad (8)$$

$$u_r \frac{u_z}{r} + \frac{u_z^2}{z} \sim -\frac{1}{\rho_a} \frac{p}{z} + \nu_a \left( \frac{u_z}{r^2} + \frac{u_z}{z^2} \right) \quad (9)$$

where  $u_r$  and  $u_z$  should be regarded as characteristic velocity of the flow field around the recirculation zone. Similarly,  $r$  and  $z$  are characteristic length.

Substituting Equation (7) into (8) and (9), then eliminating pressure term gives

$$\left[ \left( \frac{r}{z} \right)^2 - 1 \right] u_z^2 \sim \nu_a \left[ \frac{1}{r^2} + \frac{1}{z^2} \right] \left[ \left( \frac{r}{z} \right)^2 - 1 \right] u_z z \quad (10)$$

The solutions are

$$\frac{r}{z} \sim 1 \quad (11)$$

$$u_z \sim \nu_a \left[ \frac{1}{r^2} + \frac{1}{z^2} \right] z \quad (12)$$

Now for the flow around the recirculating zone, from the mean velocity distribution along the centerline reported in the literature (e.g., Ref. 11, 13 and 22), it may be assumed that

$$u_z \sim V_{AO};$$

$$r \sim \frac{D_1}{2} \sim D_1;$$

$$\text{and} \quad z \sim L_{rz}.$$

Thus, Equation (11) becomes

$$\frac{L_{rz}}{D_1} \sim 1 \quad (13)$$

and Equation (12) leads to

$$v_{ao} \sim v_a \left( \frac{1}{D_1^2} + \frac{1}{L_{rz}^2} \right) L_{rz}$$

or

$$\frac{D_o - D_1}{D_1} \frac{L_{rz}}{D_1} - R_a \frac{L_{rz}}{D_1} + \frac{D_o - D_1}{D_1} \sim 0 \quad (14)$$

where  $R_a = \frac{v_{ao}(D_o - D_1)}{v_a}$ . Therefore, the solutions of Equation (14) are obtained if it is assumed that  $R_a \gg \frac{D_o - D_1}{D_1}$ , which is always true in this study:

$$\frac{L_{rz}}{D_1} \sim \frac{D_1}{D_o - D_1} R_a$$

and

$$\frac{L_{rz}}{D_1} \sim \frac{D_o - D_1}{D_1} \frac{1}{R_a}$$

or

$$\frac{L_{rz}}{D_1} = C_1 R_a \quad (15)$$

and

$$\frac{L_{rz}}{D_1} = \frac{C_1^{-1}}{R_a} \quad (16)$$

Thus, the three solutions are:  $\frac{L_{rz}}{D_1} = C_1 R_a$ ,  $\frac{C_1^{-1}}{R_a}$ ,  $C_2$  ( $C_2 = O(1)$ ), where  $C_1$  is a function of the geometries,  $C_2$  is a function of the blockage ratio and forebody shape. When compared with Figure 4, it seems that Equation (15) is suitable for the laminar flow in which case the length of the recirculating zone increases with  $R_a$ . Equation (15) shows that if  $R_a = 0$ , i.e.,  $v_{ao} = 0$ , no recirculating zone could exist. Equation (16) appears to be valid for the transition flow region, and Equation (13) appears to be valid when the flow is fully turbulent ( $R_a \rightarrow \infty$ ). For example, some authors like Durão and Whitelaw (Ref. 11) reported that for very large  $R_a$  (about  $10^5$ ),  $\frac{L_{rz}}{D_1}$  was constant. The transition region and fully turbulent flow region (Equations (13) and (16))

will be combined as

$$\frac{L_{rz}}{D_i} = (C_2 + \frac{C_1^{-1}}{R_a})$$

Thus, there are two adjustable constants ( $C_1$  and  $C_2$ ). Fig. 4 shows the results when  $C_1$  is set equal to 0.006 and  $C_2$  to 0.934. These results are in general agreement with the experiments.

## 7.2 Cold Reacting Flow

Because of the fact that the region of subatmospheric pressure behind a bluff body, formed by bending streamlines, is set up by the annular air jet, it may be valid to assume that for both jets, the pressure gradients in the  $r$ -direction which cause the annular streamlines to converge radially inward and the central jet streamlines to diverge outward are at the same order of magnitude (they are comparable), i.e.,

$$(\frac{\partial p}{\partial r})_a \sim (\frac{\partial p}{\partial r})_c \quad (17)$$

Again using scaling arguments, the following assumptions for the central flow are made:

$$u_{cz} \sim V_{co};$$

$$z \sim L;$$

and  $r \sim D_j.$

Thus, Equations (4) and (5) become

$$\frac{u_{cr}}{D_j} \sim \frac{V_{co}}{L} \quad (18)$$



$$u_{cr} \frac{u_{cr}}{D_j} + v_{co} \frac{u_{cr}}{L} \sim - \frac{1}{\rho_c} \left( \frac{\partial p}{\partial r} \right)_c + v_c \left( \frac{u_{cr}}{D_j^2} + \frac{u_{cr}}{L^2} \right) \quad (19)$$

where  $L$  is the location of the forward stagnation point along the  $z$  axis.

Likewise, for the annular air jet, it is assumed that

$$u_{az} \sim V_{ao} ;$$

$$r \sim D_1 ;$$

$$\text{and } z \sim L_{rz} .$$

Thus, applying Eqs. (4) and (5) to the annular jet leads to

$$\frac{u_{ar}}{D_1} \sim \frac{V_{ao}}{L_{rz}} \quad (20)$$

$$u_{ar} \frac{u_{ar}}{D_1} + v_{ao} \frac{u_{ar}}{L_{rz}} \sim - \frac{1}{\rho_a} \left( \frac{\partial p}{\partial r} \right)_a + v_a \left( \frac{u_{ar}}{D_1^2} + \frac{u_{ar}}{L_{rz}^2} \right) \quad (21)$$

Combining Equations (18) with (19), and (20) with (21), then using relation (17) gives the following equation:

$$R_c^2 \frac{L}{D_j} - R_c \left( \frac{L}{D_j} \right)^2 + 1 \sim \frac{1}{E^2} \left( \frac{L}{D_j} \right)^3 ; R_a^2 \left( \frac{D_1}{D_o - D_1} \right)^2 \frac{D_1}{D_1^3} - R_a \left( \frac{D_1}{D_o - D_1} \right) \left( \frac{D_1}{D_1^3} \right) ; \quad (22)$$

$$\text{where } R_c = \frac{V_{co} D_j}{v_c} , \quad R_a = \frac{V_{ao} (D_o - D_1)}{v_a} , \quad E = \frac{v_c}{v_a} \frac{\rho_c}{\rho_a} \frac{1}{L^2}$$

and  $L_{rz}$  has been replaced by  $D_1$  since from the measurements  $\frac{L_{rz}}{D_1}$  is order of unity and changes only slightly (e.g., see Figure 8).

Now if  $R_c \gg \frac{L}{D_j} + \frac{D_1}{L}$  (which it is), the second term is negligible compared with the first term on the left hand side of the Equation (22). Likewise, if  $R_a \gg \frac{D_o - D_1}{D_1}$  (which it is), the second term on the right hand side of the same equation can be neglected compared with the first term. Thus, Equation (22) reduces to

$$R_c^2 \sim \frac{1}{E^2} \frac{L}{D_j} R_a^2 \frac{D_1}{D_o - D_1} \sim \frac{D_1}{D_1} \sim 1$$

$$\text{or } \frac{L}{D_j} \sim E R_c R_a^{-1} \frac{D_o - D_1}{D_1} \sim \frac{D_1}{D_j} \sim 1.5 \quad (23)$$

It is remarkable to note that Eq. (23), our very simplified analytical result, appears to be exactly the same as that obtained from the experimental data, Eq. (3). From the definition of E

$$E = \frac{\mu_c / \rho_c^{0.5}}{\mu_a / \rho_a^{0.5}} \\ = \frac{\mu_c / \rho_a^{0.5}}{\mu_a / \rho_c^{0.5}}$$

where  $\mu_c$  and  $\mu_a$  are the dynamic viscosities of the fluids in the annular and central jets, respectively. It has been shown here that the constant A in Eq. (3) is a function of the physical properties of the fluids in the two jets as presented before, i.e.,

$$A = BE$$

where B is a constant. Using the equation of state for the perfect gas, we have

$$\frac{\rho_a}{\rho_c} = \frac{M_a}{M_c}$$

where  $M_a$  and  $M_c$  are the molecular weights of the fluids flowing in the annular and central jets. Table 3 gives the values of  $\mu$  (from Ref. 35) and  $M$  (from Ref. 36) for propane, air and methane corresponding to the fluids used in the experiments of this study, Tankin (Ref. 27) and Namazian (Ref. 28). The values of A, B, and E corresponding to these studies are given in Table 4 where the

value of A is taken from Table 2. The value of B as shown in Table 4 is almost constant if one considers the uncertainty of the experiments. Thus, Eq. (23) could be expressed in a more general form:

$$\frac{L}{D_j} = B \left( \frac{u_c}{u_a} \right)^{0.5} \left( \frac{D_a}{D_c} \right)^{1.5} \left( \frac{R_c}{R_a} \right)^{0.5} \left( \frac{D_1}{D_j} \right)^{1.5} \left( \frac{D_0 - D_1}{D_1} \right) \quad (24)$$

Table 3. Values of  $\mu$  and  $M$  for Propane, Air and Methane

Fluid	$\mu^*$ (at 30°C)	$M$
Propane	84	44.097
Air	186	28.96
Methane	113	16.04

\*The unit of  $\mu$  is  $10^{-7}$  gm cm sec.

Table 4. Values of A, B and E

Authors	Fluid in Central Jet	A	E	B
Present	Propane	1.700	0.3660	4.644
Tinkin Ref. 17	Air	3.125	1.0000	3.125
Namazian Ref. 7	Methane	3.183	1.4163	3.777

#### 4. Conclusions

The following conclusions may be extracted from this study:

The denigrating zone length has a maximum around 700-800 mm.

Reynolds number and tends to approach a constant value of the order of unity for large annular Reynolds number in the case of the pure annular air flow.

(2) For the cold reacting flow, an empirical formula for the axial location of the forward stagnation point in terms of the exit flow conditions and nozzle diameters is found:

$$\frac{L}{D_j} = A \frac{R_a}{R_j} \left( \frac{D_i}{D_j} \right)^{1.5} \frac{D_o - D_i}{D_i}$$

The introduction of the central jet into the recirculating zone causes the aft stagnation point to move downstream and increases the size of the recirculating zone. However, if the annular air velocity is less than 0.5 m/sec, no regular, orderly recirculating zone could be formed.

(3) If the annular air velocity is less than 1.6 m/sec, the flame is always attached to the combustor surface, if the annular air velocity is greater than 1.6 m/sec, the flame is attached for the low central fuel velocity, detached if the central fuel velocity is increased over a certain value, and then reattached to the combustor for further increase in the central fuel velocity. This was an unexpected and unexplained result. The structures of the central jet and the recirculating zone are greatly different for these attached, detached and reattached flames.

4. In the presence of the attached flame, the forward and aft stagnation points are much closer to the combustor than in the corresponding cold flow. For the detached flame, the forward stagnation point moves upstream considerably whereas the aft stagnation point moves downstream slightly when compared to the corresponding cold reacting flow.

5. For the attached flame, the vortices due to the annular jet are more orderly, stationary and intense than those in the cold reacting flow. These

are also true for the vortices due to the central jet. For the detached flame, usually no orderly vortices could be observed, occasionally the unsteady vortices shed at the tip of the central jet disturb the whole flow field significantly. Only the well-organized vortices due to the annular jet could be observed near the combustor for the reattached flame. Thus, it seems that the large-scale well-organized annular jet vortices are crucial to the flame reattachment.

More work is needed to understand the flame stabilization processes and flow field dynamics. In the future, it would be very fruitful to correlate the visualization of vortex dynamics with the results of simultaneous pointwise measurements made with advanced diagnostic techniques such as laser Doppler anemometer and coherent anti-stokes Raman spectroscopy as being undertaken at the Aer. Propulsion Laboratory at Wright-Patterson AFB.

# Nomenclature

- $L$  - the height of the central jet, or the distance between the forward stagnation point and the combustor surface
- $L_p$  - length of the recirculation zone when the central jet penetrates through it
- $L_{rz}$  - length of the recirculation zone
- $M$  - molecular weight
- $r$  - radial coordinate
- $R_a = \frac{1}{2} V_{ao} (D_o^2 - D_i^2) \rho_a$
- $R_{oi} = \frac{1}{2} V_{ao} D_i^2 \rho_a$
- $R_o = \frac{1}{2} V_{ao} D_o^2 \rho_o$
- $u$  - velocity
- $u_{ao}$  - velocity of the annular jet at the outer nozzle exit
- $u_{oi}$  - velocity of the central jet at the inner nozzle exit
- $u_{oz}$  - velocity of the central jet when it penetrates through the recirculation zone; i.e., when  $L = L_{rz} = L_p$
- $\alpha = \frac{\frac{1}{2} u_{oi}^2 D_i^2 \rho_o}{\frac{1}{2} V_{ao}^2 (D_o^2 - D_i^2) \rho_a}$  momentum ratio of the central jet to the annular
- $z$  - vertical coordinate
- $\mu$  - density of fluid
- $\nu$  - kinematic viscosity
- $\nu_o$  - kinematic viscosity
- $\rho$  - density
- $\rho_a$  - annular jet
- $\rho_o$  - central jet
- $D_o$  - diameter at the outer nozzle exit
- $D_i$  - diameter of recirculation
- $D$  - diameter of orifice

## References

1. Beer, J. M., Chigier, N. A. and Lee, K. B. (1963), Modeling of the Double Concentric Burning Jets, Ninth Symposium (International) on Combustion, The Combustion Institute, Academic Press, New York, p. 892.
2. Glassman, I. (1977), Combustion, Academic Press.
3. Roquemore, W. M. and Tankin, R. S., et al., The Role of Vortex Shedding in a Bluff Body Combustor, Symposium on Experiments and Techniques in Turbulent Reactive and Non-Reactive Flows, ASME 105th Winter Annual Meeting.
4. Roquemore, W. M., et al. (1983), Influence of the Vortex Shedding Process on a Bluff-Body Diffusion Flame, AIAA-83-0335.
5. Switzer, G. L., et al. (1983), Simultaneous CARS and Luminosity Measurements in a Bluff-Body Combustor, AIAA-83-1481.
6. Kyoji, Kimoto, et al. (1981), Structure of Turbulent Jet Flame Stabilized in Annular Air Jet, Combustion Science and Technology, Vol. 25, pp. 31-41.
7. Namazian, M., et al. (1985), Flow and Combustion in Bluff-Body stabilized Flames, presented at the Combustion Institute, San Antonio, Texas, Paper No. 2-1B.
8. Scott, J. M. and Hankey, W. K. (1983), Numerical Simulation of Cold Flow in an Axisymmetric Centerbody Combustor.
9. Craig, R. R., et al. (1984), A General Approach for Obtaining Unbiased LDV Data in Highly Turbulent Non-Reacting and Reacting Flows, AIAA-84-0366.
10. Lysaght, A. J. R., Bilger, R. W. and Kent, J. H. (1982), Visualization of Mixing in Turbulent Diffusion Flames, Combustion and Flame 46, pp. 105-108.
11. Durão, D. F. G. and Whitelaw, J. H. (1978), Velocity Characteristics of the Flow in the Near Wake of a Disk, J. Fluid Mech., Vol. 85, Part 2, pp. 369-385.
12. Taylor, A. M. P. K. and Whitelaw, J. H. (1984), Velocity Characteristics in the Turbulent Near Wakes of Confined Axisymmetric Bluff Bodies, J. Fluid Mech., Vol. 139, pp. 391-416.
13. Davies, T. W. and Beer, J. M. (1971), Flow in the Wake of Bluff-Body Flame Stabilizers, Proc. 13th Int. Symp. Combustion, p. 361.
14. Pope, S. B. and Whitelaw, J. H. (1976), The Calculation of Near-Wake Flows, J. Fluid Mech., Vol. 73, Part 1, pp. 9-32.

15. Winterfeld, G. (1965), On Processes of Turbulent Exchange Behind Flame Holders, Proc. 10th Int. Symp. Combustion, pp. 1265-1275, Combustion Institute, Pittsburgh.
16. Fujii, S., Gomi, M. and Eguchi, K. (1978), Cold Flow Tests of a Bluff-Body Flame Stabilizer, Trans. ASME I: J. Fluids Engng. 100, pp. 323-333.
17. Bradbury, L. J. S. (1976), Measurements with a Pulsed-Wire and a Hot-Wire Anemometer in the Highly Turbulent Wake of a Normal Flat Plate, J. Fluid Mech. 77, pp. 473-497.
18. Carmody, T. (1964), Establishment of the Wake Behind a Disc, Trans. ASME D: J. Basic Engng. 86, pp. 869-882.
19. Tankin, R. S. (1984), Study of Forward and Aft Stagnation Points in Cold Reacting and Combusting Flows, Proposal to Southeastern Center of Electrical Engineering Education.
20. Chigier, N. A. and Beer, J. M. (1964), The Flow Region Near the Nozzle in Double Concentric Jets, J. Basic Engng. 86, pp. 797-804.
21. Strehlow, R. A. (1984), Combustion Fundamentals, McGraw-Hill Co.
22. Calvert, J. R. (1967), Experiments on the Low-Speed Flow Past Cones, J. Fluid Mech., Vol. 27, Part 2, pp. 273-289.
23. Law, C. K., et al. (1982), On the Opening of Premixed Bunsen Flame Tips, Combustion Science and Technology, Vol. 28, pp. 89-96.
24. Beer, J. M. and Chigier, N. A. (1972), Combustion Aerodynamics, Halsted Press Division, John Wiley & Sons, Inc., New York.
25. Abramovich, G. N. (1963), The Theory of Turbulent Jets, MIT Press, Cambridge, Massachusetts.
26. Zukoski, E. E. and Marble, F. E. (1956), Gasdynamics Symposium, p. 205, Northwestern University, Evanston, Illinois.
27. Tankin, R. S. (1984), unpublished notes.
28. Dyer, M. J. and Crosley, D. R. (1982), Optics Letters, Vol. 7, p. 382.
29. Lewis and von Elbe, Combustion, Flames and Explosions of Gases, 2nd Ed., (1961), Academic Press, Inc.
30. Fujii, S. and Eguchi, K. (1981), A Comparison of Cold and Reacting Flows Around a Bluff-Body Flame Stabilizer, J. Fluid Engng., Vol. 103, p. 328.
31. Bejan, A. (1984), Convection Heat Transfer, John Wiley & Sons.
32. Ramohalli, et al. (1981), Some Experimental Data on Liftoff Characteristics in Turbulent Jet Flames, Combustion Science and Technology, Vol. 36, pp. 199-203.



33. Libby, P. A. and Williams, F. A., Eds. (1980), Turbulent Reacting Flows, Springer-Verlag, Berlin, pp. 65-113.
34. Sirignano, W. A., et al. (1971), The Effect of High-Frequency Periodic Disturbances on Axisymmetric Wake Diffusion Flames, Combustion Science and Technology, Vol. 2, pp. 351-364.
35. Kanury, A. M. (1975), Introduction to Combustion Phenomena, Gordon Breach.
36. Rossini, F. D., et al. (1953), Selected Values of Physical and Thermodynamic Properties of Hydrocarbon and Related Compounds, API Research Project 44, Carnegie Institute of Technology, Pittsburgh, Pennsylvania.

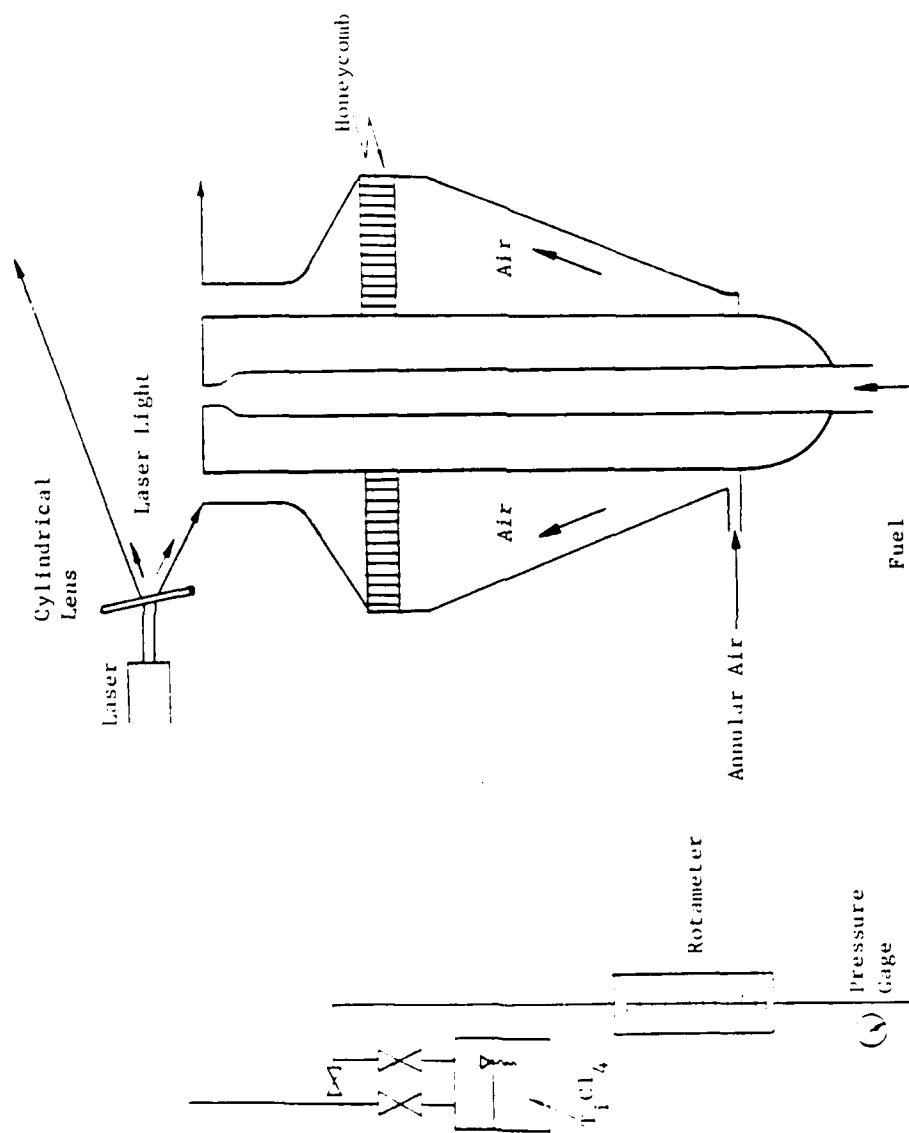


Fig. 1. Illustration of the experimental set-up.

$$D_o = 53.2 \text{ mm}$$

$$D_i = 38.5 \text{ mm}$$

$$D_j = 6.35 \text{ mm}; 9.45 \text{ mm}; 12.7 \text{ mm}$$

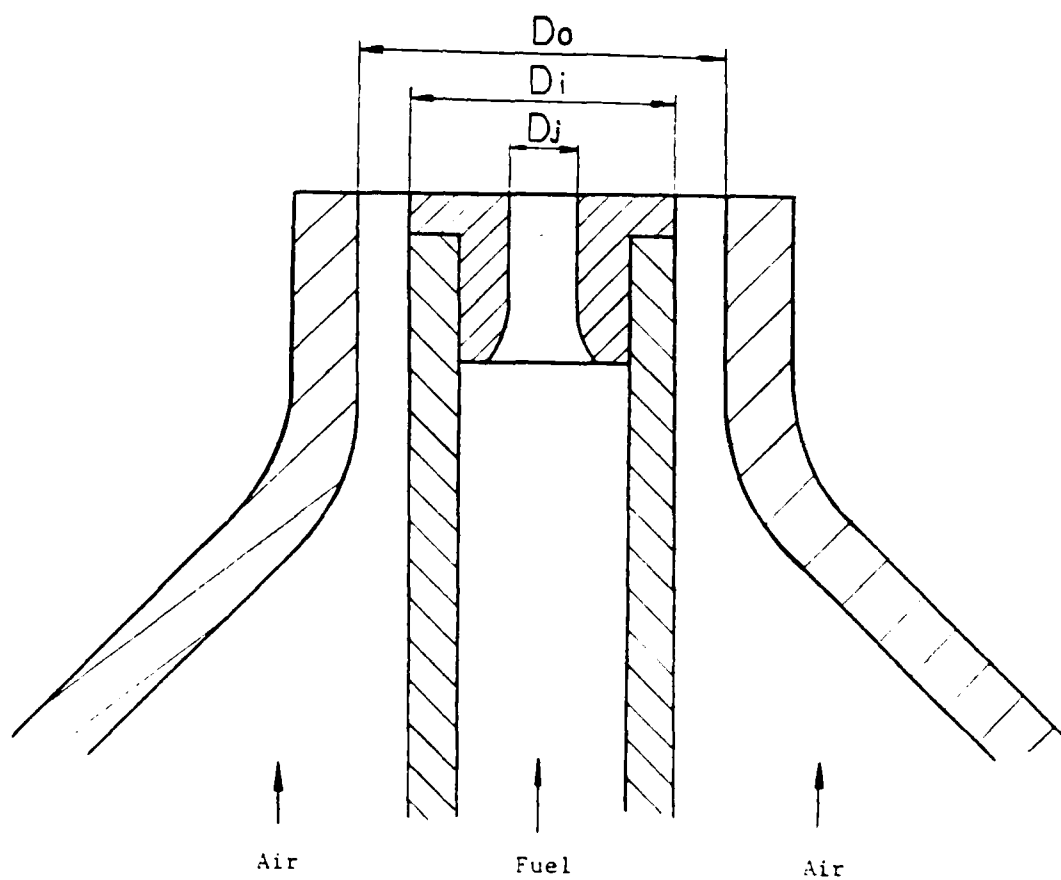


Fig. 2a. Schematic drawing of fuel and air nozzles used in Test 1.

$D_o = 53.2 \text{ mm}$

$D_i = 45.2 \text{ mm}$

$D_j = 6.35 \text{ mm}; 9.45 \text{ mm}; 12.7 \text{ mm}$

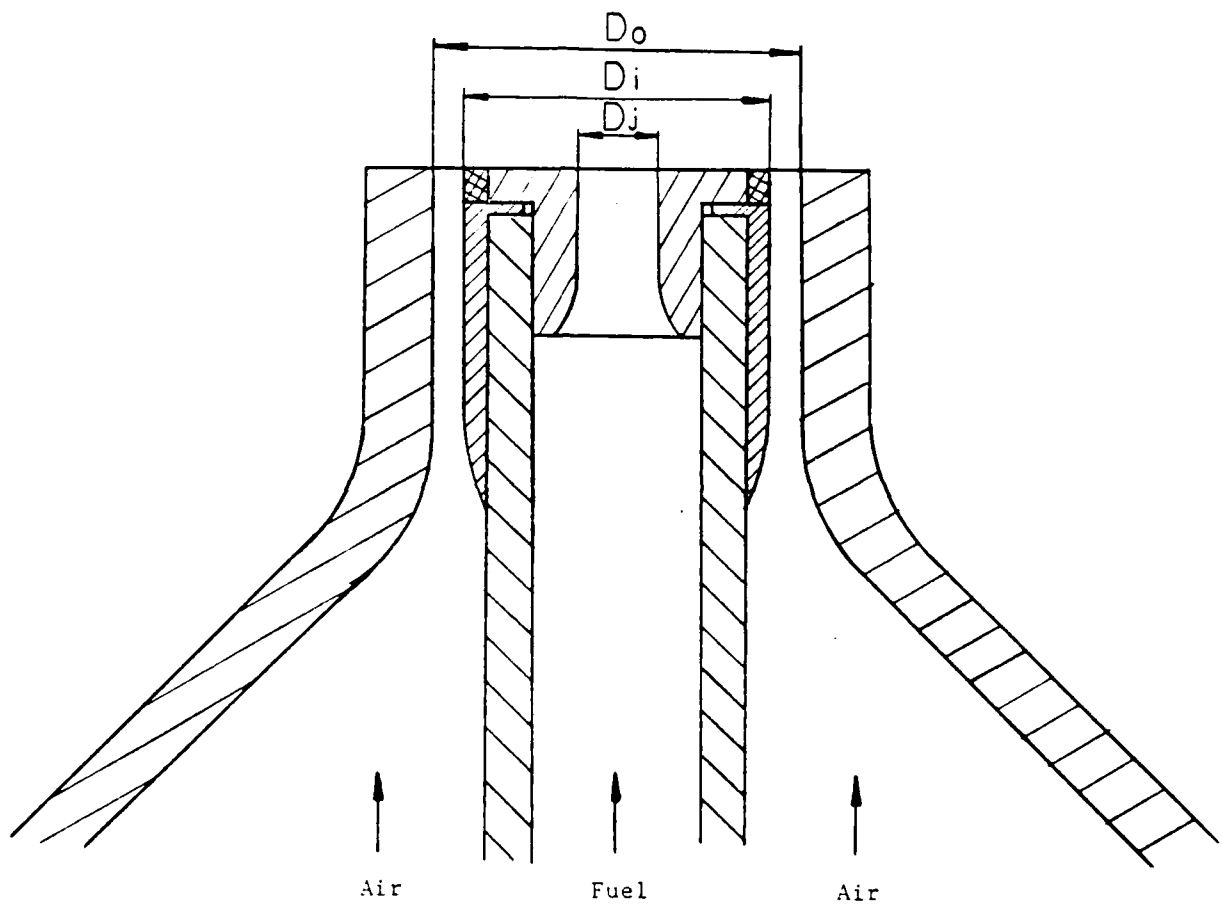


Fig. 2b. Schematic drawing of fuel and air nozzles used in Test II.

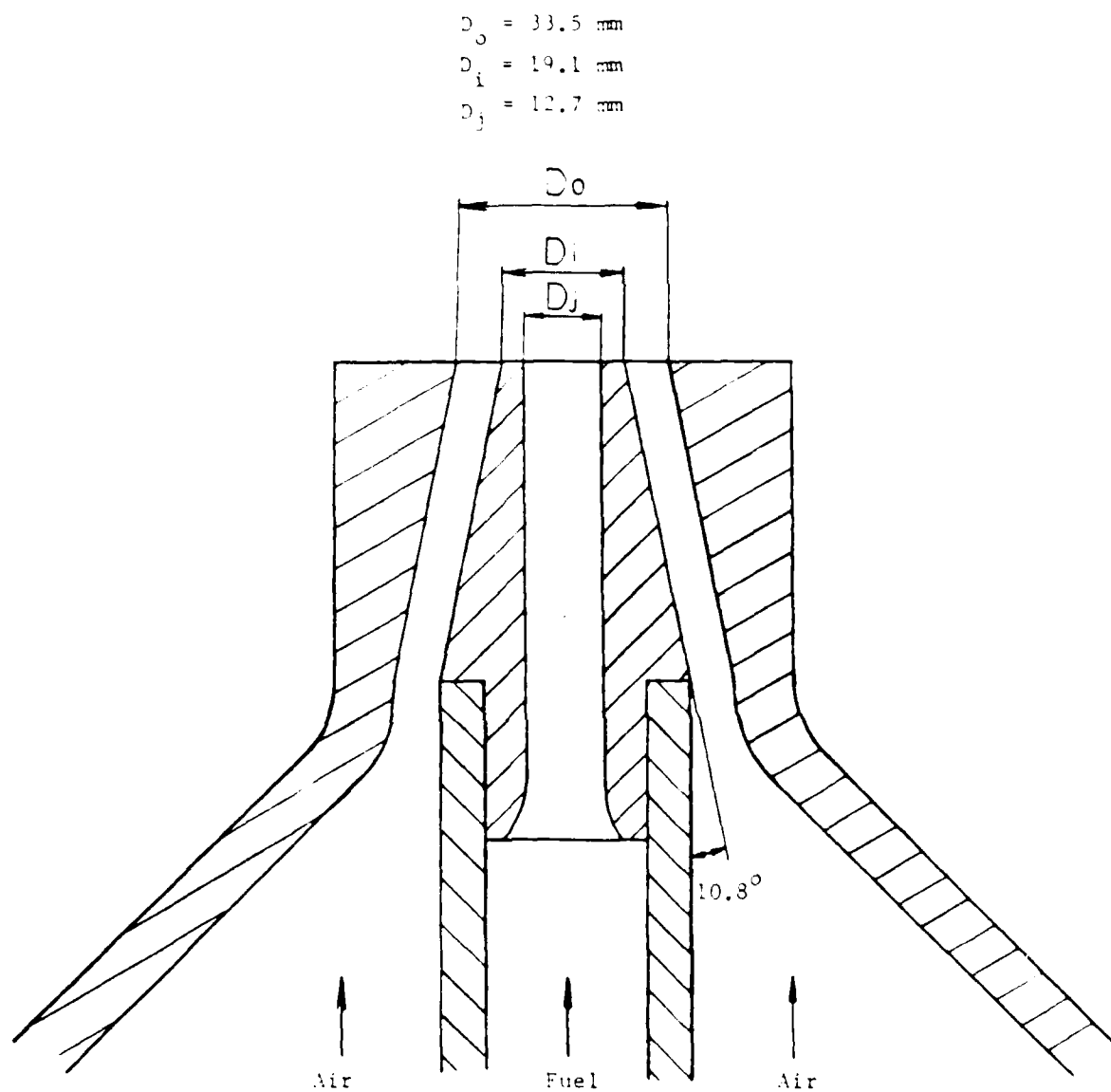
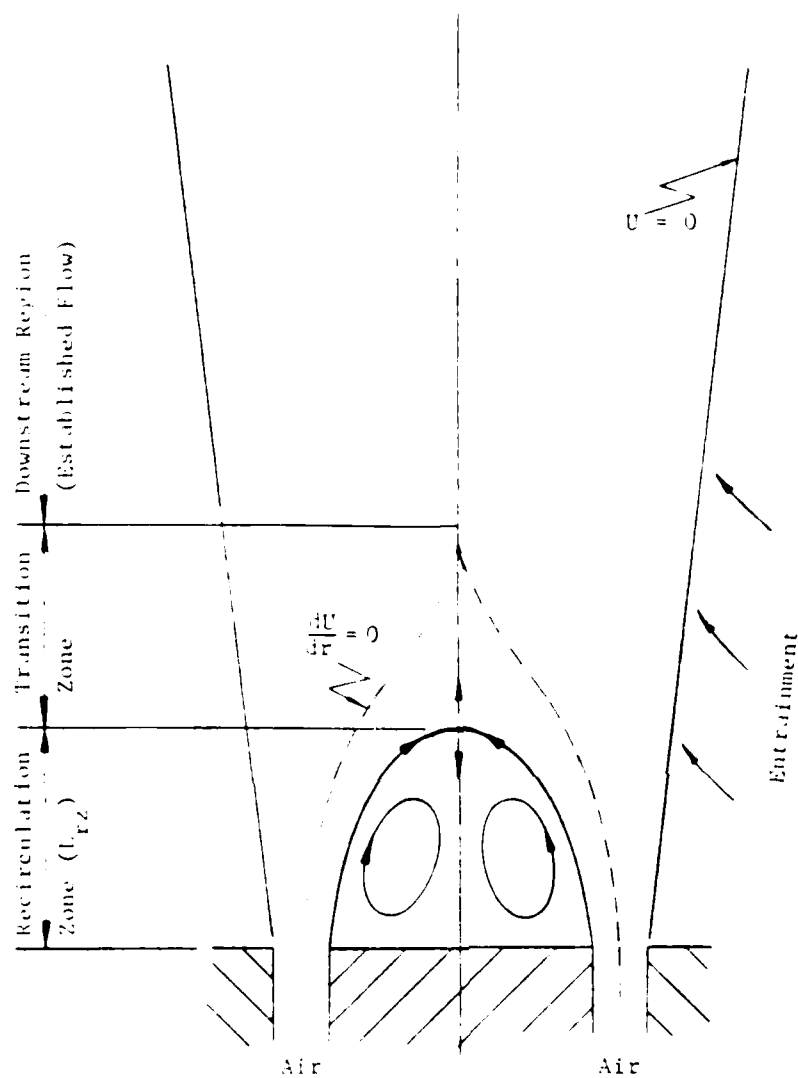


Fig. 2c. Schematic drawing of the fuel and air nozzles used in Test III.



$u$  - Mean axial velocity

$r$  - Radial distance

Fig. 3. Flow diagram for the pure annular air jet.

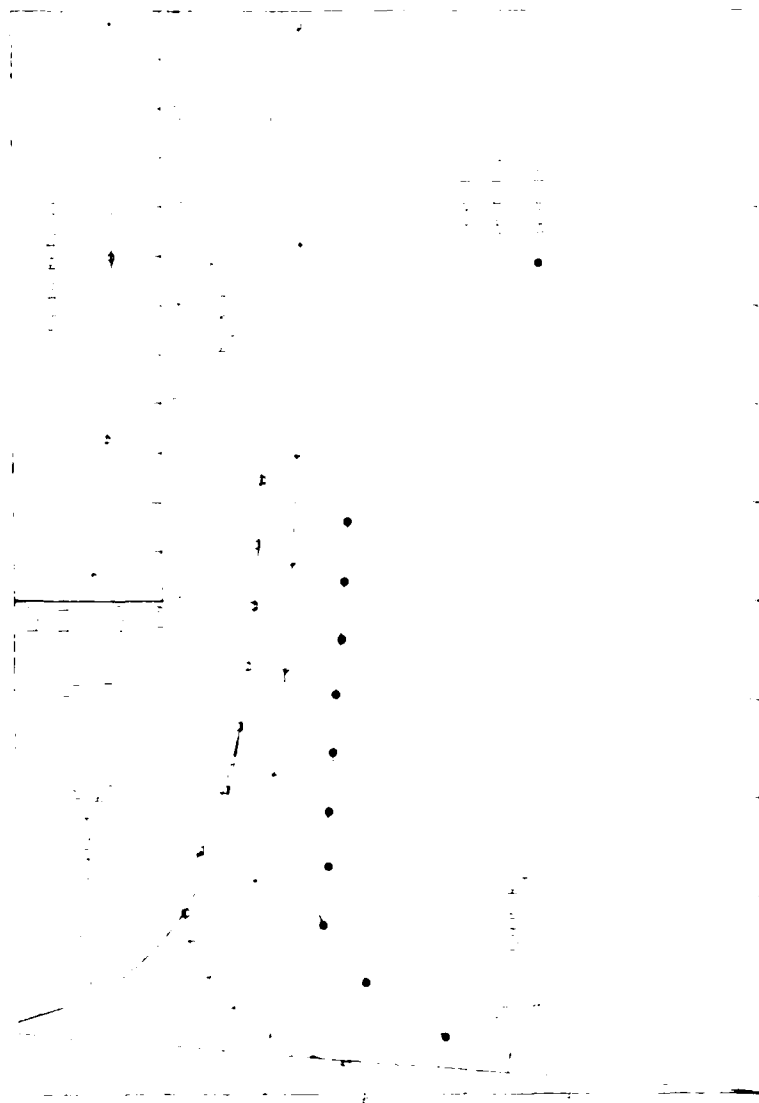
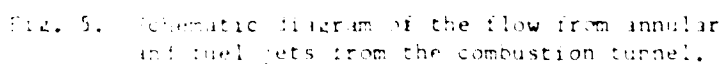


Fig. 1. Dependence of the rate of polymerization on the concentration of the initiator.





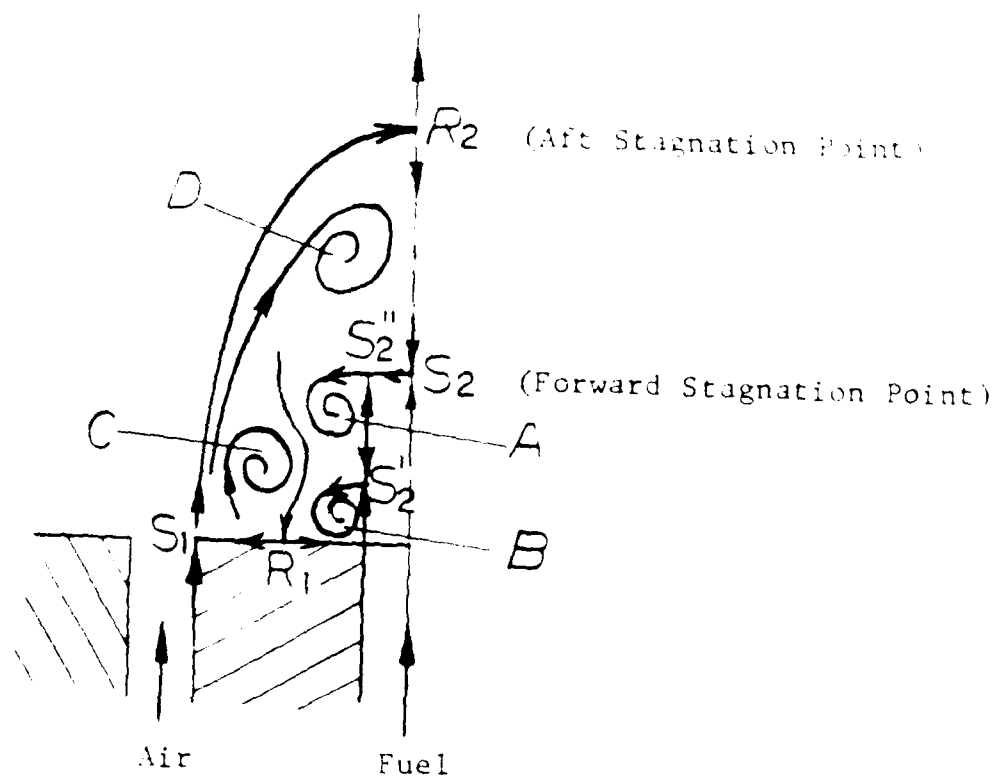
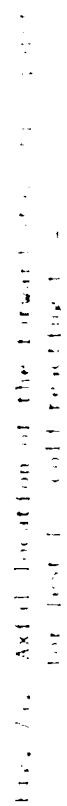


Fig. 6. Typical S and R saddle points (also see Plate 3a).



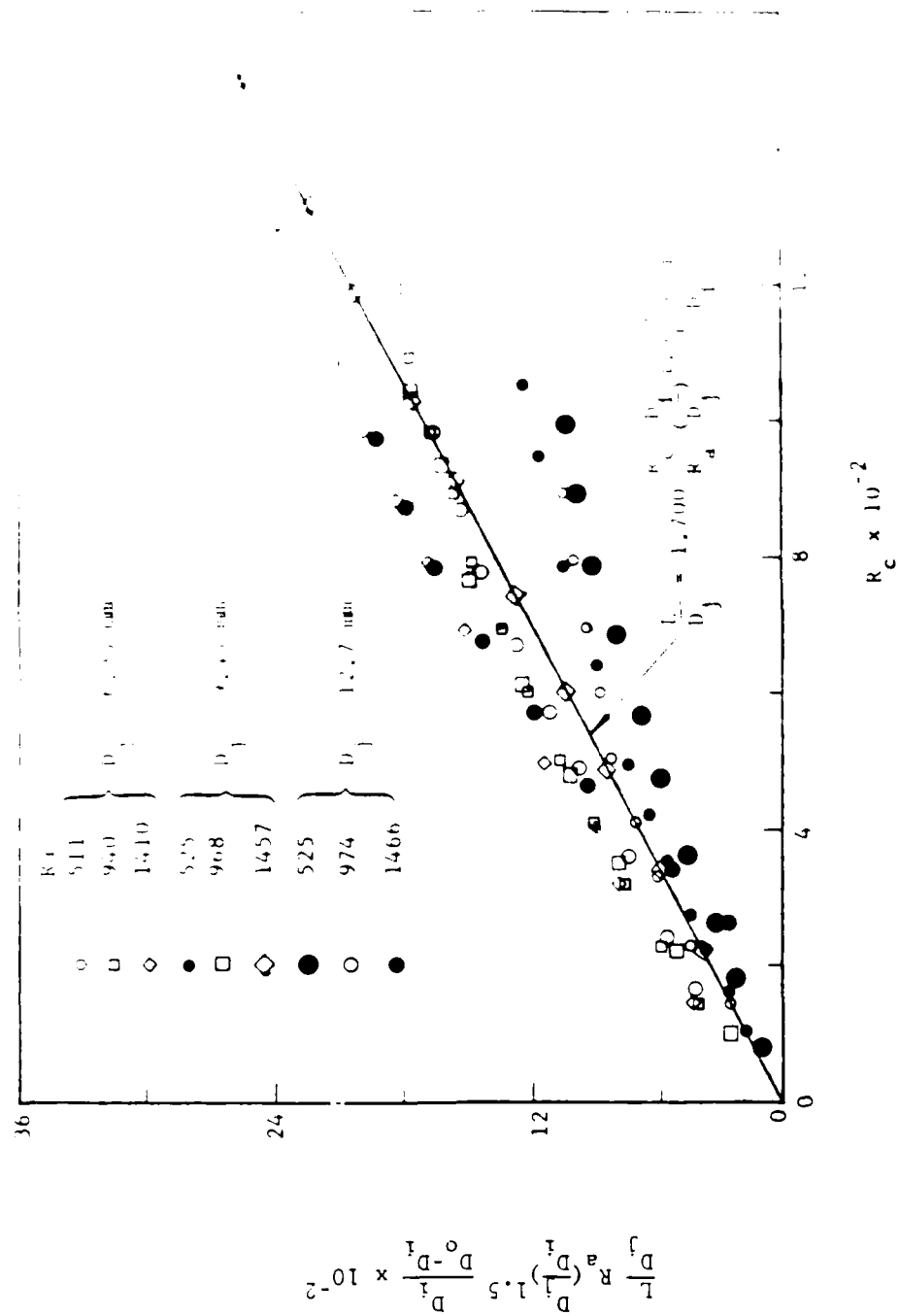
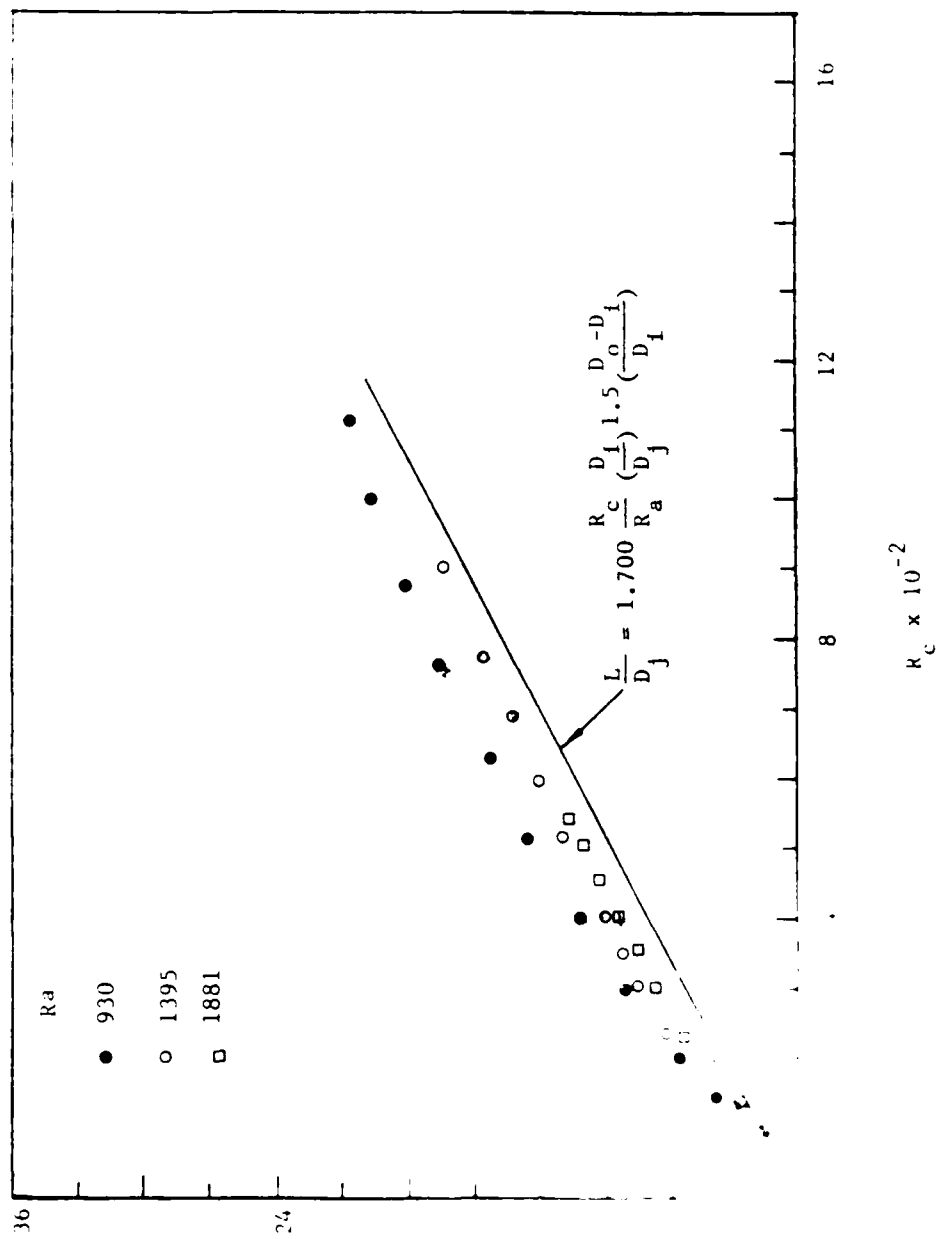


Fig. 7b. Axial location of the forward stagnation point for Test II - cold reacting flow.



Location of the forward stagnation point,  $\frac{L}{D}$ ,  
cold reacting flow.

AD-A186 490

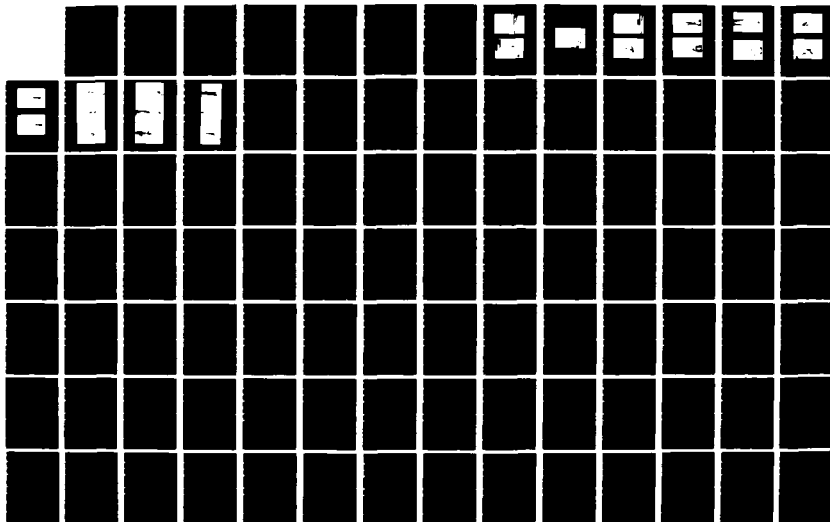
UNITED STATES AIR FORCE RESEARCH INITIATION PROGRAM  
1984 RESEARCH REPORTS (U) SOUTHEASTERN CENTER FOR  
ELECTRICAL ENGINEERING EDUCATION INC S W D PEELE

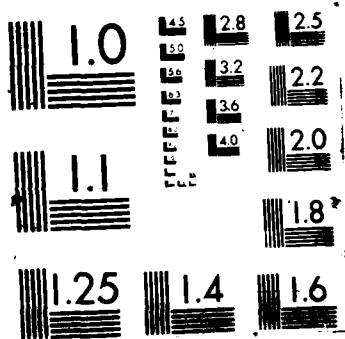
08/11

UNCLASSIFIED

MAY 86 AFOSR-TR-87-1721 F49628-82-C-0035 F/G 15/1

NL





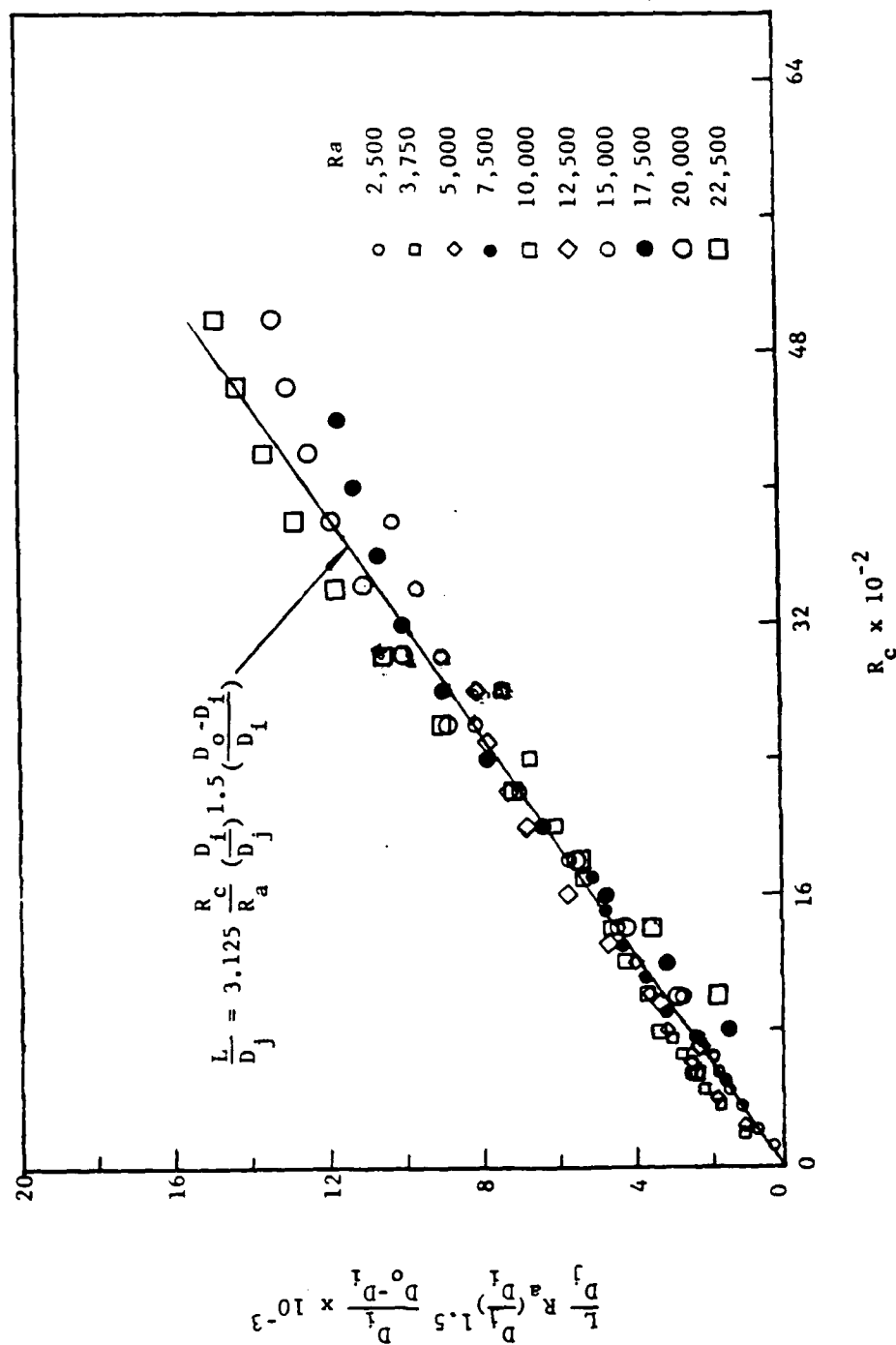


Fig. 7d. Axial location of the forward stagnation points,  $\frac{L}{D_j}$ , for data in reference 27.

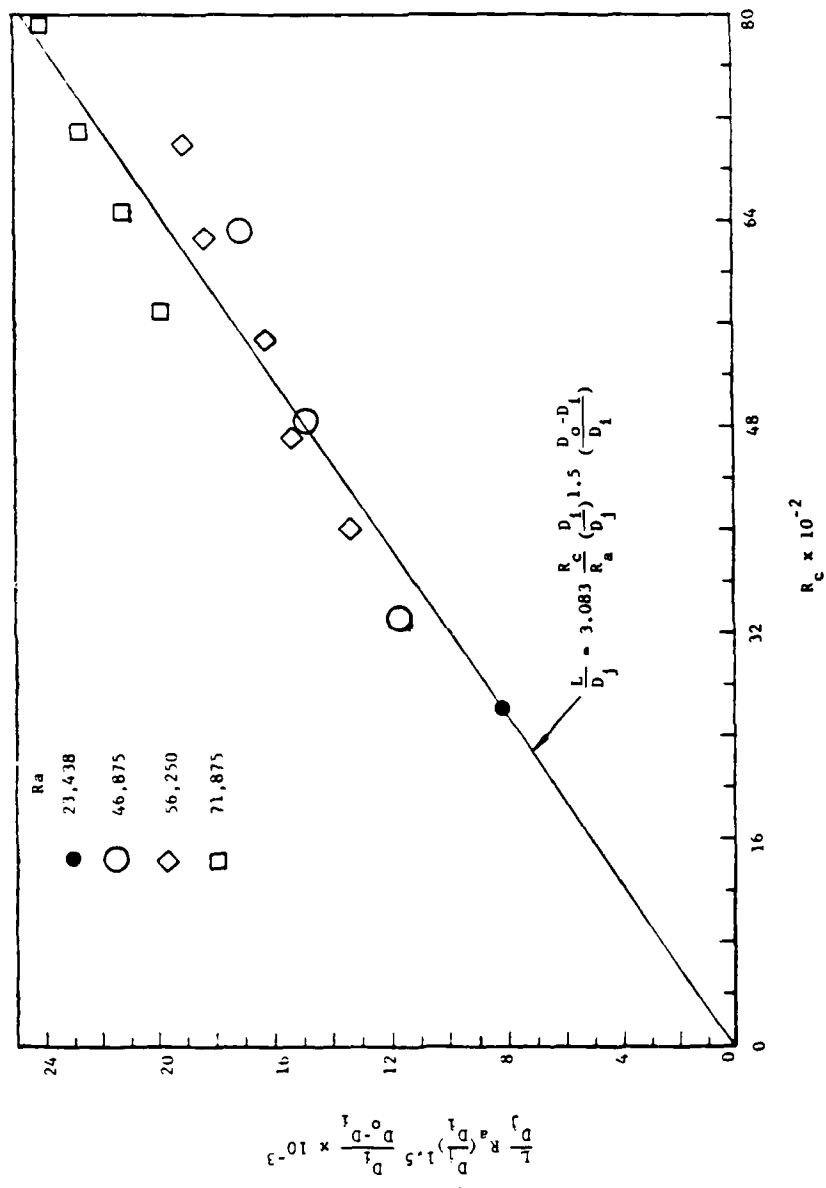


Fig. 7e. Axial location of the forward stagnation points,  $L/D_j$ , for Namazian's data (Ref. 7).



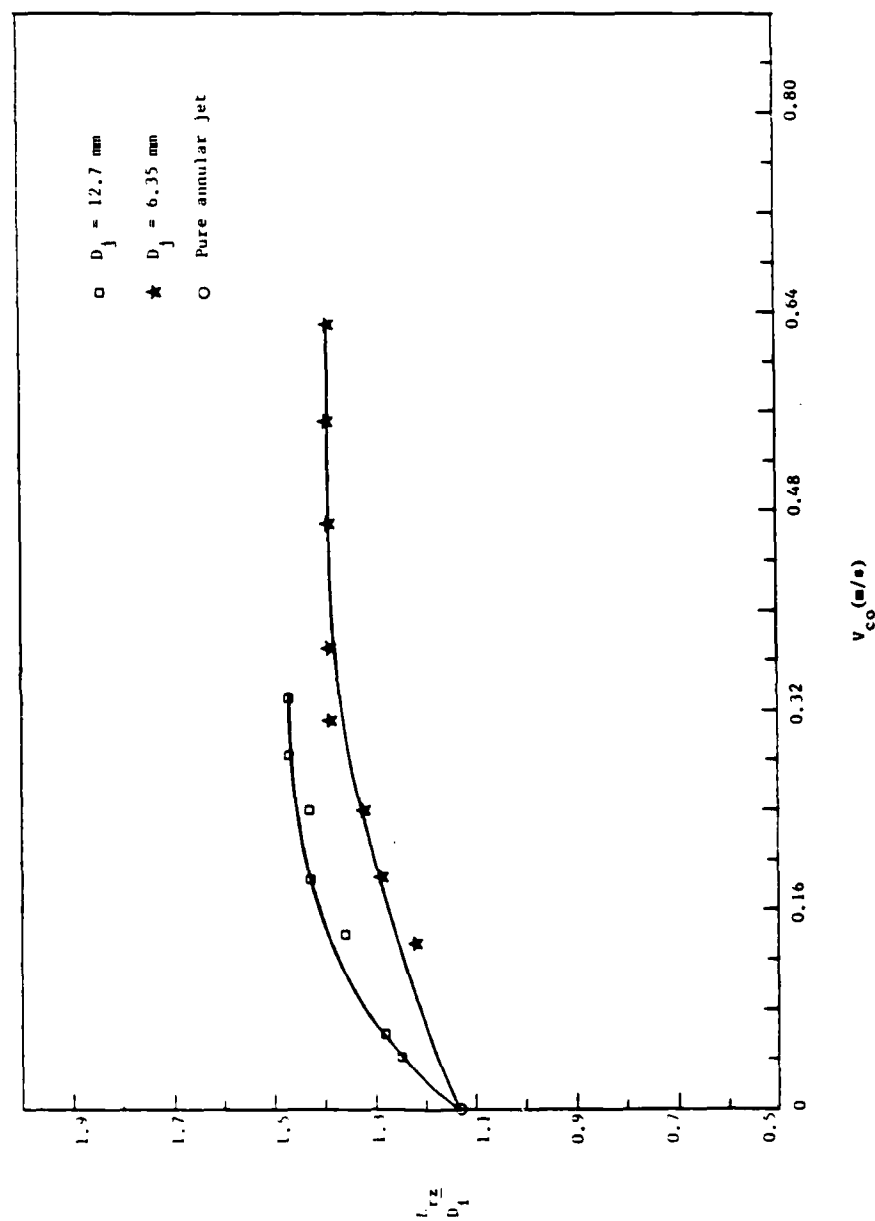


Fig. 8. The length of the recirculation zone,  $\frac{L_{rz}}{D_j}$ , vs. the exit velocity of the central jet,  $V_{co}$ , at the annular air velocity,  $V_{ao}$ , equal to 1.0793 m/s for Test I.

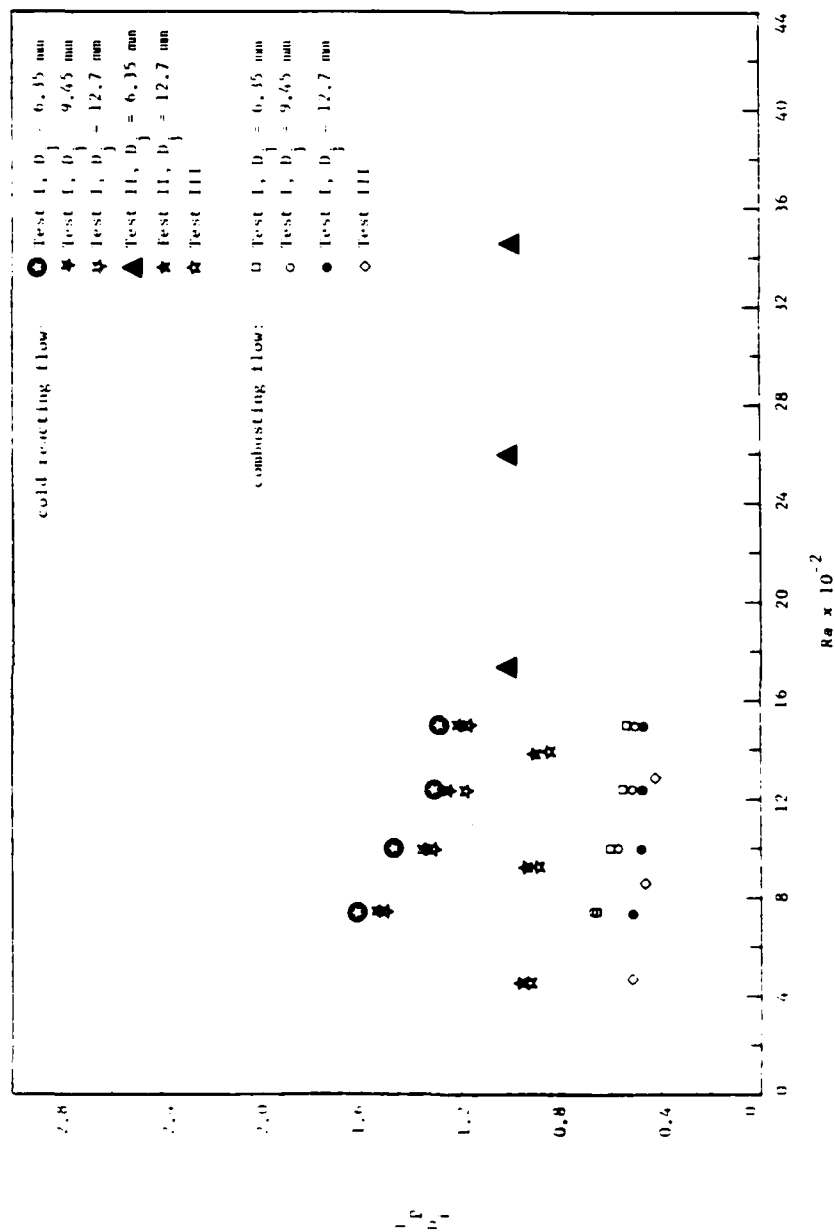


Fig. 9. Penetration length,  $\frac{l_p}{D_i}$ , vs. annular air Reynolds number,  $Ra$ , for the cold reacting flow and combustor flow (attached flame only).

PLOT OF THE NONDIMENSIONALIZED DATA SET 4

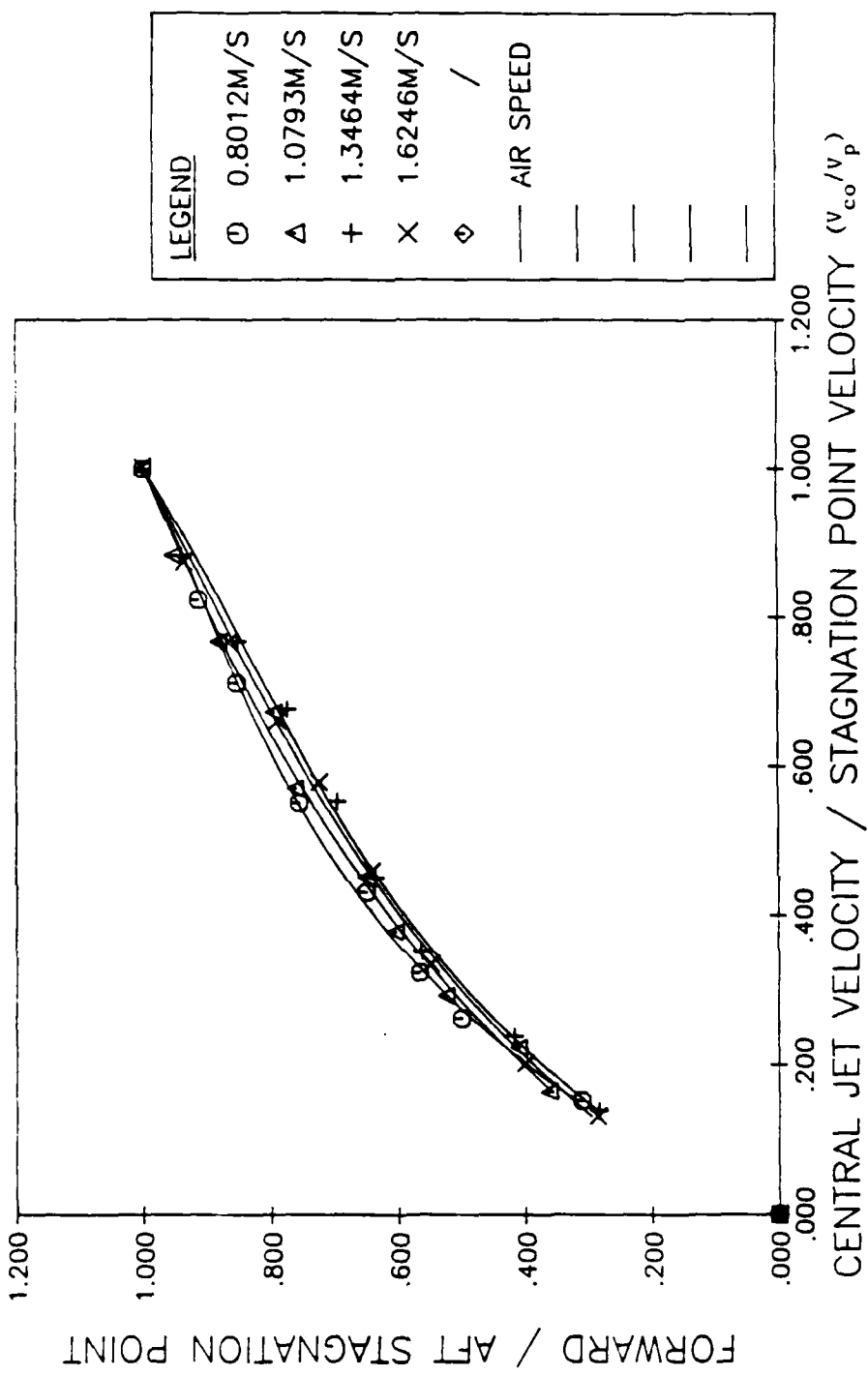


Fig. 10. Plot of  $L/L_{rz}$  versus  $V_{co}/V_p$  for Test I with  $D_j = 6.35$  mm - cold reacting flow.

# PLOT OF THE NONDIMENSIONALIZED DATA SET 4

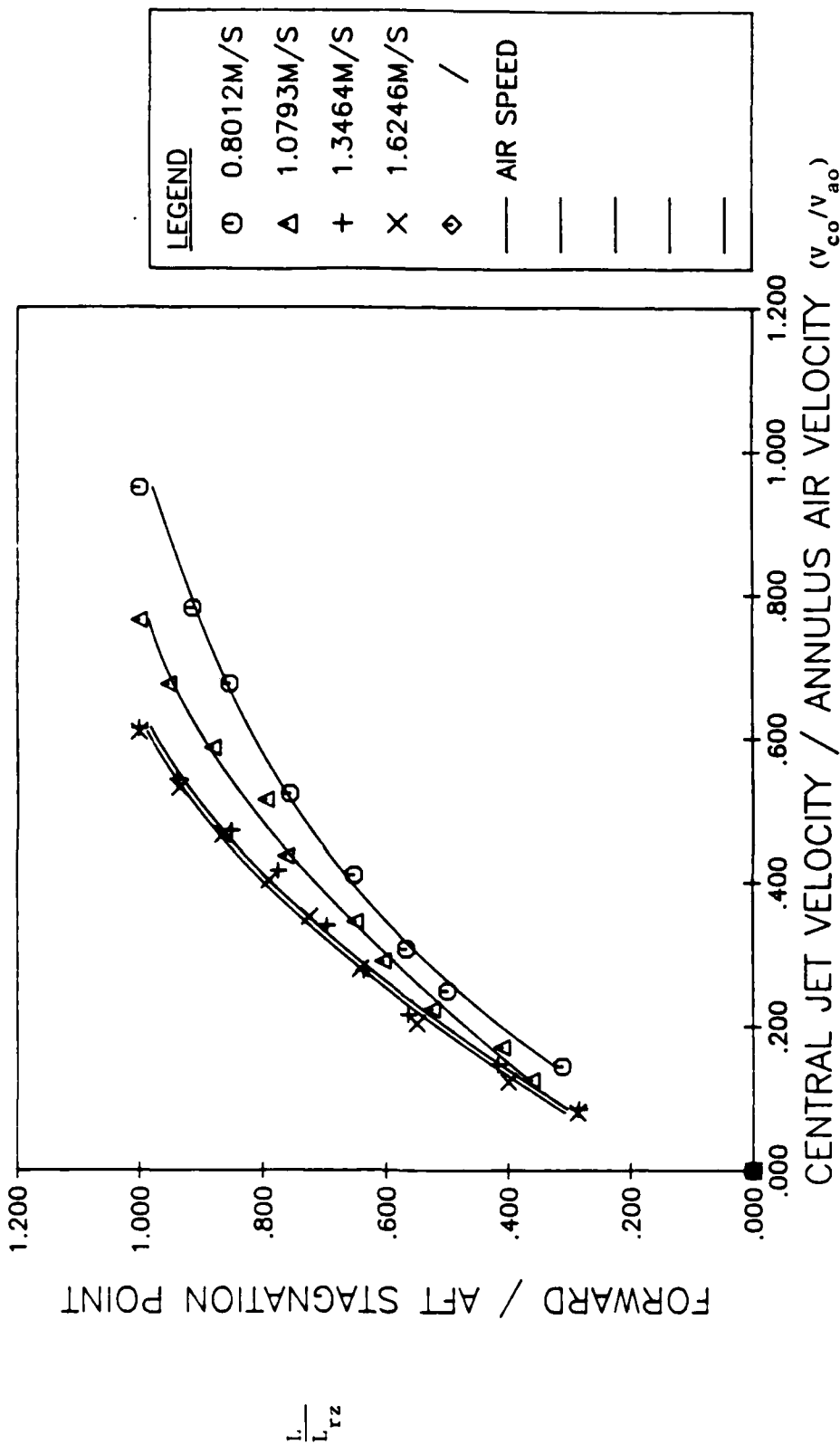


Fig. 11. Plot  $L/L_{rz}$  versus  $V_{co}/V_{ao}$  for Test I with  $D_j = 6.35$  mm - cold reacting flow.



Plate 1b. Photograph of sheet-lighted cold flow  
for Test 111; air velocity 0.4821 m/sec,  
fuel velocity 0.0076 m/sec.

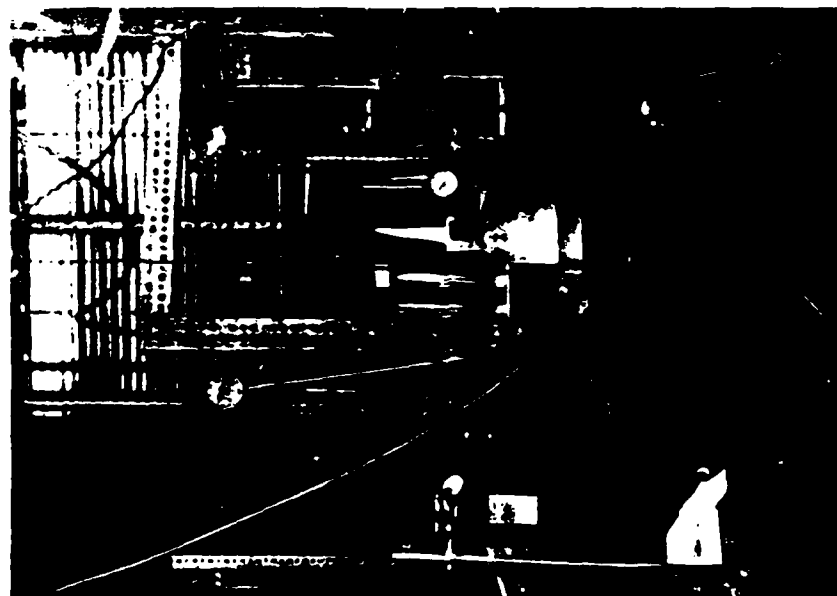


Plate 1a. Photograph showing experimental  
set-up.



Plate 1c. Photograph showing the measurement of the length of the recirculation zone for pure annular air flow.

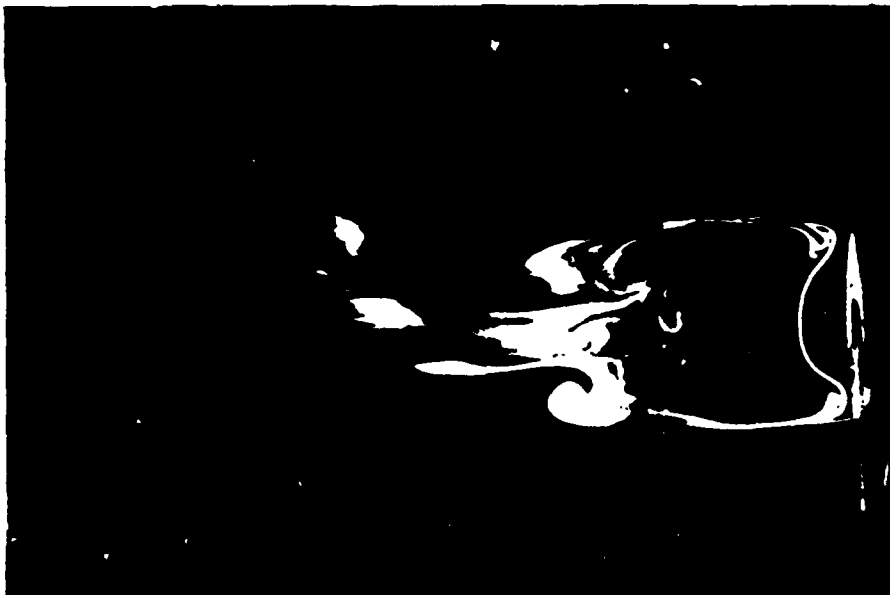


Plate 2a. Photograph of sheet-lighted cold flow for Test I; air velocity 0.534 m/sec, fuel velocity 0.111 m/sec, and  $D_j = 12.7$  mm

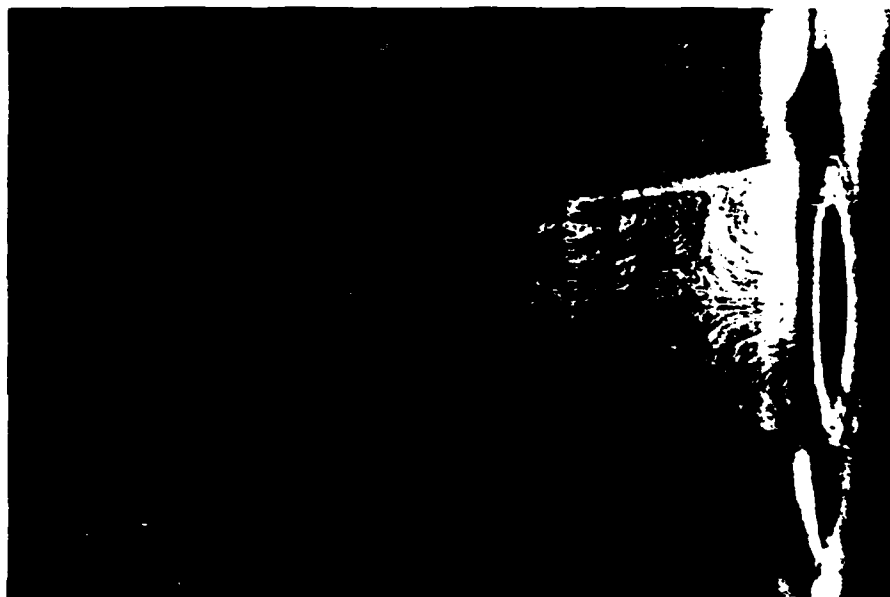


Plate 2b. Photograph of sheet-lighted cold flow for Test III; air velocity 0.964 m/sec and fuel velocity 0.050 m/sec.



Plate 3a. Photograph of sheet-lighted cold flow for Test I; air velocity 0.801 m/sec, fuel velocity 0.236 m/sec, and  $D_j = 9.45$  mm.



Plate 3b. Photograph of sheet-lighted cold flow for Test I; air velocity 1.892 m/sec, fuel velocity 0.279 m/sec, and  $D_j = 12.7$  mm.





Plate 6a. Photograph of sheet-lighted cold flow for Test 1; air velocity 0.401 m/sec, fuel velocity 0.201 m/sec, and  $p_1 = 12.7$  mm

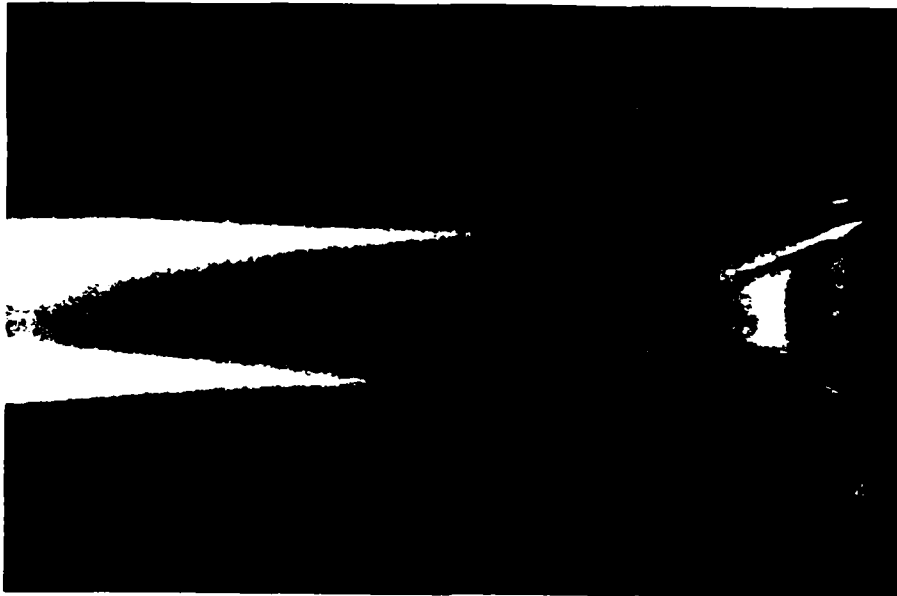


Plate 6b. Photograph of sheet-lighted combustor flow with filter for Test 11; air velocity 0.963 m/sec, fuel velocity 0.050 m/sec,



Plate 5a. Photograph of combustive flow (no sheet-lighting)  
for Test I; air velocity 1.08 m/sec, fuel velocity  
0.0258 m/sec.



Plate 5b. Photograph of sheet-lighted flow with filter for  
same conditions as in Plate 5a.



Plate 6a. Photograph of combustion flow (no sheet-lighting) for Test 4; air velocity 1.76 m/sec, fuel velocity 0.0077 m/sec, and  $D_0 = 9.55$  mm.



Plate 6b. Photograph of combustion flow with sheet-lighting for same conditions as in Plate 6a.

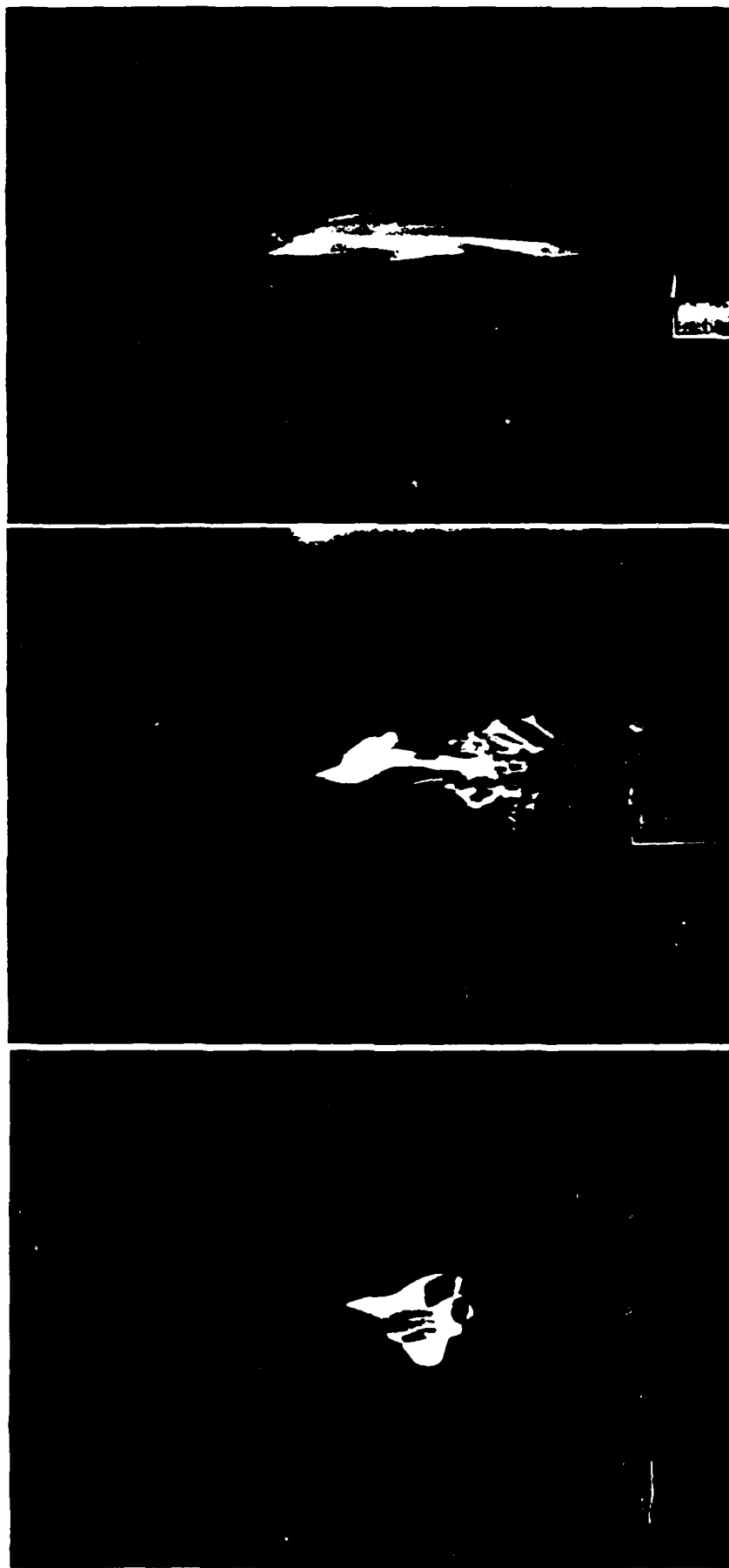


Plate 7. Photographs of detached flame for Test 1; air velocity 1.76 m/sec, fuel velocity 0.446 m/sec, and  $d = 9.45$  mm. Plate 7a is without laser sheet-lighting; Plate 7b is with sheet-lighting; Plate 7c is with sheet-lighting and filter.

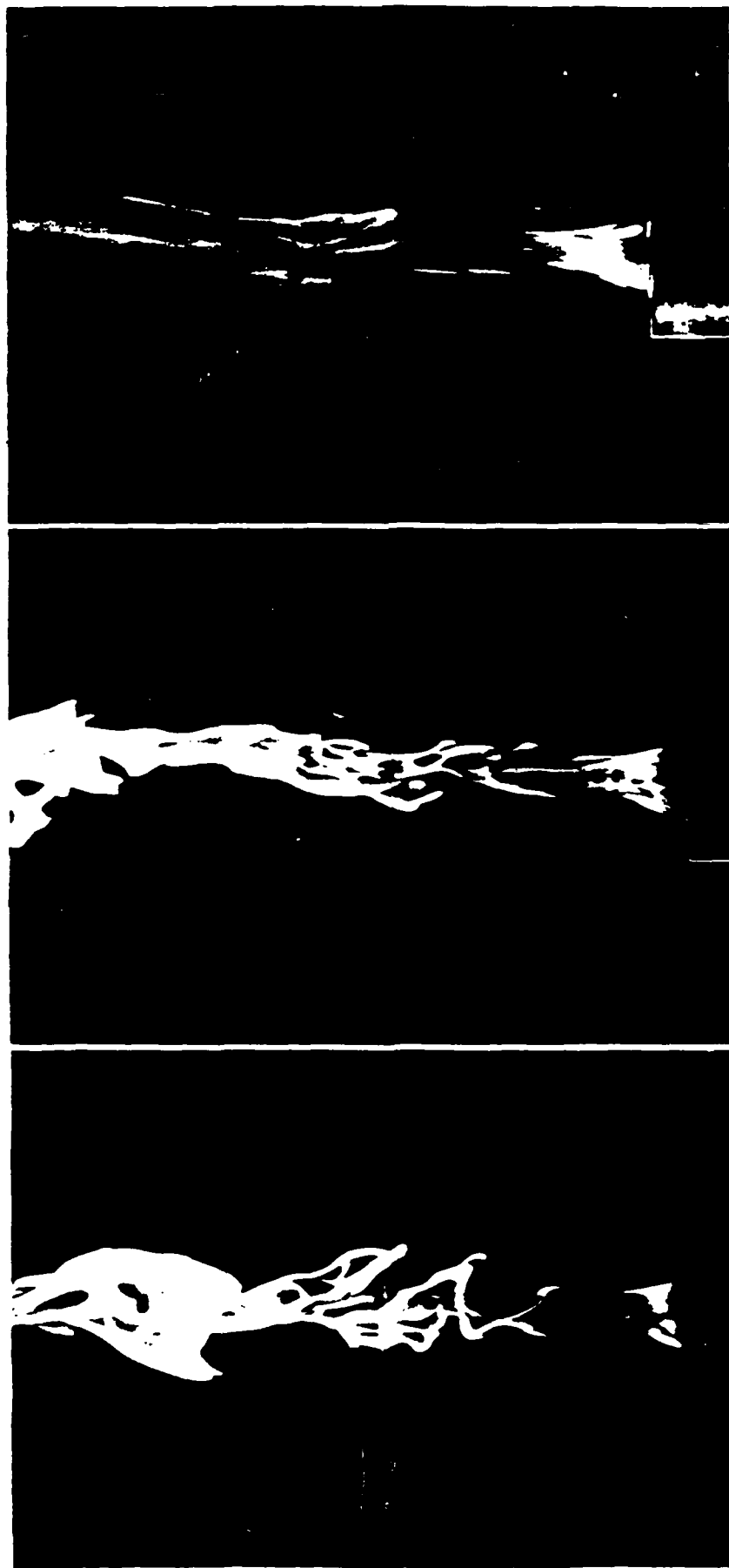


Plate 8. Photographs of reattached flame for Test I; air velocity 1.76 m/sec (same as in plate 7), fuel velocity 0.700 m/sec, and  $D_j = 9.45$  mm. Plate 8a is without laser sheet-lighting; plate 8b is with sheet-lighting; plate 8c is with sheet-lighting and filter.

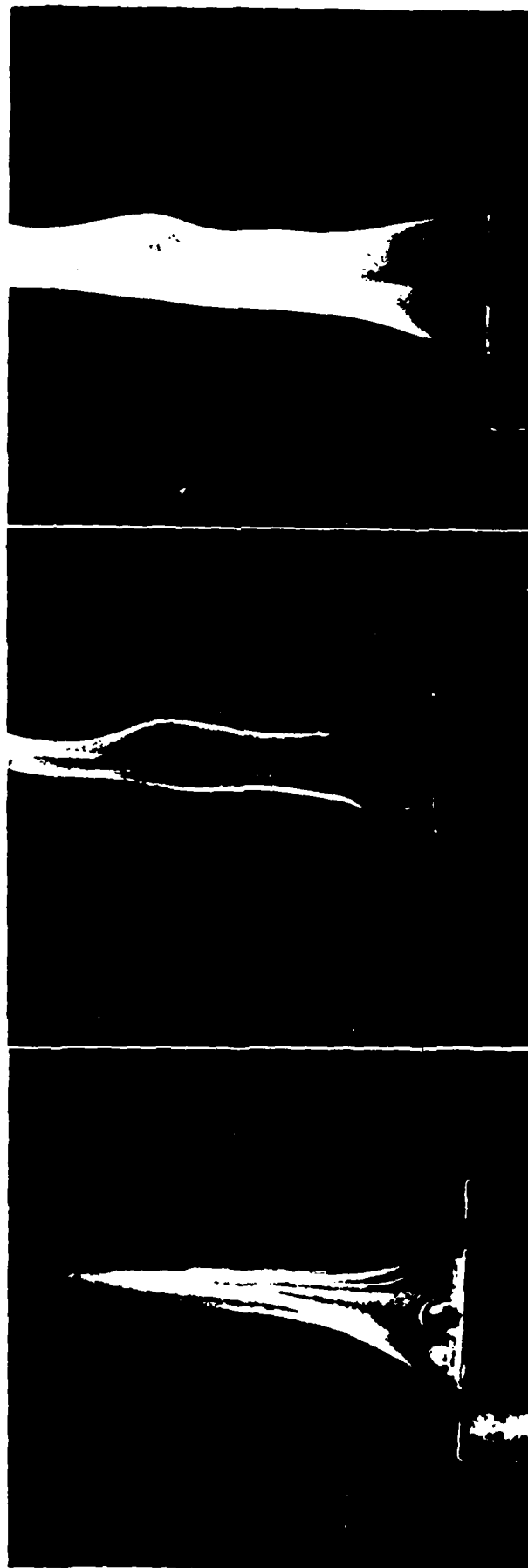


Plate 9. Photographs illustrating the effect of  $D_j$  for similar flow conditions. Flame is sheet-lighted and nozzles are Test 1. Plate 9a, the air velocity is 1.08 m/sec, the fuel velocity is 0.142 m/sec and  $D_j = 6.35$  mm. Plate 9b, the air velocity is 1.08 m/sec, the fuel velocity is 0.140 m/sec and  $D_j = 9.53$  mm. Plate 9c, the air velocity is 1.08 m/sec, the fuel velocity is 0.138 m/sec and  $D_j = 12.7$  mm.

Appendix A: Calibration Curve of the Piezometer  
for the Annular Air Flow

Air

Scalar  
division

100

90

80

70

60

50

40

30

20

10

0

0 0.5 1 1.5 2 2.5 3 3.5 4 4.5 5 5.5 6

$\frac{\text{ft}^3}{\text{min}}$



```

310 C      IF ITYP=3, PUTS OUT LEAST SQUARE FIT WITHOUT PLOTTING
320 C      IF ITYP=4, PUTS OUT LEAST SQUARE FIT WITH PLOTTING.
330 C
340 C      DATA IM, ITYP/5, 4/
350 C      CALL DRIVE(IM, ITYP)
360 C      STOP
370 C      END
380 C
390 C      *****
400 C
410 C      SUBROUTINE DRIVE(IM, ITYP)
420 C
430 C      DRIVE
440 C      *****
450 C
460 C      CONTROL THE FLOW OF THE WHOLE PROGRAM
470 C
480 C      SUBROUTINE CALLED
490 C      *****
500 C
510 C      VARIABLES
520 C      *****
530 C
540 C      IM  --NUMBER OF THE EXPERIMENTAL DATA SETS
550 C      ITYP--VALUE OF ITYP CONTROLS THE PRINTOUT(SEE MAIN PROGRAM)
560 C      N    --NUMBER OF MEASUREMENT POINTS FOR EACH EXPERIMENTAL DATA SET
570 C      SCALEA--SCALE READING OF FLOWMETER FOR AIR
580 C      T    --TEMPERATURE OF THE LAB(°C)
590 C      AREIN--AREA OF INNER NOZZLE(IN**2)
600 C      AREOT--AREA OF OUTER NOZZLE(IN**2)
610 C      WFUM --WEIGHT OF FUEL MOLECULE, FOR PROPANE, WFUM=44.097
620 C      HEIMAX, HEIF--MAXIMUM HEIGHT AND HEIGHT OF FUEL JET,
630 C      RESPECTIVELY (IN)
640 C      SCALEF, SCALEP--MAXIMUM SCALE READING AND SCALE READING OF
650 C      FLOWMETER FOR FUEL
660 C      P, PM--FUEL GAUGE PRESSURE AT FLOWMETER, OR FOR PENETRATION (KPA)
670 C      VORL, VORP--HEIGHTS OF LEFT, RIGHT VORTICES (IN)
680 C
690 C      DIMENSION M(5), X(100,10), Y(100,10)
700 C      COMMON /VALUE2/ X, Y
710 C      DATA X, Y /1000*0.0, 1000*0.0/
720 C
730 C      DO 500 I1=1, IM
740 C      READ(5, *) N, SCALEA, T, D1
750 C      M(I1)=N
760 C
770 C      D1=4.0*ATAN(1.0)
780 C      D2=1.514
790 C      D3=2.094
800 C      AREOT=(D3*D3-D2*D2)*PI/4.0
810 C      AREIN=PI*D1*D1/4.0
820 C      WFUM=44.097
830 C
840 C      CALL CONV(AREIN, AREOT, 2)
850 C      CALL CONV(AREOT, AREOT, 2)
860 C      CALL AIRVEL(SCALEA, AREOT, VELAMS)
870 C
880 C      READ(5, *) HEIMAX, SCALEF, PM
890 C      CALL GENFV(SCALEF, PM, T, AREIN, VELMAX, WFUM, 2)
900 C      DO 10 I=1, N
910 C      READ(5, *) SCALEF, P, VORL, VORP, HEIF
920 C      CALL NONDIM(HEIF, HEIMAX, HEINON)
930 C      CALL GENFV(SCALEF, P, T, AREIN, VELFMS, WFUM, 2)
940 C      CALL NONDIM(VELFMS, VELMAX, FULNON)
950 C      CALL STORE2(FULNON, HEINON, I, I1)
960 C      CALL CONV(HEIF, HEIFMS, 1)

```

```

970 CALL CONV(VOFL,VOFLF,1)
980 CALL CONV(VOPR,VOPRG,1)
990 CALL STORE1(VELFMS,HEIFMS,VOFLF,VOPRG,HEINON,I)
1000 10 CONTINUE
1010 CALL RESTOR(N)
1020 CALL PRINT(N,AREADT,AREAIN,VELAMS,I1)
1030 IF(ITYP.EQ.2) CALL DRAW(N,0,2,I1)
1040 500 CONTINUE
1050 GO 600 I1=1,I1
1060 M=M(I1)
1070 IF(ITYP.GE.3) CALL FCTDET(N,I1,ITYP,I1)
1080 600 CONTINUE
1090 RETURN
1100 END
1110 C
1120 C *****
1130 C SUBROUTINE AIRVEL(SCALE,AREADT,VELAMS)
1140 C
1150 C CALCULATION OF VELOCITY OF ANNULAR AIR FROM SCALE READING OF
1160 C FLOWMETER
1170 C
1180 C VARIABLES
1190 C *****
1200 C
1210 C SCALE --SCALE READING OF FLOWMETER FOR ANNULAR AIR
1220 C AREADT--AREA OF OUTER(ANNULAR) NOZZLE (CM**2)
1230 C VELAMS--VELOCITY OF AIR (M/SEC)
1240 C
1250 C DIMENSION VOLFR(10)
1260 C DATA VOLFR/0.6,1.2,1.8,2.425,3.025,3.65,4.25,4.95,5.45,6.075/
1270 C
1280 C DO 100 I=1,10
1290 C IF(SCALE/10.EQ.I) THEN
1300 C VOL=VOLFR(I)
1310 C GO TO 200
1320 C ENDF
1330 100 CONTINUE
1340 200 AB=0.3048
1350 C VELAMS=VOL*AB*AB*AB/60.0/AREADT*10000.C
1360 C M/SEC FT**3-->M**3 MIN-->SEC CM**2-->M**2
1370 C RETURN
1380 C END
1390 C
1400 C *****
1410 C SUBROUTINE GENFV(SCALE,P,T,AREAIN,VELFMS,WFUM,ISIZE)
1420 C
1430 C CALCULATION OF VELOCITY OF CENTRAL FUEL JET FROM THE SCALE
1440 C READING OF GILMONT FLOWMETER , CATALOG NO. 1100,SIZE 1,IF
1450 C ISIZE=1;OR,CATALOG NO. F1200,SIZE 2,IF ISIZE=2;OR,CATALOG NO.
1460 C F1300,SIZE 3,IF ISIZE=3.
1470 C
1480 C VARIABLES
1490 C *****
1500 C
1510 C SCALE --SCALE READING FROM FLOWMETER
1520 C P --GAUGE PRESSURE AT FLOWMETER (KPA)
1530 C T --TEMPERATURE INSIDE LAB (°C)
1540 C AREAIN--AREA OF INNER (CENTRAL)NOZZLE (CM**2)
1550 C VELFMS--VELOCITY OF FUEL (M/SEC)
1560 C WFUM --WEIGHT OF FUEL MOLECULE,FOR PROPANE WFUM=44.097
1570 C
1580 C FOR THE FORMULA USED HERE,PLEASE SEE GILMONT FLOWMETER
1590 C SPECIFICATION FOR SIZE 1 OR 2,OR 3.
1600 C
1610 C P1=101325.0+P*1000.0
1620 C T1=T+273.15

```

Appendix B: Computer Program Run on Cyber 71

Plotting Curves  $\frac{L}{T_{50}}$  vs.  $\frac{T_{50}}{T_{90}}$  or  $\frac{T_{50}}{T_{10}}$



```

310 C          IF ITYP=3, PUTS OUT LEAST SQUARE FIT WITHOUT PLOTTING
320 C          IF ITYP=4, PUTS OUT LEAST SQUARE FIT WITH PLOTTING.
330 C
340 C      DATA IM, ITYP/5, 4/
350 C      CALL DRIVE(IM, ITYP)
360 C      STOP
370 C      END
380 C
390 C      *****
400 C
410 C      SUBROUTINE DRIVE(IM, ITYP)
420 C
430 C      DRIVE
440 C      *****
450 C
460 C      CONTROL THE FLOW OF THE WHOLE PROGRAM
470 C
480 C      SUBROUTINE CALLED
490 C      *****
500 C
510 C      VARIABLES
520 C      *****
530 C
540 C      IM  --NUMBER OF THE EXPERIMENTAL DATA SETS
550 C      ITYP--VALUE OF ITYP CONTROLS THE PRINTOUT(SEE MAIN PROGRAM)
560 C      N   --NUMBER OF MEASUREMENT POINTS FOR EACH EXPERIMENTAL DATA SET
570 C      SCALEA--SCALE READING OF FLOWMETER FOR AIR
580 C      T    --TEMPERATURE OF THE LAB(°C)
590 C      AREIN--AREA OF INNER NOZZLE(IN**2)
600 C      AREOT--AREA OF OUTER NOZZLE(IN**2)
610 C      WFUM --WEIGHT OF FUEL MOLECULE, FOR PROPANE, WFUM=44.097
620 C      HEIMAX, HEIF--MAXIMUM HEIGHT AND HEIGHT OF FUEL JET,
630 C                   RESPECTIVELY (IN)
640 C      SCALEM, SCALEF--MAXIMUM SCALE READING AND SCALE READING OF
650 C                   FLOWMETER FOR FUEL
660 C      P, PM--FUEL GAUGE PRESSURE AT FLOWMETER, OR FOR PENETRATION (KPA)
670 C      VORL, VORR--HEIGHTS OF LEFT, RIGHT VORTICES (IN)
680 C
690 C      DIMENSION X(5), X(100, 10), Y(100, 10)
700 C      COMMON /VALUE2/ X, Y
710 C      DATA X, Y /1000*0.0, 1000*0.0/
720 C
730 C      DO 500 I1=1, IM
740 C      READ(5, *) N, SCALEA, T, D1
750 C      M(I1)=N
760 C
770 C      PI=4.0*ATAN(1.0)
780 C      D2=1.514
790 C      D3=2.094
800 C      AREOT=(D3*D3-D2*D2)*PI/4.0
810 C      AREIN=PI*D1*D1/4.0
820 C      WFUM=44.097
830 C
840 C      CALL CONV(AREIN, AREAIN, 2)
850 C      CALL CONV(AREOT, AREAOT, 2)
860 C      CALL AIRVEL(SCALEA, AREAOT, VELAMS)
870 C
880 C      READ(5, *) HEIMAX, SCALEM, PM
890 C      CALL GENFV(SCALEM, PM, T, AREAIN, VELMAX, WFUM, 2)
900 C      DO 10 I=1, N
910 C      READ(5, *) SCALEF, P, VORL, VORR, HEIF
920 C      CALL NONDIM(HEIF, HEIMAX, HEINON)
930 C      CALL GENFV(SCALEF, P, T, AREAIN, VELFMS, WFUM, 2)
940 C      CALL NONDIM(VELFMS, VELMAX, FULNON)
950 C      CALL STJPE2(FULNON, HEINON, I, I1)
960 C      CALL CONV(HEIF, HEIFMS, 1)

```

```

970      CALL CONV(T,VORL,VORLFT,1)
980      CALL CONV(VORR,VORRIG,1)
990      CALL STORE1(VELFMS,HEIFMS,VORLFT,VORRIG,HEINON,I)
1000 10   CONTINUE
1010      CALL RESTOR(N)
1020      CALL PRINT(N,AREACT,AREAIN,VELAMS,I1)
1030      IF(ITYP.EQ.2) CALL DRAW(N,0,2,I1)
1040 500   CONTINUE
1050      DO 600 I1=1,IM
1060      N=M(I1)
1070      IF(ITYP.GE.3) CALL FCTDET(N,I1,ITYP,IM)
1080 600   CONTINUE
1090      RETURN
1100      END
1110 C
1120 C *****
1130 C SUBROUTINE AIRVEL(SCALE,AREACT,VELAMS)
1140 C
1150 C CALCULATION OF VELOCITY OF ANNULAR AIR FROM SCALE READING OF
1160 C FLOWMETER
1170 C
1180 C VARIABLES
1190 C *****
1200 C
1210 C SCALE --SCALE READING OF FLOWMETER FOR ANNULAR AIR
1220 C AREACT--AREA OF OUTER(ANNULAR) NOZZLE (CM**2)
1230 C VELAMS--VELOCITY OF AIR (M/SEC)
1240 C
1250 C DIMENSION VOLFR(10)
1260 C DATA VOLFR/0.6,1.2,1.8,2.425,3.025,3.65,4.25,4.95,5.45,6.075/
1270 C
1280 C DO 100 I=1,10
1290 C IF(SCALE/10.EQ.I) THEN
1300 C VOL=VOLFR(I)
1310 C GO TO 200
1320 C ENDIF
1330 100   CONTINUE
1340 200   AB=0.3048
1350 C VELAMS=VOL*AB*AB*AB/60.0/AREACT*10000.0
1360 C M/SEC FT**3-->M**3 MIN-->SEC CM**2-->M**2
1370 C RETURN
1380 C END
1390 C
1400 C *****
1410 C SUBROUTINE CENFV(SCALE,P,T,AREAIN,VELFMS,WFUM,ISIZE)
1420 C
1430 C CALCULATION OF VELOCITY OF CENTRAL FUEL JET FROM THE SCALE
1440 C READING OF GILMONT FLOWMETER , CATALOG NO. 1100,SIZE 1,IF
1450 C ISIZE=1;OR,CATALOG NO. F1200,SIZE 2,IF ISIZE=2;OR,CATALOG NO.
1460 C F1300,SIZE 3,IF ISIZE=3.
1470 C
1480 C VARIABLES
1490 C *****
1500 C
1510 C SCALE --SCALE READING FROM FLOWMETER
1520 C P --GAUGE PRESSURE AT FLOWMETER (KPA)
1530 C T --TEMPERATURE INSIDE LAB (°C)
1540 C AREAIN--AREA OF INNER (CENTRAL)NOZZLE (CM**2)
1550 C VELFMS--VELOCITY OF FUEL (M/SEC)
1560 C WFUM --WEIGHT OF FUEL MOLECULE,FOR PROPANE WFUM=44.097
1570 C
1580 C FOR THE FORMULA USED HERE,PLEASE SEE GILMONT FLOWMETER
1590 C SPECIFICATION FOR SIZE 1 OR 2,OR 3.
1600 C
1610 C P1=101325.0+P*1000.0
1620 C T1=T+273.15

```

```

2290 C      VALMES--THE VALUE TO BE NONDIMENSIONALIZED
2300 C      VALMAX--THE REFERENCE VALUE WITH RESPECT TO WHICH
2310 C              VALMES WILL BE NONDIMENSIONALIZED
2320 C      VALNON--NONDIMENSIONALIZED VARIABLE
2330 C
2340 C      VALNON=VALMES/VALMAX
2350 C      RETURN
2360 C      END
2370 C
2380 C      *****
2390 C      SUBROUTINE STORE2(FULNON,HEINON,I,I1)
2400 C
2410 C      STORE HERE ALL THE NONDIMENSIONALIZED VARIABLES WHICH
2420 C      WILL BE PLOTTED.
2430 C
2440 C      VARIABLES
2450 C      *****
2460 C
2470 C      FULNON--FUEL VELOCITY
2480 C      HEINON--HEIGHT OF CENTRAL JET
2490 C      VERNON--MEAN HEIGHT OF VORTICES
2500 C      I      --NUMBER OF ACTUAL DATA SET TO BE STORED
2510 C
2520 C      COMMON
2530 C      *****
2540 C      VALUE2--X(MAXDAT,10) : X-VALUE FOR THE SCATTERGRAMS AND
2550 C              THE CURVE FITTINGS
2560 C      Y(MAXDAT,10) : Y-VALUE FOR THE SAME THING AS ABOVE
2570 C
2580 C      PARAMETER(MAXDAT=100)
2590 C      DIMENSION X(MAXDAT,10),Y(MAXDAT,10)
2600 C      COMMON / VALUE2 / X,Y
2610 C      X(I,I1)=FULNON
2620 C      Y(I,I1)=HEINON
2630 C      RETURN
2640 C      END
2650 C
2660 C      *****
2670 C      SUBROUTINE STORE1(VELFUL,HEIMS,VORLMS,VORRMS,PEN,I)
2680 C
2690 C      STORE ALL THE PHYSICAL VALUES IN THE COMMON 'SAVE1'
2700 C
2710 C      VARIABLES
2720 C      *****
2730 C
2740 C      VELFUL--VELOCITY OF THE FUEL
2750 C      HEIMS  --HEIGHT OF THE CENTRAL JET
2760 C      VORLMS--HEIGHT OF THE LEFT VORTEX
2770 C      VORRMS--HEIGHT OF THE RIGHT VORTEX
2780 C      PEN    --PENETRATION
2790 C      I      --NUMBER OF ACTUAL DATA SET TO BE STORED
2800 C
2810 C      COMMON
2820 C      *****
2830 C
2840 C      SAVE1(5,MAXDAT)--CONTAIN ALL THE PHYSICAL DATA TO BE PRINTED
2850 C
2860 C      PARAMETER(MAXDAT=100)
2870 C      DIMENSION SAVE1(5,MAXDAT)
2880 C      COMMON / VALUE1 / SAVE1
2890 C      SAVE1(1,I)=VELFUL
2900 C      SAVE1(2,I)=HEIMS
2910 C      SAVE1(3,I)=VORLMS
2920 C      SAVE1(4,I)=VORRMS
2930 C      SAVE1(5,I)=PEN
2940 C      RETURN

```

```

2950      END
2960 C      *****
2970      SUBROUTINE PESTOR(MAX)
2980 C
2990 C      REARRANGE THE EXPERIMENTAL DATA STORED IN COMMON 'VALUE1'
3000 C      SUCH THAT THE VELOCITY VALUES ARE IN AN INCREASING ORDER.
3010 C
3020 C      VARIABLES
3030 C      *****
3040 C
3050 C      MAX--NUMBER OF DATA SETS STORED IN VALUE1
3060 C
3070 C      COMMON
3080 C      *****
3090 C
3100 C      VALUE1--SAVE1(5,MAXDAT) : THE EXPERIMENTAL DATA TO BE PRINTED
3110 C
3120      PARAMETER(MAXDAT=100)
3130      DIMENSION SAVE1(5,MAXDAT) ,TEMP(5)
3140      LOGICAL LOG
3150      COMMON / VALUE1 /SAVE1
3160      DO 500 I=1,1000
3170          LOG=.TRUE.
3180          DO 100 J=2,MAX
3190              IF(SAVE1(1,J).LT.SAVE1(1,J-1)) THEN
3200                  DO 10 K=1,5
3210                      TEMP(K)=SAVE1(K,J)
3220                      SAVE1(K,J)=SAVE1(K,J-1)
3230                      SAVE1(K,J-1)=TEMP(K)
3240 10          CONTINUE
3250              LOG=.FALSE.
3260          ENDIF
3270 100      CONTINUE
3280          IF(LOG) GOTO 510
3290          CONTINUE
3300 510      CONTINUE
3310      RETURN
3320      END
3330 C      *****
3340      SUBROUTINE PRINT(MAX,AREACT,AREAIN,VELAIR,J)
3350 C
3360 C      CREATE A TABLE OF VALUES FOR EACH EXPERIMENTAL DATA SET
3370 C
3380 C      VARIABLES
3390 C      *****
3400 C
3410 C      MAX    --NUMBER OF DATA SETS STORED IN COMMON 'VALUE1'
3420 C      AREACT-- AREA OF OUTER NOZZLE
3430 C      AREAIN--AREA OF INNER NOZZLE
3440 C      VELAIR--VELOCITY OF AIR
3450 C      I      --NUMBER OF THE ACTUAL EXPERIMENTAL SET
3460 C
3470 C      COMMON
3480 C      *****
3490 C
3500 C      VALUE1--SAVE1(5,MAXDAT) : PHYSICAL VALUES TO BE PRINTED
3510 C
3520      PARAMETER(MAXDAT=100)
3530      DIMENSION SAVE1(5,MAXDAT)
3540      CHARACTER*3 PEN
3550      COMMON / VALUE1 / SAVE1
3560      WRITE(6,('1'))
3570      WRITE(5,901)
3580      WRITE(5,905) 'TABLE OF VALUES FOR EXPERIMENTAL DATA SET ',J
3590      WRITE(6,901) '*****'
3600      WRITE(5,901)

```



```

3610 WRITE(6,901)
3620 WRITE(6,902) 'AREA OF OUTER NOZZLE',AREAO, ' CM**2'
3630 WRITE(6,902) 'AREA OF INNER NOZZLE',AREAI, ' CM**2'
3640 WRITE(6,902) 'VELOCITY OF AIR',VELAIP, ' M/SEC'
3650 WRITE(6,901)
3660 WRITE(6,901)
3670 WRITE(6,901)
3680 WRITE(6,903) 'VELOCITY', 'HEIGHT OF',
3690 Q 'HEIGHT OF', 'HEIGHT OF'
3700 WRITE(6,903) 'OF FUEL', 'CENTRAL JET',
3710 Q 'LEFT VORTEX', 'RIGHT VORTEX'
3720 WRITE(6,903) '[ M/SEC ]', '[ MM ]',
3730 Q '[ MM ]', '[ MM ]'
3740 WRITE(6,901)
3750 DO 100 I=1,MAX
3760 PEN=' '
3770 IF(SAVE1(5,I).GT.0.9) PEN='(*)'
3780 WRITE(6,904) (SAVE1(K,I),K=1,4),PEN
3790 100 CONTINUE
3800 WRITE(6,901)
3810 WRITE(6,901) 'THE PENTRATION POINT IS SIGNED BY (*)'
3820 RETURN
3830 901 FORMAT(2X,A)
3840 902 FORMAT(2X,A,F10.4,A)
3850 903 FORMAT(4X,4(A,5X))
3860 904 FORMAT(1X,4(F10.4,8X),A)
3870 905 FORMAT(2X,A, I2)
3880 END
3890 C
3900 C *****
3910 C SUBROUTINE DRAW(NMES,NPTS,I,N)
3920 C
3930 C CREATE THE SCATTERGRAM OF THE NONDIMENSIONALIZED
3940 C DATA AND THE PLOTS OF THE CURVES
3950 C
3960 C VARIABLES
3970 C *****
3980 C
3990 C NMES--NUMBER OF MEASUREMENT POINT
4000 C NPTS--NUMBER OF POINTS FOR THE PLOT OF THE CURVE
4010 C I --NUMBER OF PLOTS TO BE MADE
4020 C N --NUMBER OF THE ACTUAL EXPERIMENT
4030 C
4040 C COMMON
4050 C *****
4060 C
4070 C VALUE2--X(MAXDAT,10) : X-VALUES OF THE POINTS TO BE PLOTTED
4080 C Y(MAXDAT,10) : Y-VALUES OF THE POINTS TO BE PLOTTED
4090 C
4100 C PARAMETER(MAXDAT=100)
4110 C CHARACTER*20 LEGEND(10)
4120 C CHARACTER*60 XAXIS,YAXIS
4130 C CHARACTER*60 TITLE
4140 C DIMENSION X(MAXDAT,10),Y(MAXDAT,10),NSYMB(10),KCHAR(10),L(10)
4150 C COMMON / VALUE2 /X,Y
4160 C LEGEND(1)= '0.5341M/S'
4170 C LEGEND(2)= '0.8012M/S'
4180 C LEGEND(3)= '1.0793M/S'
4190 C LEGEND(4)= '1.3464M/S'
4200 C LEGEND(5)= '1.6246M/S'
4210 C LEGEND(6)= 'AIR SPEED'
4220 C LEGEND(7)= ' '
4230 C LEGEND(8)= ' '
4240 C LEGEND(9)= ' '
4250 C LEGEND(10)= ' '
4260 C XAXIS= 'CENTRAL JET VELOCITY / STAGNATION POINT VELOCITY'

```

```

4270 YAXIS= FORWARD / AFT STAGNATION POINT
4280 WRITE(TITLE,901) N
4290 DATA NSYMB / 5*-1,5*0/
4300 DATA KCHAR / 1,2,3,4,5,5*1/
4310 L(1)=NMES
4320 L(2)=NMES
4330 L(3)=NMES
4340 L(4)=NMES
4350 L(5)=NMES
4360 L(6)=NPTS
4370 L(7)=NPTS
4380 L(8)=NPTS
4390 L(9)=NPTS
4400 L(10)=NPTS
4410 CALL NAMPLT
4420 CALL MRANGX(0.0,1.2)
4430 CALL MPANGY(0.0,1.2)
4440 CALL MOIV(6.0,6.0)
4450 CALL MSTARTA(X,L,MAXDAT,TITLE,XAXIS,1,I,1,2.0,6.0)
4460 CALL MLINEA (X,L,Y,MAXDAT,I,YAXIS,LEGEND,1,NSYMB,KCHAR)
4470 CALL ENOPLT
4480 RETURN
4490 901 FORMAT(1X, 'PLOT OF THE NONDIMENSIONALIZED DATA SET ',I2)
4500 END
4510 C *****
4520 C SUBROUTINE FCTDET(NMES,N,ITYP,IM)
4530 C
4540 C CONTROL THE FLOW OF THE SUBROUTINES TO FIND THE CONSTANTS
4550 C OF A FUNCTION BY A LEAST SQUARE METHOD
4560 C
4570 C
4580 C VARIABLES
4590 C *****
4600 C
4610 C NMES--NUMBER OF MEASUREMENT POINTS IN COMMON 'VALUE2'
4620 C N --NUMBER OF ACTUAL EXPERIMENT
4630 C
4640 C COMMON
4650 C *****
4660 C
4670 C VALUE2--X(MAXDAT,10) : X-VALUES OF EXPERIMENTAL DATA AND
4680 C THE CURVE FITTING
4690 C Y(MAXDAT,10) : Y-VALUES OF THE ABOVE
4700 C
4710 C SUBROUTINES CALLED
4720 C *****
4730 C
4740 C FCTFIT--DETERMINE THE CONSTANTS
4750 C FCTPRT--PRINT THE FUNCTION AND THE CONSTANTS
4760 C FCTPLT--FIND THE X AND Y-VALUES OF THE CURVE FITTING
4770 C
4780 C
4790 C PARAMETER(MAXDAT=100,MAXCON=10)
4800 C DIMENSION X(MAXDAT,10),Y(MAXDAT,10),A(MAXCON)
4810 C COMMON / VALUE2 /X,Y
4820 C NPTS=50
4830 C CALL FCTFIT(X(1,N),Y(1,N),MAXDAT,NMES, A,ERR,IERR,IT)
4840 C IF(IERR.LT.0) THEN
4850 C WRITE(6,901) 'NO LEAST SQUARE FITTING POSSIBLE '
4860 C WRITE(6,902) 'IERR= ',IERR
4870 C RETURN
4880 C ENDIF
4890 C CALL FCTPRT(A,ERR,IT)
4900 C CALL FCTPLT(X(1,N),Y(1,N),A,NPTS,NMES,X(1,N+5),Y(1,N+5))
4910 C IF((ITYP.EQ.4).AND.(N.EQ.IM)) CALL DRAW(NMES,NPTS,10,N)
4920 C RETURN
4930 901 FORMAT(2Y,4)

```

```

4930 202  FORMAT(2X,1,15)
4940      END
4950 0      *****
4960      SUBROUTINE FCFIT(X,Y,MAXDAT,NMES,A,ERR,IERR,IT)
4970 0
4980 0      DETERMINE THE CONSTANTS OF THE FUNCTION
4990 0
5000 0      VARIABLES
5010 0      *****
5020 0
5030 0      X(MAXDAT,*)--X-VALUES OF THE EXPERIMENTAL DATA
5040 0      Y(MAXDAT,*)--Y-VALUES OF THE EXPERIMENTAL DATA
5050 0      MAXDAT--MAXIMUM NUMBER OF EXPERIMENTAL DATA (ONLY USED
5060 0              FOR DIMENSION)
5070 0      NMES  --ACTUAL NUMBER OF EXPERIMENTAL DATA SETS
5080 0      A(MAX)--VECTOR CONTAINING THE CONSTANTS
5090 0      ERR   --LEAST SQUARE ERROR NORM
5100 0      IERR  --NUMBER SHOWING HOW FCFIT WORKED
5110 0              IERR>0 : FCFIT GOT RESULTS
5120 0              IERR<0 : SOME KIND OF ERROR WITHIN FCFIT
5130 0
5140 0      SUBROUTINES CALLED
5150 0      *****
5160 0
5170 0      FCT --CONTAIN THE FUNCTION AND ITS PARTIAL DERIVATIVES
5180 0      ELIM--SOLVE A SET OF EQUATIONS
5190 0
5200      PARAMETER(MAX=100,MAXP1=11)
5210      DIMENSION X(MAXDAT,*),Y(MAXDAT,*),A(MAX),F(MAX),W(MAX),
5220 0      XSAVE(MAX),FSAVE(MAX),ARR(MAX,MAXP1)
5230      CHARACTER *50 STRING
5240      LOGICAL FINISH
5250      CALL FCT(A,F,X,Y,W,1,NCONST,STRING,ERR,MAXIT,DELTA,
5260 0      XTOL, FTOL,0)
5270      IF(MAXIT.LT.0) MAXIT=50
5280      IF(DELTA.LT. 0.0) DELTA=.01
5290      IF(XTOL.LT.0.0) XTOL=.0001
5300      IF(FTOL.LT.0.0) FTOL=.0005
5310      NP1=NCONST+1
5320      DO 500 IT=1,MAXIT
5330          DO 10 I=1,NCONST
5340              XSAVE(I)=A(I)
5350 10      CONTINUE
5360          CALL FCT(A,F,X,Y,W,NMES,NCONST,STRING,ERR,P,P,P,R,
5370 0      2)
5380          FINISH=.TRUE.
5390          DO 20 I=1,NCONST
5400              IF(ABS(F(I)).GT.FTOL) FINISH=.FALSE.
5410              FSAVE(I)=F(I)
5420 20      CONTINUE
5430          IF(FINISH) THEN
5440              IERR=2
5450              RETURN
5460          ENDIF
5470          DO 100 J=1,NCONST
5480              A(J)=XSAVE(J)+DELTA
5490              CALL FCT(A,F,X,Y,W,NMES,NCONST,STRING,ERR,P,P,P,R,
5500 0      2)
5510          DO 150 I=1,NCONST
5520              ARR(I,J)=(F(I)-FSAVE(I))/DELTA
5530 150      CONTINUE
5540          A(J)=XSAVE(J)
5550 100      CONTINUE
5560          DO 200 I=1,NCONST
5570              ARR(I,NP1)=-FSAVE(I)
5580 200      CONTINUE

```

```

F530      CALL ELIN(ARR,NCONST,NP1,MAX)
F540      DO 300 I=1,NCONST
F510          IF (ABS(ARR(I,I)).LE.0.0000001) THEN
F520              IERR=-2
F530              RETURN
F540          ENDIF
F550 300    CONTINUE
F560      FINISH=.TRUE.
F570      DO 400 I=1,NCONST
F580          A(I)=XSAVE(I)+ARR(I,NP1)
F590          IF (ABS(ARR(I,NP1)).GT.XTOL) FINISH=.FALSE.
F600 400    CONTINUE
F610      IF (FINISH) THEN
F620          IERR=1
F630          RETURN
F640      ENDIF
F650 500    CONTINUE
F660      IERR=-1
F670      RETURN
F680      END
F690      *****
F700      SUBROUTINE FCT(A,F,X,Y,OVDG,MAX,NCONST,STRING,
F710      Q      EPSQ,MAXIT,DELTA, XTOL, FTOL, ITYP)
F720      C
F730      C      CONTAIN THE FUNCTION AND ITS PARTIAL DERIVATIVES WITH RESPECT TO
F740      C      CONSTANTS A(I)
F750      C
F760      C      VARIABLES
F770      C      *****
F780      C
F790      C      A(NCONST)--VECTOR CONTAINING THE CONSTANTS A1...AN OF THE
F800      C      FUNCTION
F810      C      F(NCONST)--VECTOR CONTAINING THE SUM FOR ALL GIVEN
F820      C      EXPERIMENTAL DATA OF THE PARTIAL DERIVATIVES OF
F830      C      THE FUNCTION WITH RESPECT TO THE CONSTANTS A(I)
F840      C      X(MAX)  --VECTOR CONTAINING THE X-VALUES OF THE
F850      C      EXPERIMENTAL DATA
F860      C      Y(MAX)  --FOR ITYP=1 : FOR THE GIVEN X-VALUES ARE Y-VALUES
F870      C      COMPUTED WITH THE FUNCTION AND STORED IN Y
F880      C      FOR ITYP=2 : Y CONTAINING THE Y-VALUES OF THE
F890      C      EXPERIMENTAL DATA CORRESPONDING TO X
F900      C      OVDG(NCONST)--VECTOR CONTAINING THE PARTIAL DERIVATIVES
F910      C      OF THE FUNCTION
F920      C      MAX      --NUMBER OF EXPERIMENTL DATA (FOR ITYP=2) OR
F930      C      NUMBER OF Y-VALUES TO BE COMPUTED (FOR ITYP=1)
F940      C      NCONST  --NUMBER OF CONSTANTS
F950      C      STRING   --CHARACTER VARIABLE CONTAINING THE FUNCTION
F960      C      EPSQ    --CONTAIN LEAST SQUARE ERROR NORM FOR THE GIVEN
F970      C      FUNCTION,CONSTANTS AN EXPERIMENTAL DATA
F980      C      MAXIT   --MAXIMUM NUMBER OF ITERATIONS FOR LEAST SQUARE
F990      C      FIT
F1000      C      IF MAXIT=-1,A DEFAULT VALUE WILL BE USED
F1010      C      DELTA  --SMALL VALUE TO COMPUTE THE PARTIAL DERIVATIVES
F1020      C      FOR NEWTON METHOD OF SOLVING NONLINEAR EQUATIONS
F1030      C      IF DELTA=-1.0,A DEFAULT VALUE WILL BE USED
F1040      C      FTOL   --CONTAIN THE TOLERANCE IN THE COMPUTED VALUES OF
F1050      C      PARTIAL DERIVATIVES TO STOP THE ITERATION
F1060      C      IF FTOL=-1.0,A DEFAULT VALUE WILL BE USED
F1070      C      XTOL   --CONTAIN THE TOLERANC IN THE CONSTANTS OF THE
F1080      C      FUNCTION TO STOP THE ITERATION
F1090      C      IF XTOL =-1.0,A DEFAULT VALUE WILL BE USED
F1100      C
F1110      C      CHARACTER *50 STRING
F1120      C      DIMENSION A(*),F(*),X(*),Y(*),OVDG(*)
F1130      C
F1140      C      YOU SHOULD INSERT HERE THE VALUES FOR MAXIT,DELTA,FTOL AND XTOL

```

```

4240 C IF YOU DON'T HAVE ANY SPECIAL PURPOSES OR IF YOU ARE NOT SURE
4250 C ABOUT THEM, JUST SET THEM TO -1.0, A DEFAULT VALUE WILL BE USED
4260 C
4270 C
4280 C MAXIT=-1
4290 C DELTA=-1.0
4300 C ATOL=-1.0
4310 C FTOL=-1.0
4320 C
4330 C YOU HAVE TO INSERT HERE HOW MANY CONSTANTS YOUR FUNCTION CONTAINS
4340 C
4350 C NCONST=3
4360 C
4370 C YOU SHOULD INSERT HERE YOUR FUNCTION AS A CHARACTER STRING,
4380 C THIS WILL BE USED FOR THE OUTPUT ONLY, SO CHOOSE ANY FORM
4390 C CONVENIENT TO YOU
4400 C
4410 C STRING='Y = 1+A1*(1-X)+A2*(1-Y)**2+A3*(1-X)**3 '
4420 C
4430 C IF (ITYP.EQ.0) THEN
4440 C
4450 C YOU HAVE TO INSERT HERE THE STARTING VALUES FOR ALL YOUR
4460 C CONSTANTS A1...A2, JUST MAKE ANY GUESS FOR THEM
4470 C
4480 C A(1)=0.1
4490 C A(2)=2.3
4500 C A(3)=1.5
4510 C
4520 C ELSE IF (ITYP.EQ.1) THEN
4530 C DO 100 I=1,MAX
4540 C
4550 C YOU HAVE TO INSERT HERE THE FUNCTION WHICH IS THE BASIS FOR THE
4560 C LEAST SQUARE FIT
4570 C
4580 C Y(I)=1.0+(1.-X(I))*(A(1)+(1.-X(I))*(A(2)+A(3)*(1.-X(I))))
4590 C
4600 100 CONTINUE
4610 C ELSE IF (ITYP.EQ.2) THEN
4620 C DO 150 I=1,NCONST
4630 C F(I)=0.0
4640 150 CONTINUE
4650 C ERRSQ=0.0
4660 C DO 200 I=1,MAX
4670 C
4680 C YOU HAVE TO PROGRAM HERE YOUR FUNCTION IN THE FORM
4690 C Y(I)=(FUNCTION)
4700 C
4710 C S=Y(I)-1.0-(1.-X(I))*(A(1)+(1.-X(I))*(A(2)+A(3)*(1.-X(I))))
4720 C
4730 C YOU HAVE TO PROGRAM HERE ALL PARTIAL DERIVATIVES OF THE FUNCTION
4740 C WITH RESPECT TO CONSTANTS A1...AN.
4750 C
4760 C DVDA(1)=1.0-X(I)
4770 C DVDA(2)=(1.0-Y(I))*(1.0-X(I))
4780 C DVDA(3)=(1.0-X(I))*(1.0-X(I))*(1.0-X(I))
4790 C
4800 C DO 210 II=1,NCONST
4810 C F(II)=F(II)+0.05*DVDA(II)
4820 210 CONTINUE
4830 C ERRSQ=ERRSQ+S*S
4840 200 CONTINUE
4850 C ENDOF
4860 C RETURN
4870 C END
4880 C
4890 C *****
4900 C SUBROUTINE FOTPRPT(A,ERR,IT)
4910 C

```

```

4910 C PRINT OUT THE FUNCTION OF THE LEAST SQUARE FIT AND ITS CONSTANTS
4920 C
4930 C VARIABLES
4940 C *****
4950 C
4960 C A --VECTOR CONTAINING THE CONSTANTS
4970 C ERR--THE LEAST SQUARE ERROR NORM
4980 C IT --ITERATION INDEX
4990 C
5000 C SUBROUTINES CALLED
5010 C *****
5020 C
5030 C FCT--CONTAIN THE FUNCTION AS A CHARACTER STRING
5040 C
5050 C
5060 C PARAMETER(MAX=10)
5070 C DIMENSION P(MAX),A(MAX),AO(MAX)
5080 C CHARACTER *50 STRING
5090 C CALL FCT (AO,P,P,P,P,1,NCONST,STRING,ERRSQ,P,P,P,P,C)
5100 C WRITE(6,1('111'))
5110 C WRITE(6,901)
5120 C WRITE(6,901)
5130 C WRITE(6,901) 'FUNCTION FOR THIS DATA SET'
5140 C WRITE(6,901) '*****'
5150 C WRITE(6,901)
5160 C WRITE(6,901) 'THE VALUES ARE NONDIMENSIONALIZED BY THE RULES'
5170 C WRITE(6,901)
5180 C WRITE(6,901) ' VELOCITY OF FUEL'
5190 C WRITE(6,901) ' X = -----'
5200 C WRITE(6,901) ' PENETRATION VELOCITY '
5210 C WRITE(6,901)
5220 C WRITE(6,901) ' FORWARD STAGNATION POINT'
5230 C WRITE(6,901) ' Y = -----'
5240 C WRITE(6,901) ' AFT STAGNATION POINT'
5250 C WRITE(6,901)
5260 C WRITE(6,902) 'CONSTANTS ARE DETERMINED BY A LEAST SQUARE METHOD'
5270 C WRITE(6,901)
5280 C WRITE(6,901)
5290 C WRITE(6,902) 'FUNCTION: ' ,STRING
5300 C WRITE(6,901) '*****'
5310 C WRITE(6,901)
5320 C WRITE(6,901)
5330 C WRITE(6,906) 'INITIAL VALUES: ',A1 = ',AO(1)
5340 C WRITE(6,906) '***** ',A2 = ',AO(2)
5350 C DO 50 I=3,NCONST
5360 C WRITE(6,907) ' A',I,' = ',AO(I)
5370 C 50 CONTINUE
5380 C WRITE(6,901)
5390 C WRITE(6,901)
5400 C WRITE(6,906) 'CONSTANTS: ',A1 = ',A(1)
5410 C WRITE(6,906) '***** ',A2 = ',A(2)
5420 C DO 100 I = 3,NCONST
5430 C WRITE(6,907) ' A',I,' = ', A(I)
5440 C 100 CONTINUE
5450 C WRITE(6,901)
5460 C WRITE(6,901)
5470 C WRITE(6,909) 'LEAST SQUARE ERROR NORM: E = ',ERR
5480 C WRITE(6,901)
5490 C WRITE(6,909) 'THE SOLUTION WAS FOUND AFTER',IT,'ITERATIONS'
5500 C RETURN
5510 C 901 FORMAT(2X,A)
5520 C 902 FORMAT(2X,A,A)
5530 C 906 FORMAT(2X,A,A,G10.3)
5540 C 907 FORMAT(2X,17X,A,I1,A,G10.3)
5550 C 909 FORMAT(2X,A,G15.5)
5560 C 909 FORMAT(2X,A,I4,1X,A) 34.91

```

```

7570      END
7580      *****
7590      SUBROUTINE FCTPLT (X,Y,A,NPTS,NMES,XX,YY)
7600
7610      COMPUTE THE X- AND Y-VALUES OF THE CURVE DETERMINED BY
7620      THE LEAST SQUARE METHOD AND PLOT THEM
7630
7640      VARIABLES
7650      *****
7660
7670      X(*)    --CONTAIN THE X-VALUES OF THE EXPERIMENTAL DATA
7680      Y(*)    --CONTAIN THE Y-VALUES OF THE EXPERIMENTAL DATA
7690      A(*)    --CONTAIN THE CONSTANTS OF THE FUNCTION
7700      NPTS    --NUMBER OF THE POINTS FOR THE CURVE
7710      NMES    --NUMBER OF MEASUREMENT POINTS OF EXPERIMENTAL DATA
7720      XX(*)   --X-VALUES FOR THE CURVE
7730      YY(*)   --Y-VALUES FOR THE CURVE
7740
7750      SUBROUTINE CALLED
7760      *****
7770
7780      FCT --FUNCTION OF THE LEAST SQUARE CURVE
7790
7800      PARAMETER(MAXDAT=100)
7810      CHARACTER *50 STRING
7820      DIMENSION X(MAXDAT),Y(MAXDAT),A(*),P(1),XX(MAXDAT),YY(MAXDAT)
7830      XMIN=X(1)
7840      XMAX=X(1)
7850      DO 100 I=2,NMES
7860         IF (XMIN.GT.X(I)) XMIN=X(I)
7870         IF (XMAX.LT.X(I)) XMAX=X(I)
7880      CONTINUE
7890      STEP= (XMAX-XMIN)/(NPTS-1)
7900      DO 200 I=1,NPTS
7910         XX(I)=XMIN+(I-1)*STEP
7920      CONTINUE
7930      CALL FCT (A,P,XX,YY,P,NPTS,NCONST,STRING,ERR,
7940              P,P,P,P,1)
7950      RETURN
7960      END
7970      *****
7980      SUBROUTINE ELIM (AB,N,NP,NDIM)
7990
8000      SOLVE A SET OF LINEAR EQUATIONS
8010
8020      VARIABLES
8030      *****
8040
8050      AB(NDIM,*)--ARRAY CONTAINING THE COEFFICIENT MATRIX AND THE
8060                  RIGHT HAND SIDE OF THE MATRIX EQUATION
8070      N          --NUMBER OF EQUATIONS
8080      NP         --NUMBER OF EQUATIONS + NUMBER OF RIGHT HAND SIDE VECTORS
8090      NDIM       --MAXIMUM NUMBER OF EQUATIONS
8100
8110      REAL AB (NDIM,NP)
8120      NM1=N-1
8130      DO 35 I = 1,NM1
8140         IPVT=I
8150         IP1 = I+1
8160         DO 10 J = IP1,N
8170            IF (ABS ( AB(IPVT,I) ).LT. ABS(AB(J,I) ) ) IPVT = J
8180      CONTINUE
8190      IF (ABS(AB(IPVT,I) ) .LT. 0.0000001 ) THEN
8200         WRITE(6,901) 'MATRIX NEAR SINGULAR - PIVOT SEARCH'
8210         RETURN
8220      ENDDF

```

```

0330 IF ( IPVT,1E.1 ) THEN
0340 DO 20 JCCL = 1,NP
0350 SAVE=AB(I,JCCL)
0360 AB(I,JCCL)=AB(IPVT,JCCL)
0370 AB(IPVT,JCCL)=SAVE
0380 20 CONTINUE
0390 ENDDO
0400 DO 32 JROW=IP1,N
0410 IF (AB(JROW,I).EQ.0.0) GOTO 32
0420 RATIO=AB(JROW,I)/AB(I,I)
0430 AB(JROW,I)=RATIO
0440 DO 30 KCCL = IP1,NP
0450 AB(JROW,KCCL)=AB(JROW,KCCL)-RATIO*AB(I,KCCL)
0460 30 CONTINUE
0470 32 CONTINUE
0480 35 CONTINUE
0490 IF ( ABS(AB(N,N)).LT. 0.0000001 ) THEN
0500 WRITE(6,901) 'MATRIX NEAR SINGULAR'
0510 RETURN
0520 ENDDO
0530 NP1=N+1
0540 DO 50 KCCL=NP1,NP
0550 AB(N,KCCL)=AB(N,KCCL)/AB(N,N)
0560 DO 45 J=2,N
0570 NVBL=NP1-J
0580 L=NVBL+1
0590 VALUE=AB(NVBL,KCCL)
0600 DO 40 K=L,N
0610 VALUE=VALUE-AB(NVBL,K)*AB(K,KCCL)
0620 40 CONTINUE
0630 AB(NVBL,KCCL)=VALUE/AB(NVBL,NVBL)
0640 45 CONTINUE
0650 50 CONTINUE
0660 RETURN
0670 901 FORMAT(2X,A)
0680 END
0690 9,20.0,30.5,0.372
0700 0.75,47.1,66.0
0710 33.5,67.1,0.209,0.208,0.511
0720 45.1,66.5,0.197,0.267,0.71
0730 47.1,66.0,0.196,0.262,0.75
0740 39.5,66.5,0.190,0.233,0.632
0750 26.4,67.1,0.210,0.224,0.40
0760 20.5,67.6,0.158,0.231,0.29
0770 14.0,67.3,0.175,0.257,0.146
0780 9.50,68.0,0.1267,0.215,0.089
0790 9,30.0,29.5,0.372
0800 1.058,53.0,63.1
0810 53.0,63.1,0.200,0.206,1.058
0820 47.0,64.0,0.200,0.2515,0.985
0830 41.0,64.9,0.226,0.246,0.855
0840 27.0,65.1,0.240,0.300,0.45
0850 32.5,65.0,0.231,0.278,0.5
0860 22.0,65.9,0.226,0.348,0.389
0870 12.0,66.9,0.220,0.317,0.153
0880 9.00,68.1,0.196,0.274,0.119
0890 9,40.0,29.5,0.372
0900 0.863,53.0,63.0
0910 51.0,63.0,0.231,0.250,0.863
0920 43.0,64.1,0.256,0.275,0.77
0930 32.0,64.8,0.257,0.298,0.598
0940 24.0,65.1,0.258,0.405,0.420
0950 15.5,66.0,0.2545,0.369,0.222
0960 9.0,67.8,0.2365,0.339,0.117
0970 9,50.0,29.5,0.372
0980 0.9,50.0,61.0

```



Appendix C: Computer Program Run on Harris 800

(Plotting Curves  $\frac{L}{D_1}$  vs. Flow Conditions)

1. The purpose of this experiment is to determine the effect of the concentration of a solution on the rate of a chemical reaction. The reaction studied is the reaction between sodium thiosulfate and hydrochloric acid, which produces a precipitate of sulfur and a solution of sodium chloride and sulfuric acid. The rate of reaction is measured by the time taken for the precipitate to form and for the solution to become cloudy.

2. The reaction is carried out in a conical flask. A known volume of sodium thiosulfate solution is added to a known volume of hydrochloric acid solution. The mixture is then allowed to react for a certain period of time. The time taken for the precipitate to form is measured by a stopwatch. The time taken for the solution to become cloudy is measured by a stopwatch.

3. The results of the experiment are shown in the following table. The concentration of the sodium thiosulfate solution is varied, and the time taken for the precipitate to form and for the solution to become cloudy is measured. The results show that the rate of reaction increases as the concentration of the sodium thiosulfate solution increases.

4. The results of the experiment are shown in the following table. The concentration of the sodium thiosulfate solution is varied, and the time taken for the precipitate to form and for the solution to become cloudy is measured. The results show that the rate of reaction increases as the concentration of the sodium thiosulfate solution increases.

5. The results of the experiment are shown in the following table. The concentration of the sodium thiosulfate solution is varied, and the time taken for the precipitate to form and for the solution to become cloudy is measured. The results show that the rate of reaction increases as the concentration of the sodium thiosulfate solution increases.

6. The results of the experiment are shown in the following table. The concentration of the sodium thiosulfate solution is varied, and the time taken for the precipitate to form and for the solution to become cloudy is measured. The results show that the rate of reaction increases as the concentration of the sodium thiosulfate solution increases.

7. The results of the experiment are shown in the following table. The concentration of the sodium thiosulfate solution is varied, and the time taken for the precipitate to form and for the solution to become cloudy is measured. The results show that the rate of reaction increases as the concentration of the sodium thiosulfate solution increases.

8. The results of the experiment are shown in the following table. The concentration of the sodium thiosulfate solution is varied, and the time taken for the precipitate to form and for the solution to become cloudy is measured. The results show that the rate of reaction increases as the concentration of the sodium thiosulfate solution increases.

THE UNIVERSITY OF CHICAGO  
DIVISION OF THE PHYSICAL SCIENCES  
DEPARTMENT OF CHEMISTRY

RESEARCH REPORT  
No. 1000  
JANUARY 1961

THE UNIVERSITY OF CHICAGO  
DIVISION OF THE PHYSICAL SCIENCES  
DEPARTMENT OF CHEMISTRY

RESEARCH REPORT

No. 1000

JANUARY 1961

THE UNIVERSITY OF CHICAGO  
DIVISION OF THE PHYSICAL SCIENCES  
DEPARTMENT OF CHEMISTRY

RESEARCH REPORT

No. 1000

JANUARY 1961

THE UNIVERSITY OF CHICAGO  
DIVISION OF THE PHYSICAL SCIENCES  
DEPARTMENT OF CHEMISTRY

RESEARCH REPORT

No. 1000

JANUARY 1961

THE UNIVERSITY OF CHICAGO  
DIVISION OF THE PHYSICAL SCIENCES  
DEPARTMENT OF CHEMISTRY

[illegible]

the 1990s, the number of people in the world who are under 15 years of age is expected to increase by 1.5 billion, from 1.1 billion in 1990 to 2.6 billion in 2010. The number of people aged 65 and over is expected to increase by 1.1 billion, from 0.3 billion in 1990 to 1.4 billion in 2010. The number of people aged 15-64 is expected to increase by 1.1 billion, from 1.7 billion in 1990 to 2.8 billion in 2010. The number of people aged 65 and over is expected to increase by 1.1 billion, from 0.3 billion in 1990 to 1.4 billion in 2010. The number of people aged 15-64 is expected to increase by 1.1 billion, from 1.7 billion in 1990 to 2.8 billion in 2010.

the 1990s, the number of people in the world who are under 15 years of age is expected to increase by 1.5 billion, from 1.1 billion in 1990 to 2.6 billion in 2010. The number of people aged 65 and over is expected to increase by 1 billion, from 350 million in 1990 to 1.4 billion in 2010. The number of people aged 15-64 is expected to increase by 1.5 billion, from 1.1 billion in 1990 to 2.6 billion in 2010. The number of people aged 65 and over is expected to increase by 1 billion, from 350 million in 1990 to 1.4 billion in 2010. The number of people aged 15-64 is expected to increase by 1.5 billion, from 1.1 billion in 1990 to 2.6 billion in 2010.

[illegible]

the 1990s, the number of people in the world who are illiterate has increased from 1.2 billion to 1.5 billion. The number of illiterate people in the world is expected to reach 1.7 billion by the year 2015. The number of illiterate people in the world is expected to reach 1.7 billion by the year 2015.

Figure 1. The effect of the concentration of the inhibitor on the rate of polymerization of  $\alpha$ -methylstyrene in the presence of  $\text{SnCl}_4$  at  $25^\circ\text{C}$ .

100

[illegible]

1. *Chlorophyll a* (Chl *a*)

• *W. J. G. & J. J. G.*

1997, 1998, 1999, 2000, 2001, 2002, 2003, 2004, 2005, 2006, 2007, 2008, 2009, 2010, 2011, 2012, 2013, 2014, 2015, 2016, 2017, 2018, 2019, 2020, 2021, 2022, 2023, 2024, 2025, 2026, 2027, 2028, 2029, 2030, 2031, 2032, 2033, 2034, 2035, 2036, 2037, 2038, 2039, 2040, 2041, 2042, 2043, 2044, 2045, 2046, 2047, 2048, 2049, 2050, 2051, 2052, 2053, 2054, 2055, 2056, 2057, 2058, 2059, 2060, 2061, 2062, 2063, 2064, 2065, 2066, 2067, 2068, 2069, 2070, 2071, 2072, 2073, 2074, 2075, 2076, 2077, 2078, 2079, 2080, 2081, 2082, 2083, 2084, 2085, 2086, 2087, 2088, 2089, 2090, 2091, 2092, 2093, 2094, 2095, 2096, 2097, 2098, 2099, 2100, 2101, 2102, 2103, 2104, 2105, 2106, 2107, 2108, 2109, 2110, 2111, 2112, 2113, 2114, 2115, 2116, 2117, 2118, 2119, 2120, 2121, 2122, 2123, 2124, 2125, 2126, 2127, 2128, 2129, 2130, 2131, 2132, 2133, 2134, 2135, 2136, 2137, 2138, 2139, 2140, 2141, 2142, 2143, 2144, 2145, 2146, 2147, 2148, 2149, 2150, 2151, 2152, 2153, 2154, 2155, 2156, 2157, 2158, 2159, 2160, 2161, 2162, 2163, 2164, 2165, 2166, 2167, 2168, 2169, 2170, 2171, 2172, 2173, 2174, 2175, 2176, 2177, 2178, 2179, 2180, 2181, 2182, 2183, 2184, 2185, 2186, 2187, 2188, 2189, 2190, 2191, 2192, 2193, 2194, 2195, 2196, 2197, 2198, 2199, 2200, 2201, 2202, 2203, 2204, 2205, 2206, 2207, 2208, 2209, 2210, 2211, 2212, 2213, 2214, 2215, 2216, 2217, 2218, 2219, 2220, 2221, 2222, 2223, 2224, 2225, 2226, 2227, 2228, 2229, 2230, 2231, 2232, 2233, 2234, 2235, 2236, 2237, 2238, 2239, 2240, 2241, 2242, 2243, 2244, 2245, 2246, 2247, 2248, 2249, 2250, 2251, 2252, 2253, 2254, 2255, 2256, 2257, 2258, 2259, 2260, 2261, 2262, 2263, 2264, 2265, 2266, 2267, 2268, 2269, 2270, 2271, 2272, 2273, 2274, 2275, 2276, 2277, 2278, 2279, 2280, 2281, 2282, 2283, 2284, 2285, 2286, 2287, 2288, 2289, 2290, 2291, 2292, 2293, 2294, 2295, 2296, 2297, 2298, 2299, 2300, 2301, 2302, 2303, 2304, 2305, 2306, 2307, 2308, 2309, 2310, 2311, 2312, 2313, 2314, 2315, 2316, 2317, 2318, 2319, 2320, 2321, 2322, 2323, 2324, 2325, 2326, 2327, 2328, 2329, 2330, 2331, 2332, 2333, 2334, 2335, 2336, 2337, 2338, 2339, 2340, 2341, 2342, 2343, 2344, 2345, 2346, 2347, 2348, 2349, 2350, 2351, 2352, 2353, 2354, 2355, 2356, 2357, 2358, 2359, 2360, 2361, 2362, 2363, 2364, 2365, 2366, 2367, 2368, 2369, 2370, 2371, 2372, 2373, 2374, 2375, 2376, 2377, 2378, 2379, 2380, 2381, 2382, 2383, 2384, 2385, 2386, 2387, 2388, 2389, 2390, 2391, 2392, 2393, 2394, 2395, 2396, 2397, 2398, 2399, 2400, 2401, 2402, 2403, 2404, 2405, 2406, 2407, 2408, 2409, 2410, 2411, 2412, 2413, 2414, 2415, 2416, 2417, 2418, 2419, 2420, 2421, 2422, 2423, 2424, 2425, 2426, 2427, 2428, 2429, 2430, 2431, 2432, 2433, 2434, 2435, 2436, 2437, 2438, 2439, 2440, 2441, 2442, 2443, 2444, 2445, 2446, 2447, 2448, 2449, 2450, 2451, 2452, 2453, 2454, 2455, 2456, 2457, 2458, 2459, 2460, 2461, 2462, 2463, 2464, 2465, 2466, 2467, 2468, 2469, 2470, 2471, 2472, 2473, 2474, 2475, 2476, 2477, 2478, 2479, 2480, 2481, 2482, 2483, 2484, 2485, 2486, 2487, 2488, 2489, 2490, 2491, 2492, 2493, 2494, 2495, 2496, 2497, 2498, 2499, 2500, 2501, 2502, 2503, 2504, 2505, 2506, 2507, 2508, 2509, 2510, 2511, 2512, 2513, 2514, 2515, 2516, 2517, 2518, 2519, 2520, 2521, 2522, 2523, 2524, 2525, 2526, 2527, 2528, 2529, 2530, 2531, 2532, 2533, 2534, 2535, 2536, 2537, 2538, 2539, 2540, 2541, 2542, 2543, 2544, 2545, 2546, 2547, 2548, 2549, 2550, 2551, 2552, 2553, 2554, 2555, 2556, 2557, 2558, 2559, 2560, 2561, 2562, 2563, 2564, 2565, 2566, 2567, 2568, 2569, 2570, 2571, 2572, 2573, 2574, 2575, 2576, 2577, 2578, 2579, 2580, 2581, 2582, 2583, 2584, 2585, 2586, 2587, 2588, 2589, 2590, 2591, 2592, 2593, 2594, 2595, 2596, 2597, 2598, 2599, 2600, 2601, 2602, 2603, 2604, 2605, 2606, 2607, 2608, 2609, 2610, 2611, 2612, 2613, 2614, 2615, 2616, 2617, 2618, 2619, 2620, 2621, 2622, 2623, 2624, 2625, 2626, 2627, 2628, 2629, 2630, 2631, 2632, 2633, 2634, 2635, 2636, 2637, 2638, 2639, 2640, 2641, 2642, 2643, 2644, 2645, 2646, 2647, 2648, 2649, 2650, 2651, 2652, 2653, 2654, 2655, 2656, 2657, 2658, 2659, 2660, 2661, 2662, 2663, 2664, 2665, 2666, 2667, 2668, 2669, 2670, 2671, 2672, 2673, 2674, 2675, 2676, 2677, 2678, 26

— *Journal of the American Medical Association*, 1997

—

PROGRAM KDL1

REARRANGE EXPERIMENTAL DATA OF BLUFF BODY COMBUSTION BY  
USING REYNOLDS NUMBER.  
UNITS FOR INPUT PARAMETERS: D--INCH, VELAIF--M/SEC, T--  
F, P--PSI, W--LB/HR, L--INCH, U--M/SEC

REAL C,LDU

DATA 1.320\*2.54,100

DATA 0.750\*0.54,100

DATA 0.043\*0.000

DATA 0.014,3.14,10

DATA 0.014\*0.000

DATA 0.014\*0.000

DATA 0.014\*0.000

DATA 0.014\*0.000

DATA 0.014\*0.000

DATA 0.014\*0.000

DATA 0.014\*0.000

DATA 0.014\*0.000

DATA 0.014\*0.000

DATA 0.014\*0.000

DATA 0.014\*0.000

DATA 0.014\*0.000

DATA 0.014\*0.000

DATA 0.014\*0.000

DATA 0.014\*0.000

DATA 0.014\*0.000

DATA 0.014\*0.000

DATA 0.014\*0.000

DATA 0.014\*0.000

DATA 0.014\*0.000

DATA 0.014\*0.000

DATA 0.014\*0.000

DATA 0.014\*0.000

DATA 0.014\*0.000

DATA 0.014\*0.000

DATA 0.014\*0.000

DATA 0.014\*0.000

DATA 0.014\*0.000

DATA 0.014\*0.000

DATA 0.014\*0.000

DATA 0.014\*0.000

DATA 0.014\*0.000

DATA 0.014\*0.000

DATA 0.014\*0.000

DATA 0.014\*0.000

DATA 0.014\*0.000

DATA 0.014\*0.000

DATA 0.014\*0.000

DATA 0.014\*0.000

DATA 0.014\*0.000

DATA 0.014\*0.000

DATA 0.014\*0.000

DATA 0.014\*0.000

DATA 0.014\*0.000

DATA 0.014\*0.000

DATA 0.014\*0.000

DATA 0.014\*0.000

DATA 0.014\*0.000

DATA 0.014\*0.000

DATA 0.014\*0.000

DATA 0.014\*0.000

DATA 0.014\*0.000

DATA 0.014\*0.000

DATA 0.014\*0.000

DATA 0.014\*0.000

DATA 0.014\*0.000

DATA 0.014\*0.000

DATA 0.014\*0.000

DATA 0.014\*0.000

DATA 0.014\*0.000

DATA 0.014\*0.000

PROGRAM XGPLOT

THIS PROGRAM IS USED TO PLOT EXPERIMENTAL CURVES.

CALL INIT(30)

MIN=0.0

MAX=50.0

MINY=0.0

MAXY=10000.0

CALL PRINT(1,MIN,MAX,MINY,MAXY)

CALL PRINT(1,MIN,MAX,MINY,MAXY)

CALL MOVE(1,1)

CALL DRAW(1,1)

CALL DRAW(1,1)

CALL DRAW(1,1)

CALL DRAW(1,1)

CALL DRAW(1,1)

CALL DRAW(1,1)

CALL DRAW(1,1)

CALL DRAW(1,1)

CALL DRAW(1,1)

CALL DRAW(1,1)

CALL DRAW(1,1)

CALL DRAW(1,1)

CALL DRAW(1,1)

CALL DRAW(1,1)

CALL DRAW(1,1)

CALL DRAW(1,1)

CALL DRAW(1,1)

CALL DRAW(1,1)

CALL DRAW(1,1)

CALL DRAW(1,1)

CALL DRAW(1,1)

CALL DRAW(1,1)

CALL DRAW(1,1)

CALL DRAW(1,1)

CALL DRAW(1,1)

CALL DRAW(1,1)

CALL DRAW(1,1)

CALL DRAW(1,1)

CALL DRAW(1,1)

CALL DRAW(1,1)

CALL DRAW(1,1)

CALL DRAW(1,1)

CALL DRAW(1,1)

CALL DRAW(1,1)

CALL DRAW(1,1)

CALL DRAW(1,1)

CALL DRAW(1,1)

CALL DRAW(1,1)

CALL DRAW(1,1)

CALL DRAW(1,1)

CALL DRAW(1,1)

CALL DRAW(1,1)

CALL DRAW(1,1)

CALL DRAW(1,1)

CALL DRAW(1,1)

CALL DRAW(1,1)

CALL DRAW(1,1)

CALL DRAW(1,1)

CALL DRAW(1,1)

CALL DRAW(1,1)

CALL DRAW(1,1)

CALL DRAW(1,1)

CALL DRAW(1,1)

CALL DRAW(1,1)

CALL DRAW(1,1)

CALL DRAW(1,1)

CALL DRAW(1,1)

CALL DRAW(1,1)

CALL DRAW(1,1)

CALL DRAW(1,1)

CALL DRAW(1,1)

CALL DRAW(1,1)

CALL DRAW(1,1)

Appendix D: List of All Measurements

I: Output from Cyber 730

1. Experimental Results of Test I for  
the Cold Reacting Flow



TABLE OF VALUES FOR EXPERIMENTAL DATA SET 1  
 \*\*\*\*\*

AREA OF OUTER NOZZLE 10.6076 CM\*\*2  
 AREA OF INNER NOZZLE .3167 CM\*\*2  
 VELOCITY OF AIR .3012 M/SEC

VELOCITY OF FUEL [ M/SEC ]	HEIGHT OF CENTRAL JET [ MM ]	HEIGHT OF LEFT VORTEX [ MM ]	HEIGHT OF RIGHT VORTEX [ MM ]	
.1154	15.2400	.0000	.0000	
.1995	25.4160	.0000	.0000	
.2464	34.2900	.0000	.0000	
.3281	39.3700	.0000	.0000	
.4188	45.7200	.0000	.0000	
.5415	51.5620	.0000	.0000	
.6261	55.1942	.0000	.0000	(*)
.7600	60.4520	.0000	.0000	(*)

THE PENETRATION POINT IS SIGNED BY (\*)

FUNCTION FOR THIS DATA SET  
\*\*\*\*\*

THE VALUES ARE NONDIMENSIONALIZED BY THE RULES

$$Y = \frac{\text{VELOCITY OF FUEL}}{\text{PENETRATION VELOCITY}}$$
$$Y = \frac{\text{FORWARD STAGNATION POINT}}{\text{AFT STAGNATION POINT}}$$

CONSTANTS ARE DETERMINED BY A LEAST SQUARE METHOD

FUNCTION:  $Y = 1 + A1*(1-X) + A2*(1-X)**2 + A3*(1-X)**3$   
\*\*\*\*\*

INITIAL VALUES: A1 = .100  
\*\*\*\*\* A2 = 2.30  
A3 = 1.50

CONSTANTS: A1 = -.601  
\*\*\*\*\* A2 = .569  
A3 = -.952

LEAST SQUARE ERROR NORM: E = .68196E-03

THE SOLUTION WAS FOUND AFTER 2 ITERATIONS

FUNCTION FOR THIS DATA SET  
\*\*\*\*\*

THE VALUES ARE NONDIMENSIONALIZED BY THE RULES

$$X = \frac{\text{VELOCITY OF FUEL}}{\text{ANNULUS AIR VELOCITY}}$$
$$Y = \frac{\text{FORWARD STAGNATION POINT}}{\text{AFT STAGNATION POINT}}$$

CONSTANTS ARE DETERMINED BY A LEAST SQUARE METHOD

FUNCTION:  $Y = 1 + A1*(1-X) + A2*(1-X)**2 + A3*(1-X)**3$   
\*\*\*\*\*

INITIAL VALUES: A1 = .100  
\*\*\*\*\* A2 = 2.30  
A3 = 1.50

CONSTANTS: A1 = -.420  
\*\*\*\*\* A2 = .172  
A3 = -.707

LEAST SQUARE ERROR NORM: E = .13377E-02

THE SOLUTION WAS FOUND AFTER 2 ITERATIONS

TABLE OF VALUES FOR EXPERIMENTAL DATA SET 2  
 \*\*\*\*\*

AREA OF OUTER NOZZLE 10.6036 CM\*\*2  
 AREA OF INNER NOZZLE .3167 CM\*\*2  
 VELOCITY OF AIR 1.0793 M/SEC

VELOCITY OF FUEL [ M/SEC ]	HEIGHT OF CENTRAL JET [ MM ]	HEIGHT OF LEFT VORTEX [ MM ]	HEIGHT OF RIGHT VORTEX [ MM ]	
.1351	17.0160	.0000	.0000	
.1846	20.3200	.0000	.0000	
.2415	26.6700	.0000	.0000	
.3128	32.2580	.0000	.0000	
.3721	34.6710	.0000	.0000	
.4705	40.6400	.0000	.0000	
.5553	42.4160	.0000	.0000	
.6333	46.9900	.0000	.0000	
.7290	50.8000	.0000	.0000	(*)
.8249	53.3400	.0000	.0000	(*)

THE PENETRATION POINT IS SIGNED BY (\*)

FUNCTION FOR THIS DATA SET  
\*\*\*\*\*

THE VALUES ARE NONDIMENSIONALIZED BY THE RULES

          VELOCITY OF FUEL  
X = -----  
          PENETRATION VELOCITY  
  
          FORWARD STAGNATION POINT  
Y = -----  
          AFT STAGNATION POINT

CONSTANTS ARE DETERMINED BY A LEAST SQUARE METHOD

FUNCTION:           Y = 1+A1\*(1-X)+A2\*(1-X)\*\*2+A3\*(1-X)\*\*3  
\*\*\*\*\*

INITIAL VALUES:   A1 =     .100  
\*\*\*\*\*            A2 =     2.30  
                  A3 =     1.50

CONSTANTS:         A1 =   -.531  
\*\*\*\*\*            A2 =   .721E-01  
                  A3 =   -.428

LEAST SQUARE ERROR NORM: E =       .18074E-02

THE SOLUTION WAS FOUND AFTER   2 ITERATIONS

FUNCTION FOR THIS DATA SET  
\*\*\*\*\*

THE VALUES ARE NONDIMENSIONALIZED BY THE RULES

$$X = \frac{\text{VELOCITY OF FUEL}}{\text{ANNULUS AIR VELOCITY}}$$
$$Y = \frac{\text{FORWARD STAGNATION POINT}}{\text{AFT STAGNATION POINT}}$$

CONSTANTS ARE DETERMINED BY A LEAST SQUARE METHOD

FUNCTION:  $Y = 1 + A1*(1-X) + A2*(1-X)**2 + A3*(1-X)**3$   
\*\*\*\*\*

INITIAL VALUES: A1 = .100  
\*\*\*\*\* A2 = 2.30  
A3 = 1.50

CONSTANTS: A1 = .249  
\*\*\*\*\* A2 = -1.40  
A3 = .324

LEAST SQUARE ERROR NORM: E = .27014E-02

THE SOLUTION WAS FOUND AFTER 2 ITERATIONS

TABLE OF VALUES FOR EXPERIMENTAL DATA SET 3  
 \*\*\*\*\*

AREA OF OUTER NOZZLE 10.5036 CM\*\*2  
 AREA OF INNER NOZZLE .3167 CM\*\*2  
 VELOCITY OF AIR 1.3464 M/SEC

VELOCITY OF FUEL [ M/SEC ]	HEIGHT OF CENTRAL JET [ MM ]	HEIGHT OF LEFT VORTEX [ MM ]	HEIGHT OF RIGHT VORTEX [ MM ]	
.1151	12.7000	.0000	.0000	
.1979	19.9120	.0000	.0000	
.2916	27.9400	.0000	.0000	
.3729	31.4960	.0000	.0000	
.4576	34.4678	.0000	.0000	
.5601	38.3540	.0000	.0000	
.6359	42.1640	.0000	.0000	
.7310	46.4820	.0000	.0000	(*)
.8274	49.5300	.0000	.0000	(*)

THE PENETRATION POINT IS SIGNED BY (\*)

FUNCTION FOR THIS DATA SET  
\*\*\*\*\*

THE VALUES ARE NONDIMENSIONALIZED BY THE RULES

$$Y = \frac{\text{VELOCITY OF FUEL}}{\text{PENETRATION VELOCITY}}$$
$$Y = \frac{\text{FORWARD STAGNATION POINT}}{\text{AFT STAGNATION POINT}}$$

CONSTANTS ARE DETERMINED BY A LEAST SQUARE METHOD

FUNCTION:  $Y = 1 + A1*(1-X) + A2*(1-X)**2 + A3*(1-X)**3$   
\*\*\*\*\*

INITIAL VALUES: A1 = .100  
\*\*\*\*\* A2 = 2.30  
A3 = 1.50

CONSTANTS: A1 = -.769  
\*\*\*\*\* A2 = .532  
A3 = -.314

LEAST SQUARE ERROR NORM: E = .12735E-02

THE SOLUTION WAS FOUND AFTER 2 ITERATIONS



FUNCTION FOR THIS DATA SET  
\*\*\*\*\*

THE VALUES ARE NONDIMENSIONALIZED BY THE RULES

$$X = \frac{\text{VELOCITY OF FUEL}}{\text{ANNULUS AIR VELOCITY}}$$
$$Y = \frac{\text{FORWARD STAGNATION POINT}}{\text{AFT STAGNATION POINT}}$$

CONSTANTS ARE DETERMINED BY A LEAST SQUARE METHOD

FUNCTION:  $Y = 1 + A1*(1-X) + A2*(1-X)**2 + A3*(1-X)**3$   
\*\*\*\*\*

INITIAL VALUES: A1 = .100  
\*\*\*\*\* A2 = 2.30  
A3 = 1.50

CONSTANTS: A1 = .567  
\*\*\*\*\* A2 = -1.70  
A3 = .268

LEAST SQUARE ERROR NORM: E = .34427E-02

THE SOLUTION WAS FOUND AFTER 2 ITERATIONS

TABLE OF VALUES FOR EXPERIMENTAL DATA SET 4  
\*\*\*\*\*

AREA OF OUTER NOZZLE 10.6036 CM\*\*2  
AREA OF INNER NOZZLE .3167 CM\*\*2  
VELOCITY OF AIR 1.6246 M/SEC

VELOCITY OF FUEL [ M/SEC ]	HEIGHT OF CENTRAL JET [ MM ]	HEIGHT OF LEFT VORTEX [ MM ]	HEIGHT OF RIGHT VORTEX [ MM ]	
.1300	12.7000	.0000	.0000	
.1999	17.7300	.0000	.0000	
.3314	25.8319	.0000	.0000	
.4536	30.1498	.0000	.0000	
.5715	34.0360	.0000	.0000	
.6534	37.0940	.0000	.0000	
.7578	40.6400	.0000	.0000	
.8632	43.9420	.0000	.0000	(*)
.9897	46.9900	.0700	.0000	(*)

THE PENETRATION POINT IS SIGNED BY (\*)

FUNCTION FOR THIS DATA SET  
\*\*\*\*\*

THE VALUES ARE NONDIMENSIONALIZED BY THE RULES

$$Y = \frac{\text{VELOCITY OF FUEL}}{\text{PENETRATION VELOCITY}}$$
$$Y = \frac{\text{FORWARD STAGNATION POINT}}{\text{AFT STAGNATION POINT}}$$

CONSTANTS ARE DETERMINED BY A LEAST SQUARE METHOD

FUNCTION:  $Y = 1 + A1*(1-X) + A2*(1-X)**2 + A3*(1-X)**3$   
\*\*\*\*\*

INITIAL VALUES: A1 = .100  
\*\*\*\*\* A2 = 2.30  
A3 = 1.50

CONSTANTS: A1 = -.651  
\*\*\*\*\* A2 = .306  
A3 = -.563

LEAST SQUARE ERROR NORM: E = .94812E-03

THE SOLUTION WAS FOUND AFTER 2 ITERATIONS

FUNCTION FOR THIS DATA SET  
\*\*\*\*\*

THE VALUES ARE NONDIMENSIONALIZED BY THE RULES

$$X = \frac{\text{VELOCITY OF FUEL}}{\text{ANNULUS AIR VELOCITY}}$$
$$Y = \frac{\text{FORWARD STAGNATION POINT}}{\text{AFT STAGNATION POINT}}$$

CONSTANTS ARE DETERMINED BY A LEAST SQUARE METHOD

FUNCTION:  $Y = 1 + A1*(1-X) + A2*(1-X)**2 + A3*(1-X)**3$   
\*\*\*\*\*

INITIAL VALUES: A1 = .100  
\*\*\*\*\* A2 = 2.30  
A3 = 1.50

CONSTANTS: A1 = .598  
\*\*\*\*\* A2 = -1.71  
A3 = .265

LEAST SQUARE ERROR NORM: E = .19057E-02

THE SOLUTION WAS FOUND AFTER 2 ITERATIONS

# 4 SET DATA NONDIMENSIONALIZED OF THE PLOT

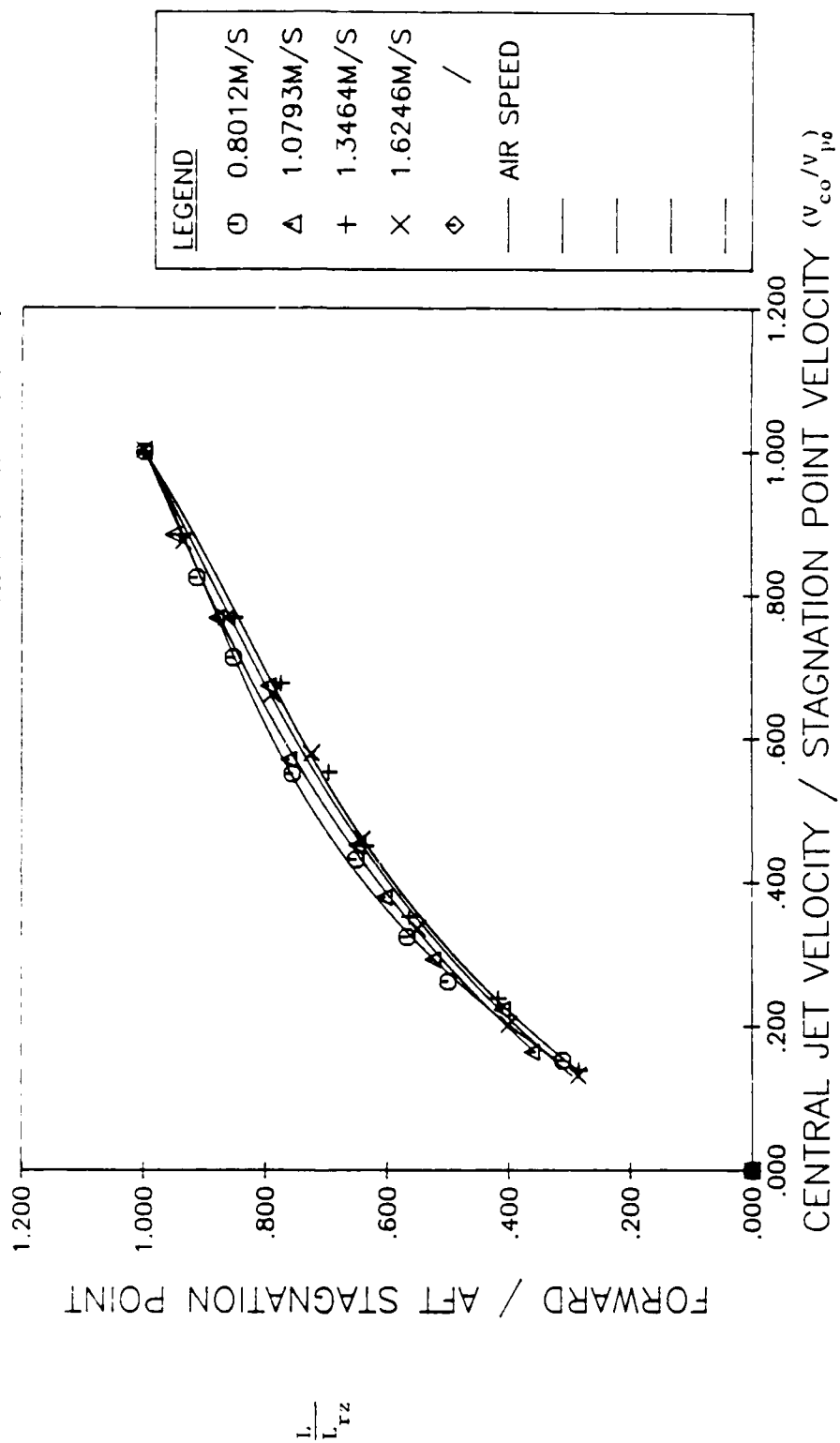


Fig. 10. Plot of  $L/L_{rz}$  versus  $V_{co}/V_p$  for Test I with  $D_j = 6.35$  mm - cold reacting flow.

# PLOT OF THE NONDIMENSIONALIZED DATA SET 4

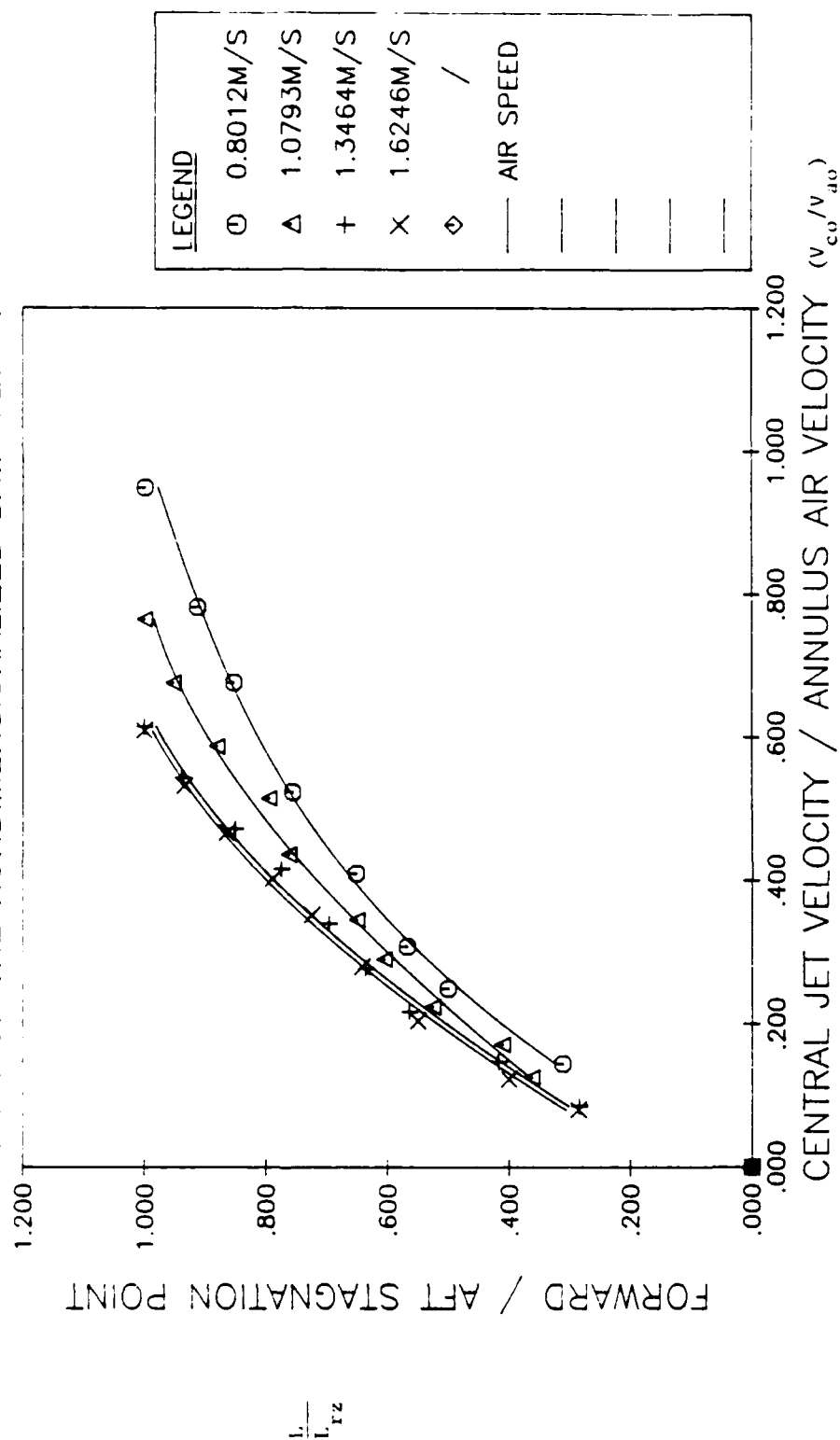


Fig. 11. Plot  $L_j/L_{rz}$  versus  $V_{co}/V_{ao}$  for Test I with  $D_j = 6.35$  mm - cold reacting flow.

TABLE OF VALUES FOR EXPERIMENTAL DATA SET 1  
 \*\*\*\*\*

AREA OF OUTER NOZZLE 10.6036 CM\*\*2  
 AREA OF INNER NOZZLE .7012 CM\*\*2  
 VELOCITY OF AIR .8012 M/SEC

VELOCITY OF FUEL [ M/SEC ]	HEIGHT OF CENTRAL JET [ MM ]	HEIGHT OF LEFT VORTEX [ MM ]	HEIGHT OF RIGHT VORTEX [ MM ]
.0405	5.5118	.0000	.0000
.1061	14.7955	.0000	.0000
.1639	22.9616	.0000	.0000
.2362	34.8488	.0000	.0000
.3044	43.1900	.0000	.0000
.3576	45.7200	.0000	.0000
.4331	49.1490	.0000	.0000
.4700	52.5780	.0000	.0000
.5264	58.4200	.0000	.0000

(\*)

THE PENETRATION POINT IS SIGNED BY (\*)

FUNCTION FOR THIS DATA SET  
\*\*\*\*\*

THE VALUES ARE NONDIMENSIONALIZED BY THE RULES

$$X = \frac{\text{VELOCITY OF FUEL}}{\text{PENETRATION VELOCITY}}$$

$$Y = \frac{\text{FORWARD STAGNATION POINT}}{\text{AFT STAGNATION POINT}}$$

CONSTANTS ARE DETERMINED BY A LEAST SQUARE METHOD

FUNCTION:  $Y = 1 + A1*(1-X) + A2*(1-X)**2 + A3*(1-X)**3$   
\*\*\*\*\*

INITIAL VALUES: A1 = .100  
\*\*\*\*\* A2 = 2.30  
A3 = 1.50

CONSTANTS: A1 = -.789  
\*\*\*\*\* A2 = .542  
A3 = -.827

LEAST SQUARE ERROR NORM: E = .43068E-02

THE SOLUTION WAS FOUND AFTER 2 ITERATIONS



FUNCTION FOR THIS DATA SET  
\*\*\*\*\*

THE VALUES ARE NONDIMENSIONALIZED BY THE RULES

$$X = \frac{\text{VELOCITY OF FUEL}}{\text{ANNULUS AIR VELOCITY}}$$
$$Y = \frac{\text{FORWARD STAGNATION POINT}}{\text{AFT STAGNATION POINT}}$$

CONSTANTS ARE DETERMINED BY A LEAST SQUARE METHOD

FUNCTION:  $Y = 1 + A1*(1-X) + A2*(1-X)**2 + A3*(1-X)**3$   
\*\*\*\*\*

INITIAL VALUES: A1 = .100  
\*\*\*\*\* A2 = 2.30  
A3 = 1.50

CONSTANTS: A1 = .248  
\*\*\*\*\* A2 = -.940  
A3 = -.341

LEAST SQUARE ERROR NORM: E = .49449E-02

THE SOLUTION WAS FOUND AFTER 2 ITERATIONS

TABLE OF VALUES FOR EXPERIMENTAL DATA SET 2  
 \*\*\*\*\*

AREA OF OUTER NOZZLE 10.6036 CM\*\*2  
 AREA OF INNER NOZZLE .7012 CM\*\*2  
 VELOCITY OF AIR 1.0793 M/SEC

VELOCITY OF FUEL [ M/SEC ]	HEIGHT OF CENTRAL JET [ MM ]	HEIGHT OF LEFT VORTEX [ MM ]	HEIGHT OF RIGHT VORTEX [ MM ]	
.0547	8.3900	.0000	.0000	
.1192	17.0180	.0700	.0000	
.1486	22.7833	.0000	.0000	
.2421	29.7020	.0700	.0000	
.3144	38.1000	.0700	.0000	
.3583	41.4020	.0000	.0000	
.4504	44.9326	.0000	.0000	
.5202	48.2600	.0000	.0000	(*)
.5902	52.3240	.0700	.0000	(*)

THE PENETRATION POINT IS SIGNED BY (\*)

FUNCTION FOR THIS DATA SET  
\*\*\*\*\*

THE VALUES ARE NONDIMENSIONALIZED BY THE RULES

VELOCITY OF FUEL  
 $X = \frac{\text{PENETRATION VELOCITY}}{\text{FORWARD STAGNATION POINT}}$   
AFT STAGNATION POINT  
 $Y = \frac{\text{AFT STAGNATION POINT}}{\text{AFT STAGNATION POINT}}$

CONSTANTS ARE DETERMINED BY A LEAST SQUARE METHOD

FUNCTION:  $Y = 1 + A1*(1-X) + A2*(1-X)**2 + A3*(1-X)**3$   
\*\*\*\*\*

INITIAL VALUES: A1 = .100  
\*\*\*\*\* A2 = 2.30  
A3 = 1.50

CONSTANTS: A1 = -.458  
\*\*\*\*\* A2 = -.293  
A3 = -.238

LEAST SQUARE ERROR NORM: E = .27204E-02

THE SOLUTION WAS FOUND AFTER 2 ITERATIONS

FUNCTION FOR THIS DATA SET  
\*\*\*\*\*

THE VALUES ARE NONDIMENSIONALIZED BY THE RULES

$$X = \frac{\text{VELOCITY OF FUEL}}{\text{ANNULUS AIR VELOCITY}}$$
$$Y = \frac{\text{FORWARD STAGNATION POINT}}{\text{AFT STAGNATION POINT}}$$

CONSTANTS ARE DETERMINED BY A LEAST SQUARE METHOD

FUNCTION:  $Y = 1 + A1*(1-X) + A2*(1-X)**2 + A3*(1-X)**3$   
\*\*\*\*\*

INITIAL VALUES: A1 = .100  
\*\*\*\*\* A2 = 2.30  
A3 = 1.50

CONSTANTS: A1 = .479  
\*\*\*\*\* A2 = -.823  
A3 = -.638

LEAST SQUARE ERROR NORM: E = .26008E-02

THE SOLUTION WAS FOUND AFTER 2 ITERATIONS

TABLE OF VALUES FOR EXPERIMENTAL DATA SET 3  
 \*\*\*\*\*

AREA OF OUTER NOZZLE 10.6036 CM\*\*2  
 AREA OF INNER NOZZLE .7012 CM\*\*2  
 VELOCITY OF AIR 1.3464 M/SEC

VELOCITY OF FUEL [ M/SEC ]	HEIGHT OF CENTRAL JET [ MM ]	HEIGHT OF LEFT VORTEX [ MM ]	HEIGHT OF RIGHT VORTEX [ MM ]	
.0467	7.5692	.0000	.0000	
.1048	14.0462	.0000	.0000	
.1819	22.5600	.0000	.0000	
.2396	27.0510	.0000	.0000	
.3224	35.9913	.0000	.0000	
.3904	38.3112	.0000	.0000	
.4380	40.1320	.0000	.0000	
.5173	43.1800	.0000	.0000	(*)
.5629	47.7520	.0000	.0000	(*)

THE PENETRATION POINT IS SIGNED BY (\*)

FUNCTION FOR THIS DATA SET  
\*\*\*\*\*

THE VALUES ARE NONDIMENSIONALIZED BY THE RULES

$$X = \frac{\text{VELOCITY OF FUEL}}{\text{PENETRATION VELOCITY}}$$
$$Y = \frac{\text{FORWARD STAGNATION POINT}}{\text{AFT STAGNATION POINT}}$$

CONSTANTS ARE DETERMINED BY A LEAST SQUARE METHOD

FUNCTION:  $Y = 1 + A1*(1-X) + A2*(1-X)**2 + A3*(1-X)**3$   
\*\*\*\*\*

INITIAL VALUES: A1 = .100  
\*\*\*\*\* A2 = 2.30  
A3 = 1.50

CONSTANTS: A1 = -.689  
\*\*\*\*\* A2 = .303  
A3 = -.618

LEAST SQUARE ERROR NORM: E = .45395E-02

THE SOLUTION WAS FOUND AFTER 2 ITERATIONS

FUNCTION FOR THIS DATA SET  
\*\*\*\*\*

THE VALUES ARE NONDIMENSIONALIZED BY THE RULES

$$Y = \frac{\text{VELOCITY OF FUEL}}{\text{ANNULUS AIR VELOCITY}}$$

$$Y = \frac{\text{FORWARD STAGNATION POINT}}{\text{AFT STAGNATION POINT}}$$

CONSTANTS ARE DETERMINED BY A LEAST SQUARE METHOD

FUNCTION:  $Y = 1 + A1*(1-X) + A2*(1-X)**2 + A3*(1-X)**3$   
\*\*\*\*\*

INITIAL VALUES: A1 = .100  
\*\*\*\*\* A2 = 2.30  
A3 = 1.50

CONSTANTS: A1 = .202  
\*\*\*\*\* A2 = .594  
A3 = -1.77

LEAST SQUARE ERROR NORM: E = .41146E-02

THE SOLUTION WAS FOUND AFTER 2 ITERATIONS

TABLE OF VALUES FOR EXPERIMENTAL DATA SET 4  
 \*\*\*\*\*

AREA OF OUTER NOZZLE 10.6036 CM\*\*2  
 AREA OF INNER NOZZLE .7012 CM\*\*2  
 VELOCITY OF AIR 1.6246 M/SEC

VELOCITY OF FUEL [ M/SEC ]	HEIGHT OF CENTRAL JET [ MM ]	HEIGHT OF LEFT VORTEX [ MM ]	HEIGHT OF RIGHT VORTEX [ MM ]
.0973	11.1506	.0000	.0000
.1170	14.0462	.0000	.0000
.2110	19.2113	.0000	.0000
.2695	23.9522	.0000	.0000
.3293	29.8196	.0000	.0000
.4116	34.8742	.0000	.0000
.4805	37.5412	.0000	.0000
.5277	39.3700	.0000	.0000
.6209	44.3564	.0000	.0000

(\*)

THE PENETRATION POINT IS SIGNED BY (\*)



FUNCTION FOR THIS DATA SET  
\*\*\*\*\*

THE VALUES ARE NONDIMENSIONALIZED BY THE RULES

VELOCITY OF FUEL  
X =  $\frac{\text{PENETRATION VELOCITY}}{\text{FORWARD STAGNATION POINT}}$   
AFT STAGNATION POINT  
Y =  $\frac{\text{AFT STAGNATION POINT}}{\text{FORWARD STAGNATION POINT}}$

CONSTANTS ARE DETERMINED BY A LEAST SQUARE METHOD

FUNCTION: Y = 1+A1\*(1-X)+A2\*(1-X)\*\*2+A3\*(1-X)\*\*3  
\*\*\*\*\*

INITIAL VALUES: A1 = .100  
\*\*\*\*\* A2 = 2.30  
A3 = 1.50

CONSTANTS: A1 = -.529  
\*\*\*\*\* A2 = -.711  
A3 = .362

LEAST SQUARE ERROR NORM: E = .43444E-02

THE SOLUTION WAS FOUND AFTER 2 ITERATIONS

FUNCTION FOR THIS DATA SET  
\*\*\*\*\*

THE VALUES ARE NONDIMENSIONALIZED BY THE RULES

$$Y = \frac{\text{VELOCITY OF FUEL}}{\text{ANNULUS AIR VELOCITY}}$$
$$Y = \frac{\text{FORWARD STAGNATION POINT}}{\text{AFT STAGNATION POINT}}$$

CONSTANTS ARE DETERMINED BY A LEAST SQUARE METHOD

FUNCTION:  $Y = 1 + A1*(1-X) + A2*(1-X)**2 + A3*(1-X)**3$   
\*\*\*\*\*

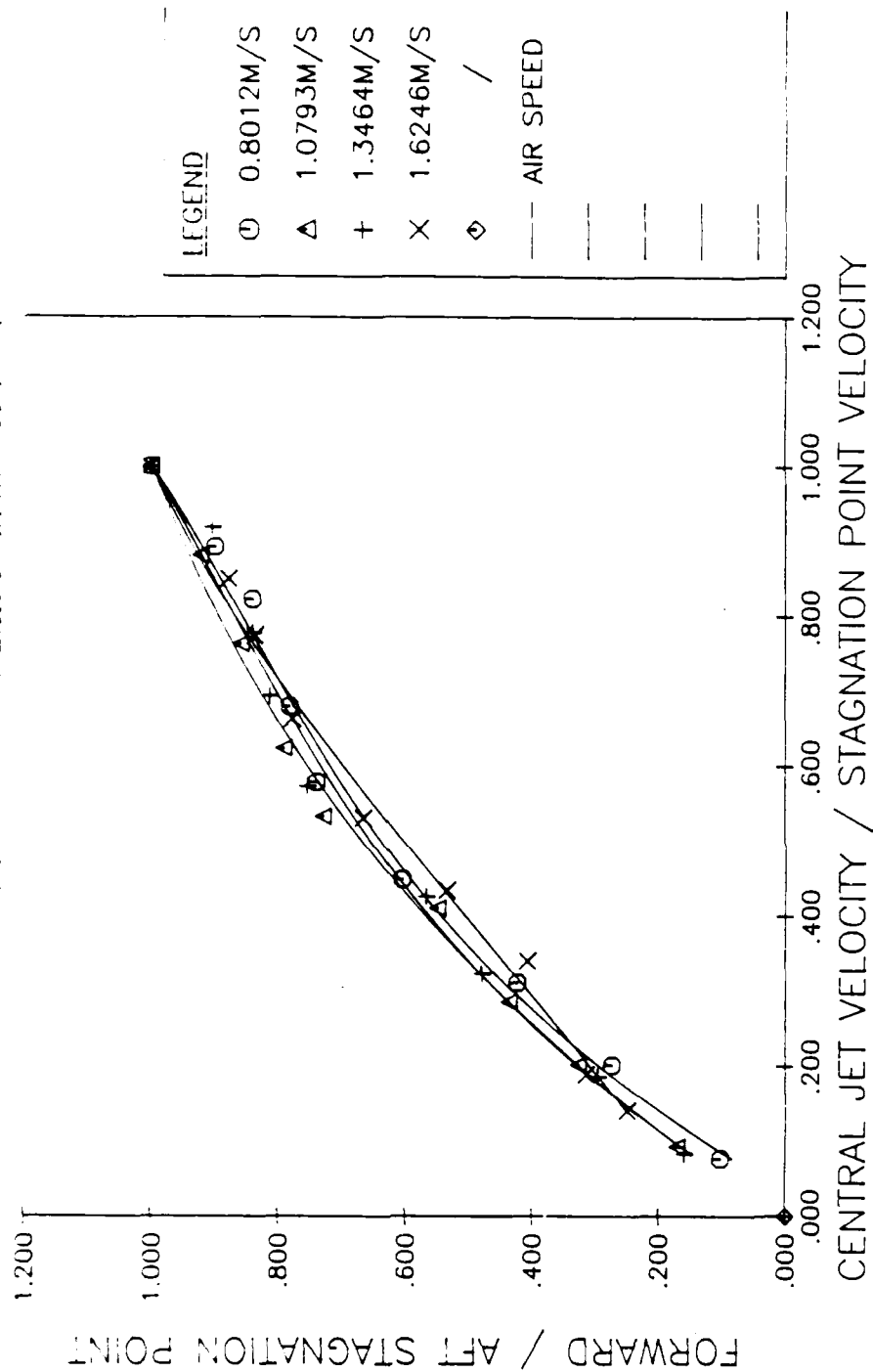
INITIAL VALUES: A1 = .100  
\*\*\*\*\* A2 = 2.30  
A3 = 1.50

CONSTANTS: A1 = 1.95  
\*\*\*\*\* A2 = -3.64  
A3 = .778

LEAST SQUARE ERROR NORM: E = .46371E-02

THE SOLUTION WAS FOUND AFTER 2 ITERATIONS

PLOT OF THE NONDIMENSIONALIZED DATA SET 4



PLOT OF THE NONDIMENSIONALIZED DATA SET 4

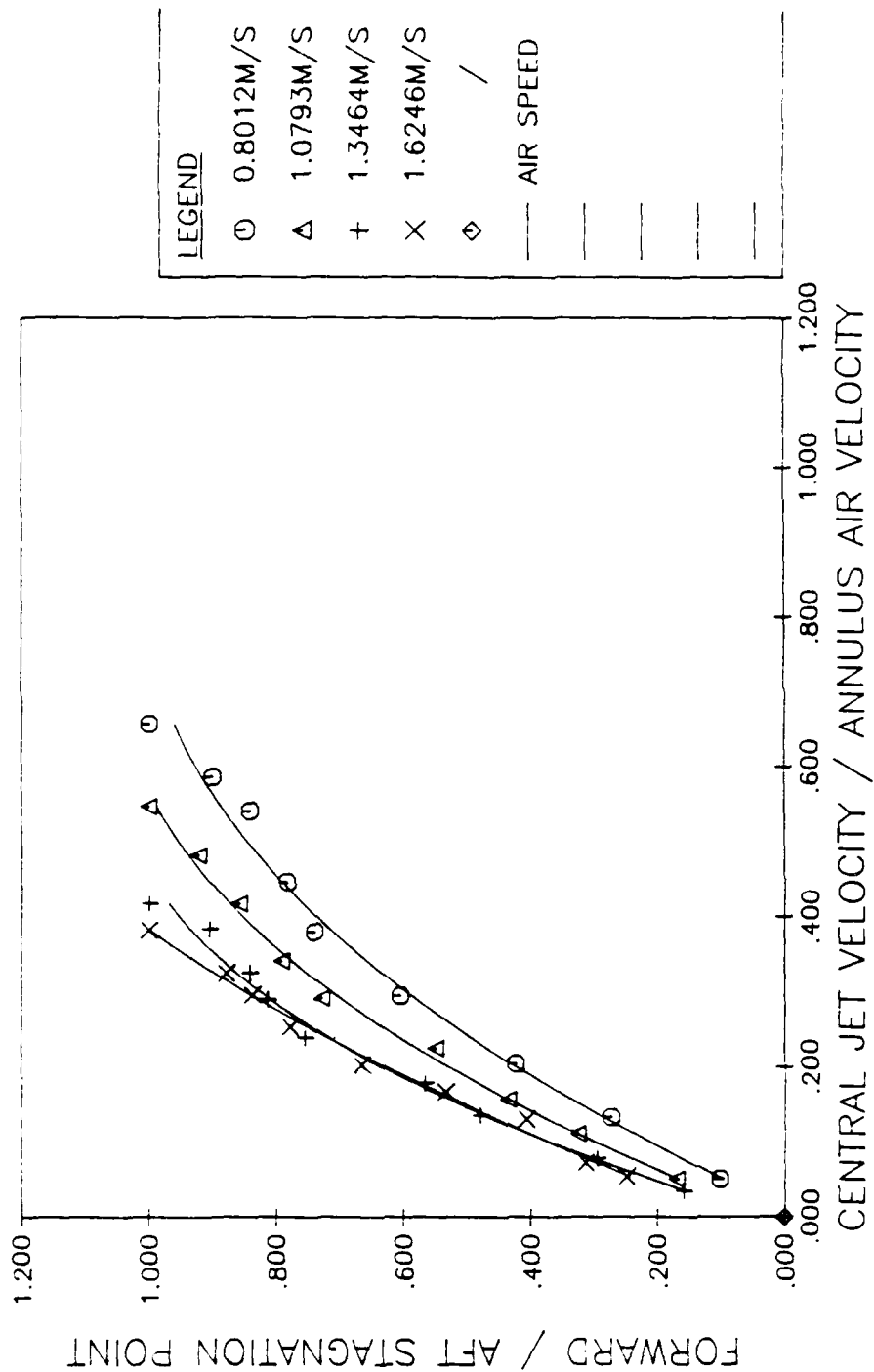


TABLE OF VALUES FOR EXPERIMENTAL DATA SET 1  
 \*\*\*\*\*

AREA OF OUTER NOZZLE 10.5036 CM\*\*2  
 AREA OF INNER NOZZLE 1.2668 CM\*\*2  
 VELOCITY OF AIR .3012 M/SEC

VELOCITY OF FUEL [ M/SEC ]	HEIGHT OF CENTRAL JET [ MM ]	HEIGHT OF LEFT VORTEX [ MM ]	HEIGHT OF RIGHT VORTEX [ MM ]
.0290	5.3086	.0000	.0000
.0465	7.1628	.0000	.0000
.0710	9.7790	.0000	.0000
.1247	13.9700	.0000	.0000
.1554	19.1770	.0000	.0000
.1849	23.6982	.0000	.0000
.2350	30.9118	.0000	.0000
.2803	35.8140	.0000	.0000
.3983	50.2031	.0000	.0000

THE PENETRATION POINT IS SIGNED BY (\*)

FUNCTION FOR THIS DATA SET  
\*\*\*\*\*

THE VALUES ARE NONDIMENSIONALIZED BY THE RULES

$$Y = \frac{\text{VELOCITY OF FUEL}}{\text{ANNULUS AIR VELOCITY}}$$
$$Y = \frac{\text{FORWARD STAGNATION POINT}}{\text{AFT STAGNATION POINT}}$$

CONSTANTS ARE DETERMINED BY A LEAST SQUARE METHOD

FUNCTION:  $Y = 1 + A1*(1-X) + A2*(1-X)**2 + A3*(1-X)**3$   
\*\*\*\*\*

INITIAL VALUES: A1 = .100  
\*\*\*\*\* A2 = 2.30  
A3 = 1.50

CONSTANTS: A1 = 1.54  
\*\*\*\*\* A2 = -5.02  
A3 = 2.56

LEAST SQUARE ERROR NORM: E = .77811E-03

THE SOLUTION WAS FOUND AFTER 2 ITERATIONS

TABLE OF VALUES FOR EXPERIMENTAL DATA SET 2  
 \*\*\*\*\*

AREA OF OUTER NOZZLE 10.6036 CM\*\*2  
 AREA OF INNER NOZZLE 1.2668 CM\*\*2  
 VELOCITY OF AIR 1.0793 M/SEC

VELOCITY OF FUEL [ M/SEC ]	HEIGHT OF CENTRAL JET [ MM ]	HEIGHT OF LEFT VORTEX [ MM ]	HEIGHT OF RIGHT VORTEX [ MM ]
.0426	6.6629	.0000	.0000
.0456	7.9502	.0000	.0000
.0604	8.1280	.0000	.0000
.0936	12.4206	.0000	.0000
.1480	15.5862	.0000	.0000
.1840	21.5900	.0000	.0000
.2414	27.9400	.0000	.0000
.2836	33.0200	.0000	.0000
.3298	39.1160	.0000	.0000

THE PENETRATION POINT IS SIGNED BY (\*)

FUNCTION FOR THIS DATA SET  
\*\*\*\*\*

THE VALUES ARE NONDIMENSIONALIZED BY THE RULES

$$X = \frac{\text{VELOCITY OF FUEL}}{\text{ANNULUS AIR VELOCITY}}$$
$$Y = \frac{\text{FORWARD STAGNATION POINT}}{\text{AFT STAGNATION POINT}}$$

CONSTANTS ARE DETERMINED BY A LEAST SQUARE METHOD

FUNCTION:  $Y = 1 + A1*(1-X) + A2*(1-X)**2 + A3*(1-X)**3$   
\*\*\*\*\*

INITIAL VALUES: A1 = .100  
\*\*\*\*\* A2 = 2.30  
A3 = 1.50

CONSTANTS: A1 = 2.80  
\*\*\*\*\* A2 = -6.84  
A3 = 3.11

LEAST SQUARE ERROR NORM: E = .64470E-03

THE SOLUTION WAS FOUND AFTER 2 ITERATIONS



TABLE OF VALUES FOR EXPERIMENTAL DATA SET 3  
 \*\*\*\*\*

AREA OF OUTER NOZZLE 10.6036 CM\*\*2  
 AREA OF INNER NOZZLE 1.2668 CM\*\*2  
 VELOCITY OF AIR 1.3464 M/SEC

VELOCITY OF FUEL [ M/SEC ]	HEIGHT OF CENTRAL JET [ MM ]	HEIGHT OF LEFT VORTEX [ MM ]	HEIGHT OF RIGHT VORTEX [ MM ]
.0577	9.1694	.0000	.0000
.0842	10.9712	.0000	.0000
.1049	13.9446	.0000	.0000
.1458	16.3576	.0000	.0000
.1798	19.7612	.0000	.0000
.2161	22.0980	.0000	.0000
.2527	23.8760	.0000	.0000
.2790	26.1620	.0000	.0000
.3017	29.6672	.0000	.0000
.3625	33.7312	.0000	.0000

THE PENETRATION POINT IS SIGNED BY (\*)

FUNCTION FOR THIS DATA SET  
\*\*\*\*\*

THE VALUES ARE NONDIMENSIONALIZED BY THE RULES

$$X = \frac{\text{VELOCITY OF FUEL}}{\text{ANNULUS AIR VELOCITY}}$$
$$Y = \frac{\text{FORWARD STAGNATION POINT}}{\text{AFT STAGNATION POINT}}$$

CONSTANTS ARE DETERMINED BY A LEAST SQUARE METHOD

FUNCTION:  $Y = 1 + A1*(1-X) + A2*(1-X)**2 + A3*(1-X)**3$   
\*\*\*\*\*

INITIAL VALUES: A1 = .100  
\*\*\*\*\* A2 = 2.30  
A3 = 1.50

CONSTANTS: A1 = 1.78  
\*\*\*\*\* A2 = -4.40  
A3 = 1.71

LEAST SQUARE ERROR NORM: E = .14186E-02

THE SOLUTION WAS FOUND AFTER 2 ITERATIONS

TABLE OF VALUES FOR EXPERIMENTAL DATA SET 4  
 \*\*\*\*\*

AREA OF OUTER NOZZLE 10.6034 CM\*\*2  
 AREA OF INNER NOZZLE 1.2668 CM\*\*2  
 VELOCITY OF AIR 1.6246 M/SEC

VELOCITY OF FUEL [ M/SEC ]	HEIGHT OF CENTRAL JET [ MM ]	HEIGHT OF LEFT VORTEX [ MM ]	HEIGHT OF RIGHT VORTEX [ MM ]
.0544	9.2550	.0000	.0000
.0825	10.6299	.0000	.0000
.1196	12.7762	.0000	.0000
.1460	13.4620	.0000	.0000
.1507	15.2908	.0000	.0000
.1845	17.3736	.0000	.0000
.2252	19.8629	.0000	.0000
.2815	22.3266	.0000	.0000
.3447	25.9080	.0000	.0000

THE PENETRATION POINT IS SIGNED BY (\*)

FUNCTION FOR THIS DATA SET  
\*\*\*\*\*

THE VALUES ARE NONDIMENSIONALIZED BY THE RULES

$$X = \frac{\text{VELOCITY OF FUEL}}{\text{ANNULUS AIR VELOCITY}}$$
$$Y = \frac{\text{FORWARD STAGNATION POINT}}{\text{AFT STAGNATION POINT}}$$

CONSTANTS ARE DETERMINED BY A LEAST SQUARE METHOD

FUNCTION:  $Y = 1 + A1*(1-X) + A2*(1-X)**2 + A3*(1-X)**3$   
\*\*\*\*\*

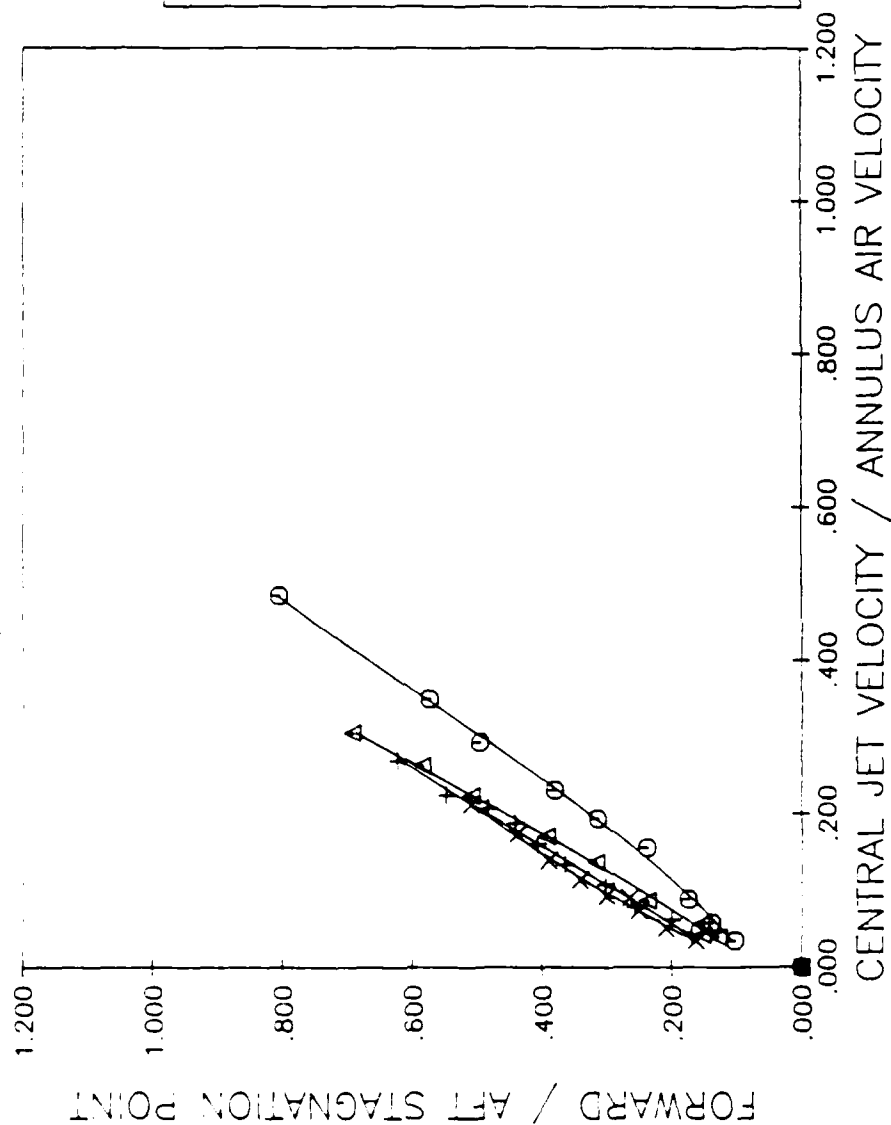
INITIAL VALUES: A1 = .100  
\*\*\*\*\* A2 = 2.30  
A3 = 1.50

CONSTANTS: A1 = -.311  
\*\*\*\*\* A2 = .395  
A3 = -1.00

LEAST SQUARE ERROR NORM: E = .75145E-03

THE SOLUTION WAS FOUND AFTER 2 ITERATIONS

PLOT OF THE NONDIMENSIONALIZED DATA SET 4



2. Experimental Results of Test I for the Combusting Flow

TABLE OF VALUES AND EXPERIMENTAL DATA SET 1  
 \*\*\*\*\*

AREA OF OUTER VORTEX 10.5134 CM<sup>2</sup>  
 AREA OF INNER VORTEX 3.147 CM<sup>2</sup>  
 VELOCITY OF AIR 1041 M/SEC

VELOCITY OF BHEL [ M/SEC ]	HEIGHT OF CENTRAL JET [ MM ]	HEIGHT OF LEFT VORTEX [ MM ]	HEIGHT OF RIGHT VORTEX [ MM ]
.0432	3.6184	4.2326	5.1562
.0497	3.1488	4.2640	5.1562
.0619	4.1047	4.2164	5.1054
.0735	4.3246	4.2414	5.3340
.0849	5.1745	4.3180	5.1562
.0973	4.0200	4.6432	5.1562
.1067	4.0040	4.4450	5.1562
.1131	11.7113	4.7750	5.1562
.1260	10.3540	4.9530	5.1308
.1447	14.3110	4.4530	5.1308
.1812	15.0120	4.7244	5.4610

(\*)

THE PENETRATION POINT IS GIVEN BY (=)

FUNCTION FOR THIS DATA SET  
 \*\*\*\*\*

THE VALUES ARE ALL LINEARIZED BY THE RULES

$$Y = \frac{\text{VELOCITY IN MPH}}{\text{PENETRATION VELOCITY}}$$

$$Y = \frac{\text{FORWARD STAGNATION POINT}}{\text{AFT STAGNATION POINT}}$$

CONSTANTS ARE DETERMINED BY A LEAST SQUARE METHOD

FUNCTION:  $Y = 1 + A1*(1-Y) + A2*(1-Y)^2 + A3*(1-Y)^3$   
 \*\*\*\*\*

INITIAL VALUES: A1 = .100  
 \*\*\*\*\* A2 = 1.30  
 A3 = 1.50

CONSTANTS: A1 = -.001  
 \*\*\*\*\* A2 = -1.00  
 A3 = .02

LEAST SQUARES PROGRAM: E = .99508E-02

THE FUNCTION WAS CALCULATED IN 2 ITERATIONS



FUNCTION FOR THIS DATA SET  
 \*\*\*\*\*

THE VALUES ARE NORMALIZED BY THE RULES

$$X = \frac{\text{VELOCITY OF FUEL}}{\text{AIR FLOW VELOCITY}}$$

$$Y = \frac{\text{FORWARD STAGNATION POINT}}{\text{AFT STAGNATION POINT}}$$

CONSTANTS ARE DETERMINED BY A LEAST SQUARE METHOD

FUNCTION:  $Y = 1 + A1*(1-X) + A2*(1-X)**2 + A3*(1-X)**3$   
 \*\*\*\*\*

INITIAL VALUES: A1 = .100  
 \*\*\*\*\* A2 = 0.30  
 A3 = 1.50

CONSTANTS: A1 = .703  
 \*\*\*\*\* A2 = .740  
 A3 = -2.70

LEAST SQUARE ERROR NORM: E = .110758-01

THE SOLUTION WAS FOUND AFTER 2 ITERATIONS

TABLE OF VALUES FOR EXPERIMENTAL DATA SET 2  
 \*\*\*\*\*

AREA OF OUTLET NOZZLE 10.116 CM<sup>2</sup>  
 AREA OF INNER NOZZLE .3157 CM<sup>2</sup>  
 VELOCITY OF AIR .1010 M/SEC

VELOCITY OF AIR [ M/SEC ]	HEIGHT OF CENTRAL JET [ MM ]	HEIGHT OF LEFT VORTEX [ MM ]	HEIGHT OF RIGHT VORTEX [ MM ]
.0441	3.0020	5.4510	7.2290
.0512	4.0144	5.0300	6.1976
.0752	7.1562	5.0035	6.0560
.0797	6.0748	4.9530	5.9690
.0937	3.0677	4.9276	5.6542
.1196	11.5570	4.7244	5.7404
.1331	10.0192	4.4530	5.8420
.1535	15.3570	4.9222	5.4102
.1757	15.3040	5.0546	5.9156
.2107	19.8100	4.6736	5.7765

(\*)

THE PENETRATION POINT IS GIVEN BY (\*)

FUNCTION: EQ. (4) DATA SET  
 \*\*\*\*\*

THE VALUES ARE INDICATED BY THE RULES

$$Y = \frac{\text{VELOCITY OF FUEL}}{\text{PENETRATION VELOCITY}}$$

$$Y = \frac{\text{FORWARD STAGNATION POINT}}{\text{AFT STAGNATION POINT}}$$

CONSTANTS ARE DETERMINED BY A LEAST SQUARE METHOD

FUNCTION:  $Y = 1 + A1*(1-Y) + A2*(1-Y)**2 + A3*(1-Y)**3$   
 \*\*\*\*\*

INITIAL VALUES:  $A1 = .100$   
 \*\*\*\*\*  $A2 = 2.40$   
 $A3 = 1.50$

CONSTANTS:  $A1 = -.357$   
 \*\*\*\*\*  $A2 = -2.74$   
 $A3 = 1.64$

LEAST SQUARE ERROR TERM:  $E = .9674 \times 10^{-2}$

THE SOLUTION WAS FOUND AFTER 2 ITERATIONS

FUNCTION FOR THIS DATA SET  
\*\*\*\*\*

THE VALUES ARE NONDIMENSIONALIZED BY THE RULES

$$Y = \frac{\text{VELOCITY OF FUEL}}{\text{ANNULAR AIR VELOCITY}}$$

$$X = \frac{\text{FORWARD STAGNATION POINT}}{\text{AFT STAGNATION POINT}}$$

CONSTANTS ARE DETERMINED BY A LEAST SQUARE METHOD

FUNCTION:  $Y = 1 + A1*(1-X) + A2*(1-X)**2 + A3*(1-X)**3$   
\*\*\*\*\*

INITIAL VALUES:  $A1 = .100$   
\*\*\*\*\*  $A2 = 2.30$   
 $A3 = 1.50$

CONSTANTS:  $A1 = 2.64$   
\*\*\*\*\*  $A2 = -2.69$   
 $A3 = -1.00$

LEAST SQUARE ERROR NORM:  $E = .13594E-01$

THE SOLUTION WAS FOUND AFTER 2 ITERATIONS

TABLE OF VALUES FOR EXPERIMENTAL DATA SET 3  
 \*\*\*\*\*

AREA OF OUTER NOZZLE 11.6034 CM<sup>2</sup>  
 AREA OF INNER NOZZLE .3127 CM<sup>2</sup>  
 VELOCITY OF AIR 1.0703 M/SEC

VELOCITY OF FUEL [ M/SEC ]	HEIGHT OF CENTRAL JET [ MM ]	HEIGHT OF LEFT VORTEX [ MM ]	HEIGHT OF RIGHT VORTEX [ MM ]
.0649	4.4450	5.5532	6.3421
.0811	5.2030	6.1466	7.1994
.0906	7.4143	6.1374	7.5692
.1017	4.7122	6.1376	7.3406
.1164	11.1253	6.1976	7.0612
.1321	11.0415	6.1976	6.7310
.1503	10.0054	6.6040	7.3660
.1785	15.0400	6.4770	7.3440
.2147	12.4150	6.3500	7.3460

(\*)

THE PENETRATION POINT IS GIVEN BY (\*)

FUNCTION FOR THIS DATA SET 2  
 \*\*\*\*\*

THE VALUES ARE NONDIMENSIONALIZED BY THE RULES

$$X = \frac{\text{VELOCITY OF FUEL}}{\text{PENETRATION VELOCITY}}$$

$$Y = \frac{\text{FORWARD STAGNATION POINT}}{\text{AFT STAGNATION POINT}}$$

CONSTANTS ARE DETERMINED BY A LEAST SQUARE METHOD

FUNCTION:  $Y = 1 + A1*(1-X) + A2*(1-X)**2 + A3*(1-X)**3$   
 \*\*\*\*\*

INITIAL VALUES: A1 = .100  
 \*\*\*\*\* A2 = 2.30  
 A3 = 1.50

CONSTANTS: A1 = -.033  
 \*\*\*\*\* A2 = .476  
 A3 = -1.06

LEAST SQUARE ERROR TERM: E = .46479E-02

THE SOLUTION WAS FOUND AFTER 2 ITERATIONS

FUNCTION FOR TWEED DATA SET 5  
\*\*\*\*\*

THE VALUES ARE NON-DIMENSIONALIZED BY THE PILES

$$X = \frac{\text{VELOCITY OF FUEL}}{\text{ANNULUS AIR VELOCITY}}$$

$$Y = \frac{\text{FORWARD STAGNATION POINT}}{\text{AFT STAGNATION POINT}}$$

CONSTANTS ARE DETERMINED BY A LEAST SQUARE METHOD

FUNCTION:  $Y = 1 + A1*(1-Y) + A2*(1-Y)**2 + A3*(1-Y)**3$   
\*\*\*\*\*

INITIAL VALUES: A1 = .100  
\*\*\*\*\* A2 = 0.30  
A3 = 1.50

CONSTANTS: A1 = -5.33  
\*\*\*\*\* A2 = 17.2  
A3 = -13.2

LEAST SQUARE ERROR NORM: E = .50443E-02

THE SOLUTION WAS FOUND AFTER 2 ITERATIONS

TABLE OF VALUES FOR EXPERIMENTAL DATA SET 4  
 \*\*\*\*\*

AREA OF OUTER NOZZLE 12.9036 CM<sup>2</sup>  
 AREA OF INNER NOZZLE .3167 CM<sup>2</sup>  
 VELOCITY OF AIR 1.0444 M/SEC

VELOCITY OF FUEL [ M/SEC ]	HEIGHT OF CENTRAL JET [ MM ]	HEIGHT OF LEFT VORTEX [ MM ]	HEIGHT OF RIGHT VORTEX [ MM ]
.0777	5.0690	6.3324	10.0584
.0955	6.7844	7.8263	11.7060
.1060	7.725	7.0104	8.6360
.1191	10.2616	6.0590	6.4912
.1284	11.4300	6.4072	8.3566
.1410	12.7432	6.7310	11.0772
.1634	10.9040	6.6348	8.0772
.1715	14.1032	6.5547	8.0772
.1730	13.1610	6.4262	8.2423

(\*)

THE PENETRATION POINT IS SIGNED BY (\*)



FUNCTION FOR THIS DATA SET IS  
\*\*\*\*\*

THE VALUES ARE NONDIMENSIONALIZED BY THE RULES

$$Y = \frac{\text{VELOCITY OF FUEL}}{\text{PENETRATION VELOCITY}}$$

$$Y = \frac{\text{FORWARD STAGNATION POINT}}{\text{AFT STAGNATION POINT}}$$

CONSTANTS ARE DETERMINED BY A LEAST SQUARE METHOD

FUNCTION:  $Y = 1 + A1*(1-X) + A2*(1-X)**2 + A3*(1-X)**3$   
\*\*\*\*\*

INITIAL VALUES:  $A1 = .100$   
\*\*\*\*\*  $A2 = 2.30$   
 $A3 = 1.50$

CONSTANTS:  $A1 = -.756$   
\*\*\*\*\*  $A2 = -.214E-01$   
 $A3 = -.656$

LEAST SQUARE ERROR NORM:  $E = .52113E-02$

THE SOLUTION WAS FOUND AFTER 2 ITERATIONS

FUNCTION FOR THIS DATA SET 1  
\*\*\*\*\*

THE VALUES ARE NONDIMENSIONALIZED BY THE RULES

$$X = \frac{\text{VELOCITY OF FUEL}}{\text{ANNULUS AIR VELOCITY}}$$

$$Y = \frac{\text{FORWARD STAGNATION POINT}}{\text{AFT STAGNATION POINT}}$$

CONSTANTS ARE DETERMINED BY A LEAST SQUARE METHOD

FUNCTION:  $Y = 1 + A1*(1-X) + A2*(1-X)**2 + A3*(1-X)**3$   
\*\*\*\*\*

INITIAL VALUES: A1 = .100  
\*\*\*\*\* A2 = 2.30  
A3 = 1.50

CONSTANTS: A1 = -10.3  
\*\*\*\*\* A2 = 24.1  
A3 = -20.1

LEAST SQUARE ERROR NORM: E = .52988E-02

THE SOLUTION WAS FOUND AFTER 2 ITERATIONS

TABLE OF VALUES FOR TIME-TAL DATA SET 5  
\*\*\*\*\*

AREA OF OUTER NOZZLE 10.000 CM<sup>2</sup>  
AREA OF INNER NOZZLE 0.0167 CM<sup>2</sup>  
VELOCITY OF AIR 1.0045 M/SEC

VELOCITY OF FUEL [ M/SEC ]	HEIGHT OF CENTRAL VFT [ MM ]	HEIGHT OF LEFT VORTEX [ MM ]	HEIGHT OF RIGHT VORTEX [ MM ]
.0740	4.6055	0.1290	.0000
.0899	7.1092	7.8740	11.1760
.1122	4.0177	7.8740	0.7790
.1193	0.4514	7.9242	0.6520
.1295	11.4516	8.0772	0.3980
.1518	13.7185	7.9175	0.5758
.1746	14.9733	8.0764	0.3523
.2072	15.0733	8.2550	0.1440
.2494	17.1410	8.0010	0.0679

(\*)

THE PENETRATION POINT IS CIRCLED BY (\*)

FUNCTION ARE THIS DATA SET  
\*\*\*\*\*

THE VALUES ARE NORMALLY SIGNALIZED BY THE RULES

$$Y = \frac{\text{VELOCITY OF FUEL}}{\text{PENETRATION VELOCITY}}$$

$$Y = \frac{\text{FORWARD STAGNATION POINT}}{\text{AFT STAGNATION POINT}}$$

CONSTANTS ARE DETERMINED BY A LEAST SQUARE METHOD

FUNCTION:  $Y = 1 + A1*(1-X) + A2*(1-X)**2 + A3*(1-X)**3$   
\*\*\*\*\*

INITIAL VALUES:  $A1 = .100$   
\*\*\*\*\*  
 $A2 = 2.30$   
 $A3 = 1.50$

CONSTANTS:  $A1 = -.485$   
\*\*\*\*\*  
 $A2 = -.505$   
 $A3 = -.432$

LEAST SQUARE ERROR NORM:  $E = .20405E-02$

THE SOLUTION WAS FOUND AFTER 2 ITERATIONS

FUNCTION FOR THIS DATA SET  
\*\*\*\*\*

THE VALUES ARE NONDIMENSIONALIZED BY THE RULES

$$Y = \frac{\text{VELOCITY OF FUEL}}{\text{ANALYSIS AIR VELOCITY}}$$
$$Y = \frac{\text{FORWARD STAGNATION POINT}}{\text{AFT STAGNATION POINT}}$$

CONSTANTS ARE DETERMINED BY A LEAST SQUARE METHOD

FUNCTION:  $Y = 1 + A1*(1-X) + A2*(1-X)**2 + A3*(1-X)**3$   
\*\*\*\*\*

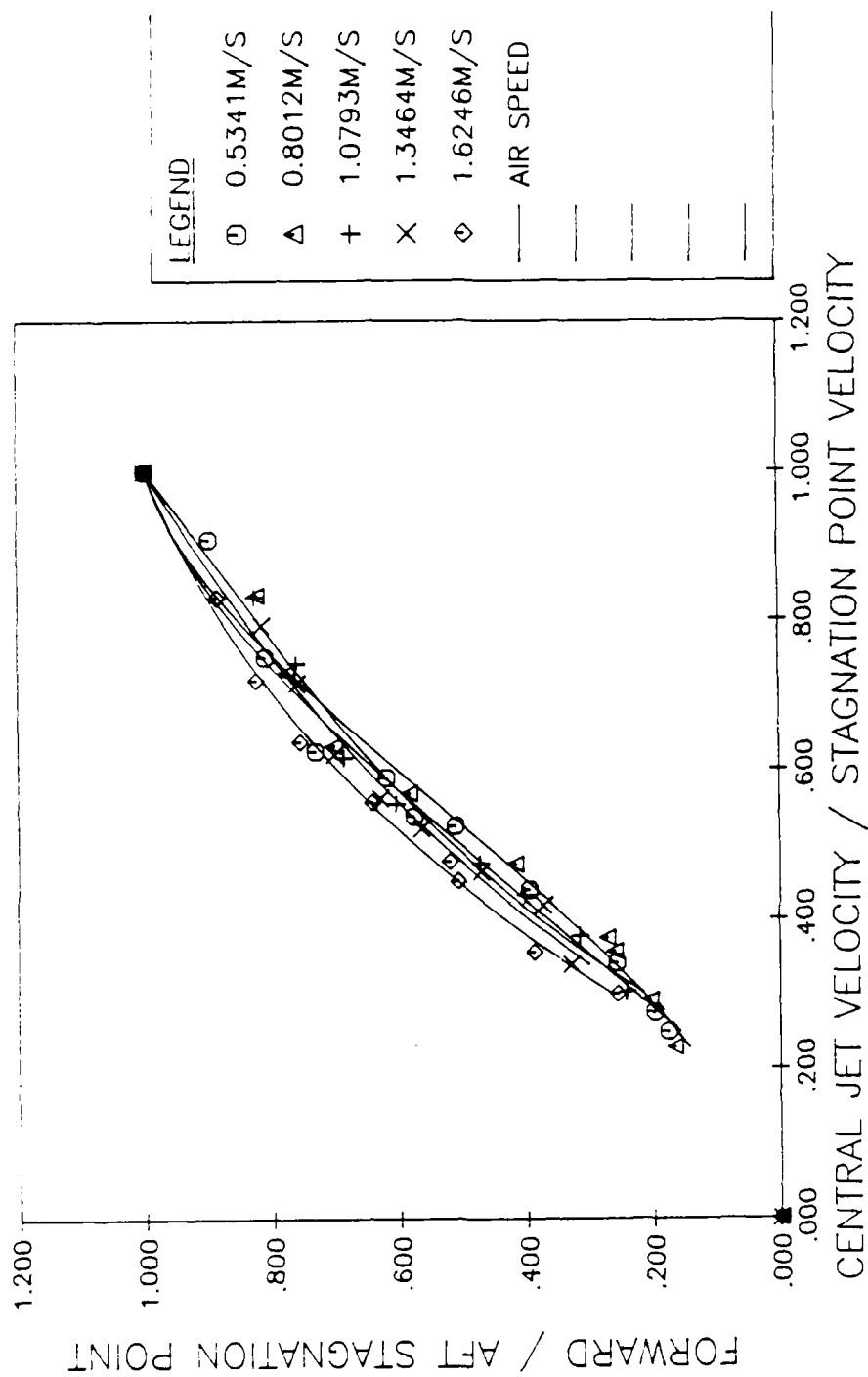
INITIAL VALUES: A1 = .100  
\*\*\*\*\* A2 = 2.30  
A3 = 1.50

CONSTANTS: A1 = -24.3  
\*\*\*\*\* A2 = 41.7  
A3 = -38.2

LEAST SQUARE ERROR NORM: E = .20639E-02

THE SOLUTION WAS FOUND AFTER 0 ITERATIONS

PLOT OF THE NONDIMENSIONALIZED DATA SET 5



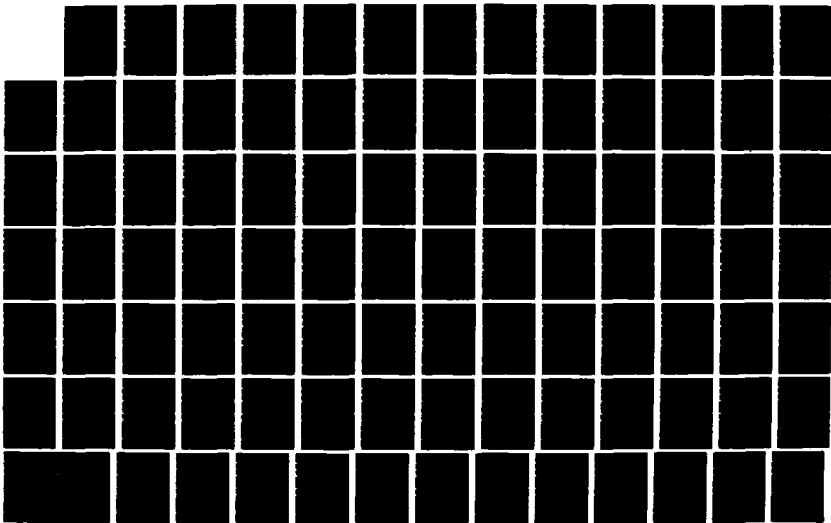
AD-A186 490

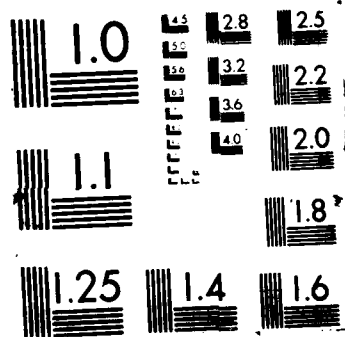
UNITED STATES AIR FORCE RESEARCH INITIATION PROGRAM  
1984 RESEARCH REPORTS (U) SOUTHEASTERN CENTER FOR  
ELECTRICAL ENGINEERING EDUCATION INC S W D PEELE  
MAY 86 AFOSR-TR-87-1721 F49620-82-C-0035 F/G 15/1

09/11

UNCLASSIFIED

ML







PLOT OF THE NONDIMENSIONALIZED DATA SET 5

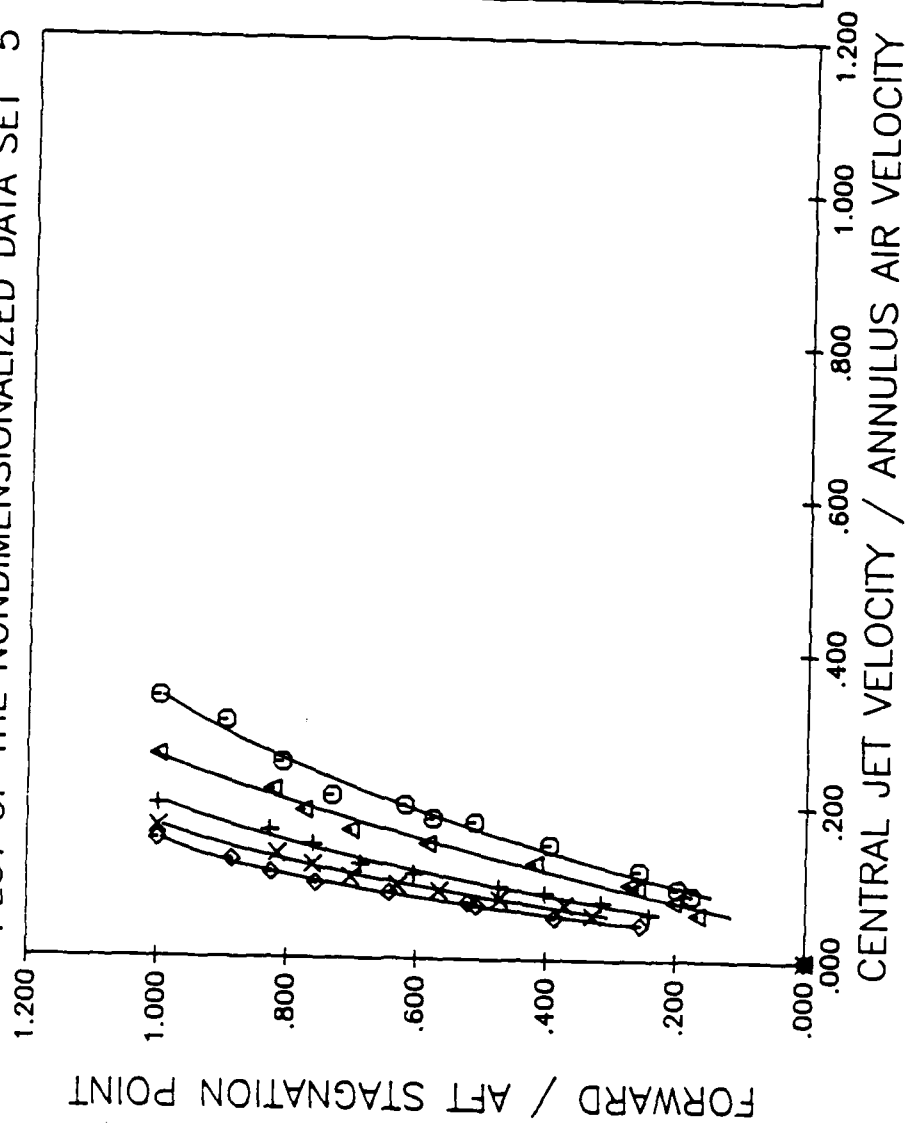


TABLE OF VALUES FOR EXPERIMENTAL DATA SET 1  
 \*\*\*\*\*

AREA OF OUTER NOZZLE 10.6036 CM\*\*2  
 AREA OF INNER NOZZLE .7012 CM\*\*2  
 VELOCITY OF AIR .9341 M/SEC

VELOCITY OF FUEL [ M/SEC ]	HEIGHT OF CENTRAL JET [ MM ]	HEIGHT OF LEFT VORTEX [ MM ]	HEIGHT OF RIGHT VORTEX [ MM ]	
.0785	3.2352	3.2182	5.4610	
.0804	3.7254	4.4450	4.5276	
.1065	7.3460	4.2672	5.8674	
.1443	10.1500	5.2340	5.6896	
.1900	12.9794	5.2932	5.2932	
.2284	15.0828	4.8250	5.9152	
.2659	13.0340	5.0738	6.7818	(*)
.2789	19.0500	4.9734	6.6548	(*)

THE PENETRATION POINT IS SIGNED BY (\*)

FUNCTION FOR THIS DATA SET /  
\*\*\*\*\*

THE VALUES ARE NONDIMENSIONALIZED BY THE RULES

$$X = \frac{\text{VELOCITY OF FUEL}}{\text{PENETRATION VELOCITY}}$$
$$Y = \frac{\text{FORWARD STAGNATION POINT}}{\text{AFT STAGNATION POINT}}$$

CONSTANTS ARE DETERMINED BY A LEAST SQUARE METHOD

FUNCTION:  $Y = 1 + A1*(1-X) + A2*(1-X)**2 + A3*(1-X)**3$   
\*\*\*\*\*

INITIAL VALUES: A1 = .100  
\*\*\*\*\* A2 = 2.30  
A3 = 1.50

CONSTANTS: A1 = -.322  
\*\*\*\*\* A2 = -.521  
A3 = .313

LEAST SQUARE ERROR NORM: E = .16658E-02

THE SOLUTION WAS FOUND AFTER 2 ITERATIONS

FUNCTION FOR THIS DATA SET  
\*\*\*\*\*

THE VALUES ARE NONDIMENSIONALIZED BY THE RULES

$$X = \frac{\text{VELOCITY OF FUEL}}{\text{ANNULUS AIR VELOCITY}}$$

$$Y = \frac{\text{FORWARD STAGNATION POINT}}{\text{AFT STAGNATION POINT}}$$

CONSTANTS ARE DETERMINED BY A LEAST SQUARE METHOD

FUNCTION:  $Y = 1 + A1*(1-Y) + A2*(1-Y)**2 + A3*(1-Y)**3$   
\*\*\*\*\*

INITIAL VALUES: A1 = .100  
\*\*\*\*\* A2 = 2.30  
A3 = 1.50

CONSTANTS: A1 = 2.02  
\*\*\*\*\* A2 = -5.35  
A3 = 2.30

LEAST SQUARE ERROR NORM: E = .16001E-02

THE SOLUTION WAS FOUND AFTER 2 ITERATIONS

TABLE OF VALUES FOR EXPERIMENTAL DATA SET 2  
 \*\*\*\*\*

AREA OF OUTER NOZZLE 10.6036 CM\*\*2  
 AREA OF INNER NOZZLE .7012 CM\*\*2  
 VELOCITY OF AIR .4012 M/SEC

VELOCITY OF FUEL [ M/SEC ]	HEIGHT OF CENTRAL JET [ MM ]	HEIGHT OF LEFT VORTEX [ MM ]	HEIGHT OF RIGHT VORTEX [ MM ]	
.0414	3.0226	4.9784	6.9596	
.0520	4.0132	5.5280	6.0513	
.1170	9.3806	5.7404	6.2392	
.1474	11.4300	6.0260	7.6200	
.1820	15.2400	5.8674	7.0612	
.2371	21.7170	5.7404	6.2484	
.2762	25.0190	5.0400	6.3881	(*)
.3152	26.8732	5.0900	5.2324	(*)

THE PENETRATION POINT IS SIGNED BY (\*)

FUNCTION FOR THIS DATA SET  
\*\*\*\*\*

THE VALUES ARE NONDIMENSIONALIZED BY THE RULES

$$X = \frac{\text{VELOCITY OF FUEL}}{\text{PENETRATION VELOCITY}}$$
$$Y = \frac{\text{FORWARD STAGNATION POINT}}{\text{AFT STAGNATION POINT}}$$

CONSTANTS ARE DETERMINED BY A LEAST SQUARE METHOD

FUNCTION:  $Y = 1 + A1*(1-X) + A2*(1-X)**2 + A3*(1-X)**3$   
\*\*\*\*\*

INITIAL VALUES:  $A1 = .100$   
\*\*\*\*\*  $A2 = 2.30$   
 $A3 = 1.50$

CONSTANTS:  $A1 = -.434$   
\*\*\*\*\*  $A2 = -1.85$   
 $A3 = 1.30$

LEAST SQUARE ERROR NORM:  $E = .24742E-02$

THE SOLUTION WAS FOUND AFTER 2 ITERATIONS

FUNCTION FOR THIS DATA SET  
\*\*\*\*\*

THE VALUES ARE NONDIMENSIONALIZED BY THE RULES

$$X = \frac{\text{VELOCITY OF FUEL}}{\text{ANNULUS AIR VELOCITY}}$$
$$Y = \frac{\text{FORWARD STAGNATION POINT}}{\text{AFT STAGNATION POINT}}$$

CONSTANTS ARE DETERMINED BY A LEAST SQUARE METHOD

FUNCTION:  $Y = 1 + A1*(1-X) + A2*(1-X)**2 + A3*(1-X)**3$   
\*\*\*\*\*

INITIAL VALUES: A1 = .100  
\*\*\*\*\* A2 = 2.30  
A3 = 1.50

CONSTANTS: A1 = 3.92  
\*\*\*\*\* A2 = -6.61  
A3 = 3.67

LEAST SQUARE ERROR NORM: E = .46121E-02

THE SOLUTION WAS FOUND AFTER 2 ITERATIONS

TABLE OF VALUES FOR EXPERIMENTAL DATA SET 3  
 \*\*\*\*\*

AREA OF OUTER NOZZLE 10.5036 CM\*\*2  
 AREA OF INNER NOZZLE .7012 CM\*\*2  
 VELOCITY OF AIR 1.0793 M/SEC

VELOCITY OF FUEL [ M/SEC ]	HEIGHT OF CENTRAL JET [ MM ]	HEIGHT OF LEFT VORTEX [ MM ]	HEIGHT OF RIGHT VORTEX [ MM ]
.0413	2.9713	6.0071	6.5852
.0741	3.6367	6.4543	9.3726
.1289	10.3966	6.5532	10.2870
.1787	15.1392	6.5276	7.5692
.2404	17.5580	6.5024	6.9850
.3157	21.0202	5.8674	6.3500

(\*)

THE PENETRATION POINT IS SIGNED BY (\*)



FUNCTION FOR THIS DATA SET 3  
\*\*\*\*\*

THE VALUES ARE NONDIMENSIONALIZED BY THE RULES

$$X = \frac{\text{VELOCITY OF FUEL}}{\text{PENETRATION VELOCITY}}$$
$$Y = \frac{\text{FORWARD STAGNATION POINT}}{\text{AFT STAGNATION POINT}}$$

CONSTANTS ARE DETERMINED BY A LEAST SQUARE METHOD

FUNCTION:  $Y = 1 + A1*(1-X) + A2*(1-X)**2 + A3*(1-X)**3$   
\*\*\*\*\*

INITIAL VALUES: A1 = .100  
\*\*\*\*\* A2 = 7.30  
A3 = 1.50

CONSTANTS: A1 = -.147  
\*\*\*\*\* A2 = -1.60  
A3 = .811

LEAST SQUARE ERROR NORM: E = .71551E-03

THE SOLUTION WAS FOUND AFTER 2 ITERATIONS

FUNCTION FOR THIS DATA SET =  
\*\*\*\*\*

THE VALUES ARE NONDIMENSIONALIZED BY THE RULES

$$Y = \frac{\text{VELOCITY OF BUFL}}{\text{ANNULUS AIR VELOCITY}}$$
$$X = \frac{\text{FORWARD STAGNATION POINT}}{\text{AFT STAGNATION POINT}}$$

CONSTANTS ARE DETERMINED BY A LEAST SQUARE METHOD

FUNCTION:  $Y = 1 + A1*(1-X) + A2*(1-X)**2 + A3*(1-X)**3$   
\*\*\*\*\*

INITIAL VALUES: A1 = .100  
\*\*\*\*\* A2 = 0.30  
A3 = 1.50

CONSTANTS: A1 = -0.268  
\*\*\*\*\* A2 = 3.42  
A3 = -4.25

LEAST SQUARE ERROR NORM: E = .21925E-02

THE SOLUTION WAS FOUND AFTER 2 ITERATIONS

TABLE OF VALUES FROM EXPERIMENTAL DATA SET 4  
 \*\*\*\*\*

AREA OF OUTER NOZZLE 10.6036 CM\*\*2  
 AREA OF INNER NOZZLE .7012 CM\*\*2  
 VELOCITY OF AIR 1.3464 "/SEC

VELOCITY OF FUEL [ "/SEC ]	HEIGHT OF CENTRAL JET [ " ]	HEIGHT OF LEFT VORTEX [ " ]	HEIGHT OF RIGHT VORTEX [ " ]	
.0443	3.6068	7.1374	10.2102	
.0840	5.9420	7.4374	9.9642	
.1229	8.0010	6.8900	13.1318	
.1725	11.6840	7.9248	7.6200	
.2299	16.7640	7.5200	7.9756	
.3092	19.3040	7.6708	7.9248	(*)
.3625	20.3200	5.7564	7.6200	(*)

THE PENETRATION POINT IS SIGNED BY (\*)

FUNCTION FOR THIS DATA SET IS  
\*\*\*\*\*

THE VALUES ARE NONDIMENSIONALIZED BY THE RULES

$$Y = \frac{\text{VELOCITY OF FUEL}}{\text{PENETRATION VELOCITY}}$$
$$Y = \frac{\text{FORWARD STAGNATION POINT}}{\text{AFT STAGNATION POINT}}$$

CONSTANTS ARE DETERMINED BY A LEAST SQUARE METHOD

FUNCTION:  $Y = 1 + A1*(1-Y) + A2*(1-Y)**2 + A3*(1-X)**3$   
\*\*\*\*\*

INITIAL VALUES:  $A1 = .100$   
\*\*\*\*\*  
 $A2 = 2.30$   
 $A3 = 1.50$

CONSTANTS:  $A1 = .234$   
\*\*\*\*\*  
 $A2 = -2.33$   
 $A3 = 1.70$

LEAST SQUARE ERROR NORM:  $E = .25552E-02$

THE SOLUTION WAS FOUND AFTER 2 ITERATIONS

FUNCTION FOR THIS DATA SET 4  
\*\*\*\*\*

THE VALUES ARE NONDIMENSIONALIZED BY THE RULES

$$Y = \frac{\text{VELOCITY OF FUEL}}{\text{ANNULUS AIR VELOCITY}}$$

$$Y = \frac{\text{FORWARD STAGNATION POINT}}{\text{AFT STAGNATION POINT}}$$

CONSTANTS ARE DETERMINED BY A LEAST SQUARE METHOD

FUNCTION:  $Y = 1 + A1*(1-Y) + A2*(1-Y)**2 + A3*(1-Y)**3$   
\*\*\*\*\*

INITIAL VALUES: A1 = .100  
\*\*\*\*\* A2 = 2.30  
A3 = 1.50

CONSTANTS: A1 = -.434  
\*\*\*\*\* A2 = 4.10  
A3 = -4.73

LEAST SQUARE ERROR NORM: E = .20361E-02

THE SOLUTION WAS FOUND AFTER 2 ITERATIONS

TABLE OF VALUES FOR EXPERIMENTAL DATA SET 5  
 \*\*\*\*\*

AREA OF OUTER NOZZLE 10.6036 CM\*\*2  
 AREA OF INNER NOZZLE .7012 CM\*\*2  
 VELOCITY OF AIR 1.5046 M/SEC

VELOCITY OF FUEL [ M/SEC ]	HEIGHT OF CENTRAL JET [ MM ]	HEIGHT OF LEFT VORTEX [ MM ]	HEIGHT OF RIGHT VORTEX [ MM ]	
.0636	5.6102	7.2508	11.9380	
.0605	7.7067	8.1280	12.1691	
.0697	9.6491	8.7312	12.5730	
.0823	11.2268	8.1534	12.3952	
.1046	14.8282	7.9248	8.6360	
.1045	14.4760	7.9756	8.9459	
.1339	17.0434	7.7478	8.2296	
.1741	18.9713	8.4074	9.3980	(*)
.2112	19.8120	7.8200	10.7315	(*)

THE PENETRATION POINT IS SIGNED BY (\*)

FUNCTION FOR THIS DATA SET 5  
\*\*\*\*\*

THE VALUES ARE NONDIMENSIONALIZED BY THE RULES

$$Y = \frac{\text{VELOCITY OF FLOW}}{\text{PENETRATION VELOCITY}}$$

$$Y = \frac{\text{FORWARD STAGNATION POINT}}{\text{AFT STAGNATION POINT}}$$

CONSTANTS ARE DETERMINED BY A LEAST SQUARE METHOD

FUNCTION:  $Y = 1 + A1*(1-Y) + A2*(1-X)**2 + A3*(1-X)**3$   
\*\*\*\*\*

INITIAL VALUES: A1 = .100  
\*\*\*\*\* A2 = 2.30  
A3 = 1.50

CONSTANTS: A1 = -.117  
\*\*\*\*\* A2 = -.362  
A3 = -.600

LEAST SQUARE ERROR NORM: E = .31984E-03

THE SOLUTION WAS FOUND AFTER 2 ITERATIONS

FUNCTION FOR THIS DATA SET 5  
\*\*\*\*\*

THE VALUES ARE NONDIMENSIONALIZED BY THE RULES

$$Y = \frac{\text{VELOCITY OF BHEL}}{\text{ANNULUS AIR VELOCITY}}$$

$$Y = \frac{\text{FORWARD STAGNATION POINT}}{\text{APT STAGNATION POINT}}$$

CONSTANTS ARE DETERMINED BY A LEAST SQUARE METHOD

FUNCTION:  $Y = 1 + A1*(1-X) + A2*(1-X)**2 + A3*(1-X)**3$   
\*\*\*\*\*

INITIAL VALUES: A1 = .100  
\*\*\*\*\* A2 = 0.30  
A3 = 1.50

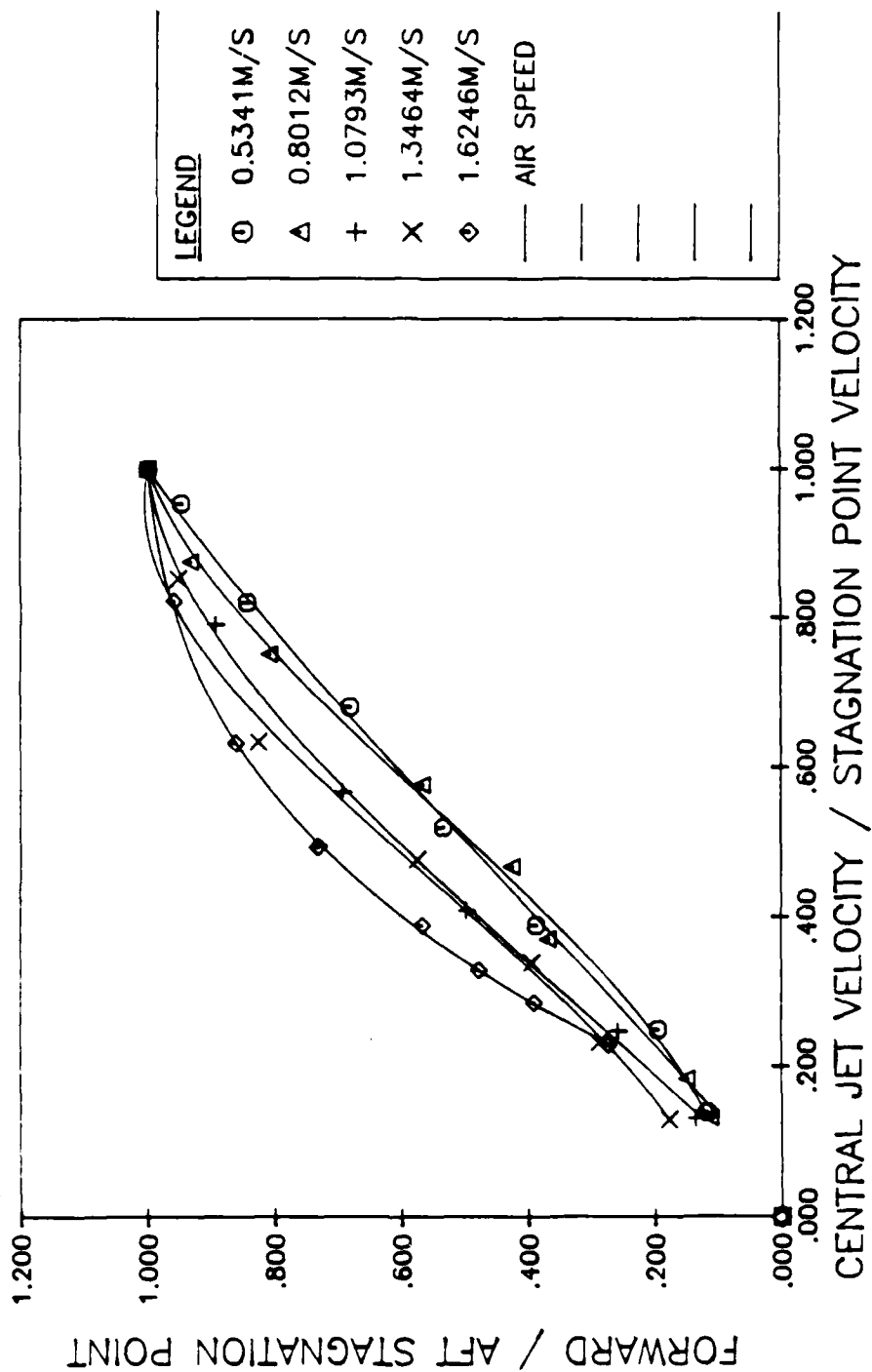
CONSTANTS: A1 = -65.5  
\*\*\*\*\* A2 = 149.  
A3 = -45.1

LEAST SQUARE ERROR NORM: E = .80839E-03

THE SOLUTION WAS FOUND AFTER 2 ITERATIONS



PLOT OF THE NONDIMENSIONALIZED DATA SET 5



PLOT OF THE NONDIMENSIONALIZED DATA SET 5

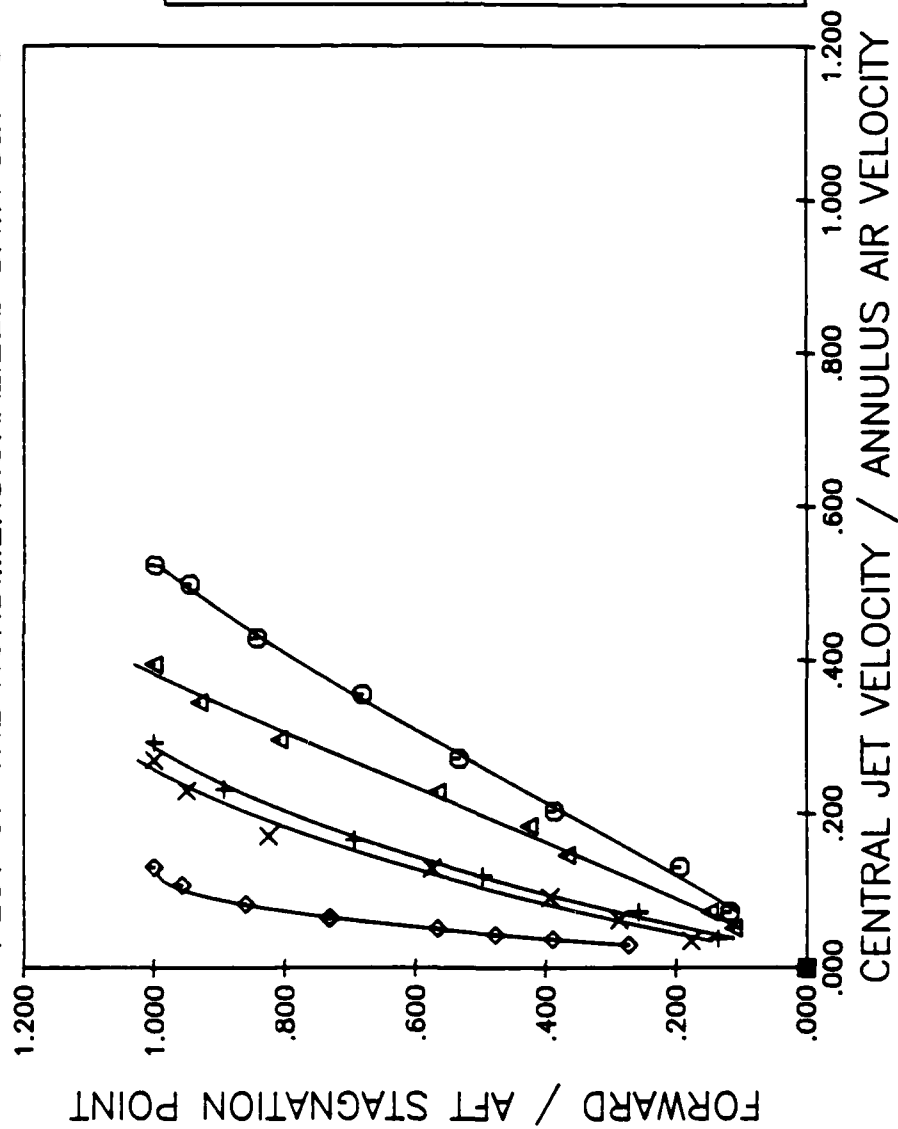


TABLE OF VALUES FOR EXPERIMENTAL DATA SET 1  
 \*\*\*\*\*

AREA OF OUTER NOZZLE 10.6036 CM\*\*2  
 AREA OF INNER NOZZLE 1.2668 CM\*\*2  
 VELOCITY OF AIR .5341 M/SEC

VELOCITY OF FUEL [ M/SEC ]	HEIGHT OF CENTRAL JET [ MM ]	HEIGHT OF LEFT VORTEX [ MM ]	HEIGHT OF RIGHT VORTEX [ MM ]	
.0239	1.9558	3.4468	4.6990	
.0375	2.9194	4.7498	5.6007	
.0643	4.2723	6.2230	7.1399	
.0894	5.7023	7.0739	7.4346	
.1096	7.5433	8.9562	10.0863	
.1209	8.3591	10.9195	11.3030	
.1403	9.6977	13.6093	13.6093	
.1595	12.1158	16.1290	16.1290	
.1834	13.5915	4.6736	5.2578	
.2044	14.7904	5.4381	5.4381	
.2205	15.2560	5.1562	5.7150	
.2584	19.8120	4.4704	5.1054	
.2841	21.5900	4.4704	5.1054	
.3410	23.4950	4.4704	5.1054	(*)
.3710	24.3840	5.0900	5.5143	(*)

THE PENETRATION POINT IS SIGNED BY (\*)

FUNCTION FOR THIS DATA SET  
\*\*\*\*\*

THE VALUES ARE NONDIMENSIONALIZED BY THE RULES

$$X = \frac{\text{VELOCITY OF FUEL}}{\text{PENETRATION VELOCITY}}$$
$$Y = \frac{\text{FORWARD STAGNATION POINT}}{\text{AFT STAGNATION POINT}}$$

CONSTANTS ARE DETERMINED BY A LEAST SQUARE METHOD

FUNCTION:  $Y = 1 + A1*(1-X) + A2*(1-X)**2 + A3*(1-X)**3$   
\*\*\*\*\*

INITIAL VALUES:  $A1 = .100$   
\*\*\*\*\*  $A2 = 2.30$   
 $A3 = 1.50$

CONSTANTS:  $A1 = -.126$   
\*\*\*\*\*  $A2 = -2.16$   
 $A3 = 1.34$

LEAST SQUARE ERROR NORM:  $E = .20902E-02$

THE SOLUTION WAS FOUND AFTER 2 ITERATIONS

FUNCTION FOR THIS DATA SET  
\*\*\*\*\*

THE VALUES ARE NONDIMENSIONALIZED BY THE RULES

$$X = \frac{\text{VELOCITY OF FUEL}}{\text{ANNULUS AIR VELOCITY}}$$
$$Y = \frac{\text{FORWARD STAGNATION POINT}}{\text{AFT STAGNATION POINT}}$$

CONSTANTS ARE DETERMINED BY A LEAST SQUARE METHOD

FUNCTION:  $Y = 1 + A1*(1-X) + A2*(1-X)**2 + A3*(1-X)**3$   
\*\*\*\*\*

INITIAL VALUES: A1 = .100  
\*\*\*\*\* A2 = 2.30  
A3 = 1.50

CONSTANTS: A1 = 1.15  
\*\*\*\*\* A2 = -4.03  
A3 = 1.89

LEAST SQUARE ERROR NORM: E = .50355E-02

THE SOLUTION WAS FOUND AFTER 2 ITERATIONS

TABLE OF VALUES FOR EXPERIMENTAL DATA SET 2  
 \*\*\*\*\*

AREA OF OUTER NOZZLE 10.5036 CM\*\*2  
 AREA OF INNER NOZZLE 1.2668 CM\*\*2  
 VELOCITY OF AIR .8012 M/SEC

VELOCITY OF FUEL [ M/SEC ]	HEIGHT OF CENTRAL JET [ MM ]	HEIGHT OF LEFT VORTEX [ MM ]	HEIGHT OF RIGHT VORTEX [ MM ]
.0190	2.0320	5.0800	7.1374
.0239	2.1590	4.8006	6.2484
.0419	2.2860	5.4102	7.8994
.0575	3.8100	5.6134	8.1280
.0891	5.0800	8.3058	9.9822
.1088	6.6040	9.7028	10.1092
.1242	7.8740	11.1760	11.7348
.1435	9.4996	13.9700	13.9700
.1594	10.4140	15.2400	15.2400
.1794	11.6586	5.3340	5.3340
.1999	13.4620	5.3340	5.3340
.2286	14.4780	5.3340	5.3340
.2706	17.2720	5.3340	5.3340
.2915	14.7960	5.5880	5.5880
.3035	19.8120	5.4864	5.5880
.3249	22.3520	5.0800	5.9690
.3874	25.4000	5.5880	6.0198

(\*)

THE PENETRATION POINT IS SIGNED BY (\*)

FUNCTION FOR THIS DATA SET  
\*\*\*\*\*

THE VALUES ARE NONDIMENSIONALIZED BY THE RULES

$X = \frac{\text{VELOCITY OF FUEL}}{\text{PENETRATION VELOCITY}}$   
 $Y = \frac{\text{FORWARD STAGNATION POINT}}{\text{AFT STAGNATION POINT}}$

CONSTANTS ARE DETERMINED BY A LEAST SQUARE METHOD

FUNCTION:  $Y = 1 + A1*(1-X) + A2*(1-X)**2 + A3*(1-X)**3$   
\*\*\*\*\*

INITIAL VALUES: A1 = .100  
\*\*\*\*\* A2 = 2.30  
A3 = 1.50

CONSTANTS: A1 = -.906  
\*\*\*\*\* A2 = -.384  
A3 = .321

LEAST SQUARE ERROR NORM: E = .45390E-02

THE SOLUTION WAS FOUND AFTER 2 ITERATIONS

FUNCTION FOR THIS DATA SET  
\*\*\*\*\*

THE VALUES ARE NONDIMENSIONALIZED BY THE RULES

$$X = \frac{\text{VELOCITY OF FUEL}}{\text{ANNULUS AIR VELOCITY}}$$
$$Y = \frac{\text{FORWARD STAGNATION POINT}}{\text{AFT STAGNATION POINT}}$$

CONSTANTS ARE DETERMINED BY A LEAST SQUARE METHOD

FUNCTION:  $Y = 1 + A1*(1-X) + A2*(1-X)**2 + A3*(1-X)**3$   
\*\*\*\*\*

INITIAL VALUES: A1 = .100  
\*\*\*\*\* A2 = 2.30  
A3 = 1.50

CONSTANTS: A1 = 2.69  
\*\*\*\*\* A2 = -6.97  
A3 = 3.21

LEAST SQUARE ERROR NORM: E = .45575E-02

THE SOLUTION WAS FOUND AFTER 2 ITERATIONS



TABLE OF VALUES FOR EXPERIMENTAL DATA SET 3  
\*\*\*\*\*

AREA OF OUTER NOZZLE 10.6036 CM\*\*2  
AREA OF INNER NOZZLE 1.2666 CM\*\*2  
VELOCITY OF AIR 1.0793 M/SEC

VELOCITY OF FUEL [ M/SEC ]	HEIGHT OF CENTRAL JET [ MM ]	HEIGHT OF LEFT VORTEX [ MM ]	HEIGHT OF RIGHT VORTEX [ MM ]	
.0221	1.7018	5.4364	7.7470	
.0370	2.3876	6.6548	9.3980	
.0479	3.0460	6.7564	9.4234	
.0641	4.0386	7.7470	10.4953	
.0825	5.2070	9.2354	11.4935	
.0938	6.4262	9.4717	12.4638	
.1305	8.4252	11.7602	13.7160	
.1434	9.8552	13.1064	15.1130	
.1641	11.8872	15.5575	15.5575	
.1822	12.8524	17.1958	17.1958	
.2039	14.6355	5.6388	6.2738	
.2293	16.3754	5.8420	5.8420	
.2629	18.3214	5.9690	6.1468	
.3049	21.1074	6.0960	6.1722	
.3325	22.5552	6.2230	6.1976	(*)
.3913	23.8760	6.8580	6.8580	(*)

THE PENETRATION POINT IS SIGNED BY (\*)

FUNCTION FOR THIS DATA SET  
\*\*\*\*\*

THE VALUES ARE NONDIMENSIONALIZED BY THE RULES

$$X = \frac{\text{VELOCITY OF FUEL}}{\text{PENETRATION VELOCITY}}$$
$$Y = \frac{\text{FORWARD STAGNATION POINT}}{\text{AFT STAGNATION POINT}}$$

CONSTANTS ARE DETERMINED BY A LEAST SQUARE METHOD

FUNCTION:  $Y = 1 + A1*(1-X) + A2*(1-X)**2 + A3*(1-X)**3$   
\*\*\*\*\*

INITIAL VALUES: A1 = .100  
\*\*\*\*\* A2 = 2.30  
A3 = 1.50

CONSTANTS: A1 = -.231  
\*\*\*\*\* A2 = -1.78  
A3 = 1.04

LEAST SQUARE ERROR NORM: E = .89464E-03

THE SOLUTION WAS FOUND AFTER 2 ITERATIONS

FUNCTION FOR THIS DATA SET  
\*\*\*\*\*

THE VALUES ARE NONDIMENSIONALIZED BY THE RULES

$$X = \frac{\text{VELOCITY OF FUEL}}{\text{ANNULUS AIR VELOCITY}}$$
$$Y = \frac{\text{FORWARD STAGNATION POINT}}{\text{AFT STAGNATION POINT}}$$

CONSTANTS ARE DETERMINED BY A LEAST SQUARE METHOD

FUNCTION:  $Y = 1 + A1*(1-X) + A2*(1-X)**2 + A3*(1-X)**3$   
\*\*\*\*\*

INITIAL VALUES: A1 = .100  
\*\*\*\*\* A2 = 2.30  
A3 = 1.50

CONSTANTS: A1 = 2.90  
\*\*\*\*\* A2 = -5.25  
A3 = 1.31

LEAST SQUARE ERROR NORM: E = .60688E-02

THE SOLUTION WAS FOUND AFTER 2 ITERATIONS

TABLE OF VALUES FOR EXPERIMENTAL DATA SET 4  
 \*\*\*\*\*

AREA OF OUTER NOZZLE 10.6036 CM\*\*2  
 AREA OF INNER NOZZLE 1.2668 CM\*\*2  
 VELOCITY OF AIR 1.3464 M/SEC

VELOCITY OF FUEL [ M/SEC ]	HEIGHT OF CENTRAL JET [ MM ]	HEIGHT OF LEFT VORTEX [ MM ]	HEIGHT OF RIGHT VORTEX [ MM ]	
.0360	2.1336	6.1722	9.0678	
.0554	2.4130	6.7818	10.1600	
.0658	3.3020	8.0772	10.3378	
.0807	3.8100	8.8900	11.1760	
.0964	5.3340	9.6520	11.6840	
.1235	7.0358	10.4648	14.6558	
.1455	9.7630	12.4206	15.6718	
.1637	10.4140	13.7150	16.0782	
.1840	12.0704	16.8556	16.8656	
.2009	13.1926	5.8420	5.8420	
.2199	14.7320	6.3500	6.8580	
.2457	16.1544	5.8420	6.7310	
.2822	17.4650	6.0960	6.7310	
.3120	18.9738	6.0960	6.0960	
.3702	20.7264	5.3594	6.1722	(*)
.3833	21.0820	6.1376	6.6294	(*)

THE PENETRATION POINT IS SIGNED BY (\*)

FUNCTION FOR THIS DATA SET  
\*\*\*\*\*

THE VALUES ARE NONDIMENSIONALIZED BY THE RULES

$$X = \frac{\text{VELOCITY OF FUEL}}{\text{PENETRATION VELOCITY}}$$
$$Y = \frac{\text{FORWARD STAGNATION POINT}}{\text{AFT STAGNATION POINT}}$$

CONSTANTS ARE DETERMINED BY A LEAST SQUARE METHOD

FUNCTION:  $Y = 1 + A1*(1-X) + A2*(1-X)**2 + A3*(1-X)**3$   
\*\*\*\*\*

INITIAL VALUES:  $A1 = .100$   
\*\*\*\*\*  $A2 = 2.30$   
 $A3 = 1.50$

CONSTANTS:  $A1 = -.380E-01$   
\*\*\*\*\*  $A2 = -2.06$   
 $A3 = 1.13$

LEAST SQUARE ERROR NORM:  $E = .41026E-02$

THE SOLUTION WAS FOUND AFTER 2 ITERATIONS

FUNCTION FOR THIS DATA SET  
\*\*\*\*\*

THE VALUES ARE NONDIMENSIONALIZED BY THE RULES

$$X = \frac{\text{VELOCITY OF FUEL}}{\text{ANNULUS AIR VELOCITY}}$$
$$Y = \frac{\text{FORWARD STAGNATION POINT}}{\text{AFT STAGNATION POINT}}$$

CONSTANTS ARE DETERMINED BY A LEAST SQUARE METHOD

FUNCTION:  $Y = 1 + A1*(1-X) + A2*(1-X)**2 + A3*(1-X)**3$   
\*\*\*\*\*

INITIAL VALUES: A1 = .100  
\*\*\*\*\* A2 = 2.30  
A3 = 1.50

CONSTANTS: A1 = .715  
\*\*\*\*\* A2 = 1.22  
A3 = -3.05

LEAST SQUARE ERROR NORM: E = .11030E-01

THE SOLUTION WAS FOUND AFTER 2 ITERATIONS

TABLE OF VALUES FOR EXPERIMENTAL DATA SET 5  
\*\*\*\*\*

AREA OF OUTER NOZZLE 10.5036 CM\*\*2  
AREA OF INNER NOZZLE 1.2668 CM\*\*2  
VELOCITY OF AIR 1.5246 M/SEC

VELOCITY OF FUEL [ M/SEC ]	HEIGHT OF CENTRAL JET [ MM ]	HEIGHT OF LEFT VORTEX [ MM ]	HEIGHT OF RIGHT VORTEX [ MM ]	
.0273	2.0320	6.9038	9.7536	
.0393	2.4638	7.1120	9.7536	
.0530	2.7940	6.8580	9.7536	
.0911	4.3358	9.0678	10.2362	
.1133	5.4356	9.0678	10.2362	
.1211	6.1976	.0000	.0000	
.1411	7.9248	.0000	.0000	
.1625	10.1270	.0000	.0000	
.1786	11.7140	.0000	.0000	
.1878	12.2428	.0000	.0000	
.2011	13.9243	.0000	.0000	
.2113	14.9352	.0000	.0000	
.2259	15.7983	.0000	.0000	
.2427	17.0742	.0000	.0000	
.2680	18.5674	.0000	.0000	
.3021	20.3200	.0000	.0000	(*)
.3967	21.0820	.0000	.0000	(*)

THE PENETRATION POINT IS SIGNED BY (\*)

FUNCTION FOR THIS DATA SET  
\*\*\*\*\*

THE VALUES ARE NONDIMENSIONALIZED BY THE RULES

$$X = \frac{\text{VELOCITY OF FUEL}}{\text{PENETRATION VELOCITY}}$$
$$Y = \frac{\text{FORWARD STAGNATION POINT}}{\text{AFT STAGNATION POINT}}$$

CONSTANTS ARE DETERMINED BY A LEAST SQUARE METHOD

FUNCTION:  $Y = 1 + A1*(1-X) + A2*(1-X)**2 + A3*(1-X)**3$   
\*\*\*\*\*

INITIAL VALUES: A1 = .100  
\*\*\*\*\* A2 = 2.30  
A3 = 1.50

CONSTANTS: A1 = .987  
\*\*\*\*\* A2 = -5.05  
A3 = 3.17

LEAST SQUARE ERROR NORM: E = .36666E-02

THE SOLUTION WAS FOUND AFTER 2 ITERATIONS



FUNCTION FOR THIS DATA SET  
\*\*\*\*\*

THE VALUES ARE NONDIMENSIONALIZED BY THE RULES

$$X = \frac{\text{VELOCITY OF FUEL}}{\text{ANNULUS AIR VELOCITY}}$$

$$Y = \frac{\text{FORWARD STAGNATION POINT}}{\text{AFT STAGNATION POINT}}$$

CONSTANTS ARE DETERMINED BY A LEAST SQUARE METHOD

FUNCTION:  $Y = 1 + A1*(1-X) + A2*(1-X)**2 + A3*(1-X)**3$   
\*\*\*\*\*

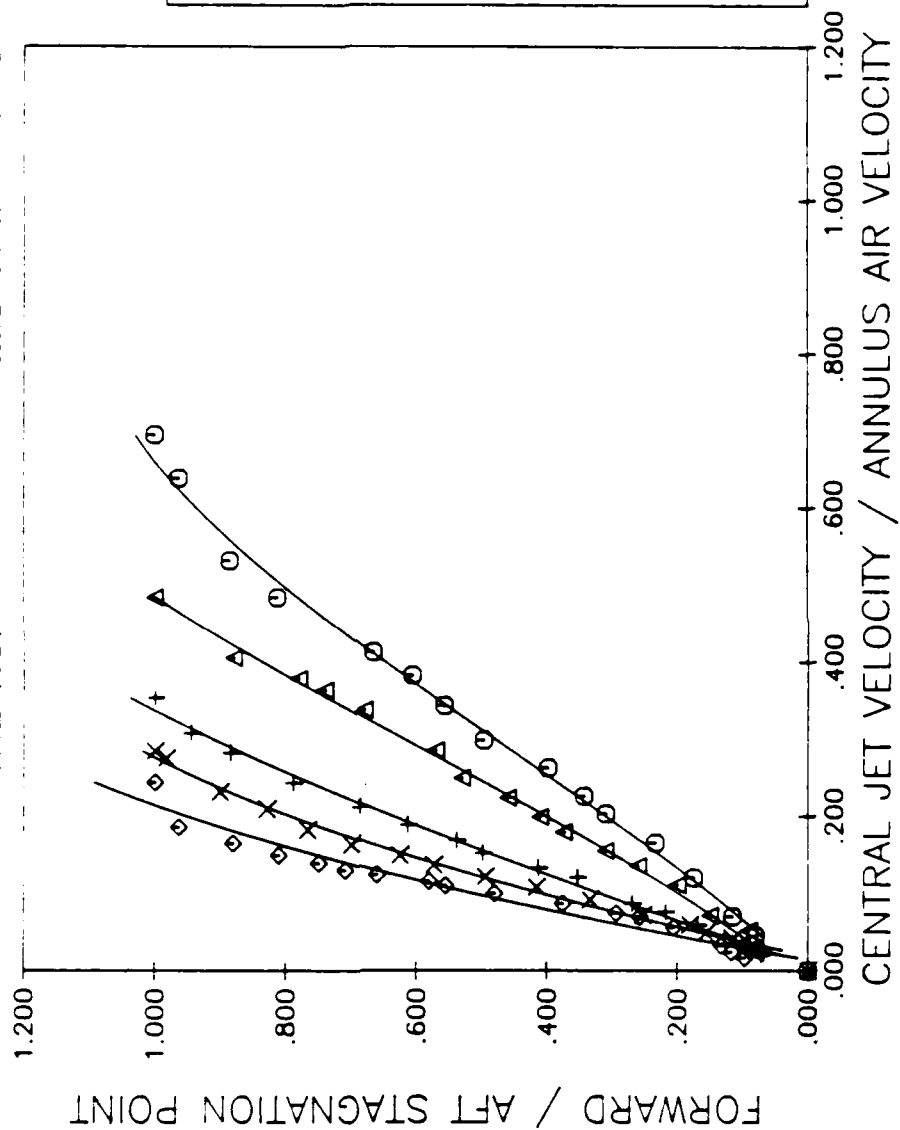
INITIAL VALUES: A1 = .100  
\*\*\*\*\* A2 = 2.30  
A3 = 1.50

CONSTANTS: A1 = .332  
\*\*\*\*\* A2 = 2.15  
A3 = -4.02

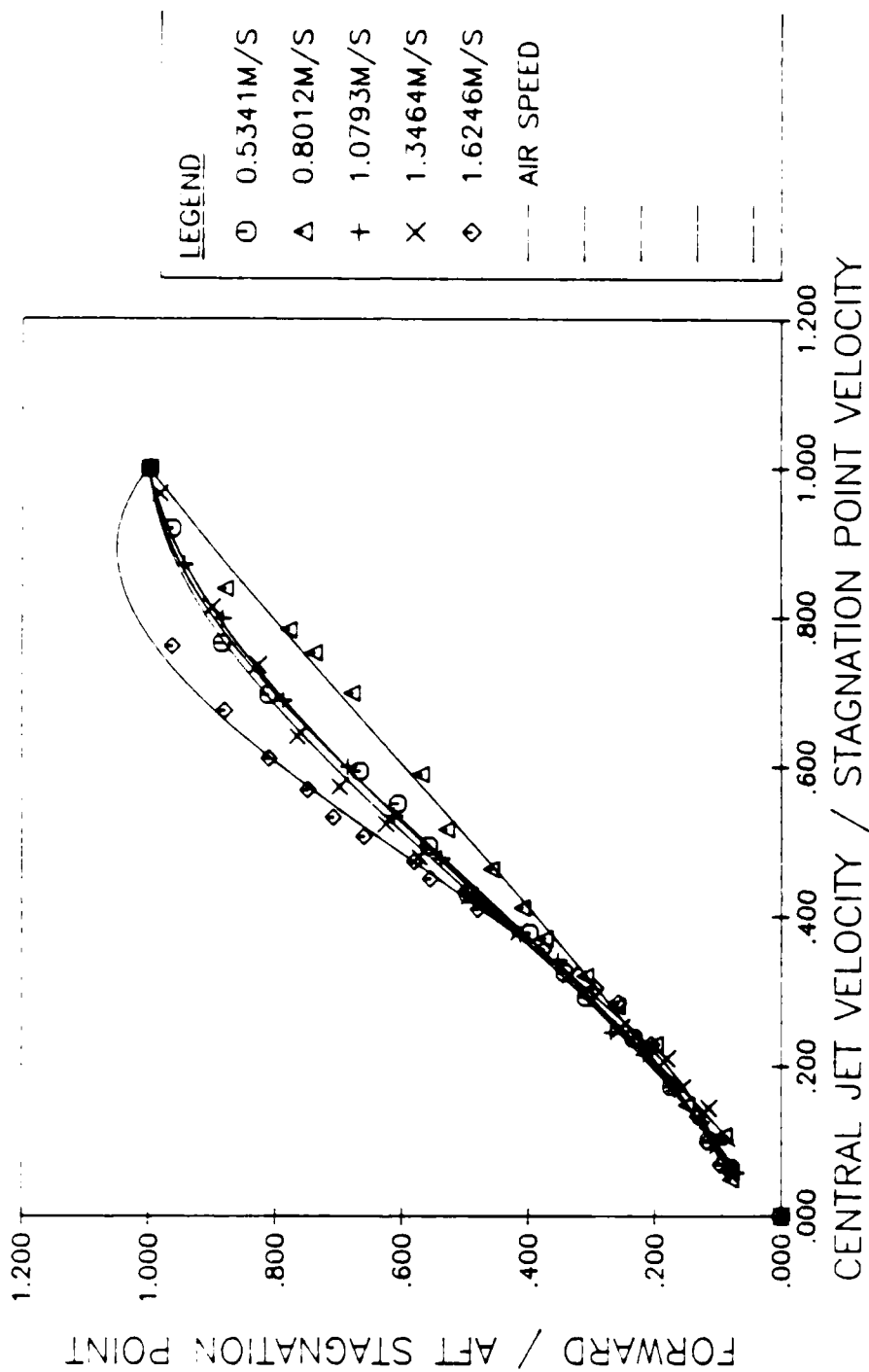
LEAST SQUARE ERROR NORM: E = .59244E-01

THE SOLUTION WAS FOUND AFTER 2 ITERATIONS

PLOT OF THE NONDIMENSIONALIZED DATA SET 5



PLOT OF THE NONDIMENSIONALIZED DATA SET 5



II: Output from Harris 800

ACCIDENT REPORT OF THE BUREAU OF THE AIR FORCE, WASHINGTON, D.C.  
NUMBER OF DATA SHEETS: 1

1. Name of the person or persons involved in the accident:  
2. Name of the person or persons who reported the accident:  
3. Name of the person or persons who investigated the accident:  
4. Name of the person or persons who approved the report:

5. Name of the person or persons who reviewed the report:  
6. Name of the person or persons who approved the report:

7. Name of the person or persons who reviewed the report:  
8. Name of the person or persons who approved the report:

9. Name of the person or persons who reviewed the report:  
10. Name of the person or persons who approved the report:

11. Name of the person or persons who reviewed the report:  
12. Name of the person or persons who approved the report:

13. Name of the person or persons who reviewed the report:  
14. Name of the person or persons who approved the report:

15. Name of the person or persons who reviewed the report:  
16. Name of the person or persons who approved the report:

104.1	0.5641
100.1	0.9140
11.9	1.263
3.7	1.117
150.7	1.100
110.5	1.200
400.7	1.100
400.0	4.000
100.1	1.130
100.0	1.000
100.0	1.121

100.0 0.5641 0.9140 1.263 1.117 1.100 1.200 1.100 4.000 1.130 1.000 1.121

100.0	0.5641
100.0	0.9140
100.0	1.263
100.0	1.117
100.0	1.100
100.0	1.200
100.0	1.100
100.0	4.000
100.0	1.130
100.0	1.000
100.0	1.121

100.0 0.5641 0.9140 1.263 1.117 1.100 1.200 1.100 4.000 1.130 1.000 1.121

100.0	0.5641
100.0	0.9140
100.0	1.263
100.0	1.117
100.0	1.100
100.0	1.200
100.0	1.100
100.0	4.000
100.0	1.130
100.0	1.000
100.0	1.121

100.0 0.5641 0.9140 1.263 1.117 1.100 1.200 1.100 4.000 1.130 1.000 1.121

100.0	0.5641
100.0	0.9140
100.0	1.263
100.0	1.117
100.0	1.100
100.0	1.200
100.0	1.100
100.0	4.000
100.0	1.130
100.0	1.000
100.0	1.121

100.0 0.5641 0.9140 1.263 1.117 1.100 1.200 1.100 4.000 1.130 1.000 1.121

NUMBER OF MEASUREMENT POINTS :

9

CURF TELLOJ

164.9	0.5200
219.2	0.6880
357.5	0.9150
481.1	1.200
549.2	1.375
667.1	1.60
775.4	1.744
883.8	1.960
979.3	2.000

REYNOLDS NO. FOR AIR FLOW 1455.4

DIAMETER OF ORIFICE (IN) : 0.50000

NUMBER OF MEASUREMENT POINTS : 9

CURF TELLOJ

164.9	0.5200
219.2	0.6880
357.5	0.9150
481.1	1.200
549.2	1.375
667.1	1.60
775.4	1.744
883.8	1.960
979.3	2.000

PRESENT RESULTS OF TEST III FOR COLD REACTING FLOW :

NUMBER OF DATA SETS : 3

FLOW NO. FOR AIR FLOW : 930.45  
 DIAMETER OF CENTRAL LET - IN : 0.50000  
 NUMBER OF MEASUREMENT POINTS : 10  
 DATA SETS :

1.14	0.1200
1.15	0.1220
1.16	0.1240
1.17	0.1260
1.18	0.1280
1.19	0.1300
1.20	0.1320
1.21	0.1340
1.22	0.1360
1.23	0.1380

FLOW NO. FOR AIR FLOW : 931.7  
 DIAMETER OF CENTRAL LET - IN : 0.50000  
 NUMBER OF MEASUREMENT POINTS : 11  
 DATA SETS :

1.14	0.1200
1.15	0.1220
1.16	0.1240
1.17	0.1260
1.18	0.1280
1.19	0.1300
1.20	0.1320
1.21	0.1340
1.22	0.1360
1.23	0.1380
1.24	0.1400

FLOW NO. FOR AIR FLOW : 932.0  
 DIAMETER OF CENTRAL LET - IN : 0.50000  
 NUMBER OF MEASUREMENT POINTS : 11  
 DATA SETS :

1.14	0.1200
1.15	0.1220
1.16	0.1240
1.17	0.1260
1.18	0.1280
1.19	0.1300
1.20	0.1320
1.21	0.1340
1.22	0.1360
1.23	0.1380
1.24	0.1400



# CONSISTING FLOW FOR TEST II

NUMBER OF DATA SETS 19

## TABLE OF VALUES FOR EXPERIMENTAL DATA SET 1 \*\*\*\*\*

APPROXIMATE NOZZLE 1.1138 CM\*\*2  
 APPROXIMATE NOZZLE 1.1137 CM\*\*2  
 DENSITY OF AIR 1.2165 G/CC  
 NUMBER OF MEASUREMENT POINTS 5

POINT NUMBER	HEIGHT OF CENTRAL JET CM**1	HEIGHT OF LEFT VORTEX CM**1	HEIGHT OF RIGHT VORTEX CM**1
1	11.0513	7.3660	7.4930
2	11.3220	7.3660	7.4930
3	12.0014	7.4168	8.0010
4	12.112	7.4930	8.0010
5	13.0010	7.3710	7.8740
6	13.3230	7.6200	7.7724

APPROXIMATE FLOW IS GIVEN BY \*\*\*

## TABLE OF VALUES FOR EXPERIMENTAL DATA SET 2 \*\*\*\*\*

APPROXIMATE NOZZLE 1.1138 CM\*\*2  
 APPROXIMATE NOZZLE 1.1137 CM\*\*2  
 DENSITY OF AIR 1.2165 G/CC  
 NUMBER OF MEASUREMENT POINTS 5

POINT NUMBER	HEIGHT OF CENTRAL JET CM**1	HEIGHT OF LEFT VORTEX CM**1	HEIGHT OF RIGHT VORTEX CM**1
1	11.0513	7.3660	7.4930
2	11.3220	7.3660	7.4930
3	12.0014	7.4168	7.8740
4	12.112	7.4930	7.7470
5	13.0010	7.3660	7.8500
6	13.3230	7.6200	8.0010
7	13.6460	7.8740	8.3900
8	13.9690	7.6200	8.0244

APPROXIMATE FLOW IS GIVEN BY \*\*\*

TABLE OF VALUES FOR EXPERIMENTAL DATA SET 3  
 \*\*\*\*\*

AREA OF OUTER NOZZLE 6.1438 CM\*\*2  
 AREA OF INNER NOZZLE 0.1167 CM\*\*2  
 VELOCITY OF AIR 1.0018 M/SEC  
 NUMBER OF MEASUREMENT POINTS 7

MEASUREMENT POINT	HEIGHT OF CENTRAL JET [ mm ]	HEIGHT OF LEFT VORTEX [ mm ]	HEIGHT OF RIGHT VORTEX [ mm ]
1	0.1030	0.0000	0.0000
2	11.0000	0.0000	0.0000
3	13.0110	0.0000	0.0000
4	14.0710	0.0000	0.0000
5	15.0810	0.0000	0.0000
6	16.1310	0.0000	0.0000
7	17.1410	0.0000	0.0000

THE PENETRATION POINT IS ASSIGNED BY \*

TABLE OF VALUES FOR EXPERIMENTAL DATA SET 4  
 \*\*\*\*\*

AREA OF OUTER NOZZLE 6.1438 CM\*\*2  
 AREA OF INNER NOZZLE 0.1167 CM\*\*2  
 VELOCITY OF AIR 1.0018 M/SEC  
 NUMBER OF MEASUREMENT POINTS 8

MEASUREMENT POINT	HEIGHT OF CENTRAL JET [ mm ]	HEIGHT OF LEFT VORTEX [ mm ]	HEIGHT OF RIGHT VORTEX [ mm ]
1	0.1030	0.0000	0.0000
2	11.0250	0.0000	0.0000
3	13.1310	10.4140	9.3900
4	14.6370	10.9000	9.7920
5	16.1100	15.2000	14.2560
6	17.6440	15.2100	20.9550
7	19.1190	14.4110	14.6050
8	20.6100	13.7110	15.2400

THE PENETRATION POINT IS ASSIGNED BY \*

TABLE OF VALUES FOR EXPERIMENTAL DATA SET 5  
 \*\*\*\*\*

MEAN OF INPUT NOISES 0.1638 \*\*\*\*\*  
 STD OF INPUT NOISES 0.3167 \*\*\*\*\*  
 MEAN OF INPUT NOISES 0.1638 \*\*\*\*\*  
 STD OF INPUT NOISES 0.3167 \*\*\*\*\*

HEIGHT OF LEFT VERTX [MM]	HEIGHT OF RIGHT VERTX [MM]	HEIGHT OF LEFT VERTX [MM]	HEIGHT OF RIGHT VERTX [MM]
0.0000	0.0000	0.0000	0.0000
0.0000	0.0000	0.0000	0.0000
0.0000	0.0000	0.0000	0.0000
0.0000	0.0000	0.0000	0.0000
0.0000	0.0000	0.0000	0.0000
0.0000	0.0000	0.0000	0.0000
0.0000	0.0000	0.0000	0.0000
0.0000	0.0000	0.0000	0.0000
0.0000	0.0000	0.0000	0.0000
0.0000	0.0000	0.0000	0.0000

THESE VALUES ARE NOT CORRECTED BY \*\*\*

TABLE OF VALUES FOR EXPERIMENTAL DATA SET 5  
 \*\*\*\*\*

MEAN OF INPUT NOISES 0.1638 \*\*\*\*\*  
 STD OF INPUT NOISES 0.3167 \*\*\*\*\*  
 MEAN OF INPUT NOISES 0.1638 \*\*\*\*\*  
 STD OF INPUT NOISES 0.3167 \*\*\*\*\*

HEIGHT OF LEFT VERTX [MM]	HEIGHT OF RIGHT VERTX [MM]	HEIGHT OF LEFT VERTX [MM]	HEIGHT OF RIGHT VERTX [MM]
0.0000	0.0000	0.0000	0.0000
0.0000	0.0000	0.0000	0.0000
0.0000	0.0000	0.0000	0.0000
0.0000	0.0000	0.0000	0.0000
0.0000	0.0000	0.0000	0.0000
0.0000	0.0000	0.0000	0.0000
0.0000	0.0000	0.0000	0.0000
0.0000	0.0000	0.0000	0.0000
0.0000	0.0000	0.0000	0.0000
0.0000	0.0000	0.0000	0.0000

THESE VALUES ARE NOT CORRECTED BY \*\*\*

TABLE OF VALUES FOR EXPERIMENTAL DATA SET 7  
 \*\*\*\*\*

NUMBER OF DATA POINTS 61118 CM\*\*2  
 AREA OF CHANNEL CROSS-SECTION 61012 CM\*\*2  
 AREA OF CHANNEL CROSS-SECTION 61012 CM\*\*2  
 AREA OF CHANNEL CROSS-SECTION 61012 CM\*\*2

DEPTH	VELOCITY	HEIGHT OF LEFT WORTLEY	HEIGHT OF RIGHT WORTLEY
0.000	0.000	0.000	0.000
0.000	0.000	0.000	0.000
0.000	0.000	0.000	0.000
0.000	0.000	0.000	0.000
0.000	0.000	0.000	0.000
0.000	0.000	0.000	0.000
0.000	0.000	0.000	0.000
0.000	0.000	0.000	0.000
0.000	0.000	0.000	0.000
0.000	0.000	0.000	0.000

WATER SURFACE ELEVATION IS 10.000 BY 10.000

TABLE OF VALUES FOR EXPERIMENTAL DATA SET 8  
 \*\*\*\*\*

NUMBER OF DATA POINTS 61118 CM\*\*2  
 AREA OF CHANNEL CROSS-SECTION 61012 CM\*\*2  
 AREA OF CHANNEL CROSS-SECTION 61012 CM\*\*2  
 AREA OF CHANNEL CROSS-SECTION 61012 CM\*\*2

DEPTH	VELOCITY	HEIGHT OF LEFT WORTLEY	HEIGHT OF RIGHT WORTLEY
0.000	0.000	0.000	0.000
0.000	0.000	0.000	0.000
0.000	0.000	0.000	0.000
0.000	0.000	0.000	0.000
0.000	0.000	0.000	0.000
0.000	0.000	0.000	0.000
0.000	0.000	0.000	0.000
0.000	0.000	0.000	0.000
0.000	0.000	0.000	0.000
0.000	0.000	0.000	0.000

WATER SURFACE ELEVATION IS 10.000 BY 10.000

◆ 歡迎各界人士踴躍投稿 ◆

[illegible]

1. The first part of the document  
 2. The second part of the document  
 3. The third part of the document  
 4. The fourth part of the document  
 5. The fifth part of the document

The following table shows the results of the experiment. The first column shows the time taken for each trial. The second column shows the distance traveled. The third column shows the average speed. The fourth column shows the standard deviation. The fifth column shows the coefficient of variation. The sixth column shows the correlation coefficient. The seventh column shows the p-value. The eighth column shows the confidence interval. The ninth column shows the power of the test. The tenth column shows the effect size. The eleventh column shows the significance level. The twelfth column shows the type of test used. The thirteenth column shows the number of trials. The fourteenth column shows the number of subjects. The fifteenth column shows the number of groups. The sixteenth column shows the number of variables. The seventeenth column shows the number of factors. The eighteenth column shows the number of levels. The nineteenth column shows the number of conditions. The twentieth column shows the number of treatments. The twenty-first column shows the number of controls. The twenty-second column shows the number of comparisons. The twenty-third column shows the number of interactions. The twenty-fourth column shows the number of main effects. The twenty-fifth column shows the number of secondary effects. The twenty-sixth column shows the number of tertiary effects. The twenty-seventh column shows the number of quaternary effects. The twenty-eighth column shows the number of quinary effects. The twenty-ninth column shows the number of senary effects. The thirtieth column shows the number of septenary effects. The thirty-first column shows the number of octenary effects. The thirty-second column shows the number of nonary effects. The thirty-third column shows the number of decenary effects. The thirty-fourth column shows the number of undecenary effects. The thirty-fifth column shows the number of duodecenary effects. The thirty-sixth column shows the number of tredecenary effects. The thirty-seventh column shows the number of quattuordecenary effects. The thirty-eighth column shows the number of quindecenary effects. The thirty-ninth column shows the number of sexdecenary effects. The fortieth column shows the number of septendecenary effects. The forty-first column shows the number of octodecenary effects. The forty-second column shows the number of nonadecenary effects. The forty-third column shows the number of vigintenary effects. The forty-fourth column shows the number of unvigintenary effects. The forty-fifth column shows the number of duovigintenary effects. The forty-sixth column shows the number of duodevigintenary effects. The forty-seventh column shows the number of tredevigintenary effects. The forty-eighth column shows the number of quattuorvigintenary effects. The forty-ninth column shows the number of quinvigintenary effects. The fiftieth column shows the number of sexvigintenary effects. The fifty-first column shows the number of septenvigintenary effects. The fifty-second column shows the number of octovigintenary effects. The fifty-third column shows the number of nonavigintenary effects. The fifty-fourth column shows the number of vigintivigintenary effects. The fifty-fifth column shows the number of untrigintenary effects. The fifty-sixth column shows the number of duotrigintenary effects. The fifty-seventh column shows the number of duodecigintenary effects. The fifty-eighth column shows the number of tredecigintenary effects. The fifty-ninth column shows the number of quattuordecigintenary effects. The sixtieth column shows the number of quinvigintenary effects. The sixty-first column shows the number of sexdecigintenary effects. The sixty-second column shows the number of septendecigintenary effects. The sixty-third column shows the number of octodecigintenary effects. The sixty-fourth column shows the number of nonadecigintenary effects. The sixty-fifth column shows the number of vigintigintenary effects. The sixty-sixth column shows the number of untrigintigintenary effects. The sixty-seventh column shows the number of duotrigintigintenary effects. The sixty-eighth column shows the number of duodecigintigintenary effects. The sixty-ninth column shows the number of tredecigintigintenary effects. The seventieth column shows the number of quattuordecigintigintenary effects. The seventy-first column shows the number of quinvigintigintenary effects. The seventy-second column shows the number of sexdecigintigintenary effects. The seventy-third column shows the number of septendecigintigintenary effects. The seventy-fourth column shows the number of octodecigintigintenary effects. The seventy-fifth column shows the number of nonadecigintigintenary effects. The seventy-sixth column shows the number of vigintigintigintenary effects. The seventy-seventh column shows the number of untrigintigintigintenary effects. The seventy-eighth column shows the number of duotrigintigintigintenary effects. The seventy-ninth column shows the number of duodecigintigintigintenary effects. The eightieth column shows the number of tredecigintigintigintenary effects. The eighty-first column shows the number of quattuordecigintigintigintenary effects. The eighty-second column shows the number of quinvigintigintigintenary effects. The eighty-third column shows the number of sexdecigintigintigintenary effects. The eighty-fourth column shows the number of septendecigintigintigintenary effects. The eighty-fifth column shows the number of octodecigintigintigintenary effects. The eighty-sixth column shows the number of nonadecigintigintigintenary effects. The eighty-seventh column shows the number of vigintigintigintigintenary effects. The eighty-eighth column shows the number of untrigintigintigintigintenary effects. The eighty-ninth column shows the number of duotrigintigintigintigintenary effects. The ninetieth column shows the number of duodecigintigintigintigintenary effects. The ninety-first column shows the number of tredecigintigintigintigintenary effects. The ninety-second column shows the number of quattuordecigintigintigintigintenary effects. The ninety-third column shows the number of quinvigintigintigintigintenary effects. The ninety-fourth column shows the number of sexdecigintigintigintigintenary effects. The ninety-fifth column shows the number of septendecigintigintigintigintenary effects. The ninety-sixth column shows the number of octodecigintigintigintigintenary effects. The ninety-seventh column shows the number of nonadecigintigintigintigintenary effects. The ninety-eighth column shows the number of vigintigintigintigintigintenary effects. The ninety-ninth column shows the number of untrigintigintigintigintigintenary effects. The hundredth column shows the number of duotrigintigintigintigintigintenary effects.

The following table shows the results of the experiment.

.....

The following table shows the results of the experiment.

The following table shows the results of the experiment.

The following table shows the results of the experiment.

.....

1. The first part of the document is a list of the names of the persons who were present at the meeting. The names are listed in alphabetical order.

Name	Address	City	State	Zip
Mr. J. H. Smith	1234 Main St.	Springfield	Ill.	62761
Mr. W. R. Jones	5678 Oak Ave.	Chicago	Ill.	60644
Mr. T. L. Brown	9012 Elm St.	Peoria	Ill.	61604
Mr. S. K. White	3456 Maple Dr.	Rockford	Ill.	61101
Mr. M. N. Black	7890 Cedar Ln.	Decatur	Ill.	62521
Mr. P. Q. Green	2345 Birch St.	Normal	Ill.	62450
Mr. R. S. Hall	6789 Pine Ave.	Urbana	Ill.	61502
Mr. V. T. King	10110 Spruce Rd.	Champaign	Ill.	61820
Mr. Y. U. Lee	4321 Ash St.	Carbondale	Ill.	62901
Mr. Z. V. Walker	8765 Willow Dr.	Macomb	Ill.	61455

\*\*\*\*\*

The second part of the document is a list of the names of the persons who were present at the meeting. The names are listed in alphabetical order.

Name	Address	City	State	Zip
Mr. A. B. Baker	11111 Main St.	Springfield	Ill.	62761
Mr. C. D. Carter	22222 Oak Ave.	Chicago	Ill.	60644
Mr. E. F. Evans	33333 Elm St.	Peoria	Ill.	61604
Mr. G. H. Green	44444 Maple Dr.	Rockford	Ill.	61101
Mr. I. J. Jackson	55555 Cedar Ln.	Decatur	Ill.	62521
Mr. K. L. King	66666 Birch St.	Normal	Ill.	62450
Mr. M. N. Lee	77777 Pine Ave.	Urbana	Ill.	61502
Mr. O. P. Olson	88888 Spruce Rd.	Champaign	Ill.	61820
Mr. Q. R. Quinn	99999 Ash St.	Carbondale	Ill.	62901
Mr. S. T. Smith	10101 Willow Dr.	Macomb	Ill.	61455

\*\*\*\*\*

\*\*\*\*\*

.....

.....

.....

.....

.....

.....

.....



the 1990s, the number of people in the world who are under 15 years of age is expected to increase from 1.1 billion to 1.5 billion. The number of people aged 65 and over is expected to increase from 200 million to 400 million. The number of people aged 15 and over is expected to increase from 3.5 billion to 4.5 billion. The number of people aged 15 and over is expected to increase from 3.5 billion to 4.5 billion. The number of people aged 15 and over is expected to increase from 3.5 billion to 4.5 billion.

.....

34.205

**Abstract**

\_\_\_\_\_

.....

.....

.....

.....

.....

.....

.....

.....

.....

1957	1958	1959	1960
1961	1962	1963	1964
1965	1966	1967	1968
1969	1970	1971	1972
1973	1974	1975	1976
1977	1978	1979	1980
1981	1982	1983	1984
1985	1986	1987	1988
1989	1990	1991	1992
1993	1994	1995	1996
1997	1998	1999	2000
2001	2002	2003	2004
2005	2006	2007	2008
2009	2010	2011	2012
2013	2014	2015	2016
2017	2018	2019	2020
2021	2022	2023	2024
2025	2026	2027	2028
2029	2030	2031	2032
2033	2034	2035	2036
2037	2038	2039	2040
2041	2042	2043	2044
2045	2046	2047	2048
2049	2050	2051	2052
2053	2054	2055	2056
2057	2058	2059	2060
2061	2062	2063	2064
2065	2066	2067	2068
2069	2070	2071	2072
2073	2074	2075	2076
2077	2078	2079	2080
2081	2082	2083	2084
2085	2086	2087	2088
2089	2090	2091	2092
2093	2094	2095	2096
2097	2098	2099	2100

.....

1957	1958	1959	1960
1961	1962	1963	1964
1965	1966	1967	1968
1969	1970	1971	1972
1973	1974	1975	1976
1977	1978	1979	1980
1981	1982	1983	1984
1985	1986	1987	1988
1989	1990	1991	1992
1993	1994	1995	1996
1997	1998	1999	2000
2001	2002	2003	2004
2005	2006	2007	2008
2009	2010	2011	2012
2013	2014	2015	2016
2017	2018	2019	2020
2021	2022	2023	2024
2025	2026	2027	2028
2029	2030	2031	2032
2033	2034	2035	2036
2037	2038	2039	2040
2041	2042	2043	2044
2045	2046	2047	2048
2049	2050	2051	2052
2053	2054	2055	2056
2057	2058	2059	2060
2061	2062	2063	2064
2065	2066	2067	2068
2069	2070	2071	2072
2073	2074	2075	2076
2077	2078	2079	2080
2081	2082	2083	2084
2085	2086	2087	2088
2089	2090	2091	2092
2093	2094	2095	2096
2097	2098	2099	2100

.....

1957	1958	1959	1960
1961	1962	1963	1964
1965	1966	1967	1968
1969	1970	1971	1972
1973	1974	1975	1976
1977	1978	1979	1980
1981	1982	1983	1984
1985	1986	1987	1988
1989	1990	1991	1992
1993	1994	1995	1996
1997	1998	1999	2000
2001	2002	2003	2004
2005	2006	2007	2008
2009	2010	2011	2012
2013	2014	2015	2016
2017	2018	2019	2020
2021	2022	2023	2024
2025	2026	2027	2028
2029	2030	2031	2032
2033	2034	2035	2036
2037	2038	2039	2040
2041	2042	2043	2044
2045	2046	2047	2048
2049	2050	2051	2052
2053	2054	2055	2056
2057	2058	2059	2060
2061	2062	2063	2064
2065	2066	2067	2068
2069	2070	2071	2072
2073	2074	2075	2076
2077	2078	2079	2080
2081	2082	2083	2084
2085	2086	2087	2088
2089	2090	2091	2092
2093	2094	2095	2096
2097	2098	2099	2100

100

1. 2. 3. 4. 5. 6. 7. 8. 9. 10. 11. 12. 13. 14. 15. 16. 17. 18. 19. 20. 21. 22. 23. 24. 25. 26. 27. 28. 29. 30. 31. 32. 33. 34. 35. 36. 37. 38. 39. 40. 41. 42. 43. 44. 45. 46. 47. 48. 49. 50. 51. 52. 53. 54. 55. 56. 57. 58. 59. 60. 61. 62. 63. 64. 65. 66. 67. 68. 69. 70. 71. 72. 73. 74. 75. 76. 77. 78. 79. 80. 81. 82. 83. 84. 85. 86. 87. 88. 89. 90. 91. 92. 93. 94. 95. 96. 97. 98. 99. 100. 101. 102. 103. 104. 105. 106. 107. 108. 109. 110. 111. 112. 113. 114. 115. 116. 117. 118. 119. 120. 121. 122. 123. 124. 125. 126. 127. 128. 129. 130. 131. 132. 133. 134. 135. 136. 137. 138. 139. 140. 141. 142. 143. 144. 145. 146. 147. 148. 149. 150. 151. 152. 153. 154. 155. 156. 157. 158. 159. 160. 161. 162. 163. 164. 165. 166. 167. 168. 169. 170. 171. 172. 173. 174. 175. 176. 177. 178. 179. 180. 181. 182. 183. 184. 185. 186. 187. 188. 189. 190. 191. 192. 193. 194. 195. 196. 197. 198. 199. 200. 201. 202. 203. 204. 205. 206. 207. 208. 209. 210. 211. 212. 213. 214. 215. 216. 217. 218. 219. 220. 221. 222. 223. 224. 225. 226. 227. 228. 229. 230. 231. 232. 233. 234. 235. 236. 237. 238. 239. 240. 241. 242. 243. 244. 245. 246. 247. 248. 249. 250. 251. 252. 253. 254. 255. 256. 257. 258. 259. 260. 261. 262. 263. 264. 265. 266. 267. 268. 269. 270. 271. 272. 273. 274. 275. 276. 277. 278. 279. 280. 281. 282. 283. 284. 285. 286. 287. 288. 289. 290. 291. 292. 293. 294. 295. 296. 297. 298. 299. 300. 301. 302. 303. 304. 305. 306. 307. 308. 309. 310. 311. 312. 313. 314. 315. 316. 317. 318. 319. 320. 321. 322. 323. 324. 325. 326. 327. 328. 329. 330. 331. 332. 333. 334. 335. 336. 337. 338. 339. 340. 341. 342. 343. 344. 345. 346. 347. 348. 349. 350. 351. 352. 353. 354. 355. 356. 357. 358. 359. 360. 361. 362. 363. 364. 365. 366. 367. 368. 369. 370. 371. 372. 373. 374. 375. 376. 377. 378. 379. 380. 381. 382. 383. 384. 385. 386. 387. 388. 389. 390. 391. 392. 393. 394. 395. 396. 397. 398. 399. 400. 401. 402. 403. 404. 405. 406. 407. 408. 409. 410. 411. 412. 413. 414. 415. 416. 417. 418. 419. 420. 421. 422. 423. 424. 425. 426. 427. 428. 429. 430. 431. 432. 433. 434. 435. 436. 437. 438. 439. 440. 441. 442. 443. 444. 445. 446. 447. 448. 449. 450. 451. 452. 453. 454. 455. 456. 457. 458. 459. 460. 461. 462. 463. 464. 465. 466. 467. 468. 469. 470. 471. 472. 473. 474. 475. 476. 477. 478. 479. 480. 481. 482. 483. 484. 485. 486. 487. 488. 489. 490. 491. 492. 493. 494. 495. 496. 497. 498. 499. 500. 501. 502. 503. 504. 505. 506. 507. 508. 509. 510. 511. 512. 513. 514. 515. 516. 517. 518. 519. 520. 521. 522. 523. 524. 525. 526. 527. 528. 529. 530. 531. 532. 533. 534. 535. 536. 537. 538. 539. 540. 541. 542. 543. 544. 545. 546. 547. 548. 549. 550. 551. 552. 553. 554. 555. 556. 557. 558. 559. 560. 561. 562. 563. 564. 565. 566. 567. 568. 569. 570. 571. 572. 573. 574. 575. 576. 577. 578. 579. 580. 581. 582. 583. 584. 585. 586. 587. 588. 589. 590. 591. 592. 593. 594. 595. 596. 597. 598. 599. 600. 601. 602. 603. 604. 605. 606. 607. 608. 609. 610. 611. 612. 613. 614. 615. 616. 617. 618. 619. 620. 621. 622. 623. 624. 625. 626. 627. 628. 629. 630. 631. 632. 633. 634. 635. 636. 637. 638. 639. 640. 641. 642. 643. 644. 645. 646. 647. 648. 649. 650. 651. 652. 653. 654. 655. 656. 657. 658. 659. 660. 661. 662. 663. 664. 665. 666. 667. 668. 669. 670. 671. 672. 673. 674. 675. 676. 677. 678. 679. 680. 681. 682. 683. 684. 685. 686. 687. 688. 689. 690. 691. 692. 693. 694. 695. 696. 697. 698. 699. 700. 701. 702. 703. 704. 705. 706. 707. 708. 709. 710. 711. 712. 713. 714. 715. 716. 717. 718. 719. 720. 721. 722. 723. 724. 725. 726. 727. 728. 729. 730. 731. 732. 733. 734. 735. 736. 737. 738. 739. 740. 741. 742. 743. 744. 745. 746. 747. 748. 749. 750. 751. 752. 753. 754. 755. 756. 757. 758. 759. 760. 761. 762. 763. 764. 765. 766. 767. 768. 769. 770. 771. 772. 773. 774. 775. 776. 777. 778. 779. 780. 781. 782. 783. 784. 785. 786. 787. 788. 789. 790. 791. 792. 793. 794. 795. 796. 797. 798. 799. 800. 801. 802. 803. 804. 805. 806. 807. 808. 809. 810. 811. 812. 813. 814. 815. 816. 817. 818. 819. 820. 821. 822. 823. 824. 825. 826. 827. 828. 829. 830. 831. 832. 833. 834. 835. 836. 837. 838. 839. 840.

[illegible]

0.0000  
0.0000  
0.0000

[illegible]

Figure 1. A schematic diagram of the experimental setup. The subject is seated in a chair, viewing a video screen. The screen displays a target (a small circle) and a starting point (a small circle). The subject's hand is positioned at the starting point. The distance between the starting point and the target is 10 cm. The subject is instructed to move their hand from the starting point to the target. The video screen is positioned 40 cm from the subject's hand. The subject's hand is positioned at the starting point. The distance between the starting point and the target is 10 cm. The subject is instructed to move their hand from the starting point to the target. The video screen is positioned 40 cm from the subject's hand.

the 1990s, the number of people in the world who are illiterate has increased from 1.2 billion to 1.5 billion. The number of illiterate people in the world is expected to reach 1.7 billion by the year 2015. The number of illiterate people in the world is expected to reach 1.7 billion by the year 2015. The number of illiterate people in the world is expected to reach 1.7 billion by the year 2015.

Appendix E: All the Experimental Data for Figure 7  
(Including the results of this study,  
Tankin (Ref. 27) and Namazian (Ref. 7))

TELETYPE UNIT - 1000

UNIT - 1000

UNIT - 1000

UNIT - 1000

UNIT - 1000

UNIT - 1000

UNIT - 1000

UNIT - 1000

1. 14.  
2. 1.  
3. 1.  
4. 1.  
5. 1.  
6. 1.  
7. 1.  
8. 1.  
9. 1.  
10. 1.

1. 14.  
2. 1.  
3. 1.  
4. 1.  
5. 1.  
6. 1.  
7. 1.  
8. 1.  
9. 1.  
10. 1.

1. 14.  
2. 1.  
3. 1.  
4. 1.  
5. 1.  
6. 1.  
7. 1.  
8. 1.  
9. 1.  
10. 1.

1. 14.  
2. 1.  
3. 1.  
4. 1.  
5. 1.  
6. 1.  
7. 1.  
8. 1.  
9. 1.  
10. 1.

1. 14.  
2. 1.  
3. 1.  
4. 1.  
5. 1.  
6. 1.  
7. 1.  
8. 1.  
9. 1.  
10. 1.

1. 14.  
2. 1.  
3. 1.  
4. 1.  
5. 1.  
6. 1.  
7. 1.  
8. 1.  
9. 1.  
10. 1.

1. 14.  
2. 1.  
3. 1.  
4. 1.  
5. 1.  
6. 1.  
7. 1.  
8. 1.  
9. 1.  
10. 1.

1. 14.  
2. 1.  
3. 1.  
4. 1.  
5. 1.  
6. 1.  
7. 1.  
8. 1.  
9. 1.  
10. 1.

|       |       |
|-------|-------|
| 534.0 | 1206. |
| 713.6 | 1501. |
| 992.0 | 1560. |
| 1041. | 1560. |
| 1144. | 1562. |
| 1145. | 1562. |

[illegible][illegible][illegible][illegible][illegible]

|   | 1 | 2 | 3 | 4 | 5 | 6 | 7 | 8 | 9 | 10 | 11 | 12 | 13 | 14 | 15 | 16 | 17 | 18 | 19 | 20 | 21 | 22 | 23 | 24 | 25 | 26 | 27 | 28 | 29 | 30 | 31 | 32 | 33 | 34 | 35 | 36 | 37 | 38 | 39 | 40 | 41 | 42 | 43 | 44 | 45 | 46 | 47 | 48 | 49 | 50 | 51 | 52 | 53 | 54 | 55 | 56 | 57 | 58 | 59 | 60 | 61 | 62 | 63 | 64 | 65 | 66 | 67 | 68 | 69 | 70 | 71 | 72 | 73 | 74 | 75 | 76 | 77 | 78 | 79 | 80 | 81 | 82 | 83 | 84 | 85 | 86 | 87 | 88 | 89 | 90 | 91 | 92 | 93 | 94 | 95 | 96 | 97 | 98 | 99 | 100 |
|---|---|---|---|---|---|---|---|---|---|----|----|----|----|----|----|----|----|----|----|----|----|----|----|----|----|----|----|----|----|----|----|----|----|----|----|----|----|----|----|----|----|----|----|----|----|----|----|----|----|----|----|----|----|----|----|----|----|----|----|----|----|----|----|----|----|----|----|----|----|----|----|----|----|----|----|----|----|----|----|----|----|----|----|----|----|----|----|----|----|----|----|----|----|----|----|----|----|----|----|-----|
| 1 | 1 | 2 | 3 | 4 | 5 | 6 | 7 | 8 | 9 | 10 | 11 | 12 | 13 | 14 | 15 | 16 | 17 | 18 | 19 | 20 | 21 | 22 | 23 | 24 | 25 | 26 | 27 | 28 | 29 | 30 | 31 | 32 | 33 | 34 | 35 | 36 | 37 | 38 | 39 | 40 | 41 | 42 | 43 | 44 | 45 | 46 | 47 | 48 | 49 | 50 | 51 | 52 | 53 | 54 | 55 | 56 | 57 | 58 | 59 | 60 | 61 | 62 | 63 | 64 | 65 | 66 | 67 | 68 | 69 | 70 | 71 | 72 | 73 | 74 | 75 | 76 | 77 | 78 | 79 | 80 | 81 | 82 | 83 | 84 | 85 | 86 | 87 | 88 | 89 | 90 | 91 | 92 | 93 | 94 | 95 | 96 | 97 | 98 | 99 | 100 |
| 2 | 1 | 2 | 3 | 4 | 5 | 6 | 7 | 8 | 9 | 10 | 11 | 12 | 13 | 14 | 15 | 16 | 17 | 18 | 19 | 20 | 21 | 22 | 23 | 24 | 25 | 26 | 27 | 28 | 29 | 30 | 31 | 32 | 33 | 34 | 35 | 36 | 37 | 38 | 39 | 40 | 41 | 42 | 43 | 44 | 45 | 46 | 47 | 48 | 49 | 50 | 51 | 52 | 53 | 54 | 55 | 56 | 57 | 58 | 59 | 60 | 61 | 62 | 63 | 64 | 65 | 66 | 67 | 68 | 69 | 70 | 71 | 72 | 73 | 74 | 75 | 76 | 77 | 78 | 79 | 80 | 81 | 82 | 83 | 84 | 85 | 86 | 87 | 88 | 89 | 90 | 91 | 92 | 93 | 94 | 95 | 96 | 97 | 98 | 99 | 100 |
| 3 | 1 | 2 | 3 | 4 | 5 | 6 | 7 | 8 | 9 | 10 | 11 | 12 | 13 | 14 | 15 | 16 | 17 | 18 | 19 | 20 | 21 | 22 | 23 | 24 | 25 | 26 | 27 | 28 | 29 | 30 | 31 | 32 | 33 | 34 | 35 | 36 | 37 | 38 | 39 | 40 | 41 | 42 | 43 | 44 | 45 | 46 | 47 | 48 | 49 | 50 | 51 | 52 | 53 | 54 | 55 | 56 | 57 | 58 | 59 | 60 | 61 | 62 | 63 | 64 | 65 | 66 | 67 | 68 | 69 | 70 | 71 | 72 | 73 | 74 | 75 | 76 | 77 | 78 | 79 | 80 | 81 | 82 | 83 | 84 | 85 | 86 | 87 | 88 | 89 | 90 | 91 | 92 | 93 | 94 | 95 | 96 | 97 | 98 | 99 | 100 |
| 4 | 1 | 2 | 3 | 4 | 5 | 6 | 7 | 8 | 9 | 10 | 11 | 12 | 13 | 14 | 15 | 16 | 17 | 18 | 19 | 20 | 21 | 22 | 23 | 24 | 25 | 26 | 27 | 28 | 29 | 30 | 31 | 32 | 33 | 34 | 35 | 36 | 37 | 38 | 39 | 40 | 41 | 42 | 43 | 44 | 45 | 46 | 47 | 48 | 49 | 50 | 51 | 52 | 53 | 54 | 55 | 56 | 57 | 58 | 59 | 60 | 61 | 62 | 63 | 64 | 65 | 66 | 67 | 68 | 69 | 70 | 71 | 72 | 73 | 74 | 75 | 76 | 77 | 78 | 79 | 80 | 81 | 82 | 83 | 84 | 85 | 86 | 87 | 88 | 89 | 90 | 91 | 92 | 93 | 94 | 95 | 96 | 97 | 98 | 99 | 100 |
| 5 | 1 | 2 | 3 | 4 | 5 | 6 | 7 | 8 | 9 | 10 | 11 | 12 | 13 | 14 | 15 | 16 | 17 | 18 | 19 | 20 | 21 | 22 | 23 | 24 | 25 | 26 | 27 | 28 | 29 | 30 | 31 | 32 | 33 | 34 | 35 | 36 | 37 | 38 | 39 | 40 | 41 | 42 | 43 | 44 | 45 | 46 | 47 | 48 | 49 | 50 | 51 | 52 | 53 | 54 | 55 | 56 | 57 | 58 | 59 | 60 | 61 | 62 | 63 | 64 | 65 | 66 | 67 | 68 | 69 | 70 | 71 | 72 | 73 | 74 | 75 | 76 | 77 | 78 | 79 | 80 |    |    |    |    |    |    |    |    |    |    |    |    |    |    |    |    |    |    |    |     |

```

*****
DE-FAULT MASS FOR Y= FLOW      1495.0
PIKE IN OF CENTER SET (IN)    0.50000
NUMBER OF MEASUREMENT POINTS :   0
NAME       =L(0)+X*(D-DI)*1.5*DI/(D-DI)

```

|      |      |        |
|------|------|--------|
| 14.3 | 4.1  |        |
| 40.3 | 40.3 | 34.212 |



|       |       |
|-------|-------|
| 348.4 | 745.5 |
| 425.3 | 795.5 |
| 439.0 | 892.2 |
| 537.4 | 1014. |
| 555.2 | 1159. |
| 820.0 | 1303. |
| 1004. | 1512. |

PRESENT RESULTS OF TEST II :

NUMBER OF DATA SETS : 9

REYNOLDS NO. FOR AIR FLOW : 511.26  
 DIAMETER OF CENTRAL POST (IN) : 0.25000  
 NUMBER OF MEASUREMENT POINTS : 9  
 COEFFICIENT OF DISPERSSION :  $1.5 \times 10^{-1}$  (DO=01)  

|       |       |
|-------|-------|
| 145.0 | 144.1 |
| 140.0 | 142.4 |
| 132.0 | 139.0 |
| 119.0 | 117.0 |
| 100.0 | 111.0 |
| 87.0  | 121.0 |
| 69.0  | 140.2 |
| 50.0  | 140.0 |
| 42.0  | 139.0 |

REYNOLDS NO. FOR AIR FLOW : 940.4  
 DIAMETER OF CENTRAL POST (IN) : 0.25000  
 NUMBER OF MEASUREMENT POINTS : 12  
 COEFFICIENT OF DISPERSSION :  $1.5 \times 10^{-1}$  (DO=01)  

|       |       |
|-------|-------|
| 143.0 | 111.0 |
| 130.0 | 100.0 |
| 120.0 | 100.0 |
| 100.0 | 100.0 |
| 80.0  | 100.0 |
| 60.0  | 100.0 |
| 40.0  | 100.0 |
| 20.0  | 100.0 |
| 10.0  | 100.0 |
| 0.0   | 100.0 |
| 10.0  | 100.0 |
| 20.0  | 100.0 |
| 40.0  | 100.0 |
| 60.0  | 100.0 |
| 80.0  | 100.0 |
| 100.0 | 100.0 |
| 120.0 | 100.0 |
| 130.0 | 100.0 |
| 143.0 | 100.0 |

REYNOLDS NO. FOR AIR FLOW : 111.0  
 DIAMETER OF CENTRAL POST (IN) : 0.25000  
 NUMBER OF MEASUREMENT POINTS : 1  
 COEFFICIENT OF DISPERSSION :  $1.5 \times 10^{-1}$  (DO=01)  

|       |       |
|-------|-------|
| 145.0 | 144.1 |
| 140.0 | 142.4 |
| 132.0 | 139.0 |
| 119.0 | 117.0 |
| 100.0 | 111.0 |
| 87.0  | 121.0 |
| 69.0  | 140.2 |
| 50.0  | 140.0 |
| 42.0  | 139.0 |

REYNOLDS NO. FOR AIR FLOW : 511.26  
 DIAMETER OF CENTRAL POST (IN) : 0.25000  
 NUMBER OF MEASUREMENT POINTS : 11  
 COEFFICIENT OF DISPERSSION :  $1.5 \times 10^{-1}$  (DO=01)

|       |       |
|-------|-------|
| 104.0 | 150.4 |
| 150.4 | 259.7 |
| 259.7 | 358.9 |
| 358.9 | 431.2 |
| 431.2 | 539.0 |
| 539.0 | 625.3 |
| 625.3 | 730.0 |
| 730.0 | 831.0 |
| 831.0 | 1032. |
| 1032. | 1117. |
| 1117. | 1230. |

[illegible][illegible][illegible][illegible]

[illegible]

PRESENT RESULTS OF TEST 111 :

NUMBER OF DATA SETS : 7

PARAMETER FOR AIR FLOW : 1000  
Diameter of central jet : 1.0000  
Number of measurement points : 10  
NAME OF FILE : \*\*\*0101\*\*\*01-00-01

|       |       |
|-------|-------|
| 11.01 | 111.0 |
| 12.01 | 112.0 |
| 13.01 | 113.0 |
| 14.01 | 114.0 |
| 15.01 | 115.0 |
| 16.01 | 116.0 |
| 17.01 | 117.0 |
| 18.01 | 118.0 |
| 19.01 | 119.0 |
| 20.01 | 120.0 |

PARAMETER FOR AIR FLOW : 1000  
Diameter of central jet : 1.0000  
Number of measurement points : 10  
NAME OF FILE : \*\*\*0101\*\*\*01-00-01

|       |       |
|-------|-------|
| 11.01 | 111.0 |
| 12.01 | 112.0 |
| 13.01 | 113.0 |
| 14.01 | 114.0 |
| 15.01 | 115.0 |
| 16.01 | 116.0 |
| 17.01 | 117.0 |
| 18.01 | 118.0 |
| 19.01 | 119.0 |
| 20.01 | 120.0 |

PARAMETER FOR AIR FLOW : 1000  
Diameter of central jet : 1.0000  
Number of measurement points : 10  
NAME OF FILE : \*\*\*0101\*\*\*01-00-01

|       |       |
|-------|-------|
| 11.01 | 111.0 |
| 12.01 | 112.0 |
| 13.01 | 113.0 |
| 14.01 | 114.0 |
| 15.01 | 115.0 |
| 16.01 | 116.0 |
| 17.01 | 117.0 |
| 18.01 | 118.0 |
| 19.01 | 119.0 |
| 20.01 | 120.0 |

WHICH RESULTS REF. 271

NUMBER OF DATA POINTS 11

NUMBER OF AIR FLOW 1270  
NUMBER OF MEASUREMENT POINTS 11  
AND CLANK OF \*\*1211 00-01

|       |       |
|-------|-------|
| 120.0 | 121.0 |
| 110.0 | 111.0 |
| 100.0 | 101.0 |
| 90.0  | 91.0  |
| 80.0  | 81.0  |
| 70.0  | 71.0  |
| 60.0  | 61.0  |
| 50.0  | 51.0  |
| 40.0  | 41.0  |
| 30.0  | 31.0  |
| 20.0  | 21.0  |
| 10.0  | 11.0  |

NUMBER OF AIR FLOW 1270  
NUMBER OF MEASUREMENT POINTS 11  
AND CLANK OF \*\*1211 00-01

|       |       |
|-------|-------|
| 120.0 | 121.0 |
| 110.0 | 111.0 |
| 100.0 | 101.0 |
| 90.0  | 91.0  |
| 80.0  | 81.0  |
| 70.0  | 71.0  |
| 60.0  | 61.0  |
| 50.0  | 51.0  |
| 40.0  | 41.0  |
| 30.0  | 31.0  |
| 20.0  | 21.0  |
| 10.0  | 11.0  |

NUMBER OF AIR FLOW 1270  
NUMBER OF MEASUREMENT POINTS 11  
AND CLANK OF \*\*1211 00-01

|       |       |
|-------|-------|
| 120.0 | 121.0 |
| 110.0 | 111.0 |
| 100.0 | 101.0 |
| 90.0  | 91.0  |
| 80.0  | 81.0  |
| 70.0  | 71.0  |
| 60.0  | 61.0  |
| 50.0  | 51.0  |
| 40.0  | 41.0  |
| 30.0  | 31.0  |
| 20.0  | 21.0  |
| 10.0  | 11.0  |

NUMBER OF AIR FLOW 1270  
NUMBER OF MEASUREMENT POINTS 11  
AND CLANK OF \*\*1211 00-01

|       |       |
|-------|-------|
| 120.0 | 121.0 |
| 110.0 | 111.0 |
| 100.0 | 101.0 |
| 90.0  | 91.0  |
| 80.0  | 81.0  |
| 70.0  | 71.0  |
| 60.0  | 61.0  |
| 50.0  | 51.0  |
| 40.0  | 41.0  |
| 30.0  | 31.0  |
| 20.0  | 21.0  |
| 10.0  | 11.0  |

NUMBER OF AIR FLOW 1270  
NUMBER OF MEASUREMENT POINTS 11  
AND CLANK OF \*\*1211 00-01

|       |      |
|-------|------|
| 100.0 | 12.0 |
| 150.0 | 14.0 |
| 200.0 | 12.0 |
| 110.0 | 10.0 |
| 130.0 | 13.0 |
| 120.0 | 11.0 |
| 140.0 | 15.0 |
| 160.0 | 17.0 |
| 180.0 | 19.0 |

[illegible][illegible][illegible]

3220.  
3221.  
3222.  
3223.  
3224.

1.11.  
1.12.  
1.13.  
1.14.  
1.15.

1.16.  
1.17.  
1.18.  
1.19.  
1.20.

1.21.  
1.22.  
1.23.  
1.24.  
1.25.

1.26.  
1.27.  
1.28.  
1.29.  
1.30.

1.31.  
1.32.  
1.33.  
1.34.  
1.35.

1.36.  
1.37.  
1.38.  
1.39.  
1.40.

1.41.  
1.42.  
1.43.  
1.44.  
1.45.

1.46.  
1.47.  
1.48.  
1.49.  
1.50.

1.51.  
1.52.  
1.53.  
1.54.  
1.55.

1.56.  
1.57.  
1.58.  
1.59.  
1.60.

1.61.  
1.62.  
1.63.  
1.64.  
1.65.

1.66.  
1.67.  
1.68.  
1.69.  
1.70.

1.71.  
1.72.  
1.73.  
1.74.  
1.75.

1.76.  
1.77.  
1.78.  
1.79.  
1.80.

1.81.  
1.82.  
1.83.  
1.84.  
1.85.

1.86.  
1.87.  
1.88.  
1.89.  
1.90.

1.91.  
1.92.  
1.93.  
1.94.  
1.95.

1.96.  
1.97.  
1.98.  
1.99.  
2.00.

2.01.  
2.02.  
2.03.  
2.04.  
2.05.

2.06.  
2.07.  
2.08.  
2.09.  
2.10.

2.11.  
2.12.  
2.13.  
2.14.  
2.15.

2.16.  
2.17.  
2.18.  
2.19.  
2.20.



Mathematics - 2000

DATE OF BIRTH : 1960  
 DATE OF DEATH :  
 PLACE OF BIRTH :  
 PLACE OF DEATH :  
 OCCUPATION :  
 RELIGION :  
 MARITAL STATUS :  
 NO. OF CHILDREN :  
 NAME OF SPOUSE :  
 NAME OF CHILDREN :

1984 USAF-SCEEE RESEARCH INITIATION PROJECT

Sponsored by the  
AIR FORCE OFFICE OF SCIENTIFIC RESEARCH

Conducted by the  
SOUTHEASTERN CENTER FOR ELECTRICAL ENGINEERING EDUCATION

Final Report

NUMERICAL MODELING OF MULTIPHASE TURBULENT RECIRCULATING  
FLOWS IN SUDDEN-EXPANSION RAMJET GEOMETRY

|                         |                                      |
|-------------------------|--------------------------------------|
| Principal Investigator: | Dr. Albert Y. Tong                   |
| Academic Rank:          | Assistant Professor                  |
| Department              | Department of Mechanical Engineering |
| University:             | University of Texas at Arlington     |
| Contract No:            | F49620-82-C-0035 (84 RIP 35)         |
| Funding Duration:       | January 1, 1986 to December 15, 1986 |

## CONTENTS

- I. Introduction
- II. Fuel Spray Model Formulation and Overall Solution Scheme
- III. Program Execution Procedure
- IV. Plotting Programs
- V. Summary
- Acknowledgement
- References
- Figures
- Appendices
  - A: Program Listing of Modified STARPIC
  - B: Program Listing of STMSORT
  - C: Program Listing of STRMPLOT
  - D. Program Listing of PLOTGEN
  - E. Program Listing of PLOTR

## 1. Introduction

The numerical modeling of multiphase flow in a sudden-expansion ramjet combustor geometry had been studied by the present author during his participation in the AFOSR/SCEEE Summer Faculty Research Program in the summer of 1984. It was part of several research efforts undertaken at the Aero Propulsion Laboratory. (Wright-Patterson AFB; Dayton, Ohio) to gain further insights into the characteristics of multiphase flow field in a ramjet dump combustor.

The basic configuration of the so-called sudden expansion dump combustor is shown in Figure 10. In this type of combustor, liquid fuel is sprayed into the ram air upstream of the dump station. It may also be injected directly into the chamber via side-wall inlets. Primary flame stabilization is provided by the flow recirculation regions, which may be supplemented with mechanical flame holding devices at the air inlet/combustor interface and/or the presence of inlet air swirl, obtained by the use of tangential injection or swirl vanes.

The goal of the summer research was to investigate via numerical modeling, the flow characteristics in a sudden-expansion ramjet combustor. The particular problem is concerned with liquid fuel spray in the combustor. The objective was to develop a computer code which can be used for the systematic study of the multiphase flow characteristics.

Liquid fuel spray plays an important role in combustion performance and emission of pollutants. Local values of air/fuel ratio are governed by trajectories of individual droplets, rates of vaporization and mixing of fuel vapor with air. Atomizers produce sprays with a wide range of droplet sizes, velocities and initial directions of flight. The droplets interact with gas streams, which can deflect the droplets from their trajectories. Vapor is released in the wakes of the droplets and these trails of vapor mix by

evaporation and diffusion with the airstreams. The rates of vaporization are governed by the temperature and species concentrations of the environment through which the droplets traverse. Since combustion efficiency and temperature distributions are directly dependent upon air/fuel ratio distributions, an accurate prediction of composition of the fuel vapor emanating at the droplet surface is important for spray combustion analysis.

The possibility of adapting and modifying developed computer codes to the present geometry and flow conditions had been considered. Several existing computer codes on fluid flow modeling available at the Aero Propulsion Laboratory had been examined. They were described briefly in [1]. It had been found that it would be most efficient to develop a custom-made droplet spray code and incorporate it into the existing STARRC code for the multiphase flow calculations. Subsequently, a droplet spray model was formulated along with an overall solution scheme (see [1]).

The present research work is a continuation of the summer work conducted by the author at the Aero Propulsion Laboratory. The goal is to implement the two-spray model along with the overall solution scheme into the STARCC code which ultimately can be used for the systematic study of the flow characteristics.

In the present study, a liquid spray model has been inserted into the STARPIC code. The details of the formulation, overall solution scheme and procedure are given in this report. More details on the liquid spray model formulation is given in [1]. Due to some programming difficulties encountered in running STARRC, STARPIC was used instead. Since STARPIC considers only the fluid dynamics, only the droplet momentum source terms are considered in the liquid spray model. However, provision has been made in the liquid spray computer code to account for the thermal energy and species source terms.

The liquid phase is modelled as a steady droplet flow from a set of ports. The ports may be at any location inside the flow field as well as at the inlet perimeter and can have arbitrary input for mass flow rate, velocity, droplet diameter and temperature. A listing of the modified STARPIC program is given in this report.

STARPIC generates tables of property data including velocity, stream function, turbulence energy and turbulent dissipation. These data are given for an array of points mapped in a grid over the length of the combustor along a plane from the centerline to the edge of the combustor. A set of computer programs (STRMPLOT, STRMSORT) have been developed to plot the streamlines. Numerical data can be hard to interpret and use, while plots can help make the interpretation easier. The procedure used to plot the streamlines can be broken down into two separate steps. In the first step, a subroutine (STRMSORT) working in the STARPIC program generates plotting points and stores these points in a data file. The second step is to plot the data using a postprocessor program (STRMPLOT) running with a Calcomp pen plotter. This set of programs is a very specialized point generating subroutines that is designed specifically for stream function plotting and is unsuitable for plotting anything but stream function. In order to plot other properties as well as stream function a more universal point generating program (PLOTGEN) is developed.

The plotting software developed in the present work can also be used with minor modifications to produce pen plots of the output of other similar programs as well. The programs are written for the user who has a mild working knowledge of Fortran 77 or similar version. The details of the theory and operation of these plotting softwares are included in this report.

## II. Fuel Spray Model Formulation and Overall Solution Scheme

In the present work, a liquid spray model has been inserted into the STARPIC Code. The liquid phase is modelled as a steady flow from a set of ports. The ports may be at any location inside the flow field and can have arbitrary input mass flow rate, velocity and temperature. The liquid flows in the form of a stream of droplets in an annular section. The model is founded on the idea of regarding the liquid phase as a source of mass, momentum and energy to the gas phase continuum. The calculation scheme utilizes the cellular approach in which each computational cell is regarded as a control volume. Eulerian conservation equations are applied to the gas phase and Lagrangian equations of droplet motion and thermal energy are applied to a finite number of droplet size ranges representing the size distribution within the spray. Recording the mass, momentum and energy of the droplets on crossing cell boundaries provide the droplet source terms for the gas flow equations.

The calculation begins by solving the gas flow field assuming no droplets are present. Using this flow field, droplet trajectories together with the size and temperature histories can be calculated as a solution to a system of ordinary differential equations developed from the Lagrangian formulation. In this program the droplet trajectory is calculated by numerical integration using a fourth order Runge-Kutta method. The droplet trajectory is followed from the port inlet to the point where it either leaves the flow domain or hits the outer wall. No attempt has been made to account for the history of the droplet after splashing off the wall. Also excluded are the possibility of the drop crossing the center line or colliding with any other droplet as reliable models for these collisions have not yet been developed. The drag forces on the droplet are computed assuming a spherical drop shape. The equation of motion of a droplet is given by

$$\frac{d\vec{V}}{dt} = \frac{3}{8} \frac{\rho_g}{\rho_d} \frac{C_D}{R} (\vec{U} - \vec{V}) |\vec{U} - \vec{V}| + \vec{g}$$

$$\frac{d\vec{X}}{dt} = \vec{V}$$

Where  $\vec{U}$  and  $\vec{V}$  are the gas and droplet velocities respectively.  $C_D$  is the drag coefficient,  $R$  is the droplet radius,  $\vec{g}$  is the gravity vector and  $\vec{X}$  is the droplet location vector. The gas phase velocity components used in the numerical integration are assumed to be constant in a given time step. The value of the gas phase velocity component is chosen as the velocity corresponding to the U or V cell that the droplet is in.

It should be mentioned that STARPIC as well as STARRC and TEACH employ a special grid system known as the staggered grid system. A schematic of the staggered grid system is given in Figure 1 where the C, U and V cells are shown. The C cells are the control volume cells for quantities such as temperature and pressure which are referenced at the grid points. The U cells are the control volume cells for the horizontal velocity components U which are referenced at midway between two neighboring horizontal grid points. Similarly, the V cells are the control volume cells for the vertical velocity components V which are referenced at midway between two neighboring vertical grid points. As shown in Figure 2, the boomerang-shaped envelope encloses a triad of points with reference location P at (I,J).

In order to correctly identify when and which C, U and V cell boundaries the droplets traverse, finer grid cells called the B cells are introduced in the present work. Basically, they are the four unit cells of a C cell. As shown in Figure 2, there are four B cells attached to a grid point. They can be categorized into types 1,2,3 and 4 as indicated in the figure. The location of a B cell relative to a grid point can then be identified once the cell type



At each integration step, a check is made to see if the droplet crosses either a C, U or V cell boundary. For example, if a drop crosses a U cell boundary, the cell it has just departed from has lost some axial momentum and the cell it has entered has gained an equal amount of momentum. This is accounted for by adjusting the source term used in the gas phase calculation. The same is true when the droplet crosses a V cell boundary. Provision has been made to account for thermal energy adjustment as the droplet crosses the C cell boundary, but this source term adjustment has not been implemented yet because STARPIC does not handle energy equation calculations.

The source terms are adjusted at each integration step, and the process is repeated for the remaining ports. Subsequently, the gas phase calculations are repeated to generate a new gas phase solution subject to the adjusted droplet source terms. The gas phase velocity distribution is checked for convergence between two consecutive solutions. A mean squared difference convergence criterion is used. Flow charts for the overall solution algorithm and the droplet calculation procedure are presented in Figures 5 and 6. is determined. The information is needed for determining the cell boundaries the droplets traverse in the source term calculations.

### III. Program Execution Procedure

In an attempt to keep as much of the original code undisturbed as possible, some of the variables that are also used in the subroutines for the liquid phase calculations are duplicated. A listing of the modified STARPIC program is given in Appendix A with the inserted sections clearly indicated. All the variables used in the liquid phase calculations are declared in two common blocks, namely DROPS and GGF. The common block GGF is used to declare the source term adjustment variables inserted in the gas phase subroutines CALCU and CALCV, and the remaining variables are declared in the common block DROPS.

The gas phase data is obtained first, and the corresponding initialization subroutines are executed. The liquid phase data is then read. The user must choose the mode to input data by assigning the value of the integer NDATA. If it is equal to 0 only the gas phase calculations are executed. If it is equal to 1 the data is read interactively from the terminal. If it is equal to 2, the data is read from a file. If it is equal to 3, the data is assigned in the program code. Thus, the program can be run both interactively or in a batch mode.

The variables to be supplied for the liquid phase are:

- (i) MAXPOR, the total number of ports from which the liquid is sprayed.  
A maximum of 10 is allowed but this can be increased by modifying the variable declaration statements.
- (ii) DRPDEN, the liquid density. The liquid from separate ports may have different densities. ( $\text{kg/m}^3$ )
- (iii) DRPDIA, the drop diameter (m)
- (iv) XDINIT and YDINIT, the axial and radial location of the port. The port may be located anywhere inside the flow domain. The location is with respect to the coordinates used in the gas phase (m).

- (v) UDINIT and VDINIT, the axial and radial velocity of the drop at injection (m/s).
- (vi) TDINIT, the initial temperature of the liquid (K).
- (vii) DRMDOT, the liquid mass flow rate from the port (kg/s).

The location of the lower left hand corner of the B-cell, XB and YB, are assigned. All flags and counters are initialized. The input data is written into a file. The integration time step and scaling factors are initialized. The droplet injection frequency is calculated from the mass flow rate.

The gas phase solution is now executed, and the equivalent gas velocity variables used in the liquid phase calculations are updated. The source term adjustment variables, RMOMU and RMOMV, are reinitialized to zero. The subroutine DROP is now invoked to perform the entire liquid phase calculations. It also returns the global convergence flag IFLAGZ. If the value of IFLAGZ returned is 1, then global convergence has been achieved. Consequently, the gas phase results are printed and the execution is terminated. If IFLAGZ is 0, the system has not converged globally and the gas phase calculations are executed again, and this is done by transferring control to statement number 2000. This causes a re-execution of both the gas phase and liquid phase calculations until either convergence is achieved or until the maximum number of iterations allowed, MAXCT, is exceeded.

Subroutine DROP is invoked by the main program, and it executes all the calculations required for the liquid phase. A brief description of the subroutines created in the present work is given in the latter part of this section. To begin, the droplet location, velocity, temperature, radius and density are initialized for the first injection port. Then, the flags and counters are initialized to zero. Subroutine FINDB is now called to obtain the B, C, U and V cells where the injection port is located. The source term adjustment variables RMOMU and RMOMV at the injection port are initialized.

UGAS and VGAS are set to the gas velocities of the mid-point of the U and V cells where the droplet is located. The numerical integration subroutine RUNGA is now called to obtain the new location and velocity for the droplet. Subroutine DOMCHK is called to check if the droplet is inside the flow domain. If the droplet has departed from the flow domain the flag IHIT is set to 1, and the control is transferred to statement number 900 to start calculations for the next port. The B cell in which the droplet is located after integration is identified by calling subroutine FINDB. The subroutine HITWAL is then called. If the droplet has hit the outside wall, IHIT is set to 1 and the control is transferred to statement number 900 to start calculations for the next port. No attempt has been made to account for the history of the droplet after splashing off the wall. Also excluded are the possibility of the drop crossing the center line or colliding with any other droplet as reliable models for these collisions have not yet been developed. If the droplet is still in the flow domain, subroutine STPCHK is called to check if the droplet has migrated to one of the eight immediate neighboring B cells. If the droplet remains inside the same B cell, the time step DT is increased by a scaling factor DTINC and the integration step is redone again with the adjusted time step to ensure that the droplet leaves the B cell in one integration step. If, however, the droplet travels beyond one of the eight neighboring cells, the integration time step is reduced by a scaling factor DTRED. As before, the integration step is redone with the adjusted time step, so that finally the droplet does move into one of its neighboring cells. The reason for this restriction is for easier bookkeeping of the droplet source term.

The integer variable NCASE which specifies the type of B cell is determined by calling subroutine FINDN. For a given value of NCASE, there are eight neighboring cells that the droplet may enter. This is shown in Figure 4. An integer variable MCASE is used to signify the relative position of the

neighboring cells. This is indicated in the figure. The value of MCASE is determined by calling subroutine FINDM.

There are all together thirty-two different cases depending on the values of MCASE and NCASE. With this information it is possible to identify exactly which C, U and V cell boundaries the droplet has crossed. If a U cell boundary has been crossed, a linearly interpolated value of the droplet axial velocity at the boundary is obtained by calling subroutine INTERP and the source term modification variables RMOMU are updated by calling subroutine UMOD. Similarly, if a V cell boundary is crossed, the variables RMOMV are updated by calling subroutine VMOD. If a C cell boundary has been crossed, subroutine CMOD is invoked. At present, subroutine CMOD has no executable statements, but it can be used to update the source terms corresponding to temperature and other variables when the thermal energy calculations for the liquid phase are implemented. Once the source term variables have been updated, the location of the droplet is stored into a file. The counter ISTEPS is incremented. If ISTEPS exceeds the maximum number of steps allowed, as would be the case if the droplet enters a recirculation zone, the calculations for the next port are initiated.

When the calculations for all the ports are completed, subroutine COMPAR is called to check for convergence by comparing the two consecutive gas phase solutions, and then control is returned to the main program.

Several spray calculations have been performed using the present modified STARPIC program. These include spray injection at the inlet perimeter as well as at the inlet center with various droplet diameters and initial velocities. In most cases, three (3) overall global iterations between gas phase and liquid phase calculations is needed.

A comprehensive documentation on STARPIC is given in [2]. Here a brief description of the various subroutines inserted in the present modified

STARPIC code is given below followed by a nomenclature list of the variables used in these subroutines.

#### Subroutine DROP

DROP is the master subroutine that when invoked by the main program, obtains the trajectories of all the droplets. A major function of this subroutine is to keep track of the droplet location with respect to the B,C,U and V cells. Whenever, the droplet crosses one of the control volume cells C,U, or V, the corresponding subroutines CMOD, VMOD and UMOD are called to adjust the source terms for these cells. The gas phase solution convergence is checked by calling subroutine COMPAR after the liquid phase calculation is completed. The flow chart for this subroutine is shown in Fig. 6.

#### Subroutine FINDB

FINDB returns the index numbers IB and JB corresponding to the B cell that the droplet is in. FINDB also returns the index numbers IC, JC, IC, JU, IV and JV corresponding to the C,U and V cells that the droplet is in.

#### Subroutine DOMCHK

DOMCHK returns a nonzero value for the flag IHIT if the drop has left the flow domain.

#### Subroutine INTERP

Performs linear interpolation between two points.

#### Subroutine FINDM

The B cell to which the droplet travels can have one of four locations in the main grid cell. FINDM returns the value of MCASE corresponding to the cell location.

#### Subroutine FINDN

FINDN returns the value of NCASE corresponding to the one of eight neighboring cells that the droplet can travel to.

#### Subroutine STPCHK

STPCHK checks if the drop travels to one of the neighboring cells. The time step is increased if the drop did not cross any cell boundary, or reduced if the drop has travelled beyond a neighboring cell.

#### Subroutine COMPAR

COMPAR checks for the global convergence of the system, and is invoked by Subroutine DROP, after the liquid phase calculations are complete. The average squared gas velocity error is used as the criterion for convergence.

#### Subroutine RUNGA

RUNGA does the numerical integration of a system of first order ordinary differential equations by fourth order Runge Kutta numerical integration, and is called by Subroutine DROP for each integration step. The derivative values are obtained by calling Subroutine XPSYS.

#### Subroutine HITWAL

The flag IHIT is set to 1 if the droplet has hit the outer wall.

#### Subroutine UMOD

The source terms for axial momentum are adjusted to account for the droplet crossing a U boundary.

#### Subroutine VMOD

The source terms for radial momentum are adjusted to account for the droplet crossing a V cell boundary.

#### Nomenclature

##### INTERGER VARIABLES:

- IB - AXIAL INDEX NUMBER FOR THE B CELL.
- IBOLD - OLD AXIAL INDEX NUMBER FOR THE B CELL.
- IC - AXIAL INDEX NUMBER FOR THE C CELL.
- ICOUNT - COUNTER FOR NUMBER OF LIQUID PHASE ITERATIONS.
- IFLAGZ - GLOBAL CONVERGENCE FLAG.
- IHIT - FLAG: 0 IF DROP IS IN THE FLOW DOMAIN.
- INTCTR - NUMBER OF RE-INTEGRATIONS.
- INTELG - INTEGRATION FLAG.
- ISTEPS - NUMBER OF STEPS TRAVELLED BY THE DROP.
- IU - AXIAL INDEX NUMBER FOR THE U CELL.
- IV - AXIAL INDEX NUMBER FOR THE V CELL.
- IB - RADIAL INDEX NUMBER FOR THE B CELL.
- IBOLD - OLD RADIAL INDEX NUMBER FOR THE B CELL.
- IC - RADIAL INDEX NUMBER FOR THE C CELL.
- IDMAX() - VARIABLE EQUIVALENT TO JMAX() IN THE MAIN PROGRAM.
- IB - RADIAL INDEX NUMBER FOR THE U CELL.
- IV - RADIAL INDEX NUMBER FOR THE V CELL.



MAXCT - MAXIMUM NUMBER OF OVERALL GAS-PHASE LIQUID-PHASE  
 ITERATIONS ALLOWED.  
 MAXPOR - MAXIMUM NUMBER OF PORTS.  
 MAXSTP - MAXIMUM NUMBER OF STEPS ALLOWED FOR DROP.  
 NPORT - PORT NUMBER.  
 NDI - VARIABLE EQUIVALENT TO NI IN THE MAIN PROGRAM.  
 NDJ - VARIABLE EQUIVALENT TO NJ IN THE MAIN PROGRAM.

REAL VARIABLES:

CDD - COEFFICIENT OF DRAG FOR THE DROPLET.  
 DRPDEN(N) - LIQUID DENSITY OF PORT NUMBER N.  
 DRPDIA(N) - DROP DIAMETER OF PORT NUMBER N.  
 DT - INTEGRATION TIME STEP.  
 DTINC - INCREMENT SCALE FACTOR FOR DT.  
 DTRED - REDUCTION SCALE FACTOR FOR DT.  
 GRAVX - AXIAL ACCELERATION FORCE COMPONENT.  
 GRAVY - RADIAL ACCELERATION FORCE COMPONENT.  
 PI - 3.14159265  
 RAD - DROPLET RADIUS.  
 RHOGAS - DENSITY OF THE GAS.  
 RMOMU - CONTRIBUTION TO AXIAL MOMENTUM SOURCE TERM.  
 RMOMV - CONTRIBUTION TO RADIAL MOMENTUM SOURCE TERM.  
 TDINIT - INITIAL TEMPERATURE OF DROPLET.  
 TDNEW - NEW TEMPERATURE OF DROPLET.  
 TDOLD - OLD TEMPERATURE OF DROPLET.  
 UDINIT - INITIAL AXIAL VELOCITY OF DROPLET.  
 UDNEW - NEW AXIAL VELOCITY OF DROPLET.  
 UDOLD - OLD AXIAL VELOCITY OF DROPLET.

UG()        - VARIABLE EQUIVALENT TO U( ) IN THE MAIN PROGRAM.  
 UGAS        - AXIAL VELOCITY OF THE GAS.  
 UGOLD()     - OLD AXIAL VELOCITY OF GAS.  
 VDINIT()    - INITIAL RADIAL VELOCITY OF DROPLET.  
 VDNEW       - NEW RADIAL VELOCITY OF DROPLET.  
 VDOLD       - OLD RADIAL VELOCITY OF DROPLET.  
 VG()        - VARIABLE EQUIVALENT TO V( ) IN THE MAIN PROGRAM.  
 VGAS        - RADIAL VELOCITY OF THE GAS.  
 VGOLD()     - OLD RADIAL VELOCITY OF GAS.  
 XB()        - AXIAL COORDINATE OF LOWER LEFT CORNER OF B-CELL.  
 XDINIT()    - INITIAL AXIAL-COORDINATE OF DROPLET.  
 XDNEW       - NEW AXIAL LOCATION OF DROPLET.  
 XDOLD       - OLD AXIAL LOCATION OF DROPLET.  
 YB()        - RADIAL-COORDINATE OF LOWER LEFT CORNER OF B-CELL.  
 YDINIT()    - INITIAL RADIAL-COORDINATE OF DROPLET.  
 YDNEW       - NEW RADIAL LOCATION OF DROPLET.  
 YDOLD       - OLD RADIAL LOCATION OF DROPLET.

#### IV. Plotting Programs

##### A. Streamline Plot

The first step of the process is to generate plotting data from the data generated in the STARPIC program. Just before the modified STARPIC program ends, the subroutine STRMSORT is called. To this subroutine, the following generated data is passed: array of stream function values for grid points, the number of i grid lines, the number of j grid lines for each i grid value, an array of the x values corresponding to each i grid line, and an array of the y values corresponding to each j grid line. The subroutine STRMSORT first generates the outer boundary line points for the combustor through the use of the IMAX and JMAX values. The maximum j value is found for each i value up to IMAX, the last i grid line within the combustor. As each outer j coordinate is found it is checked against the previous one. If it is different, then it is assumed that the expansion step has occurred between this i grid line and the last. In this case two extra points are included, defining the corners of the step, then the rest of the points. As each point is defined the boundary j value is corrected by averaging between the last active j line and the first one outside the boundary. The i and j values are converted to their corresponding x and y values respectively as each point is found. The boundary points are then written to a disk file and followed by an end of block marker, 999.9 for both x and y values to signify the end of a line definition. When the points are recorded on disk they are recorded x value first then y value for each point. This is true of all points, boundary or otherwise.

Now, the main loop of the STRMSORT is executed. A listing of the subroutine is given in Appendix B. First a stream function value is defined for the particular streamline, lines 2073 to 2079. Next the subroutine INTERP is called. As is explained later, INTERP finds the actual points with the previously defined stream-function value. Once execution has returned from the

INTERP subroutine, STRMSORT checks for the existence of two special cases. The first is no points found with the desired stream function value. If this occurs, the next value is defined and execution continues. The other special case is when the stream-function value is greater than 1.0. When this occurs, it is assumed that a loop exists and the loop sort section is executed. Once the special cases are handled, the points are converted from i,j coordinates to x,y coordinates for plotting.

The i,j to x,y conversion section, lines 2086 to 2106, first checks to see if the i coordinate is an integer. If so, then the i grid coordinate is converted directly to an x value with the appropriate number from the array 'X'. If not, then the x value is interpolated linearly between the x values of the two consecutive i grid lines surrounding the point. The y value of the point is interpolated from the j grid value in the same manner.

The sorting of the points of a loop is accomplished in lines 2114 through 2153. Since the interpolation routine selects points along set i grid lines, it is assumed that the points in a loop will occur in pairs, with the possible exception of the ends of the loop. Since the interpolation routine selects points by starting at the inlet and ending at the outlet, the points or point-pairs are in ascending order by i grid value. In these pairs of points the point with the higher j grid value occurs second because the interpolation routine checks the j grid intervals starting at the centerline and moving outward to the boundary. The first step in sorting for the loop is splitting up the pairs. In lines 2116 to 2133, a loop is executed in which the i grid value of each point is compared with the previous point. If it matches, this point is the upper point of the pair and is put at the bottom of the temporary storage array 'TEMPPTS'. The points are to be sorted so that the loop is plotted counter-clockwise starting with outer point with the highest i grid value. With this in mind, the upper points are placed in the temporary array

starting at the bottom of the array so that their order is reversed, and the lower points and any single points are placed in the temporary array in the order of occurrence starting at the top. In lines 2134 through 2143, the upper points are moved to the top of the array and the lower points are moved down with no change in order for either group. The points are now in the proper order for plotting as a loop. As a final step, the first point is added at the end to close the loop in plotting. If the first point occurs at the outlet boundary, it is not added because this would indicate that the loop continued out of the control region.

The interpolation subroutine INTERP functions as follows. Starting at the centerline and moving outward, each  $j$  grid interval is checked to see if the specified stream function value exists in it. This is carried out along each  $i$  grid line starting at the inlet and proceeding toward the outlet. If the desired stream function value is less than or equal to one, each  $j$  interval is checked until the outer value of the interval is lower than the inner value. When this occurs, the process restarts at the next  $i$  grid line. If the desired value does fall within the interval, the actual  $j$  grid value is found by linearly interpolating between the inner and outer boundary values for that interval, lines 2197 to 2201. Two special cases are handled by the interpolation routine. The first is when the desired streamline has the value one. When this occurs, the first  $i$  grid line checked is immediately following the expansion corner. Before the interpolation loop is executed, though, the lower corner point is added. If the last point is not at the outlet boundary, the last two points are used to linearly extrapolate the intersection with the outer boundary, with this point being added at the end. The second special case is when the desired stream function value is greater than one. When this occurs, the interpolation loop checks every interval out to the boundary. This is to capture the points in the recirculation region.

The plotting program STRMPLOT functions as follows. The program reads points until either the end of block marker '999.9' or the end of file marker '888.8' is read. When the end of file marker is read the points that have been read are processed and plotted. If it is the first group of points, it is considered to be the boundary points. From this group the scaling factor is determined to make the plot 10 inches long, lines 45 and 46. These scaling factors are applied to every group of points. This first group is then scaled, lines 47 to 56, and then plotted. Connecting lines to complete the boundary are then plotted using the first and last points, lines 59 to 71. An arrow is then plotted to indicate the flow direction. Each succeeding group of points is then read, scaled and plotted using smooth lines to connect the points. When the end of file marker is read the plot is ended.

Two streamline plots generated by these programs are shown in Figure 7.

#### B. Universal Plot

STRMSORT is a very specialized point generating subroutine that is designed specifically for stream function plotting and is therefore unsuitable for plotting anything but stream function. For this reason, a more universal point generating program, PLOTGEN, is developed along with a plotting post-processor, PLOTR, which is taken almost directly from its predecessor, STRMPLOT, with minor modifications allowing easier user selection of plotting options.

The assumptions and limitations in the theory behind PLOTGEN FOR are as follows. The first and most important assumption is that physical properties are continuous. It is also assumed that if two points are close enough together and the property values are known at these two points, that a point, whose property value is between the other two, can be located with sufficient accuracy by the linear proportional distance between the two previous points corresponding to the proportionality of the corresponding property values.

It is further assumed that if two points exist such that their property values are the same and the spacial intervals surrounding these two points immediately border each other, horizontally, vertically or diagonally, that these two points may be connected by a line or similar curve along which the property value is constant. PLOTGEN is limited to working with cases in which a property is a function of the physical point of interest in a two dimensional cartesian-coordinate plane.

The first step in generating the plotting data, is to find points whose property value equals the desired. To do this, the interval between each pair of grid points, that neighbor either vertically or horizontally, is checked to determine whether the desired property value occurs between these two grid points. If the value does occur between in this interval, the location of this new point is taken to correspond to the linear proportionality of the desired property value within the interval. Since both grid points have either the same x-value or the same y-value, one coordinate of the new point is known. To find the other point, the value is found through linear interpolation on the range between the two grid points. In this way, a set of points whose property value is given, can be physically located. The next step is to connect these points to produce a plot.

The method of detecting point links and of linking these points approximates the method a human would use if provided with only a group of points. The first step is to find a point in the set of points. In this case, find the lowest that is farthest to the left. With this point, there is an associated interval, between two grid points on some known grid line. Around this interval, there are eight other-bordering intervals; four diagonally, two vertically, and two horizontally. Beginning with the direction from which the current point was found, proceed in a counter-clockwise direction, checking each of these eight intervals until another point is

detected. If a point is detected, then the plot will be connected to this new point, and the intervals around this new point are checked for new points. This continues until a point is reached where no adjoining point is detected. If this occurs, the location of the first point of this plot line is checked. If this first point would have been detected here, it is repeated to close the curve. After this the process starts again with another first point until all of the points have been used. Only the intervals between active grid points are checked as outlying points could cause error.

The program PLOTGEN is written in a block style to make programming and modification easier. A listing of the program is given in Appendix D. In the setup section, the variables are defined in comment statements and declared. Here also, the point arrays and control variables are initialized. In the read section, the data table with the data to be plotted, is read into the program for processing. This section includes subsections to read from either the STARPIC or the TEACH output. Following this is the boundary definition section. Here, the physical boundaries are determined and output to the plot file. Here also, the grid boundaries for the rest of the program are set. The next sections work together in the master loop. The first section determines in which intervals the plot points are found and where within each of these intervals the point is located. Following this, the first point section searches the two interval arrays to find a first point for plotting. The succeeding points section then attempts to link up adjoining points. The last section checks for the case where the last point adjoins the location of the first point.

At the first of the setup section, there is a large group of comment statements defining the use or purpose of each variable. Following this, the arrays and variables are declared with the appropriate types. Certain variables and arrays are then loaded with the proper values. Next, the array



VALUE is initialized with the desired property values for plotting. Here the user sets NUMVALS to the number of values to be plotted. Finally, the interval arrays are set to -1 in every cell to indicate no point present.

In the read section, the data table for plotting is read according to the format type set by the variable READTYP. If READTYP equals one the data is read in the TEACH format, if two it is read in the STARPIC format.

At the beginning of the boundary definition section, the plot file is opened with the desired file name. Beginning at the left, each i grid line is checked from the bottom up until a zero value is found. This grid point is assumed to be the first beyond the wall, so the median value between this point and the previous grid point is converted to x,y coordinates and output to the plot file. This occurs at every i grid line until the first i grid line of zeroes is found. This is assumed to be the right end wall, so the value between this grid line and last is used to define the wall. The left wall was assumed to occur at an x value of zero. If a step is detected as the upper wall is being defined, the step is defined by two points whose x value equals the median of the two succeeding i grid lines and with the y values equal to that of the appropriate j grid line. After the boundary points have been output, the value 0.0 is output to close the boundary curve and the end of group marker, 999.9, and the symbol change marker, 777.7, are output.

The next four sections work together in the master loop. In the first, the point detection section, the interval to the right and the interval above each point is checked for the occurrence of each desired value. If this value is on a horizontal grid line, the proportional location of the plot point between the two end points of the interval, is stored in the interval array as type-one point and the counter of plot points found, PTNUM, is incremented. Points found in vertical intervals are stored as type-two points. Points are stored in the interval array location corresponding to either the left or

lower grid location of the interval, whichever is appropriate. If the grid location currently being checked for a plot point is at the maximum  $i$  grid line, the interval to the right of the grid point is not checked. Similarly, the intervals above grid points on the maximum  $j$  grid location of each  $i$  grid line are not checked. This is to avoid detecting phantom points at the wall.

The next block of statements checks through the interval array to find one with a point. In this case, the intervals that do not contain a point are represented by a value of -1 in the corresponding array cell. If the interval contains a point, its corresponding array cell will contain a value equal to or greater than zero and less than one. This value is the proportional location of the plot point between the two grid points at the ends of the interval. To find a point, the intervals are checked along each  $i$  grid line from left to right and from the inside  $j$  value out, with the type one cell checked first. When a point is found, its grid coordinates are converted to  $x,y$  coordinates and the point is written to the plot file. The  $i,j$  address of the interval of this point are saved along with the type of the first point and its  $x,y$  coordinates. This interval is then cleared, set to -1, and the point counter decremented, so this point will not be discovered again. Execution continues with the succeeding points section.

The succeeding points section is the heart of this plotting scheme. Here, the points are linked up to form lines, loops and other curves. Upon entering this section the  $i$ ,  $j$ , and point-type values are those of the previous point, and the direction is assumed to be three. Here the eight cells adjoining the previous point are checked for a neighboring point. The addresses of these eight cells are a function of the location of the previous point, its type, and the direction from the previous point to the cell to be checked. The type of each cell to be checked is the same as the previous point if adjoins the previous point vertically or horizontally. If the new

cell neighbors the previous cell diagonally, the new cell is of the opposite type. The  $i,j$  address of the new cell is found by adding the appropriate delta values to the  $i,j$  coordinates of the previous point. The delta  $i$  value is found from the array *DELI* and is indexed by the type of the previous point and the direction from the previous cell to the new cell. The delta  $j$  value is found similarly from the array *DELJ*. These parameters are used to check the intervals in the eight directions proceeding counter-clockwise, with the direction one being to the right. The first direction checked is one past the direction from which the previous point was found. The neighboring intervals are checked until either a new point is found or all directions have been checked. If a new point is found, its grid coordinates, one of which is on a grid line and the other is between two lines, are converted to  $x,y$  coordinates and the point is written to the plot file. The interval is then cleared and the point counter decremented. The linking procedure is then repeated with this new point being the previous value. If no point were found execution would continue at the last point section.

In the last point section, the most recently found point is checked to see if it borders the first point in this plot line. If these two points do not border or they are the same point, the end of block marker, 999.9, is written to the plot file. If point counter is greater than zero then execution continues at the first point section. If all of the points have been used, the symbol change marker, 777.7, is written to the plot file and execution continues at the start of the master loop for a new property value. If the last point and the first point do border each other, then the first point is again written to the plot file to close the curve, and the end of block marker is also written to file. Execution continues as in above, according to whether or not all of the points have been used. If this is the last point and the last property value to be plotted, the end of file marker, 888.8, is written to

file, the file closed and the program ended. Otherwise, execution continues until whole list of desired property values is exhausted.

PLOTIR is a simple plotting post-processor designed as a companion to PLOTGEN. It is composed of four major sections. The first is the set up and initialization section. Here the variables are defined and declared. The user defined parameters, with the exception of plot file name, are set. The appropriate value of LTYP is set to produce lines, symbols or a combination of the two. Following this is the master read loop. In this loop, points are read into two arrays, one each for the x and y coordinates of the plot points, until a control code is read. If the control code is 777.7, the symbol number is incremented. If the code is 999.9 and this is first group of points, control passes to the boundary plot section. If the code is 999.9 and this is not the first point group, the control passes the standard plot section. If the code 888.8 is read, the plot is ended, the plot file closed and the program ended.

In the boundary plot section, the boundary is plotted and the scaling factors are set. Since a counter of points read was kept in the read loop section, the number of points in this group is known. Since the last point of the boundary definition will be 0.0 the second to last point will have the maximum y value. With this in mind, the scaling factor for both x and y scales is set so that the maximum y value is plotted as some desired value, such as 1.5 inches. To produce a plot that is compressed or expanded in the x direction, the scaling factor for the x scale can be divided or multiplied by an appropriate factor. The boundary points are then each scaled and sent to the plotter in the order in which they occur in the plot file. A flow direction arrow is then plotted by calling the subroutine AROHD. Control then passes back to the read loop section.

In the standard plot section, the plot points representing the data table are scaled and plotted. Using the scale factors determined in the boundary plot section. Each point is scaled and then sent to plotter in the order in which it occurs in the plot file. If the value of the point counter, NUMPTS, is set to its negative in the subroutine call to FLINE, the points will be connected with a smooth curve fit to the plot points. Control is then passed back to the read loop section.

Included with this report are two sample plots. The first one shown in Figure 8 is the mixture ratio predicted by TEACH code. The inlet fuel temperature at the center is at 450 K and the air inlet temperature at the outer annular is at 300 K. The other one shown in Figure 9 is the temperature profile predicted by TEACH from the same calculation.

## VI. Summary

A fuel-spray model has been successfully implemented into the STARPIC code which allows calculations of multiphase flow in a dump combustor. While STARKO and STARPIC both belong to the TEACH, there is no foreseeable difficulty in extending the fuel-spray model developed on the present study to STARKO or TEACH.

A set of computer programs to plot the streamlines as well as other properties such as isotherms have also been developed. The plots generated by these programs can help make the interpretations of data easier. These plotting software can also be used with minor modifications to produce pen plots of the output of other similar programs.

Acknowledgement

The support of the Air Force Office of Scientific Research for this research is gratefully acknowledged.

### References

1. A. Y. Tong, "Numerical Modeling of Multiphase Turbulent Recirculating Flows in Sudden-Expansion Ramjet Geometry," USAF-SCEEE SFRP Final Report (AF49620-82-C-0035; August 1984).
2. D. G. Lilley and D. L. Rhode, "A Computer Code for Swirling Turbulent Axisymmetric Recirculating Flows in Practical Isothermal Combustor Geometries," NASA Contractor Report 3442.



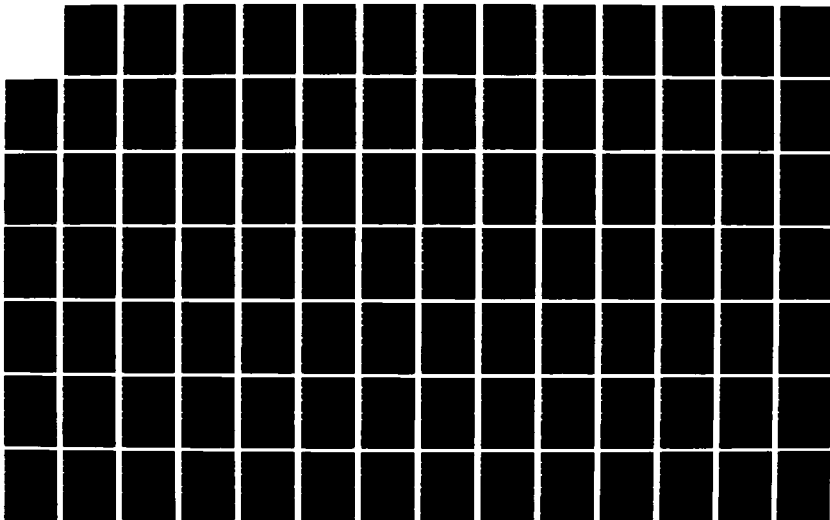
AD-A186 498

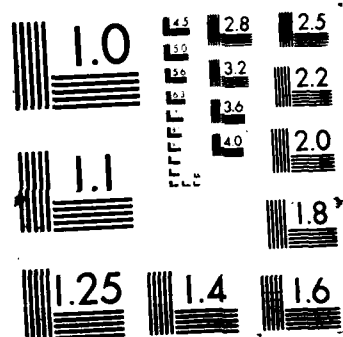
UNITED STATES AIR FORCE RESEARCH INITIATION PROGRAM  
1984 RESEARCH REPORTS (U) SOUTHEASTERN CENTER FOR  
ELECTRICAL ENGINEERING EDUCATION INC S W D PEELE  
MAY 86 AFOSR-TR-87-1721 F49620-82-C-0035 F/G 15/1

10/11

UNCLASSIFIED

NL





FIGURES

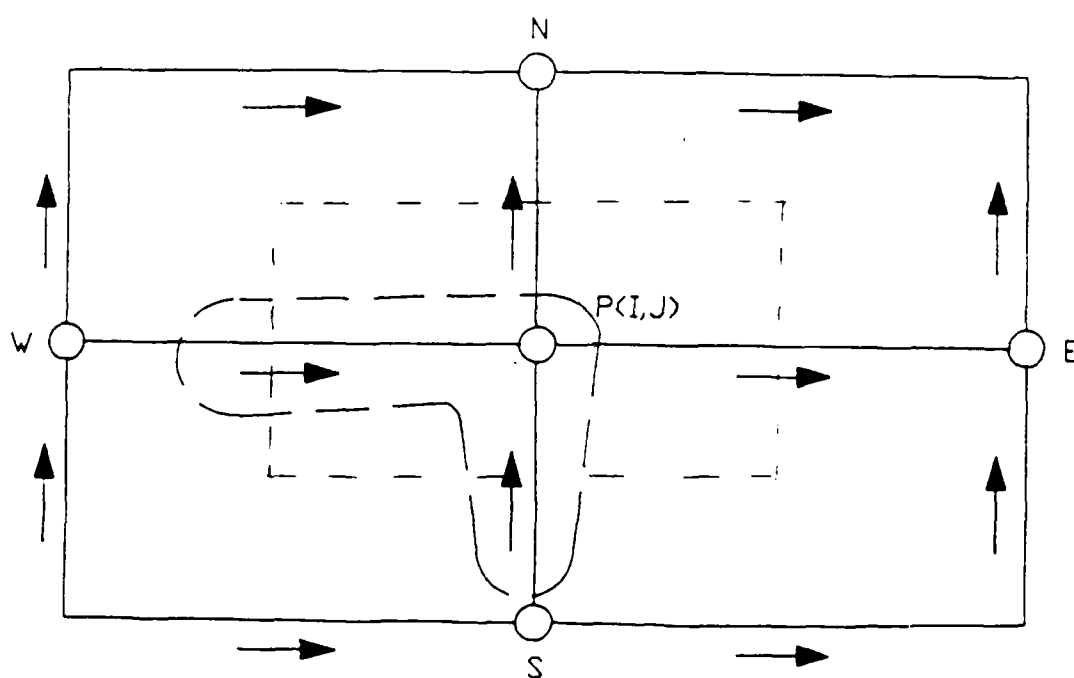
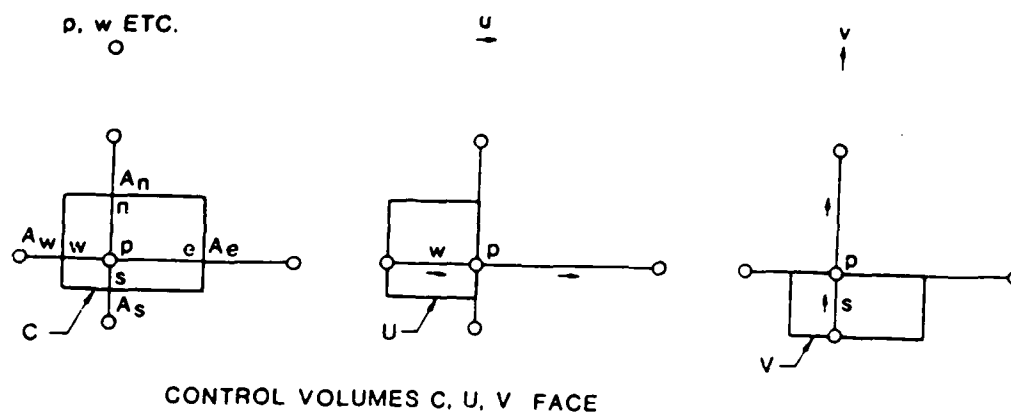


Fig. 1 Staggered grid for the computational mesh.

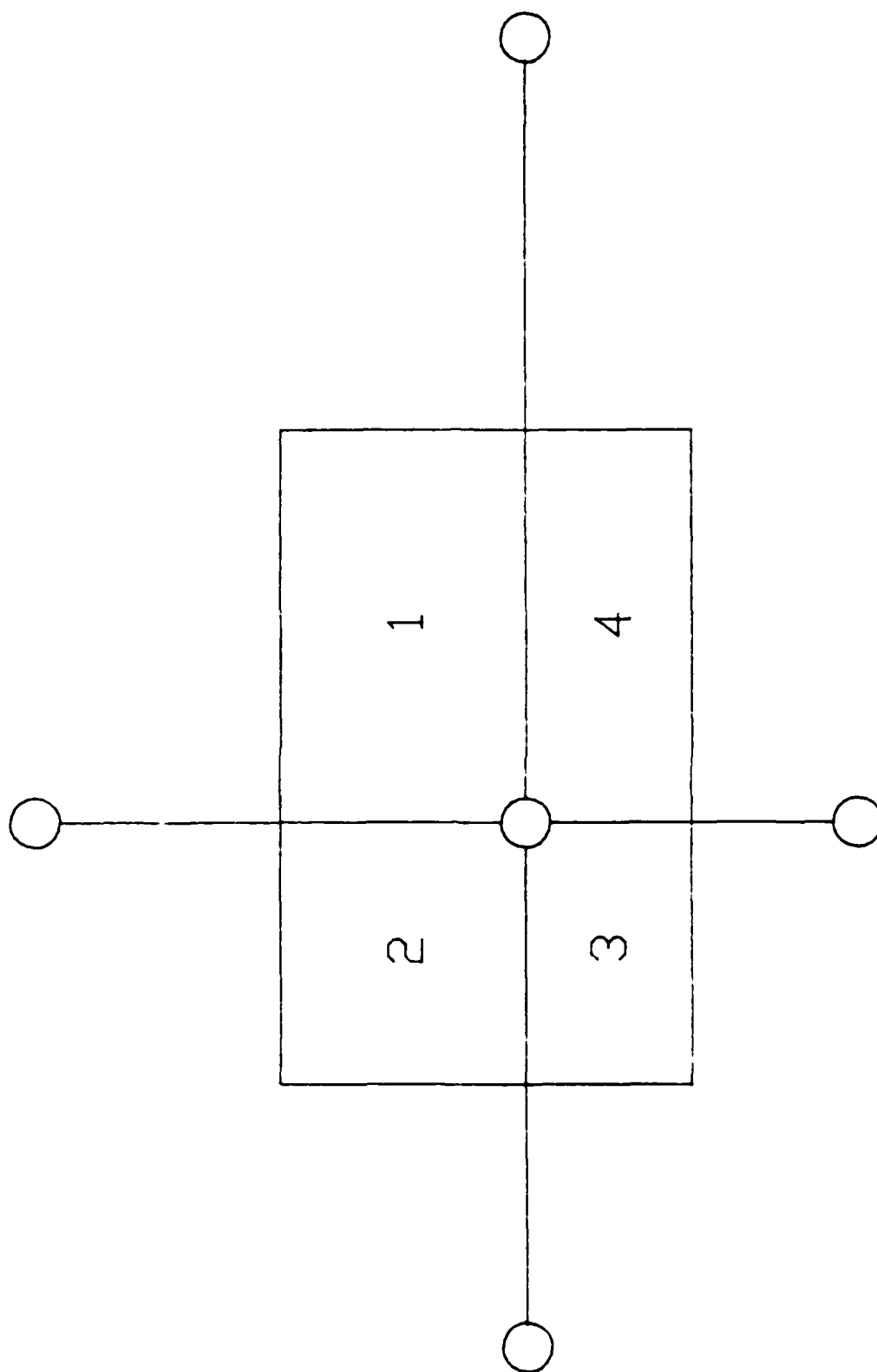


Fig. 2 The four types of B cells and their MCASE values

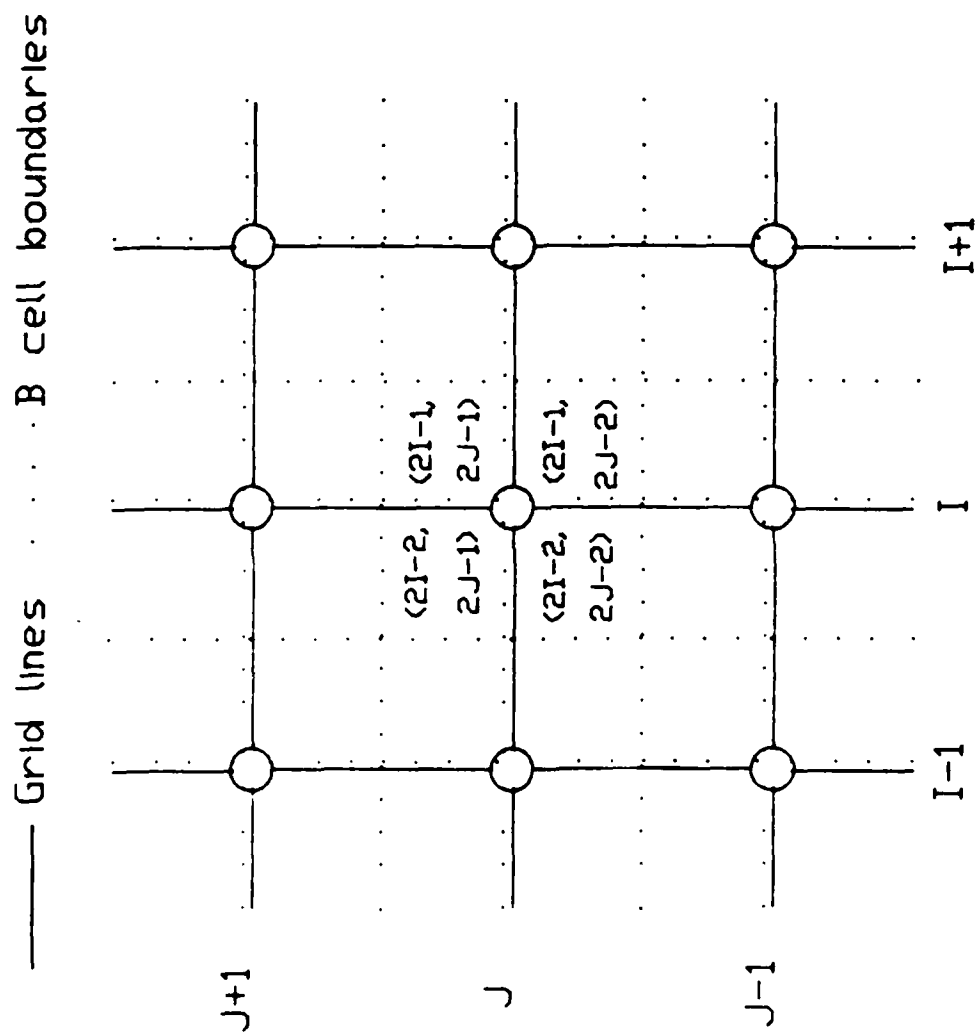


Fig. 3 B cells and their corresponding index numbers

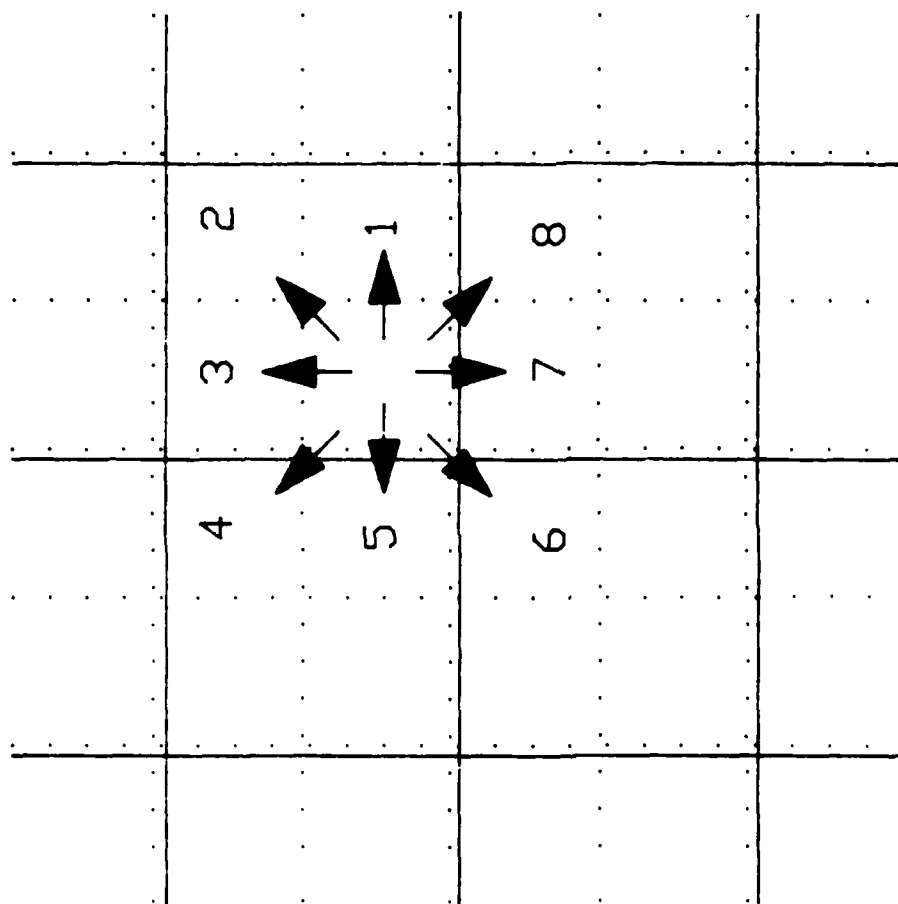


Fig. 4 The eight neighbouring B cells and their NCASE values

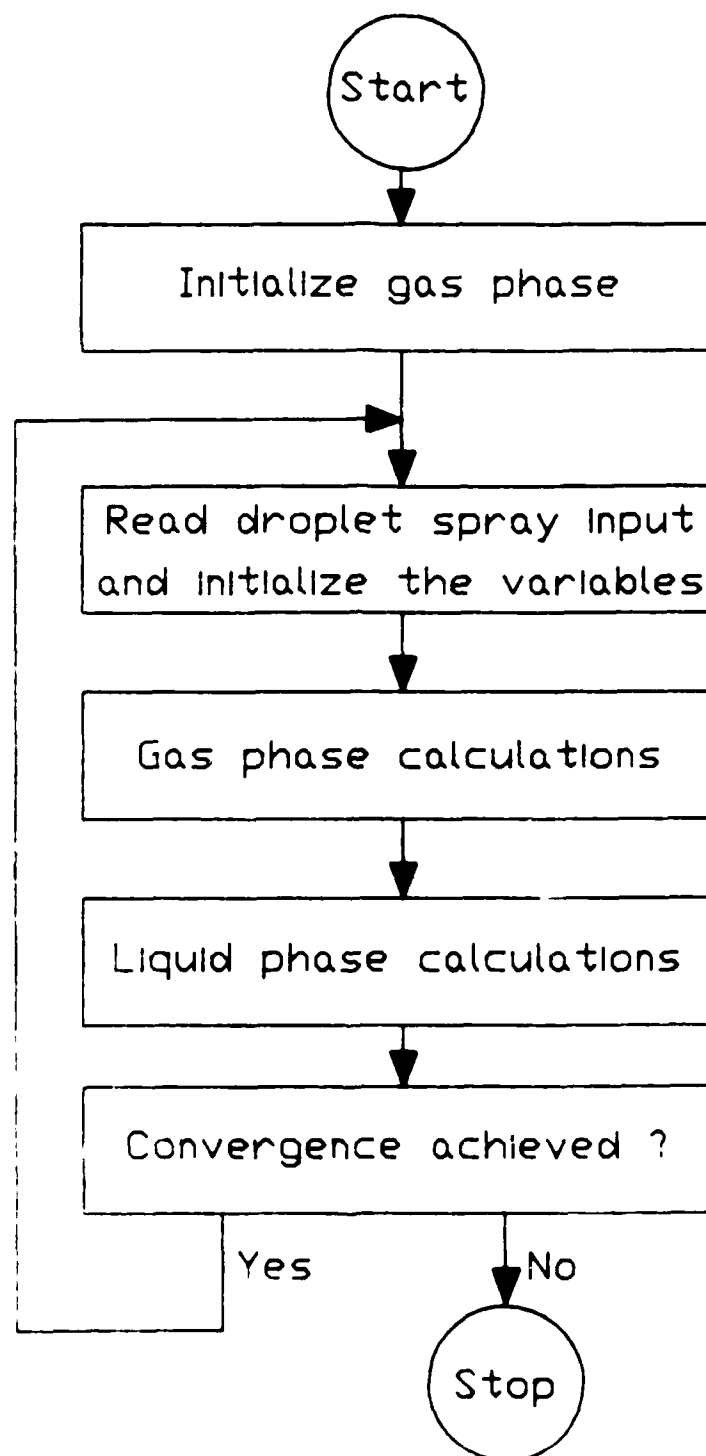


Fig. 5 Flow chart for the overall algorithm



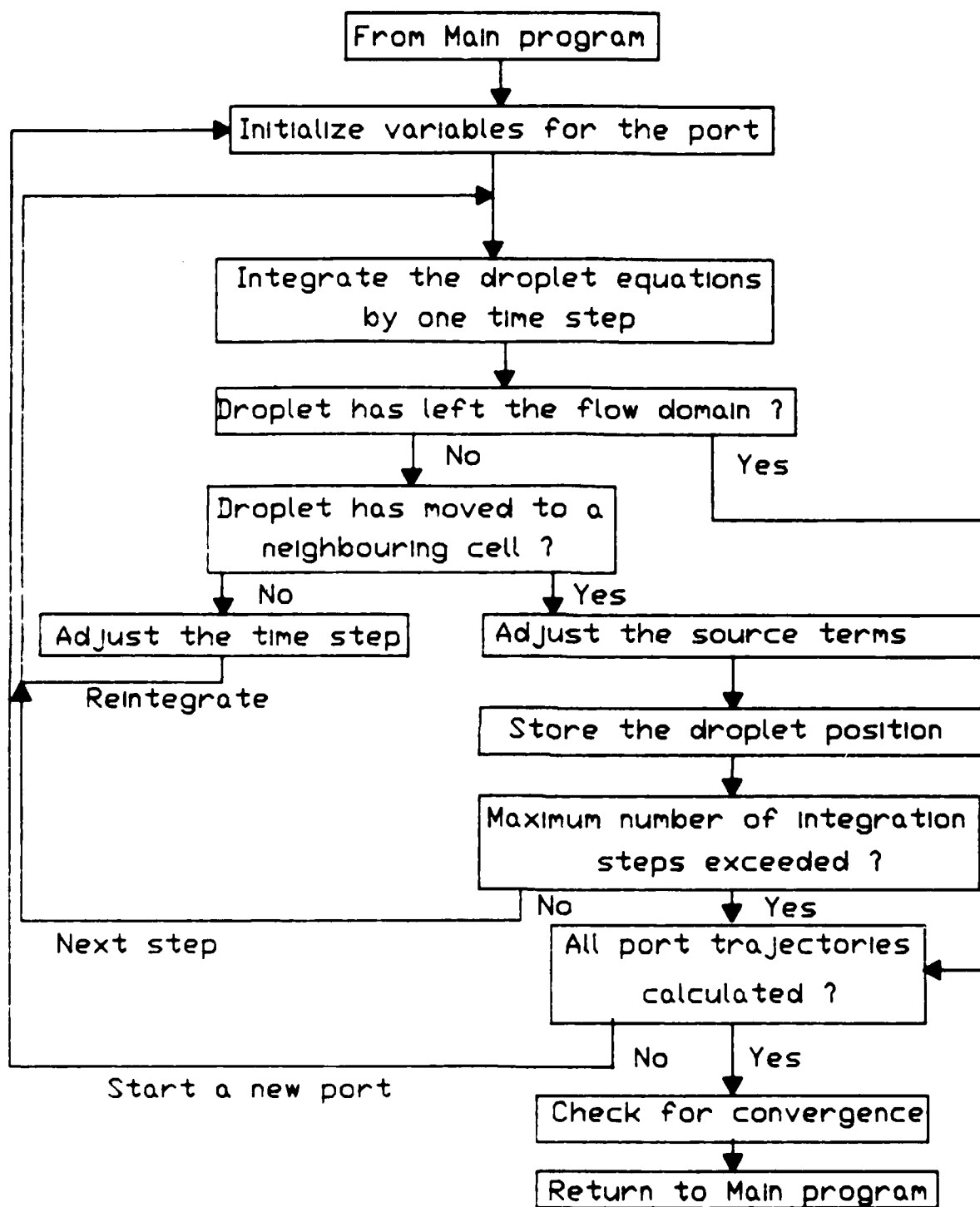
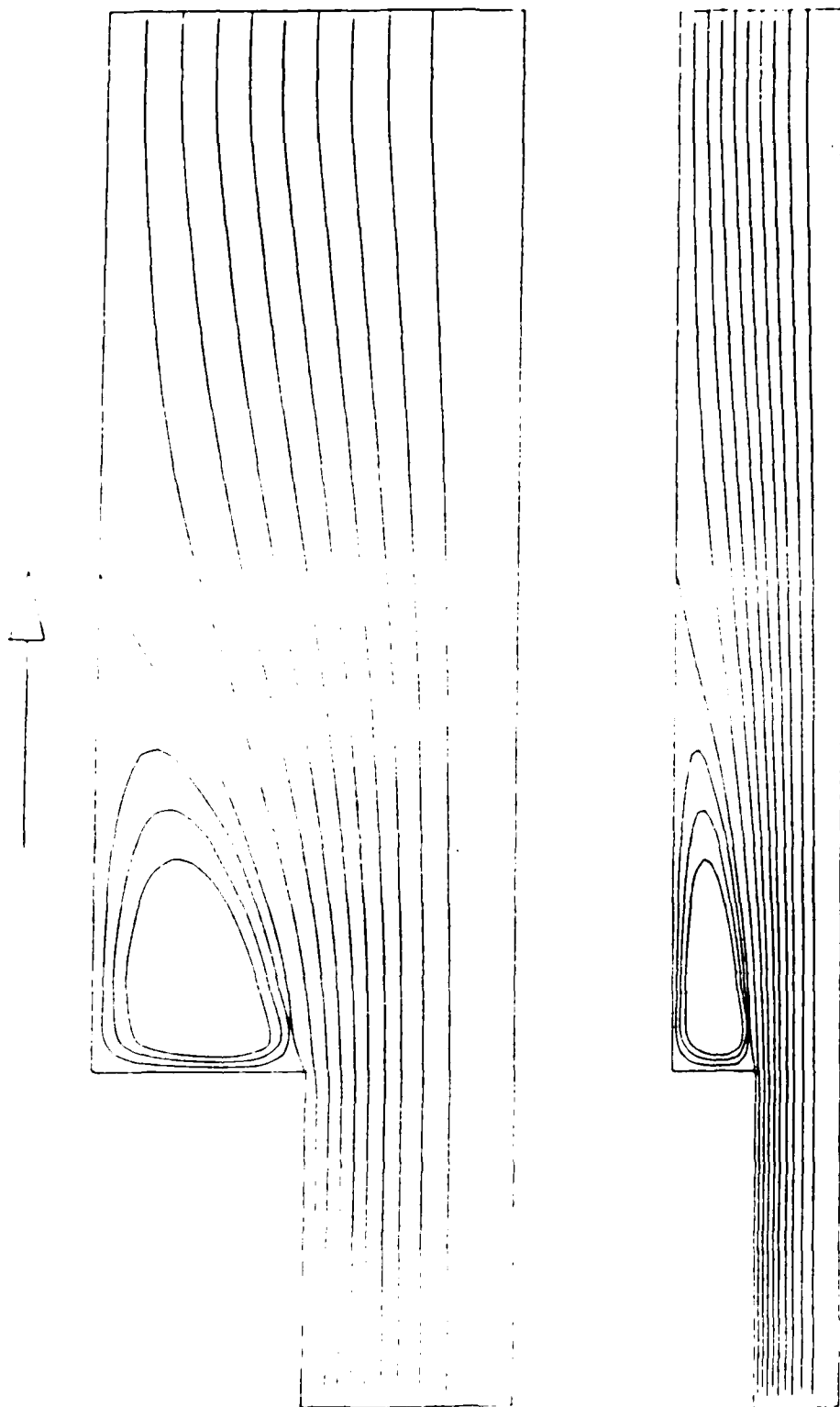


Fig. 6 Flow chart for subroutine DROP



35.39

Figure 7 Streamline plots from program STRMSORT

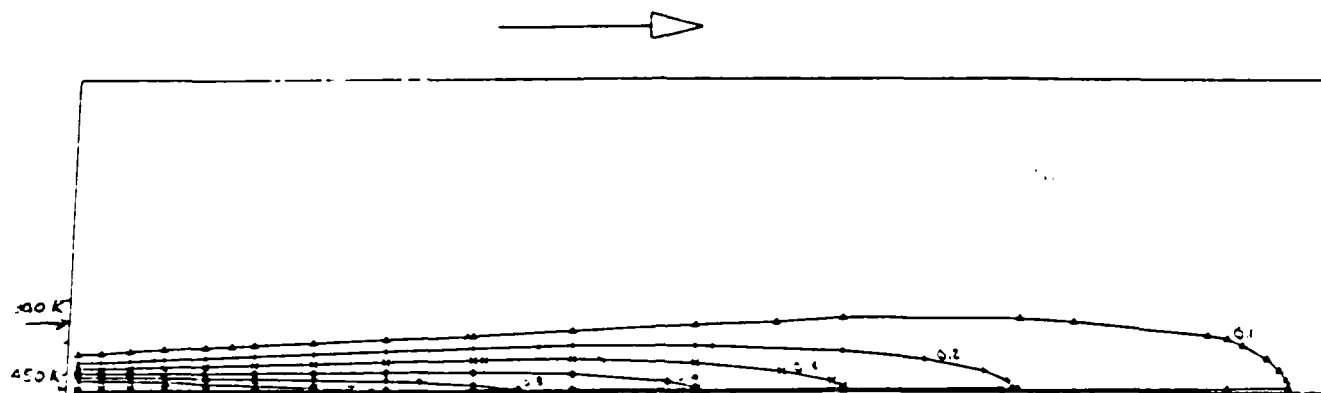


Figure 8 Mixture ratio profile from program PLOTGEN

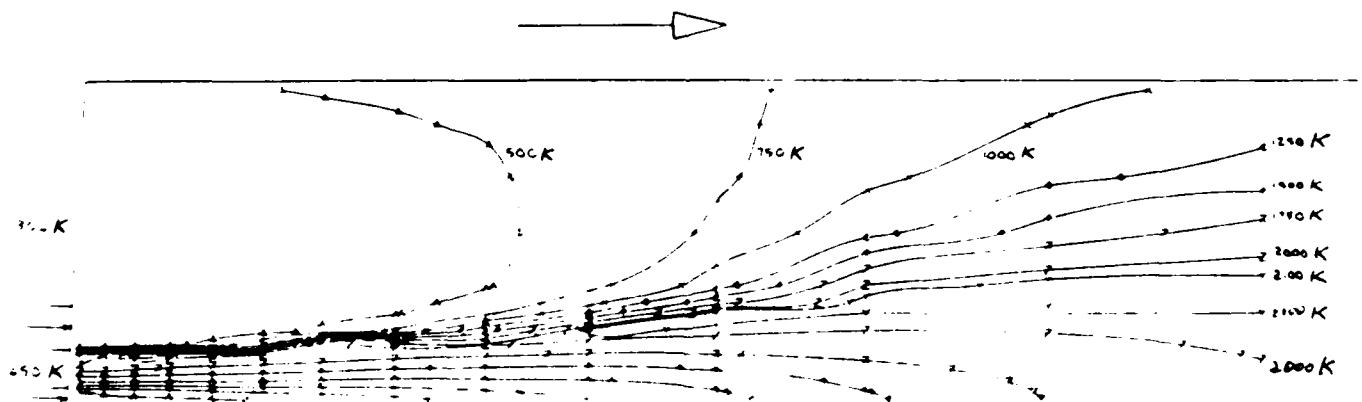


Figure 9 Temperature profile from program PLOTGEN

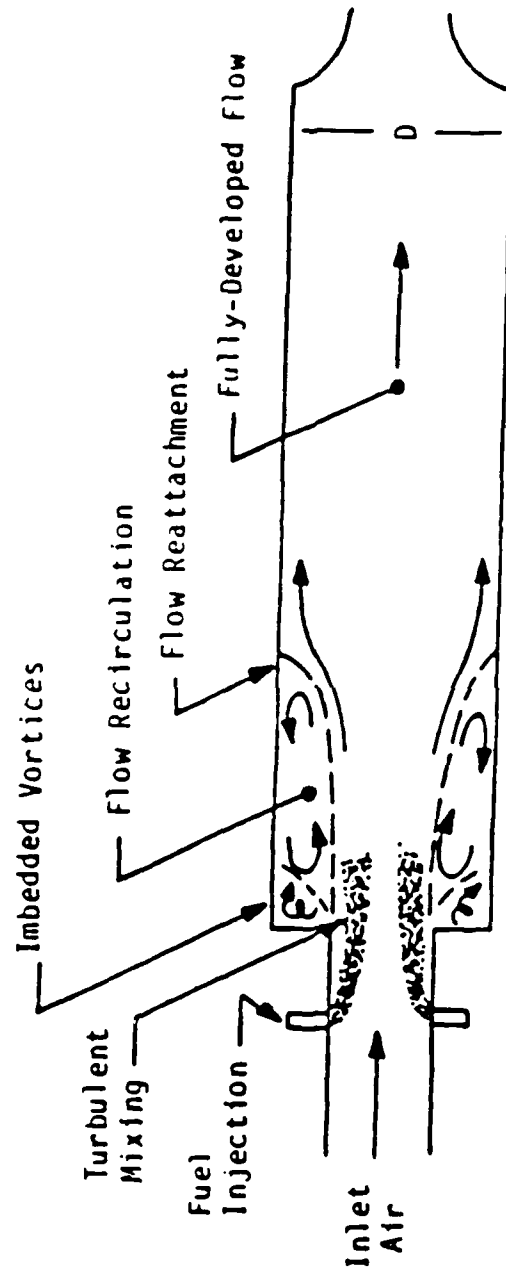


Figure 10 Ramjet Combustor Flowfield

APPENDIX A  
PROGRAM LISTING OF MODIFIED STARPIC

```

00100 C      PROGRAM MAIN
00200 C
00300 C .....
00400 C
00500 C
00600 C      A COMPUTER PROGRAM FOR TURBULENT, SWIRLING,
00700 C      RECIRCULATING FLOW IN COMBUSTION GEOMETRIES
00800 C      VERSION OF APRIL 1981 - NASA CR 3442
00900 C      D.L. RHODE AND G. LILLEY
01000 C      MECHANICAL AND AEROSPACE ENGINEERING, OKLAHOMA STATE
01100 C      UNIVERSITY, STILLWATER, OKLAHOMA 74078.
01200 C
01300 C*** BEGINNING OF INSERTED SECTION ** BEGINNING OF INSERTED SECTION ***
01400 C
01500 C      WITH LIQUID SPRAY MODEL INSERTED BY
01600 C      ALBERT Y. TUNG (FEBRUARY 1983)
01700 C      DEPARTMENT OF MECHANICAL ENGINEERING
01800 C      UNIVERSITY OF TEXAS AT ARLINGTON
01900 C      ARLINGTON, TEXAS 76019
02000 C
02100 C      INSERTED SECTIONS ARE INDICATED IN THE PROGRAM
02200 C
02300 C*** END OF INSERTED SECTION ** END OF INSERTED SECTION ***
02400 C
02500 C
02600 C .....
02700 C      CHAPTER      PRELIMINARIES
02800 C
02900 C      DIMENSION HEDC(4), HEDV(4), HEDW(4), HEDH(4), HEDT(4),
03000 C      HEDF(4), HEDL(4), HEDY(4), HEDZ(4), VANE(4), SWR(4),
03100 C      HEDCF(4), HEDCL(4), HEDCW(4), HEDCV(4), HEDCH(4),
03200 C      HEDCP(4), HEDCK(4), HEDCOL(4), HEDCDS(4)
03300 C      DIMENSION XAXES(10), SYMBOL(10)
03400 C      COMMON
03500 C      1/LEVEL/RECORG,NSWP,ORFV,DXFV(4),DXPW(4),DEW(4)
03600 C      2/VVEL/RECORG,NSWP,ORFV,DYFV(4),DYPW(4),DSW(4)
03700 C      3/XVEL/RECORG,NSWP,ORFW
03800 C      4/PCF/RECORG,NSWP,ORFW,DU(4,24),DV(4,24),IPRF,JPREF
03900 C      5/TE/RECORG,NSWP,ORFW
04000 C      6/TEIC/RECORG,NSWP,ORFW
04100 C      7/VAR/5(4,24),V(4,24),L(4,24),P(4,24),PR(4,24),
04200 C      STE(4,24),ST(4,24),STF(4,24),YOTL(4,24),OTVAL(4,24),
04300 C      IOTLR(4,24),VSTAR(4,24),WSTAR(4,24),FSTAR(4,24),
04400 C      STOTAR(4,24),YOTLW(4,24),VOTLR(4,24)
04500 C      8/WALL/IT,UT,LI,NU,NIN1,NIN2,CREAT,UTAX(4),UTAPR1(4)
04600 C      9/HEDV/1,2,3,4,X(4),Y(4),XPR(4),XPR2(4),DYP(4),YPR(4),
04700 C      B(4,24),DPR(4),XU(4),YU(4),P(4),PR(4),
04800 C      B(4,24),XPR(4),YPR(4),XPR2(4),YPR2(4),XOT(4),YOT(4),
04900 C      DYN(4),YOT(4)
05000 C      COMMON
05100 C      1/XFLURR/XFLURR,VIDOUL,CONCIT,FRANDT,DE(4,24),VID(4,24)
05200 C      2/XAGE/1/UNIT,TRIN,FRIN,FLUXIN,ALAYDA,
05300 C      3/OPALL,FLHAGD,ALI,ALD,USTEP,ISTEP,USTP,ISTP,1,ITM1
05400 C      4/ICF/XF(4,24),CD,CML,C1,C2,CAPPA,ELUC,HRED,HATE
05500 C      5/WALL/YFLUCN(4),XFLUCW(4),TAU(4),TAU(4)
05600 C      6/COEF/AR(4,24),AN(4,24),AC(4,24),AF(4,24),AW(4,24),
05700 C      7/OP(4,24)
05800 C      8/PLT/1/OTL,APLTL,APRIS,YSLPLT(10,4),XSLPLT(4),IPLOT
05900 C      LOGICAL INCALL,INCALV,INCALW,INCALP,INCALD,INCALC,INCALH,
06000 C      INCALA,INCALP,INCALC,INPLT,IXITE,IOIIM,IFRAD,INLIT,
06100 C      INITIAL,IFINL

```

```

06200 C
06300 C*** BEGINNING OF INSERTED SECTION ** BEGINNING OF INSERTED SECTION ***
06400 C
06500 COMMON /DROPS/ MAXPOR, NPORT,
06600 1 DRPDEN(10), DRPDIA(10), DRPMOUT(10), DRPERF(10),
06700 2 XDINIT(10), YDINIT(10), TDINIT(10), CDINIT(10), LDINIT(10),
06800 3 XB(50), YB(50),
06900 4 UB(40, 24), VB(40, 24), UBOLD(40, 24), VBOLD(40, 24),
07000 5 UBO, B-FAVX, GRAVY, HAD, RHOGAS, FI, UGAS, VGAS,
07100 6 ACOLD, YCOLD, TCOLD, SCOLD, DCOLD,
07200 7 XDNW, YDNW, TDNW, CDNW, VDNW,
07300 8 IT, OTING, STRED, ANGL,
07400 9 ISTEPR, INTCTR, IFLAGZ, I-IT, MAXSTE, MAXCT, I-T-LE,
07500 10 IC, UC, IV, UV, IO, OU, IB, UB, IBOLD, UBOLD, IOCNT,
07600 11 NCASE, NCASE, UDMAX(40), NDI, NCU
07700 COMMON /USE/ RNDMV(50,50), RNDVL(50,50)
07800
07900 C
08000 C*** END OF INSERTED SECTION ** END OF INSERTED SECTION ***
08100 C
08200 OPEN(UNIT=1, DEVICE='DCK:', FILE='FOR01.DAT', STATUS='OLD')
08300 C
08400 C***** ALL PRELIMINARY USER INPUTS ARE LOCATED HERE.....
08500 C
08600 DATA VAW /75.,45.,55.,60.,65.,65.,70./,
08700 BOWR/0.,.7,1.0,1.25,1.5,1.75,2.0/,
08800 DATA XAXIL /' X I' /
08900 DATA YAXIL /' Y I' /
09000 DATA XAXIC /' X I' /
09100 DATA YAXIC /' Y I' /
09200 C***** DEFINE UNDERFLOW FRACTION DECREASED, CALL TRAPD WHEN USING WATER IV
09300 C CALL TRAPD(1,1,4000)
09400 C----- GET INFLOT=TRUE, ONLY FOR STREAMLINE LINE PRINTER PLOT
09500 INFLOT=.FALSE.
09600 C----- GET IWRITE=TRUE, ONLY FOR WRITING SOLUTION ON DATA FILE
09700 IWRITE=.FALSE.
09800 C----- GET NONDIME=TRUE, ONLY FOR PRINTING DIMENSIONLESS SOLUTION
09900 NONDIME=.FALSE.
10000 C----- GET I-FADE=TRUE, ONLY FOR READING INITIAL GUESS OF ORCL
10100 I-FADE=.FALSE.
10200 C----- GET INITIAL=TRUE, ONLY FOR PRINTING INITIAL GUESS OF ORCL
10300 INITIAL=.FALSE.
10400 C----- GET IFIN=TRUE, ONLY FOR FINE GRID IN X DIRECTION
10500 IFIN=.FALSE.
10600 IF(.NOT. I-FADE) GO TO 110
10700 READ(10,*) X
10800 READ(10,*) Y
10900 100 CONTINUE
11000 NCOL= 11
11100 NROW= 1
11200 NLEN= 1
11300 NITER= 1
11400 NPRINT= NITER+30
11500 NPRINT= NITER+1
11600 LFL=1
11700 LFLMAX=1
11800 NORDER=
11900 MAXITER=1000
12000 C----- GET STATE=104 FOR MAXIT SPEC. FOR FORTHIN WIRE CAGED
12100 STATE= 1011
12200 IT= 40

```

```

12300      JT =24
12400      GREAT=1.E30
12500      NSWPU=4
12600      NSWPV=3
12700      NSWPW=3
12800      NSWPP=5
12900      NSWPK=3
13000      NSWPD=3
13100      READ(1,10) HEDU,HEDV,HEDW,HEDP,HEDT,HEDX,HEDC,HEDM,HEDL,
13200      1 HEDOF,HEDCOL,HEDOU,HEDOV,HEDOW,HEDOX,HEDCK,HEDCOL,HEDOV,
13300      210 FORMAT(9A4)
13400      C-----
13500      C--- CHAPTER 1 PARAMETERS AND PRELIMINARIES
13600      C
13700      C--- GRID
13800      ISTEP = 1
13900      JSTEP = 1
14000      INCOS= 0
14100      NJ=21
14200      NMI=NJ-1
14300      IOTF1=ISTEP+1
14400      IOTF1=JSTEP-1
14500      JOTF1=JSTEP+1
14600      JOTF1=JSTEP-1
14700      RLARGE=1.0E25
14800      ALTOT=0.375
14900      IF (IFINE) GO TO 120
15000      C--- COARSE MESH GRID LINES IN X-DIRECTION
15100      NI = 10
15200      NIMI = NI-1
15300      EPOX = 1.11
15400      IF (EPOX-1.) 13,12,13
15500      13 COMX=0.5*(EPOX** (NI-4) + (EPOX** (NI-3) -1.) / (EPOX-1.)) + .5
15600      GO TO 15
15700      12 CONTINUE
15800      COMX=NI-1
15900      14 CX=ALTOT/COMX
16000      X(1)=-.5*CX
16100      X(2)=X(1)
16200      DO 100 I = 3,NIMI
16300      X(I)=X(I-1)+CX
16400      100 CX=EPOX*CX
16500      X(NI)=X(NIMI)+((NIMI)-((NI-2)))
16600      X(21)=X(20)+(X(20)-X(1))
16700      X(22)=X(21)+(X(20)-X(1))
16800      X(23)=X(22)+(X(20)-X(1))
16900      NI=23
17000      NIMI = NI-1
17100      ALT = (X(21)+X(23))/2.
17200      ALI=0.5*(X(ISTEP)+X(IOTF1))
17300      ALL=ALTOT-ALI
17400      C----- FINE MESH GRID LINES IN X-DIRECTION
17500      IF (.NOT. IFINE) GO TO 130
17600      100 NI=30
17700      NIMI=NI-1
17800      EPOX=1.100
17900      IF (EPOX-1.) 17,16,17
18000      17 COMX=0.5*(EPOX** (NI-4) + (EPOX** (NI-3) -1.) / (EPOX-1.)) + 0.5
18100      GO TO 14
18200      16 CONTINUE
18300      COMX=NIMI-1

```



```

14400 1- DX = ALTOT/COMX
14500 X(1)=-3.5*DX
14600 X(2)=-X(1)
14700 DO 170 I=3,NIM1
14800 X(I)=X(I-1)+DX
14900 170 DX=EPDX*DX
15000 X(1)=X(NIM1)+(X(NIM1)-X(N1-1))
15100 DO 180 L=1,35
15200 1-0 X(L)=X(L-1)+(X(N1)-X(NIM1))
15300 N1 = 35
15400 NIM1=N1-1
15500 ALTOT=(X(NIM1)+X(N1))/2.0
15600 AL1 = 0.5*(X(INTER)+X(10TN1))
15700 AL2 = ALTOT-AL1
15800 C----- SPECIFY WALL CELLS (1-10-CELLS) OF COMBUSTOR
15900 C----- WALL FOR EACH I-PAID LINE
16000 150 CONTINUE
16100 DO 165 I=1,10
16200 UMAX(I)=50TSP
16300 UMAXP1(I)=0.5*UMAX(I)+1
16400 165 CONTINUE
16500 DO 168 I=11,N1
16600 UMAX(I)=100M1
16700 UMAXP1(I)=0
16800 168 CONTINUE
16900 C----- PAID LINE IN Y DIRECTION
17000 Y(1)=1.0E-5-2
17100 Y(2)=1.0E-5-3
17200 Y(3)=0.0E-5-2
17300 Y(4)=1.0E-5-2
17400 Y(5)=1.0E-5-2
17500 Y(6)=1.1E-5-2
17600 Y(7)=0.0E-5-2
17700 Y(8)=0.0E-5-2
17800 Y(9)=0.0E-5-2
17900 Y(10)=0.4E-5-2
18000 Y(11)=0.7E-5-2
18100 Y(12)=0.0E-5-2
18200 Y(13)=0.0E-5-2
18300 Y(14)=0.0E-5-2
18400 Y(15)=0.0E-5-2
18500 Y(16)=0.0E-5-2
18600 Y(17)=0.0E-5-2
18700 Y(18)=0.0E-5-2
18800 Y(19)=0.0E-5-2
18900 Y(20)=0.0E-5-2
19000 Y(21)=0.0E-5-2
19100 Y(22)=0.0E-5-2
19200 Y(23)=0.0E-5-2
19300 Y(24)=0.0E-5-2
19400 Y(25)=0.0E-5-2
19500 Y(26)=0.0E-5-2
19600 Y(27)=0.0E-5-2
19700 Y(28)=0.0E-5-2
19800 Y(29)=0.0E-5-2
19900 Y(30)=0.0E-5-2
20000 Y(31)=0.0E-5-2
20100 Y(32)=0.0E-5-2
20200 Y(33)=0.0E-5-2
20300 Y(34)=0.0E-5-2
20400 Y(35)=0.0E-5-2
20500 Y(36)=0.0E-5-2
20600 Y(37)=0.0E-5-2
20700 Y(38)=0.0E-5-2
20800 Y(39)=0.0E-5-2
20900 Y(40)=0.0E-5-2
21000 Y(41)=0.0E-5-2
21100 Y(42)=0.0E-5-2
21200 Y(43)=0.0E-5-2
21300 Y(44)=0.0E-5-2
21400 Y(45)=0.0E-5-2
21500 Y(46)=0.0E-5-2
21600 Y(47)=0.0E-5-2
21700 Y(48)=0.0E-5-2
21800 Y(49)=0.0E-5-2
21900 Y(50)=0.0E-5-2
22000 Y(51)=0.0E-5-2
22100 Y(52)=0.0E-5-2
22200 Y(53)=0.0E-5-2
22300 Y(54)=0.0E-5-2
22400 Y(55)=0.0E-5-2
22500 Y(56)=0.0E-5-2
22600 Y(57)=0.0E-5-2
22700 Y(58)=0.0E-5-2
22800 Y(59)=0.0E-5-2
22900 Y(60)=0.0E-5-2
23000 Y(61)=0.0E-5-2
23100 Y(62)=0.0E-5-2
23200 Y(63)=0.0E-5-2
23300 Y(64)=0.0E-5-2
23400 Y(65)=0.0E-5-2
23500 Y(66)=0.0E-5-2
23600 Y(67)=0.0E-5-2
23700 Y(68)=0.0E-5-2
23800 Y(69)=0.0E-5-2
23900 Y(70)=0.0E-5-2
24000 Y(71)=0.0E-5-2
24100 Y(72)=0.0E-5-2
24200 Y(73)=0.0E-5-2
24300 Y(74)=0.0E-5-2
24400 Y(75)=0.0E-5-2

```

```

24500 C1=1.49
24600 C2=1.31
24700 CAPPA=0.4147
24800 ELUG=0.773
24900 PREDEFAPPA=CAPPA/((C2-C1)/(C1+0.001))
25000 PRTE=1.0
25100 C----- BOUNDARY VALUES
25200 C1=0.0
25300 CLAR=0.0*(C2+0.001)/(C1+0.001)
25400 TURN=0.0
25500 TEIN=0.0*(C2+0.001)/(C1+0.001)
25600 ALAMDA=0.0
25700 EDIN=0.0*(C2+0.001)/(C1+0.001)
25800 VIGOR=0.0
25900 C----- PRELIMINARY CALCULATION
26000 IPREF=
26100 JPREF=
26200 C----- PRELIMINARY CALCULATION
26300 IM=0.0
26400 JMW=
26500 CORN=0.0
26600 C
26700 C-----
26800 C
26900 CALL INIT
27000 C----- INITIALIZE ALL VARIABLES AND INITIALIZE
27100 C1=0.0
27200 XND(1)=XND(1)/(C2+0.001)
27300 XND(1)=XND(1)/(C2+0.001)
27400 C1=0.0
27500 XND(1)=XND(1)/(C2+0.001)
27600 YND(1)=YND(1)/(C2+0.001)
27700 C----- INITIALIZE VARIABLE FIELD
27800 FLU=0.0
27900 ARD=0.0
28000 ARD=0.0
28100 XND(1)=0.0
28200 YND(1)=0.0
28300 ARD=0.0
28400 C
28500 C----- INITIAL WIND VELOCITY FIELD
28600 C
28700 C----- INITIAL WIND VELOCITY FIELD
28800 WIND=0.0*(C2+0.001)/(C1+0.001)
28900 C1=0.0
29000 W(1,0)=W(1,0)/(C2+0.001)
29100 C----- INITIAL WIND VELOCITY FIELD
29200 C----- INITIAL WIND VELOCITY FIELD
29300 IF(C1+0.001) THEN
29400 C----- INITIAL WIND VELOCITY FIELD
29500 WIND=0.0*(C2+0.001)/(C1+0.001)
29600 C1=0.0
29700 W(1,0)=W(1,0)/(C2+0.001)
29800 C----- INITIAL WIND VELOCITY FIELD
29900 C----- INITIAL WIND VELOCITY FIELD
30000 C1=0.0
30100 C(1,0)=0.0
30200 F(1,0)=0.0
30300 ST(1,0)=0.0
30400 AND WIND*(C1+0.001) = W(2,0)*(C1+0.001)
30500 XND(1)=XND(1)/(C2+0.001)

```

```

30600      AMOMIN = AMOMIN + ARDFM * L(2,0) * W(1,0)
30700      ANGMOM = ANGMOM + ARDFM * L(2,0) * W(1,0) * R(0)
30800      ANCENT = ANCENT + ARDFM
30900      FLOWIN = FLOWIN + ARDFM * L(1,0)
31000      UMEIN = FLOWIN / ARDFM
31100      UMEOUT = ANGMOM / (AMOMIN + AMOUL)
31200      IF (W(1,0,100) .LT. 1.0) AMOMIN = 1.0
31300      UO = UO + FLOWIN
31400      IC = UMARF(1-1)
31500      FACTOR = (Y(1,0,100) + W(1,0,100)) / (W(1,0) + W(1,0))
31600      UO = UMARF(1-1)
31700      OI = OI + FLOWIN
31800      L(1,0) = OI * FACTOR
31900      CONTINUE
32000
32100      IF (OIN .GT. 0.0) GO TO 32200
32200      GO TO 32300
32300      OI = OI + A(1)
32400      UO = UO + FLOWIN
32500      W(1,0) = W(1,0) / (1.0 + W(1,0) * (1.0))
32600      W(1,0) = W(1,0) * (1.0 / (1.0))
32700      T(1,0) = T(1,0)
32800      S(1,0) = S(1,0)
32900      GO TO 33000
33000      CONTINUE
33100      OI = OI + A(1)
33200      UO = UO + FLOWIN
33300      T(1,0) = T(1,0)
33400      S(1,0) = S(1,0)
33500      GO TO 33600
33600      CONTINUE
33700      OI = OI + A(1)
33800      UO = UO + FLOWIN
33900      T(1,0) = T(1,0)
34000      S(1,0) = S(1,0)
34100      GO TO 34200
34200      OI = OI + A(1)
34300      UO = UO + FLOWIN
34400      T(1,0) = T(1,0)
34500      S(1,0) = S(1,0)
34600      IF (OIN .GT. 0.0) GO TO 34700
34700      GO TO 34800
34800      CONTINUE
34900      OI = OI + A(1)
35000      UO = UO + FLOWIN
35100      T(1,0) = T(1,0)
35200      S(1,0) = S(1,0)
35300      IF (OIN .GT. 0.0) GO TO 35400
35400      GO TO 35500
35500      CONTINUE
35600      OI = OI + A(1)
35700      UO = UO + FLOWIN
35800      T(1,0) = T(1,0)
35900      S(1,0) = S(1,0)
36000      IF (OIN .GT. 0.0) GO TO 36100
36100      GO TO 36200
36200      CONTINUE
36300      OI = OI + A(1)
36400      UO = UO + FLOWIN
36500      T(1,0) = T(1,0)
36600      S(1,0) = S(1,0)
36700      IF (OIN .GT. 0.0) GO TO 36800
36800      GO TO 36900
36900      CONTINUE
37000      OI = OI + A(1)
37100      UO = UO + FLOWIN
37200      T(1,0) = T(1,0)
37300      S(1,0) = S(1,0)
37400      IF (OIN .GT. 0.0) GO TO 37500
37500      GO TO 37600
37600      CONTINUE
37700      OI = OI + A(1)
37800      UO = UO + FLOWIN
37900      T(1,0) = T(1,0)
38000      S(1,0) = S(1,0)
38100      IF (OIN .GT. 0.0) GO TO 38200
38200      GO TO 38300
38300      CONTINUE
38400      OI = OI + A(1)
38500      UO = UO + FLOWIN
38600      T(1,0) = T(1,0)
38700      S(1,0) = S(1,0)
38800      IF (OIN .GT. 0.0) GO TO 38900
38900      GO TO 39000
39000      CONTINUE
39100      OI = OI + A(1)
39200      UO = UO + FLOWIN
39300      T(1,0) = T(1,0)
39400      S(1,0) = S(1,0)
39500      IF (OIN .GT. 0.0) GO TO 39600
39600      GO TO 39700
39700      CONTINUE
39800      OI = OI + A(1)
39900      UO = UO + FLOWIN
40000      T(1,0) = T(1,0)
40100      S(1,0) = S(1,0)
40200      IF (OIN .GT. 0.0) GO TO 40300
40300      GO TO 40400
40400      CONTINUE
40500      OI = OI + A(1)
40600      UO = UO + FLOWIN
40700      T(1,0) = T(1,0)
40800      S(1,0) = S(1,0)
40900      IF (OIN .GT. 0.0) GO TO 41000
41000      GO TO 41100
41100      CONTINUE
41200      OI = OI + A(1)
41300      UO = UO + FLOWIN
41400      T(1,0) = T(1,0)
41500      S(1,0) = S(1,0)
41600      IF (OIN .GT. 0.0) GO TO 41700
41700      GO TO 41800
41800      CONTINUE
41900      OI = OI + A(1)
42000      UO = UO + FLOWIN
42100      T(1,0) = T(1,0)
42200      S(1,0) = S(1,0)
42300      IF (OIN .GT. 0.0) GO TO 42400
42400      GO TO 42500
42500      CONTINUE
42600      OI = OI + A(1)
42700      UO = UO + FLOWIN
42800      T(1,0) = T(1,0)
42900      S(1,0) = S(1,0)
43000      IF (OIN .GT. 0.0) GO TO 43100
43100      GO TO 43200
43200      CONTINUE
43300      OI = OI + A(1)
43400      UO = UO + FLOWIN
43500      T(1,0) = T(1,0)
43600      S(1,0) = S(1,0)
43700      IF (OIN .GT. 0.0) GO TO 43800
43800      GO TO 43900
43900      CONTINUE
44000      OI = OI + A(1)
44100      UO = UO + FLOWIN
44200      T(1,0) = T(1,0)
44300      S(1,0) = S(1,0)
44400      IF (OIN .GT. 0.0) GO TO 44500
44500      GO TO 44600
44600      CONTINUE
44700      OI = OI + A(1)
44800      UO = UO + FLOWIN
44900      T(1,0) = T(1,0)
45000      S(1,0) = S(1,0)
45100      IF (OIN .GT. 0.0) GO TO 45200
45200      GO TO 45300
45300      CONTINUE
45400      OI = OI + A(1)
45500      UO = UO + FLOWIN
45600      T(1,0) = T(1,0)
45700      S(1,0) = S(1,0)
45800      IF (OIN .GT. 0.0) GO TO 45900
45900      GO TO 46000
46000      CONTINUE
46100      OI = OI + A(1)
46200      UO = UO + FLOWIN
46300      T(1,0) = T(1,0)
46400      S(1,0) = S(1,0)
46500      IF (OIN .GT. 0.0) GO TO 46600
46600      GO TO 46700
46700      CONTINUE
46800      OI = OI + A(1)
46900      UO = UO + FLOWIN
47000      T(1,0) = T(1,0)
47100      S(1,0) = S(1,0)
47200      IF (OIN .GT. 0.0) GO TO 47300
47300      GO TO 47400
47400      CONTINUE
47500      OI = OI + A(1)
47600      UO = UO + FLOWIN
47700      T(1,0) = T(1,0)
47800      S(1,0) = S(1,0)
47900      IF (OIN .GT. 0.0) GO TO 48000
48000      GO TO 48100
48100      CONTINUE
48200      OI = OI + A(1)
48300      UO = UO + FLOWIN
48400      T(1,0) = T(1,0)
48500      S(1,0) = S(1,0)
48600      IF (OIN .GT. 0.0) GO TO 48700
48700      GO TO 48800
48800      CONTINUE
48900      OI = OI + A(1)
49000      UO = UO + FLOWIN
49100      T(1,0) = T(1,0)
49200      S(1,0) = S(1,0)
49300      IF (OIN .GT. 0.0) GO TO 49400
49400      GO TO 49500
49500      CONTINUE
49600      OI = OI + A(1)
49700      UO = UO + FLOWIN
49800      T(1,0) = T(1,0)
49900      S(1,0) = S(1,0)
50000      IF (OIN .GT. 0.0) GO TO 50100
50100      GO TO 50200
50200      CONTINUE
50300      OI = OI + A(1)
50400      UO = UO + FLOWIN
50500      T(1,0) = T(1,0)
50600      S(1,0) = S(1,0)
50700      IF (OIN .GT. 0.0) GO TO 50800
50800      GO TO 50900
50900      CONTINUE
51000      OI = OI + A(1)
51100      UO = UO + FLOWIN
51200      T(1,0) = T(1,0)
51300      S(1,0) = S(1,0)
51400      IF (OIN .GT. 0.0) GO TO 51500
51500      GO TO 51600
51600      CONTINUE
51700      OI = OI + A(1)
51800      UO = UO + FLOWIN
51900      T(1,0) = T(1,0)
52000      S(1,0) = S(1,0)
52100      IF (OIN .GT. 0.0) GO TO 52200
52200      GO TO 52300
52300      CONTINUE
52400      OI = OI + A(1)
52500      UO = UO + FLOWIN
52600      T(1,0) = T(1,0)
52700      S(1,0) = S(1,0)
52800      IF (OIN .GT. 0.0) GO TO 52900
52900      GO TO 53000
53000      CONTINUE
53100      OI = OI + A(1)
53200      UO = UO + FLOWIN
53300      T(1,0) = T(1,0)
53400      S(1,0) = S(1,0)
53500      IF (OIN .GT. 0.0) GO TO 53600
53600      GO TO 53700
53700      CONTINUE
53800      OI = OI + A(1)
53900      UO = UO + FLOWIN
54000      T(1,0) = T(1,0)
54100      S(1,0) = S(1,0)
54200      IF (OIN .GT. 0.0) GO TO 54300
54300      GO TO 54400
54400      CONTINUE
54500      OI = OI + A(1)
54600      UO = UO + FLOWIN
54700      T(1,0) = T(1,0)
54800      S(1,0) = S(1,0)
54900      IF (OIN .GT. 0.0) GO TO 55000
55000      GO TO 55100
55100      CONTINUE
55200      OI = OI + A(1)
55300      UO = UO + FLOWIN
55400      T(1,0) = T(1,0)
55500      S(1,0) = S(1,0)
55600      IF (OIN .GT. 0.0) GO TO 55700
55700      GO TO 55800
55800      CONTINUE
55900      OI = OI + A(1)
56000      UO = UO + FLOWIN
56100      T(1,0) = T(1,0)
56200      S(1,0) = S(1,0)
56300      IF (OIN .GT. 0.0) GO TO 56400
56400      GO TO 56500
56500      CONTINUE
56600      OI = OI + A(1)
56700      UO = UO + FLOWIN
56800      T(1,0) = T(1,0)
56900      S(1,0) = S(1,0)
57000      IF (OIN .GT. 0.0) GO TO 57100
57100      GO TO 57200
57200      CONTINUE
57300      OI = OI + A(1)
57400      UO = UO + FLOWIN
57500      T(1,0) = T(1,0)
57600      S(1,0) = S(1,0)
57700      IF (OIN .GT. 0.0) GO TO 57800
57800      GO TO 57900
57900      CONTINUE
58000      OI = OI + A(1)
58100      UO = UO + FLOWIN
58200      T(1,0) = T(1,0)
58300      S(1,0) = S(1,0)
58400      IF (OIN .GT. 0.0) GO TO 58500
58500      GO TO 58600
58600      CONTINUE
58700      OI = OI + A(1)
58800      UO = UO + FLOWIN
58900      T(1,0) = T(1,0)
59000      S(1,0) = S(1,0)
59100      IF (OIN .GT. 0.0) GO TO 59200
59200      GO TO 59300
59300      CONTINUE
59400      OI = OI + A(1)
59500      UO = UO + FLOWIN
59600      T(1,0) = T(1,0)
59700      S(1,0) = S(1,0)
59800      IF (OIN .GT. 0.0) GO TO 59900
59900      GO TO 60000
60000      CONTINUE
60100      OI = OI + A(1)
60200      UO = UO + FLOWIN
60300      T(1,0) = T(1,0)
60400      S(1,0) = S(1,0)
60500      IF (OIN .GT. 0.0) GO TO 60600
60600      GO TO 60700
60700      CONTINUE
60800      OI = OI + A(1)
60900      UO = UO + FLOWIN
61000      T(1,0) = T(1,0)
61100      S(1,0) = S(1,0)
61200      IF (OIN .GT. 0.0) GO TO 61300
61300      GO TO 61400
61400      CONTINUE
61500      OI = OI + A(1)
61600      UO = UO + FLOWIN
61700      T(1,0) = T(1,0)
61800      S(1,0) = S(1,0)
61900      IF (OIN .GT. 0.0) GO TO 62000
62000      GO TO 62100
62100      CONTINUE
62200      OI = OI + A(1)
62300      UO = UO + FLOWIN
62400      T(1,0) = T(1,0)
62500      S(1,0) = S(1,0)
62600      IF (OIN .GT. 0.0) GO TO 62700
62700      GO TO 62800
62800      CONTINUE
62900      OI = OI + A(1)
63000      UO = UO + FLOWIN
63100      T(1,0) = T(1,0)
63200      S(1,0) = S(1,0)
63300      IF (OIN .GT. 0.0) GO TO 63400
63400      GO TO 63500
63500      CONTINUE
63600      OI = OI + A(1)
63700      UO = UO + FLOWIN
63800      T(1,0) = T(1,0)
63900      S(1,0) = S(1,0)
64000      IF (OIN .GT. 0.0) GO TO 64100
64100      GO TO 64200
64200      CONTINUE
64300      OI = OI + A(1)
64400      UO = UO + FLOWIN
64500      T(1,0) = T(1,0)
64600      S(1,0) = S(1,0)
64700      IF (OIN .GT. 0.0) GO TO 64800
64800      GO TO 64900
64900      CONTINUE
65000      OI = OI + A(1)
65100      UO = UO + FLOWIN
65200      T(1,0) = T(1,0)
65300      S(1,0) = S(1,0)
65400      IF (OIN .GT. 0.0) GO TO 65500
65500      GO TO 65600
65600      CONTINUE
65700      OI = OI + A(1)
65800      UO = UO + FLOWIN
65900      T(1,0) = T(1,0)
66000      S(1,0) = S(1,0)
66100      IF (OIN .GT. 0.0) GO TO 66200
66200      GO TO 66300
66300      CONTINUE
66400      OI = OI + A(1)
66500      UO = UO + FLOWIN
66600      T(1,0) = T(1,0)
66700      S(1,0) = S(1,0)
66800      IF (OIN .GT. 0.0) GO TO 66900
66900      GO TO 67000
67000      CONTINUE
67100      OI = OI + A(1)
67200      UO = UO + FLOWIN
67300      T(1,0) = T(1,0)
67400      S(1,0) = S(1,0)
67500      IF (OIN .GT. 0.0) GO TO 67600
67600      GO TO 67700
67700      CONTINUE
67800      OI = OI + A(1)
67900      UO = UO + FLOWIN
68000      T(1,0) = T(1,0)
68100      S(1,0) = S(1,0)
68200      IF (OIN .GT. 0.0) GO TO 68300
68300      GO TO 68400
68400      CONTINUE
68500      OI = OI + A(1)
68600      UO = UO + FLOWIN
68700      T(1,0) = T(1,0)
68800      S(1,0) = S(1,0)
68900      IF (OIN .GT. 0.0) GO TO 69000
69000      GO TO 69100
69100      CONTINUE
69200      OI = OI + A(1)
69300      UO = UO + FLOWIN
69400      T(1,0) = T(1,0)
69500      S(1,0) = S(1,0)
69600      IF (OIN .GT. 0.0) GO TO 69700
69700      GO TO 69800
69800      CONTINUE
69900      OI = OI + A(1)
70000      UO = UO + FLOWIN
70100      T(1,0) = T(1,0)
70200      S(1,0) = S(1,0)
70300      IF (OIN .GT. 0.0) GO TO 70400
70400      GO TO 70500
70500      CONTINUE
70600      OI = OI + A(1)
70700      UO = UO + FLOWIN
70800      T(1,0) = T(1,0)
70900      S(1,0) = S(1,0)
71000      IF (OIN .GT. 0.0) GO TO 71100
71100      GO TO 71200
71200      CONTINUE
71300      OI = OI + A(1)
71400      UO = UO + FLOWIN
71500      T(1,0) = T(1,0)
71600      S(1,0) = S(1,0)
71700      IF (OIN .GT. 0.0) GO TO 71800
71800      GO TO 71900
71900      CONTINUE
72000      OI = OI + A(1)
72100      UO = UO + FLOWIN
72200      T(1,0) = T(1,0)
72300      S(1,0) = S(1,0)
72400      IF (OIN .GT. 0.0) GO TO 72500
72500      GO TO 72600
72600      CONTINUE
72700      OI = OI + A(1)
72800      UO = UO + FLOWIN
72900      T(1,0) = T(1,0)
73000      S(1,0) = S(1,0)
73100      IF (OIN .GT. 0.0) GO TO 73200
73200      GO TO 73300
73300      CONTINUE
73400      OI = OI + A(1)
73500      UO = UO + FLOWIN
73600      T(1,0) = T(1,0)
73700      S(1,0) = S(1,0)
73800      IF (OIN .GT. 0.0) GO TO 73900
73900      GO TO 74000
74000      CONTINUE
74100      OI = OI + A(1)
74200      UO = UO + FLOWIN
74300      T(1,0) = T(1,0)
74400      S(1,0) = S(1,0)
74500      IF (OIN .GT. 0.0) GO TO 74600
74600      GO TO 74700
74700      CONTINUE
74800      OI = OI + A(1)
74900      UO = UO + FLOWIN
75000      T(1,0) = T(1,0)
75100      S(1,0) = S(1,0)
75200      IF (OIN .GT. 0.0) GO TO 75300
75300      GO TO 75400
75400      CONTINUE
75500      OI = OI + A(1)
75600      UO = UO + FLOWIN
75700      T(1,0) = T(1,0)
75800      S(1,0) = S(1,0)
75900      IF (OIN .GT. 0.0) GO TO 76000
76000      GO TO 76100
76100      CONTINUE
76200      OI = OI + A(1)
76300      UO = UO + FLOWIN
76400      T(1,0) = T(1,0)
76500      S(1,0) = S(1,0)
76600      IF (OIN .GT. 0.0) GO TO 76700
76700      GO TO 76800
76800      CONTINUE
76900      OI = OI + A(1)
77000      UO = UO + FLOWIN
77100      T(1,0) = T(1,0)
77200      S(1,0) = S(1,0)
77300      IF (OIN .GT. 0.0) GO TO 77400
77400      GO TO 77500
77500      CONTINUE
77600      OI = OI + A(1)
77700      UO = UO + FLOWIN
77800      T(1,0) = T(1,0)
77900      S(1,0) = S(1,0)
78000      IF (OIN .GT. 0.0) GO TO 78100
78100      GO TO 78200
78200      CONTINUE
78300      OI = OI + A(1)
78400      UO = UO + FLOWIN
78500      T(1,0) = T(1,0)
78600      S(1,0) = S(1,0)
78700      IF (OIN .GT. 0.0) GO TO 78800
78800      GO TO 78900
78900      CONTINUE
79000      OI = OI + A(1)
79100      UO = UO + FLOWIN
79200      T(1,0) = T(1,0)
79300      S(1,0) = S(1,0)
79400      IF (OIN .GT. 0.0) GO TO 79500
79500      GO TO 79600
79600      CONTINUE
79700      OI = OI + A(1)
79800      UO = UO + FLOWIN
79900      T(1,0) = T(1,0)
80000      S(1,0) = S(1,0)

```

```

36700      WRITE(1,*)XEND
36800      237 CONTINUE
36900      IF(.NOT.IREAD) GO TO 238
37000      READ(12,*) U
37100      READ(12,*) V
37200      READ(12,*) W
37300      READ(12,*) P
37400      READ(12,*) TE
37500      READ(12,*) EC
37600      READ(12,*) VIC
37700      READ(12,*) CTEN
37800      238 CONTINUE
37900      IF(.NOT. INITIAL) GO TO 239
38000      IF(INCAL) CALL PRINT(1,1,M,N,IT,UT,X,Y,Z,HELD)
38100      IF(INCAL) CALL PRINT(1,1,M,N,IT,UT,X,Y,Z,HELD)
38200      IF(INCAL) CALL PRINT(1,1,M,N,IT,UT,X,Y,Z,HELD)
38300      IF(INCAL) CALL PRINT(1,1,M,N,IT,UT,X,Y,Z,HELD)
38400      IF(INCAL) CALL PRINT(1,1,M,N,IT,UT,X,Y,Z,HELD)
38500      239 CONTINUE
38600      C
38700      C*** BEGINNING OF INCRPTD SECTION *** BEGINNING OF INCRPTD COPY ***
38800      C
38900      C      Initialize RYMC and RYCM.
39000      C      DO 1000 I = 1, NI
39100      C      DO 1000 J = 1, NJ
39200      C      RYMC(I, J) = 0.
39300      C      RYCM(I, J) = 0.0
39400      1000 CONTINUE
39500      C
39600      C      Input the liquid data.
39700      C      DATA = 1
39800      C      IF (.DATA .EQ. 0) THEN
39900      C      To only the gas phase calculations.
40000      C      DATA = 0
40100      C      ELSE IF (.DATA .EQ. 1) THEN
40200      C      Input the data from the section 1.
40300      C      WRITE(1,*) 'INPUT THE NUMBER OF PHASE'
40400      C      READ(1,*) NPHASE
40500      C      DO 1100 I = 1, NPHASE
40600      C      WRITE(1,*) 'INPUT THE LIQUID DENSITY'
40700      C      WRITE(1,*) 'INPUT THE LIQUID VISCOSITY'
40800      C      READ(1,*) RHO_L
40900      C      WRITE(1,*) 'INPUT THE LIQUID THERMAL CONDUCTIVITY'
41000      C      READ(1,*) K_L
41100      C      WRITE(1,*) 'INPUT THE INITIAL LIQUID VELOCITY OF PHASE'
41200      C      READ(1,*) U_L
41300      C      WRITE(1,*) 'INPUT THE INITIAL LIQUID VELOCITY OF PHASE'
41400      C      READ(1,*) V_L
41500      C      WRITE(1,*) 'INPUT THE INITIAL LIQUID VELOCITY OF PHASE'
41600      C      READ(1,*) W_L
41700      C      WRITE(1,*) 'INPUT THE INITIAL LIQUID VELOCITY OF PHASE'
41800      C      READ(1,*) P_L
41900      C      WRITE(1,*) 'INPUT THE INITIAL LIQUID VELOCITY OF PHASE'
42000      C      READ(1,*) TE_L
42100      C      WRITE(1,*) 'INPUT THE LIQUID VAPOR PRESSURE'
42200      C      READ(1,*) PVP
42300      1100 CONTINUE
42400      C
42500      C      ELSE IF (.DATA .EQ. 2) THEN
42600      C      Input data from a file.
42700      C      READ(1,*) NAME

```

```

42800      DO 1200 NPORT = 1, MAXPOR
42900          READ (21, *) DRPCEN(NPORT), DRPCIA(NPORT), XINIT(NPORT),
43000      $      YINIT(NPORT), IZINIT(NPORT),
43100      $      UZINIT(NPORT), VZINIT(NPORT), DRPCUT(NPORT)
43200      1200      CONTINUE
43300      C
43400      IF (NDATA .EQ. 1) THEN
43500      C          Input data in the program.
43600          MAXPOR = 1
43700          DRPCEN(1) = 700.0
43800          DRPCIA(1) = 0.0000E
43900          XINIT(1) = 0.0
44000          YINIT(1) = 0.0
44100          IZINIT(1) = 0.0
44200          UZINIT(1) = 10.0
44300          VZINIT(1) = 0.0
44400          DRPCUT(1) = 1.0E0500E
44500      ENDIF
44600      C
44700      C
44800      C          Initialize  $\alpha$ ,  $\gamma$ , and  $\beta$  max.
44900       $\alpha$  = 1.1
45000       $\gamma$  = 1.0
45100      DO 1300 I = 1, NPT
45200           $\alpha$ (I + 1) = 1.0 +  $\alpha$ (I)
45300           $\gamma$ (I + 1) =  $\gamma$ (I) + 1
45400           $\beta$ MAX(I) =  $\beta$ MAX(1)
45500      1300      CONTINUE
45600      C
45700      C           $\alpha$ (0 + 1) = 1.0
45800       $\alpha$ (0 + 1) =  $\alpha$ (0)
45900      1400      CONTINUE
46000      C
46100      C          Initialize fluxes and counters.
46200      MAXCT = 0
46300      MAXACT = 1
46400      IZCNT = 0
46500      IZLNG = 0
46600      IZTOT = 0
46700      IZTOTL = 0
46800      C
46900      C          Store input data from a file.
47000      WRITE (1, *) MAXPOR
47100      DO 1500 NPORT = 1, MAXPOR
47200          WRITE (1, *) DRPCEN(NPORT), DRPCIA(NPORT),
47300      $      XINIT(NPORT), YINIT(NPORT), IZINIT(NPORT),
47400      $      UZINIT(NPORT), VZINIT(NPORT), DRPCUT(NPORT)
47500      1500      CONTINUE
47600      C
47700      C
47800      C          Initialize  $\alpha$ .
47900       $\alpha$ (1) = 1.0
48000      DO 1600 I = 1, NPT
48100           $\alpha$ (I + 1) =  $\alpha$ (I) + 1
48200      1600      CONTINUE
48300      1800      CONTINUE
48400      C
48500      C          Initialize time step and scale factors.
48600      TSC = 1.0
48700      DTSC = 1.0
48800      DTSC = 1.0

```

```

44900      1
44900      1      Assign gravity and drag term values.
44910      1      GCD = 0.00
44920      1      G-AYX = 0.0
44930      1      G-AYY = 0.0
44940      1      P1 = 1.141594E-
44950      1      H0DA = 1.17E-17
44960      1
44970      1      Calculate the local frequency.
44980      1      W = 17.01 * WCHT * 1.0 * WAB * 0.5
44990      1      H-CL = H-CL1 * (H-CL1 - 1) / 1.0
50000      1      H-CL = H-CL1 * (H-CL1 - 1) / 1.0
50100      1      H-CL = H-CL1 * (H-CL1 - 1) / 1.0
50200      1      H-CL = H-CL1 * (H-CL1 - 1) / 1.0
50300      1      H-CL = H-CL1 * (H-CL1 - 1) / 1.0
50400      1
50500      1      Returns three if total convergence is not achieved,
50600      1      to start a new iteration.
50700      1      CONTINUE
50800      1
50900      1      *** END OF SUBROUTINE ***
51000      1
51100      1      H-CL = H-CL1
51200      1      H-CL = H-CL1
51300      1      H-CL = H-CL1
51400      1      H-CL = H-CL1
51500      1      H-CL = H-CL1
51600      1      H-CL = H-CL1
51700      1      H-CL = H-CL1
51800      1      H-CL = H-CL1
51900      1      H-CL = H-CL1
52000      1      H-CL = H-CL1
52100      1      H-CL = H-CL1
52200      1      H-CL = H-CL1
52300      1      H-CL = H-CL1
52400      1      H-CL = H-CL1
52500      1      H-CL = H-CL1
52600      1      H-CL = H-CL1
52700      1      H-CL = H-CL1
52800      1      H-CL = H-CL1
52900      1      H-CL = H-CL1
53000      1      H-CL = H-CL1
53100      1      H-CL = H-CL1
53200      1      H-CL = H-CL1
53300      1      H-CL = H-CL1
53400      1      H-CL = H-CL1
53500      1      H-CL = H-CL1
53600      1      H-CL = H-CL1
53700      1      H-CL = H-CL1
53800      1      H-CL = H-CL1
53900      1      H-CL = H-CL1
54000      1      H-CL = H-CL1
54100      1      H-CL = H-CL1
54200      1      H-CL = H-CL1
54300      1      H-CL = H-CL1
54400      1      H-CL = H-CL1
54500      1      H-CL = H-CL1
54600      1      H-CL = H-CL1
54700      1      H-CL = H-CL1
54800      1      H-CL = H-CL1
54900      1      H-CL = H-CL1

```

```

55000 IF (HSCORE .LT. .01E+0) CREFE0.5E
55100 430 CONTINUE
55200 C----- UPDATE MAIN DEPENDENT VARIABLES
55300 IF (INCAL0) CALL CAL00
55400 IF (INCAL1) CALL CAL01
55500 IF (INCALP) CALL CAL0P
55600 IF (INCALW) CALL CAL0W
55700 IF (INCALX) CALL CAL0XF
55800 IF (INCALD) CALL CAL0CD
55900 C----- UPDATE FLUID PROPERTIES
56000 IF (INPR0) CALL PR00
56100 C----- INTERMEDIATE OUTPUT
56200 RECDRM = RECDRM/FLW00
56300 RECDUR = RECDUR/AMON0
56400 RECDV = RECDV/AMON0
56500 RECDW = RECDW/AMON0
56600 RECDRK = RECDRK/(1.0*FLW00*MEAN*MEAN)
56700 IF (WITHIN(10,1000000) GO TO 300
56800 PRINT 1, I, INT0
56900 WRITE (10) INT0, RECD, RECDUR, RECDV, RECDW, RECDRK,
7000 RECDRE, (10,1000000), V(IM,N,UMON), W(IMC,N,UMC), P(IMD,N,UNI),
7100 ALL(IM,N,UMON)
7200 IF (WITHIN(10,1000000) GO TO 300
7300 IF (INCAL0) CALL PRINT(1,1,1,NO,IT,UT,AY,Y,RECD)
7400 IF (INCAL1) CALL PRINT(1,1,1,NO,IT,UT,AY,Y,RECDV)
7500 IF (INCALW) CALL PRINT(1,1,1,NO,IT,UT,AY,Y,RECDW)
7600 IF (INCALP) CALL PRINT(1,1,1,NO,IT,UT,AY,Y,RECDP)
7700 IF (INCALD) CALL PRINT(1,1,1,NO,IT,UT,AY,Y,RECDRE)
7800 PRINT 1, I, INT0
7900 WRITE (10) IM,UMON
8000 500 CONTINUE
8100 C----- INTERMEDIATE INPUT
8200 RECDRM = RECDRM*(1.0+RECDUR*RECDV*RECDW*RECDRK)
8300 RECDUR = RECDUR*(1.0+RECDV)
8400 RECDV = RECDV*(1.0+RECDW*RECDRK)
8500 RECDW = RECDW*(1.0+RECDRK)
8600 RECDRK = RECDRK*(1.0+RECDRE)
8700 RECDRE = RECDRE*(1.0+RECDRE)
8800 C-----
8900 C-----
9000 C-----
9100 C-----
9200 C-----
9300 C-----
9400 C-----
9500 C-----
9600 C-----
9700 C-----
9800 C-----
9900 C-----
10000 C-----
10100 C-----
10200 C-----
10300 C-----
10400 C-----
10500 C-----
10600 C-----
10700 C-----
10800 C-----
10900 C-----
11000 C-----
11100 C-----
11200 C-----
11300 C-----
11400 C-----
11500 C-----
11600 C-----
11700 C-----
11800 C-----
11900 C-----
12000 C-----
12100 C-----
12200 C-----
12300 C-----
12400 C-----
12500 C-----
12600 C-----
12700 C-----
12800 C-----
12900 C-----
13000 C-----
13100 C-----
13200 C-----
13300 C-----
13400 C-----
13500 C-----
13600 C-----
13700 C-----
13800 C-----
13900 C-----
14000 C-----
14100 C-----
14200 C-----
14300 C-----
14400 C-----
14500 C-----
14600 C-----
14700 C-----
14800 C-----
14900 C-----
15000 C-----
15100 C-----
15200 C-----
15300 C-----
15400 C-----
15500 C-----
15600 C-----
15700 C-----
15800 C-----
15900 C-----
16000 C-----
16100 C-----
16200 C-----
16300 C-----
16400 C-----
16500 C-----
16600 C-----
16700 C-----
16800 C-----
16900 C-----
17000 C-----
17100 C-----
17200 C-----
17300 C-----
17400 C-----
17500 C-----
17600 C-----
17700 C-----
17800 C-----
17900 C-----
18000 C-----
18100 C-----
18200 C-----
18300 C-----
18400 C-----
18500 C-----
18600 C-----
18700 C-----
18800 C-----
18900 C-----
19000 C-----
19100 C-----
19200 C-----
19300 C-----
19400 C-----
19500 C-----
19600 C-----
19700 C-----
19800 C-----
19900 C-----
20000 C-----

```

```

61100 IF (INCALW) CALL PRINT(1,1,NI,NJ,IT,UT,X,Y,W,HECW)
61200 IF (INCALP) CALL PRINT(1,1,NI,NJ,IT,UT,X,Y,P,HECP)
61300 IF (INCALP) CALL PRINT(1,1,NI,NJ,IT,UT,X,Y,P,HECP)
61400 IF (INCALK) CALL PRINT(1,1,NI,NJ,IT,UT,X,Y,TE,HECK)
61500 IF (INCALS) CALL PRINT(1,1,NI,NJ,IT,UT,X,Y,EL,HECD)
61600 IF (INCALS) CALL PRINT(1,1,NI,NJ,IT,UT,X,Y,EL,HECD)
61700 IF (INCALS) CALL PRINT(1,1,NI,NJ,IT,UT,X,Y,STEN,HECE)
61800 IF (NOT. NONDIM) GO TO 750
61900 IF (INCALU) CALL PRINT(1,1,NI,NJ,IT,UT,XND,YND,USTAR,HECDU)
62000 IF (INCALV) CALL PRINT(1,1,NI,NJ,IT,UT,XND,YND,VSTAR,HECDV)
62100 IF (INCALW) CALL PRINT(1,1,NI,NJ,IT,UT,XND,YND,WSTAR,HECDW)
62200 IF (INCALS) CALL PRINT(1,1,NI,NJ,IT,UT,XND,YND,STVAL,YSTEND,HECDOL)
62300 IF (INCALP) CALL PRINT(1,1,NI,NJ,IT,UT,XND,YND,PSTAR,HECDP)
62400 IF (INCALK) CALL PRINT(1,1,NI,NJ,IT,UT,XND,YND,TESTAR,HECDK)
62500 IF (INCALK) CALL PRINT(5,2,NI,NJ,IT,UT,X,Y,SP,HEPL)
62600 IF (INCALK) CALL PRINT(1,1,NI,NJ,IT,UT,XND,YND,WSTAR,HECDVS)
62700 750 CONTINUE
62800 IF (NOT. IWRITE) GO TO 700
62900 WRITE(11,*) U
63000 WRITE(11,*) V
63100 WRITE(11,*) W
63200 WRITE(11,*) P
63300 WRITE(11,*) TE
63400 WRITE(11,*) EL
63500 WRITE(11,*) UIC
63600 WRITE(11,*) STEN
63700 WRITE(11,*) YSTEND
63800 700 CONTINUE
63900 C--- CALCULATION OF SHEAR STRESS COEFFICIENT ALONG LARGE DUCT WALL
64000 WRITE(11,*)
64100 DO 401 I=1,NIM1
64200 SHEAR-STRESS(I)=0.5*(U(I)-U(I+1))**2
64300 WRITE(11,*) I, SHEAR(I), DEC
64400 401 CONTINUE
64500 WRITE(11,*)
64600 C---- PLOT OF VISCERLESS STREAMLINES
64700 LATERR
64800 IF (INCALU .AND. INCALV) CALL PLOT(XOPLT,IT,VETS,XX=15,YOPLT,
64900 IMAX=10,PLTCL,YAXES,DY=0.1,LARGE)
65000 LATERR
65100 IF (INCALU .AND. INCALV) CALL PLOT(XOPLT,IT,VETS,XX=15,YOPLT,
65200 IMAX=10,PLTCL,YAXES,DY=0.1,LARGE)
65300 C---- PLOT INITIAL CONDITIONS FOR A OTHER SWIRL CASE
65400 IF (LEF .EQ. LEFTMAX) GO TO 404
65500 LEFTALF = 1
65600 LATERR
65700 J=1;ITER=1;N=0
65800 IF (ITER=1) ITER=1
65900 IF (LEF .EQ. 0) MAXITER = ITER+20
66000 IF (LEF .EQ. 0) GO TO 404
66100 WRITE(11,*) X=XOPLT/20.1+0.5*(XOPLT-LEF)*0.1
66200 X=XOPLT/20.1
66300 Y=XOPLT/20.1
66400 X=XOPLT/20.1
66500 Y=XOPLT/20.1
66600 X=XOPLT/20.1
66700 Y=XOPLT/20.1
66800 X=XOPLT/20.1
66900 Y=XOPLT/20.1
67000 X=XOPLT/20.1
67100 Y=XOPLT/20.1

```



```

67200      ANGMOM = 0.0
67300      WMONIN = 0.0
67400      C----- READ INITIAL GUESS OF NEXT SWIRL PROBLEM FROM
67500      C----- PREVIOUS SOLN. OF SIMILAR PROBLEM
67600      IF (.NOT. IREAD) GO TO 445
67700      READ(12,*) U
67800      READ(12,*) V
67900      READ(12,*) W
68000      READ(12,*) P
68100      READ(12,*) TE
68200      READ(12,*) FO
68300      READ(12,*) STEN
68400      445 CONTINUE
68500      DO 490 J=2, NSTEP
68600      ARDEN=C.5*(DEN(1,J)+DEN(2,J))+RHOV(J)*ONE(J)
68700      XMONIN=XMONIN+ARDEN*U(2,J)+U(2,J)
68800      WMONIN=WMONIN+ARDEN*U(2,J)+W(1,J)
68900      ANGMOM=ANGMOM+ARDEN*U(2,J)*W(1,J)*R(J)
69000      ARDENT=ARDEN*U(2,J)+ARDEN
69100      490 FLOWIN=FLOWIN+ARDEN*U(2,J)
69200      UMEAN=FLOWIN/XARDENT
69300      SWRLEN=ANGMOM/(XMONIN+XSMALL)
69400      IF(W(1,NSTEP).EQ.0.0) WMONIN = 1.0
69500      WRITE(13,10) IMON,UMON
69600      GO TO 300
69700      405 CONTINUE
69800      C
69900      C*** BEGINNING OF INSERTED SECTION ** BEGINNING OF INSERTED SECTION ***
70000      C
70100      IF (NDATA.EQ.0) THEN
70200      C      Liquid phase solution not required.
70300      STOP
70400      ENDIF
70500      C      Reassign gas velocities.
70600      DO 250 I = 1, NI
70700      DO 250 J = 1, NJ
70800      UGAS(I, J) = UG(I, J)
70900      VGS(I, J) = V(I, J)
71000      U(I, J) = U(I, J)
71100      V(I, J) = V(I, J)
71200      250 CONTINUE
71300      C
71400      C      Assign RHO and RHOV.
71500      DO 260 I = 1, NI
71600      DO 260 J = 1, NJ
71700      RHO(I, J) = 0.0
71800      RHOV(I, J) = 0.0
71900      260 CONTINUE
72000      C      Get the liquid phase solution.
72100      CALL LPHF
72200      IF (IFLASH.EQ.1) THEN
72300      C      The system has not converged globally so iterate again.
72400      IF (ITERP.GT. MAXIT) THEN
72500      WRITE(15,*) 'Global convergence not achieved ',
72600      $      'after 10 iterations for both phases.'
72700      STOP
72800      ENDIF
72900      NITER = 11
73000      NITER = N
73100      MAXIT = 10
73200      NITER = 0

```

```

73300      JPRINT = NITER + 300
73400      IPRINT = NITER + 1
73500      LFS = 1
73600      LFSMAX = 1
73700      NSHR = 0
73800      MAXIT = NITER + 250
73900      GOTO 2000
74000      ELSE
74100      C      System global convergence achieved.
74200      WRITE(0,312)
74300      WRITE(0,410) LFS,NGFR,SWR(LFS),VARE(LFS),SWRLNO,UMEAN,FLOWIN
74400      IF(INGALG) CALL PRINT(1,1,NI,NU,IT,UT,XL,YL,HECO)
74500      IF(INGALV) CALL PRINT(1,1,NI,NU,IT,UT,X,YV,V,HECV)
74600      IF(INGALW) CALL PRINT(1,1,NI,NU,IT,UT,X,Y,W,HECW)
74700      IF(INGALP) CALL PRINT(1,1,NI,NU,IT,UT,X,Y,P,HECP)
74800      IF(INGALR) CALL PRINT(1,1,NI,NU,IT,UT,X,Y,RF,HECR)
74900      IF(INGALK) CALL PRINT(1,1,NI,NU,IT,UT,X,Y,TE,HECK)
75000      IF(INGALL) CALL PRINT(1,1,NI,NU,IT,UT,X,Y,ED,HECD)
75100      IF(INGALO) CALL PRINT(1,1,NI,NU,IT,UT,XL,Y,OTEN,HECOF)
75200      IF(INGALS) CALL PRINT(1,1,NI,NU,IT,UT,XO,STVAL,YOTEN,HECLO)
75300      IF(.NOT. ACONDIM) GO TO 2750
75400      IF(INGALG) CALL PRINT(1,1,NI,NU,IT,UT,XUND,YND,USTAR,HECDL)
75500      IF(INGALV) CALL PRINT(1,1,NI,NU,IT,UT,XND,YVND,VSTAR,HECDV)
75600      IF(INGALW) CALL PRINT(1,1,NI,NU,IT,UT,XND,YND,WSTAR,HECDW)
75700      IF(INGALO) CALL PRINT(1,1,NI,NU,IT,UT,XUND,STVAL,YOTEND,HECDOL)
75800      IF(INGALP) CALL PRINT(1,1,NI,NU,IT,UT,XND,YND,PSTAR,HECDP)
75900      IF(INGALK) CALL PRINT(1,1,NI,NU,IT,UT,XND,YND,TESTAR,HECKK)
76000      IF(INGALK) CALL PRINT(5,2,NI,NU,IT,UT,X,Y,CF,HECKL)
76100      IF(INGALK) CALL PRINT(1,1,NI,NU,IT,UT,XND,YND,VISTAR,HECDVO)
76200      2750      CONTINUE
76300      STOP
76400      ENDIF
76500      C
76600      C--- END OF INSERTED SECTION ** END OF INSERTED SECTION ---
76700      C
76800      STOP
76900      C--- FORMAT STATEMENTS
77000      211 FORMAT(1H1,T37,'AXISYMMETRIC ISO-THERMAL, GT COMBUSTION CHAMBER
77100      FLOWFIELD SIMULATION',//T35,'USING THE STARSTEP APPROXIMATION,
77200      FOR THE CLIPPING EXPANSION WALL',//T53,'AND THE K-E TURBULENCE
77300      MODEL')
77400      225 FORMAT(///,T40,'EXPANSION ANGLE (DEG) =',T77,1PE13.3)
77500      230 FORMAT(///,T40,'NUMBER OF STARSTEP STEPS =',T61,I1)
77600      235 FORMAT(///,T40,'INLET RADIUS(M) =',T77,1PE13.3)
77700      240 FORMAT(///,T40,'COMBUSTOR RADIUS(M) =',T77,1PE13.3)
77800      245 FORMAT(///,T40,'COMBUSTOR LENGTH(M) =',T77,1PE13.3)
77900      250 FORMAT(///,T40,'INLET REYNOLDS NO.(USING DIAM) =',T77,1PE13.3)
78000      255 FORMAT(///,T40,'LAMINAR VISCOSITY(KG/M/SEC) =',T77,1PE13.3)
78100      260 FORMAT(///,T40,'DENSITY(KG/CC. M) =',T77,1PE13.3,////)
78200      310 FORMAT(13H1ITER = 0---, 1H1,2PHANOLUTE RESIDUAL SOURCE SUNG,FX,
78300      11H---1 1---,37H FIELD VALUES AT MONITORING LOCATION(,12,14,
78400      112,6H) ---12,14H NO ---, 1HUND,7X,1VMON,7X,1WMON,7X,1PMON,7X,
78500      1TKIN,7X,1HCOF,9X,1HC,9X,1HV,10X,1HW,10X,1HP,10X,1HD/)
78600      311 FORMAT(2X,14,11E11.4)
78700      312 FORMAT(1HC,59(2H-))
78800      402 FORMAT(///,7X,1H1,5X,3H//C,5X,1HC,C.COEFF.)
78900      403 FORMAT(//5X,15,C(1PE11.3))
79000      410 FORMAT(//13H SWIRL CASE WITH LFS = ,13/
79100      1H1 13H AND NSHR = ,13//
79200      13H CORRESPONDING IF NSHR = 1 TO SWIRL GENERATOR WITH SWIRL NUMBER =
79300      1,F10.1//17H OR IF NSHR = 0 TO SWIRL VANE ANGLE =,F10.1//

```

```

79400      $IX,'COMPUTED INLET SWIRL NUMBER=',F10.4//
79500      $IX,'COMPUTED INLET MEAN AXIAL VELOCITY =',F10.4//
79600      $IX,'COMPUTED INLET MASS FLOW RATE =',F10.5//)
79700      950 FORMAT(10X,6F10.5/,10X,6F10.5/,10X,4F10.5)
79800      960 FORMAT(15X,' THE SOLN. IS NOT CONVERGING')
79900      C      DEBUG UNIT(6),INIT(SUMX,EPSX,RLARGE,RSMALL,XMONIN,WMONIN,FLOWIN,
80000      C      $UMEAN,DENSIT,VISCO,UIIN), SUPCHK(ALL)
80100      END
80200      C
80300      C-----
80400      C
80500      SUBROUTINE INIT
80600      CA.....
80700      C
80800      CHAPTER      PRELIMINARIES
80900      C
81000      COMMON
81100      $/VEL/RESORW,NDWPW,URFW,CXEPW(4F),CXPW(4F),SEW(4F)
81200      $/VEL/RESORV,NDWPV,URFV,CYNPV(24),CYPV(24),SNSV(24)
81300      $/WVEL/RESORW,NDWPW,URFW
81400      $/PCOR/RESORW,NSWFP,URFP,DU(4F,24),DV(4F,24),IPRFF,URPFF
81500      $/VAR/U(4F,24),V(4F,24),W(4F,24),P(4F,24),PP(4F,24),
81600      $TE(4F,24),ED(4F,24),STFN(4F,24),YSTLN(4F,24),STVAL(24),
81700      $USTAR(4F,24),VSTAR(4F,24),WSTAR(4F,24),FSTAR(4F,24),
81800      $TESTAR(4F,24),YSTLNT(4F,24),VICTAR(4F,24)
81900      $/ALL/IT,UT,VI,VO,NIM1,NJM1,IGREAT,JMAX(4F),JMAXP1(4F)
82000      $/GEOM/INCCOS,X(4F),Y(24),CXEP(4F),CXPW(4F),CYP(24),CYPV(24),
82100      $   UNS(24),SEW(4F),XU(4F),YU(24),RU(24),RV(24),
82200      $   WFN(24),WFC(24),WFF(4F),WFW(4F),RCV(24),XUC(4F),XUNC(4F),
82300      $YND(24),YVND(24)
82400      COMMON
82500      $/FLUPR/URFV,IS,VISCO,DENSIT,FRANDT,DEN(4F,24),VIS(4F,24)
82600      $/KASE TI/UT,TEIN,EDI,FLOWIN,ALAMDA,
82700      $RSMALL,RLARGE,AL1,AL2,USTEP,ISTEP,USTP1,ISTP1,ISTM1
82800      $/TURB/SEW(4F,24),CO,CMU,C1,C2,CAPPA,ELUG,PRES,PSTE
82900      $/WALLF/YPLUG(4F),XPLUSW(24),TAUW(4F),TAUW(24)
83000      $/COEF/AF(4F,24),AN(4F,24),AS(4F,24),AE(4F,24),A(4F,24),SU(4F,24),
83100      $OP(4F,24)
83200      $/PLOT/YSTLN,PLTLN,NPTS,YOPLT(10,4F),XOPLT(4F),INPLOT
83300      C
83400      C      CHAPTER      1      CALCULATE GEOMETRICAL QUANTITIES
83500      C
83600      DO 100 J=1,NJ
83700      R(J) = Y(J)
83800      100 IF (INCCOS .EQ. 1) R(J) = 1.0
83900      CXPW(1) = 0.0
84000      CXEP(1) = 0.0
84100      DO 101 I = 1,NIM1
84200      CXEP(I) = X(I+1)-X(I)
84300      101 CXPW(I+1) = CXEP(I)
84400      CYPV(1) = 0.0
84500      CYNP(1) = 0.0
84600      DO 102 J = 1,NJM1
84700      CYNP(J) = Y(J+1)-Y(J)
84800      102 CYPV(J+1) = CYNP(J)
84900      SEW(1) = 0.0
85000      SEW(NI) = 0.0
85100      DO 103 I = 1,NIM1
85200      103 SEW(I) = 0.0*(CXEP(I)+CXPW(I))
85300      SNS(1) = 0.0
85400      SNS(NJ) = 0.0

```

```

85500      DO 104 J = 2,NUM1
85600      104 SNS(J) = 0.5*(CYNP(J)+CYPS(J))
85700      XU(1) = 0.0
85800      DO 105 I = 2,NI
85900      105 XU(I) = 0.5*(X(I)+X(I-1))
86000      DXPWU(1) = 0.0
86100      DXPWU(2) = 0.0
86200      DXEPU(1) = 0.0
86300      DXEPU(NI) = 0.0
86400      DO 106 I = 2,NIM1
86500      DXEPU(I) = XU(I+1)-XU(I)
86600      106 DXPWU(I+1) = DXEPU(I)
86700      SEWU(1) = 0.0
86800      DO 107 I = 2,NI
86900      107 SEWU(I) = X(I)-X(I-1)
87000      C----- U-VELOCITIES WEIGHTING FACTORS
87100      DO 111 I = 2,NIM1
87200      WFE(I) = SEWU(I+1)/(SEWU(I+1)+SEWU(I))
87300      IF (I .LE. 2) GO TO 111
87400      WFW(I) = SEWU(I-1)/(SEWU(I-1)+SEWU(I))
87500      111 CONTINUE
87600      YV(1) = 0.0
87700      RV(1) = 0.0
87800      DO 108 J = 2,NU
87900      RV(J) = 0.5*(R(J)+R(J-1))
88000      108 YV(J) = 0.5*(Y(J)+Y(J-1))
88100      RCY(1) = R(1)
88200      RCY(NU) = R(NU)
88300      DO 113 J=2,NUM1
88400      113 RCY(J) = 0.5*(RV(J+1)+RV(J))
88500      DYPSV(1) = 0.0
88600      DYPSV(2) = 0.0
88700      DYNPV(NU) = 0.0
88800      DO 109 J = 2,NUM1
88900      DYNPV(J) = YV(J+1)-YV(J)
89000      109 DYPSV(J+1) = DYNPV(J)
89100      SNSV(1) = 0.0
89200      DO 110 J = 2,NU
89300      SNSV(J) = Y(J)-Y(J-1)
89400      C----- V-VELOCITIES WEIGHTING FACTORS
89500      DO 112 J=3,NUM1
89600      WFSV(J) = SNSV(J+1)/(SNSV(J+1)+SNSV(J))
89700      WFSV(J) = SNSV(J-1)/(SNSV(J-1)+SNSV(J))
89800      112 CONTINUE
89900      C
90000      C-----CHAPTER 2 2 2 SET VARIABLES TO ZERO
90100      C
90200      DO 200 I = 1,NI
90300      TAU(I) = 1.0
90400      DO 200 J = 1,NU
90500      TAU(J) = 1.0
90600      U(I,J) = 0.0
90700      V(I,J) = 0.0
90800      W(I,J) = 0.0
90900      P(I,J) = 0.0
91000      PR(I,J) = 0.0
91100      TE(I,J) = 0.0
91200      ED(I,J) = 0.0
91300      DENS(I,J) = DENSIT
91400      VIS(I,J) = VISCUS
91500      DU(I,J) = 0.0

```

```

91600      DV(I,J) = 0.0
91700      SU(I,J) = 0.0
91800      SP(I,J) = 0.0
91900      STFN(I,J) = 0.0
92000      200 CONTINUE
92100      DO 300 I = 1,NI
92200      DO 300 J = 1,NSTLN
92300      YSTLN(I,J)=0.0
92400      YSTLND(I,J) = 0.0
92500      STVAL(J) = 0.0
92600      300 CONTINUE
92700      DO 400 N = 1,NPLTLN
92800      DO 400 I = 1,NI
92900      YSLPLT(N,I) = 0.0
93000      400 CONTINUE
93100      RETURN
93200      END
93300      C
93400      C-----
93500      C
93600      SUBROUTINE PROPS
93700      C.....
93800      C
93900      CHAPTER      PRELIMINARIES
94000      C
94100      COMMON
94200      $/FLUPP/JRF,VIS,VISCOG,DEN,IT,PRANDT,DEN(48,24),VIS(48,24)
94300      $/VAR/U(48,24),V(48,24),W(48,24),P(48,24),PP(48,24),
94400      $TE(48,24),ED(48,24),STFN(48,24),YSTLN(48,24),STVAL(24),
94500      $USTAR(48,24),VSTAR(48,24),WSTAR(48,24),IT-1(48,24),
94600      $TESTAR(48,24),YSTLND(48,24),VISTAR(48,24)
94700      $/ALL/IT,UT,NI,NU,NIM1,NJM1,SGREAT,JMAX(48),JWAP1(48)
94800      $/TURB/GEN(48,24),CO,CMU,C1,C2,CAPPA,ELCG,PRED,PRTF
94900      C
95000      C      CHAPTER      1      VISCOSITY
95100      C
95200      DO 100 I = 1,NIM1
95300      DO 100 J = 1,NJM1
95400      VISOLD = VIS(I,J)
95500      IF(ED(I,J).EQ. 0.0) GO TO 102
95600      VIS(I,J) = DEN(I,J)*TE(I,J)**2*CMU/ED(I,J)+VISCOG
95700      GO TO 101
95800      102 VIS(I,J) = VISCOG
95900      C      UNDERRELAX VISCOSITY
96000      101 VIS(I,J) = JRFVIS*VIS(I,J)+(1.0-JRFVIS)*VIS LD
96100      100 CONTINUE
96200      RETURN
96300      END
96400      C
96500      C-----
96600      C
96700      SUBROUTINE CALCU
96800      C.....
96900      C
97000      CHAPTER      PRELIMINARIES
97100      COMMON
97200      $/UVEL/RESORU,NSWPP,JRFU,DXFPU(48),DXFPU(48),SEWU(48)
97300      $/VVEL/RESORV,NSWPV,JRFV,DYNPV(24),DYFV(24),SNSV(24)
97400      $/PCOR/RESORP,NSWPP,JRFP,OU(48,24),DV(48,24),IPREF,JREF
97500      $/VAR/U(48,24),V(48,24),W(48,24),P(48,24),PP(48,24),TE(48,24),
97600      $ED(48,24),STFN(48,24),YSTLN(48,24),STVAL(24),USTAR(48,24),

```

```

97700 $VSTAR(46,24),WSTAR(48,24),PSTAR(48,24),TESTAR(48,24),YSTLND(48,24)
97800 $,VISTAR(48,24)
97900 $/ALL/IT,JT,NI,NU,NIM1,NUM1,GREAT,JMAX(48),JMAXP1(48)
98000 $/GEOM/INDCOS,X(48),Y(24),DXEP(48),DXPW(48),DYNP(24),DYPS(24),
98100 $SNS(24),SEW(48),XU(48),YV(24),R(24),RV(24),
98200 $WFN(24),WFS(24),WFE(48),WFW(48),RCV(24),XND(48),XUNC(48),
98300 $YND(24),YVND(24)
98400 COMMON
98500 $/FLUPR/UREVIS,VISCOS,SENSIT,PRANDT,CEN(48,24),VIS(48,24)
98600 $/COEF/AP(48,24),AN(48,24),AS(48,24),AE(48,24),AW(48,24),SC(48,24),
98700 $SP(48,24)
98800 $/KASE T1/UT,TEIV,EDIV,FLOWIV,ALAMDA,
98900 $ KSMALL,RLARGE,AL1,AL2,JSTEP,ISTEP,JUSTP1,JUSTM1,ISTP1,ISTM1
99000 COMMON/SGF/RMOMV(50,50),RMOMU(50,50)
99100 C
99200 C CHAPTER 11111 ASSEMBLY OF COEFFICIENTS
99300 DO 100 I = 3,NIM1
99400 DO 101 J = 2,NUM1
99500 C-----COMPUTE AREAS AND VOLUME
99600 AREA1 = RV(J+1)*SEWU(I)
99700 AREAS = RV(J)*SEWU(I)
99800 AREA2W = RCV(J)*SNS(J)
99900 VOL = RCV(J)*SEWU(I)*SNS(J)

```

```

00100 C----- CALCULATE CONVECTION COEFFICIENTS
00200 GN = 0.5*(DEN(I,J+1)+DEN(I,J))*V(I,J+1)
00300 GNW = 0.5*(DEN(I-1,J)+DEN(I-1,J+1))*V(I-1,J+1)
00400 GS = 0.5*(DEN(I,J-1)+DEN(I,J))*V(I,J)
00500 GSW = 0.5*(DEN(I-1,J)+DEN(I-1,J-1))*V(I-1,J)
00600 GE = DEN(I,J)*(U(I+1,J)*(1.0-WFF(I))+U(I,J)*WFE(I))
00700 GW = DEN(I-1,J)*(U(I-1,J)*(1.0-WFW(I))+U(I,J)*WFW(I))
00800 CN = 0.5*(GN+GNW)*AREAN
00900 CS = 0.5*(GS+GSW)*AREAS
01000 CE = GE*AREAEW
01100 CW = GW*AREAEW
01200 C----- CALCULATE DIFFUSION COEFFICIENTS
01300 VISN = 0.25*(VIS(I,J)+VIS(I,J+1)+VIS(I-1,J)+VIS(I-1,J+1))
01400 VISC = 0.25*(VIS(I,J)+VIS(I,J-1)+VIS(I-1,J)+VIS(I-1,J-1))
01500 CN = VISN*AREAN/DYND(J)
01600 CS = VISC*AREAS/DYDS(J)
01700 CE = VIS(I,J)*AREAEW/DXEPW(I)
01800 CW = VIS(I-1,J)*AREAEW/DXPW(I)
01900 C----- CALCULATE COEFFICIENT OF SOURCE TERMS
02000 CMP = CN-CS+CE-CW
02100 CP = AMAX1(0.0,CMP)
02200 CPO = CP
02300 C----- ASSEMBLE MAIN COEFFICIENTS
02400 AN(I,J) = AMAX1(ABS(0.5*CN),CN)+0.5*CN
02500 AS(I,J) = AMAX1(ABS(0.5*CS),CS)+0.5*CS
02600 CE = AMAX1(CE,-WFE(I)*CP,(1.0-WFE(I))*CE)
02700 CW = AMAX1(CW,WFW(I)*CP,-(1.0-WFW(I))*CW)
02800 AE(I,J) = CE-(1.0-WFE(I))*CE
02900 AW(I,J) = CW+(1.0-WFW(I))*CW
03000 CU(I,J) = AREAEW
03100 DUDXE = (U(I+1,J)-U(I,J))/DXEPL(I)
03200 DUDXW = (U(I,J)-U(I-1,J))/DXPW(I)
03300 SOURCE1 = (DUDXE*VIS(I,J)-DUDXW*VIS(I-1,J))/DEW(I)
03400 DVDXN = (V(I,J+1)-V(I-1,J+1))/SCW(I)
03500 DVDXS = (V(I,J)-V(I-1,J))/CEW(I)
03600 SOURCE2 = (U(I+1,J)*VISI+DVDXN*RW(I)+VISC+DVDXS)/(RCV(I)*DYND(J))
03700 CU(I,J) = CPO+CU(I,J)+SOURCE1*(P(I-1,J)-P(I,J))
03800 C-----
03900 C RMOM(I,J) IS THE MOMENTUM CONTRIBUTION BY THE DROPLET SPRAY TO
04000 C MAIN GAS FLOW FIELD AS A RESULT OF THE AXIAL VELOCITY.
04100 CU(I,J)=CU(I,J)+RMOM(I,J)
04200 C-----
04300 CU(I,J) = CU(I,J)+(SOURCE1+SOURCE2)*VOL
04400 SP(I,J) = -CP
04500 101 CONTINUE
04600 100 CONTINUE
04700 C
04800 C---CHAPTER 2 2.2 PROBLEM MODIFICATIONS
04900 C
05000 CALL PROMOD (2)
05100 C
05200 CHAPTER 3 FINAL COEF. ASSEMBLY AND RESIDUAL SOURCE CALCULATION
05300 C
05400 RESORU = 0.0
05500 DO 300 I = 3,NIM1
05600 DO 301 J = 2,NOM1
05700 AP(I,J) = AN(I,J)+AS(I,J)+AE(I,J)+AW(I,J)-CP(I,J)
05800 CU(I,J) = CU(I,J)/AP(I,J)
05900 RESOR = AN(I,J)+U(I,J+1)+AS(I,J)+U(I,J-1)+AE(I,J)+U(I+1,J)
06000 $ +AW(I,J)+U(I-1,J)+AP(I,J)+U(I,J)+SU(I,J)
06100 VOL = RCV(I)*CEW(I)*CNS(I)

```





```

12300      GW = 0.5*(DEN(I,J)+DEN(I-1,J))*U(I,J)
12400      GGW = 0.5*(DEN(I,J-1)+DEN(I-1,J-1))*U(I,J-1)
12500      GN = GN+AREAN
12600      GO = GO+AREAS
12700      GE = 0.5*(GE+GSE)*AREAEW
12800      GW = 0.5*(GW+GGW)*AREAEW
12900      C-----CALCULATE DIFFUSION COEFFICIENTS
13000      VICE = 0.25*(VIC(I,J)+VIC(I+1,J)+VIC(I,J-1)+VIC(I+1,J-1))
13100      VICW = 0.25*(VIC(I,J)+VIC(I-1,J)+VIC(I,J-1)+VIC(I-1,J-1))
13200      CN = VIC(I,J)*AREAN/DYNPV(J)
13300      CO = VIC(I,J-1)*AREAS/DYFV(J)
13400      CE = VICE*AREAEW/DXPR(I)
13500      CW = VICW*AREAEW/DXPR(I)
13600      C-----CALCULATE COEFFICIENTS OF SOURCE TERMS
13700      MP = CN+CO+CE+CW
13800      MP = AMAX1(0.0, MP)
13900      CP = CF
14000      C-----ASSEMBLE MAIN COEFFICIENTS
14100      CN = AMAX1(CN, -WFN(J)*CN, (1.0-WFN(J))*CN)
14200      CO = AMAX1(CO, -WFO(J)*CO, -(1.0-WFO(J))*CO)
14300      AN(I,J) = CN-(1.0-WFN(J))*CN
14400      AO(I,J) = CO-(1.0-WFO(J))*CO
14500      AE(I,J) = AMAX1(AE, 0.5*CE, CP)-0.5*CE
14600      AW(I,J) = AMAX1(AW, 0.5*CW, CP)-0.5*CW
14700      UV(I,J) = 0.5*(AREAN+AREAS)
14800      UOYE = (U(I+1,J)-U(I-1,J-1))/XNOV(J)
14900      UOYW = (U(I,J)-U(I,J-1))/XNOV(J)
15000      CORIE1 = (COOYE+VICE-COYW+VICW)/TXPR(I)
15100      UOYN = (U(I,J-1)-U(I,J))/DYNPV(J)
15200      UOYS = (U(I,J)-U(I,J-1))/DYFV(J)
15300      FORCED = (VIC(I,J)+AOV(J)+UOYN-VIC(I,J-1)+AO(I,J-1)+UOYS)
15400      * 7/(H*V(J)+INT(J))
15500      DO(I,J) = (FO*V(I,J)+OV(I,J)+(-H(I,J-1)+H(I,J))
15600      C-----
15700      C      +MMOV(I,J) IS THE MOMENTUM CONTRIBUTION BY THE DROPLET SPRAY TO
15800      C      MAIN GAS FLOW FIELD AS A RESULT OF THE RADIAL VELOCITY.
15900      DO(I,J)=DO(I,J)+MMOV(I,J)
16000      C-----
16100      D(I,J) = D(I,J)+(CORIE1-CORIE2)*VOL
16200      CH(I,J) = -P
16300      IF(INCOND.EQ.1) GO TO 101
16400      DO(I,J) = DO(I,J)+VOL*(DEN(I,J)+DEN(I,J-1))*(W(I,J)+W(I,J-1)
16500      * 3)*2/(H*V(J)+INT(J))
16600      CP(I,J) = -P(I,J)-(VIC(I,J)+VIC(I,J-1))*VOL/W(I,J)*2
16700      101 CONTINUE
16800      100 CONTINUE
16900
17000      CHAPTER 2.2.2.2.2 PROBLEM MODIFICATION
17100
17200      CALL FROMJ(3)
17300
17400      CHAPTER 2.2.2.2.3 FINAL COEF. ASSEMBLY AND RESIDUAL SOURCE CALC.
17500      RESOURV = 0.0
17600      DO 300 I = 1,NUM1
17700      DO 301 J = 1,NUM1
17800      AP(I,J) = AN(I,J)+AO(I,J)+AE(I,J)+AW(I,J)-CP(I,J)
17900      UV(I,J) = UV(I,J)/AF(I,J)
18000      RESUR = AN(I,J)*V(I,J-1)+AO(I,J)*V(I,J-1)+AP(I,J)*V(I+1,J)
18100      * +AW(I,J)*V(I-1,J)-AP(I,J)*V(I,J)+DO(I,J)
18200      VOL = -V(J)+LEW(I)*NSV(J)
18300      DERVOL = DEAT*VOL

```



```

24500 C-----CALCULATE CONVECTION COEFFICIENTS
24600 C
24700 CN = 0.5*(CEN(1,0)+CEN(1,0+1))*V(1,0+1)
24800 CU = 0.5*(CEN(1,0)+CEN(1,0+1))*V(1,0)
24900 CE = 0.5*(CEN(1,0)+CEN(1+1,0))*V(1+1,0)
25000 CW = 0.5*(CEN(1,0)+CEN(1-1,0))*V(1,0)
25100 CA = CN+CU+CE
25200 CB = CU+CE+CW
25300 CC = CN+CE+CW
25400 CD = CN+CU+CW
25500 C
25600 C-----CALCULATE DIFFUSION COEFFICIENTS
25700 C
25800 VCN = 0.5*(VIC(1,0)+VIC(1,0+1))
25900 VIC = 0.5*(VIC(1,0)+VIC(1,0+1))
26000 VCU = 0.5*(VIC(1,0)+VIC(1+1,0))
26100 VICW = 0.5*(VIC(1,0)+VIC(1-1,0))
26200 CV = VICW+VCA/VCN
26300 TC = VICW+VCE/CU
26400 CC = VICW+VCE+VCD/CD
26500 CW = VICW+VCE+VCD/CD
26600 C
26700 C-----CALCULATE MP
26800 C
26900 MP = CA+CB+CC+CW
27000 CP = AMAX1(0.0, MP)
27100 CPD = CP
27200 C
27300 C-----ASSEMBLE MAIN DIFFERENTIALS
27400 C
27500 AN(1,0) = AMAX1(CA+0.5*CN, CN)+0.5*CN
27600 AU(1,0) = AMAX1(CU+0.5*CU, CU)+0.5*CU
27700 AE(1,0) = AMAX1(CE+0.5*CE, CE)+0.5*CE
27800 AW(1,0) = AMAX1(CW+0.5*CW, CW)+0.5*CW
27900 CV = 0.5*(CA+CB+CC+CD)
28000 VAVG = 0.5*(VIC(1,0+1)+VIC(1,0))
28100 COT(1,0) = 0.5*W(1,0)
28200 IF(CV(1,0).GT.1) GO TO 101
28300 CORF1 = CV(1,0)*VAVG*W(1,0)/CV(0)
28400 CORVOL = (VIC(1,0+1)+VIC(1,0))*W(1,0)/(CV(1,0)+CV(0))
28500 COT(1,0) = 0.5*(COT(1,0)+CORF1+CORVOL)*VOL
28600 IF(1,0) = 1
28700 GO TO 100
28800 GO TO 100
28900 C
29000 C-----CALCULATE FINAL COEFFICIENTS AND REFORM MODIFICATION
29100 C
29200 CALL PRM1(4)
29300 C
29400 C-----CALCULATE FINAL COEFFICIENTS AND REFORM MODIFICATION
29500 C
29600 REFORM = 0.
29700 COT(1,0) = 0.5*W(1,0)
29800 COT(1,0) = 0.5*W(1,0)
29900 AP(1,0) = AN(1,0)+AU(1,0)+AE(1,0)+AW(1,0)+CP(1,0)
30000 REFORM = AN(1,0)+AU(1,0)+AE(1,0)+AW(1,0)+CP(1,0)+W(1,0+1)+A(1,0+1,0)
30100 E1 = AW(1,0)+W(1-1,0)+AP(1,0)+W(1,0)+COT(1,0)
30200 VOL = AT(1,0)*CN(0)+CEW(1)
30300 CORVOL = COT(1,0)*VOL
30400 IF(-CP(1,0).GT.0.01*CORVOL) REFORM = REFORM+VOL
30500 IF(CV(1,0).GT.0.01) REFORM = 0.0

```

```

30600 RESUR = RESUR + ARG(RESUR)
30700
30800 C-----UNDER-RELAXATION
30900
31000     AP(1,0) = AP(1,0)/JPF
31100     U(1,0) = (1,0)*(1,0 - JPF)*AP(1,0) + (1,0)
31200     GO1 CONTINUE
31300     GO2 CONTINUE
31400
31500 C-----SECTION OF DIFFERENCE EQUATION
31600
31700     DO 400 I = 1, N, NPM
31800     400 CALL SUB(2,2,NI,UMAX,IT,OT,UB)
31900     GO1 CONTINUE
32000     RETURN
32100
32200
32300 C-----
32400
32500 C-----
32600
32700
32800 C-----
32900
33000 C-----
33100
33200     COMMON
33300     1/ FLOW, Z, X, Y, W, XFF, YFF, U(4,24), TV(4,24), IPREF, JPF, F
33400     2/ VAX/1(4,24), V(4,24), W(4,24), P(4,24), PF(4,24),
33500     3/ TF(4,24), TT(4,24), TTF(4,24), YCTON(4,24), CT, AL(24),
33600     4/ USTAR(4,24), VSTAR(4,24), WSTAR(4,24), PSTAR(4,24),
33700     5/ TSTAR(4,24), YTLT(4,24), VTLT(4,24), WTLT(4,24),
33800     6/ ALL/IT, OT, NI, N, NIM1, NIM2, GREAT, UMAX(4), UMAXP1(4),
33900     7/ GEND/1,2,3,4, A(4), Y(24), DAP(4), DAPW(4), LYNP(24), LYNP(24),
34000     8/ DND(24), DEN(4), D(4), YV(24), F(24), RV(24),
34100     9/ WFN(4), WFD(24), WFF(4), WFW(4), RCV(24), XVF(4), XVD(4),
34200     10/ YND(24), YVDT(24)
34300     COMMON
34400     1/ FLOW, Z, X, Y, W, XFF, YFF, U(4,24), TV(4,24), IPREF, JPF, F
34500     2/ DDEF/1(4,24), D(4,24), AD(4,24), AE(4,24), AW(4,24), CU(4,24),
34600     3/ F(4,24)
34700     4/ XAGE, T1, UIN, T1IN, EDIN, FLOWIN, ALAMDA,
34800     5/ SMALL, HLA, GE, AL1, AL2, UOTFF, IOTFF, UOTF1, UOTM1, IOTF1, IOTM1
34900     RESURM = 0.0
35000
35100 C-----
35200
35300 C-----
35400
35500 C-----
35600
35700 C-----
35800
35900 C-----
36000
36100 C-----
36200
36300 C-----
36400
36500 C-----
36600

```

```

36700 C-----CALCULATE CORRECT VELOCITY
36800   A = 18000*(1,0-1)*A+AA
36900   B = 18000*(1,0)*A+AA
37000   C = 18000*(1,0)*A+AA
37100   D = 18000*(1,0)*A+AA
37200   E = 18000*(1,0)*A+AA
37300   F(1,0) = 1.0
37400   G(1,0) = 1.0
37500 C-----CALCULATE CORRECT VELOCITY
37600   H = 18000*(1,0)*A+AA
37700   I = 18000*(1,0)*A+AA
37800   J = 18000*(1,0)*A+AA
37900 C-----CALCULATE CORRECT VELOCITY
38000   K = 18000*(1,0)*A+AA
38100   L = 18000*(1,0)*A+AA
38200   M = 18000*(1,0)*A+AA
38300   N = 18000*(1,0)*A+AA
38400   O = 18000*(1,0)*A+AA
38500   P = 18000*(1,0)*A+AA
38600   Q = 18000*(1,0)*A+AA
38700   R = 18000*(1,0)*A+AA
38800   S = 18000*(1,0)*A+AA
38900   T = 18000*(1,0)*A+AA
39000   U = 18000*(1,0)*A+AA
39100   V = 18000*(1,0)*A+AA
39200   W = 18000*(1,0)*A+AA
39300   X = 18000*(1,0)*A+AA
39400   Y = 18000*(1,0)*A+AA
39500   Z = 18000*(1,0)*A+AA
39600   AA = 18000*(1,0)*A+AA
39700   AB = 18000*(1,0)*A+AA
39800   AC = 18000*(1,0)*A+AA
39900   AD = 18000*(1,0)*A+AA
40000   AE = 18000*(1,0)*A+AA
40100   AF = 18000*(1,0)*A+AA
40200   AG = 18000*(1,0)*A+AA
40300   AH = 18000*(1,0)*A+AA
40400   AI = 18000*(1,0)*A+AA
40500   AJ = 18000*(1,0)*A+AA
40600   AK = 18000*(1,0)*A+AA
40700   AL = 18000*(1,0)*A+AA
40800   AM = 18000*(1,0)*A+AA
40900   AN = 18000*(1,0)*A+AA
41000   AO = 18000*(1,0)*A+AA
41100   AP = 18000*(1,0)*A+AA
41200   AQ = 18000*(1,0)*A+AA
41300   AR = 18000*(1,0)*A+AA
41400   AS = 18000*(1,0)*A+AA
41500   AT = 18000*(1,0)*A+AA
41600   AU = 18000*(1,0)*A+AA
41700   AV = 18000*(1,0)*A+AA
41800   AW = 18000*(1,0)*A+AA
41900   AX = 18000*(1,0)*A+AA
42000   AY = 18000*(1,0)*A+AA
42100   AZ = 18000*(1,0)*A+AA
42200   BA = 18000*(1,0)*A+AA
42300   BB = 18000*(1,0)*A+AA
42400   BC = 18000*(1,0)*A+AA
42500   BD = 18000*(1,0)*A+AA
42600   BE = 18000*(1,0)*A+AA
42700   BF = 18000*(1,0)*A+AA

```

```

+2400 COMMON
+2500 S/TAH/RECOCK,NOM1,CRK
+3000 S/TAH/Z(48,24),V(48,24),W(48,24),P(48,24),PP(48,24),
+3100 STE(48,24),FT(48,24),OTF(48,24),YSTLN(48,24),STVAL(24),
+3200 S/OTAR(48,24),VOTAR(48,24),WOTAR(48,24),FOTAR(48,24),
+3300 STEOTAR(48,24),YSTLN(48,24),VOTAR(48,24)
+3400 S/ALL/IT,OTN1,NOM1,NIM1,NOM1,SEAT,OMAX(48),OMAP(48)
+3500 S/GEOM/IN(48),X(48),Y(24),TXF(48),TXPM(48),TXP(24),TXFC(24),
+3600 S TXND(24),TXM(48),TXC(48),TXV(24),R(24),RV(24),
+3700 S TXWF(24),W(48),WF(48),WF(48),RC(24),X(48),Y(24),
+3800 STN(24),TND(24)
+3900 COMMON
+4000 S/FLUPH/ZARVIT,VICCO,CONIT,FRAND,LEN(48,24),VIC(48,4)
+4100 S/HA/EIT/OTN,TE1,OTN,FLUMIN,ALAMLA,
+4200 S/SMALL,ML(48,4),AL,AL,OTEP,OTEP,OTEP1,OTM1,OTM1,OTM1
+4300 S/TAH/Z(48,24),V(48,24),W(48,24),P(48,24),PP(48,24),
+4400 S/WALL/Z(48,24),V(48,24),T(48,4),T(48,4)
+4500 S/OTEP/Z(48,24),V(48,24),W(48,24),P(48,24),PP(48,24),
+4600 S/OTEP(48,24)
+4700 S/OTEP/Z(48,24),V(48,24),W(48,24)
+4800
+4900 ***** COEFFICIENTS OF DIFFERENTIALS *****
+5000
+5100 F-T=1,
+5200 F-T=1, NIM1
+5300 F-T=1, NIM1
+5400 ***** COEFFICIENTS OF DIFFERENTIALS *****
+5500 A=1, A=1, A=1, A=1
+5600 A=1, A=1, A=1, A=1
+5700 A=1, A=1, A=1, A=1
+5800 A=1, A=1, A=1, A=1
+5900 ***** COEFFICIENTS OF DIFFERENTIALS *****
+6000 A=1, A=1, A=1, A=1
+6100 A=1, A=1, A=1, A=1
+6200 A=1, A=1, A=1, A=1
+6300 A=1, A=1, A=1, A=1
+6400 A=1, A=1, A=1, A=1
+6500 A=1, A=1, A=1, A=1
+6600 A=1, A=1, A=1, A=1
+6700 A=1, A=1, A=1, A=1
+6800 A=1, A=1, A=1, A=1
+6900 ***** COEFFICIENTS OF DIFFERENTIALS *****
+7000 A=1, A=1, A=1, A=1
+7100 A=1, A=1, A=1, A=1
+7200 A=1, A=1, A=1, A=1
+7300 A=1, A=1, A=1, A=1
+7400 A=1, A=1, A=1, A=1
+7500 A=1, A=1, A=1, A=1
+7600 A=1, A=1, A=1, A=1
+7700 ***** COEFFICIENTS OF DIFFERENTIALS *****
+7800 A=1, A=1, A=1, A=1
+7900 A=1, A=1, A=1, A=1
+8000 A=1, A=1, A=1, A=1
+8100 A=1, A=1, A=1, A=1
+8200 A=1, A=1, A=1, A=1
+8300 A=1, A=1, A=1, A=1
+8400 A=1, A=1, A=1, A=1
+8500 A=1, A=1, A=1, A=1
+8600 A=1, A=1, A=1, A=1
+8700 A=1, A=1, A=1, A=1
+8800 A=1, A=1, A=1, A=1
+8900 A=1, A=1, A=1, A=1
+9000 A=1, A=1, A=1, A=1
+9100 A=1, A=1, A=1, A=1
+9200 A=1, A=1, A=1, A=1
+9300 A=1, A=1, A=1, A=1
+9400 A=1, A=1, A=1, A=1
+9500 A=1, A=1, A=1, A=1
+9600 A=1, A=1, A=1, A=1
+9700 A=1, A=1, A=1, A=1
+9800 A=1, A=1, A=1, A=1
+9900 A=1, A=1, A=1, A=1

```

```

48900      GEN(I,J) = (2.0*(DUDX**2+DV DY**2)*(DUDY+DV DX)**2)*VIS(I,J)
49000      IF(INDCOS .EQ. 2) GEN(I,J) = GEN(I,J)*VIS(I,J)*(DUDY**2+DV DX**2)
49100      IF(RV(J) .EQ. 0.0) GO TO 110
49200      VCR = V(I,J)/RV(J)
49300      IF(INDCOS .EQ. 2) GEN(I,J)=GEN(I,J)+VIS(I,J)*0.5*(VCR+V(I,J+1)/
49400      RV(J+1))**2
49500      GO TO 120
49600      110 IF(INDCOS .EQ. 2) GEN(I,J)=GEN(I,J)+VIS(I,J)*0.5*(V(I,J+1)/
49700      RV(J+1))**2
49800      120 CONTINUE
49900      C-----ASSEMBLE MAIN COEFFICIENTS
50000      AN(I,J) = AMAX1(ABS(0.5*CN),CN)-0.5*CN
50100      AS(I,J) = AMAX1(ABS(0.5*CS),CS)+0.5*CS
50200      AE(I,J) = AMAX1(ABS(0.5*CE),CE)-0.5*CE
50300      AW(I,J) = AMAX1(ABS(0.5*CW),CW)+0.5*CW
50400      CU(I,J) = CPO*TE(I,J)
50500      CUK(I,J) = CU(I,J)
50600      SC(I,J) = CU(I,J)+GEN(I,J)*VOL
50700      CP(I,J) = -CP
50800      CPK(I,J) = CP(I,J)
50900      CP(I,J) = CP(I,J)-CD*CMC*GEN(I,J)**2*TE(I,J)*VOL/VIS(I,J)
51000      101 CONTINUE
51100      100 CONTINUE
51200      C
51300      CHAPTER 2 2 2 2 PROBLEM MODIFICATION 2 2 2
51400      C
51500      CALL PRMOC(6)
51600      C
51700      CHAPTER 3 FINAL COEFFICIENT ASSEMBLY AND RESIDUAL SOURCE CALCULATION
51800      C
51900      RESORK = 0.0
52000      DO 300 I = 2,NI*1
52100      DO 301 J = 2,NU*1
52200      AP(I,J) = AN(I,J)+AS(I,J)+AE(I,J)+AW(I,J)-CP(I,J)
52300      RESOR = AN(I,J)+TE(I,J+1)+AS(I,J)+TE(I,J-1)+AE(I,J)+TE(I+1,J)
52400      +AW(I,J)+TE(I-1,J)-AP(I,J)+TE(I,J)*CU(I,J)
52500      VOL = RV(J)*CND(J)*GEN(I)
52600      CORVOL = REAT*VOL
52700      IF(-CP(I,J) .GT. 0.5*CORVOL) RESOR = RESOR/CORVOL
52800      RESORK = RESORK+ABS(RESOR)
52900      C-----RELAXATION
53000      AP(I,J) = AP(I,J)/CPRK
53100      CU(I,J) = CU(I,J)+(1.0-CPRK)*AP(I,J)*TE(I,J)
53200      301 CONTINUE
53300      300 CONTINUE
53400      C
53500      CHAPTER 4 4 4 4 SOLUTION OF DIFFERENCE EQUATION 4 4 4
53600      C
53700      DO 400 N = 1,NC*PK
53800      400 CALL DISOL(2,2,NI,UMAX,IT,UT,TE,6)
53900      RETURN
54000      END
54100      C
54200      C-----
54300      C
54400      SUBROUTINE CALCD
54500      C.....
54600      C
54700      CHAPTER 5 5 5 5 PRELIMINARY 5 5 5 5
54800      C
54900      COMMON

```

```

55000      S/TOIS/RESORE,NSWPD,URFE
55100      S/VAR/U(48,24),V(48,24),W(48,24),P(48,24),PP(48,24),
55200      STE(48,24),ED(48,24),STFN(48,24),YSTLN(48,24),STVAL(24),
55300      SUSTAR(48,24),VSTAR(48,24),WSTAR(48,24),PSTAR(48,24),
55400      STESTAR(48,24),YSTLND(48,24),VISTAR(48,24)
55500      S/ALL/IT,UT,NI,NU,NIM1,NUM1,GRAT,JMAX(48),JMAXP1(48)
55600      S/GEOM/INOCOC,X(48),Y(24),DXEP(48),DXPM(48),DYSP(24),DYPS(24),
55700      S      DNS(24),SEW(48),XU(48),YV(24),R(24),FV(24),
55800      S      FV(24),WFS(24),WFE(48),WFu(48),FCV(24),XND(48),XUSD(48),
55900      SYND(24),YVND(24)
56000      COMMON
56100      S/FLUPR/UREVIS,VICOCOC,DENSIT,PRANDT,DEN(48,24),VIS(48,24)
56200      S/RACE TI/CIIN,TEIN,EDIN,FLOWIN,ALAMDA,
56300      SRSMALL,RLARGE,AL1,AL2,USTEP,ISTEP,JGTP1,JUSTM1,ISTP1,ISTM1
56400      S/TURB/GEN(48,24),CC,CMC,C1,CC,CAPPA,ELUS,FRED,FATE
56500      S/WALLF/YPLUS(48),YPLUSW(24),TAUN(48),TAUW(24)
56600      S/COEF/AF(48,24),AF(48,24),AS(48,24),AE(48,24),Aw(48,24),SU(48,24),
56700      SDF(48,24)
56800      S/SUCP/SCAT(48,24),SPKD(48,24)
56900      C
57000      CHAPTER 1 1 1 1 ASSEMBLY OF COEFFICIENTS 1 1 1
57100      C
57200      DO 100 I = 2,NIM1
57300      JJ = JMAX(I)
57400      DO 101 J = 2,JJ
57500      C-----COMPUTE AREAS AND VOLUME
57600      AREAN = RV(J+1)*SEW(I)
57700      AREAS = RV(J)*SEW(I)
57800      AREAEW = FCV(J)*SNS(J)
57900      VOL = FCV(J)*SNC(J)*SEW(I)
58000      C-----CALCULATE CONVECTION COEFFICIENTS
58100      GN = 0.5*(DEN(I,J)+DEN(I,J+1))*V(I,J+1)
58200      GS = 0.5*(DEN(I,J)+DEN(I,J-1))*V(I,J)
58300      GE = 0.5*(DEN(I,J)+DEN(I+1,J))*U(I+1,J)
58400      GW = 0.5*(DEN(I,J)+DEN(I-1,J))*U(I,J)
58500      CN = GN*AREAN
58600      CS = GS*AREAS
58700      CE = GE*AREAEW
58800      CW = GW*AREAEW
58900      C-----CALCULATE DIFFUSION COEFFICIENTS
59000      GAMN = 0.5*(VIS(I,J)+VIS(I,J+1))/PREC
59100      GAMS = 0.5*(VIS(I,J)+VIS(I,J-1))/PREC
59200      GAME = 0.5*(VIS(I,J)+VIS(I+1,J))/PREC
59300      GAMW = 0.5*(VIS(I,J)+VIS(I-1,J))/PREC
59400      CN = GAMN*AREAN/DYSP(J)
59500      CS = GAMS*AREAS/DYPS(J)
59600      CE = GAME*AREAEW/DXSP(I)
59700      CW = GAMW*AREAEW/DXPM(I)
59800      C-----SOURCE TERMS
59900      CMP = CN-CS+CE-CW
60000      CP = AMAX1(0.0,CMP)
60100      CPO = CP
60200      C-----ASSEMBLE MAIN COEFFICIENTS
60300      AN(I,J) = AMAX1(ABS(0.5*CN),CN)-0.5*CN
60400      AS(I,J) = AMAX1(ABS(0.5*CS),CS)+0.5*CS
60500      AL(I,J) = AMAX1(ABS(0.5*CE),CE)-0.5*CE
60600      AW(I,J) = AMAX1(ABS(0.5*CW),CW)+0.5*CW
60700      CU(I,J) = CPO*ED(I,J)
60800      SUKD(I,J) = CU(I,J)
60900      CU(I,J) = CU(I,J)+C1*CMC*GEN(I,J)*VOL*DEN(I,J)*TE(I,J)/VIS(I,J)
61000      SP(I,J) = -CF

```



```

61100      SPKD(I,J) = SP(I,J)
61200      SP(I,J) = SP(I,J)-C2*DEN(I,J)*ED(I,J)*VOL/TE(I,J)
61300      101 CONTINUE
61400      100 CONTINUE
61500      C
61600      CHAPTER 2 2 2 2 PROBLEM MODIFICATION 2 2 2 2
61700      C
61800      CALL PROMOS(7)
61900      C
62000      CHAPTER 3 3 3 COEFFICIENT ASSEMBLY AND RESIDUAL SOURCE CALCULATION
62100      C
62200      RESORE = 0.0
62300      DO 300 I = 2,NIM1
62400      DO 301 J = 2,NOM1
62500      AP(I,J) = AN(I,J)+AC(I,J)+AE(I,J)+AW(I,J)-SP(I,J)
62600      RESOR = AN(I,J)*ED(I,J-1)+AC(I,J)*ED(I,J-1)+AE(I,J)*ED(I+1,J)
62700      +AW(I,J)*ED(I-1,J)-AP(I,J)*ED(I,J)+SU(I,J)
62800      VOL = ACV(J)*CNC(J)*SEW(I)
62900      SCRVOL = GREAT*VOL
63000      IF(-SP(I,J).GT. 0.5*SCRVOL) RESOR = RESOR/SCRVOL
63100      RESORE = RESORE+ABS(RESOR)
63200      C-----UNDER-RELAXATION
63300      AP(I,J) = AP(I,J)/ORFE
63400      SU(I,J) = SU(I,J)*(1.0-ORFE)+AP(I,J)*ED(I,J)
63500      301 CONTINUE
63600      300 CONTINUE
63700      C
63800      CHAPTER 4 4 4 4 SOLUTION OF DIFFERENCE EQUATION 4 4 4 4
63900      C
64000      DO 400 I = 1,NOWPD
64100      400 CALL LISOLV(2,2,N1,UMAX,IT,UT,ED,7)
64200      RETURN
64300      END
64400      C
64500      C-----
64600      C
64700      SUBROUTINE LISOLV(ISTART,USTART,N1,UMAX,IT,UT,PHI,NCHAP)
64800      C-----
64900      C
65000      CHAPTER 5 5 5 PRELIMINARIES 5 5 5 5 5 5 5
65100      C
65200      DIMENSION PH1(IT,UT),A(4*),F(4*),C(4*),C(4*),UMAX(IT)
65300      COMMON
65400      1/THICK,TEIN,TEIN,EDIN,FLOWIN,ALAMDA,
65500      1/SMALL,FLA,FLA,ALI,ALI,USTEP,ISTEP,USTP1,USTM1,ISTP1,ISTM1
65600      1/COEF/24(4*,24),AN(4*,24),AT(4*,24),AE(4*,24),AW(4*,24),SU(4*,24),
65700      1/CP(4*,24)
65800      USM1 = USTART-1
65900      NIM1 = N1-1
66000      A(USM1) = 0.0
66100      C-----COMMON OF 1-5, 6-8
66200      DO 100 I=ISTART,NIM1
66300      C(USM1) = PH1(I,USM1)
66400      C-----COMMON OF 1- TRAVELER
66500      UI = UMAX(I)
66600      IF(NCHAP.EQ. 2) UI=UMAX(I-1)
66700      DO 101 J = USTART,UI
66800      C----- ASSEMBLE TMA COEFFICIENTS
66900      A(J) = AN(I,J)
67000      F(J) = AC(I,J)
67100      C(J) = AE(I,J)+PH1(I+1,J)+AW(I,J)+PH1(I-1,J)+SU(I,J)

```

```

67200      C(J) = AP(I,J)
67300      C----- CALCULATE COEFFICIENTS OF RECURRENCE FORMULA
67400      TERM = 1.0/(C(J)-B(J)+A(J-1))
67500      A(J) = A(J)+TERM
67600      C(J) = (C(J)+B(J)+C(J-1))*TERM
67700      101 CONTINUE
67800      C----- OBTAIN NEW PHIS
67900      DO 102 JJ = JSTART,JI
68000      J = JI+1+JDM1-JJ
68100      102 PHI(I,J) = A(J)+PHI(I,J+1)+C(J)
68200      100 CONTINUE
68300      RETURN
68400      END
68500      C
68600      C-----
68700      C
68800      SUBROUTINE PRINT(ISTART,JSTART,NI,NJ,IT,JT,X,Y,PHI,HEAD)
68900      C-----
69000      C
69100      DIMENSION PHI(IT,JT),X(IT),Y(JT),HEAD(9),STORE(49)
69200      ISKIP = 1
69300      JSKIP = 1
69400      WRITE(0,110) HEAD
69500      ISTA = ISTART - 12
69600      100 CONTINUE
69700      ISTA = ISTA+12
69800      IEND = ISTA+11
69900      IF(NI .LT. IEND) IEND = NI
70000      WRITE(0,111) (I,I=ISTA,IEND,ISKIP)
70100      WRITE(0,114) (X(I),I=ISTA,IEND,ISKIP)
70200      WRITE(0,112)
70300      DO 101 JJ=JSTART,NJ,JSKIP
70400      J = JSTART+NJ-JJ
70500      DO 120 I = ISTA,IEND
70600      A = PHI(I,J)
70700      IF(ABS(A) .LT. 1.E-20) A=0.0
70800      120 STORE(I) = A
70900      101 WRITE(0,113) J,Y(J),(STORE(I),I=ISTA,IEND,ISKIP)
71000      IF(IEND .LT. NI) GO TO 100
71100      RETURN
71200      110 FORMAT(1H0,17(2H+-),7X,9A4,7X,17(2H+-))
71300      111 FORMAT(1H0,13H      I=      ,I2,11I7)
71400      112 FORMAT(1H0,J      Y)
71500      113 FORMAT(13,OPF8.5,1X,1P,12F9.2)
71600      114 FORMAT(11H      X =      ,F9.5,11F9.5)
71700      END
71800      C
71900      C-----
72000      C
72100      SUBROUTINE PROMOD (NCHAR)
72200      C-----
72300      C
72400      CHARACTER '0' '1' '2' '3' '4' '5' '6' '7' '8' '9' 'A' 'B' 'C' 'D' 'E' 'F' 'G' 'H' 'I' 'J' 'K' 'L' 'M' 'N' 'O' 'P' 'Q' 'R' 'S' 'T' 'U' 'V' 'W' 'X' 'Y' 'Z'
72500      C
72600      COMMON
72700      1/UVEL/RECOUO,NSWPU,URFU,DXEPU(48),DXPBU(48),SEWU(48)
72800      1/VELL/R-GRV,NSWPV,URFV,DYMPV(24),DYPBV(24),SNSV(24)
72900      1/VELL/RECOFA,NSWPA,URFA
73000      1/PCOR/RECOFM,NSWPP,URFP,CU(48,24),CV(48,24),IPREF,JFREF
73100      1/VAR/U(48,24),V(48,24),W(48,24),P(48,24),PP(48,24),
73200      STE(48,24),ED(48,24),CTFN(48,24),YDTLN(48,24),STVAL(24),

```

```

73300      $USTAR(48,24),VSTAR(48,24),WSTAR(48,24),FSTAR(48,24),
73400      $TESTAR(48,24),YSTLND(48,24),VISTAR(48,24)
73500      $/ALL/IT,UT,NI,NU,NIM1,NUM1,GREAT,UMAX(48),UMAXP1(48)
73600      $/GEOM/INDCOD,X(48),Y(24),DXEP(48),DXPW(48),DYNP(24),DYPS(24),
73700      $   SNG(24),SEW(48),XU(48),YV(24),R(24),RV(24),
73800      $   WFN(24),WFS(24),WFE(48),WFW(48),RCV(24),XND(48),XVD(48),
73900      $YND(24),YVND(24)
74000      COMMON
74100      $/FLUPR/JRFVIS,VISCOS,DENSIT,PRANDT,DEN(48,24),VIS(48,24)
74200      $/KASE T1/UTN,TEIN,ECIN,FLOWIN,ALAMDA,
74300      $RSHALL,RLARGE,AL1,AL2,USTEP,ISTEP,JUSTP1,JUSTM1,ISTP1,ISTM1
74400      $/SUSP/SUKC(48,24),SPKD(48,24)
74500      $/TURB/GEN(48,24),CD,CMU,C1,C2,CAPPA,ELUG,PRED,PRTE
74600      $/WALL/YPLUSN(48),XPLUSN(24),TAUN(48),TAUW(24)
74700      $/COEF/AP(48,24),AN(48,24),AS(48,24),AE(48,24),AW(48,24),SU(48,24),
74800      $SP(48,24)
74900      IF(NCHAP .EQ. 2) GO TO 1150
75000      IF(USTEP .EQ. NUM1) GO TO 1150
75100      C-----OUT OF RANGE VALUES
75200      DO 1100 I = 2,NI
75300      IF(UMAX(I) .EQ. NUM1) GO TO 1150
75400      JU = UMAXP1(I)
75500      DO 1100 J = JU,NUM1
75600      1100 SP(I,J) = -GREAT
75700      1150 CONTINUE
75800      GO TO (1,2,3,4,5,6,7,8),NCHAP
75900      C
76000      C
76100      C
76200      CHAPTER 1 1 1 PROPERTIES 1 1 1 1 1
76300      C
76400      C
76500      1 CONTINUE
76600      C-----NO MODIFICATIONS FOR THIS PROBLEM
76700      RETURN
76800      C
76900      CHAPTER 2 1 2 2 2 2 U-MOMENTUM 2 2 2 2
77000      C
77100      2 CONTINUE
77200      C-----OUT OF RANGE VALUES
77300      IF(USTEP .EQ. NUM1) GO TO 202
77400      DO 200 I = 1,NI
77500      IF(UMAX(I-1) .EQ. NUM1) GO TO 202
77600      JU = UMAXP1(I-1)
77700      DO 200 J = JU,NUM1
77800      SP(I,J) = -GREAT
77900      200 CONTINUE
78000      202 CONTINUE
78100      C-----TOP WALL
78200      COTERM = CMU**0.25
78300      DO 210 I = 1,NUM1
78400      U = UMAX(I-1)
78500      YP = Y(U+1)-Y(U)
78600      SGRK = SQRT(0.5*(TE(I,U)+TE(I-1,U)))
78700      DENU = 0.5*(DEN(I,U)+DEN(I-1,U))
78800      YPLUSA = 0.5*(YPLUSN(I)+YPLUSN(I-1))
78900      IF(YPLUSA .LE. 11.63) GO TO 211
79000      TMULT = DENU*COTERM*SGRK/CAPPA/ALUG(ELUG*Y*YPLUSA)
79100      GO TO 212
79200      211 TMULT = VISCOS/YP
79300      212 CONTINUE

```

```

79400      205 SP(I,J) = SP(I,J)-TMULT*SEWU(I)*RV(J+1)
79500      IF(JMAX(I-1) .NE. JMAX(I)) SP(I,J) = SP(I,J)/2.0
79600      210 AN(I,J) = 0.0
79700      C----- SIDE WALL
79800      IF(JSTEP .EQ. NJM1) GO TO 214
79900      DO 225 I = 3,NIM1
80000      IF(JMAX(I-2) .GE. JMAX(I-1)) GO TO 225
80100      JU = JMAXP1(I-2)
80200      JI = JMAX(I-1)
80300      DO 220 J = JU,JI
80400      AW(I,J) = 0.0
80500      220 CONTINUE
80600      225 CONTINUE
80700      C----- SYMMETRY AXIS
80800      214 CONTINUE
80900      DO 203 I = 1,N1
81000      203 AS(I,2) = 0.0
81100      C----- OUTLET
81200      ARDEN = 0.0
81300      FLOW = 0.0
81400      DO 209 J = 2,NJM1
81500      ARDEN = 0.5*(DEN(NIM1,J)+DEN(NIM1-1,J))*RCV(J)+SNS(J)
81600      ARDEN = ARDEN*ARDEN
81700      209 FLOW = FLOW+ARDEN*U(NIM1,J)
81800      UINC = (FLOWIN-FLOW)/ARDEN
81900      DO 215 J = 2,NJM1
82000      215 U(N1,J) = U(NIM1,J)+UINC
82100      RETURN
82200      C
82300      CHAPTER      3      3      3      V-MOMENTUM      3      3      3
82400      C
82500      3 CONTINUE
82600      C----- SIDE WALL
82700      IF(JSTEP .EQ. NJM1) GO TO 314
82800      COTERM = CHU**0.25
82900      DO 325 I = 2,NIM1
83000      IF(JMAX(I-1) .GE. JMAX(I)) GO TO 325
83100      JU = JMAXP1(I-1)
83200      JI = JMAX(I)
83300      DO 320 J = JU,JI
83400      XP = X(I)-XU(I)
83500      SQRTK = SQRT(0.5*(TE(I,J)+TE(I,J-1)))
83600      DENV = 0.5*(DEN(I,J)+DEN(I,J-1))
83700      XPLUSA = 0.5*(XPLUSW(J)+XPLUSW(J-1))
83800      IF(XPLUSA .LE. 11.53) GO TO 311
83900      TMULT = DENV*COTERM*SQRTK*CAPPA/ALOG(ELCG*XPLUSA)
84000      GO TO 312
84100      311 TMULT = VISCOS/XP
84200      312 CONTINUE
84300      305 SP(I,J)=SP(I,J)-TMULT*SNSV(J)*RV(J)
84400      IF(J .EQ. JMAXP1(I-1)) SP(I,J)= SP(I,J)/2.0
84500      310 AW(I,J) = 0.0
84600      320 CONTINUE
84700      325 CONTINUE
84800      C----- TOP WALL
84900      314 CONTINUE
85000      DO 313 I=2,NIM1
85100      J = JMAX(I)
85200      313 AN(I,J) = 0.0
85300      RETURN
85400      C

```

```

85500 CHAPTER 4 4 4 PRESSURE CORRECTION 4 4 4
85600 C
85700 4 CONTINUE
85800 C----- SIDE WALL
85900 IF(JSTEP.EQ.NUM1) GO TO 414
86000 DO 412 I = 2,NIM1
86100 IF(JMAX(I-1).GE.JMAX(I)) GO TO 412
86200 JU = JMAX(I-1)
86300 JI = JMAX(I)
86400 DO 410 J = JU,JI
86500 AW(I,J) = 0.0
86600 410 CONTINUE
86700 412 CONTINUE
86800 C----- TOP WALL
86900 414 CONTINUE
87000 DO 402 I = 2,NIM1
87100 J = JMAX(I)
87200 402 AW(I,J) = 0.0
87300 C----- SYMMETRY AXIS
87400 DO 420 I = 2,NIM1
87500 AS(I,2) = 0.0
87600 420 CONTINUE
87700 C----- OUTLET
87800 DO 440 J = 2,NJM1
87900 AE(NIM1,J) = 0.0
88000 440 CONTINUE
88100 RETURN
88200 C
88300 CHAPTER 5 5 5 THERMAL ENERGY 5 5 5
88400 C
88500 5 CONTINUE
88600 C----- NO MODIFICATIONS FOR THIS PROBLEM
88700 RETURN
88800 C
88900 CHAPTER 6 6 6 TURBULENT KINETIC ENERGY 6 6 6
89000 C
89100 C
89200 6 CONTINUE
89300 C----- TOP WALL
89400 COTERM = CMU**0.25
89500 DO 610 I = 2,NIM1
89600 J = JMAX(I)
89700 LWBY = (W(I,J+1)-W(I,J-1))/(DYP(J)+DYP(J))
89800 UAVG = U(I,J)*WFE(I)+(1.0-WFE(I))*U(I+1,J)
89900 UEFF = SQRT(UAVG*UAVG+W(I,J)*W(I,J))
90000 YP = Y(J+1)-Y(J)
90100 DENS = DEN(I,J)
90200 SQRTK = SQRT(TF(I,J))
90300 VOL = RV(J)*DENS(J)*SEW(I)
90400 YPLUSN(I) = DENS*SQRTK*COTERM*YP/VISCO
90500 IF(YPLUSN(I).LE.11.63) GO TO 608
90600 TMULT = DENS*COTERM*SQRTK*CAPPA/ALOG(ELCG*YPLUSN(I))
90700 TAUX(I) = -TMULT*UEFF
90800 DITERM = DEN(I,J)*(CMU**0.75)*SQRTK*ALOG(ELCG*YPLUSN(I))/(CAPPA*YP)
90900 GO TO 609
91000 608 TAUX = -VISCO*UAVG/YP
91100 TAURW = VISCO*(-W(I,J)/YP-W(I,J)/Y(J))
91200 TAUX(I) = SQRT(TAUX**2+TAURW**2)
91300 DITERM = DEN(I,J)*(CMU**0.75)*SQRTK*YPLUSN(I)/YP
91400 609 CODY = ((U(I,J)+U(I+1,J)+U(I,J+1)+U(I+1,J+1))/4.0-
91500 1 (U(I,J)+U(I+1,J)+U(I,J-1)+U(I+1,J-1))/4.0)/SNS(J)

```

```

91600      GENCOU = TAUN(I)**2/VIS(I,J)
91700      GENRES = GEN(I,J)-VIS(I,J)*(DUDY**2+(DUDY-W(I,J)/Y(I))**2)
91800      GEN(I,J) = GENRES+GENCOU
91900      SU(I,J) = GEN(I,J)*VOL+SUKD(I,J)
92000      SP(I,J) = -DITERM*VOL+SPKD(I,J)
92100      AW(I,J) = 0.0
92200      610 CONTINUE
92300      TAUN(NI) = TAUN(NIM1)
92400      C-----SIDE WALL
92500      IF(JSTEP.EQ.NUM1) GO TO 614
92600      DO 625 I=2,NIM1
92700      IF(JMAX(I-1).GE.JMAX(I)) GO TO 626
92800      JJ = JMAX(I-1)
92900      JI = JMAX(I)
93000      DO 620 J = JJ,JI
93100      CWDX = (W(I+1,J)-W(I-1,J))/(DXPW(I)+CDEF(I))
93200      VAVG = V(I,J)*WFN(J)+(1.0-WFN(J))*V(I,J+1)
93300      VEFF = SQRT(VAVG*VAVG + W(I,J)*W(I,J))
93400      XP = X(I) - XU(I)
93500      DENV = DEN(I,J)
93600      SORTK = SORT(TS(I,J))
93700      VOL = PCV(J)*SNG(J)*CFW(I)
93800      XPLUSW(J) = DENV*SORTK+DTERM*XP/VISCOS
93900      IF(XPLUSW(J).LE.-11.63) GO TO 621
94000      TMULT = DENV*DTERM*SORTK+CAPPA/ALOG(ELCG*XPLUSW(J))
94100      TAUW(J) = -TMULT*VEFF
94200      DITERM=DENV(I,J)*(CMU**0.75)*SORTK*ALOG(ELCG*XPLUSW(J))/(CAPPA**3)
94300      GO TO 622
94400      621 TAUWR = VISCOS*VAVG/XP
94500      TAUW = VISCOS*W(I,J)/XP
94600      TAUW(J)=SQRT(TAUWR**2+TAUW**2)
94700      DITERM = DEN(I,J)*(CMU**0.75)*SORTK*XPLUSW(J)/XP
94800      622 CVDX = ((V(I,J)+V(I,J+1)+V(I+1,J)+V(I+1,J+1))/4.0-
94900      * (V(I,J)+V(I,J+1)+V(I-1,J)+V(I-1,J+1))/4.0)/SFW(I)
95000      GENCOU = TAUW(J)**2/VIS(I,J)
95100      GENRES = GEN(I,J)-VIS(I,J)*(CVDX**2+CWDX**2)
95200      GEN(I,J) = GENRES+GENCOU
95300      SU(I,J) = SU(I,J)+SUKD(I,J)+GEN(I,J)*VOL
95400      SP(I,J) = SP(I,J)+SPKD(I,J)-DITERM*VOL
95500      AW(I,J) = 0.0
95600      620 CONTINUE
95700      625 CONTINUE
95800      TAUW(NJ) = TAUW(NJM1)
95900      C-----SYMMETRY AXIS
96000      614 CONTINUE
96100      J = 2
96200      DO 630 I = 2,NIM1
96300      DUDY = ((U(I,J)+U(I+1,J)+U(I,J+1)+U(I+1,J+1))/4.0-
96400      * (U(I,J)+U(I+1,J)+U(I,J-1)+U(I+1,J-1))/4.0)/SAG(J)
96500      VOL = PCV(J)*SNG(J)*SEW(I)
96600      GEN(I,J) = GEN(I,J)-VIS(I,J)*DUDY**2
96700      SU(I,J) = SUKD(I,J)+GEN(I,J)*VOL
96800      630 AS(I,2) = 0.0
96900      C-----OUTLET
97000      DO 640 J = 2,NJM1
97100      AS(NIM1,J) = 0.0
97200      640 CONTINUE
97300      RETURN
97400      C
97500      CHAPTER 7 7 7 7 DISSIPATION 7 7 7 7
97600      C

```

```

97700      7 CONTINUE
97800      C-----TOP WALL
97900          DO 710 I = 2,NIM1
98000              U = UMAX(I)
98100              YP=Y/(U+1)-Y(U)
98200              TERM = (CMC**0.75)/(CAPPA*YP)
98300              CU(I,U) = GREAT*TERM*TE(I,U)**1.5
98400              710 SP(I,U) = -GREAT
98500      C-----SIDE WALL
98600          IF (JSTEP .EQ. NJM1) GO TO 714
98700          DO 725 I = 2,NIM1
98800              IF (UMAX(I-1) .GE. UMAX(I)) GO TO 725
98900              JU = UMAX(I-1)
99000              UI = UMAX(I)
99100              DO 720 J = JU,UI
99200                  IF (J .EQ. UMAX(I)) GO TO 720
99300                  XP = X(I)-X(J)
99400                  TERM = (CMC**0.75)/(CAPPA*XP)
99500                  CU(I,J) = GREAT*TERM*TE(I,J)**1.5
99600                  SP(I,J) = -GREAT
99700          720 CONTINUE
99800          725 CONTINUE
99900      C-----SYMMETRY AXIS

```

```

00100      714 CONTINUE
00200      DO 730 I = 2,NIM1
00300      730 AS(I,2) = 0.0
00400      C-----OUTLET
00500      DO 740 J = 2,NOM1
00600      AS(NIM1,J) = 0.0
00700      740 CONTINUE
00800      RETURN
00900      C
01000      CHAPTER 8 8 8 8 8 WIRE VELOCITY R R R R R
01100      C
01200      4 CONTINUE
01300      C-----TOP WALL
01400      CTERM = CMC*.025
01500      DO 110 I = 2,NIM1
01600      U = UMAX(I)
01700      YP = Y/(U+1)-Y(0)
01800      CORTK = CORT(TE(I,U))
01900      DENW = DEN(I,U)
02000      YPLUSA = YPLUSN(I)
02100      IF(YPLUSA.LE. 11.63) GO TO 411
02200      TMULT = DENW*CTERM*CORTK*CAPPA/ALOG(ELUG*YPLUSA)-VIS(I,U)/Y(U)
02300      GO TO 412
02400      411 TMULT = VISCOS/YP
02500      412 CP(I,U) = CP(I,U)-TMULT*DEN(I)*RV(U+1)
02600      AS(I,U) = 0.0
02700      410 CONTINUE
02800      C-----SIDEWALL
02900      IF(CTERM.LE. NOM1) GO TO 414
03000      DO 450 I = 2,NIM1
03100      IF(UMAX(I-1).GE. UMAX(I)) GO TO 455
03200      UJ = UMAXP1(I-1)
03300      UJ = UMAX(I)
03400      DO 450 J = 0,UJ
03500      KP = K(I) - KC(I)
03600      CORTK = CORT(TE(I,U))
03700      DENW = DEN(I,U)
03800      XPLUSA = XPLUSW(U)
03900      IF(XPLUSA.LE. 11.63) GO TO 451
04000      TMULT = DENW*CTERM*CORTK*CAPPA/ALOG(EL(C)*XPLUSA)
04100      GO TO 452
04200      451 TMULT = VISCOS/KP
04300      452 CP(I,U) = CP(I,U)-TMULT*ENC(U)*RCV(U)
04400      AS(I,U) = 0.0
04500      450 CONTINUE
04600      455 CONTINUE
04700      C-----SYMMETRY AXIS
04800      414 CONTINUE
04900      C-----FIX W FOR SOLID BODY ROTATION AT J=2 USING W AT J=3
05000      DO 560 I = 2,NIM1
05100      TERM = K(1,3)*R(2)/R(3)
05200      CU(I,2) = GREAT*TERM
05300      560 CP(I,2) = -GREAT
05400      C-----OUTLET
05500      DO 570 J = 2,NOM1
05600      570 AS(NIM1,J) = 0.0
05700      RETURN
05800      END
05900      C
06000      C-----
06100      C

```



```

06200      SUBROUTINE STRMFN
06300      C*****
06400      C
06500      CHAPTER 0 0 0 0 PRELIMINARIES 0 0 0 0
06600      C
06700      COMMON
06800      $/VVEL/RESORV,NSWPV,URFV,DYNPV(24),DYPSV(24),SNSV(24)
06900      $/VAR/U(48,24),V(48,24),W(48,24),P(48,24),PP(48,24),
07000      STE(48,24),ED(48,24),STFN(48,24),YSTLN(48,24),STVAL(24),
07100      $UCTAR(48,24),VSTAR(48,24),WSTAR(48,24),FSTAR(48,24),
07200      $TESTAR(48,24),YSTLNC(48,24),VISTAR(48,24)
07300      $/ALL/IT,UT,NI,NJ,NIM1,NJM1,IGREAT,UMAX(48),UMAXP1(48)
07400      $/GEOM/INCCOC,X(48),Y(24),DXEP(48),DXEPW(48),DYNP(24),DYNP1(24),
07500      $CNS(24),CFW(48),XU(48),YV(24),R(24),RV(24),
07600      $WFW(24),WFC(24),WFE(48),WFW(48),RCV(24),ANC(48),XUNC(48),
07700      $YUNC(24),YUNC(24)
07800      $/KASE/IT/UT,TEIN,EDIN,FLOWIN,ALAMDA,
07900      $RSMALL,ALARGE,AL1,AL2,UCTEP,ISTEP,USTP1,USTM1,ISTP1,ISTM1
08000      $/PLOTT/YSTLN,NPLTLN,NPTS,YSLPLT(10,48),XUCPLT(48),INPLOT
08100      LOGICAL INPLOT
08200      C
08300      CHAPTER 1 1 1
08400      CALCULATE STREAM FUNCTION BASED ON VOLUMETRIC FLOW
08500      C
08600      Q = UIN*(RSMALL**2)/C.C
08700      DO 400 I = 2,NI
08800      IF(UMAX(I-1).LT. 5) GO TO 400
08900      DTFV(I,2) = (Y(I)*R(2)*U(I,2)*C.5)/Q
09000      JU = UMAX(I-1)
09100      DO 200 J = 3,NU
09200      STFN(I,J) = STFN(I,J-1) + SNSV(J) * (R(J-1)*U(I,J-1) + R(J)*U(I,J)) * C.5/7
09300      200 CONTINUE
09400      400 CONTINUE
09500      C
09600      DO 400 I = 2,NI
09700      JU = UMAXP1(I-1)
09800      DO 700 K = 1,YSTLN
09900      AK = K-1
10000      STVAL(K) = AK*C.1
10100      JU = UMAX(I-1)
10200      DO 600 J = 2,NU
10300      IF(CTFN(I,J).GE. STVAL(K)) GO TO 650
10400      600 CONTINUE
10500      YSTLN(I,K) = RV(JU)
10600      GO TO 670
10700      650 IF(J.LE. 3) YSTLN(I,K) = C.C
10800      IF(J.EQ. 3) GO TO 670
10900      SLOPE = (STVAL(K) - STFN(I,J-1))/(CTFN(I,J) - STFN(I,J-1))
11000      YSTLN(I,K) = Y(J-1) + SLOPE*(Y(J) - Y(J-1))
11100      670 CONTINUE
11200      YSTLNC(I,K) = YSTLN(I,K)/(2.0*ALARGE)
11300      700 CONTINUE
11400      400 CONTINUE
11500      C      IF(.NOT. INPLOT) GO TO 740
11600      N = 0
11700      DO 730 K = 1,11,2
11800      N = N+1
11900      DO 730 I = 1,NIM1
12000      YSLPLT(N,I) = YSTLNC(I+1,K)
12100      730 CONTINUE
12200      DO 740 I = 1,NIM1

```

```

12300      X(1) = XONE(1)
12400      740 CONTINUE
12500      C      WRITE(14,*) *      COORDINATED      FOR      STREAMLINE*
12600      C      DO 1411 K=1,11
12700      C      WRITE(14,*) *STREAMLINE # 'A',*      VALUE = *DTVAL(K)
12800      C      DO 1411 I=1,NIM1
12900      C      WRITE(14,*) * X=COORD * XONE(I),* Y=COORD * YONE(I)
13000      C 1411 CONTINUE
13100      745 NPTS = NIM1
13200      RETURN
13300      END
13400      C
13500      C
13600      SUBROUTINE PLOT (X,ICIM,IMAX,XEND,Y,JCIM,JMAX,YARE,SYMBOL,VAR)
13700      C.....
13800      C
13900      C      X AND Y ARE ASSUMED TO BE IN ANY RANGE EXCEPT THAT NEGATIVE
14000      C      VALUES ARE PLOTTED AS ZERO
14100      C      X AND Y ARE SCALED TO THE RANGE 0 TO 1 BY DIVISION BY THE
14200      C      MAXIMA, WHICH ARE ALSO PRINTED.
14300      C      ICIM IS THE DIMENSION FOR X
14400      C      IMAX IS THE NUMBER OF X VALUES
14500      C      X-AXIS IS THE NAME OF THE X-AXIS
14600      C      JCIM IS THE VARIABLE DIMENSION FOR Y
14700      C      JMAX IS THE NUMBER OF CURVES TO BE PLOTTED (UP TO 10)
14800      C      THE ARRAY YARE(J) STORES THE NAMES OF THE CURVES
14900      C      THE ARRAY SYMBOL(J) STORES THE SINGLE CHARACTERS USED FOR PLOTTING
15000      C.....
15100      C.....
15200      DIMENSION X(ICIM),Y(JCIM,ICIM),YARE(JCIM),SYMBOL(JCIM),A(1,1),
15300      1YMAX(10),AA(20)
15400      CHARACTER A,DOT,CROSS,PLANK
15500      DATA DOT,CROSS,PLANK/'.',*,*,*,* //
15600      C-----COALING X-ARRAY TO THE RANGE 0 TO 100
15700      XMAX = 1.0E+30
15800      DO 1 I = 1,IMAX
15900      IF(X(I) .GT. XMAX) XMAX=X(I)
16000      1 CONTINUE
16100      DO 2 I = 1,IMAX
16200      A(I) = X(I)/XMAX*100.0
16300      IF(X(I) .LT. 0.0) X(I) = 0.0
16400      2 CONTINUE
16500      C-----COALING Y-ARRAY TO THE RANGE 0 TO 100
16600      DO 3 J = 1,JMAX
16700      YMAX(J) = 1.0E+30
16800      DO 4 I = 1,IMAX
16900      IF(Y(J,I) .GT. YMAX(J)) YMAX(J) = Y(J,I)
17000      4 CONTINUE
17100      DO 5 I = 1,IMAX
17200      C-----DO Y-SCALING
17300      Y(J,I) = Y(J,I)*100.0
17400      IF(Y(J,I) .GT. 100.0) Y(J,I) = 100.0*Y(J,I)
17500      IF(Y(J,I) .LT. 0.0) Y(J,I) = 0.0
17600      5 CONTINUE
17700      C-----IDENTIFYING THE VARIOUS CURVES TO BE PLOTTED
17800      WRITE(6,100) XAXIS
17900      WRITE(6,100) (YARE(I),I = 1,JMAX)
18000      WRITE(6,100) (SYMBOL(I),I = 1,JMAX)
18100      WRITE(6,100) (YMAX(I),I = 1,JMAX)
18200      DO 6 I = 1,11
18300      6 X(I)=XONE(I)

```

35.80

```

14500 100 FORMAT(11H V-AXIS: ARE,5X,10(1X,A10))
14600 101 FORMAT(11H0,2A,11F10.1)
14700 102 FORMAT(15H MAXIMUM VALUES, 10F11.3)
14800 103 FORMAT(11HIN-AXIS: 10, A3)
14900 104 FORMAT(3X,11F10.1)
15000 105 FORMAT(7H A, F5.2, 3X, 101A1, F5.2)
15100 106 FORMAT(7H SYMBOL, 11X, 10(1X, A10))
15200 107 FORMAT(7H A, F5.2, 3X, 101A1, F5.2)
15300 108 FORMAT(77, F5.2, 11ADIAL POSITION: 47(1X, 77))
15400 109 FORMAT(77, F5.2, 11ADIAL POSITION: 47(1X, 77))
15500 110 FORMAT(77, F5.2, 11ADIAL POSITION: 47(1X, 77))
15600 111 FORMAT(77, F5.2, 11ADIAL POSITION: 47(1X, 77))
15700 112
15800
15900 *** BEGINNING OF INJECTED SECTION *** BEGINNING OF INJECTED SECTION ***
16000
16100 List of variables:
16200 Integers:
16300 I - Axial index number for the i cell.
16400 J - Old axial index number for the i cell.
16500 K - Axial index number for the k cell.
16600 ICONT - Counter for number of liquid phase iterations.
16700 ICONV - Global convergence flag.
16800 ISTOP - Flag: 1 if drop is in the flow domain.
16900 IREIN - Number of re-integrations.
17000 IREINFL - Integration flag.
17100 ISTEP - Number of steps travelled by the drop.
17200 I - Axial index number for the i cell.
17300 J - Axial index number for the j cell.
17400 K - Axial index number for the k cell.
17500 L - Old radial index number for the i cell.
17600 M - Radial index number for the i cell.
17700 JMAX - Variable equivalent to JMAX in the main program.
17800 J - Radial index number for the j cell.
17900 K - Radial index number for the k cell.
18000 MAXIT - Maximum number of liquid phase iterations allowed.
18100 MAXST - Maximum number of steps allowed for drop.
18200 NPORT - Port number.
18300 N - Variable equivalent to N in the main program.
18400 N - Variable equivalent to N in the main program.
18500
18600
18700
18800
18900
19000
19100
19200
19300
19400
19500
19600
19700
19800
19900
20000
20100
20200
20300
20400
20500
20600
20700
20800
20900
21000
21100
21200
21300
21400
21500
21600
21700
21800
21900
22000
22100
22200
22300
22400
22500
22600
22700
22800
22900
23000
23100
23200
23300
23400
23500
23600
23700
23800
23900
24000
24100
24200
24300
24400
24500
24600
24700
24800
24900
25000
25100
25200
25300
25400
25500
25600
25700
25800
25900
26000
26100
26200
26300
26400
26500
26600
26700
26800
26900
27000
27100
27200
27300
27400
27500
27600
27700
27800
27900
28000
28100
28200
28300
28400
28500
28600
28700
28800
28900
29000
29100
29200
29300
29400
29500
29600
29700
29800
29900
30000
30100
30200
30300
30400
30500
30600
30700
30800
30900
31000
31100
31200
31300
31400
31500
31600
31700
31800
31900
32000
32100
32200
32300
32400
32500
32600
32700
32800
32900
33000
33100
33200
33300
33400
33500
33600
33700
33800
33900
34000
34100
34200
34300
34400
34500
34600
34700
34800
34900
35000
35100
35200
35300
35400
35500
35600
35700
35800
35900
36000
36100
36200
36300
36400
36500
36600
36700
36800
36900
37000
37100
37200
37300
37400
37500
37600
37700
37800
37900
38000
38100
38200
38300
38400
38500
38600
38700
38800
38900
39000
39100
39200
39300
39400
39500
39600
39700
39800
39900
40000
40100
40200
40300
40400
40500
40600
40700
40800
40900
41000
41100
41200
41300
41400
41500
41600
41700
41800
41900
42000
42100
42200
42300
42400
42500
42600
42700
42800
42900
43000
43100
43200
43300
43400
43500
43600
43700
43800
43900
44000
44100
44200
44300
44400
44500
44600
44700
44800
44900
45000
45100
45200
45300
45400
45500
45600
45700
45800
45900
46000
46100
46200
46300
46400
46500
46600
46700
46800
46900
47000
47100
47200
47300
47400
47500
47600
47700
47800
47900
48000
48100
48200
48300
48400
48500
48600
48700
48800
48900
49000
49100
49200
49300
49400
49500
49600
49700
49800
49900
50000
50100
50200
50300
50400
50500
50600
50700
50800
50900
51000
51100
51200
51300
51400
51500
51600
51700
51800
51900
52000
52100
52200
52300
52400
52500
52600
52700
52800
52900
53000
53100
53200
53300
53400
53500
53600
53700
53800
53900
54000
54100
54200
54300
54400
54500
54600
54700
54800
54900
55000
55100
55200
55300
55400
55500
55600
55700
55800
55900
56000
56100
56200
56300
56400
56500
56600
56700
56800
56900
57000
57100
57200
57300
57400
57500
57600
57700
57800
57900
58000
58100
58200
58300
58400
58500
58600
58700
58800
58900
59000
59100
59200
59300
59400
59500
59600
59700
59800
59900
60000
60100
60200
60300
60400
60500
60600
60700
60800
60900
61000
61100
61200
61300
61400
61500
61600
61700
61800
61900
62000
62100
62200
62300
62400
62500
62600
62700
62800
62900
63000
63100
63200
63300
63400
63500
63600
63700
63800
63900
64000
64100
64200
64300
64400
64500
64600
64700
64800
64900
65000
65100
65200
65300
65400
65500
65600
65700
65800
65900
66000
66100
66200
66300
66400
66500
66600
66700
66800
66900
67000
67100
67200
67300
67400
67500
67600
67700
67800
67900
68000
68100
68200
68300
68400
68500
68600
68700
68800
68900
69000
69100
69200
69300
69400
69500
69600
69700
69800
69900
70000
70100
70200
70300
70400
70500
70600
70700
70800
70900
71000
71100
71200
71300
71400
71500
71600
71700
71800
71900
72000
72100
72200
72300
72400
72500
72600
72700
72800
72900
73000
73100
73200
73300
73400
73500
73600
73700
73800
73900
74000
74100
74200
74300
74400
74500
74600
74700
74800
74900
75000
75100
75200
75300
75400
75500
75600
75700
75800
75900
76000
76100
76200
76300
76400
76500
76600
76700
76800
76900
77000
77100
77200
77300
77400
77500
77600
77700
77800
77900
78000
78100
78200
78300
78400
78500
78600
78700
78800
78900
79000
79100
79200
79300
79400
79500
79600
79700
79800
79900
80000
80100
80200
80300
80400
80500
80600
80700
80800
80900
81000
81100
81200
81300
81400
81500
81600
81700
81800
81900
82000
82100
82200
82300
82400
82500
82600
82700
82800
82900
83000
83100
83200
83300
83400
83500
83600
83700
83800
83900
84000
84100
84200
84300
84400
84500
84600
84700
84800
84900
85000
85100
85200
85300
85400
85500
85600
85700
85800
85900
86000
86100
86200
86300
86400
86500
86600
86700
86800
86900
87000
87100
87200
87300
87400
87500
87600
87700
87800
87900
88000
88100
88200
88300
88400
88500
88600
88700
88800
88900
89000
89100
89200
89300
89400
89500
89600
89700
89800
89900
90000
90100
90200
90300
90400
90500
90600
90700
90800
90900
91000
91100
91200
91300
91400
91500
91600
91700
91800
91900
92000
92100
92200
92300
92400
92500
92600
92700
92800
92900
93000
93100
93200
93300
93400
93500
93600
93700
93800
93900
94000
94100
94200
94300
94400
94500
94600
94700
94800
94900
95000
95100
95200
95300
95400
95500
95600
95700
95800
95900
96000
96100
96200
96300
96400
96500
96600
96700
96800
96900
97000
97100
97200
97300
97400
97500
97600
97700
97800
97900
98000
98100
98200
98300
98400
98500
98600
98700
98800
98900
99000
99100
99200
99300
99400
99500
99600
99700
99800
99900
100000

```

```

30600      C      VGAS      - Axial speed of the gas.
30700      C      VGOLD() - Old axial velocity of gas.
30800      C      VGINIT() - Initial radial speed of droplet.
30900      C      VNEW      - New radial velocity of droplet.
31000      C      VOLD      - Old radial velocity of droplet.
31100      C      VGO      - Radial velocity of gas.
31200      C      VGAS      - Radial speed of the gas.
31300      C      VGOLD() - Old radial velocity of gas.
31400      C      XH()      - Coordinates of lower left corner of
31500      C      XINIT() - Initial axial-coordinate of droplet.
31600      C      XNEW      - New axial location of droplet.
31700      C      XOLD      - Old axial location of droplet.
31800      C      YH()      - the n-cells.
31900      C      YINIT() - Initial radial-coordinate of droplet.
32000      C      YNEW      - New radial location of droplet.
32100      C      YOLD      - Old radial location of droplet.
32200
32300      .....
32400
32500
32600      SUBROUTINE DRDP
32700      COMMON /DRDP/ MAXPGR, NPORT,
32800      $   URPRDN(10), URPDIA(10), URMGOT(10), DRPREC(10),
32900      $   XINIT(10), YINIT(10), TINIT(10), UGINIT(10), VGINIT(10),
33000      $   XH(48), YH(48),
33100      $   UG(48, 24), VG(48, 24), VGOLD(48, 24),
33200      $   UGAS, VHAVAL, GRAVAL, RAD, XHOGAS, FI, GRAS, VGAS,
33300      $   XGOLD, YGOLD, TGOLD, XGOLD, YGOLD,
33400      $   XNEW, YNEW, TNEW, UNEW, VNEW,
33500      $   IT, ITHIN, ITHIN, FHOL,
33600      $   IOTERD, IOTERD, IFLAGD, ITH, MAXOTR, MAXOT, INTERL,
33700      $   IC, UC, IV, UV, IC, UC, IP, UP, IHOLD, UHOLD, IOTENT,
33800      $   UGAS, VHAVAL, UHMAX(48), XDI, YDI
33900      COMMON/GRF/RMOMV(50,50),RMOMU(50,50)
34000      INTEGER LOWER
34100      OPEN (UNIT = 12)
34200      DO 1000 NPORT = 1, MAXPGR
34300      Integrate for each port.
34400
34500      Initialize parameters for drdp.
34600      XOLD = XINIT(NPORT)
34700      YOLD = YINIT(NPORT)
34800      TOLD = TINIT(NPORT)
34900      UOLD = UGINIT(NPORT)
35000      VOLD = VGINIT(NPORT)
35100      XNEW = XINIT(NPORT)
35200      YNEW = YINIT(NPORT)
35300      TNEW = TINIT(NPORT)
35400      UNEW = UGINIT(NPORT)
35500      RAD = URPDIA(NPORT)/2.0
35600      FHOL = URPRDN(NPORT)
35700
35800      Initialize counters and flags.
35900      ITHIN = 0
36000      UHOLD = 0
36100      IOTERD = 0
36200      IOTERD = 0
36300      ITH = 0
36400      INTERL = 0
36500
36600      Initialize IC, UC, IV, UC, IC, UC, IV and UV.

```

```

36700      CALL FINDB
36800      C      Initialize drop momentum source term at injection point.
36900      C
37000      II=NPORT
37100      DELTA=4.0*PI*RHOL*RAD**3/3.0*DRFREQ(II)
37200      RMOMU(IG,JU)=DELTA*UDINIT(II)
37300      RMOMV(IV,JV)=DELTA*VDINIT(II)
37400      C
37500      IBOLD = IB
37600      JBOLD = JB
37700      100      CONTINUE
37800      C      New integration step starts here.
37900      CGAS = CG(IG, JU)
38000      VGAS = VG(IV, JV)
38100      200      CONTINUE
38200      C      Returns here for reintegration if the time step
38300      C      was incorrect.
38400      C
38500      CALL RUNGA
38600      CALL DOMCHK
38700      IF (IHIT .NE. 0) THEN
38800          WRITE (5, *) ' DOMCHK: IHIT = ', IHIT, ' NPORT = ', NPORT
38900          GOTO 800
39000      ENDIF
39100      CALL FINDB
39200      CALL HITWAL
39300      IF (IHIT .NE. 0) THEN
39400          WRITE (5, *) ' HITWAL: IHIT = ', IHIT, ' NPORT = ', NPORT
39500          GOTO 800
39600      ENDIF
39700      CALL STPCHK
39800      IF (INTELG .NE. 0) THEN
39900          C      Reintegration is required.
40000          INTCTR = INTCTR + 1
40100          IF (INTCTR .GT. 20) THEN
40200              WRITE(5, *) ' TOO MANY REINTEGRATIONS'
40300              WRITE(5, *) ' NPORT = ', NPORT, ' X = ', XOLD,
40400                  ' Y = ', YOLD, ' ICDUNT = ', ICDUNT
40500              IF (INTELG .EQ. 1) THEN
40600                  WRITE (5, *) ' TIME STEP TOO LARGE, DT = ', DT
40700                  WRITE (5, *) ' INPUT NEW TIME STEP'
40800              ELSE IF (INTELG .EQ. 2) THEN
40900                  WRITE (5, *) ' TIME STEP TOO SMALL, DT = ', DT
41000                  WRITE (5, *) ' INPUT NEW TIME STEP'
41100              ENDIF
41200              READ(5, *) DT
41300              INTCTR = 0
41400          ENDIF
41500          GOTO 200
41600      ENDIF
41700      INTCTR = 0
41800      CALL FINDB
41900      CALL FINDM
42000      WRITE(24, *) ' DROP: ', XOLD, YOLD, TOLD, UOLD, VOLD,
42100          ' XNEW, YNEW, TNEW, UNEW, VNEW,
42200          ' DT, DTINC, DTREQ,
42300          ' IOTEND, INTCTR, IFLAGZ, IHIT, MAXSTP, MAXCT, INTELG,
42400          ' IG, JU, IV, JV, IC, JJ, IB, JB, IBOLD, JBOLD, ICDUNT,
42500          ' NCASE, MCASE
42600      3      NCASE, MCASE
42700      C
42800      IF (NCASE .EQ. 0) THEN

```

```

42900      WRITE(5, *) 'ERROR: NCASE = 0'
43000      STOP
43100      ENDIF
43200      C
43300      IF (MCASE.EQ. 1) THEN
43400          IF (NCASE.EQ. 1) THEN
43500      C      0-cell vertical boundary.
43600          X1 = XCOLD
43700          X2 = XNEW
43800          X3 = XE(15)
43900          Y1 = TCOLD
44000          Y2 = TNEW
44100          IM1 = IC - 1
44200          IM2 = IC
44300          JM1 = JC
44400          JM2 = JC
44500          CALL INTERP(X1, Y1, X2, Y2, X3, Y3)
44600          CALL CM2D(IM1, IM2, JM1, JM2, Y3)
44700      C      v-cell vertical boundary.
44800          Y1 = VCOLD
44900          Y2 = VNEW
45000          IM1 = IC - 1
45100          IM2 = IC
45200          JM1 = JC
45300          JM2 = JC
45400          CALL INTERP(X1, Y1, X2, Y2, X3, Y3)
45500          CALL CM2D(IM1, IM2, JM1, JM2, Y3)
45600      C
45700      ELSE IF (MCASE.EQ. 2) THEN
45800      C      Check for path.
45900          X1 = XCOLD
46000          X2 = XNEW
46100          X3 = XE(15)
46200          Y1 = YCOLD
46300          Y2 = YNEW
46400          CALL INTERP(X1, Y1, X2, Y2, X3, Y3)
46500          IF (Y3.LT. YE(JE)) THEN
46600              LOWER = 1
46700          ELSE
46800              LOWER = 0
46900          ENDIF
47000      C      0-cell vertical boundary.
47100          Y1 = TCOLD
47200          Y2 = TNEW
47300          IM1 = IC - 1
47400          IM2 = IC
47500          IF (LOWER.EQ. 1) THEN
47600              JM1 = JC - 1
47700              JM2 = JC - 1
47800          ELSE
47900              JM1 = JC
48000              JM2 = JC
48100          ENDIF
48200          CALL INTERP(X1, Y1, X2, Y2, X3, Y3)
48300          CALL CM2D(IM1, IM2, JM1, JM2, Y3)
48400      C      v-cell vertical boundary.
48500          Y1 = VCOLD
48600          Y2 = VNEW
48700          IM1 = IC - 1
48800          IM2 = IC
48900          JM1 = JC

```

```

49000      JM2 = JV
49100      CALL INTERP(X1, Y1, X2, Y2, X3, Y3)
49200      CALL VMOD(IM1, IM2, JM1, JM2, Y3)
49300  C      C-cell horizontal boundary.
49400      X1 = YDOLD
49500      X2 = YDNEW
49600      X3 = YB(JB)
49700      Y1 = TDOLD
49800      Y2 = TDNEW
49900      IF (LOWER .EQ. 1) THEN
50000          IM1 = IC
50100          IM2 = IC
50200      ELSE
50300          IM1 = IC - 1
50400          IM2 = IC - 1
50500      ENDIF
50600      JM1 = JC - 1
50700      JM2 = JC
50800      CALL INTERP(X1, Y1, X2, Y2, X3, Y3)
50900      CALL CMOD(IM1, IM2, JM1, JM2, Y3)
51000  C      C-cell horizontal boundary.
51100      Y1 = UDOLD
51200      Y2 = UDNEW
51300      IM1 = IC
51400      IM2 = IC
51500      JM1 = JC - 1
51600      JM2 = JC
51700      CALL INTERP(X1, Y1, X2, Y2, X3, Y3)
51800      CALL CMOD(IM1, IM2, JM1, JM2, Y3)
51900  C
52000      ELSE IF (NCASE .EQ. 3) THEN
52100  C      C-cell horizontal boundary.
52200      X1 = YDOLD
52300      X2 = YDNEW
52400      X3 = YB(JB)
52500      Y1 = TDOLD
52600      Y2 = TDNEW
52700      IM1 = IC
52800      IM2 = IC
52900      JM1 = JC - 1
53000      JM2 = JC
53100      CALL INTERP(X1, Y1, X2, Y2, X3, Y3)
53200      CALL CMOD(IM1, IM2, JM1, JM2, Y3)
53300  C      C-cell horizontal boundary.
53400      Y1 = UDOLD
53500      Y2 = UDNEW
53600      IM1 = IC
53700      IM2 = IC
53800      JM1 = JC - 1
53900      JM2 = JC
54000      CALL INTERP(X1, Y1, X2, Y2, X3, Y3)
54100      CALL CMOD(IM1, IM2, JM1, JM2, Y3)
54200  C
54300      ELSE IF (NCASE .EQ. 4) THEN
54400  C      Check for path.
54500      X1 = XDOLD
54600      X2 = XDNEW
54700      X3 = XB(IB + 1)
54800      Y1 = YDOLD
54900      Y2 = YDNEW
55000      CALL INTERP(X1, Y1, X2, Y2, X3, Y3)

```



```

55100      IF (Y3 .LT. YB(JB)) THEN
55200          LOWER = 1
55300      ELSE
55400          LOWER = 0
55500      ENDIF
55600  C      U-cell vertical boundary.
55700          Y1 = UDOLD
55800          Y2 = UDNEW
55900          IM1 = IU + 1
56000          IM2 = IU
56100          IF (LOWER .EQ. 1) THEN
56200              JM1 = JU - 1
56300              JM2 = JU - 1
56400          ELSE
56500              JM1 = JU
56600              JM2 = JU
56700          ENDIF
56800          CALL INTERP(X1, Y1, X2, Y2, X3, Y3)
56900          CALL UMOD(IM1, IM2, JM1, JM2, Y3)
57000  C      C-cell horizontal boundary.
57100          X1 = YDOLD
57200          X2 = YDNEW
57300          X3 = YB(JB)
57400          Y1 = TDOLD
57500          Y2 = TDNEW
57600          IM1 = IC
57700          IM2 = IC
57800          JM1 = JC - 1
57900          JM2 = JC
58000          CALL INTERP(X1, Y1, X2, Y2, X3, Y3)
58100          CALL CMOD(IM1, IM2, JM1, JM2, Y3)
58200  C      U-cell horizontal boundary.
58300          Y1 = UDOLD
58400          Y2 = UDNEW
58500          IF (LOWER .EQ. 1) THEN
58600              IM1 = IU
58700              IM2 = IU
58800          ELSE
58900              IM1 = IU + 1
59000              IM2 = IU + 1
59100          ENDIF
59200          JM1 = JU - 1
59300          JM2 = JU
59400          CALL INTERP(X1, Y1, X2, Y2, X3, Y3)
59500          CALL UMOD(IM1, IM2, JM1, JM2, Y3)
59600  C
59700      ELSE IF (NCASE .EQ. 5) THEN
59800  C      U-cell vertical boundary.
59900          X1 = XDOLD
60000          X2 = XDNEW
60100          X3 = XR(IR + 1)
60200          Y1 = UDOLD
60300          Y2 = UDNEW
60400          IM1 = IU + 1
60500          IM2 = IU
60600          JM1 = JU
60700          JM2 = JU
60800          CALL INTERP(X1, Y1, X2, Y2, X3, Y3)
60900          CALL UMOD(IM1, IM2, JM1, JM2, Y3)
61000  C
61100      ELSE IF (NCASE .EQ. 6) THEN

```

```

61200      C          U-cell vertical boundary.
61300          X1 = XDOLD
61400          X2 = XDNEW
61500          X3 = XB(IB + 1)
61600          Y1 = UDOLD
61700          Y2 = UDNEW
61800          IM1 = IU + 1
61900          IM2 = IU
62000          JM1 = JU
62100          JM2 = JU
62200          CALL INTERP(X1, Y1, X2, Y2, X3, Y3)
62300          CALL UMOD(IM1, IM2, JM1, JM2, Y3)
62400      C          V-cell horizontal boundary.
62500          X1 = YDOLD
62600          X2 = YDNEW
62700          X3 = YB(JB + 1)
62800          Y1 = VDOLD
62900          Y2 = VDNEW
63000          IM1 = IV
63100          IM2 = IV
63200          JM1 = JV + 1
63300          JM2 = JV
63400          CALL INTERP(X1, Y1, X2, Y2, X3, Y3)
63500          CALL VMOD(IM1, IM2, JM1, JM2, Y3)
63600      C
63700      C
63800          ELSE IF (NCASE .EQ. 7) THEN
63900      C          V-cell horizontal boundary.
64000          X1 = YDOLD
64100          X2 = YDNEW
64200          X3 = YB(JB + 1)
64300          Y1 = VDOLD
64400          Y2 = VDNEW
64500          IM1 = IV
64600          IM2 = IV
64700          JM1 = JV + 1
64800          JM2 = JV
64900          CALL INTERP(X1, Y1, X2, Y2, X3, Y3)
65000          CALL VMOD(IM1, IM2, JM1, JM2, Y3)
65100      C
65200          ELSE IF (NCASE .EQ. 8) THEN
65300      C          Check for path.
65400          X1 = XDOLD
65500          X2 = XDNEW
65600          X3 = XB(IB)
65700          Y1 = YDOLD
65800          Y2 = YDNEW
65900          CALL INTERP(X1, Y1, X2, Y2, X3, Y3)
66000          IF (Y3 .LT. YB(JB + 1)) THEN
66100              LOWER = 1
66200          ELSE
66300              LOWER = 0
66400          ENDIF
66500      C          C-cell vertical boundary.
66600          Y1 = TDOLD
66700          Y2 = TDNEW
66800          IM1 = IC - 1
66900          IM2 = IC
67000          JM1 = JC
67100          JM2 = JC
67200          CALL INTERP(X1, Y1, X2, Y2, X3, Y3)

```

```

67300      CALL CMOD(IM1, IM2, JM1, JM2, Y3)
67400      C      V-cell vertical boundary.
67500          Y1 = VDOLD
67600          Y2 = VDNEW
67700          IM1 = IV - 1
67800          IM2 = IV
67900          IF (LOWER .EQ. 1) THEN
68000              JM1 = JV
68100              JM2 = JV
68200          ELSE
68300              JM1 = JV + 1
68400              JM2 = JV + 1
68500          ENDIF
68600      CALL INTERP(X1, Y1, X2, Y2, X3, Y3)
68700      CALL VMOD(IM1, IM2, JM1, JM2, Y3)
68800      C      V-cell horizontal boundary.
68900          X1 = YDOLD
69000          X2 = YDNEW
69100          X3 = YB(JB + 1)
69200          IF (LOWER .EQ. 1) THEN
69300              IM1 = IV - 1
69400              IM2 = IV - 1
69500          ELSE
69600              IM1 = IV
69700              IM2 = IV
69800          ENDIF
69900          JM1 = JV + 1
70000          JM2 = JV
70100      CALL INTERP(X1, Y1, X2, Y2, X3, Y3)
70200      CALL VMOD(IM1, IM2, JM1, JM2, Y3)
70300      ENDIF
70400      C
70500      ELSE IF (MCASE .EQ. 2) THEN
70600          IF (NCASE .EQ. 1) THEN
70700              C      U-cell vertical boundary.
70800                  X1 = XDOLD
70900                  X2 = XDNEW
71000                  X3 = XB(IB)
71100                  Y1 = UDOLD
71200                  Y2 = UDNEW
71300                  IM1 = IU - 1
71400                  IM2 = IU
71500                  JM1 = JU
71600                  JM2 = JU
71700                  CALL INTERP(X1, Y1, X2, Y2, X3, Y3)
71800                  CALL UMOD(IM1, IM2, JM1, JM2, Y3)
71900              C
72000          ELSE IF (NCASE .EQ. 2) THEN
72100              C      Check for path.
72200                  X1 = XDOLD
72300                  X2 = XDNEW
72400                  X3 = XB(IB)
72500                  Y1 = YDOLD
72600                  Y2 = YDNEW
72700                  CALL INTERP(X1, Y1, X2, Y2, X3, Y3)
72800                  IF (Y3 .LT. YB(JB)) THEN
72900                      LOWER = 1
73000                  ELSE
73100                      LOWER = 0
73200                  ENDIF
73300              C      U-cell vertical boundary.

```

```

73400      Y1 = UDOLD
73500      Y2 = UDNEW
73600      IM1 = IU - 1
73700      IM2 = IU
73800      IF (LOWER .EQ. 1) THEN
73900          JM1 = JU - 1
74000          JM2 = JU - 1
74100      ELSE
74200          JM1 = JU
74300          JM2 = JU
74400      ENCIF
74500      CALL INTERP(X1, Y1, X2, Y2, X3, Y3)
74600      CALL UMOD(IM1, IM2, JM1, JM2, Y3)
74700      C      C-cell horizontal boundary.
74800      X1 = YDOLD
74900      X2 = YDNEW
75000      X3 = YB(JB)
75100      Y1 = TDOLD
75200      Y2 = TDNEW
75300      IM1 = IC
75400      IM2 = IC
75500      JM1 = JC - 1
75600      JM2 = JC
75700      CALL INTERP(X1, Y1, X2, Y2, X3, Y3)
75800      CALL CMOD(IM1, IM2, JM1, JM2, Y3)
75900      C      C-cell horizontal boundary.
76000      Y1 = UDOLD
76100      Y2 = UDNEW
76200      IF (LOWER .EQ. 1) THEN
76300          IM1 = IU
76400          IM2 = IU
76500      ELSE
76600          IM1 = IU - 1
76700          IM2 = IU - 1
76800      ENCIF
76900      JM1 = JU - 1
77000      JM2 = JU
77100      CALL INTERP(X1, Y1, X2, Y2, X3, Y3)
77200      CALL UMOD(IM1, IM2, JM1, JM2, Y3)
77300      C
77400      ELSE IF (NCASE .EQ. 3) THEN
77500      C      C-cell horizontal boundary.
77600      X1 = YDOLD
77700      X2 = YDNEW
77800      X3 = YB(JB)
77900      Y1 = TDOLD
78000      Y2 = TDNEW
78100      IM1 = IC
78200      IM2 = IC
78300      JM1 = JC - 1
78400      JM2 = JC
78500      CALL INTERP(X1, Y1, X2, Y2, X3, Y3)
78600      CALL CMOD(IM1, IM2, JM1, JM2, Y3)
78700      C      C-cell horizontal boundary.
78800      Y1 = UDOLD
78900      Y2 = UDNEW
79000      IM1 = IU
79100      IM2 = IU
79200      JM1 = JU - 1
79300      JM2 = JU
79400      CALL INTERP(X1, Y1, X2, Y2, X3, Y3)

```

```

795 00          CALL UMOD(IM1, IM2, JM1, JM2, Y3)
796 00      C
797 00          ELSE IF (NCASE .EQ. 4) THEN
798 00      C      Check for path.
799 00          X1 = XDOLD
800 00          X2 = XDNEW
801 00          X3 = XB(IB + 1)
802 00          Y1 = YDOLD
803 00          Y2 = YDNEW
804 00          CALL INTERP(X1, Y1, X2, Y2, X3, Y3)
805 00          IF (Y3 .LT. YB(JB)) THEN
806 00              LOWER = 1
807 00          ELSE
808 00              LOWER = 0
809 00          ENDIF
810 00      C      C-cell vertical boundary.
811 00          Y1 = TDOLD
812 00          Y2 = TDNEW
813 00          IM1 = IC + 1
814 00          IM2 = IC
815 00          IF (LOWER .EQ. 1) THEN
816 00              JM1 = JC - 1
817 00              JM2 = JC - 1
818 00          ELSE
819 00              JM1 = JC
820 00              JM2 = JC
821 00          ENDIF
822 00          CALL INTERP(X1, Y1, X2, Y2, X3, Y3)
823 00          CALL CMOD(IM1, IM2, JM1, JM2, Y3)
824 00      C      V-cell vertical boundary.
825 00          Y1 = VDOLD
826 00          Y2 = VDNEW
827 00          IM1 = IV + 1
828 00          IM2 = IV
829 00          JM1 = JV
830 00          JM2 = JV
831 00          CALL INTERP(X1, Y1, X2, Y2, X3, Y3)
832 00          CALL VMOD(IM1, IM2, JM1, JM2, Y3)
833 00      C      C-cell horizontal boundary.
834 00          X1 = YDOLD
835 00          X2 = YDNEW
836 00          X3 = YB(JB)
837 00          Y1 = TDOLD
838 00          Y2 = TDNEW
839 00          IF (LOWER .EQ. 1) THEN
840 00              IM1 = IC
841 00              IM2 = IC
842 00          ELSE
843 00              IM1 = IC + 1
844 00              IM2 = IC + 1
845 00          ENDIF
846 00          JM1 = JC - 1
847 00          JM2 = JC
848 00          CALL INTERP(X1, Y1, X2, Y2, X3, Y3)
849 00          CALL CMOD(IM1, IM2, JM1, JM2, Y3)
850 00      C      U-cell horizontal boundary.
851 00          Y1 = UDOLD
852 00          Y2 = UDNEW
853 00          IM1 = IU
854 00          IM2 = IU
855 00          JM1 = JU - 1

```

```

85600      JM2 = JU
85700      CALL INTERP(X1, Y1, X2, Y2, X3, Y3)
85800      CALL UMOD(IM1, IM2, JM1, JM2, Y3)
85900      C
86000      ELSE IF (NCASE .EQ. 5) THEN
86100      C-cell vertical boundary.
86200      X1 = XDOLD
86300      X2 = XDNEW
86400      X3 = XB(IB + 1)
86500      Y1 = TDOLD
86600      Y2 = TDNEW
86700      IM1 = IC + 1
86800      IM2 = IC
86900      JM1 = JC
87000      JM2 = JC
87100      CALL INTERP(X1, Y1, X2, Y2, X3, Y3)
87200      CALL CMOD(IM1, IM2, JM1, JM2, Y3)
87300      C
87400      V-cell vertical boundary.
87500      Y1 = VDOLD
87600      Y2 = VDNEW
87700      IM1 = IV + 1
87800      IM2 = IV
87900      JM1 = JV
88000      JM2 = JV
88100      CALL INTERP(X1, Y1, X2, Y2, X3, Y3)
88200      CALL VMOD(IM1, IM2, JM1, JM2, Y3)
88300      C
88400      ELSE IF (NCASE .EQ. 6) THEN
88500      C-check for path.
88600      X1 = XDOLD
88700      X2 = XDNEW
88800      X3 = XB(IB + 1)
88900      Y1 = YDOLD
89000      Y2 = YDNEW
89100      CALL INTERP(X1, Y1, X2, Y2, X3, Y3)
89200      IF (Y3 .LT. YB(JB + 1)) THEN
89300      LOWER = 1
89400      ELSE
89500      LOWER = 0
89600      ENDIF
89700      C-cell vertical boundary.
89800      Y1 = TDOLD
89900      Y2 = TDNEW
90000      IM1 = IC + 1
90100      IM2 = IC
90200      JM1 = JC
90300      JM2 = JC
90400      CALL INTERP(X1, Y1, X2, Y2, X3, Y3)
90500      CALL CMOD(IM1, IM2, JM1, JM2, Y3)
90600      C
90700      V-cell vertical boundary.
90800      Y1 = VDOLD
90900      Y2 = VDNEW
91000      IM1 = IV + 1
91100      IM2 = IV
91200      IF (LOWER .EQ. 1) THEN
91300      JM1 = JV
91400      JM2 = JV
91500      ELSE
91600      JM1 = JV + 1
91700      JM2 = JV + 1
91800      ENDIF

```

```

91700          CALL INTERP(X1, Y1, X2, Y2, X3, Y3)
91800          CALL VMOD(IM1, IM2, JM1, JM2, Y3)
91900      C      V-cell horizontal boundary.
92000          X1 = YDOLD
92100          X2 = YDNEW
92200          X3 = YB(JB + 1)
92300          IF (LOWER .EQ. 1) THEN
92400              IM1 = IV + 1
92500              IM2 = IV + 1
92600          ELSE
92700              IM1 = IV
92800              IM2 = IV
92900          ENDIF
93000          JM1 = JV + 1
93100          JM2 = JV
93200          CALL INTERP(X1, Y1, X2, Y2, X3, Y3)
93300          CALL VMOD(IM1, IM2, JM1, JM2, Y3)
93400      C
93500          ELSE IF (NCASE .EQ. 7) THEN
93600      C      V-cell horizontal boundary.
93700          X1 = YDOLD
93800          X2 = YDNEW
93900          X3 = YB(JB + 1)
94000          Y1 = VDOLD
94100          Y2 = VDNEW
94200          IM1 = IV
94300          IM2 = IV
94400          JM1 = JV + 1
94500          JM2 = JV
94600          CALL INTERP(X1, Y1, X2, Y2, X3, Y3)
94700          CALL VMOD(IM1, IM2, JM1, JM2, Y3)
94800      C
94900          ELSE IF (NCASE .EQ. 8) THEN
95000      C      U-cell vertical boundary.
95100          X1 = XDOLD
95200          X2 = XDNEW
95300          X3 = XB(IB)
95400          Y1 = UDOLD
95500          Y2 = UDNEW
95600          IM1 = IU - 1
95700          IM2 = IU
95800          JM1 = JU
95900          JM2 = JU
96000          CALL INTERP(X1, Y1, X2, Y2, X3, Y3)
96100          CALL VMOD(IM1, IM2, JM1, JM2, Y3)
96200      C      V-cell horizontal boundary.
96300          X1 = YDOLD
96400          X2 = YDNEW
96500          X3 = YB(JB + 1)
96600          Y1 = VDOLD
96700          Y2 = VDNEW
96800          IM1 = IV
96900          IM2 = IV
97000          JM1 = JV + 1
97100          JM2 = JV
97200          CALL INTERP(X1, Y1, X2, Y2, X3, Y3)
97300          CALL VMOD(IM1, IM2, JM1, JM2, Y3)
97400          ENDIF
97500      C
97600          ELSE IF (NCASE .EQ. 3) THEN
97700              IF (NCASE .EQ. 1) THEN

```

```

97800      C      U-cell vertical boundary.
97900          X1 = XDOLD
98000          X2 = XDNEW
98100          X3 = XD(IR)
98200          Y1 = UDOLD
98300          Y2 = UDNEW
98400          IM1 = IU - 1
98500          IM2 = IU
98600          JM1 = JU
98700          JM2 = JU
98800          CALL INTERP(X1, Y1, X2, Y2, X3, Y3)
98900          CALL UMCD(IM1, IM2, JM1, JM2, Y3)
99000      C
99100      ELSE IF (NCASE .EQ. 2) THEN
99200      C      U-cell vertical boundary.
99300          X1 = XDOLD
99400          X2 = XDNEW
99500          X3 = XD(IB)
99600          Y1 = UDOLD
99700          Y2 = UDNEW
99800          IM1 = IU - 1
99900          IM2 = IU

```



```

00100      JM1 = JU
00200      JM2 = JU
00300      CALL INTERP(X1, Y1, X2, Y2, X3, Y3)
00400      CALL CMOD(IM1, IM2, JM1, JM2, Y3)
00500      C      V-cell horizontal boundary.
00600      X1 = YDOLD
00700      X2 = YDNEW
00800      X3 = YB(JB)
00900      Y1 = VDOLD
01000      Y2 = VDNEW
01100      IM1 = IV
01200      IM2 = IV
01300      JM1 = JV - 1
01400      JM2 = JV
01500      CALL INTERP(X1, Y1, X2, Y2, X3, Y3)
01600      CALL VMOD(IM1, IM2, JM1, JM2, Y3)
01700      C
01800      ELSE IF (NCASE .EQ. 3) THEN
01900      C      V-cell horizontal boundary.
02000      X1 = YDOLD
02100      X2 = YDNEW
02200      X3 = YB(JB)
02300      Y1 = VDOLD
02400      Y2 = VDNEW
02500      IM1 = IV
02600      IM2 = IV
02700      JM1 = JV - 1
02800      JM2 = JV
02900      CALL INTERP(X1, Y1, X2, Y2, X3, Y3)
03000      CALL VMOD(IM1, IM2, JM1, JM2, Y3)
03100      C
03200      ELSE IF (NCASE .EQ. 4) THEN
03300      C      Check for path.
03400      X1 = XDOLD
03500      X2 = XDNEW
03600      X3 = XB(IB + 1)
03700      Y1 = YDOLD
03800      Y2 = YDNEW
03900      CALL INTERP(X1, Y1, X2, Y2, X3, Y3)
04000      IF (Y3 .LT. YB(JB)) THEN
04100          LOWER = 1
04200      ELSE
04300          LOWER = 0
04400      ENDIF
04500      C      C-cell vertical boundary.
04600      Y1 = TDOLD
04700      Y2 = TDNEW
04800      IM1 = IC + 1
04900      IM2 = IC
05000      JM1 = JU
05100      JM2 = JU
05200      CALL INTERP(X1, Y1, X2, Y2, X3, Y3)
05300      CALL CMOD(IM1, IM2, JM1, JM2, Y3)
05400      C      V-cell vertical boundary.
05500      Y1 = VDOLD
05600      Y2 = VDNEW
05700      IM1 = IV + 1
05800      IM2 = IV
05900      IF (LOWER .EQ. 1) THEN
06000          JM1 = JV - 1
06100          JM2 = JV - 1

```

```

06200      ELSE
06300          JM1 = JV
06400          JM2 = JV
06500      ENDIF
06600      CALL INTERP(X1, Y1, X2, Y2, X3, Y3)
06700      CALL VMOD(IM1, IM2, JM1, JM2, Y3)
06800      C      V-cell horizontal boundary.
06900          X1 = YDOLD
07000          X2 = YDNEW
07100          X3 = YB(JB)
07200          IF (LOWER .EQ. 1) THEN
07300              IM1 = IV
07400              IM2 = IV
07500          ELSE
07600              IM1 = IV + 1
07700              IM2 = IV + 1
07800          ENDIF
07900          JM1 = JV - 1
08000          JM2 = JV
08100          CALL INTERP(X1, Y1, X2, Y2, X3, Y3)
08200          CALL VMOD(IM1, IM2, JM1, JM2, Y3)
08300      C
08400      ELSE IF (NCAGE .EQ. 5) THEN
08500      C      C-cell vertical boundary.
08600          X1 = XDOLD
08700          X2 = XDNEW
08800          X3 = XB(IB + 1)
08900          Y1 = TDOLD
09000          Y2 = TDNEW
09100          IM1 = IC + 1
09200          IM2 = IC
09300          JM1 = JC
09400          JM2 = JC
09500          CALL INTERP(X1, Y1, X2, Y2, X3, Y3)
09600          CALL CMOD(IM1, IM2, JM1, JM2, Y3)
09700      C      V-cell vertical boundary.
09800          Y1 = VDOLD
09900          Y2 = VDNEW
10000          IM1 = IV + 1
10100          IM2 = IV
10200          JM1 = JV
10300          JM2 = JV
10400          CALL INTERP(X1, Y1, X2, Y2, X3, Y3)
10500          CALL VMOD(IM1, IM2, JM1, JM2, Y3)
10600      C
10700      ELSE IF (NCAGE .EQ. 6) THEN
10800      C      Check for path.
10900          X1 = XDOLD
11000          X2 = XDNEW
11100          X3 = XB(IB + 1)
11200          Y1 = YDOLD
11300          Y2 = YDNEW
11400          CALL INTERP(X1, Y1, X2, Y2, X3, Y3)
11500          IF (Y3 .LT. YB(JB + 1)) THEN
11600              LOWER = 1
11700          ELSE
11800              LOWER = 0
11900          ENDIF
12000      C      C-cell vertical boundary.
12100          Y1 = TDOLD
12200          Y2 = TDNEW

```

```

12300      IM1 = IC + 1
12400      IM2 = IC
12500      IF (LOWER .EQ. 1) THEN
12600          JM1 = JC
12700          JM2 = JC
12800      ELSE
12900          JM1 = JC + 1
13000          JM2 = JC + 1
13100      ENDIF
13200      CALL INTERP(X1, Y1, X2, Y2, X3, Y3)
13300      CALL CMOD(IM1, IM2, JM1, JM2, Y3)
13400  C      V-cell vertical boundary.
13500      Y1 = YDOLD
13600      Y2 = YDNEW
13700      IM1 = IV + 1
13800      IM2 = IV
13900      JM1 = JV
14000      JM2 = JV
14100      CALL INTERP(X1, Y1, X2, Y2, X3, Y3)
14200      CALL VMOD(IM1, IM2, JM1, JM2, Y3)
14300  C      U-cell horizontal boundary.
14400      X1 = XDOLD
14500      X2 = XDNEW
14600      X3 = XB(JB + 1)
14700      Y1 = TDOLD
14800      Y2 = TDNEW
14900      IF (LOWER .EQ. 1) THEN
15000          IM1 = IC + 1
15100          IM2 = IC + 1
15200      ELSE
15300          IM1 = IC
15400          IM2 = IC
15500      ENDIF
15600      JM1 = JC + 1
15700      JM2 = JC
15800      CALL INTERP(X1, Y1, X2, Y2, X3, Y3)
15900      CALL CMOD(IM1, IM2, JM1, JM2, Y3)
16000  C      U-cell horizontal boundary.
16100      Y1 = UDOLD
16200      Y2 = UDNEW
16300      IM1 = IC
16400      IM2 = IC
16500      JM1 = JC + 1
16600      JM2 = JC
16700      CALL INTERP(X1, Y1, X2, Y2, X3, Y3)
16800      CALL CMOD(IM1, IM2, JM1, JM2, Y3)
16900  C
17000      ELSE IF (NCASE .EQ. 7) THEN
17100  C      U-cell horizontal boundary.
17200      X1 = XDOLD
17300      X2 = XDNEW
17400      X3 = XB(JB + 1)
17500      Y1 = TDOLD
17600      Y2 = TDNEW
17700      IM1 = IC
17800      IM2 = IC
17900      JM1 = JC + 1
18000      JM2 = JC
18100      CALL INTERP(X1, Y1, X2, Y2, X3, Y3)
18200      CALL CMOD(IM1, IM2, JM1, JM2, Y3)
18300  C      U-cell horizontal boundary.

```

```

18400      Y1 = UDOLD
18500      Y2 = UDNEW
18600      IM1 = IU
18700      IM2 = IU
18800      JM1 = JU + 1
18900      JM2 = JU
19000      CALL INTERP(X1, Y1, X2, Y2, X3, Y3)
19100      CALL UMOD(IM1, IM2, JM1, JM2, Y3)
19200  C
19300      ELSE IF (NCASE .EQ. 8) THEN
19400  C      Check for path.
19500          X1 = XDOLD
19600          X2 = XDNEW
19700          X3 = XB(18)
19800          Y1 = YDOLD
19900          Y2 = YDNEW
20000          CALL INTERP(X1, Y1, X2, Y2, X3, Y3)
20100          IF (Y3 .LT. YB(JB + 1)) THEN
20200              LOWER = 1
20300          ELSE
20400              LOWER = 2
20500          ENDIF
20600  C      U-cell vertical boundary.
20700          Y1 = UDOLD
20800          Y2 = UDNEW
20900          IM1 = IU - 1
21000          IM2 = IU
21100          IF (LOWER .EQ. 1) THEN
21200              JM1 = JU
21300              JM2 = JU
21400          ELSE
21500              JM1 = JU + 1
21600              JM2 = JU + 1
21700          ENDIF
21800          CALL INTERP(X1, Y1, X2, Y2, X3, Y3)
21900          CALL UMOD(IM1, IM2, JM1, JM2, Y3)
22000  C      U-cell horizontal boundary.
22100          X1 = YDOLD
22200          X2 = YDNEW
22300          X3 = YB(JB + 1)
22400          Y1 = TDOLD
22500          Y2 = TDNEW
22600          IM1 = IC
22700          IM2 = IC
22800          JM1 = JC + 1
22900          JM2 = JC
23000          CALL INTERP(X1, Y1, X2, Y2, X3, Y3)
23100          CALL UMOD(IM1, IM2, JM1, JM2, Y3)
23200  C      U-cell horizontal boundary.
23300          Y1 = UDOLD
23400          Y2 = UDNEW
23500          IF (LOWER .EQ. 1) THEN
23600              IM1 = IU - 1
23700              IM2 = IU - 1
23800          ELSE
23900              IM1 = IU
24000              IM2 = IU
24100          ENDIF
24200          JM1 = JU + 1
24300          JM2 = JU
24400          CALL INTERP(X1, Y1, X2, Y2, X3, Y3)

```

```

24500          CALL UM00(IM1, IM2, JM1, JM2, Y3)
24600      ENDIF
24700  C
24800      ELSE IF (MCASE .EQ. 4) THEN
24900          IF (MCASE .EQ. 1) THEN
25000  C      C-cell vertical boundary.
25100              X1 = XCOLD
25200              X2 = XNEW
25300              X3 = XE(18)
25400              Y1 = YOLD
25500              Y2 = YNEW
25600              IM1 = IC - 1
25700              IM2 = IC
25800              JM1 = JC
25900              JM2 = JC
26000              CALL INTERP(X1, Y1, X2, Y2, X3, Y3)
26100              CALL CM00(IM1, IM2, JM1, JM2, Y3)
26200  C      V-cell vertical boundary.
26300              Y1 = YOLD
26400              Y2 = YNEW
26500              IM1 = IV - 1
26600              IM2 = IV
26700              JM1 = JV
26800              JM2 = JV
26900              CALL INTERP(X1, Y1, X2, Y2, X3, Y3)
27000              CALL VM00(IM1, IM2, JM1, JM2, Y3)
27100  C
27200      ELSE IF (MCASE .EQ. 2) THEN
27300  C      Check for path.
27400              X1 = XCOLD
27500              X2 = XNEW
27600              X3 = XE(18)
27700              Y1 = YOLD
27800              Y2 = YNEW
27900              CALL INTERP(X1, Y1, X2, Y2, X3, Y3)
28000              IF (Y3 .LT. YE(JE)) THEN
28100                  LOWER = 1
28200              ELSE
28300                  LOWER = 0
28400              ENDIF
28500  C      C-cell vertical boundary.
28600              Y1 = YOLD
28700              Y2 = YNEW
28800              IM1 = IC - 1
28900              IM2 = IC
29000              JM1 = JC
29100              JM2 = JC
29200              CALL INTERP(X1, Y1, X2, Y2, X3, Y3)
29300              CALL CM00(IM1, IM2, JM1, JM2, Y3)
29400  C      V-cell vertical boundary.
29500              Y1 = YOLD
29600              Y2 = YNEW
29700              IM1 = IV - 1
29800              IM2 = IV
29900              IF (LOWER .EQ. 1) THEN
30000                  JM1 = JV - 1
30100                  JM2 = JV - 1
30200              ELSE
30300                  JM1 = JV
30400                  JM2 = JV
30500              ENDIF

```

```

30600      CALL INTERP(X1, Y1, X2, Y2, X3, Y3)
30700      CALL VMOD(IM1, IM2, JM1, JM2, Y3)
30800      C      V-cell horizontal boundary.
30900          X1 = YDOLD
31000          X2 = YDNEW
31100          X3 = YB(JB)
31200          IF (LOWER .EQ. 1) THEN
31300              IM1 = IV
31400              IM2 = IV
31500          ELSE
31600              IM1 = IV - 1
31700              IM2 = IV - 1
31800          ENDIF
31900          JM1 = JV - 1
32000          JM2 = JV
32100          CALL INTERP(X1, Y1, X2, Y2, X3, Y3)
32200          CALL VMOD(IM1, IM2, JM1, JM2, Y3)
32300      C
32400      ELSE IF (NCASE .EQ. 3) THEN
32500      C      V-cell horizontal boundary.
32600          X1 = YDOLD
32700          X2 = YDNEW
32800          X3 = YB(JB)
32900          Y1 = VDOLD
33000          Y2 = VDNEW
33100          IM1 = IV
33200          IM2 = IV
33300          JM1 = JV - 1
33400          JM2 = JV
33500          CALL INTERP(X1, Y1, X2, Y2, X3, Y3)
33600          CALL VMOD(IM1, IM2, JM1, JM2, Y3)
33700      C
33800      ELSE IF (NCASE .EQ. 4) THEN
33900      C      U-cell vertical boundary.
34000          X1 = XDOLD
34100          X2 = XDNEW
34200          X3 = XB(IB + 1)
34300          Y1 = UDOLD
34400          Y2 = UDNEW
34500          IM1 = IU + 1
34600          IM2 = IU
34700          JM1 = JU
34800          JM2 = JU
34900          CALL INTERP(X1, Y1, X2, Y2, X3, Y3)
35000          CALL UMOD(IM1, IM2, JM1, JM2, Y3)
35100      C      V-cell horizontal boundary.
35200          X1 = YDOLD
35300          X2 = YDNEW
35400          X3 = YB(JB)
35500          Y1 = VDOLD
35600          Y2 = VDNEW
35700          IM1 = IV
35800          IM2 = IV
35900          JM1 = JV - 1
36000          JM2 = JV
36100          CALL INTERP(X1, Y1, X2, Y2, X3, Y3)
36200          CALL VMOD(IM1, IM2, JM1, JM2, Y3)
36300      C
36400      ELSE IF (NCASE .EQ. 5) THEN
36500      C      U-cell vertical boundary.
36600          X1 = XDOLD

```

```

36700      X2 = XONEW
36800      X3 = XB(IB + 1)
36900      Y1 = UDOLD
37000      Y2 = UDNEW
37100      IM1 = IC + 1
37200      IM2 = IC
37300      JM1 = JU
37400      JM2 = JU
37500      CALL INTERP(X1, Y1, X2, Y2, X3, Y3)
37600      CALL UMCD(IM1, IM2, JM1, JM2, Y3)
37700      ELSE IF (NCASE .EQ. 6) THEN
37800  C      Check for path.
37900          X1 = XDOLD
38000          X2 = XONEW
38100          X3 = XP(IR + 1)
38200          Y1 = YDOLD
38300          Y2 = YDNEW
38400          CALL INTERP(X1, Y1, X2, Y2, X3, Y3)
38500          IF (Y3 .LT. YP(JP + 1)) THEN
38600              LOWER = 1
38700          ELSE
38800              LOWER = 0
38900          ENDIF
39000  C      U-cell vertical boundary.
39100          Y1 = UDOLD
39200          Y2 = UDNEW
39300          IM1 = IC + 1
39400          IM2 = IC
39500          IF (LOWER .EQ. 1) THEN
39600              JM1 = JU
39700              JM2 = JU
39800          ELSE
39900              JM1 = JU + 1
40000              JM2 = JU + 1
40100          ENDIF
40200          CALL INTERP(X1, Y1, X2, Y2, X3, Y3)
40300          CALL UMCD(IM1, IM2, JM1, JM2, Y3)
40400  C      U-cell horizontal boundary.
40500          X1 = YDOLD
40600          X2 = YDNEW
40700          X3 = YB(JB + 1)
40800          Y1 = TDOLD
40900          Y2 = TDNEW
41000          IM1 = IC
41100          IM2 = IC
41200          JM1 = JC + 1
41300          JM2 = JC
41400          CALL INTERP(X1, Y1, X2, Y2, X3, Y3)
41500          CALL CMCD(IM1, IM2, JM1, JM2, Y3)
41600  C      U-cell horizontal boundary.
41700          Y1 = UDOLD
41800          Y2 = UDNEW
41900          IF (LOWER .EQ. 1) THEN
42000              IM1 = IU + 1
42100              IM2 = IU + 1
42200          ELSE
42300              IM1 = IU
42400              IM2 = IU
42500          ENDIF
42600          JM1 = JU + 1
42700          JM2 = JU

```

```

42800      CALL INTERP(X1, Y1, X2, Y2, X3, Y3)
42900      CALL UMOD(IM1, IM2, JM1, JM2, Y3)
43000      C
43100      ELSE IF (NCASE .EQ. 7) THEN
43200      C-cell horizontal boundary.
43300      X1 = YDOLD
43400      X2 = YDNEW
43500      X3 = YB(JB + 1)
43600      Y1 = TDOLD
43700      Y2 = TDNEW
43800      IM1 = IC
43900      IM2 = IC
44000      JM1 = JC + 1
44100      JM2 = JC
44200      CALL INTERP(X1, Y1, X2, Y2, X3, Y3)
44300      CALL CMOD(IM1, IM2, JM1, JM2, Y3)
44400      C-cell horizontal boundary.
44500      Y1 = UDOLD
44600      Y2 = UDNEW
44700      IM1 = IC
44800      IM2 = IC
44900      JM1 = JC + 1
45000      JM2 = JC
45100      CALL INTERP(X1, Y1, X2, Y2, X3, Y3)
45200      CALL UMOD(IM1, IM2, JM1, JM2, Y3)
45300      C
45400      ELSE IF (NCASE .EQ. 8) THEN
45500      C-check for path.
45600      X1 = XDOLD
45700      X2 = XDNEW
45800      X3 = XB(IB)
45900      Y1 = YDOLD
46000      Y2 = YDNEW
46100      CALL INTERP(X1, Y1, X2, Y2, X3, Y3)
46200      IF (Y3 .LT. YB(JB + 1)) THEN
46300      LOWER = 1
46400      ELSE
46500      LOWER = 0
46600      ENDIF
46700      C-cell vertical boundary.
46800      Y1 = TDOLD
46900      Y2 = TDNEW
47000      IM1 = IC - 1
47100      IM2 = IC
47200      IF (LOWER .EQ. 1) THEN
47300      JM1 = JC
47400      JM2 = JC
47500      ELSE
47600      JM1 = JC + 1
47700      JM2 = JC + 1
47800      ENDIF
47900      CALL INTERP(X1, Y1, X2, Y2, X3, Y3)
48000      CALL CMOD(IM1, IM2, JM1, JM2, Y3)
48100      C-cell vertical boundary.
48200      Y1 = VDOLD
48300      Y2 = VDNEW
48400      IM1 = IV - 1
48500      IM2 = IV
48600      JM1 = JV
48700      JM2 = JV
48800      CALL INTERP(X1, Y1, X2, Y2, X3, Y3)

```



```

48900      CALL VMOD(IM1, IM2, JM1, JM2, Y3)
49000      C      C-cell horizontal boundary.
49100      X1 = YDOLD
49200      X2 = YDNEW
49300      X3 = YB(JB + 1)
49400      Y1 = TDOLD
49500      Y2 = TDNEW
49600      IF (LOWER.EQ. 1) THEN
49700          IM1 = IC - 1
49800          IM2 = IC - 1
49900      ELSE
50000          IM1 = IC
50100          IM2 = IC
50200      ENDIF
50300      JM1 = JC + 1
50400      JM2 = JC
50500      CALL INTERP(X1, Y1, X2, Y2, X3, Y3)
50600      CALL CMOD(IM1, IM2, JM1, JM2, Y3)
50700      C      C-cell horizontal boundary.
50800      Y1 = UDOLD
50900      Y2 = UDNEW
51000      IM1 = IC
51100      IM2 = IC
51200      JM1 = JC + 1
51300      JM2 = JC
51400      CALL INTERP(X1, Y1, X2, Y2, X3, Y3)
51500      CALL CMOD(IM1, IM2, JM1, JM2, Y3)
51600      C
51700      ENDIF
51800      ENDIF
51900      C
52000      IPOLD = IP
52100      JPOLD = JP
52200      XDOLD = XDNEW
52300      YDOLD = YDNEW
52400      TDOLD = TDNEW
52500      UDOLD = UDNEW
52600      VDOLD = VDNEW
52700      ISTEPS = ISTEPS + 1
52800      IF (ISTEPS.GT. MAXSTP) THEN
52900          WRITE(5, *) ' MAX. STEPS EXCEEDED FOR ', NPORT
53000          WRITE(5, *) ' X=', XDOLD, ' Y=', YDOLD, ' ICOUNT=', ICOUNT
53100      ELSE
53200          WRITE (22, *) XDOLD, YDOLD
53300          GOTO 100
53400      ENDIF
53500      C      Mark the end of path.
53600      900      CONTINUE
53700      DUMMY = -1.0
53800      WRITE (22, *) DUMMY
53900      C
54000      C      Re-initialize the source terms for the last cell as the
54100      C      droplet leaves the flow domain.
54200      C
54300      DELTA = 4.0 * PI * RHOL * RAD ** 3 / 3.0 * DRFREQ(NPORT)
54400      RMOMU(1, JU) = RMOMU(IU, JU) - DELTA * UOINIT(NPORT)
54500      RMOMV(1, JV) = RMOMV(IV, JV) - DELTA * VOINIT(NPORT)
54600      C
54700      1000      CONTINUE
54800      CALL COMPAR
54900      C      Mark the end of file.

```

```

55000      DUMMY = -11.0
55100      WRITE (22, *) DUMMY
55200      CLOSE (UNIT = 22)
55300      RETURN
55400      END
55500      C
55600      C .....
55700      C
55800      SUBROUTINE DCMCHK
55900      C Checks if the DFOP is within the finite
56000      C difference mesh rectangle.
56100      C
56200      COMMON /DEROPD/ MAXPOR, NPORT,
56300      1  DRPDI(10), DRPDI(10), DRMDOY(10), DRPFRQ(10),
56400      1  XDINIT(10), YDINIT(10), TDINIT(10), UDINIT(10), VDINIT(10),
56500      1  X(45), Y(45),
56600      1  UG(45, 24), VG(45, 24), UGOLD(45, 24), VGOLD(45, 24),
56700      1  CDD, GRAVX, GRAVY, RAD, RHOGAS, PI, LGAS, VGAS,
56800      1  XGOLD, YGOLD, TGOLD, UGOLD, VGOLD,
56900      1  XNEW, YNEW, TNEW, UNEW, VNEW,
57000      1  DT, DTINC, DTRED, RHOL,
57100      1  ISTERG, INTOTR, IFLAG2, IHIT, MAXSTP, MAXCT, INTFLG,
57200      1  IC, UC, IV, UV, IO, UO, IF, UF, IBOLE, UBOLE, ICDINT,
57300      1  VCASE, MCASE, UDMAX(45), NDI, NDU
57400      C
57500      IF (YNEW .GT. Y(2 * (NDI - 1))) THEN
57600      1  WRITE(5, *) * DROP OVER-TRAVELLED RIGHT*
57700      1  IHIT = 1
57800      ELSE IF (XNEW .LT. X(2)) THEN
57900      1  WRITE(5, *) * REVERSE FLOW AT ENTRANCE*
58000      1  IHIT = 2
58100      ELSE IF (YNEW .LT. Y(2)) THEN
58200      1  WRITE(5, *) * FLOW CROSSED AXIS*
58300      1  IHIT = 3
58400      ELSE IF (YNEW .GT. Y(2 * (NDU - 1))) THEN
58500      1  WRITE(5, *) * DROP OVER-TRAVELLED UP*
58600      1  IHIT = 4
58700      ELSE
58800      1  IHIT = 0
58900      1  ENDIF
59000      RETURN
59100      END
59200      C
59300      C .....
59400      C
59500      SUBROUTINE FINDP
59600      C Finds IE, JF, IC, JC, IO, JU, IV and UV for the
59700      C new p-cell.
59800      C
59900      COMMON /DEROPD/ MAXPOR, NPORT,
60000      1  DRPDI(10), DRPDI(10), DRMDOY(10), DRPFRQ(10),
60100      1  XDINIT(10), YDINIT(10), TDINIT(10), UDINIT(10), VDINIT(10),
60200      1  X(45), Y(45),
60300      1  UG(45, 24), VG(45, 24), UGOLD(45, 24), VGOLD(45, 24),
60400      1  CDD, GRAVX, GRAVY, RAD, RHOGAS, PI, LGAS, VGAS,
60500      1  XGOLD, YGOLD, TGOLD, UGOLD, VGOLD,
60600      1  XNEW, YNEW, TNEW, UNEW, VNEW,
60700      1  DT, DTINC, DTRED, RHOL,
60800      1  ISTERG, INTOTR, IFLAG2, IHIT, MAXSTP, MAXCT, INTFLG,
60900      1  IC, UC, IV, UV, IO, JU, IF, UF, IBOLE, UBOLE, ICDINT,
61000      1  VCASE, MCASE, UDMAX(45), NDI, NDU

```

```

61100 C
61200
61300
61400 100 IF (IH .GE. (L + NDI)) THEN
61500 WRITE(5, *) 'ERROR: IH OUT OF RANGE', IH
61600 STOP
61700 ENDIF
61800 IF (IB .LE. 0) THEN
61900 WRITE(5, *) 'ERROR: IB BELOW RANGE', IB
62000 STOP
62100 ENDIF
62200 IF (XNEW .LT. XH(IH)) THEN
62300 IH = IH - 1
62400 GOTO 100
62500 ELSE IF (XNEW .GE. XH(IH + 1)) THEN
62600 IH = IH + 1
62700 GOTO 100
62800 ENDIF
62900 200 IF (UH .GE. (L + NDU)) THEN
63000 WRITE(5, *) 'ERROR: UH OUT OF RANGE', UH
63100 STOP
63200 ENDIF
63300 IF (UB .LE. 0) THEN
63400 WRITE(5, *) 'ERROR: UB BELOW RANGE', UB
63500 STOP
63600 ENDIF
63700 IF (YNEW .LT. YH(UH)) THEN
63800 UH = UH - 1
63900 GOTO 200
64000 ELSE IF (YNEW .GE. YH(UH + 1)) THEN
64100 UH = UH + 1
64200 GOTO 200
64300 ENDIF
64400 IC = (IH + 2) / 2
64500 UC = (UH + 2) / 2
64600 IC = (IH + 3) / 2
64700 UC = (UH + 2) / 2
64800 IV = (IH + 2) / 2
64900 UV = (UH + 3) / 2
65000 RETURN
65100 END
65200
65300 C .....
65400 C
65500 C SUBROUTINE CHECK
65600 C Checks if the integration step size is in
65700 C the allowable range, and modifies the step size.
65800 C
65900 C COMM: / HOPS/ MAXHPS, HPORT,
66000 1 XPMOD(10), TREF(10), CRMOOT(10), TREF(10),
66100 1 XDNIT(10), YDNIT(10), IDNIT(10), UDNIT(10), IDNIT(10),
66200 1 XH(4), YH(4),
66300 1 UG(4), VU(4), UGOLD(4), VUGOLD(4),
66400 1 UGD, GRAVX, GRAVY, RAD, RHOSAS, PI, UGAS, VGAS,
66500 1 XGOLD, YGOLD, TGOLD, UGOLD, VGOLD,
66600 1 XNEW, YNEW, IDNEW, UDNEW, VDNW,
66700 1 DT, DTINC, DTRED, RHOL,
66800 1 ISTEP, INTCTR, IFLAGZ, IHIT, MAXSTP, MAXCT, INTPL,
66900 1 IC, UC, IV, UV, IG, UG, IB, UB, IBOLD, UBOLD, ICENT,
67000 1 NCASE, MCASE, UCMAX(4), NDI, NDU
67100 C

```

```

67200      IF (ABS(IB - IBOLD) .GT. 1) THEN
67300          DT = DTRED * DT
67400          IB = IBOLD
67500          JB = JBOLD
67600          INTFLG = 1
67700          RETURN
67800      ENDIF
67900  C
68000      IF (ABS(JB - JBOLD) .GT. 1) THEN
68100          DT = DTRED * DT
68200          IB = IBOLD
68300          JB = JBOLD
68400          INTFLG = 1
68500          RETURN
68600      ENDIF
68700  C
68800      IF (IB .EQ. IBOLD) THEN
68900          IF (JB .EQ. JBOLD) THEN
69000              DT = DTINC * DT
69100              IB = IBOLD
69200              JB = JBOLD
69300              INTFLG = 0
69400              RETURN
69500          ENDIF
69600      ENDIF
69700  C
69800      INTFLG = 1
69900      RETURN
70000  END
70100  C
70200  C .....
70300  C
70400      SUBROUTINE FINDN
70500  C      Returns the value of NCASE corresponding
70600  C      to the identity of the neighbouring cell
70700  C      that the CRCP travels to.
70800  C
70900      COMMON /CRCPDS/ MAXRCP, NCRST,
71000      1  CRPDI(10), CRPDIA(10), CRPDCT(10), CRPFED(10),
71100      1  CRPIT(10), CRPDIT(10), CRPDIT(10), CRPDIT(10), CRPDIT(10),
71200      1  CRP(6), CRP(4),
71300      1  CR(4), CR(4), CR(4), CR(4), IBOLD(4), JBOLD(4),
71400      1  CRD, CRAXX, CRAYY, CRD, CRD, CRD, CRD, CRD, CRD,
71500      1  CRD, CRD, CRD, CRD, CRD, CRD,
71600      1  CRNEW, CRNEW, CRNEW, CRNEW, CRNEW,
71700      1  CR, CRINC, CRRED, CRHOL,
71800      1  CRRED, CRRED, CRRED, CRRED, CRRED, CRRED, CRRED,
71900      1  CR, CR, CR, CR, CR, CR, CR, CR, CR, CR, CR, CR,
72000      1  CRD, CRD, CRD, CRD, CRD, CRD, CRD, CRD,
72100  C
72200      IF (IB .EQ. IBOLD) THEN
72300          IF (JB .GT. JBOLD) THEN
72400              NCASE = 1
72500          ELSE IF (JB .LT. JBOLD) THEN
72600              NCASE = 7
72700          ELSE
72800              NCASE = 6
72900          ENDIF
73000      ELSE IF (IB .LT. IBOLD) THEN
73100          IF (JB .GT. JBOLD) THEN
73200              NCASE = 4

```

```

73300      ELSE IF (JB .EQ. JBOLD) THEN
73400          NCASE = 5
73500      ELSE
73600          NCASE = 6
73700      ENDIF
73800  ELSE
73900      IF (JB .LT. JBOLD) THEN
74000          NCASE = 3
74100      ELSE IF (JB .EQ. JBOLD) THEN
74200          NCASE = 1
74300      ELSE
74400          NCASE = 2
74500      ENDIF
74600  ENDIF
74700  RETURN
74800  END
74900  C
75000  C .....
75100  C
75200  SUBROUTINE FINDM
75300  C      Returns the value of NCASE corresponding to
75400  C      the four possible locations of the H-cell of
75500  C      of origin, in the mesh cell.
75600  C
75700  COMMON /COMMON/ MAXPOR, IPORT,
75800  1  IPRDYN(10), IPR14(10), IPRDOT(10), IPRFREQ(10),
75900  1  XINIT(10), YINIT(10), TINIT(10), UINIT(10), VINIT(10),
76000  1  AB(20), TH(40),
76100  1  UB(40, 24), VB(40, 24), UGOLD(40, 24), VGOLD(40, 24),
76200  1  RDD, RHAVX, RHAVY, RAB, RHODAS, RI, RGAS, VGAS,
76300  1  XGOLD, YGOLD, TGOLD, UGOLD, VGOLD,
76400  1  XNEW, YNEW, TNEW, UNEW, VNEW,
76500  1  T, DTINC, DTDEC, RMOL,
76600  1  IOTPRC, IOTCTR, IFLAG2, IHT, MAXCTR, MAXCT, IATLG,
76700  1  IS, UC, IV, OV, IO, OC, IN, OH, IUGL, UGOLD, IOUNT,
76800  1  NCASE, NCASE, UCMAX(40), NDI, NCU
76900  C
77000  IF ((CMPLT = (CMOLD / 20) * 20) .EQ. 0) THEN
77100  L      CMOLD is even.
77200  IF ((CMPLT = (CMOLD / 20) * 20) .EQ. 0) THEN
77300  C      CMOLD is even.
77400  C      FLAG = 3
77500  FLAG = 3
77600  C      CMOLD is odd.
77700  C      FLAG = 1
77800  FLAG = 1
77900  ELSE
78000  C      CMOLD is odd.
78100  IF ((CMPLT = (CMOLD / 20) * 20) .EQ. 0) THEN
78200  C      CMOLD is even.
78300  C      FLAG = 4
78400  FLAG = 4
78500  C      CMOLD is odd.
78600  C      FLAG = 1
78700  FLAG = 1
78800  ENDIF
78900  ENDIF
79000  RETURN
79100  C
79200  C .....
79300  C

```

```

79400 SUBROUTINE INTER(X1, Y1, X2, Y2, X3, Y3)
79500 C The inputs are (X1, Y1), (X2, Y2) and X3.
79600 C The value of Y3 is returned, such that the
79700 C three points lie on a straight line.
79800 IF ((X2 - X1) .EQ. 0) THEN
79900 WRITE(5, *) '*** ERROR IN INTER *** : X1 = X2'
80000 STOP
80100 ENDIF
80200 Y3 = Y1 + (Y2 - Y1) * (X3 - X1) / (X2 - X1)
80300 RETURN
80400 END
80500 C
80600 C .....
80700 C
80800 SUBROUTINE CMOD(IM1, IM2, UM1, UM2, Y3)
80900 COMMON/UGF/RMOMV(50,50),RMOMU(50,50)
81000 COMMON /ZROPS/ MAXPOR, NPORT,
81100 $ ERPCEN(10), ERPCIA(10), ERPCOT(10), ERPREG(10),
81200 $ XLINIT(10), YDINIT(10), TLINIT(10), UDINIT(10), VDLIT(10),
81300 $ XR(45), YR(45),
81400 $ UG(45, 24), VG(45, 24), UGOLD(45, 24), VGOLD(45, 24),
81500 $ UDD, GRAVX, GRAVY, RAD, RHOGAS, PI, UGAS, VGAS,
81600 $ XOLD, YOLD, TOLD, UOLD, VOLD,
81700 $ XNEW, YNEW, TNEW, UNEW, VNEW,
81800 $ TI, DTINC, DTREC, RHOL,
81900 $ ISTERG, INTCTR, IFLAG2, IHIT, MAXSTP, MAXCT, INTLEN,
82000 $ IC, UC, IV, UV, IL, UL, IR, UR, IHOLD, UHOLD, ICHIT,
82100 $ NCASE, NCASE, UDMAX(45), VDI, VDU
82200 C
82300 RETURN
82400 END
82500 C
82600 C .....
82700 C
82800 SUBROUTINE CMOD(IM1, IM2, UM1, UM2, Y3)
82900 COMMON/UGF/RMOMV(50,50),RMOMU(50,50)
83000 COMMON /ZROPS/ MAXPOR, NPORT,
83100 $ ERPCEN(10), ERPCIA(10), ERPCOT(10), ERPREG(10),
83200 $ XLINIT(10), YDINIT(10), TLINIT(10), UDINIT(10), VDLIT(10),
83300 $ XR(45), YR(45),
83400 $ UG(45, 24), VG(45, 24), UGOLD(45, 24), VGOLD(45, 24),
83500 $ UDD, GRAVX, GRAVY, RAD, RHOGAS, PI, UGAS, VGAS,
83600 $ XOLD, YOLD, TOLD, UOLD, VOLD,
83700 $ XNEW, YNEW, TNEW, UNEW, VNEW,
83800 $ TI, DTINC, DTREC, RHOL,
83900 $ ISTERG, INTCTR, IFLAG2, IHIT, MAXSTP, MAXCT, INTLEN,
84000 $ IC, UC, IV, UV, IL, UL, IR, UR, IHOLD, UHOLD, ICHIT,
84100 $ NCASE, NCASE, UDMAX(45), VDI, VDU
84200 C
84300 DELTA = (4.0 * PI * RHOL * (RAD ** 3) / 3.0) * Y3
84400 $ * REPR/(16*CT)
84500 RMOMU(IM1, UM1) = RMOMU(IM1, UM1) - DELTA
84600 RMOMU(IM2, UM2) = RMOMU(IM2, UM2) + DELTA
84700 RETURN
84800 END
84900 C
85000 C .....
85100 C
85200 SUBROUTINE VMTC(IM1, IM2, UM1, UM2, Y3)
85300 COMMON/UGF/RMOMV(50,50),RMOMU(50,50)
85400 COMMON /ZROPS/ MAXPOR, NPORT,

```

```

85500      $ DRPDEN(10), DRPDIA(10), DRPDOT(10), DRFRFQ(10),
85600      $ XDINIT(10), YDINIT(10), TDINIT(10), UDINIT(10), VDINIT(10),
85700      $ XB(48), YB(48),
85800      $ UB(48, 24), VB(48, 24), UGOLD(48, 24), VGOLD(48, 24),
85900      $ CDD, GRAVX, GRAVY, RAD, RHOGAS, PI, CGAS, VGAS,
86000      $ XDOLD, YDOLD, TDOLD, UDOLD, VDOLD,
86100      $ XDNW, YDNW, TDNW, UDNW, VDNW,
86200      $ DT, DTINC, DTRED, RHOL,
86300      $ ISTEPS, INTCTR, IFLAGZ, IHIT, MAXSTP, MAXCT, INTELG,
86400      $ IC, UC, IV, UV, IS, US, IF, UR, IHOLD, UHOLD, ICONST,
86500      $ NCASE, MCASE, UCMAX(48), ADI, ADO
86600      C
86700      DELTA = (4.0 * PI * RHOL * (-RAD ** 3) / 1.0) * YI
86800      $ * DRFRFQ(NPORT)
86900      RMOMV(IM1, UM1) = RMOMV(IM1, UM1) + DELTA
87000      RMOMV(IM2, UM2) = RMOMV(IM2, UM2) + DELTA
87100      RETURN
87200      END
87300      C
87400      C .....
87500      C
87600      SUBROUTINE HITWAL
87700      C      FLAG IHIT is set to 1 if the DROP hits the wall,
87800      C      else, it is set to 0.
87900      C      COMMON /DROPE/ MAXDPR, NPORT,
88000      $ DRPDEN(10), DRPDIA(10), DRPDOT(10), DRFRFQ(10),
88100      $ XDINIT(10), YDINIT(10), TDINIT(10), UDINIT(10), VDINIT(10),
88200      $ XB(48), YB(48),
88300      $ UB(48, 24), VB(48, 24), UGOLD(48, 24), VGOLD(48, 24),
88400      $ CDD, GRAVX, GRAVY, RAD, RHOGAS, PI, CGAS, VGAS,
88500      $ XDOLD, YDOLD, TDOLD, UDOLD, VDOLD,
88600      $ XDNW, YDNW, TDNW, UDNW, VDNW,
88700      $ DT, DTINC, DTRED, RHOL,
88800      $ ISTEPS, INTCTR, IFLAGZ, IHIT, MAXSTP, MAXCT, INTELG,
88900      $ IC, UC, IV, UV, IS, US, IF, UR, IHOLD, UHOLD, ICONST,
89000      $ NCASE, MCASE, UCMAX(48), ADI, ADO
89100      C
89200      IF (UR ** 2. * UCMAX(48) / 2. + 1.0) THEN
89300      $   WRITE(*,*) 'DROP HITS THE WALL'
89400      $   IHIT = 1
89500      $   ELSE
89600      $   IHIT = 0
89700      $   ENDIF
89800      $   RETURN
89900      $   END
90000      C
90100      C .....
90200      C
90300      SUBROUTINE RUNGE4
90400      C      This routine does a fourth order Runge-Kutta integration.
90500      C      It calls the routine KPDYD which calculates the
90600      C      Runge-Kutta coefficients K0, K1, K2 and K3.
90700      C
90800      C      COMMON /DROPE/ MAXDPR, NPORT,
90900      $ DRPDEN(10), DRPDIA(10), DRPDOT(10), DRFRFQ(10),
91000      $ XDINIT(10), YDINIT(10), TDINIT(10), UDINIT(10), VDINIT(10),
91100      $ XB(48), YB(48),
91200      $ UB(48, 24), VB(48, 24), UGOLD(48, 24), VGOLD(48, 24),
91300      $ CDD, GRAVX, GRAVY, RAD, RHOGAS, PI, CGAS, VGAS,
91400      $ XDOLD, YDOLD, TDOLD, UDOLD, VDOLD,
91500      $ XDNW, YDNW, TDNW, UDNW, VDNW

```

```

91600      $ DT, DTINC, DTRED, RHOL,
91700      $ ISTEPS, INTCTR, IFLAG2, IHIT, MAXSTEP, MAXCT, INTFLG,
91800      $ IC, JC, IV, JV, IG, JG, IF, JF, ICOL, JCOL, ICD, JCD,
91900      $ MCASE, MCD, JCD, JCD, JCD, JCD, JCD, JCD, JCD, JCD,
92000      $ DIMENSION XXX(10), YYY(10),
92100      $ F1(10), F2(10), F3(10), F4(10)
92200      $
92300      XXX(1) = UCOL
92400      XXX(2) = VCOL
92500      XXX(3) = XCOL
92600      XXX(4) = YCOL
92700      IF (DT .LE. 0.0) THEN
92800          WRITE(6, *) ' INPUT THE INTEGRATION TIME STEP'
92900          READ(5, *) DT
93000          WRITE(6, *) ' INTEGRATION TIME STEP = ', DT
93100      ELSEIF
93200          DT = 0.0
93300          CALL XTIME(1, XXX, F1)
93400          DT = 1.0
93500          YYY(1) = XXX(1) + DT * F1(1)
93600          CONTINUE
93700          CALL XTIME(2, YYY, F2)
93800          DT = 1.0
93900          YYY(2) = XXX(1) + DT * F2(1)
94000          CONTINUE
94100          CALL XTIME(3, YYY, F3)
94200          DT = 1.0
94300          YYY(3) = XXX(1) + DT * F3(1)
94400          CONTINUE
94500          CALL XTIME(4, YYY, F4)
94600          DT = 1.0
94700          UCOL = (F1(1) + F2(1) + F3(1) + F4(1)) / 4.0
94800          XXX(1) = XXX(1) + DT * UCOL
94900          CONTINUE
95000
95100      $ NEW = XXX(1)
95200      $ NEW = XXX(2)
95300      $ NEW = XXX(3)
95400      $ NEW = XXX(4)
95500      $ NEW = XXX(4)
95600      $ NEW = XXX(4)
95700      $ NEW = XXX(4)
95800
95900      .....
96000
96100      $ CALL XTIME(1, XXX, F1)
96200      $ CALL XTIME(2, YYY, F2)
96300      $ CALL XTIME(3, YYY, F3)
96400      $ CALL XTIME(4, YYY, F4)
96500      $ CALL XTIME(5, YYY, F5)
96600      $ CALL XTIME(6, YYY, F6)
96700      $ CALL XTIME(7, YYY, F7)
96800      $ CALL XTIME(8, YYY, F8)
96900      $ CALL XTIME(9, YYY, F9)
97000      $ CALL XTIME(10, YYY, F10)
97100      $ CALL XTIME(11, YYY, F11)
97200      $ CALL XTIME(12, YYY, F12)
97300      $ CALL XTIME(13, YYY, F13)
97400      $ CALL XTIME(14, YYY, F14)
97500      $ CALL XTIME(15, YYY, F15)
97600      $ CALL XTIME(16, YYY, F16)
97700      $ CALL XTIME(17, YYY, F17)
97800      $ CALL XTIME(18, YYY, F18)
97900      $ CALL XTIME(19, YYY, F19)
98000      $ CALL XTIME(20, YYY, F20)
98100      $ CALL XTIME(21, YYY, F21)
98200      $ CALL XTIME(22, YYY, F22)
98300      $ CALL XTIME(23, YYY, F23)
98400      $ CALL XTIME(24, YYY, F24)
98500      $ CALL XTIME(25, YYY, F25)
98600      $ CALL XTIME(26, YYY, F26)
98700      $ CALL XTIME(27, YYY, F27)
98800      $ CALL XTIME(28, YYY, F28)
98900      $ CALL XTIME(29, YYY, F29)
99000      $ CALL XTIME(30, YYY, F30)
99100      $ CALL XTIME(31, YYY, F31)
99200      $ CALL XTIME(32, YYY, F32)
99300      $ CALL XTIME(33, YYY, F33)
99400      $ CALL XTIME(34, YYY, F34)
99500      $ CALL XTIME(35, YYY, F35)
99600      $ CALL XTIME(36, YYY, F36)
99700      $ CALL XTIME(37, YYY, F37)
99800      $ CALL XTIME(38, YYY, F38)
99900      $ CALL XTIME(39, YYY, F39)
100000     $ CALL XTIME(40, YYY, F40)

```



```

97700      DIMENSION X(N),F(N)
97800      COMMON/GGF/RMOMV(50,50),RMOMC(50,50)
97900      CONST = (RHOGAS * CDD * 3.0) / (A.0 * RHOL * RAD)
98000      * SQRT((UGAS - X(1)) ** 2 + (VGAS - X(2)) ** 2)
98100      F(1) = CONST * (UGAS - X(1)) * GRAVX
98200      F(2) = CONST * (VGAS - X(2)) * GRAVY
98300      F(3) = X(1)
98400      F(4) = X(2)
98500      RETURN
98600      END
98700
98800
98900
99000
99100      SUBROUTINE CONVAR
99200      THIS ROUTINE IS USED BY CON CHECKING FOR THE
99300      GLOBAL CONVERGENCE OF THE SYSTEM. A COM OF SQUARE
99400      DIFFERENTIALS
99500
99600
99700      COMMON / CONVAR / MERRIN, NLEFT,
99800      1  XERRN(10), XERRTA(10), TANNUT(10), GERRN(10),
99900      1  YERRN(10), YERRTA(10), TANNIT(10), GERRIT(10), YERRIT(10),

```

```

00100      $ AB(46), YB(46),
00200      $ CG(46, 24), VG(46, 24), CGOLD(46, 24), VGOLD(46, 24),
00300      $ CDD, GRAVX, GRAVY, RAD, RHOGAS, FI, CGAS, VGAS,
00400      $ XGOLD, YGOLD, TGOLD, UGOLD, VGOLD,
00500      $ XNEW, YNEW, TNEW, UNEW, VNEW,
00600      $ DT, DTINC, DTRED, RHOL,
00700      $ ISTERD, INTCY, IFLAG2, IHIT, MAXSTP, MAXCY, INTFL,
00800      $ IO, JO, IV, JV, IO, JU, IR, JR, IHOLD, UHOLD, ICOUNT,
00900      $ MOUSE, MOCASE, UCMAX(46), XDI, YDU
01000
01100
01200      ICOUNT = ICOUNT + 1
01300      IF (ICOUNT.EQ. 1) THEN
01400          Ignore the first iteration.
01500          IFLAG2 =
01600          RETURN
01700      ENDIF
01800      COMVECT =
01900      COMVECT =
02000      DO 200 J = 1, NDI
02100          DO 200 U = 1, NDU
02200              COMU = COMU + ((CGOLD(I,U) - CG(I,U)) ** 2)
02300          CONTINUE
02400      XCOM = XDI + YDU * 1.025
02500      IF (XCOM.GT. COMU) THEN
02600          IFLAG2 = 1
02700      ELSE
02800          IFLAG2 = 0
02900      ENDIF
03000      DO 300 I = 1, NDI
03100          DO 300 U = 1, NDU
03200              COMV = COMV + ((YGOLD(I,U) - YG(I,U)) ** 2)
03300          CONTINUE
03400      IF (XCOM.GT. COMV) THEN
03500          IFLAG2 = 1
03600      ELSE
03700          IFLAG2 = 0
03800      ENDIF
03900      IF (IFLAG2.EQ. 1) THEN
04000          IF (IFLAG2.EQ. 1) THEN
04100              IFLAG2 = 1
04200          ELSE
04300              RETURN
04400          ENDIF
04500      ELSE
04600          IF (DT.GT. DTMAX) THEN
04700              RETURN
04800          ELSE
04900              RETURN
05000          ENDIF
05100      ...
05200      ...

```

APPENDIX B  
PROGRAM LISTING OF STEMSORT

```

00015
00016
00017
00018
00019 SUBROUTINE STEMFIND (STEMFND,IMAX,JMAX,X,Y)
00020     Subroutine to find and record data for
00021     streamline plots.
00022     Lines from 1 to 95
00023
00024
00025 ** Variable Definitions **
00026
00027 STEMFND = stream function values at grid points
00028 POINTS = plotting points
00029 XVAL = stream function value of current stream line
00030 DVAL = interval between streamlines (xval/10)
00031 NVAL = number of values from 1 grid lines
00032 JVAL = number of values from J grid lines
00033 IOLD = distance from point to previous J grid line
00034 JOLD = distance between two succeeding J grid lines
00035 IBOUND = value of previous boundary point
00036 JBOUND = value of previous boundary point
00037 ITEMP = boundary point number in loop sort
00038 IEN = distance between two succeeding J grid lines
00039 IENOLD = distance from point to previous J grid line
00040 IMAX = number of J grid lines
00041 JMAX = number of J grid lines at each J grid value
00042 NVAL = number of points found for plotting
00043 NVALOLD = J grid value for point near boundary
00044 IENOLD = value of J grid line just past a corner
00045 IEN = J grid number in loop sort - point number
00046 IENOLD = value of previous point in loop sort
00047 IENOLD = number of points on lower side of loop
00048 IENOLD = number of points on lower side of loop
00049
00050
00051
00052
00053
00054
00055
00056
00057
00058
00059
00060
00061
00062
00063
00064
00065
00066
00067
00068
00069
00070
00071
00072
00073
00074
00075
00076
00077
00078
00079
00080
00081
00082
00083
00084
00085
00086
00087
00088
00089
00090
00091
00092
00093
00094
00095
00096
00097
00098
00099
00100
00101
00102
00103
00104
00105
00106
00107
00108
00109
00110
00111
00112
00113
00114
00115
00116
00117
00118
00119
00120
00121
00122
00123
00124
00125
00126
00127
00128
00129
00130
00131
00132
00133
00134
00135
00136
00137
00138
00139
00140
00141
00142
00143
00144
00145
00146
00147
00148
00149
00150
00151
00152
00153
00154
00155
00156
00157
00158
00159
00160
00161
00162
00163
00164
00165
00166
00167
00168
00169
00170
00171
00172
00173
00174
00175
00176
00177
00178
00179
00180
00181
00182
00183
00184
00185
00186
00187
00188
00189
00190
00191
00192
00193
00194
00195
00196
00197
00198
00199
00200
00201
00202
00203
00204
00205
00206
00207
00208
00209
00210
00211
00212
00213
00214
00215
00216
00217
00218
00219
00220
00221
00222
00223
00224
00225
00226
00227
00228
00229
00230
00231
00232
00233
00234
00235
00236
00237
00238
00239
00240
00241
00242
00243
00244
00245
00246
00247
00248
00249
00250
00251
00252
00253
00254
00255
00256
00257
00258
00259
00260
00261
00262
00263
00264
00265
00266
00267
00268
00269
00270
00271
00272
00273
00274
00275
00276
00277
00278
00279
00280
00281
00282
00283
00284
00285
00286
00287
00288
00289
00290
00291
00292
00293
00294
00295
00296
00297
00298
00299
00300
00301
00302
00303
00304
00305
00306
00307
00308
00309
00310
00311
00312
00313
00314
00315
00316
00317
00318
00319
00320
00321
00322
00323
00324
00325
00326
00327
00328
00329
00330
00331
00332
00333
00334
00335
00336
00337
00338
00339
00340
00341
00342
00343
00344
00345
00346
00347
00348
00349
00350
00351
00352
00353
00354
00355
00356
00357
00358
00359
00360
00361
00362
00363
00364
00365
00366
00367
00368
00369
00370
00371
00372
00373
00374
00375
00376
00377
00378
00379
00380
00381
00382
00383
00384
00385
00386
00387
00388
00389
00390
00391
00392
00393
00394
00395
00396
00397
00398
00399
00400
00401
00402
00403
00404
00405
00406
00407
00408
00409
00410
00411
00412
00413
00414
00415
00416
00417
00418
00419
00420
00421
00422
00423
00424
00425
00426
00427
00428
00429
00430
00431
00432
00433
00434
00435
00436
00437
00438
00439
00440
00441
00442
00443
00444
00445
00446
00447
00448
00449
00450
00451
00452
00453
00454
00455
00456
00457
00458
00459
00460
00461
00462
00463
00464
00465
00466
00467
00468
00469
00470
00471
00472
00473
00474
00475
00476
00477
00478
00479
00480
00481
00482
00483
00484
00485
00486
00487
00488
00489
00490
00491
00492
00493
00494
00495
00496
00497
00498
00499
00500
00501
00502
00503
00504
00505
00506
00507
00508
00509
00510
00511
00512
00513
00514
00515
00516
00517
00518
00519
00520
00521
00522
00523
00524
00525
00526
00527
00528
00529
00530
00531
00532
00533
00534
00535
00536
00537
00538
00539
00540
00541
00542
00543
00544
00545
00546
00547
00548
00549
00550
00551
00552
00553
00554
00555
00556
00557
00558
00559
00560
00561
00562
00563
00564
00565
00566
00567
00568
00569
00570
00571
00572
00573
00574
00575
00576
00577
00578
00579
00580
00581
00582
00583
00584
00585
00586
00587
00588
00589
00590
00591
00592
00593
00594
00595
00596
00597
00598
00599
00600
00601
00602
00603
00604
00605
00606
00607
00608
00609
00610
00611
00612
00613
00614
00615
00616
00617
00618
00619
00620
00621
00622
00623
00624
00625
00626
00627
00628
00629
00630
00631
00632
00633
00634
00635
00636
00637
00638
00639
00640
00641
00642
00643
00644
00645
00646
00647
00648
00649
00650
00651
00652
00653
00654
00655
00656
00657
00658
00659
00660
00661
00662
00663
00664
00665
00666
00667
00668
00669
00670
00671
00672
00673
00674
00675
00676
00677
00678
00679
00680
00681
00682
00683
00684
00685
00686
00687
00688
00689
00690
00691
00692
00693
00694
00695
00696
00697
00698
00699
00700
00701
00702
00703
00704
00705
00706
00707
00708
00709
00710
00711
00712
00713
00714
00715
00716
00717
00718
00719
00720
00721
00722
00723
00724
00725
00726
00727
00728
00729
00730
00731
00732
00733
00734
00735
00736
00737
00738
00739
00740
00741
00742
00743
00744
00745
00746
00747
00748
00749
00750
00751
00752
00753
00754
00755
00756
00757
00758
00759
00760
00761
00762
00763
00764
00765
00766
00767
00768
00769
00770
00771
00772
00773
00774
00775
00776
00777
00778
00779
00780
00781
00782
00783
00784
00785
00786
00787
00788
00789
00790
00791
00792
00793
00794
00795
00796
00797
00798
00799
00800
00801
00802
00803
00804
00805
00806
00807
00808
00809
00810
00811
00812
00813
00814
00815
00816
00817
00818
00819
00820
00821
00822
00823
00824
00825
00826
00827
00828
00829
00830
00831
00832
00833
00834
00835
00836
00837
00838
00839
00840
00841
00842
00843
00844
00845
00846
00847
00848
00849
00850
00851
00852
00853
00854
00855
00856
00857
00858
00859
00860
00861
00862
00863
00864
00865
00866
00867
00868
00869
00870
00871
00872
00873
00874
00875
00876
00877
00878
00879
00880
00881
00882
00883
00884
00885
00886
00887
00888
00889
00890
00891
00892
00893
00894
00895
00896
00897
00898
00899
00900
00901
00902
00903
00904
00905
00906
00907
00908
00909
00910
00911
00912
00913
00914
00915
00916
00917
00918
00919
00920
00921
00922
00923
00924
00925
00926
00927
00928
00929
00930
00931
00932
00933
00934
00935
00936
00937
00938
00939
00940
00941
00942
00943
00944
00945
00946
00947
00948
00949
00950
00951
00952
00953
00954
00955
00956
00957
00958
00959
00960
00961
00962
00963
00964
00965
00966
00967
00968
00969
00970
00971
00972
00973
00974
00975
00976
00977
00978
00979
00980
00981
00982
00983
00984
00985
00986
00987
00988
00989
00990
00991
00992
00993
00994
00995
00996
00997
00998
00999
01000

```

```

0083      IF (MAXVAL.GT.0) GOTO 50
0084      C      Sort points for loop condition...
0085      IF (BYVAL.GT.1) GOTO 50
0086      C      Convert points from grid coordinates to x,y values
0087      DO 34 J=1,NMAX
0088      IF (POINTS(J,1).GT.0) GOTO 31
0089      POINTS(J,1)=0.0
0090      31 IF (POINTS(J,2).GT.0) GOTO 32
0091      POINTS(J,2)=0.0
0092      C      Find y-value by linear interpolation
0093      32 DELX=POINTS(J,2)-INT(POINTS(J,2))
0094      DELY=Y(INT(POINTS(J,2))+1)-Y(INT(POINTS(J,2)))
0095      POINTS(J,2)=(INT(POINTS(J,2)))+DELY*DELX
0096      C      Find x-value by linear interpolation...
0097      IF (INT(POINTS(J,1)).EQ.POINTS(J,1)) GOTO 33
0098      DELX=X(INT(POINTS(J,1))+1)-X(INT(POINTS(J,1)))
0099      DELY=X(INT(POINTS(J,1))+1)-X(INT(POINTS(J,1)))
0100      POINTS(J,1)=(INT(POINTS(J,1)))+DELY*DELX
0101      GOTO 34
0102      33 POINTS(J,1)=X(INT(POINTS(J,1)))
0103      34 CONTINUE
0104      DO 35 J=1,NMAX
0105      WRITE (N,K) POINTS(J,1),POINTS(J,2)
0106      35 CONTINUE
0107      C      Write end of block marker after each group of points...
0108      WRITE (N,K) 999,999,9
0109      36 CONTINUE
0110      C      Write end of file marker after all points...
0111      WRITE (N,K) 999,9,999,9
0112      CLOSE (UNIT=N)
0113      RETURN
0114      **      Loop sort section      **
0115      C      Initialize pointers...
0116      50 INPTR=0
0117      OUTCOUNT=
0118      ILL=1
0119      DO 51 I=1,NMAX
0120      C      Sort points with duplicate y-coord values.
0121      C      Put points with higher x-value to end of
0122      C      array starting at end and moving up...
0123      IF (POINTS(I,1).EQ.0) THEN
0124      TEMPTS(NMAX+OUTCOUNT+1)=POINTS(I,1)
0125      TEMPTS(NMAX+OUTCOUNT+2)=POINTS(I,2)
0126      OUTCOUNT=OUTCOUNT+1
0127      ELSE
0128      INPTR=INPTR+1
0129      TEMPTS(INPTR+1)=POINTS(I,1)
0130      TEMPTS(INPTR+2)=POINTS(I,2)
0131      INPTR=
0132      ILL=POINTS(I,1)
0133      51 CONTINUE
0134      C      Move upper points to top of array...
0135      DO 52 I=1,OUTCOUNT
0136      POINTS(I,1)=TEMPTS(NMAX+OUTCOUNT+1+I)
0137      POINTS(I,2)=TEMPTS(NMAX+OUTCOUNT+1+I)
0138      52 CONTINUE
0139      C      Move lower points to bottom of array...
0140      DO 53 I=1,INPTR
0141      POINTS(OUTCOUNT+1+I)=TEMPTS(I,1)
0142      POINTS(OUTCOUNT+1+I)=TEMPTS(I,2)
0143      53 CONTINUE
0144      C      Add extra point to close loop...
0145      C      Unless loop is open.
0146      IF (POINTS(N+1).EQ.0) GOTO 55
0147      NMAX=NMAX+1
0148      POINTS(NMAX,1)=POINTS(1,1)
0149      POINTS(NMAX,2)=POINTS(1,2)

```

```

0147      POINTS = (MAX-1)*JMAX
0150      GO TO 30
0151      END
0152
0153      SUBROUTINE INTERP(SF,N,IJMAX,JMAX,STVAL,POINTS,PMAX,LEXP)
0154      C-- *      Sub to find grid points of streamline points
0155      C      interpolate linearly between grid points along
0156      C      lines of constant stream value...
0157      C
0158      C      ** Variable Definitions **
0159      C
0160      C      SF,N...streamfunction values for grid points
0161      C      STVAL...streamfunction value for this stream line
0162      C      POINTS...array of plotting points for stream line
0163      C      IJFOR...position of point between two grid lines
0164      C      DELI1... distance between two last points for stval=1.0
0165      C      DELI2... distance between next to last points '
0166      C      IJMAX...number of plotting points *points
0167      C      JMAX...number of j grid lines
0168      C      IJMAX...number of i grid lines at each j grid line
0169      C      LEEXP... grid line following a division
0170      C      REATTACH... Flag for reattachment point in loop
0171      C      IJMIN...lower loop boundary for stval=1.0
0172      C
0173      REAL SF(N),STVAL,POINTS(POINTS),IJFOR,DELI1,DELI2
0174      INTEGER PMAX,IJMAX,JMAX,LEEXP,REATTACH,IJMIN
0175      PMAX=0
0176      REATTACH=0
0177      C      set appropriate lower i grid value for loop
0178      IF (STVAL.EQ.1.0) THEN
0179      C      add separation point for stval=1.0 case...
0180      IJMIN=LEXP
0181      POINTS(1)=IJMIN+1
0182      POINTS(IJMAX)=IJMAX-LEXP+1
0183      PMAX=1
0184      ELSE
0185      IJMIN=1
0186      ENDIF
0187      C      add separation loop for points...
0188      DO 100 I=IJMIN,IJMAX
0189      DO 100 J=1,JMAX
0190      IF (REATTACH.EQ.1) GO TO 100
0191      IF (SF(N,I,J).LT.STVAL) PMAX = SF(N,I,J) - STVAL GO TO 100
0192      IF (SF(N,I,J).GE.STVAL) PMAX = SF(N,I,J) - STVAL GO TO 100
0193      IF (STVAL.EQ.1.0) GO TO 100
0194      IF (SF(N,I,J).LT.STVAL) PMAX = SF(N,I,J) - STVAL GO TO 100
0195      C      linear interpolation equation with divide by diff
0196      C      consideration...
0197      REATTACH = STVAL-SF(N,I,J) / (SF(N,I,LEEXP)-SF(N,I,J))
0198      PMAX=PMAX+1
0199      POINTS(PMAX)=I,J
0200      POINTS(PMAX+1)=I,LEEXP
0201      IF (J.EQ.JMAX) I=I+1,STVAL=1.0 GO TO 100
0202      C      add reattachment condition...
0203      REATTACH=1
0204      C      CONTINUE
0205      IF (STVAL.EQ.1.0) PMAX = POINTS(PMAX+1) - (JMAX-1) GO TO 100
0206      C      add reattachment point if necessary...
0207      PMAX=PMAX+1
0208      POINTS(PMAX)=IJMAX,INT(POINTS(PMAX-1)/4.5)
0209      DELI1=POINTS(PMAX)-POINTS(PMAX-1)
0210      DELI2=POINTS(PMAX-1)-POINTS(PMAX-2)
0211      POINTS(PMAX+1)=POINTS(PMAX-1) - DELI1 - DELI2
0212      GO TO RETURN
0213      END

```

APPENDIX C  
PROGRAM LISTING OF STRIPLOT

```

10.  PLOTTER FOR B475-AVT, WINARKY
20.  STEPLEXED PLOTTER
30.  JOEYSIN 00 *
40.  C H H STREAMLINE PLOTTING PROGRAM FOR DATA FROM STARRID
50.  C H H SUMMER 1955 LANCES L WINARKY
60.
70.  ***** VARIABLE DECLARATIONS
80.  C RTX, ARRAY OF PLOTTING POINT X VALUES
90.  C RTY, ARRAY OF PLOTTING POINT Y VALUES
100. C XSCALE, X AXIS SCALING FACTOR
110. C YSCALE, Y AXIS SCALING FACTOR
120. C NPTS, NUMBER OF POINTS
130. C
140. C REAL RTX, RTY, XSCALE, YSCALE
150. C INTEGER NPTS
160. C
170. C INITIALIZE PLOTTER TO STANDARD PEN
180. C CALL SDRPLT, STOP
190. C OPEN UNIT=DATA, R=OUT
200. C ** CONTROL LOOP **
210. C DO
220. C DO 100
230. C DO 100
240. C READ RTX, RTY, XSCALE
250. C ** IF X VALUES END, END PLT
260. C IF RTX(1) EQ 999.99 GO TO 100
270. C ** IF NEGATIVE Y VALUES
280. C IF RTY(1) LT 0.0 GO TO 30
290. C RTX(1) = 0
300. C DO 100 RTX(1), RTY(1), XSCALE, YSCALE
310. C ** IF X=9999 THEN PLOT POINTS READ
320. C UNATTACHED
330. C ** IF FIRST LINE GO TO BOUNDARY SECTION
340. C IF RTX(1) EQ 0.0 GO TO 400
350. C ** IF NOT FIRST LINE GO TO MAIN PLOT SECTION
360. C IF RTX(1) EQ 0.0 GO TO 400
370. C CALL SDRPLT
380. C CLOSE UNIT=DATA
390. C STOP
400. C
410. C ** BOUNDARY PLOT SECTION **
420. C ** READ BOTH SCALING FACTORS FOR ALL POINTS X
430. C
440. C ** SET SCALING FACTORS FOR DESIRED MAXIMUM PLOT SIZE
450. C DO 100 RTX(1), RTY(1), XSCALE, YSCALE
460. C DO 100 RTX(1), RTY(1), XSCALE, YSCALE
470. C ** SCALE BOUNDARY POINTS
480. C DO 100 RTX(1), RTY(1), XSCALE, YSCALE
490. C RTX(1) = RTX(1) * XSCALE
500. C RTY(1) = RTY(1) * YSCALE
510. C DO 100 RTX(1), RTY(1), XSCALE, YSCALE
520. C ** INCLUDE SCALING FACTORS IN ARRAYS FOR SUBROUTINES
530. C RTX(1) = RTX(1) * XSCALE
540. C RTY(1) = RTY(1) * YSCALE
550. C RTX(1) = RTX(1) * XSCALE
560. C RTY(1) = RTY(1) * YSCALE
570. C ** PLOT UPPER BOUNDARY LINES
580. C CALL SDRPLT, RTX(1), RTY(1), XSCALE, YSCALE
590. C ** SET UP POINTS FOR LOWER BOUNDARY LINE
600. C DO 100
610. C RTX(1) = 0
620. C RTY(1) = 100.0
630. C RTX(1) = 0
640. C RTY(1) = 0

```





APPENDIX D  
PROGRAM LISTING OF PLOTGEN

```

*****
*
*      PROGRAM FOR          DATA PLOTTING PROGRAM
*
*      GENERATION OF A FILE FOR ONE WITH PLOT4 FOR
*      OR OTHER SUITABLE PLOTTING ROUTINE
*
*      M4/86        ALL    85        JAMES L. NIERER
*
*****

```

```

C
C      ** VARIABLE DEFINITIONS **
C

```

```

C      TRASH      FOUR CHARACTER TEST STRING TO LOCATE DATA
C      JUNK       SIX CHARACTER READ STRING FOR LOCATING DATA
C      IT         ARRAY OF DATA POINTS FROM PRINT FILE
C      X          ARRAY OF X VALUES FOR I GRID LINES
C      Y          ARRAY OF Y VALUES FOR J GRID LINES
C      YB         DELTA Y VALUE FOR STARTED IN BOUNDARY PLOT
C      PVAL       VALUE OF DATA CURRENTLY BEING PLOTTED
C      PTVAL      READ POSITION VALUE FOR FIRST POINT
C      PGD        ARRAY OF READ POSITION VALUES FOR PLOT POINTS
C      XX         X VALUE OF CURRENT POINT FOR WRITE TO FILE
C      YY         Y VALUE OF CURRENT POINT FOR WRITE TO FILE
C      J          LOOP VARIABLE = I GRID VALUE
C      IG        LOOP VARIABLE = I VALUE IN READ SECTION
C      PT1I       I GRID VALUE OF FIRST POINT
C      PT1J       J GRID VALUE OF FIRST POINT
C      IMAX       NUMBER OF I GRID LINES
C      OLDJMAX     NUMBER OF J GRID LINES AT PREVIOUS I LINE
C      PTNUM      NUMBER OF POINTS FOUND FOR THIS DATA VALUE
C      I          LOOP VARIABLE = I GRID VALUE
C      K          MASTER LOOP INDEX
C      JMAX       ARRAY OF NUMBER OF GRID LINES FOR EACH I LINE
C      DIR        DIRECTION NUMBER TO LOOK FOR NEXT POINT
C      NI         I VALUE OF POSSIBLE NEXT POINT
C      NJ         J VALUE OF POSSIBLE NEXT POINT
C      NTYP       POINT TYPE OF POSSIBLE NEXT POINT
C      IYP        POINT TYPE OF CURRENT POINT
C      PT1IYP     POINT TYPE OF FIRST POINT
C      NUMI       NUMBER OF I GRID LINES TO READ FOR
C      NUMJ       NUMBER OF J GRID LINES TO READ FOR
C      FOLDI      NUMBER OF I GRID LINES ON 1ST ROW OF PRINT OUT
C      NZ         VERY SMALL NON-ZERO NUMBER
C      CHKCNTR    COUNTER FOR NUMBER OF CHECKS FOR NEXT POINT
C      DELI       DELTA I VALUE FOR CHECK FOR NEXT POINT
C      DELJ       DELTA J VALUE FOR CHECK FOR NEXT POINT
C      *----- USER DEFINED VALUES -----*
C      DUMP       CONTROL FLAG FOR POINT DUMP RUN
C      VALUE      ARRAY OF VALUES TO BE PLOTTED
C      NUMVALS    NUMBER OF DATA VALUES TO BE PLOTTED
C      READTYP    TYPE OF FILE READ
C

```

```

CHARACTER*4 TRASH
CHARACTER*80 JUNK
REAL*8 PVAL,VALUE(12),PGD(30,30,2),IT(30,30),NZ
REAL XX,YY,XX1,YY1,YB,X(30),Y(30)
INTEGER J,JJ,PT1I,PT1J,IMAX,OLDJMAX,NUMVALS,READTYP
INTEGER PTNUM,I,K,JMAX(30),DIR,NI,NJ,NTYP,IYP,PT1IYP
INTEGER CHKCNTR,DELI(3,2),DELJ(3,2),NUMI,NUMJ,FOLDI
LOGICAL DUMP
35.120
DATA NZ/0.0000001/

```



[illegible]

```

      J=0
802  IF(J.GT.JMAXCLD) GOTO 801
      IF(CPDD(I+1,J+1,D).LT.(0.00)) GOTO 804
      XX=XCLD
      YY=YCLD+Y(I+1,D)-Y(I,D)*PBDC(I+1,J+1,D)
      IY=I
      GOTO 803
804  IF(PBDC(I+1,J+1,D).LT.(0.00)) GOTO 802
      XX=XCLD+X(I+1,D)-XCLD*PBDC(I+1,J+1,D)
      Y=Y(I+1,D)
      IY=I+1
803  IF(IY=I)
      THEN
        PBDC(I+1,J+1,IY)=0
        WRITE(Z,*)'XXXXXX'
        PTNUM=PTNUM+1
        IF(PTNUM.EQ.10) GOTO 807
      ELSE
        N=KEND-SUBSTEDING-POINT+1
      ENDIF
800  IF(PTNUM.EQ.0) GOTO 803
      DIR=DIR+5
      SUBCENTRO
801  DIR=MOD(DIR,360)
      NTYP=1+MOD(DIR,NTYP+2)
      NE=1+DECEL*DIR*NTYP
      NW=1+DECEL*DIR*NTYP
      IF(PBDC(NE+1,N+1,NTYP).LT.(0.00)) GOTO 802
      SUBCENTRO=CENTR+1
      IF(1+MOD(CENTR,10).EQ.0) GOTO 803
      DIR=DIR+1
      GOTO 801
802  IF(NTYP.EQ.1) GOTO 805
      XX=XCLD+X(N+1,D)-XCLD*PBDC(NE+1,N+1,NTYP)
      XX=XCLD
801  IF(NTYP.EQ.2)
      THEN
        CC=XCLD+X(N+1,D)-XCLD*PBDC(NW+1,N+1,NTYP)
        CC=XCLD
      ELSE
        CC=XCLD
      ENDIF
      IY=NTYP
      PBDC(NE+1,N+1,IY)=0
      NW
      NE
      WRITE(Z,*)'XXXXXX'
      PTNUM=PTNUM+1
      GOTO 800
      IF(PTNUM.EQ.10) GOTO 807
803  IF(NTYP.EQ.3)
      THEN
        NTYP=1+MOD(DIR,NTYP+2)
        NE=1+DECEL*DIR*NTYP
        NW=1+DECEL*DIR*NTYP
        IF(CPDD(NE+1,N+1,NTYP).LT.(0.00)) GOTO 802
        WRITE(Z,*)'XXXXXX'
      ELSE
        CONTINUE
      ENDIF
      WRITE(Z,*)'999999999999'
      IF(PTNUM.EQ.0) GOTO 402
      GOTO 800
402  WRITE(Z,*)'ZZZZZZZZZZ'
401  CONTINUE
C      WRITE(ENDD,FILE='MAR85J123
      WRITE(Z,*)'000000000000'
      CLOSE(UNIT=2)

```



APPENDIX E  
PROGRAM LISTING OF PLOTR



```

000000   C*****
000001   C *****
000002   C *****
000003   C *****
000004   C *****
000005   C *****
000006   C *****
000007   C *****
000008   C *****
000009   C *****
000010   C *****
000011   C *****
000012   C *****
000013   C *****
000014   C *****
000015   C *****
000016   C *****
000017   C *****
000018   C *****
000019   C *****
000020   C *****
000021   C *****
000022   C *****
000023   C *****
000024   C *****
000025   C *****
000026   C *****
000027   C *****
000028   C *****
000029   C *****
000030   C *****
000031   C *****
000032   C *****
000033   C *****
000034   C *****
000035   C *****
000036   C *****
000037   C *****
000038   C *****
000039   C *****
000040   C *****
000041   C *****
000042   C *****
000043   C *****
000044   C *****
000045   C *****
000046   C *****
000047   C *****
000048   C *****
000049   C *****
000050   C *****
000051   C *****
000052   C *****
000053   C *****
000054   C *****
000055   C *****
000056   C *****
000057   C *****
000058   C *****
000059   C *****
000060   C *****
000061   C *****
000062   C *****
000063   C *****
000064   C *****
000065   C *****
000066   C *****
000067   C *****
000068   C *****
000069   C *****
000070   C *****
000071   C *****
000072   C *****
000073   C *****
000074   C *****
000075   C *****
000076   C *****
000077   C *****
000078   C *****
000079   C *****
000080   C *****
000081   C *****
000082   C *****
000083   C *****
000084   C *****
000085   C *****
000086   C *****
000087   C *****
000088   C *****
000089   C *****
000090   C *****
000091   C *****
000092   C *****
000093   C *****
000094   C *****
000095   C *****
000096   C *****
000097   C *****
000098   C *****
000099   C *****
000100   C *****

```

35.125

AD-A186 498

UNITED STATES AIR FORCE RESEARCH INITIATION PROGRAM  
1984 RESEARCH REPORTS (U) SOUTHEASTERN CENTER FOR  
ELECTRICAL ENGINEERING EDUCATION INC S W D PEELE

11/11

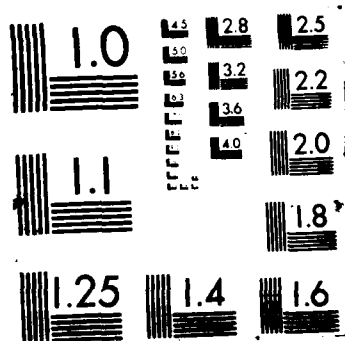
UNCLASSIFIED

MAY 86 AFOSR-TR-87-1721 F49620-82-C-0035

F/G 15/1

NL





SIC FIBER REINFORCED GLASS-CERAMIC COMPOSITES  
IN THE ZIRCONIA/MAGNESIUM ALUMINOSILICATE SYSTEM

Charles H. Drummond III  
Department of Ceramic Engineering

For the Period  
November 1, 1984 - December 15, 1985

SOUTHEASTERN CENTER FOR ELECTRICAL ENGINEERING EDUCATION  
Management Office, Central Florida Facility  
11th & Massachusetts Avenue  
St. Cloud, FL 32769

SubContract No. 84 RIP 36

April 1986

SiC Fiber Reinforced Glass-Ceramic Composites in the  
Zirconia/Magnesium Aluminosilicate System

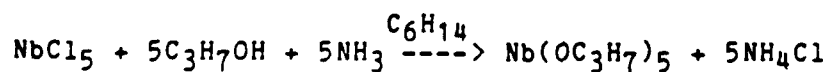
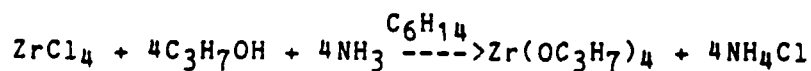
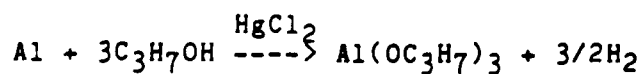
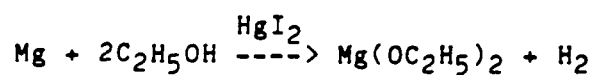
Charles H. Drummond III  
Dept. of Ceramic Engineering, The Ohio State University  
Columbus, Ohio 43210  
ABSTRACT

Glass-ceramic matrix compositions derived from metal alkoxides were vacuum hot-pressed. The compositions were nominally cordierite with variations in silica content and additions of up to 30% zirconia. Composites fabricated by vacuum hot-pressing the matrix compositions with SiC Nicalon<sup>®</sup> fibers were also studied. Variations in pressing conditions and subsequent heat treatments were examined. Crystalline phase development, bend strength and fracture toughness were evaluated as a function of hot-pressing parameters.

EXPERIMENTAL PROCEDURES

The matrix compositions investigated were primarily from the magnesia, alumina, zirconia and silica system. Each composition also contained a 5 weight percent Nb<sub>2</sub>O<sub>5</sub> addition which has been purported to provide barrier protection to the SiC fibers. The compositions were studied for phase development with and without the SiC fibers.

The matrix compositions were synthesized from the base metal or metal chloride from the following reactions:



The silica was added to the composition in the form of commercially available  $\text{Si}(\text{OC}_2\text{H}_5)_4$  (TEOS). The organic solutions were dropwise acid hydrolyzed in water. In order to study the matrix material only, part of the slurry was vacuum dried. The dried material was then calcined in air at  $600^\circ\text{C}$  to remove the bulk of the organics from the material. The calcined material was vacuum hot-pressed into inch round discs which were evaluated by XRD. The samples were then cut and polished for 4 point bend testing and indentation toughness using the Marshall, Noma and Evans indentation toughness method.<sup>1</sup>

The materials not processed into discs for the matrix material studies were slurry coated onto fibers which were then dried and calcined to  $450^\circ\text{C}$  prior to vacuum hot-pressing. These composite samples were evaluated for XRD. The study at this point is incomplete in the areas of composite mechanical properties. TEM studies are also planned for the composite and matrix only samples.

#### COMPOSITION SELECTION

Composition ZSPIN lies nearly midway between cordierite [ $2\text{MgO} \cdot 2\text{Al}_2\text{O}_3 \cdot 5\text{SiO}_2$ ] and spinel [ $\text{MgAl}_2\text{O}_4$ ] for its magnesia, alumina and silica content. The second composition studied was ZCOR which had a magnesia, alumina, and silica content corresponding to stoichiometric cordierite. ZMAS and MAS compositions contained excess silica beyond stoichiometric cordierite. These compositions are plotted on the magnesia, alumina, and silica ternary phase diagram in Figure 1.<sup>2</sup>

The MAS (magnesia, alumina, and silica) system has been

detailed by McMillan <sup>3</sup> to yield particularly high strengths when formed into glass-ceramics . The microstructure of glass-ceramics generally produces a very fine grained and dense material with superior strength to ceramics formed by traditional powder processing methods. The MAS system contains minerals that form platey and elongated grains that further enhance the strength due to the microstructure of the resulting glass-ceramic.

It has been shown by Faber and Evans <sup>4</sup> that the interweaving structure of elongated grains produces enhanced strength and toughness over the same mineral phases developed with lower resulting aspect ratios. Cordierite [ $2\text{MgO} \cdot 2\text{Al}_2\text{O}_3 \cdot 5\text{SiO}_2$ ] is an example of a mineral capable of forming platey and elongated grains consistent with the Faber and Evans model.

The thermal expansion of cordierite is less than the SiC fibers used in the composite. The choice of cordierite in the matrix was to enhance the formation of residual compressive forces in the matrix material while distributing the tensile load to the fibers. Spinel was chosen as a possible second phase in the Z6PIN composition due to its higher tensile strength than cordierite.

Each of the compositions in this study contained additions of  $\text{ZrO}_2$ . These additions were intended to act as a nucleation catalyst and as a means of transformation toughening to the matrix. It was understood in this study that critical conditions for successful transformation toughening were not optimized. The grain size and amount of the tetragonal zirconia phase are examples of two critical parameters regarding the toughening mechanism that were not optimized in this study.



## PHASE DEVELOPMENT IN THE MATRIX MATERIAL

Experiments determined that the first phases formed from the starting ZSPIN composition (without SiC) glass were spinel, sapphirine (a spinel type structure with formula  $Mg_7Al_{18}Si_3O_{40}$ ) and the tetragonal form of zirconia. These phases formed at temperatures of about 600°C. Zircon and cordierite formation were observed at 1300°C or greater. This temperature for zircon formation is consistent with the study of Conrad<sup>5</sup> regarding a glass-ceramic with a 10%  $ZrO_2$  content and a magnesium aluminosilicate composition between ZSPIN and ZCOR. The amount of zircon formed was found to increase with prolonged heating. After over an hour at 1300°, only about half the zirconia had been transformed to zircon. The amount of cordierite appeared to decrease as zircon was formed. Both cordierite and zircon form at the expense of sapphirine.

Kinetics appear to favor the formation of spinel, sapphirine and tetragonal zirconia for the ZSPIN composition. Sapphirine is similar in composition to cordierite and, therefore, likely enhances the kinetics of cordierite formation in the ZSPIN composition. Zircon, though favored in a free energy analysis, is slow to form.<sup>6,7,8</sup> From additional heatings at 1300°, it appeared that zircon and spinel would be the predominant final equilibrium phases. The kinetics of the zircon formation appear to be the rate limiting process in the reactions occurring at temperatures above 1250°C.

The objective of the composition ZSPIN was to develop spinel, cordierite and zirconia in the tetragonal structure. Equilibrium conditions would likely not allow the coexistence of these phases for the ZSPIN composition. The difference between the more rapid cordierite formation kinetics and the zircon kinetics was not sufficient to form cordierite without a significant amount of zircon for the ZSPIN composition utilized in this study.

The ZSPIN matrix material strength (no SiC fibers added) in a 4 point bend test showed the strength decreased rapidly as the cordierite and zircon phases formed. The samples with spinel, sapphirine and tetragonal zirconia phases exhibited 22 to 24 KSI strength with up to  $2.2 \text{ MPam}^{1/2}$  toughness. Bend bars with spinel, cordierite, zircon and the remaining tetragonal zirconia had only 7.5 to 13 KSI strength with the toughness values averaging approximately 1.6. This strength degradation can be readily explained when viewing a polished matrix material sample magnified at 100X. With the formation of zircon, a large number of significant flaws were readily apparent within the samples. Zircon represents roughly a 20% density increase over spinel (or sapphirine) and a 30% density increase over cordierite. No appreciable shrinkage occurred during hot-pressing in the temperature range of the zircon formation. It is apparent that the formation of the higher density zircon phase caused the resultant flaws observed on the low strength samples.

Experimentally, ZCOR and ZMAS compositions were found to contain primarily cordierite with tetragonal zirconia.

At 1300° and above, zircon began to form. This pattern of zircon formation parallels the situation found in ZSPIN and the Conrad study.<sup>5</sup> It appears that the zircon formation mechanism is not sensitive to modest variations in zirconia or silica concentration.

The transition from 1250°C to 1300°C not only introduced zircon but cordierite was observed to transform from the  $\mu$  to the  $\alpha$  form. This transformation also accompanied the disappearance of sapphirine. Tetragonal zirconia remained, since the reaction to form zircon was sluggish. The tetragonal zirconia content was not only being diminished by the zircon formation, but a portion of the tetragonal phase appeared to become destabilized and monoclinic zirconia was then observed. The monoclinic zirconia formation at 1300°C corresponded to the disappearance of sapphirine and the formation of spinel only as the ternary component. Since spinel contains a higher magnesia content than sapphirine, it is likely that a portion of the magnesia which had been a stabilizer for the tetragonal zirconia had reacted with the sapphirine to form spinel which in turn freed silica for the zircon formation.

From the compositions studied in these experiments, a simplified nonequilibrium isothermal ternary section can be approximated. With  $\text{MgAl}_2\text{O}_4$  being considered as a single component and the aid of the  $\text{ZrO}_2$ - $\text{SiO}_2$  phase diagram<sup>9</sup>, these compositions and their resulting phases can be illustrated semiquantitatively. Figures 2 and 3 illustrate the spinel-zirconia-silica nonequilibrium ternary isothermal section at 1250°C and 1300°C.

Sapphirine cannot be properly depicted on the 1250° metastable ternary as shown with spinel, zirconia, and silica components. However, a combination of spinel and sapphirine appeared to be present at 1250°. Since structurally and compositionally spinel and sapphirine are very similar and the ternary provides a useful tool in visualizing the phase development of these materials, sapphirine is included on the isothermal section with spinel.

The metastable ternary section shown in Figure 2 indicates that even though the composition ZSPIN was unable to form cordierite and spinel with tetragonal zirconia without the formation of zircon, a slightly higher silica content composition than ZSPIN may cross out of the two phase region between spinel and zirconia that was observed at 1250°C. From examining the diagram, it is inferred that a metastable coexistence between spinel, cordierite and zirconia could be achieved with a composition of slightly higher silica content than ZSPIN.

#### DENSIFICATION

The matrix materials (without SiC fibers) densified most rapidly at 1200°C through 1250°C. The final density was dependent upon the applied pressure and the rate of temperature increase or hold time in this temperature range. Compositions ZSPIN and ZCOR were the most extensively studied for densification characteristics. ZSPIN densified up to 95% of theoretical when hot-pressed at 10°C/minute heating rate and 15 minutes at 1250°C under 1100 psi applied pressure. Crystalline phase development appeared to be unaffected by the applied pressure when varied from 0 to 1100 psi. Composition ZCOR was

extremely difficult to densify. At 1700 psi applied pressure, a 10°C/ minute heating rate and 15 minutes at top temperatures of 1250°C and 1300°C, the density appeared to be near 90% of theoretical.

Densification appeared to be one of the major difficulties encountered with the not only the matrix material without the SiC fibers but also in the composite materials as well. The composite materials required a densification temperature of approximately 1300°C. This relatively high densification temperature requirement also corresponds to a temperature range that has been reported by Mah et al <sup>11,12</sup> to seriously degrade the integrity of the SiC fibers.

In short, densification of the matrix material with and without the SiC fibers is a major reason for the poor mechanical properties exhibited in the compositions studied and would be a significant barrier for their use in any practical application. A fluxing additive to the matrix composition appears to be necessary in order to overcome the densification barrier of these materials.

#### ZIRCONIA TRANSFORMATION TOUGHENING

Comparing the strength and toughness of the samples prepared in this study with data from a Claussen<sup>13</sup> study (shown in table 1), it appears the transformation toughening was not realized in these experiments. The low density of the samples distorts the evaluation of the effectiveness of the zirconia toughening. Since the toughness measurement was conducted using an indenter method, the indenter location could be chosen to minimize the

crack interaction with the porosity. The toughness of the samples as well as the strength appears to be more consistent with non-toughened ceramics. A planned microscopy study of these materials should provide insight regarding the apparently unsuccessful toughening.

TABLE 1: Strength and Toughness

| Primary Phases                                | Data Source            | (MPa)   | $K_{IC}$ (MPa <sup>m</sup> <sup>1/2</sup> ) |
|---|------------------------|---------|---|
| Spinel, ZrO <sub>2</sub> t                    | Powers, Dryummond      | 110-165 | 2.0-2.4                                     |
| Spinel  | Claussen <sup>13</sup> | 180     | 2.0   |
| Spinel, ZrO <sub>2</sub> t<br>(toughened)     | Claussen <sup>13</sup> | 350-500 | 4-5   |
| Cordierite, ZrO <sub>2</sub> t                | Powers, Dryummond      | 60-85   | 1.4-1.6                                     |
| Cordierite                                    | Claussen <sup>13</sup> | 120     | 1.4   |
| Cordierite, ZrO <sub>2</sub> t<br>(toughened) | Claussen <sup>13</sup> | 300     | 3   |

#### PHASE DEVELOPMENT IN THE SiC FIBER COMPOSITE

The final composite was comprised of between 30% to 50% fibers. The fibers were the ceramic grade Nicalon<sup>®</sup>. The fibers were continuous and approximately 13 microns in diameter. The as received fibers were coated with a sizing. The sizing was removed by a rapid heat treatment at under 600°C before slurry coating the matrix material onto the fibers. The heat treatment time was less than a minute in an air atmosphere.

The major phases developed in the composites are illustrated in Figure 4. The matrix compositions appeared to contain a higher silica content than the matrix material alone. Since the fibers used contained a significant SiO<sub>2</sub> fraction, the higher silica matrix was not surprising.

The phase development in the composites appeared to be sluggish compared to the matrix material without the fibers. Comparing the composite metastable ternary at 1300°C with that of

the matrix only material (figures 4 and 3 respectively), it is apparent that the  $\mu$  to  $\alpha$  transformation is retarded and the zircon formation region is reduced in the composite materials. The mechanical properties evaluation of these composites is not yet complete to correlate with phase development.

It has been shown by Brennan<sup>14</sup> that  $\text{Nb}_2\text{O}_5$  precipitates as  $\text{NbC}$  near the fiber surface with a high carbon content material surrounding the fiber. Analytical microscopy is planned for the composites fabricated in this study. Results are not yet available to add to the observations made by Brennan. However, to understand the driving forces behind the role of the  $\text{Nb}_2\text{O}_5$  in the formation of  $\text{NbC}$  or carbon in the  $\text{SiC}$  fiber composites, a  $\text{Nb-Si-C-O}$  stability diagram was constructed. By examining a large number of potential reactions between  $\text{Nb}$ ,  $\text{Si}$ ,  $\text{C}$  and  $\text{O}$ , a diagram for the condensed phases stable at a given oxygen partial pressure and temperature was constructed. This diagram can be seen in Figure 5.

This stability diagram was constructed from data available in the JANAF thermochemical tables.<sup>7</sup> The data available in these tables do not consider the nonstoichiometric character of  $\text{Nb}_2\text{O}_5$  at high temperatures<sup>15</sup> nor of  $\text{NbC}$ .<sup>16</sup> Intermetallic compounds of  $\text{Nb}$  and  $\text{Si}$  as shown by Kocherzhinskiy et al<sup>18</sup> also do not have available the required thermochemical data, therefore, the lowest oxygen partial pressure region of the stability diagram is left unlabeled and is therefore incomplete.

The stability diagram shows some general trends:

1. Carbon can be stable in the presence of niobia and silica.
2. Niobia is not stable in the presence of its own carbide.

If both species are present, this would indicate localized variations in oxygen partial pressure within the composite exist. Such localized regions would suggest a diffusion barrier layer exists.

3. The oxides of niobium are not stable in the presence of SiC. The large free energy release for the formation of silica from SiC will drive the niobia-SiC reaction.

4. Silica is stable in the presence of carbon and niobium oxides at higher oxygen pressures and stable with NbC at lower oxygen pressures. The coexistence of carbon or niobia with NbC is separated by SiO<sub>2</sub> if the SiO<sub>2</sub> is acting as an oxygen or carbon diffusion barrier.

The stability diagram agrees with experimental evidence by supporting the potential existence of carbon between the SiC fiber surface and the matrix material. NbC would not be expected to coexist with carbon except at the oxygen partial pressure boundary which separates the NbC and C containing regions. Since the stability diagram does not illustrate the nonstoichiometric character of NbC, the boundary between NbC and C may actually be a region of nonstoichiometry rather than a distinct line.

#### CONCLUSIONS

The compositions investigated in general showed a substantial change in the crystalline phases formed between 1250°C and 1300°C. Accompanying this change was the development of zircon at the expense of the zirconia and the transformation of cordierite from the  $\mu$  to the  $\alpha$  form. The formation of



zircon coincided with the formation of large flaws in the matrix material which greatly degraded the material strength.

Metastable ternary isothermal diagrams at 1250°C and 1300°C were constructed for the compositions used in this study. The resulting diagram should be extremely useful in selecting future compositions for study.

Crystalline phase development of the composite samples seemed to lag behind that of the matrix material without the SiC fibers. The  $\mu$  to  $\alpha$  transformation of cordierite and the formation of zircon were two examples of lagging reactions. An isothermal section for the composite materials was estimated based on the experimental XRD diffraction data and is shown in Figure 4.

By utilizing available thermochemical data, a Nb-Si-O-C stability diagram was calculated. This stability diagram is offered as an aid in understanding the role of Nb<sub>2</sub>O<sub>5</sub> in SiC fiber composites.

## References

1. Marshall, D.B., Noma, T., Evans, A.G. "A Simple Method for Determining Elastic Modulus-to-Hardness Ratios using Knoop Indentation Measurements". Communications of the American Ceramic Society, Oct. 1982, C175-176.
2. Osborn, E.F., Muan, A. "MgO-Al<sub>2</sub>O<sub>3</sub>-SiO<sub>2</sub>", Fig. 712, Phase Diagrams for Ceramists, The American Ceramic Society.
3. McMillan, P.W., Glass-Ceramics, Academic Press London, 1979.
4. Faber, K.T. and Evans, A.G. "Crack Deflection Processes", Acta Metall. Vol. 31 [4], 565-584.
5. Conrad, M.A. "Phase Transitions in a Zirconia Nucleated MgO Al<sub>2</sub>O<sub>3</sub> 3SiO<sub>2</sub> Glass-Ceramic", Journ. Material Science 7, 1972, 527-530.
6. Besmann, T.M., "SOLGASMIX-PV, A Computer Program to Calculate Equilibrium Relationships in Complex Chemical Systems", Oak Ridge National Laboratory Report No. ORNL/TM-5775, Oak Ridge, Tenn. 37830, 1977.
7. JANAF Thermochemical Tables, NSRDS-NBS37 1971 edition and 1975 Supplement. Stull, D.R. and Prophet, H. Eds.
8. Geological Survey Bulletin #1452, "Thermodynamic Properties of Minerals and Related Substances", 1979, Robie, R., Hemingway, B. and Fisher, J. Eds., U.S. Government Printing Office, Washington, D.C. 1978.
9. Geller, R.F. and Lang, S.M. "SiO<sub>2</sub>-ZrO<sub>2</sub> Phase Diagram", Levin, E.M., Robbins, C.R., McMurdie, H.F. and Reser, M.K. Eds., NBS, American Ceramic Society, Columbus 1974.
10. Claussen, N., Ruhle, M. Heuer, A.H. Advances in Ceramics, Vol. 12, Science and Technology of Zirconia II.
11. Mah, T., Mendiratta, M.G., Katz, A.P., Ruh, R. and Mazdiasni, K.S. "Room-Temperature Mechanical Behavior of Fiber-Reinforced Ceramic-Matrix Composites", Communications of the American Ceramic Society, Journ. Am. Cer. Soc., 68 [1] C-27-30 (1985).
12. Mah, T., Hecht, N.L., McCullum, D.E., Hoenigman, J.R., Kim, H.M., Katz, A.P. and Lipsitt, H.A. "Thermal Stability of SiC Fibres", Journ. Material Science 1984 [19], 1191-1201.
13. Claussen, N. "Strengthening Strategies for ZrO<sub>2</sub>-Toughened Ceramics at High Temperatures" Materials Science and Engineering, 71 (1985) 23-38.

14. Brennan, J.J. "Additional Studies of SiC Fiber Reinforcement Glass-Ceramic Composites", Annual Report R83-916018-2 on ONR Contract N00014-82-C-0096, 14 Feb. 1983.
15. Balachandran, U., Eror, N.G. "Nonstoichiometric Disorder in Alpha  $\text{Nb}_2\text{O}_5$  at Elevated Temperatures", Journ. Mater. Sci. 1982 17 [5] 1286-96.
16. Samsonov, G.V., Upadkhaya, G.Sh. "Physical Properties of the Monocarbides of the Transition Metals in their Homogeneity Regions I.  $\text{TiC}_{1-x}$  and  $\text{NbC}_{1-x}$ " Sov. Pow. Met. and Met. Cer. 1969, 5, 394-398.
17. Kruger, J. Vacuum Metallurgy, Winkler, O. and Bakish, R. Eds., Elsevier Publishing Company, Amsterdam 1971, 165-167.
18. Kocherzhinskiy, Yu.A., Yupko, L.M. and Shishkin, E.A. "The Nb-Si Phase Diagram", Russian Metallurgy 1980 [1], 184-188.

Figure 1:  $\text{MgO}-\text{Al}_2\text{O}_3-\text{SiO}_2$  Diagram taken from that of E.F. Osborn and A. Muan. Figure 712, Phase Diagrams for Ceramists, The American Ceramic Society.

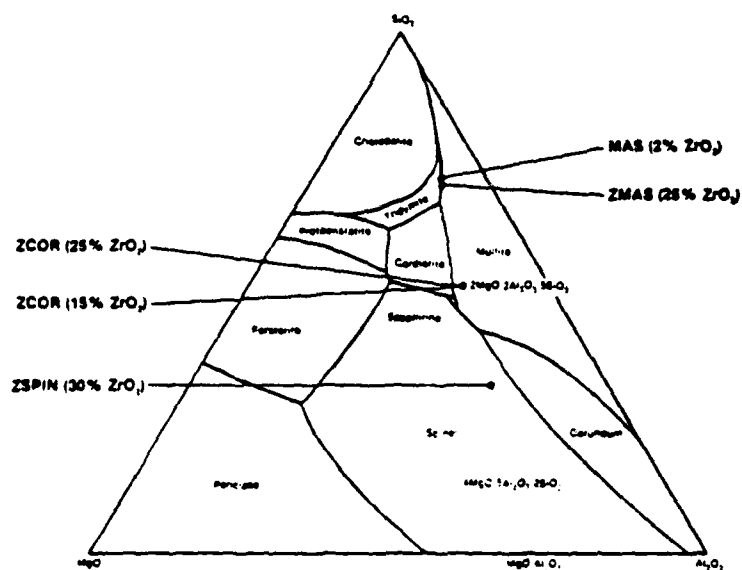


Figure 2:

**Predominant Crystalline Phases at 1250°C, 15 min.**

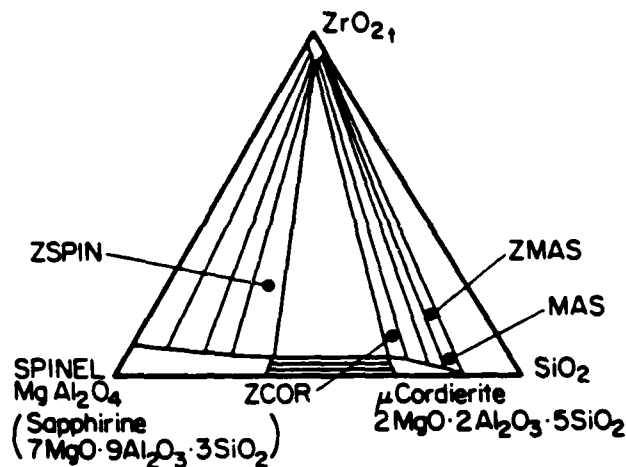


Figure 3:

**Predominant Crystalline Phases at 1300°C**

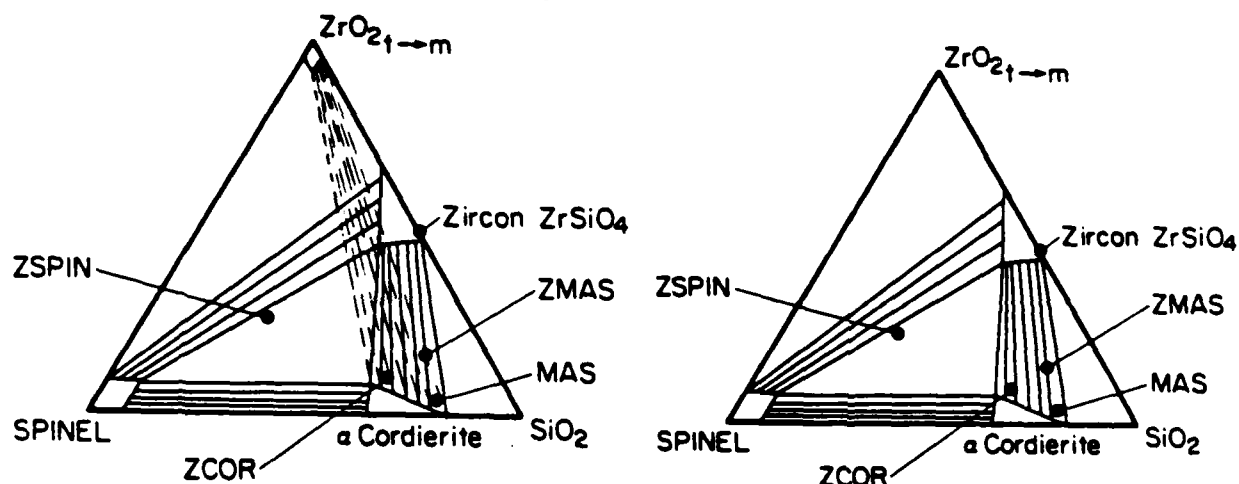


Figure 3 Left shows the major phases formed after 15 min. at 1300°. The dotted lines indicate that  $ZrO_2$  remains. Figure 3 Right indicates the expected final phases after extended heat treatment times.

Figure 4:

**Matrix & SiC fibers at 1300°C, 15 min.**

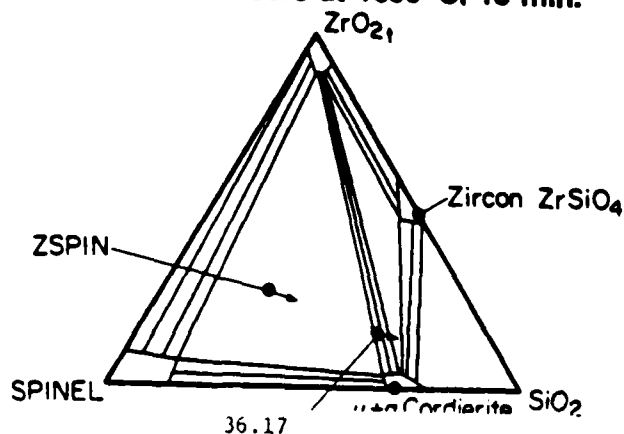
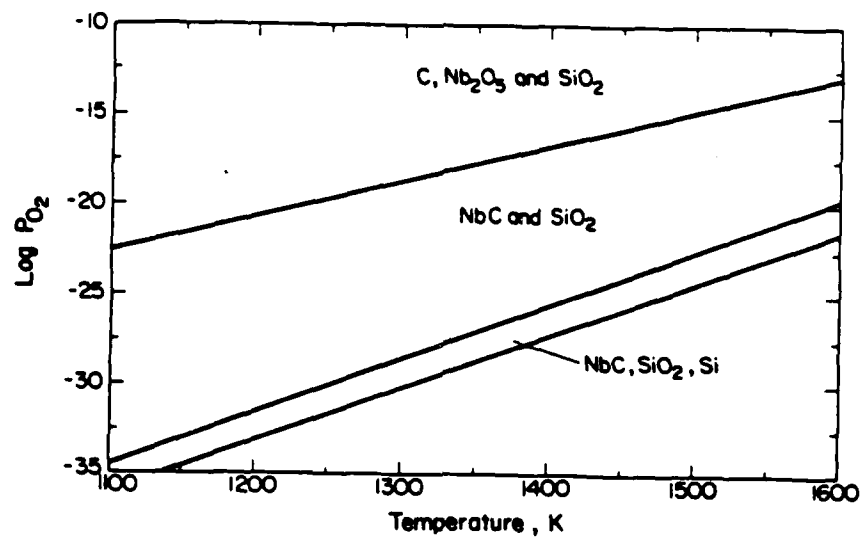


Figure 5: Nb-Si-O-C System Stability Diagram



END

DATE

FILM

JAN  
1988